NIGERIAN SOCIETY OF CHEMICAL ENGINEERS

(A Divisions of Nigerian Society of Engineers)

49th Annual CONFERENCE (KADA 2019)

PROCEEDINGS OF 49th ANNUAL CONFERENCE (KADUNA 2019) OF NIGERIAN SOCIETY OF CHEMICAL ENGINEERS

NIGERIAN SOCIETY OF CHEMICAL ENGINEERS

(A Divisions of Nigerian Society of Engineers)

Proceedings

49th Annual CONFERENCE (KADA 2019)

THEME:

ENHANCEMENT OF AGRICULTURAL VALUE CHAIN FOR ECONOMIC DEVELOPMENT: THE ROLE OF CHEMICAL ENGINEERING

13TH - 16TH NOVEMBER, 2019

www.nsche.org.ng

NIGERIAN SOCIETY OF CHEMICAL ENGINEERS

(a Division of Nigerian Society of Engineers)

PROCEEDINGS of the 49th NSChE Annual Conference (KADA 2019)

THEME:

ENHANCEMENT OF AGRICULTURAL VALUE CHAIN FOR ECONOMIC DEVELOPMENT: THE ROLE OF CHEMICAL ENGINEERS

www.nsche.org.ng

13th - 16th November 2019

Typeset and Printed in Nigeria for the Nigerian Society of Chemical Engineers (NSChE)

This Document was collated and produced by the Technical/Editorial Sub-Committee of the Local Organising Committee for the Annual Conference/General Meeting of the Nigerian Society of Chemical Engineers (KADA, 2019) holding at Kaduna, Nigeria

Technical/Editorial Sub-Committee of the 2019 Annual Conference

1.	Engr. Prof. B. O. Aderemi	-	Chairman
2.	Engr. Prof. B. J. El-Yakub	-	Member
3.	Engr. Dr. S. N. Mumah, FNSChE	-	"
4.	Engr. Dr. M. D. Jibrin	-	"
5.	Engr. Dr. A. Hamza	-	"
6.	Engr. Dr. S.M. Waziri	-	"
7.	Engr. M. L. Funtua	-	"
8.	Engr. Dr. H. F. Akande	-	Member/ Technical Secretary

BOARD OF DIRECTORS AND OFFICIALS

Chairman of the Board/National President
Engr. Onochie A. Anyaoku, FNSChE

Deputy National President
Engr. Saidu Aliyu Mohammed, FNSChE

DIRECTORS

Immediate Past President	Prof. Sam. S. Adefila, FNSChE
Publicity Secretary	Engr. Donatus Uweh, MNSChE
Asst. Publicity Secretary	Engr. Ben Akaakar, FNSChE
National Treasurer	Engr. Anthony Ogheneovo, MNSChE
Asst. National Treasurer	Engr. Dr. (Mrs.) Edith E. Alagbe, MNSChE
Executive Secretary	Samuel O. Bosoro, MNSChE

INTERNAL AUDITORS
Engr. Dr. (Mrs.) G. Akujobi-Emetuche, FNSChE
Engr. E. N. Ikezue, FNSChE

NATIONAL SECRETARIAT
Infinite Grace House, Plot 4, Oyetubo Street, Off Obafemi Awolowo Way, Ikeja, Lagos State
E-mail: nationalhqtrs@nsche.org.ng
nsche_headquarters@yahoo.com
Website: http://www.nsche.org.ng

2019 AGM/Conference Local Organizing Committee (LOC) Members

S/No	Name	Position	Address
1.	Engr. Prof. I. M. Bugaje , FNSChE	Chairman	Rector, Kaduna Polytechnic, Kaduna
2	Engr. C.O. Ezem	Co- Chairman	NNPC, Kaduna
3	Engr. G. T. Muhammad	Co- Chairman	NNPC, Kaduna
4	Engr .Prof. I. A. Mohammed-Dabo	Chapter Chairman	Ahmadu Bello University, Zaria
5	Engr. Prof. B. O. Aderemi	Member	Ahmadu Bello University, Zaria
6	Engr. Dr. M. K. Abdullahi	Member	Rector, Nuhu Bamalli Polytechnic, Zaria
7	Engr. E. A. Adebayo	Member	Kaduna Polytechnic, Kaduna
8	Engr. N.M. Inuwa	Member	Kaduna Polytechnic, Kaduna
9	Engr. Dr. B. H. Diya'udeen	Member	Ahmadu Bello University, Zaria
10	Engr. Dr. S. N. Mumah, FNSChE	Member	Kaduna Polytechnic, Kaduna
11	Engr. Prof. A. S. Ahmed	Member	Ahmadu Bello University, Zaria
12	Engr. Prof. B. J. El-Yakub	Member	Ahmadu Bello University, Zaria
13	Engr. Dr. A. Hamza	Member	Ahmadu Bello University, Zaria
14	Engr. I. Muazu	Member	Kaduna Polytechnic, Kaduna
15	Engr. M. L. Funtua	Member	NNPC
16	Engr. Dr. S. M. Waziri	Member	Ahmadu Bello University, Zaria
17	Engr. S. I. Lamido	Member	Kaduna Polytechnic, Kaduna
18	Engr. Dr. I. Haruna	Member	NARICT, Zaria
19	Engr. O. Safariel (Mrs.)	Member	NNPC
20	Engr. A.S. Anwar	Member	Kaduna Polytechnic, Kaduna
21	Engr. E. G. Kefas	Chapter /LOC Secretary	Kaduna Polytechnic, Kaduna

LOC Advisory Committee

S/No	Name	Position
1.	Engr. S. Bello	Former National President
2.	Engr. S. I. Sodangi	Former National President
3.	Engr. A. L. Yar'adua	Former National President
4.	Engr. A. Bukar	Immediate Past Chapter Chairman

Finance Sub-Committee

S/No	Name	Position
1	Engr. O. C. Ezem -	Chairman
2	Engr. Prof. I. M. Bugaje	Member
3	Engr. G. T. Muhammad	Member
4	Engr .Dr. M. K. Abdullahi	Member
5	Engr Dr. F. U. Nwafulugo (Mrs.)	Member
6	Engr. A.S. Anwar	Member
7	Engr. M. L. Funtua	Secretary

Technical/Editorial Sub-Committee

S/No	Name	Position
1.	Engr. Prof. B. O. Aderemi	Chairman
2.	Engr. Prof. B. J. El-Yakub	Member
3.	Engr. Dr. S. N. Mumah	Member
4.	Engr. Dr. A. Hamza	Member
5.	Engr. Dr. S.M. Waziri	Member
6.	Engr. Dr. H. F. Akande	Secretary

Welfare Sub-Committee

S/No	Name	Position
1.	Engr. G. T. Muhammad Chairman	Chairman
2.	Engr. I. Muazu	Member
3.	Engr. O. Safriel (Mrs.)	Member
4.	Engr. M. Abubakar (Mrs)	Member
5.	Engr. H. S. Zubair (Mrs.)	Secretary

Logistics/Protocol Sub-Committee

S/No	Name	Position
1	Engr. Dr. M. K. Abdullahi	Chairman
2	Engr. Dr. V. Kurah	Member
3	Engr. J. Waziri	Member
4	Engr. S. Haske	Member
5	Engr. P. O. Nwosibe	Member
6	Engr. M. Shehu.	Member
7	President Students' Chapter ABU Zaria	Member
8	President Students' Chapter Kadpoly	Member
9	Engr. S. Musa	Secretary

Publicity Sub-Committee

S/No	Name	Position
1	Engr. N. M. Inuwa	Chairman
2	Engr. G. Mohammed	Member
3	Engr. M. Baba	Member
4	Engr. U. Musa	Member
5	Engr. A. U. Alhassan	Member
6	Engr. S. I. Lamido	Secretary

Exhibition Sub-Committee

S/No	Name	Position
1	Engr. E. A. Adebayo	Chairman
2	Engr. A. U. Alhassan	Member
3	Engr. M. Murtala	Member
4	Engr. K. Lawal	Secretary

Security Sub-Committee

S/No	Name	Position
1	Engr. Dr. B.H. Diya'udeen	Chairman
2	Engr. M. H. Abdulkadir	Member
3	Engr. S. Lawal	Member
4	Engr. I. Muazu	Member
5	Engr. T. Nyam	Secretary

Registration Sub-Committee

S/No	Name	Position
1	Engr. Prof. I. A. Mohammed-Dabo	Chairman
2	Engr. E. G. Kefas	Member
3	Engr. N. M. Inuwa	Member
4	Engr. S. Mohammed	Member
5	Engr. I. Muazu	Member
6	Engr. S. Musa	Member
7	Engr. S. I. Lamido	Member
8	President Students' Chapter ABU	Member
9	President Students' Chapter Kadpoly	Member
10	Engr. S.M. Shuwa	Member
11	Engr. Dr. I. Haruna	Member
12	Engr. M. Murtala	Secretary

Synopsis of the Conference

As advances are made in Chemical Engineering, the Chemical Industry will be able to produce more useful products economically on a large scale from agriculture-based inputs. Value-addition to agricultural produce is the magic wand for transforming the nation's economy and providing meaningful employment for the teeming youth. The pivotal role of Chemical Engineering as the engine of growth for the economy is indispensable. To contribute to this critical area, at this time in our national development, the Nigerian Society of Chemical Engineers (NSChE) organized a National Conference on the theme, "*Enhancement of Agricultural Value Chain for Economic Development: The Role of Chemical Engineering"*. The Conference, KADA 2019, was aimed at bringing together participants from policy makers, industrialists, the academia, research institutes, the private and public sectors, etc., to brainstorm and proffer solutions to challenges in the agricultural downstream sector and galvanize efforts to ensure the revamping of our economy through the multiplier effect of value-addition to agricultural produce.

It is the hope of the Organisers of this important Conference that the recommendations of the Conference/AGM if implemented, will pave the way for the nation to attain self-sufficiency in food production, increased foreign exchange earnings, higher GDP and better balance of trade.

The Nigerian Society of Chemical Engineers is therefore pleased to present this Book of Proceedings to all Chemical Engineers and other stakeholders for the advancement of the Profession and the growth of the Economy.

TABLE OF CONTENTS

Proceedings of the 49th NSChE Annual Conference
KADA 2019: pp 1-7

PIA-01: EFFECT OF DRYING ON THE FOOD PROPERTIES OF TIGER NUTS

***Akhihiero E.T, Ebhodaghe S.O, Agbahowe S.E**
Department of Chemical Engineering, University of Benin, Benin
***Corresponding author**: thelma.akhihiero@uniben.edu, +234-8063980390

ABSTRACT
Effective storage conditions can resolve the challenge of food scarcity and extinction of certain food species. Since temperature is one of the most important variables that affect food preservation and food quality, this study is investigating the changes in the food properties and mineral composition of tiger nuts at different temperature variations. Required quantities of fresh tiger nuts were collected for different individual experiments. The results showed that while the temperature of 55^0C had significant effect on the retention of water, crude protein and carbohydrate contents of tiger nuts, fats were better retained at 80^0C. Irrespective of storage method, most food nutrients and properties of tiger nuts are better retained at temperatures $\geq 50^0$C.

1.0 INTRODUCTION
Tiger nut is a monocotyledonous plant with about 4000 species with high contents of starch, fat, sugar, protein, phosphorus, potassium and vitamins E and C (Belewu and Belewu, 2007; Ekeamyanwu and Ononogbu, 2010). Since it has high nutritional and low viscosity values, it is mostly cultivated for food and biodiesel production in the Valencia region of Spain, Australia, North and South America, Europe and Egypt (Ezeh et al, 2014; Adel et al, 2015). Though African countries are major producers and exporters of tiger nuts (Barminas et al, 2001), it can however be grown in most regions of the world. This is because of its' good water retention capability, suitability to different soils and short maturity period (www. nwtf.org/conservation/bulletins/bulletin_07.pdf).

Though current research are actively investigating food sources (Wells et al, 2017; Zhenzhang et al, 2019), extraction of food products (Chemat et al, 2017; Chen et al, 2019; Arya et al, 2019) and food processing techniques (Chemat et al, 2017; Barbosa-Canovas et al, 2019; Jones et al, 2019), food security should be given more attention due to the growing world population and consequences of neglect. To address this potential threat to human existence, researchers have investigated the effect of several factors on food supply. Few of the researched factors are the effect of pesticide residues (Carvalho 2017; Bonner and Alavanja 2017; Popp and Nagy 2012), and climatic conditions (Baethgen and Magrin 1995; Rosenzweig et al, 1994; Parry et al, 2004). Temperature is a climatic factor that most research has found to limit the maximum yield of crops (Davis et al, 2017).

For this reason, researchers have previously investigated the impact of temperature variation on wheat production (Parry et al, 2004). Parry et al (2004) showed that temperature increase affected wheat production more than rainfall. Therefore, they concluded that crop yields dramatically decrease with increase in temperature. Though it has generally been accepted that temperature affects crop yields (Parry et al, 2004; Davis et al, 2017), more research is needed to examine the effect of temperature variation on other edible crops. This will determine the optimal temperature condition of storing fresh tiger nuts in order to preserve its food and mineral components.

To this end, this study is investigating the changes in the food properties and mineral composition of tiger nuts at different temperature conditions. To achieve this, several samples of tiger nuts dried at different temperatures will be analyzed for the food properties of

moisture content, crude protein and carbohydrate contents. In addition, the mineral compositions of the fresh and sun dried samples will be determined.

2.0 METHODOLOGY

2.1 Preparation and Analyses of fresh tiger nuts

Samples were washed with distilled water to remove impurities. The proximate composition analysis was carried out for the moisture content, crude protein content and carbohydrate contents of the tiger nuts.

In addition, the mineral and vitamin content analyses of tiger nuts samples were carried out. The samples were analyzed for several minerals such as potassium, calcium, iron, copper and vitamins C and E contents.

2.2 Calculation Procedure

The drying rate calculation for each samples at different temperatures were carried out using the formula:

$$W = \frac{hA\Delta T}{\lambda}$$

Where:

$Area, A = \frac{4}{D} \times \sqrt{1 - a2}$ (Kolev, 2011).

Diameter of tiger nut, D = 6.27mm (Sanchez et al, 2012).
Heat transfer coefficient, h= 20.442 (Perry chemical engineering handbook)
Latent heat of vaporization of water = 22.6$\times 10^5$J/Kg (Vaclavik and Christian, 2008).

3.0 RESULTS

Table 3.1 Proximate composition of tiger nuts

Components	Sample A @ 23^{0}C	Sample B @ 55^{0}C	Sample C @ 40^{0}C	Sample D @ 80^{0}C	Sample E @ 100^{0}C	Sanchez et al, 2012	Adel et al, 2015	Ogunlade et al, 2015
Moisture Content (%)	**20.60**	**12.50**	**5.40**	**4.52**	**3.62**	**26.00**	**7.30**	**27.00**
Crude Protein (%)	**2.70**	**2.20**	**1.16**	**1.60**	**1.35**	**5.04**	**4.33**	**1.67**
Carbohydrate (%)	**11.40**	**9.65**	**4.61**	**6.20**	**8.71**	**43.30**	**48.12**	**48.30**
Fats and oils (%)	**1.36**	**1.21**	**1.24**	**1.31**	**1.06**	**24.49**	**…**	**…**

Table 3.2 Calculated drying rate of tiger nuts

Samples	A	B	C	D	E
Drying Rate	1.5221	1.7706	1.7567	1.9905	2.1130

3.1 Effect of drying on crude protein content

The results show that the highest protein content of tiger nuts is when it is freshly harvested at normal room temperature of 23^{0}C. Protein content was decreased at temperatures of 55,

40, 80 and 100^{0}C. However, protein content was better retained at 55^{0}C. The results of this research study agreed with findings of a study conducted by Seow and Gwee (1997), who reported that at temperatures greater than 80^{0}C, protein was generally destroyed. According to Tangsuphoom and Coupland (2005), some proteins are destroyed when heated even at 70^{0}C, even though Hartati et al. (2018) found that protein content was best retained at 70^{0}C.

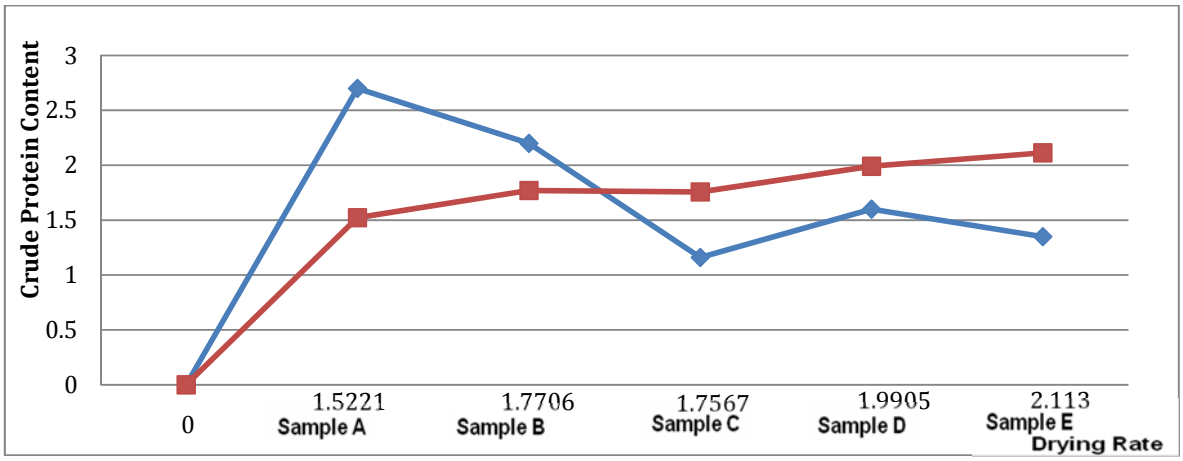

Figure 3.2 Effect of drying on crude protein content

3.2 Effect of drying on moisture content

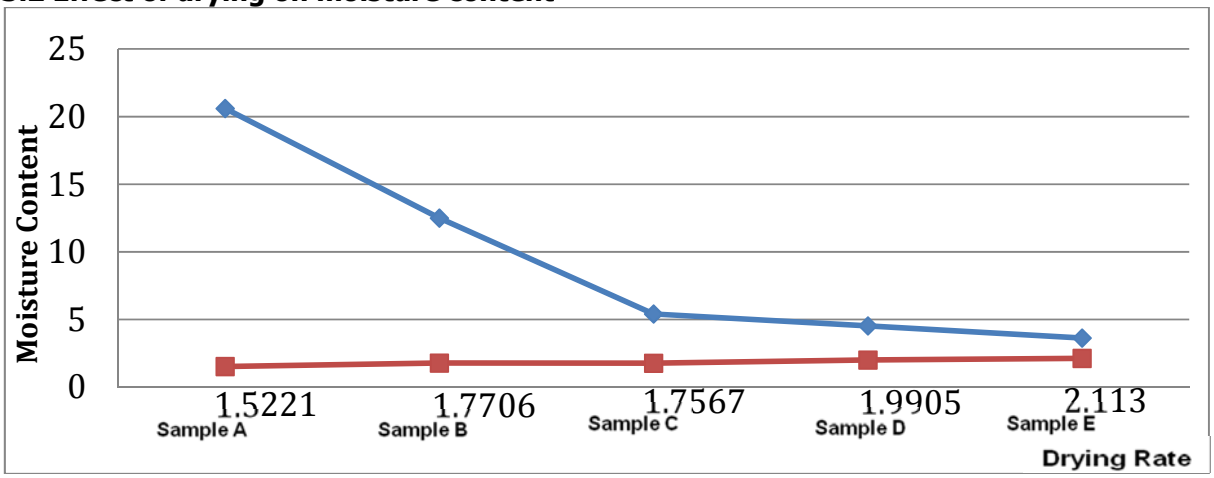

Figure 3.1 Effect of drying on moisture content

Since drying at temperatures above 70^{0}C increases the dissolved solids due to protein denaturation, the water content as shown in the effect of drying on moisture content in Figure 3.1 decreases. The water content was best retained at a temperature of 55^{0}C. This result agrees with that of Hartati et al (2018) when they found that the water content of laksan sauce was best retained at a temperature of 60^{0}C.

3.3 Effect of drying on carbohydrate content

The results showed that the highest carbohydrate content was found in fresh tiger nuts at 23^{0}C. Negligible losses were observed in sample B with drying at 55^{0}C and the lowest at 40^{0}C. It is shown that drying at 55^{0}C best preserved the carbohydrate content with a negligible loss of 2.75mg relative to the fresh sample at 23^{0}C. A recent study conducted by Hartati et al, 2018 agrees with this finding. They showed from their results that the highest carbohydrate content was at 60^{0}C.

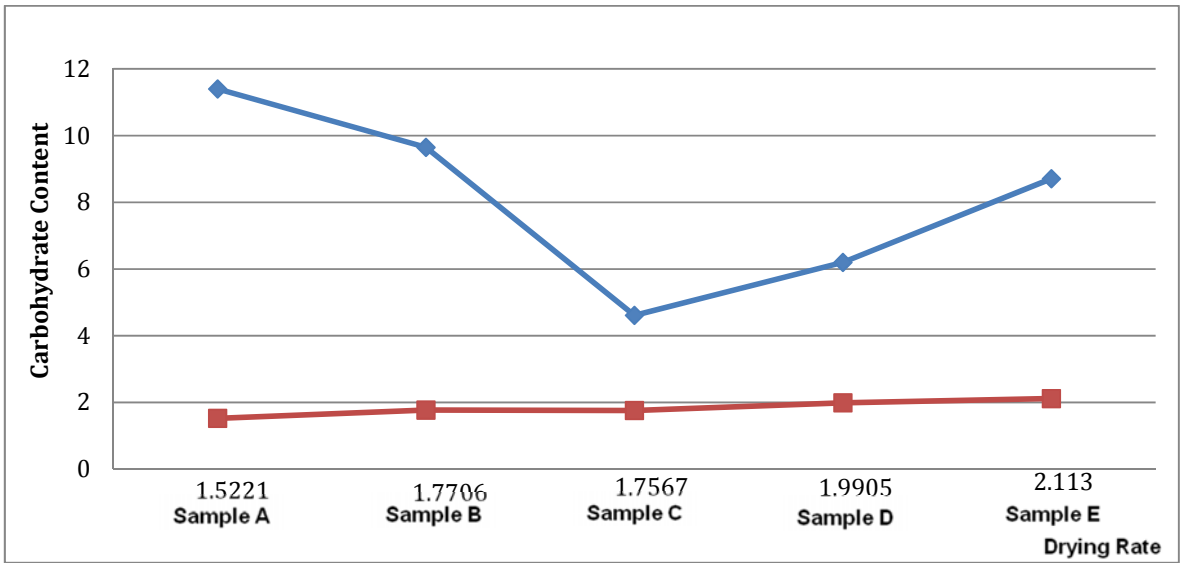

Figure 3.3 Effect of drying on carbohydrate content

3.4 Effect of drying rate on fats content

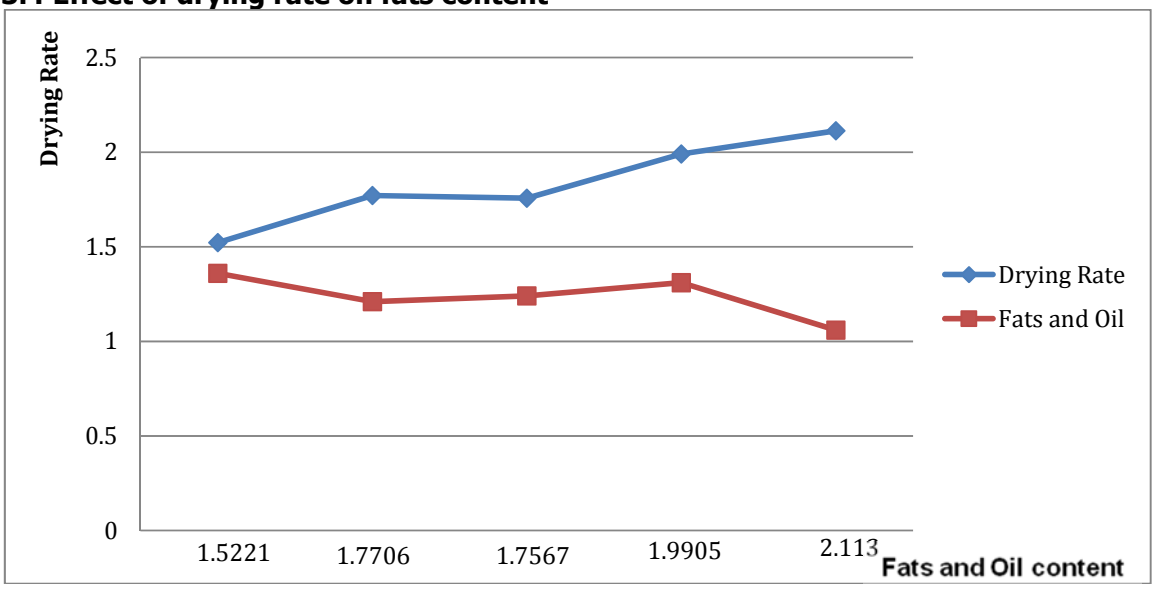

Figure 3.4 Effect of drying on fats and oil content

The results of this study showed that the highest fat content was at 23^0C. However, when subjected to different temperature conditions, the fats contents were better retained at 80^0C in comparison to other temperature conditions. When subjected to this temperature, only a negligible loss of 0.05g was observed. Similarly, Hatati et al, (2018) obtained the maximum lipid content at 70^0C in their experiment.

3.4 Mineral compositions of tiger nuts

The effect of a specific temperature of 23^0C on the mineral composition of fresh tiger nuts is shown in Figure 3.4. It is shown that the properties of calcium, sodium and potassium are in significant amounts in freshly harvested tiger nuts when compared to presence of copper and iron.

Table 3.3: Mineral properties of tiger nuts

Mineral Components (mg/100)	Sample A @ 23^{0}C Fresh	Sample B @ 55^{0}C *Sun-dried	Ogunlade et al, 2015	
			Fresh	Dry
Na	22.73	19.27	101.30	101.17
K	128.49	322.47	122.40	122.90
Ca	20.05	31.46	83.00	91.60
Fe	1.72	3.39	3.60	3.80
Cu	0.21	0.59	0.20	0.30

*Sun-drying temperature at 55^{0}C was from literature (Tunde and Oke, 2011).

3.4.1 Effect of drying on mineral composition (Sample A)

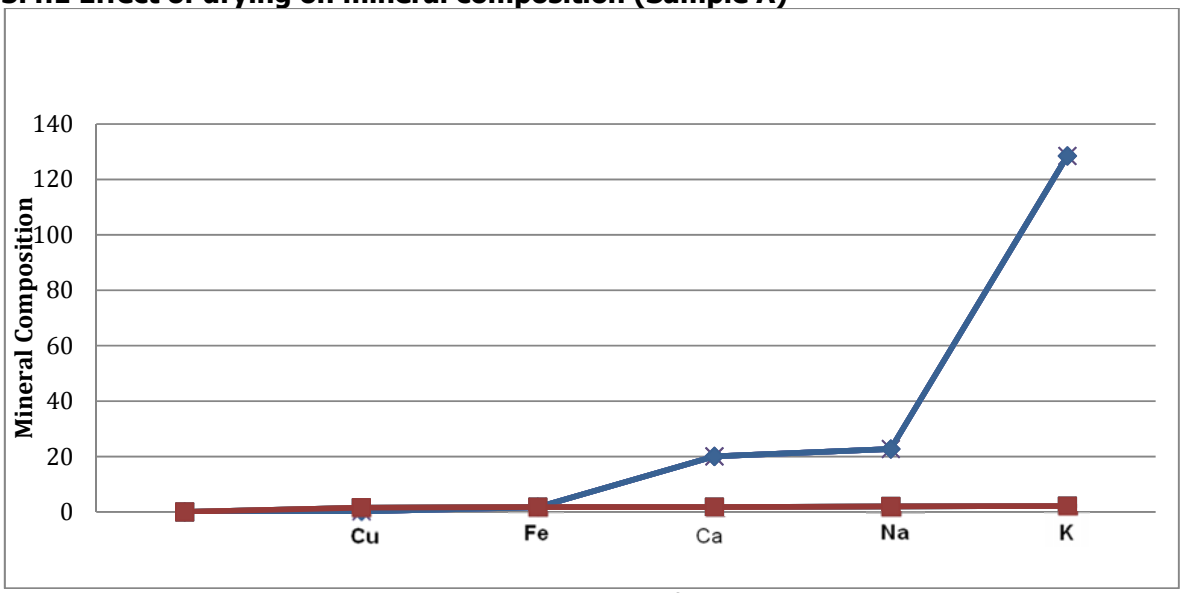

Figure 3.4: mineral properties of tiger nuts at 23^{0}C

3.4.2 Effect of drying on mineral composition (Sample B)

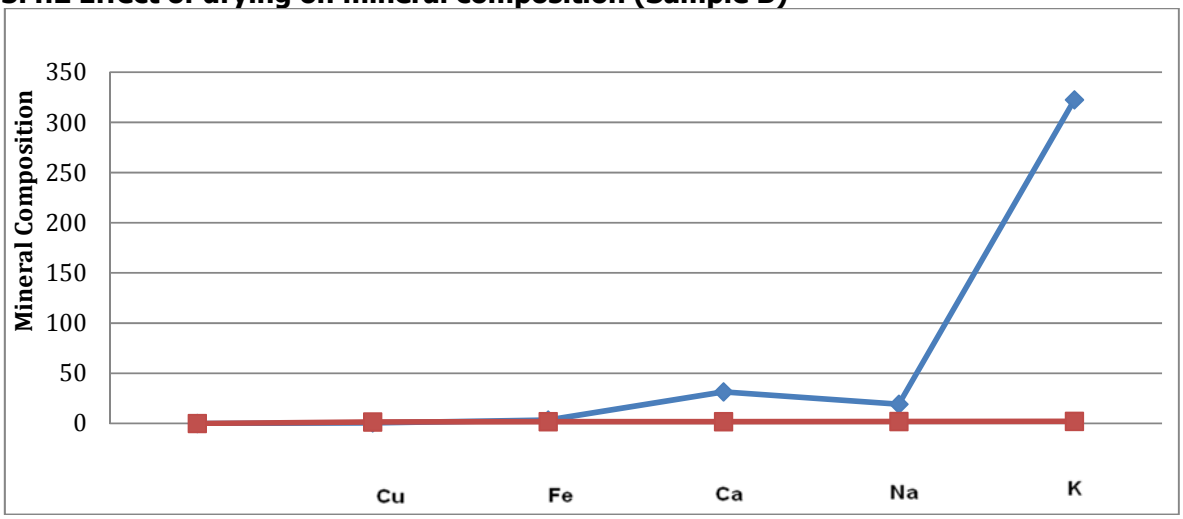

Figure 3.5: mineral properties of tiger nuts at 55^{0}C

The mineral composition of tiger nuts dried at 55^0C is shown in Figure 3.5. Even with an increase in temperature from 23^0C to 55^0C, calcium, sodium and potassium are still the major constituents of tiger nuts though the amount of sodium present has reduced.

From the effect of temperature increase (23-55^0C) on the mineral compositions of tiger nuts, the examined food minerals (Cu, Fe, K, Ca) increased by 0.38mg, 1.67mg, 193.98mg, and 11.41mg respectively, while sodium decreased by 3.46mg. Therefore, increase in temperature enhances the mineral composition of most properties of tiger nuts.

4.0 CONCLUSION

The results of this study showed that temperature had a significant effect on the food properties and mineral composition of tiger nuts. Drying at 55^0C produced the best results in the properties of crude protein, moisture content and carbohydrate, in comparison to 40, 80 and 100^0C. However, heating at 80^0C was best for maximum fats and oil retention. Since tiger nut is a source of food supply, this study has shown the optimal temperature conditions ($\geq 55^0$C) of storage, in order to preserve its' essential food components. Storage at the right condition will prevent the challenge of food scarcity and loss of essential nutrients. Future research can examine the effect of other process variables on a wider range of food properties of other common foods.

REFERENCES

Adel A.A.M, Awad A.M, Mohamed H.H, Iryna S. (2015). Chemical composition, physicochemical properties and fatty acid profile of Tiger nut (Cyperus esculentus L.) seed oil as affected by different preparation methods. International Food Research Journal, 22(5): 1931-8

Arya S.S, Kaimal A.M, Chib M, Sonawane S.K, Show P.L. (2019). Novel, energy efficient and green cloud point extraction: technology and applications in food processing. Journal of Food Science and Technology, 56(2); 524-34. DOI: 10.1007/s13197-018-3546-7

Baethgen W.E, Magrin G.O. (1995). Assessing the impacts of climate change on winter crop production in Uruguay and Argentina using crop simulation models. 207-228.

Barminas J, Maina H, Tahir S, Kubmarawa D, Tsware K. (2001). A Preliminary investigation into the biofuel characteristics of tiger nut (Cyperus esculentus) oil. Bioresource technology, 79; 87-9.

Barbosa-Canovas G.V, Zhang H. (2019). Pulsed electric fields in food processing: Fundamental aspects and applications. CRC Press.

Belewu M.A, Belewu K.Y. (2007). Comparative physicochemical evaluation of tiger nut, soybean and coconut milk sources. International Journal of Agriculture and Biology, 5; 785-7.

Bonner M.R, Alavanja M.C.R. (2017). Pesticides, human health and food security. Food and Energy Security. DOI: 10.1002/fes3.112. 6(3): 89-93.

Brenneman R, Daniel H. Turkey Gold. http://www.nwtf.org/conservation/bulletins/bulletin_07.pdf

Burden D. (2012). Chufa. http://www.agmrc.org/commodities_products/grains_oilseeds/chufa/

Carvalho F.P. (2017). Pesticides, environment and food safety. Food and Energy Security. DOI: 10.1002/fes3.108. 6(2): 48-60.

Chemat F, Rombaut N, Meullenriestre A, Turk M, Perino S, Fabiano-Tixier A.S, Abert-Vian M. (2017). Review of green food processing techniques: Preservation, transformation, and Extraction. Innovative Food Science and Emerging technologies, 41; 357-77. DOI: 10.1016/j.ifset.2017.04.016

Chemat F, Rombaut N, Meullenriestre A, Turk M, Perino S, Fabiano-Tixier A.S, Abert-Vian M. (2017). Ultrasound- assisted extraction of food and natural products. Mechanisms,

techniques, combinations, protocols and applications: A review. Ultrasonic Sonochemistry, 34; 540-60. DOI: 10.1016/j.ultsonch.2016.06.035

Chen J, Ying G.G, Deng W.J. (2019). Antibiotic residues in food: Extraction, Analysis, and Human Health Concerns. Journal of Agricultural and Food Chemistry, 67; 7569-86. DOI: 10.1021/acs.jafc.9bo1334

Davis K.F, Rulli M.C, Seveson A, Odorico P.D. (2017). Increased food production and reduced water use through optimized crop distribution. Natural Geoscience. DOI: 10.1038/s41561-017-0004-5

Ekeamyanwu R.C, Ononogbu C.I (2010). Nutritive value of Nigerian tiger nut (Cyperus esculentus L.). Agricultural Journal 5; 297-302.

Ezeh O, Gordon M.H, Niranjan K. (2014). Tiger nut oil (Cyperus esculentus L.): A review of its' composition and physico-chemical properties. European Journal of Lipid Science Technology. 116, 0000-0000.

Hartati Y, Priyanto G, Yuliati K, Pambayun R. (2018). Effect of temperature and drying time on chemical and proximate characteristics of Laksan Sauce as a Palembang Traditional Food. Pakistan Journal of Nutrition, 17: 64-70

Jones J.M. (2019). Food processing: Criteria for dietary guidance and public health. Proceedingss of the Nutrition Society. Cambridge University Press, 78(1), 4-18. DOI: 10.1017/s002966511800.2513

Kolev N.I. (2011). Heat and Mass transfer at the film/gas interface. In: Multiphase flow dynamics 3. Springer. DOI: 10.1007/978-3-642-21372-4_13. Pp 319-57.

Ogunlade I, Adeyemi B.A, Aluko O.G. (2015). Chemical compositions, antioxidant capacity of tiger nut (Cyperus esculentus) and potential health benefits. European Scientific Journal. ISSN: 1857-7881. 217-24

Parry M.L, Carter T.R, Konijn N.T. (1988). The impact of climatic variations on agriculture. Volume 1

Popp J, Peto K, Nagy J. (2013). Pesticide productivity and food security. A review. Agron. Sustain. Dev. DOI: 10.1007/s13593-012-0105-x. Vol. 33:243-55.

Perry R.N, Green D.W. (1999). Perry's chemical engineers' handbook 7th Edition. McGraw-Hill Companies, Inc.

Pereira L.S. (2017). Water, Agriculture and Food: Challenges and Issues. Water Resources Management. DOI: 10.1007/s11269-017-1664-z

Rosenzweig C, Parry M.L. (1994). Potential impact of climate change on world food supply. Nature. Vol. 367. Pp 133-8.

Seow, C.C, and Gwee C.N. (1997). Coconut milk: Chemistry and technology. International Journal of Food Science and Technology, 32: 189-201

Sanchez-Zapata E, Juana F, Jose A.P. (2012). Tiger nut (Cyperus esculentus) commercialization: Health aspects, composition, properties and food applications. Comprehensive Reviews in Food Science and Food Safety. DOI: 10.1111/j.1541-4337.2012.00190.x; Vol. 11; 366-77

Tangsuphoom, N and Coupland J.M. (2005). Effect of drying and homogenization on the stability of coconut milk emulsions. Journal of Food Science, 70: e466-e470.

Tunde-Akintunde T.Y, Oke M.O. (2011). Thin-layer drying characteristics of tiger nut (Cyperus esculentus) seeds. Journal of Food Processing and Preservation. DOI: 10.1111/j.1745-4549.2011.00604.x

Vaclavik V.A, Christian E.W. (2008). Water. Essentials of Food Science. In: Food Science Texts Series. Springer. DOI: 10.1007/978-0-387-69940-0_2. Pp 21-31.

Wells M.L, Potin P, Craigie J.S, Raven J.A, Merchant S.S, Heliwell K.E, Smith A.G, Camire M.E, Brawley S.H. (2017). Algae as nutritional and functional food sources: revisiting our understanding. Journal of Applied Phycology, 29; 949-82. DOI: 10.1007/s10811-016-0974-5.

Proceedings of the 49th NSChE Annual Conference
KADA 2019: pp 8-13

P1A-02: DEVELOPING OF ONION VALUE CHAIN IN NIGERIA

[1*]Abdulazeez Y. Atta, [2]Sirajo Musa, [2]Ozonyia G. Ngozichukwuka and [2]Hussaini I. Ibrahim
[1]Department of Chemical Engineering, Ahmadu Bello University, Zaria
[2]Raw Materials Research and Development Council, Abuja
***Corresponding author**: zeezoatta@gmail.com

ABSTRACT
Onions are grown in very large quantity in Nigeria. However, dehydrated powdered onions are currently imported mainly from China and India. The powdered onions have industrial applications as additive in production of sauce (Maggi, Knorr, etc), food condiment, noodles, etc. Development of onion value chain is envisioned to link the growing of onions to the industrial needs in Nigeria. In this proposed strategic plan to develop onions value chain in Nigeria, the focus is on three important areas; (1) Domestication of powdered onion production technology, (2) Development of framework for best agronomy practice in onion cultivation and (3) Linking entrepreneurs to onion cultivation and powdered onion production in Nigeria. It is envisaged that the implementation of the strategic plan would spur the domestication of powdered onion production in Nigeria thereby reducing the importation of powdered onions. In addition, a clear framework to improve the current agronomy practices in onion cultivation to meet the specifications for industrial application is expected to be developed.

1.0 INTRODUCTION
Nigeria government is actively pursuing economic diversification. The recent Economic Recovery Growth Plan (ERGP) is intended at growing national output via broadening production (ERGP, 2017). Along this line, the Nigerian Industrial Revolution Plan (NIRP), which is focused specifically on industrial transformation, is designed to accelerate industrial capacity and diversification (NIRP, 2014). To achieve this objective, the plan is centered on developing four key industrial groups in which Nigeria already possesses clear advantage: agri-business and agro-allied; solid minerals and metals; oil and gas related industries; construction, light manufacturing and services (NIPR, 2017). Agri-business and agro-allied industrial sector is envisaged to build an end-to-end integrated value chain via boosting local production to meet domestic demand and reducing country's requirement on import of processed food products.

Agricultural sector is gradually and steadily being transformed in Nigeria. This is evidenced from the successful Central Bank of Nigeria Anchor Borrowers' Programme, which provides linkages between companies involved in processing rice and smallholder farmers, have spurred the production of rice in Nigeria (CBN, 2016). Consequence of this initiative and the progress recorded, according to PricewaterhouseCoopers (2018) report, rice production peaked at 3.7 million tons in 2017 and with appropriate agricultural practice in the next 5 years rice production in Nigeria is expected hit 7.2 million tons.

The success achieved in rice production in Nigeria can be replicated for major crops such as sorghum, soya beans, maize, onions, etc. which when processed serve direct industrial applications. For example, Onions when dehydrated into flakes or powder form are used as additive in production of sauce (Maggi, Knorr, etc) and food condiment and so on.

Onion is most commonly grown in North-west and North-central regions of Nigeria with states like Kebbi, Sokoto, Kano, Kaduna, Jigawa and Plateau states. From 2012 data, Nigeria ranks

sixth nation behind major producers such as China and Japan with 240 thousand tons of green onions and 1.3 million tons of dry (Indorama, 2014).

In Nigeria postharvest and poor storage are the major challenges associated with the production of onions. For Nigeria to maximize the benefit of growing onions and drastically reduce the 50% postharvest best agronomy practices must be introduced. The farmers must be provided with extension services to choose the appropriate varieties that have long shelf life, suitable soil condition and application of fertilizer at correct time and use the correct quantity. After harvesting, the onions must be classified to remove undeveloped onions that may potential be the source of spoilage (Olanipekun, 2018).

Postharvest losses in onions could also be reduced by transforming via value addition to products such as onion powder, onion flakes, onion sauce, etc. Despite the huge potential likely to be achieved through the development and deployment of an onion powder production process, there is no existing onion powder production plant in Nigeria.

The goal is to demonstrate the technical and economic viability of domesticating production of powdered onion from local onion raw material. The production of powdered onions from local raw material will entail the following key objectives:

1. Domestication of powdered onion production technology in Nigeria.
2. Spur import substitution of powdered onions currently imported.
3. Develop framework to improve the current agronomy practice in onion cultivation to meet the specifications for industrial application.

2.0 STRATEGIC PLAN

2.1 Domestication of Powdered Onion Production Technology

Currently in Nigeria, the powdered and flake onions utilized by the industries are imported predominantly from India and China. Although no data available from the key government agencies (Central Bank of Nigeria and National Bureau of Statistic) on the quantity and amount of powdered onion imported into the country, however, companies that produce sauce, food condiment and so on, import the product from Asia.

Maggi, Knorr, etc. produced by various companies are collectively referred to as bouillon cubes. In production of bouillon, powdered onion is a key raw material. At this moment, the following companies produce the bouillon in Nigeria (Table 1); Nestle Nigeria Limited, Unilever Nigeria Limited, PZ Nigeria, etc.

Table 1: Companies Producing Bouillon Cubes

S/No	Company	Bouillon Cubes Brand Name
1	Nestle Nigeria Limited	Maggi
2	Unilever Nigeria Limited	Knorr and Royco
3	PZ Nigeria	Mamador
4	Pramasidor	Onga
5	Doyin Group of Companies	Doyin and Prime
6	Daily Nigeria Limited	Suppy
7	NASCON Allied Industries Plc, (a subsidiary of the Dangote Industries Limited)	Dan-Q
8	TGI Distri Limited	Terra

According to Nestlé, the Central West Africa Region is the largest MAGGI cube producing market in Nestlé and sells over 100 million cubes in the Central West Africa Region daily. Nigeria is the major contributor in the growth of bouillon cube market in this region.

Another group of companies in Nigeria that utilize powdered onions is the producers of noodles. Noodles are now very common instant meal in Nigerian homes. According to World Instant Noodles Association (WINA), Nigeria is currently 12th largest consumer of noodles in the world with 1.82 billion serving noodles in 2018 (WINA, 2019). In-fact, Nigeria consumes 7 times than the amount consumed in South Africa.

The sauce that normally comes along with the noodles contains powdered onions. There are several companies in Nigeria that produce noodles, hence, these companies import the powdered onions additive. Indomie noodles produced by Dufil Prima Foods Plc are reported to control about 75% of the market share. Other notable producers of noodles are Golden Noodles Company Limited (Golden Noodle).

In essence, there is a large market demand for powdered onions in West Africa, particularly Nigeria that is being supplied for primarily by importation. Therefore, domestication of this technology will not only improve the shelf lives of onions and reduce their wastages in the country, but will also go a long way in providing import substitution for the product and ultimately create jobs for the vast unemployed populace in the country.

2.2 Strategies

The key strategies in domestication of production of powdered onions (DPPO) in Nigeria are presented in Table 2.

2.3 Outcomes

The outcomes from the domestication of the production of powdered onions in Nigeria are:

1. A functional plant for the production of powdered onions from local raw materials.
2. Demonstration of economic and technical viability of production of powdered onions in Nigeria.

3.0 DEVELOPMENT OF FRAMEWORK FOR BEST AGRONOMY PRACTICE IN ONION CULTIVATION IN NIGERIA

The onion cultivation in Nigeria is associated with huge postharvest loss. As stated earlier, about halve of the onion produced are lost to poor agronomy practices by farmers such as lack of appropriate storage facilities (Olanipekun, 2018). In meeting the need of onion processors, postharvest loss must be drastically reduced and the problem of storing onions for extended time needs to be addressed.

The reduction of the postharvest loss begins at the start of cultivation and application of appropriate agronomy practices. Suitable varieties with longer shelf life must be made available to the farmers and application of appropriate fertilizer (Olanipekun, 2018).

3.1 Strategies

The key strategies in development of framework for best agronomy practice in onion cultivation in Nigeria are presented Table 3:

Table 2: Strategies for Domestication of Powdered Onion Production Tachnology

S/No.	Strategies	Key Activities	Stakeholders	Lead Agency
1	Formation of RMRDC Stirring Committee for the DPPO	1. Selection of RMRDC staff for DPPO Stirring Committee 2. Inauguration of the DPPO committee 3. Meeting to adopt the work plan for DPPO 4. Harmonize the DPPO activities with the current effort of RMRDC in Sokoto 4. Reengineering and developing of the Sokoto Plant in Zaria	RMRDC, Consultant	RMRDC
2	Stakeholders Meeting to Review the Plan for the DPPO	1. Workshop to review and adopt the work plan for DPPO	RMRDC, FMARD, FMST, CBN, NIRSAL, BOI, BOA, SON, NAFDAC, State Governments, related food industries, organized onion farmers association, Agricultural research institutes, NACIMA	RMRDC

Table 3: Strategies for Development of Best Agronomy Practice

S/N	Strategies	Key Activities	Stakeholders	Lead Agency
1.	To develop appropriate framework for onion cultivation in Nigeria.	1. Meeting of the Stirring Committee Members with key stakeholders (State Goverments, FMARD, IAR and CBN) 2. Preparation of a draft document for the workshop. 3. Validation of the draft financial package document	Sokoto, Kebbi, Zamfara, Kano, Jigawa and Kaduna State Governments, FMARD, RMRDC, IAR Zaria, UDU Sokoto	FMARD
2.	Demonstration of best practices of onion cultivation to onion farmers at the proposed Sokoto site.	1. Identification of farmers that will be involved in the demonstration farm. 2. Provision of appropriate onion variety to the farmers. 3. Extension services to the farmers' prior-cultivation, during cultivation and after harvesting. 4. Demonstration of appropriate storage techniques	Sokoto State Government, FMARD, RMRDC, IAR Zaria, UDU Sokoto	IAR Zaria

3.2 Outcomes

The outcomes from the development of framework for best agronomy practice in onion cultivation in Nigeria are:

1. A document clearly stating the best approach in cultivation of onions in Nigeria.
2. Demonstration of the best agronomy practice at the Sokoto site of the proposed plant.

4.0 LINKING ENTREPRENEURS TO ONION CULTIVATION AND POWDERED ONION PRODUCTION

There several government agencies with experience and expertise in developing financial packages that link entrepreneurs with appropriate funding arrangements. Some these agencies include CBN, BOI and BOA. It is paramount to tap into these know-how and skills in development of financial packages for the entrepreneurs that will take-up the production of powdered onions and also cultivation of onions.

The public-private company, The Nigeria Incentive-Based Risk Sharing system for Agricultural Lending (NIRSAL), is well suited in providing tailor made financial solution for agriculture enterprises. NIRSAL have already demonstrated this with its acclaimed successes achieved in the rice value chain. It is expected to be at center of providing solution for the onion value chain.

4.1 Strategies

The key strategies in linking entrepreneurs to onion cultivation and powdered onion production in Nigeria are shown in Table 4:

Table 4: Strategies in Linking Entrepreneurs to Onion Cultivation and Powdered Onion Production

S/No.	Strategies	Key Activities	Stakeholders	Lead Agency
1	To develop appropriate financial packages for onion cultivation and powdered onion production.	1. Meeting of the Stirring Committee Members with financial stakeholders (CBN, NIRSAL, BOI and BOA) 2. Preparation of a draft document for the workshop. 3. Validation of the draft financial package document	CBN, NIRSAl, BOI, BOA and RMRDC	NIRSAL

4.2 Outcomes

The expected outcomes from linking entrepreneurs to onion cultivation and powdered onion production in Nigeria are:

1. Development of financial instruments for potential investors in onion cultivation and powdered onion production.

5.0 CONCLUSION

The development of onion value chain in Nigeria that encompassed best agronomy practice, appropriate onion powder technology and linking entrepreneurs is envisioned to lead into production of powdered onion locally, reduce current loss associated with growing onions in Nigeria and serve as a model were other crops (ginger, pepper, etc) value chain could also be developed.

Acronyms

ABU: Ahmadu Bello University

BOA: Bank of Agriculture
BOI: Bank of Industry
CBN: Central Bank of Nigeria
DPPO: Domestication of Production of Powdered Onions
FMARD: Federal Ministry of Agriculture and Rural Development
FMST: Federal Ministry of Science and Technology
IAR: Institute of Agriculture, Ahmadu Bello University
NIPR: Nigerian Industrial Revolution Plan
NIRSAL: Nigeria Incentive-Based Risk Sharing system for Agricultural Lending
UDU: Usman Danfodio University
RMRDC: Raw Materials Research and Development Council

REFERENCES

Anchor Borrowers' Programme Guideline, Development Finance Department, Central Bank of Nigeria, Abuja (2016).

Boosting Rice Production Through Increased Mechanisation, PricewaterhouseCoopers Limited, Nigeria (2018).

Economic Growth and Recovery Plan, 2017-2020, Ministry of Budget and National Planning, Federal Government of Nigeria (2017).

Global Demand for Instant Noodles, World Instant Noodles Association. https://instantnoodles.org/en/noodles/market.html (2019).

Maggi: A history of Everyday Home Cooking. https://www.nestle-cwa.com/en/en/brands/culinary/maggi (2019).

Nigeria Industrial Revolution Plan, Ministry of Industries, Trade and Investment, Federal Republic of Nigeria (2014).

Olanipekun, C.I. Building an Improved Onion Storage Facility in Sokoto, World Vegetable Center. https://avrdc.org/building-an-improved-onion-storage-facility-in-sokoto/ (2018).

Onion Crop Management Practices, Indorama Fertilizer Nigeria Limited

Proceedings of the 49th NSChE Annual Conference
KADA 2019: pp 14-23

P1A-03: DESIGN, CONSTRUCTION AND TESTING OF A MEAT GRINDING MACHINE

[1]*Bako Sunday, [2]Ezra P. Mijinyawa, [3]Mohammed B. Ndaluiman, [3]Katsina C. Bala
[1]Department of Mechanical Engineering, Nuhu Bamalli Polytechnic Zaria
[2]Department of Technical Education, Nuhu Bamalli Polytechnic, Zaria
[3]Department of Mechanical Engineering, Federal University of Technology, Minna
***Corresponding Author**; s2bako@yahoo.com

ABSTRACT
Meat is an essential nutritious food item needed for human consumption from which high quality proteins, minerals and essential vitamins are derived. However, certain categories of consumers such as the children, elderly and sick people might not be able to provide the requisite biting force for chewing of the meat. Thus they would only be able to consume meat in their grinded form. In order to address this problem, it becomes necessary to have a meat grinding machine. Meat grinders are either motorized or manually operated. This paper presents the design, construction and testing of an efficient single meat grinding machine with both manual and motorized mode of operation. To avoid failure of the machine, the calculated working stress of 21MN/m^2 of the machine is kept within the value of the machine ultimate stress of 30MN/m^2 and the calculated factor of safety of 1.4 is within accepted range for factor of safety which indicates that the design is safe. A functional test carried out on the machine shows that it has an efficiency of 69% and 73% for manual and motorized operation respectively. The utilization of this machine would enhance meat processing thereby creating employment. The machine can be used in the urban, rural area and with or without electricity.

Keywords: Design, Construction Assembling, Meat Grinding and Testing.

1.0. INTRODUCTION
The preferred solution to meat processing is to introduce a mechanical and hygienic method of processing meat. The machine is used to force meat by means of rotating shaft under pressure through a horizontal mounted cylinder (shaft housing). At the end of the shaft housing there is a cutting system consisting of a cross-shaped knives rotating with the shaft and a stationary perforated disc (hole plate). The perforation of the hole plate normally range from 1 to 13mm. The meat is compressed by the rotating shaft, forced through the cutting system and extrudes through the hole of the hole plate after being cut by the revolving knives. The degree of grinding is determine by the size of the holes of the hole plate (Principles of Meat Processing Technology, 2014).

This paper presents the design of an efficient single meat grinding machine with both manual and motorized mode of operation, which can be used (in the urban and rural area) and with or without electricity. This design provides the kinematic arrangement of forces, materials selection and proportion of parts to ensure maximum strength and functionality of the machines. Meat grinders are either motorized or manually operated. This paper presents the design, construction and testing of an efficient single meat grinding machine with both manual and motorized mode of operation. The concept of the paper came as a measure to design and construct a machine which can be used for grinding meat into a very smaller piece. This is as to encourage the processing of meat and the establishment of meat processing industries in Nigeria, especially in the northern parts where there is high availability of beef as a raw material.

2.0. METHOD

This work invokes design of a manual and motorized meat grinding machine. Design of individual component of the machine was carried. After the design, various fabrication methods such cutting, welding, grinding, drilling and casting were used for construction of the various components of the meat grinding machine. The individual components of the machine were assembled to form a single meat grinding machine. The manual and motorized operation of the machine was tested using equal mass of meat.

3.0. DESIGN ANALYSIS

The material selection and positioning of components were controlled by the material strength, rigidity, corrosion resistance and the construction method.

3.1. Selection of the V-belt and Calculation of Torque

The machine was designed to use two horse power (2hp) electric motor. Since the power of the electric motor was 1.402kW; a "A" type of V-belt with a power range of 0.7-3.5 kW, a top width (b) of 13mm and thickness (c) of 8mm was selected according to Indian Standard (IS: 2494-1974).

Torque transmitted by electric motor, T_t is given by;

$$T_t = \frac{P}{\omega} \quad (1)$$

,

P = Power transmitted by electric motor, ω = Angular speed of the electric motor

ω = Speed of rotation of electric motor = 1420rev/min

3.2. Calculation of the Tightening Belt Tension T_1 and Slackening Belt Tension T_2,

Figure 1; shows the shaft loading and the power transmission on the manual and motorized meat grinding machine.

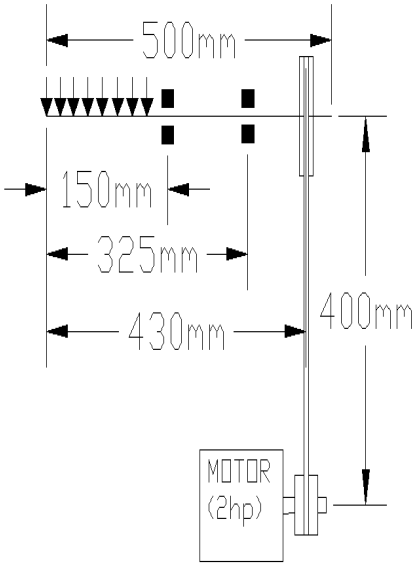

Figure. 1: Meat Grinder Power Transmission

The weight of the pulley W_p is given by;

$$W_P = mg \quad (2)$$

Vertical load $V_l$on the shaft is given by;

$$V_l = (T_1 - T_2)Sin60° \quad (3)$$

Horizontal load H_l on the shaft is given by;

$$V_l = (T_1 - T_2)Cos60° \quad (4)$$

Torque supplied T_t is given by;

$$T_t = (T_1 - T_2)r \quad (5)$$

r = radius of the smaller pulley

Peripheral Velocity V is given by;

$$V = \omega r \quad (6)$$

Mass/unit length of belt m is given by;

$$m = PgA \quad (7)$$

p = Density of the belt = 980kg/m^2

g = Acceleration due to gravity = 9.8m/s^2, A = Cross-sectional area of belt m^2

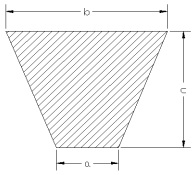

Figure 2: Belt Cross Sectional View

Cross-sectional area A of the belt is given by;

$$A = \frac{1}{2}(a + b)c \quad (8)$$

Centrifugal Tension T_c is given by;

$$T_c = MV^2 \quad (9)$$

$$\frac{T_1 - T_C}{T_2 - T_C} = e^{\frac{\mu \propto_1}{sin\theta/_2}} \quad (10)$$

μ = Coefficient of friction between belt and pulley = 0.2

θ = Groove angle for V-belt = 30^O, ρ = Density of belt materials = 980kg/m^3,

$\propto_1$ = Angle of wrap for smaller pulley (rad) $= 180^0 - 2Sin^{-1}\frac{R-r}{c}$

C = Centre distance between pulley

R = Larger pulley radius r = Small pulley radius

$$But, D = \frac{N_1 d}{N_2}.$$

N_1 = Speed of the electric motor or small pulpy (r.p.m) N_2 = Speed of the larger pulley (r.p.m)

d = Diameter of the smaller pulley (m) D = Diameter o the larger pulley (m)

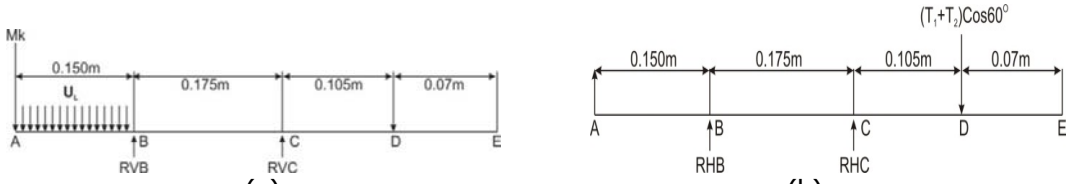

(a) (b)

Figure 3: (a) Vertical Loading on the Shaft. (b) Horizontal Loading on the Shaft

Mk = Weight of the knife U_L = Uniform distributed load

RVB = Reaction of the bearing at B, RVC = Reaction of the bearing at C,

Figure 4.0 shows the hear force and the bending moment diagram for the vertical and horizontal loading respectively.

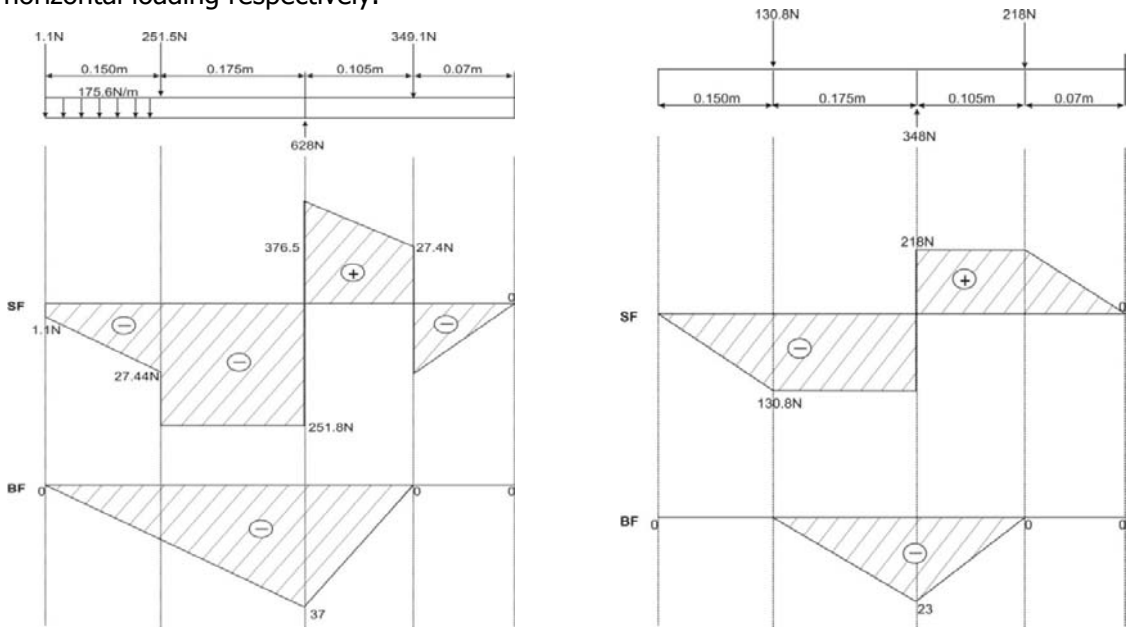

(a) (b)

Figure 4: Bending Moment and Shear Force Diagram for; (a) Vertical loading. (b) Horizontal Loading.

3.3. Calculation of the Resultant Maximum Bending Moment, Mmax

$$M_{max} = \sqrt{M_h^2 + M_V^2} \qquad 11$$

M_H = Maximum bending moment for horizontal loading
M_v = Maximum bending moment for vertical loading

3.4. Calculation of the Shaft Diameter d_0,

In actual practice shafts are subjected to fluctuating torque and bending moment. For shafts subjected to combine bending and torsion, the shaft diameter, d_o is given by;

$$d_o = \frac{16}{\pi\tau_s}\sqrt{(K_b M_{max})^2 + K_t T_t)^2} \qquad 12$$

The shaft is design to have the maximum allowable shear stress of $\tau_s = 30 \times 10^{-6} N/m$.

T_t = Torque Transmitted by electric motor

K_b and K_t are Combine shock and fatigue factors for bending and torsion. The recommended value for K_t and K_b are 1.5 and 1.0 for steady loading (Khurmi, 2005). π = 3.142.

3.4. Calculation of Belt Length

The belt length is given by;

$$L = \sqrt{4C \quad -(D-d)^2 + \frac{1}{2}(D\alpha_2 + d\alpha_1)} \qquad 13$$

Where;

L = Belt length (m) D = Diameter of the larger pulley (m)
D = Diameter of the smaller pulley (m) C = Centre distance between the two pulley (m)
α_1 = Wrap angle of the smaller pulley (rad) α_2 = Wrap angle of the larger pulley (rad)

3.5. Calculation of the Centre Distance between Pulleys C

The Centre distance between the two pulleys is given by;

$$C = \frac{L}{4} - \frac{\pi(D-d)}{8} + \sqrt{\frac{L}{4} - \frac{(D-d)^2}{8} - \frac{(D-d)^2}{8}} \qquad 14$$

3.6. Bearing Selection,

The resultant radial force (F) and the dynamic loading (C) are calculated.

$$F = \sqrt{F_H^2 + F_V^2} \qquad 15$$

$$F_H = RHC \qquad F_V = RVC$$

3.7. Calculation of the Factor of Safety, F_S,

$$F_S = \frac{Ultimate\ Stress}{Working\ Stress} \qquad 16$$

$$Working\ Stress = \frac{16T}{\pi d^3} \qquad 17$$

T = Twisting Moment (Maximum Bending Moment) D = Shaft Diameter

According to Sharma and Aggarwal (2006), the Factor of Safety (F_S) is between 1.25 to 1.5 for exceptionally reliable material used under controlled condition and subjected to loads and stresses that can be determine certainly. Therefore since the Factor of Safety of this machine wass within the range (1.25 to 1.5). Therefore the design was safe.

3.8. Key Design

In this design, a round key inform of a bolt was used. The height (h) and the width (b) of the key was determined by using the empirical design code relation for different types of keys.

3.8.1. Calculation of the Width/Diameter of the Key b

b = nd 18

n = Ratio of the key width to the shaft diameter. The recommended value of n is 0.25

d = Shaft diameter

3.8.2. Calculation of the Depth/Height of the Key h

h = mb 19

m = Ratio of height of the key to the key width. The recommended value of m was 1.30
Therefore, a bolt of 6mm in diameter (width) and the more than 7mm height was selected.

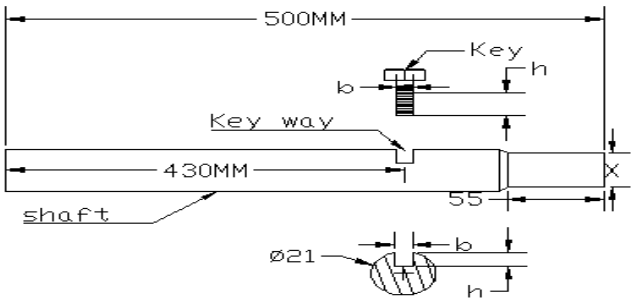

Figure 5: Shaft Design

3.9. Handle Design

The average of 170.6N effort is assigned to operate the machine during the manual operation. The maximum force required for a single person to operate the handle is 400N with the handle length of 300mm, (Khurmi, 2005).

3.9.1. The Maximum Bending Moment of the Handle M_L,

$$M_L = P \times \frac{2l}{3} \quad 20$$

3.9.2. The Section Modulus of the Handle Z,

$$Z = \frac{\pi}{32} d^3 \quad 21$$

Where, d = diameter of the handle

The diameter of the handle is proportioned as 25mm for single person with the effort of 400N.

3.9.3. The Constant Twisting Moment T,

$$T = {}^{2}/_{3} \times p \times l \quad 22$$

3.9.4. The Maximum Bending Moment M_L,

$$M_L = p \times L \quad 23$$

The length of the lever, L is 86mm

3.9.5. The Width near the Boss B,

$$B = 2t \quad 24$$

t = Thickness of the lever

The section modulus Z for the level arm is also given by;

$$Z = \frac{1}{6} \times t \times B^2 \qquad 25$$

3.9.6. The Dimension or Length of the Square End, of the Handle x

$$x = \sqrt{\frac{D^2}{2}} \qquad 26$$

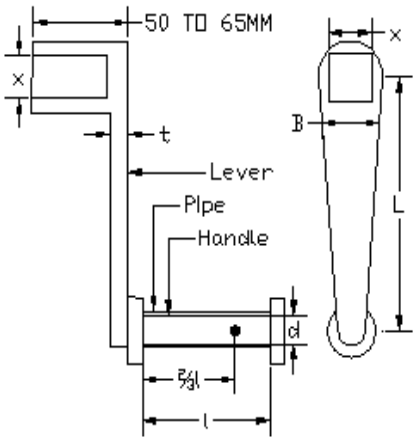

Figure 6: Handle Design

4.0 CONSTRUCTION

The Table 1 summarized the construction process involved with the construction of this machine. The engineering drawing of the individual components and their respective materials are shown in the appendix.

Table 1: Component and Construction Operations

S/N	COMPONENT	MATERIAL	OPERATION
1	Hopper	Mild steel	Cutting to size, folding wielding and grinding
2	Shaft Housing	Galvanized steel	Cutting ti size, threading, wielding, and grinding
3	Hole Plate	Aluminum	Casting and drilling
4	Knife	Stainless steel	Cutting to size, wielding and grinding
5	Shaft	Stainless steel	Cutting to size, turning, wielding, hand forging and grinding
6	Bearing Holder	Mild steel bolts and nuts	Cutting to size. Welding and grinding
7	Ring Screw	Aluminum	Casting and threading
8	Grinder Stand	Mild steel	Cutting to size, welding. Drilling and grinding
9	Handle	Mild steel	Cutting to size, welding and grinding
10	Grinder Stand	Mild Steel Pipe	Cutting to size
11	Grinder Base	Mild Steel Plate	Cutting to size

5.0 Assembling

A number of components were permanently joined together using arc welding to form a sub-assembly. The sub-assembly and other components were temporarily joined together using bolts and nuts to form a complete structure of the meat grinding machine. The assembly and individual components drawing are shown in the appendix.

Table 2: Components and Orthographic Drawing

Components and Orthographic drawing
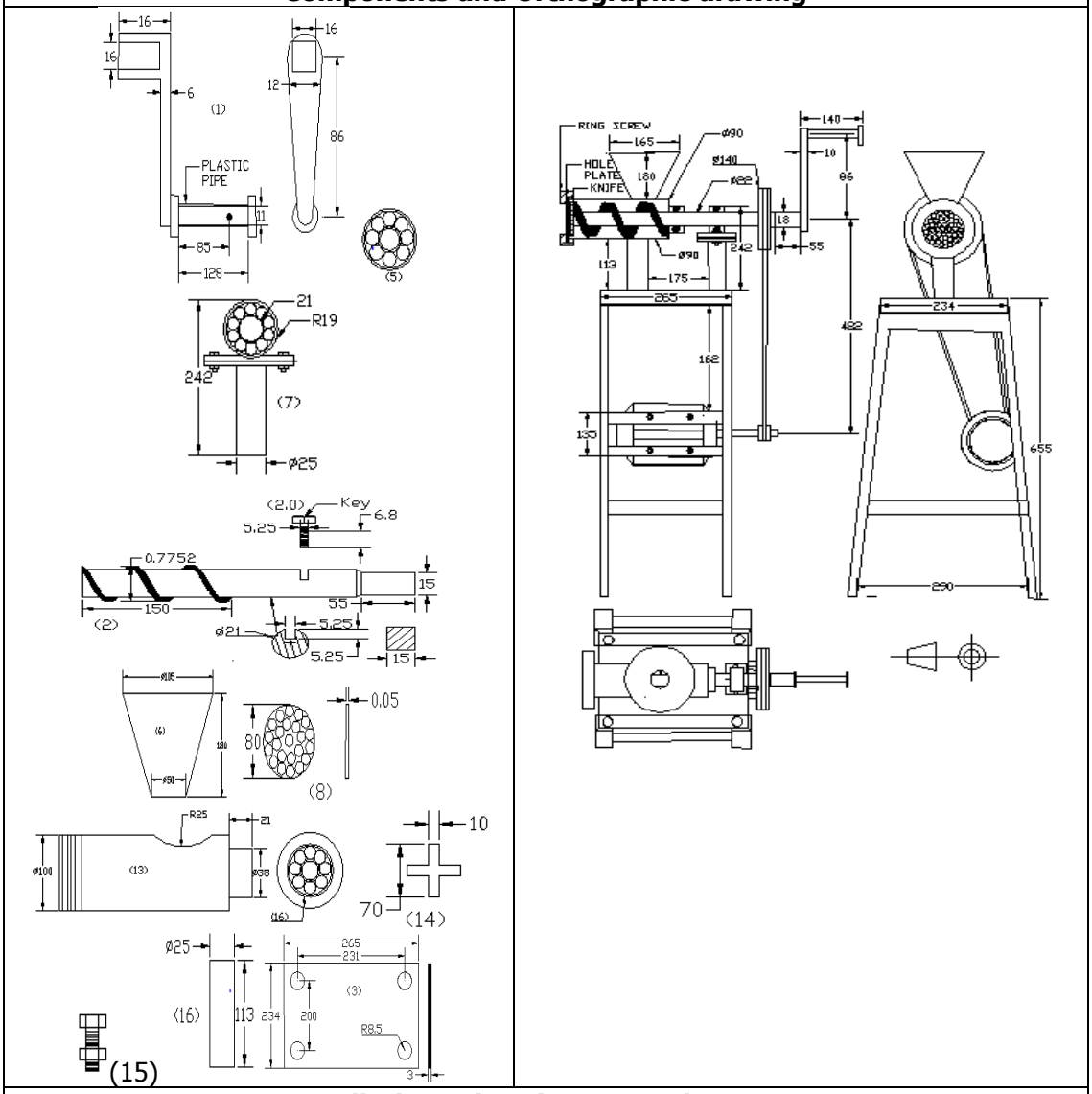
All Dimensions in mm, Scale 1:1

Table 3: Assembling Drawing

The Assembly Drawing				
	S/N	**Component**	**Material**	**Qty**
	1	Handle	MS, P	1
	2	Shaft and Key	SS,MS	1
	3	Grinder Base	MS	1
	4	Motor Pulley	MS	1
	5	Bearing	SS	2

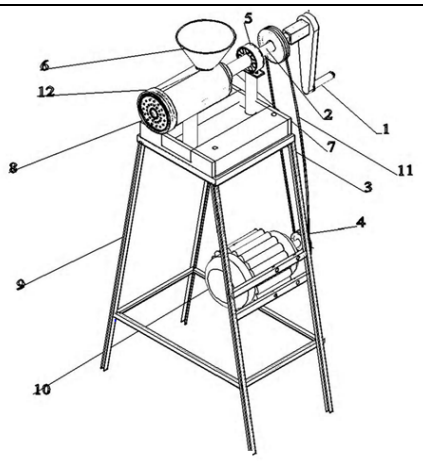

6	Hopper	SS	1
7	Bearing Stand	MS	2
8	Hole Plate	A	3
9	Grinder Stand	Ms	1
10	Electric Motor	MS, R	!
11	V-belt	R, C, R	1
12	Ring Screw	A	1
13	Shaft Housing	SS	1
14	Knife	SS	1
15	Bolt and Nut M12x1,25 M16x1,5	 MS MS	 6 4
16	Grinder Leg	MS	1

All Dimensions in mm, Scale 1:1

6.0 TESTING

The machine was tested for performance in terms of Meat Grinding Rate and Meat Grinding Efficiency of the meat grinder.

6.1. Meat Grinding Rate (MGR)

This is the total quantity of meat grinder per unit time, which passes through the hole plate. It is measured in kilogram per second.

$$\text{Meat Grinding Rate(MGR)} = \frac{\text{Mass of Mear after Grinding}}{\text{Meat Grinding Time}} \qquad 23$$

6.2. Meat Grinding Efficiency (MGE)

This is used to show the proportion of the output (mass of meat after grinding) in respect to the input mass of meat before grinding.

$$\text{Meat Grinding Efficiency (MGE)} = \frac{\text{Mass of Meat after Grinding}}{\text{Mass of Meat before Grinding}} \times 100 \qquad 24$$

6.3 Testing Procedure

A 2.2kg of meat (1.1kg each) free from bones, muscles and fat was purchased from the market. The meat was washed and cut into strips for easy grinding. The machine was set up and the meats were grinded electrically and manually with 1.1kg of meat respectively. The time required and the mass of the meat after grinding were also noted and recorded.

6.4 Results and Discussion

Time required to grind 1.1kg of meat by manual operation T_m = 75sec
Time required to grind 1.1kg of meat by electrical (motorized) operation. T_e = 15sec
Mass of Meat before Grinding M = 1.1kg, Mass of meat after manual operation M_m = 0 .76kg
Mass of meat after electrical (motorized) operation M_e = 0.8 kg.

MGR (for manual operation) = $\frac{M_m}{T_m}$ = $\frac{0.76}{75}$ = 0. 010 kg/sec

MGR (for electrical operation) = $\frac{M_e}{T_e}$ = $\frac{0.8}{15}$ = 0.0 53 kg/ sec

MGE (for manual operation) $=\frac{M_m}{M} \times 100 = \frac{0.76 \times 100}{1.1} = 69\%$

MGE (for electrical operation) $\frac{M_e}{M} \times 100 = \frac{0.8 \times 100}{1.1} = 73\%$

The manual operation of the meat grinder had a meat mincing rate of 0.010kg/esc, while the electrical/motorized operation had 0.0.053kg/sec. This indicates the quantity of meat that can be grinded per second by the manual and motorized method. The motorized method had a high grinding rate due to the high speed of the electric motor. The manual and motorized method had high [69% and 73%] efficiency.. This shows that the manual and motorized meat grinder has a very low [27%and 31%] possibility of being inefficiency.

From Alaba international market, Lagos, the cost of a motorized meat grinding machine is ninety Thousand naira (#90,000.00). One of the objectives of this paper is to design and construct a single meat grinding machine with both manual and motorized mode of operation using simple available tools and materials in order to provide a local alternative. The cost of construction of the manual and motorized neat grinding machine was sixty-two thousand naira (#62.000.00, which is less than the imported meat grinding machines.

7.0 CONCLUSION

From the Shear Force (SF), Bending Moment (BM) diagram and the value of the Factor of Safety (F_S), It can be concluded that the design was safe. The manual operation of the machine had a meat grinding rate of 0.010kg/sec, while the motorized operation has a meat grinding rate of 0.053kg/sec. These indicate the quantity of meat that can be grinded per second by the manual and motorized method respectively. The manual and motorized operation of the machine had a high efficiency (69% and73%) indicating that the machine had a good working condition.

REFERENCES

Khurmi R.S. Machines design. Eurasia Publishing House. Ram Nagar, New Delhi. Pp 4-5, 52-57, 568-571, 716-719, 728-729,1012-1015. 2005.

Khurmi R.S. Theory of machines. Eurasia Publishing House, Ram Nagar, New Delhi. Delhi, Pp 341-345. 2005.

L. Robert Mott. Machine Element in Mechanical Design. Fourtt Edition. Upper Saddle River, New Jessey. Pp 548-551. 2004.

O. Robert and Parmley P.E. Illustrate Source of Mechanical Components.McGraw Hill Company Inc. Pp 4-5. 2000.

P.C. Sharma and Aggarwal D.K. Machine Design. Eleventh edition. S.K. Kataria and Son. Pp 390, 492, 641-644. 2006.

Principles of Meat Processing Technology. Available at; www.foa.org/dcrep/010/ai407e/ai407e04.htm. cited December 2014.

Proceedings of the 49th NSChE Annual Conference
KADA 2019: pp 24-35

P1A-04: REDUCING FOOD LOSS AND WASTE IN NIGERIA AGRICULTURAL VALUE CHAIN

***Nwosibe, P.O[1]; Idika, Kenneth[2]; Omale, Sunday[3]; Nyam, Tobias[4]**
[1.2]African Save Food Initiative, No 42 Onitsha Street Area 11 Garki, Abuja, Nigeria
[1,3,4]Department of Chemical Engineering, Kaduna Polytechnic, Kaduna
Correspondence: Email: patnwosibe@gmail.com, Phone: + 2348037710269.

ABSTRACT
This study investigates the present status of food losses in Nigeria. The causes of food losses and wastage in Nigeria can be hinged on inadequacies or attitudes that revolve around financial, managerial and technical limitations in harvesting techniques, processing and transportation systems, storage and cooling facilities in difficult climatic conditions, infrastructure, packaging, and marketing systems. Reduction in food losses can be achieved by systematic analysis of and awareness creation within the entire food supply chain spanning through producers, retailers and consumers on how to better use food that is now thrown away. To adequately tackle the problem of food losses in Nigeria requires a systematic and holistic approach that will involve all the stakeholders. It is recommended that the save food initiative as an inescapable alternative be harnessed to address the malady, it has the ultimate goal reducing loses and wastages over 60% and value addition not only to food but perceived waste as well.

Keywords: Food Losses, Current Status, Food Chain, Food Security, Nigeria

1.0 INTRODUCTION

According to the predictions of FAO, with an expected population rise to about 9 billion in 2050, food demand is expected to increase by 60% (Alexandratos and Bruinsma, 2012). However, merely increasing food production will not solve the problem of food demand; this is because reports (Gustavasson, *et al.* 2011) have shown that about 13 billion tons (one-third) of the total food production in the world are lost through food loss or wastage. Although limited farmland, water shortage and increasing variability of weather due to climate change are limiting factors to food production; food loss or wastage is another big barrier to food security that should be squarely tackled. Food loss is the decrease in edible food material through the entire supply chain; from production to transportation, postharvest and processing. Food losses that occur at the market level or final consumption are referred to as food waste, which relates to retailers' and consumers' attitudes (Parfitt *et al.*, 2010). The term food waste or loss concerns only products that are meant for human consumption, excluding feed and non-edible products. Therefore, food materials that were originally meant for human consumption but which get out of the human food supply chain are considered as food loss or waste even if finally used for other purposes such as feed or bioenergy. This definition gives the difference between planned non-food uses to unplanned non-food uses, which are hence regarded as losses. Then, postharvest food loss is the measurable qualitative and quantitative food loss along the supply chain, starting from harvest until the food is consumed or used for other purposes (De Lucia and Assennato,1994; Hodges, Buzby and Bennett, 2011). It was reported that about 30% of farm produce is lost in India while in sub-Saharan Africa, the annual value of grain loss is estimated at USD4 billion, which is enough to feed 48 million people for one year.

Food availability and accessibility can be increased by increasing production, improving distribution, and reducing the losses. Thus, the reduction of post-harvest food losses is a critical component of ensuring future global food security.

According to Mundial (2008) and Trostle (2010) reduction in these losses would increase the amount of food available for human consumption and enhance global food security. This has become a growing concern especially with the rising food prices owing to increasing consumer demand, competing demands for biofuel and other industrial uses, and increased weather variability. A reduction in food loss also improves food security by increasing the real income for all the consumers (World Bank, 2011). In addition, crop production contributes a significant proportion of typical incomes in certain regions of the world (70 percent in Sub-Saharan Africa) and reducing food loss can directly increase the real incomes of the producers (World Bank, 2011). Not only do food losses reduce available food for human consumption, but it also increases the cost of waste management, increases greenhouse gas production and loss of scarce resources used in producing the food. Food loss is estimated to be equivalent to 6-10 percent of human-generated greenhouse gas emissions (Gustavasson, *et al.* 2011; Vermeulen, *et al.* 2012). A significant contributor to this problem is through methane gas generation in landfills where food waste decomposes anaerobically (Buzby and Hyman, 2012). The US Environmental Protection Agency reports that in the United States about 31 million MT of food waste accounted for 14% of the 2008 solid waste produced in the country (EPA, 2011) whose costs is roughly 1.3 billion dollars to landfill (Schwab, 2010; Buzby and Hyman, 2012).

2.0 PAST EFFORTS TO INCREASE AGRICULTURAL PRODUCTION IN NIGERIA WITHOUT COMMENSURATE EFFORTS TO MINIMIZE FOOD LOSS AND WASTAGE

In Nigeria, many efforts have been made by the national and state governments as well as international organizations to increase food production from pre-independence era till date (Table 1).

Table 1: Past Nigerian government and other efforts towards increased food production

S/N	Government Project/Programme	Year Established	Mandate
1	First National Plan for Agriculture	1962-1968	Introduction of more modern agricultural methods through farm settlements, co-operative plantations, the supply of improved farm implements and expanded agricultural extension service
2	National Accelerated Food Production Programme (NAFPP)	1972/73	A voluntary scheme launched in Nigeria to make the country self-sufficient and food secured.
3	The Agricultural Development Project (ADP)	The 1970s	Increase crop production through rural development through improved technologies, increased supplies of farming inputs, and improvement of infrastructure.
4	National Seed Service (NSS)	1975	Producing certified seeds as well as to arrange for seed certification
5	Operation Feed the Nation (OFN)	1976	Increase local food production and reduce food imports by encouraging citizens to cultivate unused plots of land to boost agricultural production.

6	The River Basin Development Authorities (RBDA)	1976	Undertake the development of groundwater resources and maintain dams, dikes, wells or boreholes, irrigation, and drainage systems to boost agricultural production.
7	National Food Reserve Agency of Nigeria (NFRA)	1977	Feed the Nigerian nation, export food to other countries, and produce processed agricultural products that would do well in the international market.
8	Agricultural Credit Guarantee Scheme (ACGS)	1977	Provide guarantee on loans granted by banks to farmers to boost agricultural production and agro-allied processing.
9	Green Revolution	1980	Self-sufficiency in food production through modern technologies applied to the Nigerian agricultural sector
10	Directorate of Food, and Rural Infrastructure (DFFRI)	1986	Improve the performance of agricultural-related projects in rural areas to boost food production.
11	Structural Adjustment Programme (SAP)	1986	Aimed at restructuring and diversifying the production base of the economy so as to reduce the over-dependency on the oil sector and imports.
12	National Seed Policy (NSP)	1992	Provide guidelines for the development of seed subsector, to support the improvement of varieties, testing, registration, release, multiplication of released seed varieties, and improve the quality of seeds sold to farmers
13	Nigerian Agricultural Cooperative and Rural Development Bank (NACRDB)	2000	Financing agricultural enterprises at both the micro and macro levels to foster an increase in food production and subsequent food security
14	National Agricultural Development Fund (NADF)	2002	To be involved in agricultural research and development, and to promote the development of the agricultural sector
15	Government-World Bank assisted Fadama project	2005	Enhance agricultural production and value addition to smallholders and rural entrepreneurs in the states by providing support for water management systems in low lying flood plains, so that farming can continue in the dry seasons

16	Agricultural Transformation Agenda (ATA)	2012	Repositioning agriculture to drive Nigeria's economy through deregulation of seed and fertilizer sectors, marketing reforms to structure markets, innovative financing for agriculture and new agricultural investment framework
17	Research Institutes ✓ Institute for Agricultural Research,	1924	Take care of genetic improvement and development of production and utilization technologies for sorghum, cowpea, cotton, groundnut, and sunflower and the improvement of farm-based farming systems in Nigeria.
	✓ National Institute for Oil Palm Research	1937	Research into the genetic improvement, production, and processing of oil palm, date palm, coconut, and ornamental palms.
	✓ Lake Chad Research Institute	1960	Genetic improvement and development of production technologies for wheat, millet, and barley.
	✓ Cocoa Research Institute of Nigeria	1964	Genetic improvement of the production and local utilization of cocoa, cashew, kola nut, coffee, and tea.
	✓ National Cereal Research Institute	1975	Genetic improvement and production of soybean, rice, sugarcane, and sesame.
	✓ National Root Crop Research Institute	1976	Genetic improvement of yam, cassava, cocoyam, Irish and sweet potato and ginger.
	✓ National Animal Production Research Institute	1977	Carry out research into the production of food animals' species and forages.

However merely increasing food production will not totally achieve the required food security for Nigeria. Complementary efforts must be made to ensure that food losses and wastages are reduced to the barest minimum. This will definitely reduce the over-dependence on imported food. Through the above mentioned previous local and foreign efforts, domestic food production is on the rise in Nigeria but it is not enough to meet the national food demand. Worse still, losses of produced crops are on the rise because processing and storage of crops are not adequately done.

3.0 FOOD SECURITY ISSUES AND THE PRESENT STATUS OF FOOD LOSS/WASTAGE IN NIGERIA

A report by West Africa Insight in 2010 estimated that the number of hungry people ie people living in less than two dollars a day in Nigeria to be over 53 million, which is about 30% of the country's total population, while another study (Venkat, 2011) stated that about 84% of Nigeria's population is living below poverty level of less than USD 2 per day. Nigeria is reported to be the 7th most populated country in the world with a total population of about 190 million people and about 51% live in the urban area. Furthermore, it is predicted that in 2050, Nigeria will be the 3rd most populated country in the world after India and China; with a total population between 230 and 430 million people. In recent times food security for the increasing population of Nigerian people has been an issue of great concern to all stakeholders. In 2009, the Federal Ministry of Agriculture estimated that Nigeria was spending over USD3 billion to import food every year. However, food losses and wastages are part of the greatest challenges to food security in Nigeria and have been of great concern to stakeholders including the government policymakers, international organizations like World Bank, UNDP, etc. researchers, extension workers and the farmers themselves. The World Food Summit in 1996 made attempts to achieve 4% annual increase in food production so as to reduce the number of hungry people to half its value then of 800 million by 2015. To achieve this feat would not only require increase in the area of land cultivated, cropping intensities and yield but also deliberate efforts at minimizing, to the barest minimum, food loss and wastage presently bedeviling the food security of the country.

The food problem in Nigeria is due largely to the inability to preserve food surpluses during the short harvest periods rather than to low production. According to FAO when compared to other African countries, Nigeria has one of the highest per capita food output; it accounts for about 70% of world production of yams and 19% of global market share for cassava (FAO, 2001). According to Earth Trends, Nigeria produces 8.41%, 1.09%, 2.85%, and 0.38% of world production of root and tubers, cereals, legumes, and meat respectively. Food losses have a great bearing on food availability and security. Nkana *et al* (1994) painted a dire picture of the situation when they posit that 20%-30%, 5%, 10%-20%, and 20%-67% of maize, rice, cassava, and yam are lost respectively at post-harvest- stored levels in Nigeria. Furthermore, they maintained that 35%-100%, 20% - 80%, 20%-95%, 20%-50%, 70%, and 40%- 100% of plantain, banana, citrus, tomatoes, pineapple, and pawpaw are lost respectively at post-harvest levels. From the foregoing, we can say categorically that more efforts should be channeled towards food storage in Nigeria rather than to production since available statistics show that an alarming percentage of crops that are produced in Nigeria is lost at one stage or the other at post-harvest–storage levels.

Despite all efforts of the government and other international agencies to increase food production, the present situation of food losses and wastage in Nigeria for certain crops are presented in Tables 2 to 5. The tables reveal serious food security issues that demand attention and targeted efforts if Nigeria is to tackle the problem of hunger effectively. Shimada (1999) reported that the increase in the production of rice, cassava, maize, and yam since the 1980s has been very high; also Hall (1968), Adeniyi (1977) and Agboola (1980) are of the opinion that self-sufficiency in food in Nigeria can only be achieved if all effort at increasing crop production is matched with greater effort at postharvest technology to save crops that are produced from spoilage and wastage. It is further reported that Nigeria is one of the leading producers of plantain, okra, tomatoes, yams, and cassava but 30%-50% of these are lost due to poor post-harvest practices (Aworh, 2010).

Table 2. Estimated Annual Production and Postharvest Losses of Stored Cereals in Nigeria (X 10^3MT)

Commodity	Production	Postharvest Losses (%)
Maize	4186.60	20 – 30
Millet	1955.40	20 – 30
Sorghum	5751.10	20 – 30
Rice	6831.19	5

Annual Losses of Cereals: 2378.90 – 3767.90 (10^3MT)
Source: Ministry of Agriculture, Benue State (2010)

Table 3. Estimated Annual Production and Postharvest Losses of Roots and Tubers in Nigeria (X 10^3MT)

Commodity	Production	Postharvest Losses (%)
Cassava	106,785.00	10 – 25
Yam	86, 229.00	20 – 67
Cocoyam	336.00	10 – 40
Sweet potato	5853.00	50 – 80
Ginger	8.10	5

Annual Losses of Roots and Tubers: 30, 884.40 – 89286.91 (10^3MT)
Source: Ministry of Agriculture, Benue State (2010)

Table 4. Estimated Annual Production and Postharvest Losses of Legumes and Oilseeds in Nigeria (X 10^3MT)

Commodity	Production	Postharvest Losses (%)
Soybeans	5090.40	30 – 40
Cowpea	809.70	30 – 40
Bambara nut	371.10	30 – 40
Beniseed/ Sesame seed	7685.50	20 – 50
Melon	874.80	10 – 30
Groundnut	10748.10	30 – 40
Pigeon Pea	196.80	10 – 15
Palm nuts	2555.10	10 – 15

Annual Losses of Legumes and Oilseeds: 30, 884.40 – 89286.91 (10^3MT)
Source: Ministry of Agriculture, Benue State (2010

Table 5. Estimated Annual Production and Postharvest Losses of Fruits and Vegetables in Nigeria (X 10^3MT)

Commodity	Production	Postharvest Losses (%)
Citrus	32, 013.90	20 – 95
Mango	29,590.50	20 – 80
Garden egg	739.80	40 –100
Okra	893.70	30 – 70
Pepper	304.20	10 – 20
Tomatoes	565.50	20 – 50

Annual Losses of Fruits and Vegetables: 20, 839.44 – 45,910.40 (10^3MT)
Source: Ministry of Agriculture, Benue State (2010)

4.0 CAUSES OF FOOD LOSS IN NIGERIA

Generally speaking, factors that may contribute to food losses are numerous and may include biological and environmental factors, socioeconomic factors, mechanization of production and harvesting practices, handling, transportation, infrastructure, processing, weather conditions, government policies, lack or shortage of relevant tools/machines/skills, inadequate maintenance culture, lack of information, management decisions, sorting and grading problems, consumer attitudes and marketing. The quantity of losses occurring at each stage depends on so many factors including available skills, technologies adopted in the supply chain and organization efficiency. In many places in Nigeria, food losses occur mainly with crops such as vegetables, fruits, roots, and tubers; losses occurring at the stage of processing and drying of cereals: Therefore, causes of food loss in Nigeria may be summarized as inadequate methods and attitudes during or due to:

- *Transportation*

  Many Nigeria roads and transport means are not adequate for efficient transport of Farm produce from the farm to either the market or processing and or storage units. Due to the low capital base and farm size, most Nigerian farmers cannot afford to own personal transport vehicles. Public transport vehicles are usually not in the best state to give the best service and also the cost can become unprofitable considering the quantity of crop produced and the price being offered in the market.

- *Handling*

  Improved post-harvest handling procedures are not fully recognized in less developed countries and as a result of post-harvest losses of food, especially fruits and vegetables, are more serious in developing countries like Nigeria due to the use of crude harvesting tools and poor handling technologies. It is distressing to note that so much time is being devoted to the culture of the plant, so much money spent on irrigation, fertilization, and crop protection measures only to be wasted about a week after harvest. It is, therefore, important that post-harvest procedures be given as much attention as production practices.

- *Processing*

  Lack of processing facilities causes high food losses in developing countries, especially, in Nigeria. In many situations, the food processing industry doesn't have the capacity to process and preserve fresh farm produce to be able to meet the demand. Part of the problem stems from the seasonality of production and the cost of investing in processing facilities that will not be used year-round. Governments should develop contract farming linkages between processors and farmers to stimulate the private sector to invest in the food industry and to work more closely with farmers to address supply issues.

- *Poor Maintenance culture*

  This is undoubtedly one of the key reasons why most Nigerian government and foreign interventions to solve the problem of food security in Nigeria have always failed either in the short or long run. As will be briefly highlighted later, there have been some projects, equipment, facilities, interventions that were built or established some years ago but are currently either completely out of use or seriously underutilized owing to poor maintenance, unavailability of equipment and machine spare and lack of follow up. The problem of inadequate maintenance is more pronounced with public-sector facilities and government projects. Therefore, for any similar new projects towards reducing food losses to be sustainable; adequate plans and funds to support maintenance and to ensure success and extended usefulness must be included in the overall plan at the onset of the project or intervention.

- *Lack of required tools and equipment*

  Many needed tools and equipment for proper handling, processing, and storage may not be readily available in the local markets. Most of the tools are usually imported and may not be the inadequate quantity to meet the demand of local farmers. Where available, may be very expensive and uneconomical to the farmer.

- *Storage*

  Agridem Consultant, a private organization, estimated the marketing distribution losses in 1994 for maize, rice, sorghum, millet, cowpea, groundnut, yam, cassava, plantain and fruits as 1.6%, 1.8%, 1.76%, 1.65%, 2.81%, 1.63%, 3.7%, 2.38%, 2.22% and 3.83% respectively. In his previous works, Okigbo advocated good, efficient handling abilities to reduce the cost of perishables. At the present time; Nigeria is still battling with primitive ways of handling farm produce. A visit to a loading point will show a pitiable sight.

- *Inadequate marketing/price system*

  There are very few wholesale, supermarket and retail facilities providing suitable storage and sales conditions for food products in Nigeria. The available wholesale and retail markets are often small, overcrowded, unsanitary and lacking storage equipment. This problem is further exacerbated by inadequate communication and information flow between producers, middlemen and consumers, and lack of market information. Improved market facilities will help to minimize food losses by ensuring that the commodities produced by farmers reach the consumers in an efficient way. Also, there is a need for production incentives in terms of favorable pricing linked with efficient marketing facilities, if losses are to be reduced. However, in Nigeria, such incentives are generally minimal or non-existent.

- *Inadequate fund and information system*

  The cause of food losses in low-income countries, like Nigeria, is mainly connected to financial, managerial and technical limitations in harvesting techniques, processing and transportation systems, storage and cooling facilities and as a result most handlers involved directly in harvesting, packaging, transporting, and marketing in Nigeria have little appreciation for maintaining high quality. Effective educational, training and extension programs on these aspects are continually required. Communicating more of this required information through multimedia will be an important step in the right direction, especially with the increasing awareness and use of the internet in Nigeria.

- *Consumer attitudes and preferences*

  It is very apparent in Nigeria that consumer attitudes and preferences are major causes of high food waste just as witnessed in industrialized countries. IN Nigeria, consumer food waste occurs at the household level and in food service institutions such as restaurants, schools, and hospitals. In the USA, a lot of restaurants serve buffets at fixed prices, which encourages people to fill their plates with more food than they can actually eat. Retail stores offer large packages and "getting one for free" bargains. Likewise, food manufacturers produce oversized ready to eat meals (Stuart, 2009).

- *Management decisions*

  The proportion of *food loss* that occurs in Nigeria is partly a *result* of poor *management decisions*. An enormous amount of food is wasted unnecessarily in Nigeria due to this problem. The negative impact this waste has on our economy and environment is significant. While the majority of food loss and wastage occurs at the consumer level, improving the management of agri-food value chains would have the greatest long-term

impact on reducing food waste, and the resulting economic and environmental impacts. Studies by the Value Chain Management Centre showed where lack of coordination along the chain resulted in at least 25% of Ontario peaches being wasted annually (Gooch et al, 2009).

- *Research and Development*
  Weak RandD capacity and ineffective means of transferring outcomes of R and D to end-users. Besides, more effective research is needed in the field of food waste and loss, and in relation to international trade, as many food products are produced, transformed and consumed in Nigeria and then there should be effective means of transferring the results of the research to the users and the local farmers.

- *Government agricultural policies and policy implementation*
  In Nigeria, government regulations and legislation (if any) on the price of farm produce are not effective and not pronounced. Although in developed countries, government controls on wholesale and retail prices originally designed to protect the consumer can become counter-productive, as producers may lower the quality of products in order to break even. However, government regulations on proper handling procedures and public health issues such as food safety during marketing are very useful if properly implemented.

5.0 PROPOSAL FOR MANAGING AND MINIMIZING FOOD LOSSES IN NIGERIA

To adequately tackle the problem of food losses in Nigeria requires a systematic and holistic approach that will involve all the stakeholders. It has been noted also that minimizing postharvest losses of already produced food is more sustainable than increasing production to compensate for these losses. Therefore, the following steps are outlined for reducing or totally eradicating food losses in Nigeria. They include:

1. Identify a particular crop of interest;
2. Form a team to look into it comprising of researchers, government representatives at the three-tier levels, relevant industry representatives, interested private investors, and relevant banks
3. Carry out a systematic analysis of the entire stages of the supply chain, from production up to marketing and the final consumer to identify the causes of loss
4. Locate, interact and interview the workers involved in each of the stages of the supply chain to appreciate the problems by first-hand information
5. Take each of the loss situations and carefully describe the problem, the cause, possible remedies (which should address each of the causes of loss identified), and proposal of an action plan towards either totally eradicating the losses or minimizing them as much as possible
6. Carry out a cost-benefit analysis of each recommended solution strategy, highlighting the returns on investment for technologies and methods recommended
7. Set up a reliable marketing system for agricultural product price assurance which will serve as a motivation to investors and farmers. Also, the system should be able to provide facilities for accumulating, preparing and transporting produce to markets
8. Collate and summarize the report of investigation for each of the crops, pointing out causes of loss, solution action plans, cost-benefit analysis and a clearly defined role of each stakeholder
9. Organize a workshop/conference of all stakeholders to present and discuss the report of the investigation on each crop and to set up the implementation process
10. Set up a monitoring team to supervise and check the implementation of the solution action plan
11. Organize a periodic workshop for all stakeholders to present progress reports and to carry

out a possible review of any of the solution strategies

12. Active participation in international agreements that promote trade and food safety.

6.0 AN EXAMPLE FROM INDIA

A cue could be taken from the Food Corporation of India, which has played a significant role in transforming the Indian food economy. It operates through a countrywide network of institutions and infrastructures at zonal, regional and district level. The following are the steps taken by India to tackle the problem of food losses in their country:

- **Indigenous manufacture, promotion, and adoption of indigenous technologies**
  One way to reduce agricultural losses is to apply indigenous technologies including effective ways of coordinating research, disseminating results and demonstrations to encourage wider adoption;
- **Price control and assurance for agricultural products**
  The issue of price assurance must be addressed so that the farmer can increase production to levels that will ensure the stability of supplies to meet both normal and emergency requirements;
- **Involvement of private investors**
  Incentive packages to compensate for the opportunity cost of capital tied down must be evolved if the private sector is to continue holding stocks. Such incentives should include fees or commissions for storing on behalf of the government and entitlements to credit at favourable interest rates;
- **Active involvement of the three tiers of government**
  The local government is closest to the farmer and so should be at the forefront in preventing losses by promoting the maintenance of food stocks at household and enterprise levels. Food storage at the government level is a buffer to ensure price stability in the system;
- **Emphasis on the quality of agricultural produce**
  To enhance demand and farm income, it is essential to focus on customers and to improve the quality of produce. Even a slight improvement can affect the marketability of produce quite dramatically and hence reduce loss;
- **Consistency and sustainability of government policies on agriculture**
  Current policies in Nigeria are *ad hoc*, conflicting and inconsistent. Only good policies can ensure viable national farm factors, which will provide food for the people, raw materials for agro-industries and exports and protection for the environment. Agricultural production is complex and multi-disciplinary so a holistic, integrated approach must be adopted in shaping policies and plans, determining strategies, formulating programs and managing their implementation. Only then can consistency and compatibility among sectors be achieved.
- **Development and maintenance of rural farming community infrastructure**
  Roads and electricity must be built to convey the large amounts of farm produce now wasting away in the fields because of the lack of transport facilities.
- **Continuous training and re-training of farmers and agricultural workers**
  Institutions, the government, and other organizations should arrange regular workshop training for farmers and those who operate agricultural machinery.

6.0 SAVE FOOD INITIATIVE

Nigeria should also take a cue from the global initiative on food loss and waste reduction which is presently being led by FAO and Messe Düsseldorf, a leading trade fair organizer. Since 2011, it has worked with donors, development agencies, financial institutions and the private sector (particularly the food packaging industry) to develop and implement a program to reduce food loss and waste. The program rests on four pillars:

1) Awareness-raising;

2) Collaboration with like-minded initiatives;
3) Policy, strategy, and program development; and
4) Support for food supply chain actors and organizations involved in food loss and waste reduction (http://www.save-food.org).

7.0 CONCLUSION

An enormous amount of food is wasted unnecessarily in Nigeria. The negative impact of this wastage on our economy and environment is significant. The causes of these losses are numerous and occur at the stages of production, processing, retailing and consumption. Thus, food losses and wastage occur at all stages of the food supply chain in Nigeria, and improving the management of agri-food value chains would have the greatest long-term impact on reducing food wastage, and the resulting economic and environmental impacts. Therefore, food supply chains in Nigeria should be strengthened, amongst others by diversifying and up-scaling the production and marketing of small farmers, and by (public and private) investments in infrastructure, transportation, processing, storage, food and packaging industries.

REFERENCES

Adeniyi, M.O (1977). Status of plant protection in the operation feed the Nation program, presidential address delivered at its 7th annual conference at Institute of Agricultural Research and Technology (IARandT), Moore plantation in Ibadan, page 10-17

Agboola S.D. (1980). The role of the Nigerian Stored Products Research Institute in Nigeria March towards self-sufficiency in food NSPRI occasional paper series NO 17, page 25-29.

Agricultural and Rural Co-operation Netherland (ARCN) (1998). Bi-monthly publication of the Technical Center for Agriculture and Rural Co-operation. Netherland: No. 77. October issue.

FAO (1988). Food Security Assessment, Food and Agricultural Organization Bulletin Rome.

Alexandratos Nikos and Bruinsma Jelle, (2012). World agriculture towards 2030/2050: the 2012 revision. FAO: Agricultural Development Economics Division. (Available from www.fao.org/economic/esa)

Aworh O.C. (2010). Reducing postharvest losses of horticultural commodities in Nigeria through improved packaging. The world of food science.

Buzby, J. C., and J. Hyman. (2012). "Total and per capita value of food loss in the United States." Food Policy, 37(5), 561-570.

DE Lucia, M.andA Ssennato, D. (1994). Agricultural Engineering in Development: Post-harvest Operations and Management of Food grains. FAO Agricultural Services Bulletin No. 93. Rome: FAO.

Earth Trends country profiles (2003). Agriculture and Food-Nigeria. HTTP: earthtrends.wri.org.

EPA.(2011). Municipal Solid Waste in the United States: 2011 Facts and Figures.

Food and Agricultural organization (2011). Global food losses and waste: Extent causes and prevention. A study conducted for the International Congress (FAO) Rome.

Food and Agricultural organization, (1997). The state of food and agriculture 1997 (FAO) Rome.

Food and Agricultural organization (2001). Production yearbook. Vol .1.55 (FAO) Rome.

Gooch, M., Laplain, D., Stiefelmeyer, K., Marenick, N., Felfel, A., Ingratta, F., Martin, L., Siren, C., Lamb, T., Dent, B., MacTavish, J.; (2009). Consumer Market Research Strategic Study for Fresh Grapes and Fresh and Processed Apples and Tender Fruit and Orchard Fruit and Vineyard Quality Assessment throughout the Value Chain. Value Chain Management Centre; George Morris Centre. Available online: http://www.vcmtools.ca/pdf/Vineland%20Final%20111009.pdf

Gustavsson, J, Cederberg C, Sonesson, U., Van Otterdijk, R., Meybeck, A., (2011). "Global Food Losses and Food Waste: Extent Causes and Prevention." Rome: Food and Agriculture

Organization of the United Nations (FAO). (Available from http://www.fao.org/fileadmin/user_upload/ags/publications/ GFL_web.pdf)

Hall F.W. (1968). Prevention of waste of agricultural produce during handling, storage, and transportation. Tropical stored institute pp 15-23.

Hillocks R (2002). Cassava in Africa. In hillocks R., Thresh J and Bellotti AC (eds). Cassava biology, production, and utilization. CABI publishing**.**

Hodges, R. J., Buzby J. C., and Bennett, B., (2011). Postharvest losses and waste in developed and less developed countries: opportunities to improve resource use. *Journal of Agricultural Science* (2011), 149, 37–45. (Available from http://ucanr.edu/datastoreFiles/234-2203.pdf) .

Mundial, B. (2008). "Double Jeopardy: responding to high food and fuel prices." Cumbre Hokkaido-Toyako del G, 8, 2.

Nkana I, Adamu DJM and Igene J.O., (1994). Food loss and conservation under arid environment. *Annals of Borno Journals*, 11(12):191-204.

Oriole E.O. (2009). Irrigation agriculture. An option for achieving the Millennium Development Goals (MDGs) in Nigeria. *Journal of Geography and Regional Planning* vol 2(7); 176-181

Osunde Z.D. (2008). Minimizing post-harvest losses in Yam (*Discorea* spp): Treatments and Techniques. International union of food science and technology.

Parfitt, J., Barthel, M., Macnaughton, S., (2010). Food waste within food supply chains: quantification and potential for change to 2050. *Philosophical Transactions of the Royal Society B: Biological Sciences* 365(1554):3065-3081.

Shimada S. (1999). A study of increased food production in Nigeria: the effect of the structural adjustment program on the local level. African study monographs 20(4): 175-227, Dec 1999.

Trostle, R. 2010. "Global Agricultural Supply and Demand: Factors Contributing to the Recent Increase in Food Commodity Prices." (Rev. DIANE Publishing).

Venkat K. (2011). Climate change and economic impacts of food waste in the United States. *International Journal of Food System Dynamics* 2(4):431-446.

Vermeulen SJ, Campbell BM, Ingram J SI. (2012). Climate change and food systems. *Annual Review of Environmental Resources* 37. (Available from http://www.annualreviews.org/doi/abs/10.1146/ annurev-environ-020411-130608).

West Africa Insight (2010). Concerning Food Security in Nigeria December 2010 Farming.

World Bank (2011). Missing Food: The Case of Postharvest Grain Losses in Sub-Saharan Africa. Economic and Sector Work. Washington, The World Bank.

Proceedings of the 49th NSChE Annual Conference
KADA 2019: pp 36-41

P1A-05: PHYSICOCHEMICAL PROPERTIES OF COCONUT OIL EXTRACT FROM IMOPOLY PLANTATION SEED

***[1]Offurum, J.C.; [2]Ahamefula K.; [3]Iheme C. and [4]Mbadike A.C.**
[1,3,4]Department of Chemical Engineering, Imo State Polytechnic, Umuagwo-Ohaji
[2]Centre for Technology Management, Amas-soma, Bayelsa State
E-mail of Corresponding Author: jullyengine@yahoo.com

ABSTRACT
The present research work focused on the analysis of physicochemical composition of coconut oil extracted from coconut seed (cocosnucifera linn). This was motivated by the need to know if the artificially-budded specie of IMOPOLY plantation conforms to the generally existing characteristics of coconut oils. The sample was produced using the solvent extraction method (with N-hexane as the solvent). The results obtained from the analysis of physicochemical parameters showed that the acid value, perioxide value, saponification value, iodine value, free fatty acid, pH, cetane number, specific gravity, viscosity, density and crude protein are 2.40gNaOH/100g, 25.00meqKOH/g, 46.28mgKOH/g, 8.88mgI_2/g, 1.2%, 5.33, 162.23, 0.9063 (at 15^{0}C kglm$^{3)}$, 341.35 mpas^{-1}, 0.88773, and 5.25% respectively. These results were found to be within standard specifications as was recommended by the American standard testing method (ASTM) and the Analysis of association of official Analytical Chemists (AOAC) for edible oil, as well as within the limits of other results of similar researchess. However, the percentage yield of the oil (58.87%) could be said to be satisfactory and within acceptable range (30 – 65%) for coconut oils, which basically depends largely on the quantity of coconut seed, species of coconut and extraction method used.

Keywords: Physicochemical, Coconut oil, Characteristics, IMOPOLY Plantation.

1.0 INTRODUCTION
The coconut oil is an edible vegetable oil produced from the kernel (meat) or endocarp of matured coconut seed. The coconut oil has been found to be very useful domestically, medically and industrially as cooking (baking) oil, skin moisturizer, as a hair supplement and anti-oxidant (Bawalan, 2011)). It is a good lubricant/fuel, and can be used also to power generators and diesel engines, reasons which are not far-fetched from its potential chemical and physical properties/characteristics. Predominantly coconut oil is composed of saturated fatty acids (about 94%). The presence of these free fatty acids makes it slow to oxidize, thus resistant to rancidification, lasting up to more than six months without spoilage (Bawalan, 2011)). This saturated fatty acid is a parameter readily not available in most edible oil in the market. However, many health organizations have advised against the usefulness of coconut oil because of its high level of saturated fat.

This research seeks to harness the raw material potentials of the coconut oil due to huge demands of products (directly and indirectly) made from it. The pressing method was employed during preliminary generation of coconut oil, as the method is considered viable because of its high oil yield and specifications.

2.0 MATERIALS AND METHODS

Sample Preparation for Extraction
The basic sample used for this study is the coconut seed. Matured coconut fruits, (three in number), were harvested from the coconut farm/plantation at the 'Otammiri' Area of Imo State Polytechnic, Umuagwo-Ohaji, and was peeled off, to obtain the browny coconut seed.

The seeds were dehusked and deshelled to obtain the coconut meat. The coconut meat was scrapped to remove the browny part. Immediately, it was cut to smaller sizes, washed and ground (pulverized). Using an oven dryer at 70^0C, it was demoisturized in preparation for extraction process; the dried coconut cake obtained is the 'Copra'.

Extraction Procedure

Solvent method of extraction was adopted by means of *soxhlet extractor* and hexane (as solvent). Initially, 50.21g of sample (copra) was introduced into the extractor, and 300ml of hexane was poured into the solvent flask. The extractor (receiver tube) was then connected to soxhlet flask with the aid of an adaptor to make it air tight. Also, a reflux condenser was connected to a water reservoir and water flowed continuously through the condenser, to supply cooling to the system. The heating mantle was then switched on (at a temperature of 70^0C); the *N–hexane* gradually boiled, and its vapour condensed by the reflux condenser. The condenser dripped through the copra (sample), contained in the extractor tube and gradually percolates it, while the oil was absorbed by the solvent. The oil-solvent mixture goes up (with time) to the top of the extractor discharge. At this point, the solvent was refluxed into the flask. This process continued until a colourless condensate was noticed, which indicate no traces of oil; then, heating process was stopped. The oil-solvent mixture was distilled thereafter to recover the coconut oil with no trace of hexane. For further purifications, the coconut oil produced was transferred into a beaker and heated to completely evaporate the solvent from mixture, and the sample from the extractor was finally removed.

Physicochemical Characteristics of Coconut Oil

Standard methods of analysis of association of official analytical chemist, AOAC (1997) were used in all analysis.

Determination of Percentage Yield of Oil: The weight of the ground copra, W_1 was taken, as well as that of the oil extract, W_2. This was done according to the solvent used for the extraction. The percentage oil yield is given by equation (1).

$$Percentage\ Yield = \frac{W_2}{W_1}\ \mathrm{X}\ \ \frac{100}{1} \qquad (1)$$

Determination of Crude Protein: The crude protein in the sample was determined using kjeldhal method. 0.5g of the sample was weighed into a digestion flask, containing 10ml of concentrated H_2SO_4, and 8g of digestion mixture was added, that is K_2SO_4 : $CuSO_4$ (8:1) . Then the flask was swirled for proper mixture of the contents. A blue-green colouration indicates the completion of digestion. The digest was cooled and transferred to 100ml volumetric flask, which contains 25ml of distilled water. The digest was then distilled with 10ml of 0.5N NaOH; the distillation continued, and the NH_3 formed (as NH_4OH) was collected in 20ml of 4% boric acid. Using methyl-red indicator, the distillate was titrated against standard 0.1N HCl till the appearance of a pink colour; the blank was also ran using the same steps at each case. The percent crude protein is given by equation (2).

$$Crude\ Protein = 6.75\ \mathrm{X}\ \mathrm{YoN}\ (\mathrm{Concentration\ Factor}) \qquad (2)$$

Determination of Specific Gravity: 50ml pyrometer bottle was washed thoroughly with a detergent, ionized water and rinsed with petroleum ether. It was then filled with the coconut oil sample and weighed. The specific gravity was determined using equation (3).

$$S.G. = \frac{M_2 - M_1}{W_2 - W_1} = \frac{\mathrm{Mass\ of\ Substance}}{\mathrm{Mass\ of\ equal\ Vol.\ of\ Water}} \qquad (3)$$

Where (M_2-M_1) = Mass difference of Oil

(W_2-W_1) = Mass difference of equal volume of water

Results were expressed as relative density at 20^0C/20^0C or 40^0C/40_0C.

Determination of pH Value: The pH meter was used to determine the pH value of the coconut oil. 2g of sample (coconut oil) was poured into a clean dry 25ml beaker, and then 13ml of hot ionized was added to the sample in the beaker and stirred slowly. The mixture of oil and water (hot) was allowed to cool in a cold water bath to 25^0C. Then the pH electrode was standardized with buffer solution and the electrode immersed into the sample and the value was read and recorded.

Determination of Viscosity: NDJ-5S digital rotary viscometer was used for determining the liquid viscosity of the oil. The liquid (oil) to be measured was kept for enough time under an unchanged temperature in order to obtain stable measuring result. Then, the required speed and spindle number was selected. The knob was pressed to start measuring viscosity. The result is displayed on the digital viscometer in mpa/s.

Determination of Saponification Value (SV) in Oil: Saponification value was determined by weighing 0.5g of the sample into a conical flask. 25ml of potassium hydroxide was then added with 5 granules of anti-bumping chips. The system was attached to reflux air condenser, and was refluxed for 30minutes until saponification was complete.

1ml of phenolphthalein indicator was added into the hot soap solution and slowly titrated against 0.5NHCl until the pink colour of the indicator disappears; the same procedure was used for the blank. The saponification value, SV is given by Equation 3.3.

$$SV = \frac{56.1\ \mathrm{N}(V_1 - V_2)}{\mathrm{W}} \qquad (4)$$

Where V_1 = Vol. of acid used in blank solution
V_2 = Vol. of acid used in the sample
N = Actual normality of the HCl used
W = weight of the sample (in gram).

Determination of Acid Value: 25ml of diethyl ether was mixed with 25ml of ethanol (neutralized solvent). 1ml of phenolphthalein solution was added. 1g of oil was weighed and dissolved in the neutralized solvent. This was titrated using 0.1m NaOH to a pink end point. The acid vale was calculated using equation (5).

$$Acid\ Value = \frac{56.9\ \mathrm{X\ Titre\ X\ M}}{\mathrm{W}} \qquad (5)$$

Where: W = mass of sample used
M = Molarity of the Base (NaOH)
V = titre value

Determination of Free Fatty Acid (FFA): The same procedure for acid value was used to determine the free fatty acid content of sample (coconut oil), as contained in Equation (6).

$$\text{Free Fatty } Acid\ Value = \frac{56.9 \text{ X Titre X M}}{2 \text{ X W}} \qquad (6)$$

Determination of Iodine Value : 0.4g of the test sample was weighed into a conical flask and 20ml of carbon tetrachloride was added to dissolve in it. 25ml of Dam's reagent (Wig's iodine) was then added using a safety pipette. The stopper was inserted and the content of the flask was vigorously swirled. The flask was then placed in the dark for 2hours, 30mins. At the elapse of the time, 20ml of 10% aqueous potassium iodide and 125ml of water were added using a measuring cylinder. The content was then titrated with 0.1N of sodium thiosulphate solution until the yellow colour almost disappeared. At this point, few drops of 1% starch indicator were added and the titration continued by drop-wise addition of more sodium thiosulphate until the blue colour formed disappears (after vigorous shaking). The same procedure was used for the blank test, and the iodine value, IV is given by Equation (7).

$$IV = \frac{12.69 \text{ C } (V_1 - V_2)}{\text{M}} \qquad (7)$$

Where, C = concentration of sodium thiosulphate used
V_1 = Vol. of sodium thiosulphate used for blank
V_2 = Vol. of sodium thiosulphate used for the determination.
M = Mass of sample.

Determination of Peroxide Value: A blank determination of the reagents were conducted, where 5.00 (10.05g) of coconut oil sample was weighed into a 250ml glass stoppered Erlenmeyer flask. The weight was recorded to meet the nearest 0.0lg. Using graduated cylinder. Then 30ml of acetic acid chloroform solution was added in the ratio 2:1. The flask was swirled until the sample was completely dissolved (that is 5g to 5ml of water). Then using Mohr pipette, 0.5ml of saturated potassium iodide solution was added. Then the flask was stoppered, the contents of the flask swirled for exactly l minute, and it was then heated. Immediately, using graduted cylinder, 30ml of ionized water was heated, stoppered and shaked vigorously to liberate the iodide from the chloroform. Finally, the burette was filled with 0.lN sodium thiosulphate and titrated slowly until the deep red-orange colour was observed. Using a dispensing device, lml of starch indicator was adopted, added and titrated until the blue-gray colour of the indicator disappeared in the aqueous (upper) layer. The peroxide value was evaluated using Equation (8).

$$PV = \frac{200(V_1 - V_2)\text{N}}{\text{M}} \qquad (8)$$

Where: V_1 = titre value of sample
V_2 = titre value of blank
N = normality of the thiosulphate
M = Mass of oil used

Cetane Number: The cetane number was evaluated by simple substitution of the saponification value and iodine value as stated in Equation (9).

$$\text{Centane Number} = 46.3 \frac{5458}{\text{SV}} - 0.225 \text{ X IV} \qquad (9)$$

Where;
SV is the saponification value
IV is the iodine value.

3.0 RESULTS AND DISCUSSION

The results of Percentage oil yield, physical assessment of oil extract from coconut seed and those of chemical assessment of oil extract from coconut seed are presented in Tables 1, 2 and 3 respectively.

Table 1: Percentage oil yield

Properties	Coconut oil
Weight of oil extracted	150.3lg
Weight of sample (Copra)	255.32g
% yield of oil	58.87

Table 2: Physical assessment of oil extract from coconut seed

S/N	CHARACTERISTICS	COCONUT OIL
1	Colour	Colourless
2	Odour	Smell of coconut
3	Taste	Bland
4	Texture	Smooth feel
5	State	Liquid at 25^{o}C
6	Specific gravity 15^{0}C kglm^{3}	0.9063
7	Kinematic viscosity at 40^{0}C	341.35 mpas^{-1}
8	Density	0.8773
9	pH	5.33
10	Water absorption capacity	Insoluble in water at room temperature.

Table 3: Chemical assessment of oil extract from coconut seed.

S/N	CHARACTERISTICS	COCONUT OIL
1	Acid value	2.40g NaOH/100g
2	Peroxide value	25.00 meq KOHlg
3	Saponification value	46.26 mg KOHlg
4	Iodine value	8.88mgI_2lg
5	Free fatty acid (FFA)	1.2%
6	Protein	5.25%
7	Ceta number	162.23

The yield of the oil (58.87%), as presented in table 1, could be identified as being within satisfactory (acceptance) limit when compared with relevant information from literature (Bezard *et al*, 1997). The percentage yield of coconut oil is attributed to the quantity of coconut seed used, the specie of the seed, the method of extraction and solvent used. *N-hexane* used for the extraction of the oil is a non-polar solvent, and is capable of dissolving fats coupled with prolonged exposure to heat at 70^{0}C. Hexane, which is largely unreactive, is easily evaporated at a very low energy, and is capable of extracting high quantity of coconut oil. It is selective and leaves the protein, FFA and some undesired gums largely undisturbed in coconut oil.

Table 2 shows the physical characteristics of coconut oil extract from coconut seed. The coconut oil extracted formed a white homogenous mixture when *beaten* well in water, otherwise it insoluble at room temperature. It is colourless, has a smell of coconut, highly viscous at 40^{0}C, slightly acidic, and is denser than water (at 15^{0}C).

The chemical characteristics of coconut oil extract from coconut seed (table 3) indicate that the free fatty acid of coconut oil is high (with FFA of 1.2%); this implies low rancidity of the

oil, thus viable as edible oil (FAO, 2009; Aten *et al*, 1958; APCC, 2009). The iodine value of 8.88I_2/100g falls within acceptable limit of l0*meq* peroxide/kg FAO, 2009), which signifies high oxidative stability. The saponification value of 46.28mg KOH/lg, makes the oil suitable for soap production, detergents and shampoo products. The cetane number of 162.23 signifies that the oil can serve as alternative source of biodiesel. This is high and good for improved burning ability, better fuel consumption, reduced engine noise, lower emission, wider energy release spectrum (due to slower burning), hence torque and power output characteristics (Dreamer *et al*, 2005; Bello and Agge, 2011).

4.0 CONCLUSION

The coconut oil was successfully produced from coconut seed, using *N-hexane* (as solvent) and soxhlet extraction unit. The results obtained from the physical and chemical analysis were found to be within standard specifications, as was recommended by ASTM and AOAC, for edible oil. The utilization of coconut seed in the area of production of products, made both directly and indirectly from coconut, has widely expanded the importance of the plant in respect to industrial applications. Therefore, there is need for more research in the area of improving the shelf life of the oil produced from coconut seed, in order to exploit its massive application opportunities in our industries.

5.0 REFERENCES

AOAC (1997). Methods of Analysis of Association of Official Analytical Chemist, 14th Ed, Washington DC; PP 576-624.

APCC (2009). Quality Standard of Virgin Coconut Oil; Available at www.APCC.org/APCCsec/admin/file.hvco standard flyer.pdf; pp 5-6.

Aten, A., Mami A. and Cooke F.C. (1958). Copra Processing in Rural Industries; FAO Agric.

Bawalan D.D. (2011). Processing Manual for Virgin Coconut Oil, its Products and By-products for Pacific Island Countries and Territories; Available at: http://www.spc.int.

Bello E.I. and Agge M. (2011). Production, Characterization and Evaluation of Castor Oil Biodiesel as Alternative Fuel for Diesel Engines; Journal of Emerging Trend in Engineering and Applied Sciences; 2(3): 525-530.

Bezard J.J., Bugat M. and Clement G. (1997). Triglyceride Composition of Coconut Oil; Journal of American Oil Chemists Society; 48(3): 134-139.

Dreamer T., Newell R., Deamer Z., Deamer E. and White J. (2005). Issues in using Coconut Oil as Fuel in Vanuatu: National Workshop Towards Increased Use of Liquid Biodiesels in the FijiIsland, Suva-Fiji; 16th– 17th March.

FAO (2009). Codex Alimentarius Standard; 2001 Standards for Named Vegetable Oils; Available at: http:// www.fao.org/fao-who-codex alimentarious/en/.

Proceedings of the 49th NSChE Annual Conference
KADA 2019: pp 42-48

P1A-06: DIARY INDUSTRY - CONVERSION OF RAW MILK IN A TRIPPLE-EFFECT EVAPORATOR

Folahan P. Ibitoye[1*] and Mojirade M. Oloruntoba[1,2]
[1]Prototype Engineering Development Institute (PEDI), Ilesa, Nigeria.
[2]Department of Chemical Engineering, University of Lagos, Akoka, Lagos, Nigeria.
***Corresponding author**: E-mail: folaibitoye@yahoo.com

ABSTRACT
In order to achieve a good concentration of milk, Matrix Laboratory (MATLAB®) was used to model a triple-effect evaporator for a 30 ton/h processed milk initially at 5% concentration to 81% concentration. The steam economy (SE) was reduced to 4.1 at an interval of 0.4 to study its effect on the outlet milk concentration. Based on some thermodynamic assumptions, the effect of varying some input variables on the output parameters was studied. Other values of SE were later assumed and the process repeated until the desired 81% milk concentration was obtained. The desired concentration was obtained in the third effect when a steam economy of 2.5 was used. With this SE of 2.5, the concentration of milk obtained in first effect is 7%; second effect is14% while the target concentration of 81% is obtained in the third effect. It was concluded that most of the output parameters, such as milk concentration; water removed; volumetric flow rate; and area decrease with increasing SE; only mass of flow rate increases with increasing SE. Also, the milk concentration increases as the number of effect increases; with a milk concentration of 81% obtained in the third effect. The choice of SE and the number of effects should be properly considered before the design of milk production facility.

Keywords: evaporator, steam economy, milk, facility, concentration

NOMENCLATURES
x1 : Inlet composition of milk feed
x2 : Outlet composition of concentrated powdered milk
SE : Steam economy
MF : Mass flow rate of milk feed (kg/h)
TF : Temperature of milk feed (K)
TS : Temperature of saturated steam to first effect (K)

1.0 INTRODUCTION
The various activities of the Nigerian diary industry have been going on in the country for over 60 years. These activities are however unorganised except for the relatively few processing firms that produce and market reconstituted milk products from imported powdered milk. Diary industry represents an important component of the agricultural sector of the economy with great economic, nutritional and social implications.

Livestock play a very important role in Nigerian agriculture contributing about 12.7% of the agricultural GDP (CBN, 1999). The livestock subsector is dominated by traditional systems of production, processing and marketing. Evaporation is a process by which a liquid brought to its boiling point by external heating transforms water into vapour which escapes from the surface of the liquid. The evaporation of water from milk requires special attention because of heat sensitivity. Limited literature exists specifically on falling-film evaporator modeling for milk applications. Winchester and Marsh (1999) proposed a first-principles model of an evaporator based on the physical laws of thermodynamics. More recently, Medhat *et al.* (2015)

developed both "lumped" and "distributed" dynamic models for an industrial multi-effect whole milk evaporator.

However, a wide variety of evaporator models can be found in the literature for other food applications. Russell *et al.* (2000) presented three types of evaporator models for a general evaporation process: an artificial neural network model; an analytically-derived model; and a linear regression model; and Bhargava *et al.* (2008) presented a non-linear mathematical model for concentrating black liquor in a paper mill. Moreover, various studies have investigated: flow regimes (Silveira *et al.,* 2015); heat transfer coefficient distribution (Gong *et al.,* 2015); pressure drop and friction factor modelling (Mura and Gourdon, 2017); and modelling of heat and mass transfer in falling film evaporators (Bourouni *et al.*, 1998). In this work, a simulation approach was proposed to model the effect of input variables on the concentration of 30ton/h processed milk in a triple-effect evaporator.

2.0 METHODOLOGY

In order to achieve maximum profitability, manufacturers of powdered milk need processing equipment that is modular in construction and versatile enough to handle a wide range of products. Also, since energy can be saved by reusing vapour formed from one effect to the other, a triple-effect evaporator is considered for this study for a 30,000 Kg/hr milk initially at a concentration of 5% to a concentration of 81%. Changes to product quality that result from relatively severe heat treatment are minimized by the design and operation of the equipment. For this study, the evaporator therefore works at reduce pressure and temperature (significantly below 100°C). The reduced pressure is obtained by combining condensers with vacuum pumps to the vapour from the evaporator.

For this work, mass flow rate of product for each effect and the water removed in each effect were calculated. Mass of steam required to achieve separation was also calculated by assuming SE values. MATLAB was used in analyzing the design and operation of the triple-effect evaporation system by initially testing with a SE of 2.5 (based on previous report by some authors) in order to study its effect on the outlet concentration and then reducing and assuming new values of SE from 3.7 (at an interval of 0.4) each time until desired product concentration is obtained. The area, number of tubes and volumetric flow rate of the pump in each effect was also calculated. The methodology adopted is similar to the modeling conducted by Oloruntoba *et al.*, 2016. Equations (1-11) describe the mass and energy balance for all effects.

$$m_F = m_P + m_E \quad \text{.....(1)}$$

$$m_s = {}^{m_E}/_{SE} \quad \text{.....(2)}$$

1st Effect

$$m_F = m_{P1} + m_{E1} \quad \text{.....(3)}$$

$$Q_F + Q_S = Q_{C1} + Q_{P1} + Q_{E1} \quad \text{.....(4)}$$

$$[m_F * C_F * \Delta T] + [m_s * \lambda_S] = [m_{C1} * C_{C1} * \Delta T] + [m_{P1} * C_{P1} * \Delta T] + [m_{E1} * \lambda_{E1}] \quad \text{.....(5)}$$

2nd Effect

$$m_{P1} = m_{P2} + m_{E2} \quad \text{.....(6)}$$

$Q_{P1} + Q_{E1} = Q_{C2} + Q_{P2} + Q_{E2}$.....(7)

$[m_{P1} * C_{P1} * \Delta T] + [m_{E1} * \lambda_{E1}] = [m_{C2} * C_{C2} * \Delta T] + [m_{P2} * C_{P2} * \Delta T] + [m_{E2} * \lambda_{E2}]$.....(8)

3rd Effect

$m_{P2} = m_{P3} + m_{E3}$.....(9)

$Q_{P2} + Q_{E2} = Q_{C3} + Q_{P3} + Q_{E3}$.....(10)

$[m_{P2} * C_{P2} * \Delta T] + [m_{E2} * \lambda_{E2}] = [m_{C3} * C_{C3} * \Delta T] + [m_{P3} * C_{P3} * \Delta T] + [m_{E3} * \lambda_{E3}]$.....(11)

where,

C_F = specific heat of the feed (kcak/kg°C)
C_{P1}, C_{P2}, C_{P3} = specific heat of Product in effect 1 to 3 (kcak/kg°C)
C_{C1}, C_{C2}, C_{C3} = specific heat of Condensate in effect 1 to 3 (kcak/kg°C)
λ_S = Latent heat of steam (to 1st effect)kcal/kg
λ_{E1},λ_{E2},λ_{E3} =Latent heat of water evaporated (kcal/kg).
m_F = mass flow rate of feed (kg/hr)
m_E = Total water evaporated (kg/hr)
SE = Steam Economy
m_S = mass flow rate of steam (kg/hr)
m_{E1}, m_{E2}, m_{E3} = mass flow rate of water removed in effects 1 to 3 (kg/hr)
m_{P1}, m_{P2}, m_{P3} = mass flow rate of product in effects 1 to 3 (kg/hr)
m_{C1}, m_{C2}, m_{C3} = mass flow rate of condensate in effects 1 to 3 (kg/hr)

2.1 Assumptions

1. The raw milk in the evaporator is assumed to be completely mixed
2. The milk entering the evaporator and the milk leaving the evaporator has the same composition.
3. The heat recovery and preheating process ensures the milk enters the first effect 1 at 81.5°C, and 50 kPa.
4. The specific heat (Cp) of milk at 5% concentration is taken as 3.2 kJ/kg K
5. No heat is lost by radiation or convection

2.2 Mathematical Modeling of the Triple-Effect Evaporator

The known parameters for the process are given in Table 1.

Table 1. Known parameters for the triple-effect evaporator

SN	PARAMETER	VALUE
1	No of Effects	3
2	M_F	30000 kg/hr
3	T_F	81.5 °C
4	X_1	0.05
5	X_2	0.81
6	T_S	100.0 °C

3.0 RESULTS AND DISCUSSION

The results obtained for the output parameters for a steam economy of 2.5 are given in Table 2. It can be seen from the table that a target milk concentration of 81% was obtained from the third effect. It is observed that the milk concentration increases as the number of effect increases. Also the mass flow rate of product decreases as the number of effect increases which is similar to results obtained from Oloruntoba *et al.,* 2016 and Medhat *et al.,* 2015. A plot of milk concentration against steam economy for the different effects is shown in Figure 1.

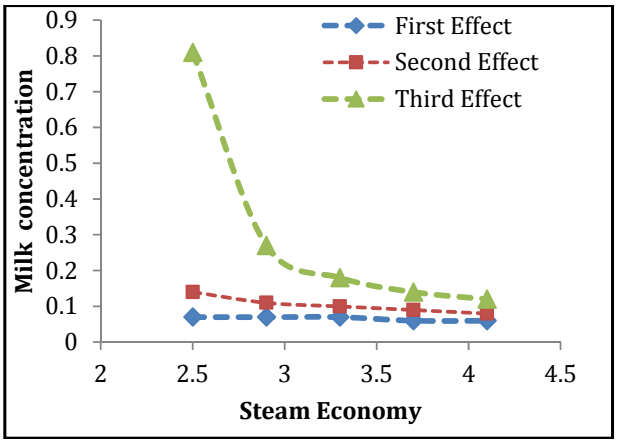

Figure 1. Milk concentration versus steam economy for the different effects

It can be seen that the milk concentration increases with decreasing steam economy. The target milk concentration of 81% was obtained in the third effect when the steam economy of 2.5 was used. There is no remarkable change in concentration of milk in first effect with different changes in steam economy. With a steam economy of 2.5, the concentration of milk obtained in first effect is 7%; second effect is 14% while the target concentration of 81% is obtained in the third effect.

Figures. 2 to 5 show the plots of some output parameters against SE for the different effects. The profiles for first effect, second effect and third effect show similar trends as shown in the plots. Most of the output parameters, such as milk concentration; water removed; volumetric flow rate; and area decrease with increasing SE; only mass of flow rate increases with increasing SE as shown in Figure 3. Close values were noticed at SE of 2.9, 3.3, 3.7 and 4.1 in first, second and third effect for the water removed; as shown in Figure 2. The above deductions is due to the fact that multiple-effect evaporator using a particular number of effect increases the steam economy but decreases the heat flux per effect by a factor of inverse of the number of effect relative to single effect operation under same conditions.

4.0 CONCLUSION

The implementation of MATLAB to model a Triple-effect evaporator for a 30 ton/h processed milk initially at 5% concentration to 81% milk concentration was studied. Steam economy (SE) was reduced from 4.1 at an interval of 0.4 to check its effect on the concentration obtained. The desired milk concentration of 81% was obtained in the third effect when a steam economy of 2.5 was used. With this SE of 2.5, the concentration of milk obtained in first effect is 7%; second effect is 14% while the target concentration of 81% was obtained in the third effect. The choice of SE and the number of effects should be properly considered before the design of milk production facility.

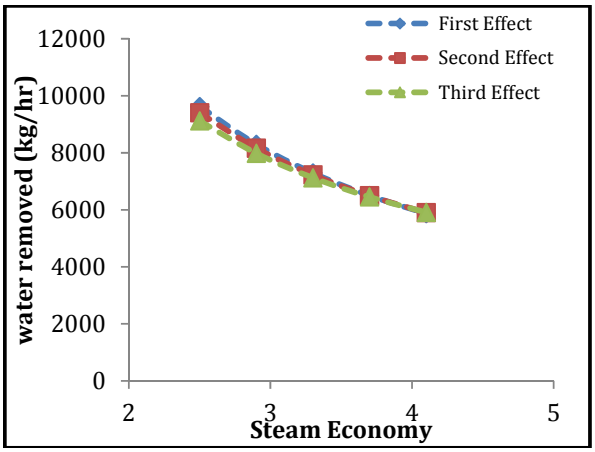

Figure 2. Water Removed versus Steam Economy for the different effects

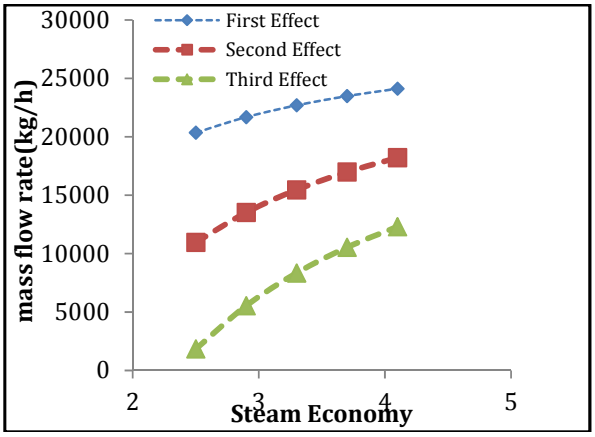

Figure 3. Mass Flow Rate versus Steam Economy for the different effects

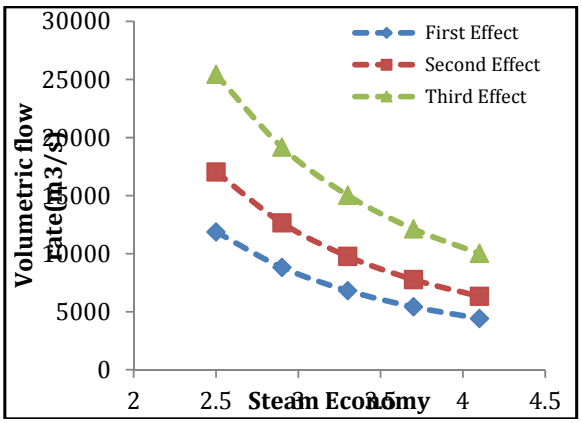

Figure 4. Volumetric Flow Rate versus Steam Economy for the different effects

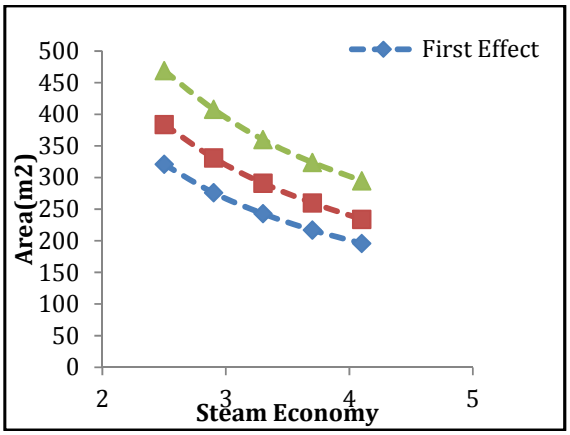

Figure 5. Area versus Steam Economy for the different effects

Table 2. The results obtained as output parameters for steam economy of 2.5

Parameters	Values
The mass of flow rate of product obtained in first effect is:	20375.27 kg/h
The water removed in first effect is:	9624.72 kg/h
The mass of flow rate of product obtained in second effect is:	10970.46 kg/h
The water removed in second effect is:	9404.81 kg/h
The mass of flow rate of product obtained in third effect is:	1850.12 kg/h
The water removed in third effect is:	9120.34 kg/h
The area in first effect is:	320.73 m^3
The area in second effect is:	384.14 m^3
The area in third effect is:	469.42 m^3
The number of tubes in first effect is:	925
The number of tubes in second effect is:	1108
The number of tubes in third effect is:	1354
The volumetric flow rate of the pump in first effect is:	11880.05 m^3/s
The volumetric flow rate of the pump in second effect is:	17040.78 m^3/s
The volumetric flow rate of the pump in third effect is:	25442.96 m^3/s
The reduced concentration in first effect is:	0.07
The reduced concentration in second effect is:	0.14
The reduced concentration in third effect is:	0.81

REFERENCES

Bhargava, R., Khanam, S., Mohanty, B., Ray, A.K., 2008. Simulation of flat falling film evaporator system for concentration of black liquor. Comput. Chem. Eng. 32 (12), 3213 - 3223.

Bourouni, K., Martin, R., Tadrist, L., Tadrist, H., 1998. Modelling of heat and mass transfer in a horizontal-tube falling-film evaporator for water desalination. Desalination 116 (2), 165 - 183.

CBN (Central Bank of Nigeria). 1999. Annual report 1999. Central Bank of Nigeria, Lagos, Nigeria.

Medhat, B., Fateme, Fanaei, M.A., Zohreie, H., 2015. Mathematical modelling and dynamic simulation of multi-effect falling-film evaporator for milk powder production. Math. Comput. Model. Dyn. Syst. 21 (4), 336 - 358.

Mura, E., Gourdon, M., 2017. Pressure drop in dairy evaporators: experimental study and friction factor modelling. J. Food Eng. 195, 128 - 136.

Oloruntoba, M. M., Olunlade, B. A., Ibitoye, F. P., 2016. Effects of Input Variables on the Conversion of 5Ton/h Processed Tomato Juice in a Triple-Effect Evaporator. Biotechnology Journal International, 16(4): 1-8, Article no.BJI.29320.

Russell, N.T., Bakker, H.H.C., Chaplin, R.I., 2000. A comparison of dynamic models for an evaporation process. Chem. Eng. Res. Des. 78 (8), 1120 - 1128.

Silveira, A.C.P., Tanguy, G., Perrone, I.T., Jeantet, R., Ducept, F., de Carvalho, A.F., Schuck, P., 2015. Flow regime assessment in falling film evaporators using residence time distribution functions. J. Food Eng. 160, 65 - 76.

Winchester, J.A., Marsh, C., 1999. Dynamics and control of falling film evaporators with mechanical vapour recompression. Chem. Eng. Res. Des. 77 (5), 357 - 371.

Proceedings of the 49th NSChE Annual Conference
KADA 2019: pp 49-55

P1A-07: DELIGNIFICATION OF CORN COB FOR THE SYNTHESIS OF LACTIC ACID

H. A. Alhafiz[1*], M. T. Isa[1], B. Sallau[2], A. O. Ameh[1]
[1]Department of Chemical Engineering, Ahmadu Bello University, Zaria, Nigeria
[2]Department of Biochemistry, Ahmadu Bello University, Zaria, Nigeria
*Corresponding Author: sadiyalhafeez@gmail.com. +2348038103443

ABSTRACT
In view of the environmental and sustainability issues associated with petroleum-based polymers, corn cob was pretreated for the synthesis of lactic acid. Lactic acid is the base material for poly lactic acid synthesis production. The corn cob (Zea mays) which contains 79.73% holocellulose and 16.24% lignin was subjected to oxalic acid pretreatment in order to remove lignin. With the aid of Central Composite Design (CCD) on Design-Expert 6.0.6 Software, the pretreatment was optimized at a temperature range of 25-120 °C and a time range of 30-60 min. Optimization studies revealed that the optimum temperature and time for oxalic acid treatment was 25 °C/30 min, holocellulose content improved from 79.73% to 85.565% and expectedly lignin content reduced from 16.24% to 9.91%. Fermentation with Bacillus coagulans at a temperature of 50 °C, a pH of 6.0 and a time span of 48 hr produced lactic acid with a yield 82%. This implies that oxalic acid pretreatment of corn cob is effective for the synthesis of lactic acid.

1.0 Introduction
Biodegradable and renewable polymers have drawn much interest owing to the environmental and sustainability issues associated with petroleum based polymers (Ren, 2010). Poly lactic acid (PLA) is a biodegradable and renewable polymer used in plastics for packaging and in medicine for implants (Averous, 2008). PLA is derived from lactic acid, a naturally occurring acid that is produced by chemical synthesis or by biochemical process. The chemical synthesis of lactic acid has a major drawback because it leads to a racemic mixture (Rafael, 2010). On the other hand, the biochemical process involves the use of microorgansms such as *Rhizopus oryzae*, *Lactobacillus delbruki* and *Lactobacillus casei* to ferment monomeric sugars. Another microorganism that has been used for lactic acid fermentation is *Bacillus coagulans*, it is a microorganism with thermophilic growth characteristic, a strong ability for pentose and hexose homofermentation and a robust tolerance to inhibitors (Maas *et al*., 2008).

Monomeric sugars are found in carbohydrates such as cassava, rice, sweet potato, raw starch, sugar cane molasses as well as corn starch (Afolabi *et al.,* 2012; Lu *et al*., 2008; Panda and Ray 2008; Thongchul 2005). In addition to these carbohydrate sources, there exist lignocellulosic biomass also termed agro residue that can be employed in the production of lactic acid. These materials are abundant, cheap and do not compete as food source, thereby striking out the food versus raw material conflict that arise when carbohydrates are used (Hadar, 2014). Hence some agro residues have received attention in the production of lactic acid, these include: wheat straw, corn fiber, corn stover, cane molasses and corn cob (Maas *et al*., 2008; Bischoff *et al*., 2010; Zhao *et al*., 2013; Srivastava *et al*., 2014; Ali *et al*., 2006). Lignocellulosic materials are composed of cellulose and hemicellulose which are cemented together by lignin. This lignin component acts as a barrier that makes cellulose and hemicellulose inaccessible by microorganisms. In order to break this barrier, lignocellulosic materials have to undergo pretreatment prior to processing. This pretreatment which can be by physical, chemical, physicochemical or biological means decreases the crystallinity of cellulose as well as improves its porosity (Harmsen, 2010). Chemical pretreatment using oxalic acid is non-toxic and produces low amounts of inhibitory products when compared with sulphuric acid which is widely used (Lee and Jeffries 2011). The choice of pretreatment

method relies on the raw material to be used and the by-products generated (Kumar *et al.,* 2009).

In order to break down the lignin barrier on corn cob as a lignocellulosic biomass, this study focused on chemical pretreatment precisely oxalic acid pretreatment of corn cob for the synthesis of lactic acid. Optimization studies were carried out to determine the optimum time and temperature for the pretreatment.

2.0 Materials and Method

2.1 Materials

The corn cob that was used for this study was obtained from a farm land in Dan-Alhaji, Lere local government, Kaduna State, Nigeria. It was identified at the Herbarium of the Department of Botany, Ahmadu Bello University as *Zea mays* with a voucher number 01824 belonging to the family Poaceae. The corn was harvested, dried and separated from the corb. The corn cob was cleaned to remove foreign materials, grinded to a particle size of 0.5 mm and dried at 103 ^{o}C until a moisture content of less than 10 wt. % was achieved. The holocellulose composition of the untreated and treated corn cob was based on the Technical Association of Pulp and Paper Industry (TAPPI) Standard 211 –om 85. Oxalic acid by Fizmerk India with 99% purity and a melting point of 101^{o}C was purchased from Emaco Chemicals Kaduna State. Sodium Hydroxide with 99% purity produced by Merck India was purchased from Hadis Chemicals Zaria Kaduna state. Design Expert 6.0.6 was used to carry out the experimental design and optimization.

2.2 Experimental design

This was carried out on design-expert 6.0.6 software. The design was with Central Composite Design (CCD) and a study type Response Surface Methodology (RSM) was adopted. Two factors (variables) and a response were considered. The factors were A (Time) in minutes and B (Temperature) in ^{o}C. The response was the holocellulose composition of con corb in %. The lower and upper bounds for the time were 30 and 60 min respectively. While for the temperature, 25 and 120 ^{o}C were the lower and upper limits respectively. Eventually, 10 number of experimental runs were generated.

2.3 Pretreatment with Oxalic Acid

30 g of corn cob was immersed in 300 ml of oxalic acid solution with a concentration of 5 wt.%. Subsequently, the corn cob was washed with distilled water until a neutral pH was achieved and it was then dried at 103 ^{o}C for 10 hr.

2.4 Fermentation of Treated Corn cob

At the end of pretreatment with oxalic acid, the holcellulose content of the 10 experimental runs were fed back into design expert software in order to determine the optimum pretreatment condition. The determined optimum condition was used to pretreat corn cob that was subsequently used for the fermentation. The fermentation methodology by Hu *et al*. (2015) was modified and adopted. *Bacillus coagulans* inoculum (seed culture) was prepared in YEX medium containing 10 g/l xylose and 10 g/l yeast extract at a pH of 6.0, a temperature of 50 ^{o}C for a time span of 24 hr. Fermentation was carried out by introducing 10 % (w/w) oxalic acid treated corn cob, 10 g/l yeast extract and 10% (v/v) of the inoculum to 100 ml of the fermentation medium (50 g/l glucose and 10g/l yeast extract) in 150 ml Erlenmeyer flask. The fermentation was accomplished in an Incubator Shaker Water Bath at a temperature of 50 ^{o}C, pH of 6.0, agitated at 100 r.p.m for 48 hr. The fermentation process was maintained at a pH of 6.0 by charging 10 M NaOH solution. The concentration of lactic acid produced

from the start to the end of the experiment was determined and the yield calculated using Equation 1.

$$LA\ Yield = \frac{[LA]\times V - [LA_o]\times V_o}{f \times Wcc \times 1.111} \times 100\% \quad (1)$$

Where LA = Lactic acid, [LA] = Lactic acid concentration at the end of the fermentation (g/L), [LAo] = Lactic acid concentration at the start of the fermentation (g/L), V = Volume of fermentation broth at the end of the fermentation (L), V_o = Volume of fermentation broth at the end of the fermentation (L), f = Cellulose fraction of dried corn cob (g/g), Wcc = Weight of dried corn cob used in fermentation (g), 1.111 = Conversion factor for cellulose to equivalent glucose.

2.5 Characterization of Lactic Acid Produced

The lactic acid produced was characterised using FTIR. The analysis was carried out with SHIMADZU FTIR-8400S. The spectra were documented between a range of 4000 and 650 cm^{-1} at a resolution of 8 cm^{-1}. In addition, Kelling's test using Iron (III) chloride was used to confirm the presence of lactic acid. Furthermore, the boiling point and specific gravity were determined to further confirm that lactic acid was produced.

3.0 Results and Discussion

3.1 Composition of Untreated Corn Cob

Table 1 shows the composition of untreated corn cob. The corn cob used for this study had a holocellulose composition of 79.73% which is higher than that of Zhang (2016) and lower than that of Pointer et al. (2014) and Gusman (2010). The variation in holocellulose is due to the fact that the composition of a lignocellulosic biomass depends on the location of growth, condition of the soil and fertilizers applied as well as the analytical procedure utilized (Kumar *et al.*, 2009).

Table 1: Composition of untreated corn cob

	Location	Cellulose (%)	Hemicellulose (%)	Holocellulose (%)	Lignin (%)
This Study	Kaduna, Nigeria	70.00	9.725	79.73	16.24
Pointer *et al.* 2014	Austria	38.80	44.40	83.20	11.90
Gusman 2010	Ames, Iowa	32.30	41.30	85.40	13.90
Zhang 2016	Hubei, China	37.26	29.05	66.31	19.60

3.2 Composition of Corn Cob after Pretreatment

Table 2 shows the composition of corn cob in terms holocellulose and lignin after pretreating it with oxalic acid. There was a substantial increase in holocellulose and a corresponding decrease in lignin. A similar result was obtained in the work of Zhang *et al.* (2016) where the holocelluse content of corn cob increased after pretreatment. This increase in holocellulose implies the availability of more monomeric sugar for subsequent processing or for digestion

by microorganisms. The holocellulose composition which is the response for the pretreatment was run on design expert 6.0.6 software in order to arrive at the optimum pretreatment conditions (time and temperature). Table 3 shows the Analysis of Variance (ANOVA) for the pretreatment. The model was a quadratic model with a 'prob>f' value of 0.001 which is less than 0.05. This implies that the model is significant and adequately fits the response.

Table 2: Composition of Oxalic Acid Treated Corn Cob

Time	Temperature	Holocellulose	Lignin
30	25.0	85.78	10.40
60	25.0	85.19	11.08
30	120.0	85.18	11.08
60	120.0	85.20	11.08
24	72.5	85.60	10.56
66	72.5	85.59	10.62
45	5.3	86.32	9.91
45	139.0	85.33	11.00
45	72.5	86.38	9.88
45	72.5	85.37	10.85

Figure 1 shows the parity plots for the pretreatment. This compares the actual experimental values with the values predicted by Design expert software. The R^2 value from the parity curve describes how well the model describes the process. It ranges from 0 to 1. An R^2 value of 1 means the model perfectly describes the process. The R^2 value for oxalic acid treatment is 0.9848, this means the model perfectly describes the process.

Table 3: Summary of Analysis of Variance (ANOVA) for Oxalic Acid Treated Corn Cob

Parameter Model	Prob > F	
Model	0.0010	Significant
A	0.8955	
B	0.0014	
A^2	0.2411	
B^2	0.0057	
AB	0.0002	

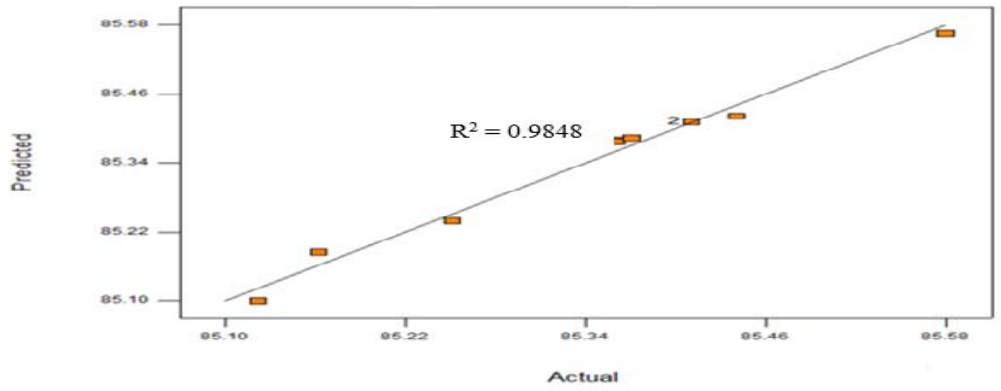

Figure 1: Predicted Versus Actual Holocellulose Values for Oxalic Acid Treated Corn Cob

The result of the optimization is shown in Table 4. The optimum time and temperature for oxalic acid synthesis is 30 min and 25 °C respectively.

Table 4: Optimization Result for Oxalic Acid Pretreatment of Corn Cob

Solution No.	Time (Minutes)	Temperature (^{0}C)	Holocellulose (%)	Desirability	
1	30.00	25.00	85.5646	0.967	Selected
2	30.79	25.00	85.5576	0.951	
3	60.00	106.65	85.4254	0.664	
4	60.00	107.02	85.4254	0.664	

3.3 Concentration and Yield of Lactic Acid after Fermentation

During the course of fermentation, the concentration of sugars (glucose and xylose) and lactic acid were determined. In addition, the concentration of acetic acid was determined. This is the most encountered inhibitor during pretreatment. Figure 2 shows the concentrations of glucose, xylose, lactic acid and acetic acid from the beginning to the end of fermentation. Also, the concentration of lactic acid during fermentation with oxalic acid treated corn cob increased from zero at the start of fermentation to 77.34 g/L at the end of the fermentation (48 hr). Glucose and xylose were utilized by *Bacillus coagulans* to produce lactic acid. Acetic acid was present in low amounts, the highest concentration throughout the 48 hours of fermentation was 0.015 g/L. The yield of lactic acid at the end of the fermentation was calculated as 82%.

3.4Characterization of Lactic Acid

Figure 3 shows the FTIR spectra of standard lactic acid and produced lactic acid. The spectra of the lactic acid produced was similar to the spectrum of standard lactic acid. From the spectra, the stretch between wavenumber 3000 and 3500 cm^{-1} indicates the presence of O-H bond. Furthermore, the stake-shaped bond located between wavenumber 1500 and 2000 cm^{-1} (1718.3 precisely) corresponds to C = O bond. The functional groups observed in the lactic acid produced matches those present in standard lactic acid spectrum as shown in Figure 3. Kelling's test with Iron (III) chloride gave a yellow colouration, indicating the formation of ferric lactate (Sood, 2006). The boiling point of the lactic acid produced was 125 °C. The specific gravity calculation revealed a value of 1.02. These values (boiling point and specific gravity) are close to literature values of 122 °C and 1.12 (Ren, 2010).

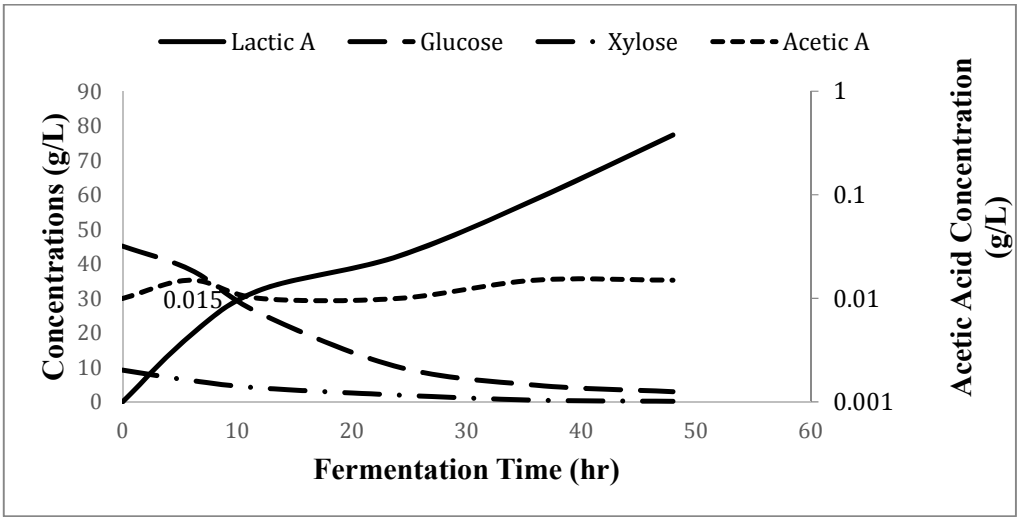

Figure 2: Concentrations of Sugars, Lactic Acid and Acetic Acid during Fermentation

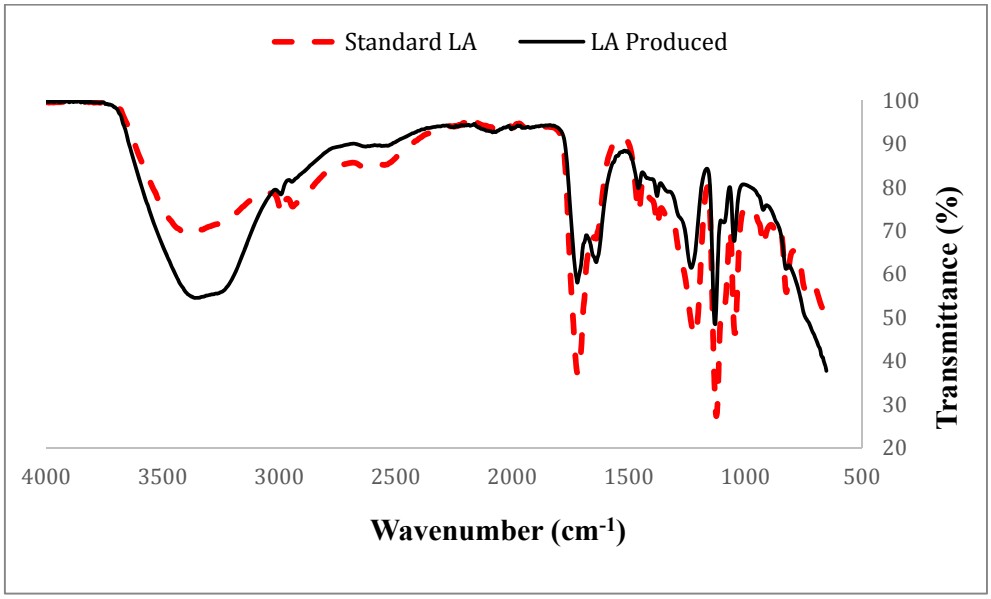

Figure 3: FTIR Spectra of Lactic Acid Produced

4.0 Conclusion

In this study, oxalic acid was used to treat corn cob which was subsequently used for the synthesis of lactic acid. The treatment was optimised leading to an optimum time and temperature of 30 min and 25 ^{0}C respectively. The treatment reduced lignin from 16.24% to 9.91% thereby making holocellulose increase from 79.73% to 85.565%. The fermentation with *Bacillus coagulans* produced lactic acid with a yield of 82%. The boiling point of lactic acid produced was 2.5% higher than that in literature. Also the specific gravity was 9.8% less than the literature value.

References

Afolabi, A. S., Sosu-mobee, O., and Abdulkareem, A. S. (2012). Production of Lactic Acid from Cassava Starch Hydrolysate using Immobilized Lactobacillus Casei in a Fibrous Bed Bioreactor, *III*, 4–7.

Ali, Z., Anjum, F. M., and Zahoor, T. (2009). Production of lactic acid from corn cobs hydrolysate through fermentation by Lactobaccillus delbrukii. *African Journal of Biotechnology*, *8*(17), 4175–4178. https://doi.org/http://dx.doi.org/10.5897/AJB2009.000-9403

Bischoff, K. M., Liu, S., Hughes, S. R., and Rich, J. O. (2010). Fermentation of corn fiber hydrolysate to lactic acid by the moderate thermophile Bacillus coagulans. *Biotechnology Letters*, *32*(6), 823–828. https://doi.org/10.1007/s10529-010-0222-z

Gusman, B., and Campo, D. (2010). Corncob dry matter loss in storage as affected by temperature and moisture content.

Hadar, Y. (n.d.). Sources for Lignocellulosic Raw Materials for the Production of Ethanol. https://doi.org/10.1007/978-3-642-37861-4_2

Harmsen, P. F. H., Huijgen, W., Bermudez, L., and Bakker, R. (2010). Literature review of physical and chemical pretreatment processes for lignocellulosic biomass. *Energy Research Centre of the Netherlands*, (September), 10–13. Retrieved from https://www.researchgate.net/profile/Wouter_Huijgen/publication/254853217_Literature_review_of_physical_and_chemical_pretreatment_processes_for_lignocellulosic_biomass/links/02e7e5252cf3686b63000000.pdf%0Ahttps://www.ecn.nl/docs/library/report/2010/e10013.p

Hu, J., Zhenting, Z., Yanxu, L., Shumiao, Z., Yuxia, M., Yunxiang, L. N. P. (2015). High-titer lactic acid production from NaOH-pretreated corn stover by Bacillus coagulans LA204 using fed-batch simultaneous saccharification and fermentation under non-sterile condition, 182, 251-257.

Kumar, P., Barrett, D. M., Delwiche, M. J., and Stroeve, P. (2009a). Methods for pretreatment of lignocellulosic biomass for efficient hydrolysis and biofuel production. *Industrial and Engineering Chemistry Research*, *48*(8), 3713–3729. https://doi.org/10.1021/ie801542g

Kumar, P., Barrett, D. M., Delwiche, M. J., and Stroeve, P. (2009b). Methods for pretreatment of lignocellulosic biomass for eficient hydrolysis and biofuel production. *Industrial and Engineering Chemistry*, *48*(8), 3713–3729. https://doi.org/10.1021/ie801542g

Lu, Z. H., Peng, H. H., Cao, W., Tatsumi, E., and Li, L. T. (2008). Isolation, characterization and identification of lactic acid bacteria and yeasts from sour Mifen, a traditional fermented rice noodle from China. *Journal of Applied Microbiology*, *105*(3), 893–903. https://doi.org/10.1111/j.1365-2672.2008.03814.x

Maas, R. H. W., Bakker, R. R., Jansen, M. L. A., Visser, D., and Jong, E. De. (2008). Lactic acid production from lime-treated wheat straw by Bacillus coagulans: neutralization of acid by fed-batch addition of alkaline substrate, 751–758. https://doi.org/10.1007/s00253-008-1361-1

Minmunin, J., Limpitipanich, P., and Promwungkwa, A. (2015). *Delignification of Elephant Grass for Production of Cellulosic Intermediate*. *Energy Procedia* (Vol. 79). Elsevier B.V. https://doi.org/10.1016/j.egypro.2015.11.468

Panda, S. H., and Ray, R. C. (2008). Direct conversion of raw starch to lactic acid by Lactobacillus plantarum MTCC 1407 in semi- solid fermentation using sweet potato (Ipomoea batatas L .) flour. *Industrial Research*, *67*(July), 531–537. Retrieved from http://www.scopus.com/inward/record.url?eid=2-s2.0-55349138790andpartnerID=40

Pointner, M., Kuttner, P., Obrlik, T., Jäger, A., and Kahr, H. (2014). Composition of corncobs as a substrate for fermentation of biofuels, *12*(2), 391–396.

Rafael A. Auras, Loong-Tak Lim, Susan E. M. Selke, H. T. (2011). *Poly(lactic acid): Synthesis, Structures, Properties, Processing, and Applications*. *Bio-Based Plastics: Materials and Applications*. https://doi.org/10.1002/9780470649848

Ren, J. (2010). *Biodegradable Poly(Lactic Acid): Synthesis, Modification, Processing and Applications*. https://doi.org/10.1007/978-3-642-17596-1

Sanjay, A., Sinha, K., and Dhanraj, R. R. (2017). Response Surface Optimization of Rice Straw Treatment with Oxalic Acid For Production Of Xylose, Cellulose And Lignin, *9*(2), 163–174.

Sood (2006). Textbook of Medical Laboratory Technology. JaypeeBrothers Publishers. P.444. ISBN 978-81-8061-591-7.

Srivastava, A. K., and Tripathi, A. D. (2014). Production, optimization and characterization of lactic acid by Lactobacillus delbrueckii NCIM 2025 from utilizing agro-industrial byproduct (cane molasses). https://doi.org/10.1007/s13197-014-1423-6

Thongchul, N. (2005). Lactic acid production by immobilized Rhizopus oryzae in a rotating fibrus bed bioreactor, 265.

Wyman, C. E., Dale, B. E., Elander, R. T., Holtzapple, M., Ladisch, M. R., and Lee, Y. Y. (2005). Comparative sugar recovery data from laboratory scale application of leading pretreatment technologies to corn stover. *Bioresource Technology*, *96*(18 SPEC. ISS.), 2026–2032. https://doi.org/10.1016/j.biortech.2005.01.018

Zhang, Z., Xie, Y., He, X., Li, X., Hu, J., and Ruan, Z. (2016). Comparison of high-titer lactic acid fermentation from NaOH- and NH 3 -H 2 O 2 -pretreated corncob by Bacillus coagulans using simultaneous saccharification and fermentation. *Nature Publishing Group*, (April), 1–10. https://doi.org/10.1038/srep37245

Zhao, K., Qiao, Q., Chu, D., Gu, H., Dao, T. H., Zhang, J., and Bao, J. (2013). Bioresource Technology Simultaneous saccharification and high titer lactic acid fermentation of corn stover using a newly isolated lactic acid bacterium Pediococcus acidilactici DQ2. *Bioresource Technology*, *135*, 481–489. https://doi.org/10.1016/j.biortech.2012.

Proceedings of the 49th NSChE Annual Conference
KADA 2019: pp 56-72

P1A-058: THE EFFECT OF SYNTHESIZED NPK LOADED SURFACTANT MODIFIED ZEOLITE A BASED FERTILIZER IN TOMATO *(LYCOPERSYCUM ESCULENTUM)* CULTIVATION

[1]Salako. O., *[1]A.S. Kovo,[1] A.S. Abdulkareem, [2]Yusuf S.T, [1]Afolabi, E.A. and [1]Manase Auta

[1]Department of Chemical Engineering, Federal University of Technology, Minna
[2]Department of Crop Production, Federal University of Technology, Minna
*Corresponding author: Kovo@futminna.edu.ng, 08094059107

ABSTRACT

The surface of an optimized zeolite A synthesised from Ahoko kaolin was modified by quaternary ammonium compound, HDTMA and was used as fertilizer carrier. Characterization techniques such as SEM, FTIR and BET were used to characterise the zeolite loaded samples and the subsequent adsorption process. The maximum adsorption capacity of 7.55mg/g was obtained at initial concentration of 162.6 mmol/L, contact time 16 h, and temperature 25 ^{o}C. The initial HDTMA concentration is the most significant term that influences the adsorption capacity of zeolite A. The interactive effect that contributes significantly to the maximum adsorption capacity (6.27 mg/g) of the zeolite occurs between initial HDTMA concentration (243.80 mmol/l) and adsorption temperature 25.21^{o}C as predicted by the Design Expert software applied for this work. The surfactant modification of the surface of zeolite A reverses the negative charges on the framework to positive and allows the adsorption of oxyanions such as nitrates and phosphates. The results indicated a reduction in the BET surface area of HDTMA modified Zeolite A with 65 m^2/g to 46.72 m^2/g and 62.27 m^2/g for Phosphate zeolite A and Nitrate loaded zeolite A based fertilizers respectively. Conventional NPK 15:15:15 and the NPK loaded zeolite A based fertilizer was applied on tomato crop. The result of a higher leaf count (growth parameter) of zeolite A based fertilizer with mean (54.2) compared with NPK 15:15:15 with mean (25.7) at 11 WAT indicated the slow release property and nutrient retention of Zeolite A based fertilizer. The zeolite A based fertilizer had a higher fruit yield with mean (84.69) compared with NPK 15:15:15 fertilizer with mean (69.34).

Keywords: Zeolite A, Surfactant Modified Zeolite A, Optimization, Zeolite A based slow release fertilizer, Plant growth, fruit yield.

Introduction

The application of excessive high soluble inorganic fertilizers has resulted to agronomic and pollution problems. Zeolite based slow release fertilizers signify an endeavour to answer the drawback of low nutrient retention capacity and nutrient leaching which causes low crop yields and contamination. Zeolites are hydrated crystalline aluminosilicates of alkali and alkaline earth cations with 3 – dimensional framework channelled by pores and channels (Notario del pino *et al*., 1995). The negative charge framework of zeolites creates the prospect for the surface modification of zeolites by functional groups such as cationic surfactants. This surface functionalization of zeolites improves its activity in the sorption of anionic species (Thirunavukkarasu and Subramanion, 2014).

Baniswal *et al*. (2006) reported the use of modified synthetic zeolite on environmental applications especially for the adsorption of anionic nutrients such as phosphate, nitrate and nitrite. Surfactant modified zeolite (SMZ) have been known for its high sorption capacity for phosphates, nitrates, sulphates, and chromates (Li *et al*., 1988). Studies on zeolites are increasing because of their high cation exchange capacity which subsequently increases the fertility of the soil. They are also used as inexpensive carriers of plant nutrients because of their slow release property (Ramesh *et al*., 2015).

Baniswal *et al.*, 2006 observed that the phosphorous released from fertilizer loaded SMZ was available even after 1080 h of continuous percolation whereas phosphorous release from KH_2PO_4 was exhausted in 264 h. The result suggests that SMZ could be used as carriers for slow release fertilizers (SRF) to control phosphate release.

Jakkula *et al.*, 2011 reported that synthetic phillipsite had a high affinity towards ammonium ion when it was used as a soil amendment in comparison to natural phillipsite. Synthetic phillipsite could be suggested to be a potential slow release fertilizer based upon its high selectivity and high affinity towards ammonium ion.

Li (2003) also reported using surfactant-modified zeolite (SMZ) as fertilizer carrier to control nitrate release. Results indicated that the adsorption of nitrate to SMZ increased as the HDTMA loading on SMZ increased. The result further showed that 30 – 40 % of adsorbed nitrate still remained on SMZ after 100 pore volumes of distilled water was used to desorb the nitrate from SMZ. The result indicate that slow release of nitrate is achievable.

Li and Zhang (2010) reported the practicality of using SMZ as fertilizer additives to control sulphate release in batch and column leaching experiments. Batch results indicated an almost instantaneous and partially reversible sulphate release while 70 % and 85 % of the loaded sulphate was still remaining on SMZ modified to 150 % and 200 % External cation exchange capacity (ECEC) respectively. The initial sulphate concentration of leachate was reduced by a factor of three.

Tomato is grown in low fertile soils in Nigeria because of continuous cropping with no added inputs to enhance soil fertility (Mofuka *et al.*, 2007). FAO (2012) reported that the yield level of tomato in Nigeria is low in comparison to producing countries like Ethiopia and Niger with a mean yield of 7.11 t ha^{-1}. Past researches on the effect of NPK zeolite based SRF on plant growth, fruit yield and soil nutrient efficiency on tomato crops focused only the natural forms of zeolite, natural zeolite use as a soil amendment and the use of one variable at a time (OVAT) experimental design in the synthesis of zeolite from kaolin. However, this paper reports the optimized surfactant modified zeolite synthesised from kaolin and the effects of NPK loaded zeolite A based SRF on tomato growth and fruit yield.

Materials and Methods

Preparation of Hexa-decytrimethyl ammonium bromide (HDTMA) modified zeolite

Zeolite A has been produced from Ahoko Kaolin through a process of metakaolization, gel formation and zeolitization by hydrothermal method as reported by (Salako *et al.*, 2017). The surfactant modified zeolite A sample was prepared according to a procedure described by Schick *et al.* (2010) by treating 5g of raw zeolite A by 25ml of 25 - 299mmol/l surfactant (HDTMA) solution at temperature between 60 °C to 120 °C for a period of 8 to 24 hours using a central composite design. The mixture was continuously stirred at 150 rpm to achieve equilibrium. After filtration, the sample was washed with 50ml distilled water to remove the excess of HDTMA and dried at 80 °C overnight.

PHOSPHATE AND NITRATE LOADING ON SURFACTANT MODIFIED ZEOLITE A

KH_2PO_4 was used as the reagent to carry out ion exchange for phosphate on surfactant modified Zeolite A. 25 ml of KH_2PO_4 solution was added to 5 g of surfactant modified zeolite A and stirred continuously at 150 rpm in a conical flask for 16 hours at room temperature as also reported by Vijay *et al.* (2011). 1 mole of ammonium nitrate solution was added to 5 g for of HDTMA modified zeolite A in a 250ml conical stoppered flask. The mixture was placed

in a mechanical shaker and agitated at 150 rpm for 16 h. Each of the solutions was filtered and washed with 50 ml of distilled water to wash off the excess soluble nutrients loaded on the extra lattice framework and dried at temperature of 40 °C for 24 h (Zhaohu *et al*., 2013). The phosphate and nitrate loaded phillipsites were blended to give the NPK loaded zeolite A based slow release fertilizer.

EVALUATION OF THE EFFECTS OF ZEOLITE A BASED SLOW RELEASE FERTILIZER APPLICATION ON GROWTH, FRUIT YIELD OF TOMATO (*LYCOPERSYCUM ESCULENTUM*) IN POT EXPERIMENT

A pot experiment was conducted in the teaching and research farm of the Federal University of Technology, Minna in 2018 to evaluate the efficacy of the synthesized zeolite A based fertilizer on the growth, fruit yield of two cultivars of tomato (Roma VF and UC82B). Treatment consists of four levels each of the synthesized zeolite A based fertilizer, and NPK 15:15:15 fertilizer laid out in completely randomized design (CRD) with three replications. Soil samples were initially collected from a depth of 20 cm, processed and subjected to physico-chemical analysis. The tomato seeds were initially sown in germination trays and later transplanted into pots 3 week after sowing the seeds. Application of the synthesized zeolite A based fertilizers and NPK 15:15:15 at four levels of treatment (Soil alone 0 % as control, 0.66 g, 1.33 g, 2.66 g which is equivalent to 0, 150, 300 and 600 kg/ha) took place 5 weeks after transplanting. At 6 weeks after transplanting (6WAT), data on growth parameters viz; number of leaves, plant height, plant girth, number of flowers, number of fruits and fruit yield on a weekly basis. At crop maturity and following the ripening of the tomato fruit, harvesting were carried out and fruit yields on treatment basis were determined accordingly.

All data generated through the experiment were subjected to statistical analysis engaging Statistical Analysis Software (SAS). The Means were separated by Duncan's Multiple Range Test (DMRT) at 5 % level of probability.

RESULTS AND DISCUSSION

Analysis Of Zeolite A and HDTMA Modified Zeolite A.

The Fourier transform infra-red spectroscopy (FTIR) was mainly employed to understand the interaction between the zeolite and the cationic surfactant. The spectrum of the synthesized zeolites in Figure 1 and 2 showed vibrational bands with different types of functional groups present. The overall spectrum of FTIR is divided into two general regions: 4000 –1300 cm^{-1} (the functional group region) and 1300 – 400 cm^{-1} (the fingerprint region). The frequency assignment approach was used for the interpretation of the spectrum. The FTIR spectrum demonstrated that HDTMA had completely adsorbed on zeolite A surface as observed from HDTMA-Modified Zeolite A in Figure 2. The absorption bands near 3488 cm^{-1} represent OH groups for the surfaces of zeolite A and HDTMA-modified Zeolite A. This showed that zeolites are hydrated materials. The OH in Figure 2 also suggests that HDTMA only adsorbs on partial surface of the zeolites. The weak absorbance of signal near 1000 cm^{-1} for the zeolite A and HDTMA modified zeolite A in Figure 3 and 4 represents the presence of asymmetric stretching vibration modes of internal T-O bonds in TO_4 tetrahedral (T = Si and Al) on the surface. The strong absorbance signal near 1000 cm^{-1} for the HDTMA modified zeolite A is considered as the CN group on the surface. The absorbance of the HDTMA modified zeolite located in the region below 1000 cm^{-1} might have resulted from the alkyl groups of HDTMA on the zeolite surface. It is important to note that HDTMA molecules adsorb on the external surface of the zeolite and do not react completely with all the surface hydroxyl groups and HDTMA molecules are too big to enter the internal pores of zeolite A. The net effect leads to HDTMA modified

zeolite A having the positive charge on the external surface and also the negative charge on the internal pore surface.

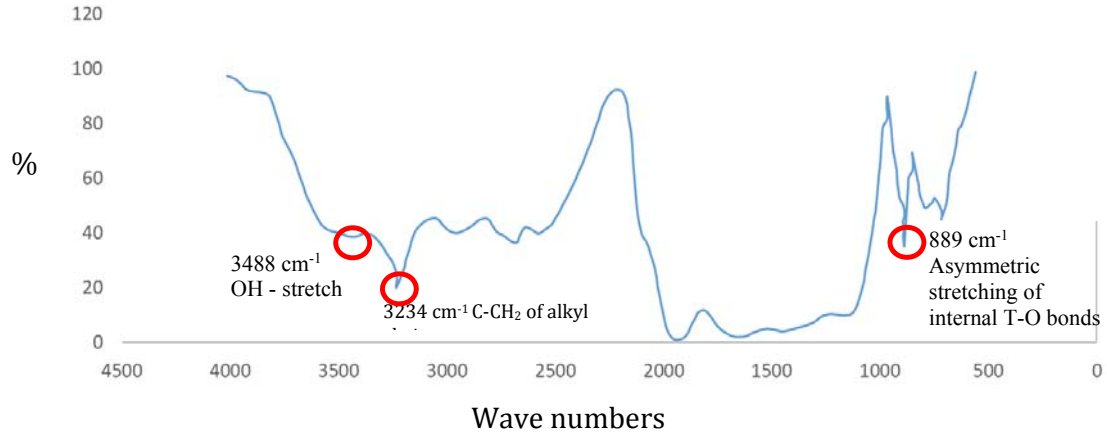

Figure 1: FTIR spectrum of the synthesized zeolite A

The bands observed at 3488 cm^{-1} and 2978 cm^{-1} in Figure 2 were attributed to symmetrical stretching vibration of $C\text{-}CH_2$ of alkyl chain while the band around 1404 cm^{-1} was assigned to the trimethylammonium quaternary group vibration $C\text{-}N(CH_3)_3$ (Aroke and El-Nafaty, 2014; Maina, 2016). These spectra bands could be correlated with antisymmetric and symmetric C-H stretching of the methylene group. The extra peaks suggest that the HDTMA surfactant successfully modified the zeolite surface. There was no change in band positions after modification in Zeolite A and this showed that the basic zeolite structure was kept unchanged (Aseidu, 2016).

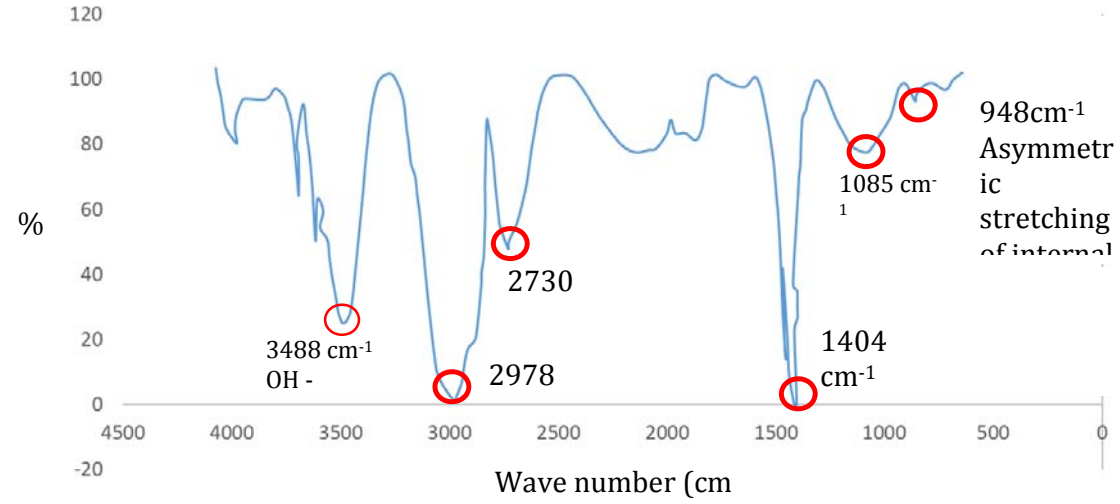

Figure 2: FTIR spectra of the HDTMA modified Zeolite A

TEXTURAL ANALYSIS BY NITROGEN ADSORPTION

Surface areas and porosity are important characteristics responsible for the description of the adsorption process in zeolites. The BET surface area analysis was performed on the synthesized zeolite A and its modification as shown in Table 2. The samples were degassed under vacuum at 250 ^{o}C for 3 h to remove any residual moisture. It was observed that the specific surface areas of Zeolite A reduced with HDTMA modification. Subsequent loading of Phosphate ions (KH_2PO_4) and Nitrate ions (NH_4NO_3) loading on the HDTMA-zeolite A modification reduced the surface areas further. This result is similar to the trend observed by Fungaro and Magdalena (2014) that the modified zeolites show lower total BET surface area than the unmodified zeolite. The authors further reported that the addition of the external surface area and micropore surface area gave the total BET surface area. The internal area of the zeolites was blocked and the micropore surface area decreased when the bulky molecules of the HDTMA are adhered on the external surface and pore openings of the zeolites. Similar trend was observed in reduction in the cation exchange capacity of the zeolites when surface modification took place as shown in Table 1.

Table 1: BET results of Specific surface area, Pore volume and Pore size

	Specific Surface Area (m^2/g)	**Pore Volume (cm^3/g)**	**Pore Size (nm)**
Zeolite A	296.178	0.137	0.4523
Modified Zeolite A	65.257	0.017	0.3488
Phosphate loaded Zeolite A	46.724	0.014	0.3469
Nitrate loaded Zeolite A	62.272	0.018	0.3423

ADSORPTION OPTIMIZATION USING RANDOM SURFACE METHODOLOGY (RSM)

The porous nature of zeolite confers on it high adsorptive and cation exchange and carrier property. The negatively charged porous surface of zeolite A makes it to easily attract and carry alkaline metals in its pores by ion exchange mechanism. The process of carrying oxyanions (phosphates and nitrates) requires reverting the negative surface charge of the zeolite A to positive in order to cause an intense attraction between the surfactant (HDTMA) and the zeolite A adsorbent. It is this adsorptive process that requires optimization in the development of a zeolite based slow release fertilizer. The adsorption process is further enhanced by the statistical design of experiment using Random surface methodology to provide the optimum conditions for the efficient utilization of the adsorbent. The desired product with its optimum conditions is obtained with fewer experimental runs using central composite design, a tool used to optimize any process especially multiple variables with their interactive effects on the response indicators. Table 2 shows the experimental design matrix for the adsorption of HDTMA on to zeolite A.

Table 2: Experimental design matrix of the adsorption of HDTMA on Zeolite A

Std	HDTMA conc mmol/ kg	Temp °C	Contact time hours	Adsorption Capacity (q) mg /kg
1	81.3	25	8	3.75
2	243.9	25	8	5.95
3	81.3	70	8	0.5
4	243.9	70	8	2
5	81.3	25	24	0.5
6	243.9	25	24	5.25
7	81.3	70	24	0.35
8	243.9	70	24	2
9	25.87	47.5	16	1.95
10	299.33	47.5	16	5.85
11	162.6	25	16	7.55
12	162.6	85.34	16	1.3
13	162.6	47.5	2.55	0
14	162.6	47.5	29.45	0.6
15	162.6	47.5	16	1.1
16	162.6	47.5	16	0.7
17	162.6	47.5	16	1.35
18	162.6	47.5	16	0.6
19	162.6	47.5	16	1
20	162.6	47.5	16	1.25

The central composite design with four independent variables are concentration of HDTMA, adsorption temperature and contact time gave a total of 20 experimental runs in a standard order as shown in Table 2 of the test results. The analysis of variance (ANOVA) results is presented in Table 3.

Table 3: Analysis of variance of the response surface model for HDTMA adsorption on Zeolite A

Source	**Sum of Squares**	**df**	**Mean Value**	**F Prob > F**	**P- value**	
Model	89.97	9	10.00	22.85	<0.0001	significant
A	20.32	1	20.32	46.46	< 0.0001	
B	32.63	1	32.63	74.61	< 0.0001	
C	0.70	1	0.70	1.60	0.2347	
AB	1.80	1	1.80	4.13	0.0696	
AC	0.91	1	0.91	2.08	0.1795	
BC	1.80	1	1.80	4.13	0.0696	
A2	12.47	1	12.47	28.50	0.0003	
B2	17.94	1	17.94	41.01	< 0.0001	
C2	1.69	1	1.69	3.87	0.0775	
Residual	4.37	10	0.44			
Lack of Fit	3.93	5	0.798.83	0.0160		

The Model F-value of 22.85 implies the model is significant. There is only a 0.01 % chance that a "Model F-Value" this large could occur due to noise. The values of "Prob > F" less than 0.0500 indicate that the model term significantly influence the adsorption capacity response. Table 2 shows A, B, A^2, B^2 as significant model terms. The values greater than 0.1000 indicate the model terms do not significantly influence the adsorption capacity**.** The "Lack of Fit, F-value" of 8.83 implies the Lack of Fit is significant which indicates that the model does not fit all the experimental data. There is only a 1.60 % chance that a "Lack of Fit F-value" this large could occur due to noise. The guiding rule is that significant lack of fit should be low for a model to fit. The coefficients of the response surface as given by Equation 1 were evaluated and the p-values showed that linear coefficients A and B were more significant than their quadratic terms and interractive terms. The final regression model based on coded factor values representing the adsorption process of HDTMA on Zeolite A was found to fit into the second order polynomial equation as shown in Equation 1.

$$q = +1.01 +1.22\ A -1.55B -0.23C -0.48AB +0.34AC + 0.48BC + 0.93\ A^2+1.12B^2- 0.34C^2 \quad (1)$$

where q is the Adsorption capacity.

Given that A = HDTMA concentration, B = Adsorption temperature and C = Contact time. Equation 1 is valid within the range of HDTMA concentration of 25.87 to 299.33mmol/kg, Adsorption temperature of 25 – 60 ° C and contact time of 2.55 to 29.45h

The Adequate Precision measures the signal to noise ratio. Patil and Deng (2009a and b) reported a statistical analysis that showed a ratio greater than 4 was desirable. The ratio of 15.194 obtained with the model indicated an adequate signal. The model can therefore be used to navigate the design space. The coefficient of determination (R^2) with value 0.9536 obtained for the model indicated that only 95.36% of the experimental data are well represented within the range of the study. The optimized conditions obtained from the design expert software were suitable for the various types of adsorption process carried out. The value of coefficient of variation (CV) of 30.37 indicated a better precision and reliability of the experimental runs (Karmakar and Ray, 2011)

Std. Dev.	0.66	R-Squared	0.9536
Mean	2.18	Adj R-Squared	0.9119
C.V. %	30.37	Pred R-Squared	0.6652
PRESS	31.59	Adeq Precision	5.194

The "Predicted R-Squared of 0.6652 is not as close to the Adjusted R-Squared of 0.9119 as one might normally expect. This may indicate a large block effect with the model.

THE MAIN EFFECTS OF HDTMA CONCENTRATION, TEMPERATURE AND CONTACT TIME ON ADSORPTION CAPACITY OF ZEOLITE A

The observation shown in Figure 3a revealed that as the concentrations of HDTMA increased from 81.3- 243.90 mmol/kg, the adsorption capacity of zeolite A also increased from 0.72 – 3.16mg/g indicating a positive main effect on adsorption capacity. This trend is similar to Demircvi and Saygili (2014) who reported that HDTMA sorption percentages on vermiculite, perlite, and zeolite clays increased with increasing the initial concentration of HDTMA. It was also observed in Figure 3b that as temperature increased from 25° C to 60 ° C, the adsorption capacity of the Zeolite A decreased from 3.68 to 0.58 This increase in temperature had a main negative effect on adsorption capacity on Zeolite A. This trend is similar to Jin *et al*. (2008) who reported that though the optimum temperature was found to be 25 ° C, there was

variation of adsorbed Methylene Blue with increasing temperature for SDS – modified zeolite. Figure 3c showed the plot of adsorption capacity and contact time. It was observed that there was a slight increase in adsorption from 8 h to 13.78 h and thereafter a noticeable decrease in adsorption capacity as contact time increased from 16h to 24 h. The reduced adsorption capacity at higher HDTMA concentration may have been as a result of excess, loosely bound HDTMA from ad micelles on the organo-zeolite into the aqueous solution (Haggerty and Bowman, 1994).

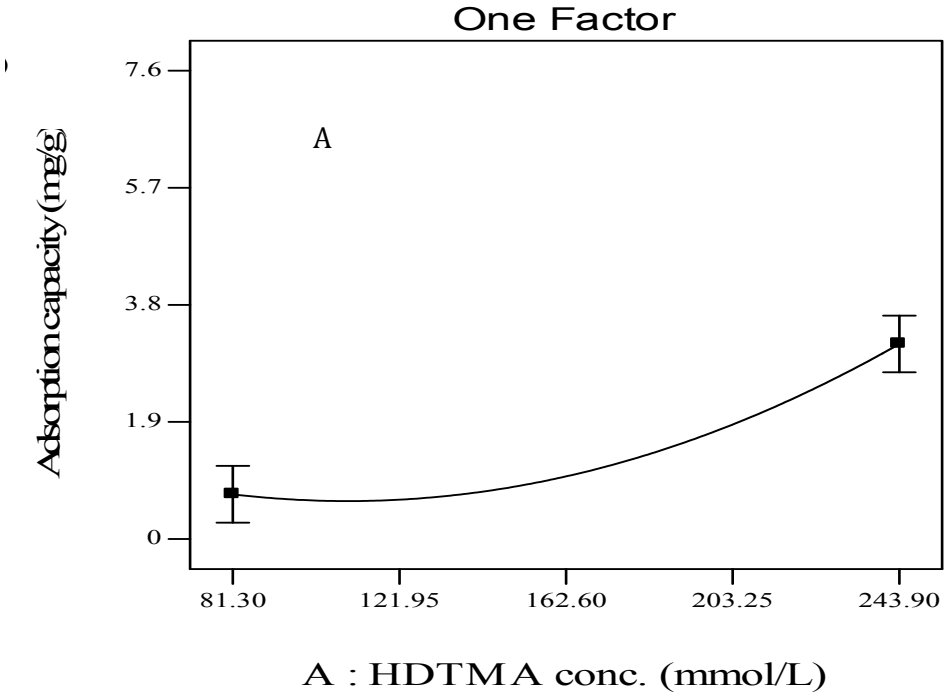

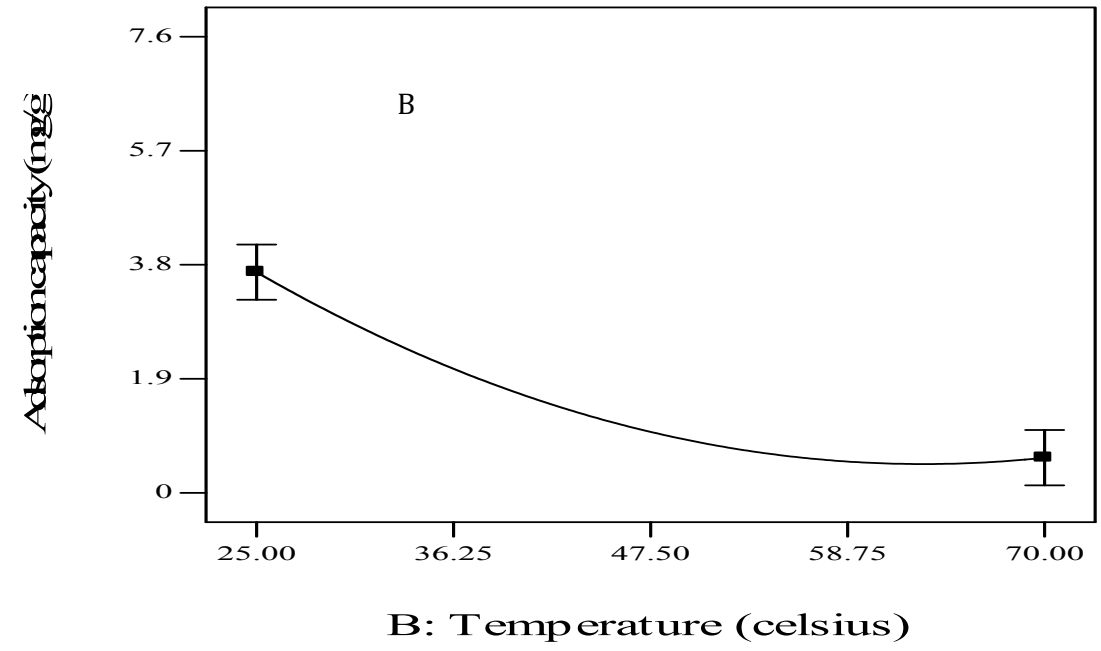

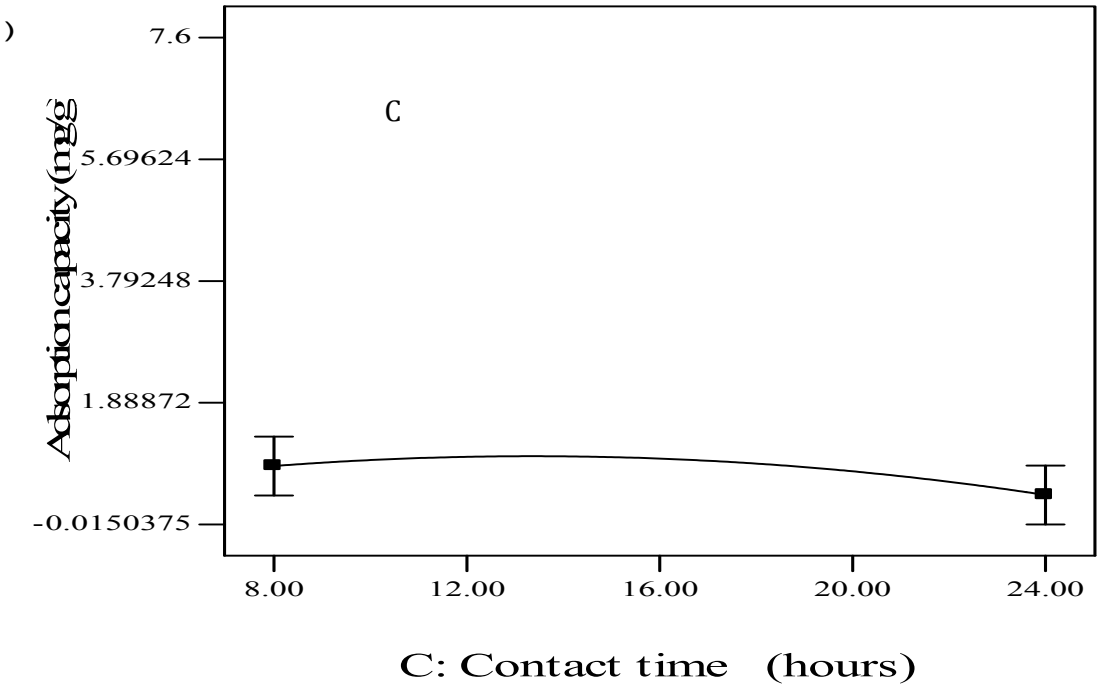

Figure 3(a, b and c) Main effects of variables of HDTMA concentration, Temperature and contact time on Adsorption capacity of Zeolite A

THE EFFECT OF INTERACTIVE VARIABLES ON ADSORPTION CAPACITY OF ZEOLITE A

Random Surface Methodology is a statistical approach used to maximize the adsorption process by optimization of operational variables. The interactive effects among the adsorption process were also determined by this statistical technique in contrast to conventional methods which could not determine interactive effects among adsorption process variables.

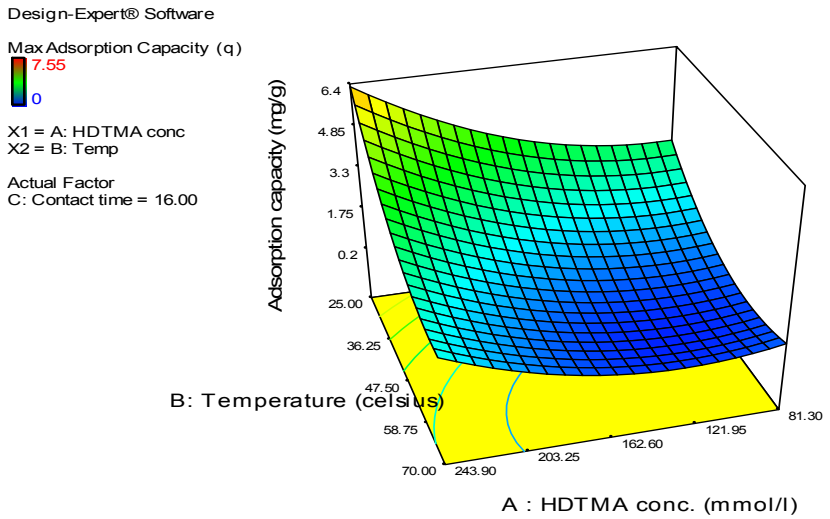

Figure 4a: 3D response surface plot showing the interactive effect of temperature and HDTMA concentration on the adsorption capacity of Zeolite A

The Figure 4a showed the relationship between adsorption capacity, temperature and concentration of HDTMA on zeolite A. The 3D plot showed that as temperature increased from 25 °C to 70 °C and concentration of HDTMA increased from 81.30 to 243.90 mmol/L, there

was generally an increase in the adsorption capacity of zeolite A. The maximum adsorption capacity for the interactive effect was 6.27 mg/g when the HDTMA concentration was 243.80 mmol/L and temperature was 25.21 ° C.

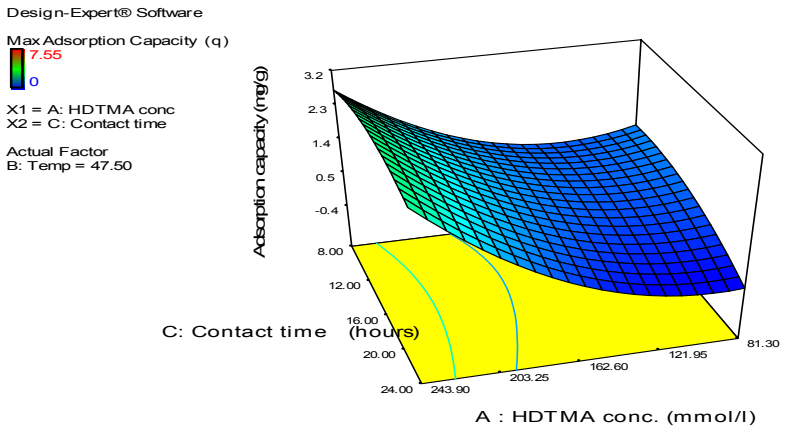

Figure 4b A 3D response surface plot of contact time and concentration of HDTMA on the adsorption capacity of zeolite A

Figure 4b showed the interactive effects of contact time and HDTMA concentration on adsorption capacity of Zeolite A. The response surface showed that as contact time increased from 8 to 24 h, the adsorption capacity of zeolite A decreased simultaneously as the HDTMA concentration increased from 81.30 – 243.90 mmol/l. The maximum effect of these two variables interaction resulted to an adsorption capacity of 3.72 mg/g when HDTMA concentration was 243.75mmol/l and contact time was 8.15 h.

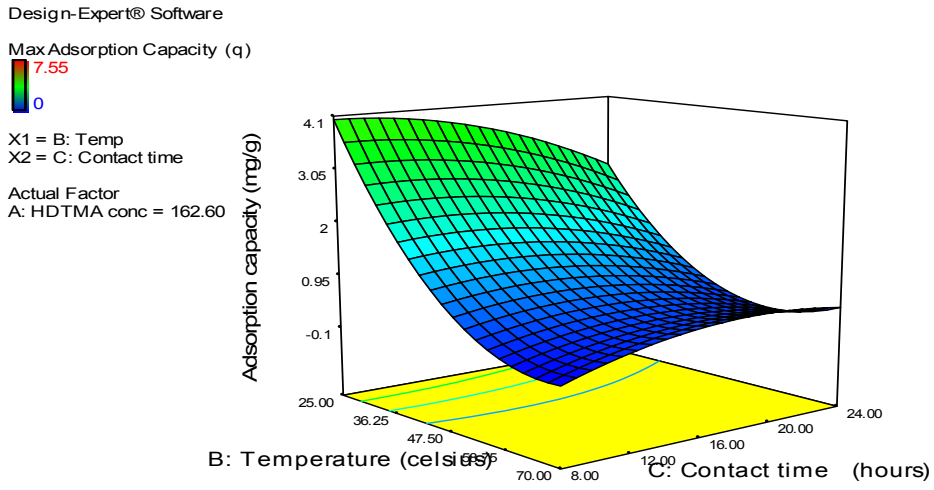

Figure 4c A 3D response surface plot of the interactive effect of contact time and temperature on the adsorption capacity of zeolite A

Figure 4c showed the interactive effects of constant time and temperature on the adsorption capacity of zeolite A. It was observed that as temperature increased from 25 ° C to 70°C, the adsorption capacity reduced as contact time increased from 8 to 24 h. However, it was observed that the maximum interactive effect of the two variables gave an absorption capacity of 4.02 mg/g when contact time was 8.05 h and temperature was 25.09 ° C.

Analysis of Result of Evaluation of the effects of zeolite A based slow release fertilizer application on growth, fruit yield of tomato.

The evaluation of the synthesized NPK loaded surfactant modified Zeolite A based fertilizer was done when it was applied to two varieties of tomato crop in a completely randomized design to determine their effects on the growth parameters such as the leaf count, plant height, stem girth, branch count, fruit count and fruit yield as presented in Tables 4 to 8.

EFFECT OF VARIETIES, FERTILIZER SOURCES AND RATES OF APPLICATION ON THE LEAF COUNT OF TOMATOES FOR 5 -11 WEEKS AFTER TRANSPLANTING (WAT) 1.0

In Table 4, it was generally observed that the mean of UC82b variety were higher than the Roma VF variety in the leaf counts from 5 to 10 weeks after transplanting. However, there was no significant difference between the leaf counts of the two varieties. There was generally an increase in the number of leaves from week 5 to 9 with respect to the two fertilizer sources; however, there was generally a drop in the leaf counts from 10 and 11 WAT. This trend might be traceable to the fact that the plant diverts nutrients to the development of the fruits. Interestingly, at the 11 WAT, the zeolite A based fertilizer treatment plants were observed to have greener leaves than the conventional NPK fertilizer treated plants. The means of zeolite A based fertilizer was found to be significantly different from the mean of the conventional NPK fertilizer. It was observed that the leaves of the conventional NPK fertilizer were wilting and dying. The greener leaves on the plants with zeolite based fertilizer application indicated the presence of more nutrients retained in the soil by the zeolite A carrier in the fertilizer. The zeolite A based fertilizer releases their nutrients slowly for a longer period of time than the conventional fertilizers. In the conventional NPK fertilizer, nutrient carriers or fillers have no adherence to the plant nutrients and therefore nutrients leach easily beyond the root zone with percolated water. The consequence is the cutting off of the supply of nutrients to the leaves. The rates of application were not significantly different at 150, 300 and 600 kg/ha at 11 WAT. Statistical significance was only observed for interaction between fertilizer and rate of application.

Table 4: Effect of varieties, fertilizer sources and rates of application on the leaf count of tomatoes for 5 -11 Weeks after transplanting (WAT)

	Weeks After Transplanting (WAT)						
Treatment	**5**	**6**	**7**	**8**	**9**	**10**	**11**
Variety(V)							
UC82b	98.70a	124.92a	131.85a	137.56a	124.54a	80.35a	41.6a
Roma Vf	96.12a	120.94a	128.39a	133.54a	123.16a	79.19a	32.2a
SE±	5.53	5.74	5.55	5.53	5.00	1.84	5.65
Fertilizer Source							
Zeolite A based fertilizer	78.33b	99.56b	107.76b	113.17a	104.38b	81. 35a	54.2a
NPK15:15;15	93.75a	122.22a	128.07a	133.19a	120.47a	82.36a	25.7b
SE±	4.51	3.36	3.25	3.13	2.94	2.37	7.44
Rate (kg/ha)							
0	86.45b	111.54b	118.29b	123.67b	110.67b	78.45ab	31.5a
150	103.04a	129.83a	137.88a	143.17a	130.14a	83.87a	46.58a
300	94.63a	119.38a	127.04a	131.79ab	122.05ab	72.53b	32.21a
600	105.54a	130.96a	137.29a	143.37a	132.43a	84.25a	37.29a
SE±	6.75	7.36	7.04	6.92	6.66	2.52	6.43

Interactions							
V*F	NS	NS	NS	NS	NS	NS	NS
V*L	NS	NS	NS	NS	NS	NS	NS
F*L	*	*	*	*	*	NS	NS
V*F*L	NS	NS	NS	NS	NS	NS	NS
CV (%)	22.92	19.03	17.43	16.60	16.86	14.51	15.09

Means with unlike letter(s) in columns or rows are significantly different at p≤0.05 by Duncan's Multiple Range Test (DMRT), NS stands for not significant

THE EFFECT OF VARIETIES, FERTILIZER SOURCES, RATES OF APPLICATION ON THE PLANT HEIGHT OF TOMATO FOR 5 -10 WEEKS AFTER TRANSPLANTING (WAT)

The result of analysis of variance for plant height did not significantly differ for the two varieties (Roma VF and UC82b) from 5 – 10 WAT in Table 5 though Roma VF variety had a higher mean of 64.8 than UC82b with 63.3. The effect of the NPK fertilizer source on the plant height of tomato showed it was statistically significant only at 5WAT and 9 WAT and not statistically significant for 6, 7, 8, and 10 WAT respectively. However, it was observed that at 5 WAT, zeolite A based fertilizer was not statistically different. The maximum plant height with mean of 69.53 was recorded at 7 WAT with NPK 15:15:15 beyond which the plant height decreases. The minimum plant height with mean of 44.13 was recorded at 5 WAT for Zeolite A based fertilizer. The effect of plant height with rate of application showed no statistical difference at 5, 6, and 7 WAT while statistical difference was recorded at 8, 9 and 10 WAT. Generally, there was a growing trend in the plant heights from 5 -10 WAT with increase in rates of the different fertilizer application. This is expected because of the proportion of fertilizers that was added per level of application was also increasing. It was further observed that the interaction between fertilizer and the rates of application were statistically significant for 5 WAT to 10 (WAT).

Table 5: Effect of fertilizer sources, rates and varieties on the Plant height of tomato for 5 -10 Weeks after transplanting (WAT)

	Week After Transplanting (WAT)					
Treatment	**5**	**6**	**7**	**8**	**9**	**10**
Variety (V)						
Uc82b	45.03a	52.26a	59.15a	62.14a	62.83a	63.33a
Roma VF	45.56a	53.05a	60.64a	63.94a	64.66a	64.85a
SE±	0.83	1.04	0.96	0.83	0.98	0.85
Fertilizer Source						
Zeolite A based fertilizer	44.13ab	52.73a	58.56a	61.55a	67.87a	63.06a
NPK15:15:15	45.83a	50.67a	69.53a	62.03a	62.67b	62.82a
SE±	0.92	1.21	1.45	1.32	1.36	1.23
Rates (kg/ha)						
0	45.83a	53.13a	58.73a	60.97b	61.33b	61.55b
150	45.73a	53.15a	58.97a	62.34ab	63.00b	63.44ab
300	45.45a	51.84a	59.96a	63.44ab	64.48ab	65.13a
600	45.86a	52.76a	62.04a	65.42a	66.18a	66.57a
SE±	1.36	1.37	1.43	1.14	1.25	1.13
Interaction						
V*F	NS	NS	NS	NS	NS	NS
V*L	NS	NS	NS	NS	NS	NS
F*L	*	*	*	*	*	*
V*F*L	NS	NS	NS	NS	NS	NS

CV (%)	11.05	10.48	8.74	8.11	8.00	7.93

Means with unlike letter(s) in columns or rows are significantly different at p≤0.05 by Duncan's Multiple Range Test (DMRT)

THE EFFECT OF VARIETIES, FERTILIZER SOURCES AND RATES OF APPLICATION ON THE FLOWER COUNT OF TOMATOES FOR 5 – 10 WEEKS AFTER TRANSPLANTING (WAT)

The result of analysis of variance for the number of flower counts showed that the main effect of variety and rates were all not statistically significant (Table 6). Moreover, fertilizer sources showed statistically significant difference only at 6 WAT. However, results indicated that there was an increase in the mean values of flower count from the 5 WAT to the 6 WAT and there after a decrease till the 10 WAT for varieties UC82b and Roma VF tomato. UC82b variety had the highest mean value for flower count at 6 WAT with a value of 4.12 and the lowest mean value of 0.02 for the flower count at 10 WAT. There was no significant difference for both varieties. It was however observed that zeolite A based fertilizer maintained high mean values above 3.07 for the flower count at 6 – 7 WAT. The NPK fertilizer produced flower counts above 1.24 at the 8 WAT. The trend in decrease in mean values of flower count can be linked to the slow release property of the zeolite A based fertilizer. The sharp drop at 7 WAT with mean value of 3.01 to 0.76 at 8 WAT for the conventional NPK fertilizer can be traced to the lack of barrier or slow release property. Generally, increase in rate of application led to increase in flower count at 6 -7 WAT though they were not statistically significant. There was interactive effect between the fertilizer and the rate of application as illustrated in 6 WAT.

Table 6 Effect of varieties, fertilizer sources and rates of application on the flower count of tomatoes for 5 -10 Weeks after Transplanting (WAT)

	Weeks after transplanting					
Treatment	**5**	**6**	**7**	**8**	**9**	**10**
Variety (V)						
UC82b	1.64a	4.12a	3.25a	0.82a	0.14a	0.02a
Roma VF	1.06a	4.04a	3.64a	0.44a	0.36a	0.02a
SE±	0.37	0.34	0.36	0.31	0.16	0.01
Fertilizer Source						
Zeolite based fertilizer	0.87a	3.36b	3.07a	1.47a	0.32a	0.00a
NPK15:15:15	1.84a	4.24a	3.01a	0.76a	0.15a	0.04a
SE±	0.37	0.37	0.47	0.25	0.11	0.00
Rate (kg/ha)						
0	0.96a	3.65a	3.86a	0.98a	0.04a	0.04a
150	1.15a	4.23a	3.21a	1.04a	0.24a	0.00a
300	1.31a	3.92a	3.45a	1.02a	0.45a	0.00a
600	1.85a	4.46a	3.23a	1.59a	0.35a	0.04a
SE±	0.32	0.57	0.57	0.35	0.22	0.00
Interaction						
V*F	NS	NS	NS	NS	NS	NS
V*L	NS	NS	NS	NS	NS	NS
F*L	NS	*	NS	NS	NS	NS
V*F*L	NS	NS	NS	NS	NS	NS
CV (%)	29.91	45.67	36.32	64.22	26.74	24.64

Means with unlike letter(s) in columns or rows are significantly different at p≤0.05 by Duncan's Multiple Range Test (DMRT)

THE EFFECT OF VARIETIES, FERTILIZER SOURCES AND RATES OF APPLICATION ON TOMATO FRUIT COUNT FOR 5 -10 WEEKS AFTER TRANSPLANTING (WAT)

It was observed from Table 7 that Tomato variety, UC82b had the highest fruit count at 10 WAT with a mean value of 2.65 while Roma VF variety had a mean value of 2.53 at 10 WAT. There was no significant difference between the means of the two varieties from 5 – 10 WAT. Zeolite A based fertilizer produced the highest fruit count at 7 WAT with a mean of 2.48. The NPK fertilizer had its highest fruit count with a mean value of 2.12 at 9 WAT. The difference in mean values of the zeolite A based fertilizer to the conventional NPK fertilizers is traceable to the steady nature the zeolite A based fertilizer releases its nutrients to the plant. Leaching of plant nutrients is reduced largely because the plant nutrients are occluded in the pores of the zeolite framework and not exposed easily as conventional NPK are mainly supported by fillers for handling purposes. It was also observed that the rate of application of 300 kg/ha which was the recommended rate for applying NPK 15: 15:15 produced the highest fruit count at 9 and 10 WAT (Isah *et al.*, 2014). There was no interactive effect from 5 – 10 WAT.

Table 7 Effect of varieties, fertilizer sources and rates of application on tomato fruit count for 5 -10 Weeks after Transplanting (WAT)

	Weeks after transplanting					
Treatment	5	6	7	8	9	10
Variety(V)						
UC82b	0.00a	1.02a	2.05a	2.57a	2.62a	2.65a
Roma VF	0.00a	0.32b	2.02a	2.54a	2.55a	2.53a
SE±	0.00	0.13	0.25	0.26	0.26	0.22
Fertilizer Source						
Zeolite based fertilizer	0.00a	0.59a	2.48a	2.26a	2.33a	2.36a
NPK15:15:15	0.00a	0.70a	1.83a	2.00a	2.12a	2.11a
SE±	0.00	0.24	0.26	0.22	0.27	0.23
Rates of application (kg/ha)						
0	0.00a	0.47a	1.83a	2.29a	2.22b	2.22b
150	0.00a	0.56a	2.16a	2.57a	2.52ab	2.54ab
300	0.00a	0.83a	2.17a	2.86a	3.06a	3.05a
600	0.00a	0.94a	2.24a	2.54a	2.56ab	2.53ab
SE±	0.00	0.34	0.33	0.31	0.30	0.30
Interaction						
V*F	NS	NS	NS	NS	NS	NS
V*L	NS	NS	NS	NS	NS	NS
F*L	NS	NS	NS	NS		
V*F*L	NS	NS	NS	NS	NS	NS
CV (%)	0.00	16.43	37.94	23.16	38.77	38.77

Means with unlike letter(s) in columns or rows are significantly different at p≤0.05 by Duncan's Multiple Range Test (DMRT

THE EFFECT OF VARIETIES, FERTILIZER SOURCES AND RATES OF APPLICATION ON TOMATO FRUIT YIELD FOR 5 -10 WEEKS AFTER TRANSPLANTING (WAT

The mean values of the fruit yield of tomato variety shown in Table 8 illustrate that UC82b produced the highest fruit yield with mean value of 92.71 while Roma VF produced the lowest yield with mean value of 87.66. The mean values of the two varieties were not significantly different. It was observed that Zeolite A based fertilizer produced the highest fruit yield with

a mean value of 84.69. The fruit yield of NPK 15:15: 15 was lowest with a mean value of 69.34. The increase observed in Zeolite A based fertilizer is traceable to its slow release property of the adsorption between the plant nutrients and the pores of the zeolite carrier. The rate of application of fertilizer (300 kg/ha) had the highest mean value of 103.57 and it was statistically different from rate of application (600kg/ha). It was also observed that the interactive effect occurred between the fertilizer and the rate of application.

Table 8 :Effect of varieties, fertilizer sources and rates of application on tomato fruit yield for 5 -10 Weeks after Transplanting (WAT)

Treatment	**Fruit yield** (g/plant)
Variety (V)	
UC82b	92.71a
Roma VF	87.66a
SE±	7.58
Fertilizer Source	
Zeolite A based fertilizer	84.69a
NPK15:15:15	69.34a
SE±	4.93
Rates of application (kg /ha)	
0	70.36b
150	97.57a
300	103.57a
600	89.25ab
SE±	12.19
Interaction	
V*F	NS
V*R	NS
F*R	*
V*F*R	NS
CV (%)	25.30

Means with unlike letter(s) in columns or rows are significantly different at p≤0.05 by Duncan's Multiple Range Test (DMRT)

Conclusions

The study investigated the sorption of quaternary amine compound, HDTMA and oxyanions such as nitrates and phosphates on optimized zeolite A synthesised from an Ahoko Kaolin using central composite design. The initial concentration of HDTMA (162.6 mmol/l) equivalent to its external cation exchange capacity (ECEC) was adsorbed to zeolite A surface by coulombic interactions. The study further evaluated the application of synthesized NPK loaded Zeolite A based fertilizer and conventional NPK 15:15:15 fertilizer on the growth and fruit yield of tomato crop. Tomato crop treatments with NPK loaded Zeolite A based fertilizer showed much greener leaves than the conventional NPK fertilizer source with less greener leaves at 11 weeks thereby explaining the better retention of plant nutrients and the slow release property of the carrier, surfactant modified zeolite A. The fruit yield from the NPK loaded zeolite A based fertilizer also showed higher fruit yield than the conventional NPK based fertilizer indicating that plant nutrients which might have leached beyond the root zone in the NPK fertilizer were utilized in the zeolite A based fertilizer to giver higher fruit yields.

References

Aroke, U. O., and El-Nafaty, U. (2014). XRF, XRD and FTIR properties and characterization of HDTMA-Br surface modified organo-kaolinite clay*. International Journal of Emerging Technology and Advanced Engineering, 4(4), 817-825*

Asiedu, O. (2016). Removal of Fluoride from water using Surfactant Modified Synthetic Zeolites (Doctoral dissertation), Kwame Nkrumah University of Science and Technology, Kumasi, Ghana.

Bansiwal, A. K., Rayalu, S. S., Labhasetwar, N. K., Juwarkar, A. A., and Devotta, S. (2006). Surfactant-modified zeolite as a slow release fertilizer for phosphorus. *Journal of Agricultural and Food Chemistry*, 54, 4773-4779.

Demirçivi, P.,and Saygılı, G. (2014). Sorption isotherms and modeling studies of HDTMA for adsorption onto vermiculite, perlite and zeolite clays. *Sigma Journal of Engineering and Natural Sciences*, *32*, 311-320

Food and Agricultural Organization FAO (2012).Faostat. Retrieved December 29th 2012 from http://faostat.fao.org/site/339/defalt.aspx

Fungaro, D. A. and Magdalena, C. P. (2014). Counterion Effects on the Adsorption of Acid Orange 8 from Aqueous Solution onto HDTMA-Modified Nanozeolite from Fly Ash. *Environment and Ecology Research*, *2*(2), 97-106

Haggerty, G.M., Bowman, R.S., (1994). Sorption of inorganic anions by organo-zeolites, *Environmental Science and Technology*, 28 (3), 452-458.

Isah, A. S., Amans, E.B., Odion, E. C. and Yusuf, A. (2014). Growth rate and yield of two tomato varieties (*lycopersiconesculentum Mill*) under Green Manure and NPK Fertilizer rate, Samaru Northern Guinea Savanna, *International Journal of Agronomy,*(2014) 8.http://dx.doi.org/10.1155/2014/932759

Jin, X., Jiang, M. Q., Shan, X. Q., Pei, Z. G., and Chen, Z. (2008). Adsorption of methylene blue and orange II onto unmodified and surfactant-modified zeolite. *Journal of Colloid and Interface Science*, 328(2), 243-247.

Jakkula, V. S., Williams, C. D., Hocking, T. J., and Fullen, M. A. (2011). High selectivity and affinity of synthetic Phillipsite compared with natural Phillipsite towards ammonium (NH4+) and its potential as a slow release fertilizer. *Archives of Agronomy and Soil Science*, *57*(1), 47-60.

Karmakar, M., and Ray, R. R. (2011). Current trends in research and application of microbial cellulases. *Journal of Microbiology Research*6(1), 41.

Li, Z., Roy, S. J., Zou, Y., and Bowman, R. S. (1998). Long-term chemical and biological stability of surfactant-modified zeolite. *Environmental Science and Technology*, 32(17), 2628-2632.

Li, Z. (2003). Use of surfactant-modified zeolite as fertilizer carriers to control nitrate release. *Microporous and Mesoporous Materials*, 61, 181-188

Li, Z., and Zhang, Y. (2010). Use of surfactant-modified zeolite to carry and slowly release sulfate. *Desalination and Water Treatment*, *21*(1-3), 73-78.

Maina, E. W. (2016). Studies on photo stabilization of pyrethrum flower extracts using clay, Master of Science (Chemistry), Jomo Kenyatta University of Agriculture and Technology, Kenya

Mofuka, M. M., Nsomb, M., Nkasa C., Ibwenzi, K and Taba, K. (2007).Effect of combining organic biomass and inorganic fertilizer on tomato yield and nematode control in Arenosal in Kinshasha. In: A Betonoed (ed)., Advances in Integrated Soil Fertility Management in sub-Saharan African. *Challenges and Opportunities*. 359-363 Springer.

Notario, P., Arteaga, J. S., Padron, I. J., Gonzalez M., M. M. and Garcia, H., (1995). Phosphorous and potassium release from phillipsite based slow release fertilizers. *Journal of Controlled Release*, 34, 25 – 29

Ramesh, V., James G., Jissy S., Jyothi., and Shibli, S.M.A. (2015). Effect of Zeolites on Soil quality, Plant growth and Nutrient uptake efficiency in Sweet Potato. *Journal of Root Crops*, 41(1), 25 -31.

Salako, O., Kovo, A.S., Abdulkareem, A.S., Yusuf, S.T.(2017): Synthesis of LTA Zeolite from Ahoko Kaolin: Application of Statistical Analysis. Proceedingss of 2nd International Engineering Conference, Federal University of Technology, Minna, Niger State, Nigeria, 17th -19th October, 2017, pp 39-47

Schick, J., Caullet, P., Paillaud, J. L., Patarin, J., and Mangold-Callarec, C. (2010). Batch-wise nitrate removal from water on a surfactant-modified zeolite. *Microporous and Mesoporous Materials*, 132(3), 395-400

Thirunavukkarasu, M. and Subramanian, K.S. (2014). Surface modified nano-zeolite used as carrier for slow release of sulphur. *Journal of Applied and Natural Science* 6 (1), 19-26.

Zhaohui, L., Yingpeng, Z and Yan, L. (2013). Zeolite as slow release fertilizer on spinach yields and quality in a greenhouse test, *Journal of Plant Nutrition*, 36:10, 1496-1505, DOI: 10.1080/01904167.2013.790429.

Proceedings of the 49th NSChE Annual Conference
KADA 2019: pp 73-82

P1A-09: UTILIZING LNG AS FEEDSTOCK FOR AMMONIA UREA FERTILIZER DEVELOPMENT TO BOLSTER AGRICULTURAL PRODUCTION IN NIGERIA

Nwosi H.[a*], Appah, Dulu[b], Kinigoma B. S.[b] Ndubuisi E. C. [ab]

[a] World Bank African Centre for Excellence, (ACE), University Port Harcourt

[b] Department of Petroleum and Gas Engineering, University of Port Harcourt, Nigeria

Corresponding Author: dulu.appa@uniport.edu.ng, boma.kinigoma@uniport.edu.ng

ABSTRACT

Worldwide, farmers are dealing with the problem of feeding an increasing population; to meet this growing demand requires producing extra food on smaller acres through fertilizers application and profuse yields. To vertically integrate the agricultural value chain for economic advancement, we must first tackle multiple hitches encountered by farmers. In northern Nigeria, with vast acres yet with moribund state of fertilizer plants or no access to fertilizers apart from those from Notore and Ndorama or importation in view of this dilemma, this paper examines how LNG can be used to produce fertilizer due to its availability in domestic market. Natural gas as most popular feedstock of fertilizer production is found in abundance in Nigeria and 70% of this is currently flared. In this work, skid mounted fertilizer plant is designed to feed on 23MT of LNG truck. Using ANSYS the LNG of -162^{0}C, 259^{0}F was introduced into an installed heater of ammonia plant and the temperature was increased to 50^{0}C-250^{0}C for primary reformer. After regasification, total volume of 13800mcf of NG was recorded and 2760 mcf/d was utilized as feed-stock, which yields 500MT ammonia and urea.

Keywords: LNG-Feedstock; Fertilizer Production; Agricultural; Nigeria.

1.0 INTRODUCTION

Nigeria holds an immense reserve of natural gas, likely in surplus of 160 tcf. Ranked the 9th position in terms of proven associated and non–associated natural gas reserves around the globe with about 70% of gas flared. With 22 MT of LNG production capacities yet not a drop of these LNG is utilized in the nation's local marketplace. The largest parts of the country are presently excluded from natural gas pipeline and distribution until the advent of the Greenville LNG virtual network distribution. The accessibility of LNG as feed stock for fertilizer plants will be of immense benefit to farmers in Nigeria more especially those from the northern region. Previously natural gas has been used as feed for fertilizer production before the introduction of LNG. Hence with lack of basic infrastructure such as natural gas pipeline to meet the demands of various process plants, from the southern region where natural gas is produced to northern region where most fertilizer plants are situated has instigated the application of virtual LNG pipeline delivery network. The first fertilizer plant in Nigerian was established in 1973, between these periods to 1999, we have recorded a total of thirty two (32) fertilizer production plant. A good number of these production plant are moribund, in fact 90 percent of these fertilizer production plant has not been functional due to several challenges. Prominent among the issues that lead to poor performance of these plants are lack of natural gas supply as there is no natural gas pipeline for gas supply and technical issues, political and above all recurrent shortages of the plant feedstock which is basically natural gas (IFDC, 2018). The Federal Superphosphate Fertilizer Company (FSFC) was among the first fertilizer plants that were established in the country that is not functional till date. This plant was set up to produced NPK and SSP, with an installed capacity of 100,000 located in Kaduna but has been at moribund. Before the establishment of Notore and Indorama fertilizer companies, the country has been relying on importation of fertilizers which has consumed large sum of funds from the federal government. Although there has been several effort to ensure food security in Nigeria and this has been in line with some agricultural strategies and policies. These policies

have progressively developed significantly in line with the country's population, which is expanding in geometric propulsion independence. In Nigeria, around 1998 some of the agricultural strategies that were abandoned by successive government were revisited and revived to guarantee food security for the growing population by increasing local production capacity. Prominent amongst these policies are the Nigerian "*New Agricultural Policy Thrust,"* issued in 2001, with the *National Fertilizer Policy for Nigeria*, (FMARD, 2008) as some of the subsector which are fundamental for the realization of a national food security agenda. The *National Fertilizer Policy for Nigeria,* adopted in 2006, is an all-inclusive broad idea of "facilitating farmers' with an appropriate access to sufficient quantity and quality of fertilizers at ready for action and reasonably priced prices." The agricultural value chain can be improved for economic advancement; if we undertake the manifold drawbacks encountered by farmers in Nigeria (Nagy *et al,* 2002). Farmers in Nigerian Struggle for almost everything within each the segment of the agricultural value chain, farmers in northern region of the country with vast land and big farms but little or no access to fertilizers apart from purchase from southern part where the only two fertilizer plants are situated (Notore and Ndorama) or importation are faced with numerous challenges; prominent among these challenges are lack of access to high-quality fertilizer. Natural gas as the most popular feedstock to fertilizer production is found in abundance in Nigeria and 70% is flared hence there is need to encourage farmers in northern Nigeria to establish their own fertilizer plant based on the new era of LNG distribution in the Nigerian domestic market by Greenville. Prior to this time natural gas that is composed of 75% to 95% methane and other components has been used directly to produce fertilizer hence the idea of utilizing LNG is based on the availability of LNG delivery system. Hence to establish a skid mounted modular fertilizer plant of 500MTPD for the production of ammonia and urea in some of the big farms in northern Nigeria is well thought-out or conceives. Nigeria as country spend billions annually to imports fertilizer for farmers while the natural resource for feedstock for the fertilizer production is found in Nigeria is large proportion and there is new development in LNG distribution today in Nigeria fertilizer feedstock will no long be a problem.

2.0 MATERIALS AND METHODS

The material used for the realization of the aim and objectives of the paper was, the LNG sample to apply LNG as feedstock for ammonia and urea production as against the normal direct natural gas method with normal atmospheric temperature the research will consist the application of heat and mass transfer computer aided engineering software to model the process of elevating the temperature of LNG to meet the required primary reformer unit temperature for the production of the feed gas to synthesis gas. The LNG sample used was received from the downstream gas companies such Greenville LNG downstream company. This is done because each gas company field gas properties data differ from company to company based on different reservoir conditions. The method followed a series of data collection, process design consideration and the software application. The data of the volume of LNG feed day that would generate the 500MTPD of liquid ammonia and 500MTPD urea chips was estimated. Cost analysis and profit merging for produced fertilizer and foreign fertilizer will be calculated in further studies. Figure 1 (Notore Process Plant Manual 2006) is a schematic description of the 500MTPD ammonia plant with an LNG stream, heater as stream one to enhance LNG temperature and gas filter to further remove mechanical impurities in order to meet the design specification of 250^0C temperature and purity to primary reformer processes.

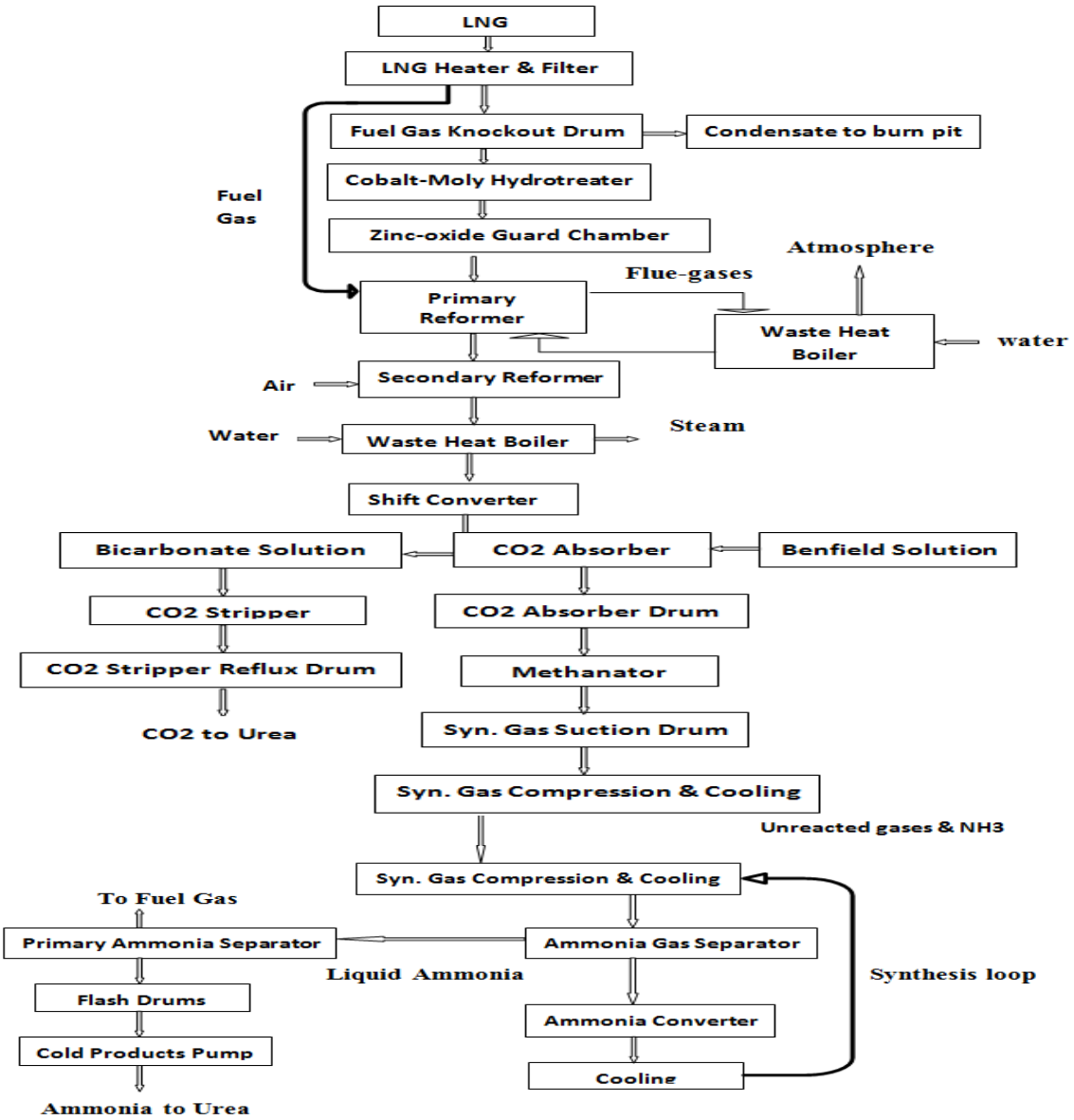

Figure 1 Schematic description ammonia process plant.

The LNG stream heating vessel conditions, properties and value for the inlet and outlet streams are defined in Table 1 with the LNG inlet stream pressure set at 10 bar while the temperature is set at -162^{0}C and the outlet pressures is calculated at 25bar and the outlet temperature is recorded to be 250^{0}C with a mass flow rate of 300 kg mole per hour showed in Table 1.

Table 1 LNG Heating Vessel operating Conditions

Table 1 LNG Heating Vessel operating Conditions	
Property	Values
Inlet Pressure	10bar
Inlet Temperature	-162^{o}c
Outlet Pressure	25bar
Outlet Temperature	250^{o}c
Flow Rate	3000kgmole/hr

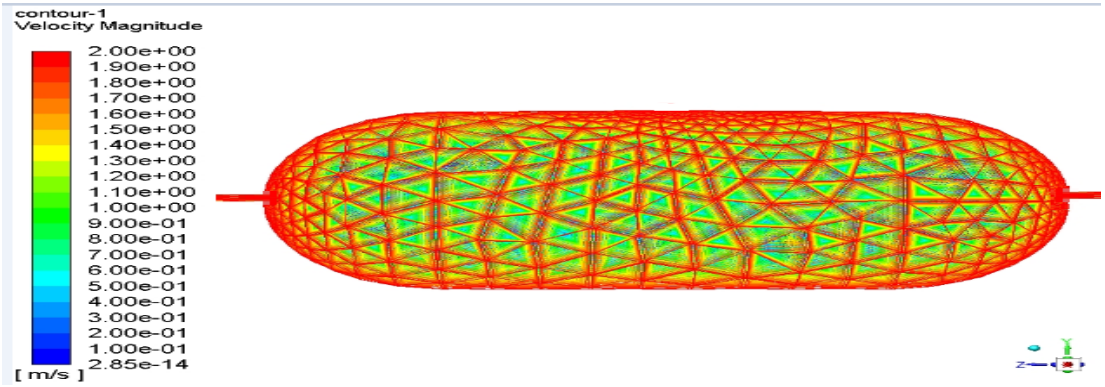

Figure 2 ANSYS Simulation of the LNG Heating Vessel before entering the Primary Reformer

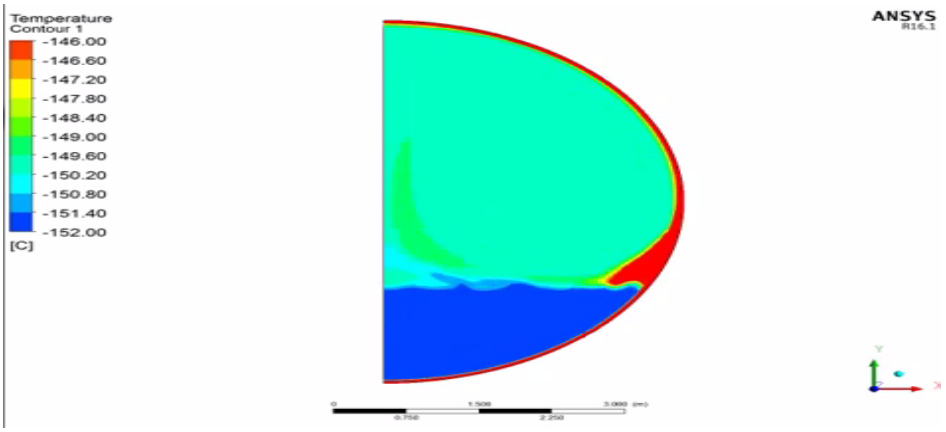

Figure 3 ANSYS CFD LNG Heater Internal Temperature Increase from -152^{0}C to 250^{0}C

$$\frac{\partial(\rho E)}{\partial t}+\nabla\cdot\left[\vec{V}(\rho E+p)\right]=\nabla\cdot\left[k_{\text{eff}}\nabla T-\sum_j h_j J_j+\left(\bar{\bar{\tau}}_{\text{eff}}\cdot\vec{V}\right)\right]+S_h \quad (1.)$$

The Equation 1 is used to determine the heat transfer per unit mass, at the wall of the simulated heater. As part of the enabler Equation within the ANASYS simulation environment for heat transfer analysis of the LNG evaporation and Boil-off formation. Equation 2 is used to enable the analysis of the liquid gas flow, as applied directly and the computer aided engineering simulation process utilized, the equation to determine heat conduction, gas molecule or species diffusion and the viscous dissipation of the fluid to predict gas dynamics parameters from LNG to natural gas. Equation 2 is also used to determine the rate at which LNG will be converted back to natural gas in the LNG heater vessel as a result of heating system in order to serve as feed stock in the gaseous form to the primary reformer.

$$BOR=\frac{V_{BOG}.24}{V_{LNG}.P}=\frac{Q.3600.24}{\Delta H.V_{LNG}.P}.100$$

(2.)

Description and operating conditions of the Ammonia Process Ammonia plant consists of four major units; the reforming unit, CO_2 removal unit, Compression unit, and Synthesis unit, Feedstock used in ammonia plant include: natural gas, water, steam, air, chemicals, and power, Desulphurization: Sulphur is removed from Natural gas using zinc oxide catalyst (ZnO),

because it is poisonous to Nickel catalyst used in the primary reformer. The minimum amount of sulphur content in NG for efficient reforming is 0.2ppm.

$ZnO + H_2S \; ZnS + H_2O$ (3.)

Primary Reformer: the reaction in the primary reformer is highly endothermic and involves both thermal and catalytic cracking. Natural gas and medium pressure steam reacts over Nickel catalyst and burner of about 1000^0C using NG to break down the hydrocarbon into hydrogen, carbon oxides inert gases and about 10% methane.

$$CH_{4(g)} + H_2O_{(g)} \longrightarrow CO_{(g)} + 3H_{2(g)} \quad (4.)$$

$$CO_{(g)} + H_2O_{(g)} \longrightarrow CO_{2(g)} + H_{2(g)} \quad (5.)$$

The products from the primary reformer (CO, CO_2, H_2, CH_4, Ar) is then sent to the secondary reformer for the final cracking of hydrocarbon. Secondary Reformer: Air is introduced into the secondary reformer to add Nitrogen to the synthesis gas for Ammonia production. In this vessel, both endothermic and exothermic reaction takes place. The burning of hydrogen is exothermic, producing a pop sound.

$$2H_{2(g)} + O_{2(g)} \longrightarrow 2H_2O_{(g)} \quad (6.)$$

The reforming of the 10% methane left from the primary reformer is endothermic.

$$CH_{4(g)} + H_2O_{(g)} \longrightarrow CO_{(g)} + 3H_2 \quad (7.)$$

The water Gas shift is endothermic converting carbon monoxide to carbon dioxide and hydrogen.

$$CO_{(g)} + H_2O_{(g)} \longrightarrow CO_2 + H_{2(g)}$$

Shift Converters (H.T.S and L.T.S): From the secondary reformer, the gas passes through a two stage shift converter, the High temperature shift converter(H.T.S) which uses iron oxide with chromium (Fe_2O_3)as catalyst and Low temperature shift converter(L.T.S) which uses copper oxide on zinc oxide or alumina, to convert $CO_{(g)}$ to $CO_{2(g)}$ and $H_{2(g)}$. The first stage converts CO to about 3% while the second stage converts to about 0.2-0.3%.

H.T.S Reaction

$$CO + H_2O \rightleftharpoons CO_2 + H_2 \text{ (exothermic)}$$

$$\left.\begin{array}{l} 3Fe_2O_3 + H_2 \rightleftharpoons 2Fe_3O_4 + H_2O \\ 3Fe_2O_3 + CO \rightleftharpoons 2Fe_3O_4 + CO_2 \end{array}\right\} \text{ Slightly exothermic reaction} \quad (8.)$$

If steam is not present, there will be further reduction of Fe3O4 to metallic iron, Fe which is undesirable because it catalyses a highly exothermic reaction.

$$Fe3O4 + H2 \rightleftharpoons Fe + H2O \quad (9.)$$

$$Fe3O4 + CO \rightleftharpoons Fe + CO2$$

(10.) Metallic iron will catalyse the following reaction

$$CO + 3H2 \rightleftharpoons CH_4 + H_2O \quad (11.)$$

$$2CO \rightleftharpoons C + CO_2 \quad (12.)$$

L.T.S Reaction

$CuO + H_2 \longrightarrow Cu + H_2O$ (highly exothermic) (13.)

$CO + H_2O \longrightarrow CO_2 + H_2$ (exothermic) (14.)

The efficiency of the plant was determined by the efficiency of the L.T.S. Process Condensate Separator: here condensate is removed from the process gas and sent the condensate for treatment at the utility plant.

The Benfield System: this is where a solution of potassium carbonate is prepared and used to absorb CO_2 in the CO_2 absorber. The compositions of the Benfield solution are: potassium carbonate in water ($K_2CO_3 + H_2O$), diethanol amine as organic activator, and vanadium pentaoxide (V_2O_5) as corrosion inhibitor. CO_2 Removal system: This consists of CO2 Absorber, knock out drum and stripper. The process gas enters the absorber from the bottom and goes out from the top to the knock out drum, while the Benfield solution enters the absorber from the top and goes out from the bottom to the stripper for regeneration. The CO2 is stripped off the solution and sent to urea plant.

Reaction in the absorber:

$CO_2 + H_2O \longrightarrow H_2CO + O_2$ (15.)

$H_2CO + K_2CO_3 \longrightarrow 2KHCO_3$ (16.)

$OHC_2H_4\text{-}NH\text{-}C_2H_4OH + CO_2 \longrightarrow C_4H_{10}NCOOH$ (17.)

$C_4H_{10}NCOOH + K_2CO_3 + H_2O \longrightarrow C_2H_4OHNH + 2KHC0_3$ (18.)

Methanator: left over of oxygenated species in the process gas is methanated to avoid poisoning of ammonia synthesis catalyst and formation of ammonium carbonate in the synthesis loop which may deposit and cause stress corrosion in the compressor.

$CO_2 + H_2 \longrightarrow CO + H_2O$ (19.)

$CO + 3H_2 \longrightarrow CH_4 + H_2O$ (20.)

$CO_2 + 4H_2 \longrightarrow CH_4 + 2H_2O$ (21.)

Synthesis Gas Compressor: this compressor runs at about 700rpm and it compresses the synthesis gas to a pressure of about 150kg/cm^2. Synthesis loop exchangers: the compressed gas passes through exchangers, to be cooled using liquid ammonia. This occurs through a refrigeration cycle having the liquid ammonia as the refrigerant. For every refrigeration cycle, 12.5% of liquid ammonia is formed from the gaseous ammonia. Ammonia liquefies at -33^{o}c of which is pumped and stored in a 500MT storage capacity. In order to maintain the liquid phase of the ammonia in the plant and prevent solidification, burners are attached at the bottom of the tank to keep warm. The vapour formed at the storage tank is then recycled back for refrigeration.

Urea Plant

The urea plant was designed to produce 500MT/D of urea. The feedstock is carbon dioxide (CO_2) and ammonia (NH_3), both from ammonia plant. The plant can be divided into three units; CO_2 compressor unit, synthesis unit and granulation unit. Urea formation occurs in two step reaction as below.

$2NH_{3(g)} + CO_{2(g)} \leftrightarrow NH_4COONH_{2(aq)}$ (22.)

$NH_4COONH_{2(aq)} \leftrightarrow NH_2CONH_{2(aq)} + H_2O_{(aq)}$ (23.)

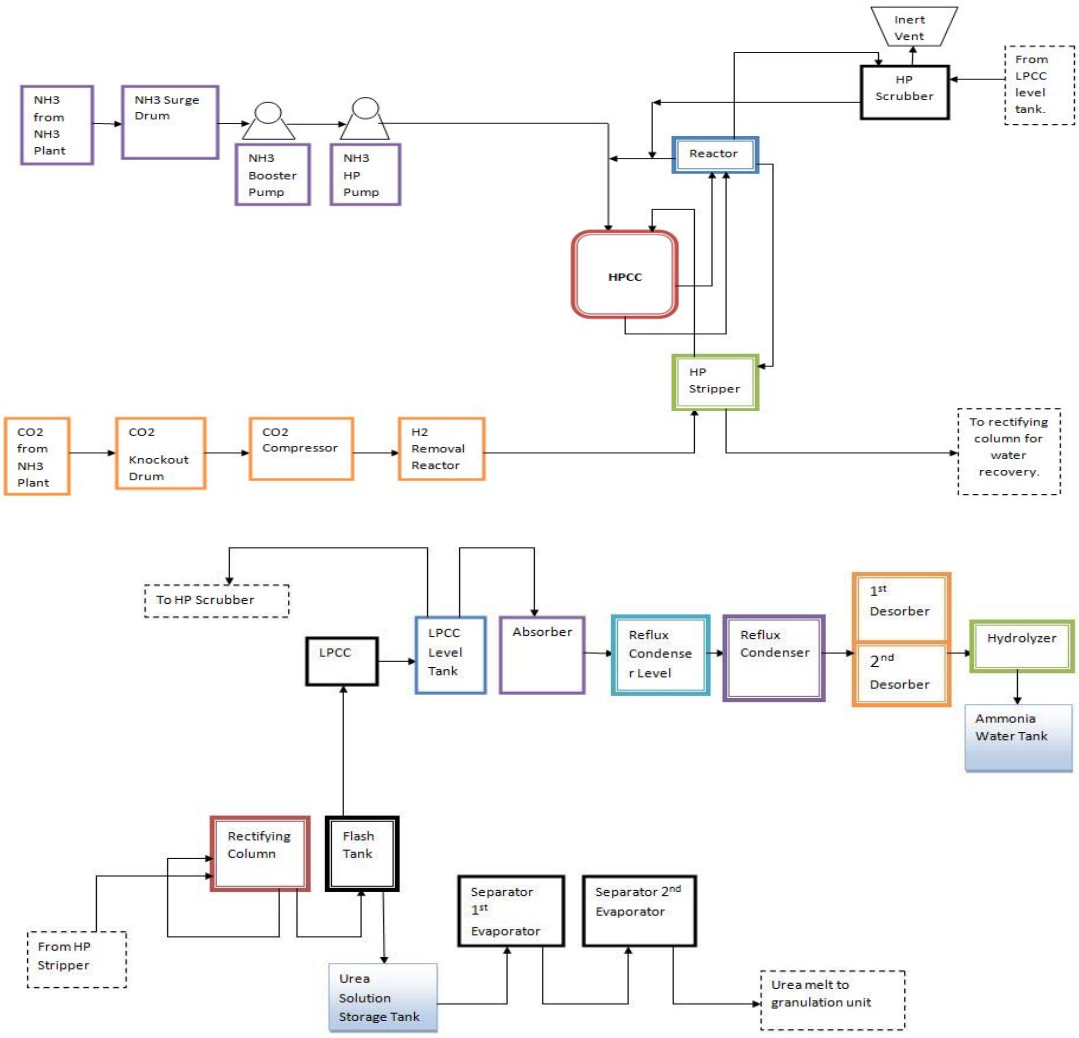

Figure 4: Continuation of Schematic Plant Designed Process for 500MT/D of Urea

Compressor Unit

Carbon dioxide which is a by-product is taken directly from the desorbers in the ammonia plant without undergoing purification and it is sent to the knock-out drum through the battery limit entrance. The carbon dioxide contains about 1.35% (by volume) of hydrogen, water, traces of methane and carbon monoxide and enters the plant at a low pressure of 0.60kg/cm^2 and at a temperature of 38°C. The CO_2 goes to the knock-out drum for the purpose of separation. Air from the atmosphere is introduced into the drum using a pressure air blower and the air is filtered using the air filter (to remove impurities). It goes to the high pressure carbon dioxide cooler where the temperature is decreased to 120°C. At the outlet of the CO_2 cooler analyzers are installed to measure the oxygen and CO_2 content. The CO_2 goes to the high pressure stripper where unreacted gases are stripped from the CO_2. Thereafter the CO_2 goes into the high pressure carbamate condenser (HPCC).

Synthesis Unit

Apart from the formation of urea in this unit, the unit also consists of process operations such as evaporation, desorption and hydrolysis. It constitutes four major vessels for the synthesis of urea; reactor, high pressure stripper, high pressure carbamate condenser (HPCC) and the high pressure scrubber. The rectifying section steps down the pressure from high to low and

removes water by utilizing the evaporator (two stages). The water separated is recovered from ammonia and urea in the desorber and hydrolyser (desorption unit). Stripper, it receives lean CO_2 from the compressor at 140-145 Kg/cm^2 and urea (the stream actually contains CO_2, unreacted carbamate, NH_3, CO_2 and inert) from the reactor. HPCC, Ammonia from ammonia plant is received in the surge drum at pressure of 11.2Kg/cm^2 and temperature of$30℃$. It is pumped from the surge drum by ammonia booster pump which increases the pressure to about 16Kg/cm^2 (allowable inlet pressure for high pressure pump to operate) and temperature is$70℃$. The high pressure Ammonia pump takes over from the booster pump and pumps the NH_3 into the high pressure carbamate condenser (HPCC). The HPCC is the vessel where the reaction between ammonia and carbon dioxide to form ammonium carbamate occurs.

$$2NH_{3(g)} + CO_{2(g)} \leftrightarrow NH_4COONH_{2(aq)} \qquad \Delta H = -ve \qquad (24.)$$

It is the first step in the formation of urea and as shown above, the reaction is reversible and exothermic. The forward reaction is favoured at high pressure and high temperature of 140-145Kg/cm^2 and $180℃$ respectively. Reaction between NH_3 reacts and CO_2 (the stream also contains carbamate and ammonia) from the stripper to form carbamate is exothermic. The heat released in the reaction is collected in two steam drums attached to the HPCC to produce low steam pressure (3.2- 3.5Kg/cm^2). The formation of urea and the completion of carbamate formation reaction take place in the reactor vessel.

$$NH_4COONH_{2(aq)} \leftrightarrow NH_2CONH_{2(aq)} + H_2O_{(aq)} \qquad \Delta H = +ve \qquad (25.)$$

Urea formation is endothermic while carbamate formation is exothermic. The heat required for urea formation is gotten from the heat released from the carbamate formation reaction. The urea solution overflows into the stripper through the down-comer, the gases (inert, unreacted CO_2 and NH_3) are sent to the scrubber. Scrubber, the scrubber makes use of water in cooling the gases thereby venting out the inert through the inert vent and sends back the unreacted gases back to the reactor. Rectifying column, the pressure of the urea solution is stepped down from 150Kg/cm^2 to 2.5Kg/cm^{2}via the help of stripper level control valve. In the rectifying column, the solution dissociates gases from liquid as a result of pressure that is lowered. The unreacted gases escape through the overhead to the low pressure carbamate condenser (LPCC) where it is converted to ammonium carbamate. It overflows through a nozzle into the LPCC level tank, the high pressure carbamate pump discharges the carbamate at a pressure of 150Kg/cm^2 into the high pressure scrubber where inert gases are removed and the carbamate goes into the reactor for reaction. The solution is taken from the hydrolyser heat exchanger to the hydrolyser where it is subjected to an extraction steam of 23.5-24kg/cm^2 pressure so as to breakdown the urea into ammonia and carbon dioxide, it is then sent to the second desorber where 3.5kg/cm^2 steam is applied at a temperature of $145℃$. So by then you have pure water which you drain out.

Granulation Unit

This is where urea is coated with formaldehyde and made into granules. The coating is done to prolong the life of the urea granules, minimize leaching and ensure moderate release of urea into the soil on application.

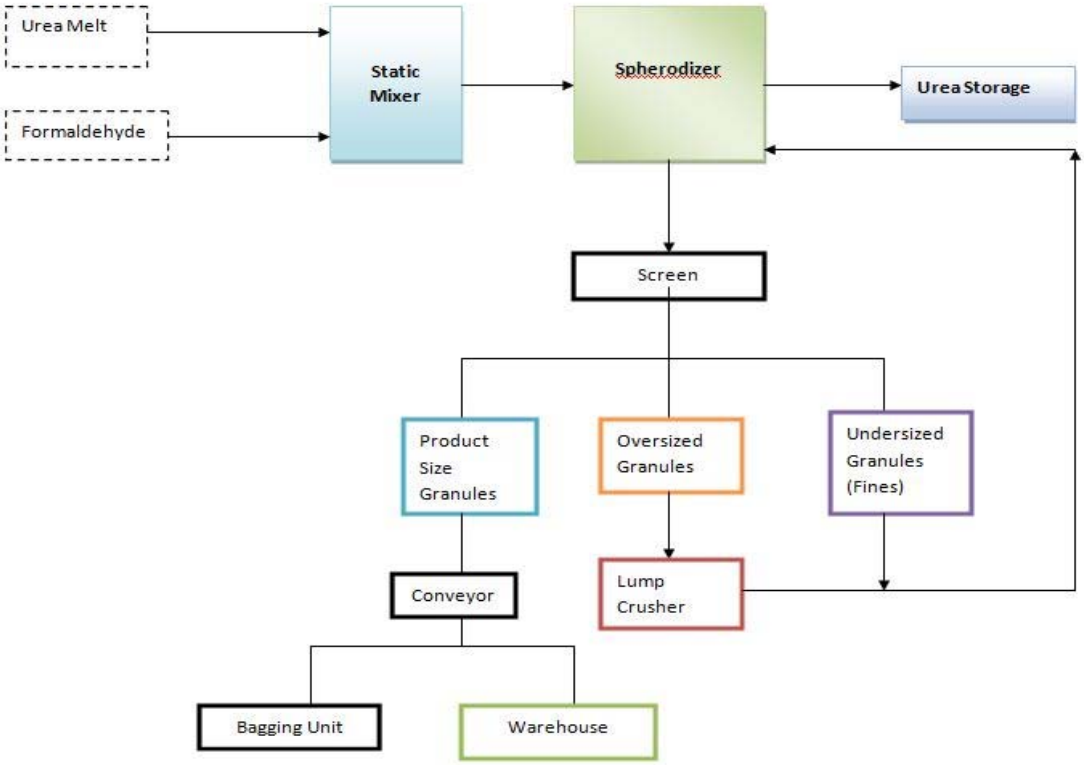

Figure 5: Schematic of Granulation Unit Plant Designed Process

There are four granulators in this unit and they are linked to a common exhaust stack. Urea melt is pumped from the urea evaporator in the urea synthesis plant through steam jacketed lines to the static mixer where it is mixed with formaldehyde. The hot urea melt at about 135^0C is then sent to the spherodizer granulation drums (rotating at about 7.5 rpm) where it is sprayed through four specially designed nozzles onto rolling beds of undersized granules. The undersized granules become content with the urea formaldehyde to form a bed of spherical semi-plastic particles. The Exhauster provides draft for the eliminated dusts to rise up the exhaust stack. A sump tank, sump pumps, steam ejector and urea filter are provided for collecting pump drains, drains from the stack and exhausters and re-dissolving little quantities of urea granules from bulk storage. The re-dissolved urea is then returned to the urea solution tank. Air Heater Coil: prevents ambient air of high relative humidity from being drawn through the drum causing 'internal sweating' and caking of the urea bed. Air Cooling Coil: uses ammonia to cool the air duct to the granulation drum.

3.0 RESULTS AND DISCUSSION

LNG can be utilized as an alternative to natural gas in teams of feedstock for fertilizer production in Nigeria. As clearly shown in this work, a fertilizer plant was developed to feed on LNG and that a total volume of 23MT/5d of LNG used to feed a 500MTPD of ammonia and urea plant and a total volume 2760 Scm^3 the plant daily consumption for five operational days and the expected product was realized. The LNG of -162^0C, 259F was increased to 50^0C-250^0C for the primary reformer. After the regasification, a total volume of 13800 $Scfm^3$ of natural gas was recorded and 2760 scm^3/d was utilized as feedstock which yields 500mt/d ammonia and urea. From figure 2.6, graph above shows the LNG temperature increase from 50^0C to 250^0C versus the time taken for the heat supply the required energy to raise the temperature to the plant design specification.

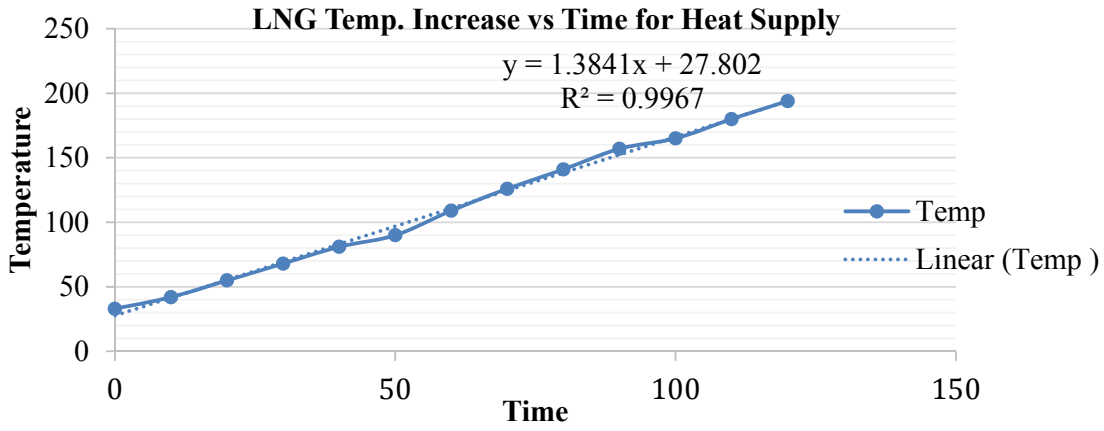

Figure 3.1 Results and Discussion

4.0 CONCLUSIONS

In conclusion, LNG can be used as feed stock for fertilizer production plants in Nigeria and to enhance the agricultural value chain for economic development: the role of chemical engineering would include tackling farmers' technical issues and d*eveloping* technologies for agriculture to gain its own share of the abundant natural resource found in Nigeria. Today LNG is readily accessible in the downstream sector as the Greenville LNG refuelling stations are tactically situated across Nigeria. LNG is being utilized in several sectors of the economy not only for transportation for sales through shipment or for power plants but as feed stock for a good number of industries. These include cement industries, the breweries, asphaltic plants and even vehicle fuels. Utilizing LNG to produce fertilizers will help us achieve agricultural competitiveness and sustain agricultural produce, retain the soil nutrient, boost bountiful yields, safeguard the public health and the environment.

REFERENCES

Agricultural Research Council of Nigeria (ARCN) *Agriculture in Nigeria: the New Policy Trust*, <www.lisabi.org/arcn/pubs/Agricultural%20Policy%20in%20Nigeria.pdf>.

ANSYS Heat transfer modelling, an Introduction to Fluent Training Material 2006

Assessment of Nigeria Seed and Fertilizer Market; Federal Ministry of Agriculture and Rural Development, Federal Fertilizer Department, 2008 *National Fertilizer Policy for Nigeria*, Draft.

IFDC/PROMIDIA 2008 *An Assessment of the Nigeria Seed and Fertilizer Markets,* IFDC internal draft report.

Nagy, J.G., and O. Edun (2002) *Assessment Nigerian Government Fertilizer Policy and Suggested Alternative Market-Friendly Policies*, IFDC

Nwosi, H. A., Appah, D., and Kinigoma, B. (2018) the new-Dawn for Liquefied Natural Gas Utilization: Empowering the Transportation Sector in Nigeria. Society of Petroleum Engineers doi: 10.2118/193437-MS

The New Nigerian Agricultural Policy www.nipc.gov.ng/opportunities.html

Vitale S.A., 2012. LNG and Gas Thermodynamics Vol. II. GT

Yang C.C., Huang Z., (2004) Lower Emission LNG Vaporization LNG Journal Nov./Dec. 2004.

Zhang N., Lior N., 2006. A novel near-zero CO2 emission thermal cycle with LNG cryogenic exergy utilization Energy,

Mokhatab, S., Mak, J. Y., Valappil, J. V. and Wood, D. A. (2014), Handbook of LiquefiedNatural Gas, Elsevier.

National Bureau of Statistics (NBS) 2017 technical report

Proceedings of the 49th NSChE Annual Conference
KADA 2019: pp 83-92

P1B-01: DEVELOPMENT AND APPLICATION OF LOW-TEMPERATURE THERMAL ARC PLASMA REACTOR FOR WASTEWATER SLUDGE TREATMENT

Abubakar M. Ali[1*], Bala I. Abdulkarim[2] and Ephraim G. Kefas[3]
[1,3] Department of Chemical Engineering, Kaduna Polytechnic, Kaduna, Nigeria
[2] Department of Chemical Engineering, University of Abuja, Nigeria
E-mail*: abualimoh67@gmail.com, balisa76@yahoo.com and egkefas@yahoo.com*

ABSTRACT
A large quantity of wastewater sludge is generated yearly. Traditional disposal methods are short of providing the much needed benign treatment. Thermal plasma is a promising treatment technique to address this problem. A 20 cm^3 capacity laboratory-scale thermal-arc plasma reactor was developed using a 4.5 kW TIG welding torch and was used to treat wastewater sludge. The design was based on a DC transferred-arc torch with argon gas as plasma forming gas. The reactor was tested with wastewater sludge from the petroleum industry. The plasma arc temperature was in the range of 356 – 1694 °C at an arc current of 100 – 190 A. Two products, flue gas and a vitreous slag were obtained. A mass reduction of 36.87 – 91.40 % of the sludge was achieved in at an arc current 150 – 190 A which correspond to a plasma temperature range of 539 – 1603 °C. The mass reduction increased with treatment duration from 2 – 8 min. The mass reduction also increased with increasing arc current from 150 – 190 A at an interval of 20 A. Reduction in total organic carbon (TOC) is between 74.03 – 75.83%. The metal elements in the wastewater sludge were enriched after the plasma treatment. The composition of the flue gas was H_2, CO, O_2, CO_2, CH_4 and C_2 hydrocarbons. CO was the major component accounting for over 74%. The concentration of greenhouse gases (CH_4 and CO_2 combined) was less than one. The system was able to gasify the organics in the wastewater sludge to combustible gases and vitrified the inorganics into a slag.

Keyword: Thermal plasma, wastewater sludge, plasma temperature, mass reduction, TOC, carbon conversion

1.0 INTRODUCTION
Thermal arc plasma technology has become a prominent waste treatment technique for a wide variety of waste because of the shortcomings of traditional waste disposal methods (Ali *et al.*, 2016). The plasma arc treatment technology has been identified as a potentially effective tool for producing less harmful by-products which can be used in building and road construction (Kourti *et al.*, 2011; Tu *et al.*, 2008). The innovative plasma technique involves subjecting waste material to high-temperature arc plasma such that the organics and the volatile species are gasified while the inorganics and non-volatiles are chemically bonded in a vitreous matrix, thereby making them resistant to leaching of heavy metals (Agon, 2015). Thermal arc plasma provides a suitable treatment technique for special waste disposal requirements. Advantages of thermal arc plasma treatment technique over conventional incineration include high-temperature regime, high waste volume reduction, low gas throughput, process flexibility in either oxidizing or a reducing environment, and can effectively treat a wide variety of waste types (Heberlein, 2002).

There is an increase in the documented research, in the last two decades, concerning the destruction of hazardous wastes using thermal arc plasma technique. The growing interest of academic research in such an area cannot be unrelated to the ability of the technique to reduce

waste volume by over 80% and produce benign byproducts (Ali *et al.*, 2016; Heberlein and Murphy, 2008). The plasma gasification of the organic portion of sludge has attracted interest as a source of energy and spawned process developments for the treatment of sludge from different sources (Bień *et al.*, 2013; Celary and Sobik-Szołtysek, 2014; Cubas *et al.*, 2014; Kim and Park, 2004; Leal-Quirós and Villafañe, 2007; Li *et al.*, 2007; Li *et al.*, 2012; Li *et al.*, 2015a; Li *et al.*, 2015b; Mohai and Szépvölgyi, 2005; Mountouris *et al.*, 2008; Ramachandran and Kikukawa, 2002; Shie *et al.*, 2014; Sobiecka and Szymanski, 2014). Factors like treatment efficiency, plasma gas flow-rate, the treatment period of a batch operation, feed flowrate of continuous operation and inter-electrode separation were subject of investigation.

Feasibility studies involving design and fabrication of thermal arc plasma reactors for hazardous waste destruction are also documented in the literature. In the USA a laboratory-scale thermal arc plasma reactor consisting of a highly instrumented furnace equipped with a 75 kW transferred arc plasma torch, was developed and used to study the physical and chemical behaviour of metal-spiked waste (nickel and chromium) in a high-temperature plasma regime (Cortez *et al.*, 1996). In Thailand, a 20 kW laboratory-scale, atmospheric-air DC plasma reactor was designed and fabricated using a non-transferred plasma torch and its performance was evaluated using electronic waste (Tippayawong and Khongkrapan, 2009). A research team in Brazil developed a small-scale, continuous-flow plasma reactor consisting of a torch with graphite electrodes and an integrated nebulization furnace. The reactor was used to eliminate carbon-tetrachloride from liquid waste (Cubas *et al.*, 2005). In the Durgapur city of West Bengal, a 20 kg/hr plasma reactor for the treatment of waste plastic was developed, and its performance on the pyrolysis of waste plastic and energy generation was studied (Punčochář *et al.*, 2012). Other similar studies involving the design and evaluation of thermal plasma reactor for hazardous waste destruction were reported (Barcza, 1986; Khongkrapan *et al.*, 2013; Szałatkiewicz *et al.*, 2012, 2013; Tang *et al.*, 2003; Townsend and Oehmig, 2014; Zhao *et al.*, 2001).

It is obvious from the above discussion that waste treatment using thermal plasma technology has gained ground, and laboratory/pilot scale plasma reactors have been developed and their performances for the destruction of hazardous waste were studied. However, it is not available to the knowledge of the authors, any attempt to develop a thermal arc plasma reactor that treats wastewater sludge from the petroleum industry. The wastewater sludge from the petroleum industry is unique in its composition due to the presence of hydrocarbons, phenols and dissolved minerals (Diya'uddeen *et al.*, 2011). Thus, the present investigation was geared towards bridging this gap. In this study, a 20 cm^3 capacity laboratory-scale thermal-arc plasma reactor was developed and used to treat wastewater sludge from the petroleum industry. Design parameters and result from the testing of the reactor is presented.

2. MATERIALS AND METHOD

2.1. Thermal Plasma Reactor

The development of the plasma reactor for the treatment of wastewater sludge from the petroleum industry passes through a series of design, construction, testing, redesigning, reconstruction and retesting process. Major problems encountered at different stages of the development include difficulty in arcing, difficulty in machining high-temperature stable material and stability of the plasma arc to mention but a few. The thermal plasma process system consists of a DC power source, a transferred arc plasma torch, a reaction chamber and a gas cooling and cleaning system. The process flow diagram of the system is shown in Figure1. The equipment

power rating and reactor capacity were based on a commercially available torch and 20 g of sludge respectively. The DC power source is a TIG (master weld, model: TP-2000) used commercially for arc welding, it supplies a voltage of 63 V and a variable current of 5 – 200 A to the plasma torch.

The transferred arc plasma torch was a Ø 2.4 mm tungsten rod (98% purity) inserted into the centre of a nozzle ejector. The torch was connected to the negative terminal of the DC power source. The nozzle ejector had an orifice opening through which argon gas (the plasma forming gas) flows. The torch was supported vertically at 10 cm above the anode electrode. The anode was a tungsten rod of Ø 10 mm and 35 mm length, placed concentrically at the centre of the reaction chamber. The reactor furnace was an aluminium block with a sculptured conical shaped chamber at the inner side and a cooling water jacket surrounding the chamber. The block had a dimension of 99 mm by 95 mm rectangular bottom and a height of 116 mm. The conically shaped chamber had a dimension of Ø 42 mm top, Ø 13 mm base and 20 mm depth. The furnace had a flue gas outlet and a glass window for temperature measurement. The gas cooling and cleaning system consisting of a cooling coil and particle gas filter were connected to the gas outlet. Photographs of the equipment components and the reactor setup are shown in Plate I. Specifications for TIG master weld and reactor system are shown in Tables 1 and 2 respectively

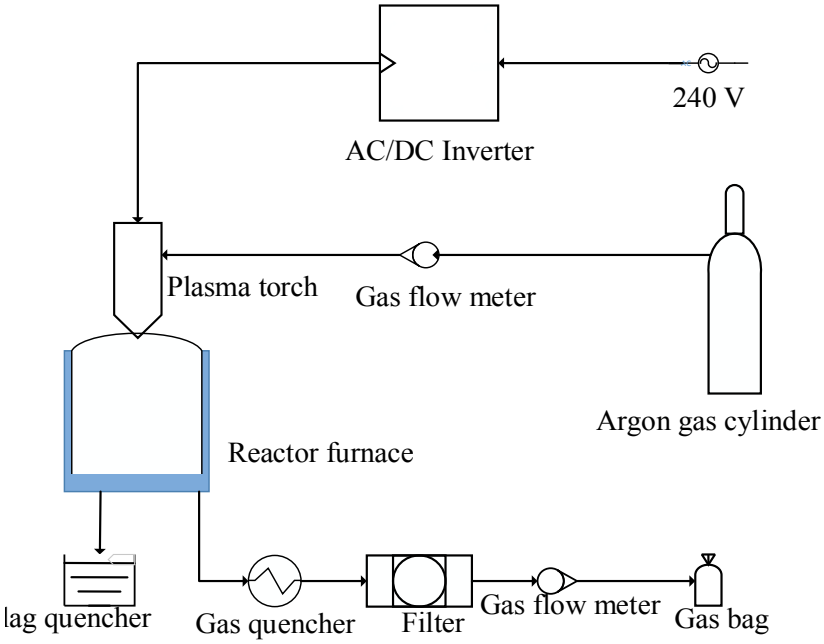

Figure 1: Process flow diagram of the setup for plasma treatment of sludge

Plate I: Photographs of the equipment components and the reactor setup

Table 1: TIG master weld specifications

Specification	Input rating	Output rating
Model	TP – 2000	
Efficiency (%)	80	
Power (kW)	4.7	
Voltage (V)	220/230/240	63
Current (A)	31	5 – 200

2.2. Plasma Treatment of Wastewater Sludge

A current of 100 A and argon flow-rate of 10 L/min were supplied to ignite and generate the arc plasma. The supplied current was increased gradually using a control nob while the plasma temperature was measured at intervals using an infrared thermometer (temperature range of 200 – 2200 ^{o}C). The same procedure was repeated with argon flow-rate of 5 L/min and 15 L/min. The result of temperature measurement is presented in Figure 2. Samples of wet wastewater sludge were treated batch-wise in the thermal arc plasma generated at arc currents of 150, 170 and 190 A respectively. At each of the operating current 20 g of the sludge was treated for 2, 4, 6, 8 and 10 min respectively. The flue gas, after passing through the cooling coil and the particle dust filter, was collected in a Teflon gas bag and analyzed in an offline residual gas analyzer (model: MKS Cirrus 2). The reactor was allowed to cool to room temperature. The slag collected, weighed and analyzed using TOC analyzer (Model SSM-5000A) and AAS machine (model: Perkin Elmer, PinAAcle 900T).

Table 2: Reactor parts and specifications

Reactor furnace: rectangular aluminium block
Dimension: 99 mm by 95 mm bottom, 116 mm height
Reaction chamber: conical shape
Dimension: Ø 42 mm top, Ø 13 mm base and 20 mm depth
Reactor inner volume: 20 cm^3
Cathode: long tungsten rod (98% purity)
Dimension: Ø 2.5 mm and length 150 mm
Anode: tungsten rod (98% purity)
Dimension: Ø 10 mm and length 35 mm

3. RESULT AND DISCUSSION

3.1. Plasma Arc Temperature Profile

The thermal arc plasma ignited at an arc current of 100 A. Bellow 100 A only vibration was observed. At an argon gas flow-rate of 15 L/min, when the plasma arc current was increased from 100 – 190 A, the plasma arc temperature increased from 356 – 1694 ^{o}C. This increase in temperature was not uniform all through. Between 100 – 140 A, the increase in temperature was gradual, from 372 – 627 ^{o}C respectively. However, from 140 – 190 A, the plasma arc temperature increased from 627 – 1694 ^{o}C. This trend of increased plasma arc temperature with increased plasma arc current was equally observed with argon gas flow-rate of 10 and 5 L/min as depicted in Figure2. The plasma temperature also increased when the argon gas flow-rate increased from 5 – 15 L/min.

Previous research by Kim *et al.* (2003) reported a temperature of range of 1520 – 1570 K in a steam plasma used for the treatment of polychlorinated biphenyls (PCBs). Similarly, Tang

and Huang (2005) observed an increased in temperature from 1073 – 1773 K in a high-frequency (HF) plasma reactor used for pyrolysis of waste tyre powder.

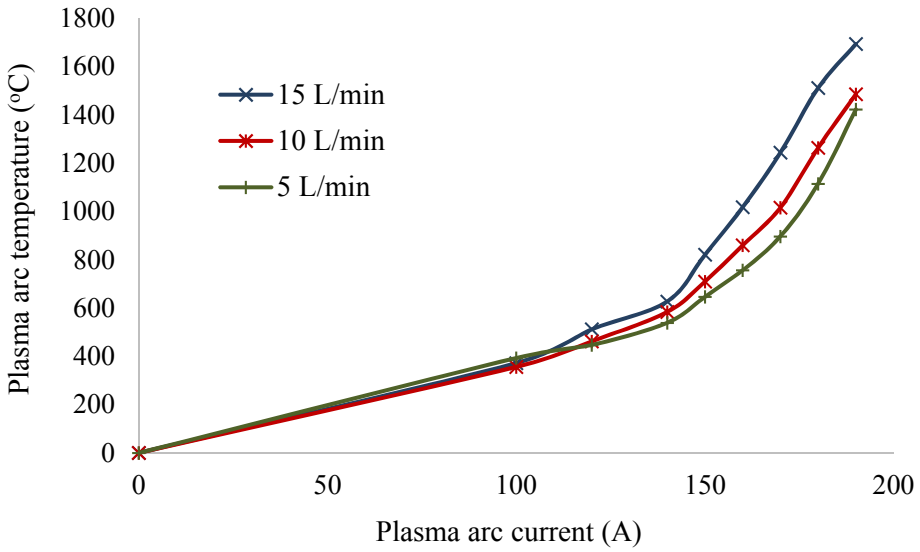

Figure 2: Effect of plasma arc current and gas flow-rate on plasma temperature

3.2. Mass and Volume Reduction

The mass reduction achieved through the thermal plasma treatment of wastewater sludge from the petroleum industry was in the range of 36.87 – 91.40 %. The obtained mass reduction was achieved at a relatively high plasma arc current (150 – 190 A). At 150 – 190 A, the plasma temperature ranges between 539 – 1603 °C. The high-temperature plasma environment decomposed the bulk of the sludge (the organic fraction) leaving behind small fraction (the inorganic) as a byproduct. There is a general increase in the mass reduction of the wastewater sludge with an increase in the plasma treatment duration as shown in Figure3. At a plasma arc current of 190 A, the mass reduction increased from 44.78 – 91.40% when the plasma treatment duration increased from 2 – 10 min. Likewise, at 170 and 150 A, the mass reduction increased with increased plasma treatment duration.

The increase in the mass reduction is associated with the elevated temperature in the thermal plasma regime coupled with the limited amount of oxygen in the reaction chamber. The hydrocarbons in the wastewater sludge were gasified in the reducing environment by the elevated temperature plasma, into flue gases. Thereby, leaving the inorganics and heavy metals in the vitreous slag. The mass reduction was most significant between the 2nd and the 8th min, suggesting that the hydrocarbons were mostly gasified within the first 8 min of treatment. Similarly, mass reduction increased with increasing arc current from 150 – 190 A at an interval of 20 A. At constant applied voltage, the current is proportional to the power. Thus, higher arc current leads to a higher power, which yielded more decomposition of the hydrocarbons.

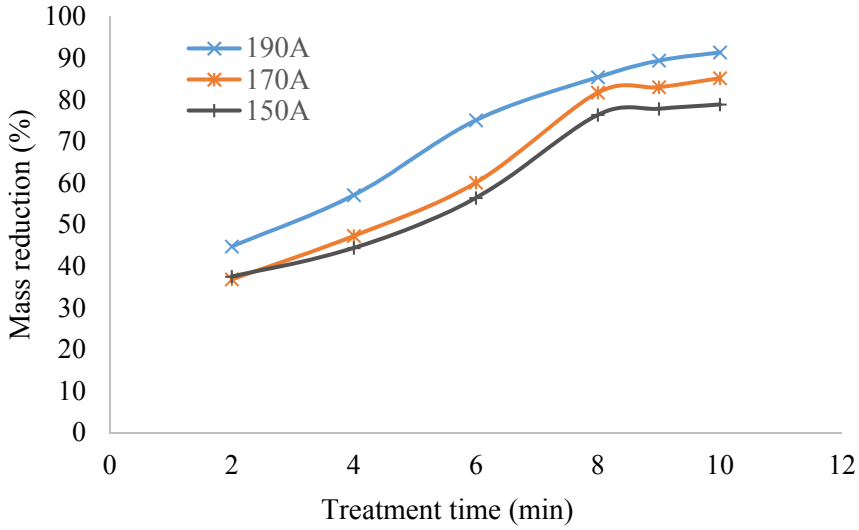

Figure 3: Effect of treatment duration and arc current on mass reduction of sludge

3.3. Total Organic Carbon and Metal Composition

The measurement of the total organic carbon (TOC) in both the wastewater sludge and the product slag was conducted via the Total Organic Carbon-Solid Sample Module (TOC-SSM) machine (Model: SSM-5000A) (Ali *et al.*, 2017). Glucose was used as a standard for total carbon (TC) measurement while sodium carbonate was used as a standard for inorganic carbon (IC) measurement. Finally, TOC was calculated as the difference between the results of the measurements of TC and IC. The effectiveness of the thermal plasma reactor in treating the wastewater sludge was evaluated by determining the percentage carbon conversion using Equation 1. Carbon conversions of 74.03%, 75.83% and 75.86% were achieved with 150, 170 and 190 A respectively as shown in Table 3. These high carbon conversions are evidence of effective gasification of the hydrocarbon in the wastewater sludge by the thermal plasma. A similar result was reported by Li *et al.* (2015a) where a 100% carbon conversion of hydrocarbons was obtained when storm water sludge was treated in an integrated thermal plasma system.

$$Carbon\ conversion(\%) = \left[1 - \frac{TOC\ of\ product\ slag}{TOC\ of\ sludge}\right] \times 100 \qquad (1)$$

Table 3: Carbon conversion achieved in the treated wastewater sludge

Plasma arc current	TOC of sludge (%)	TOC of product slag (%)	Carbon conversion (%)
150	54.48	14.15	74.03
170	54.48	13.17	75.83
190	54.48	13.15	75.86

The metal concentrations in both the raw wastewater sludge and the product slag were determined via acid digestion according to US EPA method 3050 B as reported by Ali *et al.* (2019), the results are shown in Table 4. The metal elements in the wastewater sludge in major quantities were Al, K and Fe. Three other metal elements, Na, Mg and Zn were in small quantities while Cr, Mn, Ag and Hg were in trace quantities. After the thermal plasma treatment, the concentrations

of the metals elements, except K, were significantly increased. The presence of large quantities of hydrocarbons in the wastewater sludge suppressed the concentration of the inorganics. After the gasification of the hydrocarbons, the inorganics became paramount in the products. The reduced concentration in the case of K could be as a result of vapourization of the metal because of its low melting point when compared with the other metals present.

3.4. Flue Gas Analysis

The composition of the flue gas obtained from the plasma treatment of wastewater sludge from the petroleum industry is shown in Table 5. The gas consists of H_2, CO, O_2, CO_2, CH_4 and C_2 hydrocarbons. The CO is the major component accounting for over 74%. At high temperature and in the presence of moisture (H_2O) hydrocarbon was converted to CO through water-gas reaction as shown in Equation 3. The concentration of oxygen in the flue gas is between 15 – 19%. There was the possibility of air getting into the reactor since it was not airtight. Concentrations of greenhouse gases (CO_2 and CH_4 combined) was very low, less than 1%. Even though there may be oxygen in the system, CO_2 was not stable at a temperature above 1400 ^oC and any quantity formed at the beginning of the process, when the temperature was lower than 1400 ^oC, may be converted to CO through Boudouard reaction shown in Equation 4.

$$C + H_2O \leftrightarrow CO + H_2 \quad (3)$$

$$C + CO_2 \leftrightarrow 2CO \quad (4)$$

Table 4: Metal concentrations in the wastewater sludge and the product slag

	Concentration (ppm)	
Metals	**Wastewater sludge**	**Product slag**
Na	21	34.4467
Mg	15.09	27.9125
Al	95.83	193.047
K	183.667	75.2154
Cr	1.6197	2.05181
Mn	0.1372	0.3487
Fe	327	620.989
Zn	12.4	25.5033
Ag	0.4630	0
Hg	1.3908	0.34387

4.0 Conclusion

A laboratory-scale thermal arc plasma reactor was developed to treat 20 g per batch of wastewater sludge from the petroleum industry. The reactor was used to treat petroleum waste-water sludge. Temperature profile inside the plasma reactor increased with an increasing arc current and also with an increasing argon gas flowrate. A mass reduction of between 36.87 – 91.10% was achieved at a plasma temperature of 539 – 1603 ^oC. The mass reduction increased with an increase in the duration of treatment. The mass reduction also increased with an increase in plasma arc current from 150 – 190 A. A TOC reduction of 74.03%, 75.83% and 75.86% was obtained at an arc current of 150, 170 and 190 A respectively. The concentration of metals in the wastewater sludge increased after the plasma treatment. CO is the major component in the flue gas, accounting for over 74%. The concentration of greenhouse gases (CH_4 and CO_2 combined) was less than 1. The thermal plasma reactor gasifies the wastewater sludge from the petroleum

industry into flue gases with slag as a byproduct. The CO richen flue gas can be enriched with hydrogen to produce syngas.

Table 5: Composition of the flue gas

Component	Concentration (mol %)	
	1st run	2nd run
H_2	0.0051	0.0023
N_2	1.1729	1.3976
CH_4	0.5083	0.5125
CO	78.1940	74.5410
C_2^+	0.0195	0.0140
O_2	15.6388	18.6352
Ar	1.9549	1.8635
CO_2	0.0782	0.1398
NO_2	0	0.0056
SO_2	0.0043	0

5.0 Recommendation

Further research should look into the effect of cathode diameter on plasma temperature.

References

Agon, N. (2015). *Development and study of different numerical plasma jet models and experimental study of plasma gasification of waste.* Ghent University.

Ali, A. M.Abu-Hassan, M. A.Ibrahim, R. R. K.Zaini, M. A. A.Abdulkarim, B. I. Hussein, A. S.Su, S. M. and Mohd-Halim, M. I. (2017). Characterization of Petroleum Sludge from Refinery Industry Biological Wastewater Treatment Unit. *The International Journal of Engineering and Science (IJES), 6*(9), 61 - 65. doi: 10.9790/1813-0609016165

Ali, A. M.Abu Hassan, M. A. and Abdulkarim, B. I. (2016). Thermal Plasma: A Technology for Efficient Treatment of Industrial and Wastewater Sludge. *IOSR Journal of Environmental Science, Toxicology and Food Technology (IOSR-JESTFT), 10*(11), 63 - 75. doi: 10.9790/2402-1011046375

Ali, A. M.Abu Hassan, M. A.Ibrahim, R. R. K.Jalil, A. A.Mat Nayan, N. H.Abdulkarim, B. I. and Sabeen, A. H. (2019). Analysis of Solid residue and Flue Gas from Thermal Plasma Treatment of Petroleum Sludge. *Journal of Environmental Chemical Engineering, 7*(4), 103207. doi: https://doi.org/10.1016/j.jece.2019.103207

Barcza, N. (1986). The development of large-scale thermal-plasma systems. *J. S. Afr. Inst. Min. Metall., 86*(8), 317-333.

Bień, J.Celary, P.Morzyk, B.Sobik-Szołtysek, J. and Wystalska, K. (2013). Effect of Additives on Heavy Metal Immobilization During Vitrification of Tannery Sewage Sludge. *Environment Protection Engineering, 39*(2). doi: 10.5277/EPE130204

Celary, P. and Sobik-Szołtysek, J. (2014). Vitrification as an alternative to landfilling of tannery sewage sludge. *Waste Management, 34*(12), 2520-2527. doi: http://dx.doi.org/10.1016/j.wasman.2014.08.022

Cortez, R.Zaghloul, H. H.Stephenson, L. D.Smith, E. D.Wood, J. W. and Cahil, D. G. (1996). Laboratory scale thermal plasma arc vitrification studies of heavy metal-laden waste. *Journal of the Air and Waste Management Association, 46*(11), 1075-1080.

Cubas, A. L. V.Carasek, E.Debacher, N. A. and De-Souza, I. G. (2005). Development of a DC-Plasma Torch Constructed with Graphite Electrodes and an Integrated Nebulization System for Decomposition of CCl4. *J. Braz. Chem. Soc., 16*(3B), 531-534.

Cubas, A. L. V.Machado, M. D.-M.Machado, M. D.-M.Gross, F.Magnago, R. F.Moecke, E. H. S. and De-Souza, I. G. (2014). Inertization of Heavy Metals Present in Galvanic Sludge by DC Thermal Plasma. *Environmental science and technology, 48*(5), 2853-2861. doi: 10.1021/es404296x

Diya'uddeen, B. H.Wan-Daud, W. M. A. and Abdul-Aziz, A. R. (2011). Treatment technologies for petroleum refinery effluents: a review. *Process Safety and Environmental Protection, 89*(2), 95-105.

Heberlein, J. (2002). New approaches in thermal plasma technology. *Pure and Applied Chemistry, 74*(3), 327-335.

Heberlein, J. and Murphy, A. B. (2008). Topical review: Thermal plasma waste treatment. *Journal of Physics D: Applied Physics, 41*, 1-20. doi: 10.1088/0022-3727/41/5/053001

Khongkrapan, P.Thanompongchart, P.Tippayawong, N. and Kiatsiriroat, T. (2013). Fuel gas and char from pyrolysis of waste paper in a microwave plasma reactor. *International Journal of Energy And Environment, 4*(6), 969 - 974.

Kim, H. and Park, D. (2004). Characteristics of Fly Ash/Sludge Slags Vitrified by Thermal Plasma. *J. Ind. Eng. Chem., 10*(2), 234-238.

Kim, S. W.Park, H. S. and Kim, H. J. (2003). 100 kW steam plasma process for treatment of PCBs (polychlorinated biphenyls) waste. *Vacuum, 70*(1), 59-66. doi: http://dx.doi.org/10.1016/S0042-207X(02)00761-3

Kourti, I.Devaraj, A. R.Butos, A. G.Deegan, D.Boccaccini, A. R. and Cheeseman, C. R. (2011). Geopolymers prepared from DC plasma treated air pollution control (APC) residues glass: Properties and characterisation of the binder phase. *Journal of Hazardous Materials, 196*, 86-92. doi: http://dx.doi.org/10.1016/j.jhazmat.2011.08.081

Leal-Quirós, E. and Villafañe, C. R. (2007). An Assessment of the Power Generated With Plasma Processing of Sludge From Wastewater Treatment Plants. *IEEE Transactions On Plasma Science, 35*(6), 1622 - 1627.

Li, C.Lee, W.Huang, K.Fu, S. and Lai, Y. (2007). Vitrification of Chromium Electroplating Sludge. *Environmental science and technology, 41*(8), 2950-2956. doi: 10.1021/es062803d

Li, O. L.Guo, Y.Chang, J. S.Urashima, K. and Saito, N. (2012). Treatment of Non-point Sources by a Thermal Plasma System Under DC Partial Transferred Mode. *International Journal of Plasma Environmental Science and Technology, 6*(1), 63 - 67.

Li, O. L.Guo, Y.Chang, J. S.Urashima, K. and Saito, N. (2015a). A new approach of nonpoint source pollution/stormwater sludge treatment by an integrated thermal plasma system. *International Journal of Environmental Science and Technology, 12*(5), 1769-1778. doi: 10.1007/s13762-014-0570-7

Li, O. L.Guo, Y.J.S., C. and Saito, N. (2015b). Thermal plasma treatment of stormwater sediments: comparison between DC nontransferred and partially transferred arc plasma. *Environ Technol, 36*(13), 1672-1679.

Mohai, I. and Szépvölgyi, J. (2005). Treatment of particulate metallurgical wastes in thermal plasmas. *Chemical Engineering and Processing, 44*, 225-229.

Mountouris, A.Voutsas, E. and Tassios, D. (2008). Plasma gasification of sewage sludge: Process development and energy optimization. *Energy Conversion and Management, 49*(8), 2264-2271. doi: http://dx.doi.org/10.1016/j.enconman.2008.01.025

Punčochář, M.Ruj, B. and Chatterj, P. K. (2012). Development of Process for Disposal of Plastic Waste Using Plasma Pyrolysis Technology and Option for Energy Recovery. *Procedia Engineering, 42*, 420-430. doi: http://dx.doi.org/10.1016/j.proeng.2012.07.433

Ramachandran, K. and Kikukawa, N. (2002). Thermal Plasma In-Flight Treatment of Electroplating Sludge. *IEEE Transactions On Plasma Science, 30*(1), 310-317.

Shie, J.Liau, Y.Lin, K. and Chang, C. (2014). *Thermal Treatment of Paper Sludge Using Torch Plasma.* Paper presented at the 2014 4th International Conference on Future Environment and Energy, IACSIT Press, Singapore.

Sobiecka, E. and Szymanski, L. (2014). Thermal plasma vitrification process as an effective technology for fly ash and chromium-rich sewage sludge utilization. *Journal of Chemical Technology and Biotechnology, 89*(7), 1115-1117. doi: 10.1002/jctb.4221

Szałatkiewicz, J.Szewczyk, R.Budny, E.Missala, T. and Winiarski, W. (2012). Determination of PID control parameters of plasmatron plasma reactor. *Journal of Applied Computer Science Methods, 4*(2), 31--39.

Szałatkiewicz, J.Szewczyk, R.Budny, E.Missala, T. and Winiarski, W. (2013). Construction Aspects of Plasma Based Technology for Waste of Electrical and Electronic Equipment (WEEE) Management in Urban Areas. *Procedia Engineering, 57*(Supplement C), 1100-1108. doi: https://doi.org/10.1016/j.proeng.2013.04.139

Tang, L. and Huang, H. (2005). Treatment of Waste Tyre Powder Using a High-frequency Capacitively Coupled Plasma Reactor. *Chinese Journal of Process Engineering, 5*(3), 295-300.

Tang, L.Huang, H.Zhao, Z.Wu, C. Z. and Chen, Y. (2003). Pyrolysis of Polypropylene in a Nitrogen Plasma Reactor. *Ind. Eng. Chem. Res., 42*, 1145-1150.

Tippayawong, N. and Khongkrapan, p. (2009). Development of a laboratory scale air plasma torch and its application to electronic waste treatment. *Int. J. Environ. Sci. Tech., 6*(3), 407-414.

Townsend, T. and Oehmig, W. (2014). *Development of a Bench-Scale Plasma Arc Vitrification Unit and the Exploration of Element Behavior in High Temperature Plasma Vitrification.* (PhD), University of Florida, Hinkley Center for Solid and Hazardous Waste Management. (Report # 81839)

Tu, W. a.Shie, J. L.Chang, C. Y.Chang, C. F.Lin, C. F.Yang, S. Y.Kuo, J. T.Shaw, D. G. and Lee, D. J. (2008). Pyrolysis of Rice Straw Using Radio-Frequency Plasma. *Energy and Fuels, 22*(1), 24-30. doi: 10.1021/ef7002848

Zhao, Z.Huang, H.Wu, C.Li, H. and Chen, Y. (2001). Biomass Pyrolysis in an Argon/Hydrogen Plasma Reactor. *Eng. Life Sci., 1*(5), 197 - 199.

Proceedings of the 49th NSChE Annual Conference
KADA 2019: pp 93-99

P1B-02: SYNTHESIS, CHARACTERIZATION, AND APPLICATION OF KAOLIN-BASED ZSM-5 ZEOLITE FOR WATER DESALINATION.

Aliyu, Usman Mohammed*, Sudesh Rathilal, and Yusuf Makarfi Isa
Chemical Engineering, Durban University of Technology, P.O. Box 1334, Durban 4000, South Africa.
***Corresponding author**: usmanaliyumohammed@gmail.com

ABSTRACT
ZSM-5 was produced after the metakaolinization of South African clay and the use of NaOH, TPABr, $Na_2SiO_3.9H_2O$ solution and deionized water with a molar composition of $50SiO_2 : Al_2O_3 : 20Na_2O : 2TPABr: 2000H_2O$. The synthesized product was characterized by XRD, SEM, TGA and BET surface area. The characterization results confirmed that the sample produced was of ZSM-5 phase. The product has a specific surface area, pore size and pore volume of 179.9 m^2/g, 49.262A and 0.05 cm^3/g respectively. The effect of zeolite dosage, (1.0, 2.5, 4.0, and 6.0g) on salinity reduction of seawater was investigated via adsorption study. The result revealed that effectiveness salinity (ES) increases with the increase of the sorbent dose. At 1.0g dose, the salt removal value is 1.04 ppt (SR) which is 3.64% effectiveness salt removal. At ZSM-5 dose of 2.5, 4.0, and 6.0 g, the SR values are 3.29, 6.46, and 8.12 ppt which correspond with ES value of 9.40, 18.40, and 23.20%. ZSM-5 zeolite synthesized from kaolin of South African origin has shown great prospect as natural abundant sorbent material for desalination of synthetic seawater.

Introduction
Global water shortage has progressively become a great opposition to human exploit, agricultural growth and industrial activities (Zhu *et al.*, 2016). Availability of potable water is vital for human needs and it scarce is threatened in many areas across the globe more especially in developing countries and arid regions (Shannon *et al.*, 2008; Zhao *et al.*, 2014). Oceans and seas water comprises of more than 71% of earth surface and 97% of it is saline and cannot be used as potable water, industries as well as agricultural purposes (Von-kiti, 2012). To curb and subdue this salinity problem and ensure the accessibility of freshwater a right strategy has to be adapted. South Africa is located between two great oceans, Atlantic and Indian and water crisis is usually emanating in some part of Cape Town province. Therefore, seawater desalination is a choice and potential technology to subjugate the water crisis in the future (Wibowo *et al.*, 2017).

Desalination of seawater is a process whereby dissolved salts and minerals are removed to produce fresh potable water (Zhao *et al.*, 2013; Wang *et al.*, 2016; Wenten *et al.*, 2016). Nowadays, there are many types of seawater desalination technology – including RO (Greenlee *et al.*, 2009) and thermal processes like multi-effect distillation (MED) (Abu-Zeid *et al.*, 2015), membrane vacuum distillation (MVC) (Pérez-González *et al.*, 2012) and multi-stage flash distillation (MSF) (Khawaji *et al.*, 2008). These processes produce potable water but the technology is expensive to operate, so a cheaper way of alternative methods cannot be overemphasis.

Sorption is a process in which one substance takes up or holds another by either absorption or adsorption. Sorption technique is the potential presume process for seawater desalination. Sorption technology is coherence and highly productive with a varied range of materials which influence its potentiality and less expensive method of desalination of seawater (Wibowo *et al.*, 2017). The adsorption process is considered as the most sufficient technology for desalination of

seawater environmentally and economically. Many sorbent materials such as eggshell, fly ash and clay mineral (Aliyu *et al.*, 2017) and natural zeolites were applied to treat saline water (Wibowo *et al.*, 2017). Kaolin-based zeolite is appraised as cheap and abundant sorbent material (Lijalem Ayele Regassa, 2016). In this study, kaolin-based zeolite was synthesized and applied as an absorbent for the desalination of seawater. The salinity reduction (RS) and the effectiveness of salinity reduction (ES) of seawater after treatment were determined and the effect of the seawater on salinity reduction with an increase of zeolite dosage was evaluated.

Materials and methods.

As received kaolin from GandW minerals resources located in the Western Cape region of South Africa was calcined at 650℃ for 2h with Si/Al ratio 2.91 applied as a source of silica and alumina (66.58% SiO_2 and 22.81 % Al_2O_3 respectively). Seawater solution (0.35 w%) used for the adsorption studies were prepared from analytical seawater (Na, K, Ca, and Mg) salts from Sigma-Aldrich. Sodium silicate 26.5% SiO_2 and 10.6% Al_2O_3 composition solution and TPABr. All the chemicals were purchased from Sigma Aldrich except Nitric acid 55% which is sourced from Ace enterprises chemical association. The chemicals were applied as received with no additional purification.

Synthesis of kaolin-based ZSM-5 zeolite.

In the preparation of kaolin-based ZSM-5, the required amount of GandW metakaolin and sodium hydroxide were dissolved in deionized (DI) water and TPABr were also mixed separately with the required amount of DI water. The solution of NaOH/Kaolin and sodium silicate solution were added simultaneously to the solution of the TPABr while stirring. Nitric acid was used to control the pH until the solution mixture is homogenous. The synthesized gel was transferred to stainless steel Teflon lined autoclave cup and was hydrothermally treated at 180℃ for two days. The resulting product was washed with DI until the pH is less than 8. The sample was dried overnight at 80℃ and calcined for 5 hours at 550℃. The resulting powder was characterized.

Characterization.

X-ray diffraction (XRD) patterns and average crystallite size were collected with Bruker AXS, D8 Advance equipped with Tube (Cu-Ka radiation (lKa_1=1.5406Å) and Detectors Lynx Eye (Position sensitive detector) at 40kV, 40mA and V20 variable slit. The measurements were carried out with a step width of 0.5° to 130° 2θ with an increment (Δ2θ of 0.034° and a scan rate of 0.5 sec per step. The diffraction data were analyzed using OriginPro 2018 software to give the estimation of the amount of each phase in the sample. The morphology was characterized by using scanning electron microscopy FEI Nova NanoSEM 230 with a field emission gun equipped with a high-resolution immersion lens. The EDS detector is an Oxford X-Max, using INCA software. Surface area, pore size, and pore volume measurements and analysis were determined by BET machine. Thermal analysis was done using thermogravimetric analyzer/differential scanning calorimetry (TGA/DSC 1) STAR System Mettle Toledo.

Adsorbate and Batch Adsorption studies

The adsorption of Na, Ca, K and Mg from the synthetic seawater containing NaCl, $CaCl_2$, KCl, and $MgSO_4$ with an average salinity of 35g/L or 35,000mg/L were conducted in the laboratory using linear shaker 262 apparatus experiment. The experimental runs were conducted by dispersing a required amount of kaolin-based ZSM-5 into a 100mL synthetic seawater solution. The sorbent material (kaolin-based ZSM-5) dosage was varied at 1, 2.5, 4.0, and 6.0g and dispersed in the seawater sample using a linear shaker apparatus for 180 min at room temperature and 7.8 pH in

order to determine the optimum dosage and salt reduction. The adsorbent was filtered out with Whitman filter paper No. 5 after each run and the salinity of the water after adsorption was estimated by **YSI** Pro Plus Multi-Parameter Water Quality Meter. The effectiveness of salt removal (*ES*), salt removal (*SR*), and adsorbent dosage was analyzed.

From a study by the school of ocean science and technology in 2015, Table 1 shows the major salt ions found in seawater of salinity 35g/L and their respective percentage total and mass concentrations. Chlorine (Cl^-) has the highest percentage of 55.29% and 19.353gms/kg while potassium (K^+) has the least with 1.14% and 0.399gms/kg. other ions in descending order of percentage total and concentrations are sodium (Na^+): 30.74% and 10.76gms/kg, Sulphate (SO_4^{2-}): 17.75% and 2.712gms/kg, Magnesium (Mg^{2+}): 3.69% and 1.292gms/kg, Calcium (Ca^{2+}): 1.18% and 0.412gms/kg.

Table 1. Major ions in seawater of salinity 35g/L

Symbol	Name	% of total	mmoles	gms/kg
CL^-	Chlorine	55.29	546	19.353
Na^+	Sodium	30.74	469	10.76
Mg_{2+}	Magnesium	3.69	53	1.292
SO_4^{2-}	Sulphate	7.75	28	2.712
Ca_{2+}	Calcium	1.18	10.3	0.412
K^+	Potassium	1.14	10.2	0.399

(School of Ocean Science and Technology, 2015).

The amount of salt ion adsorbed (RS) at equilibrium was evaluated by

$$RS = c_i - c_e \qquad 1.$$

Where C_i and C_e are initial and equilibrium adsorbate concentration respectively. The percentage of salt ions removal (%ES) was evaluated using.

$$\%\, ES = \frac{Ci - Ce}{Ci} * 100 \qquad 2.$$

Results and Discussion

X-ray diffraction (XRD) studies

The XRD pattern of ZSM-5 crystalline at 180℃ for 2days using metakaolin that calcined at 650℃ for 2hour is shown in Figure (1a). The characteristic peaks of ZSM-5 in the ranges of 7.9 to 23.1° 2θ which show nucleation with a sizable amount of quartz as an impurity at 20.9 and 26.6° 2θ clearly confirmed the formation of crystalline ZSM-5 phase (Salou *et al.*, 2001; Mohiuddin *et al.*, 2016). The percentage (%) crystallinity and the average crystal (grain) size was evaluated using OriginPro 2018 version and found to be 87% crystallinity and 28 nm respectively The two parameters are key to the sorption process. The specific surface area, pore size and pore volume of 179.9 m^2/g, 49.262A and 0.05 cm^3/g respectively were deduced using BET surface area analyzer. The crystal size of the sorbent rises the specific surface area and intense surface porosity increases the outer surface area of the zeolite (Wibowo *et al.*, 2017). The incorporation of the two parameters together influences the effective surface area. This shows that synthesized

kaolin-based ZSM-5 with a good surface area would promote high sorption potential and proficiency. Consequently, it will be applied as a sorbent medium in seawater desalination.

Scanning electron microscopy (S.E.M.) studies

SEM is a technique used to interpret the morphology and distribution of crystals size of the zeolite phase. Typically, the configuration, formation, and structure of ZSM-5 crystals were highly controlled and depend on synthesis parameters such as crystallization temperature, time and aging. Mohiuddin 2015, conducted a study on the synthesis of ZSM-5 using impure kaolin under various parameters resulting in different morphologies. The image of kaolin-based ZSM-5 nanocrystals synthesized under 180℃ temperature for 2 days' crystallization time and 2 days aging were performed in this study Figure 1(b). It can be seen clearly that the kaolin-based ZSM-5 is obviously orthogonal shape and highly crystallized with an average crystals size of 28 nm indicated that there is an intergrown crystal with some amorphous material clearly observed. The orthogonal nanocrystals are as a result of the aggregation of their high surface Gibbs free energy (Wu *et al.*, 2013). The TGA results depicted in Figure 1(c). show the stability of the synthesized kaolin-based ZSM-5. The graph demonstrated that water and other volatile material are removed from the sample at around 45 to 180℃ and the material became stable through the ranges of temperature until it is about 950°C from where phase change was noticed as it's approaching its a melting point which is 1000°C and above.

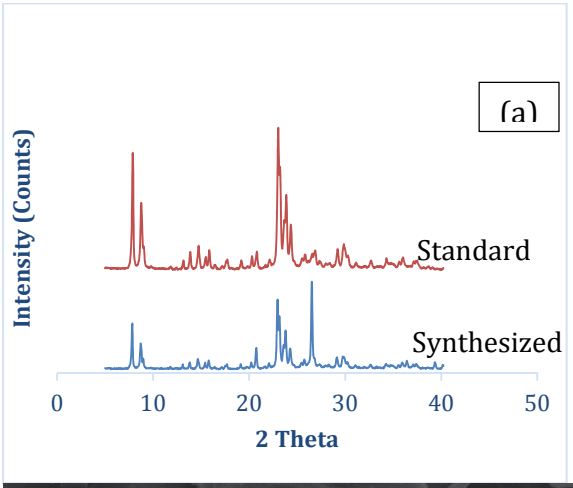

(b)

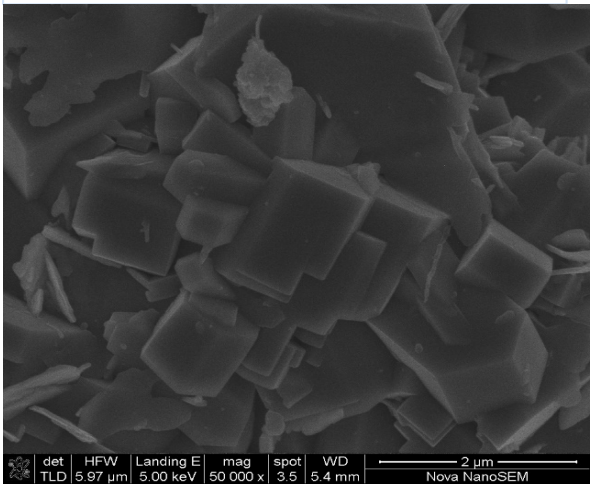

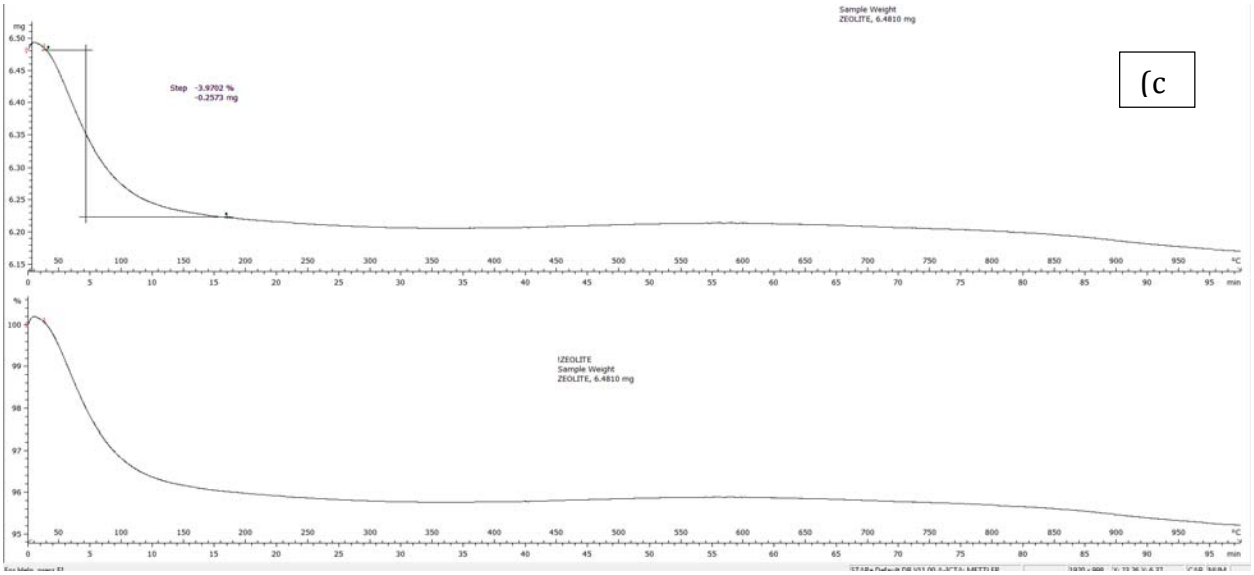

Figure 1(a). XRD pattern of standard and kaolin-based ZSM-5 zeolite and (b). SEM image of synthesized kaolin-based ZSM-5 zeolite (c)TGA of the synthesized kaolin-based ZSM-5.

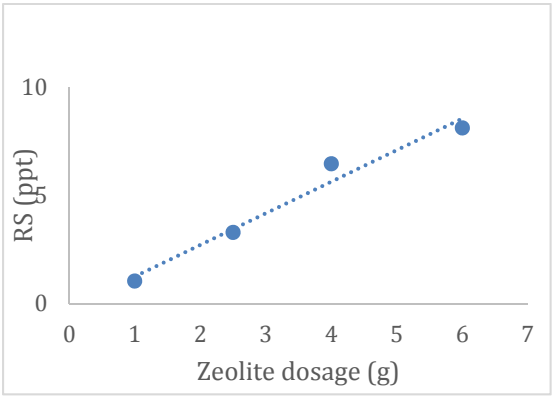

Figure 2. Salinity reduction with an increase of zeolite dosage.

Effect of Adsorbent Dosage.

The effect of adsorbent dose on the adsorption of salt from seawater onto kaolin-based ZSM-5 zeolite revealed that the seawater was desalinated and there is a reduction of salinity after treatment. The salinity reduction (effectiveness) rises with an increase in an adsorbent dose which shows that the adsorption sites are capable of absorbing more salt ions. By increasing the adsorbent dose, the sorption active area is adequately accessible for the adsorbate to utilize. The effectiveness of the adjusted ZSM-5 zeolite dosage for the desalination process is depicted in Figure 1. We applied different zeolite dosage of 1.0, 2.5, 4.0, and 6.0g to investigate the salinity reduction of seawater after treatment with the different dosage of the adsorbent. At 1.0g dose, the salt removal effectiveness value is 1.04 ppt which is 3.64% salt removal (SR). At ZSM-5 dose of 2.5, 4.0, and 6.0 g, the ES values are 3.29, 6.46, and 8.12 ppt which correspond with RS value of 9.40, 18.40, and 23.20%. However, It was reported by Mekonnen et al (2015) that adsorption of Cr(iv) onto some selected adsorbents that, adsorbent dose above the equilibrium stage does not ameliorate adsorption due to the accessibility of surplus adsorption sites than that of sorbent

considering that the adsorption sites per unit mass of adsorbent remain constant. They reported that with an increase in sorbent dosage, removal is increasing exponentially rather than linearly. The behavior of kaolin-based ZSM-5 presents a different tendency. This shows that the desalination of seawater using synthesized ZSM-5 is a function of sorbent dosage. The interaction of seawater-ZSM-5 reveals that desalination can be better as the sorbent dose increases. Therefore, it can be concluded that the behavior of sorbent is a result of sorbate-sorbent interaction. This implies that each sorption materials have a different characteristic reaction (Wibowo *et al.*, 2017)

Conclusion

Kaolin-base ZSM-5 from South African local kaolin with specific surface area, pore size and pore volume of 179.9 m^2/g, 49.262A and 0.05 cm^3/g respectively were successfully synthesized and applied as sorbent material to desalinate synthetic seawater. The values of *RS* are found to increase as dosage increases 1.0, 2.5, 4.0, and 6.0 as 1.04, 3.29, 6.40, and 8.12 ppt respectively. whereas *ES* values are 3.64, 9.40, 18.40, and 23.20 % at 1.0, 2.5, 4.0, and 6.0 g. ZSM-5 zeolite synthesized from kaolin of South African origin has shown great prospect as low-cost sorbent material for desalination of synthetic seawater.

Acknowledgment: The authors wish to appreciate and acknowledged the financial support from Umgeni water, Durban, KZN South Africa and the Durban University of Technology.

References

Abu-Zeid, M. A. E. R., Zhang, Y., Dong, H., Zhang, L., Chen, H. L. and Hou, L. 2015 A comprehensive review of vacuum membrane distillation technique, *Desalination*. Elsevier B.V., **356**, pp. 1–14. doi: 10.1016/j.desal.2014.10.033.

Aliyu, A., Abdulkareem, A., Kovo, A., Abubakre, O., Tijani, J. and Kariim, I. 2017 Synthesize multi-walled carbon nanotubes via catalytic chemical vapour deposition method on Fe-Ni bimetallic catalyst supported on kaolin, *Carbon letters*, **21**, pp. 33–50. doi: 10.5714/CL.2017.21.033.

Greenlee, L. F., Lawler, D. F., Freeman, B. D., Marrot, B. and Moulin, P. 2009 Reverse osmosis desalination: Water sources, technology, and today's challenges, *Water Research*. Elsevier Ltd, **43**(9), pp. 2317–2348. doi: 10.1016/j.watres.2009.03.010.

Khawaji, A. D., Kutubkhanah, I. K. and Wie, J. M. 2008 Advances in seawater desalination technologies, *Desalination*, **221**(1–3), pp. 47–69. doi: 10.1016/j.desal.2007.01.067.

Lijalem Ayele Regassa 2016 Synthesis and Characterization of Zeolite A from Kaolin of Ethiopia : Studies of its application as a detergent builder and in tannery wastewater treatment Lijalem Ayele Regassa A Thesis Submitted to Department of Chemistry Presented in Fulfillment of the R.

Mekonnen, E., Yitbarek, M. and Soreta, T. R. 2015 Kinetic and Thermodynamic Studies of the Adsorption of Cr (VI) onto Some Selected Local Adsorbents, *South African Journal of Chemistry*, **68**, pp. 45–52. doi: 10.17159/0379-4350/2015/v68a7.

Mohiuddin, E., Isa, Y. M., Mdleleni, M. M., Sincadu, N., Key, D. and Tshabalala, T. 2016 Synthesis of ZSM-5 from impure and beneficiated Grahamstown kaolin: Effect of kaolinite content, crystallization temperatures and time, *Applied Clay Science*, **119**(November), pp. 213–221. doi: 10.1016/j.clay.2015.10.008.

Pérez-González, A., Urtiaga, A. M., Ibáñez, R. and Ortiz, I. 2012 State of the art and review on the treatment technologies of water reverse osmosis concentrate, *Water Research*, **46**(2), pp. 267–283. doi: 10.1016/j.watres.2011.10.046.

Salou, M., Kooli, F., Kiyozumi, Y. and Mikamizu, F. 2001 Effect of aluminum source and content

on the synthesis of zeolite ZSM-5 from kanemite solid-state transformation, *Journal of Materials Chemistry*, **11**(5), pp. 1476–1481. doi: 10.1039/b008126o.

School of Ocean Science and Technology 2015 Chemical composition of seawater, *Chemical Oceanography*, p. 26. Available at: http://www.soest.hawaii.edu/oceanography/courses/OCN623/Spring2012/Salinity2012web.pdf.

Shannon, M. A., Bohn, P. W., Elimelech, M., Georgiadis, J. G., Marinas, B. J. and Mayes, A. M. 2008 Science and technology for water purification in the coming decades, *Nature (London, U. K.)*, **452**(March), pp. 301–310. doi: 10.1038/nature06599.

Von-kiti, E. 2012 *SYNTHESIS OF ZEOLITES AND THEIR APPLICATION TO THE*, *Msc.thesis Knust*.

Wang, Q., Li, N., Bolto, B., Hoang, M. and Xie, Z. 2016 Desalination by pervaporation: A review, *Desalination*, **387**, pp. 46–60. doi: 10.1016/j.desal.2016.02.036.

Wenten, I. G. and Khoiruddin 2016 Reverse osmosis applications: Prospect and challenges, *Desalination*. Elsevier B.V., **391**, pp. 112–125. doi: 10.1016/j.desal.2015.12.011.

Wibowo, E., Sutisna, Rokhmat, M., Murniati, R., Khairurrijal and Abdullah, M. 2017 Utilization of Natural Zeolite as Sorbent Material for Seawater Desalination, *Procedia Engineering*. The Author(s), **170**, pp. 8–13. doi: 10.1016/j.proeng.2017.03.002.

Wu, G., Wu, W., Wang, X., Zan, W., Wang, W. and Li, C. 2013 Nanosized ZSM-5 zeolites: Seed-induced synthesis and the relation between the physicochemical properties and the catalytic performance in the alkylation of naphthalene, *Microporous and Mesoporous Materials*. Elsevier Inc., **180**, pp. 187–195. doi: 10.1016/j.micromeso.2012.11.011.

Zhao, L., Chang, P. C. Y. and Ho, W. S. W. 2013 High-flux reverse osmosis membranes incorporated with hydrophilic additives for brackish water desalination, *Desalination*. Elsevier B.V., **308**, pp. 225–232. doi: 10.1016/j.desal.2012.07.020.

Zhao, L. and Ho, W. S. W. 2014 Novel reverse osmosis membranes incorporated with a hydrophilic additive for seawater desalination, *Journal of Membrane Science*. Elsevier, **455**, pp. 44–54. doi: 10.1016/j.memsci.2013.12.066.

Zhu, Y., Gupta, K. M., Liu, Q., Jiang, J., Caro, J. and Huang, A. 2016 Synthesis and seawater desalination of molecular sieving zeolitic imidazolate framework membranes, *Desalination*. Elsevier B.V., **385**, pp. 75–82. doi: 10.1016/j.desal.2016.02.005.

Proceedings of the 49th NSChE Annual Conference
KADA 2019: pp 100-106

P1B-03: THERMAL STABILITY OF WATER SOLUBLE BIO-POLYMERS

Eiroboyi, I.[a]*; Ikiensikimama, S. S.[b]; Oriji, B. A.[c]; Okoye, I.P.[d]
[a]World Bank Africa Centre of Excellence, University of Portharcourt, Rivers State
[b,c]Department of Petroleum Engineering, University of Portharcourt, Rivers State
[d]Department of Pure and Industrial Chemistry, University of Portharcourt, Rivers State
*__Corresponding author__: ebitoh@yahoo.com

ABSTRACT
The work studies the thermal stability of some biopolymers (Xanthan gum, Guar gum, Carob bean gum, Gum Arabic and locally sourced Carob bean gum) to ascertain their degree of stability for use in polymer flooding. It was done by analysing the rheology prior to thermal analysis, then the polymers were subjected to varying degree of temperature from 50 °C to 150 °C to ascertain their stability at high temperatures, after which a final rheological characterisation was done on the polymers. Some of the polymers showed increased stability between 80 °C to 90 °C over the commercial Xanthan gum with a thermal stability at 70 °C used in the industry for polymer flooding.

Keywords: Polymer, Xanthan gum, HPAM, temperature, viscosity, LBG

INTRODUCTION
Naturally derived polymers like Xanthan gum, Guar gum and also synthetic polymers like the partially Hydrolyzed polyacrylamide (HPAM) have been used mostly for the purpose of increasing the viscosity of water while reducing the mobility of water for polymer flooding. Most synthetic polymers like partially hydrolyzed polyacrylamide (HPAM) and its derivatives have been used widely for most large-scale field application basically because it is less costly (Chang, 2011). HPAM is mostly used than xanthan gum because of its low-price, good solubility in water and viscous properties (Changhong, 2014).

However, results from field applications showed that the viscosity of Polyacrylamide (PAM) decreased rapidly with increase in water salinity. Nevertheless, shear degradation at the wellhead chokes results in 25 to 50% loss in polymer viscosity (Morel et al. 2008). Also, field application have shown that PAM and HPAM have poor shear resistance (Martin, 1984) this is due to the fact that polymer molecular chain breaks invariably reducing the polymer viscosity when polymer solution passes through the pump, pipeline as well as perforations at high speed. Also, thermal degradation is another form of degradation that can affect polymers under the influence of high temperature, polymers tend to lose their viscosity under increasing temperature as such it can affect their ultimate recovery..

Another issue with the use of HPAM in produced water (back produced water) after polymer flooding in oil and gas industry includes difficulty in oil - water separation; the treatment of back produced water from polymer flooding (PWPF) is much difficult to separate than oily wastewater without HPAM (Zhang, 2010; Bao, 2010; Deng, 2002) because the HPAM residual component dissolved in water increases the viscosity of wastewater making it difficult to attain an effective separation (Duan, 2014). Furthermore, the HPAM in the wastewater can degrade naturally into toxic acrylamide monomers can endanger human and the environment.

However, Xanthan gum, a commercial biopolymer shows excellent viscosifying ability, high tolerance to salinity and temperature (Guo X., 1999), Also, good shear stability and great ability to thicken at high salinity are major advantages of Xanthan gum over HPAM (Sun, 2012). Shear thinning in xanthan gum recovers rapidly once the shearing force is removed. The major disadvantages of this biopolymer are its high cost and difficulty in preparing uniform solutions such that it does not plug the pores within the reservoir. The occurrence of pore plugging can be avoided by using good quality water and filtration of the polymer solution before injection that is the use of microfilters (Chang, 1978). Micro-filtration is one method of conditioning; Enzyme clarification and diatomaceous earth (DE) filtration are usually implemented for treatment process of polymer solutions prior to flooding. Xanthan gum is a biopolymer released by the micro-organism *Xanthomonas campestris*, which is manufactured commercially by the fermentation process. The molecular weight distribution ranges from 2 x 10^6 to 20 x 10^6 Da. (Casas, 2000). Xanthan gum is a heteropolysaccharide with a structure consisting of repeated pentasaccharide units formed by two glucose units, two mannose units, and one glucuronic. acid unit (Garcia-Ochoa, 2000). Aqueous solutions of xanthan gum are very viscous owing to the existence of double helix and triple helix structure of the polymer chain with polar side chains that promote extensive hydrogen bonds (Chatterji, 1981). Xanthan exhibits high viscosity at a low shear force.

Guar gum is derived as extracts from the seed of the guar plant (*Cyamopsis tetragonolobus).* Grinding the endosperm of the guar bean produces relatively pure guar gum. The backbone of the polymer is composed of mannose and galactose units as known as the "galactomannan." There are no ions in the polymer structure; thus, the polymer is termed "non-ionic". Guar solutions have almost a constant viscosity over pH range of about 1.0-10.5. This stability is believed to be due to non-ionic, uncharged nature of the molecule. (Chatterji, 1981).

Carob (locust) bean gum (LBG) is mainly consisting of the high molecular weight approximately from 50,000-3,000,000 Daltons. The polysaccharides is composed of galactomannans and is obtained from the endosperm of the seed of the carob (locust) tree also known as Ceratonia siliqua. The gum is a white to yellowish, nearly odourless powder. Carob bean gum is insoluble in most organic solvents for example ethanol. It is partially soluble in water at ambient temperature and soluble in hot water. Carob bean gum typically needs heating to above 85°C for complete solubility (Chatterji, 1981; Gaisford 1986; Mathur 2005). The Carob bean gum is used as thickeners, stabilizrs and emulsifiers in the food, pharmaceutical, cosmetic, agricultural industries e.t.c

Gum Arabic also called Acacia Senegal, is produced as tear-drop-shaped globules exuding from bark wounds of Acacia trees. The viscosity of solutions of gum Arabic changes due to the presence of ionic charges, the gum is highly water soluble. (Glicksman, 1983). Gum Arabic solution is slightly acidic and it is principally used in the food and pharmaceutical industries as stabilizer, thickener, suspending and binding agent.

In line with the principles of green chemistry which is aimed at designing safe biodegradable chemicals while considering the impact of the use of these chemicals on the environment by employing different principles including; minimizing waste production, use of hazardous materials, less use of non-renewable resources, reducing risks, hazards as well as costs. This work study the thermal stability of biopolymers: Xanthan gum, Guar gum, commercial Locust bean gum, Gum Arabic as well as locally sourced LBG and also the conditions under which they can function.

EXPERIMENTAL PROCEDURE

The analysis was done using 1wt% of Xanthan gum and Guar gum which were obtained from Fufeng group, China while Locust bean gum was from Will powder, 1wt% and 8wt% of Gum Arabic from the Kano State, as well as Locally sourced LBG from Kaduna State, Nigeria, see Figure 1, 2, 3, 4, 5 and 6. The polymers were hydrated in water separately for each specific temperature. The solutions were stirred gently to achieved homogeneity in order to avoid the formation of fish eye; this was then allowed to hydrate for a period of 24hrs. An initial rheological characterisation was done using Fann Viscometer to determine the rheology at different speeds from (600, 300, 200, 100 6, 3) rpm.

Figure 1: Xanthan gum

Figure 2: Guar gum

Figure 3: Locust Bean (Imported)

Figure 4: Gum Arabic

Figure 6: Locust Bean gum (Locally sourced)

Thermal analysis was carried out using the Roller Oven at 26°C, 50°C, 80°C, 100°C, 130°C and 150°C, the temperature conditions were considered to study the resistance of the polymer at increasing temperatures. Finally, a rheological characterisation was carried out again to determine the degree of stability after the effect of temperature.

RESULTS AND DISCUSSION

This study captures the thermal behaviour of imported polymers at lower and higher temperatures which have not really been addressed by other literature so as to understand the behaviour of the polymers under high temperatures. The results presented in figure 7 show that the viscosity of Xanthan gum's solution was stable up to 70°C. Afterwards, there was a gradual reduction in the viscosity at increasing temperature, this agrees with Chang, 1978 in which he reported that Xanthan's thermal stability is averagely 160°F (71°C).

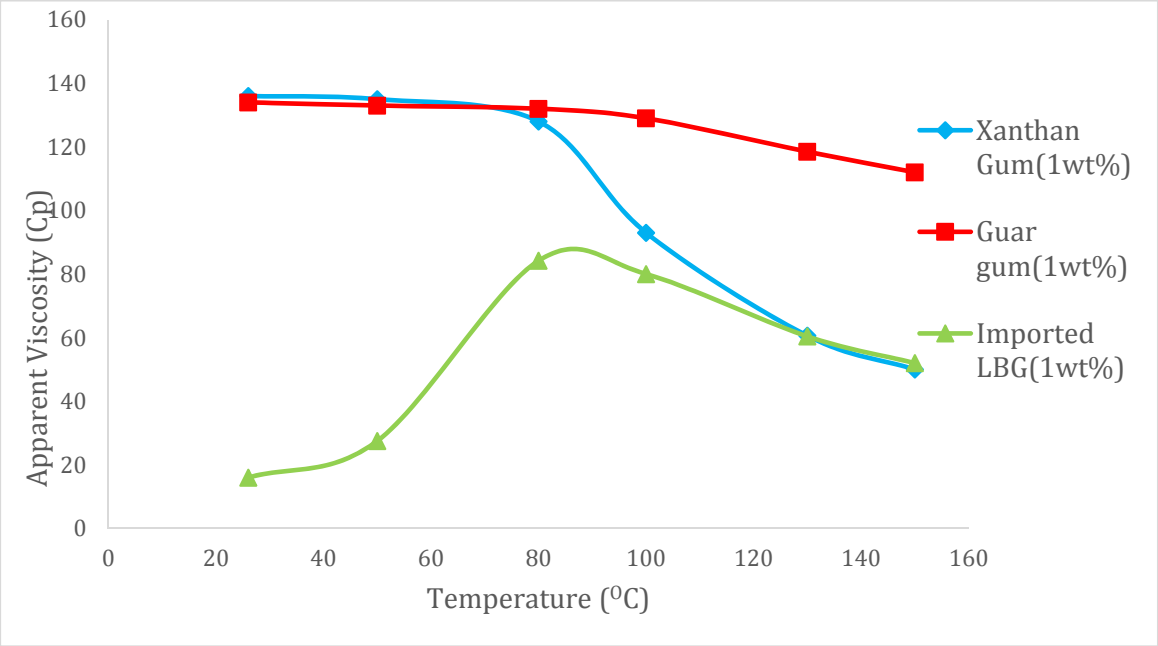

Figure 7: Thermal stability of the imported polymers at 300rpm

Guar gum was stable over a wide range of temperature, it was stable to about 80°C after which above 80°C, it reflected a slight drop in viscosity, the stability displayed by this gum can be attributed to the nature of its molecular structure (Figure 7) and also this agrees with the result reported by Chatterji et al. 1981 and Mathur et al. 2005 where they stated that Guar gum based on the nature of its molecular structure, it has about 60 to 70% solubility in cold water, hence when subjected to the effect of heat, its mannan chains that were initially not soluble in water at room temperature are made available for interaction hence the increase in viscosity. Also Gaisford, 1986 mentioned the heating of the gum to 80°C is needed for complete dissolution of the gum, it means the viscosity of the gum will increase as the temperature increase to 80°C for it to attain complete dissolution, its optimum viscosity is at 80°C. The viscosity loss produced by Xanthan is more than that produced by Guar gum, it implies that Guar gum displayed a stronger thermal resistance that the conventional Xanthan gum.

The imported LBG showed improvement with respect to increasing temperature, as can be observed from figure 7, the viscosity of the solution increased tremendously with increasing temperature up to 90°C before it started dropping again just like the Guar gum, though, the similar behaviour is understood because they are both Galactomannans however, the increase in viscosity generated by the locust bean gum was much higher compared to the increase in viscosity produced by Guar gum. This agrees with Gaisford et al, 1986 and Hui and Neukom, 1964. The gain in viscosity can be related to analogy from literature which establishes that LGB is partially soluble in cold water, it has about 30% solubility, requiring solutions to be heated to at least 80°C for full hydration. Again, LBG has the lowest galactose content and is the least soluble among the other galactomannans (Fenugreek gum, Guar gum and Tara gum). The heating of LBG aqueous dispersions up to about 80 to 90°C is necessary to obtain a complete dissolution of the gum (Casas, 2000; Gaisford et al, 1986).

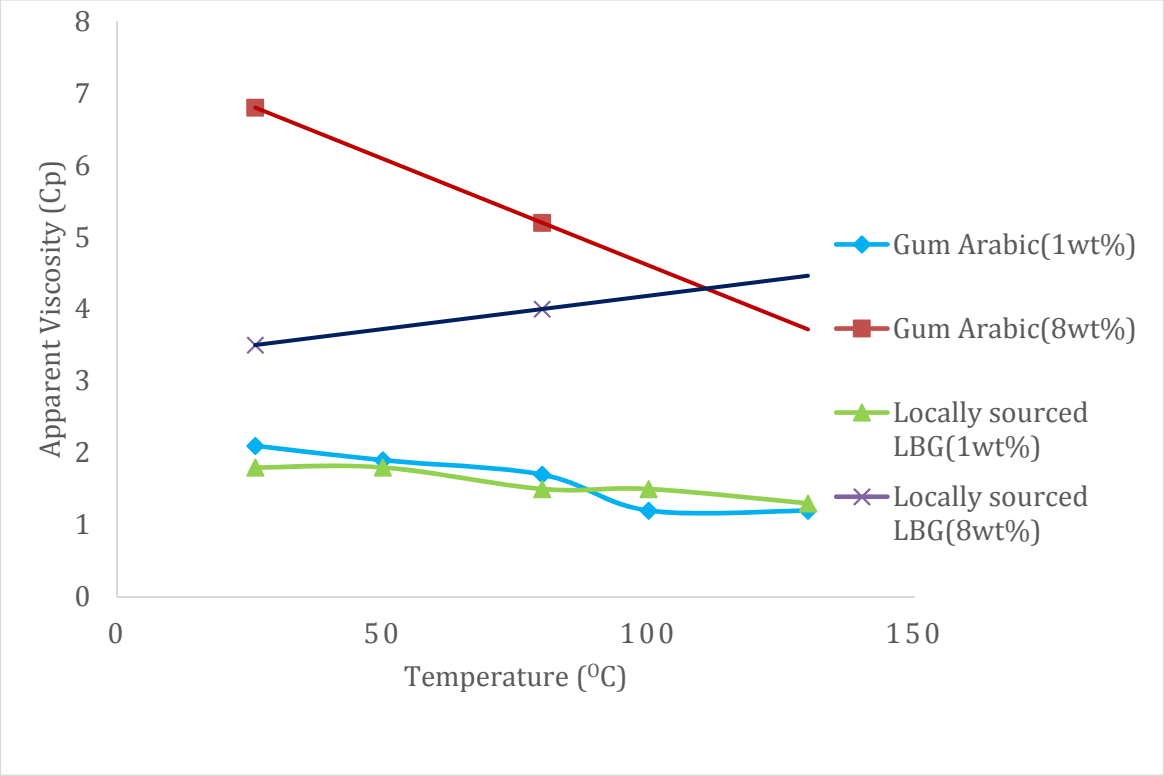

Figure 8: Thermal stability of the locally sourced polymer blend at 300rpm

Based on figure 8, the effect of temperature on Gum Arabic using 1wt% and 8wt% resulted in reduction in viscosity. According to Muller 1981, the hydrolysis of a polymer solution is the cumulative effect of the pH and the temperature. Based on this, the loss of viscosity can be related to the hydrolysis of the polymer chain which is a function of the pH of Gum Arabic solution which was acidic ranging from pH of 4 to 5, this implies that the pH of Gum Arabic solution is strongly responsible for the loss in viscosity encountered. Nevertheless, the Locally sourced LBG (1wt%) did not show much increase in viscosity upon increasing temperature, however, the effect of increasing temperature on a higher concentration of LBG (8wt%) was very significant as this led to increase in viscosity at about 80°C (figure 8) which is synonymous to the rheological behaviour of the imported LBG. According to Gaisford et al., 1986 and Hui et al., 1964, LBG has both hot water and cold water soluble component, increasing the temp of the locust bean solution will dissolve the bonds that were initially not soluble in cold water, thus increasing the viscosity at increasing temperature.

CONCLUSION

The water soluble polymers considered in work proved to be viscous and soluble in water, it can be said conclusively that:

i. All polymers are water soluble and produced significant appreciable viscosities at increasing concentrations.

ii. Xanthan gum had the highest viscosity at 26°C because it showed great ability to viscosify at very little concentration which is an indication of its commercial value in the oil and gas industry especially in polymer flooding. However, Xanthan gum was stable up to 70°C.

iii. Guar gum showed strong thermal stability more than Xanthan gum, this is evident by its strong thermal stability at 80°C.
iv. Significantly interesting is the thermal stability of the locust bean gum, LBG displayed the strongest thermal stability up to 90°C because at each temperature increase, it displayed a significant increase in thermal resistance.
v. Gum Arabic did not give much stability at high temperatures, even at increasing concentration. This can be attributed to the slightly acidic nature of Gum Arabic solution.
vi. Locally sourced LBG at higher concentration displayed a similar rheological behaviour like the imported LBG, its viscosity increased with increase in temperature.
vii. Based on the results above, it implies that a blend of Xanthan gum and Guar gum or Xanthan gum and LBG would likely produce increasing thermal resistance.

REFERENCES

Bao, M., Chen Q., Li Y., and Jiang G., (2010), Biodegradation of partially hydrolyzed polyacrylamide by bacteria isolated from production water after polymer flooding in an oil field. Journal of Hazardous Materials, 184 105–11

Chang, H. G., (2011), Scientific research and field applications of polymer flooding in heavy oil recovery. J Petrol Explor Prod Technol, 1:65–70. DOI 10.1007/s13202-011-0014-6.

Changhong Gao., Jing S. and Fangjian Z. ((2014)), Successful polymer flooding and surfactant-polymer flooding projects at Shengli Oilfield from 1992 to 2012.

Chatterji, J., and Borchardt, J., (1981), Applications of water-soluble polymers in the oil field. J Pet Technol, 33:2,042–042,056. doi:10.2118/9288-PA.

Chang H. L. (1978) Polymer flooding technology yesterday, today, and tomorrow. J Pet Technol 30:1,113–111,128. doi:10.2118/7043-PA.

Deng, S., Bai, R., Chen, J.P., Jiang, Z., Yu, G., Zhou, F., and Chen, Z., (2002), Produced water from polymer flooding process in crude oil extraction: characterization and treatment by a novel crossflow oil–water separator. Sep. Purif. Technol., 29 207–216.

Duan, M., (2014), Treatment of wastewater produced from polymer flooding using polyoxyalkylated polyethyleneimine. Separation and Purification Technology, 133 160–16.

Casas, J. A., Mohedano, A. F., and Garcıa-Ochoa F. (2000) Viscosity of guar gum and xanthan/ guar gum mixture solutions Journal of the Science of Food and Agriculture J Sci. Food Agric 80:1722 – 1727

Gaisford, S. E., Harding, S. E., Mitchellt, J. R. and Bradley, T. D. (1986) A Comparison Between the Hot and Cold Water Soluble Fractions of Two Locust Bean Gum Samples. Carbohydrate Polymers, 6, 423-442

Glicksman, M., and Sand, R. E., (1973), Gum Arabic. In:Industrial gums (Whistler RL ed). New York Academic Press, NY, USA, pp. 197-263.

Guo X. H., Li D. W., Tian J., Liu Y. Z., (1999), Pilot test of xanthan gum flooding in Shengli oilfield. In: SPE 57294 presented at SPE Asia Paciûc improved oil recovery conference, Kuala Lumpu

Ibrahim, S. M., Mousaa, I. M., and Ibrahim, M. S., (2014), Characterization of gamma irradiated plasticized carboxymethyl cellulose (CMC)/gum arabic (GA) polymer blends as absorbents for dyestuffs. Indian Academy of Sciences, Bull. Mater. Sci., Vol. 37, No. 3, pp. 603–608.

Martins F.D., "Mechanical Degradation of Polyacrylamide Solutions in Core Plugs from Several Carbonate reservoirs," Paper SPE 12651 presented at the 1984 SPE/DOE symposium on Enhanced Oil Recovery, Tulsa, April 15-18.

Marthur V. and Mathur. N. K. (2005). Fenugreek and other lesser known legume galactomannan-polysaccharides: Scope for development. Journal of scientific and Industrial research, Vol 64, pp 475 to 481.

Rellegadla, S., Prajapat, G., and Agrawal, A., (2017), Polymers for enhanced oil recovery: fundamentals and selection criteria. Appl Microbiol Biotechnol, DOI 10.1007/s00253-017-8307-4.

Sun, Y., Laila, S., and Baojun, B., (2012), Measurement and Impact Factors of Polymer Rheology in Porous Media. Petroleum Engineering Program, Missouri University of Science and Technology, Rolla, Missouri, USA.

Zhang, Y. Q., Gao B.Y., and Lu, L., (2010), Treatment of produced water from polymer flooding in oil production by the combined method of hydrolysis acidification dynamic membrane bioreactor–coagulation process. J. Pet. Sci. Technol, 74 14–1.

Proceedings of the 49th NSChE Annual Conference
KADA 2019: pp 107-116

P1B-04: VALORISATION OF SUNFLOWER (*TITHONIA DIVERSIFOLIA*) STALK FOR THE REMOVAL OF PB(II) AND FE(II) FROM AQUEOUS SOLUTIONS

Omodele A. A. Eletta[1], Fisayo Oyepeju Ayandele[1], Adewale George Adeniyi[1] and Joshua O. Ighalo[1*]

[1]Chemical Engineering Department, Faculty of Engineering and Technology, University of Ilorin, Ilorin, P. M. B. 1515, Nigeria

*Corresponding author: oshea.ighalo@yahoo.com

ABSTRACT

Sunflower (Tithonia diversifolia) stalk was harnessed as a precursor in preparing adsorbents for the removal of Pb(II) and Fe(II) from aqueous solutions. The biomass was acid activated by wet impregnation with phosphoric acid and carbonised at 500°C. The adsorbent was characterised using Fourier Transform Infra-Red Spectroscopy (FTIR), Branueur Emmet and Teller analysis (BET), Scanning Electron Microscopy with Energy Dispersion Spectroscopy (SEM-EDS) and X-ray Diffraction (XRD). The surface area of the adsorbent obtained was 325.375 m^2/g. The effect of metal ions concentration, adsorbent dosage and contact time was studied for both Pb(II) and Fe(II) uptake. The best fit isotherm model for Pb(II) and Fe(II) was Langmuir and Freundlich Models respectively. The monolayer adsorption capacity of the adsorbent to Pb(II) and Fe(II) was 31.55 mg/g and 35.84 mg/g respectively. The pseudo second order was the best fit kinetic model. The study was able to reveal that Sunflower (Tithonia diversifolia) stalk can be used to prepare cost effective adsorbents for water treatment.

Keywords: Adsorption, *Tithonia diversifolia*, Heavy metals, Kinetics, Isotherm

1.0 INTRODUCTION

The treatment of polluted industrial wastewater remains an area of global concern among engineers and researchers since wastewater collected from municipalities, communities and industries must be returned to receiving waters or to the land (Salam *et al.*, 2011). Heavy metals are introduced into the environment majorly through anthropogenic activities. They are adulterant and their toxicity is a major problem from ecological, evolutionary, nutritional and environmental perspectives (Jaishankar *et al.*, 2014). Heavy metals accumulate and persist in the ecosystems because they cannot be degraded or destroyed (Kano, 2015; Pinho and Ladeiro, 2012). Industrial waste water mostly contain heavy metals like arsenic, cadmium, chromium, iron, copper, lead, nickel, and zinc which could have adverse effect on human health (Jaishankar *et al.*, 2014).

Various methods have been implemented in the treatment of wastewater among which are: chemical precipitation, solvent extraction, ion exchange, electrolytic techniques, coagulation, sedimentation, filtration, membrane process and adsorption techniques (Balcıoğlu and Ötker, 2003; Kano, 2015). Adsorption is a widely used technique for wastewater treatment and activated carbon is a commonly used adsorbent for the process, The usefulness of this method lies in the benefits of cleaner, easy controlled process, more efficient and cost-effective technology (Cherdchoo *et al.*, 2019). Agricultural lignocellulosic based adsorbents have also been gaining worldwide attention as a result of their characteristics which includes renewability, biodegradability, environmentally friendliness, low cost and availability (Ling Pua *et al.*, 2013). In recent times, activated carbons with very high surface area, high porosity, and high adsorptive

capacity have been obtained by chemical activation method which have been extensively used for the removal of pollutants (Üner *et al.*, 2015; Yahya *et al.*, 2015).

Many studies have been carried out to utilise agricultural by-products as adsorbent material in wastewater treatment: peanut husk (Salam *et al.*, 2011), rice husk (Hegazi, 2013), *Delonix regia* (Babalola, 2018), *Amaranthus hybridus* (African spinach) stalk (Egila *et al.*, 2011), *Carica papaya* (pawpaw) (Egila *et al.*, 2011), groundnut shell (Isah and Yusuf, 2012), tea leaves and pumpkin seeds (Francis, 2015), orange peel (Geremew, 2017), almond shell (Largitte *et al.*, 2016), mango peel (*Garcinia mangostana*) (Foo and Hameed, 2012), bamboo (Awoyale *et al.*, 2013), coconut shell (Achaw, 2012; Babarinde and Onyiaocha, 2016), cassava peel and waste bamboo (Omotosho and Amori, 2016), physic nut seed hull (Yakub *et al.*, 2013), dates stone (Alhamed, 2006), guava seeds (Largitte *et al.*, 2016), coffee (Rattanapan *et al.*, 2017), sugarcane bagasse (Geremew, 2017), watermelon rind (Üner *et al.*, 2015), fox nut(Kumar and Jena, 2016) and a host of others. The aim of this study is to evaluate the removal of Pb^{2+} and Fe^{2+} from wastewater by treating with a cost-effective adsorbent prepared from *Tithonia diversifolia.*

2.0 MATERIALS AND METHOD

2.1 Preparation Of Adsorbent

Sun flower stalk (*Tithonia diversifolia*) was sourced from within the premises of the university of Ilorin, Kwara State, Nigeria. The stalks were rinsed with tap water and distilled water to remove dirt and dust and sundried for 24 h to reduce the moisture content prior to oven drying. It was then oven dried at 105 ^oC until no weight loss was observed (Bello and Ahmad, 2011). The dried biomass was pulverized with a ball milling machine and sieved to 100 µm size (Odubiyi *et al.*, 2012). H_3PO_4 was used for chemical activation with impregnation ratio of 1:2 acid-biomass. The mixture was stirred continuously using magnetic hot plate stirrer at ambient temperature for 1 hour and left to age for 24 h. The mixture was filtered and dried in the oven at 110^oC for 24 h. The sample was taken to a muffle furnace and heated at 500 ^oC for 1 h to produce activated carbon. Finally, the powdered sample was washed with 0.5 M of KOH and distilled water to remove residual acids until washing solution become neutral. The samples were then dried overnight at 100 ^oC and cool to room temperature to obtain H_3PO_4 activated carbon (Krishna, 2014). The samples was grinded with mortar and pestle and sieved to obtain maximum particle size of 100 µm (Krishna, 2014).

2.2 Adsorbent Characterisation

FTIR spectrometer used to identify the functional groups responsible for the heavy metals uptake and bonding present on the surface of the adsorbents. The scan range was set to 650-4000 cm^{-1}. The sample was placed on the sample holder and the sample was scanned to obtain the spectrum. BET analysis was employed to determine the surface area, pore size and pore volume of the adsorbent. The surface properties of the soot sample were done using Multipoint BET surface area and DR (Dubinin-Radushkevic) method for the pore volume and width (diameter) respectively. SEM was used for morphological structure such as size and shape of the adsorbent. The sample stub was placed on a charge reduction sample holder and introduced into the column of the SEM machine. On the SEM machine, it was viewed from a NavCam before being sent to SEM mode. Different magnifications were obtained after adjustment of brightness and contrast. XRD was employed to investigate the physical properties of the adsorbent as it relates to the crystallinity of the material. The XRD was operated with Cu Kα emission (ƛ = 1.54105 Å, 45 kV, 40 mA per sec).

2.3 Batch Adsorption Experiments

The experiments were performed using 50 ml of synthetic wastewater (pH 6.4) at 30°C and 150 rpm for maximum of 180 mins. The choice of Pb(II) and Fe(II) for the experiments was based on an earlier characterisation of a real paint industry wastewater which highlighted the high levels of those metals. All adsorption experiments were performed in 250 ml conical flasks with 50 ml of wastewater, varying any one of the parameters and keeping the other parameters constant. The parameters studied were adsorbent dosage (1 – 6 g/l), initial Pb(II) and Fe(II) concentration (25 – 150 mg/L), contact time (30 – 180 minutes). The equilibrium isotherm experiments were done at 30 ^{o}C, initial metal concentration (C_i) was 25 – 150 mg/L and contact time of 60 minutes. The adsorbent dosage was 5 g/L. For the kinetic studies, the temperature was set at 30 ^{o}C, initial metal concentration (C_i) was set at 100 mg/L and dosage of 5 g/L and contact time was varied from 30-180 mins.

3.0 RESULTS AND DISCUSSION

3.1 Adsorbent Characterisation

3.1.1 FTIR

Figure 1 revealed that activated carbon from *Tithonia diversifolia* shows a weak N-H stretch of 3652.8 cm^{-1} which is assigned to amines group, it also shows a strong band of C-H stretch of alkanes and alkyls at 2918.5 cm^{-1} which is similar to what was obtained by Cherdchoo *et al.* (2019). The band at 3123.5 cm^{-1} indicates weak medium =C-H stretch of alkenes group. The band at 2750.8 cm^{-1}, 3123.5 cm^{-1}, 2918.5 cm^{-1} are assigned to strong broad O–H stretching of hydroxyl groups from carboxylic acid (Kumar and Jena, 2016). 2344.5 cm^{-1} indicates amino group (Cherdchoo *et al.*, 2019). The bands at 805 cm^{-1} is assigned to strong C-H bend of aromatics compound group (Kumar and Jena, 2016). The band region between 900 and 1300 cm^{-1} depicts the characteristic of phosphorous and phosphorous carbonaceous compounds present in the phosphoric acid activated carbon (Kumar and Jena, 2016). N-H and O-H groups have been shown to be important functional groups for the sorption of heavy metals (Farhan *et al.*, 2012) and especially Pb(II) (Fauzia *et al.*, 2018).

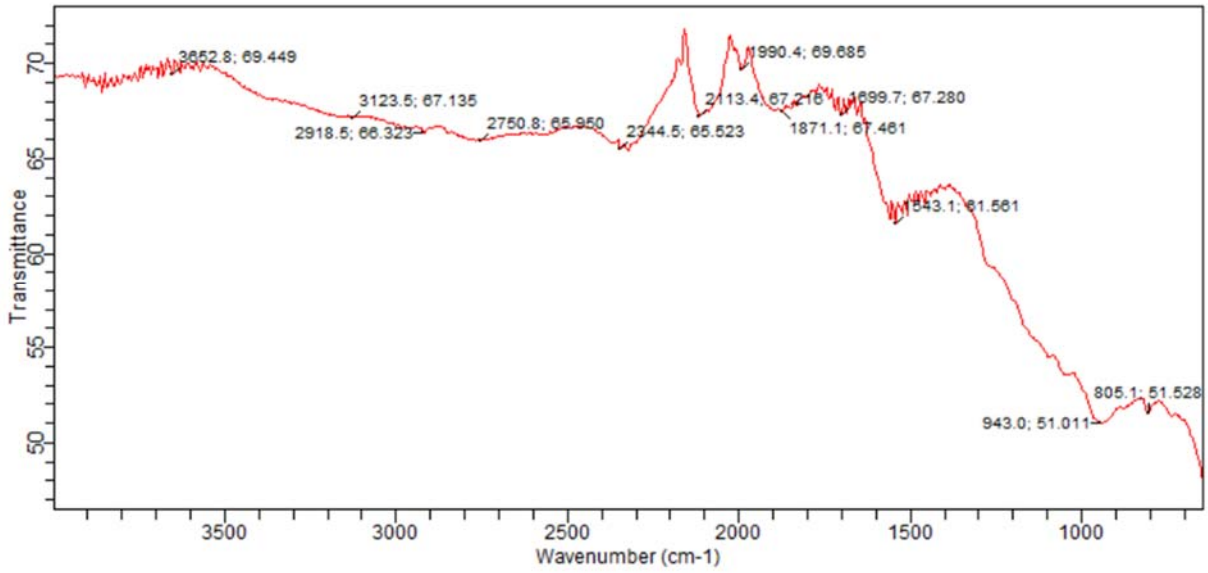

Figure 1. FTIR spectra of *Tithonia diversifolia* activated carbon

3.1.2 BET

The specific surface area of the *Tithonia diversifolia* AC was 325.375 m^2/g based on the Branueur-Emmett-Teller (BET) standard method which was higher when compared with peanut shell (Al-Othman *et al.*, 2012), mixed waste tea and coffee ground (Cherdchoo *et al.*, 2019). The total pore volume obtained was 0.136 cc/g. The pore size width obtained was 5.749 nm suggesting a mesoporous structure (Cherdchoo *et al.*, 2019). The prepared activated carbon has well-developed pores which can be attributed to the activation with H_3PO_4 during carbonisation of the adsorbent at 500°C, H_3PO_4 also act as dehydrating agents that inhibit the formation of tar as well as volatile substances during the process, which enhance the yield from the process (Kumar and Jena, 2016).

Table 1. BET analysis of *Tithonia diversifolia* activated carbon

Surface area (m^2/g)	Pore volume (cc/g)	Pore size distribution (nm)
325.375	0.136	5.749

3.1.3 SEM-EDS

Figure 2 showed small pieces and pores, this is due to the fact that during carbonisation, organic materials were volatilized from the biomass leading to the formation of many pores which led to higher BET surface area. The higher surface area can also be due to the interaction of H_3PO_4 during impregnation. *Tithonia diversifolia* (sunflower) activated carbon contained 59.43% carbon, 27.24% oxygen, 2.04% nitrogen, 10.01% phosphorous and others as shown in Figure 3. SEM image shows rough surface, some clouded white substances on the morphological surface of the sample and agglutinative flakes of *Tithonia diversifolia*, this suggests that the adsorbent has heterogeneous surface which makes it very suitable for use as an adsorbent.

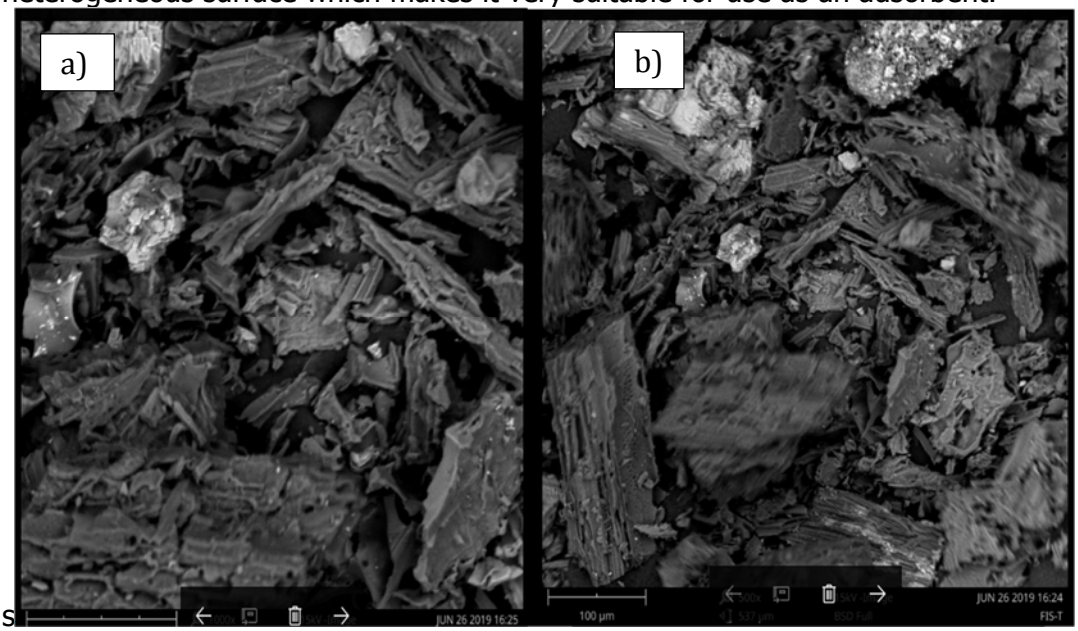

Figure 2. SEM image of *Tithonia diversifolia* activated carbon (a) ×1,500 (b) ×1,000

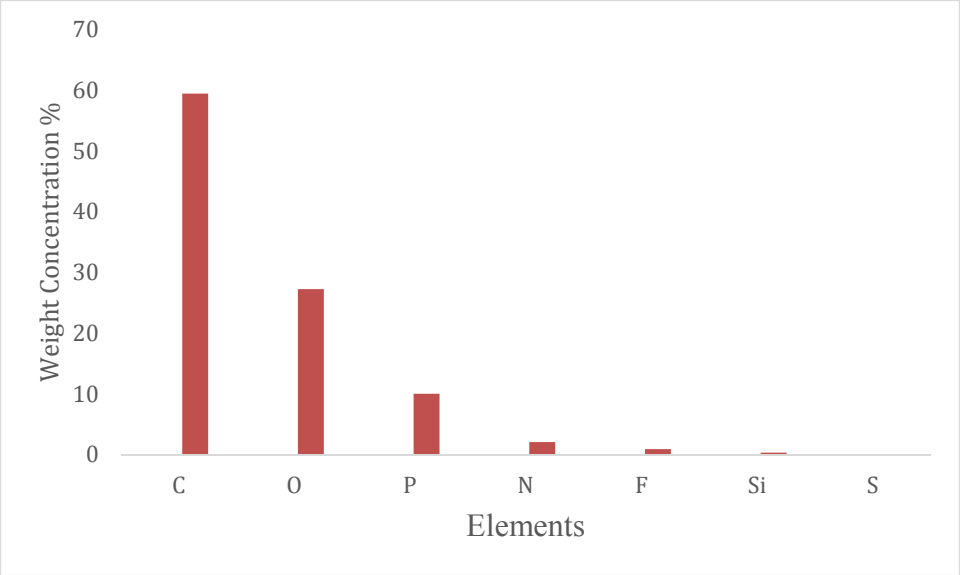

Figure 3. EDS plot of *Tithonia diversifolia* activated carbon

3.1.4 XRD

Figure 4 shows a clear pattern of the characteristic peaks for Fe_3O_4 at 18.32°, 30.14°, 35.48°, 37.19°, 43.12°, 53.47°, 57.01°, 62.61°, 71.11°, and 74.08° confirming the presence of traces of magnetite of spinel group (Datta *et al.*, 2017). It also shows a clear pattern of the characteristic peaks for $MgCO_3$ at 32.41° and 46.50° confirming the presence of traces of magnesite of the spinel group. In summary, the presence of the sharp peaks reveals that the adsorbent is crystalline.

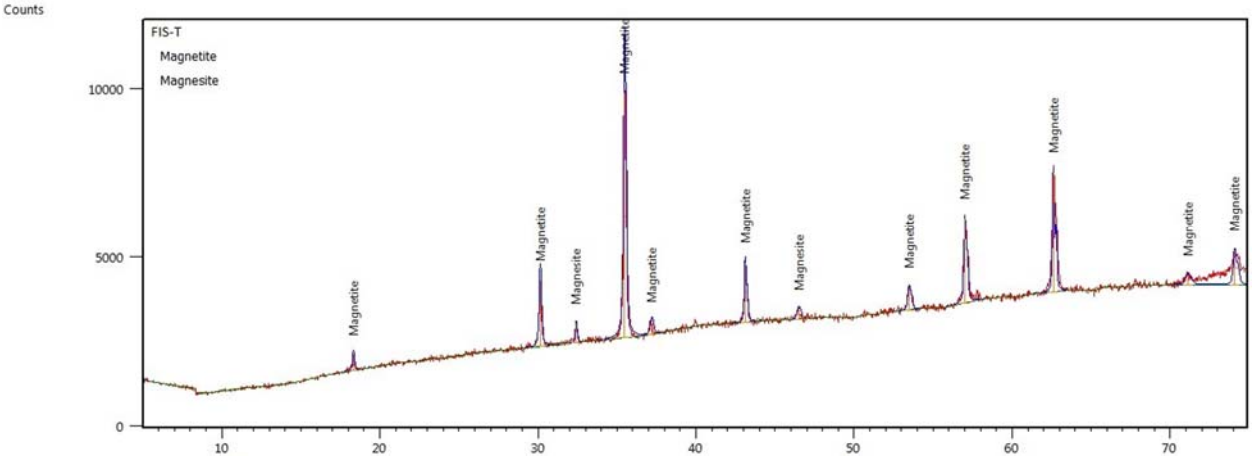

Figure 4. XRD spectra for *Tithonia diversifolia* activated carbon

Parametric studies

3.2.1 Effect of Initial concentration

The effect of different initial concentrations of Fe(II) and Pb(II) was investigated. It was observed that there was a decrease of adsorption of Pb(II) and Fe(II) with an increase in concentrations of Pb(II) and Fe(II) in the study. Adsorption efficiency decreased as metal ion concentrations increased which depicts saturation at the adsorbent surface site. The ratio of surface active sites

to total amount of metal ions was higher in lower metal ion concentrations compared with higher metal ions. Rate of metal ion adsorption decreases when approaching equilibrium.

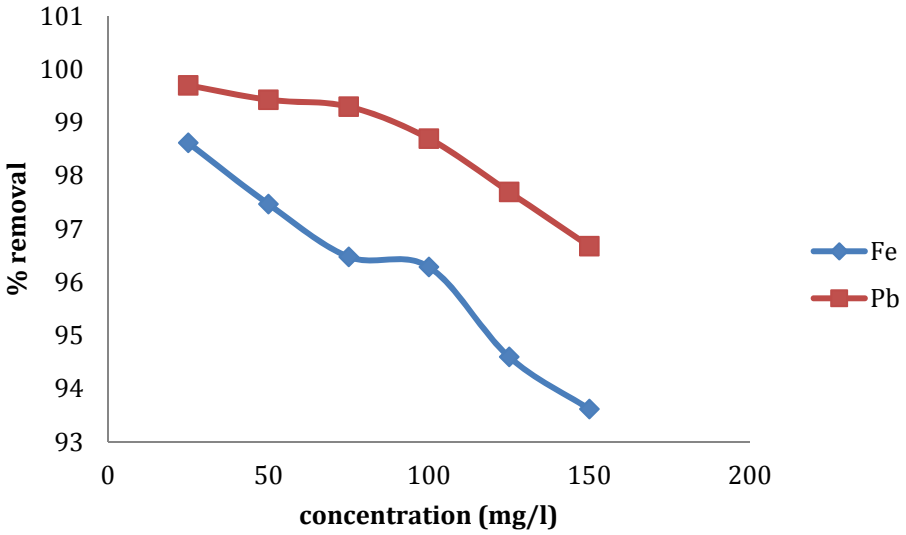

Figure 5. Effect of initial concentration on Pb(II) and Fe(II) Adsorption onto *Tithonia diversifolia* activated carbon

3.2.2 Effect of Adsorbent Dosage

Different adsorbent doses (0.05–0.3 g/50 mL) on adsorption of Pb(II) and Fe(II) were analysed at a constant initial concentration of Pb(II) and Fe(II) solution (100 mg/L) under fixed parameters: pH = 6.4 and contact time 60 minutes. The percentage removal of Fe(II) and Pb(II) increased from 88.28 % to 98.04 % and 96.25 % to 99.38 % as shown in Figure 6. This showed that as adsorbent dose increased more surface area was available which exposed more active sites for binding metal ions.

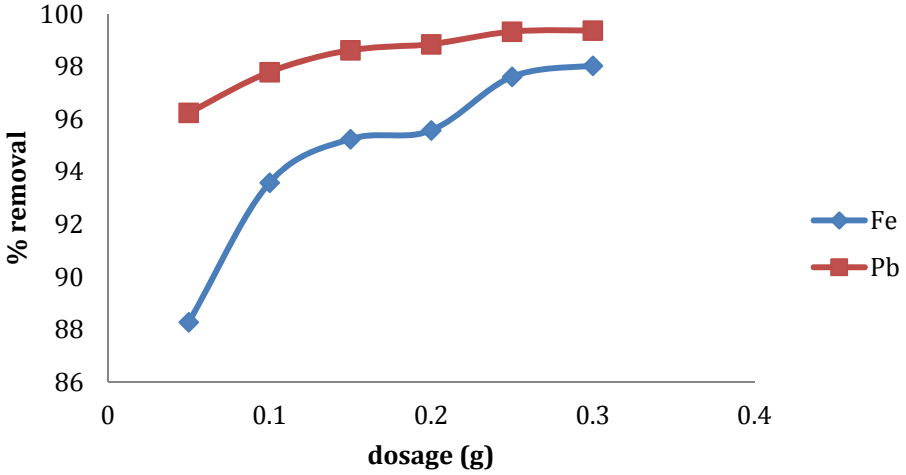

Figure 6. Effect of adsorbent dosage on Pb(II) and Fe(II) adsorption onto *Tithonia diversifolia* activated carbon

3.2.3 Effect of Contact Time

The effect of contact time on the adsorption of Fe(II) and Pb(II) was investigated. 93% of Fe(II) and 98.2% of Pb(II) was adsorbed at equilibrium, though the percentage removal increased from 90.15% to 95.28 and 96.78% to 99.2% between 30-180mins for Fe(II) and Pb(II) respectively. It can be seen from Figure 7 that the adsorption rate increased rapidly because the adsorption sites are readily available on the adsorbent but adsorption approaches equilibrium as the sites becomes saturated after 60 and 120 minutes for Pb(II) and Fe(II) respectively (Odubiyi *et al.*, 2012; Tao *et al.*, 2015).

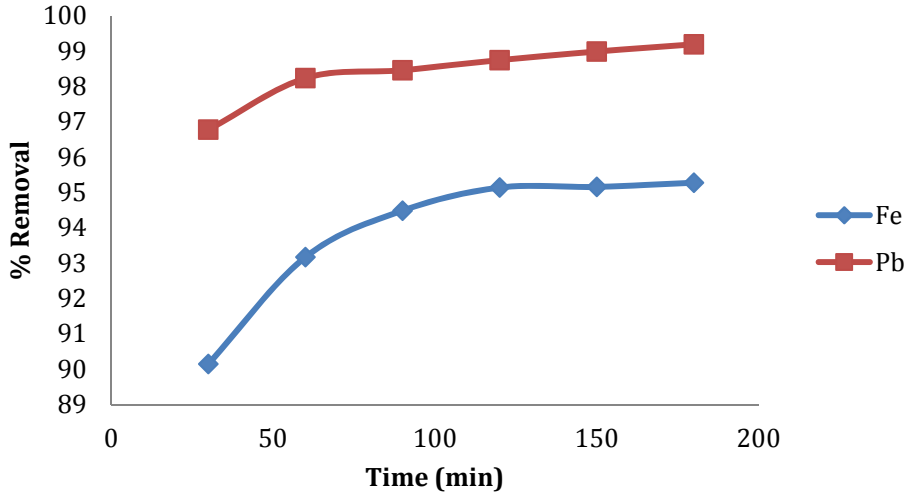

Figure 7. Effect of Contact Time on Pb(II) and Fe(II) Adsorption onto *Tithonia diversifolia* activated carbon

3.2.4 Equilibrium Isotherm

Adsorption isotherms are criteria used in optimizing the use of adsorbents as they describe the nature of interaction between adsorbate and adsorbent. Langmuir, Freundlich and Temkin were used to study the adsorption of Pb(II) and Fe(II) under the conditions of (5 g/l dosage, 100 mg/L initial metal concentration, pH = 6.4, t = 60 mins. The three models were in support of the study but Langmuir model fitted better than Freundlich and Temkin model except for the adsorption of Fe(II) on TD-AC which gives R^2 of 0.995 and n of 1.8822 for Freundlich model. The main characteristic of Langmuir equation is a dimensionless constant called equilibrium parameter (R_L). The results obtained revealed 0.1113 for Fe(II) and 0.00619 for Pb(II) R_L values, which indicates a favourable condition and optimum adsorption (Albadarin *et al.*, 2014; Cherdchoo *et al.*, 2019). The maximum adsorption capacity was 31.55 mg/g for Pb(II) and 35.84 mg/g for Fe(II) while the maximum correlation coefficient is 0.9911 for Fe(II) and 0.9983 for Pb(II).

3.2.5 Adsorption Kinetics

The adsorption kinetics depends greatly on the physical and or chemical characteristics of the adsorbent and on the mass transfer process. The experimental data of adsorption of Pb(II) and Fe(II) onto the adsorbent at different time intervals were examined with pseudo-first-order and pseudo second-order models, using the plots of Log ($q_e - q_t$) against t and t/q_t versus t, respectively. The Pseudo second order gave a higher coefficient of determination >0.99, which implies that the basic adsorption is chemisorption involving sharing of electrons between the adsorbate and surface of the adsorbent. There is also a close range between $q_{e\ exp}$ and $q_{e\ calc}$

which suggested that the adsorption of Pb(II) and Fe(II) was consistent with pseudo second order kinetic model.

Table 2. Adsorption isotherm data for *Tithonia diversifolia* activated carbon

Model	Parameter	Metal ion	
		Pb(II)	**Fe(II)**
Langmuir	q_{max} (mg/g)	31.55	35.84
	B	0.6058	0.3195
	R_L	0.0062	0.1113
	R^2	0.9921	0.9691
Freundlich	K_F (L/mg)	16.49	8.7478
	N	2.402	1.8822
	1/n	0.4164	0.5313
	R^2	0.9635	0.995
Temkin	α (L/mg)	5.88	4.28
	β (kJ/mol)	6.9765	1.1043
	R^2	0.9478	0.7865

Table 3. Adsorption kinetic data for *Tithonia diversifolia* activated carbon

Model	Parameters	Metal ion	
		Pb(II)	**Fe(II)**
	$q_{m,}$ exp (mg/g)	19.83	19.05
Pseudo first order	k_1 (min^{-1})	0.0341	0.0191
	$q_{e,}$ calc (mg/g)	2.9	0.7619
	R^2	0.9593	0.9701
Pseudo second order	k_2 (g/mg.min)	0.0529	0.0261
	$q_{e,}$ calc (mg/g)	19.92	19.31
	R^2	1.000	1.000

4.0 CONCLUSION

Sunflower (*Tithonia diversifolia*) stalk was harnessed as a precursor in preparing adsorbents for the removal of Pb(II) and Fe(II) from aqueous solutions. The biomass was acid activated by wet impregnation with phosphoric acid and carbonised at 500°C. Transform Infra-Red Spectroscopy (FTIR) revealed the presence of several key functional groups needed for the adsorption of heavy metals such as N-H and O-H groups. Branueur Emmet and Teller analysis (BET) revealed that the adsorbent was mesoporous with and has a surface area of 325.375 m^2/g. Scanning Electron Microscopy with Energy Dispersion Spectroscopy (SEM-EDS) revealed that the adsorbent has a highly heterogeneous surface which is favourable for adsorption. X-ray Diffraction (XRD) revealed that the adsorbent is crystalline. The effect of pollutant concentration, adsorbent dosage and contact time was studied for both Pb(II) and Fe(II) uptake. The best fit isotherm model for Pb(II) and Fe(II) was Langmuir and Freundlich Models respectively. The monolayer adsorption capacity of the adsorbent to Pb(II) and Fe(II) was 31.55 mg/g and 35.84 mg/g respectively. The pseudo second order was the best fit kinetic model. The study was able to reveal that Sunflower (*Tithonia diversifolia*) stalk can be used to prepare cost effective adsorbents for water treatment.

REFERENCES

Achaw, O.-W. (2012). A study of the porosity of activated carbons using the scanning electron microscope *Scanning Electron Microscopy*: InTech.

Al-Othman, Z. A., Ali, R., and Naushad, M. (2012). Hexavalent chromium removal from aqueous medium by activated carbon prepared from peanut shell: adsorption kinetics, equilibrium and thermodynamic studies. *Chemical Engineering Journal, 184*, 238-247. doi: http://dx.doi.org/10.1016/j.cej.2012.01.048

Albadarin, A. B., Mo, J., Glocheux, Y., Allen, S., Walker, G., and Mangwandi, C. (2014). Preliminary investigation of mixed adsorbents for the removal of copper and methylene blue from aqueous solutions. *Chemical engineering journal, 255*, 525-534.

Alhamed, Y. A. (2006). Activated carbon from dates' stone by ZnCl2 activation. *JKAU Eng Sci, 17*, 75-100.

Awoyale, A., Eloka-Eboka, A., and Odubiyi, A. (2013). Production and experimental efficiency of activated carbon from local waste bamboo for wastewater treatment. *International Journal of Engineering and Applied Sciences, 3*(2), 8-10.

Babalola, B. (2018). *Investigating adsorption characteristics of Delonix regia for heavy metals removal in wastewater and its potential for remediating contaminated soils.* Lancaster University.

Babarinde, A., and Onyiaocha, G. O. (2016). Equilibrium sorption of divalent metal ions onto groundnut (Arachis hypogaea) shell: kinetics, isotherm and thermodynamics. *Chem. Int, 2*(3).

Balcıoğlu, I. A., and Ötker, M. (2003). Treatment of pharmaceutical wastewater containing antibiotics by O3 and O3/H2O2 processes. *Chemosphere, 50*(1), 85-95.

Bello, O. S., and Ahmad, M. A. (2011). Adsorptive removal of a synthetic textile dye using cocoa pod husks. *Toxicological and Environmental Chemistry, 93*(7), 1298–1308.

Cherdchoo, W., Nithettham, S., and Charoenpanich, J. (2019). Removal of Cr (VI) from synthetic wastewater by adsorption onto coffee ground and mixed waste tea. *Chemosphere, 221*, 758-767.

Datta, D., Kerkez Kuyumcu, Ö., Bayazit, Ş. S., and Abdel Salam, M. (2017). Adsorptive removal of malachite green and Rhodamine B dyes on Fe3O4/activated carbon composite. *Journal of Dispersion Science and Technology, 38*(11), 1556-1562.

Egila, J., Dauda, B., Iyaka, Y., and Jimoh, T. (2011). Agricultural waste as a low cost adsorbent for heavy metal removal from wastewater. *International Journal of Physical Sciences, 6*(8), 2152-2157.

Farhan, A. M., Salem, N. M., Ahmad, A. L., and Awwad, A. M. (2012). Kinetic, Equilibrium and Thermodynamic Studies of the Biosorption of Heay Metals by Ceratonia Siliqua Bark. *American Journal of Chemistry, 2*(6), 335-342.

Fauzia, S., Aziz, H., Dahlan, D., and Zein, R. (2018). *Study of equilibrium, kinetic and thermodynamic for removal of Pb(II) in aqueous solution using Sago bark (Metroxylon sago).* Paper presented at the Proceedingss of the 3rd International Symposium on Current Progress in Mathematics and Sciences (ISCPMS2017).

Foo, K., and Hameed, B. (2012). Factors affecting the carbon yield and adsorption capability of the mangosteen peel activated carbon prepared by microwave assisted K2CO3 activation. *Chemical engineering journal, 180*, 66-74.

Francis, M. M. (2015). Aluminophosphates Derived From Tea Leaves And Pumpkin Seeds Ashes For Removal Of Selected Heavy Metals From Contaminated Water.

Geremew, B. (2017). A Review on Elimination of Heavy Metals from Wastewater Using Agricultural Wastes as Adsorbents. *Science Journal of Analytical Chemistry, 5*, 72-75. doi: http://dx.doi.org/10.11648/j.sjac.20170505.12

Hegazi, H. A. (2013). Removal of heavy metals from wastewater using agricultural and industrial wastes as adsorbents. *HBRC journal, 9*(3), 276-282.

Isah, U., and Yusuf, A. (2012). Adsorption of lead ions on groundnut shell activated carbon. *Der Chemica Sinica, 3*(6), 1511-1515.

Jaishankar, M., Tseten, T., Anbalagan, N., Mathew, B. B., and Beeregowda, K. N. (2014). Toxicity, mechanism and health effects of some heavy metals. *Interdisciplinary toxicology, 7*(2), 60-72.

Kano, N. (2015). Adsorption of Heavy Metal onto the Materials Prepared by Biomass *Biomass Production and Uses*: InTech.

Krishna, C. (2014). A Research On Cocoa Pod Husk Activated Carbon For Textile Industrial Wastewater Colour Removal. *International Journal of Research in Engineering and Technology, 3*, 731-737.

Kumar, A., and Jena, H. M. (2016). Preparation and characterization of high surface area activated carbon from Fox nut (Euryale ferox) shell by chemical activation with H3PO4. *Results in Physics, 6*, 651-658.

Largitte, L., Brudey, T., Tant, T., Dumesnil, P. C., and Lodewyckx, P. (2016). Comparison of the adsorption of lead by activated carbons from three lignocellulosic precursors. *Microporous and Mesoporous Materials, 219*, 265-275.

Ling Pua, F., Sajab, M. S., Chia, C. H., Zakaria, S., Rahman, I. A., and Salit, M. S. (2013). Alkaline-treated cocoa pod husk as adsorbent for removing methylene blue from aqueous solutions. *Journal of Environmental Chemical Engineering, 1*(3), 460-465.

Odubiyi, O. A., Awoyale, A. A., and Eloka-Eboka, A. C. (2012). Wastewater Treatment with Activated Charcoal Produced from

Cocoa Pod Husk. *International Journal of Environment and Bioenergy, 4*(3), 162-175.

Omotosho, O., and Amori, A. (2016). Effect of zinc chloride activation on physicochemical characteristics of cassava peel and waste bamboo activated carbon. *International Journal of Chemical, Molecular, Nuclear, Materials and Metallurgical Engineering, 10*(6).

Pinho, S., and Ladeiro, B. (2012). Phytotoxicity by lead as heavy metal focus on oxidative stress. *Journal of Botany, 2012*.

Rattanapan, S., Srikram, J., and Kongsune, P. (2017). Adsorption of Methyl Orange on Coffee grounds Activated Carbon. *Energy Procedia, 138*, 949-954.

Salam, O. E. A., Reiad, N. A., and ElShafei, M. M. (2011). A study of the removal characteristics of heavy metals from wastewater by low-cost adsorbents. *Journal of Advanced Research, 2*(4), 297-303.

Tao, H.-C., Zhang, H.-R., Li, J.-B., and Ding, W.-Y. (2015). Biomass based activated carbon obtained from sludge and sugarcane bagasse for removing lead ion from wastewater. *Bioresource Technology, 192*, 611-617.

Üner, O., Geçgel, Ü., and Bayrak, Y. (2015). Preparation and characterization of mesoporous activated carbons from waste watermelon rind by using the chemical activation method with zinc chloride. *Arabian Journal of Chemistry*.

Yahya, M. A., Al-Qodah, Z., and Ngah, C. Z. (2015). Agricultural bio-waste materials as potential sustainable precursors used for activated carbon production: A review. *Renewable and sustainable energy reviews, 46*, 218-235.

Yakub, I., Mohammad, M., and Yaakob, Z. (2013). *Effects of zinc chloride impregnation on the characteristics of activated carbon produced from physic nut seed hull.* Paper presented at the Advanced Materials Research.

Proceedings of the 49th NSChE Annual Conference
KADA 2019: pp 117-126

P1B-05: KINETIC COEFFICIENTS OF SUBSTRATE UTILIZATION AND BIOMASS GROWTH IN THE BIO-DEGRADATION OF PETROLEUM REFINERY WASTEWATER IN AN ACTIVATED SLUDGE PROCESS

O. J. Momoh*, P.C Okonkwo and L.C Edomwonyi-Otu
Department of Chemical Engineering, Ahmadu Bello University, Zaria
Corresponding Author: ojamesmomoh@gmail.com

ABSTRACT
A study of the kinetics of petroleum refinery wastewater biodegradation in an activated sludge process was carried out in a 25 L volume bio-reactor, operated for a time range of 2-10 hours hydraulic retention. Substrate utilization and microbial growth rate was monitored at various hydraulic retention time which shows corresponding increase in microbial growth and coliform count with substrate utilization. Analysis of the results obtained using the Monod and the modified Monod kinetic model gave the following bio-kinetic parameters for petroleum refinery wastewater bio-degradation in an activated sludge process: Maximum Substrate Utilization Rate= 4.4 day^{-1}, Half Saturation Constant=275 mg/L, Yield Coefficient=0.5083 mgVSS/mg BOD and Endogenous Decay Constant=0.003 day^{-1}.

1.0 Introduction
The ever-increasing world population and industrial development have led to the introduction of different types of chemical substances to the environment, leading to considerable deterioration in environmental quality (Taghreed and Muftah, 2018). Petroleum refinery generates enormous wastewater that requires effective treatment before discharge into the environment. A typical petroleum refinery generates wastewater 0.4-1.6 times the volume of crude oil processed (Coelho *et al.*, 2006) which is potentially harmful to man and the environment if not well treated before discharge. According to Qin *et al.* (2007) biological treatment of petroleum refinery wastewater by an activated sludge process is viable, as it is generally the most economical method for reducing both wastewater toxicity and dissolved organic constituents, although the process is faced with challenges in terms of performance. Previously, activated sludge process designs were not based on kinetic data but recently, a more rational solution for the design of activated sludge process has been under studies. Process modeling of the activated sludge process as it is currently conceived requires experimental assessment of kinetic and stoichiometry coefficients, these coefficients vary for different wastewater (Tchobanoglous *et al.*, 2003).

Previously Ambreen *et al.* (2013) used a laboratory-scale reactor to obtain the following kinetic coefficients for diary wastewater: maximum specific growth rate (μ_{max}) =4.46 day^{-1}, saturation constant (Ks) =534 mg/l, yield coefficient (Y) =0.714 mgVSS/mg sCOD and decay coefficient (Kd) =0.038. Similarly Haydar and Aziz (2009) used a laboratory scale completely mixed continuous flow reactor to generate the following kinetic data for tannery wastewater: maximum substrate utilization rate, half velocity constant, cell yield coefficient and decay coefficient of 3.125 day-^{1}, 488 mg/L, 0.64 and 0.035 day^{-1}, respectively.

For petroleum refinery wastewater, Carlos *et al.* (2013) reported rate constant (*k*) values of 0.055 and 0.059 L mg^{-1} VSS day^{-1}, with and without biomass recirculation, respectively for the removal of organic matter in petroleum refinery wastewater treatment in ASP. Fazel (2016) treated a simulated petroleum refinery wastewater in an aerobic film bioreactor integrated with a UV reactor and obtained saturation constant (K_B) and maximum utilization rate (U_{max}) of 110.67 g/Lday and 90.90 g/Lday respectively.

In the present work actual petroleum refinery wastewater was treated in ASP to obtain maximum substrate utilization rate, half saturation constant, yield coefficient and Endogenous decay constant. The determinations of these kinetic parameters are helpful in understanding the kinetics of substrate utilization, sludge production and design of activated sludge process for wastewater treatment (Haydar and Aziz, 2009).

Mechanism and Kinetics of Activated Sludge Process

The mechanism of the activated sludge process is such that microorganism takes in oxygen and feed on the organic materials in the wastewater which enables reproduction of more microorganisms. According to Tchobanoglous *et al.* (2003), reaction (1), (2) and (3) represent the biochemical reaction in the activated sludge process which involves bacterial cell respiration and synthesis using organic pollutants as substrate. Reaction (3), the endogenous respiration stage is the last phase in the process; it takes place when new cells begin to consume their own cell tissue to obtain energy for their cells maintenance and simultaneously release carbon dioxide, water.

Oxidation (Catabolism)

$$Organics + Oxygen \xrightarrow{Micro-organism} CO_2 + H_2O + Energy \ldots\ldots\ldots\ldots\ldots\ldots\ldots\ldots\ldots.\ldots\ldots\ldots\ldots.(1)$$

S**ynthesi**s (Anabolism)

$$Organics + Oxygen + Nutrients \xrightarrow{Micro-organism} New\ cells + CO_2 + H_2O \ldots\ldots\ldots\ldots\ldots\ldots..(2)$$

Endogenous Respiration (Endogenous metabolism)

$$Cell\ matter + Oxygen \xrightarrow{Micro-organism} CO_2 + H_2O + Nutrient + Energy \ldots\ldots\ldots\ldots\ldots\ldots.\ldots(3)$$

Generally substrate utilization and cell growth rate in an activated sludge process can be related as described by Sperling (2007) in Equations 4 to 16.

$$r_{su} = \frac{kSX}{K_s + S} \ldots\ldots\ldots\ldots\ldots\ldots\ldots\ldots\ldots\ldots\ldots\ldots\ldots\ldots\ldots\ldots\ldots\ldots\ldots\ldots\ldots\ldots\ldots\ldots\ldots\ldots\ldots(4)$$

Where r_{su}= rate of substrate concentration change due to utilization, S=substrate concentration, k=maximum specific substrate utilization rate, X=biomass (microorganism) concentration, K_s = half saturation coefficient. The bacteria growth rate is dependent on the rate at which the substrate is utilized; making the bacterial growth rate maximum at maximum substrate utilization rate.

$$u_{max} = kY \ldots\ldots\ldots\ldots\ldots\ldots\ldots\ldots\ldots\ldots\ldots\ldots\ldots\ldots\ldots\ldots\ldots\ldots\ldots\ldots\ldots\ldots\ldots\ldots\ldots\ldots\ldots\ldots(5)$$

Where, $\mu_{max} = \text{maximum specific growth rate}$, Y is the yield coefficient.

Therefore,

$$k = \frac{u_{max}}{Y} \ldots\ldots\ldots\ldots\ldots\ldots\ldots\ldots\ldots\ldots\ldots\ldots\ldots\ldots\ldots\ldots\ldots\ldots\ldots\ldots\ldots\ldots\ldots\ldots\ldots\ldots\ldots(6)$$

The rate of substrate utilization can be further expressed as:

$$r_{su} = \frac{\mu_{max} SX}{Y(K_s + S)} \quad (7)$$

The specific growth rate is related to substrate utilization rate as follows:

$$\mu = Y\frac{r_{su}}{X} \quad (8)$$

Therefore,

$$\mu = \mu_{max}\frac{S}{K_s+S} \quad (9)$$

Equation (9) is the Monod kinetic model which relates the microbial growth with the substrate concentration. Considering microbial death rate, r_d.

$$r_d = -(k_d)(X) \quad (10)$$

Where k_d=endogenous decay coefficient, the endogenous decay coefficient accounts for the loss in cell mass. Growth rate of biomass is proportional to the substrate utilization rate by the synthesis yield coefficient, and biomass decay is proportional biomass present (Sperling, 2007). Net rate of growth can be obtained as follows:

$$r_g = -(Y)(r_{su}) - (k_d)(X) \quad (11)$$

Therefore equation (9) becomes:

$$r_g = \frac{(\mu_{max})(S)(X)}{K_s + S} - (K_d)(X) \quad (12)$$

Or as $r_g = Y\frac{kSX}{K_s+S} - K_d X$ (13)

Specific biomass growth rate, $\mu = \frac{r_g}{X}$ (14)

The corresponding expression for the net specific growth rate is written as:

$$\mu = \mu_{max}(\frac{S}{K_s + S}) - (K_d) \quad (15)$$

Or in terms of Y as

$$\mu = Y\frac{kS}{K_s + S} - K_d \quad (16)$$

Equations (4), (9), (10) and (15) are useful equations to obtain the following kinetic coefficients data: k, K_s, K_d and Y, which can be used in the prediction of the rate of substrate utilizations and biomass growth rate in an activated sludge process (Haydar and Aziz, 2009). Understanding of the dynamic nature of substrate utilization and microbial growth rate in ASP is essential, as it can be used as diagnostics tool to improve process performance.

2.0 Methodology

Petroleum refinery wastewater sample was collected from the wastewater treatment plant of Kaduna Refining and Petrochemical Company (KRPC) Kaduna. The study was carried out in a 25 L activated sludge process reactor shown in Figure 1. The reactor was seeded with 2 L sludge obtained from the bio-filter unit of KRPC wastewater treatment plant. An air compressor was used to supply air at a rate of 10 L/min into the reactor for aeration and to maintain intimate contact between the influent wastewater and the microbes. The process was operated at a hydraulic retention time (HRT) of 2,4,6,8 and 10 Hrs, at the end of each HRT, effluent was taken for BOD, biomass growth and coliform count analysis using the America Public Health Association (APHA) Standard Method for the Examination of Water (APHA, 2017).

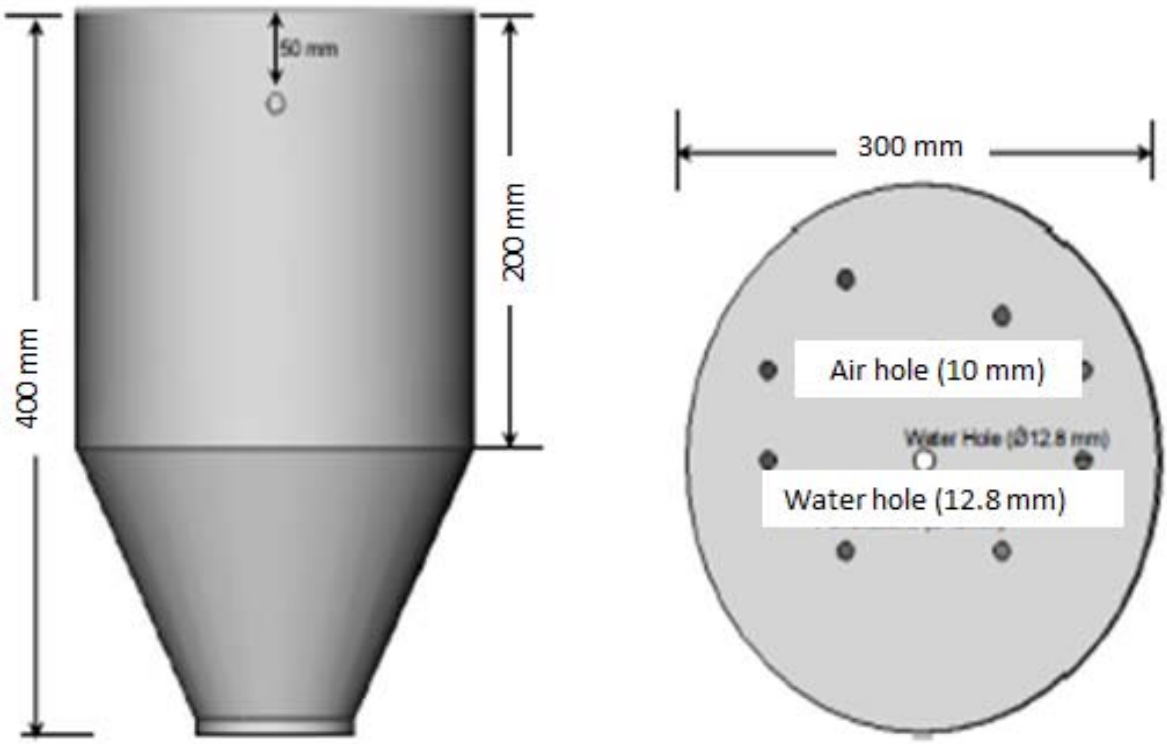

Figure 1: Activated Sludge Bio-reactor

Equations (4) and (16) were linearized to obtain Equation (17) and (18) as shown in Table 1, which were plotted to arrive at the kinetic coefficients (Haydar and Aziz (2009) and Ambreen *et al.* (2013)).

$$\frac{X\theta}{So-S} = \frac{Ks}{k}\frac{1}{S} + \frac{1}{k} \quad \text{(17)}$$

$$\frac{1}{\theta} = \frac{So-S}{X\theta}Y - K_d \quad \text{(18)}$$

Where X is mass of microorganisms, S is mass of organic matter used as food by the microorganisms (BOD), and Y is the cell yield coefficient, which is the ratio of the mass of cells formed to the mass of substrate consumed. K_d represents the proportion of the total mass of microorganisms that self-degrades (endogenous respiration) per unit time, K is the maximum rate of substrate utilization per unit mass of microorganisms, and K_s is the half saturation constant,

which is the substrate concentration at one half of the maximum growth rate, mass per unit volume.

Table 1: Monod and modified Monod Kinetics

S/N	Rate Expression	Kinetics	Integrated Form	Plot
1	$\frac{ds}{dt} = \frac{KsX}{(Ks+S)}$	Monod Kinetics	$\frac{X\theta}{So-S} = \frac{Ks}{K}\frac{1}{S} + \frac{1}{K}$	Plot of $\frac{X\theta}{So-S}$ versus $\frac{1}{S}$
2	$\frac{dX}{dt} = \mathrm{Y}\frac{dS}{dt} - K_d X$	Modified Monod	$\frac{1}{\theta} = \frac{So-S}{X\theta}Y - kd$	Plot of $\frac{1}{\theta}$ versus $\frac{So-S}{X\theta}$

3. Results and Discussion

3.1. Cell growth and substrate utilizations

Figure 2 shows that cell growth rate is proportional to the cell concentration X with gradual utilization of the substrate. Bacteria growth count also shows in Figure 1 that there is a steady increase in bacteria growth from 1.1×10^5 to 6.4×10^5 cfu after 10 hours of aeration.

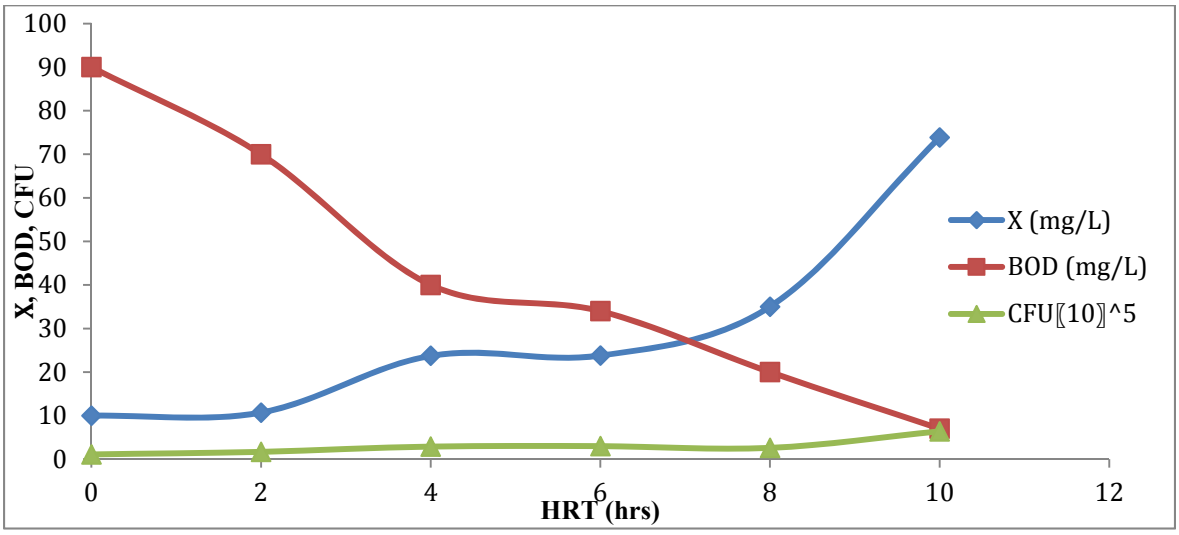

Figure 2: Cell Growth and Substrate Utilization

Figure 3 is the Food-to-Microorganism Ratio (F/M) obtained at various HRT; this indicates how much food is available at a particular time for microorganism to consume. An appropriate F/M ratio is necessary to obtain proper performance from the activated sludge process.

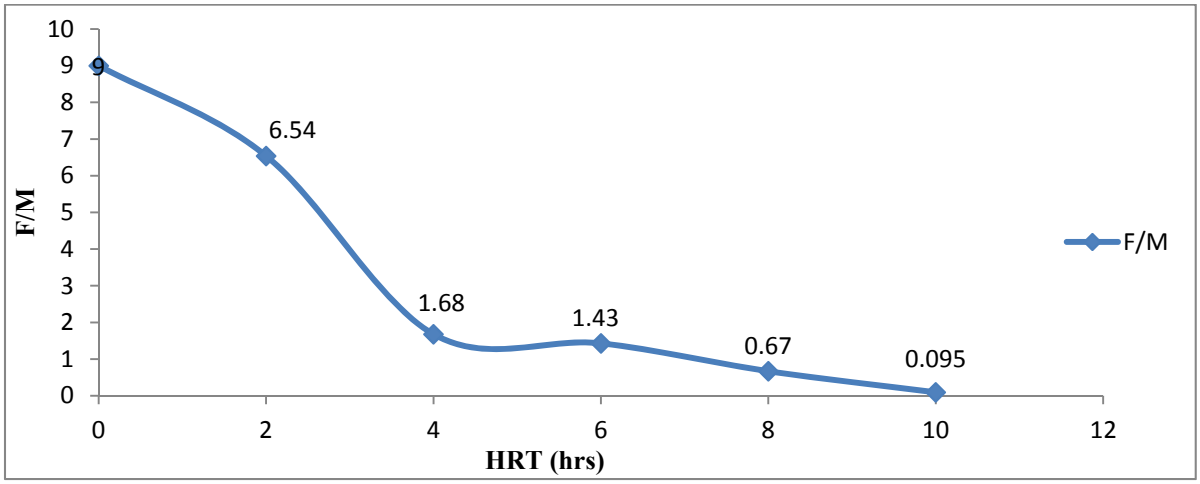

Figure 3: Food-to-Micro-organism ratio

The highest value of 9.0 was obtained at the start of the process when the food (BOD) was very high but it gradually reduces as treatment progresses and more food has been used up for metabolism by the microorganism.

3.2. Determination of bio-kinetic coefficients

Figure 4 and 5 is the plots of the linearized Monod and modified Monod equations in Table 1 which were used to determine the bio-kinetic coefficients for petroleum refinery wastewater bio-degradation in the activated sludge process. Using the Line-Weaver approach, a linear regression line is fitted to the plotted data. The intercept on the y-axis and the slope of this line is used to find K and K_s. From the linearized Equation 17 and Figure 4, K = 4.4 day^{-1}, Ks =275 mg/L.

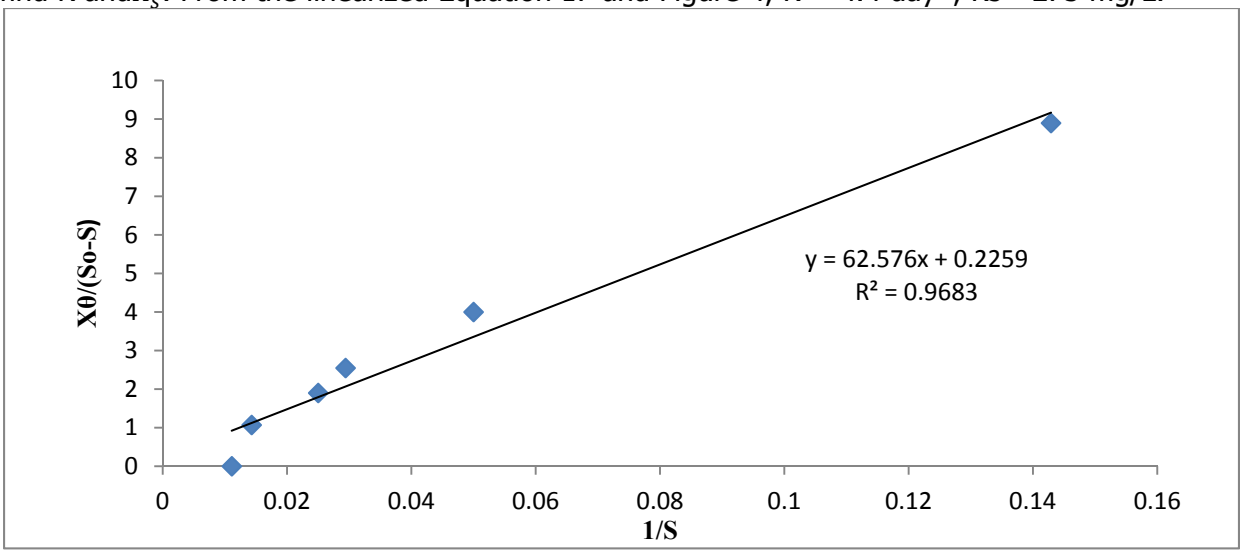

Figure 4: Determination of K and K_s

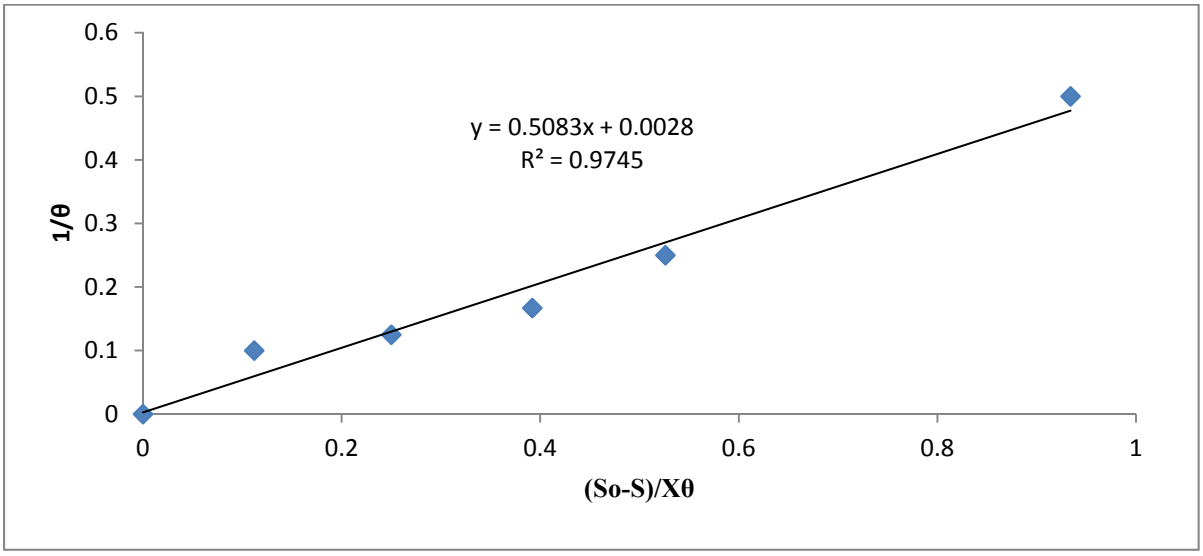

Figure 5: Determination of K_d and *Y*

Figure 5 is the plot of the linearized form of the modified Monod equation which was used to obtain K_d and *Y.* A plot of 1/θ against (So-S)/Xθ, gives an intercept which represents K_d, while the slope represents Y. Therefore, an Endogenous Decay Constant (K_d) and Yield Coefficient (Y) of 0.0028 and 0.5083 respectively were obtained for this study as seen in Figure 5

Kinetic parameters vary for different industrial wastewater based on the nature of raw materials processed and the nature of wastewater effluent. Table 2 shows a fit of the obtained kinetic coefficients in Equation (4), (5), (9), (10) and (15) for substrate utilization rate, maximum bacterial growth rate, bacterial growth rate, microbial death rate and net biomass production rate respectively.

Table 2: Parameters for Substrate Utilizations and Biomass Growth Prediction

	Parameter	Equation	Predictive Equation
1	Substrate utilization rate	$r_{su} = \frac{kSX}{K_s + S}$	$r_{su} = \frac{4.4SX}{275 + S}$
2	Maximum bacterial growth rate	μ_{max}=kY	u_{max}=4.4×0.5083= 2.236
3	Bacterial growth rate	$\mu = \mu_{max}\frac{S}{K_s + S}$	$\mu = 2.236\frac{S}{275 + S}$
4	Microbial death rate	$r_d = -(k_d)(X)$	$r_d = -(0.003)(X)$
5	Net biomass production rate	$r_g = Y\frac{kSX}{K_s + S} - K_dX$	$r_g = 0.5083\frac{4.4SX}{275 + S} - 0.003X$

Table 3 presents the summary of kinetic parameters of petroleum wastewater treatment in activated sludge process obtained in this work and previous works.

Table 3: Obtained Kinetic Coefficients and Previous Works

S/N	Author	Wastewater	K (day^{-1})	K_s (mg/l)	Y mgVSS/mg sCOD	K_d (day^{-1})
1	**This work**	**PRWW**	**4.4**	**275**	**0.5083**	**0.003**
2	Ambreen *et al.*(2013	Dairy	4.46	534	0.714	0.038
3	Mardani *et al.* (2011).	Municipal	0.95-0.98	52-71	0.48-0.8	0.0189-0.026
6	Haydar and Aziz (2009)	Tannery	3.125	488	0.64 mgVSS/mgBOD	0.035

3.3 Kinetic parameters obtained and their significance

3.3.1 Maximum Rate of Substrate Utilisation (K)

K is the maximum rate of substrate utilization per unit mass of microorganisms. K value of 4.4 was obtained for petroleum refinery wastewater treatment in a pilot scale activated sludge process. Although there is no previously reported K value for petroleum refinery wastewater treatment in an activated sludge process, a value of 0.216 was reported for fertilizer industry wastewater by Gupta and Sharma (1996). A higher value of 3.125 was obtained by Haydar and Aziz (2009) for tannery wastewater. Ambreen *et al.* (2013) obtained a close value of 4.46 for diary wastewater. K value affects the volume of the reactor in a biological system. The greater the value of k, the smaller will be the size of the reactor (Benefield and Randall, 1980).

3.3.2 Half Saturation Constant (K_s)

Half Saturation Constant which is K_s in the Monod Model and analogues to the Half Velocity Constant (Vmax) in the Michealis-Menten Model. K_s is the substrate concentration at which specific substrate utilization rate is half of maximum substrate utilization rate. In this work K_s was obtained to be 275. A large value of K_s shows that the maximum specific yield of bacteria occurs at high substrate concentration in the case of dairy industry and other industrial wastewaters (Ambreen *et al.*, 2013).

K_s is one of the coefficients that are normally determined, yet it has no direct application in the process design, the only significance of K_s is more of a theoretical nature and gives an idea about change in specific growth rate of bacteria with a change in the concentration of growth limiting substrate (Benefield and Randall, 1980). In view of the above it may be said that the change in specific growth rate of bacteria with a change in the concentration of growth limiting substrate for petroleum refinery wastewater treatment in an activated sludge system is 275.

3.3.3 Biomass Yield (Y)

Yield Coefficient or Biomass Yield is the mass of cells produced per unit of substrate utilized which may be measured as mgVSS/mgCOD, it may also be described as how biomass is produced against substrate utilized. A value of 0.5083 was obtained for this work as shown in Figure 4.19. Yield coefficient of 0.714 mg VSS/mg sBOD was reported by Ambreen *et al.* (2013). Typically yield coefficient ranges from 0.4-0.8 (Sperling, 2007). Haydar and Aziz (2009) reported 0.64 for tannery wastewater treatment in activated sludge process, none was found reported for petroleum refinery wastewater.

The significance of Y in process design is that it gives an estimate of the sludge produced as a result of wastewater treatment. The greater the value of Y, the greater will be the amount of sludge, and the size of sludge handling facility. Preliminary cost estimates for sludge handling can be found out once the size is known (Ambreen *et al.*, 2013).

3.3.4 Endogenous Decay Coefficient (K_d)

K_d Endogenous decay coefficient is the fraction of the cells oxidized by endogenous respiration per unit of time. An endogenous decay coefficient of 0.003 was obtained in this study. The range of K_d generally for wastewater treatment is 0.06-0.100 (Sperling, 2007). Haydar and Aziz (2009) reported a value of 0.035 for tannery wastewater while Ambreen *et al* (2013) also reported another close value of 0.038 for diary industry wastewater. High value of K_d is an indication of high bacterial decay rate.

K_d has a reasonable significance in the design of activated sludge process as it is used in the evaluation of net sludge production in activated sludge process. According to Benefield and Randall (1980), it can be used to fine-tune the size of sludge handling facilities resulting in some economic benefits in the cost reduction.

4.0 Conclusion

Petroleum refinery wastewater biodegradation in an activated sludge process gave the following kinetic coefficients: Maximum substrate utilization rate= 4.4 mgBOD per mgVSS per day, half saturation constant= 275 mgBOD per liter, yield coefficient= 0.5083 mgVSS/mgBOD_5 and endogenous decay constant=0.003 day^{-1}. These kinetic coefficients are useful as predictive and diagnostic tool for further design and control of activated sludge process for optimal process performance.

References

Ambreen L., Muhammad , N.C and , Shazia, I. (2013). Biological treatment of dairy wastewater using activated Sludge. *ScienceAsia, 29*, 179-185.

APHA (2017) *Standard Methods for the Examination of Water and Wastewater*. 21st Edition, American Public Health Association/American Water Works Association/Water Environment Federation, Washington DC.

Benefield LD, Randall CW (1980). Biological Process Design for Wastewater Treatment, Prentice Hall, Inc., Englewood Cliffs.

Carlos E. Santo, Vítor J.P. Vilar, Amit Bhatnagar, Eva Kumar, Cidália M.S. Botelho and Rui A.R. Boaventura (2013) Biological treatment by activated sludge of petroleum refinery wastewaters, *Desalination and Water Treatment*, 51:34-36, 6641-6654.

Coelho, A., Castro, A.V., Dezotti, M., and Sant'Anna Jr., G.L. (2006). Treatment of Petroleum Refinery Sourwater by Advanced Oxidation Processes. *J. Hazard. Mater*. 137, 178–184.

Fazel Dolati (2016). Kinetics Study of Organic Removal in a Biological Treatment of Refinery Wastewater by Activated Sludge, *6th Conference 0n Energy Management and the Environment,* Iranian Scientific Society of Thermal Engineering, Energy Seminar Kimia, 2016,Volume 6

Gupta SK, Sharma R (1996) Biological oxidation of high strength nitrogenous wastewater. *Water Resources,* 30, 593–600.

Haydar, S., and Aziz, J.A. (2009). Kinetic Coefficients for the Biological Treatment of Tannery Wastewater using Activated Sludge Process. *Pak. J. Engg and Appl. Sci., 5*, 39-43.

Mardani, Sh., Mirbagheri, A., Amin, M.M and Ghasemian, M. (2011). Determination of Biokinetic Coefficients for Activated Sludge Processes on Municipal Wastewater ., 2011, Vol. 8, No. 1, pp. 25-34. *Iran. J. Environ. Health. Sci. Eng, Vol. 8,* (No. 1), 25-34.

Qin, J.-J., Oo, M.H., Tao, G., Kekre, K.A., 2007. Feasibility study on petrochemical wastewater treatment and reuse using submerged MBR. Journal of Membrane Science 293, 161-166.

Sperling, M. V. (2007). *Activated Sludge and Aerobic Biofilm Reactor* (Vol. 5). London, U.K: IWA Publishing, Alliance House.

Taghreed A and Muftah, H. E (2018). Organic Contaminants in Refinery Wastewater: Characterization and Novel Approaches for Bio-treatment. *Recent Insights in Petroleum Science and Engineering.*

Tchobanoglous, G., Burton, F. L., Stensel, H. D., and Metcalf and Eddy. (2003). *Wastewater Engineering: Treatment and reuse*. Boston: McGraw-Hill.

Proceedings of the 49th NSChE Annual Conference
KADA 2019: pp 127-138

P1B-06: MIL-53(Fe)/COW BONE CHAR COMPOSITE FOR CHROMIUM REMOVAL FROM TANNERY WASTEWATER

[a]Ajayi O. A.,[a] Shindangi N and [b]Oladipo A.A
Department of Chemical Engineering, Ahmadu Bello University, Zaria. Kaduna State.
Department of Environmental Engineering, Cyprus Science University, Girne,
TRCN Mercin 10, Turkey.

ABSTRACT
MIL-53(Fe)/Cow bone char composite, prepared via the sol-gel method was used for the removal of chromium from real tannery effluent having an initial concentration of 40mg/L. The characteristics of MIL-53(Fe)/Cow bone char were studied using X-ray diffraction (XRD), Fourier transform infrared spectroscopy (FTIR), thermo gravimetric analysis (TGA) Boehm titration and scanning electron microscopy (SEM-EDX). Adsorption capacity of MIL-53(Fe)/Cow bone char composite for chromium was 19.61mg/g with a removal efficiency of 87.8% at an optimal bed height of 2.4cm (2.0g) for MIL-53(Fe)/Cow bone char composite, time of 2 minutes and pH_{pzc}=5.4.The kinetic studies showed that the adsorption data were fitted well to the pseudo second-order model with high correlation coefficient R^2=0.9911. Furthermore, the adsorption isotherm equilibrium studies confirmed that the Langmuir model best described the adsorption process of chromium onto MIL-53(Fe)/Cow bone char composite. A result from analysis of data with Dubinin–Radushkevich and Temkin isotherms showed that adsorption of chromium onto MIL-53(Fe)/Cow bone char composite is physical in nature.

Introduction
Wastewater discharge from industrial sectors such as agriculture, textile, tanneries, pulp and paper contribute largely to environmental pollution when untreated. Some of which contain heavy metals like cadmium and chromium that are toxic, mutagenic, carcinogenic and cause hormonal disorder to human life. Tannery waste is generated in huge amount during the tanning process by leather industries all over the world (Mohammed *et al*., 2017). The used and non-useable hides and skins along with the excess chemicals and water used in the process constitute solid and liquid wastes in the tannery (Mohammed *et al*., 2017), which when untreated affect streams, groundwater, land and sewers in which they are discharged. Important pollutants associated with the tanning industry include chlorides, tannins, chromium, sulphate, sulphides and increasing use of synthetic chemicals such as pesticides, dyes and finishing agents.

Several adsorbents have been investigated including zeolite, cow bone, activated carbon, banana peel, sugarcane bagasse, rice husk, palm kernel shell, coconut shell etc. Modern technology employs the use of composites that have extraordinary combination of properties (Araoye, 2015). One of the materials used are the metal organic framework (MOFs) with carbon-based materials. Recently, metal of organic framework materials (MOFs) with high porosity and high surface area have gained application in adsorption, membrane separation, sensing, catalysis and proton conduction, owing to their water stable structure (Wang *et al*., 2016). They have adjustable surface properties, and have more abundant and controllable porous structures compared to conventional porous materials such as zeolite, silica and activated carbon (Jiao *et al*., 2017).

Cow bones used in this research constitutes a waste of natural resources especially in developing countries. Cow bones which are obtainable from slaughtered cows in abattoirs are readily available in Nigeria and are usually burnt or sold to feed mill for the production of animal feeds.

Cow bone char consists mainly of 57–80% tricalcium phosphate,6–10% calcium carbonate and 7–10% carbon (Fawell, 2006).

The use of MIL-53(Fe)/cow bone char composite for the removal of chromium in tannery wastewater through the process of adsorption has not been harnessed and thus, will be used in this present study.

Materials and Methods

Materials and Instruments

All chemical reagents, namely: Iron (III) chloride hexahydrate ($FeCl_3.6H_2O$). Terephthalic acid (H_2BDC) N,N'-Dimethylformamide (DMF, 99.8%), Ethylene glycol and Sodium hydroxide were of analytical grade (≥98%). Cattle bones were collected at Zango abattoir, Zaria, Nigeria. Deionized water was obtained from the PTDF Laboratory, Department of Chemical Engineering Ahmadu Bello University, Zaria. The tannery wastewater wascollected from the Nigerian Institute of Leather and Science Technology (NILEST), Zaria, Nigeria.

Synthesis of MIL-53(Fe)

MIL-53(Fe) powder was prepared via a modified previously reported method (Dan *et al.*, 2017; Oladipo, 2018). A mixture of Iron (III) chloride hexahydrate ($FeCl_3.6H_2O$) (1.35g), 1,4-benzenedicarboxylic acid (H_2BDC) (0.83g), and N,N'-Dimethylformamide (DMF) (112 ml) were mixed and stirred at room temperature using a magnetic stirrer until it became clear, then the reaction mixture was transferred into a 100ml Teflon-lined stainless steel autoclave and heated at 180°C for 10h. After the heat treatment, the autoclave was allowed to cool to room temperature and the resultant suspension was filtered and the orange MIL-53(Fe) powder residue was washed with 200ml deionized water and allowed to dry at 150^0C in the oven overnight in order to remove the DMF in the pores. The resulting sample was stored at room temperature in a covered glass container until the time of study. The functional groups, surface morphology, crystal structure and surface area were determined using FTIR spectrophotometer, SEM, XRD and BET respectively for the as-prepared MIL-53(Fe).

Preparation of bone char

Cow bone char was prepared via a previously reported method (Patel *et al.*, 2015). Cattle bones collected at Zango abattoir, Zaria, Nigeria were parboiled with NaOH, washed thoroughly with water several times, dried at 100^0C for 1h. The dried bones were carbonized at a temperature of 500^0C for a residence time of 1h resulting into bone char. The bone char was further ground to powder using a ceramic mortar and pestle followed by sieving to a particle size of 75µm with an electric sieve shaker.

Synthesis of MIL-53(Fe)/Cow bone char composite

The composite was prepared via a previously reported method (Oladipo, 2018). 4.2g of the as-prepared MIL-53(Fe) was suspended into 100 ml ethylene glycol in a flask and stirred for 1h. And then, 3.2 g of cow bone powder was added to the above suspension, followed by continuous stirring with heat for 190mins at 100^0C for solvent evaporation. The resulting solid was washed severally with 160ml deionized water and 40ml ethanol and decanted with a suction pump and sinter glass. It was further dried in the oven at 80^0C for 5h and finally calcined at 500^0C for 1h and cooled, sieved and stored in desiccator.

Treatment of tannery wastewater by fixed-bed system

The dynamic sorption studies were carried out in a plastic column of 1.2cm in diameter and 7.5cm in length. Different masses of 0.5g, 1.25g and 2.0g of composite was packed into the column, achieving a bed height of 0.6cm, 1.5cm and 2.4cm respectively. The tannery wastewater with an initial concentration of 40mg/L was allowed to pass over the adsorbent bed at different times of 2mins to 16mins. The initial and final chromium concentration in the effluent samples was determined by atomic absorption spectroscopy (SHIMADZU, Model-AA6800 AAS).The amount of heavy metal adsorbed (q_t) at any given time (t) and at equilibrium (q_e) can be expressed as equations 1 and 2 respectively (Chowdhury *et al.*, 2013; Agoyi *et al.*, 2015).

$$q_t = \left(\frac{C_o - C_t}{m} \right) V \quad (1)$$

$$q_e = \left(\frac{C_o - C_e}{m} \right) V \quad (2)$$

While the percentage of heavy metal adsorbed is expressed as equation 3:

$$\% = 100 \left(\frac{C_o - C_t}{C_o} \right) \quad (3)$$

Where:
C_0 is the initial chromium concentration (mg/L)
C_t is the chromium concentration at time t (mg/L)
C_e is the molar equilibrium concentration of the solute remaining after adsorption (mg/L)
M is the mass of the adsorbent (g)
V is the volume of solution used (L)

Column desorption of MIL-53(Fe)/cow bone char composite and regeneration studies

Desorption studies were performed with MIL-53(Fe)/cow bone char composite that was saturated with tannery wastewater of pre-determined chromium concentrations. The flow rate was adjusted to 5ml/min at a bed height of 2.4cm. After the column had reached exhaustion, the exhausted MIL-53(Fe)/cow bone char composite was regenerated using 0.05M NaOH. After elution, the bed was washed with distilled water until the pH stabilised close to neutral (7.0). Three cycles of sorption-desorption-regeneration were carried out to evaluate the MIL-53(Fe)/cow bone char composite capacity. The chromium removal percentage was determined in each cycle.

Results and Discussion

Physicochemical characteristics of tannery wastewater

From Table 1, the total suspended solids concentration in the sample tannery wastewater was 5920mg/l which classifies it as strong wastewater. Hence tannery industrial waste cannot be discharged into the environment. Similarly, total dissolved solid concentration was 7160mg/l indicating that the tannery wastewater contain soluble solids as well as floating solids. The result of Table 1 shows a COD and BOD concentration of 1600mg/l and 170mg/l respectively. This is due to the use of inorganic chemicals that are oxygen demand in nature. The pH of wastewater

is the strength of acidity or alkalinity of the wastewater, which is the measure ofhydrogen ion concentration in the wastewater (Oke *et al.*, 2006).

Table 1: Physicochemical Parameters of Tannery Wastewater

S/N	Parameter	Unit	Result
1	pH	-	6.8
2	Dissolved Oxygen (DO)	mg/l	210
3	Biological Oxygen Demand	mg/l	170
4	Total Dissolved Solids	mg/l	7160
5	Total Suspended Solids	mg/l	5920
6	Chemical Oxygen Demand	mg/l	1600
7	Total Chromium Concentration	mg/l	40
8	Electrical Conductance	µmhos/cm	190
9	Color	Hazen Unit	1200

Characterization of samples

Figure 1 presents the XRD pattern of the synthesized MIL-53(Fe), the diffraction lines appeared at 2θ of 8.9 (101), 11.2, 14.5, 17.5 (002), 23.5 (302), were identical to those reported for standard MIL-53(Fe) (Araya *et al.,* 2017; Oladipo, 2018) and no other lines were observed indicating that the pure crystalline phase of MIL-53(Fe) was synthesized. The XRD pattern of bone char is consistent with the standard crystalline hydroxyapatite and distinct diffraction peaks were observed at the 2θ of 26.3°, 28.2°, 32.1°, 37.9°, 43.2°, 47.8°, 49.4°, 50.4° and 62° which is agrees with the JCPDS card no: 82-1943. The XRD pattern of the MIL-53 (Fe)/char exhibits the coexistence of both MIL-53 (Fe) and bone char phases, no any impurity peaks detected, and thus indicated the high purity of the composite. While the characteristic diffraction peaks of MIL-53(Fe) reduced in intensity in the composite with no shift, the retained bone char peaks became more crystalline in nature in the composite and the structure of MIL-53(Fe) remain unchanged after the deposition of CBC (Hu *et al.*, 2017).

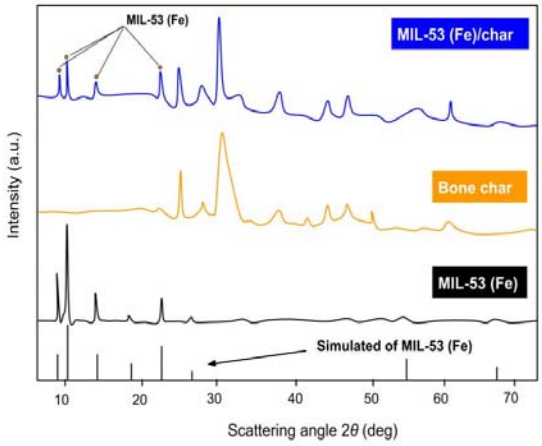

Figure 1: XRD patterns for samples

The morphology and spectra of elemental analysis of cow bone char, MIL-53(Fe) and MIL-53(Fe)/cow bone char composite are reported in Figure 2. The micrograph for cow bone char clearly shows that the sample had undergone significant structural changes due to the thermal

treatment at 500^{0}C which indicates that the thermal treatment creates more pores on the surface and increases the surface area (Mendoza-Castillo *et al*., 2014). Cow bone char exhibits a distinct morphology from the MIL-53 (Fe). As seen, the cow bone char is characterized by a highly dense continuous fibrous-like structure with crunchy textural surface and its chemical composition includes the presence of carbon, oxygen, phosphorus, and calcium, which are the main components of hydroxyapatite (Mendoza-Castillo *et al*., 2014) with minor traces of sodium, iron and magnesium. These results are consistent with the results of X-ray diffraction (see Figure 1).

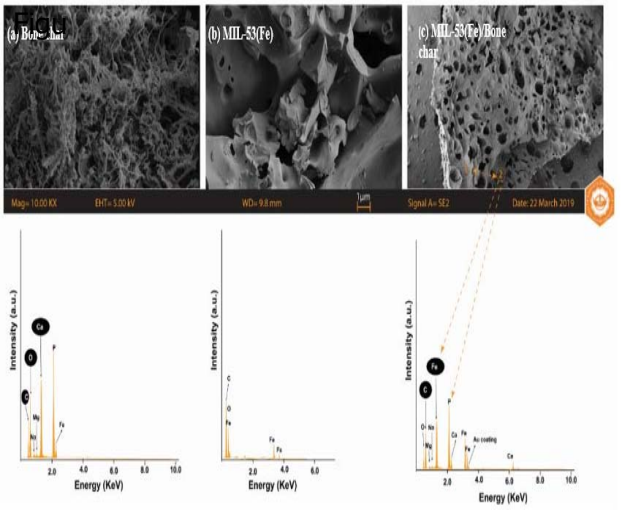

Figure 2: SEM-EDX images for samples

In contrast, the MIL-53 (Fe) morphology is homogeneous and characterized by well-defined smooth surface and pronounced polyhedron-like crystalline structure and its chemical composition include the presence of Iron (Fe), carbon and oxygen as depicted on the physicochemical characteristic for the sample in Table 2 as reported by Oladipo *et al*. 2017).

The surface of the MIL-53(Fe)/cow bone char is relatively smooth with heterogeneous meso and micro-pores and thick cuticle-like edges because of hetero-junctions of the pores of cow bone char onto the MIL-53(Fe) structure and the thermal treatment of the composite, which increased the porosity of the structure. Its chemical composition includes the presence of carbon, oxygen, phosphorus, calcium from the hydroxyapatite structure of cow bone char and Iron with minor traces of sodium, iron and magnesium.

The FTIR spectra are shown in Figs. 3, 4 and 5 respectively. For the MIL-53(Fe), a broad vibration at around 3480 cm^{-1}was attributed to the stretching vibrations of the O–H of water molecules adsorbed on the surface. The asymmetric (γ_{as} C-O)and symmetric (γ_s C-O) stretching of carboxyl group could be described by the appearance of sharp vibrations at 1525 cm^{-1} and 1380 cm^{-1} respectively indicating the presence of dicarboxylate linkers within the framework (Oladipo, 2018). The carbonyl groups (C=O) of the carboxylate ligand (COO) were visible at 1696 cm^{-1}, whereas a very sharp peak at 750 and 696 cm^{-1} corresponds to the Csp^2-H (C=C-H) bending vibrations, which belong to the benzene rings of carboxylates. The characteristic coordination bonds between Fe^{3+} cations and -OOC-C_6H_4-COO- carboxylate anions were observed at a very low wave number of 545 cm^{-1} which implies the existence of a Fe-oxo-bond present in the MIL-

53(Fe) structure that exists between the carboxylic group of terephthalic acid linker and the inorganic iron(III) metal (Zhang *et al.*, 2016; Oladipo, 2018). The MIL-53(Fe) spectrum clearly exhibited the characteristic absorption peaks and thus confirms the formation of MIL-53(Fe) structure (Oladipo, 2018).

For the cow bone char, the C-O stretching vibrations at 1453 with a shoulder at 1421cm^{-1} has been assigned to CO_3^{2-} group indicating that CO_3^{2-} is present (Patel *et al.*, 2015). The bands at 1041 and 962 cm^{-1} has been assigned to the P-O stretching vibrations of PO_4^{3-} group. The bands at 600, 561 and 475cm^{-1} corresponds to PO_4^{3-} bending vibrations (Patel *et al.*, 2015).

The intensity of the characteristic absorption peaks of MIL-53 (Fe) were decreased, the peak at 1380 cm^{-1} become narrower and the Fe-O band was widened at 545cm^{-1} (Oladipo, 2018). The bands at 1026 and 963 cm^{-1} is seen to also appear which is assigned to the P-O stretching vibrations of PO_4^{3-} group from the hydroxyapatite structure of the bone char. The broad vibration from the MIL-53(Fe) is seen to disappear in the spectra of the composite as a result of sintering at 500^{0}C and thus, becoming broader.

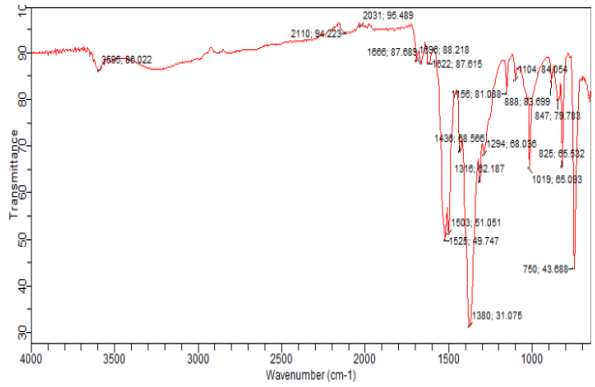

Figure 3: FTIR for MIL-53(Fe)

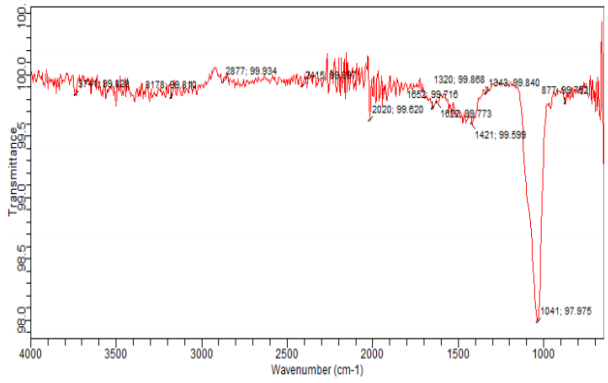

Figure 4: FTIR for Cow bone char

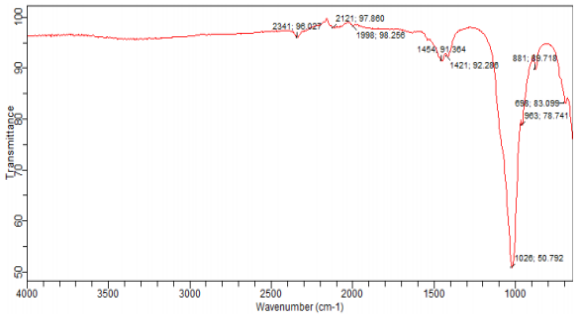

Figure 5: FTIR for MIL-53(Fe)/Cow bone char composite

Analysis of samples

Table 2 shows the results for ultimate and proximate analysis of all samples as well as specific surface area and pore parameters of the samples. The prepared cow bone char has a high surface area of 108.2m^2 g^{-1}compared to that of MIL-53(Fe) with 69.5m^2 g^{-1}, while the composite recorded 125.6m^2 g^{-1}. In terms of pore size, the synthesized MIL-53(Fe) has a higher value of 13.9nm compared to that of cow bone char of 8.94nm which explains the network structure of MIL-53(Fe) as highly flexible and opens up its pores to guest host (breathing effect), though having a small surface area compared to other metals (Janiak and Jana, 2010; Oladipo, 2018). And on introduction of cow bone char to the composite structure, there was a reduction in the pore size to 11.2nm. The results obtained

The results obtained confirm that the composite have mesoporous structures suitable for the entrapment of the reactive species, chromium and subsequent enhancement of the adsorption process reactive species, chromium and subsequent enhancement of the adsorption process (Oladipo, 2018). The elemental analysis indicates the presence of P_2O_5 higher in cow bone char than in the MIL-53(Fe)/cow bone char composite having 38.66% and 22.78% respectively with an absence in MIL-53(Fe) structure. This result is depicted on the SEM-EDX analysis of the samples. The percentage content of Iron (Fe) is seen to be higher in MIL-53(Fe) with 8.16% and MIL-53(Fe)/bone char composite with 8.23% compared to bone char having 0.07% of Fe.

Table 2: Properties of Samples

Property	**Cowbone char**	**MIL-53(Fe)**	**MIL-53(Fe)/Char**
Total surface area (m^2 g^{-1})	108.2	69.5	125.6
Pore size (nm)	8.94	13.9	11.2
Total pore volume (cm^3 g^{-1})	0.589	0.789	0.981
Micropore volume (cm^3 g^{-1})	0.237	0.396	0.325
Density (g cm^{-3})	0.69	0.89	1.12
Carbon content (%)	13	15.3	22.4
pHpzc (zero point charge)	6.7	4.5	5.4
P_2O_5 (%)	38.66		22.78
N_2 (%)	0.89		0.32
Fe (%)	0.07	8.16	8.23
Ca (%)	26.55		11.89
Mg (%)	0.67		0.23
SO_4 (%)	0.89		0.23
S(%)	0.38		0.004
Cation exchange capacity (meq g^{-1})	7.5	4.56	6.56

Adsorption column studies

Effect of time of collection

The contact time was determined for different flow rates of 5ml/min and 15ml/min as shown in Figures 9 and 10. The percentage removal of chromium increased up to 4 minutes having a maximum removal at 87.9% and 80.94% respectively following a reduction up to 14 minutes and there after no further changes was observed.

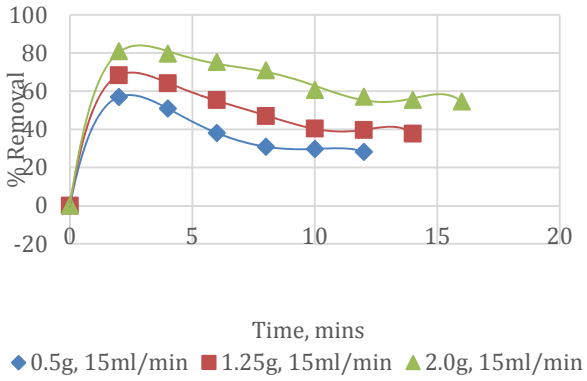

Figure 9: Chromium removal with time (5ml/min)

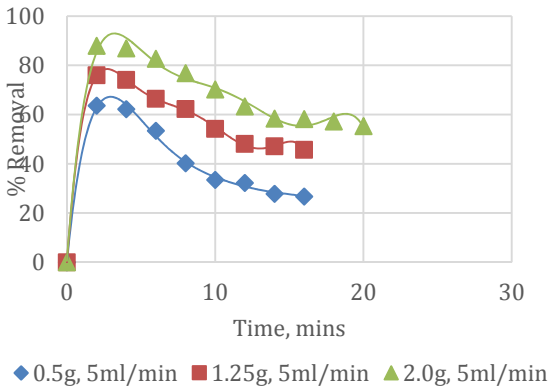

Figure 10: Chromium removal with time (15ml/min)

Effect of flow rate on breakthrough curve

The breakthrough curve in Figure 11 showed that at lower flow rate of 5ml/min, the surface of the composite was readily available for adsorption and more molecules were adsorbed as there was sufficient contact time with chromium molecules. Thus, having a higher adsorption percentage as well as a shallow adsorption zone and breakthrough and exhaustion were not quickly reached. While at higher flow rate, there was an increase in rate of mass transfer, shorter contact time and a steeper curve with relatively early breakthrough and exhaustion time which resulted in less adsorption uptake was observed. The observations drawn is in agreement with those reported by (Ghribi and Chlendi, 2011; Chowdhury *et al.*, 2013; 2015; Dutta and Basu, 2014).

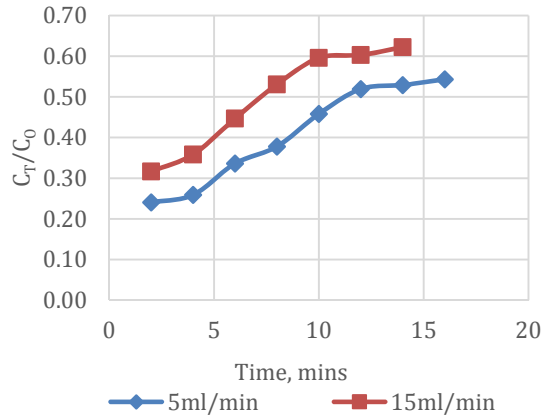

Figure 11: Breakthrough curve for chromium removal

Effect of bed height on chromium adsorption

Figure 12 shows the effect of bed height on chromium adsorption obtained for three different bed depths of 0.6cm, 1.5cm and 2.4cm at 5ml/min with an inlet concentration of 40mg/L. A higher uptake was observed at a higher bed height of 2.4cm, as more adsorbate was passed down the bed, the adsorbent bed became saturated at which there was a reduction in the individual bed efficiency to about 58%. This observation is in agreement with those reported by (Ghribi and Chlendi, 2011; Chowdhury *et al.*, 2013; 2015).

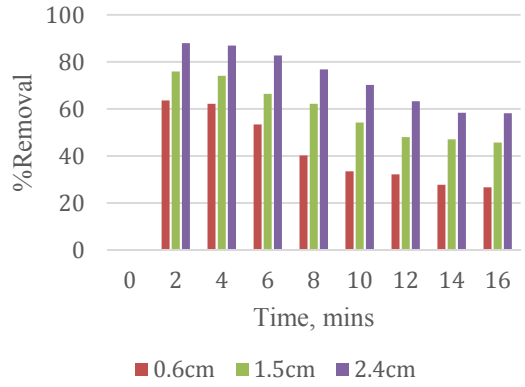

Figure 12: Bed height effect on adsorption of chromium

Equilibrium adsorption isotherm study

Tables 3 and 4, the determination of coefficients (R^2) of the linear form of Langmuir model turned out to be satisfactory having an R^2> 0.9893 and 0.9933 respectively at a bed height of 2.4cm. Also, the maximum monolayer adsorption capacity of 19.61mg/g was found at this same bed height of 2.4cm compared to other bed heights which indicate uniform monolayer coverage. $R_L$values determined were found to be in the range $0<R_L<1$ which explains that the chromium ions is favorably adsorbed and the values of the equilibrium constant K_L were lower than unity which quantitatively reflects the strong affinity between the chromium ions and the MIL-53(Fe)/cow bone char composite.

K_F was determined to be 13.5515mg/g, 6.63461mg/g and 4.8759mg/g which explains the random distribution of cow bone char between the crystallites of MIL-53(Fe) which may introduce heterogeneity onto the surface (Ghanizadeh *et al.*, 2012) and a favorable sorption capacity.

From the Temkin plot, the heat of adsorption of chromium ions onto the composite was seen to be higher at 0.6cm and reduced at 1.5cm with a slight increase at 2.4cm for both flow rates indicating an exothermic process. Also, the b values are lower than 80kJ/mol which indicates that the adsorption of chromium ions onto MIL-53(Fe)/cow bone char composite is a physical adsorption process and consistent with FTIR analysis.

The mean energy of adsorption for chromium onto MIL-53(Fe)/cow bone char composite were all below 8kJ/mol withR^2values all at 0.9 and demonstrates that the adsorption of chromium onto MIL-53(Fe)/cow bone char is physisorption and plays an important role.

Table 3: Isotherm parameters for chromium adsorption onto MIL-53(Fe)/CBC composite

Isotherm	**Kinetic Parameters, 0.6cm, 5ml/min**	**Kinetic Parameters, 1.5cm, 5ml/min**	**Kinetic Parameters, 2.4cm, 5ml/min**
Langmuir	Q_m=4.2753mg/g K_L=0.087L/mg R_L= 0.22273 R^2=0.9579	Q_m=8.326mg/g K_L=0.170L/mg R_L= 0.12807 R^2=0.9850	Q_m=19.61mg/g K_L=0.368L/mg R_L=0.06361 R^2=0.9893
Freundlich	K_F=13.5515 1/n=1.20 n=0.830 R^2=0.9696	K_F=6.63461 1/n=0.62 n=1.596 R^2=0.9735	K_F=4.8759mg/g 1/n=0.35 n=2.824 R^2= 0.9608
Temkin	A_T=49.9198L/g b_T=196.586 B=12.603J/mol R^2= 0.9942	A_T=75.8987L/g b_T=275.601 B=8.9897J/mol R^2= 0.9896	A_T=174.354L/g b_T=246.206 B=10.063J/mol R^2= 0.978
Dubinin-Radushkevich	β=0.00004 Q_m=5.5384mg/g E=111.8J/mol R^2=0.9056	β=0.00001 Q_m=10.4093mg/g E=223.6J/mol R^2=0.8805	β=0.000002 Q_m=14.0202mg/g E=500J/mol R^2=0.8019

Kinetics of adsorption

Three kinetic models were employed to describe the sorption rates for chromium and obtained results are presented in Table 5.

The equilibrium adsorption of chromium onto MIL-53(Fe)/cow bone char composite could be best described with the pseudo-second order kinetic model judging by the R^2 values depicted in Table 5.

Table 4: Isotherm parameters for chromium adsorption onto MIL-53(Fe)/CBC composite

Isotherm	Kinetic Parameters, 0.6cm, 15ml/min	Kinetic Parameters, 1.5cm, 15ml/min	Kinetic Parameters, 2.4cm, 15ml/min
Langmuir	Q_m=3.88048mg/g K_L=0.074L/mg R_L= 0.25306 R^2=0.9767	Q_m=6.21891mg/g K_L=0.116L/mg R_L= 0.17683 R^2=0.9811	Q_m=17.67mg/g K_L=0.259L/mg R_L= 0.08792 R^2=0.9933
Freundlich	K_F=17.374mg/g 1/n=1.37 n=0.726 R^2=0.9829	K_F=9.053mg/g 1/n=0.88 n=1.135 R^2=0.9782	K_F=6.857mg/g 1/n=0.46 n=2.183 R^2= 0.9818
Temkin	A_T=47.7674L/g b_T=182.55 B=13.572J/mol R^2= 0.9969	A_T=58.1506L/g b_T=226.345 B=10.946J/mol R^2= 0.9937	A_T=110.757L/g b_T=201.691 B=12.284J/mol R^2= 0.9910
Dubinin-Radushkevich	β=0.00006 Q_m=4.8105mg/g E=91.2871J/mol R^2=0.9446	β=0.00002 Q_m=7.87505mg/g E=158.114J/mol R^2=0.9133	β=0.000005 Q_m=12.59mg/g E=316.228J/mol R^2=0.9011

Table 5: Kinetic model parameters for chromium adsorption onto MIL- 53(Fe)/CBC composite.

Model	Kinetic parameters
Lagergren Pseudo First-order	k_1 (min^{-1})= 0.2096 q_1 (mg/g)=14.047 R^2=0.963
Pseudo second-order	k_2 ($gmg^{-1}min^{-1}$)=0.04304 q_2 (mg/g)=12.3762 R^2=0.9911
Intraparticle diffusion	k_{ad}($mgg^{-1}min^{-1(1/2)}$)=3.0312 C_i(mg/g)=26.353 R^2=0.9503

Conclusions

In the present work, MIL-53(Fe)/Cow bone charcoal composite, was successfully prepared via the sol-gel method and was tested for the removal of chromium from real tannery effluent. The adsorption process was found to be efficient below the pH_{pzc} of 5.4. The kinetic studies showed that the adsorption data were fitted well to the pseudo second-order model with high correlation coefficient R^2=0.9911. The adsorption isotherm equilibrium studies confirmed that the Langmuir model best described the adsorption process of chromium onto MIL-53(Fe)/Cow bone char composite. Adsorption capacity of MIL-53(Fe)/Cow bone char composite for chromium was 19.61mg/g with a removal efficiency of 87.8% at an optimal bed height of 2.4cm (2.0g) for MIL-53(Fe)/Cow bone char composite. A result from analysis of data with Dubinin–Radushkevich and Temkin isotherms showed that adsorption of chromium onto MIL-53(Fe)/Cow bone char composite is physical in nature.

References

Agoyi O.R., Igboro S.B., Okuofo C.A. (2015). *Performance of Cow bone Char in Fixed-Bed Column for the Treatment of Industrial Wastewater.* Kaduna State: Department of Water Resources and Environmental Engineering, Ahmadu Bello University, Zaria.

Araoye, B. O. (2015). A Study of the Development, Characterisation and Degradability of Polyester/Nano-Locust Bean Pods Ash Composite. Ahmadu Bello University, Zaria, Department of Metallurgical and Materials Engineering.

Chowdhury, T, L. Zhang , J. Zhang and S. Aggarwal. (2018). Removal of Arsenic(III) from Aqueous Solution Using Metal Organic Framework-Graphene Oxide Nanocomposite. *Nanomaterials (8)*, 1-18.

Chowdhury, Z. Z., Zain,S.M., Rashid,A. K., Rafique,R. F., and Khalid, K. (2013). Breakthrough Curve Analysis for Column Dynamics Sorption of Mn(II) Ions from Wastewater by Using Mangostana garcinia Peel-Based Granular-Activated Carbon. *Journal of Chemistry*, 1-8. doi:http://dx.doi.org/10.1155/2013/959761

Fawell, J. (2006). Fluoride in drinking-water (1st published. ed.). *WHO ISBN 9241563192.*, 47.

Ghader Ghanizadeh, Ghorban Asgari, Abdol Motaleb Seid Mohammadi and Mohammad Taghi Ghaneian. (2012). Kinetics and Isotherm Studies of Hexavalent Chromium Adsorption from Water using Bone Charcoal. *Fresenius Environmental Bulletin*, 1296-1302.

Janiak, C and Jana K. V.. (2010),. MOFs, MILs and more: concepts, properties and applications for porous coordination networks (PCNs). *New Journal of Chemistry, 34*, Pages 2337–2684. Retrieved from www.rsc.org/njc

Mohammed, SSD; Orukotan, AA; Abdullahi, H. (2017). Physicochemical and Bacteriological Assessment of Tannery Effluent from Samaru-Zaria, Kaduna State, Nigeria. *Journal of Applied Science and Environmental Management (4), 21*, 734-740. doi:10.4314/jasem.v21i4.14

Oke,I. A., Otun, J. A., Okuofu,C. A. and Olarinoye,N. O. (2006). Characteristics of Tanning Industries in Nigeria for Aquatic Animals and Plants. *Research Journal of Agriculture and Biological Sciences, 2(5)*, 209-217.

Oladipo, A. A. (2018). MIL-53 (Fe)-based photo-sensitive composite for degradation of organochlorinated herbicide and enhanced reduction of Cr(VI). *Process Safety and Environmental Protection (116)*, 413-423.

Proceedings of the 49th NSChE Annual Conference
KADA 2019: pp 139-152

P1B-07: ISOTHERM, KINETIC STUDIES, MODELLING AND OPTIMIZATION OF ADSORPTION PROCESSES FOR CRUDE OIL REMOVAL FROM WATER USING CHITOSAN.

Oseke Godwin Gbenga*., Isa M. Tijjani, Galadima Muhammad Sani and Ameh Alewo Opuada
[1]Chemical Engineering Department, Ahmadu Bello University, Zaria.
*Corresponding author: osechemtechy@gmail.com

ABSTRACT
Crude oil spill remediation in the rivers, seas and oceans of exploration zones is on major issue of concern. The cost implication of clean up processes using synthetic adsorbent is on high side alongside the negative impact on the environment. Chitosan, a biopolymer was prepared from prawns' shells waste sourced from the Atlantic Ocean The chitosan was characterized using FTIR, XRD, AAS and proximate analysis and was used to remove crude oil spill from simulated crude oil contaminated water using batch adsorption. The chitosan yield was 20.33%. Degree of deacetylation using C/N ratio and FTIR peaks were 85.70% and 86.27% respectively. Design Expert 6.06 was used to design the adsorption experiment. Model was significant with R^2 value of 0.8488 and ANOVA model result of P>F value of <0.0001. Maximum adsorption capacity of 18.34 g g^{-1} which shows that the synthesized chitosan is a good adsorbent for crude oil spill.

Keywords: Chitosan; Batch studies, Adsorption isotherms; Adsorption kinetics, Design Expert.

1.0 Introduction
Oil pollution among many others is one of the most serious environmental problems in oil exploration regions and its becoming increasingly inevitable. The transportation of crude oil and its derivatives usually cause their spillage on water bodies and the contaminated water produces undesirable taste and odour which affect its consumption and environment. It becomes important to ensure that water sources must be well protected and necessary actions should be taken to remove these pollutants to ensure balance in the environment (Abdul *et al.,* 2012: Abdulwadud *et al.,* 2013: Aisien *et al.,* 2003: Aisien *et al*., 2006).

Crude oil tends to form insoluble layers with water as a result of its hydrophobicity, which can be easily separated from seawater by gravity and skimming. Much more difficulties are experienced when there is oil-water emulsion due to mixing. Report has shown that spraying of expanded graphite and chalk, in-situ burning of oil with wicks, use of chemical dispersant, mechanical skimming, gelling, sinking and absorbing, disposing of oil with detergent, application of mechanical floating barriers, booms or skims, use of polymeric foams and other sorbents, and enhanced biodegradation are some methods used in remediation of such contamination (Abdulwadud *et al.,* 2013: Amita and Suresh., 2011). However, these materials, over time are limited in biodegradability, efficiency, usage, cost and regeneration.

Bio-sorption, a biological method of environmental control using biomass for adsorption separation process can be an alternative to conventional adsorbents for removal of crude oil spill from water surface. Natural biopolymers are industrially attractive because of their capability to float and adsorb liquid to their pore spaces. Biopolymers are used for this bio-adsorption process because they are cheap and are widely available engineering materials that can be converted to useful materials from there raw state (Aisien *et al.,* 2003: Sun *et al*., 2002: Sun *et al*., 2003).

Raw rice husk has been used for oil removal in simulated contaminated water with sorption capacity of about 5g/g adsorbent (Yang *et al.,* 2005). Thermally treated rice husk silica at 700 ^{o}C has also been used for crude oil sorption (Kudaybergenov *et al*., 2012) with sorption capacity of 15.2g/g of adsorbent.

Chitosan, which occurs naturally in the environment in large quantities and only second in abundance to cellulose, has been used for adsorption purposes. It has an amine functional group which is strongly reactive with metal ions for crude oil adsorption (Annunciado *et al.,* 2005). Acetylated rice husk was used by Nwankwere *et al*., 2012 to carry out crude oil sorption studies with sorption capacity of 10.31g/g of adsorbent. The work of Sewvandi and Adikary., 2010 has the uptake of metal ions.

In this present research work, the effect of contact time, chitosan dosage and oil water ratio have been investigated under simulated contamination with Design Expert software to optimize the process and obtain a model equation for the adsorption.

2.0 Materials and methods

2.1 Adsorbent preparation

Common estuarine prawn shells as locally called (Hastatus spp) were sourced as waste from fishermen at River Nun, Atlantic Ocean of Bayelsa state, Nigeria. The shells obtained were washed thoroughly with distilled water and dried in an oven to constant weight at a temperature of 35^{0}C for an hour. The dried shells were size- reduced to 75µm. The demineralization of the biomass involved treating the shells with 1M HCl (1:10 w/v) at ambient temperature (approximately 28^{0}C) for 6 hours after which it was washed in the acid until no bubbles were seen and no colour change was observed. This was followed by thorough washing with distilled water to completely remove all traces of hydrochloric acid. Deproteinization was done to remove protein and sugar in the sample thus isolating the crude chitin attached to the demineralized samples by treating it with 1 M sodium hydroxide solution at solute to solvent ratio of 1:10 (w/v) for 16 hours in 250 ml conical flasks at ambient temperature (28 ℃). Washing with distilled water to pH of 7.3 removed all traces of sodium hydroxide. Chitin from this step was treated in 25 M of Sodium hydroxide (NaOH) solution of 1:10 (w/v) for 20 hours at a temperature of 115 ℃ and atmospheric pressure using a Bunsen burner in order to further leach out the undissolved proteins and remove the acetyl groups from the chitin.

The extracted chitosan samples were washed thoroughly with distilled water to pH of 7.4, filtered and then dried to constant weight using an oven at 35 ℃ for an hour.

2.2 Chitosan Characterization

Chitosan surface morphology were obtained using SEM machine for Phenom TM Pro X. Chitosan was inserted into Quorium (Q15OR ES) where it was coated with a thin layer of gold operated at voltage of 10kV. Chitosan crystallinity was measured using X-ray diffraction (XRD) on a Rigaku MiniFlex II X-ray diffractometer using Cu Kα radiation. The anode was operated at 40 kV and 40 mA. X-Ray. The catalysts were scanned in continuous mode at wavelength Kalpha1=1.540562, Kalpha2=1.544390 and Kbeta=1.3922182 from 0^{o}-75^{o} at scanning speed of 12°/min°.

2.3 Batch adsorption experiment

Batch biosorption experiments were conducted to investigate the influence of physiochemical parameters such as contact time, oil-water initial concentration ratio and adsorbent dosage using Design Expert 6.06. For adsorption process, 0.25 grams of chitosan was put into a beaker containing the calculated 0.25% v/v oil/water ratio for five minutes. It was agitated under these designed conditions keeping the pH of the medium at 2.0 (acidic) of the medium and agitating the mixture for 200 r.p.m using mechanical shaker for each runs. The same procedure was repeated for several designed conditions of chitosan dosages, time and adsorbate concentration. The mixture was poured into a sieve and allowed to drain to get the new weight of the added adsorbent. The best adsorbent and adsorbate concentration which happen to be the optimized dosage was used to carry out these tests at different time intervals which followed the same adsorption process.

The oil sorption capacity (OSC) of the sorbents was determined by Equation 1.
The OSC of the sorbents were obtained with the formula.

$$OSC = \frac{Weight\ Gain}{Original\ Weight} \quad (1)$$

2.3 Isotherm and kinetic studies

Theory

The amount of oil adsorbed into the adsorbent is designated by q in g/g of the adsorbent and given by the formula

$$q = \frac{V}{W}(C_o - C_e) \quad (2)$$

Where C_o and C_e (g/mL) are the concentration of oil at initial and equilibrium respectively, W is the weight of the adsorbent used in grams and V is the volume of the solution in litres

Langmuir adsorption isotherm

Langmuir is the simplest type of theoretical isotherms. Langmuir adsorption isotherm describes quantitatively the formation of a monolayer of adsorbate on the outer surface of the adsorbent, and after that no further adsorption takes place. Therefore, the Langmuir represents the equilibrium distribution of adsorbate between the solid and liquid phases (Tsai *et al.*, 2001; Dada *et al.*, 2012).

The Langmuir isotherm assume that the ability of molecule to bind and adsorb is independent of whether or not neighbouring sites are occupied. This means that there will be no interactions between adjacent molecules on the surface and immobile adsorption. It also infers that trans-migration of the adsorbate in the plane of the surface is prevented. Langmuir adsorption is represented in Equation

$$\frac{C_e}{q_e} = \frac{1}{q_m} Ce + \frac{1}{q_m b} \quad (3)$$

where Ce= equilibrium concentration qe= the amount of adsorbate adsorbed for unit mass.

The plot of $\frac{C_e}{q_e}$ against Ce will help determine q_m and b are related to standard monolayer adsorption capacity and the Langmuir constant, respectively.

A dimensionless separation factor or equilibrium parameter, R_L was proposed by (Hall *et al.,* 1966), as an essential feature of the Langmuir Isotherm to predict favourability of adsorption which is defined in Equation 4 as:

$$R_L = \frac{1}{1+bC_0} \quad (4)$$

Co= reference fluid-phase concentration of adsorbate (mg/l) (initial adsorbate concentration)
b= Langmuir constant (ml/mg)

Freundlich adsorption isotherm

Freundlich isotherm is commonly used to describe the adsorption characteristics for the heterogeneous surface. It represents an initial surface adsorption followed by a condensation effect resulting from strong adsorbent-adsorbate interaction. Freundlich isotherm curves is in the opposite way of Langmuir isotherm and is exponential in form. The heat of adsorption, in many instances, decreases in magnitude with increasing extent of adsorption. This decline in heat is logarithmic implying that the adsorption sites are distributed exponentially with respect to adsorption energy. This isotherm does not indicate an adsorption limit when coverage is sufficient to fill a monolayer (Dada *et al.*, 2012). It is given by Equation 5.

$$\log q_{e=} \frac{1}{n} logC_e + logK_f \quad (5)$$

K_f= Freundlich constant related to maximum adsorption capacity (mg/g). It is a temperature-dependent constant.

n= Freundlich constant related to surface heterogeneity (dimensionless). It gives an indication of how favourable the adsorption processes.

Temkin adsorption isotherm

Temkin isotherm contains a factor that explicitly takes into the account of adsorbent –adsorbate interactions. By ignoring the extremely low and large value of concentrations, the model assumes that heat of adsorption (function of temperature) of all molecules in the layer would decrease linearly rather than logarithmic with coverage (Temkin and Pyzhev., 1940; Dada *et al.*, 2012). Its equation is given as:

$$q_e = \frac{RT}{b_T} lnCe + \frac{RT}{b_T} lnK_T \quad (6)$$

Where K_T =Temkin isotherm equilibrium binding constant (L/g)
b_T = Temkin isotherm constant R= universal gas constant (8.314J/mol/K)
T= Temperature at 298K. B = $\frac{RT}{b_T}$ is constant related to heat of sorption (J/mol)

Pseudo-first-order kinetics

The linear form of pseudo-first-order equation is given by Equation 7

$$\log(q_e - q_t) = log q_e - \frac{k_1 t}{2.303} \quad (7)$$

Where, qe and qt are the amounts of adsorbate adsorbed g/g at equilibrium time and at any instant of time, t respectively, and k_1l $min^{-1}$is the rate constant of the pseudo first-order adsorption operation (Qiu *et al.,* 2009).

Second order-kinetic model

The second order-kinetic model is shown in Equation 8; it is often used for chemical reaction in kinetics and chemical reaction engineering, but can also be applied for adsorption processes (Qiu *et al.,* 2009).

$$\frac{1}{C_e} = k_2 t + \frac{1}{C_o} \quad (8)$$

Pseudo-second-order kinetics

Pseudo-first-order kinetics differs from a true first order equation in two ways: (i) the parameter $k_1(q_e - q_t)$ does not represent the number of available sites, and (ii) the parameter log (qe) is an adjustable parameter and often found not to be equal to the intercept of the plot of log $(q_e - q_t)$) versus t, whereas in a true first order log q_e should be equal to the intercept (Qiu *et al.,* 2009). In such cases, applicability of the second order kinetics should be tested with the rate equation given by Equation 9.

$$\frac{t}{q_t} = \frac{1}{h} + \frac{t}{q_e} \quad (9)$$

Elovich model

Elovich model is applicable for chemisorption processes. The equation is often valid for adsorption surface that is heterogeneous. Equation 10.

$$q_t = \frac{1}{b} In(ab) + \frac{1}{b} ln\ t \quad (10)$$

Where a is the initial adsorption rate (mg/gmin) and b is related to the extent of surface coverage and the activation energy for chemisorption (g/mg). A plot of q_t against *Int* gives a straight line with a slope of $\frac{1}{\mathrm{b}}$ and an intercept of $\frac{1}{b}$In(ab) with correlation coefficients (Qiu *et al.,* 2009).

3.0 Results and discussion

3.1 Characteristics of adsorbent

The AAS elemental composition is as given in Table 1.

Table 1: Elemental analysis of materials

Materials	Ca mg/g	Fe mg/g	Nitrogen %	Carbon%
Shrimps	18.7427	0.9413	11.9	20.54

Chitosan	1.3339	1.7200	2.81	15.14

Carbon and nitrogen percentage of chitosan as shown Table 1 are 15.14% and 2.81% respectively. Isa *et al.,* 2012 reported similar carbon and nitrogen value of 13.32% and 2.29% respectively where chitosan was produced from mussel shell. The differences may be due to the extent or degree of deacetylation and specie of shrimps. The demineralization of chitosan in terms of calcium removal was effective of about 92.88%.

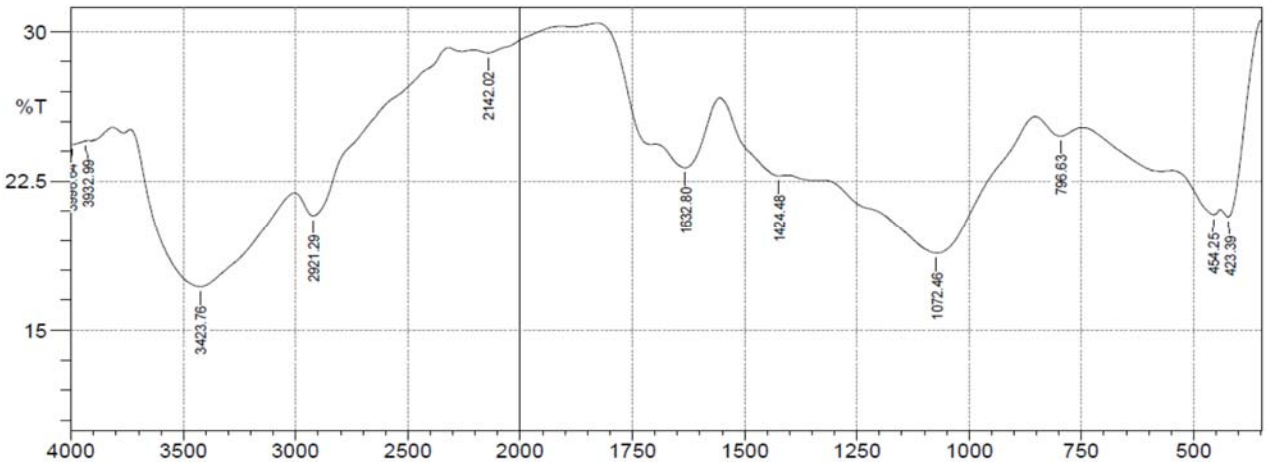

Figure 1: FTIR spectroscopy analysis Chitosan

Figure 1 shows the wide band of $-NH_2$ at 3423.76 cm^{-1} corresponded to N-H stretching vibrations of free amino groups. Likewise, the band observed at 2921.29 cm^{-1} corresponded to CH stretching vibrations. The band at 1072.46 cm^{-1} is as a result of stretching of primary hydroxyl groups of tertiary O-H stretching. The band at 1632.80 cm^{-1} corresponded C=O stretch of the carbonyl group, a structural feature of chitosan and the occurrence of deacetylation. This functional group attracts anionic ions such as OH−to bind and bridge. Due to this reason, oil has more affinity to be adsorbed on the surface of chitosan flakes. Electrostatic forces of attraction are created between this positive charge on chitosan surface and the negative charge of fatty acids in oils (Suresh and Amita, 2012).

The XRD pattern of the produced chitosan is as shown in Figure 2 which exhibited sharp diffraction peaks at 2θ = 10º, 20º and 28º . Bangyekan *et al*., 2006 and Isa *et al*., 2012 reported that these are the two typical identities and characteristic peaks of semi-crystalline chitosan.

The SEM micrograph of produced chitosan in Plate 1 has smooth close-fitting surface morphology with minimum residues. Isa *et al*., (2012) gave similar report of chitosan showing prominent sheath-like layers. This could probably be as result of deacetylation of the chitin which removes some bonding agents and exposing more sheaths in the chitosan.

3.2 Effects of influencing parameters

The adsorption capacities were calculated for each batch of experimental runs as given by Design Expert 6.06 software and presented in Table 2.

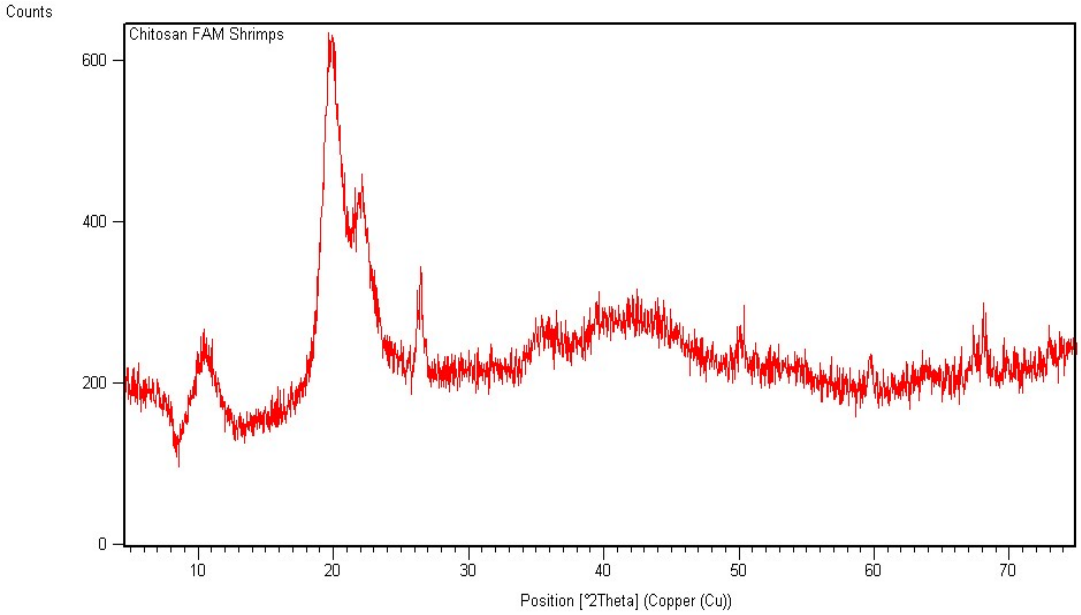

Figure 2: XRD Pattern of Chitosan Extracted From Shrimp Shells

Plate 1: SEM image of Chitosan

The ANOVA Table 3 indicated that the model was significant due to the P>F value of <0.0001. Significant model terms were A and C due to their P>F value of <0.0001 respectively. Being significant means the model will fit into experimental data.

Table 2: Chitosan Adsorption Experimental Runs

Run	Chitosan Dosage (g)	Contact Time(mins)	Oil/Water %v/v	Oil Sorption Capacity g/g
1	1.13	32.50	0.14	9.31
2	1.13	32.50	0.14	9.29
3	1.13	32.50	0.14	9.31
4	2.00	5.00	0.02	1.425
5	1.13	78.75	0.14	9.32
6	1.13	32.50	0.14	9.31
7	0.25	60.00	0.02	11.4
8	1.13	32.50	0.14	9.3
9	1.13	32.50	0.33	9.32
10	2.00	5.00	0.25	6.715
11	1.13	32.50	0.14	9.31
12	0.25	5.00	0.25	23.08
13	2.60	32.50	0.14	4.2
14	1.13	32.50	0.06	4.54
15	0.25	5.00	0.02	11.4
16	2.00	60.00	0.25	8.175
17	1.13	13.75	0.14	9.13
18	0.25	60.00	0.25	23.9
19	2.00	60.00	0.02	1.425
20	0.35	32.50	0.14	13.17

Table 3: ANOVA response for square root 2FI model to identify the significant contributing factors.

Source	Sum of Squares	DF	Mean Square	F Value	Prob>F
Model	13.48	3	4.49	29.94	< 0.0001*
A	9.29	1	9.29	61.91	< 0.0001*
B	0.012	1	0.012	0.080	0.7809
C	4.18	1	4.18	27.84	< 0.0001*
Residual	2.40	16	0.15		
Lack of Fit	2.40	11	0.22	1.160E+005	< 0.0001*
Pure Error	9.408E-006	5	1.882E-006		
Cor Total	15.88	19			

Standard Deviation: 0.39; R-Squared: 0.8488 *significant variable

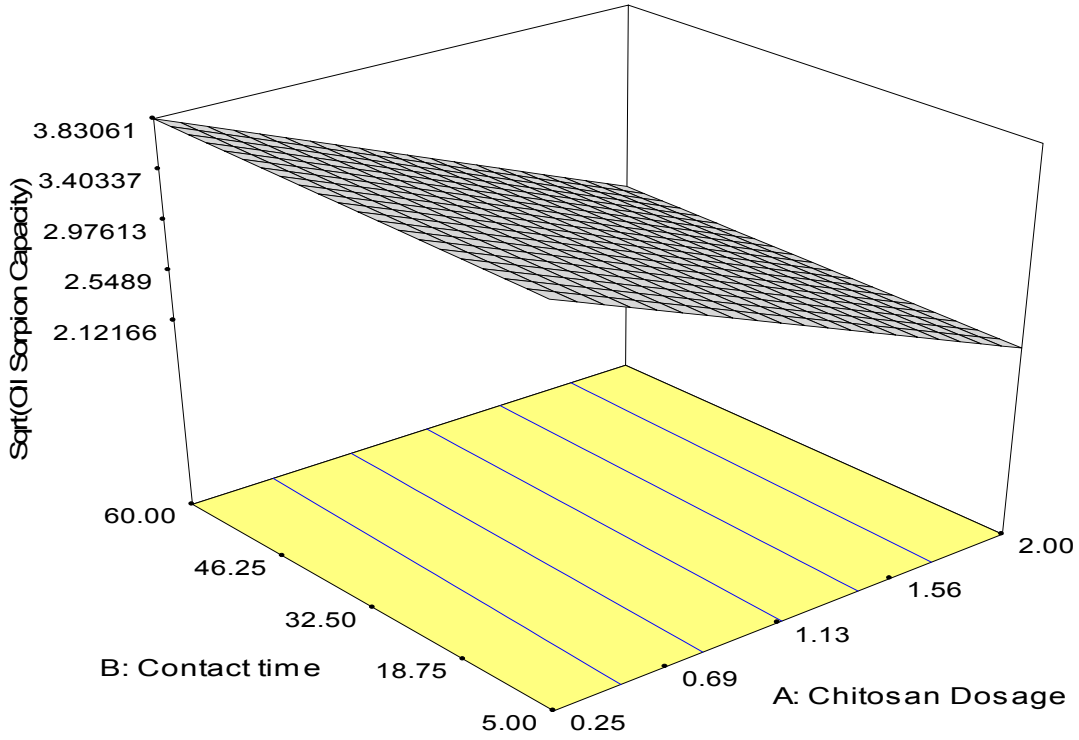

Figure 2: Response surface 3D plot of OSC versus Contact time and Chitosan dosage

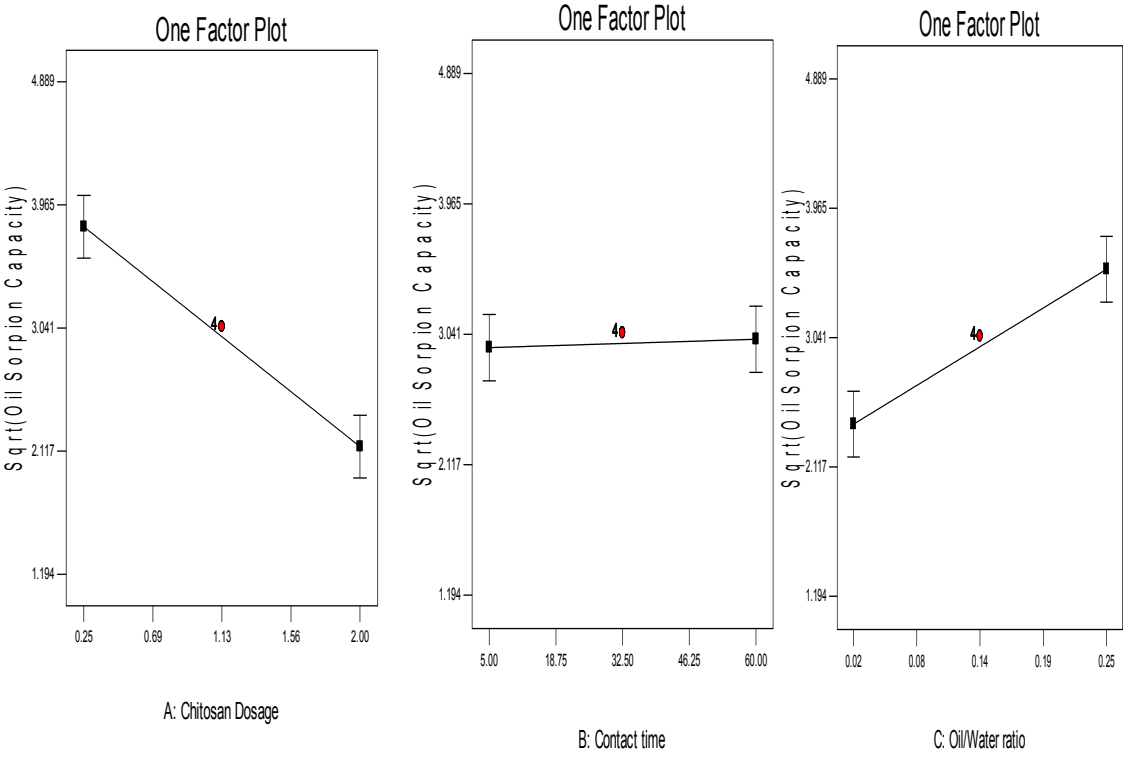

Figure 3: Effect of influencing parameters

The 3D-Figure 2 and 3 shows the response (Oil sorption capacity) with two combined influencing factors and single variable respectively. It can be deduced that oil sorption capacity of chitosan increased with increase in contact time and oil water ratio while it decreased with amount of adsorbent concentration (dosage). The decrease in adsorption capacity by increasing the adsorbent amount is basically due to the sites remaining unsaturated during the adsorption process. It thus follows that if adsorbent dosage is increased by keeping the adsorbate concentration constant, the amount of adsorbate taken up per unit dosage of adsorbent showed a decrease due to availability of less amount of oil per unit mass of the adsorbent. Annunciado *et al.*, 2005 reported that adsorption capacity of chitosan also to decrease with increase in adsorbent dosage because of the smaller quantities of oil present to be adsorbed per unit mass of adsorbent dosage.

The proposed model equation is given as:

$$OSC = (+35222 - 0.94265 * A + 1.07855E - 003 * B + 4.80985 * C)^2 \quad (2)$$

where A= chitosan dosage, B= contact time and C=oil/water concentration
The model was optimised for chitosan adsorption giving 0.25, 60.0, 0.25, 4.384 and 0.863 as Chitosan dosage, Contact time, Oil/Water ratio, Sqrt(OSC) and Desirability respectively.
The isotherm studies of chitosan are shown in the Figures 4, 5 and 6 while the kinetic and isotherm parameters are also as presented in Table 4.

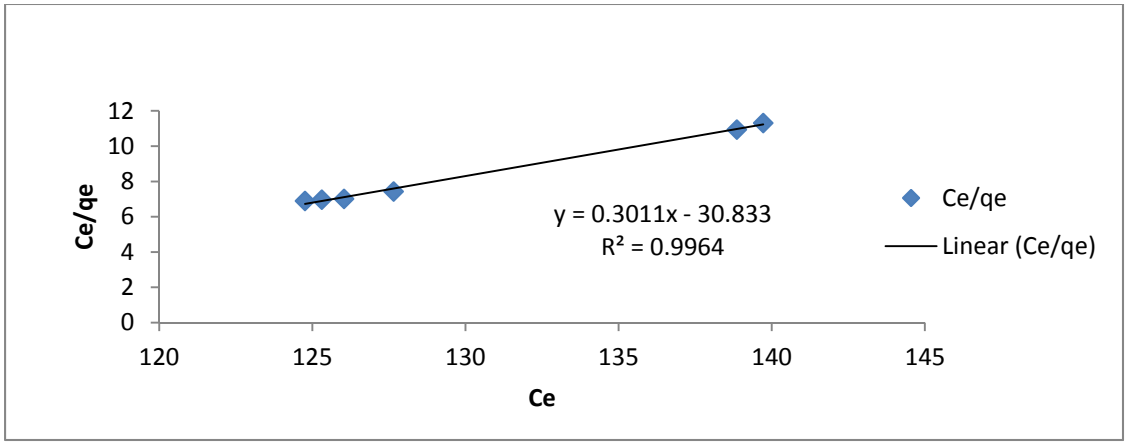

Figure 4: Chitosan Langmuir isotherm plot

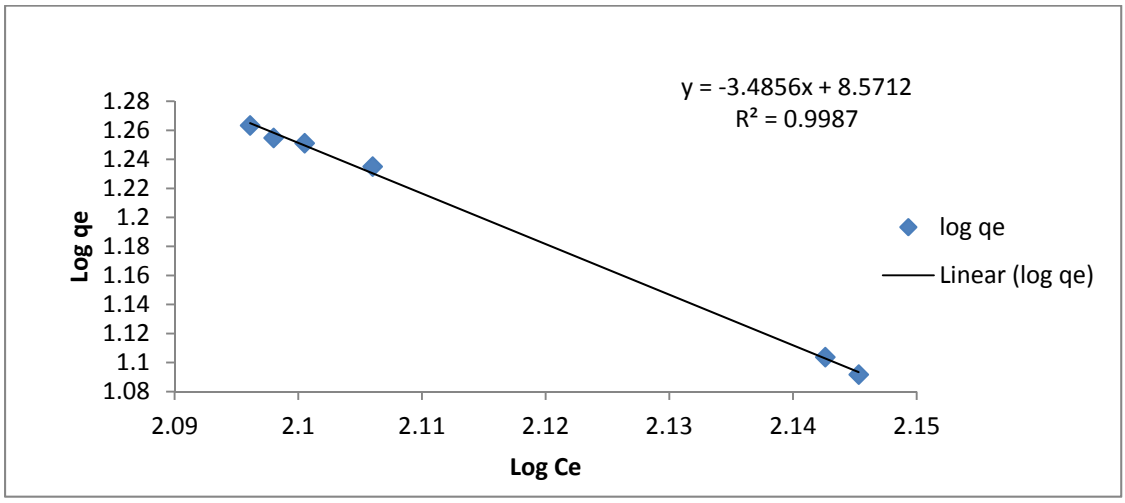

Figure 5: Chitosan Freundlich isotherm plot

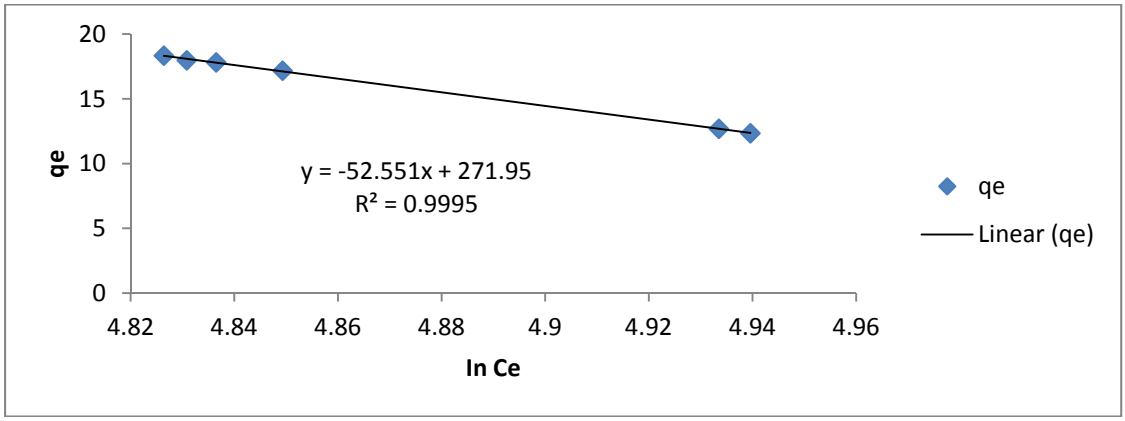

Figure 6: Chitosan Temkin isotherm plot

Temkin isotherm best fit the adsorption with R-squared value of 0.9995, heat of adsorption b_T value -47.146 J/mol is very low signifying that it is physisosorption. R_L value for Langmuir isotherm is 0.05376 with R-squared value of 0.9964 (favourable adsorption isotherm studies). Table 4 presents the calculated isotherm parameter values.

Table 4: Chitosan adsorption isotherm value

Isotherm	Parameter	Value
Langmuir	b	0.0983
	R_L	0.05376
	R^2	0.9964
Freundlich	K_f	19.055
	1/n	-3.4856
	R^2	0.9987
Temkin	K_T	0.6835
	b_T	-47.146
	R^2	0.9985

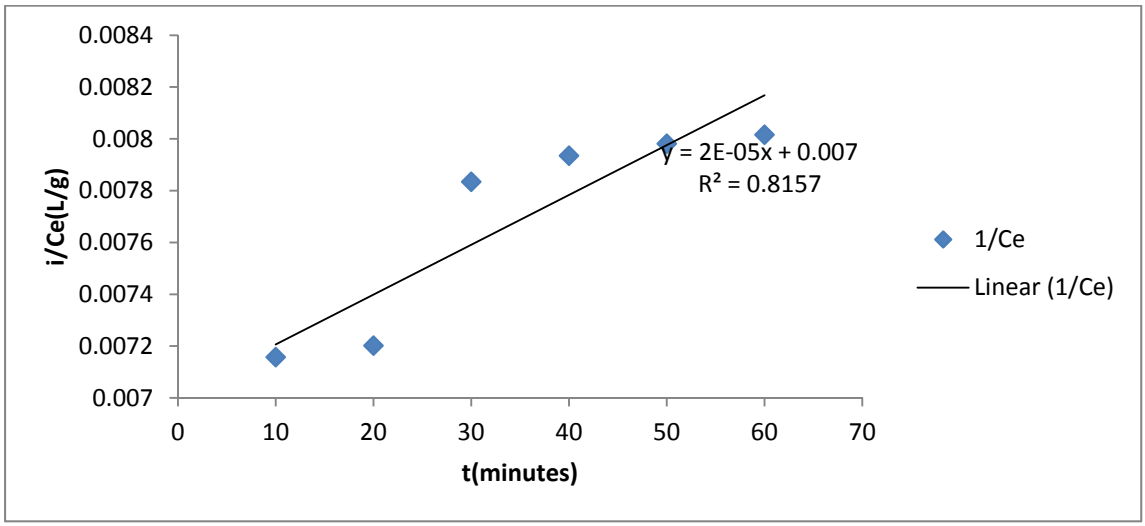

Figure 7: Chitosan Second order kinetic model.

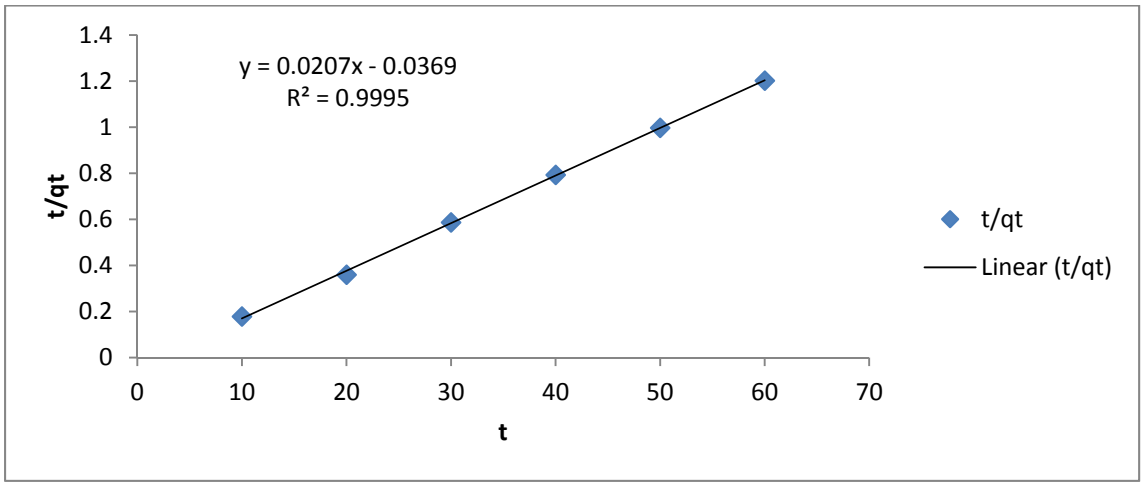

Figure 8: Chitosan Pseudo-second order kinetic model

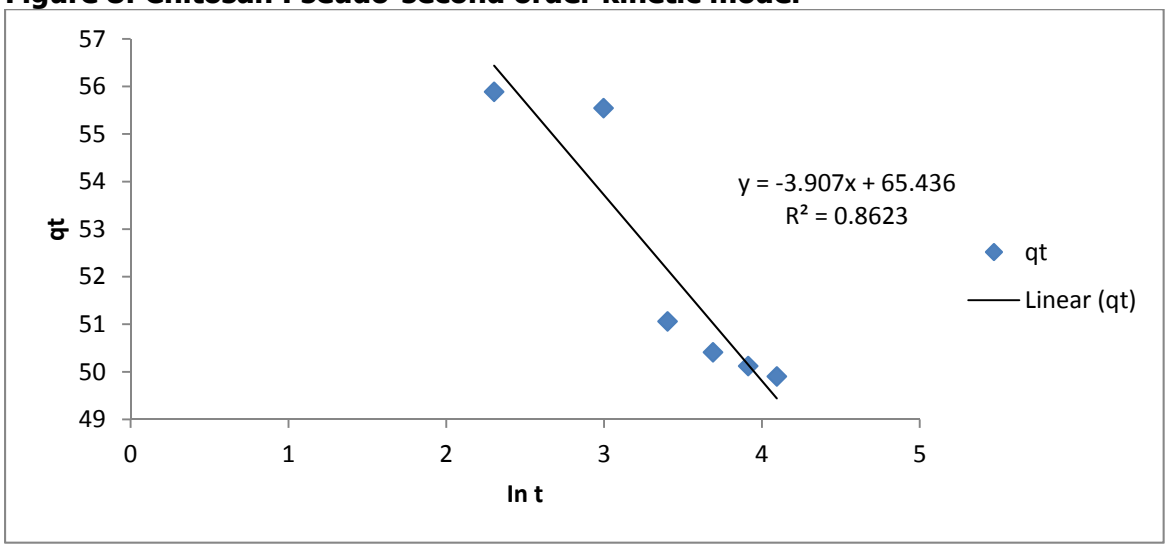

Figure 9: Chitosan Elovich kinetic model

Figures 7-9 present second order,pseudo-second order and Elovich kinetic models for chitosan respectively. The kinetic data best fit into pseudo-first order kinetic model with highest R^2 value of 0.9995.Data generated are presented in Table 5

Table 5: Evaluated constants obtained from the tested kinetic model for chitosan

Kinetic model	R^2	Intercept	K	Other constants
Second order	0.8157	0.007l	0.00002	C_o=142.8572
Pseudo-second order	0.9995	0.0369	0.065778	q_e=27.1003
Elovich	0. 8623	65.436	b=-0.256	a=5.3243E-08

Conclusion

Chitosan prepared from prawn shell waste was suitable for oil removal from oil water solution. Equilibrium data are well fitted with the Temkin isotherm. Models for the prediction of adsorption capacity of chitosan was successfully developed by application of response surface methodology of Design Expert Software with R^2 value of 0.8488, 0. ANOVA model results was significant with P>F value of 0.0001. The maximum adsorption capacity is obtained as 18.34 g g^{-1}.

The heat of adsorption b (kJmol-1) obtained from Temkin isotherm studies was low, indicating physisorption of adsorbents to the crude oil. The rate kinetics of oil adsorption on chitosan is best represnted by pseudo-second order with R^2 value 0.9995.

References

Abdul A. A, Abdulrauf R. A, Enamul H. M. (2012). 'A Novel Sustainable Oil Spill Control Technology' Dept. of Petroleum Engineering, King Fahd University of Petroleum and Minerals, Dhahran 31261, Saudi Arabia

Abdulwadud, A., Isa, M. T., Abdulsalam, S., Muhammad, A. J., and Ameh, A. O. (2013). Extraction and characterisation of chitin and chitosan from mussel shell. Extraction, 3(2), 108-114.

Aisien, F. A., Hymore, F. K., and Ebewele, R. O. (2003). Potential application of recycled rubber in oil pollution control. Environmental monitoring and assessment, 85(2), 175-190.

Aisien, F. A., Hymore, F. K., and Ebewele, R. O. (2006). Comparative absorption of crude oil from fresh and marine water using recycled rubber. Journal of Environmental Engineering, 132(9), 1078-1081.

Amita, U. and Suresh G. (2011). Characteristics and kinetic study of chitosan prepared from seafood industry waste for oil spills clean-up. J. 44 Taylor and Francis Group. Birla Institute of Technology and Science (BITS), Pilani-333031, Rajasthan, India.

Annunciado, T. R., Sydenstricker, T. H. D., and Amico, S. C. (2005). Experimental investigation of various vegetable fibers as sorbent materials for oil spills. Marine pollution bulletin, 50(11), 1340-1346.

Bangyekan, C., Aht-Ong, D. and Srikulkit, K., (2006). Synthesis and Characterisation of Chitosan from Shrimp Shells Carbohydrate. International Journal of Basic and Applied Sciences IJBAS-IJENS Vol: 11 No: 01 Polymer. 63(1**):** 61-71.

Isa, M. T., Ameh, A. O., Gabriel, J. O., and Adama, K. K. (2012). Extraction and Characterization of Chitin from Nigerian Sources'. Leonardo Electronic Journal of Practices and Technologies, 21, 73-81.

Isa, M.T., Ameh, A.O., Tijjani, M. and Adama, K.K. (2012) 'Extraction and Characterisation of Chitin and chitosan from Nigerian Shrimps', International Journal of Biological and chemical Sciences, vol. VI, no. 1, pp. 446-453.

Kudaybergenov, K. K., Ongarbayev, Y. K., and Mansurov, Z. A. (2012). Thermally treated rice husks for petroleum adsorption. International Journal of Biology and Chemistry, (3), 3-12.

Sewvandi, G.A. and Adikary S.U. (2010). Removal of Heavy Metals from Wastewater Using Chitosan. Department of Materials Science and Engineering, University of Moratuwa, Moratuwa,Sri Lank

Sun, X. F., Sun, R. C., and Sun, J. X. (2003). A convenient acetylation of sugarcane bagasse using NBS as a catalyst for the preparation of oil sorption-active materials. Journal of Materials Science, 38(19), 3915-3923.

Sun X.F., Sun R. and Sun, J. X., (2002), Acetylation of rice straw with or without catalysts and its characterization as a natural sorbent in oil spill clean-up, Journal of Agricultural and Food Chemistry, 50(22), 6428.

Temkin, M., and Pyzhev, J. A. V., (1940). Kinetics of ammonia synthesis on promoted iron catalysts. Acta Physiochim 12: 217-222.

Tsai W.T., Chang C.Y., Wang S.Y., Chang C.F., Chien S.F., and Sun H. F., (2001), Utilization of agricultural waste corncob for the preparation of activated carbon, Journal of Environmental Science and Health, 5B (36), 677-686.

Hall, K. R., Eagleton, L. C., Acrivos, A., and Vermeulen, T. (1966). Pore-and solid-diffusion kinetics in fixed-bed adsorption under constant-pattern conditions. Industrial and Engineering Chemistry Fundamentals, 5(2), 212-223.

Yang, H., Viola, D., Belinda, J., Rmbo, X. and Tony, S. Rice husks and oil pollution. Fall 2005, Roskilde University.

Nwankwere, E.T., Gimba C.E, Kagbu, J.A. and Nale, B. (2012). Sorption studies of crude oil on acetylated rice husks. Chemistry Dept. Ahmadu Bello University, Zaria Nigeria.

Dada, A. O., Olalekan, A. P., Olatunya, A. M., and Dada, O. J. I. J. C. (2012). Langmuir, Freundlich, Temkin and Dubinin–Radushkevich isotherms studies of equilibrium sorption of Zn2+ unto phosphoric acid modified rice husk. IOSR Journal of Applied Chemistry, 3(1), 38-45.

Qiu, H., Lv, L., Pan, B. C., Zhang, Q. J., Zhang, W. M., and Zhang, Q. X. (2009). Critical review in adsorption kinetic models. Journal of Zhejiang University-Science A, 10(5), 716-724.

Proceedings of the 49th NSChE Annual Conference
KADA 2019: pp 153-162

P1B-08: IRON IMPREGNATED RICE HUSK ASH ADSORBENT FOR CYANIDE REMOVAL FROM CASSAVA PROCESSING EFLLUENT

M.S. Olakunle, O. A. Ajayi, H.S. Ajoge* K. Lawal
Department of Chemical Engineering, Ahmadu Bello University Zaria-Nigeria.
*Corresponding author: haruna.ajoge@gmail.com

ABSTRACT
Rice husk (RH) was calcined and the resultant ash (RHA) was impregnated with Fe, (Fe-RHA). Both were used to adsorb cyanide from simulated cyanide solution and effluents from cassava processing. X-ray fluorescence (XRF) and Scanning Electron Microscope (SEM) were used to characterize the RH, RHA and Fe-RHA, while UV spectrophotometer was used to monitor the cyanide concentrations. BET results for surface area, pore volume and pore width are 552 m^2/g, 0.625 cm^3/g, and 3.17 nm respectively for RHA while those for Fe-RHA are 475.6 m^2/g, 0.2253 cm^3/g, and 2.128 nm respectively. To determine the best set of parameters (impregnation ratio, calcination temperature and calcination time) for the synthesis of Fe-RHA, the Central Composite Design (CCD) in Response Surface Methodology (RSM) was employed using the simulated cyanide water in batch adsorption experiments, with constant conditions of 50 mL each of 80 mg/L cyanide solutions, contact time of 40 minutes, adsorbent dosage of 2 g, pH of 8, and at room temperature. Adsorption efficiencies of Samples A, B and C were: 64.71%, 60.37% and 63.03% respectively when Fe-RHA adsorbent was used. The efficiencies when RHA was used were: 45.10.10%., 40.09% and 58.18% respectively. Sample A is the juice extracted from cassava tubers; Sample B is the effluent from cassava processing plant, and Sample C is the effluent from cassava plant after sedimentation. However, higher adsorption efficiencies were recorded when simulated cyanide solutions having the same concentrations with the real effluents (Samples A, B and C) were contacted with the adsorbents at the same adsorption conditions. The adsorption efficiencies when Fe-RHA adsorbent was contacted on simulated A, B and C were: 86.27%, 76.04%, and 86.06% respectively, while 78.43%, 58.99% and 67.27% efficiencies were achieved when RHA adsorbent was used on the simulated samples.

The analysis of the adsorption data using the Langmuir and Freundlich models showed that the data was consistent with Langmuir model for monolayer adsorption with adsorption capacity of 4.2 mg/g and a correlation coefficient (R^2) of 0.9924.

Keywords: Adsorption, Cyanide, Effluent, Impregnation, Calcination, Response Surface Methodology (RSM).

1.0 Introduction
Wastes are generated in every facet of life including the industrial activities of man. Wastes emanating from local food processing industries are becoming challenging, especially in developing countries where such activities are encouraged to alleviate poverty and provide food for the populace. The disposal of the wastes has followed varied routes from proper disposal to designated landfills and incinerators to indiscriminate disposal on streets, drainages and water bodies (Eletta *et al.,* 2016).

Cassava (*Manihot esculenta Crantz*) is a very important food crop in tropical countries and it is one of the most widely distributed food crops having high content of cyanogenic glycosides According to Food and Agriculture Organization of the United Nations, cassava production in

Nigeria is the largest in the World. Cassava is an important staple crop and in the tropical world it ranks fourth in importance after rice, wheat and maize. In Nigeria, '*gari*- a grated, fermented and dehydrated cassava food product is one of the most popular staple foods produced from cassava, which provides a major source of calories for families because of its high starch content. The increased importance of cassava in agricultural and economic development and in food security particularly in Africa has given its processing and waste handling a new attention (Okunade *et al.,* 2014). The process of washing, grating and moisture extraction by pressing; results in the production of wastewater. There are environmental and human health implications of the whole '*gari* processing procedure especially on the disposal of wastewater resulting therefrom (Okunade *et al.,* 2014).

Cassava processing, especially in areas where the industry is highly concentrated, is regarded as polluting and a burden on natural resources. Some forms of processing, particularly for starch, have developed beyond traditional methods and are now water intensive. By its nature, cassava processing for starch extraction produces large amounts of effluent high in organic content. Other forms of processing, despite not requiring water, generate very visible dust waste. As a consequence of the visual display of pollution, cassava is often perceived by local populations as contributing significantly to environmental damage and water deficit (Okunade *et al.,* 2014).). As an environmentally protective measure, the Environmental Protection Agency (EPA) has placed rigorous limitations on the permitted cyanide concentrations levels in industrial wastewater effluent streams. The toxic effects of cyanide are so momentous to cause nerve damage and thyroid glands malfunctioning and the established toxicity level should be as low as 0.1mg/l. Adsorption and biodegradation are the effective methods of removal of cyanide ion from wastewater. These two techniques are considerable methods for treatment of wastewater containing cyanide complexes to a tolerable level, operated either separately or simultaneously, but the choosing of the better treatment method is based on the benefit, cost and concentration of cyanide ion in wastewater (Mohammed *et al*, 2014).

Rice is an important staple food for approximately half of the world population (Kumar *et al*, 2013). Rice husk is one of the most widely available agricultural wastes in many rice producing countries of the world. Rice hulls (or rice husks) are the hard protecting coverings of grains of rice and removed from rice seed as a by-product during the milling process. It possesses various properties that make them suitable for bioethanol production. Rice husk biomass is made up of three polymers like cellulose, hemicelluloses and lignin. Rice husk like other lignocellulosic biomass feedstock has been explored as the cheapest feedstock for bio-ethanol production. It is essentially free as waste product from agricultural sector. Utilization of these wastes could solve the disposal problem and reduce the cost of waste treatment. When rice husk is incinerated, ash is obtained called rice husk ash. Rice husk contains 75-90% organic matter such as cellulose, lignin etc, and the rest being mineral components such as silica, alkalis and trace elements. Rice husk is unusually high in ash compared to other biomass fuels in the range 10-20%. The ash is 87-97% silica, highly porous and light- weight, with a very high external surface area (Kumar *et al.*, 2013). Presence of high amount of silica makes it a valuable material for use in industrial application. Other constituents of Rice Husk Ash (RHA), such as K_2O, Al_2O_3, CaO, MgO, Na_2O, Fe_2O_3 are available in less than 1 %. Rice husk also have bulk density of 96-160 kg/m^3, oxygen 31-37%, nitrogen 0.23- 0.32%, sulphur 0.04-0.08% (Kumar *et al.*, 2013).

The aim of this investigation is to develop of rice husk, synthesize the husk, and impregnate the ash with iron (Fe), and then use it to remediate cyanide loaded cassava processing effluents

(CPE) using batch adsorption method. The comparison between the real effluent (CPE) and simulated (cyanide simulated water) in terms of their adsorptions were also studied; likewise the adsorption capacities of rice husk ash (RHA) and the iron loaded rice husk ash (Fe-RHA) were determined.

2.0 Materials and Methods

2.1 Preparation of Rice Husk Ash (RHA)

The rice husk was sourced from *Dariya* Rice processing mill *Kakuri*, Kaduna state. 100 g of the husk was weighed into 1000 mL measuring cylinder and mixed with 1 mole HCl. The content was heated to a temperature of 100 ^{o}C for 2 hour. After decanting, the content was then washed with deionized water. The pH was monitored using HANNA pocket-sized pH meter until pH of 7 was reached. The residue was then transferred into an electric oven (DHG9030 model) operated at a temperature of 110 ^{o}C for 5 hour. The dried chemically treated RH was calcined in a muffle furnace at a temperature of 700 ^{o}C for 2 hour. The result is the RHA which was cooled in a desiccator and packed in air-tight container.

2.2 Preparation of Iron loaded Rice Husk Ash (Fe-RHA)

2 g of the RHA was weighed into a beaker and a known molar concentration (based on the design of experiment) of $FeSO_4.7H_2O$ was prepared and mixed with the RHA for wet impregnation process. This was thoroughly mixed and allowed for 24 hour before filtering with filter paper (Whatman 1). The residue was then transferred into an electric oven for drying. The oven was operated at a temperature of 110 ^{o}C for 30 minute. The content was then transferred into a muffle furnace and heated for a known temperature and time (based on the design of experiment). The resultant product was Iron loaded rice husk ash (Fe-RHA).

2.3 Design of Experiment (DOE)

RSM is an approach to achieving optimum values for any method where multiple factors affect the response of interest (Dutta *et al,* 2011). Three steps were followed to perform the optimization that is: perform the experiments that were designed statistically, estimate the coefficients using the mathematical model, predict the response, and study the model's effectiveness. An RSM model allows input (X_i) and output variable (Y) to be linked as shown in Eq. (1).

$$Y = f(X_{1,} X_2 X_{3,} \dots\dots\dots\dots\dots, X_{n,}) \quad (1)$$

Central Composite Design (CCD) is an RSM design method, which was used to fit surface (quadratic) and thus optimize the active parameters with a minimum possible number of experiments. It also helps in studying the relationship between the parameters (Sen *et al,* 2018). The CCD largely consists of 2^n factorial runs with 2n axial runs and n_c central runs (Chaterjee *et al,* 2012). Experimental errors and the repeatability of the experiment were gotten with the aid of centre points. Therefore, the synthesis process having three numeric factors (impregnation temperature, calcination temperature and calcination time), the total experiments performed are given by Eq. (2):

$$N = 2^n + 2n + n_c = 2^3 + (2x3) + 6 = 20 \quad (2)$$

Design Expert software version 10; was used and the generated twenty set of runs is as shown in Table 3. Therefore, twenty sets of Fe-RHA were synthesized, and in other to determine the best sets of parameters, they were subjected to adsorption process using 50 mL of simulated water prepared from sodium cyanide (NaCN) at a concentration of 80 mg/L, Fe-RHA dosage of 2 g, and pH of 8. To each of the set up; after 40 minute and at room temperature the content was centrifuged operated at 4,500 revolutions per minute for 5 minute, the content is decanted and tested for final cyanide concentration using UV Spectrophotometer. The percentage cyanide removals were entered as responses as shown in Table 3. The optimum parameters were then used to prepare the optimized Fe-RHA.

2.4 Comparative study on cyanide removal using real effluent and simulated cyanide water

Three cassava effluents were sourced and tagged Samples A, B and C. Sample A is the juice extracted from cassava tubers purchased from *Kawo* market Kaduna, while Sample B is the direct effluent from a cassava processing plant located at *Goningora* Kaduna, and Sample C is the effluent obtained from the same plant but after sedimentation was carried out by the operators. The samples were then subjected to adsorption process using the same conditions as described in section 2.2 above. Both RHA and Fe-RHA were used as the adsorbents to each sample, and in each case, both the initial and final cyanide concentrations were measured.

Pure sodium cyanide (NaCN) solution with the same concentrations as the samples (A, B and C), were then prepared. These prepared solutions were subsequently treated with RHA and Fe-RHA adsorbents under the same conditions to determine their percentage cyanide removals.
The adsorption efficiency or CN removal percentage was calculated using Eq. (3) (Eletta *et al.,* 2016).

$$Adsorption\ Efficiency\ (\%) = \frac{C_0 - C_t}{C_0} x100 \quad (3)$$

Where, C_o and C_t are initial and final cyanide concentrations respectively in mg/L.

3.0 Results and Discussion

3.1 X-Ray Fluorescence analysis

X-ray fluorescence (XRF) was used to determine the metallic oxides in the Rice husk (RH), Rice husk ash (RHA), and Fe impregnated rice husk ash (Fe-RHA) as shown in Table 1. It is observed that the percentage weight compositions of most the oxides in RHA and Fe-RHA are lower compared with that of RH; this is as a result of chemical and thermal treatments given to the RH.

This is in agreement with the finding of Gad *et al.,* (2012) which reported that acid treatment reduces the cellulose and hemicelluloses as well as the traces of the metals in the husk. The silica content was improved as a result of acid pre-treatment followed by thermal treatment which reduces the carbonaceous materials. The impregnation of Fe onto the RHA was successful as shown in the table because it increased from 0.083 in RHA to 2.025 in Fe-RHA.

Table 1 XRF result of the samples

		PERCENTAGE COMPOSITION (wt. %)		
S/N	**COMPONENTS**	**RH**	**RHA**	**Fe-RHA**
1	CaO	6.21	0.529	0.528
2	SiO_2	52.4	94.873	92.043
3	Al_2O_3	4.72	0.101	0.115
4	Cr_2O	0.17	0.001	0.001
5	CuO	0.14	ND	ND
6	MgO	0.62	0.379	0.492
7	P_2O_3	0.51	0.214	0.22
8	NiO	0.18	ND	ND
9	SO_3	10.25	0.002	0.127
10	K_2O	5.12	0.22	0.22
11	TiO_2	0.41	0.087	0.093
12	MnO	0.31	0.04	0.04
13	Fe_2O_3	1.89	0.083	2.025
14	Na_2O	5.25	ND	ND
15	ZnO	0.14	0.05	0.047

ND= Not detected

3.2. SEM analysis

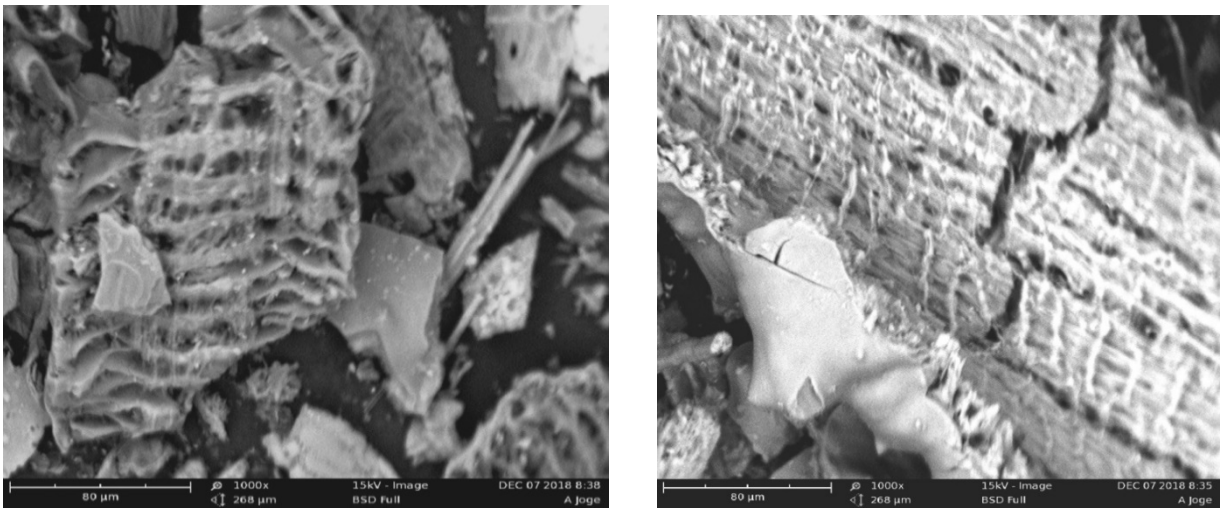

(a) (b)

Figure 1: SEM morphological image for (a) RHA and (b) Fe-RHA

Scanning electron microscopy (SEM) analysis was carried out to characterize the surface morphology of the samples as shown in Figure 1. An examination of Figure 1 reveals different pore sizes in the samples. The pore sizes in the RHA sample shown in Figure 1a are more

pronounced than those in Fe-RHA (Figure 1b) because of the anchoring of Fe on RHA which partially blocks the pores thus reducing their sizes and also increasing the surface roughness.

3.3 Brunauer - Emmett - Teller (BET) Analysis

The pore size distribution and surface area analysis were carried out using BET as shown in Table 2. The BET analysis is considered to be the most extensively used method for estimating surface area (Naveen *et al,* 2014). The results in Table 2 reveal that the adsorbents (RHA and Fe-RHA) are mesoporous (2-50 nm) in nature.

Table 2 BET results

S/N	Parameters	Fe-RHA	RHA	Lit. Value (RHA)*
1	Surface area (m^2/g)	475.6	552.1	653
2	Pore volume (cm^3/g)	0.2253	0.625	0.64647
3	Pore width (nm)	2.128	3.17	1.98

(*Hassan *et al.,* 2013)

According to International Union of Pure and Applied Chemistry (IUPAC) nomenclature, the pore size classification range of 2-50 nm is a mesoporous material, if less than 2 nm is microporous and above 50 nm is macroporous (Katsuhiko *et al*, 2012). The parameters for Fe-RHA is lower than RHA, this is because the pores and the surface are slightly covered as a result of the deposition or anchoring of the impregnating chemical ($FeSO_4.7H_2O$). In comparison with Hassan *et al.,* (2013), there is a relative agreement despite the fact that they employed sol gel method for their RHA nano-silica powder production. The BET surface area and pore volume were: 475.6 m^2/g and 0.2253 cm^3/g respectively for Fe-RHA and 552.1 m^2/g and 0.625 cm^3/g respectively for RHA. Hence, these properties make them a good adsorbent.

3.4 Experimental Design and Responses for Fe-RHA Optimization

The percentage cyanide removals obtained from the experiments conducted using simulated water were inputted as responses as shown in Table 3. Central Composite Design (CCD) was used for the Design of Experiment (DOE). The Response Surface Methodology (RSM) was applied to analyse these values leading to the quadratic model equation suggested by the software:

$$\%CN\ Removal = 85.83 + 11.07A + 6.42B + 4.61C + 2.79AB - 2.77AC - 2.00BC - 4.34A^2 - 1.54B^2 \quad (4)$$

Where; A is the impregnation ratio, B is the calcination temperature and C is the calcination time. The model equation signifies that impregnation ratio (A) having the highest coefficient is the dominant factor.

3.5 Analysis of Variance (ANOVA)

The analysis of variance of the model shown in Table 4 indicated the significance values of the F- values which show the adequacy of the model.

Table 3 CCD matrix and responses for Fe-RHA Optimization

S/No.	Impreg. Ratio (mol/l)	Calcination Temp. (°C)	Calcination Time (min)	Cyanide Removal (%)
1	0.073	550	20	92.11
2	0.04	550	20	85.01
3	0.04	550	36.81	88.71
4	0.02	450	30	74.29
5	0.04	550	20	81.13
6	0.06	650	30	98.47
7	0.02	650	10	66.97
8	0.04	381.82	20	69.11
9	0.02	450	10	54.61
10	0.06	450	30	82.96
11	0.04	718.17	20	90.12
12	0.06	650	10	97.87
13	0.04	550	20	84.78
14	0.04	550	20	86.11
15	0.04	550	20	85.21
16	0.04	550	3.18	73.42
17	0.02	650	30	76.97
18	0.06	450	10	76.01
19	0.006	550	20	51.27
20	0.04	550	20	87.01

Table 4 ANOVA Table

Source	Sum of Squares	DF	Mean Square	F Value	p-Value Prob > F	
Model	2975.80	9	330.64	81.81	< 0.0001	**Significant**
A-Imp. Ratio	1672.98	1	1672.98	413.93	< 0.0001	
B-Cal. temp.	563.75	1	563.75	139.48	< 0.0001	
C-Cal. Time	290.11	1	290.11	71.78	< 0.0001	
AB	62.33	1	62.33	15.42	0.0028	
AC	61.22	1	61.22	15.15	0.0030	
BC	32.12	1	32.12	7.95	0.0182	
A^2	271.76	1	271.76	67.24	< 0.0001	
B^2	34.20	1	34.20	8.46	0.0156	
C^2	15.23	1	15.23	3.77	0.0809	
Residual	40.42	10	4.04			
Lack of Fit	20.17	5	4.03	1.00	0.5017	**not significant**

The square of the coefficient of regression of the model is 0.98 suggesting that the model is significantly high. All the parameters and their interactions as shown in the table are significant because their p-values are less than 0.05 except the C^2. The predicted R^2 (0.9389) is in reasonable agreement with the adjusted R^2 (0.9745) because the difference is less than 0.2.

3.6 Comparative Studies

The results of the batch adsorption experiments carried out on the three samples of cassava effluents are presented in Table 5a

Table 5a Cassava effluent's cyanide removal efficiencies

	SAMPLE (A)		SAMPLE (B)		SAMPLE(C)	
	RHA	**Fe-RHA**	**RHA**	**Fe-RHA**	**RHA**	**Fe-RHA**
C_o	***1.02***	***1.02***	***2.17***	***2.17***	***1.65***	***1.65***
C_t	0.56	0.36	1.3	0.86	0.69	0.61
$C_o - C_t$	0.46	0.66	0.87	1.31	0.96	1.04
Ads. eff. (%)	**45.10**	**64.71**	**40.09**	**60.37**	**58.18**	**63.03**

As observed from this table, the measured adsorption efficiency of RHA with sample A (juice extracted from cassava tubers) was 45.10% and increased to 64.71% when Fe-RHA adsorbent was used. Similarly, for sample B (effluent from cassava processing plant) the adsorption efficiency increased from 40.09% when RHA adsorbent was used to 60.37% when the effluent was treated with Fe-RHA.

Also Sample C (effluent from cassava plant after sedimentation) showed the same trend with the adsorption increasing from 58.18% to 63.03% respectively when the effluent was contacted with RHA and Fe-RHA adsorbents.

In other to identify the distinction between actual effluent and the simulated effluent, the same concentrations of the real effluents were simulated and the same adsorption conditions were applied, the result is as presented in Table 5b.

Table 5b Simulated water cyanide removal efficiencies

	SIMULATED (A)		SIMULATED (B)		SIMULATED (C)	
	RHA	**Fe-RHA**	**RHA**	**Fe-RHA**	**RHA**	**Fe-RHA**
C_o	***1.02***	***1.02***	***2.17***	***2.17***	***1.65***	***1.65***
C_t	0.22	0.14	0.89	0.52	0.54	0.23
$C_o - C_t$	0.80	0.88	1.28	1.65	1.11	1.42
Ads. eff. (%)	**78.43**	**86.27**	**58.99**	**76.04**	**67.27**	**86.06**

Higher efficiencies were achieved in each case compared to when real effluents were used; this may be because cassava effluent contains some other organic matters which compete with cyanide for the adsorption active site, whereas the simulated solutions were prepared using deionized water and analytical grade NaCN, hence the level of purity is higher.

The improved adsorption efficiencies recorded while using Fe-RHA adsorbent against RHA adsorbent may be as a result of ferrous ions which react with free cyanide to form ferocyanide complex. Therefore, with respect to this investigation, the mechanism is surface adsorption as well as ionic exchange.

3.7 Adsorption Isotherms for Fe-RHA

Isotherm is of significance to this research because it does not only reveals solute-surface relationship but also gives the idea about the extent of adsorbate accumulation on the surface of the adsorbent (Shelja *et al.,* 2019). The results obtained from the cyanide adsorption equilibrium experiments were fitted to Langmuir and Freundlich adsorption isotherm models. The linearized models were plotted as shown in Figure 2.

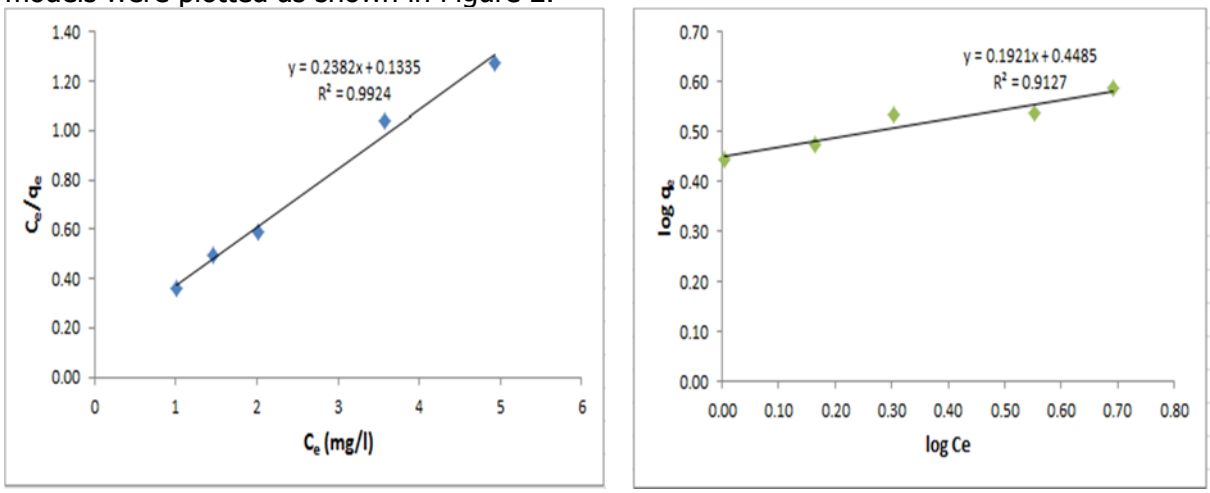

(a) (b)

Figure 2: Adsorption Isotherms for (a) Langmuir and (b) Freundlich.

The Langmuir isotherm model describes monolayer adsorption of adsorbate onto a homogeneous surface of the adsorbent, whereas Freundlich isotherm model describes multilayer adsorption of adsorbate onto the surface of the adsorbent and also assumes that the stronger binding sites are occupied first and that the binding strength decreases with the increasing degree of site occupation (Shelja *et al.,* 2019).

The Figure 2a (Langmuir isotherm) has a value of correlation coefficient (R^2=0.9924) with adsorption capacity of (q_m=4.2 mg/g) while that of Freundlich isotherm model (Figure 2b) has correlation coefficient (R^2=0.9127). Therefore, with the K_F value of 1.5 mg/g and 1/n value of 0.1921 which is less than 1 indicates that Langmuir isotherm model can explain the experimental data better.

4.0 Conclusions

i. Rice husk was beneficiated with HCl and thermally treated to improve its properties needed for cyanide adsorption.
ii. RSM was used to synthesize the Fe-RHA and from the mathematical model developed the impregnation ratio showed to be the dominant factor.
iii. The characterizations carried out on the Fe-RHA proves the potential of its applicability such as the large surface area of 475.6 m^2/g, silica oxide content of 92.043 wt% , and Fe_2O_3 of 2.025 wt%.

iv. The Fe-RHA gave better adsorption efficiencies than RHA in each of the samples investigated, i.e. 30.3%, 33.6% and 7.7% increment for samples A, B and C respectively.
v. The analysis of the adsorption data using the Langmuir and Freundlich models showed that Langmuir model is suitable with adsorption capacity of 4.2 mg/g and a correlation coefficient (R^2) of 0.9924 while that of Freundlich is 1.57 mg/g with a correlation coefficient (R^2) of 0.9127.

References

Chaterjee S, Kumar A, Basu S, Dutta S (2012) ''Application of response methodology for methylene blue dye removal from aqueous solution using low cost adsorbent". *Chem Eng J* 181:289–299.

Dutta S, Bhattacharyya A, Ganguly A, Gupta S, Basu S (2011). ''Application of response surface methodology for preparation of low cost adsorbent from citrus fruit peel and for removal of methylene blue" *Desalination* 275:26-31

Eletta O.A.A.A, Ajayi O. A, Ogunleye O.O, Akpan I.C. (2016) ''Adsorption of Cyanide from aqueous solution using calcinated eggshells: Equilibrium and Optimization Studies" *Journal of environmental chemical engineering*. 4(2016):1367-1375.

Gad H.M, Borai E.H, and El-Khalafawy A.M. (2012) '' Sorption and Desorption of Strontium using Silica extracted from Acid Treated Rice Husk. I: Effect of pH and Interfering Ions" *Arab Journal of Nuclear Sciences and Applications.* 45(2): 142-154

Kumar S., Sangwan P., Dhankhar R. Mor V., and Bidra S. (2013). ''Utilization of Rice Husk and Their Ash: A Review" *Research Journal of Chemical and Environmental Sciences* 1 Issue 5.126-129

Mohammed N.A, Firas S. A, Suha I. (2014) '' Cyanide removal from wastewater by using banana peel" *Journal of Asian Scientific Research* 4(5): 239-247

Naveen D., Chandrajit B.,and Prasenjit M. (2014) ''Study for the Treatment of Cyanide Bearing Wastewater using Bio-adsorbent Prunus Amygdalus (Almond Shell)" *International Research Journal of Environment Sciences*. Volume 3(1) page 23-30

Okunade D. A. and Adekalu K.O. (2014) ''Characterization of Cassava-waste Effluents Contaminated Soils in Ile-Ife, Nigeria" *European International Journal of Science and Technology Vol. 3 No. 4:173:182*

Sen S., and Nandi S, Dutta S (2018) ''Application of RSM and ANN for Optimization and modeling of biosorption of chromium (VI) using cyanobacterial biomass". Appl Water Sci 8(5):148

Shelja A,, Sabyasachi P., Ajanur R., Kartik C., and Susmita D. (2019) ''A Cost-effective approach for abatement of cyanide using iron-impregnated activated carbon: Kinetic and Equilibrium study" Journal of *Applied water science* (2019), 9:74

Proceedings of the 49th NSChE Annual Conference
KADA 2019: pp 163-175

P1B-09: VALOURISATION OF COTTON HULL FOR THE DECONTAMINATION OF KAGARA MINING WASTEWATER

Y. Ibrahim[a], [a]M.D. Yahya[*], A.G. Olugbenga[a], Usman Garba[b] and J.M. Oyelude[c]
[a]Department of Chemical Engineering, Federal University of Technology, Minna, Nigeria
[b]Department of Chemical Engineering, School of Engineering and Environmental Design, Usmanu Danfodiyo University Sokoto, Sokoto State, Nigeria
[c]Department of Chemical Engineering, Ladoke Akintola University of Technology, Ogbomosho
* Corresponding Author: muibat.yahya@futminna.edu.ng, +234 8032854148

ABSTRACT
In this work, a fixed bed adsorption column was used in the decontamination of Pb (II) ions from illegal gold mining wastewater of Kagara mines, Niger State, North Central Nigeria. Flame Atomic Absorption Spectrometer analysis of the waste solution showed a high concentration of Pb (II) ion of 85 mg/L. Fourier Transform Infra-Red (FT-IR) spectroscopy revealed the presence of OH, C-O, C=O, C-O-H and CH_2 functional groups in cotton hull. Brauneur-Emmet Teller (BET) test results indicated surface area of 139.8 m^2/g and micropores size and radius of <2 nm and 9.237 Å respectively, while the Scanning Electron Microscope micrographs revealed the presence of pores on the raw adsorbent. Column adsorption scale-up data for the 120 L/hr of Kagara mining wastewater shows that 607.2 L of the effluent can be treated of Pb (II) in 5.06 hours using 4.75 kg of the cotton hull adsorbent. The maximum adsorption capacity of 27.65 mg/g, with correlation coefficients within 0.7674 and 0.9551 has an average experimental value of 23.09 mg/g and theoretical of 21.60 mg/g adsorption capacities of the cotton hull adsorbent (CHA) which signify that Thomas kinetics model fit the experimental data.

INTRODUCTION
The rapid industrialization and population growth rate of industries, agriculture, and mining activities have led to the increased disposal of toxic substances such as heavy metals into the environment (Mengistie *et al.* 2008). The presence of these heavy metals in the environment is a challenge for remediation because of the inability to degrade and bio-accumulation tendency. (Ruparelia *et al*. 2008). Metals which are specifically toxic to human beings and ecological environment include Copper (Cu), Nickel (Ni), Pb (II) (Pb), Cadmium (Cd), Chromium (Cr), Zinc (Zn), and Mercury (Hg) to mention a few. They are toxic, cause severe disorder, illness to plants, animal and human. Pb (II) (Pb) II, for example, is one of the heavy metals when exposed to children at low level causes blindness, low intellect quotient, learning disabilities, attention deficit disorder, stunted growth, impaired hearing, and kidney damage. At high levels of exposure, a child may become mentally retarded, fall into a coma, and even die from Pb (II) poisoning. In adults, Pb (II) can cause fertility problems, nerve disorders, muscle and joint pain, irritability, and memory or concentration problems (Farghali *et al.* 2012). Recent reports have shown that exposure to Pb (II) contaminated soil and dust resulting from battery recycling and mining has caused mass Pb (II) poisoning and multiple deaths in young children in Senegal and Nigeria (WHO, 2015). Saturnism/Pb (II) poisoning is one of the most common and best-recognized childhood diseases of toxic environmental origin. It accounts for about 0.6% of the global burden of disease (WHO, 2010).

In May 2015 the World Health Organisation, WHO (2015) reported that in Rafi Local Government Area of Niger State, North Central Nigeria where the Kagara Mines was located, a devastating

effect of Pb (II) poisoning from illegal mining activities has caused the death of 28 young children and 65 others affected with many domestic animals lost to the tragedy.

The removal of heavy metals from contaminated soils can be achieved by various treatment methods such as chemical precipitation, ion exchange, and electrochemical removal. These processes which are generally known as conventional treatment methods have several disadvantages mainly due to high energy requirements and capital cost and low efficiency (Barakat, 2011). Biosorption has recently attracted a considerable amount of attention as an alternative method used for the removal and recovery of toxic metals due to numerous advantages such as low sludge production, low investment, and operational cost and above all higher efficiency (Eckenfelder, 2000). Thus, locally generated agricultural wastes such as cotton seed hull have been tested in the production of activated carbon in many developing countries, though very few research works have been published in this regard.

Cotton (*Gossypiumhirsutum*) is an important cash crop for several developing countries at both local and national levels. After oil and a few agriculture products, cotton is one of the largest industries in Nigeria with the country's alarmingly decreasing production put at 235,000 bales (183.43 kg/bale) for the year 2019 by the United States Department of Agriculture (2019). Cotton/textile activities are widespread in the country, largely in the Savannah geographical regions (https://www.cotton.org/oubs/cottoncounts/fieldfabric/uses.cfm). Production of cotton depends on various factors ranging from vagaries of weather, cotton price, problems of the textile industries.

In cotton production operations two products are of paramount importance. The cotton fibre used in textile industries and the kernel (meat) for refinery oil production. In cotton oil refineries, once the seed lint is removed, it is dehulled, by loosening the inner meat (kernel) from cotton hull which forms the tough outer part covering surrounding the seed (Heuzé *et al.*2015). The hull is turned out as waste to dump sites. In processing operations, the cotton seed products yield per ton of seed crushed are crude oil, 16%; hull, 27%; meat, 45%; lint, 8%; cotton residues 4% (American National Cotton seed Products Association, 2000).

This study focusses on the use of plant-based adsorbent produced from cotton seed hull for the adsorption characteristics of Pb (II) ions found in gold mining liquid effluent. Since cotton seed hull can be regarded as a potentially promising cost-effective, sustainable source of adsorbent for the removal of harmful metallic waste from mining wastewater yet to be fully explored. Column flow experiment was conducted to investigate the effect of flow rate, bed height, and initial metal ion concentrations on breakthrough curves as well as adsorption kinetics of the Pb (II) ions in the mining waste solution onto the adsorbent.

MATERIALS AND METHODS

Collection of Mining Waste Water Sample

Waste water was gotten from three different mining waste water points and stored in three containers of about 25 liters. These were analyzed using atomic absorption spectrophotometer and a mean value deduced.

Preparation of Cotton Hull Adsorbent

Cotton seeds hull were gotten from a local market in Katsina State, it was sun dried for ten days in accordance with the method established by Biradarpatil (2009). The seeds lint was removed with H_2SO_4 at 100 ml/kg cotton seeds for 3 mins to have a complete removal of the fuzz. The seeds were instantly removed and rinsed several times with deionized water. The seeds were neutralized in 2% Na_2CO_3 solution for 15 minutes and it was thoroughly washed with deionized water. The seeds were separated and dried in an oven; it was then dehulled after being dried at constant weights of 12% moisture content. The cotton hull was separated from the inner kernel using sieve aperture of 2 mm and 1 mm mesh size (Biradarpatil (2009).

The cotton hull gotten was then rinsed thoroughly with deionized water and sun dried for 5 days. The dried cotton hull was grinded and sieved to 500 μm size and sun dried for another 2 days. The adsorbent powder was oven dried for 12 hours at 105^{o}C, cooled in a desiccator for 30 minutes.

Characterization of cotton hull adsorbent.

The prepared cotton hull was characterized to determine the important properties such as BET surface area test, FT-IR, SEM analysis and apparent density.

Scanning Electron Microscope (SEM) Analysis

Scanning electron microscope (model- DSM 9872 Gemni) was used to examine the surface morphology of cotton hull adsorbent. The SEM of the carbon was recorded at 5000 magnification through which a thin layer of the adsorbent was mounted on aluminum specimen holder coated with gold (Au) at a thickness of about 30 nm.

Fourier Transform Infra-Red (FT-IR) Spectroscopy

Diamond ATR Agilent Cary 630 infra –red spectrometer was used to carry out the FTIR of cotton hull adsorbent. The adsorbent sample was placed on cleaned crystal window and the overhead press tip was adjusted until the desired pressure put forth onto the introduced sample material. The system analyzed the sample being placed and a displayed graph result showed the intensity of the sample measurement within spectral range of 4000 cm^{-1} to 650 cm^{-1}.

BET (Brunauer Emmett and Teller) Surface Area Analysis

The prepared adsorbent was outgassed under vacuum for 3 hours at 300^{0}C to get rid of moisture contents and contaminants from the solid surface. The degassed sample was cooled and transferred, firmly fixed in the analysis station of the equipment. Then nitrogen adsorption at 77K by the surface area analyzer was used to determine the pore volume and the surface area of the outgassed carbon samples.

Apparent Density of Cotton Hull Adsorbent

The sample earlier dried in an oven at 105^{o}C was put into a 25 ml cylinder used to carry out the apparent density. It was then compacted by tapping on the bench top till the volume of the sample stopped decreasing of about 1 -2 minutes. The volume, mass and density were calculated and this procedure was repeated for three times to get the average value.

$$\text{Apparent density} = \frac{\text{dry weight of adsorbent(g)}}{\text{volume of packed sample}}$$

Sample Preparation for Pb (II) Adsorption

50 ml of the mining waste water was measured into nine sterile 250ml glass stoppered flasks, little portion of 0.1M HCl solution was added. The pH was adjusted within the range of 2 to10. 250 g of cotton hull adsorbent was measured into the nine sample flasks and the mixture agitated using a multi-purpose flask shaker at 200 rpm for 120 minutes at pre- determined time intervals. The resultant mixture was filtered and the filtrate analysed using AAS to evaluate the resultant Pb (II) concentrations.

Column Adsorption Procedure

A glass column of internal diameter 3 cm, 30 cm length was used to carry out the column study in which particle size of 500 µm was used. The prepared adsorbent was packed into the column with glass wool acting as support at the top and bottom ends of the bed. The bed heights were varied at 2, 4 and 7 cm and waste water was supplied by a peristaltic pump into the adsorption column at constant flow rate of 5, 7.5 and 10 ml/min while the initial adsorbate concentrations were varied 50, 65 and 85 mg/l. The targeted heavy metal is Pb (II) ions as it was extremely high and the major cause of the death and ill health of the community. Atomic Absorption Spectrophotometer, model Accusys 211 from Buck Scientific, USA was used to determine the resulting concentration and the effluent samples were collected at various time intervals. The experiment was discontinued when the exhaustion of column was reached.

RESULTS AND DISCUSSION

Chemical Composition of Kagara Mining Effluent

Atomic absorption spectrophotometer was used to determine the composition of Kagara mining effluent. The effluent indicates that the Pb (II) ions content is extremely high (85 mg/l) and its release poses significant harm to the environment. The threshold value for Pb (II) is 0.5 mg/L (NIS, 2007). Other potentially harmful elements found in significant quantities in the effluent include copper (2.5861 mg/l) and zinc (0.4281 mg/l).

Scanning Electron Microscopy

The scanning electron micrographs before adsorption Figure 1A revealed that the surface texture and morphology of biosorbent at high (× 5000) magnifications. The morphology was that of smooth surface with no presence of metals seen, when untreated cotton hull carbon with metal ions were seen under SEM. In Figure1B after the adsorption of Pb (II), it was observed that the fresh adsorbent discloses spots of microscopic pores and crevices indicated with white arrow headlines on the raw cotton hull adsorbent micrographs. Pb (II) metal adsorption by the fresh adsorbent were attained from the SEM results which displayed that the mapping of Pb (II) ions onto biomass surface are spotted with some red arrows on the surface of cotton hull on the micrograph. The micrograph of the ion loaded carbon adsorbent also displayed that the formation of white layers on the surface was because of the adsorption of Pb (II) ions. From this SEM analysis of cotton adsorbent after the adsorption of Pb (II), more uneven and rough surface morphology existed in the adsorbents. The irregular surface outlook could be due to ions and foreign molecules deposition emanating from the contaminated fluid containing the adsorbate onto the carbon surface. Hence, the micrograph structures of the cotton hull attained from SEM represented a large surface area for heavy metal ion adsorption which indicates the difference between before and after loading of ions on the biomass surface.

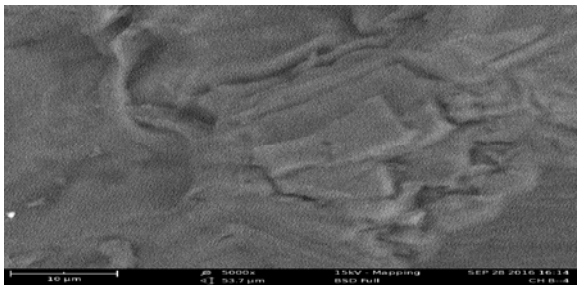

Figure1A: Micrographs of cotton hull

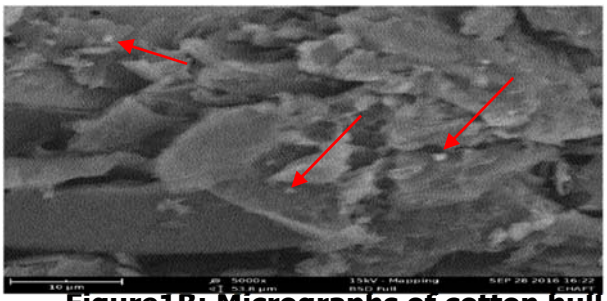

Figure1B: Micrographs of cotton hull after Pb (II) equilibration

FT-IR Spectrum Analysis of Cotton Hull Adsorbent

Figures 2 and 3 respectively shows FTIR carried out before and after Pb (II) ions. At adsorption ranges of 4000 to 650 cm^{-1}which shows shift in the wave number of emerging peaks associated with the plots after adsorption process. The raw adsorbent showed five energy bands within the range of 3947.3 and 3503.7 wave number which are broad but short peaks. The absorbance is associated with stretching variations of O-H groups found in polysaccharides, absorbed water, hemicellulose and lignin. This corresponded to free hydroxyl and carboxylic acids on the surface of the adsorbent (Blanes *et al*. 2016), the presence of the OH^- group enhanced the removal of Pb (II) through the surface reaction between the hydroxyl terminal and the Pb (II) (Icoranu *et al*., 2018) C-H stretching vibration was indicated from 2639-2516 cm^{-1}, C≡C symmetric variation for 2366.9 -2050 cm^{-1}, also 2016.5 – 1986.7 cm^{-1} for C=C asymmetric stretch while 1848.8 cm^{-1} is attributed to C = O stretch in the xylan tissue of the organic adsorbent. The peak at 1420.1 cm^{-1} represented H-C-H and O-C-H in plane bending vibrations. The almost flattened spectra from Figure 3 at 3333.2 cm^{-1} is broadened and responsible for the sorption of the Pb (II) ions on the surface of the cotton hull. Also, present is the C-H bending vibrations of H-C-C and C-O-H at 1364.2 cm^{-1} as well as frequencies at 1200.2 and 1155.5 cm^{-1}. The lone pairs of electrons oxygen in C-O-H and C = O further increase the rate of adsorption of the Pb (II) ion by attracting the Pb (II) (II) ions from the effluent (Wahi *et al*., 2009). Comparing the two figures showed that there was either a complete disappearance or a major shift of dominant peaks. Figure 3 justifies the feasibility of the adsorption (metal binding) process taking place at the surface of the spent cotton hull adsorption.

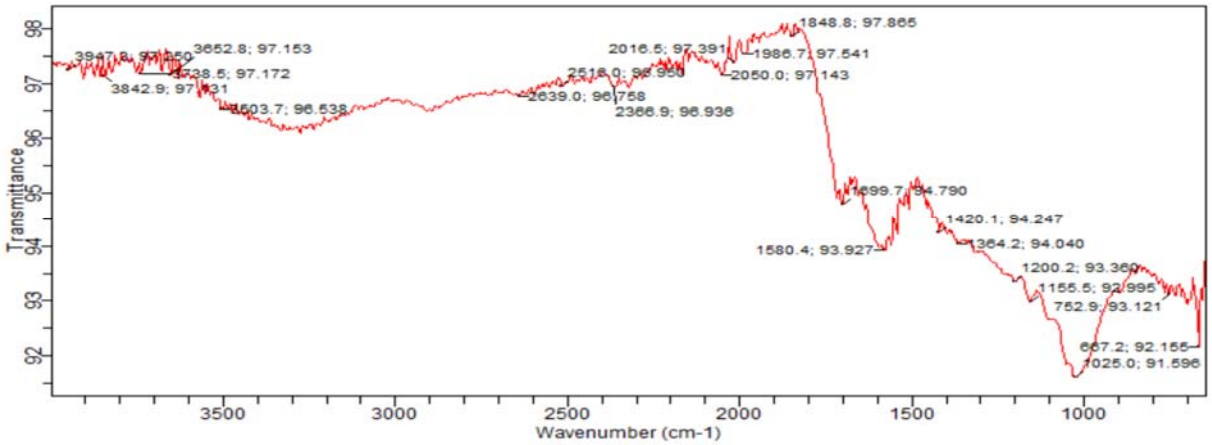

Figure 2: FTIR spectrum of cotton hull before Pb (II) ions adsorption

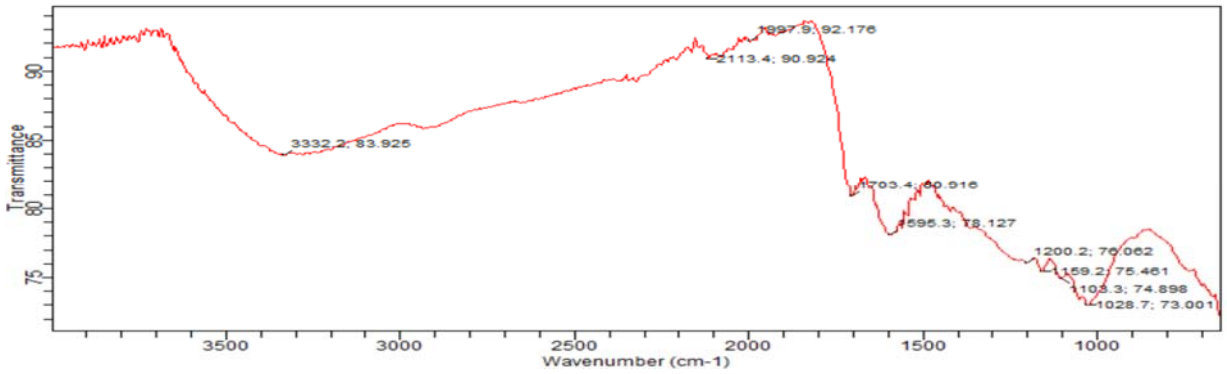

Figure 3: FTIR spectrum of cotton hull after Pb (II) ions adsorption

Evaluation of BET Analysis

The BET result for the cotton hull material showed relatively high surface area of 139.8 m^2/g as compared to some untreated agricultural adsorbents such as soy meal hull with 0.7623 m^2/g (Arami *et al,* 2006); cotton seed shells with specific surface area 124.35 m^2/g (Thinakaran *et al.* (2008); banana peel with 20.6–23.5 m^2/g (Annadurai *et al.* (2002) and orange peel with 20.6–23.5 m^2/g (Annadurai *et al*. (2002). The specific surface contributed greatly to the Pb (II) ions adsorption onto the cotton hull. The micro-pore volume and pore radius values were provided. The adsorbent characterized by important micro porosity of 9.237Ă (< 2nm) in this adsorbent are responsible for adsorption of metallic ions from solutions. Micro porosity is needed in adsorbing lower molecular weight material like Pb (II) atom (3 Ă diameter) and trace organics in water to a non – detectable level. The adsorbent has a low volume of micro pores radius of 0.0217 cm^3/g. The values got i.e. 9.237 Ă for micro pore radius and 139.8 m^2/g for cotton hull surface area material makes it a suitable adsorbent.

Evaluation of Apparent Density.

The apparent density had a value of 0.42 g/ml which showed that the material is good for water treatment process. The value is relatively high compared to other agricultural adsorbents such as empty palm oil fruit bunches of 0.21 g/ml (Wahi *et al.,* 2009) and is not likely to pose challenge of being trapped and suspended in water during application Wahi *et al.* (2009).

Effect of pH on Pb (II) adsorption

It is clear from the results represented graphically in Figure 4 that with the increase in pH, the Pb (II) removal increased gradually from its initial value of 2. At low pH of 2, the acidity of the medium shows high competition between hydrogen ions and Pb (II) ions in solution This is because at lower pH values, biosorption of metal ions was inhibited since the cell wall of the cotton hull contains various functional groups. The positively charged functional groups increase competition between protons and metal cations for binding active sites of cotton hull, resulting in decreasing the metal cations adsorption on its surface as explained by Yalcin (2014). At higher pH values of 5, several hydroxides low – soluble species such as Pb $(OH)_2$ was formed. Hence, considering the pH value of 5 requires little acid solution, it has minimal effect on both the processing equipment and the environment. Also, it gives optimum removal of Pb (II) from aqueous solution. This result is in agreements with the findings of Rahman and Sathasivam (2015) for heavy metal adsorption onto *Kappaphycus sp*. From aqueous solutions.

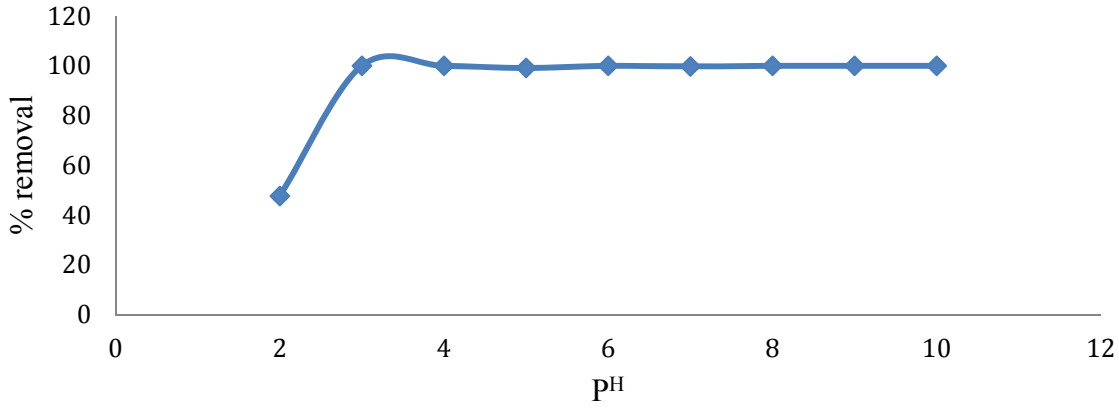

Figure 4: Effect of *pH* on Removal of Pb (II) (II) ions from solution

Column Adsorption Parameters

Effect of Feed Flow Rate

This was investigated by varying the feed flow rate at a constant bed height of 4 cm and an initial concentration of 50 mg/l. The breakthrough time obtained are 721, 480 and 240 minutes for flow rate values of 5, 7.5 and 10 ml/min respectively which indicated that the breakthrough time decreased with increasing flow rates. Also, there was a decrease in total percentage removal of Pb (II) ions in the fluid bed operations from 50.68% to 29.14% with increasing flow rate from 5 -10 ml/min. Similarly, increase in initial metal concentration with decreasing time from 3120 to 1920 minutes was observed. Hence, the contact time between the ions and cotton hull adsorbent decreases with increasing feed flow which results in decrease in adsorption capacity from 27.65 mg/g to 19.56 mg/g. This can be explained by the lack of sufficient residence time of the solute to diffuse into the pores of the cotton and thus reduces the volume of the water treated and the solute left the column before equilibration. This finding is in line with that of Nwabanne and Igbokwe (2012) for the removal of Pb (II) ions using oil palm fibre and that of Nouri and Ouederni (2013) for the adsorption of phenol from an aqueous solution on an activated carbon.

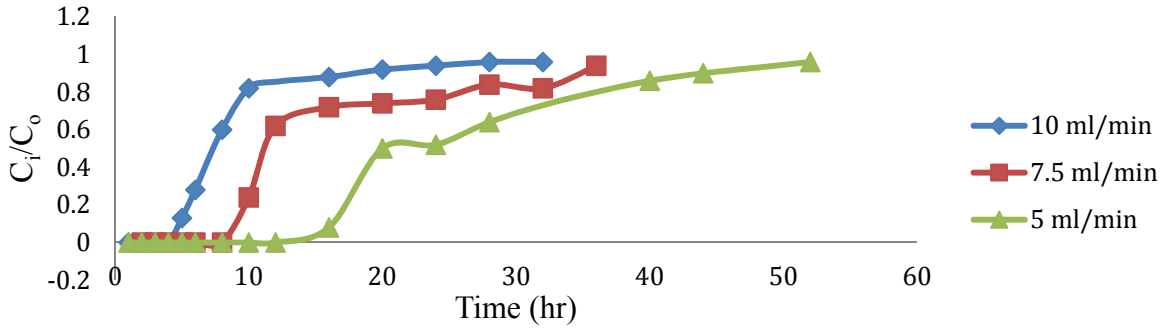

Figure 5: Effect of flow rate on breakthrough curve for Pb (II) adsorption on CHA

Effect of concentration

The effluent flow rate of 5 ml/min with a fixed bed of depth 4 and concentration of (50, 65 and 85 mg/l) were used to evaluate the effect of concentration on adsorption. It was observed from Figure 6 that as the effluent concentration increased, the breakthrough curves became sharper and the column with the highest inlet concentration saturated faster. That is from 3120 to 1920 minutes saturation. Also, a lower concentration gradient results in a slower transport because of decrease in the diffusion coefficient or the mass transfer coefficient as explained by Sivakumar and Palanisamy (2009) as well as Baek *et al*, (2007).

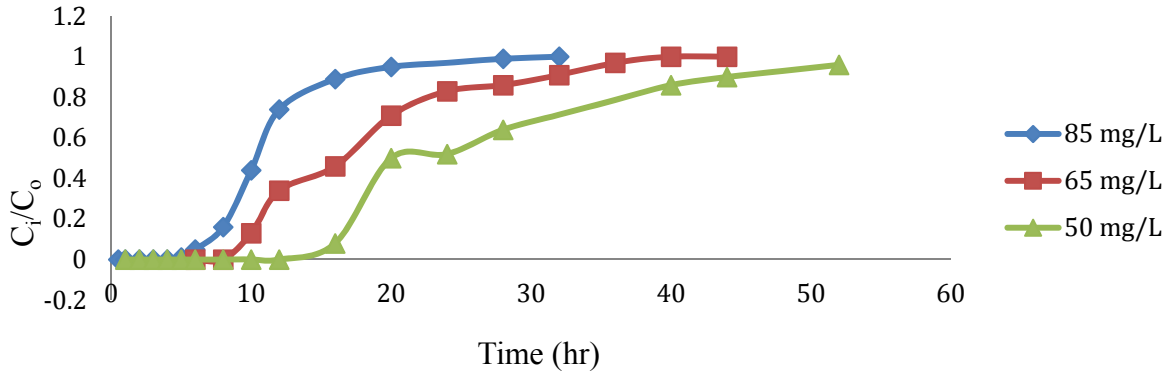

Figure 6: Effect of change in feed concentration on adsorption of cotton hull adsorbent with raw effluent

Effect of Adsorbent Bed Height

The effect of cotton hull bed length varied from 2.7 – 7 cm plots shown in Figure 7. The plots showed that the slope gradient of the breakthrough curves was slightly different with variation in bed depths with an earlier exhaustion for lower bed lengths. The results shown on Table 2 indicates that the breakthrough time of the adsorption increased sharply from 62 to 1212 mins with slight increase in the adsorbent bed height from 2.7 to 7 cm. This reveals that the cotton hull adsorbent had more contact time with the Pb (II) ion as the bed height was increased from 2.7 to 7 cm. Also, this may be due to the increase in the number of sorption sites (Radhika *et al.*, 2018). The increase in the adsorption capacity with increase in the bed height further suggested that at smaller bed height, the effluent adsorbate concentration ratio decreased more rapidly than for a higher bed height. Furthermore, low amount of the adsorbent in the column corresponds to smaller bed height and hence, less saturation time (Nwabanne *et al.*, 2012). The decrease in the slope of the breakthrough curves with increase in bed height observed may be due to the broadened movement of the influent at the mass transfer zone (Sekhula *et. al.* 2012).

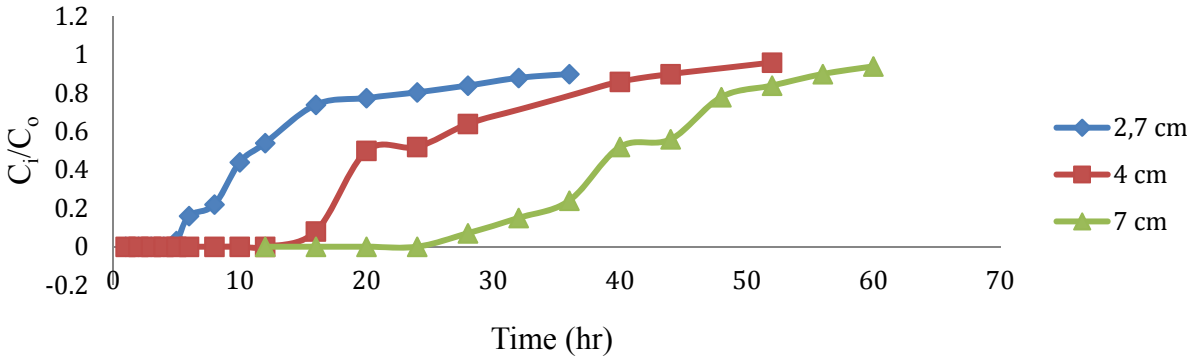

Figure 7: Effect of bed heights on column adsorption at constant concentration

Table 2 Evaluation of Column efficiency using experimental data

Q (ml/min)	conc.(mg/)	Bed (cm)	$q_{e,exp}$(mg/g)	t_{total}(min)	V_b(ml)	t_{break}(min)	q_{total}(mg)	% removal	R_a (mg/ml)
5	50	4	27.65	3120	3605	721	780	50.68	3.967
7.5	50	4	25.58	2160	3600	480	810	45.16	3.972
10	50	4	19.56	1920	2400	240	960	29.14	5.958
5	65	4	24.01	2400	2400	480	780	44.02	5.958
5	85	4	20.05	1920	905	181	816	35.14	15.8
5	50	2.7	20.95	2160	310	62	540	41.12	34.19
5	50	7	23.81	3600	6060	1212	900	69.83	4.356

q_e experimental average =23.09 mg/g and q_e theoretical average =21.60 mg/g

Column flow Adsorption Models

Three models (Thomas, Yoon-Nelson, and Adams- Bohart models) were used to analyse the column performance.

Application of Thomas Model

The behavior of the column was modelled using the Thomas model. Effect of bed heights and flow rate of the raw water on the removal of the Pb (II) by the cotton hull adsorbent were studied. This model is highly suitable for processes where external and internal diffusion will not be limiting step (Yahaya *et al.,* 2012) the results obtained are shown on table 2, the initial concentration increases with the value of k_{th} increasing from 0.042 to 0.068 ml/mg.min. The initial sorption capacity decreases with increasing initial concentration. This as a result of the slow mass transfer at lower concentration (Tor *et al.*, 2009), this was also reported in the modelling of the biosorption of Pb (II) by residue allspice (Cruz *et al.,* 2013). The q_{th} values decreases as the coefficient k_{th} increases when the fluid flow was increased. When the fluid flow rate increases from 5 to 7 ml/min, there was high system turbulence which reduces the effects of film diffusion and lower solute ions uptake q_{th}. Also, it was observed that the Thomas bed capacity, q_{th} gradually rises and the coefficient k_{th} decreases with an increase in bed length. The qth metal uptake is 21.60 mg/g compared with the experimental uptake of 23.09 mg/g. The correlation values are high ($0.7674 \leq R^2 \leq 0.9551$). Therefore, R^2 values and the closeness of predicted adsorption capacity to experimental data indicated the fitness of Thomas model to the experimental data. The relationship between the model and the initial concentration is to provide information on the adsorbent capacity, volume of contaminant treated and the total time needed to attain equilibrium. It is a suitable kinetic model to describe Pb (II) ions adsorption in a fixed bed column of cotton hull adsorption, Baek *et al.* (2007) and Nwabanne and Igbokwe (2012) but in contrast with the report of Sivakumar and Palamisamy (2009).

Application of Yoon – Nelson Model

Yoon–Nelson was used to examine the breakthrough behavior of Pb (II) ions on cotton hull adsorption. The values of k_{YN} and τ were determined from the plot of $L_n[C_i / C_o - C_i]$ against time at different operating conditions, to predict the rate constant and time required for 50% adsorbate breakthrough. The results obtained are shown on table 3. As initial concentration was increased at constant bed height and flow rate, the k_{YN} and τ decreased and increased respectively with increase in the initial concentration of the adsorbate. As the bed height increase, the values of τ increases from 1098.03, 1559.29, 2572.29 minutes for 2.7, 4 and 7 cm beds respectively. This

is similarly reported on the study of adsorption of Cu (II) onto maize tassel-PVA beads (Sekhula *et al.*, 2012), removal of perchlorate using modified activated carbon (Redhika *et al.*, 2018). This further suggests that increase in the bed height increased the contact time of the adsorbent on the adsorbate. The predicted τ obtained from the Yoon-Nelson model are closed to the experimental values. The regression coefficient R^2 values ($0.7661 \leq R^2 \leq 0.9551$) provide a good fit for the model, this agrees with the report provided by Radhika *et al.*, 2018. Therefore, Yoon-Nelson model could give depiction of an adsorption process for a single component Pb (II) adsorption of cotton hull adsorbent.

Table 2: Thomas model Parameters at different flow rates, initial concentrations and bed heights

Q_f (ml/min)	Conc.(mg/l)	Bed ht(cm)	t_{total}(min)	V_{eff} (ml)	K_{TH} (ml/mg.min)	q_{Th} (mg/g)	q_e, exp(mg/g)	R^2
5	50	4	3120	15600	0.042	27.25	27.65	0.9021
7.5	50	4	2160	16200	0.036	18.93	25.58	0.7883
10	50	4	1920	19200	0.054	14.90	19.56	0.7741
5	65	4	2400	12000	0.046	23.02	24.01	0.9551
5	85	4	1920	9600	0.068	22.92	20.05	0.9028
5	50	2.7	2160	10800	0.070	19.70	20.95	0.7674
5	50	7	3600	18000	0.068	24.46	23.81	0.9261

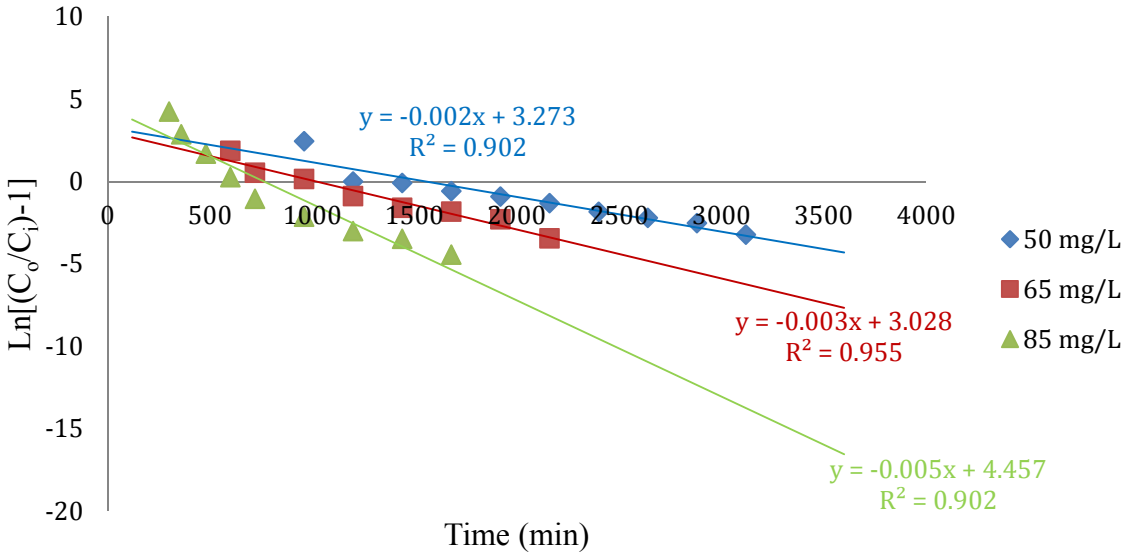

Figure 8: **Linear plot of Thomas model with experimental data at different concentrations and fixed** bed heights and initial metal ions concentrations

Table 3: Yoon-Nelson model Parameters at different flow rates, initial concentration, and bed heights.

Qf (ml/min)	Conc. (mg/L)	Bed height(cm)	K_{YN} (1/min)	$T_{Predicted}$ (min)	R^2	T_{exp} (min)
5	50	4	0.0021	1559.2857	0.9031	1442
7.5	50	4	0.0017	751.8823	0.7881	960
10	50	4	0.0027	417.6296	0.7661	480
5	65	4	0.003	1009.4667	0.9551	960
5	85	4	0.0058	768.5345	0.9028	362
5	50	2.7	0.0034	1098.0294	0.7865	124
5	50	7	0.0034	2572.2941	0.9244	2424

Key: T_{exp}= $T_{experiment}$

Application of Adams –Bohart Model

From table 4, adsorption capacity of adsorbent, No increased from 21358 to 42025 mg/l. The increase of adsorption capacity of the adsorbent with increase in bed height was similarly reported by Asif and Chen (2015), Yahuza *et al.*,(2017) while the kinetic constant of the model, *Kab* decrease with incresing adsorbent height (2.7 – 7 cm). It was observed that adsorption capacity of the adsorbent N_o decreased from 23140 to 13623 mg/l with increasing flow rate (5-10 ml/min). The R^2 value decreased with increase in flow rate at constant concentration and bed height. For instance, at 10, 7.5 and 5 ml/min, the R^2 were 0.4692, 0.5424 and 0.5698 respectively. At higher concentrations, the bed capacity has no defined pattern. This probably indicates that the model is not fit for a process at a very high flow rate (Yagub *et al,* 2014).

Table 4: Application of Adams-Bohart model to the experimental Data

Q_f(ml/min)	Conc. (mg/L)	Bed h_t(cm)	K_{AB} (ml/mg.min)	N_o (mg/L)	R^2
5	50	4	0.016	23140	0.5698
7.5	50	4	0.012	16932	0.5424
10	50	4	0.016	13623	0.4692
5	65	4	0.011	26290	0.679
5	85	4	0.023	22753	0.578
5	50	2.7	0.046	21358	0.606
5	50	7	0.04	42025	0.7282

CONCLUSION

Cotton seed hull is an economically viable adsorbent for the removal of Pb (II) ions from mining waste waters. Three models were used to evaluate the behavior of the experimental adsorption. Thomas model showed the comparison between the average experimental adsorption capacity of 23.09 mg/g and a theoretical value of 21.60 mg/g as well as a reasonably high correlation ($0.7674 \leq R^2 \leq 0.9551$). The Yoon–Nelson model showed the data regression analysis results also high linear correlation ($0.7661 \leq R^2 \leq 0.9551$). Hence, the Yoon – Nelson model is suitable model to

foretell the behavior of the experimental adsorption. Adams –Bohart model predicts poor efficiency of fixed – bed column. Characterizations of the untreated adsorbent carried out which included FTIR, SEM and BET. FTIR showed that the adsorbent has functional groups such as OH, C-O, C=O, C-O-H and CH_2. The SEM result showed that the micrograph structures of raw cotton hull carbon represent a large surface area for heavy metal ions adsorption. The BET provided a summary of specific surface area (139.8 m^2/g), micro-pore volume (0.0217 cm^3/g), micro pores (< 2 nm) and pore radius (9.237 Å). Column adsorption scale-up data for the 120 L/hr of Kagara mining wastewater shows that 607.2 L of the effluent can be treated of Pb (II) in 5.06 hours using 4.75 kg of the cotton hull adsorbent. Also, the column adsorption parameters investigated which included initial metal ions concentration, pH, feed flow rate, apparent density (0.42 g/ml) indicated that cotton hull as an adsorbent has high potential for removing heavy metal ions especially Pb (II), from aqueous solutions.

REFERENCES

American National Cotton seed Products Association (2000). Retrieved from https://www.bloomberg.com/profile/company/0759886D:US on 13th June 2014.

Annadurai G., Juang, R.S. and Lee, D. J. (2002). Use of Cellulose-Based Wastes for Adsorption of Dyes from Aqueous Solutions, J. Hazard. *Mater*. 92, 263–274.

Arami, M., Limaee, N.Y., Mahmoodi, N.M. and Tabrizi, N.S. (2006). Equilibrium and kinetics studies for the adsorption of direct and acid dyes from aqueous solution by soy meal hull, J. Hazard. *Mater* 135, 171–179.

Asif, Z. and Chen, Z. (2015). Removal of arsenic from drinking water using rice husk. Applied Water Science, 7(3), 1449–1458. doi:10.1007/s13201-015-0323-x

Baek, K., Song, S., Kang, S., Rhee, Y., Lee, C., Lee, B., Hudson, S. and Hwang, T. (2007). Adsorption kinetics of boron by anion exchange resin in packed column bed. J. Ind. Eng. Chem., 13(3), 452-456.

Barakat, M.A. (2011). New Trends in Removing Heavy Metals from Industrial Waste Water. *Arabian Journal of Chemistry*, 4, 363, doi:10.1016/j.arabjc.2010.07.019.

Biradarpatil, N. K. and Sangeeta, M. (2008). Effect of Dosages of Sulphuric Acid and Duration of Delinting on Seed Quality in Desi Cotton. *Karnataka Journal of Agricultural Science*, 22(4), 896.

Cruz-Olivares, J., Pérez-Alonso, C., Barrera-Díaz, C., Ureña-Nuñez, F., Chaparro-Mercado, M. C. and Bilyeu, B. (2013). Modeling of Pb (II) (II) biosorption by residue of allspice in a fixed-bed column. Chemical Engineering Journal, 228, 21–27.doi:10.1016/j.cej.2013.04.101

Eckenfelder, W. W. (2000). Industrial Water Pollution Control: McGraw-Hill Series in Pollution, New York: McGraw-Hill 138, 360.

Farghali, A.A., Bahgat, M., Abdelaal,A.A. and Khedr, M. H. (2013). Adsorption of Pb(II) ions from aqueous solutions using copper oxide nanostructures. *Beni-Suef University Journal Of Basic And Applied Sciences* 2 (2013) pp 61-71. DOI: 10.1016/j.bjbas.2013.01.001

Heuzé, V., Tran, G., Hassoun, P., and Lebas, F. (2015). Cotton seed Meal. Feedipedia: *Animal Feed Resources Information System*, 1.

Iconaru, S.L., Heino, M.M., Guegan, R., Beuran, M., Costescu, A. and Predoi, D. (2018). Adsorption of Pb (II) Ions onto Hydroxyapatite Nanopowders in Aqueous Solutions. J. Material, doi:10.3390/ma11112204

Mengistie , A.A, Rao,T.S., Rao, A.V. P. and Singanan,M. (2008). Removal of Pb (II)(II) Ions from Aqueous Solutions using Activated Carbon from Militia Ferruginea Plant Leaves. *Bulletin of Chemical Society of Ethiopia*, 22(3), 349-360.

Nouri, H. and Ouederni, A. (2013). Modeling of the Dynamics Adsorption of Phenol from an Aqueous Solution on Activated Carbon Produced from Olive Stones. *International Journal of Chemical Engineering and Applications*, 4 (4), 254-261.

Nwabanne, J. T. and Igbokwe, P. K. (2012). Adsorption Performance of Packed Bed Column for the removal of Pb (II) (II) using Oil Palm Fibre. *International Journal of Applied Science and Technology,* 2 (5), 106 -115.

Radhika, R., Jayalatha, T., Rekha Krishnan, G., Jacob, S., Rajeev, R. and George, B. K. (2018). Adsorption Performance of Packed Bed Column for the Removal of Perchlorate Using Modified Activated Carbon.Process Safety and Environment Protection, 117, 350-362. https://doi.org/10.1016/j.psep.2018.04.026.

Rahman, M.S. and Sathasivam, K.V. (2015). Heavy Metal Adsorption onto Kappaphycus sp. From Aqueous Solutions: The Use of Error Functions for Validation of Isotherm and Kinetics Models. BioMed Research International, Volume 2015. http://dx.doi.org/10.1155/2015/126298.

Ruparelia, J.P., Duttagupta, S.P., Chatterjee, A.K. and Mukherji, S. (2008). Potential of Carbon Nanomaterials for Removal of Heavy Metals from Water. *Desalination* 232(1):145-156. DOI: 10.1016/j.desal.2007.08.023.

Sekhula, M.M., Okonkwo, J.O., Zvinowanda1, C.M., Agyei N.N. and Abdul J.C. (2012).
Fixed bed Column Adsorption of Cu (II) onto Maize Tassel-PVA Beads, J. of Chem. Eng.
and Process Technology, 3(2), 131. http://dx.doi.org/4172/2157-7048.1000131

Sivakumar, P. and Palanisamy, P. N. (2009). Adsorption Studies of Basic Red 29 by A Non-Conventional Activated Carbon Prepared from Euphorbia Antiquorum L. *International Journal* of Chem. Tec. Research, 1 (3), 502-510.

Thinakaran, N., Panneerselvam, P., Baskaralingam, P. Elango, D. and Sivanesan, S. (2008). Equilibrium and Kinetic Studies on the Removal of Acid Red 114 from Aqueous Solutions using Activated Carbons Prepared from Seed Shells, *J. Hazard*. *Mater*. 158, 142–150.

Tor, A., Danaoglu, N., Arslan, G. and Cengeloglu, Y. (2009). Removal of fluoride from water by using granular red mud: batch and column studies, J. Hazard. Mater. 55, 77–93.

United States Department of Agriculture (2019). Retrieved form https://www.indexmundi.com/agriculture/?country=ngandcommodity=cottonandgraph=production.

World Health Organization, WHO. (2010). Childhood Pb (II) Poisoning. WHO Library Cataloguing-in-Publication Data 12.

World Health Organization, WHO. (2015). Pb (II) Poisoning and health. WHO Fact sheet N°379, Media Centre. https://reliefweb.int/report/nigeria/Pb (II)-poisoning-nigeria-15-may-2015.

Yagub, M. T., Sen, T. K., Afroze, S., and Ang, H. M. (2014). "Dye and its removal from aqueous solution by adsorption: A review,"*Adv. Colloid Interfac.,*209: 172-184.

Yahuza, K. M., Ibrahim, M. B., Ayuba, A. M., Hamza, R. (2017). Fixed-bed column Adsorption of methyl blue using carbon derived from axle-wood (*anogeissus leiocarpus)* stem as adsorsent. Bayero Journal of Pure and Applied Sciences: 10(1), 304 – 310. doi.org/10.4314/bajopas.10i1.61S

Yalcin, S. (2014). The Mechanism of Heavy Metal Biosorption on Green Marine Macroalga Enteromorpha Linza, *Clean—Soil, Air,Water*, 42 (3) 251–259. \

Yahaya, N., Abustana, I., Latiffa, M., Bello, O.S. and Ahmad, M. A. (2011). Fixed-bed column study for Cu (II) removal from aqueous solutions using rice husk based activated carbon. International Journal of Engineering and Technology, 11, 248-252.

Proceedings of the 49th NSChE Annual Conference
KADA 2019: pp 176-185

P1C-01: EXPERIMENTAL EVALUATION OF AGRO PRODUCT AS FLUID LOSS CONTROL AGENT IN CEMENTING OPERATIONS

Ndubuisi, E. C. [a,b], O. F. Joel[a,b], A. Dosunmu[b], I. Okoye[c] Nwosi H. A[a]
[a] World Bank African Centre of Excellence, Centre for Oilfield Chemicals Research, University of Port Harcourt, Port Harcourt, Nigeria.
[b] Department of Petroleum, University of Port Harcourt, Port Harcourt, Nigeria.
[c] Department of Pure and Industrial Chemistry, University of Port Harcourt, Port Harcourt
Corresponding authors: elizabeth.ndubuisi@uniport.edu.org; ndubuisi.elizabeth@aceuniport, ndu5fc@gmail.com, hezekiahandrews@yahoo.com

ABSTRACT
The devastating effect of the operational failure of a cementing job is enormous. Additives used for cement slurry recipe contribute substantially to the total cause of an operational failure. Therefore, it is imperative that a paradigm shift that addresses the challenges of cementing failure be considered. A comparative analyses were performed with imported polymer (Hydroxyethylcellulose) as against local polymers (cassava starch) for cement slurry design to determine fluid loss. Polymer's concentration of 0.1% by weight of cement was used for the cement slurry design, in order to characterize their fluid loss. Experimental study of cement slurry density of 14ppg and 15.8ppg at temperatures of 80°F (29°C) and 190°F (88°C) and the result of the local-based polymers (cassava starch), namely; 96/1632 (PG1); 98/0505 (PG2) and 92/0057 (PG3) were ascertained; for 96/1632 (PG1) as temperature increased then decreased in fluid loss, 289 to 95 cc/30min; for 98/0505 (PG2) the fluid loss decrease from 293 to 98 cc/30min; for 92/0057 (PG3) it decreases from 346 to 105 cc/30min and HEC decreased from 247 to 91 cc/30min. A cement slurry density of 15.8ppg of the same concentration and temperatures, results showed that for 96/1632 (PG1) as temperature increased there was a corresponding decreased in fluid loss from 103 to 43 cc/30min; for 98/0505 (PG2) the fluid loss decreased from 121 to 53 cc/30min; for 92/0057 (PG3) the fluid loss decreased from 136 to 61cc/30min and for HEC the fluid loss decreased from 151 to 69 cc/30min.

Keywords: Cement-slurry; fluid-loss; Hydroxyethylcellulose; Green Chemistry; Cassava starch

1.0 Introduction
Zonal isolation is obtained in oil and gas wells by cementing operation thus, creating a strength zone against the physical and chemical forces in well from the underground environment. Constant research by the Oil and Gas industry towards improving the properties of that strength zone is continues. According to Nelson (1990), certain parameters help to control this zone isolation and they are classified into four categories; First one is related to all parameters provided by cement sheath on the reservoir, affecting the well performance; Second one is considering parameters of design works for cement slurry to maintain desired physical and chemicals properties for each individual well condition; The third one is capturing various aspects of cementing job for different purposes including pre-job works, like squeeze cementing, foamed cement or horizontal well cementing; and the fourth is, considering all cementing job evaluation for short term and long term after the placement of cement slurry. As stated above, the first and second categories and parameters define main quantities to control the cement-reservoir interactions and cement slurry design work, thus, these are key issues for the oil and gas industry. After a conventional drilling operation, depending on the depth and casing design parameters, each section is definitely isolated from the other sections. Not only from the reservoir part but

also from the cement slurry part should be hydraulically sealed. Zonal isolation preserves the reservoir conditions including permeability for the vicinity of wellbore but more importantly, zonal isolation preserves cement slurry against unwanted fluid migration from the reservoir. Baroghel-Bouny et al. (2009) disclosed that the durability of oil or gas well is dependent on the absolute binding of the cement structures and should be able to serve the purposes for which they were built throughout their service life. The authors further stated that safety, economy and environmental factors are major issues in the long-term durability of structures. "The restriction of fluid movement between zones and protection of casing from corrosion as well as closing non-productive well could be achieved by the used of cement in drilling operations" (Roshan, H. et al. 2010). Santra et al. (2007) noted that formation fluid influx into cement slurries presents not only short term problems like losing appropriate composition by shallow water influxes but also present long term problems by gas migration. There exist very large numbers of well that leak or have sustained casing pressure (SCP). In Central Europe and the Middle East, there are hundreds of wells with reports of trapped pressure that cannot be bled off. In the USA and Canada, there are thousands of wells leaking to the surface which may or may not be discharged to the atmosphere.

Because of complex conditions downhole, several chemicals referred to as additives are usually needed in the design of optimum cement slurries to improve desired American Petroleum Institute (API) properties. At different temperature conditions of oil or gas well, firm and absolute placement of cement slurries are required along the wellbore and an even filled with the annular volume. However, fluid loss additives are needed to prevent water encroachment in or out the formation, while free water additive is a key ingredient of cement slurry design towards achieving zero percent free water at formation temperature.

Keller, S.R. et al (1987) affirmed that free water is the most important factor that should be as low as possible after cement sets. Yield point, plastic viscosity, fluid loss, gel strength, and the dynamic settling characteristics of the cement slurry are other important parameters. The proper slurry design is of extreme importance, not only to prevent particle settling but also to help cover appropriate rheology for efficient placement and mud removal, as well as providing zero free water to help provide top-side integrity in the annulus. Cement slurries that have free water and/or settling tendencies can result in water channels on the top side of a horizontal annulus, or an area of reduced compressive strength cement which may not provide the annular seal required for zonal isolation during stimulation treatments. It is necessary that well-suspended, zero free water slurries be used in horizontal cementing applications. Free fluid may show up not as clear water, but as a thin portion of the cement-colored fluid containing well-dispersed cement fines. This type of slurry should be rejected or adjusted to eliminate this phenomenon because the less dense portion at the top may not provide the strength required for a proper seal, and may provide a path for well fluid movement. This could also leave the casing exposed to corrosion from downhole water contact.

Field experience has shown that cement behavior remains very difficult to predict and extensive design and testing is required to adjust and optimize almost each and every job. Nelson and Guillot, 2006 stated that sometimes variability can be so dramatic that some additives performance can be completely lost in some cement grades thus, there is usually dramatic effects in fluid loss at any slight temperature increase.

Sabins and Sutton noted that cement response to additives is closely monitored at every stage of a job implementation. Fluid loss is essential to allow an even placement of cement and ensure acceptable cement hydration. It is advocated that once the cement is placed, the water to cement ratio is kept within acceptable limits and cement hydration, for instance, consolidation will take place as designed and that mechanical properties will develop as scheduled.

The focus of this study is on fluid loss control during placement; cement, in this case, is at the very early stages of its hydration and within the induction period. According to Scrivener *et al.* (2015), during the pre-induction period, fast dissolution and precipitation processes occur and modify the surfaces of all mineral phases present in the cement. Of course, most times the pre-induction period lasts a few minutes. It was observed that a very limited reaction activity of very slightly hydrated cement enters the induction period. Cement is pumped downhole and placed against the formation during this induction phase. Nelson and Guillot, (2006) stated that for high-temperature application, retarders are added in order to maintain cement in the induction phase throughout the pumping time. Rao and Burkhalter (1985), Persinski, Cook, and Adams (1977) disclosed that conventional copolymers generally comprises 2-Acrylamido-2-methyl propane sulfonic acid (AMPS). Study on the mechanism of action of these polymers was carried out by Plank, et al (2006), Recalde L and Plank (2012) and it was discovered that the performance is directly linked to adsorption of the polymer on the cement surface. Again this adsorption is electro-statically driven, anionic sulfonate groups from the "AMPS" monomeric units adsorbs onto the cationic sites on the cement (Nagele 1985, Plank and Hursch 2007).

The objective of this study is to evaluate the effectiveness of storage amylose/amylopectin based polymer such as cassava starch as cementing additive to control fluid loss and compare it with the structural cellulose-based polymer such as hydroxyethylcellulose-HEC). The benefit of the storage polymer is that it promotes the principle of green chemistry, however, the benefits are not only health and environment-related, but also economical, as the costs of storage, regulation and protecting workers and the public from exposure to hazardous chemicals are reduced.

2.0 Material and Methods

Raw samples were collected from the South-East geopolitical zone of Nigeria. Preparation of the raw samples was done in accordance with the Food and Agricultural Organization procedures. Thereafter, laboratory analyses were conducted to ascertain American Petroleum Institute, standard to ensure it meets specifications prior to usage.

2.1 Cement Slurry Design

The first concern in designing cement systems for oil and gas wells is to ensure that the slurries are suitable for field applications. This means that they can easily be mixed and pumped with conventional surface equipment, and placed at the required depth with proper thickening time. The slurry must also remain stable during the whole process. For this purpose, optimization is carried out for each system. Therefore, Proper slurry design is critical to the success of a cementing job.

Dry samples of three cultivars were used for the experiments. Two different cement slurry densities; 14 and 15.8ppg were prepared with 0.10% BWOC polymer concentration as shown in Table 2.1 Samples were weighed and then blended uniformly before added to the mixing fluids. Standard CTC constant speed mixer (Model-7000) of 1.2L capacity was used to an obtained homogenous mixture. The mixer motor was turned on and maintained at (4000±200 rpm)

according to API RP10-2B procedure (API Edition, 2009). Water and fluid additives were then stirred above rotational speed to thoroughly disperse them prior to cement addition. The cement and solid additives blend were added at a uniform rate, in not more than 15 seconds. After the addition of all dry materials to the mix water, the mixing speed was increased to 12000±500 rpm for 35 seconds. Dry materials (cement and solid additives) and water temperature should be kept at 23±1.10C prior to the mixing.

2.1.1 API Fluid Loss Test

Static fluid loss experiments were performed and conditioned for 20 minutes at temperatures ranging from 80°F (29°C) to 190°F (88°C) using atmospheric consistometer according to API standard (ANSI, API 2005). A standard 175ml filtration cell fitted with a 45µm (325) mesh screen supplied by OFI Testing equipment (Houston, USA) was used. The operating procedure and test conditions are detailed in API 10-B norm (API 2013). The conditioned slurry was placed in the preheated fluid loss cell (the fluid loss cell was heated in the heating jacket prior to conditioning). Nitrogen was used to apply 1000psi (60 bars) on top of the cell. The test started when the bottom outlet was opened to atmospheric pressure. The filtrate was collected, measured and plotted against time. It was ensured that filtration lasted for 30minutes without nitrogen breakthrough.

Calculation of fluid loss

If however, filtration proceeds for 30minutes without nitrogen breakthrough, then;

$$V_{API} = 2 \text{ X } V(t_{30})$$

In the case of nitrogen blowout, the test was stopped and reported API volume was calculated as:

$$V_{API} = 2 \text{ X } V(_{breakthrough}) \text{ X} \sqrt{\frac{30}{t_{breakthrough}}}$$

2.2 Materials

Cement and Additives

The cement grade used for the study is the certified HSR class G cement and corresponds to AOI specifications (API 10 A), derivatized imported polymer (Hydroxyethylcellulose-HEC) and local polymers (cassava starch), antifoam (FP-30L) and freshwater.

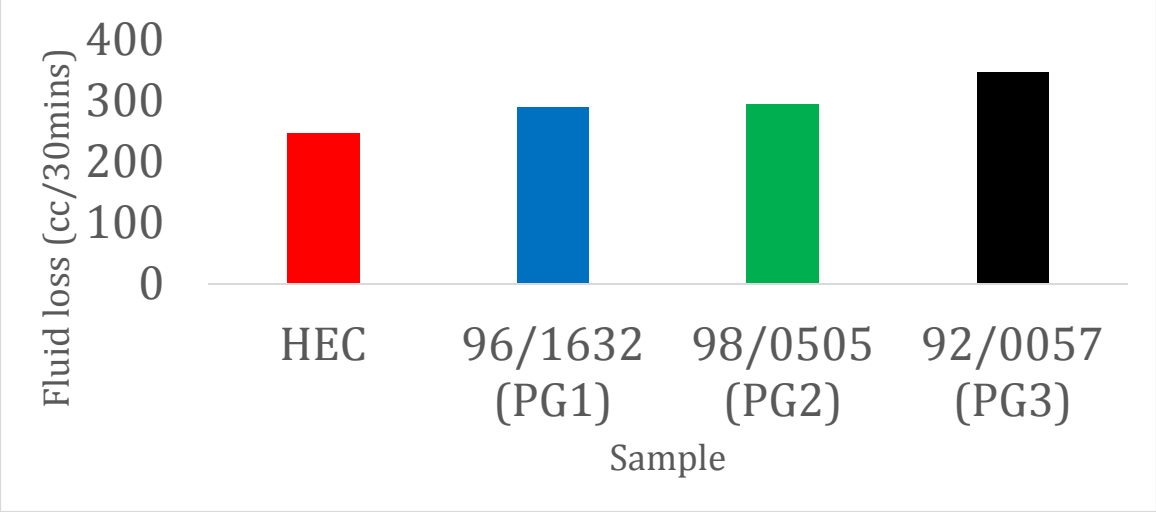

Figure 1: Fluid loss of different samples of polymers at 80°F (29°C) of 14ppg cement slurry

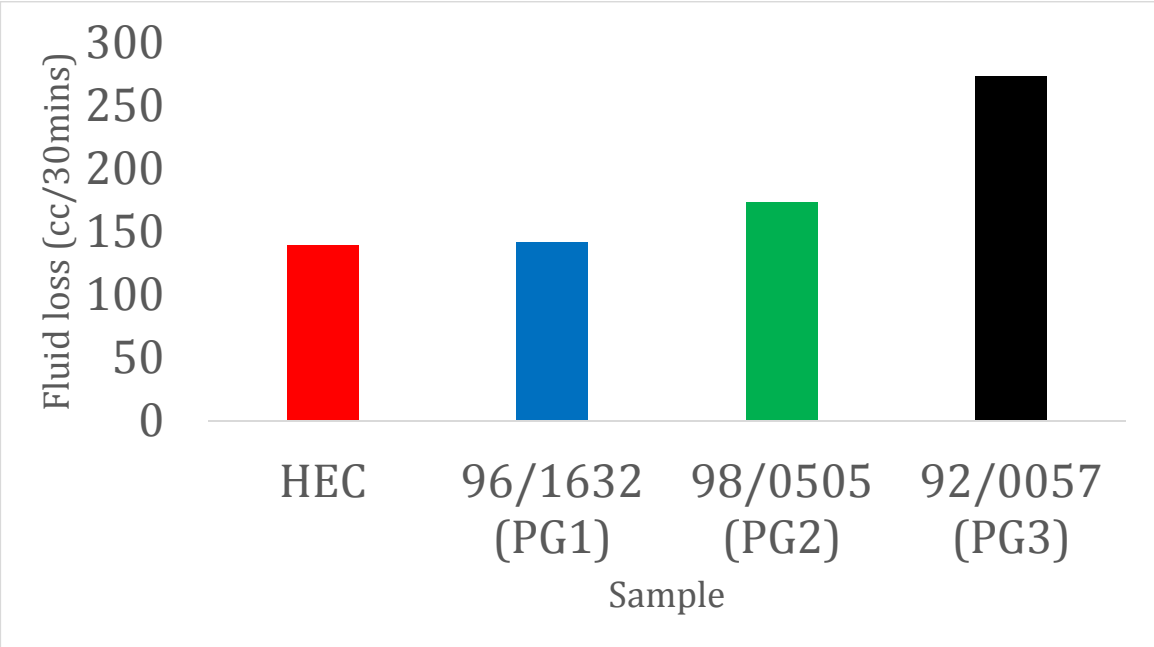

Figure 2: Fluid loss of different samples of polymers at 120°F (49°C) of 14ppg cement slurry

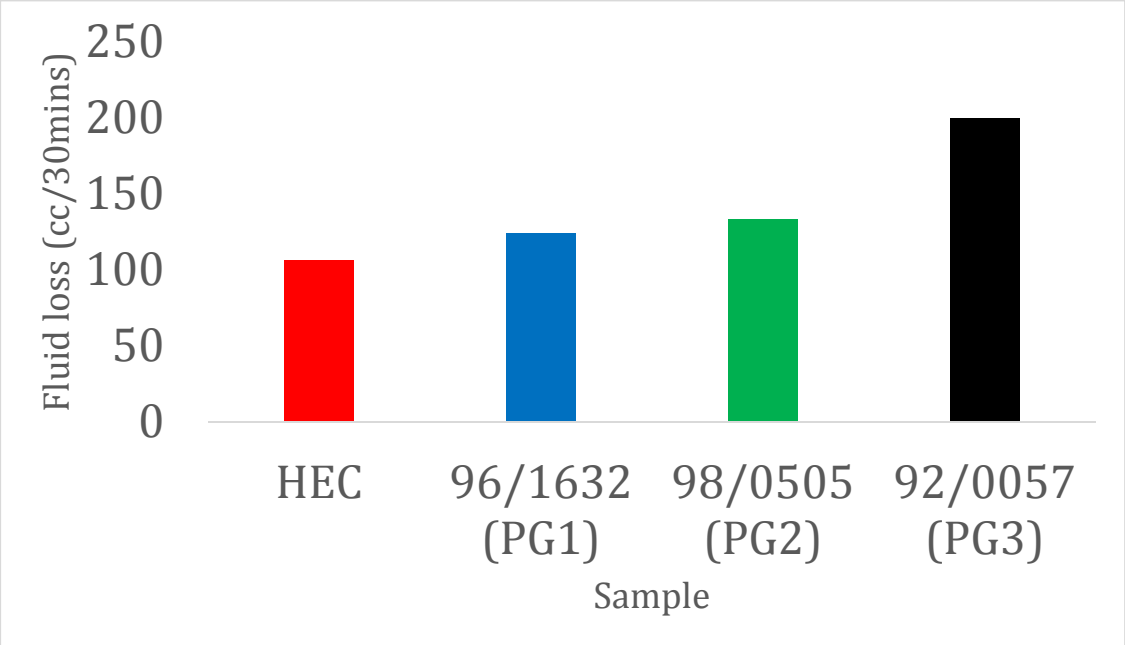

Figure 3: Fluid loss of different samples of polymers at 150°F (66°C) of 14ppg cement slurry

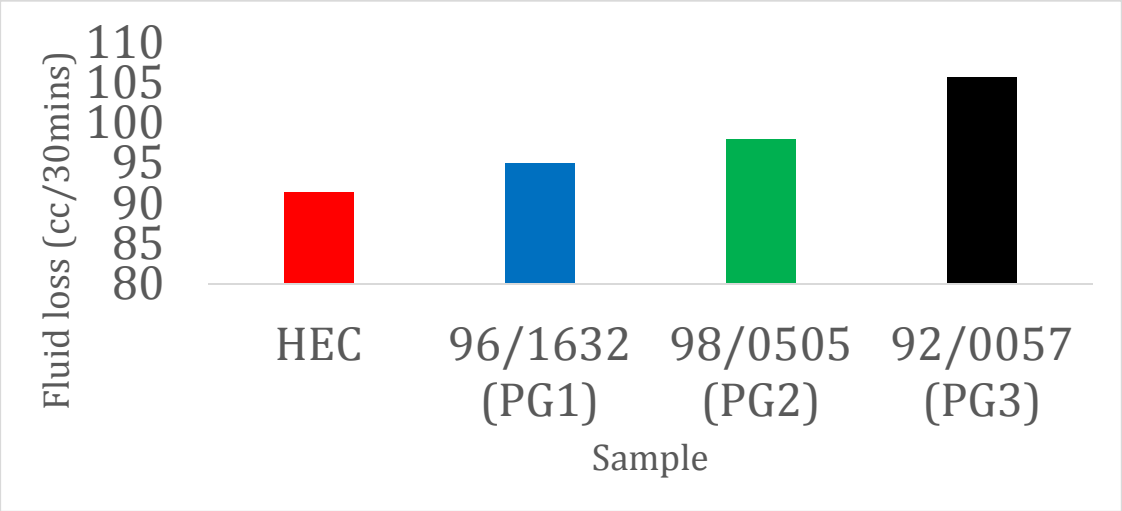

Figure 4: Fluid loss of different samples of polymers at 190°F (88°C) of 14ppg cement slurry

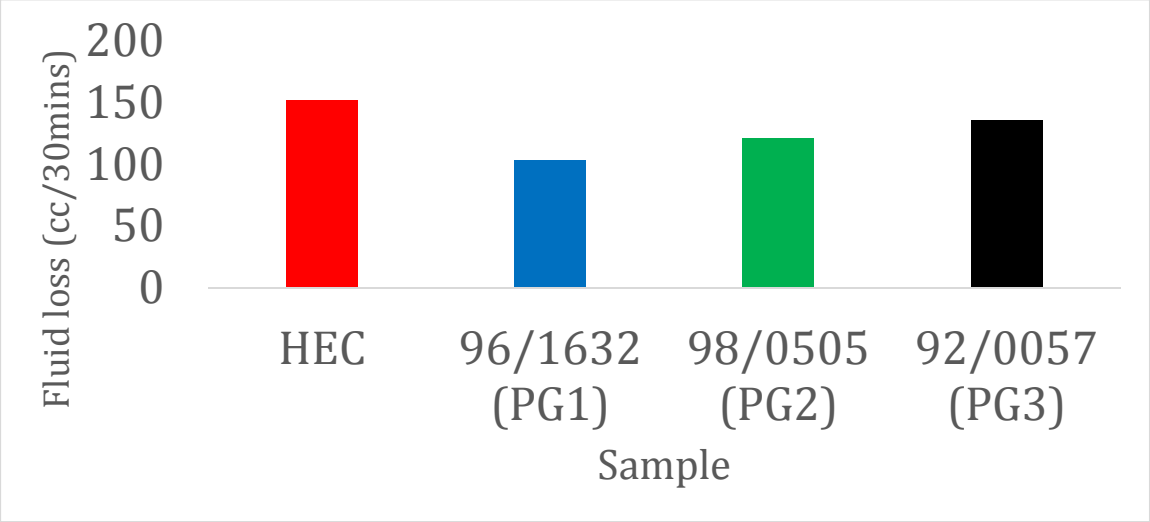

Figure 5: Fluid loss of different samples of polymers at 80°F (29°C) of 15.8ppg cement slurry

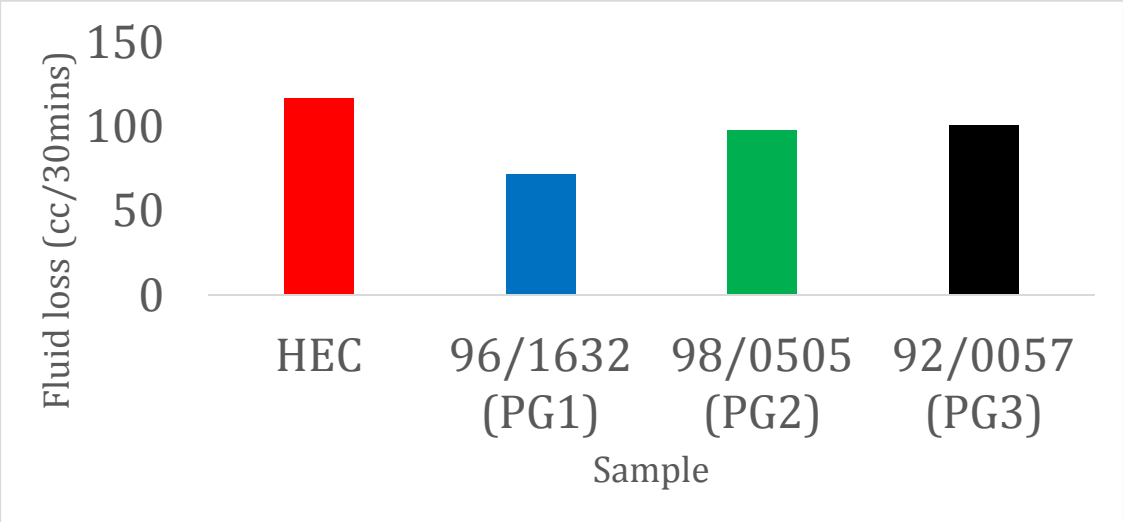

Figure 6: Fluid loss of different samples of polymers at 120°F (49°C) of 15.8ppg cement slurry

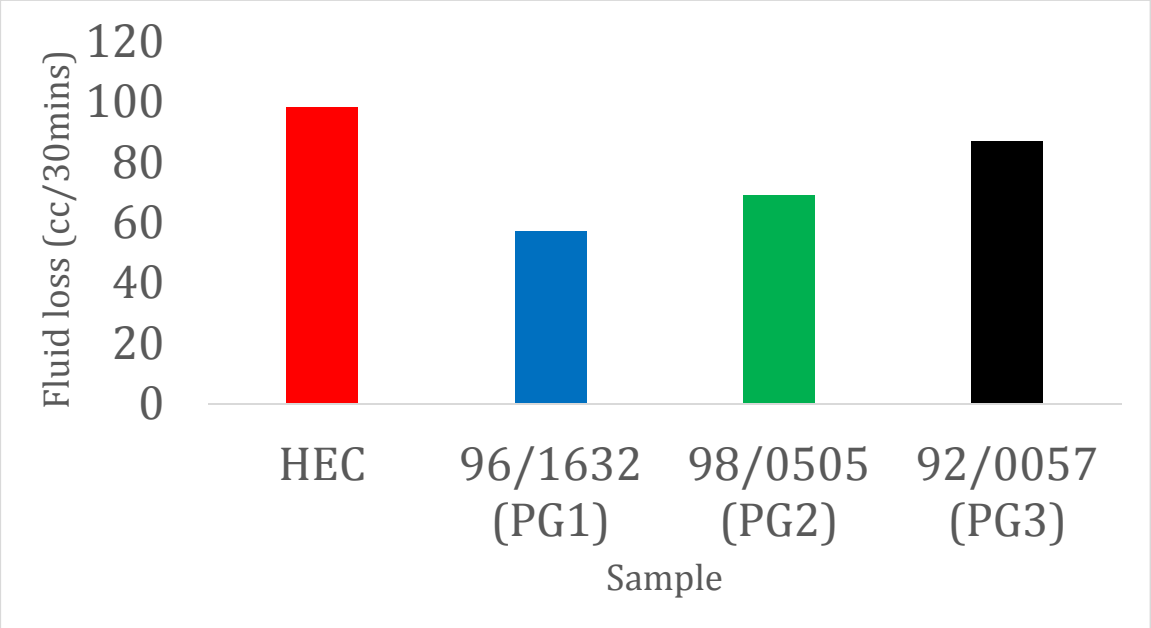

Figure 7: Fluid loss of different samples of polymers at 150°F (66°C) of 15.8ppg cement slurry

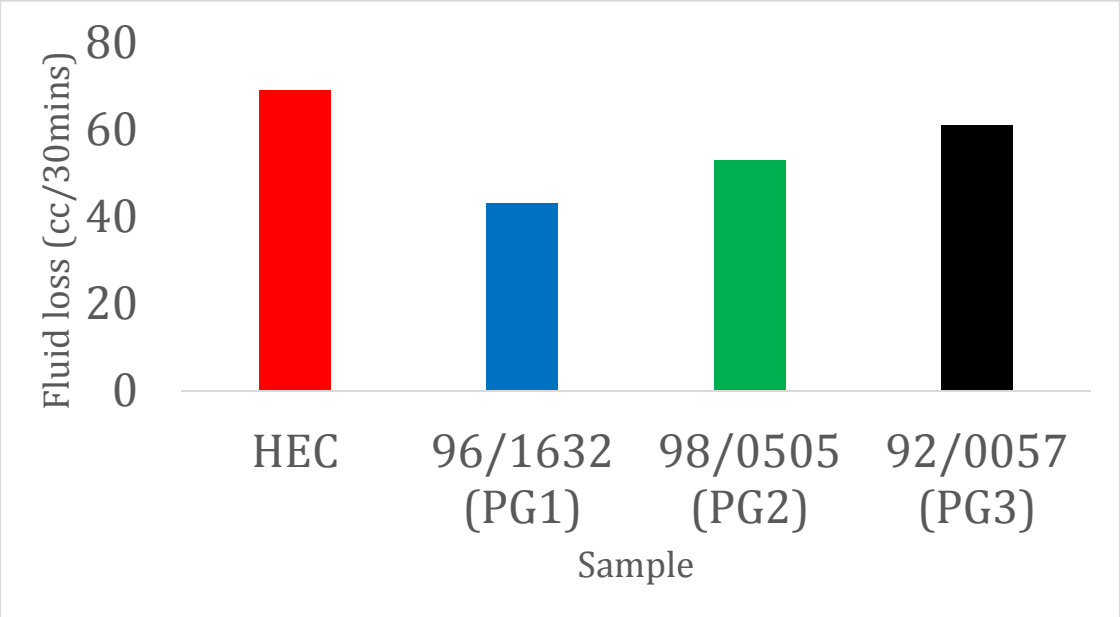

Figure 8: Fluid loss of different samples of polymers at 190°F (88°C) of 15.8ppg cement slurry

2.3 Impact of Imported and Local Polymers on Cement Slurries Fluid loss

Fluid loss control through cement slurry is essential for cementing operations, especially to prevent fluid migration and fluid segregation. The performance of three samples of local-based polymers (cassava starch), namely; 96/1632 (PG1); 98/0505 (PG2) and 92/0057 (PG3) were ascertained by analyzing the products and then compared with hydroxyethylcellulose (HEC) based polymer to determine their effectiveness with respect to fluid loss as shown in Figures 2.1 to 2.8. For cement slurry density of 14ppg, at temperatures of 80°F (29°C) to 190°F, results showed that for 96/1632 (PG1) as temperature increased there was a corresponding decreased in fluid loss from 289 to 95 cc/30min; for 98/0505 (PG2) the fluid loss decrease from 293 to 98 cc/30min; for 92/0057 (PG3) it decreases from 346 to 105 cc/30min and HEC decreased from 247 to 91 cc/30min. A cement slurry density of 15.8ppg of the same concentration and temperatures, results showed that for 96/1632 (PG1) as temperature increased there was a corresponding decreased in fluid loss from 103 to 43 cc/30min; for 98/0505 (PG2) the fluid loss decreased from 121 to 53 cc/30min; for 92/0057 (PG3) the fluid loss decreased from 136 to 61cc/30min and for HEC the fluid loss decreased from 151 to 69 cc/30min. Experimental results here have shown that cassava starch compared favourably with hydroxyethylcellulose. It should be noted that, field experience in a number of application shows that most operators will accept fluid loss values below 200 to 250 cc/30min. as reasonably good for fluid loss control agent, however, for critical jobs like narrow annulus liner or casing job across permeable hydrocarbon zones, values below 50 or even 15 are required for fluid loss., Nelson and Guillot, (2006) stated that a basic 15.8 ppg cement slurry with no chemicals to improve fluid loss will usually have a fluid loss value higher than 1500 ml./30 min. Therefore, the result of this work proves that cassava starch could be a good substitute as fluid loss reducers for cement slurry design.

The local-based cement slurry polymer cassava starch (96/1632 (PG1) performed favorably with the imported based cement slurry polymer ((Hydroxyethylcellulose - HEC), with local based cement slurry polymers 98/0505 (PG2) and 92/0057 (PG3) having better fluid loss control. The

study revealed that local polymers (cassava starch) reduced fluid loss in cement slurry density of 14ppg and 15.8ppg. However, 0.1% by weight of cement of cassava starch reduced fluid loss with increase in temperature.

2.7 Analysis of Variance of Fluid loss of Imported and Local Based Cement Slurry Polymers

Table 2.1 result showed that for cement slurry design of 14 ppg, the average fluid loss of HEC was 145.93 (SD = 70.25), while the average of PG1, PG2, and PG3 were 162.63 (SD = 86.71), 174.48 (SD = 85.22) and 231.38 (SD = 103.04) respectively. Thus indicating no significant difference between the fluid loss of the four different polymers used as viscosifier. This result pretty indicates that PG1, PG2, and PG3 polymer can be used as a substitute for HEC. Results from a further investigation using SPSS 22 software showed that for fluid loss there was no significant difference among the polymers. Similar results were also noticed for cement slurry design for 15.8 ppg, with no significant difference.

Table 2.1: Analysis of Variance for Fluid loss

Polymer	Cement Slurry Design for 14ppg Fluid loss (cc/30min)	Cement slurry design for 15.8ppg Fluid loss (cc/30min)
HEC	145.93[a]	108.9[a]
PG1	162.63[a]	68.78[a]
PG2	174.48[a]	85.25[a]
PG3	231.38[a]	96.25[a]

Conclusions

A fluid loss in cement slurry was minimized with Local cassava starch (96/1632 (PG1) when compared with imported polymer (Hydroxyethylcellulose – HEC). Also, cassava starches 98/0505 (PG2) and 92/0057 (PG3) minimized the fluid loss in cement slurry but little below when compared with an imported polymer. As the temperature increased from 80°F to 190°F there was a corresponding decrease in fluid loss. Local cassava starch exhibited excellent fluid loss at cement slurry density of 15.8ppg because it was below 200 cc/30mins which is in line with field acceptable value stated by other investigators and researchers. However, for critical jobs like narrow annulus liner or casing job across permeable hydrocarbon zones, values below are required for fluid loss. Also, at cement slurry density of 14ppg, the fluid loss was minimized at temperatures of 120°F to 190°F.

Statistical analysis obtained revealed that there was no significant difference between the imported polymer (Hydroxyethylcellulose-HEC) and local polymers (cassava starches). Local cassava starch 98/0505 (PG2) had the highest mean plastic viscosity at 14ppg. This shows that local cassava starch PG2 was slightly better than imported polymer Hydroxyethylcellulose (HEC). This product is unique in that apart from its ability to reduce fluid loss with an increase in temperature, it is self-active, and also supports the principle of green chemistry due to its environmental friendliness.

Acknowledgments

Authors wish to acknowledge World Bank Africa Centre of Excellence in Oilfield Chemicals Research (ACE-CEFOR), University of Port Harcourt Nigeria for support. Thanks to Baker Hughes Incorporated, Nigeria and Pollution Control and Environmental Management (POCEMA) Limited, Port Harcourt, where experimental work was conducted. This research work was supported by National Root Crop Research Institute (NRCRI), Umudike for providing, and conducting the extraction and analysis of the starches.

References:

ANSI, API (2005): RP 10B-2 Recommended Practice for Testing Well Cementing, 1st addition

API-RP 10B-2. (2009): "Recommended practice for testing well cement". Washington, DC, 22-02.

Baroghel-Bouny, V., Nguyen, T. Q., and Dangla, P. (2009): Assessment and prediction of RC structure service life by means of durability indicators and physical/chemical models. Cement and Concrete Composites, 31, 522–534.CrossRefGoogle Scholar

Keller, S.R. et al.: "Deviated-Wellbore Cementing: Part 1.Problems," JPT (Aug. 1987) 955-60; Trans., AIME 283.

Nagele E. (1985): The zeta-potential of cement (in cement and concrete Research 15 (3). 453-462. http

Nelson E. B, Baret J. F, Michaux M (1990): "Cement Additives and Mechanism of Action in Well Cementing". Nelson Elsevier Science Publishers Amsterdam 3-37.

Nelson E.B. and Guillot D. (2006): "Well Cementing" 2nd edition.

Plank J., Brandl Y and Zhai (2006): Adsorption behavior and effectiveness of poly (N, N-dimethylacrylamide-co-Ca2-acrylamido-2-methylpropanesulfonate) as cement fluid loss additive in the presence of acetone-formaldehyde-sulfite dispersant (in English) Journal of Applied Polymer Science 102 (5): 4341-4347

Plank J and Hursch C. (2007): "Impact of zeta potential of early cement hydration phases on superplasticizer adsorption" (in English). Cement and Concrete Research 37 (4): 537-542

Rao S. P and Burkhalter J. (1985): Hydrolytically stable polymers for use in oil field cementing methods and compositions. US Patent No

Recalde Lummer N. and Plank J. (2012): "Combination of lignosulfonate and AMPSand-co-NNDMA water retention agent. An example of dual synergistic interaction between admixtures in cement" (in English). Cement and Concrete Research 42 (5): 728-735.

Roshan H, Asef M. R (2010): "Characteristics of Oil Well Cement Slurry Using CMC". Journal of Society of Petroleum Engineers Drilling and Completion SPE 25: 328-335

Sabins, Frd L., David L. Sutton. The Relationship of Thickening Time, Gel Strength and Compressive Strength of Oilwell Cement

Santra, A., Reddy B.R. and Antia M. (2007): "Designing Cement Slurries for Preventing Formation Fluid Influx after Placement" paper SPE 106006 presented at the 2007 SPE International Symposium on Oilfield Chemistry held in Houston, Texas, U.S.A., 28 February-2 March

Scrivener, K. L., Juilland P., and Monteiro P. J. M. (2015): "Advances in understanding hydration of Portland cement (in Cement and Concrete Research" 78: 38-56

Proceedings of the 49th NSChE Annual Conference
KADA 2019: pp 186-192

P1C-02: PYROLYSIS CHARACTERIZATION AND KINETICS OF YAGBATA BITUMEN USING A TGA

A.G. Olugbenga[1*], A. G. Audu[2], M. U. Garba[3] and P. B.O. Pagu[4]
[1,2,3]Department of Chemical Engineering, School of Infrastructure, Process Engineering and Technology, Federal University of Technology P.M.B 65, Minna Niger State, Nigeria.
Corresponding Autors: [1]giwaabel@yahoo.com,[2]grace.adeola@futminna.edu.ng, [3]umar.garba@futminna.edu.ng, [4]realobd@gmail.com

ABSTRACT
Pyrolysis kinetics of thermal decomposition of bitumen was investigated by thermogravimetric analysis (TGA). TGA experiments were conducted at multiple heating rates of 5, 10, 20°Cmin^{-1} up to 800°C to obtain the pyrolysis characteristics of bitumen. Weight loss curve from TGA shows that three different stages occurred during bitumen pyrolysis. Weight loss profile and the final amount of coke formed changes with the heating rate. Differential method has been used for determining the kinetic parameters and the best fit for the order of reaction was found based on the R^2 values. Kinetics results confirm the presence of three different stages in bitumen pyrolysis with varying kinetic parameters. The average activation energy for the first, second and third stages was 27, 78 and 84 kJ mol^{-1}, respectively.

Keywords: Nigeria, bitumen, thermogravimetric analysis, thermal cracking, pyrolysis, kinetics,

List of Acronym

R^2	*Regression squared*
TGA	Thermo gravimetric analysis
TG	Thermogravimetry
α	Degree of conversion
$m0$	weights *before* the reaction,
mf	weights after reaction at time t,
Ea	apparent activation energy (J mol−1).
A	pre-exponential factor (min−1);
R	is universal gas constant (J mol−1 K−1).
T	heating temperature (K).
B	heating rate (K/°C)
DTA	differential thermal analysis

INTRODUCTION
The Nigeria bitumen belts are large deposits of bitumen, located in southwestern state of Ondo, Lagos, Ogun, and Edo State. The bitumen deposit in Nigeria is in huge quantity and recorded as the largest deposit in Africa and second largest deposit in the world. The bitumen is hosted within the eastern Dohomey basin, of which has been of much geological interest as a result of the occurrences of bitumen, limestone, glass sands and phosphates (Nton, 2001). This bitumen remains untapped because of inadequate knowledge of the oil exploration and exploitation. With the rise of price of crude oil the need for the development of alternative and or additional sources of energy has become urgent. Bitumen has become an unconventional energy resource due to a huge source of solid fossil hydrocarbon compound in the form of bitumen on the surface of the earth. Consequently the need for a viable energy sources have become imperative.

Bitumen (tar or asphalt) is a natural polymer and the lowest grade of crude oil. Bitumens have much higher viscosities and heteroatom compositions than conventional light crude oils. For many years, it has been used for paving applications, construction and maintenance of roads. Due to increasing demands and performance, bitumen is now often blended with polymer.

Bitumen–polymer blends have a better resistance to cracking in low temperatures, as well as lower flow and deformation in higher temperatures, than that of bitumen alone (Masson *et al.*, 2003). After oil sand is mined, the bitumen has to be recovered from the oil sand in order to upgrade and transport to refiners. At present, several methods may be applied to recover bitumen from oil sand, such as water-based extraction, solvent extraction and pyrolysis (Park *et al.*, 2009). Among these methods, pyrolysis is widely used by many researchers for the characterization of the heavy oils using in situ combustion (Kok *et al.*, 1998; Meng *et al.*, 2006).

Pyrolysis is a process of thermal decomposition of coal, biomass and oil shale in the absence of oxygen to obtain an array of char, oil and gaseous products. Several thermal analysis techniques have been used to obtain the experimental data. The most common and suitable for fundamental kinetic characterization are thermogravimetry (TG). Due to the simplicity of the instrument and calculation methods, the authors have used these techniques to successfully estimate the kinetics of many processes such as pyrolysis of coal (coal), crude oil (Murugan et al., 2009) and bitumen. Many researchers have used the thermogravimetric analyser to study the thermal decomposition of Alberta oil sand (Park *et al.*, 2009), Indonesian bitumen and Canadian bitumen (Alshareef et al., 2010).

The thermal stability of bitumen is a significant property to be considered in selection of the best processing conditions, depending on the quality of the products, and to fit their performances to the proper final applications. Many applications of bitumen involve a high temperature that requires a fundamental knowledge about thermal kinetics. Hence, the pyrolysis kinetics of bitumen was studied in this work using thermogravimetric analysis (TGA) under an inert atmosphere at different heating rates. In addition, the effects of different reservoir sand on bitumen pyrolysis were also studied.

EXPERIMENTAL

The bitumen used in this work was recovered from Yagbata Ondo State sand reservoir. The experimental setup consisting of Perkin Elmer STA 6000 Thermogravimetric analyser. This instrument has a capability of simultaneously measuring TG and differential thermal analysis (DTA). This unit includes built-in mass flow controller that monitors and controls the purge flow rates. About 20mg of the sample was used for all the experiments. Initially the sample was kept at room temperature for 5 min and then heated up to 800 ^{o}C with multiple heating rates from 5 to 20^{o}C. The experiments were conducted under the nitrog flow rate of 45mLmin−1 throughout the furnace. The weight change with respect to the temperature was measured by TGASTA 6000 and saved to the PC through pyris module interface.

Kinetics theory

Non-isothermal kinetics of thermogravimetric analyses was usually performed by a differential method and integral method. In this work, differential method was used based on the empirical expression of Arrhenius. The different stages during the bitumen pyrolysis were determined based on the number of levels of the TG curve and on the number of peaks of the DTG curve. The rate of thermal devolatilisation of a solid can be expresses as follows (Benbouzid and Hafsi, 2008):

$$\frac{d\alpha}{dt} = Aexp\ (-\frac{E}{RT})(1-\alpha)^{\mathrm{n}} \quad (1)$$

The variable"α" is the degree of conversion of the stage *i*.

$$\alpha = \frac{\mathrm{m_o - mt}}{\mathrm{m_o - mf}} \quad (2)$$

where *m*0, *m*f and *m*t are the weights *before* the reaction, after the reaction and at time *t*, respectively. *E*ai is the apparent activation energy (J mol−1). *A*i is the pre-exponential factor (min−1); *R* is universal gas constant (J mol−1 K−1). *T* is the heating temperature (K). At a given heating rate β, we have:

$$\frac{d\alpha}{(1-\alpha)^{\mathrm{n}}} = \frac{\mathrm{A}}{\beta} exp(-\frac{E}{RT})\ \mathrm{dT} \quad (3)$$

The plot of ln[(dα/dT)/(1−αi)^{ni}] versus 1/*T* at different *n*i is a straight line from which the activation energy and the preexponential factor can be determined. The optimum value of *n*i gives the highest value of R^2.

RESULTS AND DISCUSSION

3.1. Pyrolysis characteristics of oil sand bitumen

Figure shows the TG/DTG of bitumen at 5 °C/min. Figure 2 (a) and (b) represent TG results showing weight loss and the rate of weight loss as a function of temperature, respectively, for raw bitumen, which were obtained by the release of volatiles during the non-isothermal pyrolysis at different heating rates of 5,10, and 20 °C/min. It is observed that the TG and DTG curves shifted to higher temperatures as the heating rate increased. This phenomenon, called as thermal lag, was caused by limited heat transfer to the sample, resulting in the temperature difference between the sample and the thermocouple (Anca-Couce *et al.*, 2014, Park et al., 2006). In Figure 2(a), it can be seen that bitumen lost approximately 93 % of original weight and yielded 7 wt% coke after the pyrolysis reaction was terminated. It is noticeable that the curves of weight loss rate for bitumen show one narrow peak and two shoulder peaks as shown in Figure 2(b). This probably indicates that multiple reactions were involved in the pyrolysis of bitumen, and it was assumed that the nonisothermal pyrolysis of bitumen consists of three reaction stages (light volatilization, main volatilization and continuous volatilization). In general, TGA can be used to investigate chemical reactions or physical transitions occurring with weight changes, and then the shape of TGA curve is considered characteristic and identification of chemical reactions. Prior to the first stage, a small weight loss appeared in TG/DTG curve near 100 °C, probably caused by evaporation of water (Bai et al., 2015). The first shoulder peak from ambient temperature to about 320 °C (at the heating rate of 1◦C/min) in the DTG curve corresponds to light volatilization reactions which entail the desorption of light hydrocarbon volatiles with a weight loss of 29 %. From the boiling point distribution in Figure 1, it can be observed that bitumen at boiling point lower than 400 °C contains about 28 % distillates. This indicates that a part of oil sand bitumen vaporized during the heating process of non-isothermal pyrolysis before main cracking reaction occurred. Therefore, it can be considered that volatile gases were generated by vaporization of light compounds in the first stage. Volatilization can be caused by the formation of light gases from primary pyrolysis, cross-linking reactions, and coke formation reactions (Caprariis et al.,

2012). The second shoulder peak which arrower temperature of the range 370 °C to 470 °C in the DTG curve corresponds to evolution of volatiles is probably due to thermal cracking with a weight loss of 34 %. The continuous evolution of volatiles at high temperature (470 °C -600 °C) is probably due to thermal cracking of organic matter.

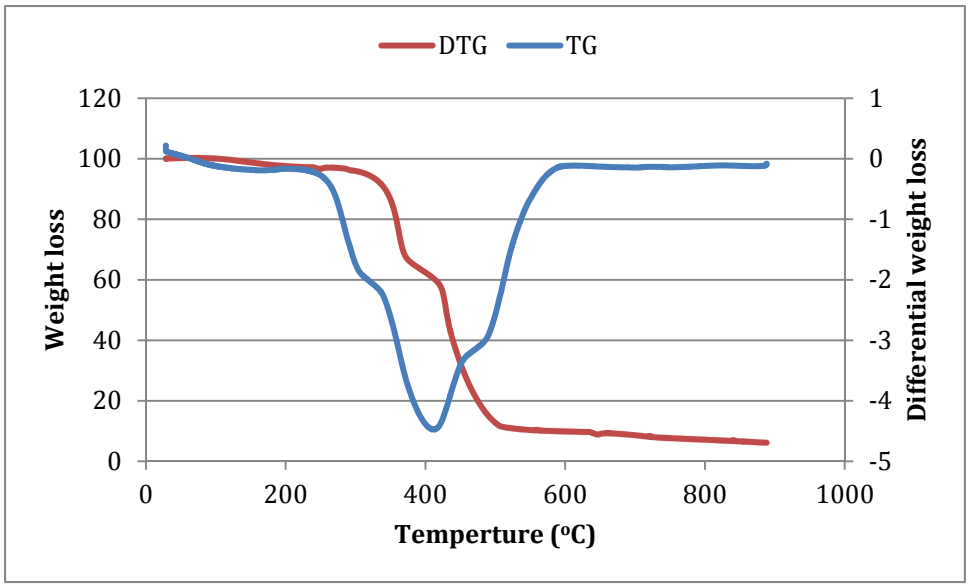

Figure 1. TGA analysis of Yagbata bitumen

3.2 Effect of heating rates

The TG and DTG curves for bitumen at different heating rates (5, 10 and 20 °C min−1) indicate the presence of three stages (Figures 2a and b). As the heating rate increased from 5 to 20 °C min⁻1, the curves are displaced to higher temperatures. At the final temperature of 800 °C, the amount of residue produced after pyrolysis increased as heating rate increased such as 6 %, 11.7 % and 14.6 % for 5, 10 and 20 °C min−1, respectively. The difference in the amount of residue produced indicates the influence of heating rate in bitumen pyrolysis. At lower heating rates, the heating of the bitumen occurred more slowly, leading to a more effective heat transfer to the inner portions and throughout the sample (Mani *et al.*, 2010). As a result of the improved heat transfer, more efficient cracking took place, causing more weight loss in the form of volatiles. Therefore, as the heating rate increased, the residue at the end of the pyrolysis reactions also increased. Based on these results, it is noted that at lower heating rate (5 °C min−1) of bitumen pyrolysis, thermal cracking occurred efficiently resulting in a lesser amount of residue compared to other heating rates. The DTG curves for different heating rates of bitumen pyrolysis also exhibit the difference in curves, more specifically at the peak points such as 435, 445 and 465 °C for 5, 10 and 20 °C min−1, respectively. The details of three stage bitumen pyrolysis characteristics are given in Table 1. The occurrence of three stages in this study is different from two different stages in the pyrolysis curve has been determined by Benbouzid and Hafsi (2008) for the pyrolysis of pure and oxidized bitumens.

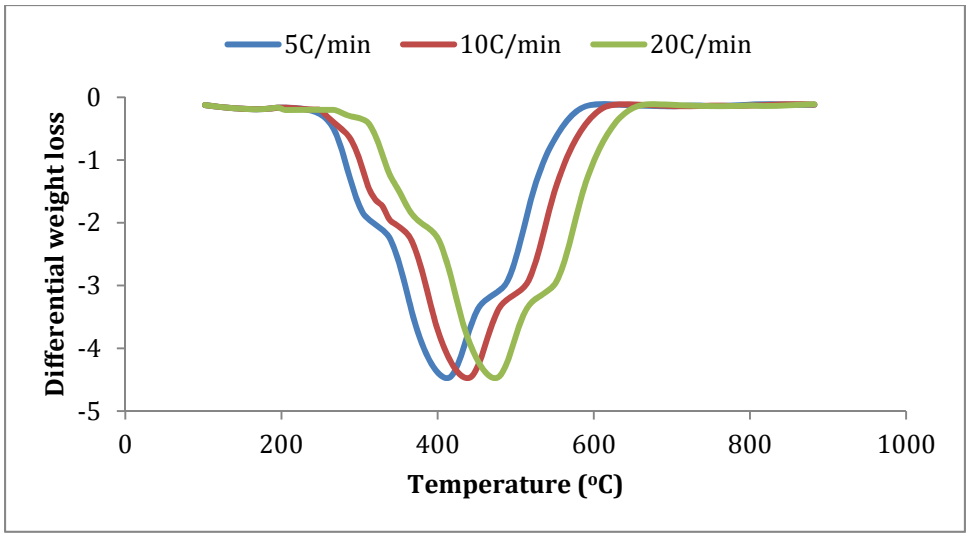

Figure 2a. DTG analysis of Yagbata bitumen at different heating rates.

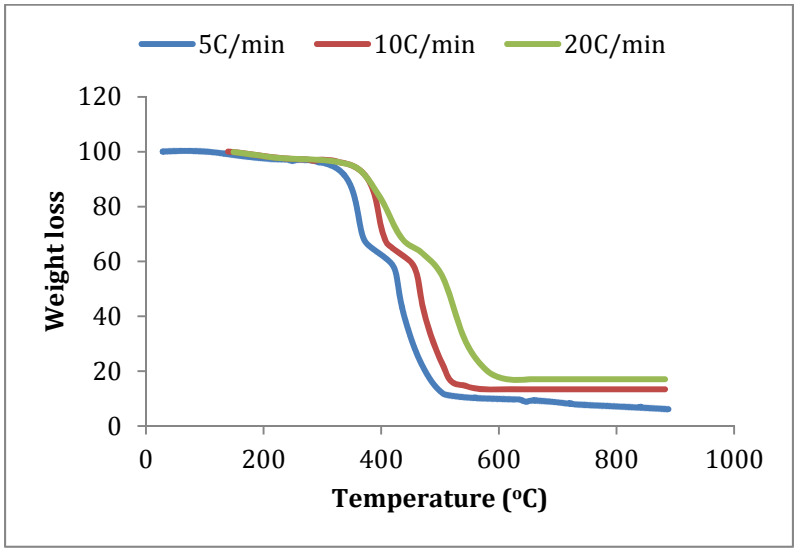

Figure 2b. TG analysis of Yagbata bitumen at different heating rates.

Table 1. Analysis of the thermogravimetric results of the bitumen

	β ((◦Cmin−1))		
Pyrolysis characteristics	5	10	20
Number of stages	3		
Temperature interval (◦C)			
Stage 1	150-340	150-352	150-363
Stage 2	340-456	352-471	363-489
Stage 3	456-589	471-601	489-609
Maximum temperature (◦C)	451	459	468
Final temperature (◦C)	932	938	946

3.3 Kinetic analyses

Kinetic analyses were performed individually for the three heating rates using TG data. The order of the reaction that provides minimum residuals between experimental and predicted data was chosen as the optimum value of *n*. The corresponding activation energy and frequency factor were determined based on the optimum order of reaction. The results of kinetic study for the first stage are different from the second and third stages (Table 2). The activation energy increased (i.e. 27, 31 and 33 kJ mol−1 for 5, 10 and 20 °C min−1, respectively) as the heating rate increased in the first stage of pyrolysis, indicating the minimum activation energy at 5°C min−1. The reason for lowest activation energy at low heating rate could be explained by several factors including total weight loss being lowest at this heating rate, or longer residence times at a given temperature, which will influence the conversion positively.

In the first stage of bitumen pyrolysis, increase in activation energy with respect to heating rate also reveals that for the initial weight loss, more heat is required, which is in contrast to the second stage of pyrolysis. During the second stage, the activation energy decreased (i.e. 78.3, 42.4 and 30.6 kJ mol−1 for 5, 10 and 20 ^{0}C min−1, respectively) with increase in the heating rate that indicates the requirement of less energy at the end of the pyrolysis process. Due to high heating rate, the molecules heated up quickly that makes the diffusion fast, and therefore leading to lower energy demand for the final conversion.

During the first stage of bitumen pyrolysis average of 25 % of the weight loss occurred with low activation energy and high reaction order; while in the second stage, average of 75 % of the weight loss was observed with higher activation energy and lower reaction order compared to the first stage. The significant difference observed between the two stages indicates that the volatiles present in bitumen might be of two different categories with varying degrees of volatilization.

Table 2. Kinetic parameters of the bitumen pyrolysis at different heating rates

	β ((°Cmin−1))		
Pyrolysis characteristics	5	10	20
Number of stages	3	3	3
Stage 1			
N			
Ea (kJ mol^{-1})	27	31	33
A (min−1)	7.5	24	105
R^2	0.976	0.976	0.967
*C*1 (%)			
Stage 2			
N			
Ea (kJ mol−1)	78.3	42.4	30.6
A (min−1)	1.2×10^5	673	37
R^2	0.982	0.977	0.969
*C*1 (%)			
Stage 2			
N			
Ea (kJ mol−1)	84.1	51.8	34.3
A (min−1)	1.3×10^5	703	41
R^2	0.9977	0.987	0.976
*C*1 (%)			

CONCLUSIONS

A two-stage first-order model is inferred to define the pyrolysis of asphalt. In this, the activation energy, E, is different for each stage, but is independent of the type of bitumen and the rate of heating. The frequency factor depends on the heating rate and is independent of the bituemen. The final yield of volatiles depends on the type of bitumen. The pyrolysis of bitumen exhibits three stages during devolatilisation process. The kinetic results were varied considerably between the stages and also for the different heating rates. Average activation energy for the first stage was lower than the second stage. About 25 % of the weight loss occurred in the first stage and the remaining 75% weight loss occurred during the second and third stages of bitumen pyrolysis.

REFERENCES

Murugan, P., N. Mahinpey, T. Mani and N. Freitag, "Pyrolysis and Combustion Kinetics of Fosterton Oil Using Thermogravimetric Analysis," Fuel **88**, 1708–1713 (2009a).

Masson, J.-F., P. Collins, G. Robertson, J. R. Woods and J. Margeson, "Thermodynamics, Phase Diagrams, and Stability of Bitumen-Polymer Blends," Energy Fuels **17**, 714–724 (2003).

Nton ME (2001) Sedimentological and geochemical studies of rock units in the eastern Dahomey basin, south western Nigeria, unpublished Ph.D thesis, University of Ibadan, pp 315

Park, Y. C., J.-Y. Paek, D.-H. Bae and D. Shun, "Study of Pyrolysis Kinetics of Alberta Oil Sand by Thermogravimetric Analysis," Korean J. Chem. Eng. **26**(6), 1608–1612 (2009).

Meng, X., C. Xu and J. Gao, "Secondary Cracking of c4 Hydrocarbons From Heavy Oil Catalytic Pyrolysis," Can. J. Chem. Eng. **84**(3), 322–327 (2006).

Kok, M. V., O. Karacan and R. Pamir, "Kinetic Analysis of Oxidation Behaviour of Crude Oil SARA Constituents," Energy Fuels **12**, 580–588 (1998).

Benbouzid, M. and S. Hafsi, "Thermal and Kinetic Analyses of Pure and Oxidised Bitumens," Fuel **87**, 1585–1590 (2008).

Anca-Couce, A., Berger, A., Zobel, N. (2014) How to determine consistent biomasspyrolysis kinetics in a parallel reaction scheme, Fuel 123, 230–240.

Park, H.Y. Kim, T.H. (2006) Non-isothermal pyrolysis of vacuum residue (VR) in a thermogravimetric analyzer, Energy Convers. Manag. 47, 2118–2127.

Bai, F., Guo, W., Lü X., Liu, Y., Guo M., Li Q., Sun Y., (2015) Kinetic study on the pyrolysisbehavior of Huadian oil shale via non-isothermal thermogravimetric data,Fuel 46, 111–118.

Cai J., Wu W., Liu R. (2014) An overview of distributed activation energy model and its application in the pyrolysis of lignocellulosic biomass, Renew. Sustain.Energy Rev. 36,236–246.

Caprariis B. de, De Filippis P., Herce C., N. Verdone (2012) Double-Gaussian distributed activation energy model for coal devolatilization, Energy Fuels 26, 6153–6159.

Proceedings of the 49th NSChE Annual Conference
KADA 2019: pp 193-201

P1C-03: SYNTHESIS OF HIERARCHICAL Zn-ZSM-5 USING ɣ-Al_2O_3 FROM KANKARA KAOLIN

T. J. Mamman[1], B. Mukhtar[1], A. Y. Atta[1]*, A.S. Kovo[2], B. O. Aderemi[1] and B. Y. Jibril[1]
[1]Chemical Engineering Department, Ahmadu Bello University Zaria, Nigeria2
[2]Chemical Engineering Department, Federal University Technology, Minna, Nigeria
*Corresponding author: zeezoatta@gmail.com

ABSTRACT
Hierarchical ZSM-5 zeolite was successfully synthesized via hydrothermal synthesis using ***ɣ-Al_2O_3*** *from Kankara kaolin. Crystallization was carried out in an oven at 95^{0}C for 7days using the kinetic-control method. After ion exchange using 1M solution of NH_4Cl for 7 hours, extra framework incorporation of zinc was done in $ZnNO_3$ solution using wet incipient impregnation method. The samples were characterized using Fourier-transform infrared spectroscopy (FTIR), X-Ray fluorescence (XRF), X-ray diffraction (XRD), and Brunauer, Emmett and Teller (BET). Synthesized hierarchical HZSM-5 with 1 wt. % zinc loading was the best among the prepared catalyst samples based on the specific surface area (381.49 m^2/s), mesoporosity (55.8625 %) and hierarchy factor (0.197)*

1.0 Introduction
Zeolites are crystalline aluminosilicate materials in which the silicon and aluminum are arranged in tetrahedral coordination and are linked by oxygen atoms (Nada and Larssen 2017). The zeolite structure contains micropores of molecular dimensions. The uniform molecular sized pores and channel provide shape and size selectivity, advantages exploited in catalysis, adsorbents development and emerging fields such as CO_2 capture (Siriwardane *et. al.,* 2005; Davis 2002)
ZSM-5, a pentasil-type zeolite, with high surface area, high thermal stability and intrinsic acidity serves as choice catalyst in several processes. The structure of ZSM-5 is three dimensional with two kinds of intersecting channels, straight channels and zigzag channels, that are formed by 10-ring pores with pore diameters of 0.55 nm (Petushkov *et. al*., 2011). An inherent disadvantage of the comparable size of the micropores and hydro- carbon reactants with respect to zeolite crystal dimensions is slow mass transport. This can suppress the reaction rate. Moreover, coke formed by side-reactions can rapidly block the pores near the external surface, prematurely deactivating the zeolite catalyst (Meng *et. al*., 2018).

The amorphous framework nature, poor acidity and unstable structure of ordered mesoporous materials (OMM) lead to unsatisfied activity in acid catalyzed reactions even though OMM solved the problem of diffusion limitations associated with microporous zeolites (Li *et al*., 2007); thus, it is apparently difficult to improve the catalysis performance simply through the production of analogous materials to settle the diffusion issues. On the other hand, nanosized zeolites with short intracrystalline path length have been developed to solve the diffusion problem, but recycling these nanocatalysts after heterogeneous catalysis, (Tosheva and Valtchev, 2005) difficulty in crystallization during synthesis and their hydrothermal stability have been a challenge (Tao *et. al.,* 2006). Therefore, development of hierarchical zeolites with an extra pore system in addition to the micropores in zeolite crystals has become a major research area in view of the fact that hierarchical zeolites have the potential to overcome the aforementioned challenges (*Holms et,al*, 2011; Feliczak-Guzik *et. al 2018*).

Hierarchical zeolites have the advantages of traditional zeolites while enjoying the merits of introduced mesopores, and this has greatly expanded their applications in catalysis, benefiting

from the increased external surface area, abundant surface acid sites, decreased diffusion path length, and good hydrothermal stability (Fang *et. al.,* 2006, *Egeblad*. *et. al.* 2007, Fan *et. al*., 2008). Past works on performance of hierarchical zeolites have shown that they are more robust with regards to deposition of coke (*Ni et. al., 2011;* Al-Yassir *et. al.;* 2012, Ogunrombi *et. al*., 2015*)*.

Generally, there are two main methods of synthesis of hierarchical zeolites: 'bottom-up', which include - hard templating, soft templating and non-templating and "top-down", such as demetallation, recrystallization, delamination and pillaring (*Zhang* 2013). The post synthesis (top-bottom) approach is a facile method to obtain hierarchical zeolites, i.e. dealumination and desilication; however, the mesopores created by dealumination are commonly of intercrystalline, and desilication always leads to the decrease of the crystallinity and the hydrothermal stability (*Pérez-Ramírez et al., 2008). By* removing the framework atoms, it adversely affects structure stability and surface acidity. The templating approaches induce the formation of mesopores avoiding the damage of framework properties to a large extent (Chen *et. al*., 2011, *Möller et. al., 2011*). Hard templates such as activated carbon, carbon fibers, aerogels, and polymer aerogel and soft templates such as cationic polymers, amphiphilic organosilane surfactants, and silylated polymers have been used as mesoporogens in the production of hierarchical zeolites (Fan et. al., 2008, Yang *et. al*,, 2004).

It is important that the mesoporogen has hydrophobic groups to expand space to provide conditions for the formation of mesopores, and also should have a steady connection method with zeolite precursor during the process of crystallization (*Choi et, al., 2006)*. CTAB as a soft-template in this work possesses a ternary ammonium in the center which is connected with three hydrophobic short alkyl chains, and three silicon atoms that are distributed terminally at each alkyl chain, and each silicon atom is connected with three methoxy- groups ($–OCH_3$). It was proposed that the formation of these hierarchical zeolites takes place by means of a liquid-crystal 'templating' mechanism, in which the silicate material forms inorganic walls between ordered surfactant micelles. CTAB formed micelles in the solution and the micelles further formed a two dimensional hexagonal mesostructure. The silicon precursor begins to hydrolyze between the micelles and finally fills the gap with silicon dioxide. The template could be further removed by calcination and leaves a pore structure behind. The pores mimic exactly the structure of mesoscale soft template and lead to highly ordered mesoporous silica materials (Chen *et. al.,* 2003). The introduction of mesoporosity in zeolites is frequently accompanied with a lowered micropore volume. The interplay between the catalytic function located in the micropores (active sites) and the accessibility function provided by the mesopores should be finely balanced. This trend sparked the development of the generic tool termed the hierarchy factor (HF) (Pe´rez-Ramı´rez *et. al.,* 2009; Ahmadpour and Taghizadeh,, 2015).The HF is expressed as the relative mesopore surface area (S_{meso}/S_{total}) multiplied by a relative microporosity (V_{micro}/V_{total}), and can be used to classify the porous characteristics of any material (Verboekend and Pe´rez-Ramı´rez, 2011)

Zeolites are synthesized under highly alkaline hydrothermal conditions, from mixed solutions of silica and alumina containing different cationic or other organic structure-directing species. Under such conditions, a variety of silicate and/or other anions have been observed to be present in solution and have been studied with respect to their roles in zeolite crystallization. Quantitative analysis of the different silicon species in the Si NMR data indicates that the intermediate amorphous aluminosilica formed during aging has a significantly lower Si/Al ratio (i.e., higher Al

content) than the final zeolite product and that Si/Al ratios increase continuously during crystallization (Ogura *et. al.,* (2003). This finding suggests that zeolite crystallization may not occur solely by conversion of amorphous aluminosilica gel intermediates, but may involve the incorporation of siliceous solution-phase species and other solution-phase species from the reaction mixture along with depletion of Al species from the gel back into solution. This implies that for successful synthesis of zeolites the nature and reactivity of the ammonia used is principal. The different phases of alumina are Alpha (α), Beta (β) and gamma (γ). γ-Al_2O_3 is composed of minute colorless cubic crystals with sp. gr. about 3.6 that are transformed to the alpha form at high temperatures. γ-Al_2O_3 is the most important among the different alumina available because of its applications compared to other phases. it is used in catalyst formulation, due to its high surface area, thermal stability, outstanding mechanical properties and nature of interaction with zeolite active phases (Paranjpe 2017, Wang *et al.*,2006). In this work, γ-Al_2O_3 (which was used in previous research as active matrix) produced from Kankara kaolin in Nigeria was used in synthesizing hierarchical Zn-ZSM-5 zeolite.

Herein, we report the use of synthesized alumina from Kankara clay and CTAB as mesoporogen to successfully synthesize hierarchical ZSM-5 catalyst. Previous works used laboratory grade alumina but with the abundant kaolin in Nigeria, it becomes important to harness it for the production of the alumina.. In addition, it has been shown that the presence of extra- framework metals (eg Zn, Pt, Ga) in HZSM-5 can enhance the dehydrogenation ability of the catalyst (Ogunrombi *et. al.,* 2015). However, the deactivation and hydrogenolysis of Pt/HZSM-5 and high cost of gallium encourages the use of Zn/HZ5M-5 as the system of interest (Choudhary *et. al.,* 2000).

2. Experimental

2.1 Catalyst Synthesis

H-ZSM-5 was synthesized using the hydrothermal procedure; from a gel (pH 10) consisting of, sodium hydroxide, aluminum oxide (synthesized from Kankara Kaolin from Katsina State, Nigeria), tetrapropyl ammonium bromide (TPABr), zinc nitrate, sulfuric acid, silica sol, CTAB, and deionized water in an oven at 95^0C. In a typical synthesis, 2 g of NaOH was dissolved in 25ml of de-ionized water, 0.15g of active alumina was added with additional 4g of NaOH, (mixture 'A'). TPABr was added to 50ml of water and 1.7ml of 96wt.% H_2SO_4 (mixture 'B'). 24 ml of silica sol was prepared (mixture 'C'). The mixtures A and B obtained were then simultaneously added to 'C' and stirred for 30 minutes. The resulting mixture was then aged for 2 days in an oven at 95^oC then CTAB added and the mixture was again put into the oven for 5 days, that is, the kinetic control crystallization method was adopted. The solid component at the bottom was washed with de-ionized water. Then, the sample was calcined at 550^oC for 5hrs to remove the template. The acid form HZSM- 5 for five samples with different zinc loading was obtained by ion-exchange with 1.0 M ammonium chloride using a ratio of 5 g sample: 250 ml ammonium chloride solution. This process was repeated twice to ensure maximum exchange. Then, the solid was filtered, washed, dried at 95^0C for 8 hrs and calcined at 550^0C for another 5 hrs. It was then converted to Zn-HZSM-5 using $ZnNO_3$ employing wet impregnation method. In a typical procedure, 0.55g of zinc nitrate was dissolved in 10ml of deionized water and the solution was poured into deionized water containing 7.5g of the zeolite sample.. The water of this mixture was vaporized using a magnetic stirrer at 60^0C with constant stirring. The catalyst was dried at 95^0C for 8 hrs and calcined at 550^0C for another 5 hrs.

2.2 Catalyst Characterization

Infrared spectra were recorded on a FT-IR spectrophotometer (Shimadzu model 8400 S) instrument with a MCT detector (64 scans, 4 cm−1). Approximately 20 mg of catalyst was weighed and put in an infrared cell with KBr windows for treatments and the spectra were recorded. The powder X-ray diffraction (XRD) patterns were obtained on a Rigaku MiniFlex II X-ray diffractometer using Cu *K*α radiation. The anode was operated at 40 kV and 40 mA. The catalysts were scanned in continuous mode at wavelength Kalpha1=1.540562, Kalpha2=1.544390 and Kbeta=1.3922182θ from 3°-70° at scanning speed of 12°/min°.

The textural properties (surface area, pore size and pore volume), of the products were determined using BET method by N_2 adsorption at -196°C using 3Flex 3.02 Micrometrics equipment. JEM-2100 Plus was used for the transmission electron microcopy of the samples.

3.0 Results and Discussion

3.1 Characterization of the ɣ-Al_2O_3

The XRD pattern of the prepared ɣ-Al_2O_3 (Figure 1) showed broad peaks at d-spacing of 1.43Å, 1.99Å and 2.43Å which largely matched with the commercial and standard XRD pattern of ɣ-Al_2O_3 (Samain *et. al.,* 2014). The diffractogram with broad peaks indicates that the alumina used is amorphous and therefore reactive in the synthesis of zeolite.

The chemical composition of the ɣ-Al_2O_3 obtained from the XRF analysis showed that the Al_2O_3 content was 85.02% with 4.76% SO_3 and 5.16% loss on ignition. This suggested that there were SO_3 and water still left in the structure.

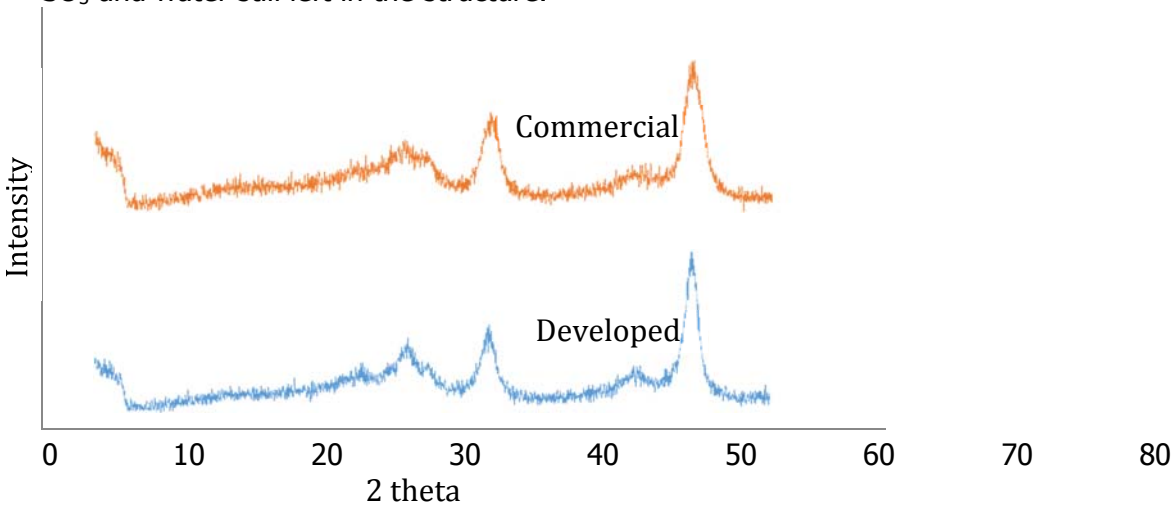

Figure 1: X-ray Diffraction Pattern of ɣ-Al_2O_3

3.2. Elemental Composition of the Synthesized Hierarchical ZSM-5

The elemental composition of the synthesized hierarchical ZSM-5 is shown in Table 1. The silica to alumina ratio of all the samples is approximately 20. This value is significant because the activity of an aluminosilicate zeolite is mainly dependent on its acidity and the acidity depends on the alumina content of the zeolite framework (Asaftei, *et. al,.* 2015). For ZSM-5, the brönsted acid sites directly correspond to the number of tetrahedrally coordinated Al atoms in the MFI framework. The stability of the zeolite is also a function of the silica to alumina ratio, a high ratio

implies high stability However, there is a trade-off between activity of zeolite and its stability. So, a ratio of 20 is considered a fair balance between activity and stability.

Table 1: XRF Elemental Composition of the Synthesized Hierarchical ZSM-5

Elements	Zn loading	% Silica	% Alumina	SiO_2/Al_2O_3
HZSM-5 (sample G)	0	94.50	3.25	50
Sample Z(0)	0	90.84	7.75	20
Sample Z(0.5)	0.5	88.00	7.40	20
Sample Z(1)	1	85.66	7.20	20
Sample Z(2)	2	88.60	7.25	20
Sample Z(3)	3	86.60	7.31	20

Figure 2a shows the FTIR patterns for all the samples. The bands at 1100cm^{-1} and 450cm^{-1} are typical of highly siliceous materials and have been assigned to the asymmetric stretching and bending modes of the SiO_4/AlO_4, tetrahedra respectively. The band at 550 cm^{-1} is caused by the double five-membered rings of tetrahedra in the framework, containing two parallel faces of nearly planar five-membered rings. The most prominent band covering the range of about 3000 - 3700 cm^{-1} in the functional group region is due to the vibrations of O-H bond, a functional group of ZSM-5. The absorption bands from all Five (5) samples indicate the successful synthesis of ZSM-5.

The XRD pattern of the conventional ZSM-5 and synthesized ZSM-5 with varying extra-framework incorporated zinc loading is shown in Figure 2b. The peaks of the synthesized ZSM-5 are in agreement with those of the conventional ZSM-5 i.e. they occur at about the same 2 theta position which confirmed the production of ZSM-5. There are no visible peaks identified as zinc or zinc oxide peaks because the zinc loading is below 4 wt% (Van Der Borght *et. al.,* 2015). CTAB that promotes mesoporosity, undesirably also induces amorphosity, which leads to synthesized ZSM-5 having lowered peaks than the conventional ZSM-5. In Figure 2c, it is shown that crystallinity increased from loading of 0.5 wt% to the zenith (82.1%) at 2 wt% zinc loading, then it decreased to 55.7% at 3 wt%, indicating that 2 wt% loading gave the maximum crystallinity.

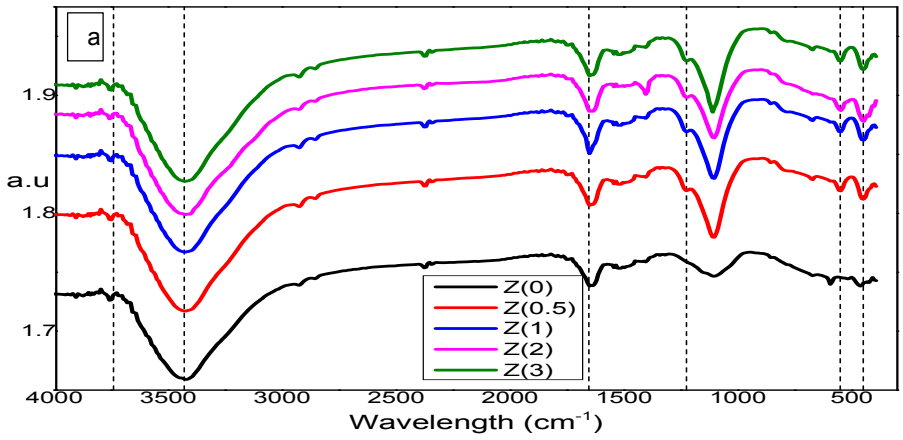

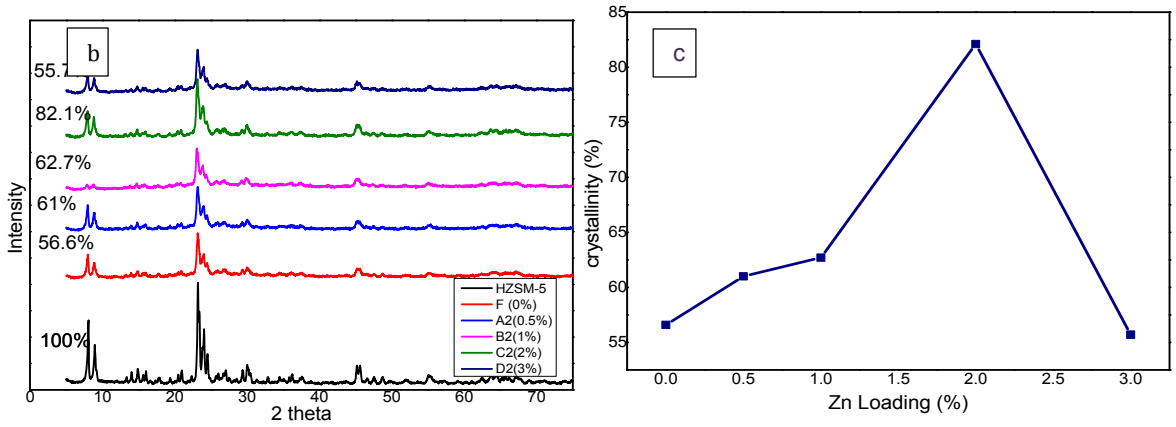

Figure 2: (a) FTIR patterns, (b) XRD patterns and (c) percentage crystallinity of synthesized zinc (0.5-3% loading) extra-framework incorporated Hi-ZSM-5.

The BET surface area of the hierarchical Zn-HZSM-5 samples in Table 2 shows that sample Z(1) has the highest specific surface area and mesoporosity of 381.49 m²/g and 55.86% respectively. Though HZSM-5 has a high mesoporosity (51.52%) above the expected for microporous HZSM-5, it is noteworthy that this its mesoporosity is below the average of the synthesized hierarchical zeolite (56%). HZSM-5 also showed pore size of 3.3nm, which is lower than the average pore size of the synthesized hierarchical zeolites with an average of about 4.3nm. The foregoing observations implied that the HZSM-5 used in this research is indeed hierarchical and commercial companies are fast moving from microporous to hierarchical owing to the overwhelming advantages of hierarchical over microporous. The mesoporosity and pore size of the synthesized zeolites indicate that varying the zinc loading does not significantly affect its hierarchical properties.

The hierarchy factor has a proportional relationship with activity and performance of a catalyst which means that sample Z(1) with the highest hierarchy factor is the best among the prepared catalyst samples. This also shows that the micropore framework was not severely tempered with and hence crystallinity of sample Z(1) was not compromised.

Table 2. Morphological properties of the synthesized hierarchical ZSM-5

. Sample (%Zn loading)	HZSM-5	Z(0)	Z (0.5)	Z (1)	Z(2)	Z (3)
BET (m²/g)	415.51	377.58	369.54	381.49	372.79	369.71
Mesopore area (m²/g)	214.05	217.07	205.51	213.11	205.04	203.25
Percentage mesoporosity	51.52	57.49	55.62	55.86	55.54	54.98
Pore size (nm)	3.30	4.17	4.5608	4.30	4.52	4.57
Hierarchy Factor	0.186	0.15	0.14	0.20	0.14	0.14

The pore size distribution shown in Figure 3a confirmed the hierarchical nature of the zeolite samples with a spread of pore size from 0.1 to about 10nm . The isotherms in Figure 3b showed that a major uptake of nitrogen occurred at low relative pressure less than 0.02 and hysteresis loops at relative pressure of 0.45–0.95, and this signifies the presence of both micropores and mesopores. The nature of hysteresis loop indicates that they are highly mesoporous and of the type IV i.e. sample have slit pores of uniform size formed from the aggregation or agglomeration of the particles. ZSM-5 are of the slit pore shape category.

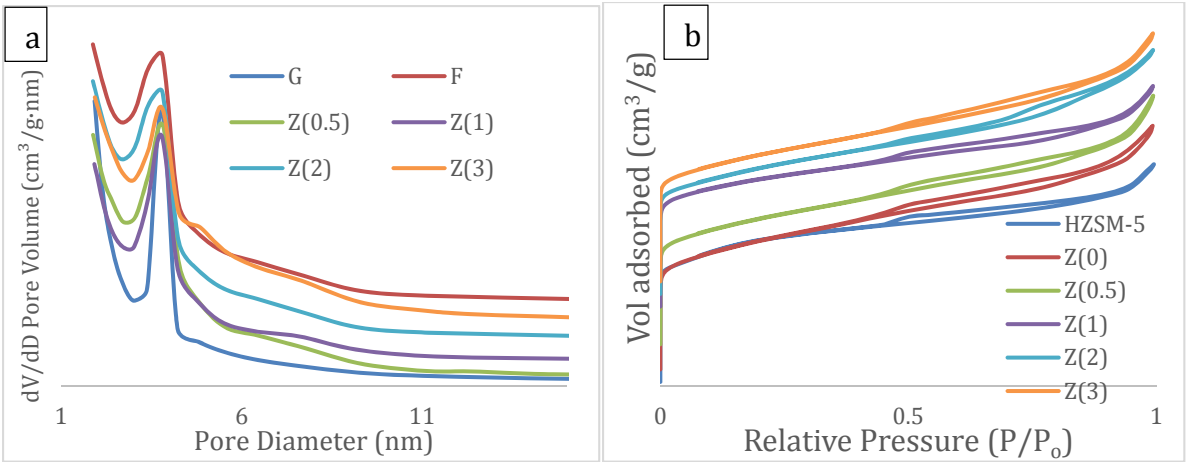

Figure 3: (a) Pore size distribution of the synthesized hierarchical ZSM-5 (b) Isotherms of the synthesized hierarchical ZSM-5

4.0 Conclusions

Hierarchical Zn-ZSM-5 catalyst samples with different zinc loading were successfully synthesized via hydrothermal method using ɣ-Al_2O_3 from Kankara kaolin. Based on the characterization results obtained using FTIR, XRD, BET and TEM, the hierarchical HZSM-5 with 2 wt.% zinc loading had the highest crystallinity (82.1%) while the hierarchical HZSM-5 with 1 wt. % zinc loading showed the best specific surface area (381.49 m^2/g), mesoporosity (55.86%) and hierarchical factor (0.20). The catalyst sample with the 1 wt. % zinc loading has the potential for highest catalytic activity.

References

Ahmadpour, J., and Taghizadeh, M. (2015). One-pot synthesis of hierarchically mesoporous ZSM-5 using different combinations of mesogenous templates, *3174*(12). https://doi.org/10.1080/15533174.2015.1004433

Al-Yassir, N., Akhtar, M. N. N., Ogunronbi, K., and Al-Khattaf, S. (2012). Synthesis of stable H-galloaluminosilicate MFI with hierarchical pore architecture by surfactant-mediated base hydrolysis, and their application in propane aromatization. Journal of Molecular Catalysis A: Chemical, 360, 1–15. https://doi.org/10.1016/j.molcata.2012.04.005

Asaftei, I. V., Earar, K., Birsa, L. M., Sandu, I. G., and Lungu, N. C. (2015). Conversion of Light Hydrocarbons with Butanes and Butenes from Petroleum Refining Processes Over Zn-HZSM-5 and ZnO / HZSM-5 Catalysts, 963–971.

Chen, L. H., Li, X. Y., Tian, G., Li, Y., Rooke, J. C., Zhu, G. S., ... and Su, B. L. (2011). Highly Stable and Reusable Multimodal Zeolite TS-1 Based Catalysts with Hierarchically Interconnected Three-Level Micro–Meso–Macroporous Structure. *Angewandte Chemie International Edition*, *50*(47), 11156-11161.

Cheng, W., Dong, S., and Wang, E. (2003). Synthesis and self-assembly of cetyltrimethylammonium bromide-capped gold nanoparticles. *Langmuir*, *19*(22), 9434-9439.

Choi, M., Cho, H. S., Srivastava, R., Venkatesan, C., Choi, D. H., and Ryoo, R. (2006). Amphiphilic organosilane-directed synthesis of crystalline zeolite with tunable mesoporosity. *Nature materials*, *5*(9), 718.

Choudhary, V. R., Mantri, K., and Sivadinarayana, C. (2000). Influence of zeolite factors affecting zeolitic acidity on the propane aromatization activity and selectivity of Ga/H–ZSM-5. *Microporous and mesoporous materials*, *37*(1-2), 1-8.

Davis, M. E. (2002). Ordered porous materials for emerging applications. *Nature*, *417*(6891), 813.

Egeblad, K., Christensen, C. H., Kustova, M., and Christensen, C. H. (2007). Templating mesoporous zeolites. *Chemistry of Materials*, *20*(3), 946-960.

Fan, W., Snyder, M. A., Kumar, S., Lee, P. S., Yoo, W. C., McCormick, A. V., and Tsapatsis, M. (2008). Hierarchical nanofabrication of microporous crystals with ordered mesoporosity. *Nature materials*, *7*(12), 984.

Fang, Y., and Hu, H. (2006). An ordered mesoporous aluminosilicate with completely crystalline zeolite wall structure. *Journal of the American Chemical Society*, *128*(33), 10636-10637.

Feliczak-Guzik, A. (2018). Hierarchical zeolites: synthesis and catalytic properties. *Microporous and Mesoporous Materials*, *259*, 33-45.

Holm, M. S., Taarning, E., Egeblad, K., and Christensen, C. H. (2011). Catalysis with hierarchical zeolites. *Catalysis Today*, *168*(1), 3-16.

Van Der Borght, K., Galvita, V. V., and Marin, G. B. (2015). Ethanol to higher hydrocarbons over Ni, Ga, Fe-modified ZSM-5: Effect of metal content. *Applied Catalysis A: General*, *504*, 621–630. https://doi.org/10.1016/j.apcata.2015.06.03

Li, C., Zhang, H., Jiang, D., and Yang, Q. (2007). Chiral catalysis in nanopores of mesoporous materials. *Chemical Communications*, (6), 547-558.

Meng, L., Zhu, X., Wannapakdee, W., Pestman, R., Goesten, M. G., Gao, L., … Hensen, E. J. M. (2018). A dual-templating synthesis strategy to hierarchical ZSM-5 zeolites as efficient catalysts for the methanol-to-hydrocarbons reaction. *Journal of Catalysis*, *361*, 135–142. https://doi.org/10.1016/j.jcat.2018.02.032

Möller, K., Yilmaz, B., Jacubinas, R. M., Müller, U., and Bein, T. (2011). One-step synthesis of hierarchical zeolite beta via network formation of uniform nanocrystals. *Journal of the American Chemical Society*, *133*(14), 5284-5295.

Nada, M. H., and Larsen, S. C. (2017). Microporous and Mesoporous Materials Insight into seed-assisted template free synthesis of ZSM-5 zeolites. *Microporous and Mesoporous Materials*, *239*, 444–452. https://doi.org/10.1016/j.micromeso.2016.10.040

Ni, Y., Sun, A., Wu, X., Hai, G., Hu, J., Li, T., and Li, G. (2011). Preparation of hierarchical mesoporous Zn/HZSM-5 catalyst and its application in MTG reaction. *Journal of Natural Gas Chemistry*, *20*(3), 237-242.

Ogunronbi, K. E., Al-Yassir, N., and Al-Khattaf, S. (2015). New insights into hierarchical metal-containing zeolites; synthesis and kinetic modelling of mesoporous gallium-containing ZSM-5 for propane aromatization. *Journal of Molecular Catalysis A: Chemical*, *406*, 1–18. https://doi.org/10.1016/j.molcata.2015.05.005

Ogura, M., Kawazu, Y., Takahashi, H., and Okubo, T. (2003). Aluminosilicate species in the hydrogel phase formed during the aging process for the crystallization of FAU zeolite. *Chemistry of materials*, *15*(13), 2661-2667.

Paranjpe, K. Y. (2017). Alpha, Beta and Gamma Alumina as a catalyst -A Review. *The Pharma Innovation Journal*, *6*(11), 236–238.

Pe´rez-Ramı´rez, J., Verboekend, D., Bonilla, A., and Abello, S. (2009). Zeolite Catalysts with Tunable Hierarchy Factor by Pore-Growth Moderators, 3972–3979. https://doi.org/10.1002/adfm.200901394

Pérez-Ramírez, J., Christensen, C. H., Egeblad, K., Christensen, C. H., and Groen, J. C. (2008). Hierarchical zeolites: enhanced utilisation of microporous crystals in catalysis by advances in materials design. *Chemical Society Reviews*, *37*(11), 2530-2542.

Petushkov, A., Yoon, S., and Larsen, S. C. (2011). Synthesis of hierarchical nanocrystalline ZSM-5 with controlled particle size and mesoporosity. *Microporous and mesoporous materials*, *137*(1-3), 92-100W.

Samain, L., Jaworski, A., Edén, M., Ladd, D. M., Seo, D. K., Garcia-Garcia, F. J., and Häussermann, U. (2014). Structural analysis of highly porous γ- Al_2O_3. *Journal of solid state chemistry*, *217*, 1-8.

Siriwardane, R. V., Shen, M. S., Fisher, E. P., and Losch, J. (2005). Adsorption of CO2 on zeolites at moderate temperatures. *Energy and Fuels*, *19*(3), 1153-1159.

Tao, Y., Kanoh, H., Abrams, L., and Kaneko, K. (2006). Mesopore-modified zeolites: preparation, characterization, and applications. *Chemical reviews*, *106*(3), 896-910.

Tosheva, L., and Valtchev, V. P. (2005). Nanozeolites: synthesis, crystallization mechanism, and applications. *Chemistry of materials*, *17*(10), 2494-2513.

Verboekend, D., and Pe´rez-Ramı´rez*, J. (2011). Design of hierarchical zeolite catalysts by desilication. *Catalysis Science and Technology*, *1*(6). https://doi.org/10.1039/c1cy00150

Wang, H., and Pinnavaia, T. J. (2006). MFI zeolite with small and uniform intracrystal mesopores. *Angewandte Chemie International Edition*, *45*(45), 7603-7606.

Wang, L. J., Wen, M. F., Li, Y. S., Yang, D., Chen, J., and Song, C. L. (2006). Preparation of high surface area, large pore volume alumina by using beta-cyclodextrin as a non-surfactant template. *Chinese Chemical Letters*, *17*(9), 1239.

Yang, Z. X., Xia, Y. D., and Mokaya, R. (2004). Zeolite ZSM-5 with unique supermicropores synthesized using mesoporous carbon as a template. *Advanced Materials*, *16*(8), 727-732.

Zhang, Z., Han, Y., Xiao, F. S., Qiu, S., Zhu, L., Wang, R., ... and Sun, H (2001). Mesoporous aluminosilicates with ordered hexagonal structure, strong acidity, and extraordinary hydrothermal stability at high temperatures. *Journal of the American Chemical Society*, *123*(21), 5014-5021.

Proceedings of the 49th NSChE Annual Conference
KADA 2019: pp 202-213

P1C-04: DISPERSION MODELLING OF AIR EMISSION FROM RICE-HUSK FIRED PARBOILING BOILER

Funso Alaba Akeredolu[1], Jacob Ademola Sonibare[1], Bamidele Sunday Fakinle[2*] and Lukuman Adekilekun Jimoda[3]

[1]Department of Chemical Engineering, Obafemi Awolowo University, Ile-Ife, Nigeria.
[2]Department of Chemical Engineering, Landmark University, Omu-Aran, Kwara State, Nigeria.
[3]Department of Chemical Engineering, Ladoke Akintola University of Technology, Ogbomoso
Corresponding authors: xdales@yahoo.com, fakinle.bamidele@lmu.edu.ng

ABSTRACT

*The study investigated the air quality impacts of a Rice Mill using the ISC-AERMOD View. Contributions of a steam boiler and three electric power generators in the mill to ground level concentrations of criteria air emissions were established.The maximum ground level concentrations of air pollutants presently emitted by the steam boiler are 1-hour averaging period concentrations of 1.4 – 177.3 µg/m^3 with 24-hour level of 0.3 – 43.5 µg/m^3. Simultaneous operations of the steam boiler and electric power generators give 1-hour averaging period concentrations of 29.7 – 257.8 µg/m^3 with 24-hour levels of 8.8 – 95.8 µg/m^3 . The simultaneous operations of the steam boiler and the electric power generators add about 0.41 – 84.78% of the respective investigated air pollutants limits to the ambient air quality of the host environment. Occasionally the daily NO_X limits from this **scenario 2** could breach the ambient limit whenever all the three electric power generators are simultaneously operated with the steam boiler.*

Keywords: rice mill, criteria pollutants, dispersion modelling, air quality, rice husk.

1.0 Introduction

Rice is a very important staple food in Nigeria and the world at large. It is one of the major sources of carbohydrates, which is an essential element for energy, human development and body growth (Adegun, 2012). In agricultural history, the domestication and cultivation of rice is one of the most important event. According to Okeke (2017) the raw material needed for commercial production of rice is the rice seeds or seedling.

Rice grain consist of husk and brown rice. The brown rice contains bran which comprises the outer layer and the edible portion. The rice mill operation is the removal of husk (dehusking) and bran to obtain the edible portion for consumption. The milling is wherein the rice grain is transformed into the form that is suitable for consumption. The extent of rice recovery during milling depends on many factors like variety of rice, degree of milling required, quality of equipment used and the operators (Poonam, 2014).

Due to increase population growth rate as well as consumers' demand of rice in Nigeria, the country has become the highest rice producing country in West Africa and the third largest in Africa. (WARDA, 1996). During rice processing, several streams of materials are generated which include the husks, the bran and the milled rice kernel. The rice kernel is further processed for consumption while the bran and the husk biomass waste generated are of environmental concern.

The availability of energy for rice processing is of outermost concern. One of the major sources of energy in Nigeria is the fossil fuel which it utilization has caused serious environmental impact such as global warming by greenhouse gases and acidification by SOx and NOx. In this study the

environmental impact assessment of a rice milling facility located in Nigeria was carried out. This was with the view of determining the impact of the rice milling company activities on the ambient environment base on the source of energy used for its operation.

2.0 Methodology

2.1 Study Area Description

This Study is conducted in an Agro-allied Industries Limited which is an agricultural products processing company. The company currently owns and operates a 50 MT per day Rice processing Mill producing parboiled head rice and delivers to the final customer through its distributors. It is located in Kwara State, a location of about 7 km from Ajese-ipo and 4 km from Offa (Figure 1). The site accommodates the Factory, the administrative building and a warehouse which occupy about ten (10) hectares of the total land size (100 hectares). The Rice Mill has 2 x 1500 tonnes bulk storage silos with tempering bins. There is a Mechanical reception hopper that allows fast sack tipping before movement to the Cleaning and destoning section in the Mill. Four soaking/steaming tanks are present with continuous flow drier and holding bin to rice mill and tempering bins. Inside the Double Flow, the parboiled paddy is dried carefully and efficiently with low, un-compacted, bed. There is also a low volume air that slowly cools the paddy in resting bins after which there follows distribution of paddy, water and steam to the tanks. In the multistage rice mill are husking, paddy separation, whitening, polishing, sifting, optical sorting and sacking. Also located in the mill is an air conditioned room on platform for optical sorter with overhead bins and sacking station. The husk fired steam boiler that assists in steam generation. It operates in the factory with husk store, ash settling chamber in brickwork and fan equipped with cyclone and chimney. The Rice Mill operates 2 - 3 shifts per day.

Figure 1: The Rice Mill Facility Site and Area of Influence

2.2 Emission Inventory

A very important step in air emission dispersion modelling is the air emission inventory. This is to identify sources of air emissions in a facility on which dispersion modelling is carried out. It was carried out in this study and with it sources of air emissions in the Rice Mill were identified. The identified major point sources of air emissions in the Rice Mill include the steam boiler where rice

husk is used to generate steam for parboiling and utilities that consist of the three diesel-powered electric power generators where electricity is generated to meet its power requirements.

Criteria air pollutants of interest in this study are: carbon monoxide (CO), oxides of nitrogen (NO_X), suspended particulate matter (SPM), and sulphur dioxide (SO_2). Emission rates and stack parameters used as model input were obtained from project details. The emissions sources obtained in the study are as summarized in Table 1.

Table 1: Air Emission Source Characteristics of the Rice Mill Project

Air Emission Source	Coordinates		Exit Temp (°C)	Air Pollutant	Emission (g/s)	Release Height (m)	Stack Diameter (m)	Exit Velocity (m/s)
	Latitude (North)	Longitude (East)						
Husk fired steam boiler cyclone stack	08° 12.404′N	004° 46.432′E	750	PM*	0.5000	11.6	0.36	15
				NO_{X*}	0.0352			
				SO_{2*}	0.0204			
				CO*	2.6000			
500 kva Generator (1)	08° 12.410′N	004° 46.408′E	110	PM	0.0010	3.0	0.3	8.94
				NO_X	0.1182			
				SO_2	0.0136			
				CO	0.0086			
500 kva Generator (2)	08° 12.412′N	004° 46.410′E	110	PM	0.0010	3.0	0.3	8.94
				NO_X	0.1182			
				SO_2	0.0136			
				CO	0.0086			
200 kva Generator	08° 12.414′N	004° 46.412′E	100	PM	0.0004	2.5	0.2	6.40
				NO_X	0.0473			
				SO_2	0.0054			
				CO	0.0034			

Calculated from rice husk emission factors reported by Irfan et al., (2014) for gases and Mantananont and Patumsawad (2016) for particulates

2.3 Emission Modelling

The ISC-AERMOD View was used to investigate the air emission dispersion modelling. It is a user-friendly interface for four U.S. EPA air dispersion models: ISCST3, ISC-PRIME, AERMOD and MET developed for Microsoft Windows which uses pathways consisting runstream file as basis for functional organization. The ISC-AERMOD version 8.2.0 with serial number AER00005543, licensed to the Environmental Engineering Research Laboratory, Department of Chemical Engineering, Obafemi Awolowo University, Ile-Ife, Nigeria was used.

The identified point emission sources with all the parameters listed in Table 1 were considered as input parameters into the modelling while Table 2 was used to investigate their impacts on the ambient air quality. From the identified sources of air emission in the Rice Mill project, two air emissions scenarios were considered to establish potential ground level concentrations of air pollutants within the site and surroundings. The operating scenarios investigated were Scenario 1 where process air emissions from the Rice Mill were considered where operation was assumed to be full with rice husk fired steam boiler in the Mill and Scenario 2 which assumed full operation of the rice-husk-fired steam boiler simultaneously in operation with the three diesel-fired electric power generators.

Table 2: Standards of Ambient Air Quality

Air Pollutants	Averaging Period	Maximum Concentration (µg/m³)	
		FMENV[a]	World Bank[b]
CO	1 – Hr	-	30,000
	8 – Hr	22,800	10,000
	24 – Hr	11,400	-
NO_X	1-Hr	-	200
	24 – Hr	75 – 113	-
	Annual	-	40
PM	1-Hr	600	
	24-Hr	250	
SO_2	1-Hr	260	
	24-Hr	26	

[a]Source: FEPA (1991); [b]Source: World Bank (2007

2.4 Meteorological Parameters

Meteorological information is essential in ISCST air dispersion modelling. Both the surface and upper air observations were compiled using meteorological data from the Lakes Environmental meteorological observations on the study area (Met Data Order # MET 134283). It has winds having prevalence for a south-westerly direction (Figure 2).

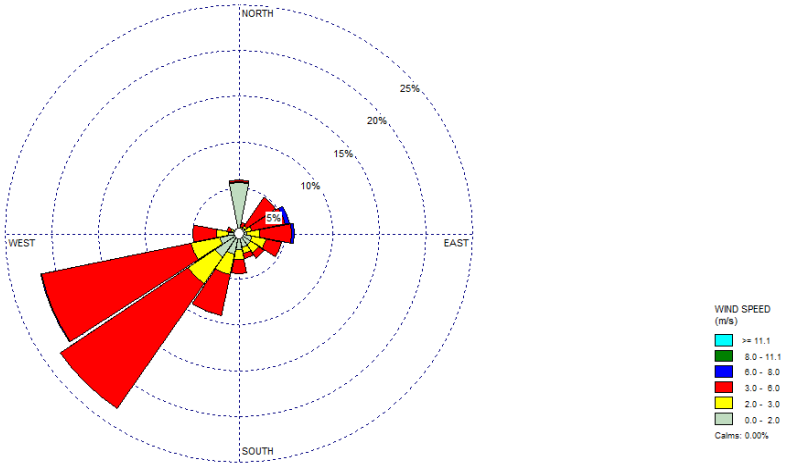

Figure 2: Generated Windrose from the Wind Data used for the Study

3.0 Results and Discussion

3.1 Ground Level Concentrations of Criteria Pollutants

Presented in Figure 3 the present 1-hour averaging period CO concentrations from the Rice Mill Steam Boiler as investigated in ***scenario 1*** are 41.5 – 177.3 µg/m³ while its 8-hour and 24-hour averaging period concentrations are 7.0 – 97.5 µg/m³ (Figure 4) and 2.5 – 43.5 µg/m³ (Figure 5). Its 1-hour ground level NO_X are 0.56 – 2.40 2.5 – 43.5 µg/m³ (Figure 6) with 24-hour and annual averaging period concentrations of 0.03 – 0.59 2.5 – 43.5 µg/m³ (Figure 7) and 0.0019 – 0.1814 2.5 – 43.5 µg/m³ (Figure 8) respectively. While its 1-hour SPM are 7.99 – 34.09 µg/m³ (Figure 9) the 24-hour levels are 0.47 – 8.37 µg/m³ (Figure 10). This ***scenario 1*** emits 1-hour

SO_2 concentrations of 0.33 – 1.39 µg/m^3 (Figure 11) with 24-hour levels of 0.02 – 0.34 µg/m^3 (Figure 12).

From the simultaneous operations of both the steam boiler and the diesel electric power generators in the Rice Mill as investigated in ***scenario 2***, the 1-hour averaging period ground level CO are 43.5 – 185.1 µg/m^3 (Figure 13) with 8-hour and 24-hour levels of 7.1 – 99.3 µg/m^3 (Figure 14) and 2.5 – 46.8 µg/m^3 (Figure 15) respectively. Their 1-hour, 24-hour and annual NO_X averaging period concentrations are respectively 34.0 – 257.8 µg/m^3 (Figure 16), 2.0 – 95.8 µg/m^3 (Figure 17) and 0.2 – 21.0 µg/m^3 (Figure 18). Their 1-hour SPM are 8.2 – 35.0 µg/m^3 (Figure 19) with 24-hour levels are 0.48 – 8.75 µg/m^3 (Figure 20). Both their 1-hour and 24-hour SO_2 averaging period concentrations are respectively 3.95 – 29.67 µg/m^3 (Figure 21) and 0.2 – 11.0 µg/m^3 (Figure 22).

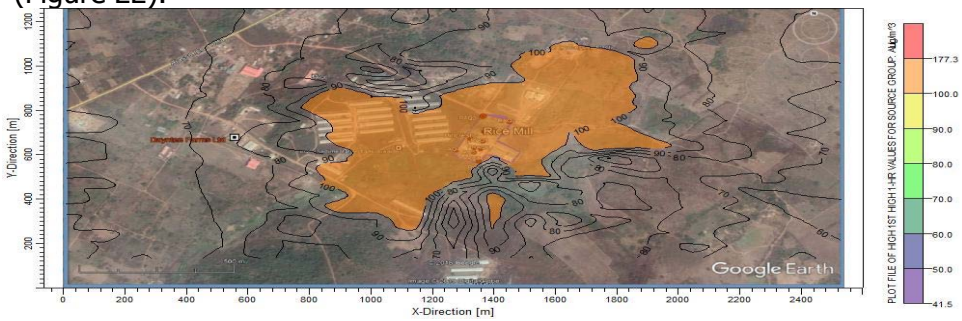

Figure 3: Isopleth of 1-Hour Ground Level CO from the Rice Mill Boiler (Scenario 1)

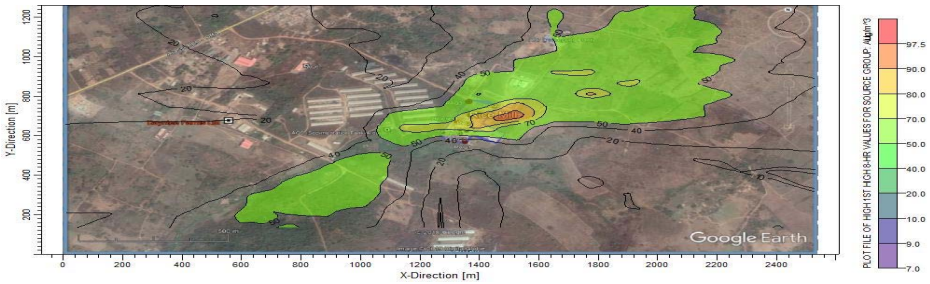

Figure 4: Isopleth of 8-Hour Ground Level CO from the Rice Mill Boiler (Scenario 1)

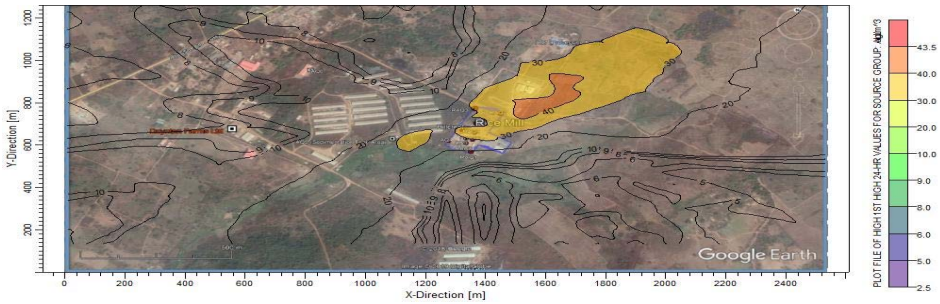

Figure 5: Isopleth of 24-Hour Ground Level CO from the Rice Mill Boiler (Scenario 1)

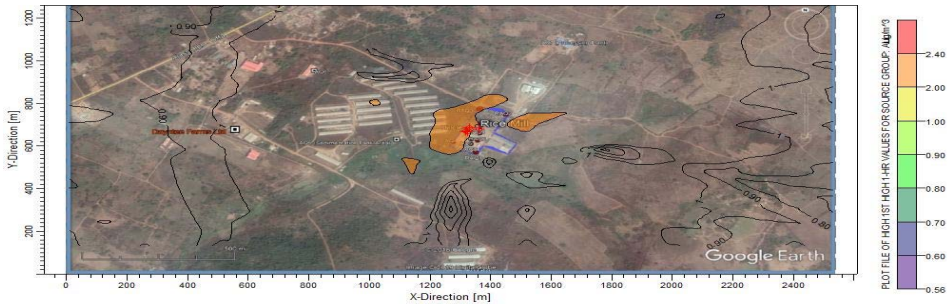

Figure 6: Isopleth of 1-Hour Ground Level NOX from the Rice Mill Boiler (Scenario 1)

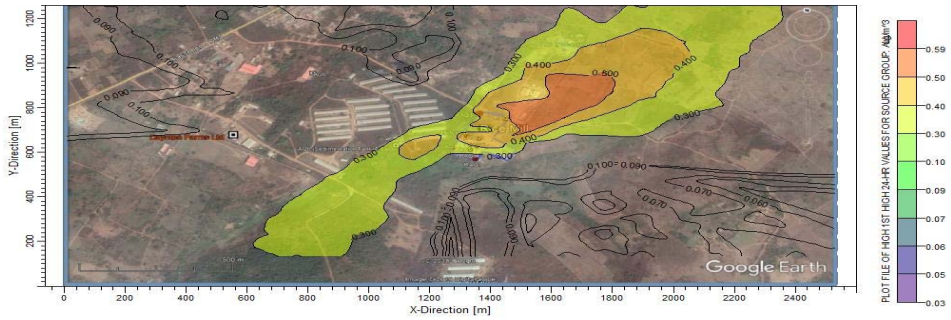

Figure 7: Isopleth of 24-Hour Ground Level NOX from the Rice Mill Boiler (Scenario 1)

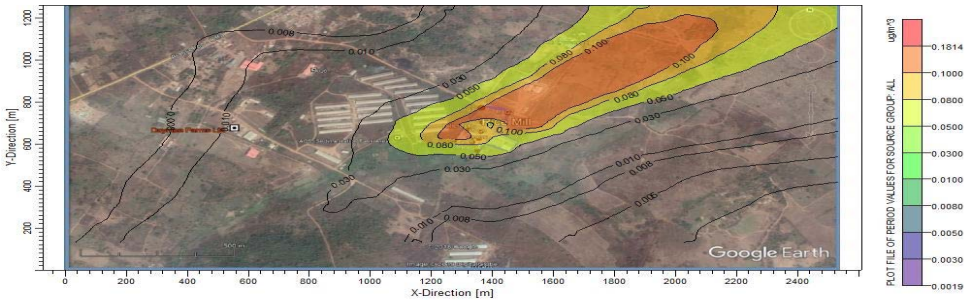

Figure 8: Isopleth of Annual Ground Level NO_X from the Rice Mill Boiler (Scenario 1)

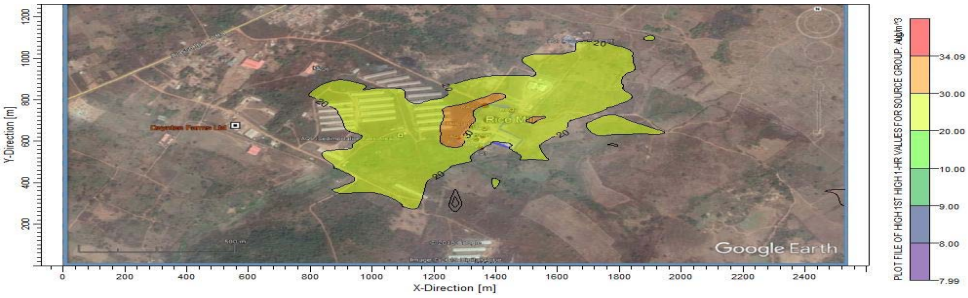

Figure 9: Isopleth of 1-Hour Ground Level SPM from the Rice Mill Boiler (Scenario 1)

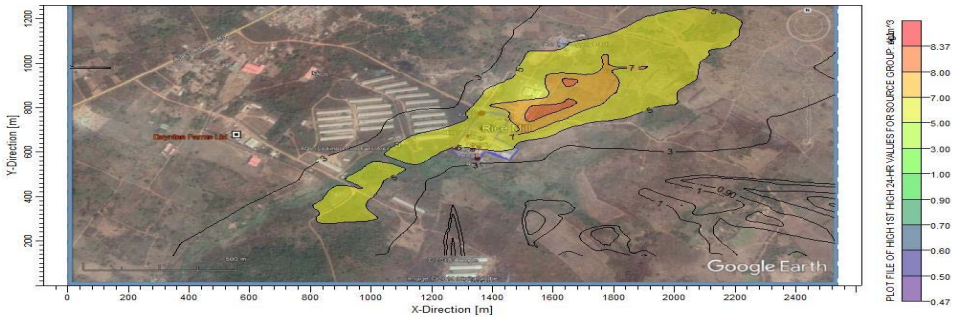

Figure 10: Isopleth of 24-Hour Ground Level SPM from the Rice Mill Boiler (Scenario 1)

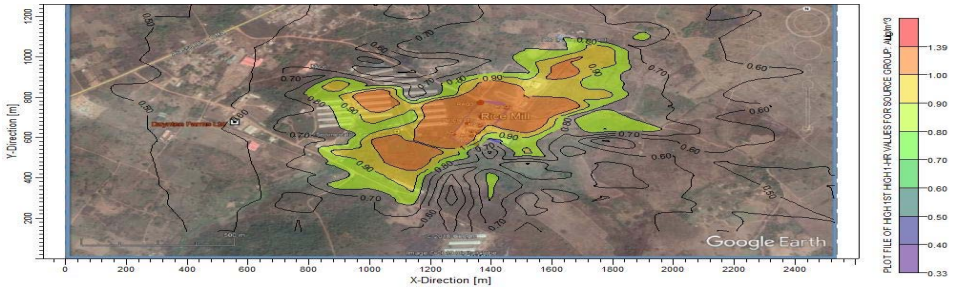

Figure 11: Isopleth of 1-Hour Ground Level SO_2 from the Rice Mill Boiler (Scenario 1)

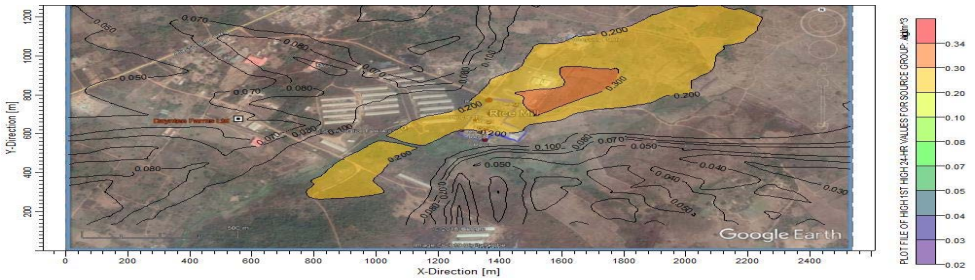

Figure 12: Isopleth of 24-Hour Ground Level SO_2 from the Rice Mill Boiler (Scenario 1)

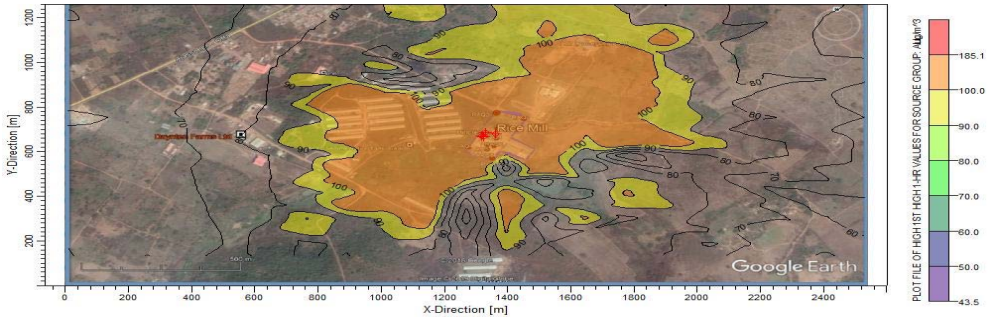

Figure 13: Isopleth of 1-Hour Ground Level CO from the Boiler and Power Generator (Scenario 2)

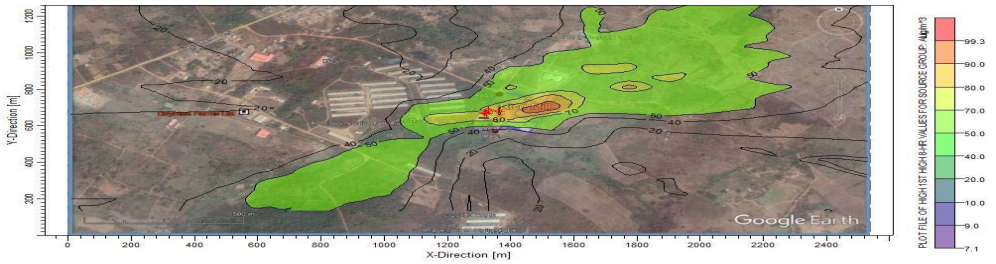

Figure 14: Isopleth of 8-Hour Ground Level CO from the Boiler and Power Generator (Scenario 2)

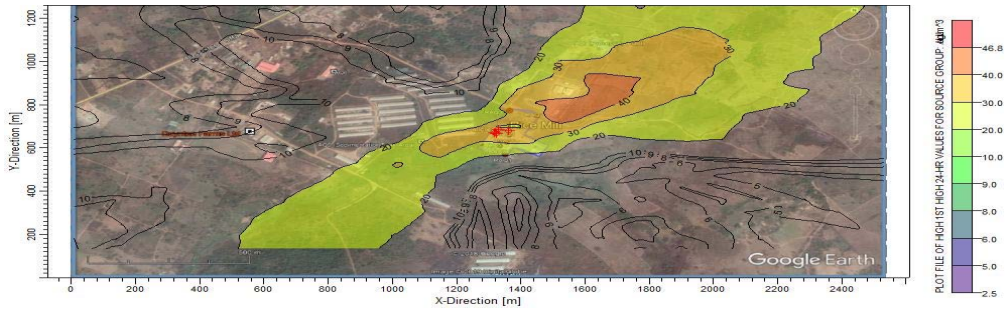

Figure 15: Isopleth of 24-Hour Ground Level CO from the Boiler and Power Generator (Scenario 2)

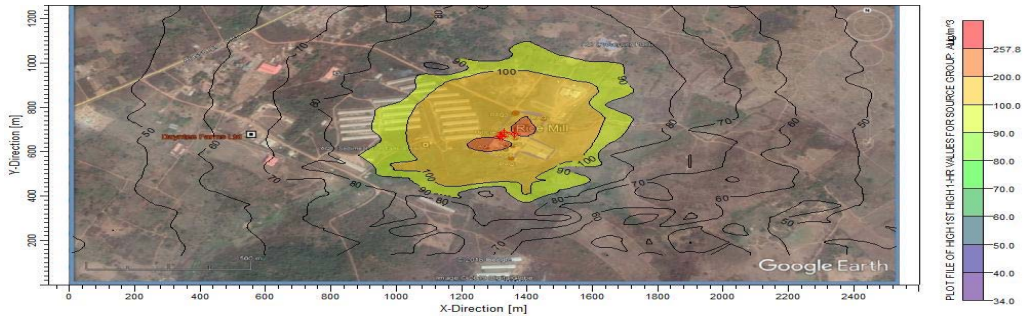

Figure 16: Isopleth of 1-Hour Ground Level NO_X from the Boiler and Power Generator (Scenario 2)

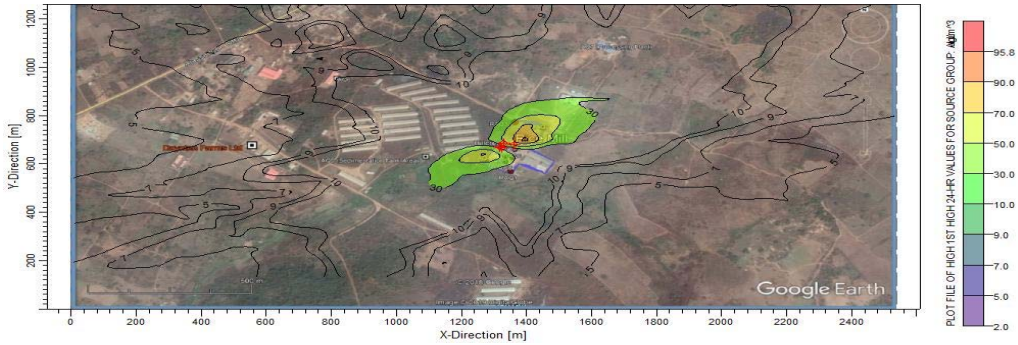

Figure 17: Isopleth of 24-Hour Ground Level NO_X from the Boiler and Power Generator (Scenario 2)

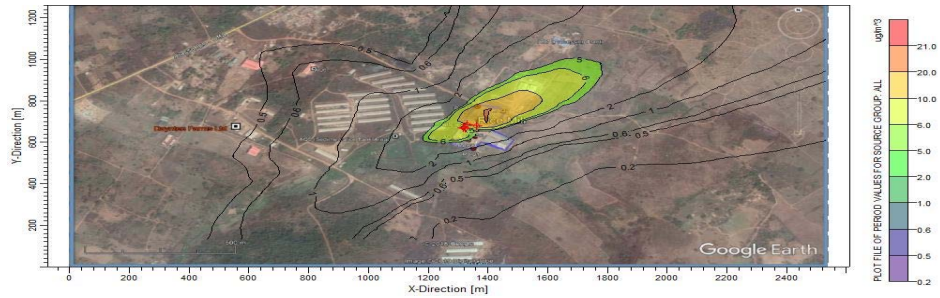

Figure 18: Isopleth of Annual Ground Level NO_X from the Boiler and Power Generator (Scenario 2)

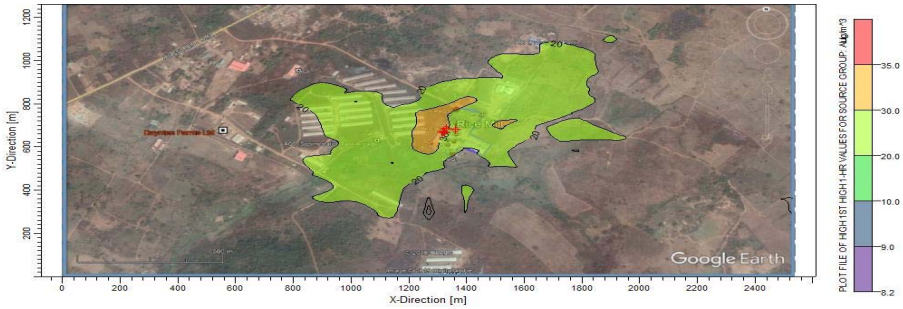

Figure 19: Isopleth of 1-Hour Ground Level SPM from the Boiler and Power Generator (Scenario 2)

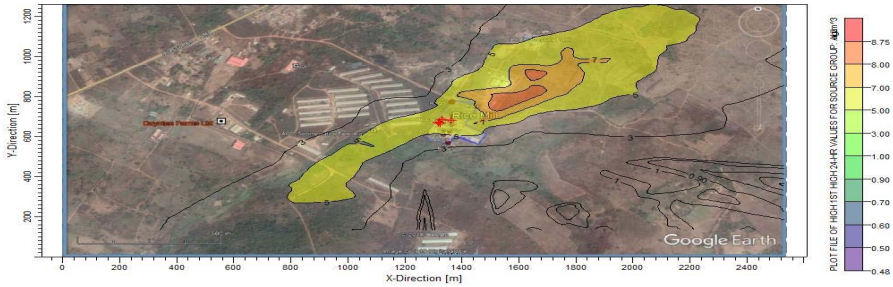

Figure 20: Isopleth of 24-Hour Ground Level SPM from the Boiler and Power Generator (Scenario 2)

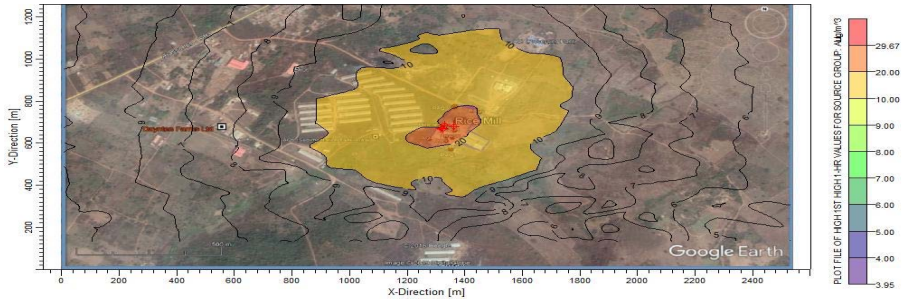

Figure 21: Isopleth of 1-Hour Ground Level SO_2 from the Boiler and Power Generator (Scenario 2)

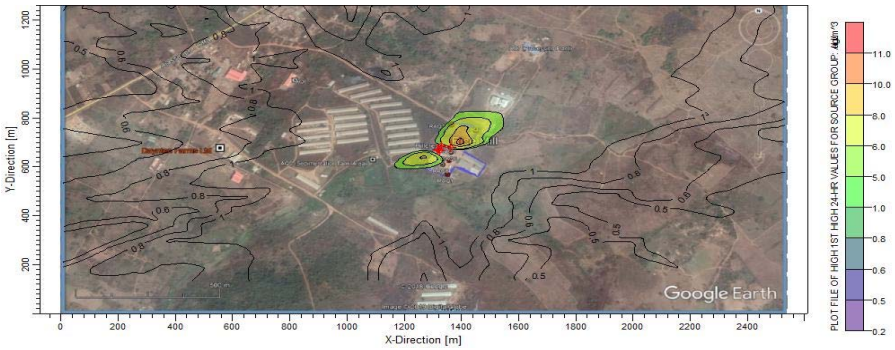

Figure 22: Isopleth of 24-Hour Ground Level SO_2 from the Boiler and Power Generator (Scenario 2)

3.2 Maximum Ground Level Concentrations Impact on Ambient Air Quality

Summarized in Table 3 are the maximum ground level concentrations of air pollutants presently emitted by the Rice Mill. From the steam boiler as investigated in scenario 1, the maximum 1-hour averaging period concentrations are 1.4 – 177.3 µg/m^3 with 24-hour averaging period maximum ground level concentrations of 0.3 – 43.5 µg/m^3 which are respectively 0.54 – 5.68% and 0.38 – 3.36% of their respective limits. While the minimum of these is from SO_2 the maximum is from CO. These maximum concentrations are around the boiler with the minimum in the northeast end of the Mill. The 1-hour averaging period cumulative maximum ground level concentrations of air pollutants from simultaneous operations of the steam boiler and the three diesel electric power generators as investigated in scenario 2 are 29.7 – 257.8 µg/m^3 with 24-hour levels of 8.8 – 95.8 µg/m^3 which are 0.62 – 11.42% and 0.41 – 84.78% of their respective limits. All these maximum concentrations of ground level air pollutants from the Rice Mill are within the set limit except in scenario 2 where the simultaneous operations of both the steam boiler and the diesel generator emits the 1-hour ground level NO_X concentrations of about 128% of the limit.

3.3 Impacts of the Rice Mill Project on the Host Airshed

As obtained from scenario 1, steam boiler of the Rice Mill presently adds about 0.38 – 5.68% of the respective investigated air pollutants limits to its host environment. Similarly simultaneous operations of the steam boiler and the electric power generators of the Rice Mill add about 0.41 – 84.78% of the respective investigated air pollutants limits to the ambient air quality of the host environment. Occasionally the daily NO_X limits from this ***scenario 2*** could breach the ambient limit.

Table 3: Maximum Ground Level Concentrations of Air Pollutants from the Rice Mill

Air Pollutant	Averaging Period	Concentration		Designation/Nearest Community
		Predicted ($\mu g/m^3$)	% of Standard	
Scenario 1 (Rice Mill Boiler)				
CO	1 – Hour	177.3	0.59	Within the Rice Mill
	8 – Hour	97.5	0.98	East End of the Rice Mill
	24 – Hour	43.5	0.38	Around the Boiler
NO_X	1 – Hour	2.4	1.20	Around the Boiler
	24 – Hour	0.59	0.52	East End of the Rice Mill
	Annual	0.18	0.45	Southwest End of the Mill
PM	1 – Hour	34.1	5.68	Southwest End of the Mill
	24-Hour	8.4	3.36	Northeast End of the Mill
SO_2	1 – Hour	1.4	0.54	Around the Boiler
	24-Hour	0.3	1.15	Northeast End of the Mill
Scenario 2 (Rice Mill Boiler and Diesel Generators)				
Air Pollutant	**Averaging Period**	**Concentration**		**Designation/Nearest Community**
		Predicted ($\mu g/m^3$)	**% of Standard**	
CO	1 – Hour	185.1	0.62	Generator House
	8 – Hour	99.3	0.99	Northeast End of Rice Mill
	24 – Hour	46.8	0.41	Northeast End of Rice Mill
NO_X	1 – Hour	257.8	128.90	Generator House
	24 – Hour	95.8	84.78	Northeast End of Rice Mill
	Annual	21.0	52.50	Generator House
PM	1 – Hour	35.0	5.83	Generator House
	24-Hour	8.8	3.52	Northeast End of Rice Mill
SO_2	1 – Hour	29.7	11.42	Generator House
	24-Hour	11.0	42.31	Northeast End of Rice Mill

CONCLUSIONS

The ISC-AERMOD View version 8.2.0 has been used in this study to determine the actual contribution of steam boilers and electric power generators in a Rice Mill to air pollutants of its host environment. Ground level concentrations of Carbon Monoxide (CO), Oxides of Nitrogen (NO_X), Particulate Matter (PM) and Sulphur Dioxide (SO_2) associated with the project were estimated. All the anticipated maximum ground level concentrations of air pollutant associated with the Rice Mill are within their respective limits except NO_X that could occasionally breach its limit. Continuous adherence of the Mill to its present attitude of keeping one of the electric power generators on standby will assist to keep the daily NO_X within its set standard.

References

Adegun, I. K., Adepoju, S. A. and Aweda, J. A. (2012) A Mini Rice Processing Machine for Nigeria Farmer. Journal of Agricultural Technology 8(4): 1207 – 1216

FEPA. (1991). Guidelines to Standards for Environmental Pollution Control in Nigeria. Federal Environmental Protection Agency (FEPA), Lagos.

NESREA (2007) National Environmental Standards and Regulations Enforcement Agency (Establishment) Act, 2007. Federal Republic of Nigeria.

NESREA (2013) National Environmental (Air Quality Control) Regulations, National Environmental Standards and Regulations Enforcement Agency, Abuja.

Okeke, C. G. and Oluka, S. I. (2017) A Survey of Rice Production and Processing in Southeast Nigeria. Nigerian Journal of Technology. 36(1): 227 – 234

Poonam, D. (2014) Rice Milling. IOSR Journal of Engineering. 4(5): 34 – 42.

USEPA (2000) EPA. Compilation of Air Pollutant Emission Factors Volume I: Stationary Point and Area Sources, 5th ed. United States Environmental Protection Agency, Office of Air Quality Planning and Standards. Research Triangle Park NC 27711, USA, 1995.

WARDA (1996) West Africa Rice Development Association Annual Report.

World Bank (2007) Pollution Prevention and Abatement Handbook WORLD BANK GROUP, Washington DC.

World Bank (2016) Environmental, Health, and Safety Guidelines for Annual Crop Production. WORLD BANK GROUP, Washington DC.

Irfan, M., Riaz, M., Afif, M.S., Shahzad, S.M., Saleem, F., Rahman, N., Berg. L.V.D and Abbas F. (2014) Estimation and characterization of gaseous pollutant emissions from agricultural crop residue combustion in industrial and household sectors of Pakistan. Atmospheric Environment, 189 - 197

Mantananont, N and Patumsawad, S (2016) Particulate matter and gaseous emission rate from combustion of Thai lignite and agricultural residues in a fixed-bed combustor. Energy Sources, Part A: Recovery, Utilization, and Environmental Effects. 38:4, 478-484, DOI: 10.1080/15567036.2013.783655

Proceedings of the 49th NSChE Annual Conference
KADA 2019: pp 214-222

P1C-06: CHARACTERIZATION OF KAOLIN FROM NARAGUTA CLAY DEPOSIT IN JOS NORTH LOCAL GOVERNMENT AREA OF PLATEAU STATE FOR THE PRODUCTION OF CERAMIC MATERIAL

H.F. Akande*, S.N. Mumah, K.Y. Mudi and Francis Samuel
Department of Chemical Engineering, Kaduna Polytechnic, Kaduna, Nigeria
***Corresponding author**: hassan.akande@kadunapolytechnic.edu.ng, +234-8033686645

ABSTRACT
Clay Samples from Naraguta deposit in Jos North Local Government Area of Plateau State, Nigeria have been studied for its application as raw material for ceramic material production. Naraguta clay, a soft white in lumped form were obtained randomly from different points within each deposit from underground local mines pit at a depth of 10, 20 and 30 cm and labelled samples 1,2 and 3 respectively. The samples were air-dried for several days and crushed using a crusher. Each crushed sample was thoroughly mixed, coned and quartered. The samples were subsequently ball milled to form a powder. The powder was pressed to form pellets which were dried at 105 °C until constant weight was achieved. The samples were then heated to temperature 600, 800, 1000, 1200, 1300 and 1400 °C in a furnace, respectively at a rate of 5 °C/min with soaking time of 1h at each maximum temperature. The chemical analysis was carried out using x-ray fluorescence (XRF) and x-ray diffraction (XRD) while the physical property tests such as bulk density, apparent porosity, compressive strength and shear stress were carried out using standard techniques such as American Society for Testing and Materials (ASTM 2016). The effects of firing temperature on the physical properties were also studied. The results of the chemical analysis revealed that the clays were composed majorly of silica (SiO_2), 49 – 51%; alumina (Al_2O_3), 31.494 – 33.301%; and other oxides. The XRD spectra of the clay showed that the components of the clay samples were predominantly kaolinite constituting about 80% of the particles with some traces of mica and quartz. The physical properties (bulk density, compressive strength and shear strength) of the clay sample initially increased with increased firing temperature from 750 °C to 800 °C, and then the properties decreased with further increase in firing temperature until it reached the minimum at 950 °C because of the transformation of the clay due to dehydroxylation of kaolin into kaolinite. The results of both the physical and chemical analysis fall within the acceptable standards for materials for ceramic material production.

Key Words: Kaolin, Ceramic Material, Chemical and Physical Analysis, X-Ray fluorescence, X-Ray Diffraction

Introduction
Ceramics are inorganic and nonmetallic solids with a range of useful properties, including very high hardness and strength, extremely high melting points, and excellent electrical and thermal insulation. The best-known ceramics are pottery, glass, brick, porcelain, and cement (Emmanuel 2015) Clay remains the major raw material in the ceramic industry. It has also found wide applications in the paint and paper industries. This versatility depends principally on the composition and physical properties. The properties of a particular ceramic depend not just on the materials from which it is made but also on the way they are joined together—in other words, on its crystalline structure**.** The clay used for the production of ceramics should have the following specifications; plastic enough for shaping, dry without excessive cracking and warping, have low and wide vitrification range, low carbonate content, and a good spread in particle size. (Angelica *et al.*, 2008). Low and wide vitrification range is desirable for favourable unit firing cost and for

ease of firing. Because the fluxing action of carbonates tends to shorten the firing range and trigger localized flux spots, the low carbonate content is desirable, and CaO and MgO resulting from the firing of typical carbonate-bearing clay can hydrate relatively easily with no damage to the fired material.

In the fabrication of ceramic products, raw materials selection plays a vital role in the final product. The properties of the components present in the clay and the firing temperature affect critically the physicochemical properties of the resulting ceramics (Jordan et al., 1999). The sintering process has been widely used in producing ceramic components. Sintering processes can be divided into two types: solid-state sintering and liquid phase sintering. Solid-State Sintering (SSS) happens when the powder compact is fully densified in a solid-state at sintering time, whereas fluid phase sintering occurs when the powder compact is still in a liquid phase during sintering (Kang, 2005).

Sintering of ceramic mass is therefore critical in adjusting desired properties and occurs in general during liquid-phase formation. The presence of components such as low-melting clays is significant in the process. Fluxes (alkaline oxides, mainly K_2O and Na_2O), in reaction with silica and alumina, promote liquid phase formations and therefore assist densification process (Hamisi *et al.*, 2014). Evaluating the phase transformations which take place during the firing process is therefore crucial in determining the quality of the clay used in the formulation of ceramic materials (Sousa and Holanda, 2005).

Nigeria is immensely endowed with ceramic raw materials like alumina, coal, clay, feldspar, kaolin, quartz, silicon, and zirconium, located throughout the country's geographical zones. Local demands for ceramic products are very high considering our population which is presently about 180 million, yet the supply is met mostly through importation. Despite the fact that both raw materials and human capacity are available for research, production and development of high-quality ceramic products of international standard, the country imports more than 50 containers a day (Emmanuel, 2015). The demand for ceramic products in Nigeria is quite high with the real estate sector leading in the drive for demand with ceramic tiles which are used for floor, walls, ceiling and even roof. Next is the power sector with its high demand for electrical porcelain insulators. Another area worth considering is ceramics for home use. This includes dinner wares, pottery wares and decorative wares. Other products such as spark plug ceramics, beryllium oxide ceramics, chemical or refractory porcelain, engine and turbine combustion chambers can be categorized for industrial applications (Emmanuel, 2015).

It makes economic sense to invest in the production of ceramics in Nigeria at this time with all these demands in the different sectors, even as the raw materials are readily available in commercial quantities. This will not only help meet the growing demand for these products but will also help create jobs for our young people and help the state economy to grow. Clay bodies are widely distributed on the Precambrian basement complex of Nigeria. Clay occurs in deposits of greatly varying nature. No two deposits have the same clay, and frequently different samples of clay from the same deposit differ. Due to its small size, complex structural structure and relative slow kinetics of forming and transition, clay can be difficult to define.

Naraguta clay deposit is located in Jos North Local Government Area of Plateau State, North Central Nigeria. Clay samples were collected from three different locations in the upper part of the area.The study areas are bounded between latitudes 8°30E and 9°00E and longitudes9°30N

and 10°00N. Fresh samples in lump form were obtained randomly from different points within each deposit.

This work is therefore to evaluate the properties of kaolin from Naraguta clay deposit in Jos North Local Government Area of Plateau State, Nigeria to determine its suitability for ceramic materials production.

Experimental Procedure

Sample Preparation

The material preparation was carried out using the procedure adopted by Ituma *et al*. (2018) and Lydia *et al*. (2018). In this experiment, 5 kg of fresh samples in lump form were obtained randomly from different points within each deposit from underground local mines pit at a depth of 10, 20 and 30 cm and labelled samples 1,2 and 3 respectively. The samples were air-dried for several days and crushed using a set of Denver crushers by Denver Equipment Co. England. Each crushed sample was thoroughly mixed, coned and quartered. These were packaged in small polythene bags as representatives of the samples for the required test. Clay sample was subsequently ball milled to form a powder. The powder was pressed to form pellets which were dried at 105^{O}C until constant weight was achieved. The samples were then heated to 600, 800, 1000, 1200, 1300 and 1400 ^{o}C, respectively at a rate of 5^{O}C/min with soaking time of 1h at each maximum temperature.

Sample Characterization

The chemical compositions of the clay samples were determined using X-ray fluorescence (XRF). The clay samples were mixed inside a cleansed crucible and heated to 500 ^{o}C for 8 min and allowed to cool at room temperature until the sample fused and later used for the analysis. The chemical composition of the sample is presented in Table 1.

The X-Ray Diffraction (XRD) patterns and phase identifications of the samples were carried out using X-ray diffractometer (XRD); PW 1800 diffractometer, Philips, the Netherlands with graphite monochromatized copper Kα-radiation.

Apparent porosity

Apparent porosity of the clay material was carried out by preparing a clay brick measuring 5x5x4 cm. The brick was then dried in an oven at 100^{o}C, fired in a furnace at a temperature of 900 ^{o}C. The fired specimen was cooled and then transferred into a desiccator, and the dry weight noted and recorded as x. The specimen was then immersed in a water-filled beaker, allowed to soak in boiled water for 30 minutes while being agitated to free trapped air bubble. The specimen was then allowed to cool in a desiccator and then soaked weight recorded as y. The specimen was weighed suspended in water using beaker placed on a balance, and the suspended weight noted and recorded as z. The apparent porosity was calculated using equation (1) (Abubakar *et al*., 2014)

$$\text{Apparent porosity} = \frac{y-x}{y-z} \times 100\% \quad (1)$$

Bulk density

The samples were dried for 24 hours, the test pieces were put in an oven and dried at a temperature of 110 ^{o}C for 6 hr. They were allowed to cool and weighed by means of weighing

balance and their dried weights (D) recorded in turn. They were transferred to a beaker and heated for 40 min and then cooled, the soaked weight was recorded. Water was put in another beaker and each of the test pieces suspended in the water so that their suspended weights were recorded. The equation for calculating bulk density is given by Equation 2. (Ovat and Bisong 2017).

$$\text{Bulk density} = \frac{D\rho W}{w-s} \quad (2)$$

Where D = Dried weight
W = Soaked weight
S = Suspended weight
ρW =Density of water

Loss of ignition

The loss of ignition was calculated by measuring 50 g of the sample, dried in an oven at 110 ^{o}C and cooled in a desiccator. A porcelain crucible was cleaned, dried and weighed (A). The dried sample was introduced into the crucible and weighed (B). The crucible containing the sample was placed in a muffle furnace and heated to a temperature of 900 ^{o}C for 3 hours, cooled in a desiccator and then weighed (C). The loss of ignition was calculated from Equation (Abubakar *et al.*, 2014)

$$\text{LOI} = \frac{B-A}{B-C} \quad (3)$$

Compressive and Shear Strength of the Kaolin Sample

Clay samples were ball milled to form a powder. The powders were pressed to form pellets which were dried at 105^{O}C until constant weight was achieved. The samples were then transferred into a furnace and heated to temperature of 600, 800, 1000, 1200, 1300 and 1400 ^{o}C, respectively at a rate of 5^{O}C/min. The samples were cooled to room temperature. The samples were placed on a compressive tester and load was applied by turning the handwheel of the tester at a uniform rate until failure occurred. The manometer readings were recorded, and the compressive strength (CS) and Shear strength were calculated from equation 4. (Abubakar *et al.*, 2014)

$$CS = \frac{maximum\ laod\ (N)}{cross\ sectional\ area\ (m^2)} \quad (4)$$

Results and Discussion

The chemical composition of kaolin is essential because of its influence on the behaviour of ceramic masses during thermal treatment. Table 1 shows the chemical compositions of the clay samples.

From Table 1, it could be deduced that the silica contents of the samples are 49.038, 51.102 and 50.673% of clay sample 1, 2 and 3 respectively. This shows that all the clay samples met the requirements for the manufacture of ceramics as reported by Abubakar *et al.*, (2014). In their work, they reported that a clay material having silica contents of between 40 – 65 % satisfies the requirements for the manufacture of refractory bricks and ceramics. This may be due to the presence of higher bond impacted into the matrix of the clay by the silica content.

Table 1: Chemical Composition of the Kaolin Sample

Oxide	Kaolin Sample 1	Kaolin Sample 2	Kaolin Sample 3
CuO	0	0	0
NiO	0	0	0
Fe_2O_3	0.483	0.387	0.694
MnO	0	0	0
Cr_2O_3	0.011	0.009	0.017
TiO_2	1.112	0.801	1.483
CaO	0.083	0.106	0.093
Al_2O_3	31.494	32.878	33.301
MgO	0.328	0.317	0
ZnO	0.004	0.004	0.006
SiO_2	49.038	51.102	50.673
Total	82.553	85.604	86.267
LOI	17.447	14.396	13.733

An Al_2O_3 content higher than 30 % is necessary for increasing the refractory and mechanical resistance (Benea and Gorea, 2004). From Table 1, it could be deduced that the alumina contents of the clay samples were found to be between 31 – 33%, an indication that the samples fall within the range of standards for the manufacturing of ceramics (above 30%) and refractory bricks (25 – 44%). From Table 1 also, it could be seen that the Fe_2O_3 contents of the clay samples are 0.483, 0.387 and 0.694 % for sample 1, 2 and 3 respectively. These values of the Fe_2O_3 contents also falls within the range of standards (0.4 – 2.4 %) for the manufacture of refractory bricks. Such level of Fe_2O_3 usually alters the colour of the clay to reddish-brown, thereby making it attractive as a ceramic material as reported by Marcel and Bernea (2004). Marcel and Bernea (2004) reported that the Fe_2O_3 content of clay influenced the high-temperature characteristics of the clay such as the fired strength.

The Loss on Ignition (LOI) values of the clay samples were found between 13.733 – 17.447%. The values, which fall within the range of 8 – 18 % for ceramics and refractory bricks products as reported by Omowumi, (2000). Omowumi (2000) reported in her work that the LOI characteristics of the clay materials should be low to impact adverse effects on the porosity of the materials especially those used for refractory bricks.

The bulk density, compressive strength and shear stress of the fired clay are presented in Table 2, 3 and 4, respectively.

From Tables 2 - 4, it could be observed that the physical properties (bulk density, compressive strength and shear strength) of the fired bricks produced from the kaolin sample initially increased with increased firing temperature from 750^{o}C to 800^{o}C and then the properties decreased with further increase in firing temperature until it reached the minimum at 950 ^{o}C for the considered firing temperatures. The explanation for this is that transformation of the sample type of clay used for producing ceramic from one phase to another has occurred as the dehydration of kaolinite completes by ~150^{o}C, followed by dehydoxylation at ~500-600^{o}C and its structural breakdown occurs in the temperature range ~800-900^{o}C, depending upon the particle size and amount and type of the impurities present (Francisca, 2014). Also the bulk density of 1.56

g/cm^{3}obtained at fired temperature of 950^{o}C shows that the sample is suitable for producing ceramic materials.

The apparent porosity of the clay samples is presented in Table 5

Table 2: Compressive Strength of the Kaolin Sample

Temperature (^{o}C)	Compressive Strength (N/m^2)
750	7.86
800	7.88
850	7.32
900	7.43
950	8.21

Table 3: Shear Strength of the Kaolin Sample

Temperature (^{o}C)	Shear Strength (N/m^2)
750	1.76
800	2.27
850	1.24
900	1.23
950	2.86

Table 4: Bulk Density of the Kaolin Sample

Temperature (^{o}C)	Bulk Density (g/cm^3)
750	1.55
800	1.63
850	1.59
900	1.6
950	1.56

Table 5: Apparent porosity of the clay sample

Clay samples	**1**	**2**	**3**
Apparent porosity	4.1	5.8	8.2

The apparent porosity of the clay samples as revealed in table 5 were found to be 4.1, 5.8 and 8.2 for samples 1, 2 and 3, respectively. These low porosities exhibited by these clay materials also fall within the standard for the production of fired clay and refractories as reported by Tiffo *et al.* (2015). Tiffo *et al.* (2015) reported that low porosity found in a clay sample leads to increase in their mechanical strength. Therefore, these samples are found suitable for the manufacture of refractories, ceramic materials and siliceous fired clays.

The phases present in the clay samples and their crystallinity were identified using XRD, as shown in Figures 2a to 2c.

The results as presented in Figure 2a - c, show eleven major peaks at diffraction angles, 2θ of 10.2, 20, 24.9, 26.6, 28.0, 35.0, 38.3, 50.1, 60.2, 68.9 and 74°. The presence of mica and quartz was as a result of silicate minerals present in the kaolin sample. The XRD study confirmed that the major component present in the clay samples were predominantly kaolinite constituting about 80 % of the particles. Other components include mica and quartz. The average lattice parameters from indexing of the peaks in the XRD were calculated to be 9.9882A. The particle diameter of the kaolin sample was calculated using the Debye-Sherrer Equation;

$$D = \frac{0.9\lambda}{\beta\cos\theta} \quad (5)$$

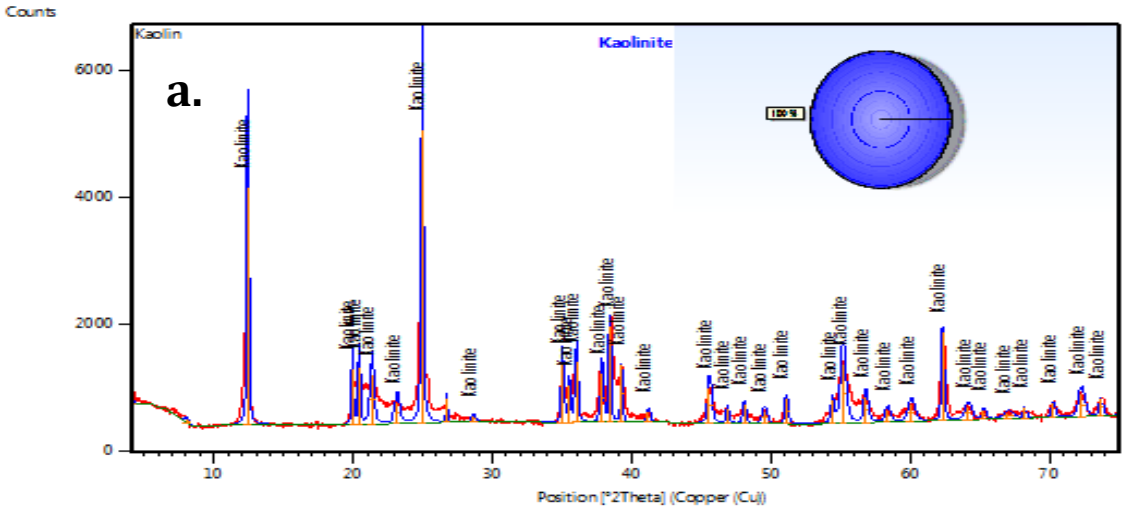

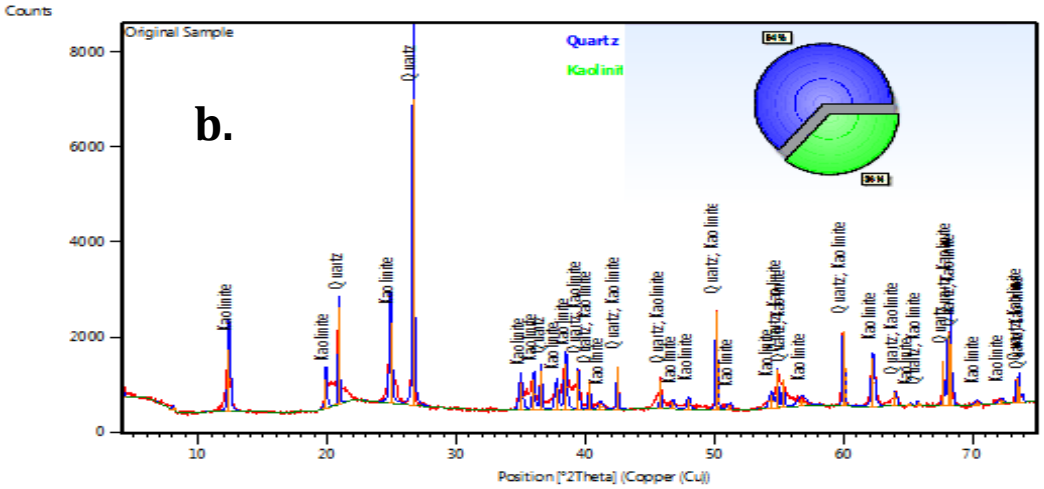

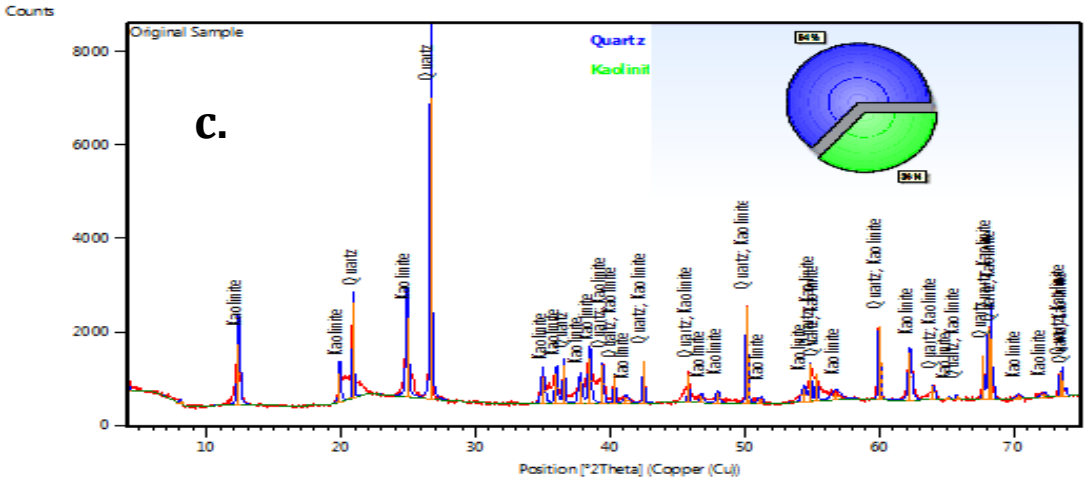

Figure 2: XRD Spectrum of Jos clay samples

Where λ is the wavelength of the x-ray (0.1541 nm) β is the full width at half maximum (FWHM), θ is the diffraction angle in radian, and D is the particle diameter size. The interspacing between the atoms (d) was calculated using the Bragg's law given as;

$$d = \frac{\lambda}{2\sin\theta} \quad (6)$$

The average interspacing between the atoms, average crystal size and average lattice parameters of the study clay samples calculated are 0.3764 nm, 17.480 nm and 10.03 A respectively. These indicated that the clay samples used shows characteristic that is of less spaces between the particles of the clay samples. This wider angle between the unit cells of the kaolin crystal of 10.03A is more than general well crystallized kaolinites having a graphitic line of 001 d spacing of 7.1 to 7.2 as reported by Aroke *et al.* (2013). The difference could be connected with a small amount of interlayer water within the kaolin crystals. However, there are some incompleteness and imperfections in some patterns in Figure 2, indicating the overshadowing amounts of other minerals of clay size with the kaolin. Some peaks related to crystallized phase were also detected, which is attributed to quartz, and mica initially present in the kaolin. This is in line with the work of Francisca (2014).

Conclusion

Clay Samples from Naraguta deposit in Jos North Local Government Area of Plateau State were prepared and characterized using physical and chemical analysis. The results of the chemical analysis showed that kaolinite was the major components of the clay with the composition of silica (SiO_2), 49 – 51%; alumina (Al_2O_3), 31.494 – 33.301%; and other oxides. The bulk density, compressive strength and shear strength of the clay was stable at a temperature of 950^oC due to dehydroxylation of kaolin. It was found that the physical properties and chemical compositions of the clays are within the acceptable standard ranges for the manufacture of ceramics.

References

Abubakar I., Birninyauri, U.A., Faruq, U.Z., Noma, S.S and Sharif, N. (2014). Characterization of Dabagi clay deposit for its ceramic potential.*African Journal of Environmental Science and Technology*. 8 (8), 455 – 459.

Angelica, M.P. (2008); Mixtures of fine-grained minerals – kaolinite and carbonate grains; Clays and Clay Minerals 56(6):599-611 · December 2008

Aroke, U. O., El-Nafaty, U. A., andOsha, O. A. (2013).Properties and Characterisation of Kaolin Clay from Alkaleri, North-Eastern Nigeria. *International Journal of Emerging Technology and Advanced Engineering.3,* (11), 387-392. Retrieved from https://www.researchgate.net/.../281378945

Benea, M. And M. Gorea (2004) Mineralogy and Technological Properties Of Some Kaolin Types Used In The Ceramic Industry; Studia Universitatis Babeş-Bolyai, Geologia, Xlix, 1, Pg 33-39

3 EMMANUEL, E (2015) PRODUCTION OF CERAMIC PRODUCTS THROUGH SUSTAINABLE EXPLOITATION OF RICH CLAY DEPOSITS IN CROSS RIVER. *, CROSS RIVER WATCH*, 9

Francisca, U. N. (2014).Application Of Zeolite 4a – Metakaolin Matrix for the Removal of Some Heavy Metals from Crude Oil Tank Farm Wastewater. Zaria, Nigeria. Ph.DThesis.Ahmadu Bello University.Unpublised.

Hamisi (2014).Influence of Firing Temperature on Physical Properties of Same Clay and Pugu Kaolin for Ceramic Tiles Application .*International Journal of Materials Science and Applications.*Vol. 3, No. 5, 2014, pp. 143-146.

Ituma, C.G., Etukudoh, A.B., Abuh, M.A., Akpomie, K.G and Obioha, C.I. (2018). Utilization of Nkpuma-Akpatakpa clay in ceramics: characterization and microstructural Studies. *Journal of Applied Science, EnvironmentalManagement.*22 (1) 47-53

Jordan,M., A. Boix, T. Sanfeliu, and C. De la Fuente, "Firing transformations of cretaceous clays used in the manufacturing of ceramic tiles," *Applied Clay Science,* vol.14, pp. 225-234, 1999.

Kang, S.L. (2005) Densification, Grain Growth and Microstructure; in Sintering, Elsevier, Ltd, pg 3-8

Lydia, S.J., Alexander, A.J., Okon, E.E and Aliyu, J. (2018). Investigating the Industrial Potentials of Some Selected Nigerian Clay Deposits. *Journal of Minerals and Materials Characterization and Engineering*, 2018, 6, 569-586

Omowumi, O. J. (2001). Characterization of some Nigerian clay as refractory materials for furnace lining.Mineral Raw Materials Department, Federal Institute of Industrial Research, Ikeja, Lagos, Nigeria.

Ovat, F. A andBisong M. A. (2017). Assessment of the Industrial Potentials of some Nigerian Kaolinitic Clay Deposits.*European Journal of Engineering and Technology*. 5 (2) 48

Sousa, S. and J. Holanda, "Sintering Behavior of Porous Wall Tile Bodies During Fast Single-Firing Process," *Materials Research,* vol. 8, pp. 197-200, 2005.

Tiffo.E., Antoine, E., Joseph, D. M and Arlin, B.T (2015). Red Ceramics Produced from mixtures of Kaolinite clay and waste glass. *Brazilian Journal of Science and Technology*. 2:4

Omowumi O.J. (2000). Characterizatioin of some Nigerian clays as refractory materials for furnace lining*. Nigerian Journal of Engineering Management*. 1-4

Proceedings of the 49th NSChE Annual Conference
KADA 2019: pp 223-226

P1C-07: PHENOMENON OF OIL DISPERSED SYSTEM AND ITS INFLUENCE ON REFINING PROCESSES (2).

[1] C.S Ajimomoh; [1] O.R. Momoh; [2]M.K.Ogheaejobor; [1]M.S. Galadima
[1]Department of Chemical Engineering, Ahmadu Bello University, Zaria, Nigeria.
[2]Department of Chemical Engineering, Delta State University, Nigeria.
*Corresponding author: collinajinomo@yahoo.com, Tel: 07037251392, 08054516816

ABSTRACT
Oil samples were activated via ozone interaction, at specific ozone input of 1.1, 1.8, 4.3, 4.4 and 5.8g 0_3/kg feed, prior to distillation. It was observed that the optimal fractions obtained at ozone input of 4.4g/kg feed was 25.6 wt%, compare to 21.0wt% of raw sample. Mechanical vibration action was deployed in destroying oil interface barrier before distillation and the fractional yield was 52.8%. Storage yield of 61.4 wt% at vibration a duration of 45 minutes compare to raw sample of 52.8% yield. Storage of micro-wave activated oil sample prior to distillation favors the formation of heavy oil product such as light and heavy gas oil. All the methods of activating oil samples leads to reduction in formation of lighter hydrocarbon product during their distillation.

Keywords: Distillate Yield, Distribution, Fractions, Hydrocarbons, Interface, Oil Components

Introduction
Modern trend of oil refining focused on resolving the potential of resources through the studies of complex oil nature. Oil complex nature has been investigated by various scholars from various direction (Wenger, Speit, Pokonov, 1982, Krasnogorskaya, Andreeva, 1987). The most recent interpretation of the complex oil nature is the version of it paramagnetic properties. From oil colloidal point of view (Safeeva, 1998), that it consist of dispersed system of a continuous dissociation phase. The work (Wenger, Andreeva, 1995) emphasized much more on the homolytic dissociation theory of oil system.

The modern perspectives of oil nature constitute on the evidence of long-life free radicals exhibiting high spin interaction potentials, whose nature leads to changes in colloidal phase of the oil structure, (Lickterova et al 2005). Such periodic changes in the oil structure exposed it to further interactions (or pretreatment).

Various pretreatment on oil system has proved to effectively intensified its refining direction as reported, via methods of ozone interaction on oil (Lunin et al 2003, Ajinomoh 2016,), method of polar solvent dissolution prior to refining (Momoh *et al.*, 2011). In addition to the various physical and chemical pretreatments, the pretreated oil show some interesting anomalous in the result of the processed oil, (Ajinomoh *et al.*, 2015, 2012).

Methods
Series of independent experiments are conducted:
1. via ozone initiation- Ozonation or ozonolysis of oil residue (fraction > 350^0), at a specific ozone input of 1.5 till 5.8g 0_3/kg feed at 40 – 50^0c, in a fluidised reactor type, according to the method (Lunin et al 2003), then followed by thermolysis of the sample at 180^0C, for duration of 60 minutes at atmospheric pressure. Later, distillations are carried out at atmospheric and vacuum pressure for fractions, IBR – 180, 240 – 280, and 180 – 450^0c at vacuum pressure.

2. A domestic microwave (Model WM 224R) was modified for activating 89.3g of Ural crude oil at 560 watts; then part of the treated sample was stored for 1-6days and the remaining was fractionated (table3); later the stored sample was fractionated for the yield of fractions, IBP-180, 220- 240, 240–360^{0}C, (Ajinomoh et.al,2012,Abdullah et al.2010).
3. Escravo crude oil was subjected to mechanical vibration pretreatment at a constant frequency of 450Hz for duration of 20, 30, and 45 minutes, before subjecting the samples to atmospheric distillation, (Ajinomoh el.al, 2010).

All the outcomes of the series of experiment are subjected to mass, IR-spectral analysis, octane rating analysis, elementary sulfur analysis.

Result and Discussion

The first service of experiment is presented in table1, it is observed that gasoline fraction appears after ozone treatment and increase proportionately with ozone input, the same scenario occurs with fraction 240 – 350^{0}C.

In the next series of experiment (effect of vibration Table 2, for oil sample, Escravors), a remarkable increment in yield for fractions up till 350^{0}C was recorded. From the analysis, there are noticeable distribution of hydrocarbon component toward heavy hydrocarbon chain. But in the case of microwave activation and subsequent storage, it is was observed that there is partial increment, but on storage the yield in fractional yield decrease; and this can be trace to the process of recombination of hydrocarbon components after activation.

Conclusion

1. Pretreatment of oil sample via ozonation leads to increase in yield of fractions.
2. Mechanical activation leads to higher yield of lighter fractions.
3. Microwave radiation lead to fractured yield but on storage reduces the yield.
4. Applying all the three forms of activation there are drastic reduction in $C_1 – C_4$

Table 1. Fractions obtain before and after ozonation treatment

Fractions, ^{0}C	**Yield, % wt**					
	Initial sample	**Number of sample**				
		1	**2**	**3**	**4**	**5**
		Specific ozone {input} g/O_3/kg feed				
		1.1	1.8	4.3	4.4	5.8
Up to 180	-	4.2	4.7	2.7	7.0	3.1
180 – 240	-	-	-	-	-	0.6
240 – 350	6.0	5.35	5.2	4.7	5.3	8.1
350 – 420	15.0	16.0	14.2	13.7	13.3	13.1
> 420 (Residue)	77.4	72.4	74.5	77.4	72.5	72.8
$\sum distillate$	21.0	25.7	24.1	21.1	25.6	24.9
Losses	1.6	1.6	1.4	1.5	1.9	2.3
Fraction increase	0	4.7	3.0	0.1	4.6	3.9

Table 2: Effect of vibration on the yield of fuel fractions from Escravos crude oil sample.

Fractions	Fractional yield, % wt			
	Non vibrated sample	Vibration duration, min		
		20	30	45
IBP – 180^{0}C	28.49	29.54	30.83	33.39
180 – 240^{0}C	16.21	16.38	16.54	17.37
240 – 360^{0}C	8.09	9.55	10.42	10.64
> 360^{0}C (Res.)	41.08	38.66	36.91	33.46
Losses (C_1 – C_5)	6.13	5.88	5.31	5.13
Fraction	52.79	55.47	57.79	61.40
Increase	0	5.08	9.47	16.31

Table 3 Fractional yield, % wt from Ural crude oil sample before activation and after activation and storage

Fraction, ^{0}C	Fractional yield before activation, after activation and storage % wt.							
	Before activation	0day	1day	2 days	3 days	4days	5 days	6 days
Up to 180	12.458	19.792	18.542	17.914	16.771	16.667	16.617	16.594
180 – 245	15.563	18.229	15.844	15.073	15.638	15.429	15.221	15.104
245 – 345	25.000	25.521	24.927	25.292	25.646	25.753	26.047	26.047
345 – 360	9.271	8.333	9.531	9.958	9.958	10.053	10.282	10.262
>360	37.396	27.604	31.146	30.719	31.258	31.577	31.588	31.785
Losses C_1 – C_5	0.313	0.521	1.016	1.041	0.729	0.521	0.245	0.208

References

Ajinomoh C.S//Phd Dissertation. Physicio-chemical Methods of Activating Heavy Crude Oil Residue. Moscow Academic of Pure Chemical Technology. Moscow Russian. Pp. 105. 2005

Ajinomoh S.C. Ikpeamarize A.C. Hamza A, Igbagara P.W.// Effect of Storage Time in the Composition of Fuel Fractions of Micro-Waved Activated Heavy Crude Oil. Nigerian Society of Chemical Engineering 2012. Abuja.

Likhterova N.M, Lunin V.V, Torkhorvsky V.N., Fionov A.V, Ajinomoh S.C.// Imitation of Vis-Breaking Process of Bottom Oil by the Action of Election Irradiation. Russian Journal of Chemistry and Technology of Fuels and Lubricant Oil. 2005. V.5. 10-19 P.

Lunin V.V, Likhterova N.M., Torhovrsky V.N, Fionov A.V. Ajinomoh C. S. Ozone technology and heavy Oil Residue. Materials. 16th World Congress of International Ozone Association. Las Vegas USA 2003 p 1271-1289.

Mohammad A.D., Muhammad I.A., Ajinomoh S.C.Effect of microware dissertation on Heavy Petroleum and Based Distillate Yield. Journal of Nigerian Society of Chemical Engineers 26 (2). 2011. p 108-120.

Momoh O.R., Ahmad A.K, Mohammed. I.A, Ajinomoh C.S //Enhancement of Light Ends Recovery Through joint Atmospheric Distillation of Heavy Crude Oil and Used Engine Oil Nigerian journal of Engineering Sciences. 2011. P. 96-106.

Speit J. Pokonova Yu.V. Petro-Chemistry, 1982, V.55 N.P, P.3.

Wenger F.G, Andrew W.N., Fundamental Aspect of Oil Chemistry and Nature of Resin and Asphaltenes. Norosibirisk: Nauka Siberia Region, Russian Academy of Sciences 1995, P.192

Wenger F.G., Krasnogorskaya N.P, Andreva L.I/ Role of Paramagnetic Molecules in Inter- phacial Interaction if Oil Disputed System, Reprint N.P, Tomsk: Academic Science of Soviet Union, Tomsk Region. 1987. p. 46

Proceedings of the 49th NSChE Annual Conference
KADA 2019: pp 227-237

P1C-08: INFLUENCE OF SYNTHESIS METHODS ON TEXTURAL PROPERTIES OF CUZN/MCM-41

Opeoluwa O. Fasanya[a,b*], Abdulazeez Y. Atta[b], Kovo Abdulsalami[c], Baba Y. Jibril[b]
[a] Petrochemical and Allieds Department, Nat. Research Institute for Chemical Technology, Zaria.
[b] Department of Chemical Engineering, Ahmadu Bello University, Zaria
[c] Department of Chemical Engineering, Federal University of Technology, Minna
[*] **Corresponding author**: opefas@gmail.com

ABSTRACT
A series of CuZn/MCM-41 catalysts were synthesized by three different synthesis techniques; co-impregnation, serial impregnation and Copper impregnated MCM-41 with Zn in the framework. The preparation methods were found to greatly influence the physical-surface properties such as porosity, arrangement of pores and surface area, and pore volume. BJH data obtained from surface area analysis showed that the catalyst prepared by co-impregnation had the largest pore width of 5.1 nm, while that prepared by serial impregnation had the smallest pore width of 3.88 nm. The catalysts synthesized by serial impregnation however presented the largest surface area of 415 m^2/g while co impregnated and Zn- intra framework catalysts had surface areas of 284 and 246 m^2/g respectively. Scanning electron microscopy and Transmission electron microscopy micrographs were captured to study the morphology of the synthesized catalysts.

1.0 INTRODUCTION
Traditionally at laboratory scale, impregnation, co-precipitation, combustion synthesis, ion exchange and hydrothermal synthesis are some of the popular methods of catalyst synthesis. Understanding the effects of synthesis route on the final nature of an intended catalyst ensures that these catalysts can be engineered to improve properties such as surface area, pore volume, crystallinity, metal dispersion and many other factors which can affect activity, selectivity and stability of catalysts during reactions. The final properties of any catalyst is strongly affected by the route taken in preparing these materials. The method of synthesis (Das, Llorca, Dominguez, and Gayen, 2015; Hosseini, Haghighi, and Ajamein, 2016; Ning, Shen, and Liu, 2001), nature and morphology of support(Danwittayakul and Dutta, 2012, 2013; Nakajima, Lee, Lee, and Grigorpoulos, 2016), metal source(Qin, Liu, Qing, Hou, and Gao, 2017) and the addition of promoters(Agrell et al., 2003; Minaei, Haghighi, Jodeiri, Ajamein, and Abdollahifar, 2017; Sanches, Flores, Avillez, and Silva, 2012; Toyir, Ramírez de la Piscina, and Homs, 2015) have been explored by various groups in order to improve the activity of catalysts. The use of some external factors can also be applied to tweak the synthesis route such as sonication(Hosseini et al., 2016), use of microwaves(Ajamein and Haghighi, 2016), hydrothermal synthesis (Danwittayakul and Dutta, 2014), combustion synthesis and UV exposure(Danwittayakul, Lakshman, Al-Harthi, and Dutta, 2014). Thermal stability and surface area are greatly affected by the method of synthesis.

The importance of mesoporous materials in engineering cannot be overstated. Research and development in this class of nanostructured materials has witnessed enormous growth in recent times. This is due to the large surface areas, pore volumes and pore sizes which they possess(Morsi and Mohamed). MCM-41 is a mesoporous silica compound which can be synthesized by different methods. Since its discovery in the late 1980's(Kresge, Vartuli, Roth, and Leonowicz, 2004), it has been extensively investigated and utilized as catalyst support, adsorbent, hydrogen storage, drug delivery and for electronic and optical devices(Lin, Wong, Mou, and Tang, 2000). The large surface area; sometimes

up to 1000 m^2/g and tunable pore sizes make them an attractive material for many catalytic applications. Recently some of the catalytic applications of MCM-41 have included alcohol steam reforming for hydrogen production(Gunduz and Dogu, 2012; Kosaraju, Rahman, and Duncan, 2014), methanol production from carbon dioxide(Siriworarat, Deerattrakul, Dittanet, and Kongkachuichay, 2016), and synthesis of imidazoles(Shekouhy, Moaddeli, and Khazaei, 2017) to name a few.

The synthesis of MCM-41 has been conducted in a variety of ways. Each method altering properties such as pore size or the nature in which pores are ordered. The introduction of metals to the MCM-41 structure can cause significant changes to its textural properties. One of such properties is surface area and pore volume. Several reports have shown significant reduction in the surface area due to metal introduction (Abrokwah, Deshmane, and Kuila, 2016; Reddy, Davydov, and Smirniotis, 2002). In some investigations, reports have been made of significant alterations to crystallinity and also slight shifts in the characteristic d(100) peak of MCM-41 which can be observed by X-Ray Diffraction(Getle, Belay, Chandra Reddy, and Belay, 2017; Gunduz and Dogu, 2012; Kruk, Jaroniec, Kim, and Ryoo, 1999; La-Salvia, Lovón-Quintana, Lovón, and Valença, 2017). Bimetallic catalysts made of Cu, Zn and MCM-41 have been applied to numerous processes. Some of these include; acetylation hydration(Wang et al., 2018), synthesis of 6-substituted 2,4-diamino-1,3,5-triazines(Shekouhy, Moaddeli, and Khalafi-Nezhad, 2017; Shekouhy, Moaddeli, and Khazaei, 2017), as a catalyst for the reduction of NO(Imyen et al., 2016; Imyen et al., 2019) and also for the hydrogenation of CO_2(Siriworarat, Deerattrakul, Dittanet, and Kongkachuichay, 2017).

Investigations into the effect of some synthesis techniques have revealed better ways to engineer materials especially in the aspect of chemical catalysis. In comparing the properties of Pd-Cu-Zn/MCM-41 prepared by flame spray pyrolysis(FSP) and sol-gel methods, Siriworarat and co-workers reported more spherical shapes and lower surface area in the catalysts prepared by FSP(Siriworarat et al., 2016). The effect of synthesis technique of production Mn-MCM-41 for alkene epoxidation has also been reported(Qi et al., 2014). The authors showed the physical and chemical variations between the catalysts synthesized by wet impregnation, template ion exchange, direct hydrothermal methods and *in situ* reduction methods.

In this paper, the effect of three synthesis methods on some textural properties of CuZn/MCM-41 is presented. Three sets of catalysts were synthesized by co impregnation, serial impregnation and Zn-intra framework synthesis. The same amount of metal precursors was used in the synthesis of these catalysts. The catalysts were characterized by surface area analysis, X-Ray Diffraction(XRD), X-Ray Fluorescence(XRF), Scanning electron microscopy(SEM), and Transmission Electron Microscopy(TEM).

2.0 MATERIALS AND METHODS

2.1 Materials

Cetyl TrimethylAmmonium Bromide (BDH), Zinc Nitrate (BDH), Copper Nitrate (BDH), tetraethylorthosilicate (Sigma Aldrich) and ammonium hydroxide(BDH) were used for the synthesis of CuZn/MCM-41 catalysts.

2.2 Catalyst Synthesis

To synthesize MCM-41, 2.2g of the surfactant; Cetyl Trimethyl Ammonium Bromide (CTAB) was dissolved in water and stirred for 30 minutes till a clear solution was formed. 11.6g of Ammonium hydroxide was then added to the mixture and it was further stirred for another thirty minutes. 8.66g of TEOS was then added drop-wise to the solution and stirred for 6 hours. The solution was then aged for 48 hours at 110 ^{o}C. The precipitate was filtered and washed thoroughly with deionized water after which it was dried overnight at 95 ^{o}C. The dried powder was then calcined at 550 ^{o}C for 6 hours at a heating rate of 1 ^{o}C/min to completely remove all traces of CTAB.

For the co-impregnation the required concentration of copper nitrate solution and zinc nitrate solution was simultaneously added to a solution of MCM-41 and heated at a temperature of 70 ^{o}C while being stirred. The solution was heated at this temperature till all the water evaporated. The resulting powder was dried overnight at 95 ^{o}C after which calcination was carried out at 550 ^{o}C for 6 hours. For serial impregnation, a solution of zinc nitrate was added to a solution of MCM-41 at 70 ^{o}C. Stirring and heating continued at this temperature until dryness was achieved. The powder was then dried overnight at 95 ^{o}C to remove water trapped within the pores of the powder after which it was calcined for 6 hours at 550 ^{o}C. The calcined powder was then dissolved in deionized water and a solution of copper nitrate was added to the mixture while it was heated and stirred at 70 ^{o}C till dryness. After drying overnight at 95 ^{o}C the powder was also calcined at 550 ^{o}C for 6 hours.

The procedure of synthesis of Zn- intra framework was somewhat different. Zinc metal nitrate was also added to the liquor during MCM-41 synthesis. Ageing, drying and calcination of the resulting powder was carried out at the same conditions as stated in previous paragraphs, Copper was then introduced via impregnation and subsequently calcined after drying overnight. For all the catalysts, a copper concentration of 9% and Zinc concentration of 3% was used in synthesis.

2.3 Catalyst Characterization

The crystalline structure properties of the synthesized catalysts were evaluated using a Rigaku MiniFlex300 XRD analyser. Scans were taken at room temperature with two theta values ranging between 2 and 80 degrees with radiation source operating at 30kv and 30 mA. The average crystallite size were estimated using the Scherrer equation from main diffractions of d(100). N_2 adsorption-desorption measurements were conducted on a ASAP 2420 surface area and porosity analyser at 77K. X-ray fluorescence was carried out using a hand held Niton^{TM} XL3t analyser. The surface areas were calculated by BET method and BJH method was used for analysis of pore analysis. SEM micrographs were captured using JEOL JSM-6301F field emission scanning electron microscope. While TEM images were captured using JEOL JEM-2100Plus transmission electron microscope.

3.0 RESULTS AND DISCUSSION

The three synthesized catalysts exhibited type IVa isotherms with H4 hysteresis loops based on IUPAC classification(Thommes et al., 2015) when subjected to surface area analysis as seen in Figure 1. These isotherms are typical of MCM-41(Gunduz and Dogu, 2012; Kosaraju et al., 2014; Selvaraj, Pandurangan, and Sinha, 2004) and other mesoporous materials. The H4 hysteresis loops are indicative of narrow slit pores and possibly irregular shaped and interconnecting pores. Previous work has shown that MCM-41 is typically characterized by H1 hysteresis loop(Morsi and Mohamed). The deviation from this can be attributed to defects which were introduced into the

structure during synthesis. The defects are meant to create channels between the pore network so as to facilitate transport of reacting species when used as a catalyst.

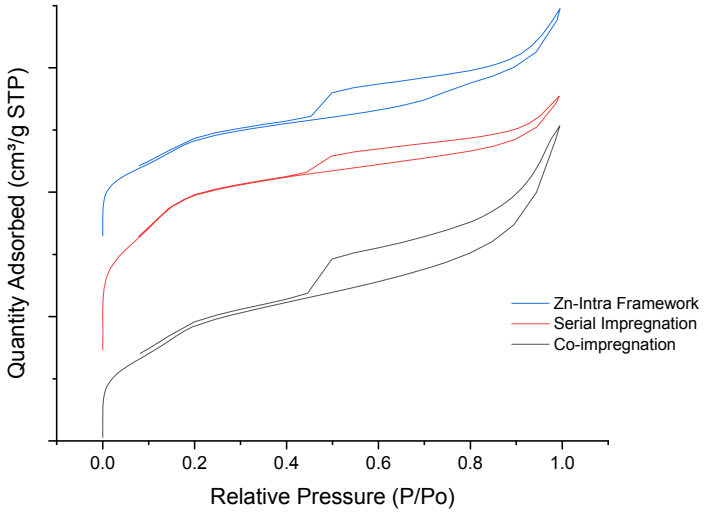

Figure 1 Adsorption desorption isotherms of synthesized CuZn/MCM-41

The shape of the hysteresis loops is often a good indicator as to the presence of defects which could be caused by the amount of water used during synthesis of the MCM-41(Lin et al., 2000). The H4 loops are also indicative of the presence of micropores within the structure(Oliveira and Andrada, 2019). It is observed that all three isotherms exhibit different widths of hysteresis loops. The variation in width points to differences in the diameter of the pores. The width of the hysteresis loop is indicative of dimensions of the pore diameter suggesting that the catalyst synthesized by co-impregnation has the largest pore size, while serial impregnation has the smallest size. The correlation between the hysteresis loop width and pore diameter is confirmed in Table 1 and Figure 2 where the co-impregnated catalyst had an average pore size of 5.1 nm. The pore diameter is also directly proportional to the pore volume as also shown in Table 1.

Table 1 Textural properties of synthesized catalysts

	pore width (nm)[a]	BET surface area (m^2/g)	pore volume (cm^3/g)[b]	d-spacing[c]	a_0(unit cell parameter)[c]	Cu/Zn[d]	Cu Crystallite size[c]
Zn-Intra Framework	4.29	246	0.238	34.75	4.01	6.63	23.23
Co Impregnation	5.1	284	0.359	33.95	3.92	3.15	25.19
Serial Impregnation	3.88	415	0.214	37.75	4.28	3.70	34.15

[a]BJH desorption average pore diameter [b]BJH desorption pore volume [c]calculated from XRD [d]Obtained from XRF

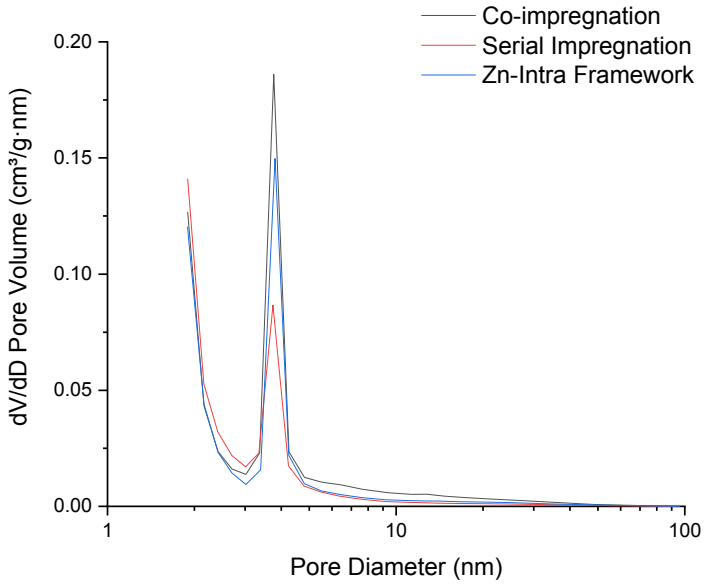

Figure 2 pore size distribution for the synthesized CuZn/MCM-41 catalysts

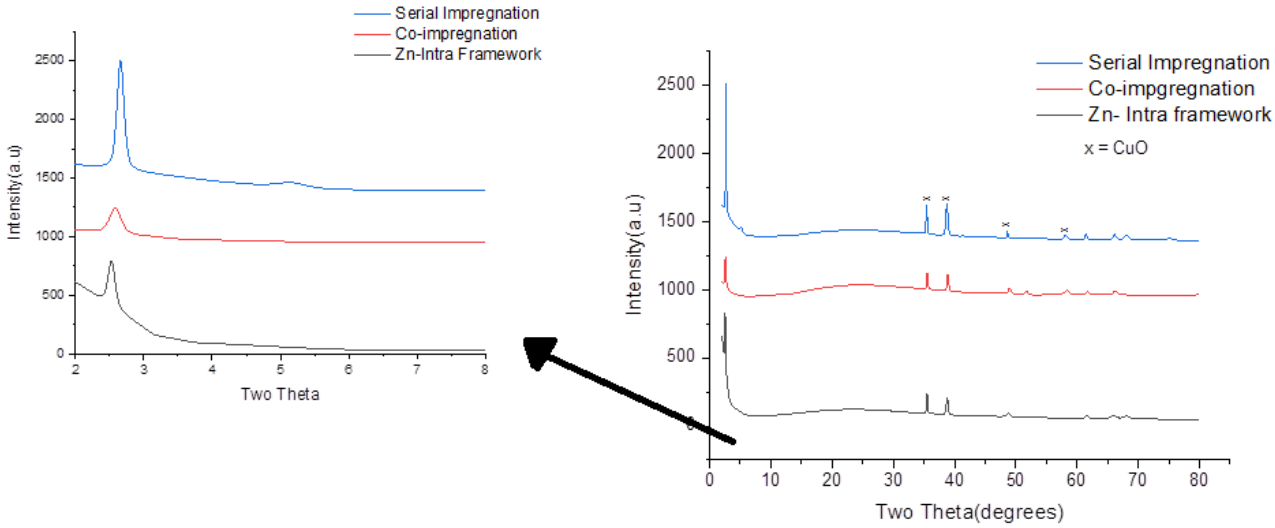

Figure 3 XRD patterns of the synthesized CuZn/MCM-41 catalysts

The patterns recorded show that all catalysts exhibit a sharp peak between 2 and 3 theta which is characteristic of MCM-41(Gunduz and Dogu, 2012). This peak is related to the d(100) diffraction plane. The position of this peak allows for the determination of the center-center distance between two adjacent tubes a_0 within the MCM-41 structure(Costa et al., 2014) as given in Equation (1) and (2). Table 1 shows the computed values for a_0 and d.

$$a_0 = \left(2/\sqrt{3}\right)d \quad - \qquad (1)$$

The intensities of the peaks however vary suggesting that the method of synthesis invariably has altered the structure of the final powder. The catalyst, Zn- Intra framework deviates the most from typical MCM-41 patterns. This means that the presence of Zn in the synthesis broth has altered the structure of MCM-41 somewhat. The least altered pattern is that prepared by serial impregnation. It is possible that the initial impregnation by Zinc and subsequent calcination at 550 ^{o}C may have resulted in a protective coating around the MCM-41 partially filling and sealing off pores. This can be observed in the SEM micrographs in Figure 4b. The elemental analysis carried out via XRF showed close proximity to the targeted Cu:Zn ratio of 3 for both coimpregnation and serial impregnation. The larger ratio observed for Zn- intra framework suggests that not all of the zinc found its way into the framework of MCM-41 during synthesis.

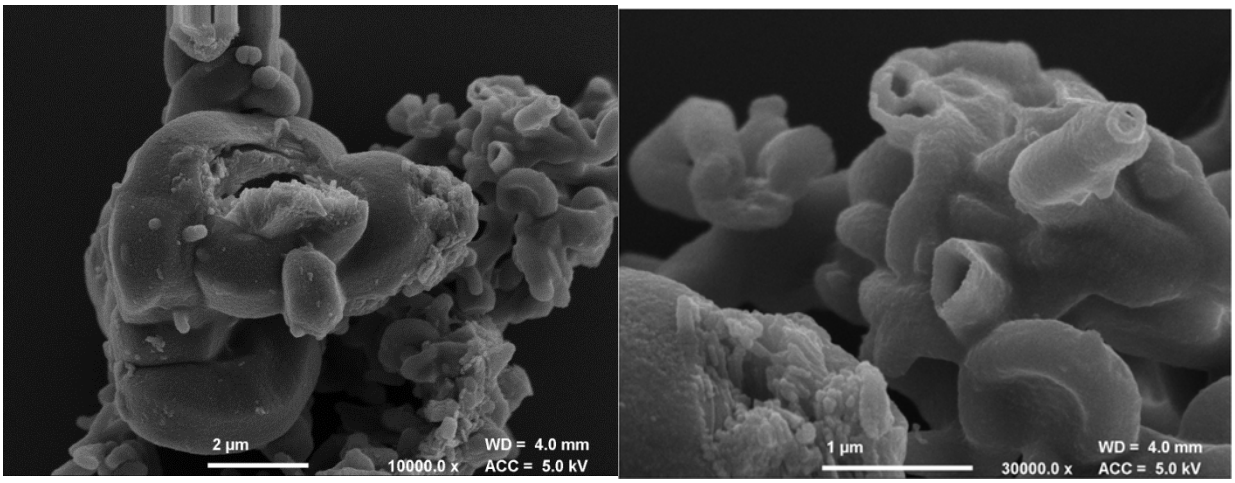

4a) SEM micrographs of CuZn/MCM-41 Catalysts synthesized by co-impregnation

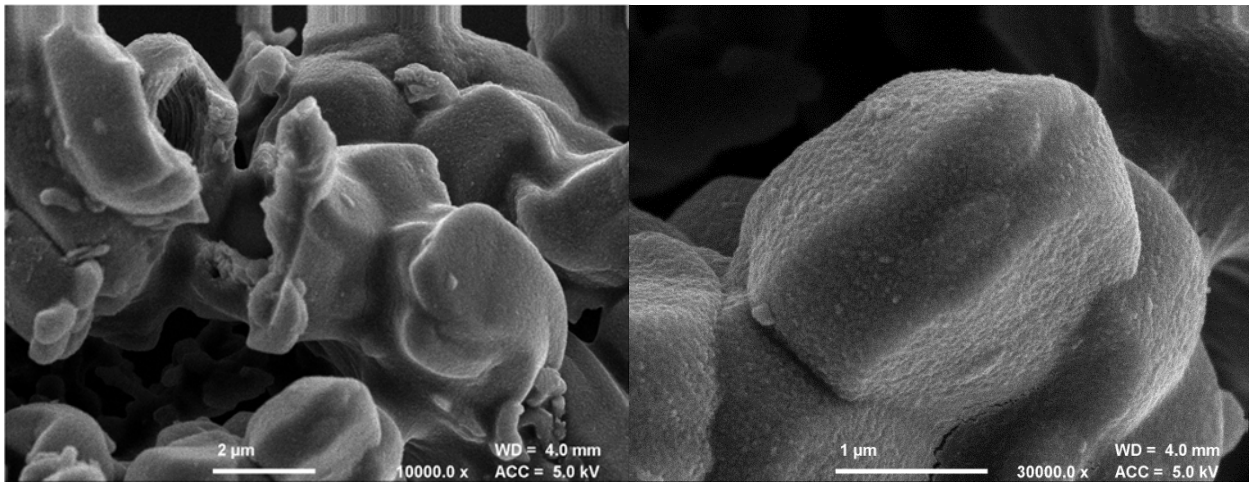

4b) SEM micrographs of CuZn/MCM-41 Catalysts synthesized by serial impregnation

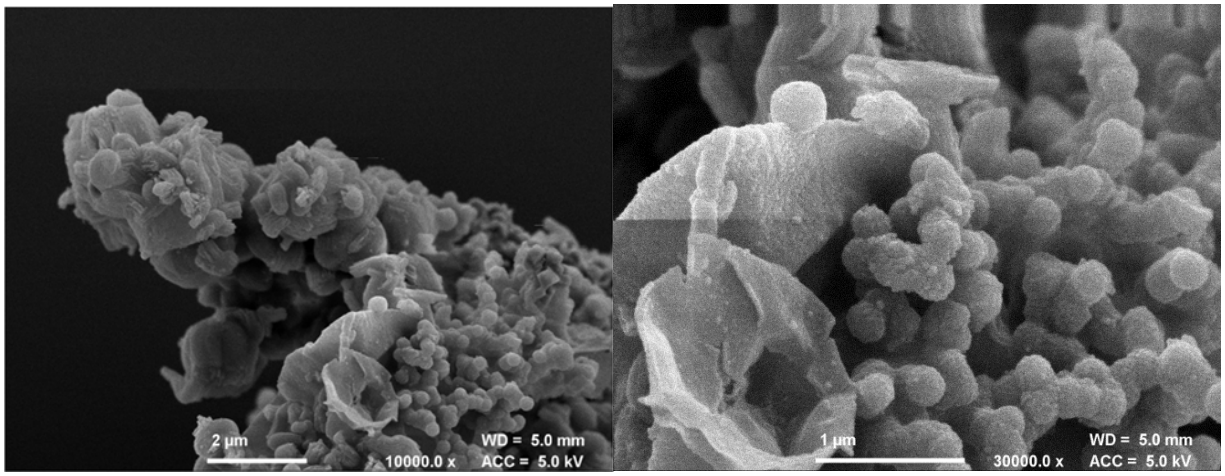

4c) SEM micrographs of CuZn/MCM-41 Catalysts synthesized by Zn- Intra frame work synthesis

The SEM micrographs presented in Figure 4 show the differences in the morphology of catalysts synthesized by the three different routes. Catalysts prepared by co-impregnation and serial impregnation shown in Figures 4a and 4b are relatively similar in nature. They are both characterized by relatively smooth surfaces with large "chunks" of particles. It is however observed that Figure 4a exhibits the presence of tunnel like structures twisted together. The catalysts prepared by serial impregnation on the other hand do not show such properties to the same degree. This is possibly as a result of zinc melting at 550 ^{o}C and filling up or blocking most of the pores. This postulation is in agreement with the pore width presented in Table 1 and Figure 2 acquired from surface area analysis. The catalyst synthesized by the Zn- Intraframe work method deviates strongly from the other two. It is characterized by small ball-like agglomerations scattered all over the surface.

The TEM micrographs shown in Figure 5 support the data shown in the XRD patterns in Figure 3. In Figures 5a and 5b representing co-impregnation and serial impregnation respectively, the ordered arrays which are characteristic of MCM-41 can be seen. For co-impregnation, it is observed in the bottom right of the image while the patterns are more visible in Figure 5b for serial impregnation. This agrees with the XRD patterns which showed that serial impregnation had the least deviation from typical MCM-41 patterns. Whilst in the co-impregnation a suppression of the d(100) peak was observed. The Cu and Zn metals could be observed as they were below the detection limit of the machine.

The TEM micrograph for Zn- Intra framework did show the typical hexagonal pore like structure of MCM-41. Even though the arrays could not be observed in the structure it is highly probable that the introduction of Zn in the synthesis liquor disrupted the formation of ordered arrays.

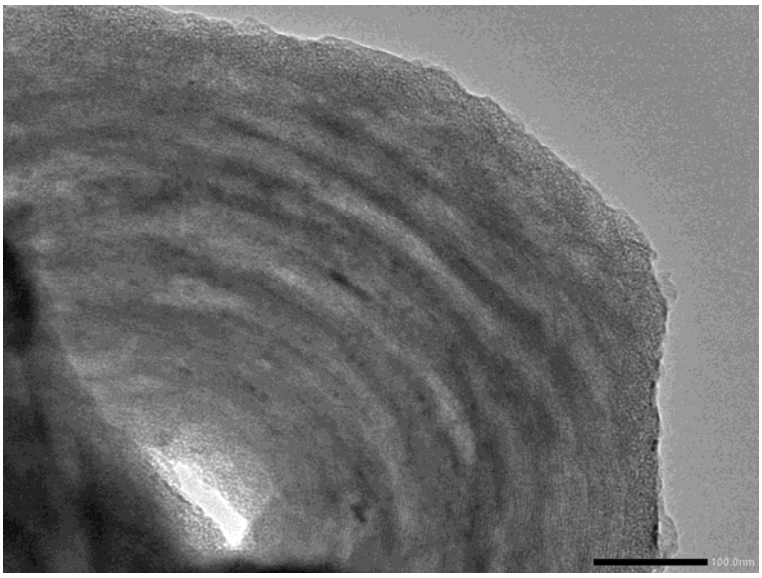

Figure 5a TEM micrograph of CuZn Co-impregnated MCM-41

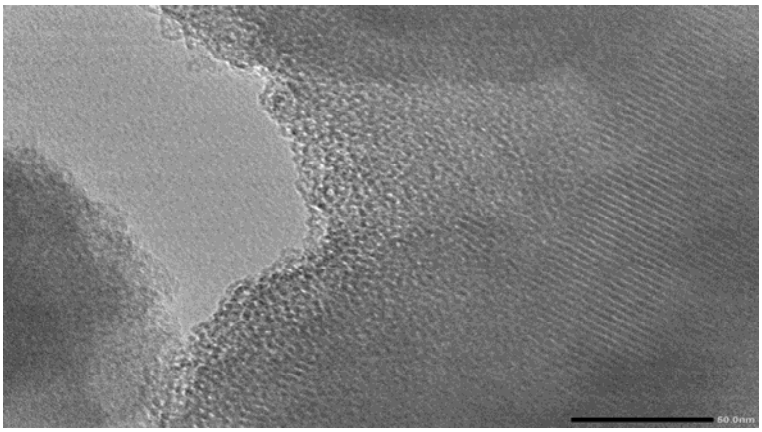

Figure 5b TEM micrograph of Serial impregnated CuZn/MCM-41

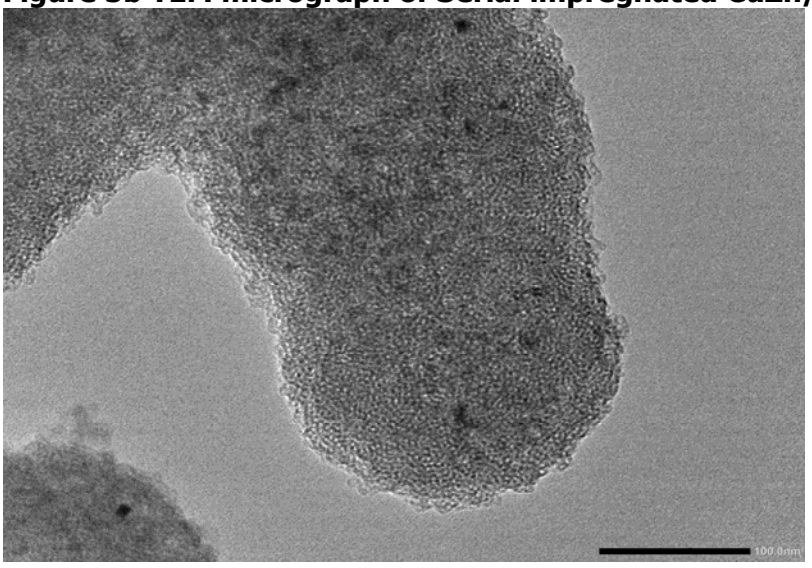

Figure 5c TEM micrograph of copper impregnated Zn-intra framework MCM-41

4.0 CONCLUSION

CuZn/MCM-41 catalysts were successfully synthesized by three different routes. Characterization of the samples revealed marked differences between all three catalysts. The catalysts prepared by co-impregnation had the largest pore size and subsequently pore volume as shown by BJH data obtained from surface area analysis. While the catalyst prepared by serial impregnation deviated the least from typical MCM-41 structure as revealed by TEM micrographs and XRD analysis. The presence of large pore size makes the catalyst prepared by co-impregnation suggests that it will have better performance when used as a catalyst. The larger pore sizes will allow for reduced effect of intracrystalline diffusivity.

REFERENCES

Abrokwah, R. Y., Deshmane, V. G., and Kuila, D. (2016). Comparative performance of M-MCM 41 (M: Cu, Co, Ni, Pd, Zn and Sn) catalysts for steam reforming of methanol. *Journal of Molecular Catalysis A: Chemical, 425*, 10-20.

Agrell, J., Birgersson, H., Boutonnet, M., Melián-Cabrera, I., Navarro, R. M., and Fierro, J. L. G. (2003). Production of hydrogen from methanol over Cu/ZnO catalysts promoted by ZrO_2 and Al_2O_3. *Journal of Catalysis, 219*(2), 389-403. doi:https://doi.org/10.1016/S0021-9517(03)00221-5

Ajamein, H., and Haghighi, M. (2016). On the microwave enhanced combustion synthesis of CuO–ZnO–Al_2O_3 nanocatalyst used in methanol steam reforming for fuel cell grade hydrogen production: Effect of microwave irradiation and fuel ratio. *Energy Conversion and Management, 118*, 231-242. doi:http://dx.doi.org/10.1016/j.enconman.2016.04.002

Costa, J. A. S., Garcia, A. C. F. S., Santos, D. O., Sarmento, V. H. V., Porto, A. L. M., Mesquita, M. E. d., and Romão, L. P. C. (2014). A new functionalized MCM-41 mesoporous material for use in environmental applications *Journal of the Brazilian Chemical Society, 25*, 197-207.

Danwittayakul, S., and Dutta, J. (2012). Zinc Oxide nanorods based catalysts for hydrogen production by steam reforming of methanol. *International Journal of Hydrogen Energy, 37*, 5518-5526.

Danwittayakul, S., and Dutta, J. (2013). Two step copper impregnated zinc oxide microball synthesis for the reduction of activation energy of methanol steam reformation. *Chemical Engineering Journal*(223), 204-308.

Danwittayakul, S., and Dutta, J. (2014). Controlled growth of zinc oxide microrods by hydrothermal process on porous ceramic supports for catalytic application. *Journal of Alloys and Compounds, 586*, 169-175.

Danwittayakul, S., Lakshman, K., Al-Harthi, S., and Dutta, J. (2014). Enhanced hydrogen selectivity via photo-engineered surface defects for methanol steam reformation using zinc oxide-copper nanocomposite catalysts. *Applied Catalysis A: General, 471*, 63-69.

Das, D., Llorca, J., Dominguez, M., and Gayen, A. (2015). Single step combustion synthesized $Cu/Ce_{0.8}Zr_{0.2}O_2$ for methanol steam reforming: structural insights from in situ XPS and HRTEM studies. *Catalysis, Structure and Reactivity, 1*(4), 174-182. doi:10.1080/2055074X.2015.1105616

Getle, S., Belay, A., Chandra Reddy, A., and Belay, Z. (2017). Synthesis and Characterization of Zinc Oxide Nanoparticels for Antibacterial Applications. *Journal of Nanomedicine and Nanotechnology, S8*(004).

Gunduz, S., and Dogu, T. (2012). Sorption-Enhanced Reforming of Ethanol over Ni- and Co-Incorporated MCM-41 Type Catalysts. *Industrial and Engineering Chemistry Research, 51*(26), 8796-8805. doi:10.1021/ie201852f

Hosseini, T., Haghighi, M., and Ajamein, H. (2016). Fuel cell-grade hydrogen production from methanol over sonochemical coprecipitated copper based nanocatalyst: Influence of irradiation power and time on catalytic properties and performance. *Energy Conversion and Management, 126*, 595-607. doi:http://dx.doi.org/10.1016/j.enconman.2016.07.056

Imyen, T., Yigit, N., Dittanet, P., Barrabés, N., Föttinger, K., Rupprechter, G., and Kongkachuichay, P. (2016). Characterization of Cu–Zn/Core–Shell Al-MCM-41 as a Catalyst for Reduction of NO: Effect of Zn Promoter. *Industrial and Engineering Chemistry Research, 55*(51), 13050-13061. doi:10.1021/acs.iecr.6b03990

Imyen, T., Yigit, N., Poo-Arporn, Y., Föttinger, K., Rupprechter, G., and Kongkachuichay, P. (2019). Promotional Effects of Zn Doping on Cu/Core Shell Al-MCM-41 for Selective Catalytic Reduction of NO with NH_3. *Journal of Nanoscience and Nanotechnology, 19*(2), 743-757. doi:10.1166/jnn.2019.15756

Kosaraju, K., Rahman, A., and Duncan, M., Tatineni, B., Basova, Y., Deshmane, V., Abrokwah, R., Hosseinnezhad, S., King, J., Ilias, S., Kuila, D. (2014). *Bimetallic nanocatalysts in mesoporous silica for steam reforming reactions to produce H_2 for fuel cells*. Paper presented at the 2013 International Conference on Future Energy, Environment, and Materials, FEEM 2013, Hong Kong; China. Conference Paper retrieved from

Kresge, C. T., Vartuli, J. C., Roth, W. J., and Leonowicz, M. E. (2004). The discovery of ExxonMobil's M41S family of mesoporous molecular sieves. In O. Terasaki (Ed.), *Studies in Surface Science and Catalysis* (Vol. 148, pp. 53-72): Elsevier.

Kruk, M., Jaroniec, M., Kim, J. M., and Ryoo, R. (1999). Characterization of Highly Ordered MCM-41 Silicas Using X-ray Diffraction and Nitrogen Adsorption. *Langmuir, 15*(16), 5279-5284. doi:10.1021/la990179v

La-Salvia, N., Lovón-Quintana, J. J., Lovón, A. S. P., and Valença, G. P. (2017). Influence of Aluminum Addition in the Framework of MCM-41 Mesoporous Molecular Sieve Synthesized by Non-Hydrothermal Method in an Alkali-Free System %J Materials Research. *20*, 1461-1469.

Lin, H.-P., Wong, S.-T., Mou, C.-Y., and Tang, C.-Y. (2000). Extensive Void Defects in Mesoporous Aluminosilicate MCM-41. *The Journal of Physical Chemistry B, 104*(38), 8967-8975. doi:10.1021/jp001569p

Minaei, S., Haghighi, M., Jodeiri, N., Ajamein, H., and Abdollahifar, M. (2017). Urea-nitrates combustion preparation of CeO_2-promoted $CuO/ZnO/Al_2O_3$ nanocatalyst for fuel cell grade hydrogen production via methanol steam reforming. *Advanced Powder Technology, 28*(3), 842-853. doi:https://doi.org/10.1016/j.apt.2016.12.010

Morsi, R. E., and Mohamed, R. S. Nanostructured mesoporous silica: influence of the preparation conditions on the physical-surface properties for efficient organic dye uptake. *Royal Society Open Science, 5*(3), 172021. doi:10.1098/rsos.172021

Nakajima, H., Lee, D., Lee, M.-T., and Grigorpoulos, C. P. (2016). Hydrogen production with CuO/ZnO nanowire catalyst for a nanocatalytic solar thermal steam-reformer. *International Journal of Hydrogen Energy*(41), 16927-16931.

Ning, W., Shen, H., and Liu, H. (2001). Study of the effect of preparation method on CuO-ZnO-Al_2O_3 catalyst. *Applied Catalysis A: General, 211*(2), 153-157. doi:http://dx.doi.org/10.1016/S0926-860X(00)00871-1

Oliveira, D. M., and Andrada, A. S. (2019). Synthesis of ordered mesoporous silica MCM-41 with controlled morphology for potential application in controlled drug delivery systems %J Cerâmica. *65*, 170-179.

Qi, B., Lou, L.-L., Wang, Y., Yu, K., Yang, Y., and Liu, S. (2014). Comparison of different prepared Mn-MCM-41 catalysts in the catalytic epoxidation of alkenes with 30% H2O2. *Microporous and Mesoporous Materials, 190*, 275-283. doi:http://dx.doi.org/10.1016/j.micromeso.2014.02.018

Qin, F.-j., Liu, Y.-j., Qing, S.-j., Hou, X.-n., and Gao, Z.-x. (2017). Cu-Al spinel as a sustained release catalyst for H_2 production from methanol steam reforming: Effects of different copper sources. *Journal of Fuel Chemistry and Technology, 45*(12), 1481-1488. doi:https://doi.org/10.1016/S1872-5813(17)30065-8

Reddy, E., Davydov, L., and Smirniotis, P. (2002). Synthesis and characterization of TiO_2 loaded Cr-MCM-41 catalysts. *Studies in Surface Science and Catalysis - STUD SURF SCI CATAL, 141*, 487-494. doi:10.1016/S0167-2991(02)80580-8

Sanches, S. G., Flores, J. H., Avillez, R. R. d., and Silva, M. I. P. d. (2012). Influence of preparation methods and Zr and Y promoters on Cu/ZnO catalysts used for methanol steam reforming. *International Journal of Hydrogen Energy, 37*, 6572-6579.

Selvaraj, M., Pandurangan, A., and Sinha, P. K. (2004). Comparison of Mesoporous Zn−Al−MCM-41 and Al−MCM-41 Molecular Sieves in the Production of p-Cymene by Isopropylation of Toluene. *Industrial and Engineering Chemistry Research, 43*(10), 2399-2412. doi:10.1021/ie0340084

Shekouhy, M., Moaddeli, A., and Khalafi-Nezhad, A. (2017). A novel one-pot three component approach to 6-substituted 2,4-diamino-1,3,5-triazines using nano-sized copper/zinc-modified MCM-41 (Cu/Zn-MCM-41) as a new heterogeneous mesoporous catalyst. *Journal of Industrial and Engineering Chemistry, 50*, 41-49. doi:https://doi.org/10.1016/j.jiec.2017.01.001

Shekouhy, M., Moaddeli, A., and Khazaei, A. (2017). *Nano-sized Cu/Zn-modified MCM-41 (Cu/Zn-MCM-41): preparation, characterization and catalytic application in a new more atom efficient synthesis of tetrasubstituted imidazoles* (Vol. 25).

Siriworarat, K., Deerattrakul, V., Dittanet, P., and Kongkachuichay, P. (2016). Production of Methanol from carbon dioxide using palladium-copper-zinc loaded on MCM-41: Comparison of catalysts synthesized from flame spray pyrolysis and sol-gel method using silica source from rice husk ash. *Journal of Cleaner Production, 142*. doi:10.1016/j.jclepro.2016.07.099

Siriworarat, K., Deerattrakul, V., Dittanet, P., and Kongkachuichay, P. (2017). Production of methanol from carbon dioxide using palladium-copper-zinc loaded on MCM-41: Comparison of catalysts synthesized from flame spray pyrolysis and sol-gel method using silica source from rice husk ash. *Journal of Cleaner Production, 142*, 1234-1243. doi:https://doi.org/10.1016/j.jclepro.2016.07.099

Thommes, M., Kaneko, K., Neimark Alexander, V., Olivier James, P., Rodriguez-Reinoso, F., Rouquerol, J., and Sing Kenneth, S. W. (2015). Physisorption of gases, with special reference to the evaluation of surface area and pore size distribution (IUPAC Technical Report). In *Pure and Applied Chemistry* (Vol. 87, pp. 1051).

Toyir, J., Ramírez de la Piscina, P., and Homs, N. (2015). Ga-promoted copper-based catalysts highly selective for methanol steam reforming to hydrogen; relation with the hydrogenation of CO2 to methanol. *International Journal of Hydrogen Energy, 40*(34), 11261-11266. doi:http://dx.doi.org/10.1016/j.ijhydene.2015.04.039

Wang, Q., Zhu, M., Xu, C., Zhang, H., Wang, X., Dai, B., and Zhang, J. (2018). Zn–Cu bimetallic catalysts supported on pure silica MCM-41 for acetylene hydration reaction. *New Journal of Chemistry, 42*(8), 6507-6514. doi:10.1039/C8NJ00707A

Proceedings of the 49th NSChE Annual Conference
KADA 2019: pp 238 -245

P2A-01: SOLUTIONS TO ENERGY CHALLENGES IN AGRO ALLIED INDUSTRIES

Abubakar Aliyu Aliyu
National Metallurgical Development Center, Jos. (NMDC) Zaria Road Jos Nigeria.
Correspondence: abubakar.aliyu77@yahoo.com

ABSTRACT
This report examines the challenges of energy use and efficiency in Agro-allied industries and proffers possible solution in sustainable energy options across the sector. Focusing on and in unlocking greater energy efficiency within the sector. Energy demand across the sector is projected to grow steadily, both in agriculture and agro-allied industries. Increasing dependence on energy usage (mainly fossil fuels) throughout the entire Agricultural value chain raises concerns about the impact of high or variable energy prices on production costs, competitiveness, the final price of the product for the consumer, greenhouse gas emissions, as well as concerns about energy security.

1.0 INRODUCTION
Agro allied industries are industries, which depend on agriculture for their raw materials so as to operate successfully in the production of, finished goods that are useful to livestock and humans. Industries produce machineries and equipment for agricultural uses. Agriculture and industry compete for labour. Industries provide a large range of products that the rural dwellers (mostly famers) want to buy and produce agro-chemicals for agricultural uses e.g. pesticides, fertilizers, vaccines, and herbicides. Agriculture is a source of food for, consumption by man, feed for animals, and raw materials for agro-allied industries (Edoumiekumo and Audu, 2009; Oji-Okoro, 2011). Central Bank of Nigeria (2016) noted that agricultural sector's contribution to the gross domestic product in Nigeria is 24.18 percent. Over 70 percent of the informal sector jobs created in the Nigerian economy were related to rural agriculture. Most experts were also of the view economic sectors will not stand without the practice of agriculture. This is due to the fact that it is the major raw materials for the functioning of those sectors. The agro-allied industry is regarded as an extended arm of agriculture. Its development could help to stabilize and make agriculture more lucrative, thereby creating employment opportunities both at the production and marketing stages (NPCS, 2000). The importance of agriculture extends beyond the provision of food for man and animals, but also the provision of basic raw materials for industrial purpose, such that other products which are not directly utilized could be transform into usable materials.

Ajila (2014) further explained that the agro-allied industries bring about diversification and commercialization of agriculture and also enhance the income of farmers and create food surpluses. It is in this sense that the agro-industry is an important and vital part of the manufacturing sector in developing countries (NPCS, 2000). In the same line, Chengappa (2004) reported that agro-processing offers great scope for conversion of farm produce to consumer commodity and in the process, reduce wastage, increase shelf-life resulting in value addition and higher income transfer to the farmers from different classes of consumers as the processed commodities have wider market outlets. Developing agriculture is one of the means of developing the rural communities as it is the primary occupation of most people in the rural areas and a major source of national income for most African countries (Mahmood, 2011). Agro-allied industries have been viewed as a safety valve that needs to be built within rural areas to absorb surplus labour and provide relief to the problem of large scale unemployment. Thus, inadequate attention paid to the agro-processing sector in the past, puts both producer and the consumer at

a disadvantage and this hurts the economy of the country (Kachru, 2008). Rural dwellers stand to enjoy some benefits with the existence of agro-allied industries in the rural areas. The populace in the rural areas where the industries are sited begin to enjoy benefits such as availability of market for the rural farmers, this further increases their production level and thus generates more income with which the living conditions of the people can be improved. Besides the above benefits, they enjoy infrastructural amenities like good roads, water supply, electricity, schools, and hospitals. All of these benefits describe some of the impact of agro-allied industries on the rural dwellers. An impact analysis, according to Iheanacho (2012), can be carried out from three different approaches; the before and after approach, with and without approach, and the benchmark or set target approach. The focus of this study, however, is on the with and without approach which shows the comparison between areas where agro-allied industries are sited and areas that do not have agro-allied industries. There is therefore, a link between agriculture, agro-allied industries, and rural dwellers in that without agriculture, the agro-allied industry will not have the availability of resources to carry out it performance. The rural communities which constitute a greater percentage of the labour force in the agricultural sector also have an opportunity to increase their production because of the availability of a good market outlet brought about by the agro-industrial sector.

2.0 METHODOLOGY

In carrying out this study, the following methods were used to get information from the target industries:

i. On Spot Assessment and Inspection Visits were paid to the factory of selected companies for an —on the spot assessment. In doing this, the physical conditions of the factory units operations and other energy intensive units were inspected including the working environment. The problems that workers were having in each sub-division were also noted.
ii. Personal Interviews were conducted with some of the cadres and sections of the companies. This included the, administrative director/accountant, factory manager, heads of production, fabrication sub-divisional heads, etc. These were able to shed light on area of enquiry.

3.0 RESULTS AND DISCUSSION

The private sector and the government are paying increased attention towards the importance of energy efficiency due to growing awareness of the limitations of fossil fuels for sustainable productivity, of the implications of GHG emissions and of variable and rising energy prices on competitiveness and productivity. Indeed, energy efficiency is increasingly being recognized as one of the most important and cost-effective solutions to reduce GHG emissions and other important air pollutants (IEA, 2014a; Masanet et al., 2012). However important progress has been made by the private sector to improve energy efficiency in the agro-allied sector through innovation, investments in more efficient technologies and adoption of more energy-efficient management practices. But more is anticipated, and more can still be done.

3.1 Challenges

3.1.1 The challenge of Increasing Energy Usage.

Agricultural value chains are diverse and highly complex with many final products drawing on inputs from a variety of industries. The type of and the way energy is used in the Agriculture value chain can influence the extent to which the food system in a country will be able to support growth and productivity objectives in an environmentally sustainable manner. This is the case as energy is used throughout the entire processes involved: in the production of crops, fish,

livestock, and forestry products; in post-harvest operations; in food storage and processing; in food transport and distribution; and in food preparation. Moreover, energy contributes to the transformation and reuse of the various forms of by products and waste which the production process generates.

Agricultural product is a composite and perishable product and the amount of energy for processing it varies greatly from one product to another. Even when considering the same type of product, the Energy "cost" differs notably, reflecting changes on cultivation area, farming practices, efficiency of processing and storage, season of production and/or consumption, transportation needs, etc. Moreover, in most countries, supply chains have evolved in multi-stage production and processing operations with varying degrees of vertical and horizontal integration. In addition, the diversity of product-specific chains means that a precise accounting of energy consumed in the production is extremely challenging.

Most Agro-allied products have a specific life-cycle which involves a combination of direct energy use at specific stages of the cycle (e.g. drying process) plus indirect energy use related to the production of other intermediate inputs that ultimately go into a final product. The more complex a product life-cycle, the less adequate direct measures become in measuring total energy consumption. For example, with regard to the agro-allied industries, direct energy for production would include electricity, heating fuel and machinery fuel used in the production, grain drying, animal and animal production, heating/cooling of animal incubator, transportation of products and personal energy use . Indirect energy would consist of the energy consumed in the production, packaging and transport to the gate of fertilizers, pesticides, farm machinery and buildings (CAEEDAC, 2000).

3.1.2 The Challenge of Measuring Energy Usage

Tracking trends in energy efficiency and comparing the performance of countries is made challenging by the lack of a single indicator to measure energy efficiency levels and changes. Instead, in the energy balance for a given production process, a variety of indicators may serve and support energy efficiency analysis (IEA, 2014b). Possible indicators include: primary energy per area or per tone of agricultural product, or energy contained in the products divided by the energy consumed (OFAG, 2015). Although the area is often used as a denominator, the link between this variable and energy consumption is not very strong. For example, in the EU, energy use by agriculture per cultivation area in hectares was highest in the Netherlands, which is mainly due to intensive greenhouse farming.

The quantitative assessment of energy flows in Agriculture value chain systems is most often carried out following one of two approaches: the life cycle analysis (LCA) and the input-output (IO) accounting (Burney, 2001). These two approaches differ fundamentally in both the conception and the data inputs, and therefore it is not surprising that results often differ. From the variety of metrics it is clear that energy analysis has nevertheless not evolved into an exact science, and this explains the few comprehensive studies of any sector let alone one as complex as Agriculture value chain. Challenges and ultimately subjective decisions lay in determining boundaries, aggregating different forms of energy, and defining energy credits for by-products.
LCA, as a product-focused methodology, takes into consideration all energy inputs along the full production (and disposal) chain, wherever these occur and as such it isolates the direct and indirect energy requirements of specific products. All the steps involved in creating a certain product are analyzed, starting from raw material extraction and conversion, then manufacture

(process) and distribution, to the final use and/or consumption. LCA also includes re-use, recycling of materials, energy recovery and ultimate disposal. Interest in forms of LCA, particularly energy use and emissions, has recently increased as retailers attempt to develop consistent "energy foot printing" labels for their products.

LCA, however, needs detailed data on product "history" and is sensitive to the definition of the boundaries of the production system and to the methodology used for allocating the embodied energy among co-products or by-products. LCA remains challenging when applied to large economic sectors as apparently "similar" products can be enormously diverse in reality.

Numerous LCA studies have shown the cumulative energy intensity of food products (e.g. de Vries and de Boer 2010; Carlsson-Kanyama et al. 2003; Heller and Keoleian, 2000).6 However, when comparing across studies an important methodological caveat is the boundary of the analysis can often vary.

The I-O analysis is a tool that can be used to provide estimates of inputs (including energy) per unit of final product based on how various sectors of an economy are linked and exchange resources (including energy) and can provide very precise results down to a certain level of aggregation, taking into account direct and indirect contributions. Nevertheless, I-O needs to be complemented with exogenous data as far as process steps taking place outside the studied economic area are concerned. However, the accuracy of this approach is also dependent on the accuracy of input-output data, which are prone to become outdated. COM/TAD/CA/ENV/EPOC (2016)19/FINAL

3.1.3 Unpredictable Government Actions

There is high level of uncertainty and lack of confidence in government and its intentions in the business sector especially with the inability to predict government policy. Uncertainty basically rises as a result of the conflicting objectives of government agencies. For instance Federal Ministry Of Agriculture and Rural Development has the mandate of supervising farming activities and Federal Ministry of Industry oversees the Agribusiness Firms and large Industries. But because of inter-ministerial relations are almost nonexistent leading to implementation conflicts and this one reason for policy inconsistencies in the Nigerian agribusiness environment.

3.2 SUSTAINABLE ENERGY SOLUTIONS IN AGRO ALLIED INDUSTRIES

"Tackling the challenges of food security, economic development and energy security in a context of ongoing population growth will require a renewed andre-imagined focus on agricultural enhancement. Agriculture value chain can and should become the backbone of tomorrow's green economy. It's time to stop treating Agriculture value chain and energy as separate issues and tackle the challenge of intelligently balancing the needs of these two sectors, building on synergies, finding opportunities to reduce waste and identifying ways that can be shared and reused rather than competed for "Climate-smart systems that make efficient use of resources like water and energy must become the basis of tomorrow's agricultural economy .In practice, most of the technologies and other options needed for providing sustainable energy solutions in ago-allied industries already exist. The suggested measures have been described many times, and importantly, components of such system, have been available.

3.2.1 Energy Efficiency and Energy Conservation

Improving energy efficiency and energy conservation in agro-allied are essential to reduce energy demand and therefore reduce costs. Improving energy efficiency, and thus reducing reliance on fossil fuels, will further reduce greenhouse gas emissions. In addition, it must be taken into consideration that a reduced energy demand will also proportionally reduce investment costs for shifting from fossil fuels to sustainable energy sources. Everywhere in agriculture where energy is used, its demand can be reduced. For example, it has been shown that fossil energy use in the current food system could be significantly reduced by appropriate technology changes. It is estimated (Pimentel, *et al*., 2008) that the total energy in agricultural products production could be reduced by more than 50% with the following changes of practices: (i) using smaller machinery and less fuel; (ii) replacing commercial nitrogen with livestock manure and (iii) adopting alternative and conservation techniques. Pellizzi*et al*. (1988) showed that with improved management and operation, energy saving of around 12–15% of present consumption can be realistically obtained for agro-allied industrial machine. Brown and Elliot (2005) found that the largest energy savings are available in motorized systems, Pathakand Bining (1985) showed that in agricultural processes, fuel savings of over 50% were feasible through improvements in equipment and water management practices. It not only makes a significant contribution to global food production but it also contributes significantly to national economies.

3.2.2 Cooling and Heating

There is a considerable requirement for heating and cooling in agro-allied industries. For example, greenhouse heating may be essential to the year-round production of fertilizers, vegetables, fruit and disinfectant chemicals. Temperature controlled storage and refrigeration systems also consume large amounts of electricity and thereby contribute greatly to the running costs of businesses which have considerable cooling requirements, particularly in the horticulture and vegetable industry. Improvements to technical elements and operation of modern refrigeration systems have the potential to reduce energy consumption by 15–40%. This will become more important as a price is placed on greenhouse gas emission and as energy prices rise. Improved thermal insulation to reduce the costs of heating and cooling would result in reduced demand for energy, while the on-farm production of energy and can produce more energy than is needed. The energy efficiency of all electrical devices used in agriculture processing can also be continuously increased. For example, energy consumption in the lighting sector can be reduced by shifting to energy-saving appliances. At the same time, increasing temperature may reduce the need for heating in many places as well. These emissions could be eliminated where they stem from electricity generated from fossil fuels, if zero emissions electricity sources were to replace current infrastructure.

There are many agricultural production processes, the energy efficiency of which can further be Increased.

3.2.3 Use of biomass and Biomass Waste for Production of biofuel and Electricity.

Biomass can be produced by cultivating suitable crops and used for production of different types of biofuels. Bio-ethanol can be used to replace gasoline, and biogas to substitute natural gas. Biodiesel and pure plant oils can be produced from oil-rich plants. This biodiesel can substitute for fossil-fuel based diesel used in many agricultural processing activities and requires only minor changes to the diesel engines. These biofuels can also be used for electricity production, which is a very economic option, in particular in off-grid applications. Compared with biodiesel, pure plant oil can be easily produced without great technical effort. Older diesel engines, which are

often used in developing and transitioning countries to supply electricity, can often run without conversion with pure plant oils as fuel. However, modern diesel engines require technical conversions to befueled with pure plant oils (Fell, 2012).Therefore, biofuels can reduce the need for agricultural installations to purchase expensive fossil fuels, which must often be transported over long distances, and hence significantly reduce production costs.. An example is given by Fell (2012) from Brazil where annually 100 megatons of sugar is produced from about 1 gigaton of sugar cane. About 90% of the sugar cane crop is burned without any further use. Such biomass waste can be used either for biofuel production and, if needed, electricity. Alternatively, after converting it to bio-coal it can be use. All in all, such measures increase economic benefits and contribute to climate protection.

3.2.4 Decentralized Renewable Energy Systems (solar, wind, geothermal)

Many processes and applications in agro-allied industries require energy either in the form of heat, mechanical energy or electricity, which can be provided by solar, wind and/or geothermal energy, depending on the local sources and the specific application. For example, wind and solar energy can economically produce electricity to power off-grid machinery such as pumps for pumping of fluids; wind energy can also be used as mechanical energy for pumping; solar heat can be used directly for space heating/cooling and warm water production while solar and geothermal heat can economically power thermal water desalination and the treatment of agro-allied effluents. Electricity produced from wind and solar energy sources can also be used for water desalination using membrane technologies but at higher cost than thermal methods. Geothermal heat with temperature differences of a few degrees centigrade to the ambient temperature can be used through heat pumps for space heating/cooling. Depending on the temperature of the available resource, geothermal heat has many applications in agro-allied such as for dehydration of products, and heating for greenhouses. Biomass produced onsite can also provide an energy source as biofuel for machinery, as heat or as electricity produced from it.

3.2.5 Governments Have a Role to Play in Encouraging Energy Efficiency

Capturing economic incentives for efficiency improvements requires transparent energy pricing, information on opportunities to improve efficiency and investments in research and development. In these areas, governments have an important role to play. Governments can play a decisive role in boosting energy efficiency in the food-chain by putting in place appropriate business-enabling policies, in order to allow the private sector to realize its full potential. The key drivers of energy efficiency – namely investment and innovation – require the creation of enabling policy frameworks in which private sector-led and collaborative investment and innovation initiatives can thrive. This requires an approach in which policy coherence and partnerships with the private sector are key aspects.

The private sector response to the challenges of improving energy efficiency can be enhanced if firms are able to benefit from the business opportunities that this can create. However, there are many challenges to improving energy efficiency in the food-chain that can be identified. They include, among others, market distortions, lack of information, co-ordination and risk aversion elements. Energy efficiency in the agro-food chain also has to be considered alongside other factors that drive investment decisions such as new product development, market growth and production location decisions to meet those markets.

In addition, firms are likely to intensify their efforts to increase energy efficiency of food products if consumers respond by purchasing energy-efficient products. Greater government-led

awareness raising campaigns and knowledge sharing in all parts of the agro-food chain – including consumers, as well as the role of regulation and explicit or implicit taxes to internalize the external environmental effects of production and consumption decisions, are very important. Policy makers must bear in mind that improving energy efficiency may save less energy than expected due to a "rebound" of energy use and may, in some cases, actually lead to an increase in energy use. As energy consumers save on energy cost through energy efficiency, they may spend their savings on other energy-intensive activities, or increase their demand for the new service, thereby countering the potential savings of energy. For example, consumers buying more energy-efficient household appliances may then use them more frequently because they are cheaper to run (Gillingham, Rapson and Wagner, 2015; Sorrell and Dimitropoulos, 2008; Tollefson, 2011).

Further, policy makers must take into account that improving energy efficiency does not necessarily translate into reduced CO2 emissions: the savings depend on the type of energy. If the energy is supplied from fossil fuels, then improved efficiency will cut emissions. But if the energy is supplied by a low-carbon source such as renewable, then improving efficiency may have little impact on emissions.5 Nonetheless, improving energy efficiency overall is a key tool for reducing CO2 emissions, alongside energy conservation and low-carbon energy sources such as renewable, carbon capture and storage. Additionally, if reducing energy use is the policy goal, then energy efficiency is only one of a number of factors that impact energy use, and energy conservation may or may not be associated with an increase in energy efficiency – depending on the input-output relationship. This is, energy consumption may be reduced with or without an increase in energy efficiency, and energy consumption may increase alongside an increase in energy efficiency. COM/TAD/CA/ENV/EPOC(2016)19/FINAL

4.0 CONCLUSIONS

Agro-allied industries are typically highly reliant on fossil fuels and energy is a significant input cost to production. Production of food and other agricultural products accounts for 70% of global freshwater withdrawals. In addition, in the 2010–2035 periods, world primary energy demand is forecasted to rise by one-third and electricity demand by 70% increasing the cost of energy and production. Some of these demands will be met from bioenergy which will in turn intensify competition for resources, particularly water for food and fiber production and therefore the need to maximize the efficient use of these resources becomes increasingly important. As fossil fuel costs continue to increase, so does the focus on energy efficiency to help minimize the impacts of rising energy costs on profitability and competitiveness. This includes a growing number of renewable energy sources that could be considered as alternatives to fossil fuels. Renewable energy sources may include solar, wind, hydropower, biomass, biogas and geothermal power. Where the opportunities are appropriate, integrating renewable energies into the arming operations is likely to save energy, costs, and greenhouse gas emissions. Examples of specific applications include solar drying, solar space and water heating and using biomass for heating purpose and electricity generation. Other applications include wastewater treatment, communication and remote equipment operation and others. Overall, the long-term future for renewable energy is definitely positive, since the prices of fossil fuels will continue to rise as the resources are depleted while the prices of renewable energy will continue to decrease. There are already a good number of successful examples of application of alternative energy.

REFERENCES

Alexandratos, N. and Bruinsma, J(2013).World agriculture towards 2030/2050: the 2012 revision. ESA Working paper No. 12-03, Food and Agriculture Organization of the United Nations (FAO), Rome, Italy.

Antonietti, M., Murach, D. and Titirici, M.M.(2010).Opportunities for technological transformations: From climate change to climate management? In: H.-J. Schellnhuber (ed): Global sustainability*:* A nobel cause. Cambridge University Press, Cambridge, UK. pp. 319–330.

Barber, A. (2004).Seven case study farms: total energy and carbon indicators for New Zealand arable and vegetable production. Agrilink New Zealand Limited, Auckland, New Zealand.

Chen, G., Baillie, C. and Kupke, P.(2009). Evaluating on-farm energy performance in agriculture. Austral. J. Multi Discipl. Eng. 7: pp. 55–61.

Chen, G., Baillie, C, Eady, S. and Grant, T.(2013).Developing life cycle inventory for life cycle assessment of Australian cotton: Australian Life Cycle Assessment Conference.

EWG (Energy Watch Group).(2007). Crude oil:The supply outlook. EWG-Series http://www.energywatchgroup.org/fileadmin/global/pdf/EWG_Oilreport_10-20019

FAO (Food and Agriculture Organization of the United Nations).(2009) : How to feed the world in 2050. Food and Agriculture Organization of the United Nations, Rome, Italy, www.fao.org/fileadmin/ntemplates/wsfs/docs/expert_paper/How_to_Feed_the_World_in_2050.

Jochen, B. and Guangnan, C.(2018). Sustainable Energy Development:Sustainable Energy Solution in Agriculture. University of Southern Queensland Toowomba, Australia.: pp .3-13.

Organization For Economic Co-operation and Agriculture and Enviroment: Improving Energy Efficiency In the Agro-Food chain.pp.8-17.

Segun,F. and Barau, A.d. .Role of Agro-Industries in increasing food production in Nigeria

Proceedings of the 49th NSChE Annual Conference
KADA 2019: pp 246 - 258

P2A-02: SIMULATION OF PRESSURE SWING ADSORPTION SYSTEM FOR SEPARATION OF HYDROGEN FROM CATALYTIC REFORMING EFFLUENT GAS

***Eyitayo A. Afolabi and Israel I. Audu**
Department Of Chemical Engineering, Federal University Of Technology, Minna, Nigeria.
Corresponding author: elizamos2001@yahoo.com

ABSTRACT
A numerical simulation for the separation of hydrogen gas from effluent gas mixture in a catalytic reforming unit of Port Harcourt Refining and Petrochemical Company (PHRC) is presented for a basic two bed pressure swing adsorption (PSA) process. The model equations adopted involve partial differential equations (PDEs) in time and space with periodic boundary conditions that link the processing steps together. MatlabR 2014a software was then used to simulate the model equations and the simulation results validated with the experimental data obtained from the PSA system used for the separation of effluent gas mixture in Port Harcourt Refining and Petrochemical Company (PHRC). It was observed that the simulation results compared favourably. Based on the simulation results, the effect of adsorption pressure, cycle time, feed temperature and adsorption duration on hydrogen purity and recovery were investigated and optimum values of these process parameters proposed in order to maximize the product purity and recovery.

Keywords: Hydrogen, Simulation, Pressure Swing Adsorption, Catalytic Reforming, Effluent gas

Introduction
In chemical industry, an important unit operation is the purification and separation of hydrogen from gas mixtures by pressure swing adsorption and membrane technology (Al Ghafri, 2007). Four basis techniques for gas separation and purification in process technology are distillation and condensation, absorption, adsorption and diffusion. While distillation, condensation and absorption are often classified as traditional methods for gas separation, diffusion and adsorption are developing technologies in term of their commercial applications (Ruthven *et al.,* 1994; Ruthven, 1984). The demand for hydrogen is increasing day by day in various fields such as fuel cells, semi conductor processing and petrochemical industry (Whysall and Picioccro, 1998). This is mainly due to the fact that hydrogen is generally regarded as an ecologically clean and renewable energy source. In addition, there is an increase in demand of hydrogen as the world's consumption of refinery products increases with the ever growing industrialization (Sircar and Golden, 2000). Hydrogen can be recovered from steam reformers, dry reformers, tri-reformers, thermal crackers, catalytic crackers, ethylene plants etc. to satisfy the demand. Hydrogen-rich gas mixture produced via reforming or gasification contains 40-70% hydrogen and a variety of contaminants including carbon monoxide, carbon dioxide, nitrogen, methane, water, sulphur, and possibly tar and ash (Baksh and Ackley, 2002).

The need for alternatives to fossil fuel has been explored due to its environmental concerns in the last decades. For an alternative fuel to be acceptable, it has to be technically feasible, economically competitive, environmentally satisfactory and readily accessible. Many authors have suggested several alternative fuels such as hydrogen, biodiesel, natural gas, liquefied petroleum gas (LPG), solar fuels, electricity, methanol and ethanol. (James and Gleen, 2001; Jee *et al.,* 2001). Hydrogen possess some unique features that single it out among alternative fuel suggested and these include its availability in the universe, higher specific energy content when

compared with other fuels (Ankit *et al.,* 2010). Hydrogen is widely used in many chemical process industries as hydrocracking, hydrogenation of fats and oils, methanol production, manufacture of silicon (Cavenati, *et al.,* 2006).

The use of the Pressure swing adsorption (PSA) process has seen tremendous growth during the last two decades mainly due to its simplicity and low operating costs. Basically, a PSA system is made up of at least two beds alternately pressurized and depressurized according to a programmed system order. A number of modifications have subsequently been developed based on the Skarstrom cycle, vastly enlarging the area of practical applications of the process. From an operational point of view, PSA is an intrinsic dynamic process operating in a cyclic manner with each bed undergoing the same sequence of steps (Jee et al; 2001).

In the times past, several models have been developed and numerical simulation carried out with the sole aim of improving the efficiency of separation of hydrogen and enhancing its recovery. Tanczyk and Warmuzinski (1997) developed a model that incorporates the basic steps of PSA system in two- and multi-column installations for the separation of hydrogen gas from coke gas. In addition, the bed configuration is made up of two different layers of adsorbents and the PSA system used were connected in series. Tanczyk andWarmuzinski (1998) developed non isothermal, non equilibrium, and non adiabatic models for the separation of hydrogen gas using layered beds, PSA process. They compared their numerical simulation result with experimental profiles obtained from small scale PSA system. The performance of a pressure swing adsorption (PSA) system used for the separation and production of high purity hydrogen from a mixture of methane and hydrogen gases were simulated by Sircar (2000). He considered an adiabatic PSA model with activated carbon as the adsorbent used for the selective adsorption of methane over hydrogen. The influences of various process variables such as feed gas pressure and composition, purge gas pressure and quantity, configuration of process steps on the, hydrogen production capacity, hydrogen recovery and purity as the major dependent process variables are evaluated. The PSA system designed produced high pure hydrogen with the hydrogen recovery of about 74%.

Park *et al;* (2003) adopted a four bed PSA process for the purification of hydrogen from a typical cracked gas mixture. An ideal adsorbed solution (IAS) model was used to represent the multicomponent adsorption equilibrium and the simulation results include the effects of the superficial velocity and heat-transfer resistance on the process performance. Most of the other research works reported centered on application of more that 2 beds and 4 steps in the PSA system. This research paper aimed at simulation of the separation of hydrogen gas from the effluent gas of catalytic reforming process of Port Harcourt Refining and Petrochemical Company (PHRC) using Pressure swing adsorption (PSA) method. It is achieved by the following objectives. (1) selection of relevant model equations to represent flow behaviour of gas mixture in a PSA system from the literatures. (2) numerical simulation of a two bed, four steps PSA system for the separation of hydrogen gas from effluent gas using MATLAB software. (3) validation of the simulated results with the experimental data obtained from the separation of effluent gas mixture of catalytic reforming process of PHRC. (4) investigating the effects of total cycle time, adsorption pressure, feed flow rate and the product rate on the product purity and recovery of hydrogen gas in order to obtain their optimal values and maximize the product purity and recovery.

2.0 Methodology

2.1 Mathematical Models

The continuous adsorption/desorption of the adsorbate in the PSA system automatically make its processes transient. The operation of four steps PSA process is described by a set of partial differential equations, which require an appropriate solution procedure. In this work, a number of simplifying assumptions adopted is a nonisothermal model for two bed process operating with Skarstrom cycle were taken from the work of Yang *et al.,* 1998; Yang and Lee, 1997). These include;

a. Gas behaves as an ideal gas.
b. The flow pattern is described by axially dispersed plug-flow model.
c. Adsorbing properties throughout the tower would remain constant and unchanged.
d. Radial gradient is to be negligible.
e. The equilibrium relation is described by the Langmuir correlation
f. Mass transfer rate is expressed by linear driving force equation.
g. Thermal equilibrium between gas and solid phases is assumed.
h. Pressure drop along the bed is calculated by the Ergun's equation.

The flow through an adsorption column in a PSA system may be adequately represented by the axial dispersed plug flow model. Overall and component mass balances for the bulk phase over a differential volume element in the adsorption bed are (Mofarahi and Shokroo, 2013; Ankit *et al.,* 2010);

$$\frac{\partial C_i}{\partial t} - D_L \frac{\partial^2 C_i}{\partial z^2} + \frac{\partial (C_i . \mathcal{U})}{\partial z} + \rho_{\mathrm{P}} . \left(\frac{1-\varepsilon}{\varepsilon}\right) . \frac{\partial \bar{q}_i}{\partial t} = 0 \qquad (1)$$

$$\frac{\partial C}{\partial t} - D_L \frac{\partial^2 C}{\partial z^2} + \frac{\partial (C . \mathcal{U})}{\partial z} + \rho_{\mathrm{P}} . \left(\frac{1-\varepsilon}{\varepsilon}\right) . \sum_{i=1}^{N} \frac{\partial \bar{q}_i}{\partial t} \qquad (2)$$

When the ideal gas law ($C_i = y_i {}^{\mathrm{P}}/_{RT}$ and $C = {}^{\mathrm{P}}/_{RT}$) is applied to equations (1) and (2), the component and overall mass balances can be represented as follows,

$$- D_L \frac{\partial^2 y_i}{\partial z^2} + y_i . \frac{\partial \mathcal{U}}{\partial z} + \mathcal{U} \cdot \left(\frac{\partial y_i}{\partial z} + y_i . \left(\frac{1}{\mathrm{P}} \cdot \frac{\partial \mathrm{P}}{\partial z} - \frac{1}{T} \cdot \frac{\partial T}{\partial z} \right) \right) + \frac{\partial y_i}{\partial t} + y_i \left(\frac{1}{\mathrm{P}} \cdot \frac{\partial \mathrm{P}}{\partial t} - \frac{1}{T} \cdot \frac{\partial T}{\partial t} \right) + \left(\frac{\rho_{\mathrm{P}} . R . T}{P} \right) \cdot \left(\frac{1-\varepsilon}{\varepsilon} \right) \cdot \frac{\partial \bar{q}_i}{\partial t} = 0 \qquad (3)$$

$$\frac{\partial \mathrm{P}}{\partial t} + \mathrm{P} \frac{\partial \mathcal{U}}{\partial z} + \mathcal{U} \frac{\partial \mathrm{P}}{\partial z} + \mathrm{PT} . \left(\frac{\partial}{\partial t} \left(\frac{1}{T} \right) \mathcal{U} \frac{\partial}{\partial z} \left(\frac{1}{T} \right) \right) - \rho_{\mathrm{P}} . R . T . \left(\frac{1-\varepsilon}{\varepsilon} \right) . \sum_{i=1}^{N} \frac{\partial \bar{q}_i}{\partial t} = 0 \qquad (4)$$

In this system, energy balance for the gas and also heat transfer to the bed wall is included (Malek and Farooq, 1997). This is due to temperature variation caused by heat of adsorption and desorption occur.

$$-K_l \frac{\partial^2 T}{\partial z^2} + \varepsilon.\rho_g.c_{\mathrm{P,g.}}\left(\mathcal{U}\frac{\partial T}{\partial z} + T\frac{\partial u}{\partial z}\right) + \left(\varepsilon_t.\rho_g.c_{P,g} + \rho_B.c_{\mathrm{P,s}}\right).\frac{\partial T}{\partial t} - \rho_B.\sum_{i=1}^{N}\left(\frac{\partial \overline{q_l}}{\partial t}.\left(-\overline{\Delta H_l}\right)\right) + \frac{2h_i}{R_{B,i}}(T - T_w) = 0 \quad (5)$$

To evaluate heat loss through the walls and the accumulation of energy, corresponding to energy balance has also been used, (Malek and Farooq, 1998).

$$\rho_w.c_{\mathrm{P},w.}A_w \frac{\partial T_w}{\partial t} = 2\pi \mathrm{R_{B,i}} h_{i(T-T_w)} - 2\pi R_{B,o} ho(T_w - T_{atm}) \quad (6)$$

where,

$$A_w = \pi\left(R_{B,o}^2 - R_{B,i}^2\right) \quad (7)$$

Initial conditions

$c_i(x) = 0 x = (0, L)$ (8)

$T(x) = T_f \quad x = (0, L)$ (9)

$q_i(x) = 0 \quad z = (0, L)$ (10)

where T_f is the feed temperature

Boundary conditions

For the adsorption step

At $x = 0$, $c = c_0$, $u = u_f$ (11)

$\left.\frac{dc}{dx}\right| x = L$ is equal to zero (12)

Where, L is the column height.

Also

$\frac{dT}{dx} = 0$ at x = L (13)

For the depressurisation step

At $x = 0$, $u = 0$ (14)

$\left.\frac{dc}{dx}\right| x = 0 = 0$ (15)

The pressure is assumed as a second order function of the time which is adapted to the literature (Jee *et al.,* 2001).

$$\mathrm{P}(t) = a..t^2 + b.t + c \quad (16)$$

In the above equation a, b and f(t) parameters defined regarded to duration and initial and final pressures of each step.

To consider the pressure drop effect across the bed, Ergun's equation was introduced as a momentum balance.

$$-\frac{dP}{dz} = a.\mu.u + b.\rho.u|u| \quad (17)$$

$$a = \frac{150}{4R_p^2}.\frac{(1-\varepsilon)^2}{\varepsilon^2}; b = 1.75\frac{(1-\varepsilon)}{2R_p\varepsilon} \quad (18)$$

Where u is the interstitial velocity.

The multi-component adsorption equilibrium was predicted by the following Langmuir isotherm.

$$q_{i=}\frac{q_{m,i}.B_i.\mathrm{P_i}}{1+\sum_{j=1}^{N}B_j.\mathrm{P_j}} \qquad (19)$$

Where,

$$q_{m,i=\mathrm{k_1+\kappa_2\cdot T;B_i=k_3.exp}\left(\mathrm{k_4}/_{\mathrm{T}}\right)} \qquad (20)$$

The sorption rate into an adsorbent pellet is described by LDF model with a simple lumped mass-transfer parameter (Cavenati *et al.,* 2006; Ankit *et al.,* 2010).

$$\frac{\partial\bar{q_i}}{\partial t}=\omega_i.(q^{\cdot}-\bar{q});\omega_i=\frac{15D_{ei}}{r_c^2} \qquad (21)$$

where

$$\frac{15D_{ei}}{r_c^2}=c_{i\ .p}p_r^{0.5}.(1+B_i.\mathrm{P_i})^2 \qquad (22)$$

The adsorption isotherm parameters and diffusion rate constant of H_2, CH_4 , CO_2 and CO over activated carbon and Zeolite 5A are shown in Table 1. In Table 2, physical properties of the adsorption bed for both activated carbon and Zeolite 5A are indicated.

Table 1: Rate parameters of H_2 , CO, CH_4 and CO_2 on Activated Carbon and Zeolite 5A (Se-Il *et al;*2008).

Adsorbent		k_1 **{mmol/g}**	k_2 **{1/atm}**	k_3 **{K}**	k_4 **{mmol/g}**	k_5 **{1/atm}**	k_6 **{K}**
Activated Carbon	H_2	0.01910	1.90E-05	1170.00	8.73 E-04	4.98E-06	1901.46
	CO	0.00423	1.43E-05	2407.68	7.40 E-04	2.29E-03	1760.96
	CH_4	0.00576	7.44E-05	2157.02	7.09 E-04	2.73E-02	1467.70
	CO_2	0.00764	1.28E-04	2228.63	1.62 E-03	2.53E-02	1724.50
Zeolite 5A	H_2	0.00064	1.14E-04	1665.08	3.61 E-06	1.96E-16	20848.3
		0.00231	1.17E-04	2652.03	2.54 E-03	4.29E-08	3755.31
	CO						
	CH_4	0.00220	2.08E-04	2298.51	7.31 E-04	1.98E-12	7282.80
	CO_2	0.00356	3.01E-03	2923.79	8.23 E-04	5.78E-09	5478.58

Table 2: Physical properties of adsorbents and bed (Malek and Farooq, 1998, 1997).

Properties		Activated Carbon	Zeolites 5A
Average pellet size	{mm}	1.15	1.57
Pellet density	{g/cm^3}	0.85	1.16
Bulk density	{g/cm^3}	0.482	0.764
Heat capacity	{cal/g.K}	0.25	0.21
Bed			
Length	{m}		1.2
Inside diameter	{m}		0.0246
Outside diameter	{m}		0.034
Heat capacity of the column	{cal/g.K}		0.12
Density of column	{g/cm^3}		7.83
Internal heat transfer coefficient	{KJ/s.m^3 K}		0.0385
External heat transfer coefficient	{KJ/s.m^3 K}		0.0142
Bulk density	{g/cm^3}	0.532	0.744
Void fraction		0.433	0.357
K_{H_2}	s^{-1}		0.1
K_{C_O}	s^{-1}		0.3
K_{CH_4}	s^{-1}		0.4
K_{CO_2}	s^{-1}		1.0

Table 3: H_2 PSA system operating condition (PHRC, 1984).

Mole fraction	Feed	Product
H_2	0.835	0.9999
CO	0.000015	Balance
CH_4	0.15	Balance
CO_2	0.01	Balance
Unit Recovery (%)	75	
Pressure (Bar)	30	22.5
Flow Rate (N.m^3/h)	16000	10050

It is evidently clear from Table 3 that the plant under consideration is a separation process because the impurities in the feed flow are more than 10 percent. Two major parameters used in measuring the efficiency of a PSA system, are product purity and percent recovery. The recovery measures the amount of component that is contained in the product stream divided by the amount of the same component in the feed mixture. Gomes and Yee (2002) give an expression to calculate the percent recovery of H_2 as;

$$\text{Percent recovery (\%)} = \frac{Product_i}{Feed_i} \times 100 \qquad \text{where i= 1,2 ....} \qquad (23)$$

Product Purity gives an idea about percentage of desired component in the product stream. Gomes and Yee (2002) expressed the average purity of H_2 in the product as the mole percent of H_2 using the following expression:

Product purity (%) = $\frac{Product_i}{\sum_{i=1}^{c} Product_i}$ x 100 where i= 1,2 .... (24)

2.2 Solution Methodology

Pressure swing adsorption modelling involves partial differential equations (PDEs) in time and space with periodic boundary conditions that link the processing steps together. The solution of these coupled stiff PDE systems are governed by steep fronts moving with time. However, solving these partial differential equations analytically is difficult; therefore, the numerical method using finite difference technique was used to solve the model equations in order to obtain the product purity, recovery, and concentration profile along the adsorption bed. The partial differential equations were first converted into ordinary differential equations-initial value problems (ODE-IVPs) by discretization along the bed length (Ankit *et al;*2010). Then after, a set of differential-algebraic equations (DAEs) were obtained and solved using MatlabR 2014a software.

3.0 Results and Discussion

The developed model which is a partial differential equation was simulated using MATLAB R-2014a software. The effectiveness of the developed model was then determined by comparing the simulated with the data obtained from the Port Harcourt refining and Petrochemical Company under the same operating conditions. The effect of the variation of various parameters on the purity and recovery of hydrogen gas using the pressure swing adsorption model was also studied.

3.1 Validation of the Numerical Simulation Results

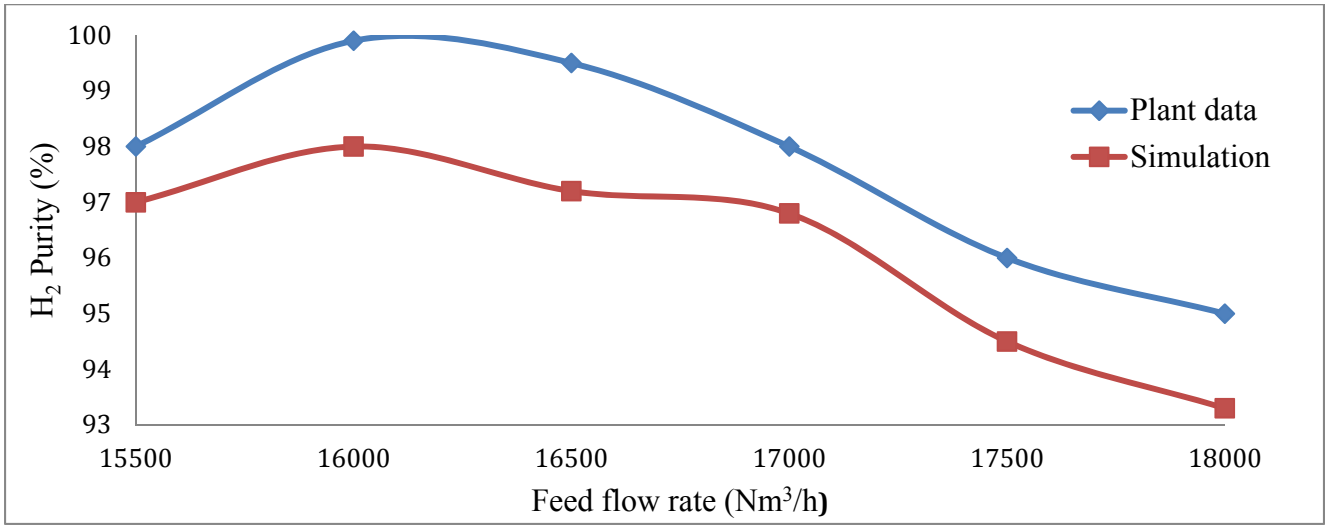

Figure1: Comparison between Simulation Results and Experimental Data at Different Feed Flow Rates.

In validating the simulation results, the results of this work were compared with experimental data obtained from PSA system used in separating hydrogen from the effluent gas of catalytic reforming process of Port Harcourt Refining and Petrochemical Company (PHRC). The results of this work were compared with the experimental data as shown in Figure 1, where hydrogen purity is plotted against feed flow rate. It can be seen that the simulation results indicated a very good agreement with the experimental data. For example, at 16000 Nm^3/h hydrogen purity of the experimental data and simulated results were found to be 99.99% and 98.0% respectively. The largest and smallest deviations between the experimental data and simulation results are found to be 2.5% and 1% for flow rates of 16500 Nm^3/h and 15500 Nm^3/h respectively. This comparison

clearly showed that the model equations predict the PSA system adopted in this study with a relatively high accuracy.

3.2 Investigating the Effects of Process Variables

The validity of the numerical simulation of the PSA system used for hydrogen separation from the effluent gas of catalytic reforming process at Port Harcourt Refining and Petrochemical Company (PHRC) can be used as a basis to investigate the effects of some important operating parameters on the performance of the PSA system. In order to establish the optimum values of the process variables, adsorption pressure, cycle time, adsorption duration and feed temperature were selected to study their effects on hydrogen purity and recovery. The reference process operating conditions were selected and only one parameter was changed at a time.

3.2.1 Adsorption pressure

The effect of adsorption pressure against hydrogen purity and recovery are plotted in Figures 2 and 3 respectively. There is a gradual increase in the purity of hydrogen as adsorption pressure increased from 1 to 3 Pa, and this is due to large amount of impurities such as CO, CO_2 and CH_4 adsorbed in the PSA beds. However, as the adsorption pressure exceeds 3 Pa there was a gradual decrease in hydrogen purity. This is due to the possibility that the adsorption bed is fully saturated, thereby resulting in less impurities being adsorbed and reduction in the product purity. For example, product purity of 92.5 and 88 % were achieved at an adsorption pressure of 3 Pa and above respectively. The same trend is observed as shown in Figure 4.3 where at initial stage, an increase in the adsorption pressure leads to increase in hydrogen recovery. However, as adsorption pressure exceeds 3 Pa, there is a gradual decrease in the percentage of hydrogen recovered. This trend of product purity and recovery is observed in the previous works carried out by Al Ghafri (2007) and Ankit *et al.* (2010). However, their optimum adsorption pressure is different possibly due to the fact that the PSA adopted in their work is operating at different feed composition, adsorbents and operation steps. Therefore, the adsorption pressure of 3 Pa should be maintained for this PSA system.

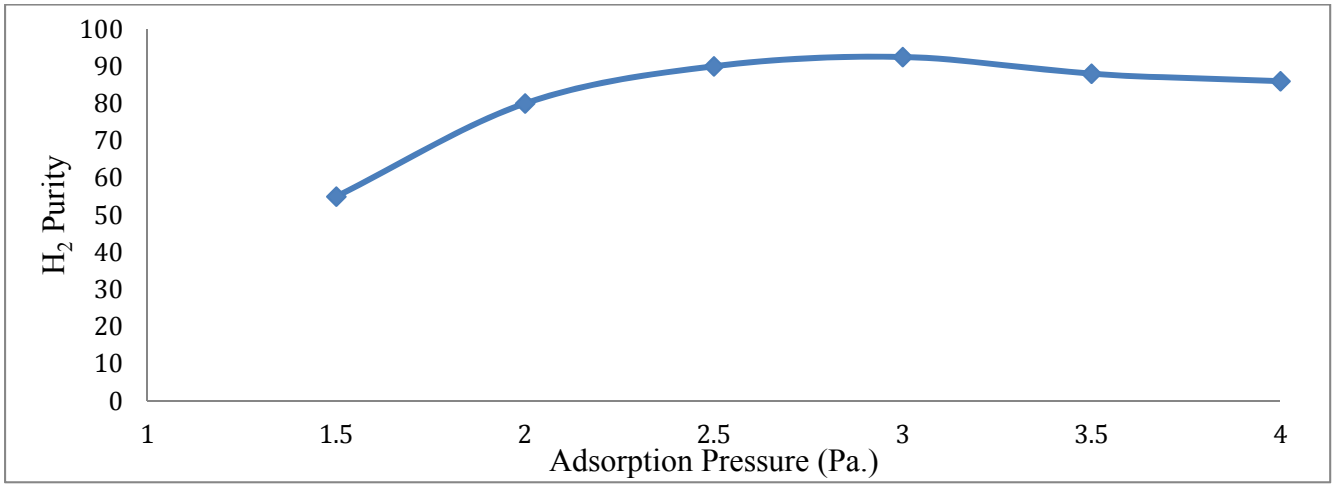

Figure 2: Effects of Adsorption Pressure on Hydrogen Purity

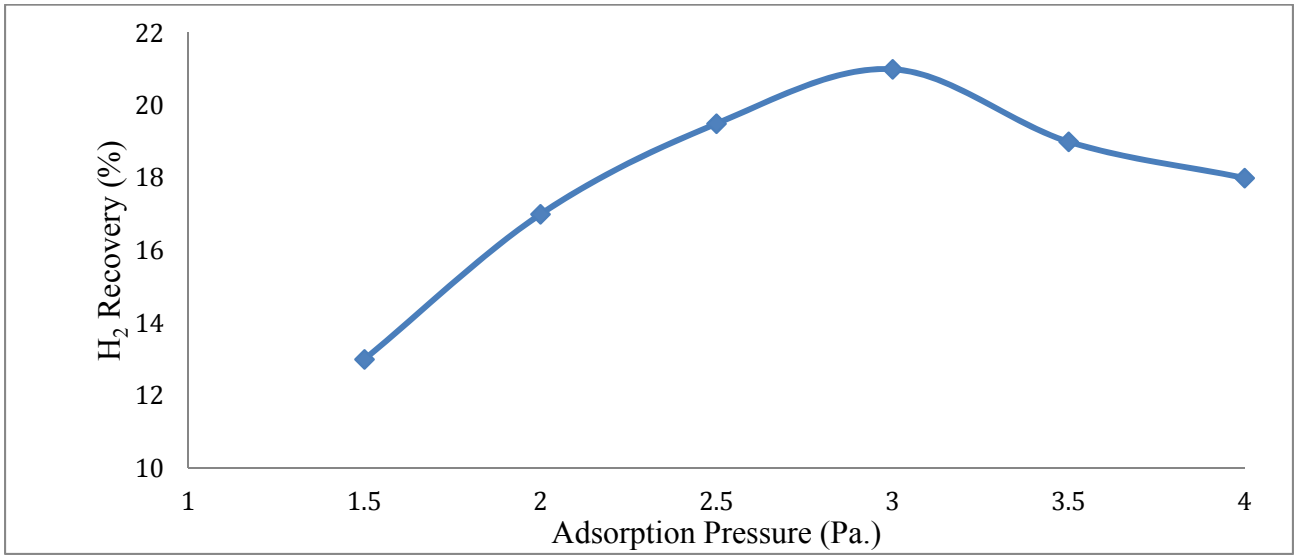

Figure 3: Effects of Adsorption Pressure on Hydrogen Recovery.

3.2.2 Cycle time

In determining the effect of cycle time, the ratio of operation times of all the four steps in a cycle were kept constant, i.e. adsorption, blowdown, purging, and pressurization times were kept in the ratio of 4:1:1:4. Figures 5 and 6 show the effect of cycle time on hydrogen purity and recovery respectively. It can be observed that the percentage purity and recovery of hydrogen through PSA system gradually increases as cycle time increases. This means, there is a sufficient time for adsorption to take place thereby making the bed to adsorbed more impurities and invariably increases the product purity and recovery. However, as the cycle time exceeds 200 second, a gradual decrease in the percent hydrogen purity and recovery is observed. This implies, the adsorption bed is fully saturated as cycle time exceeds 200 seconds. Once the bed become saturated, the yet to be adsorbed impurities reduces the purity and recovery of the product stream. Therefore, a cycle time of 200 second or less is expected to produce optimum product purity and recovery.

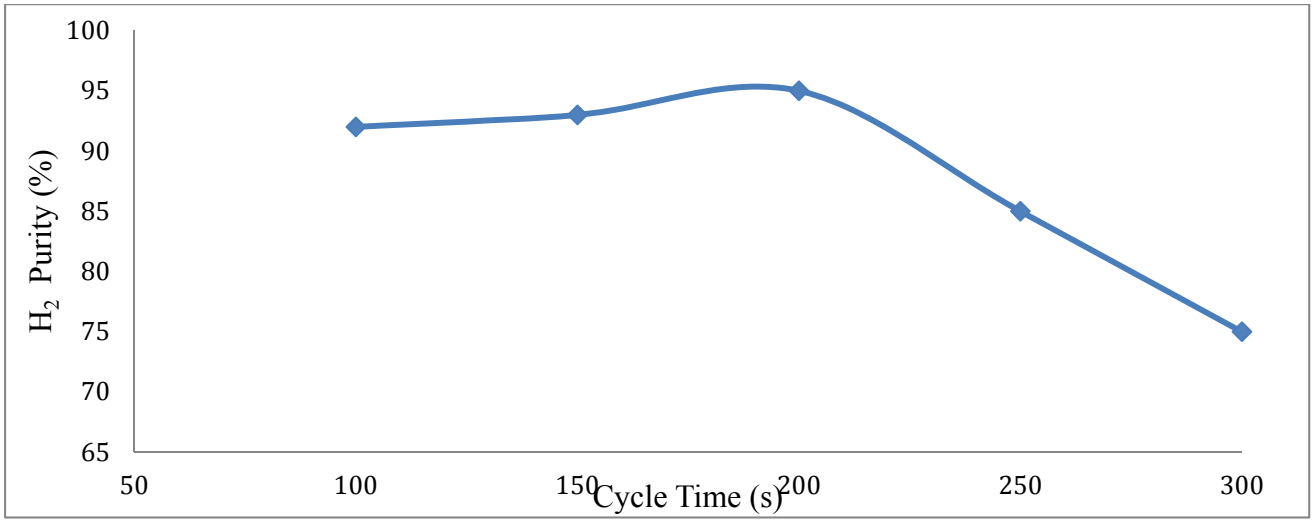

Figure 4: Effects of Cycle Time on Hydrogen Purity

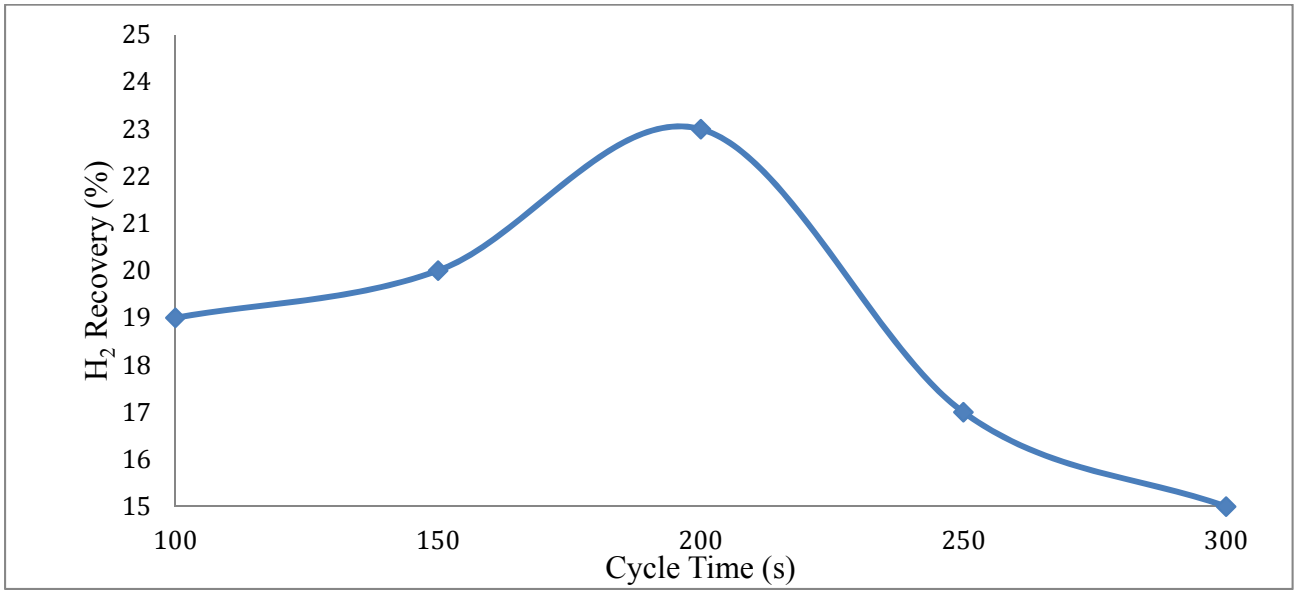

Figure 5: Effects of Cycle Time on Hydrogen Recovery

3.2.3 Adsorption duration

In investigating the effect of adsorption duration, Ankit *et al*; (2010) suggested that total cycle should be assumed constant while adsorption time, purging time and pressurization time were taken to be equal. The effect of adsorption duration on hydrogen purity and recovery is showed in Figures 6 to 7. It can be observed that as adsorption time increases, the percentage of hydrogen purity and recovery increases up till 40% of the total cycle time for adsorption step. However, after 40% of total cycle time, the product purity and recovery gradually started to decrease with an increase in adsorption duration. This behaviour is believed to be due the fact that an increased in the adsorption time is associated with corresponding increase in purging time and therefore, the bed is in more cleaned condition after purging.

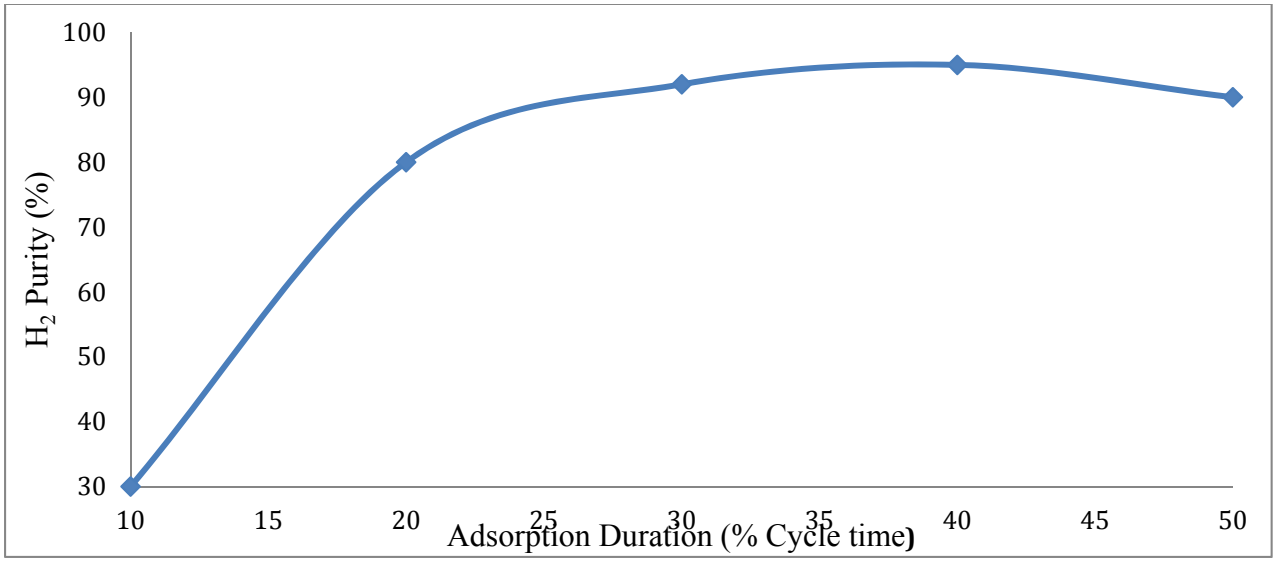

Figure 6: Effects of Adsorption Duration on Hydrogen Purity

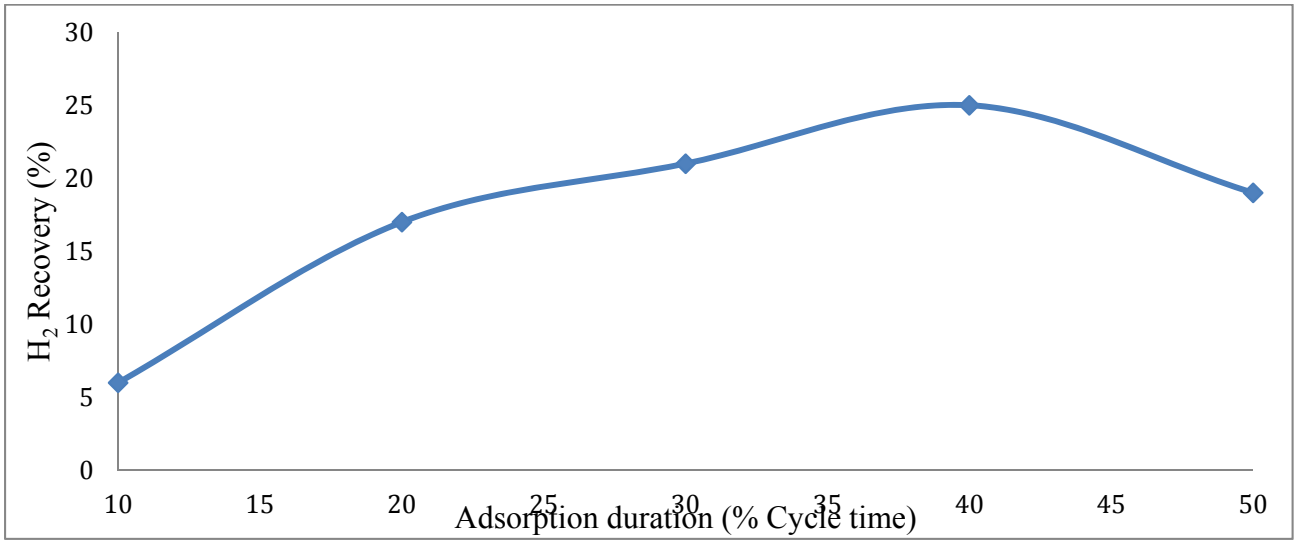

Figure 7: Effects of Adsorption Duration on Hydrogen Recovery

This trend is in agreement with the work of Ankit *et al*; (2010) who observed that at 30% of total cycle time for adsorption step, maximum values of 95.45 and 20.55% were achieved for product purity and recovery respectively. However, in this work the maximum values of 95.0 and 25% were obtained for product purity and recovery respectively.

3.2.4 Feed temperature

The effect of feed temperature on H_2 purity and recovery is showed in Figures 8 and 9. It can be seen from Figures 8 and 9 that increasing of the feed temperature is resulting in reduction of the hydrogen purity and an increment in the hydrogen recovery. Shokroo *et al;* (2014) observed that the adsorption process in a PSA system is an inherently exothermic phenomenon; therefore, a decrease in the purity of hydrogen at the product stream as feed temperature increases is expected. They suggested that an increase in hydrogen recovery

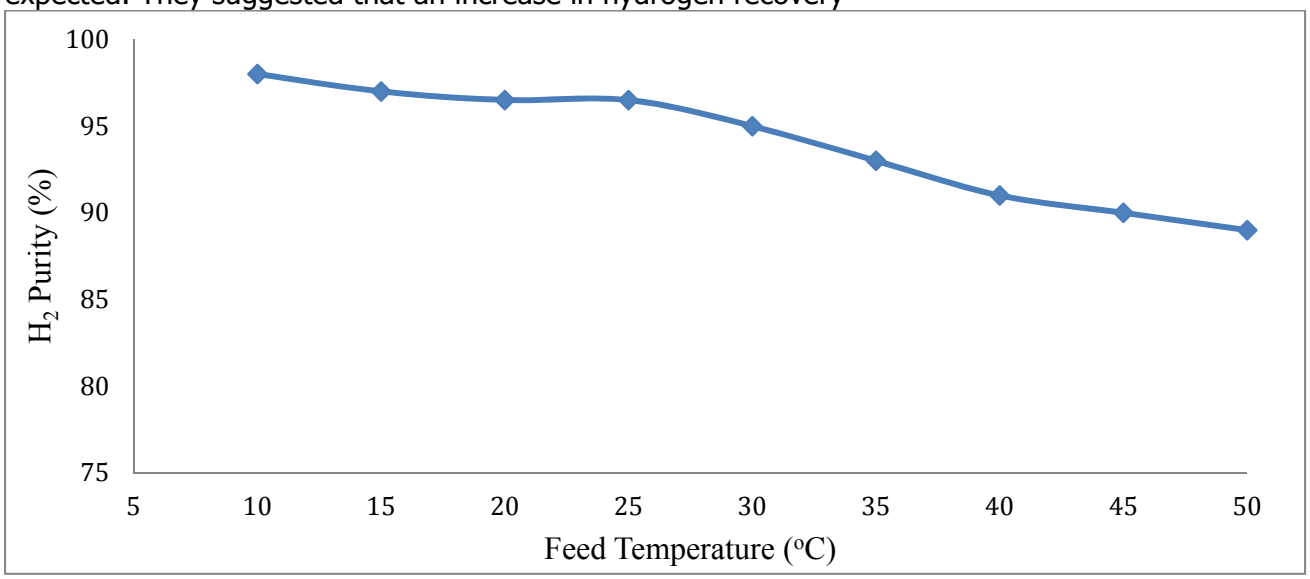

Figure 8: Effects of Feed Temperature on Hydrogen Purity

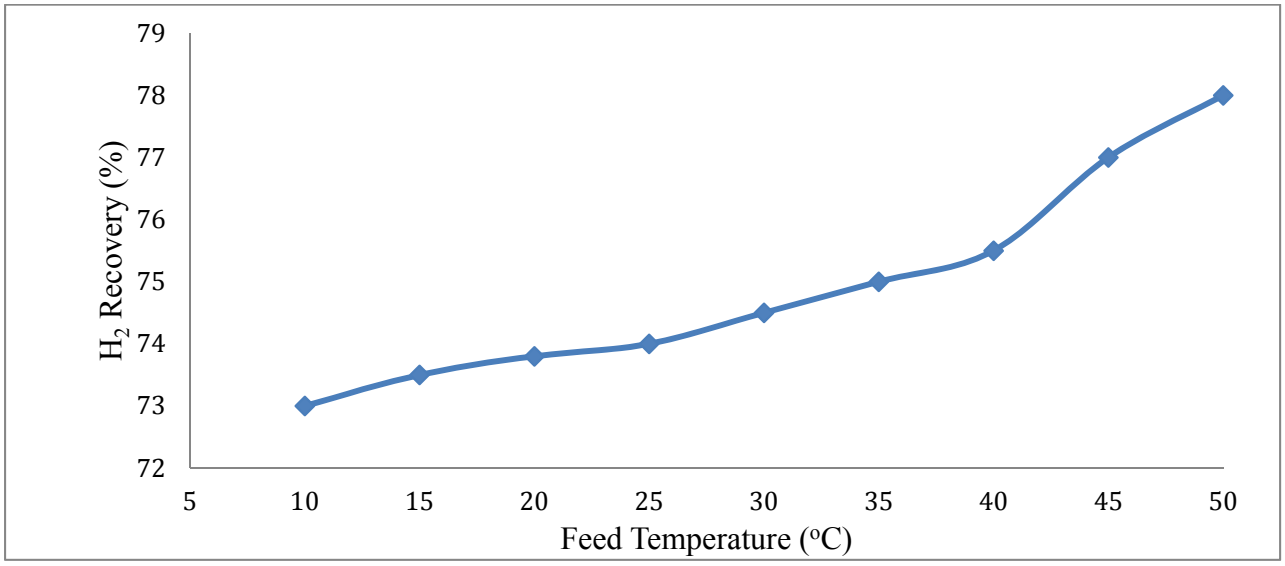

Figure 9: Effects of Feed Temperature on Hydrogen Recovery

through the increase of the feed temperature is due to gaseous molar volume expansion in the adsorption step, which leads to an increase in the hydrogen molar flow in the product stream. In general, adsorption of all compounds in the bed decreases as the feed temperature increases and invariably the molar flow of all components increases in the product stream. In addition, this increase in the hydrogen molar flow in the product stream automatically increases the hydrogen recovery. However, impurities increase rapidly in the product stream as the hydrogen molar flow increases and subsequently, hydrogen purity will decrease.

4.0 Conclusions

By using a Matlab R 2014a software to simulate the separation of hydrogen from effluent gas coming from the catalytic reforming unit of Port Harcourt Refining and Petrochemical Company (PHRC), the results are summarized as follows:

(a) The model equations used in this work adequately described the flow behaviour of the separation of hydrogen from the effluent gas mixture in a PSA system.

(b) The simulation result compared favourably with the experimental data obtained from catalytic reforming unit in Port Harcourt Refining and Petrochemical Company (PHRC). The largest and smallest deviation between the simulation result and experimental data were found to be 2.5% and 1% at flow rates of 16500 Nm^3/h and 15500 Nm^3/h respectively. This comparison clearly showed that MatlabR 2014 software can be used effectively for numerical simulation of hydrogen from effluent gas mixture.

(c) The effect of adsorption pressure, cycle time, feed temperature and adsorption duration on hydrogen purity and recovery has been studied numerically and their optimum values obtained. In order to maximize the product purity and recovery, it can be concluded that for hydrogen separation from gas effluent of catalytic reforming process, operating parameters of the PSA unit with adsorption pressure of 3 Pa, cycle time of 200 s, feed flow rate of 16000 $N.m^3/h$ and feed temperature of 35 °C yield optimal results of hydrogen purity and recovery of 95.0 and 75.2% respectively.

References

Al Ghafri, S. (2007), "Modelling and Optimisation of Hydrogen Production by Hybrid PSA-Membrane System", MSc Thesis, Imperial College of Science, Technology and Medicine, London

Ankit K. B, Singh, A.K., Kailash; V, Kumar, R. K. , Shashi, K. S. (2010), "Parametric studies and simulation of PSA process for oxygen production from air", *Polish Journal of Chemical Technology*, 12(2), Pp18-28.

Baksh, M. S. A and Ackley, M. W. (2002); "Pressure Swing Adsorption Process for the Production of Hydrogen", US Patent 6340382.

Cavenati S., Grande C. A., Rodrigues A. E. (2006), "Separation of CH4/CO2/N2 Mixtures by Layered Pressure Swing Adsorption for Upgrade of Natural Gas". *Chemical Engineering Science*, 61, Pp.3893-3906.

Gomes, V. G. and Yee, K. W. K. (2002), *"Pressure swing adsorption for carbon dioxide sequestration from exhaust gases"*. Separation and Purification Technology 28(2), 161 – 171. DOI: 10.1016/S1383-5866(02)00064-3.

James, M.K and Gleen, U. (2001), *Petroleum Refining Technology and Economics*, Mercel Dekker Inc. New York, Pp. 56-71.

Jee, J.-G;.Kim, M.-B and Lee, C.-H. (2001). *Adsorption Characteristics of Hydrogen Mixtures in a Layered Bed: Binary, Ternary, and Five-Component Mixtures*, *Ind. Eng. Chem. Res.* no. 3, 868(878).

Malek A., Farooq , S. (1998), "Hydrogen Purification from Refinery Fuel Gas by Pressure Swing Adsorption". *AIChE Journal* , 44, Pp. 1985.

Mofarahi, M and Shokroo, E. J. (2013), "Comparison of Two Pressure Swing Adsorption Processes for Air Separation Using Zeolite 5A and Zeolite 13X", *Petroleum and Coal* 55 (3) Pp.216-225.

Park, J.H, Jong-Nam, K, and Soon-Haeng, C. (2003), "Performance Analysis of Four-Bed H2 PSA Process Using Layered Beds", *Korea Institute of Energy Research,* Yusungku, Taejon 305-343.

PHRC Operational Manual (1984): Project Specialization UOP, C.C.R Plat Forming Process Technology

Ruthven, D. M., (1984). *"Principles of Adsorption and Adsorption Processes",* John Wiley, New York.

Shokroo, E. J. Shahcheraghi, M and Farniaei, M (2014), "Numerical Simulation of a H2 –PSA. The JAM petrochemical Industrial plant in the Southern Pars Zone", *Petroleum and Coal,* 56(1) Pp. 110-115.

Ruthven D. M., Farooq S. and Knaebel K. S. (1994). "*Pressure Swing Adsorption*," New York: VCH Publishers, Inc.

Sircar, S., and T. Golden (2000), "Purification of hydrogen by pressure swing adsorption," *Separation Science and Technology*, 35, 667

Tanczyk, M., and Warmuzinski, K. (1997). "Multicomponent Pressure Swing Adsorption: I

Modelling of Large-Scale PSA Installations," *Chemical Engineering Process*, 37, Pp.89

Whysall M. and Picioccro K.W (1998), "*Selection and Revamp of Hydrogen Purification Processes"*, UOPLLC Dec Plains IIIiniois

Yang R. T. (1987). "*Gas Separation by Adsorption Processes"*. London: Butterworth, Reprinted by Imperial College Press.

Yang J., Lee C-H. (1997). "Separation of Hydrogen Mixtures by a Two-Bed Pressure Swing Adsorption Process Using Zeolite 5A." *Industrial Engineering Chem. Res.*, 36,Pp 2789-2798.

Proceedings of the 49th NSChE Annual Conference
KADA 2019: pp 259 - 270

P2A-03: HYDROGEN FUEL FROM BIOMASS GASIFICATION-COST EFFECTIVE ENERGY FOR DEVELOPING ECONOMY

Kehinde A. BABATUNDE[1], Funmilayo N. OSUOLALE[1],* Oluseye O. AGBEDE[1], Akinfenwa F. OLAWUNI[1], Ayodeji J. FATUKASI[1], Adekunle E. ADEWUNMI[1], Christiana J. OLADIPO[1] and Olukorede M.OSUOLALE[2]

[1]Department of Chemical Engineering, Ladoke Akintola University of Technology, Ogbomoso, Oyo State, Nigeria

[2]Department of Civil Engineering, Ladoke Akintola University of Technology, Ogbomoso, Oyo State, Nigeria

*__Corresponding author__: fnosuolale@lautech.edu.ng; Tel.: +234-813-901-0453

ABSTRACT

Hydrogen has the potential to be a clean and sustainable alternative to fossil fuel especially if it is produced from renewable sources such as biomass. Gasification is the thermochemical conversion of biomass to a mixture of gases including hydrogen. The percentage yield of each constituent of the mixture is a function of a number of factors. This article highlights various parameters such as operating conditions; gasifier type; biomass type and composition; and gasification agents that influence the yield of hydrogen in the product gas. Economic evaluation of hydrogen from different sources was also presented. The hydrogen production from gasification process appears to be the most economic process amongst other hydrogen production processes considered. The process has the potential to be developed as an alternative to the conventional hydrogen production process.

INTRODUCTION

Biomass is the largest renewable energy and it has a major share of about 90% of the total energy supply in the remote and rural areas of developing world (Demirbas, 2001). While burning of fossil fuel converts carbon that has been confined underground (as crude oil, coal and gas) to CO_2 thereby increases CO_2 in circulation and hence the greenhouse gas (GNG) effects, the combustion of biomass recycles the CO_2 captured during photosynthesis and thus maintains the CO_2 balance in the atmosphere (Ahmad et al., 2016). Biomass can therefore be said to possess a zero CO_2 net emission (Mohammed et al., 2011).

Most often, biomass is from agricultural by products but sometimes, it could be directly cultivated (McKendry, 2002a). The routes to convert biomass into useful products will depend on the form of the biomass. For agricultural residues, forest residues and wood, thermo-chemical conversion routes are the widely-used methods to extract energy from biomass. Thermochemical processes can be categorized into combustion, pyrolysis and gasification where the syngas and bio-oil produced as intermediate products can be subsequently converted to valuable fuels and chemicals. Combustion is the direct burning of biomass in air to convert the chemical energy in biomass to heat, electricity or mechanical power. The energy efficiency of this process is between 10-30% (Ni et al; 2006). Pyrolysis is the burning of biomass in the absence of air. Slow pyrolysis gives high yield of charcoals whereas rapid heating of biomass at high temperature (fast pyrolysis) give products in the liquid, gaseous and solid states. Gasification is the conversion of biomass into a combustible gas mixture (syngas) by heating in a gasification medium such as air, oxygen or steam. Gasification of biomass leads to the production of syngas of which carbon monoxide, methane, and hydrogen are some of the constituents.

Of all the three thermochemical routes, Gasification is being considered in this research work as a promising technology to treat biomass. This is because it produces minimal emissions, can be easily adapted to treat different materials and the process conditions can be altered selectively to isolate different gaseous products. Furthermore, gasification is likely to be commercially viable based on the consideration of overall conversion efficiency and proven operational history and performance.

Hydrogen- one of the constituents of syngas has been dubbed the energy carrier of the future and has gained reputation as a potential substitute to fossil fuels. This is because Hydrogen when combusted or used in a fuel cell does not emit greenhouse gas, it has a high energy content on a mass basis when compared to gasoline or natural gas and it can be easily and efficiently converted to electricity using fuel cells. Hydrogen as a high efficiency low polluting fuel can be used for transportation, heating and power generation (Orhan et al, 2011). Hydrogen is also a raw material for chemical, petroleum and agro-based industries (Lewis et al, 2009 and Naterer et al, 2010).

Converting biomass to aqueous and gaseous fuel most especially hydrogen could be a more efficient way of utilizing biomass. This is good for developed nations because the problem of greenhouse gas (GHG) emissions will be dealt with and for developing nations with power generation problems by providing access to electricity and power supply from relatively available sources.

This study is focused on highlighting the potential of hydrogen generated from biomass gasification to be effective solution to the menace of inadequate power supply in rural areas and for both small and medium scale industries. It is much more apt for a developing nation like Nigeria which has an agrarian based economy. The vast amount of biomass as agricultural byproducts and abundant virgin land that could be put to use for more cultivation of biomass is a great motivation for this study. The work is presented as follows. Section 2 highlights various sources of producing hydrogen. In section 3 gasification of biomass and factors that affect hydrogen production is discussed. Section 4 presents the implications of hydrogen fuel in terms of usage, economy and challenges. Section 5 concludes the write up.

2.0 Hydrogen Production

Although abundant on earth as an element, hydrogen is almost always found as part of another compound, such as water (H_2O) and some other compounds and must be separated from the compounds that contain it. Once separated, hydrogen can be used in diverse ways. In addition, Hydrogen can be produced using diverse resources. The environmental impact and energy efficiency of hydrogen depends on how it is produced. Figure 1 depicts some sources through which hydrogen can be generated.

2.1 Production from natural gas: Hydrogen can be produced from natural gas through three different chemical processes. Steam reforming involves the endothermic conversion of methane and water vapour into hydrogen and carbon monoxide as given in equation 1. The product gas CO can be further converted to $CO_2$and H_2 through the water-gas shift reaction (Equation 2)

$$CH_4 + H_2O + heat \rightarrow CO + 3H_2 \quad (1)$$

$$CO + H_2O \rightarrow CO_2 + H_2 + heat \quad (2)$$

Partial oxidation involves the production of hydrogen through the partial combustion of methane with oxygen rich gas to yield carbon monoxide and hydrogen (equation 3). The CO can be further converted through the water-gas shift reaction (Equation 2)

$$CH_4 + \frac{1}{2}O_2 \rightarrow CO + 2H_2 \quad (3)$$

Autothermal reforming is a combination of both steam reforming and partial oxidation.
This method of producing hydrogen has developed technology and has been commercialized. However, the hydrogen generated from this source can only be sustainable if it is from renewable source such as biogas or syngas.

2.2 Electrolysis: An electric current splits water into hydrogen and oxygen. If the electricity is from renewable sources, such as solar or wind, the resulting hydrogen will be considered renewable as well, and have numerous environmental benefits

$$H_2O + electricity \rightarrow H_2 + \frac{1}{2}O_2 \quad (4)$$

Figure 1: Some hydrogen production sources

2.3 Solar based Hydrogen Production: solar energy is available readily at no cost to produce hydrogen; therefore, it may lead to a future clean alternative fuel (hydrogen) for transportation. Direct solar water decomposition, or photolytic, processes use light energy to split water into hydrogen and oxygen. These processes are currently in the very early stages of research but offer long-term potential for sustainable hydrogen production with low environmental impact such as the threatening global warming effects. (U.S. Department of energy, 2004).

2.4 Biological processes: Microbes such as bacteria and microalgae can produce hydrogen through biological reactions, using sunlight or organic matter. These technology pathways are at an early stage of research, but in the long term have the potential for sustainable, low-carbon hydrogen production. Biological hydrogen can be produced in an algae bioreactor. (Hemschemier et al., 2009).

2.5 Thermochemical Water Decomposition for Hydrogen Production: This is an emerging and promising technology for large-scale production of hydrogen and it is commonly called thermochemical cycles. This is done using intermediate compounds and sequence of chemical reactions to split water into hydrogen and oxygen without polluting the atmosphere (Naterer et al 2009). Many thermochemical cycles have been identified but only a few has been proven to be feasible (McQuillan, 2002).

2.6 Gasification: This conversion route is the focus of the study. It is discussed extensively in the next section.

3.0 Biomass Gasification

Gasification is the conversion of biomass into a gaseous product that mainly consist of Hydrogen (H_2), and carbon monoxide (CO) with lower amounts of methane(CH_4), carbon dioxide (CO_2), water(H_2O), Nitrogen(N_2) and higher hydrocarbon(C+) in the presence of gasifying agents. The gasifying agents could be air, oxygen or steam or a mixture of these components. Gasification is carried out at temperatures between 500 and 1400 ^{0}C and at atmospheric pressure of 101.325kPa up to an elevated pressure of 3300kPa (Ciferno and Marano, 2002). The reactions taking place in the gasifier are summarized in equations 5-7 (Mckendry, 2002b).

$$C + \frac{1}{2}O_2 \leftrightarrow CO \text{ (partial oxidation)} \quad (5)$$

$$C + O_2 \leftrightarrow CO_2 \text{ (complete oxidation)} \quad (6)$$

$$C + H_2O \leftrightarrow CO + H_2 \text{ (water gas reaction)} \quad (7)$$

The hydrogen and steam can undergo further reaction during gasification as given in Equations 8 and 9

$$CO + H_2O \leftrightarrow CO_2 + H_2 \text{ (water gas shift reaction)} \quad (8)$$
$$CO + 3H_2 \leftrightarrow CH_4 + H_2O \text{ (Methane formation)} \quad (9)$$

The arrows indicate that the reactions are in equilibrium and can proceed in either direction depending on the conditions of reaction (temperature, pressure and concentration)
Main products of gasification are synthesis gas, char and tars. The content depends on the feedstock, oxidizing agent and the conditions of the process. The gas mainly consists of CO, CO_4, H_2O, CH_4 and other hydrocarbons. The gasification process can be summarized as given in equation 10

$$\gamma C_a H_b O_c + \varphi H_2O \xrightarrow{heat} d\ H_2 + eCO + fCO_2 + gCH_4 + tar \quad (10)$$

where $\gamma C_a H_b O_c$ is the general chemical representation of the biomass.

The syngas produced consist of a mixture of CO_2 (8-10%), H_2 (18-20%), CO (18-20%), CH_4 (2-3%) and traces of other light hydrocarbon and steam (Simonyan and Fasina, 2013). This can be burnt directly or used as a fuel for gas engines and gas turbines in generating electricity (Ben-Iwo et al., 2016).

A few parameters have effects on the quality and quantity of the syngas production during gasification. These are discussed as follows.

3.1 Effect of temperature

Temperature appears to have the greatest influence on the performance of the gasifiers. The composition of the volatiles produced from a gasifier depends on the degree of the equilibrium attained by various gasification reactions. All the gasification reactions are normally reversible and the equilibrium point of any of the reaction can be shifted by changing the temperature. Hydrogen productions reactions (water gas shift reaction) is endothermic, a higher gasification temperature will favor the production of Hydrogen (Nanda et al, 2016).

A study of steam gasification of almond shells in a continuous fluidized bed reactor reported the yield of hydrogen at above 50% of the syngas composition (Rapagna and Latif, 1997). The temperature was increased from 600 to 800 ^{0}C. Similarly, Lv et al 2004 reported an increase in Hydrogen production from 21-39 vol.% when the gasification temperature was varied from 700 to 900 ^{0}C. Sawdust and fluidized bed reactor were the feedstock and type of gasifier respectively. For all cases considered, the higher temperature favoured higher concentrations of syngas and Hydrogen yield but lower concentration of char and heavy tar. The increase was due to tar thermal cracking reaction which also decrease the tar concentration (Skoulou et al, 2009). The gasification temperature needed to be selected carefully as a tradeoff between the char conversion and the H_2 output. However, other research shows that high H_2 yield can be obtained at low temperature (600^{o}C) by using 90% steam content (Gao, Li, Quan, & Gao, 2008). Table 1 gives indication of the influence of temperature on hydrogen yield for selected biomass.

Table 1: Hydrogen production of biomass at different gasification temperature (Source: Nanda et al; 2016a; Safari et al, 2018; Lu et al, 2008; Nanda et al, 2016b)

Biomass	Temperature	Hydrogen yield (mol/kg)
Orange peel	400	0.08
Orange peel	500	0.58
Orange peel	600	0.91
Pine wood	300	0.22
Pine wood	400	0.69
Pine wood	500	1.14
Almond shell	380	3.95
Almond shell	400	4.55
Almond shell	420	5.43
Almond shell	440	6.45
Almond shell	460	7.85
Corn cob	550	2.55
Corn cob	600	5.31
Corn cob	650	9.08

3.2 Effect of biomass feed stock

Table 2 shows the hydrogen production from gasification of different biomass subjected to the same conditions. The type of feed stock can be seen to affect the yield of hydrogen at the same process conditions. Sugarcane bagasse from table 2 yielded 1.66mol/kg Hydrogen while coconut shell yielded 2.17mol/kg Hydrogen at the same process conditions. The general chemical representation of biomass as given in equation 10 indicates that the chemical composition of varying biomass is not the same. Ultimate analysis is often used for the chemical analysis of biomass feedstock. The chemical analysis usually lists the carbon, hydrogen and oxygen of the dry biomass sample on a weight percentage basis. The composition of hydrogen in the biomass feedstock may influence the yield of Hydrogen in the gasified biomass.

Method of gasification also influences the yield of hydrogen. In the table, supercritical water gasification of biomass yield of hydrogen is much lower than steam gasification of the same biomass. For example the yield of hydrogen for cotton stalk is 4.19 with supercritical water gasification while steam gasification of the same biomass yielded 8.26 mol/kg of hydrogen, about 97% increment. The same goes for corn stalk with about 111% increment in hydrogen yield for steam gasification process.

Table 2: Hydrogen production from different biomass subjected to the same conditions. (Source: Nanda et al, 2016; Yanik et al, 2007, Wei et al, 2014; Pala et al, 2017)

Biomass	Hydrogen(mol/kg)	Conditions
Sugarcane bagasse[#]	1.66	400^0C
Coconut shell[#]	2.17	400^0C
Cotton stalk[#]	4.19	500^0C
Corn stalk[#]	4.15	500^0C
Cotton stalk*	8.26	650^0C
Sawdust*	9.02	650^0C
Corn stalk *	8.79	650^0C
Wood residue	27.86	900^0C
Coffee bean husk	34.32	900^0C

[#]supercritical water gasification **Steam gasification*

3.3 Effect of equivalence ratio

The ratio between the theoretical and practical air demand in steam gasification process utilizing air or O_2 is termed the equivalence ratio (ER). For each kind of biomass, there is a theoretical O_2 demand needed to achieve the combustion based on its contents of combustible materials and since in most cases, gasification is based on realizing relatively partial combustion, a fraction of this ratio is only used. A ratio of 0.15-0.35 has been investigated (Mohammed, 2010). The tar and char yields was discovered to decrease as the ER increases. This is because more oxygen in the gasifier causes the oxidation of the char and tar and leading invariably to producing more of CO and CO_2 and less of H_2. Optimum value of the ER for a particular gasification process should be noted. Beyond this optimum, carbon conversion efficiency and gasification efficiency will start to decrease (Gao et a.l, 2012; Zhao et al, 2010; Xiao et al, 2006).

3.4 Effects of Steam/biomass ratio

The steam biomass ratio could be varied either by changing the biomass feed rate while keeping the steam flow constant or vice versa. Result from previous researches show an increase in

Hydrogen production as the ratio increases. However, when S/B ratio is further increased beyond a certain point, production declined. The critical S/Bs are generally between 0.70 and 3.41 depending on the conditions (Zhang et al 2016b). Previous researches by Mahishi and Goswami, 2007; Kalinci et al, 2009; Inayat et al, 2010 and Moneti et al, 2016 obtained optimum yield of hydrogen at steam/biomass ratios of 3, 0.6-10, 2, and 2-3 respectively. Increasing the S/B ratio decreases slightly the CO and favours the water gas shift reaction that results in more hydrogen production. Operating the gasifier at a very high S/B might not be energy efficient since the increase in the production of hydrogen at this state may not justify the cost in increasing the steam (Pallozzi et al, 2016).

3.5 Effects of gasifier

Gasifiers are classified mainly on the basis of their gas solid contacting mode and gasifying medium. Based on the gas solid contacting mode, gasifiers are broadly divided into three principal types:

(i) fixed or moving bed gasifier
(ii) fluidized bed gasifier
(iii) entrained-flow bed gasifier

Each type of gasifier has different ranges of appropriate reaction condition and feedstock. There is an appropriate range of application for each. The moving-bed (updraft and downdraft) type often used for smaller units (10 MW) contains a large amount of tars in its product gas due to flow of biomass and the produced gas (Luo et al, 2009; Li et al, 2009). The fluidized-bed (bubbling and circulating) type is more appropriate for intermediate units (100 MW). Feed stock with high ash content can cause stickiness in the fluidized agent and reduce the fluidity of the inert bed material (Siedleck, 2011). The entrained-flow reactors are used for large capacity units (500 MW). The operating temperatures and pressure of the entrained flow reactor are higher than that of the fluidized bed and the fixed bed (Ghassemi et al, 2016). Several studies have compared the advantages and various gasifiers using different criteria such as use of material, energy efficiency, technology and enviromental impacts. The general consensus is that there was no significant advantage of one reactor type over the other. However, for decentralized power generation and distribution to remote and rural areas as well as for small scale industries fixed bed gasifier such as downdraft gasifier which are typically small scale unit with power generation capacity of up to 10 MW could be used.

3.6 Effects of catalyst and biomass composition

Reactions catalysts have positive effects on the yield of Hydrogen. Previous works indicates increase in the yield of Hydrogen when a catalyst was added to the reaction (Nanda et al, 2016; Gong et al 2014). The catalysts are known for cracking tars to produce gaseous products. Biomass are essentially made of three major polymers; the lignin, cellulose and hemicellulose. Experiments have shown that compared with lignin, cellulose and hemicellulose produced gases more rapidly with higher CO and CH_4 but lower H_2 and CO_2 concentrations, and higher temperature is needed for optimum hydrogen production. Lignin produced more hydrogen than cellulose and hemicellulose cell (Tian et al., 2017).

4. 0 Implications of Hydrogen fuel

Hydrogen as an energy carrier can be converted into useful forms of energy. For combustion in internal combustion engines, jet engines and rocket engines; Hydrogen powered combustion engines are about 20% more efficient than gasoline engines. This is because the thermal

efficiency of internal combustion engine can be improved by either increasing the compression ratio or the specific ratio both of which are higher in hydrogen engines. Hydrogen combusted with pure oxygen can generate steam with a temperature in the flame zone of above 3000^0C. Hydrogen steam generators can be used for industrial steam power supply, for electricity generation and in power plants. Hydrogen steam generator is close to 100% efficient since there are little or no thermal losses and there is no emission other than steam. Hydrogen can be combined with oxygen in an electrochemical reaction in fuel cell to produce electricity. In the typical IC engine vehicle optimized for a hydrocarbon fuel, only about 15% of the fuel value ends up as kinetic energy moving the vehicle down the road. This value increases to about 25% for an IC engine/electric hybrid. Fuel cell vehicles operating on compressed hydrogen have the potential of achieving over 30% and, unlike the hybrids, would be classed as zero emission vehicles.

Other energy conversion route of Hydrogen includes catalytic conversion to produce heat and conversions involving metal hydrides. Analysis of biomass gasification options has shown that production of hydrogen is the most economic route for the conversion of syngas to transportation fuels (Spath and Dayton, 2003). An economic and efficiency evaluation of hydrogen from biomass is therefore important for the implementation of the technologies of the gasification processes. Table 3 lists the hydrogen production costs from biomass gasification using different gasifiers and from other sources for previous studies. Biomass gasification seems to be the most cost effective for the production of hydrogen and power aside from Steam Methane Reforming (SMR). SMR is a mature technology that uses natural gas which has a well-defined non varying composition and is delivered via pipeline. However, SMR uses fossil fuel which is prone to depletion, enviromental pollution and greenhouse gas (GHG) emission. Biomass gasification on the other hand uses renewables which is available and sustainable. Infact, it has been viewed as an important technology for reducing GHG.

The U.S Department of Energy (U.S. DOE) has set a cost goal for hydrogen at $2-$3/kg including production, transportation and delivery for hydrogen to be cost competitive with fossil fuel. The goal for production cost only was set at $1.10/kg. None of the gasification process presented in table 3 met up with this goal. One way to reduce cost of production is to use renewable from nonfood biomass such as, agricultural residues; energy crops; woody crops; forestry, mill and wood wastes.

Hydrogen energy technologies are particularly interesting for the developing countries that do not have huge energy infrastructures in place. Cost for distribution such as power transmission lines, pipelines, transportation infrastructure might work against centralized production in developing economy. Developing countries may adopt dispersed renewable energy sources using both traditional and advanced technologies for their utilization. Hydrogen can be produced from low cost biomass to supply off grid electricity to homes using a portable fuel cell power systems. Technology improvements of gasification process may reduce the cost of producing hydrogen from biomass. Advances in biotechnology that will produce high yield, low-cost energy crops is one of such ways. Improvement actions leading to an increase in process efficiency that would significantly enhance the system's performance is another way. This is because increase in hydrogen production from gasification of biomass has been linked to improved exergy efficiency of the gasification process. (Zhang et al; 2019)

Table 3: Hydrogen Production cost

Process	H_2 production cost	References
Air gasification in a fluidized bed	2.11USD/kg	Mohamed et al, 2011
steam gasification in fluidized bed with in-situ co2 capture	1.91 USD/kg	Inayat et al, 2011
Oxygen gasification in a Fixed bed and CO-shift at atmospheric pressure	1.69USD/kg	Lv et al (2008)
Large scale gasification	1.38USD/kg	Spath et al, 2005
Fuel cell hydrogen	2.76USD/kg	Ogden, 1999
Eletrolysed hydrogen	10USD/kg	Iwasaki, 2003
Biomass pyrolysis with high pressure	4.28USD/kg	Iwasaki, 2003
Steam methane reforming	1.25USD/kg	NREL, 2011

5.0 CONCLUSION

Hydrogen energy system from biomass gasification is a coherent, comprehensive and permanent solution to global energy-economic-environmental problems, and as such deserves support from individual governments, industrial organizations and research institutes. Adopting gasification technology for the main purpose of producing hydrogen may seem expensive but in the long run its benefit might be unquantifiable.

REFERENCES

Ahmad, A. A, Zawawi, N. F, Kazim, F. H, Inayat, A. and Khasri A. (2016). Assessing the gasification performance of biomass: A review on biomass gasification process conditions, optimization and economic evaluation. *Renewable and Sustainable Energy Reviews,* 53: 1333-1347.

Ben-Iwo, J., Manovic, V., Longhurst P. (2016). Biomass resources and biofuels potential for the production of transportation fuels in Nigeria, *Renewable and sustaianble energy reviews*, 63: 172-192.

Ciferno, J. P, Marano, J .J. (2002) Benchmarking biomass gasification technologies for fuels, chemicals and hydrogen production. U.S. Department of Energy National Energy Technology Laboratory (Washington, DC); 2002.

Demirbas A. (2001) Biomass resource facilities and biomass conversion processing for fuels and chemicals. *Energy conversion management* 42(11): 1357-1378.

Gao, N., Li, A., Quan, C., and Gao, F. (2008). Hydrogen-rich gas production from biomass steam gasification in an updraft fixed-bed gasifier combined with a porous ceramic reformer. *International Journal of Hydrogen Energy , 33* (20): 5430-5438.

Gao N, Li A, Quan C, Qu Y, Mao L. (2012). Characteristics of hydrogen-rich gas production of biomass gasification with porous ceramic reforming. *Int J Hydrog Energy*, 37:9610–9618

Ghassemi H, Mostafavi S. M, Shahsavan-Markadeh R.(2016) Modeling of high-ash coal gasification in an entrained-flow gasifier and an IGCC plant. J Energy Eng, 40:150-152.

Gong M, Zhu W, Zhang H.W, Ma Q, Su Y, Fan Y.J. (2014) Influence of NaOH and Ni catalysts on hydrogen production from the supercritical water gasification of dewatered sewage sludge *International Journal of Hydrogen Energy,* 39:19947-19954.

Hemschemeier, A., Melis, A., Happe, T., (2009), Analytical approaches to photobiological hydrogen production in unicellular green algae. Photosynthesis Research 102 (2–3): 523–540.

Inayat A, Ahmad MM, Abdul Mutalib MI, Yusup S. (2010) Effect of process parameters on hydrogen production and efficiency in biomass gasification using modelling approach. *J Appl Sci*, 10:3183–3190.

Inayat, A., Ahmad M.M, Mutalib M.A, Yusup S. (2011). Heat integration analysis of gasification process for hydrogen production from oil palm empty fruit bunch. *Chem Eng Trans* 25:971–976.

Iwasaki W. (2003). A consideration of the economic efficiency of hydrogen production from biomass. *Int J Hydrogen Energy*, 28:939–44.

Kalinci Y, Hepbasli A, Dincer I. (2009) Biomass-based hydrogen production: a review and analysis. *Int J Hydrogen Energy*, 34:8799–8817.

Lewis M.A., Ferrandon M.S., Tatterson D. F, Mathias P.,(2009), Evaluation of alternative thermochemical cycles-part III further development of the Cu-Cl cycle, Int J Hydrogen Energy, 34, 4136-4145.

Li J, Yin Y, Zhang X, Liu J, Yan R. (2009) Hydrogen-rich gas production by steam gasification of palm oil wastes over supported tri-metallic catalyst. *Int J Hydrog Energy*, 34:9108–9115.

Lu Y, Jin H, Guo L, Zhang X, Cao C, Guo X. (2008). Hydrogen production by biomass gasification in supercritical water with a fluidized bed reactor. *Int J Hydrogen Energy*, 33:6066-6075.

Luo S, Xiao B, Hu Z, Liu S, Guo X, He M.(2009) Hydrogen-rich gas from catalytic steam gasification of biomass in a fixed bed reactor: influence of temperature and steam on gasification performance. *Int J Hydrog Energy*, 34:2191–2194.

Lv P, Wu C, Ma L, Yuan Z. (2008) A study on the economic efficiency of hydrogen production from biomass residues in China. *Renewable Energy*, 33:1874–1879.

Lv P. M, Xiong Z. H, Chang J, Wu C. Z, Chen Y, Zhu J. X. (2004). An experimental study on biomass air–steam gasification in a fluidized bed. *Bioresour Technol* , 95(1):95–101

Mahishi M.R, Goswami D.Y. (2007) Thermodynamic optimization of biomass gasifier for hydrogen production. *Int J Hydrogen Energy* 32:3831–3840.

McKendry, P. (2002a). Energy production from biomass (part 2): conversion technologies. *Bioresource Technology , 83*: 47-54.

McKendry, P. (2002b). Energy production from biomass (part 3): gasification technologies. *Bioresource Technology , 83*: 55-63.

McQuillan B.W., Brown L.C., Besenbruch G.E., Tolman R., Cramer T., Russ B.E. (2002). High efficiency generation of hydrogen fuels using solar thermochemical splitting of water. Annual Report, GA-A24972, General Atomics, San Diego, CA

Mohammed M.A.A, Salmiaton A, Wan Azlina WAKG, Mohammad Amran M.S, Fakhru'l-Razi A. (2011). Air gasification of empty fruit bunch for hydrogen-rich gas production in a fluidized-bed reactor. *Energy Conversion Management*, 52(2), 1555–1561.

Moneti M, Di Carlo A, Bocci E, Foscolo P.U, Villarini M, Carlini M. (2016) Influence of the main gasifier parameters on a real system for hydrogen production from biomass. *Int J Hydrogen Energy*, 1–9.

Nanda, S, Isen J, Dalai A K, Kozinski J A.(2016a). Gasification of fruit wastes and agro-food residues in supercritical water. *Energy Convers Manag*, 110:296-306.

Nanda, S. Reddy S.N, Dalai AK, Kozinski JA.(2016b) Subcritical and supercritical water gasification of lignocellulosic biomass impregnated with nickel nanocatalyst for hydrogen production. *Int J Hydrogen Energy* 41:4907-4921.

Naterer, G.F., Suppiah, S., Stolberg, L., Lewis, M., Wang, Z., Daggupati, V., Gabriel, K., Dincer, I., Rosen, M. A, Spekkens, P., Lvov, S., Fowler, M., Tremaine, P., Mostaghimi, J., Easton, E.B., Trevani, L., Rizvi, G., Ikeda, B.M., Kaye, M.H., Lu, L., Pioro, I., Smith, W.R., Secnik, E., Jiang, J., Avsec, J., (2010). Canada's program on Nuclear Hydrogen Production and the Thermochemical Cu-Cl cycle, *Int J Hydrogen Energy*, 35: 10905-10926.

National renewable energy laboratory(NREL) (2011). Hydrogen production cost estimate using biomass asification. www.nrel.gov.

Ni, M, Leung DY, Leung MK, Sumathy K. (2006). An overview of hydrogen production from biomass, *Fuel Process Technol*, 87: 461-472.

Ogden, J. M. (1999) Prospects for building a hydrogen energy infrastructure. *Annu Rev Energy Envision*, 24:227–73.

Orhan, M. F., Ibrahim D., Marc A.R., (2011), Simulation and Exergy Analysis of a Copper-Chlorine Thermochemical Water Decomposition Cycle for Hydrogen Production, *Intl Journal of Hydrogen Energy*, 36, 11309-11320.

Pala, L.P.R, Wang Q, Kolb G, Hessel V.(2017). Steam gasification of biomass with subsequent syngas adjustment using shift reaction for syngas production: an Aspen Plus model. *Renew Energy,* 101:484-492

Pallozzi V, Di Carlo A, Bocci E, Villarini M, Foscolo, P.U, Carlini M. (2016) Performance evaluation at different process parameters of an innovative prototype of biomass gasification system aimed to hydrogen production, *Energy Conversion and Management* 130: 34–43

Rapagnà S, Latif A. (1997). Steam gasification of almond shells in a fluidised bed reactor: the influence of temperature and particle size on product yield and distribution. *Biomass Bioenergy*, 12(4):281– 288

Safari F, Javani N, Yumurtaci Z. (2018) Hydrogen production via supercritical water gasification of almond shell over algal and agricultural hydrochars as catalysts. *Int J Hydrogen Energy*, 43:1071-1080

Siedlecki M, de Jong W, Verkooijen A.H.M.(2011) Fluidized bed gasification as a mature and reliable technology for the production of bio-syngas and applied in the production of liquid transportation fuels-a review. Energies, 4:389–43

Simonyan K, Fasina O. (2013). Biomass resources and bioenergy potentials in Nigeria, *Afr J Agric*., 8:4975–4989.

Skoulou V, Swiderski A, Yang W, Zabaniotou A. (2009). Process characteristics and products of olive kernel high temperature steam gasification (HTSG). *Bio resour. Technol*. 100(8):2444–2451

Spath P.L, Dayton D.C. (2003). Preliminary Screening} Technical and Economic Assessment of Synthesis Gas to Fuels and Chemicals with Emphasis on the Potential for Biomass- Derived

Syngas. National Renewable Energy Laboratory: Golden, CO, TP-510-34929

Spath PL, Aden A, Eggeman T, Ringer M, Wallace B, Jechura J. (2005). Biomass to Hydrogen Production Detailed Design and Economics Utilizing the Battelle Columbus Laboratory Indirectly Heated Gasifier. National Renewable Energy Laboratory: Golden, CO, TP-510-3740

Tian T Li Q, He R. Tan Z. and Zhang Y(2017) Effects of biochemical composition on hydrogen

production by biomass gasification*, International Journal of Hydrogen Energy* 42 (31) 19723-1973

Valente A, Diego R. and Dufour J. (2019). Life cycle sustainability assessment of hydrogen from biomass gasification: A comparison with conventional hydrogen, *International Journal of*

Hydrogen Energy, 44(38) 21193-21203

Wei L, Yang H, Li B, Wei X, Chen L, Shao J, Chen H.(2014). Absorption-enhanced steam gasification of biomass for hydrogen production: effect of calcium oxide addition on steam

asification of pyrolytic volatiles. *Int J Hydrogen Energy* 2014;39:15416e23.

iao R, Jin B, Zhou H, Zhong Z, Zhang M. (2007) Air gasification of polypropylene plastic waste in fluidized bed gasifier. *Energy Convers Manag*., 48:778–86.

Yanik J, Ebale S, Kruse A, Saglam M, Yuksel M. (2007). Biomass gasification in supercritical water: Part 1. Effect of the nature of biomass. *Fuel*, 86:2410-2415.

Zhao Y, Sun S, Zhou H, Sun R, Tian H, Luan J, (2010). Experimental study on sawdust air gasification in an entrained-flow reactor. *Fuel Process Technol*, 91:910–914

Zhang Y. Li L, Xu P, Liu B, Shuai Y. and Li B (2019). Hydrogen production through biomass gasification in supercritical water: A review from exergy aspect, *International Journal of Hydrogen Energy*, 44(30):15727-15736.

Zhang Y. Li L, Xu P, Liu B, Shuai Y. and Li B (2019). Exergy analysis of hydrogen production from steam gasification of biomass: A review*, International Journal of Hydrogen Energy*, 44(28), pp 14290-14302.

Proceedings of the 49th NSChE Annual Conference
KADA 2019: pp 271-286

P2A-04: STUDY OF METHANOL FUEL PRODUCED BY ELECTROCHEMICAL PROCESS USING PROTON EXCHANGE MEMBRANE (PEM).

Sampson Ojon Nwovu*, O.M.O Etebu[1], P. I. Okoye[2] and Alasdair Cairns[3]

*and1)Department of Mechanical Engineering, African Centre of Excellence, Centre for Oilfield Chemical and Research, University of Port Harcourt, Rivers State, P.M.B. 5323, Nigeria;
2)Department of Pure and Applied Chemistry, University of Port Harcourt, Rivers State, Nigeria.
3)Department of Mechanical Engineering, Nottingham University, Room C48 Coates, University Park, Nottingham, NG7 2RD, UK.

ABSTRACT

Methanol fuel was produced by electrochemical process using Proton Exchange Membrane (PEM). Carbonated alkaline solution of potassium hydroxide ($KHCO_3$) and water were the major feedstocks used. Cu and Zn electrodes were used as catalysts for cathode and anode respectively. The electrolysis of water and reduction of $KHCO_3$ to methanol occurred simultaneously in a single unit electrochemical set-up. Methanol synthesis occurred at cathodic half-cell when the proton produced by water in anodic half-cell reacted with $KHCO_3$. The synthesized methanol was separated from its solution by distillation. The membrane was prepared using Paraffin Wax, Silica Gel, and Sodium Dodecyl/Lauryl Sulphate (Surfactant). $KMnO_4$, FTIR and GC-MS were used for confirmatory tests on the synthesized methanol. The FTIR percentage transformation and GC-MS library results were analysed in comparison with analytical methanol purchased from chemical suppliers. The tentatively identified compounds in GC-MS's library have similarity indices of 97% and 95% to the synthesized methanol.

KEY WORDS: Carbon (IV) Oxide (CO_2), Water, Potassium Hydroxide (KOH), Methanol Fuel, Proton Exchange Membrane (PEM), Cu and Zn.

1.0 INTRODUCTION

Methanol is a colorless, volatile, flammable, poisonous and polar liquid at room temperature with the formula CH_3OH (also abbreviated as MeOH). It can also be called methyl alcohol, wood alcohol/spirit and carbinol. As published by National Center for Biotechnology Information; Fiedler et al., (2000); Cappelletti et al., (2012); Khirsariya and Mewada, (2013) pure methanol was first separated by Robert Boyle in 1661. Mr. Robert Boyle produced the chemical (i.e., Methanol) through the distillation of boxwood. The chemical was then called "pyroxylic spirit". Thereafter, French Chemists, Jean-Baptiste Dumas and Eugene Peligot determined its elemental composition in 1834.

Methanol is the simplest in the series of alkanol/hydroxyl group of organic compounds known as alcohols. The hydroxyl group (OH) is attached to a methyl group (CH_3). The term "methyl" was derived from the word "methylene" which was conceived by Dumas and Peligot in 1840 (Rossi, 1890 and Wisniak, 2009). It was then applied to describe "methyl alcohol". The International Conference on Chemical Nomenclature shortened this to "methanol" in 1892. Thereafter, the German Chemists, Alwin Mittasch and Mathias Pier developed a means to convert synthesis gas into methanol which was patented on January 12, 1926 (Alwin and Mathias, 1926).

However, the primeval Egyptians obtained methanol from pyrolysis of wood. Pyrolysis is a thermal treatment which results in the production of char, liquid and gaseous products (Maschio et al.,

1992). They mixed methanol in the substances which they used in embalming process. As published in https://thechemco.com/chemical/methanol/, in the early 1970s, Mobil developed a methanol to gasoline process for producing vehicle ready gasoline. One of the facilities was built in New Zealand at Motunui in the 1980s. Harvey-Smith and Cohen, (2006) reported that Astronomers at Jodrell Bank Observatory used Merlin array of radio telescopes to discover a large-scale of methanol in space, 300 billion miles across.

Presently, methanol fuel is among the renewable energy and alternative fuels presented by researchers and automobile manufacturers as replacement to gasoline in line with Sustainable Development Goals (SDGs). Due to its combustion characteristics, it is one of the most widely suggested alternative fuels (Atul and Atsushi, 2014; Olah, 2005; Olah et al., 2008a; Olah et al., 2008b and Goeppert et al., 2018). Accordingly, Olah and others promoted methanol economy as an excellent replacement to petroleum-based fuels and chemicals. For instance, methanol produced from wood or other organic materials ("bioalcohol") has been recommended as renewable alternative to petroleum-based hydrocarbons. In some countries (e.g., Europe and China), the use of methanol in existing vehicles involves blending it with proper cosolvents and corrosion inhibitors. As published in (https://thechemco.com/chemical/methanol/), the European Fuel Quality Directive (EFQD) permits up to 3 percent methanol with an equal amount of cosolvent to be blended in gasoline sold in Europe. Whereas China uses more than one billion gallons of methanol per year as transportation fuel in existing vehicles and vehicles designed to accommodate the use of methanol fuels.

Methanol fuel has advantages such as high octane rating and cleaner-burning properties amongst others than gasoline. It also has disadvantages such that a coal-based methanol economy could increase amongst others the water shortages, net carbon dioxide emissions, and volatility to regional and global coal prices. Moreover, methanol is toxic in nature as published by De Schweinitz, 1901. The publication by "thechemicalcompany Global Bonds in Chemistry" reported that in humans, methanol has high toxicity such that a little quantity of about 10mL if drank can destroy the optic nerve. The resultant effect on the human is permanent blindness. However, the effects of methanol toxicity can take hours before the patient begins to feel the symptoms. Meanwhile, if effective antidotes are administered to the patient, permanent damage can easily be prevented.

Nevertheless, alcohol fuels with carbon atom of C2 to C4 other than methanol as published by (Vafamehr et al., 2016; Moxey et al., 2014; Stansfield et al., 2012; Nwovu et al., 2018; and Kar et al., 2008) are also good alternatives to gasoline. Other suggested alternative to gasoline vehicle is electric vehicles. Yet, in electric vehicles, high-cost price and lack of suitable battery remain serious challenges. Meanwhile, the development of Lithium-ion and Lithium-Polymer battery that have two-to-three energy density of lead/acid batteries as reported by (Stone, 1999) is an improvement in the battery technology.

To ensure sustainable production of methanol and in commercial quantity, many researchers proposed different and promising preparation techniques. Amongst techniques are the capturing, recycling, and transformation of CO_2 to methanol and its by-products (example, Dimethyl ether, Alkanes, Alkenes, Dimethyl carbonate, and Olefin). This was published by (Sorenson, 2001; Atul and Atsushi, 2014).

In 1950s, Grubb introduced Proton Exchange Membrane (PEM) also called Polymer Electrolytic Membrane whereby the generation of proton (H^+) and reduction of CO_2 to methanol occur simultaneously in an electrochemical setups. This was not fully given the needed attention by researchers until 20th and 21st Centuries.

The use of high-pressure with reduced temperature catalytic technique as published by (Lee, 2007; and Bansode and Urakawa, 2014) was among the promising techniques of interest. But the technique negates the economic value associated with a reaction operated at a reduced pressure. The reason is because of higher energy (ΔG^o = 3.30KJmol^{-1}) involved during the high-pressure reaction (Fujitani et al., 1997; Jadhav et al., 2014; and Bahruji et al., 2016). As an improvement to the high-pressure, (Razali et al., 2012) reported that with a high-performance catalyst, the activation energy of CO_2 can be reduced. Nevertheless, the recent report on hydrogenation of CO_2 to methanol by (Tidona, 2013) showed the electrolysis of water as a major stage of high energy demand while the remaining stages are virtually pressure independent.

However, the concept of high-pressure methanol production is not new. In 1923, BASF commercialized the first methanol production using a mixture of syngas at pressure of 250 to 350 bar. Ipatieff and Monroe (1945) carried out CO_2 hydrogenation at high-pressure up to 412 bar using Cu/Al_2O_3 catalysts in a fixed bed reactor. They obtained remarkable selectivity of methanol and high conversion of CO_2. Atul and Atsushi (2014) reported high-pressure up to 360 bar CO_2 hydrogenation to methanol using co-precipitated $Cu/ZnO/Al_2O_3$ catalysts at high GHSV of 182,000h^{-1}. The authors improved on the catalyst compared to earlier reporters and recorded the first ever outstanding one-pass CO_2 conversion (>95%).

Low-pressure and temperature techniques were also developed by researchers as alternative to high-pressure hydrogenation of CO_2 to methanol. The concept of Low Pressure Methanol (LPM) originated in the late 1960s with the technology by Johnson Matthey, the leading licensor of methanol technology (Sheldon, 2017). Consequently, Wang et al., (2013) amongst others developed and operated successfully lower reaction pressure of about 50 to 100 bar at comparably lower temperatures in the presence of Cu/Zn-based catalysts. At a pressure of 15 bar and temperature of 250^{o}C, Deerattrakul et al., (2016) achieved methanol productivity of 591$mg_{meOH}^{-1}g_{cat}^{-1}h^{-1}$ using Nitrogen-doped (N-doped) reduced graphene oxide (N-rGO) in Cu-Zn catalysts. This is an improvement to the work of Atul and Atsushi, 2014 and earlier publishers. Interestingly, the concept of Proton Exchange Membrane (PEM) also called Polymer Electrolytic Membrane further addresses the issue of low temperature and pressure in methanol production.

Subsequently, in 2017, Abdelaziz and co-workers developed an optimum process technology that resulted in methanol production of 0.625 t-per-tonne of CO_2 waste gas supply. Andika, et al., (2018) made a comparison of methanol production from H_2-CO (from co-electrolysis) and H_2-CO_2 mixtures (from electrolysis). In their findings, they predicted that methanol production pathways from electrolysis if given favourable attention can lead to methanol production in a commercial quantity.

Presently, it is on record that China is in the frontrunner towards actualization of methanol economy (Chi-Jen and Robert, 2011). This is because from 2006 to 2011, China built an industry of coal-based methanol and dimethyl ether (DME) that is competitive in price with petroleum-based fuels (Chi-Jen and Robert, 2011). The publication by (Li-Wang et al., 2013) showed that most of the methanol produced in China are primarily utilized in the synthesis of formaldehyde,

alternative fuels and acetic acid, with the equivalent percentages of 35.0%, 33.0% and 8.0%. In terms of transportation, (Li-Wang et al., 2013) reported that China transported approximately 82.6% of methanol by overland freight, 9.0% by sea and 8.4% by train. Further remarkable trends in methanol fuel production and utilization is reported by Gong, et al., (2018); Iaquaniello, et al., (2017); Liu, et al., (2017); Liu, et al., (2019); Śliwińska, et al., (2017); Luu et al., (2015); Milani, et al., (2015); Szima and Cormos, (2018); Toyir, et al., (2009); Yang, et al., (2012); and Yao, et al., (2018).

2.0 Improved Combustion Characteristics of Alcohol Fuels in a SI Engine.

The use of alcohol fuels in internal combustion engines started since the onset of mechanically driven automotive transportation (Moxey et al., 2014). Most of the alcohols utilization in the current SI engines are gasoline-ethanol blends, with 5 to 10% volume alcohol typically allowed. Ikoma et al., (2006) and Zhu et al., (2008) reported that ethanol among other alcohol fuels is a good alternative transportation fuel for replacement of gasoline. Research proved alcohol fuels to have higher potential to increase engine performance, and ultimately improve knock resistance over gasoline because of its rapid rise in charge temperature during combustion events (Vafamehr et al., 2016 and Yacoub et al., 1998). At high temperature and pressure conditions in a SI engine operating on gasoline, there are high tendencies for occurrence of auto-ignition of the unburned gases ahead of the flame. The auto-ignition comes with irregular and uncontrollable pre-ignition with high-intensity knocking combustion (Kalghatgi and Bradley, 2012; Pan et al., 1998; and Basshuysen and Schäfer, 2004). Such auto-ignition often appears in different modes as reported by (Stone, 1999; König et al., 1990; and GU et al., 2003).

Alcohol fuels also have high latent heat of vaporization and lower unburned gas temperatures which help to cool the charge temperature during combustion compared to gasoline. In terms of injector deposit formation, Cairns et al., (2009) and Taniguchi et al., (2007) published that ethanol blends have a reduced injector deposit formation at an increased compression ratio due to lower nozzle temperatures and single component nature of the fuel. In terms of wear and corrosion in fuel pumps for gasoline-alcohol engines, (Rovai et al., 2005) reported that wears due to abrasion were dominant when using E22 with more corrosion damage when using fuel with increased alcohol content. Therefore, in the design of modern SI engines that can operate on alcohol fuels, there is need to consider the power cell materials selection, compression ratio and thermodynamic properties. This will validate the prediction by (Cowart et al., 1995 and Pearson et al., 2011) that engine output may be raised by 10 to 15% with potential additional gains for dedicated alcohol operation in the future.

Therefore, this study provides insight in methanol fuel production by electrochemical process using proton exchange membrane (PEM).

3.0 Materials and Method

3.1 Materials

The materials used during the study are described below.

Code A. Distilled water – *used to generate proton (H^+) at the anodic half-cell during electrolysis.*

Code B. Carbonated Potassium Hydroxide (KOH) Solution (i.e., Potassium Hydrogen Trioxocarbonate (IV)) produced by the reaction of CO_2 and KOH – *used to synthesize the methanol at the cathodic half-cell when reacted with the H^+ from the anodic half-cell*.

Code C. Proton Exchange Membrane (PEM) Materials – *used to promote transport of H^+ from anodic half-cell to cathodic half-cell.* It consists of the following materials:

I. Paraffin Wax.

Functions:

i. Repelled flow of water from anodic half-cell to the cathodic half-cell and vice-versa.
ii. Acted as a good binder.
iii. Attracted/captured the produced proton from water as a result of hydrogen bond interaction.
iv. Facilitated the transport of H^+ from anodic half-cell to cathodic half-cell through "domino effect".

II. Silica Gel (SiO_2).

Functions:

i. Worked together with paraffin wax to improve H+ transport.
ii. Provided pathway for proton transport. This is because, during the electrochemical reactions, the lone pair electron of Oxygen atom in the covalently bonded molecules of silica gel tends to attract a proton from the anodic half-cell. To attain suitability, it releases the attraction proton to the cathodic half-cell on continuous basis till the reaction is completed.

III. Sodium Dodecyl/Lauryl Sulphate (SDS/SLS) (Surfactant)
$CH_3(CH_2)10CH_2(OCH_2CH_2)nOSO_3Na$

Functions:

i. Served as an electron conductor through the membrane. This is because of the release of Na^+ from its molecule during the electrochemical reactions.
ii. Improved the conductivity of the membrane since paraffin wax and silica gel are not conductors.

Code D. Acidified Potassium Permanganate ($KMnO_4$) – *used to carryout qualitative and confirmatory test for presence of methanol*.

Code E. Polypropylene Container – *used as a lid to the component parts and also houses the solid electrolyte pile (i.e., proton exchange membrane).*

Code F. Cell – *was used to house the carbonated KOH solution (i.e., $KHCO_3$) and water which served as the electrolytes*.

Code G. Zinc electrode (positive/anode electrode) – *the electrode in which water was electrolyzed to generate hydrogen ion (H^+)/proton in the anodic half-cell*.

Code H. Copper electrode (negative/cathode electrode) – *the electrode in which carbonated KOH solution (i.e., $KHCO_3$) reacted with H^+ from the zinc electrode to produce methanol*.

4.0 Experimental Procedures

4.1 First Step: Preparation of the Proton Exchange Membrane (PEM)

i. 30g of paraffin wax was weighed into a beaker and heated until it melted.
ii. 15g of silica gel was weighed into another beaker.
iii. 5g of SLS/SDS was added into **"ii"** above and mix properly to obtain a homogenous mixture.
iv. The mixture in **"iii"** above was poured into the molten paraffin wax and stirred for 5minutes to ensure proper mixture.
v. The mixture in **"iv"** above was poured into a mould and allowed to cool/solidify for 30minutes.
vi. The mould was removed to obtain the formed PEM. See the Figure 1 below.

Figure 1 PEM made of paraffin wax/SLS/silica gel

4.2 Second Step – The cells were arranged as shown in Figure 2 below.

Figure 2 View of the half-cell compartments with Zinc and Copper electrodes

4.3 Third Step – The complete set up was packaged as shown in the Figure 3 below.

Figure 3 Packaging of the electrochemical set-up

4.4 Fourth Step – The electrochemical test was carried out as shown in Figure 4 below.

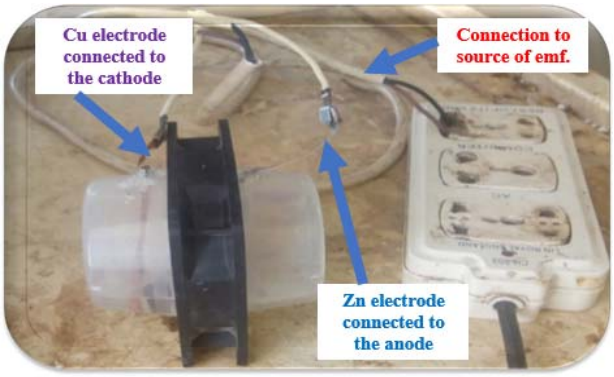

Figure 4 Electrochemical set up

4.5 The Reaction Processes

In the electrochemical set up, the CO_2 was fed into the electrochemical cell as a carbonated alkaline solution in the cathodic half-cell as illustrated in Equation (1) below.

$$\mathbf{CO_{2_{(g)}} + KOH_{(aq)} \rightarrow \quad KHCO_{3_{(aq)}} - - - \quad (1)}$$

(Carbonated alkaline solution)

Scheme 1: Solvation of CO_2 in an Alkaline Solution.

The carbonated alkaline solution which is represented as $KHCO_3$ for the purpose of simplification can be selectively reduced into any of the product shown in the scheme below (i.e., equations 2, 3 and 4) as reported by (Kuhl et al. 2014 and Olah et al. 2009). The availability of protons and electrons that act as limiting factors determine which of the preferred products are obtained.

$$\mathbf{CO_{2_{(g)}} + 2H^{+}_{(aq)} \xrightarrow{+2e^{-}} CO_{(g)} + 2H_2O_{(l)} - \quad (2)}$$

$$\mathbf{E_v = -0.76V}$$

$$\mathbf{CO_{2_{(g)}} + 6H^{+}_{(aq)} \xrightarrow{+6e^{-}} CH_3OH_{(aq)} + 2H_2O_{(l)} - (3)}$$
$$\mathbf{E_v = -0.62V}$$

$$\mathbf{CO_{2_{(g)}} + 8H^{+}_{(aq)} \xrightarrow{+8e^{-}} CH_{4_{(aq)}} + 2H_2O_{(l)} - (4)}$$
$$\mathbf{E_v = -0.48V}$$

Scheme 2: Overall electrochemical equations for the reduction of carbonated alkaline solution into methanol.

From the electrochemical point of view, the overall reaction for the conversion of the carbonated alkaline solution into methanol is presented in the equations 5, 6 and 7 below:

$$\text{Cathode: } KHCO_{3_{(aq)}} + 6H^{+}_{(aq)} \rightarrow KOH_{(aq)} + CH_3OH_{(aq)} + 2H_2O_{(l)} --- (5)$$

$$\text{Anode: } 6H_2O_{(l)} + 6e^{-} \rightarrow 6H^{+}_{(aq)} + O_{2_{(g)}} --------- (6)$$

$$\text{Overall Reaction: } KHCO_{3_{(aq)}} + 4H_2O_{(l)} + 6e^{-} \rightarrow KOH_{(aq)} + CH_3OH_{(aq)} + O_{2_{(g)}} --- (7)$$

As demonstrated in scheme 1, the efficiency of this process is grossly dependent on the transfer of protons from one half-cell to another. The proton transfer was achieved using the Proton Exchange Membrane (PEM).

4.6 Schematic of the Experimental Set-Up

Figure A in the Appendix shows the schematic of the experimental set-up.

5.0 Results and Discussion

The experiment was allowed to run for 1 hour and the following trends were observed:

i. For the first 10 to 15minutes, there was an observable concentration of a yellowish spot within the cathodic half-cell electrolyte.
ii. After 30 minutes, the yellowish spot disappeared thereby leaving the electrolyte solution in its initial colourless state.
iii. After 1 hour, we disconnected the power source and poured some sample of the electrolytic solution from the cathodic half-cell into a beaker shown in Figure 5 below for a qualitative test to confirm the presence of methanol.

Figure 5 Sample of $KHCO_3$ solution after the electrochemical reaction

iv. Acidified $KMnO_4$ was added in drops and then in excess to the collected sample of $KHCO_3$ solution and the colour changes were observed for 4minutes. At different time intervals, different colour changes were recorded till the sample solution became completely **"yellowish"** which confirmed the presence of **"methanol fuel"**.

5.1 FTIR Comparison of the Synthesized Methanol with Analytical Methanol purchased from Chemical Suppliers.

For more confirmatory test on the synthesized methanol, further analysis was performed using Fourier Transform Infrared Spectrophotometer (FTIR). At this stage, the percentage transformation of the synthetic methanol was compared to that of analytical methanol and the results demonstrated equivalent characteristics. Presented in Figure 6 is a computer generated graphical comparison of the synthesized and analytical methanol. Also, Figure 7 presents graphical comparison of generated data from the test results of synthetic and analytical methanol.

5.2 GC-MS Analysis Report on the Synthesized Methanol

To determine experimentally the molecular weight and structure of the synthesized methanol, GC-MS test was also carried out.

However, the calibration of the machine (SHIMADZU GC-MS - QP2010 PLUS) used for the GC-MS test could only analyze and detect organic/alcohol compounds from butanol (C4) and above.

Therefore, from the library results, the Tentatively Identified Compounds (TIC) are butanol and pentanol with highest Similarity Indices (SI) of **97%** and **95%** respectively to the unknown sample under test. The mass spectra of the TIC are shown in Figures 8 and 9 for butanol and pentanol respectively.

The high SI of the TIC to the unknown sample indicates that if worked backwards using their respective molecular structures, the original structure of methanol can be determined. The interpretation of the GC-MS library results is similar to crime detection by detectives who compares the fingerprint of an unknown crime suspect to a library of known fingerprint.

Therefore, from the library results of the GC-MS test, FTIR comparison test and qualitative test using KMnO4, it is established that the unknown sample is methanol.

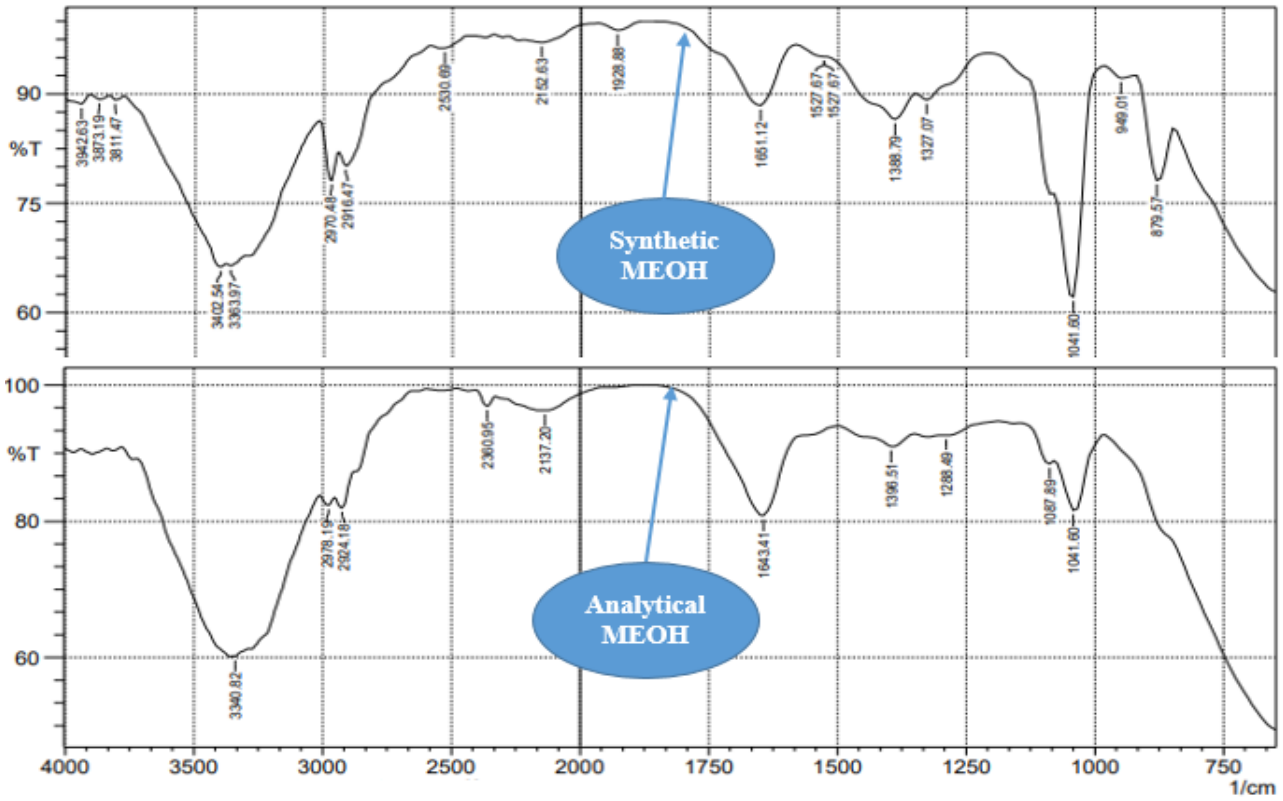

Figure 6 FTIR computer generated graphical comparison of the synthesized and analytical methanol

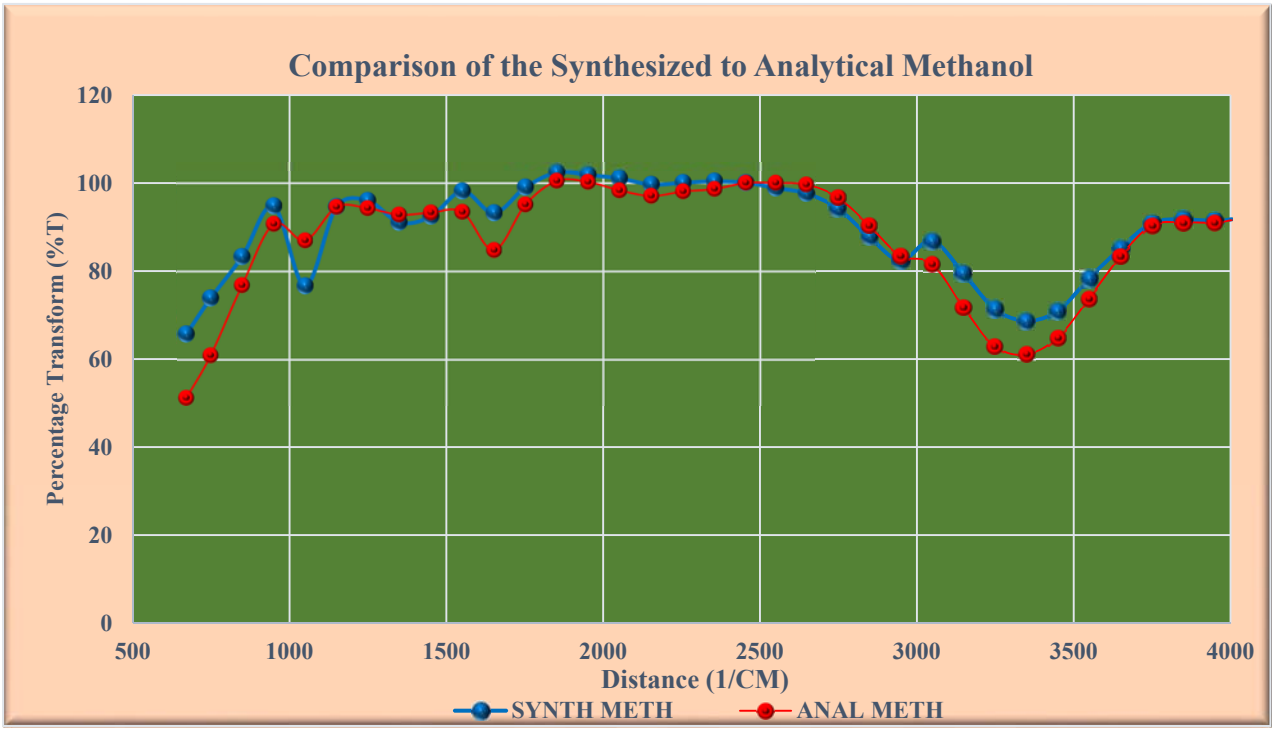

Figure 7 Graphical comparison of generated data from the test results of synthetic and analytical methanol

5.3 Library Result of GC-MS Test.

Entry 444 Library for butanol:
NIST08s.LIB; SI: **97**; Formula: $C_4H_{10}O$; CAS: 78-83-1; Mol Weight: 74; Ret Index: 597; Comp Name: 1-Propanol, 2-methyl- $$ Isobutyl alcohol $$ Isobutanol $$ Isopropylcarbinol $$ 2-Methyl-1-propanol $$ iso-C4H9OH $$ Fermentation butyl alcohol.

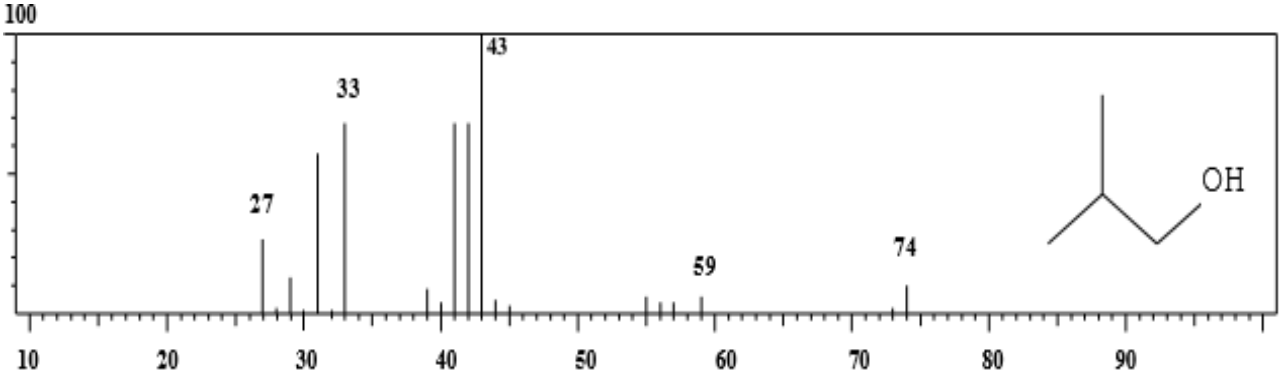

Figure 8: GC-MS test library result with butanol similarity index of 97%Entry 1060

Library for pentanol:

NIST08s.LIB; SI: **95**; Formula: $C_5H_{12}O$; CAS: 123-51-3; Mol. Weight: 88; Ret Index: 697; Comp Name: 1-Butanol, 3-methyl- $$ Isopentyl alcohol $$ Fermentation amyl alcohol $$ Fusel Oil $$ Isoamyl alcohol $$ Isoamylol $$ Isobutyl carbinol $$ Is.

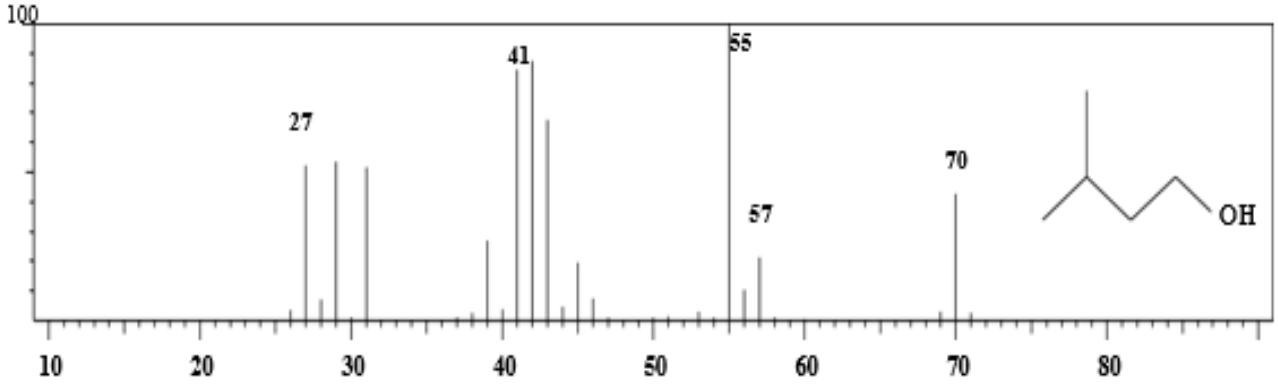

Figure 9: GC-MS test library result with pentanol similarity index of 95%

6.0 CONCLUSION

From the confirmatory tests, observations and results, the conclusion drawn are as follows:

i. 3.5litres of methanol fuel was synthesized. This shows that increased capacity of the electrochemical set-up, Proton Exchange Membrane (PEM), Carbonated alkaline solution and water will produce methanol of commercial quantity.
ii. Methanol can be produced from carbonated alkaline solution and water by electrochemical process using appropriate PEM materials.
iii. This study discovered that paraffin wax, silica gel and sodium lauryl/dodecyl sulphate (SDS) are optimum materials for PEM preparation. Therefore, PEM made up of combination of paraffin wax, silica gel and sodium lauryl/dodecyl sulphate (SDS) provides suitable conduit for proton and electron transport in an electrochemical process of methanol production.

iv. The use of Potassium permanganate ($KMnO_4$), Fourier Transform Infrared Spectrophotometer (FTIR) and GC-MS are good confirmatory tests for the presence of methanol in a given solution.
v. Copper and zinc electrodes are good catalysts for reductive hydrogenation of carbonated alkaline solution in an electrochemical reaction to produce methanol fuel.

7.0 RECOMMENDATION

From the conclusion derived from this study, it is recommended that further studies should aim at improving the capacity and effectiveness of the proton exchange membrane to achieve methanol production in commercial quantity.

Acknowledgement

The authors would like to acknowledge the Petroleum Technology Development Fund (PTDF) for its financial support through award of Scholarship to the corresponding author in the year 2016. We would also like to acknowledge the World Bank for establishing a Centre of Excellence at University of Port Harcourt, Rivers State, Nigeria wherein this study took place. Our appreciations also go to Abubakar Tafawa Balewa University, Bauchi State, Nigeria that provided all the supporting equipment and enabling environment that led to the success of this study.

APPENDIX

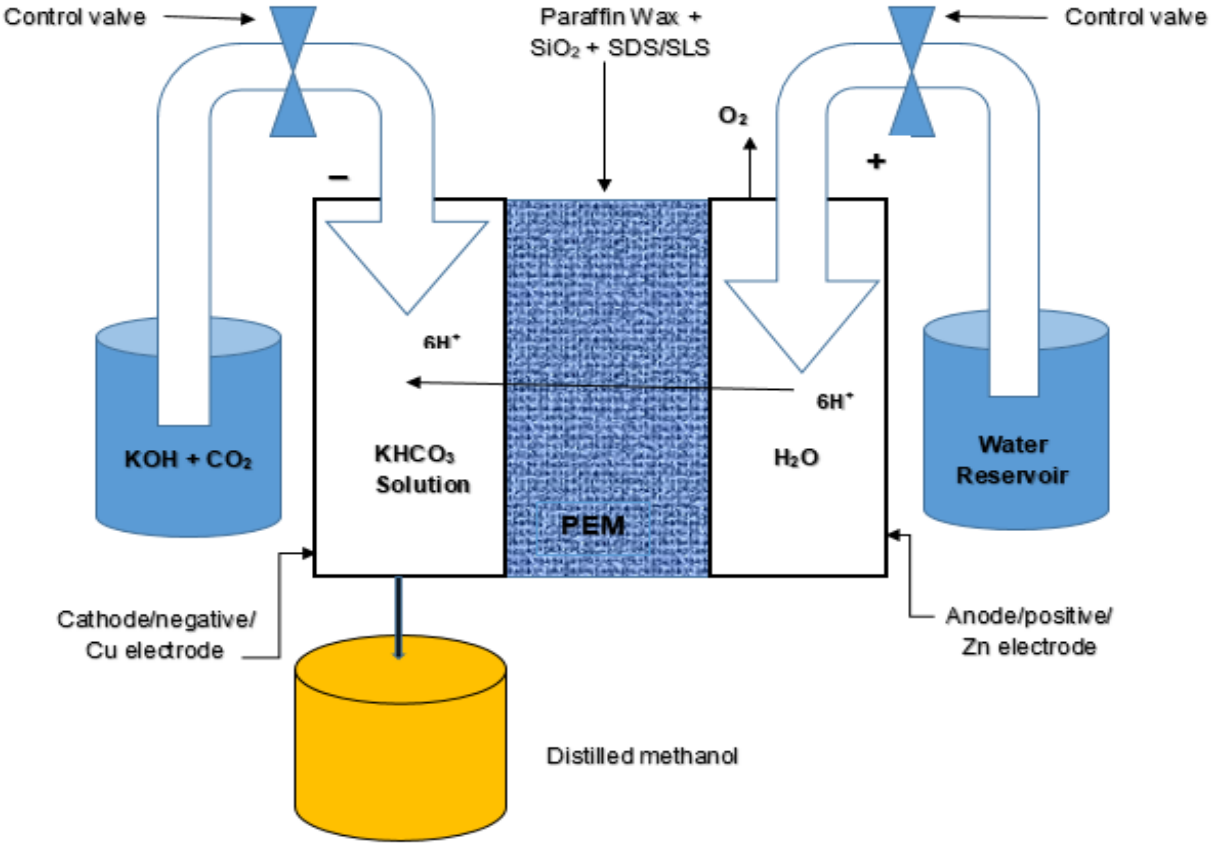

Figure A: Schematic of the experimental set-up

REFERENCES

Abdelaziz, O.Y., Hosny, W.M., Gadalla, M.A., Ashour, F.H., Ashour, I.A. and Hulteberg, C.P., (2017). Novel process technologies for conversion of carbon dioxide from industrial flue gas streams into methanol. *Journal of CO_2 Utilization*, ***21***, pp.52-63.

Andika, R., Nandiyanto, A.B.D., Putra, Z.A., Bilad, M.R., Kim, Y., Yun, C.M. and Lee, M., (2018). Co-electrolysis for power-to-methanol applications. *Renewable and Sustainable Energy Reviews*, ***95***, pp.227-241.

Alwin, M., and Mathias, P. (1926). *U.S. Patent No. 1,569,775*. Washington, DC: U.S. Patent and Trademark Office.

Bansode, A. and Urakawa, A., (2014). Towards full one-pass conversion of carbon dioxide to methanol and methanol-derived products. *Journal of catalysis*, ***309,*** pp.66-70.

Bahruji, H., Bowker, M., Hutchings, G., Dimitratos, N., Wells, P., Gibson, E., Jones, W., Brookes, C., Morgan, D. and Lalev, G., (2016). Pd/ZnO catalysts for direct CO_2 hydrogenation to methanol. *Journal of catalysis*, ***343***, pp.133-146.

Cairns, A., Stansfield, P., Fraser, N., Blaxill, H., Gold, M., Rogerson, J., and Goodfellow, C. (2009). A study of gasoline-alcohol blended fuels in an advanced turbocharged DISI engine. *SAE International Journal of Fuels and Lubricants*, *2*(1), 41-57.

Cappelletti, D., Candori, P., Falcinelli, S., Albertì, M., and Pirani, F. (2012). A molecular beam scattering investigation of methanol–noble gas complexes: Characterization of the isotropic potential and insights into the nature of the interaction. *Chemical Physics Letters*, *545*, 14-20.

Cowart, J. S., Boruta, W. E., Dalton, J. D., Dona, R. F., Rivard, F. L., Furby, R. S., ... and Takai, R. M. (1995). Powertrain development of the 1996 Ford flexible fuel Taurus. *SAE transactions*, 2092-2105.* (2016). CO2 hydrogenation to methanol using Cu-Zn catalyst supported on reduced graphene oxide nanosheets. *Journal of CO2 Utilization*, ***16***, pp.104-113.

De Schweinitz, G. E. (1901). *A case of methyl-alcohol amaurosis, the pathway of entrance of the poison being the lungs and the cutaneous surface*. RR Donnelly and Sons, printers.

Fiedler, E., Grossmann, G., Kersebohm, D. B., Weiss, G., and Witte, C. (2000). Methanol. *Ullmann's encyclopedia of industrial chemistry*.

Goeppert, A., Olah, G.A. and Prakash, G.S., (2018). Toward a sustainable carbon cycle: the methanol economy. In *Green Chemistry* (pp. 919-962). Elsevier.

Gong, C., Huang, W., Liu, J., Wei, F., Yu, J., Si, X., Liu, F. and Li, Y., (2018). Detection and analysis of formaldehyde and unburned methanol emissions from a direct-injection spark-ignition methanol engine. *Fuel*, ***221***, pp.188-195.

Gu, X. J., Emerson, D. R., and Bradley, D. (2003). Modes of reaction front propagation from hot spots. *Combustion and flame*, *133*(1-2), 63-74.

Harvey-Smith, L., and Cohen, R. J. (2006). Discovery of large-scale methanol and hydroxyl maser filaments in W3 (OH). *Monthly Notices of the Royal Astronomical Society*, *371*(4), 1550-1558.

Iaquaniello, G., Centi, G., Salladini, A., Palo, E., Perathoner, S., and Spadaccini, L. (2017). Waste-to-methanol: *Process and economics assessment. Bioresource Technology,* ***243***, 611-619

Ikoma, T., Abe, S., Sonoda, Y., Suzuki, H., Suzuki, Y., and Basaki, M. (2006). *Development of V-6 3.5-liter engine adopting new direct injection system* (No. 2006-01-1259). SAE Technical Paper

Ipatieff, V. N., and Monroe, G. S. (1945). Synthesis of methanol from carbon dioxide and hydrogen over copper-alumina catalysts. Mechanism of reaction. *Journal of the American Chemical Society,* ***67(12),*** 2168-2171.

Jadhav, S. G., Vaidya, P. D., Bhanage, B. M., and Joshi, J. B. (2014). Catalytic carbon dioxide hydrogenation to methanol: a review of recent studies. *Chemical Engineering Research and Design,* ***92(11),*** 2557-256.

Kalghatgi, G. T., and Bradley, D. (2012). Pre-ignition and 'super-knock' in turbo-charged spark-ignition engines. *International Journal of Engine Research*, *13*(4), 399-414.

Kar, K., Last, T., Haywood, C., and Raine, R. (2008). Measurement of vapor pressures and enthalpies of vaporization of gasoline and ethanol blends and their effects on mixture preparation in an SI engine. *SAE International Journal of Fuels and Lubricants,* ***1(2008-01-0317),*** 132-144.

Khirsariya, P., and Mewada, R. K. (2013). Single step oxidation of methane to methanol–towards better understanding. *Procedia Engineering*, *51*, 409-415.

König, G., Maly, R. R., Bradley, D., Lau, A. K. C., and Sheppard, C. G. W. (1990). Role of exothermic centres on knock initiation and knock damage. *SAE transactions*, 840-86.

Kuhl, K.P., Hatsukade, T., Cave, E.R., Abram, D.N., Kibsgaard, J. and Jaramillo, T.F., (2014). Electrocatalytic conversion of carbon dioxide to methane and methanol on transition metal surfaces. *Journal of the American Chemical Society*, ***136*****(40)**, pp.14107-14113.

Lee, S., (2007). Methanol synthesis from syngas. In *Handbook of alternative fuel technologies* (pp. 313-338). CRC Press

Liu, F., Hua, Y., Wu, H., Lee, C., and Shi, Z. (2017). Experimental and kinetic studies of soot formation in methanol-gasoline coflow diffusion flames. *Journal of the Energy Institute*.

Liu, H., Wang, Z., Qi, Y., He, X., Wang, Y., and Wang, J. (2019). Super-knock suppression for highly turbocharged spark ignition engines using the fuel of propane or methanol. *Energy,* ***169***, 1112-1118.

Luu, M. T., Milani, D., Bahadori, A., and Abbas, A. (2015). A comparative study of CO_2 utilization in methanol synthesis with various syngas production technologies. *Journal of CO_2 Utilization,* ***12****, 62-76*.

Maschio, G., Koufopanos, C., and Lucchesi, A. (1992). Pyrolysis, a promising route for biomass utilization. *Bioresource technology*, *42*(3), 219-231.

Milani, D., Khalilpour, R., Zahedi, G., and Abbas, A. (2015). A model-based analysis of CO_2 utilization in methanol synthesis plant. *Journal of CO2 Utilization,* ***10***, 12-22.

Moxey, B.G., Cairns, A. and Zhao, H., (2014). A study of turbulent flame development with ethanol fuels in an optical spark ignition engine (**No. 2014-01-2622**). *SAE Technical Paper*

Nakamura, I., Uchijima, T., Nakamura, J. and Fujitani, T., (1997). The kinetics and mechanism of methanol synthesis by hydrogenation of CO 2 over a Zn-deposited Cu (111) surface. *Surface Science*, ***383*****(2-3),** pp.285-298.

National Center for Biotechnology Information. PubChem Database. Methanol, CID=1031, https://pubchem.ncbi.nlm.nih.gov/compound/Methanol (accessed on July 13, 2019

Nwovu, S.O., Cairns, A. and Vafamehr, H., (2018), August. Effects of Direct Injection DI on Knocking Combustion in Spark Ignition SI Engine Operated on 75-RON and Ethanol Fuels. In *SPE Nigeria Annual International Conference and Exhibition*. Society of Petroleum Engineers.

Olah, G.A., (2005). Beyond oil and gas: the methanol economy. *Angewandte Chemie International Edition*, ***44*****(18),** pp.2636-2639.

Olah, G.A., Goeppert, A. and Prakash, G.S., (2008a). Chemical recycling of carbon dioxide to methanol and dimethyl ether: from greenhouse gas to renewable, environmentally carbon neutral fuels and synthetic hydrocarbons. *The Journal of organic chemistry*, ***74*****(2),** pp.487-498.

Olah, G.A. and Aniszfeld, R., University of Southern California (USC), (2008b). *Method for producing methanol, dimethyl ether, derived synthetic hydrocarbons and their products from carbon dioxide and water (moisture) of the air as sole source material*. U.S. **Patent 7,378,561**.

Olah, G. A., Goeppert, A., and Prakash, G. S. (2009). Chemical recycling of carbon dioxide to methanol and dimethyl ether: From greenhouse gas to renewable, environmentally carbon neutral fuels and synthetic hydrocarbons. The Journal of Organic Chemistry, **74(2),** 487-498.

Pan, J., Sheppard, C. G. W., Tindall, A., Berzins, M., Pennington, S. V., and Ware, J. M. (1998). End gas inhomogeneity, autoignition and knock. *SAE transactions*, 1748-1762.

Pearson, R. J., Eisaman, M. D., Turner, J. W., Edwards, P. P., Jiang, Z., Kuznetsov, V. L., ... and Taylor, S. G. (2011). Energy Storage via Carbon-Neutral Fuels Made From CO $ _ {2} $, Water, and Renewable Energy. *Proceedingss of the IEEE*, *100*(2), 440-460.

Razali, N. A. M., Lee, K. T., Bhatia, S., and Mohamed, A. R. (2012). Heterogeneous catalysts for production of chemicals using carbon dioxide as raw material: a review. *Renewable and Sustainable Energy Reviews, **16(7)**,* 4951-4964.

Rossi, A. J. (1890). EUGENÈ MELCHIOR PÉLIGOT. *Journal of the American Chemical Society*, *12*(5), 128-130.

Schafer, F., and Van Basshuysen, R. (Eds.). (2004). *Internal combustion engine handbook: basics, components, systems, and perspectives*. SAE International.

Sheldon, D. (2017). *Methanol Production - A Technical History. Johnson Matthey Technology Review, 61(3), 172–182.*

Śliwińska, A., Burchart-Korol, D., and Smoliński, A. (2017). Environmental life cycle assessment of methanol and electricity co-production system based on coal gasification technology. *Science of the Total Environment, **574***, 1571-1579.

Sorenson, S. C. (2001). Dimethyl ether in diesel engines: progress and perspectives. *Journal of Engineering for Gas Turbines and Power, **123(3),*** 652-658.

Stansfield, P.A., Bisordi, A., OudeNijeweme, D., Williams, J., Gold, M. and Ali, R., 2012. The Performance of a Modern Vehicle on a Variety of Alcohol-Gasoline Fuel Blends. *SAE International Journal of Fuels and Lubricants*, ***5*(2),** pp.813-822.

Stone, R., 1999. *Introduction to internal combustion engines* (**Vol. 3**). London: Macmillan.

Szima, S., and Cormos, C. (2018). Improving methanol synthesis from carbon-free H_2 and captured CO_2: A techno-economic and environmental evaluation. *Journal of CO_2 Utilization, **24***, 555-563.

Taniguchi, S., Yoshida, K., and Tsukasaki, Y. (2007). Feasibility study of ethanol applications to a direct injection gasoline engine. *SAE Transactions*, 695-70

The chemicalcompany Global Bonds in Chemistry https://thechemco.com/chemical/methanol/ (last accessed: 17th July 2019).

Tidona, B., Koppold, C., Bansode, A., Urakawa, A., and von Rohr, P. R. (2013). CO2 hydrogenation to methanol at pressures up to 950 bar. *The Journal of Supercritical Fluids, **78***, 70-77.

Toyir, J., Miloua, R., Elkadri, N., Nawdali, M., Toufik, H., Miloua, F., et al. (2009). Sustainable process for the production of methanol from CO_2 and H_2 using Cu/ZnO-based multicomponent catalyst. *Physics Procedia, **2(3),*** 1075-1079.

Vafamehr, H., Cairns, A., Sampson, O., and Koupaie, M. M. (2016). The competing chemical and physical effects of transient fuel enrichment on heavy knock in an optical spark ignition engine. ***Applied Energy**, 179*, 687-697.

Wang, Q., An, N., Bai, Y., Hang, H., Li, J., Lu, X., Liu, Y., Wang, F., Li, Z. and Lei, Z., 2013. High photocatalytic hydrogen production from methanol aqueous solution using the photocatalysts CuS/TiO2. *International Journal of Hydrogen Energy*, ***38*(25),** pp.10739-10745

Wisniak, J. (2009). Eugène Melchior Peligot. *Educación química*, *20*(1), 61-69.

Yacoub, Y., Bata, R., and Gautam, M. (1998). The performance and emission characteristics of C1-C5 alcohol-gasoline blends with matched oxygen content in a single-cylinder spark ignition

engine. *Proceedingss of the Institution of Mechanical Engineers, Part A: Journal of Power and Energy*, *212*(5), 363-379.

Yang, C., and Jackson, R. B. (2012). China's growing methanol economy and its implications for energy and the environment. *Energy Policy, **41**,* 878-884.

Yao, Y., Chang, Y., Huang, R., Zhang, L., and Masanet, E. (2018). Environmental implications of the methanol economy in china: Well-to-wheel comparison of energy and environmental emissions for different methanol fuel production pathways. *Journal of Cleaner Production, **172***, 1381-1390.

Zhu, G., Stuecken, T., Schock, H., Yang, X., Hung, D. L., and Fedewa, A. (2008). *Combustion characteristics of a single-cylinder engine equipped with gasoline and ethanol dual-fuel systems* (No. 2008-01-1767). SAE Technical Paper.

Proceedings of the 49th NSChE Annual Conference
KADA 2019: pp 287-298

P2A-05: DYNAMIC SIMULATION OF METHANE PRODUCTION FROM FOOD WASTE

Abdulwahab Giwa[1,*], Hamdalah Omosalewa Ibraheem[2], Idowu Iyabo Olateju[3] and John Olusoji Owolabi[4]

[1,2,3,4]Chemical and Petroleum Engineering Department, College of Engineering, Afe Babalola University, Afe Babalola Way, Ado-Ekiti, Ekiti State, Nigeria

[1,*]agiwa@abuad.edu.ng, [2]hamdyx7@gmail.com, [3]iolateju@abuad.edu.ng, [4]owolabijohn@abuad.edu.ng

[*]Corresponding author

ABSTRACT

This research has been carried out to study the dynamics simulation of methane production from anaerobic digestion of food waste with the aid of MATLAB/Simulink. The models used were obtained from literature and converted to a Simulink model of the process. The Simulink model was simulated with the aid of MATLAB mfile program. The dynamic responses were obtained by varying the retention time, specific death rate of methane-forming bacteria and influent biodegradable volatile solid concentration. It was revealed from the results obtained that methane can be produced from food waste because its amount was found to increase within the time of 7 days considered. Also, the amount of methane obtained from the process was found to be affected by the retention time and the specific death rate of methane-forming bacteria whereas the effect of concentration of influent biodegradable volatile solid was negligible.

Keywords: Methane, anaerobic digestion, bio-digester, dynamics, MATLAB, Simulink.

4 NOMENCLATURE

AD Anaerobic Digestion
BVS Biodegradable Volatile Solids
VFA Volatile Fatty Acid
VS Volatile Solids
S_0 Concentration of influent biodegradable volatile solid
θ Retention time
k_{dc} Specific death rate of methane-forming bacteria

1.0 INTRODUCTION

Anaerobic digestion is the process of molecular breakdown of biodegradable material using microorganisms under a controlled environment to generate biogas in form of an energy source from organic matter. This technique of generating energy was noted in the 17th century. Furthermore, in the 19th century, the consistency of the produced biogas as a renewable energy was explored. Most recently in the 20th century, anaerobic bacteria for commercial digestion have been discovered (Gantulga and McKenna, 2015).

Anaerobic digestion (AD) was practiced in the 10th century for heating baths in Assyria by biogas (gas produced by the breakdown of organic matters). In the 17th century, Jan Baptita Van Helmont of Belgium discovered that decaying organic matters produce flammable gas. In 1808, the British Chemist, Sir Humphry Davy, discovered that methane gas was present in cow manure (Ibraheem, 2018).

This process conserves nutrients and reduces pathogens in organic matter. According to Wellinger *et al.* (2013), 1000 lbs of human waste can produce 0.6 cubic meters of biogas.

Anaerobic digestion involves breaking down of organic material by bacteria in four major processes: hydrolysis, acidogenesis, acetogenesis, and methanogenesis. Hydrolysis is the process in which carbohydrates, proteins, fats are converted to sugars, fatty acids, and amino acids. Acidogenesis is the process in which the sugars, fatty acids, and amino acids are converted to carbon dioxide, ammonia, and carbonic acids. Acetogenesis is the process that creates acetic acid and carbon dioxide. The final process, methanogenesis, is the one that gives rise to the formation of biogas, which is a mixture methane and carbon dioxide gases. The extracted methane from this process can serve as a fuel for heat and electricity (Cakir and Stenstrom, 2005).

There are two common types of digesters used for anaerobic treatment: batch and continuous. Batch digesters are the simpler of the two because the material is loaded in the digester and then allowed to digest. Once the digestion is complete, the effluent is removed, and the process is repeated (Verma, 2002). Continuous digesters can be used for large commercial purposes. Either in a batch or a continuous mode, anaerobic digestion occurs as a controlled biological degradation process and allows for efficient capturing and utilization of biogas (approximately 60% methane and 40% carbon dioxide) for energy generation. The digestate from anaerobic digesters contains many nutrients and can be used as plant fertilizer and soil amendment (Ibraheem, 2018).

Researches have been carried out on the production of methane from food waste by anaerobic digestion, but few are in the area of modelling and simulation. Bala and Satter (1991) presented a dynamic model of biogas production. The model, which was solved using DYNAMO, had four coupled nonlinear first-order differential equations, two microbial growth equations and the resulting equation for biogas production. The predictive ability of the model was determined by comparing the model output with the observed values reported. The sensitivity analysis carried out in the work showed that gas production was sensitive to influent concentration and retention time. Adak *et al.* (2011) developed a simplistic mathematical model for anaerobic digestion of municipal solid waste in a continuous flow reactor unit under homogeneous steady-state condition by assuming that the kinetics of biomass growth and substrate utilization rate followed first order reaction kinetics. In the work, design table and charts were able to be prepared for ready use in actual plant operations. Masebinu *et al.* (2014) simulated a biogas upgrading plant operation that was using gas permeation technique for methane enrichment of biogas by studying the effect of recycling permeate stream on methane recovery, and it was discovered that recycling of the permeate stream improved the methane recovery of the simulated process. Contreras-Andrade *et al.* (2015) proposed a model, in form of differential equations, of a digester to study the dynamic simulations of biogas generation using Vensim software by taking the main factors of the biogas production to be the retention time and the methanogen mortality ratio. It was discovered in the work that the best yield of biogas could be obtained when the mortality ratio in methanogen and acidogenic bacteria were lower than 0.2 and the retention time was 30 h. Manjusha and Beevi (2016) used the Anaerobic Digestion Model 1 (ADM1), which gives complete information about the physicochemical reactions in the anaerobic process, that was solved with the aid of MATLAB, to model and simulate anaerobic digestion of solid waste in order to investigate how biogas production was affected by different parameters such as pH and volatile fatty acid (VFA).

This work has been carried out to contribute to biogas development by simulating the anaerobic digestion of food waste for the production of methane with the aid of MATLAB/Simulink using the dynamic models obtained from the literature.

2.0 METHODOLOGY

The version of MATLAB used in this work was R2018a (Mathworks, 2018), and the system used to carry out the simulation was Core(TM) -i5 6200U CPU @ 2.30 GHz.

The models used for the simulation of the anaerobic digestion of food waste for methane production in this work were obtained from the works of Bala and Satter (1991) and Contreras-Andrade *et al.* (2015). The steps involved in the production of methane by solid waste decomposition were analysed using differential equations. Thus, to model the quantity of solid waste flow in the system, an equation relating the solid material feed and its quantity in the reactor was used, and it was expressed as the biodegradable volatile solids (BVS) in the digester as in Equation (1),

$$\frac{dS}{dt} = \frac{S_0 - S}{\theta} - \frac{\mu M}{Y} \tag{1}$$

where S_0 is the concentration of influent biodegradable volatile solids (g VS/liter), S is the concentration of biodegradable volatile solids in the digester (g VS/liter), M is the concentration of acid-forming bacteria (g organism/liter), θ is the retention time (day), μ is the specific growth rate of acid-forming bacteria (day^{-1}), Y is the yield coefficient of acid-forming bacteria (g organism/g BVS) and t is the process time (day).

Also, an expression for describing the quantity of fatty acids available for methanogen bacteria was obtained in form of volatile fatty acids (VFA) in the digester to be as expressed in Equation (2),

$$\frac{dAC}{dt} = \frac{AC_0 - AC}{\theta} + \mu M Y_a - \frac{\mu_c M_c}{Y_c} \tag{2}$$

where AC_0 is the concentration of influent volatile fatty acids (g VFA/liter), AC is the concentration of volatile fatty acids in the digester (g VFA/liter), Y_a is the yield of volatile fatty acids from acid-forming metabolism (g VFA/g organism), μ_c is the specific growth rate of methane-forming bacteria (day^{-1}), M_c is the concentration of methane-forming bacteria (g organism/liter), Y_c is the yield coefficient of methane-forming bacteria (g bacteria/g VFA).

The expression for the dynamics of concentration of acid forming bacteria (acidogen) and methane forming bacteria (methanogen) were given as in Equations (3) and (4) respectively,

$$\frac{dM}{dt} = \left(\mu - k_d - \frac{1}{\theta}\right) M \tag{3}$$

$$\frac{dM_c}{dt} = \left(\mu_c - k_{dc} - \frac{1}{\theta}\right) M_c \tag{4}$$

where k_d is the specific death rate of acid-forming bacteria (day^{-1}) and $k_d c$ is the specific death rate of methane-forming bacteria (day^{-1}).

Since the quantity of biogas produced is a direct function of the quantity of methanogen in the bio-digester, it was deemed necessary to add a proportionality constant to this factor in order to obtain a correlation for the dynamics of the biogas production. The rate of biogas production, which was considered to be dependent on the concentration of methane-forming bacteria, was expressed as given in Equation (5),

$$\frac{dm}{dt} = \beta \mu_c M_c \tag{5}$$

where m is the amount of methane produced (liter/liter digester volume) and β is the proportionality constant.

The model set was setup with the aid of MATLAB/Simulink version R2018a as shown in Figure 1 and simulated by running an *mfile* containing codes written in MATLAB using some parameters (Table 1) obtained from the work of Bala and Satter (1991). Other parameters (Table 2) used were selected until acceptable output values, which were non-negative, were obtained.

Table 1. Parameter values of the model obtained from the work of Bala and Satter (1991)

Parameter	Values	Unit
μ	0.40	day^{-1}
μ_c	0.40	day^{-1}
k_d	0.04	day^{-1}
Y	0.10	g organism/g BVS
Y_c	0.05	g organism/g VFA
Y_a	9.00	g VFA/g organism

Table 2. Other chosen parameters used for the simulation

Parameter	Values	Unit
θ	1	day
β	0.5	-
S_0	40	g VS/litre
M_0	4	g organism/litre
MC_0	2	g organism/litre
AC_0	3	g VFA/litre
P_0	1.5	litre/litre digester volume

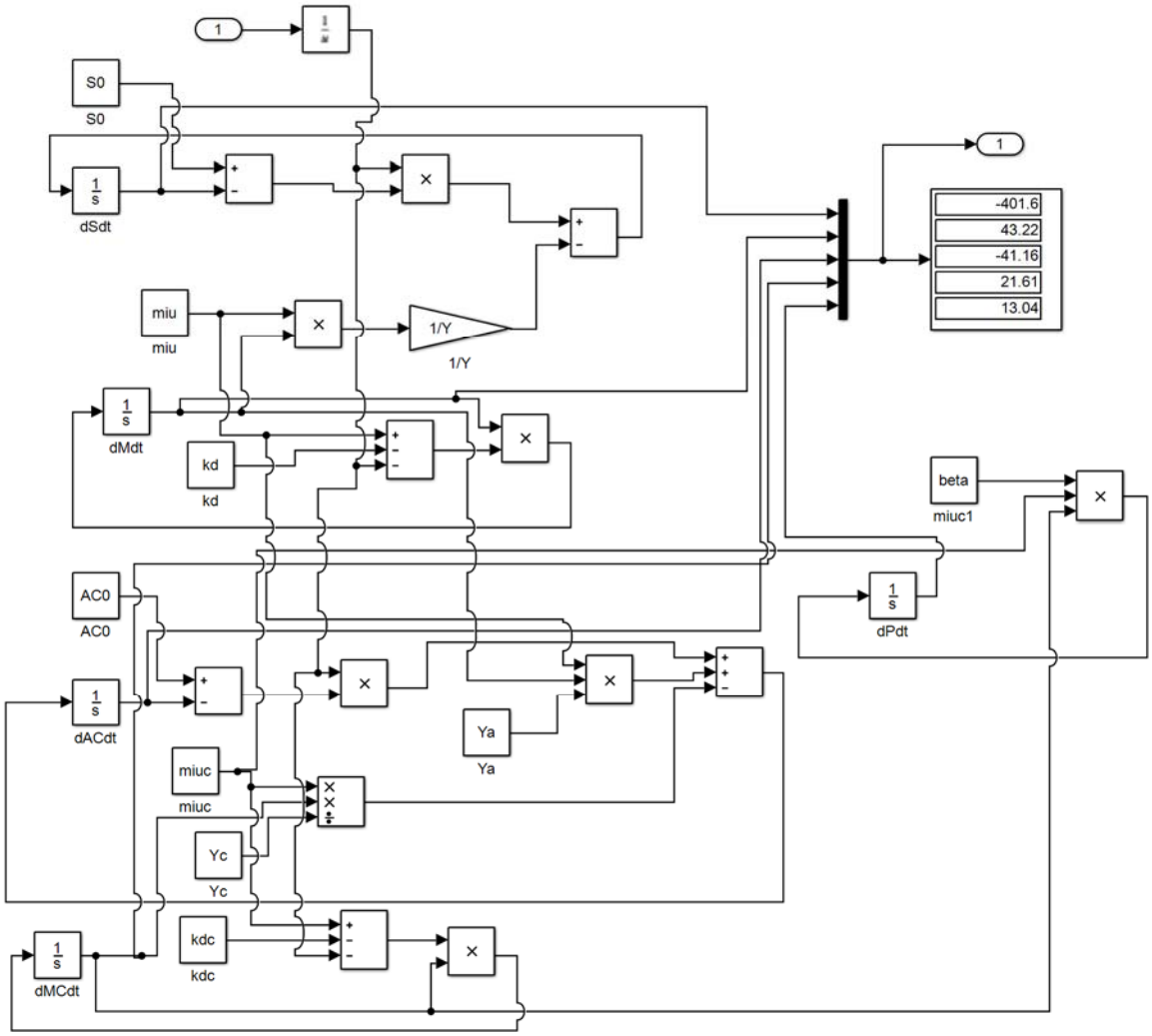

Figure 1: Simulink model for anaerobic digestion of food waste for methane production

Finally, the dynamic responses of the model were obtained while varying the retention time (θ), the specific death rate of methane-forming bacteria (k_{dc}), and the concentration of influent biodegradable volatile solids (S_0). The value of θ were varied arbitrarily between 10 and 50 day with a step size of 10 day, that of k_{dc} were between 0.25 and 0.75 day^{-1} with a step size of 0.25 day^{-1} while that of S_0 were from 40 to 120 (g VS/litre) with a step size of 20 (g VS/litre).

3.0 RESULTS AND DISCUSSION

The results obtained from the dynamic simulation of the model developed for the production of methane from food waste are as outlined and discussed thus. Figure 2 shows the dynamic responses of influent volatile fatty acid concentration when the retention time was varied. According to the results shown in Figure 2, the change in the retention time of the process gave rise to changes in the concentration of the influent volatile fatty acid, and it was noticed that the higher the retention time the higher the final concentration of the influent volatile fatty acid. Also noticed from the results shown in Figure 2 was that as the retention time was increasing from 10 to 50 days, the difference between the final concentration of the influent fatty acid for the different retention times was decreasing from about 23 to about 24.5 gVFA/liter.

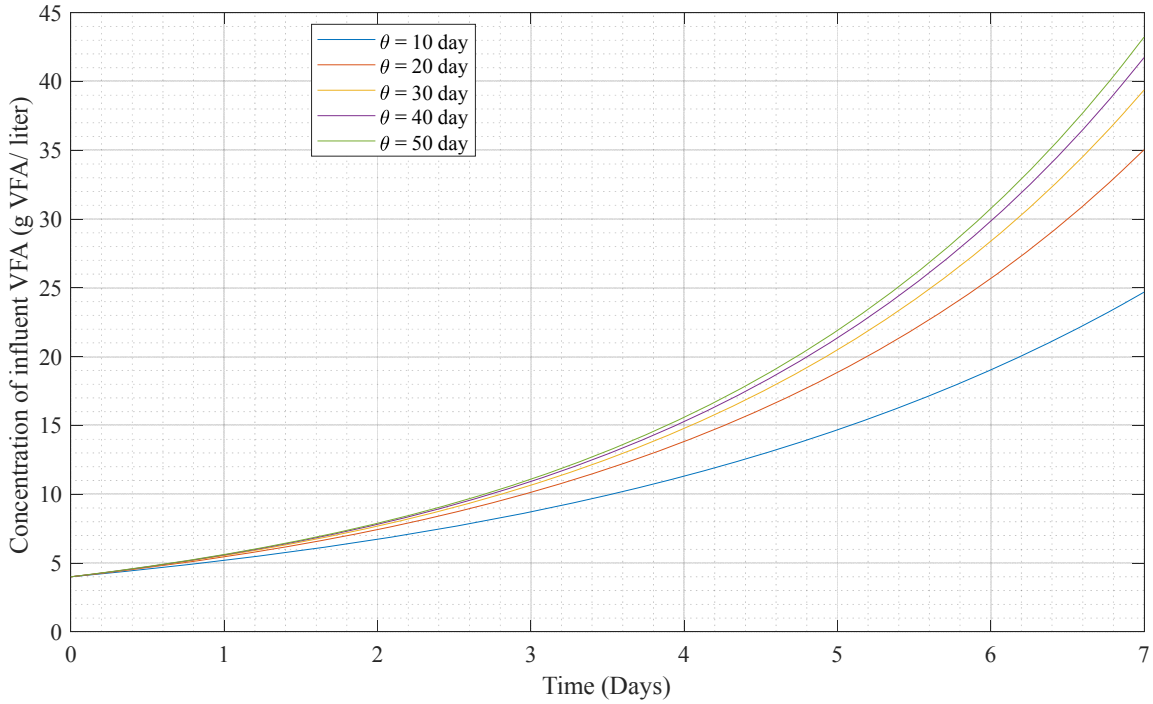

Figure 2. Dynamic concentration of influent volatile fatty acid (g VFA/ liter) at different retention times

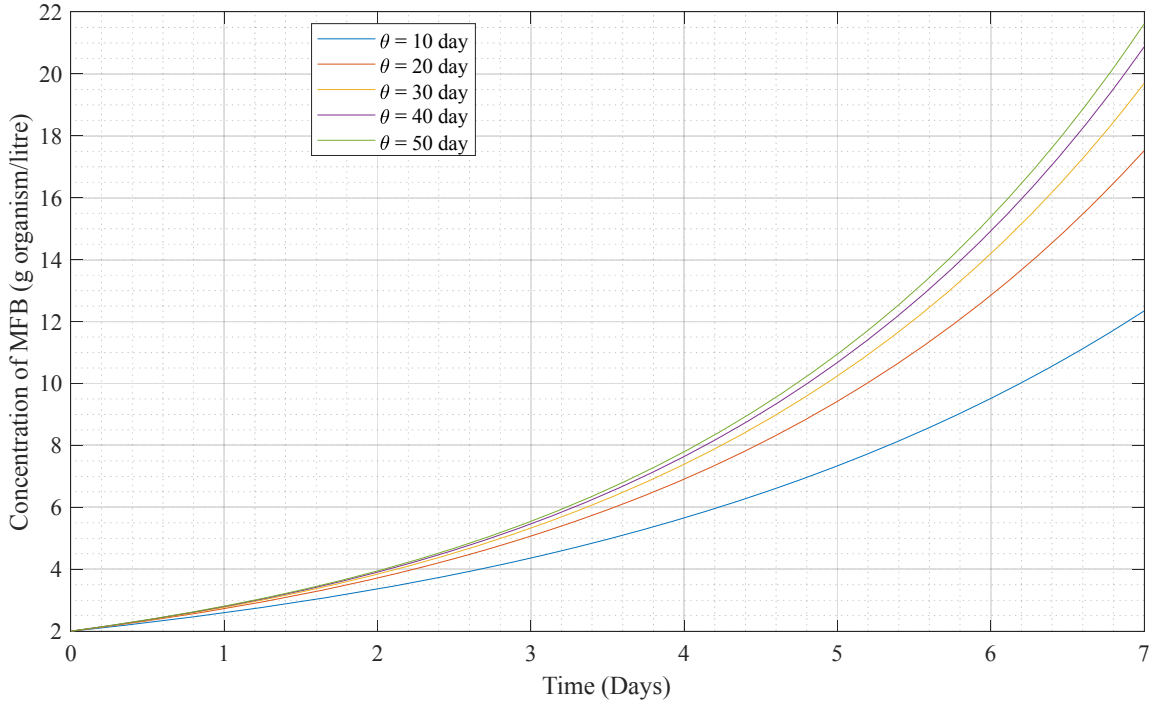

Figure 3. Dynamic concentration of methane-forming bacteria (g organism/litre) at different retention times

Similar observations to those of the results given in Figure 2 were made in the case of Figure 3 in which the dynamic responses of the concentration of methane-forming bacteria were shown at different retention times. However, the final values of the concentration of methane-forming bacteria were found to be different from those of the concentration of influent volatile fatty acid.

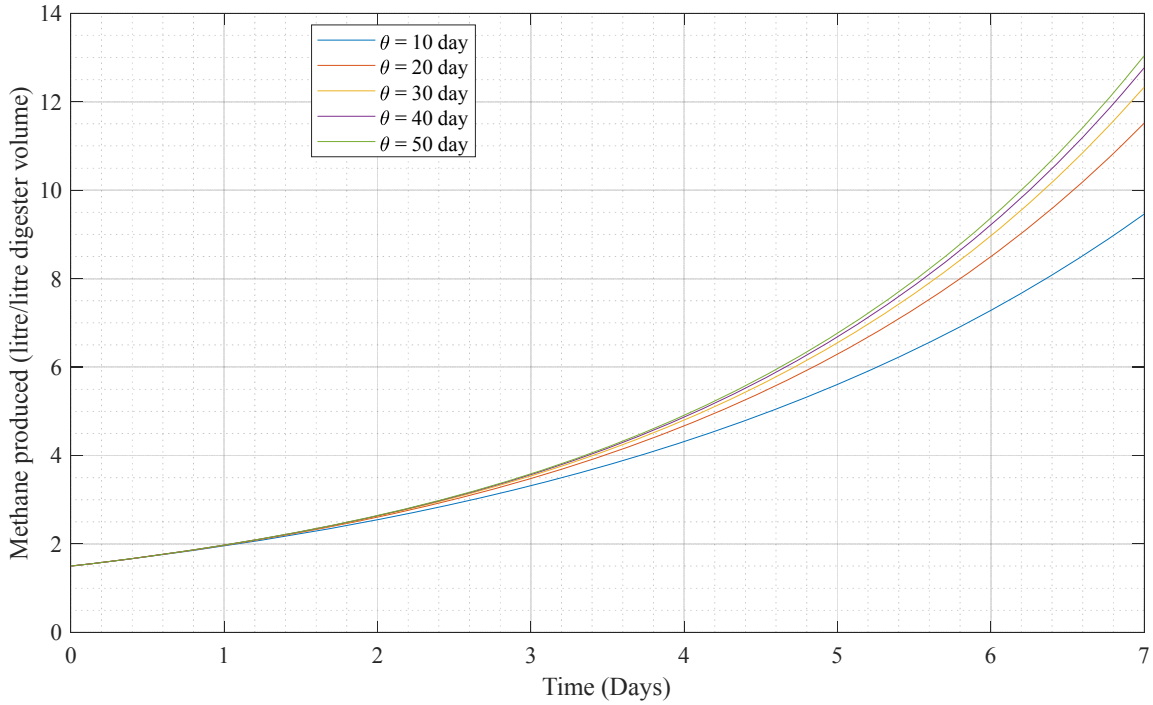

Figure 4. Dynamic response of methane produced (litre/litre digester volume) at different retention times

The dynamic responses of the amount of methane produced from the process is given in Figure 4. It can be seen from the figure that the amount of the methane was observed to vary as the process retention time was being varied. Also noticed from the results shown in the figure was that, despite the fact that the initial values of the simulation at the different retention times used were the same, the final values of the amount of methane produced were different, although the difference was becoming lesser as the retention time was increasing.

Furthermore, the effects of different specific death rates of methane-forming bacteria on the dynamic responses of some variables of this process were also investigated, and the results obtained were as given in Figures 5-7.

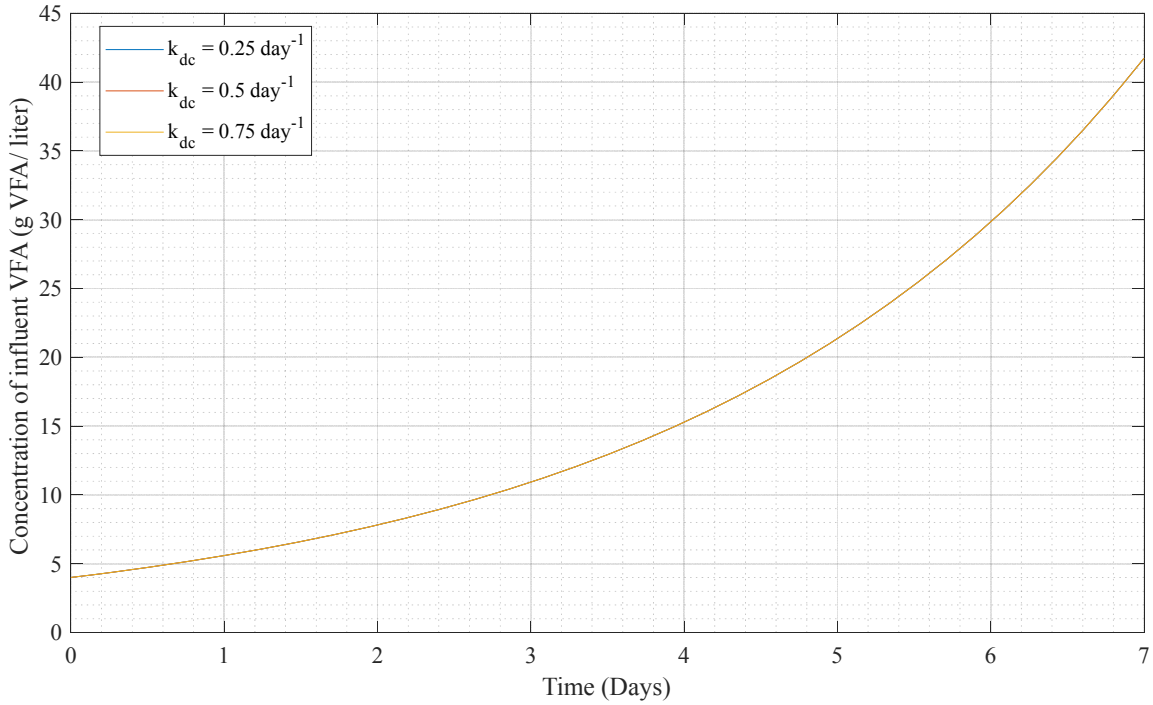

Figure 5. Dynamic concentration of influent volatile fatty acid (g VFA/ liter) at different specific death rate of methane-forming bacteria

Figure 5 shows the dynamic concentration of influent volatile fatty acid at different specific death rates (0.25, 0.50 and 0.75 per day) of methane-forming bacteria. It was observed from the results shown in the figure that the three responses obtained were found to overlap, and that was the reason for the appearance of a single curve on the figure. The implication of this is that the values of the specific death rate of the methane-forming bacteria at this instance has not any effect on the concentration of influent volatile fatty acid of the process.

The results obtained as the dynamic response of the concentration of methane-forming bacteria with variation in the specific death rate of the bacteria is shown in Figure 6. As can be observed from the results, the concentration of the methane-forming bacteria was found to increase with days when the specific death rate was 0.25 per day because the death rate was not high enough to hinder the formation of the bacteria for methane production. When the death rates were 0.5 and 0.75 per day, the concentrations of methane-forming bacteria were observed to decrease owing to the fact the rates were high enough then for the hindrance of the formation of the bacteria.

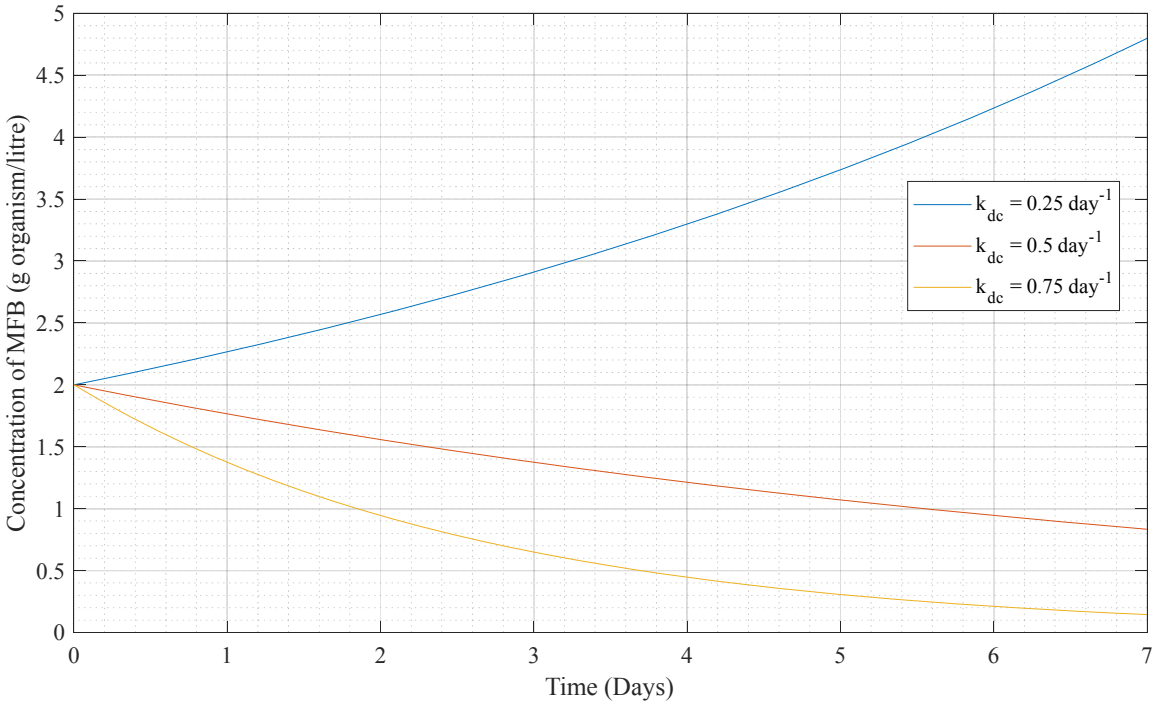

Figure 6. Dynamic concentration of methane-forming bacteria (g organism/litre) at different specific death rate of methane-forming bacteria

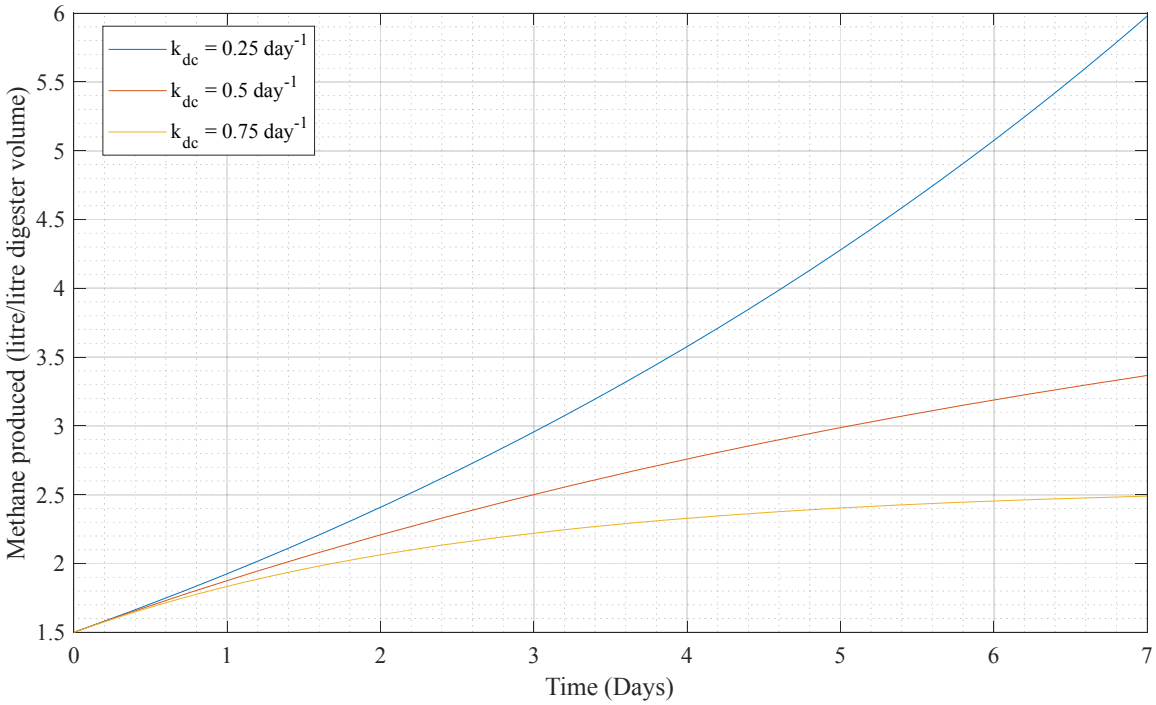

Figure 7. Dynamic concentration of produced methane (litre/litre digester volume) at different specific death rate of methane-forming bacteria

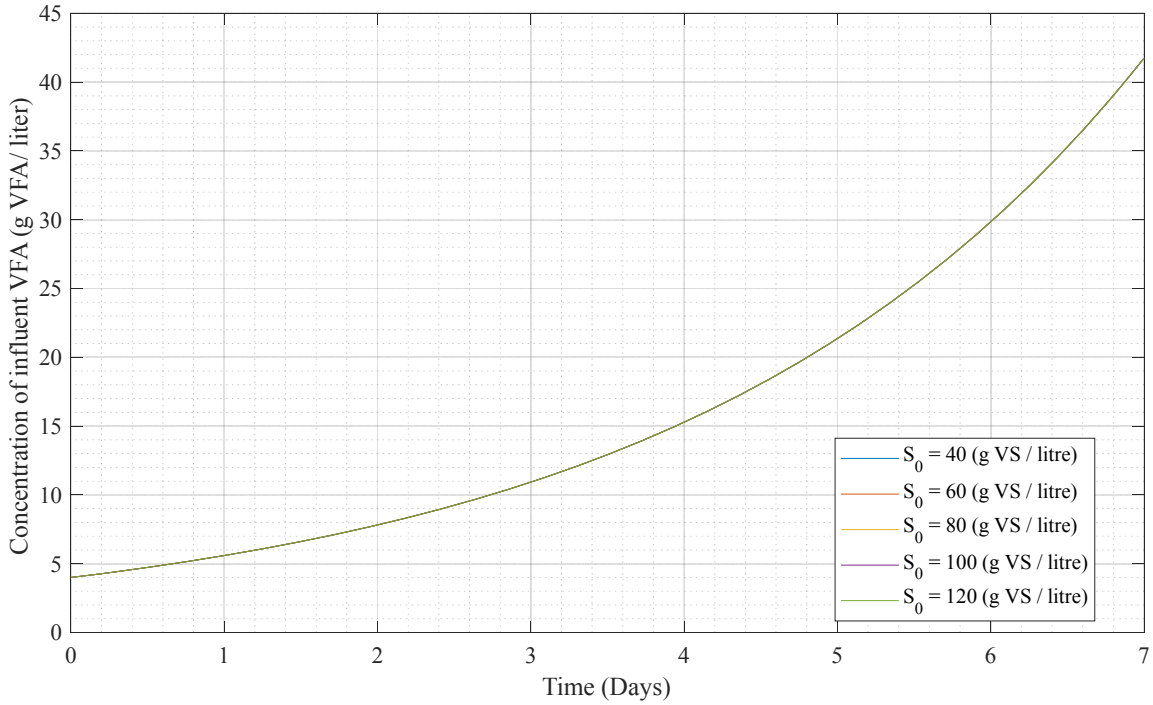

Figure 8. Dynamic concentration of influent volatile fatty acid (g VFA/ liter) at different concentration of influent biodegradable volatile solid

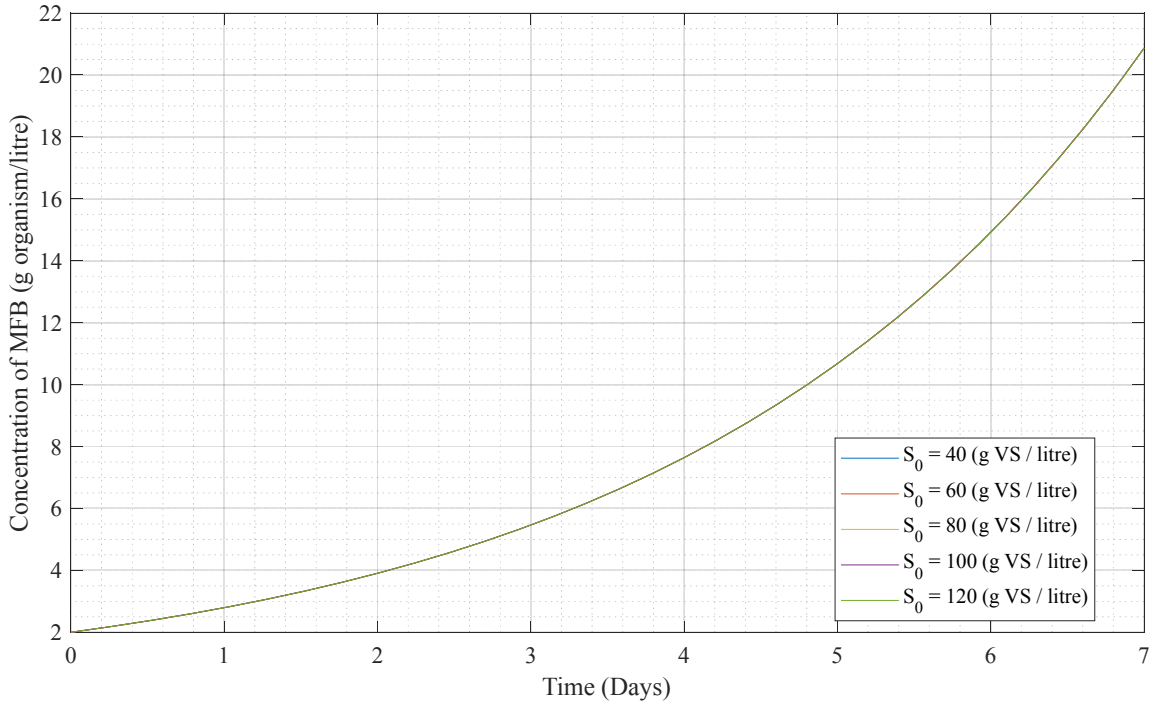

Figure 9. Dynamic concentration of methane-forming bacteria (g organism/litre) at different concentration of influent biodegradable volatile solid

Figure 7 shows the dynamic responses of the methane produced at different specific death rates of methane-forming bacteria. Using a simulation time of 7 days, the highest amount of methane

was observed to be obtained when the death rate was 0.25 followed by that of 0.5 and the least value was given by the death rate of 0.75. Also, within the simulation time considered, the three responses were found to be increasing. However, the amount of methane produced from the process was found to decrease as the specific death rate of the bacteria was increasing because the higher the death rate the less the bacteria that would be available for methane formation.

The dynamic responses of the influent volatile fatty acid concentration, methane-forming bacteria concentration and amount of methane produced obtained from the simulation of the process was carried out with variation in the concentration of influent biodegradable volatile solid were as shown in Figures 8, 9 and 10 respectively.

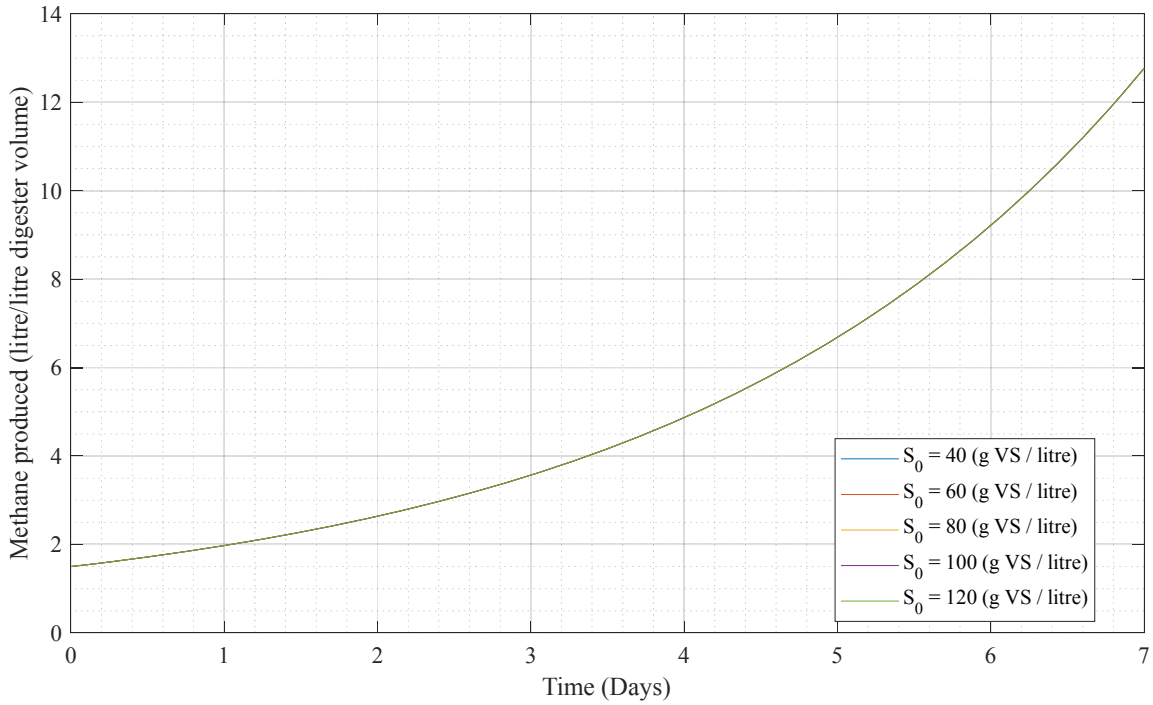

Figure 10. Dynamic concentration of produced methane (litre/litre digester volume) at different concentration of influent biodegradable volatile solid

According to the results (Figures 8-10), the concentration of influent biodegradable volatile solid was discovered not to have any effect on the selected process variables (influent volatile fatty acid concentration, methane-forming bacteria concentration and amount of methane produced) because the same dynamic responses were given for each of them, and this made the response curves to overlap one another.

The results obtained in this work were found to compare well with those obtained in the researches of Bala and Satter (1991) and Contreras-Andrade *et al.* (2015).

4.0 CONCLUSION

The results obtained from the simulation carried out in this work for the process producing methane from food waste with the aid of MATLAB/Simulink revealed that methane can be produced successfully from food waste because, with all the input parameters, the amount of methane in the digester was found to increase within the simulation time of 7 days considered.

The retention time and the specific death rate of methane-forming bacteria were found to have effects on the amount of methane produced from the process. For instance, as the retention time was varied from 10 to 50 days, the concentration of methane-forming bacteria was found to vary from about 12.5 to 21.5 at the end of the simulation period of 7 days. It is recommended that experiments should be carried out to validate the simulation responses obtained in this work.

ACKNOWLEDGEMENT

Special thanks go to Aare Ambassador Afe Babalola, LL.B, FFPA, FNIALS, FCIArb, LL.D, SAN, OFR, CON – The Founder and President, and the Management of Afe Babalola University, Ado-Ekiti, Ekiti State, Nigeria for providing a very conducive environment and the necessary materials that enabled the accomplishment of this research work.

REFERENCES

Adak, A., Mazumder, D., and Bandyopadhyay, P. (2011). Simulation of a process design model for anaerobic digestion of municipal solid wastes. *International Journal of Environmental and Ecological Engineering*, 5(8), 671-676

Bala, B., and Satter, M. (1991). System dynamics modelling and simulation of biogas production systems. *Renewable Energy*, 1(5-6), 723-728.

Cakir, F.Y., and Stenstrom, M.K. (2005). Greenhouse gas production: a comparison between aerobic and anaerobic wastewater treatment technology. *Water Research*, 39(17), 4197-4203.

Contreras-Andrade, I., Parra-Santiago, J., and Guerrero-Fajardo, C.A. (2015). Simulation of biogas production from solid organic wastes. *Journal of Chemistry and Chemical Engineering*, 9, 107-112.

Gantulga, D., and McKenna, J.R. (2015). *Anaerobic digestion of food waste including the impact of the commercial food waste disposal ban in Massachusetts*. An interactive Qualifying Project Report. Worcester Polytechnic Institute, Worcester, USA.

Ibraheem, H.O. (2018). *Dynamic simulation of methane production from food waste*. Bachelor of Engineering (B.Eng.) Project Report. Afe Babalola University, Ado-Ekiti, Ekiti State, Nigeria.

Manjusha, C., and Sajeena, B.B. (2016). Mathematical Modeling and Simulation of Anaerobic Digestion of Solid Waste. *Procedia Technology*, 24, 654-660

Masebinu, S.O., Aboyade, A.O., and Muzenda, E. (2014). Operational Study and Simulation of a Biogas Upgrading Plant. Proceedingss of the World Congress on Engineering, Vol II (pp. 1-7). London, United Kingdom

MathWorks (2018). MATLAB, The Language of Technical Computing, The MathWorks, Inc., Natic

Verma, S. (2002). *Anaerobic digestion of biodegradable organics in municipal solid wastes*. Master of Science Degree Thesis. Columbia University, New York City

Wellinger, A., Murphy, J., and Baxter, D. (Ed.). (2013). *The biogas handbook: Science, production and applications* (3rd Ed.). Sawston, United Kingdom: Woodhead Publishing.

Proceedings of the 49th NSChE Annual Conference
KADA 2019: pp 299-315

P2A-06: MODELLING OF BIOREFINERY SUPPLY CHAIN PROBLEMS: A CASE STUDY OF THE PROPOSED NNPC-KOGI BIOREFINERY PROJECT

M. O. Oladipo[1], S. M. Waziri[1*], U. A. Zaria[1], and A. A. Hamisu[1]
[1]Department of Chemical Engineering, Ahmadu Bello University Zaria, Nigeria
[*]**Corresponding author**: smwaziri@abu.edu.ng

ABSTRACT

This paper addresses challenges associated with biorefinery supply chain under economic, environmental and social objectives. The economic objective is expressed as the total supply chain cost, the environmental objective is expressed as greenhouse gas (GHG) emission and the social objective is measured as the total number of accrued jobs. A multi-objective mixed-integer non-linear (mo-MINLP) based optimization model was developed which accounted for the feedstock cost, feedstock transportation cost, unit production cost of bioethanol, bioethanol distribution cost to demand centres, energy consumption from the production of bioethanol, emission from waste generated in the bioethanol production, GHG emission from the transportation of feedstock to the biorefinery and transportation of bioethanol todemand zones. Also accounted for in the mo-MINLP is the social productivity coefficient, which isa measure of the social objective. The mo-MINLP model was solved using non-dominated sorting genetic algorithm-II (NSGA-II) which reveals a pareto-frontier within the economic, environmental and social objectives. A case study of the proposed NNPC-Kogi biorefinery project using Kabba-Bunu, Yagba-West and Bassa as potential locations of biorefinery was conducted. Bagasse sourced from Kabba-Bunu, Yagba-West, and Bassa harvesting sites and corn stover sourced from Kabba-Bunu, Dekina and Bassa harvesting sites were used as potential feedstocks. Kaduna refinery and petrochemical company (KRPC) and Port Harcourt refinery company (PHRC) were used as the target demand centres. The optimised results show a global optimal value of $1.24/litre which is 21.8% more than the local optimal value obtained from literature value of $1.24/litre. This difference was due to the location factor of 2.2 as assigned to Nigeria. Model acceptability and replication of the model in Nigeria and other countries of location factor of 2.2 with respect to USA location factor of 1; the production cost should be ≤ 21.8%.

Keywords: multi-objective optimization; Nonlinear programming, Supply Chain, Biorefinery Environmental and social objectives; Costs

INTRODUCTION

Fossil fuels have for decades been a dominant source of world energy supply. Fossil-fuel by-products are the world's most significant contributor to worldwide CO_2 emissions (Perera, 2017). 2009). Energy derived from biomass resources, known as bioenergy, is seen as an alternative energy resource. These biomass resources are categorized as: monomer of first-generation biofuel (food plants and animal fats), monomer of second-generation biofuel (animal waste, grass, corn-stover, crop residue) and third-generation (algae and bio-engineered feedstock) (Tembo *et al.,* 2003).

In 2018, the Nigerian National Petroleum Corporation (NNPC) signed a memorandum of understanding with Kogi state government to develop 84 million liters per annum biorefinery in Kabba-Bunu (Kogi state). The feedstocks to be used are cassava (a first-generation biofuel monomer) and bagasse (a second-generation biofuel monomer) (NNPC, 2018). To avoid competition with food security, secondary generation biofuel monomer is used.

The biorefinery supply chain has peculiar problems which include: location of harvesting sites, required amount of feedstock to be harvested, optimal route biomass logistics to the biorefinery, location, production processes, and production capacity of the bio-refinery, biofuel logistics and finally the number and location of target consumers (Cristina*et al.*, 2017). These problems need to be addressed to simultaneously minimize the overall biorefinery supply chain cost, minimize the GHG emission and to maximize the number of jobs accrued per annum.

The following are some related works that concentrate on mo-MINLP based models for biorefinery supply chain optimization. Guillen-Gosalbez and Grossmann (2009) looked at the optimal design and planning of chemical supply chains underuncertainty.In their work, they optimized the design and planning of chemical processes under uncertainty in the life cycle inventory bydeveloping a bi-objective MINLP based on stochastic assumption. Maximization of the economic objective function which is the net present value (NPV) and minimization of the environmental objective function based on the greenhouse gas (GHG) emission were successfully carried out.
Following the work of Corsano *et al.* (2011) an MINLP model was developed incorporating bioethanol supply chain cost and detailed plant design. for the simultaneous optimization of supply chain and plant design for producing ethanol from sugar cane as a feedstock was proposed. The model takes into account a detailed formulation for the ethanol plants considered in thesupply chain. It was deduced that residual recycle and derivative products are needed to attain sustainable designs of ethanol plants.

Based on the work by Yue and You (2014), presented a single objective MINLP model for fair profit allocation withtransfer price and revenue sharing: for cellulosic biofuel supply chains. Their results showed that anoptimal profit of 129.88 million dollars per yearwas obtained for the entire supply chain under the coordination of the revenue sharing policy. Gong and You (2014) considered the optimal design and planning of sustainable chemical supply chains underuncertainty. They proposed anMINLPmodel to minimize the unit CO_2 sequestration and utilizationcost subject to mass balance constraints, energy balanceconstraints, techno-economic constraints, and LCA (life cycle analysis) constraints.

A closely related article is in the work of Ivanovski (2014), where he considered a mo-MINLP based optimization model in his thesis titled "Multi-objective Optimization for Sustainable Supply Chain Network Design". His work failed to address the case study of a biorefinery supply chain network and also the optimal locations of demand centres where bioethanol will be delivered.

Based on the articles highlighted it was observed that more research is needed on mo-MINLP based optimization models in which economic, environmental and social objective functions are integrated into the optimization formulation for possible application to biorefinery supply chain questions and using global optimization technique. The aim of this work is to develop a multi-objective MINLP model to address bio-refinery supply chain problems with the view to optimizing the total supply chain network, taking into account the costs, GHG emission (environmental considerations) and social factors (such as the number of accrued local jobs). This is carried out by i) the design of a superstructurewhich shows all the possibilities of material flow from harvesting sites to biorefineries and to final demand centres ii) MINLP model development ii) solving of the MINLP using NSGA-II and iv) testing the performance of the model. However, this research is limited to the neighbourhood of material flow representation, steady-state assumption of the model development, stochastic based approach for the optimization and using second-generation biofuel as a feedstock to the biorefinery.

2.0 METHODOLOGY

This section comprises of the procedure in the research, superstructure assumptions, and model development assumptions and solution techniques.

2.1 Research Procedure

The procedure for carrying out the research is shown in Figure 1, which represents the flow chart ofthe schematic steps of the research.

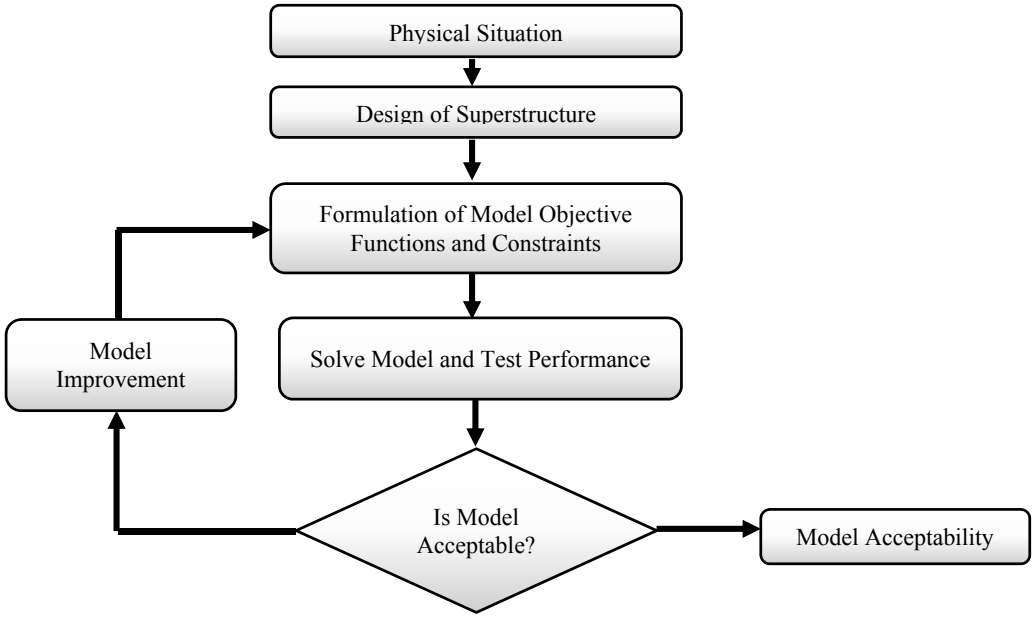

Figure 1: Flowchart of research methodology

The physical situation represents system to optimize which is the biorefinery supply chain using NNPC/Kogi biorefinery as a case study.The design of the superstructure entails possible locations of the harvesting sites, biorefineries and demand centers.It also gives the possible route to be taken for the delivery of biomass to the biorefineries and distribution of the product (bioethanol) to the final demand centers.

A multi-commodity flow model was used in the development of the economic objective function and corresponding constraints with improvement on the choice location on the demand centres; the approach on the environmental objective of the mo-MINLP was on the waste reduction model (WARM) proposed by "Environmental Protection Agency of United States" (EPA, 2014b); the social objective function was based on the job productivity of the individual biorefinery.
The solving of the model followed after the development of the model was done. Mo-MINLP can be solved generally by classical methods (as shown in table 1 with their respective disadvantages) and evolutionary algorithm (NSGA-II).

Table 1: Classical methods in solving mo-MINLP and their disadvantages

Category	Types	Shortcomings	Source
Traditional	Weighted-sum method	• Difficulty in setting the weight vectors to obtain a pareto-optimal solution in a desired region in an objective space • Does not calculated global optimum variables • Computationally expensive when the number of objectives and constraints increases	Shahryar and Yasaman, 2019
	Epsilon (ε)-constraint method	• The ε vector has to be chosen carefully so that it is within the minimum or maximum values of the individual objective function which can lead to an infeasible solution when the ε vector is not carefully selected which also depends on the expertise of the user • Computationally expensive when the number of objectives and constraints increases	Kaveh *et al.,* 2013
	Goal Programming	• Finding the highest quality set of solutions can be nevertheless a complex task, due to the fact the deviations from the goal levels can mislead the decision-maker, namely because of the conflicting functions and dependence between variables. • Computationally expensive when the number of objectives and constraints increases	Murshid *et al.,* 2018

The NSGA-II algorithm is computationally inexpensive when dealing with many objective functions and corresponding constraints. The solutions generated are insensitive to weights, constraints definitions and goal settings as attributed to the weighted-sum method, epsilon constraints method and the goal programming method respectively (Seada and Deb, 2018). It also ensures globalization (the least extremal value of the entire function) of the output. The objective functions and corresponding constraints were coded in MATLAB; MATLAB implementation of the NSGA-II was used to solve the mo-MINLP.

2.2 Superstructure assumptions

i. Two biomass feedstocks (corn-stover and bagasse) were considered. Bagasse and cassava are the proposed design feedstock for the Kogi/NNPC biorefinery (NNPC, 2017). Cassava was not chosen due to its potential to compete in food security in Nigeria. Furthermore, the scope of the research is limited to second-generation biofuel monomer where corn-stover and bagasse falls.

ii. Kabba-Bunu, Yagba-West, Bassa and Dekina were considered to be potential harvesting sites. Bagasse is harvested from Kabba-Bunu, Yagba -West and Bassa due to their availability of sugar-cane produce in their localities (NSDC, 2018). Bassa, Dekina and Kabba-Bunu are potential biomass sites for harvesting corn-stover due to its availability and these sites are located within the agricultural zones.
iii. No collection/storage facilities prior to transportation to the biorefineries.
iv. Kabba-Bunu, Yagba-West and Bassa were considered as the potential locations of the biorefineries, this is due to:
    a. Kabba-Bunu is considered as the design potential location of the biorefinery (NNPC, 2018)
    b. Kabba-Bunu, Yagba-West and Bassa are considered having large harvesting power in sugar production which produces bagasse as intermediate.
v. Kaduna refinery and petrochemical company (KRPC) and Port-Harcourt refinery company (PHRC) all subsidiaries of NNPC were considered as the demand zones due to proposed installation of blending unit in the refineries.

The unoptimized case for the design superstructure is shown in Figure 2, this shows the possible unoptimized biorefinery supply chain design, this case includes five potential harvestings sites located in Kabba-Bunu, Yagba-West (bagasse), Bassa(bagasse and corn-stover) and Dekina (corn-stover), with potential biorefineries co-located in Kabba-Bunu, Yagba-West, Bassa, it also shows the potential demand zones located in Kaduna and Port-Harcourt

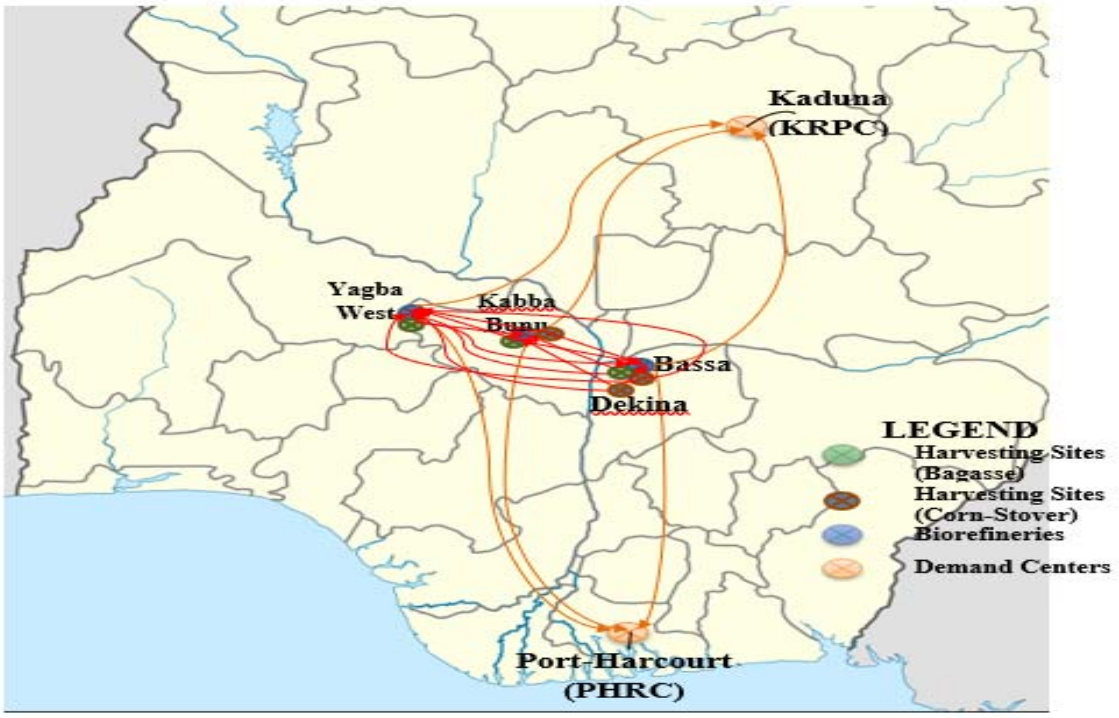

Figure 2: Design superstructure for the biorefinery supply chain (unoptimized Case)

2.3 Model development assumptions

Certain assumptions were, these assumptions were needed in setting up the boundaries of the model. Therefore, the following assumptions were made prior to the model development:

i. Steady-state assumption (single-period) of the model was considered

ii. Mixed-integer non-linear optimization model was used.
iii. A multi-objective optimization model consisting of minimization of economic, minimization of environmental objective function and the maximization of the social objective function.
iv. Harvesting sites' capacity can satisfy the production demand for feedstock.
v. Demand for product is known.
vi. Transportation and distribution distances between units in the supply chain model are known.
vii. Uniform mode of transportation of feedstock between harvesting site and biorefineries and distribution of product from biorefineries to demand zones were taken.
viii. Parameters associated with environmental objective function were based on GHG CO_2emission, which is a quantifiable basis in establishing the parameters associated with the environmental objective function (EPA, 2018).
ix. A single technology type (Biochemical conversion) was considered: the biochemical conversion process is close to commercialization and had better economic feasibility compared to thermochemical conversion in the production of bioethanol from corn and bagasse (You *et al.,* 2011, Cardona *et al.,* 2018, García *et al.,* 2019).
x. Single product type (bioethanol) was considered.

3.0 RESULTS AND DISCUSSION

This section presents the model development and results interpretation obtained from the solutions generated.

3.1 Model development

A mo-MINLP was developed in the modelling of biorefinery supply chain consisting of economic, environmental and social objective functions and corresponding constraints. The Indices used for the model development are shown below.

Indices/Set

R=set of biomass feedstocks indexed by r
I=set of harvesting sites indexed by i
J = set of biorefineries indexed by j
K = set of demand centres indexed by k

The following gives the list of the parameters as indicated below

COE_j = Cost of Opening a biorefinery (j), using biochemical conversion technology producing bioethanol
$CRM_{i,r}$= Cost of raw material(r) from harvesting site (i) to produce bioethanol
$CTRM_{r,i,j}$= Cost of transporting raw material (r) from harvesting site (i) to biorefinery (j)
CP_j= Cost of producing bioethanol form biorefinery (j) using technology type (g)
$CTPR_{j,k}$= Cost of transporting bioethanol to demand centers (k) from biorefinery (j)
ENV_j= Energy consumption per bioethanol produced in biorefinery (j) with biochemical conversion technology
WSE_j= waste generated from bioethanol produced in biorefinery (j) with biochemical conversion technology
$GHGTRM_{r,i,j}$= GHG emission from transportation of one unit of feedstock (r), from supplier (i) to production facility (j)
$GHGTPR_{j,k}$=GHG emission from transportation of one unit of bioethanol, from biorefinery (j) to customer (k)

$SIMPC_j$= Social coefficient of biorefinery (j) with biochemical conversion technology for producing bioethanol

D_k= demandforbioethanol from customer (k)

CAP_j = capacity of facility (j) with biochemical conversion technology for producing bioethanolfrom biorefinery (j)

Integer variables

The binary (integer) variables which allows decision to be made on the location of harvesting sites, biorefineries and demand centres

$H_{i,j}$ = Binary Variable for the location of harvesting site (i) distributing feedstock to biorefinery (j)

B_j = Binary Variable for the location of biorefinery (j) with biochemical conversion technology for producing bioethanol

$M_{j,k}$ = Binary Variable for the distribution of bioethanol to demand zone (k) from biorefinery (j)

Continuous variables

The continuous variables give the amount of feedstock and bioethanol that can be harvested from the harvesting sites and biorefineries respectively in the biorefinery supply chain

AMP_j= Amount of bioethanol produced from biorefinery (j) using biochemical conversion technology

$AMRT_{r,i,j}$= Amount of raw material(r) transported to biorefinery (j) from harvesting site (i)

$AMPT_{j,k}$= Amount of bioethanol transported to demand centre (k) from biorefinery (j)

3.1.1 Economic objective function

The economic objective function was based upon capital and operational costs of the lignocellulosic biorefinery supply chain from the feedstock procurement to product (bioethanol) distribution to final demand centers. This model is presented in equation 1

$$minimise \sum_j COE_j * B_j + \sum_r \sum_p \sum_i CRM_{i,r,p} * \sum_j AMRT_{r,i,j} + \sum_j CP_j * AMP_j + \sum_i \sum_j \sum_r CTRM_{r,i,j} * AMRT_{r,i,j} + \sum_j \sum_k CTPR_{j,k} * AMPT_{j,k} \quad (1)$$

The first term in equation 1 represents Fixed cost of construction and commissioning of every potential biorefinery based on its location and biochemical conversion technology type; the second term represents costs of feedstock purchased from every harvesting site based on the flow of material between the nodes harvesting sites – biorefinery; the third term represents variable costs of production; the fourth term gives the costs for transporting feedstock from suppliers to biorefinery; the last term represents the costs of distributing the bioethanol from biorefinery to final demand centers.

3.1.2 Environmental objective function

The model adopted in developing the environmental objective function is the "Waste Reduction Model (WARM)" developed by the "Environmental Protection Agency of United States" (EPA, 2018). WARM is a life-cycle methodology that is assessing the GHG emission throughout the whole life cycle of a product, from raw materials extraction, until the end of life disposals. The unit adopted for this objective function is GHG emissions which is available in the WARM model proposed by US environmental protection agency (EPA, 2018). The environmental objective function is given in Equation 2

$$minimise \sum_{j} ENV_j * B_j + \sum_{j} WSE_j * AMP_j \sum_{i} \sum_{j} \sum_{r} GHGTRM_{r,i,j} * AMRT_{r,i,j} + \sum_{j} \sum_{k} GHGTPR_{j,k} * AMPT_{j,k} \quad (2)$$

The first term in Equation 2 represents the electricity used per bioethanol produced, based on biochemical technology adopted in a particular biorefinery; the second term signifies the amount of waste generated per bioethanol from production processes, based on the amount of bioethanol produced and biochemical conversion technology adopted in a particular biorefinery; the third term denotes GHG emission from transportation between harvesting sites and biorefineries; the last term explains the GHG emission from transportation between biorefineries and demand centres

3.1.3 Social objective function

Ivanovski (2014) proposed a new model of describing the social objective function based on the social coefficient a production facility can have. In our case, a production facility is the biorefinery. The term social coefficient "$SIMPC_{j,g,p}$" is aimed at modeling the social impact of a new biorefinery. It is derived from the ratio of bioethanol produced and the projected productivity, based on the technology adopted and the workforce located in a particular biorefinery. The adopted model for the social objective function is given in equation 3

$$maximise \sum_{j} SIMPC_j * B_j \quad (3)$$

3.1.4 Constraints

The constraints employed for the three objective functions are shown in equation 4 to 10. Equation 4 ensures that there is demand satisfaction of every customer per bioethanol transported. Equation 5 gives that amount of bioethanol produced should be equal to the amount of bioethanol distributed to the customers. Equation 6 ensures that a biorefinery cannot produce more bioethanol than its capacity. Material balance in the biorefinery as regards to the inflow of feedstock transported to biorefinery from the harvesting site to the bioethanol produced in each biorefinery is given in equation 7. Equations 8 to 10 ensures non-negative values of the continuous variables are produced which signifies positive variables

From the model analysis, we could deduce that six decision variables are contained in the mo-MINLP model of which three are binary ($H_{i,j}, B_j \; and \; M_{j,k}$) and three are continuous variables ($AMP_j, AMRT_{r,i,j}$and $AMPT_{j,k}$), respectively

$$\sum_{j} AMPT_{j,k} * M_{j,k} \geq * D_k \quad (4)$$

$$\sum_j B_j * AMP_j = \sum_k AMPT_{j,k} \quad (5)$$

$$\sum_j AMP_j * B_j \leq CAP_j \quad (6)$$

$$\sum_i \sum_r H_{i,j} * AMRT_{r,i,j} = \sum_j B_j * Con_j * AMP_j \quad (7)$$

$$AMP_j \geq 0 \quad (8)$$

$$AMRT_{r,i,j} \geq 0 \quad (9)$$

$$AMPT_{j,k} \geq 0 \quad (10)$$

3.2 Model testing

The model testing is done by imputing model parameters into the model for testing the performance of the model. The data obtained are primarily gotten from information on the chosen case study which is the Kogi/NNPC proposed biorefinery project. For the purpose of this project information obtained from the MOU signed by Kogi state and the management of NNPC include the capacity of the plant (84 million liters per annum of bioethanol), location of the proposed biorefinery/potential location of the harvesting site (Kabba-Bunnu), proposed design feedstock (cassava and bagasse) (NNPC, 2018).

The cost of opening potential biorefineries and unit cost of bioethanol production were obtained from You *et al*. (2011). However, these cost values were calculated using CEPCI values for 2011 and 2019 as shown in equation 11

$$Cost_{2019} = Cost_{2011} \times \frac{Cost\ Index_{2019}}{Cost\ Index_{2011}} \quad (11)$$

To determine the final equivalent cost obtained in Nigeria, location factor is incorporated due to political stability, banking systems, business ethics, legal systems and geographical location. The location factor of 2.2 in Nigeria was recorded (Humphreys, 2005) with U.S.A having a location factor of 1. Using equation stipulated by (Oladapo and Aibinu, 2008) as shown in Equation 12

$$\frac{Cost_{U.S.A}}{Cost_{Nigeria}} = \frac{Lf_{U.S.A}}{Lf_{Nigeria}} \quad (12)$$

In estimating the cost of the design capacity of 84 million liters of ethanol, we employ the ballpark estimate which is expressed in Equation 13,

$$C_{ISBL@\ new\ capacity} = C_{ISBL@\ old\ capacity} \times \left(\frac{new\ capacity}{old\ capacity}\right)^n \quad (13)$$

Projected productivity is established to predict the productivity of workers within a year in the biorefinery as stipulated by Ivanovski (2014). The environmental, data were obtained from the USA EPA. These values were obtained based on $KgCO_2$ -equivalent (EPA, 2018). Transportation and distribution distances were calculated with the aid of google maps (Google Maps, 2019)

3.3 Pareto frontier generations

The pareto frontier was generated for 300 generations, these fonts were calculated for the three objective functions (economic, environmental and social) which were simultaneously solved by the NSGA-II. Each font (represented by the blue marks on individual generations) gives optimised solution of sets of genes corresponding to individual objective function fonts. Thegenes based on the principle of NSGA-II represent the optimised decision variables both binary and continuous variables with model definition of $H_{i,j}, B_j \; and \; M_{j,k}$ (binary) and $AMP_j, AMRT_{r,i,j} \; and AMPT_{j,k}$ (continuous). Selected pareto frontiers are given in Figure 3 to Figure 6.

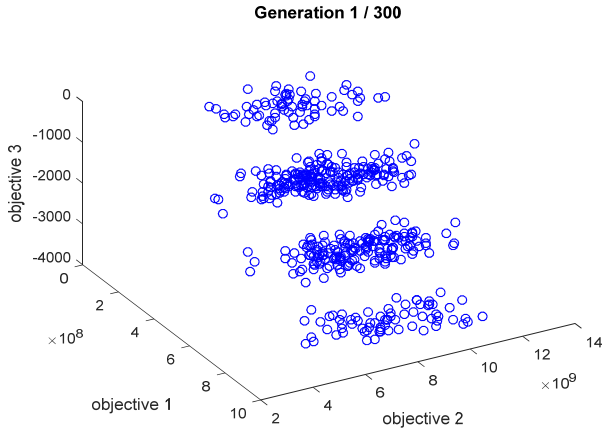

Figure 3: MATLAB generation for 1

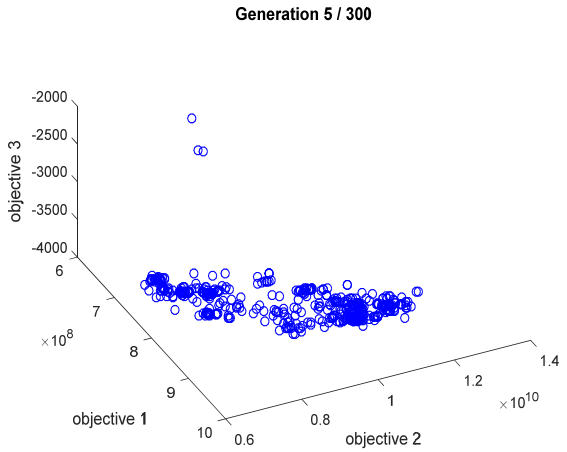

Figure 4: MATLAB generation for 5

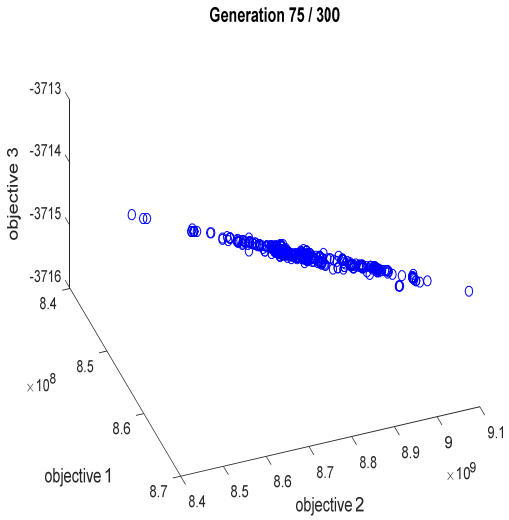

Figure 5: MATLAB generation for 75

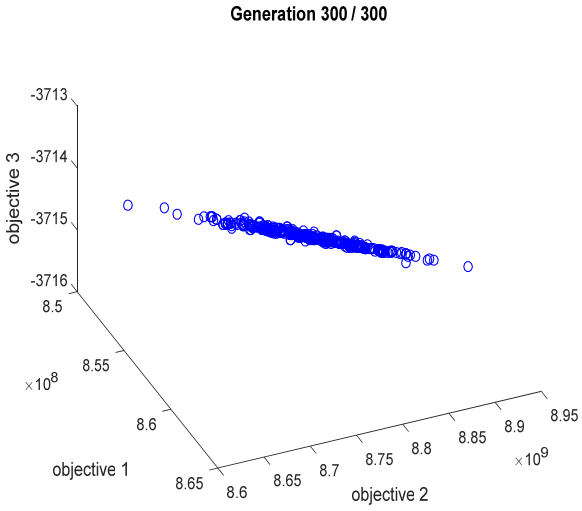

Figure 6: MATLABgeneration for 30

The non-correlated data (scattered) diagram in Figure 3 explains the first iteration of the algorithm, the initial population was defined by a random selection of data from the lower and upper bounds. This was done since no previous optimization existing was used. As it is shown in Figure 3 to Figure 6, convergences increase as we progress in the generation, this is in consonant with the principle of NSGA-II, the optimization stops when no considerable change in the optimal values of the objective functions (economic, environmental and social). The objective functions objective 1, objective 2 and objective 3 represents the social, environmental and economic objective functions respectively. The negative values for the objective 1 have to do with MATLAB code which signifies maximization of the objective function (social objective function). The values considered and treated as positive values. We can also see from Figure 3 to Figure 6, as it relates to the economic and social objective functions, that an increase in total jobs increases the total biorefineries installed. It implies that regional economy can benefit from installing more biorefineries especially within other local government areas in Kogi state.

3.4 Trade-off analyses

The trade-off analysis is done on individual objective function to ascertain the highest occurring values (fronts) in the entire generations. These are expressed as frequency to fronts occurrence. These are done for the cost, environmental and social objective function.

3.4.1 Cost distribution

Figure 7 shows the cost distribution of the fonts generated for the 300 generations. The distribution shows that the optimal solution for the overall supply chain for the biorefinery supply chain is mostly within the range of 850 million dollars to 859 million dollars. This range is within the economic viability of the overall biorefinery supply chain cost.

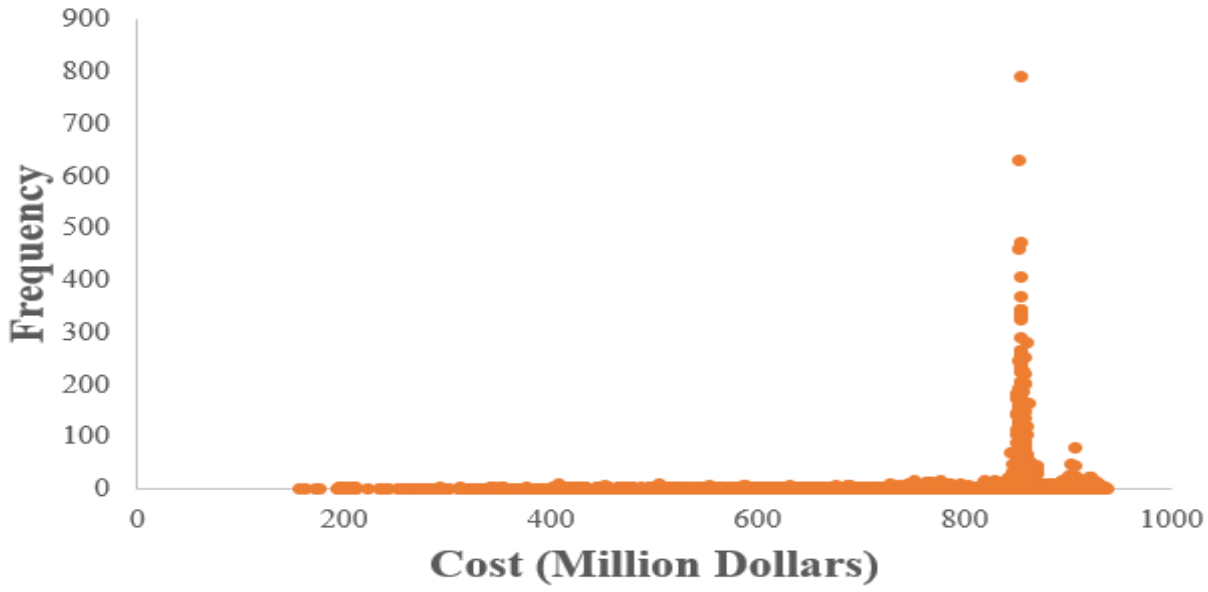

Figure 7: Cost distribution

3.4.2 Environmental distribution

The distribution of the GHG emission is shown in Figure 8, it can be seen the range of optimality is within 8652 ktonCO$_2$-Eq to 8729 ktonCO$_2$-Eq, with optimal solution of 8725ktonCO$_2$-Eq; which reflects the good solution selected by the NSGA-II algorithm in each of the generations.

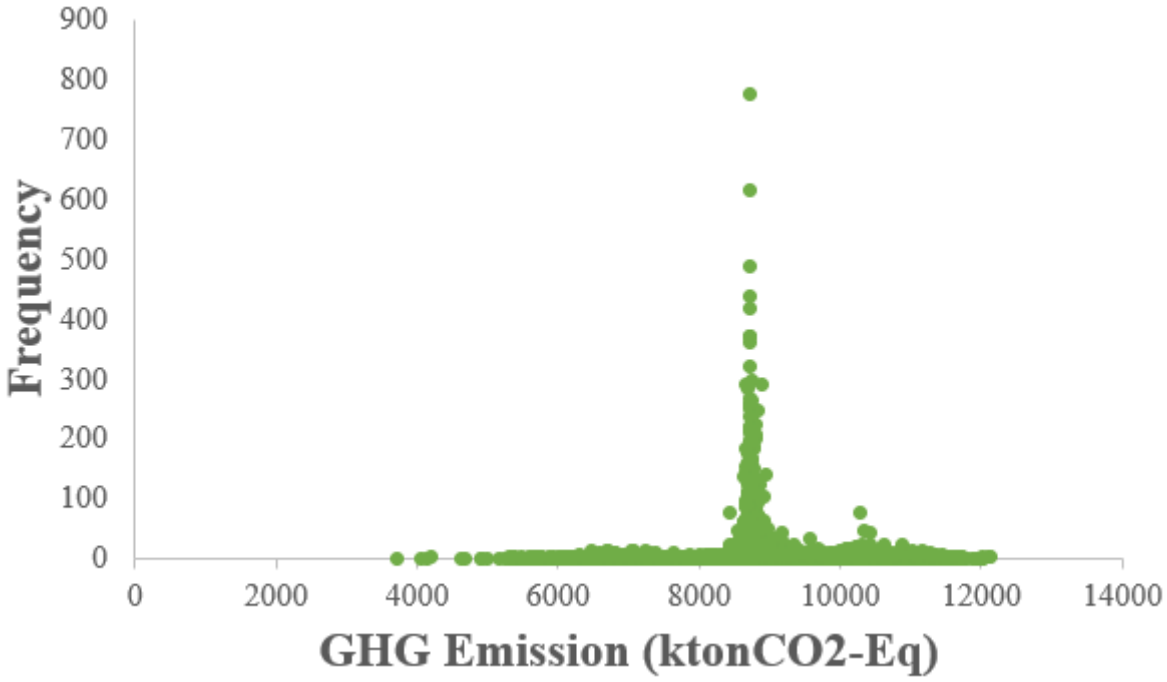

Figure 8: GHG emission distribution

3.4.3 Social distribution

Table 1 shows the social objective function distribution in terms of the total accrued jobs in a year. The optimal value of 3714 was obtained having the highest frequency. It should also be noted that the values of 1238, 2476 and 3714 local jobs per annum are for scenarios when one, two and three biorefineries are located

Table 2: Social objective function frequency distribution

No. of Accrued Jobs	Frequency
1238	341
2476	698
3714	148834

3.5 Optimised results for the decision variables

The optimised results for the decision variables considering the three objective functions are given. These results are selected from the tradeoff-analysis of the MOO optimization using the NSGA-II algorithm, it was calculated thus, that a value of 854 million dollars, 8725ktonCO$_2$-Eq and 3714 jobs were calculated simultaneously to optimised solutions for the economic, environmental and social objective functions respectively. The corresponding decision variables were thus obtained. The optimal solutions for their corresponding constraints are shown in table 3a Table 3b

Table 3a: Optimised decision variables

Variable	Optimised Value (Location*)
Bassa Biorefinery	1
Kabba-Bunu Biorefinery	1
Yagba-West Biorefinery	1
Harv-Bassa [Bagasse]	1
Harv-Kabba_Bunu [Bagasse]	0
Harv-Yagba_West [Bagasse]	1
Harv-Kabba_Bunu [Corn-Stover]	0
Harv-Dekina [Corn-Stover]	0
Harv-Bassa [Corn-Stover]	1
Bioethanol-Dist-frm-Bassa-Biorefinery-to-Kaduna	1
Bioethanol-Dist-frm-Bassa-Biorefinery-to-PH	1
Bioethanol-Dist-frm-Kabba-Bunu-Biorefinery-to-Kaduna	0
Bioethanol-Dist-frm-Kabba-Bunu-Biorefinery-to-PH	0
Bioethanol-Dist-frm-Yagba-West-Biorefinery-to-Kaduna	1
Bioethanol-Dist-frm-Yagba-West-Biorefinery-to-PH	0

* 1 = yes, 0 = No

Table 3b: Optimised decision variables

Variable	Optimised Value (Million litres)
Bioethanol-Bassa Biorefinery	78.00
Bioethanol-Kabba_Bunu Biorefinery	47.70
Bioethanol-Yagba_West Biorefinery	38.23
Harv-Bassa- BiorefBassa[Bagasse]*a	67.00
Harv-Bassa- BiorefKabba-Bunu[Bagasse]	28.92
Harv-Bassa- BiorefYagba_West[Bagasse]	84.03
Harv-Kabba_Bunu- BiorefBassa[Bagasse]	0
Harv-Kabba_Bunu-BiorefKabba_Bunu[Bagasse]	0
Harv-Kabba_Bunu-BiorefYagba-West[Bagasse]	0
Harv-Yagba_West- BiorefBassa[Bagasse]	23.84
Harv-Yagba_West-Bioref Kabba_Bunu[Bagasse]	41.63
Harv-Yagba_West- BiorefYagba-West[Bagasse]	51.86
Harv-Kabba_Bunu- BiorefBassa[Corn-Stover]*b	0
Harv-Kabba_Bunu-BiorefKabba_Bunu[Corn-Stover]	0
Harv-Kabba_Bunu-BiorefYagba-West[Corn-Stover]	0
Harv-Dekina- BiorefBassa[Corn-Stover]	0
Harv-Dekina- BiorefKabba-Bunu[Corn-Stover]	0
Harv-Dekina- BiorefYagba-West[Corn-Stover]	0

Harv-Bassa- BiorefBassa[Corn-Stover]	29.53
Harv-Bassa- BiorefKabba-Bunu[Corn-Stover]	81.76
Harv-Bassa- BiorefYagba_West[Corn-Stover]	35.24
Demand-Kaduna-BiorefBassa[Bioethanol]*c	22.67
Demand-Kaduna-BiorefKabba-Bunu[Bioethanol]	0
Demand-Kaduna-BiorefYagba-West[Bioethanol]	17.14
Demand-PH-BiorefBassa[Bioethanol]	30.51
Demand-PH-BiorefKabba-Bunu[Bioethanol]	0
Demand-PH-BiorefYagba-West[Bioethanol]	0

**a Harv-Bassa- BiorefBassa[Bagasse]= amount of bagasse transported from Bassa harvesting site to Bassa biorefinery, *bHarv-Kabba_Bunu- BiorefBassa[Corn-Stover] = amount of corn-stover transported from Kabba-Bunu harvesting site to Bass biorefinery,*cDemand-Kaduna-BiorefBassa[Bioethanol]= amount of bioethanol transported from Bassa biorefinery to Kaduna demand zone.*

Further explanation on the optimised results can be deduced from the optimised superstructure as shown in Figure 9

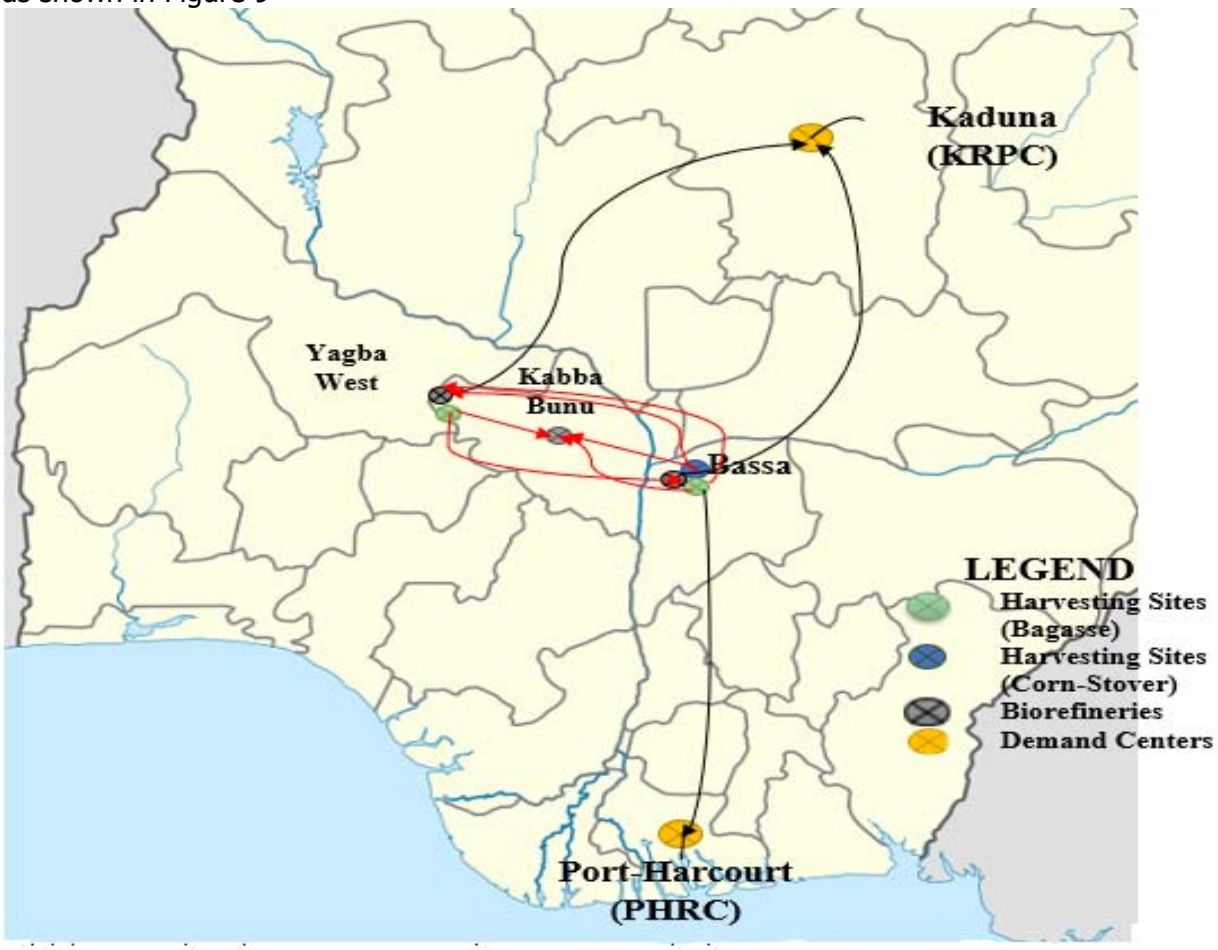

Figure 9: Design superstructure for the biorefinery supply chain (optimized case)

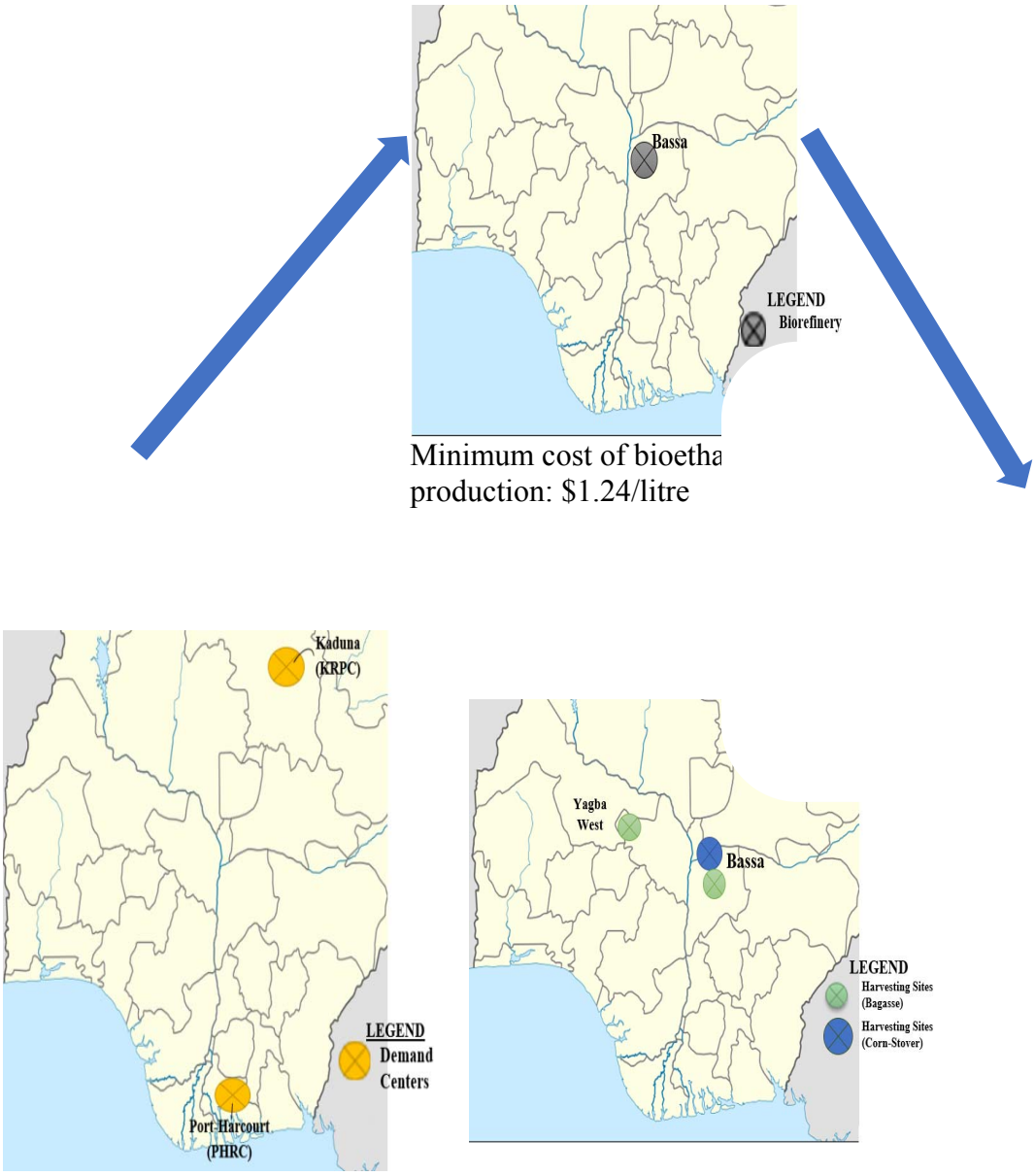

Figure 10: Global optimum cost of production of bioethanol fromthe biorefinery supply chain

As shown in Figure 10, Bassa biorefinery was selected as the optimal biorefinery location since it was able to satisfy the demand in Kaduna and Port-Harcourt demand centres respectively. Feedstock selection was from Bassa (bagasse and corn-stover) and Yagba-West (bagasse).

3.6 Model validation

The validation of the model was done to ascertain the acceptability of the model, this was done by the comparison of the optimized value of $1.24/litre of minimum production cost to that obtained from You *et al.,* 2011 (a production cost of $0.97/litre), which is 21.8% more than the literature value. The global optimal value calculated ($1.24/litre) should be less than the local optimal value of $0.97/litre obtained from literature; this deviation is due to the location factor of 2.2 as expressed in equation 12.

This can be deduced that for model acceptability and replication of the model in Nigeria and other countries of location of 2.2 with respect to USA location factor of 1, the production cost should be ≤ 21.8%.

A price of Nigeria gasoline of $0.375/litre (Ogbon *et al.,* 2018) is below the production cost of optimised value of $1.24/litre which shows the economic infeasibility of the bioethanol from second-generation (bagasse and corn-stover) biofuel monomer. Therefore, government incentives are required to offset the economic infeasibility.

4.0 CONCLUSIONS

Based on the model developed (equation 1 to 10) and optimization results obtained, the following conclusions were deduced:

i. A mo-MINLP model (economic, environmental and social objective functions) for the biorefinery supply chain was successfully developed which took into account biorefinery supply chainlogistics, production cost, biorefinery supply chain environmental parameters and social productivity coefficient.
ii. The multi-objectives (economic, environmental and social) MINLP model developed was simultaneously solved using NSGA-II algorithm.
iii. The optimised results show a global optimal value of $1.24/litre which is 21.8% more than the local optimal value obtained from literature value of $1.24/litre (You *et al.,* 2011). This difference was due to the location factor of 2.2 as assigned to Nigeria.
iv. Raw material logistics suggests that feedstock should be sourced from Bassa (Bagasse),
v. Yagba-West (Bagasse) and Bassa (Corn-Stover).
vi. Bassa biorefinery was calculated as optimal location in siting the biorefinery and bioethanol will be distributed to Kaduna and Port-Harcourt demand centres.
vii. The model acceptability and replication of the model in Nigeria and other countries of location of 2.2 with respect to USA location factor of 1; the production cost should be ≤ 21.8%.

REFERENCES

Cardona Alzate, C. A., Solarte Toro, J. C., and Peña, Á. G. (2018). Fermentation, thermochemical and catalytic processes in the transformation of biomass through efficient biorefineries. Catalysis Today, 302, 61–72. doi:10.1016/j.cattod.2017.09.034

Corsano, G., Vecchietti, A. R., andMontagna, J. M. (2011). Optimal design for sustainable bioethanol supply chain considering detailed plant performance model. Computers and Chemical Engineering, 35(8), 1384–1398. doi:10.1016/j.compchemeng.2011.01.0

Cristina, A.; Paulo, F.; Maria, S.; Huy, S.; and Truong, Q. (2017), "Supply chain management and quality management integration A conceptual model proposal", International Journal of Quality and Reliability Management, Vol. 34 Issue 1 pp. 53 – 67.

EPA, 2018. Greenhouse Gas Equivalencies Calculator [WWW Document]. URL http://www.epa.gov/cleanenergy/energy-resources/calculator.html

García-Velásquez, C. A., and Cardona, C. A. (2019). "Comparison of the biochemical and thermochemical routes for bioenergy production: A techno-economic (TEA), energetic and environmental assessment". Energy. doi:10.1016/j.energy.2019.01.073

Gong, J. and You, F. (2014) "Optimal Design and Planning of Sustainable Chemical Supply Chains Under Uncertainty" ACS Sustainable Chemistry and Engineering 2(1):49–61, DOI:10.1021/sc400267t

Google Maps http://map.google.com/.

Guillen-Gosalbez, G. and Grossmann, I. E. (2009) "Optimal Design and Planning of Sustainable Chemical Supply Chains Under Uncertainty" AIChE Journal 55(1):99 – 121 DOI:10.1002/aic.11662

Ivanovski, D. (2014), "Multi-objective Optimization for Sustainable Supply Chain Network Design" (Masters dissertation, POLITECNICO DI MILANO, Milan, Italy). Retrieved from https://www.polimi.it/en/

Jamet, S. and Corfee-Morlot, J. (2009), "Assessing the Impacts of Climate Change: A Literature Review", OECD Economics Department Working Papers, No. 691, OECD publishing, © OECD. doi:10.1787/224864018517

Khalili-Damghani, K., Nojavan, M., andTavana, M. (2013). "Solving fuzzy Multidimensional Multiple-Choice Knapsack Problems: The multi-start Partial Bound Enumeration method versus the efficient epsilon-constraint method." Applied Soft Computing, 13(4), 1627–1638. doi:10.1016/j.asoc.2013.01.014

Murshid Kamal , Syed Aqib Jalil, Syed MohdMuneeb, Irfan Ali (2018) "A Distance Based Method for Solving Multi-objective Optimization Problems" Journal of Modern Applied Statistical Methods, 17(1). DOI: 10.22237/jmasm/1532525455

NNPC, Available at https://www.nnpcgroup.com (accessed November 1, 2018).

NSDC, Available at https://www.nsdcnigeria.org/ (accessed November 6, 2018)

Ogbon, N. O., Otanocha, O. B., and Rim-Rukeh, A. (2018). "An assessment of the economic viability and competitiveness of modular refinery in Nigeria". Nigerian Journal of Technology, 37(4), 1015. doi:10.4314/njt.v37i4.22

Perera, F. (2017). "Pollution from Fossil-Fuel Combustion is the Leading Environmental Threat to Global Pediatric Health and Equity; Solutions Exist". International Journal of Environmental Research and Public Health, 15(1), 16. doi:10.3390/ijerph15010016

Seada, H., and Deb, K. (2018). "Non-dominated Sorting Based Multi/Many-Objective Optimization: Two Decades of Research and Application". Multi-Objective Optimization, 1–24. doi:10.1007/978-981-13-1471-1_

Shahryar Sorooshian, YasamanParsia (2019) . "Modified Weighted Sum Method for Decisions with Altered Sources of Information." Mathematics and Statistics , 7(3) ,57 - 60. doi: 10.13189/ms.2019.070301

Tembo, G.; Epplin, F. M. and Huhnke, R. L. (2003). "Integrative Investment Appraisal of a Lignocellulosic Biomass-to-Ethanol Industry". Journal of Agricultural and Resource Economics 2003;28(3):611-633.

You, F.; Tao, L.; Gaziano, D. J.; Seth, W.; and Synder, S. W. (2011), "Optimal Design of Sustainable Cellulosic Biofuel Supply Chains: Multiobjective Optimization Coupled with Life Cycle Assessment and Input–Output Analysis". American Institute of Chemical Engineers; 58(4): 986-1311, DOI 10.1002/aic.1263

Yue, D.; and You, F. (2014) "Fair profit allocation in supply chain optimization with transfer price and revenue sharing: MINLP model and algorithm for cellulosic biofuel supply chains" AIChE Journal 63(3): https://doi.org/10.1002/aic.14511

Proceedings of the 49th NSChE Annual Conference
KADA 2019: pp 316-329

P2A-07: DRYING OF AGRO-WASTE BIOMASS FOR BIOENERGY PRODUCTION: MATHEMATICAL MODELLING OF OPEN SUN AND SOLAR DRYING OF PULVERIZED MAIZE HUSKS

O. O. Agbede[1], K. J. Ayanniyi[1], K. A. Babatunde[1], F. N. Osuolale*[1], E. O. Oke[2], O. O. Ogunleye[1] and S. E. Agarry[1]

1. Department of Chemical Engineering, Ladoke Akintola University of Technology, Ogbomoso, Oyo State, Nigeria.

2. Department of Chemical Engineering, Michael Okpara University of Agriculture, Umudike, Abia State, Nigeria.

* Corresponding author: fnosuolale@lautech.edu.ng

ABSTRACT

The open sun and solar drying of maize husks, agro-waste biomass, were investigated. Maize husks obtained from freshly harvested maize were pulverized and dried in direct sunlight and solar dryer. The Midilli-Kucuk, Page, Logarithmic, Two-term, Wang and Singh, Approximation of diffusion, Modified Henderson and Pabis, Modified Page, Henderson and Pabis, two-term exponential, Verma et al and Weibull et al thin layer drying models were fitted to the drying data. The coefficient of determination (R^2), sum of square error (SSE), root mean square error (RMSE) and Chi-square (χ^2) were used as criteria to determine the model that best fit the drying data. The Wang and Singh model best fitted the sun drying data for all sample depths (5 – 20 mm) with highest values of R^2 (>0.993) and lowest values of SSE, RMSE and χ^2, whereas it only suitably described the solar drying data for the 15 and 20 mm samples.

Keywords: Maize husk, open sun drying, solar drying, agro-waste biomass, model, thin layer modelling

1.0 INTRODUCTION

The primary energy sources of fossil fuels (coal, crude oil and natural gas) are limited, fast depleting, highly polluting and non-renewable (Panwar *et al*., 2011; Demirbas *et al*., 2017). Biomass, on the other hand, is a renewable source of energy which is easily replenished and environmentally benign (Saxena *et al*., 2009; Ellabban *et al*., 2014). Biomass are materials derived from microorganisms, animals and plants; they include algae, energy crops, animal wastes, food wastes, wood and wood wastes, agricultural residues/agro-waste, municipal solid wastes and industrial residues (Demirbas *et al*., 2017). They are considered as a mitigation against climate change (Saxena *et al*., 2009), since they are produced by the process of photosynthesis which combines solar energy and carbon dioxide into chemical energy in the form of carbohydrates. In addition, their utilisation as a fuel is a carbon neutral process since the carbon dioxide captured by the biomass during photosynthesis is released during its combustion (Kumar *et al*., 2009).

Biomass may be combusted to generate heat and then electricity or converted to solid, liquid or gaseous biofuels (Ellabban *et al*., 2014). The conversion of biomass to biofuels or bioenergy is achieved through physicochemical, biochemical and thermochemical processes. The physicochemical process involves oil extraction e.g. from seed biomass followed by transesterification, the biochemical processes include fermentation, anaerobic digestion and biophotolysis while the thermochemical conversion processes are pyrolysis, gasification, hydrothermal liquefaction and direct combustion (Kumar *et al*., 2009; Kumar *et al*., 2015).

Thermochemical conversion of biomass to bioenergy may require the removal of the large amount of moist usually present in biomass, prior to pyrolysis, gasification and combustion conversion processes (Bennion *et al.*, 2015; Azizi, 2018).

Drying is a preservation method usually employed to reduce the moisture content of agricultural products and consequently decrease microbial and enzyme activities, thus enhancing product shelf-life and decreasing the packing and transportation cost (Mujumdar and Law 2010; Guine *et al*. 2012). Sun drying is the traditional method of drying agricultural products, but it is extremely weather dependent, takes a long time and materials are prone to contamination with dust, insect, etc. However, solar drying employs a solar dryer which shades the material from direct exposure to rainfall, dust, insects, etc., but still uses energy from sun radiation to dry the material in a chamber heated up directly or indirectly by the sun radiation. The drying of several agricultural products including fruits, vegetables and staple foods have been reported in the literature (Davishi, 2017; Doymaz, 2010; Erbay and Icier, 2010; Ojediran and Raji, 2010; Rajkumar *et al*., 2007) but little has been reported on the drying of agricultural residues or agro-waste biomass for production of bioenergy.

Drying involves simultaneous coupled heat and mass transfer (Diamante *et al*. 2010), it is a complex process which require effective mathematical models for process design, optimization and control as well as energy integration. The mathematical models employed for modelling drying process can be either distributed or lumped parameter models; the distributed models consider internal and external heat and mas transfer and predict temperature and moisture gradient whereas the lumped parameters models assume a uniform temperature distribution in the product which is the drying air temperature (Erbay and Filiz, 2010). For a uniform temperature to be correctly assumed for a lumped parameter model, the material must be dried as one layer of sample particles or slices, so that the material has a thin structure; this is generally known as thin layer drying (Akpinar, 2006; Erbay and Filiz, 2010). Thin layer drying models are easy to use and require less data compared to complex distributed models, so they have been frequently applied in the study of the drying of foods, fruits and vegetables (Toğrul and Pehlivan, 2004; Akpinar and Bicer, 2008; Doymaz, 2010; Ojediran and Raji, 2010; Doymaz and Ismail, 2011; Tunde-Akintunde, 2011). However, this useful modelling tool has not been adequately explored for the drying of biomass, therefore this study aimed to investigate the thin layer mathematical modelling of open sun and solar drying of agro-waste (maize husk) biomass.

2.0 METHODOLOGY

2.1 Sample Preparation

Maize husks were obtained from freshly harvested maize collected from a farmland in Ogbomoso. The husks were pulverized in a kitchen blender to increase the surface area of the material, prior to the drying operation.

2.2 Experimental Procedure for Drying of Maize Husks

The pulverized maize husk samples were spread uniformly in pre-weighed aluminium pans, of dimension 7.5 by 7.5 cm, which had been calibrated to depths of 5, 10, 15 and 20 mm for all the drying experiments. The initial mass of the pulverized maize husks in each of the pans was determined. A set of pans was placed in a triangular prism-shaped natural convection direct solar dryer (Figure 1), at the same time another set was placed in direct sunlight. The drying chamber

of the solar dryer has a height of 0.67 m while its rectangular base on which the aluminium drying pans were placed has a dimension of 1.2 by 0.7 m. The mass of the samples were measured at 30 min interval until constant mass was achieved, using a Citizen digital weighing balance which has an accuracy of 0.001 g. The drying experiments were performed in triplicates, in the month of October, 2018 between 10 am and 6 pm. The ambient and solar dryer temperatures were monitored.

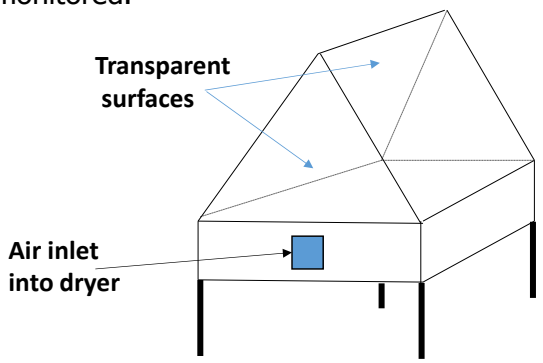

Figure 1: Schematic of a direct solar dryer

2.3 Thin Layer Drying Models

The moisture content of maize husk at time t, X_t (g water. g dry matter^{-1}) is defined as:

$$X_t = \frac{m_t - m_d}{m_d} \quad [1]$$

where m_t and m_d are mass of maize husk sample at any time t (g) and absolute dried mass of sample (g), respectively. The moisture content can be expressed as dimensionless moisture ratio (M_R):

$$M_R = \frac{X_t - X_e}{X_i - X_e} \quad [2]$$

where X_i and X_e are initial and equilibrium moisture contents (g water/g dry matter), respectively. For a long drying time the values of X_e are small compared with X_t and X_i, the moisture ratio may be simplified (Dissa *et al.*, 2011; Perea-Flores *et al.*, 2012):

$$M_R = \frac{X_t}{X_i} \quad [3]$$

Thin layer drying models describe the relationship between moisture ratio (M_R) and drying time (t). Several thin layer models have been reported in the literature, but twelve of them have been identified as the most frequently suitable models by researchers for various products; they include Midilli-Kucuk, Page, Logarithmic, Two-term, Wang and Singh, Approximation of diffusion, Modified Henderson and Pabis, Modified Page, Henderson and Pabis, two-term exponential, Verma et al and that of Weibull et al (Kucuk *et al.*, 2014).

2.3.1 Midilli-Kucuk Model

This is also called the Midilli or Midilli *et al.* model. It is a four parameter model which has an exponential term as well as a linear term (Midilli, 2002). It is given as:

$$M_R = a\exp\left(-kt^n\right) + bt \quad [4]$$

where a, k, b and n are all constants.

2.3.2 Page Model

The page model (Page, 1949) is a two parameter model, it has a single term which is entirely exponential. It is defined as:

$$M_R = \exp\left(-kt^n\right) \quad [5]$$

where k and n are constants.

2.3.3 Logarithmic Model

The logarithmic model (Chandra and Singh, 1995) is:

$$M_R = a\exp\left(-kt\right) + c \quad [6]$$

where a, k and c are model constants, c being an empirical constant that is dimensionless. This model is occasionally called the asymptotic or Yagcioglu et al. model (Yagcioglu *et al.*, 1999). It has an empirical term "c" in addition to an exponential term.

2.3.4 The Two-term Model

The two-term model (Henderson, 1974; Glenn, 1978) has two exponential terms. It has four constants and is given as:

$$M_R = a\exp\left(-k_0 t\right) + b\exp\left(-k_1 t\right) \quad [7]$$

where a, b, k_0 and k_1 are constants.

2.3.5 Wang and Singh Model

The Wang and Singh model (Wang and Singh, 1978) has two model constants and is given as:

$$M_R = 1 + at + bt^2 \quad [8]$$

where a and b are constants.

2.3.6 Approximation of Diffusion Model

The approximation diffusion model (Kaseem, 1998) has two exponential terms and four constants. It is sometimes called the diffusion approach or simplified diffusion model. It is defined as:

$$M_R = a\exp\left(-kt\right) + \left(1-a\right)\exp\left(-kbt\right) \quad [9]$$

where a, b and k are constants.

2.3.7 Modified Henderson and Pabis Model

The modified Henderson and Pabis model (Karathanos, 1999) is a three exponential term model; it has six constants and is expressed as:

$$M_R = a\exp\left(-kt\right) + b\exp\left(-gt\right) + c\exp\left(-ht\right) \quad [10]$$

where a, b, c, k, g and h are constants.

2.3.8 Modified Page Model

A modified form of the Page model generally known as Modified Page-II was proposed and used by White *et al.* (1978):

$$M_R = \exp\left(-(kt)^n\right) \quad [11]$$

2.3.9 Henderson and Pabis model

The Henderson and Pabis model (Henderson and Pabis, 1961) is a single term exponential model consisting of two model constants:

$$M_R = a\exp(-kt) \quad [12]$$

where a and k are constants.

2.3.10 Two-term Exponential Model

The two-term exponential model (Sharaf-Eldeen *et al.*, 1980) has two terms and two model constants, and is given as:

$$M_R = a\exp(-kt) + (1-a)\exp(-kat) \quad [13]$$

where a and k are constant.

2.3.11 The Verma et al. Model

The Verma *et al.* (1985) model is also called the modified two-term exponential model, it has three models constant and is defined as:

$$M_R = a\exp(-kt) + (1-a)\exp(-gt) \quad [14]$$

where a, k and g are constant.

2.3.12 The Weibull Model

It has four model constants and is defined as (Kucuk *et al.*, 2014):

$$M_R = a - b\exp(-kt^n) \quad [15]$$

where a, b, k and n are constant.

2.4 Criteria for Selecting Best Model

The coefficient of determination (R^2), sum of square error (SSE), root mean square error (RMSE) and Chi-square (χ^2) were the statistical parameter used as criteria to determine the model that best fit the moisture ratio – time data. The model that best fit the data is one that has the highest value of R^2 and lowest values of SSE, RMSE and χ^2 (Erbay and Icier, 2010; Kucuk *et al*, 2014). These criteria are given as:

$$R^2 = \frac{\sum_{i=1}^{N}\left(M_{R_{\exp,i}} - M_{R_{pred,i}}\right)^2}{\sqrt{\left(\sum_{i=1}^{N}\left(M_{R_{\exp,i}} - M_{R_{pred,i}}\right)^2\right)\left(\sum_{i=1}^{N}\left(M_{R_{\exp,i}} - M_{R_{pred,i}}\right)^2\right)}} \quad [16]$$

$$SSE = \frac{1}{N}\sum_{i=1}^{N}\left(M_{R_{\exp,i}} - M_{R_{pred,i}}\right)^2 \quad [17]$$

$$RMSE = \left[\frac{1}{N}\sum_{i=1}^{N}\left(M_{R_{pred,i}} - M_{R_{exp,i}}\right)^2\right]^{\frac{1}{2}} \quad [18]$$

$$\chi^2 = \frac{\sum_{i=1}^{N}\left(M_{R_{exp,i}} - M_{R_{pred,i}}\right)^2}{N - z} \quad [19]$$

where $M_{R_{exp,i}}$, $M_{R_{pred,i}}$, N and z are experimental moisture ratio, predicted moisture ratio, number of observations and number of constants, respectively.

The moisture ratio-drying time data obtained from experimental data for both open sun and solar drying of pulverized maize husk were fitted to the twelve thin layer drying mathematical models described in section 2.3; the criteria of section 2.4 were used to determine the model which best fit the experimental drying data. Non-linear regression analysis was employed to fit experimental data of moisture ratio (MR) versus drying time (t) to the thin layer drying models. Statistical Package for the Social Sciences (SPSS) version 20 (SPSS Inc., Chicago, Illinois), was the software used for the regression analysis. The R^2 values were computed by SPSS while SSE, RMSE and χ^2 were calculated from equations 17, 18 and 19, respectively, using Microsoft Excel.

3.0 Results and Discussion

3.1 Open Sun Drying of pulverized Maize Husks

The moisture ratio decreased progressive during the open sun drying operation as shown in the plot of moisture ratio versus drying time of Figure 2 indicating that moisture was successfully removed from the maize husk by air heated through the sun radiation. The moisture ratio decreased progressively with time during the open sun drying of all samples of the pulverized maize husks of depths 5 – 20 mm considered. As expected the drying rate decreased with increasing depth of maize husks in the pans, since the initial mass and moisture content of maize husks in the pans increased with increasing depth of husks in the pans; the drying time required for the 5, 10, 15 and 20 mm deep samples were 180, 240, 330 and 390 min, respectively.

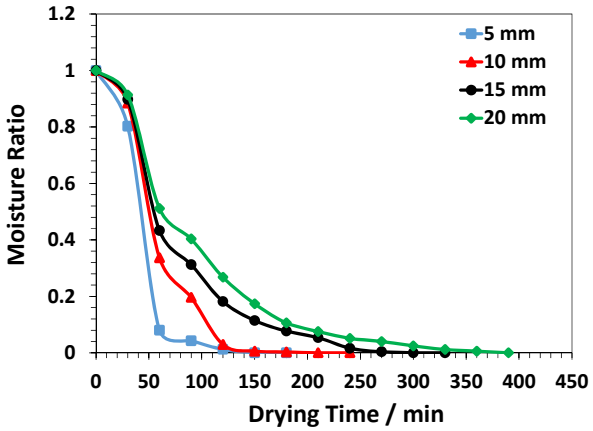

Figure 2: Plot of moisture ratio versus drying time for open sun drying of pulverized maize husks of 5, 10, 15 and 20 mm depth

The statistical parameters obtained after the twelve thin layer models were fitted to the open sun drying data are shown in Tables 1 – 4. The Wang and Singh model best fitted the drying moisture ratio – time data for all the drying operations. This model had the highest R^2 and lowest SSE, RMSE and χ^2 compared to those of the other eleven models. The R^2, SSE, RMSE and χ^2 for open sun drying of pulverized maize husks of 5 mm depth were 0.996, 0.011069692, 0.105212604, and 0.012772722, respectively. Similar high values of R^2 (>0.996) and low values of SSE (<0.02), RMSE (<0.15) and χ^2 (<0.025) were observed for the 10, 15 and 20 mm depth samples. The Wang and Singh model does not have an exponential term unlike the other eleven equations, it is a second order polynomial; this implies that a polynomial relation exists between the moisture ratio and drying time for the sun drying of pulverized maize husks. The Wang and Singh model has been reported to best fit the open sun drying of mint leaves (Akpinar, 2010) and parsley leaves (Akpinar, 2011).

Table 1: Statistical parameters for thin layer drying models for sun drying of 5 mm deep maize husks

Model	**R^2**	**SSE**	**RMSE**	**χ^2**
Midilli-Kucuk	0.428	0.088673964	0.297781738	0.120919041
Page	0.991	0.043491250	0.208545559	0.050182212
Logarithmic	0.547	0.085892917	0.293074934	0.107366146
Two-term	0.415	0.088976317	0.298288982	0.121331341
Wang and Singh	0.996	0.011069692	0.105212604	0.012772722
Approximation of diffusion	0.945	0.043491250	0.208545559	0.054364062
Modified Henderson and Pabis	0.415	0.088976317	0.298288982	0.148293861
Modified Page	0.991	0.043491250	0.208545559	0.050182212
Henderson and Pabis	0.415	0.088976317	0.298288982	0.102664981
Two-term exponential	0.945	0.043491250	0.208545559	0.050182212
Verma et al	0.986	0.043491250	0.208545559	0.054364062
Weibull et al	0.547	0.085892917	0.293074934	0.117126705

Table 2: Statistical parameters for thin layer drying models for sun drying of 10 mm deep maize husks

Model	R^2	SSE	RMSE	χ^2
Midilli-Kucuk	0.281	0.089097772	0.298492498	0.121496961
Page	0.996	0.062385172	0.249770238	0.071982890
Logarithmic	0.470	0.078481171	0.280144911	0.098101464
Two-term	0.260	0.089182238	0.298633954	0.121612143
Wang and Singh	0.997	0.009312752	0.0965026	0.010745483
Approximation of diffusion	0.979	0.062385172	0.249770238	0.077981465
Modified Henderson and Pabis	0.260	0.089182238	0.298633954	0.148637064
Modified Page	0.996	0.062385172	0.249770238	0.071982890
Henderson and Pabis	0.26	0.089097772	0.298492498	0.102805121
Two-term exponential	0.979	0.062385172	0.249770238	0.071982890
Verma et al	0.996	0.062385172	0.249770238	0.077981465
Weibull et al	0.470	0.078481171	0.280144911	0.107019779

Table 3: Statistical parameters for thin layer drying models for sun drying of 15 mm deep maize husks

Model	R^2	SSE	RMSE	χ^2
Midilli-Kucuk	0.188	0.105331045	0.324547446	0.143633243
Page	0.976	0.076466778	0.276526270	0.088230898
Logarithmic	0.445	0.090308166	0.300513171	0.112885207
Two-term	0.151	0.105331045	0.324547446	0.143633243
Wang and Singh	0.999	0.012813192	0.113195371	0.014784452
Approximation of diffusion	0.893	0.076466778	0.276526270	0.095583473
Modified Henderson and Pabis	0.151	0.105331045	0.324547446	0.175551741
Modified Page	0.976	0.076466778	0.276526270	0.088230898
Henderson and Pabis	0.967	0.064309148	0.253592484	0.074202863
Two-term exponential	0.893	0.076466778	0.276526270	0.088230898
Verma et al	0.963	0.076466778	0.276526270	0.095583473
Weibull et al	0.445	0.090308166	0.300513171	0.123147499

Table 4: Statistical parameters for thin layer drying models for sun drying of 20 mm deep maize husk

Model	R^2	SSE	RMSE	χ^2
Midilli-Kucuk	0.102	0.118473695	0.34420008	0.161555038
Page	0.974	0.092181428	0.303613946	0.106363186
Logarithmic	0.407	0.097715342	0.312594532	0.122144177
Two-term	0.056	0.118473695	0.344200080	0.161555038
Wang and Singh	0.998	0.019087366	0.138157034	0.022023884
Approximation of diffusion	0.866	0.092181428	0.303613946	0.115226785
Modified Henderson and Pabis	0.056	0.118473695	0.344200080	0.197456158
Modified Page	0.974	0.092181428	0.303613946	0.106363186
Henderson and Pabis	0.056	0.118473695	0.344200080	0.136700417
Two-term exponential	0.866	0.092181428	0.303613946	0.106363186
Verma et al	0.955	0.092181428	0.303613946	0.115226785
Weibull et al	0.407	0.097715342	0.312594532	0.133248193

3.2 Solar Drying of pulverized Maize Husks

The moisture ratio decreased progressive during the solar drying process as shown in the plot of moisture ratio versus drying time of Figure 3, which implies that moisture was also successfully removed from the pulverized maize husks by hot air within the solar dryer chamber. The moisture ratio decreased progressively with time during the solar drying of all samples of the pulverized maize husks of depths 5 – 20 mm investigated. Similar to the open sun drying, the drying time increased with increasing depth of maize husks in the pans because the initial mass and moisture content of the husks in the pans increased with increasing depth of husks. The time required for drying of the 5, 10, 15 and 20 mm deep samples were 100, 120, 180 and 210 min, respectively; these drying times are shorter than those required for open sun drying of maize husks of similar depth. It was observed that the temperature in the solar drying chamber increased to about 31 – 51 °C (depending on the time of the day) compared to the ambient temperature of 30 - 39 °C , during the drying process, which consequently increased the thermal energy available for the removal of moisture from the maize husks. This resulted into a higher drying rate in the solar dryer compared to the open sun and consequently a shorter drying time in the solar dryer.

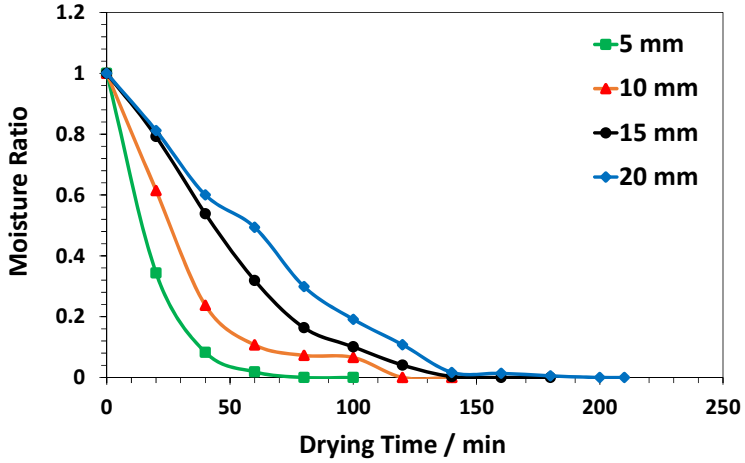

Figure 3: Plot of moisture ratio versus drying time for solar drying of pulverized maize husks of 5, 10, 15 and 20 mm depth

The statistical parameters obtained after the twelve thin layer models were fitted to the solar drying data are shown in Tables 5 – 8. The R^2, SSE, RMSE and χ^2 for Wang and Singh model for the 5 mm deep pulverized maize husks sample were 0.998, 0.731722935, 0.855408052, and 0.844295695, respectively; the corresponding values for the 10 mm deep sample were 0.997, 0.847283028, 0.920479781, and 0.977634263, respectively. The Page and modified Page models had the lowest values of SSE (0.008348702), RMSE (0.091371232) and χ^2 (0.009633118) compared to the other eleven models and R^2 value of 0.973, for the 5 mm deep sample whereas the Page model had the lowest values of SSE (0.014752447), RMSE (0.121459653) and χ^2 (0.017022055) compared to the other eleven models and R^2 value of 0.985, for the 10 mm deep sample. Although the Wang and Sing model had the highest values of R^2, for the 5 and 10 mm deep samples, this same model also had the highest values of SSE, RMSE and χ^2, compared to the other eleven models.

Alternatively, the statistical parameters for the thin layer drying models fitted to the drying data for 15 and 20 mm deep samples of the pulverized maize husks, detailed on Table 7 and Table 8 show that the Wang and Singh model had high values of R^2 (>0.993) and lowest values of SSE

(<0.011), RMSE (<0.15) and χ^2 (<0.012) compared to the other eleven models. The Weibull *et al* model had a slightly higher R^2 value of 0.999 compared to 0.996 for the Wang and Singh model but its SSE (0.476146701), RMSE (0.690033841) and χ^2 (0.649290956) values are very high compared to those of Wang and Singh model, for the 15 mm sample. Similarly, the Midilli-Kucuk model had a slightly higher R^2 value of 0.995 compared to 0.994 for the Wang and Singh model but its SSE (0.477595650), RMSE (0.691082955) and χ^2 (0.651266796) values are also much higher compared to those of Wang and Singh model, for the 20 mm sample. Hence, the Wang and Singh model is considered to suitably describe the solar drying data for the 15 and 20 mm deep samples due to the high values of R^2 (>0.993) coupled with the lowest values of SSE (<0.011), RMSE (<0.15) and χ^2 (<0.012) compared to the other models. The Wang and Singh model has also been reported to best fit the solar drying of mint leaves (Akpinar, 2010) and parsley leaves (Akpinar, 2011).

Table 5: Statistical parameters for thin layer drying models for solar drying of 5 mm deep maize husks

Model	R^2	SSE	RMSE	χ^2
Midilli-Kucuk	0.846	0.057094448	0.238944445	0.077856065
Page	0.973	0.008348702	0.091371232	0.009633118
Logarithmic	0.995	0.056483141	0.237661821	0.070603926
Two-term	0.839	0.057197769	0.239160550	0.077996957
Wang and Singh	0.998	0.731722935	0.855408052	0.844295695
Approximation of diffusion	0.913	0.008348702	0.091371232	0.010435878
Modified Henderson and Pabis	0.924	0.057197769	0.239160550	0.095329615
Modified Page	0.973	0.008348702	0.091371232	0.009633118
Henderson and Pabis	0.839	0.057197769	0.239160550	0.065997426
Two-term exponential	0.913	0.008348702	0.091371232	0.009633118
Verma et al	0.964	0.008348702	0.091371232	0.010435878
Weibull et al	0.890	0.056483141	0.237661821	0.077022465

Table 6: Statistical parameters for thin layer drying models for solar drying of 10 mm deep maize husks

Model	R^2	SSE	RMSE	χ^2
Midilli-Kucuk	0.458	0.063103426	0.251203954	0.086050127
Page	0.985	0.014752447	0.121459653	0.017022055
Logarithmic	0.646	0.054730706	0.233945947	0.068413383
Two-term	0.417	0.063103426	0.251203954	0.086050127
Wang and Singh	0.997	0.847283028	0.920479781	0.977634263
Approximation of diffusion	0.906	0.035967159	0.189650098	0.044958949
Modified Henderson and Pabis	0.417	0.063018426	0.251034711	0.105030710
Modified Page	0.985	0.035955453	0.189619231	0.041487061
Henderson and Pabis	0.417	0.063103426	0.251203954	0.072811646
Two-term exponential	0.906	0.035967159	0.189650098	0.041500569
Verma et al	0.974	0.035967159	0.189650098	0.044958949
Weibull et al	0.646	0.054730706	0.233945947	0.074632781

Table 7: Statistical parameters for thin layer drying models for solar drying of 15 mm deep maize husks

Model	**R^2**	**SSE**	**RMSE**	**χ^2**
Midilli-Kucuk	0.159	7588.736565	87.11335469	10348.27713
Page	0.989	0.070563451	0.265637819	0.081419366
Logarithmic	0.466	0.074897210	0.273673546	0.093621513
Two-term	0.106	0.093613051	0.305962499	0.127654160
Wang and Singh	0.996	0.010063471	0.100316853	0.011161697
Approximation of diffusion	0.896	0.070563451	0.265637819	0.088204313
Modified Henderson and Pabis	0.106	0.093456517	0.305706587	0.155760862
Modified Page	0.989	0.024893285	0.157776059	0.028723021
Henderson and Pabis	0.106	0.093534717	0.305834461	0.107924674
Two-term exponential	0.896	0.070563451	0.265637819	0.081419366
Verma et al	0.976	0.068981685	0.262643647	0.086227107
Weibull et al	0.999	0.476146701	0.690033841	0.649290956

Table 8: Statistical parameters for thin layer drying models for solar drying of 20 mm deep maize husks

Model	R^2	SSE	RMSE	χ^2
Midilli-Kucuk	0.995	0.477595650	0.691082955	0.651266796
Page	0.993	0.096816692	0.311153808	0.111711568
Logarithmic	0.393	0.081670234	0.285780045	0.102087792
Two-term	0.913	0.113350292	0.336675351	0.154568580
Wang and Singh	0.994	0.009830096	0.099146843	0.011342419
Approximation of diffusion	0.881	0.096816692	0.311153808	0.121020865
Modified Henderson and Pabis	0.913	0.113416759	0.336774047	0.189027932
Modified Page	0.993	0.096816692	0.311153808	0.111711568
Henderson and Pabis	0.913	0.113416759	0.336774047	0.130865491
Two-term exponential	0.881	0.096816692	0.311153808	0.111711568
Verma et al	0.978	0.096816692	0.311153808	0.121020865
Weibull et al	0.393	0.081670234	0.285780045	0.111368501

4.0 CONCLUSIONS

Maize husks were successfully dried in direct sunlight and solar dryer. The drying rate decreased with increasing depth of maize husks for both sun and solar drying; however the drying rate were higher and consequently the drying time of the maize husks were shorter in the solar dryer

compared to open sun. The Wang and Singh model best fitted the open sun drying data for all sample depths (5 – 20 mm) considered with highest values of R^2 (>0.993) and lowest values of SSE (<0.02), RMSE (<0.15) and χ^2 (<0.025), compared to the other eleven thin layer drying models. However, the Wang and Singh model only suitably described the solar drying data for the 15 and 20 mm deep samples.

References

Akpinar, E.K. (2006) Determination of suitable thin layer drying curve model for some vegetables and fruits. *Journal of Food Engineering*, 73, 75–84.

Akpinar, E. K. (2010) Drying of mint leaves in a solar dryer and under open sun: Modelling, performance analyses. *Energy Conversion and Management*, 51, 2407–2418

Akpinar, E. K. (2011) Drying of parsley leaves in a solar dryer and under open sun: modeling, energy and exergy aspects. *Journal of Food Process Engineering,* 34, 27–48.

Akpinar, E. K. and Bicer, Y. (2008) Mathematical modelling of thin layer drying process of long green pepper in solar dryer and under open sun. *Energy Conversion and Management* 49, 1367–1375.

Azizi, K., Moravejia, M. K., and Najafabadi, H. A. (2018). A review on bio-fuel production from microalgal biomass by using pyrolysis Method. *Renewable and Sustainable Energy Reviews,* 83 (3), 3046-3059.

Bennion, E. P., Ginosar, D. M., Moses, J., Agblevor, F., and Quinn, J. C. (2015). Lifecycle assessment of microalgae to biofuel: comparison of thermochemical processing pathways. *Applied Energy,* 154, 1062–71.

Chandra, P.K. and Singh, R.P. (1995). Applied Numerical Methods for Food and Agricultural Engineers. pp. 163–167. CRC Press, Boca Raton, FL.

Davishi, H. (2017) Quality, Performance Analysis, Mass Transfer Parameters and Modeling of Drying Kinetics of Soybean. *Brazilian Journal of Chemical Engineering*, 34 (1), 143 – 158.

Demirbas, A., Kabli, M., Alamoudi, R.H., Ahmad, W and Basahel, A. (2017) Renewable energy resource facilities in the Kingdom of Saudi Arabia: Prospects, social and political challenges. *Energy Sources, Part B: Economics, Planning, And Policy* 12 (1) 1, 8–16.

Diamante L. M., Ihns, R., Savage G. P., and Vanhanen, L. (2010). A new mathematical model for thin layer drying of fruits. *International Journal of Food Science and Technology,* 45 (9), 1956–1962.

Dissa, A.O., Bathiebo, D.J., Desmorieux, H., Coulibaly, O. and Koulidiati, J. (2011). Experimental characterization and modelling of thin layer direct solar drying of Amelia and Brooks mangoes. *Energy*, 36, 2517–2527.

Doymaz, I. (2010). Evaluation of Mathematical Models for Prediction of Thin-Layer Drying of Banana Slices. *International Journal of Food Properties*, 13 (3), 486–497.

Doymaz, I. and Ismail, O (2011) Drying characteristics of sweet cherry. *Food and Bioproducts Processing* 89, 31–38.

Ellabban, O., Abu-Rub, H. and Blaabjerg, F. (2014) Renewable energy resources: Current status, future prospects and their enabling technology. *Renewable and Sustainable Energy Reviews* 39, 748–764.

Erbay, Z. and Icier, F. (2010) A Review of Thin Layer Drying of Foods: Theory, Modeling, and Experimental Results. *Critical Reviews in Food Science and Nutrition* 50, 441–464.

Guine R. P. F., Francisca, H., and Barroca, M. J. (2012). Mass transfer coefficients for the drying of pumpkin (*Cucurbita moschata*) and dried product quality. *Food and Bioprocess Technology,* 5 (1), 176–183.

Glenn, T.L. (1978). Dynamic analysis of grain drying system. Ph.D. Thesis, Ohio State University, Ann Arbor, MI (unpublished).

Henderson, S.M. (1974). Progress in developing the thin layer drying equation. *Trans. ASAE*. **17**:1167–1172.

Henderson, S.M., and Pabis, S. (1961). Grain drying theory I: Temperature effect on drying coefficient. *Journal of Agricultural Engineering Research*. 6,169–174.

Karathanos, V.T. (1999).Determination of water content of dried fruits by drying kinetics. *Journal of Food Engineering*, 39:337–344.

Kaseem, A.S. (1998). Comparative studies on thin layer drying models for wheat. In 13th International Congress on Agricultural Engineering, Vol. **6**:2–6. February, Morocco.

Kucuk, H., Midilli, A. Kilic, A and Dincer, I. (2014) A Review on Thin-Layer Drying-Curve Equations. *Drying Technology: An International Journal*, 32 (7), 757-773.

Kumar, A., Jones, D. D. and Hanna, M. A. (2009) Thermochemical Biomass Gasification: A Review of the Current Status of the Technology. *Energies*, *2*, 556-581;

Kumar, A., Kumar, N., Baredar, P. and Shukla, A. (2015) A review on biomass energy resources, potential, conversion and policy in India. *Renewable and Sustainable Energy Reviews,* 45, 530–539

Midilli, A., Kucuk, H., and Yapar, Z. (2002). A new model for single-layer drying. *Drying Technology*. 20:1503–1513.

Mujumdar, A. S., and Law, C. L. (2010). Drying technology: trends and applications in post-harvest processing. *Food and Bioprocess Technology*, 3 (6), 843–8

Ojediran J. O. and Raji, A. O. (2010) Thin Layer Drying of Millet and Effect of Temperature on Drying Characteristics. *International Food Research Journal,* 17, 1095-1106.

Page, G.E. (1949). Factors *i*nfluencing the maximum rate of air drying shelled corn in thin-layers. M.S.Thesis, Purdue University, West Lafayette, Indiana.

Panwar, N. L., Kaushik, S. C., and Surendra Kothari, S. (2011). Role of renewable energy sources in environmental protection: A review. *Renewable and Sustainable Energy Reviews,* 15 (3), 1513–1524.

Perea-Flores, M.J., Garibay-Febles, V., Chanona-Pérez, J.J., and Calderón-Domínguez, G., Méndez-Méndez, J.V., Palacios-González, E. and Gutiérrez-López, G.F. (2012). Mathematical modelling of castor oil seeds (Ricinus communis) drying kinetics in fluidized bed at high temperatures. *Industrial Crops and Products*, 38, 64–71.

Rajkumar, P., Kulanthaisami, S., Raghavan, G.S.V., Gariepy, Y. and Orsat, V. (2007) Drying kinetics of tomato slices in vacuum assisted solar and open sun drying methods. *Drying Technology*, 25, 1349–1357.

Saxena, R.C., Adhikari, D.K. and Goyal, H.B. (2009) Biomass-based energy fuel through biochemical routes: A review. *Renewable and Sustainable Energy Reviews* 13, 167–178.

Sharaf-Eldeen, Y. I., Blaisdell, J.L., and Hamdy, M.Y. (1980). A model for ear corn drying. *Transaction of the ASAE*. 23:1261–1271.

Toğrul, I. T. and Pehlivan, D. (2004) Modelling of thin layer drying kinetics of some fruits under open-air sun drying process. *Journal of Food Engineering* 65, 413–425.

Tunde-Akintunde, T. Y. (2011) Mathematical modeling of sun and solar drying of chilli pepper. *Renewable Energy* 36, 2139- 2145.

Verma, L.R., Bucklin, R.A, Ednan, J.B., and Wratten, F.T. (1985). Effects of drying air parameters on rice drying models. *Transaction of the ASAE*. **28**:296–301.

Wang, C.Y., and Singh, R.P. (1978). A single layer drying equation for rough rice. ASAE Paper No. 3001.

White, G.M., Bridges, T.C., Loewer, O.J., and Ross, I.J. (1978). Seed coat damage in thin layer drying of soybeans as affected by drying conditions. ASAE paper no. 3052.

Yagcioglu, A., Degirmencioglu, A., and Cagatay, F. (1999). Drying characteristics of laurel leaves under different conditions. Proceedingss of the 7th international congress on agricultural mechanization and energy, ICAME'99, pp. 565–569, Adana, Turkey.

Proceedings of the 49th NSChE Annual Conference
KADA 2019: pp 330- 337

P2A-08: APPLICATION OF KF MODIFIED SNAILSHELL FOR SINGLE-STAGE TRANSESTERIFICATION OF NEEM OIL

[a]Ajayi O. A., [a]Abdulmalik A and [b]Oladipo A.A
Department of Chemical Engineering, Ahmadu Bello University, Zaria. Kaduna State.
Department of Environmental Engineering, Cyprus Science University, Girne, TRCN Mercin 10, Turkey.

ABSTRACT
A solid base KF/Snailshell catalyst was synthesized by wet impregnation method and applied for biodiesel production from neem oil with high FFA. The XRF and XRD analyses confirmed the presence CaO in snailshell and its crystalline nature. The parameters affecting the preparation of the catalyst were investigated using the Box-Behnken design approach of design expert. The maximum yield of CaO from snailshell was obtained at 800^{0}C snailshell calcination temperature for 3h, while the optimal synthesis condition was 32 wt. % KF dosage, 2hrs calcination time, and calcination temperature of 598^{0}C. The catalyst was applied in a single stage transesterification of neem oil having FFA of 4.2% to produce 95.5% yield of biodiesel. The biodiesel produced was characterized using FTIR and GC-MS and compared to the ASTM commercial standard. The reusability test shows that the catalyst was active recording high yield of 91.9% even after the fifth run and more efficient than KF/commercial CaO which had a biodiesel yield of 32% after the fifth run.

Introduction
Biodiesel refers to mono-alkyl esters of long chain fatty acids derived from renewable lipid feedstock. CaO is the most promising and frequently applied metal oxide catalyst for biodiesel production, due to its cheap price, relatively high basic strength and less environmental impacts (Madhu et al., 2017). The catalytic activity of CaO in transesterification is based on the existence of basic sites and their spatial dispersion defining their availability (Marinkovic et al., 2016)
Li/CaO (Kaur *et al*., 2014), CaO-KF (Liu *et al.,* 2012), KF/ZnO (Xie *et al.,* 2006) and KF/Ca–Mg–Al (Gao *et al.,* 2009) have been reported for the transesterification reactions. Heterogeneous basic catalysts performed more actively, react faster and are less corrosive in comparison with acidic heterogeneous catalyst (Helwani *et al.,* 2009), but they are unfavorable for feedstock with high FFAs and moisture content leading to saponification and hydration respectively (Wei *et al.,* 2009; Gao *et al.,* 2010; Oladipo *et al.,* 2016).

EXPERIMENTAL

2.1 Materials
2.5kg waste snailshell were collected from eateries around Kaduna and beneficiated. Neem oil having FFA of 4.2 was provided by the National Research Institute for Chemical Technology Zaria, Nigeria. Methanol, Commercial CaO and KF used were analytical grade reagents with purity level of 99%.

2.2 Method

2.2.1 Snailshell preparation/ beneficiation/activation.

The collected waste snailshell were parboiled, satisfactorily washed and dried overnight in hot air oven at 105^0C. The dried snailshell were crushed, ball milled and then sieved using a 125µm mesh sized sieve. The powdered snailshell obtained was calcined in a muffle furnace under static air condition at 800^0C at holding time of 3hr (Sani *et al.,* 2016). The highly active CaO and commercial CaO were hydrated at 60^0C, dehydrated at 600^0C for 2h to convert the hydroxide formed to a highly porous oxide.

2.2.2 Catalyst Synthesis: wet impregnation of KF/Snailshell.

20g each of the dehydrated-activated-CaO snailshell based catalysts was mixed with previously prepared aqueous solution of potassium fluoride (KF) with dosage (in wt.%) of 15 to 35. The resulting slurries were dried at 105^0C overnight in an oven and was subsequently calcined at temperatures ranging between 500^0C and 600^0C at holding times of 2 to 4hrs. These as-prepared catalysts were applied in the transesterification process to investigate their efficacies.

2.2.3 Transesterification: catalyst testing and characterization

The reaction conditions for the transesterification was obtained from (Oladipo, 2016) with little modification. The oil-methanol ratio used was 1:15, catalyst weight of 5 wt.% was employed, reaction temperature of 65°C and reaction time of 90 minutes were used with an agitation speed of 400 rpm. The raw snailshell, catalyst and biodiesel were characterized and analyzed using XRF, SEM-EDX, FTIR and XRD.

2.2.4 Comparative and Reusability tests

Based on the selected favorable conditions obtained using Design Expert, six different types of catalysts were synthesized namely; KF/snailshell, KF/Commercial CaO, snailshell, Commercial CaO, KF/snailshell-Fe_3O_4 and KF/Commercial CaO-Fe_3O_4 which were applied in consecutive transesterification reactions and reused appropriately.

3.0 RESULTS AND DISCUSSIONS

3.1 Snailshell and catalysts

The XRF analysis of the calcined snailshell in Table 2, depicts that the choice of snailshell in this study is justified by its rich content of CaO (Sani *et al.,* 2016 and Ikbar *et al.,* 2018).

Table 2: chemical composition of Raw and calcined snailshell

Composition	**CaO***	**SiO_2**	**Fe_2O_3**	**MnO**	**MgO**	**Na_2O**	**SrO**
Raw	97.017	0.628	0.409	0.12345t6yu8i9op-[=\][poiuyr43w2etyui;' ".,mnv cxAZsgbn,.	0.152	0.336	0.457
Calcined	98.017	0.467	0.357	0.2431	0.182	0.170	0.1603
Composition	**Al_2O_3**	**SO_3**	**P_2O_5**	**K_2O**	**Cr_2O_3**	**CuO**	**TiO_2**
Raw	0.180	0.073	0.004	0.212	0.083	0.015	0.005
Calcined	0.1301	0.0605	0.054	0.074	0.035	0.011	0.004

The FTIR spectra of the beneficiated snailshell and calcined shell are shown in Figure 1(a) and (b), respectively. For the beneficiated snailshell (Figure 1(a)), the major absorption band found at 1468 cm^{-1} can be ascribed to the asymmetric stretching of CO_3 molecules and the other major absorption bands found at 2524 cm^{-1} which depicts the presence of organic matter (Ikbar *et al.,* 2016) and 840 cm^{-1} which is ascribed to the out of plane vibration of CO_3^{2-} molecules.

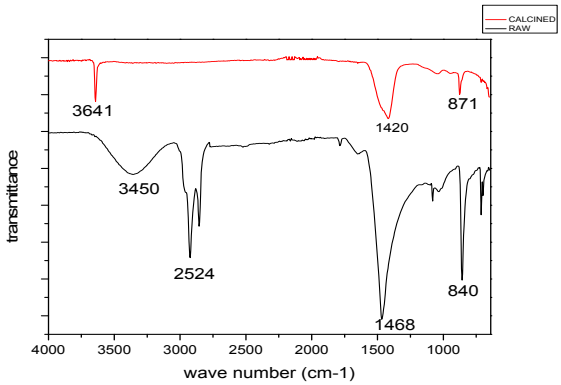

Figure 1. FTIR spectra of uncalcined (raw) and calcined snailshell

The absorption band of the organic matter obtained for the uncalcined shell at 2524cm^{-1} completely vanished after calcination of the shells at 800°C. The presence of a water molecule in the snailshell (uncalcined) was confirmed from the broad peak which appeared at 3450 cm^{-1}, and the appearance of a new peak at 3641 cm^{-1} in the calcined shell spectrum indicated the formation of $Ca(OH)_2$ from the airing of CaO. The new peak at 871 cm^{-1} is characteristics of Ca-O vibration. The SEM micrograph of the uncalcined snailshell Figure 2(a) exhibited irregular sizes of rod and spherical particles as reported by Sani et al., (2016). Calcination of the snailshell at 800°C resulted to irregular sizes of semi-spherical particles and, more importantly, porous surfaces were observed from the image in Figure 2(b).

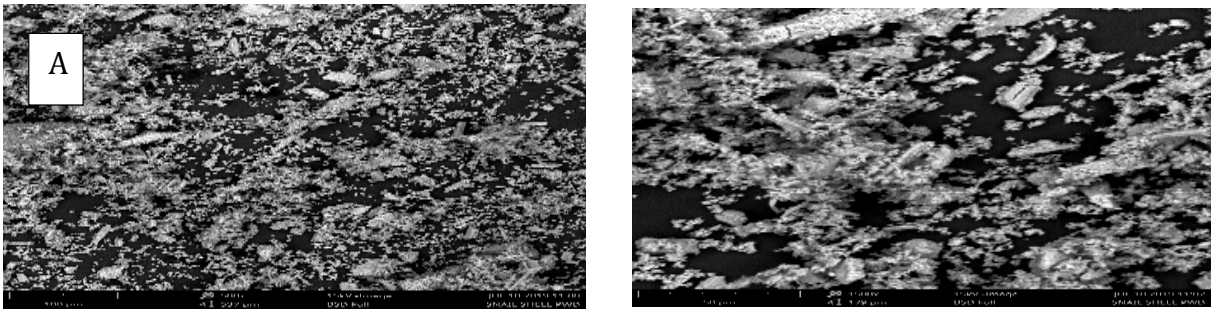

Figure2: SEM micrograph of beneficiated (A) and calcined snailshell (B)

Th transition of the catalyst and its crystalline phases and the morphology of the starting material and optimal synthesized catalyst were observed from the XRD results which shows the most intense peak occurred at 2θ = 29.32° in figure 3(a) and other peaks at 35.95°, 39.37° and 43.08° which correlates with the JCPDS card number 01-085-1108 for calcium carbonate. Thermal treatment of the calcite at the optimum operating condition assisted in the transformation of the $CaCO_3$ into CaO as depicted by Figure 3(b). Diffraction 2θ from JCPDS for calcium oxide being

used is at 32.2°, 37.3° which corresponds to the figure 3(b). The peaks corresponding to the $KCaF_3$ were consistent with the standard pattern reported in JCPDS file for KCaF3 crystal.

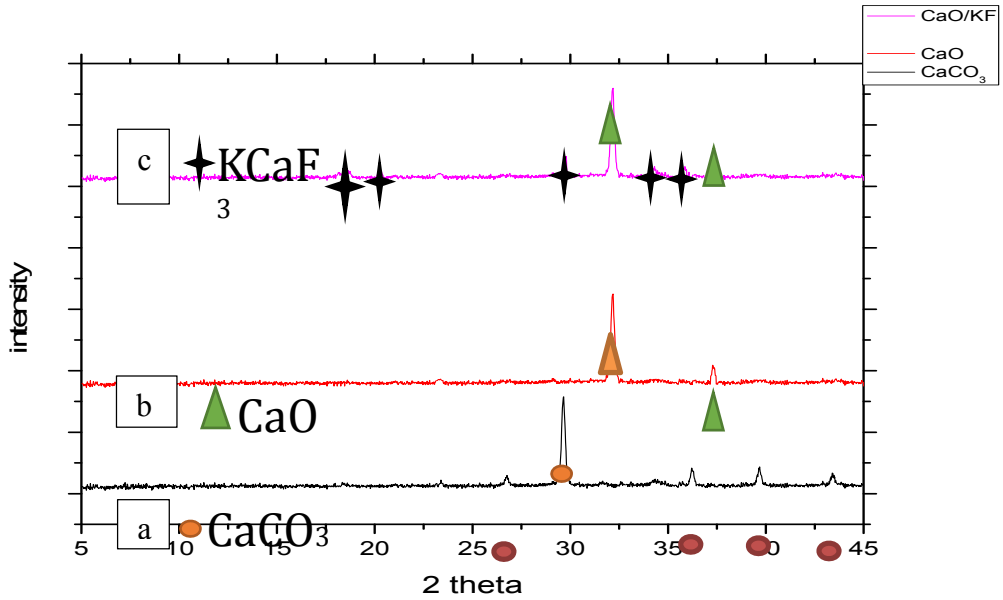

Figure 3: XRD patterns for raw snailshell (a), calcined snailshell (b) and KF/snailshell catalyst (c)

3.2 Comparative and reusability study

Figure 4 shows the biodiesel yield obtained from six different catalysts. KF impregnation significantly improved the activity of the catalyst with a biodiesel yield of 95% which can be attributed to the formation of the new specie $KCaF_3$ crystal on the surface of the catalyst which is more electronegative than CaO (Anbia *et.al.,* 2019). The reusability study conducted showed that the catalyst can be economically used for more than four runs with catalyst weight 0.89g recovered after fifth run for the KF/Snailshell-Fe_3O_4. This high catalyst weight recovery was maintained due to its magnetic nature. The commercial CaO was only used for 2 runs as no significant catalyst weight (< 0.05g) was recovered after the second run.

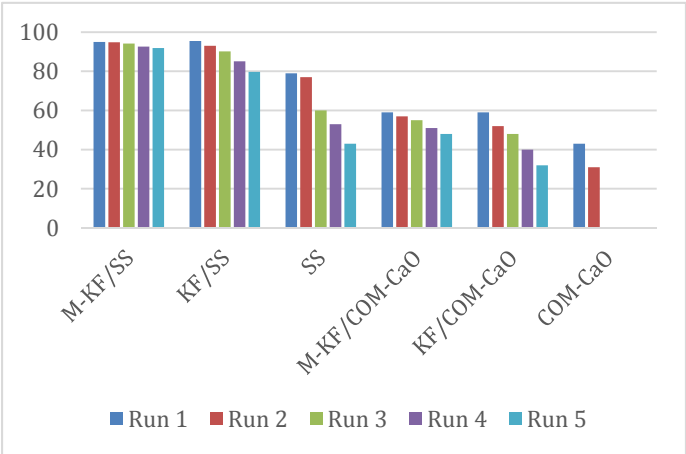

Figure 4: Biodiesel yield from different catalyst
Legend: M-KF/SS: Magnetic Potassium Fluoride/Snailshell, SS: snailshell, COM-CaO: commercial calcium oxide

The weight of catalyst recovered as result of magnetization tends to improve on the biodiesel yield obtained.

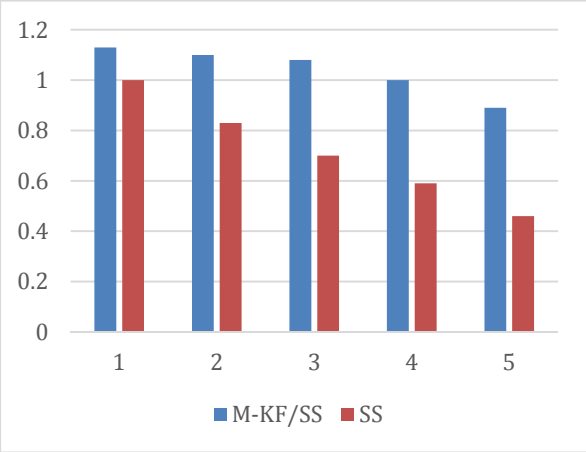

Figure 4: Weight of catalyst recovered.

3.3 Experimental design for catalyst synthesis and testing

Table 3 shows the summary of the model accuracy and the analysis of variance table. From the Table 4, a new catalyst was synthesized using the optimal selected points which was applied in a fresh batch of transesterification reactions to verify the predicted yield. Three (3) runs was carried out with biodiesel yield of 85.01, 85.28 and 84.84% respectively with an average yield of 85.043% which is close to the predicted value of 85.176%, difference observed might be due to errors during the course of the experiment.

Table 3: analysis of variance (ANOVA) for catalyst synthesis process

Full Quadratic Model					Model Accuracy	
Source	Mean Square	F-value	p-value		Correlation coefficients	**values**
Model	5.96	61.85	0.0001	Significant	R-Squared	0.9911
A-Calcination time	2.41	24.99	0.0041	Significant	Adj. R-squared	0.9751
B-KF dosage	6.99	72.54	0.0004	Significant	Pred. R-squared	0.8807
C-Calcination Temperature	5.20	53.93	0.0007	Significant	Adeq. Precision	22.4938
AB	0.0256	0.2655	0.6283	Not significant		
AC	0.0056	0.0583	0.8187	Not significant		
BC	7.45	77.30	0.0003	Significant		
A^2	22.75	235.92	< 0.0001	Significant		
B^2	4.42	45.88	0.0011	Significant		
C^2	8.33	86.40	0.0002	Significant		
Residual	0.0964					
Lack of Fit	0.1303	2.85	0.2701	Not significant		
Pure Error	0.0456					

Biodiesel yield $=79.0433 + 0.54875A + 0.935B + 0.80625C + 1.365BC + 2.48208A^2 + 1.09458B^2 + 1.50208C^2$ ..... (1)

Table 4: optimization results for catalyst synthesis process

Number	Calcination time	KF dosage	Calcination Temperature	Biodiesel yield	Desirability	
1	2.000	32.011	598.218	85.176	1.000	Selected
2	3.387	34.840	599.484	85.001	1.000	
3	2.011	34.702	588.147	84.733	0.954	
4	2.816	35.000	600.000	84.287	0.921	
5	4.000	15.000	500.000	83.947	0.828	

3.3.1 Interaction effects of catalyst synthesis factors

From Table 4, the only significant interaction among the independent variables is BC with a p-value of 0.0003. This implies that the KF loading (B) and the calcination temperature (C) plays an important role in the overall activity of the synthesized catalyst. Figure 5 shows a contour plot depicting the increase in biodiesel yield as the temperature of reaction increases and the weight of KF impregnation increases. The interaction between calcination temperature and calcination time (AC) has an insignificant effect on the overall biodiesel yield. Same was observed for the interaction (AB) which has a p-value of 0.6283.

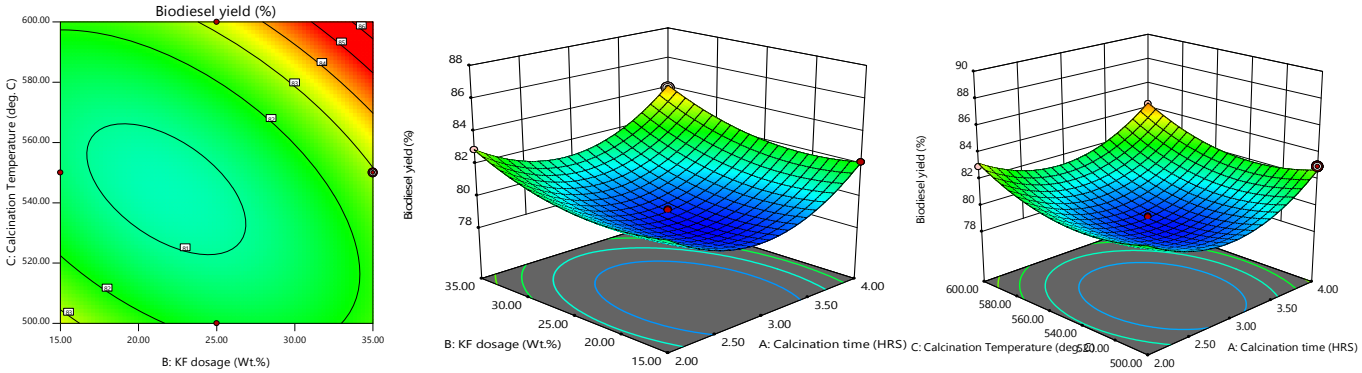

Figure 5: interaction effect of catalyst synthesis factors (BC), (AB) and (AC)

3.4 Biodiesel characterization

The FTIR result for the produced biodiesel in Figure 6 shows a distinct peak at 1740 cm^{-1} which is a characteristic peak of carbonyl ester group which shows almost complete conversion of triglycerides to methyl esters (Oladipo *et.al*, 2016). The peak observed at 1163 cm^{-1} is ascribed to C-O alkoxy ester group while the peak at 1450 and 730 cm^{-1} denotes the presence of $-(CH_2)$ methyl and methylene groups. Peaks observed at 2925 and 2854 cm^{-1} shows the presence of C-H alkanes and methylene group respectively which shows the liquid can be used as a fuel (Ismail *et. al.,* 2016). The absence of a broad peak around 3600-3300 cm^{-1} indicates the absence of water and alcohol which was as a result of the distillation of the fuel after the transesterification.

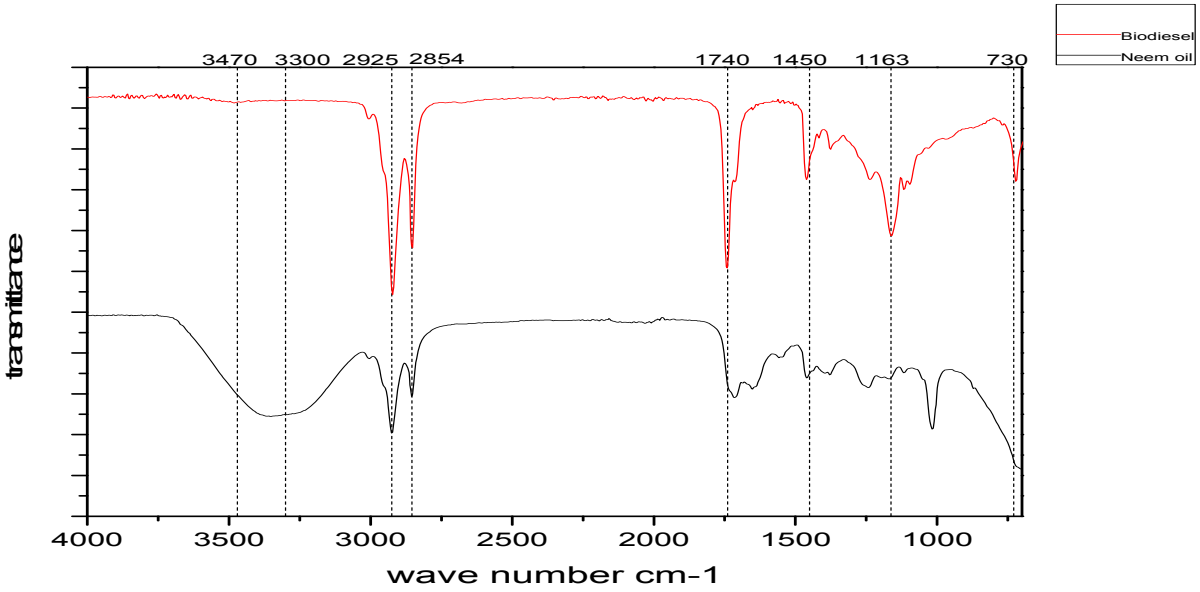

Figure 6: FTIR of neem oil and synthesized biodiesel

The physicochemical properties of the produced biodiesel show a kinematic viscosity of 3.7mm^2/sec which affect flow which in turn ensure a superior injection and atomization with the added advantage of lubricating the moving parts. High flash point temperatures for fuels ensure safe handling and storage. All the properties investigated in Table 7 were observed to fall within the ASTM standard.

Table 5: Physicochemical properties of Neem oil and Biodiesel

Parameter	**UnitUnits**	Test method	Range		**Neem ers**
Flash point	°C	D93	≥130	-	160
Kinematic viscosity (40°C)	mm^2/s	D445	1.6 – 6.0	24.89	3.70
Cloud point	°C	D2500	3 – 15		12
Pour point	°C	D2500	5 – 10		4.6
Density	g/ml	D1298	0.86 – 0.9		0.89
Acid value	mg/KOH/g	D664	≤ 0.5		0.33
Saponification value	mg/KOH/g	-	-	180.6	-

The synthesized biodiesel composition was determined by GC-MS studies and gas chromatography. It was noticed from the GC-MS results that the major FAMEs were methyl-octadecadienoate (C18:2, linoleic acid, 30.08%), methyl-hexadecanoate (C16:0, palmitic acid, 28.87%), methyl-octadecanoic (C22:0, 25.80%) and methyl stearate (C20:0, 12.36%).

Conclusions

Snailshell is a relatively cheap and organic source of $CaCO_3$ from which CaO can be synthesized as a catalyst for the single stage production of biodiesel. The best temperature for the calcination of snailshell for the production of usable CaO-catalyst in biodiesel production was established to

be 800^0C for a period of 3h. The impregnation of KF on the calcined snailshell consequentially led to the formation of $KCaF_3$ crystals with higher basic strength than CaO. The KF/snailshell synthesized after impregnation are more acid tolerant than CaO, hence usable in the transesterification of neem having FFA of 4.2%. 32 wt.% of KF was found to be the best amount needed for the impregnation, calcination of KF/snailshell at 598^0 for 2h were also found to be the optimal conditions for the preparation of the acid tolerant catalyst. The catalyst was found to be reusable up to the fifth run where a biodiesel yield of 91.9% was obtained. The addition of the magnetite helped in the recovery of the catalyst after each run using a strong bar magnet which is directly responsible for the high yield still recorded after the fifth run.

References

Ajayi, O.A., Oladipo, S.A., Ogunyemi, S.S., Nurudeen, Y., Atta, Y.A., preparation and application of KF/eggshell catalyst in Transesterification of neem oil: ovat approach. NSChe 32(2) 2017.

ASTM, D. (2002). 6751-02, Standard Specification for Biodiesel Fuel (B100) Blend Stock for Distillate Fuels. Designation D-6751-02, American Society for Testing and Materials: West Conshohocken, PA

Gao, L., Teng, G., Lv, J., and Xiao, G. (2009). Biodiesel synthesis catalyzed by the KF/Ca– Mg–Al hydrotalcites base catalyst. Energy and Fuels, 24(1), 646-651.

Helwani, Z., Othman, M. R., Aziz, N., Kim, J., and Fernando, W. J. N. (2009). Solid heterogeneous catalysts for transesterification of triglycerides with methanol: a review. Applied Catalysis A: General, 363(1), 1-10

Ikbal Bahar Laskar, Kaylani Rajkumari, Rajat Gupta, Sushovan Chatterjee" waste snail shell derived heterogeneous catalyst for biodiesel production by transesterification of soybean oil. March 2018.

Kaur, M., and Ali, A. (2014). Potassium fluoride impregnated CaO/NiO: An efficient heterogeneous catalyst for transesterification of waste cottonseed oil. European Journal of Lipid Science and Technology, 116(1), 80-88.

Lee, H.V and Y.H. Taufiq-Yap (2014). Optimization study of binary metal oxides catalyzed transesterification system for biodiesel production. Journal of Process Safety and Environmental Protection, Official Journal of European Federation of Chemical Engineering, Part B.

Liu, H., Su, L., Y, Shao and L. Zou (2012). Biodiesel production catalyzed by cinder supported CaO/KF particle catalyst. Fuel, vol. 97, 651-657

Madhu, D., Arora, R., Sahani, S., Singh, V., and Sharma, Y.C (2017). Synthesis of High-Quality Biodiesel Using Feedstock and Catalyst Derived from Fish Wastes. Journal of Agricultural and Food Chemistry 65(10):2100-2109. doi: 10.1021/acs.jafc.6b05608.

Marinković D.M., Stanković M.V., Veličković A.V., Avramović J.M., Miladinović M.R., Stamenković O.O., Veljković V.B., Jovanović D.M., Renew. Sustain. Energy Rev. 56 (2016) 1387–1408.

Sani J., Samir S., Rikot, Tambuwal A, Sanda A, "production and characterization of heterogeneous catalyst from snail shell for biodiesel production using waste cooking oil. 2017.

Wei, Z., Xu, C., and Li, B. (2009). Application of waste eggshell as low-cost solid catalyst for biodiesel production. Bioresource technology, 100(11), 2883-2885

Xie, W and X. Huang (2006). Synthesis of biodiesel from soybean oil using heterogeneous KF/ZnO catalyst. Catalysis Letters, vol. 107, Issue 1-2, 53-58

Proceedings of the 49th NSChE Annual Conference
KADA 2019: pp 338-345

P2B-01: PRODUCTION OF AVIATION FUEL FROM PLASTIC WASTES: A REVIEW

Kelechi Iheonye[a], Ifeanyichukwu Edeh[b], Ibrahim Kolawole Muritala and Ayoade Kuye[b*]

[a]World Bank African Centre of Excellence for Oil Field Chemicals Research
[b]Department of Chemical Engineering, University of Port Harcourt, Port Harcourt,
[c]Department of Solar Chemical Engineering, Institute of Solar Research, Deutsches Zentrum für Luft- und Raumfahrt (DLR)/German Aerospace Center, Linder Höhe, 51147, Köln, Germany.
[*]**Corresponding author**: ayo.kuye@uniport.edu.ng

ABSTRACT

The need to reduce the quantity of carbon monoxide (CO_2) released into the atmosphere by the aviation industry have become the driving force towards developing an alternative aviation fuel. Plastics waste currently constitute a major environmental problem since it is not bio-degradable. There is a possibility that plastic waste reduction can be achieved through the thermochemical conversion of wastes plastics to aviation fuel range alkanes. This paper reviews different technologies that are being used for such plastics waste conversion with emphasis on pyrolysis. It recommends the use of catalytic pyrolysis for the production of aviation fuel from wastes plastic materials due to its high products selectivity. It is observed that one of the challenges facing the commercialization of the catalytic pyrolysis process is the high cost of catalyst and its contamination by the feed stock.

1.0 INTRODUCTION

Plastics are materials composed of polymers which may either be thermoplastic or thermosetting (Soganocioglu et al, 2017). The most commonly used thermoplastics include polyethylene (PE), polyethylene terephtalat (PET), polypropylene (PP) and polystyrene (PS). This type of plastics is recyclable and are usually used to make containers and packing materials (Bajus and Hajekova, Gutierrez, et al., 2012). On the other hand, thermoset plastics include phenol formaldehyde and urea formaldehyde but are not recyclable as the materials cannot be modified after solidification (Aahik, et al., 2016).

Plastics play major roles in different sectors such as packaging, construction, transportation, electronics and healthcare (Anene *et al.,* 2018). This may be due to its versatility and low cost (Almeida and Marques, 2016). Annually, the global production of plastics is estimated to be about 300 million tons with its production continuously increasing every year (Miandad *et al.,* 2016). As the production of plastics increases annually, so the quantity of wastes generated also increases. This increase in plastics wastes impacts on the environment as they make the environment dirty, block drainages, pollute the water bodies and has contributed to flooding in Nigeria and around the globe. Plastic wastes are also not bio-degradable.

Over the years, various mechanisms have been used to manage plastic wastes, such as incineration, dumping them in landfills and recycling them into useful products. These methods are not enough in creating and ensuring a circular economy for plastics. The disposals of plastic waste in landfills and by incineration are expensive because plastic waste is bulky and incineration leads to release of toxic substances into the atmosphere, which pollutes the environment (Gandidi *et al.,* 2018). Conversely, values can be recovered from waste plastics in form of materials recycling or energy depending on the plastic type, ecology, ease separation from other waste

materials and cost require for processing (Panda et. al, 2010). This can be achieved through thermochemical processes such as gasification, pyrolysis, hydrocracking and catalytic cracking (Lpez, et al. 2011, Kumar et al., 2013). Although, most of these processes are expensive, require high amount of energy and might result in producing low-grade materials, pyrolysis is viable and sustainable (Xue et al., 2016).

Plastic waste oil from catalytic pyrolysis is often associated with some impurities such as sulphur, chlorine, solid residue, moisture and acids. These impurities in the raw waste plastic oil make it unsuitable for use directly as transportation fuel as well as reduces its commercial value. Thus, several researches have been carried out to upgrade waste plastic oil to different transportation fuels such as gasoline and aviation fuel.

Aviation fuel is a middle distillate of crude oil fractional distillation, specifically kerosene range (Archana *et al*, 2017). In the last decade, several developments in the use of alternative aviation fuel have led various demonstration flights by some major airlines. Concerns over the use of alternative sources of fuels for aviation operations, especially in terms of their compatibility have been a great set back. Various characteristics are expected if a fuel should be fit for aviation use. These characteristics are: high energy to maximize range, good atomization, rapid evaporation, low viscosity, extremely low freezing point, and good chemical stability as well as availability in large volumes to be able to compete economically with Jet A-1 fuels, (Chucks and Donnelly, 2014). The need to reduce the carbon emissions contributed by the aviation sector, also the exposure to crude price volatility are more reasons why researches are working on the possible alternative fuel to fossil-based aviation fuels.

Technically, the production of aviation fuel from plastic waste consists of: (a) waste plastic pyrolysis processes, (b) upgrading the waste oil and gas cleaning, (c) Fischer-Tropsch (FT) synthesis, and, finally, (d) hydro-processing and distillation of the liquid hydrocarbons. The synthetic aviation fuel produced via FT synthesis is environmentally friendly because of the lower concentrations of nitrogen, sulfur, and aromatics. Apparently, the first step is to quantify the waste plastics availability; some of the available data in this regard for Nigeria is presented in Section 2. Pyrolysis is discussed in Section 3 and some of the existing methods for producing transport fuels from waste plastic oil is presented in Section 4.

2.0 TYPICAL PLASTIC WASTE AVAILABILITY IN NIGERIA

Ikebude (2017), investigated the components of wastes generated in Port Harcourt and grouped these components as garbage, paper, plastics, scrap metal and Glass, construction waste, sludge and others. The data was collected through questionnaires, literature examination, oral interview, field survey and physical observation. Three major sampling sites were used – Borokiri, main town and GRA areas of Port Harcourt. The data obtained show that 35% of solid waste generated in Port Harcourt Metropolis is composed of paper and plastic (Figure 1). This indicates that there is a large amount of plastic wastes produced in Port Harcourt.

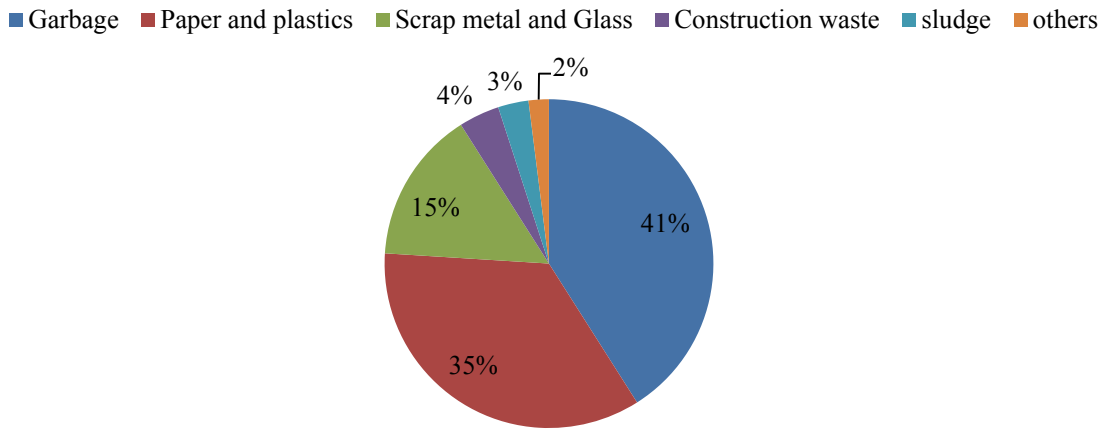

Figure1: Physical composition of solid waste generated in Port Harcourt metropolis (Ikebude, 2017)

Oghenefejiri *et al* (2016) assessed the various components of municipal wastes in Nigeria. Group discussions involving professional environmentalists and solid waste managers were used for data collection. His studies areas were the six geopolitical zones in Nigeria. The results obtained are presented in Table 1. Table 1 shows that the cities with large dumps of waste plastics are Abuja, Kano, Ota, Cross river, Delta, Lagos, Niger while States like Rivers possessed less amount of plastic wastes compared to other cities in Nigeria. Based on these results, Oghenefejiri *et al.* (2016) concluded that there are sufficiently large quantities of plastic wastes in Nigeria.

Table 1: Components of municipal solid waste in the six geo-political zones in Nigeria (Oghenefejiri *et al,* 2016**).**

Zone	States	Organics	Plastics	Paper	Glass	metal	Textile/leather	Unclassified debris
North East	Borno (Maiduguri)	28.8	18.1	7.5	4.3	9.1	3.9	31.3
North Central	Niger	31	16	13	9	11	6	14
	Nasarawa	31.5	7.25	3.5	18	6.5	1.5	31.75
	Abuja	43.57	20.97	23.11	3.23	3.79	2.77	2.56
North West	Kano (Sabon-gari)	57.5	17.5	6.7	5.7	3.9	4.5	4.2
South West	Oyo (Ibadan)	47	12.6	21.9	0.9	6	8.8	2.8
	Lagos	53	15	10	5	5	4	8
	Ogun (Ota)	42.07	21.01	8.29	9.59	1.06	7.44	10.54
South South	Rivers	63	3.5	9.9	1.9	3.4	14	4.3
	Delta	37	21	18	6	10	5	3
	Cross River (Calabar)	23.33	14.67	16	12	15.33	0	18.67
South East	Enugu	30.7	9.2	23.1	9.2	6.2	6.2	15.4

3. PYROLYSIS OF PLASTIC WASTE

Pyrolysis can be described as the decomposition of long chain hydrocarbon polymer molecules into smaller sizes monomer at a temperature range of 450-800^{0}C within a short period of time in an environment devoid of oxygen (Thahir *et al*, 2019). The pyrolysis products are in the form of carbon as residues and volatile hydrocarbons which can be condensed as liquid and non-condensable gaseous. As the temperature is increasing the weak bonds binding the polymer gets damaged, this is followed up by the formation of free radicals, these free radicals gets separated again forming stable compounds of paraffins, isoparaffins, olefins, naphthenes and aromatics (Thahir *et al*, 2019). These compounds are the major components of petroleum.

The relative amount of solid, liquid and gases produced in a typical process depends on the operating conditions. The range of the main operating parameters for pyrolysis processes are shown in Table 2. Slow pyrolysis is an ancient method used for producing charcoal (Patni *et al*, 2013). In fast pyrolysis (also called thermal pyrolysis) the material is rapidly heated to high temperatures in the absence of oxygen.

Table 2: Operation conditions for pyrolysis processes (Patni et al, 2013).

Parameter	Conventional	Fast	Flash
Pyrolysis temp. (K)	500-900	850-1250	1050-1300
Heating rate (K/s)	0.1-1	10-200	>1000
Particle size (mm)	5-50	<1	<0.2
Solid residence (s)	300-3600	0.5-10	<0.5

The liquid oil from thermal pyrolysis may contain impurities and residues. To overcome these problems catalysts are used to improve the pyrolysis process of plastic waste overall and to enhance process efficiency (Miandad et al, 2019). When catalysts are used it is called catalytic pyrolysis. Thermal and catalytic pyrolysis of waste plastics are discussed further in Sections 3.1 and 3.2.

3.1 Thermal pyrolysis

Thermal pyrolysis of plastic wastes leads to the formation of a wide range of hydrocarbons (Almeida and Marques, 2016). The reaction mechanism of thermal pyrolysis of waste plastics is complex, and this contributes to the limited commercial value of it being used as fuels. The products obtained by the thermal pyrolysis of plastic wastes are grouped into non-condensable gas fraction, liquid fraction (paraffin, olefins, Sssnaphthenes and aromatics) and the solid residue (Almeida and Marques, 2016). The liquid fraction obtained from the thermal pyrolysis are gasoline range (C_4-C_{12}), diesel range (C_{12}-C_{20}), kerosene range (C_{10}-C_{18}) and motor oil range (C_{23}-C_{45}) (Archana *et al*, 2017).

3.2 Catalytic pyrolysis

Catalysts are used to reduce the activation energy and to improve the thermal efficiency in pyrolysis process. The presence of catalyst helps secondary cracking to the solids and liquids, which results in higher pyrolytic products. Mohammed *et al* (2015a) carried out the catalytic pyrolysis by using Y-zeolite and ZSM-5 as catalyst to convert electric and electronic plastic waste into oil, the oil produced contained mainly styrene. The ratio of Si:Al in the Zeolite determined the extent of influence of the catalyst. With lower Si:Al ratio in the zeolite, a higher conversion of styrene to other aromatic products particularly benzene and toluene was observed. When Y Zeolite

catalyst was compared to ZSM-5 catalyst, a higher conversion of styrene to other aromatic products was observed with Y zeolite, this can be attributed to the larger catalyst active sites and also larger pore sizes when compared to ZMS-5 catalyst. Aida *et al* (2015) used fluidized catalytic cracking (FCC) catalyst to convert plastic waste to liquid using a pyrolysis temperature of 400 ˚C and reaction time of 2 hours, the mixed plastic waste used (polyethylene, polypropylene and polystyrene) were combined in the ratio 5:3:2 and a catalyst to waste plastic ratio of 10:90 was used. The volume of liquid product obtained was 20ml under non-catalytic condition and 35ml under catalytic condition. The energy require for this process may be decreased as the reaction temperature is reduced. This decrease is caused by the reduced activation energy of the pyrolysis reaction (Anene *et al,* 2018). The catalyst used in the process may favour the yield of lighter hydrocarbons, gasoline range and gases. The product obtained will depend on the type of polymer, their sources and structure, (Anene *et al,* 2018). The products are hydrocarbons with so many applications; the pyrolysis oil can be used as an energy source and also for producing other chemicals. The pyrolysis liquids will need to be refined and upgraded before it can be used as a transportation fuel and other petrochemical products (Ghodrat *et al,* 2019).

4.0 TRANSPORT FUEL PRODUCTION FROM WASTE PLASTIC OIL

In general, available methods for producing transportation fuels from waste plastic oil can be classified into two main groups namely: refining and blending (Miandad *et al.,* 2016). Some of these works are presented in this section.

Sharma (2014) used a Be-h desktop plastic oil system to distillate the waste plastic oil, the gasoline fraction was obtained by setting an upper and lower temperature of 195 ˚C and 175 ˚C respectively. The diesel fraction was collected by setting the upper and lower temperature at 290 ˚C and 271˚C.

Syamsiro *et al,* 2014 reports the use of FCC catalyst as a cracking catalyst, this improved the liquid, gas yields, and a high fraction of heavy hydrocarbons was in the fuel due to more cracking residue. The low thermal conductivity and high viscosity of plastic crude oil are the main challenges for designing the cracking reactor. Syamsiro *et al*. (2014) used a pilot scale two stage reactor operating a batch system consisting of a pyrolysis reactor and a catalytic reforming reactor. The gas generated from the pyrolysis reactor was reformed in the reforming reactor, the resulting liquid was condensed and the product collected. From the experiment carried out, it was reported that feed type and catalyst type have an effect on the products. Presence of catalyst promoted the formation of gaseous products, unlike the non-catalysed pyrolysis that had more yield of the liquid product.

Chen *et al.* (2014) carried out an experiment on pyrolysis using hydrolysis reactors having steam as carrier gas and Fe based catalyst, followed by the catalytic cracking reactor having Zeolite as a catalyst. This could be a positive move towards pyrolysis fuel upgrade. Using a fluidized bed reactor operating at a temperature of about 500 ˚C, the gases can be extracted before the secondary cracking takes place. This will result to a higher yield of the liquid product.

Muhammed (2015b) used a two-stage pyrolysis fixed bed reactor in his experiment to determine the product yield, composition and hydrocarbon distribution of a catalyzed pyrolysis process to convert virgin polyethylene, polypropylene, polystyrene and PET using a zeolite HZSM -5 catalyst. It was observed that the yield of the liquid product dropped in the samples where catalyst was used from 45wt% and 55wt% when it was compared to the 81wt%-97wt% obtained from

uncatalysed pyrolysis. The catalyzed pyrolysis oil was rich in aromatic hydrocarbon content. The composition of the catalyzed pyrolysis oil moved from high molecular weight hydrocarbons (C_{16}) to full range hydrocarbons (C_5-C_{15}).

.

Zhang *et al* (2019) investigated seven types of commercial and home – made activated carbon on the pyrolysis of waste plastics in a facile tube reactor, the liquid obtained had components of Jet-range hydrocarbons accounting for 28.8% aromatics and 71.8% alkanes. It was observed that activated carbon catalyst transformed low density polyethylene into Jet fuel and hydrogen gases excellently. In addition, it is important to note that these activated carbon catalysts could be sourced and prepared locally from biomass residues or agricultural wastes from available crops such as walnut shells, palm shells, coconut shells, beans husks, banana peels, tobacco stems and so on (Tadda *et.al,* 2016). Zhang *et al.* (2019) suggested a possible route to obtaining jet-fuel range hydrocarbons from low density polyethylene waste plastics, ground to a particle size of 3mm (Figure2). Unit (1) is a cylinder filled with the Nitrogen gas which was used as the carrier gas, (2) is a control valve for the nitrogen gas coming from the cylinder, (3) is a tube which carried the waste plastic (7) into the reactor (8) where pyrolysis occurred alongside with catalytic cracking with activated carbon catalyst (10), (11) is a condenser which cooled the outlet vapor to liquids in (12) and the uncondensed gases were collected in (13).

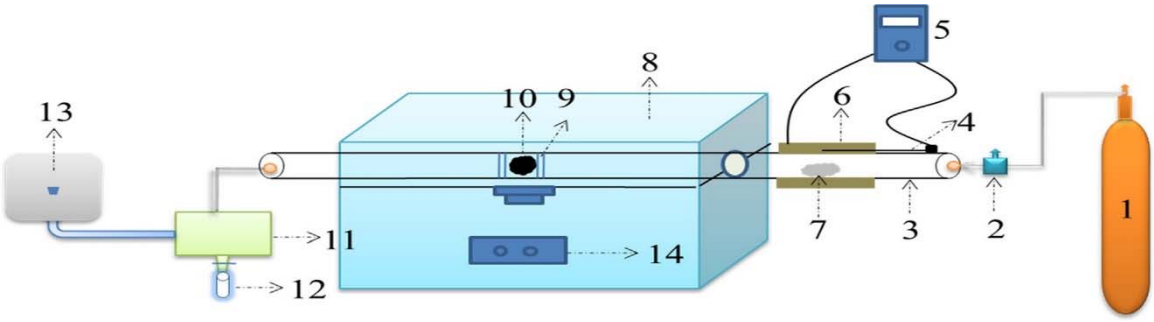

Figure2: The catalytic pyrolysis system of daily waste plastics (Zhang *et al*.2019)
1-Nitrogen gas; 2-Gas flow meter; 3-Quartz tube; 4-Thermocouple for heating tape; 5-Heating tape controller; 6-Heating tape; 7-Waste plastics; 8-Fixed bed furnace; 9-Quartz wool; 10- Activated carbon catalyst; 11-Condensor; 12- Liquid product collector; 13-Non-condensable gas collector; 14-Control panel of the furnace.

5.0 IDENTIFIED GAPS FOR FUTURE RESEARCH

From the researches reviewed so far, the followings are some of the areas that require further work:

(a) The common catalyst used for waste plastics pyrolysis is zeolite. Zeolite is very expensive (Butler, 2011). An alternative to zeolites or zeolite produced locally will greatly reduce the cost of production.

(b) Catalyst recovery after use is another issue due to the deposition of carboneous matter on the catalyst during the pyrolysis. This can lead to the deactivation of the catalyst (Syamsiro *et al.,* 2014). Integrating a catalyst regenerating unit into the design would be very useful in reducing the cost and also minimize the waste from spent catalyst.

6.0 CONCLUSION

This paper reviewed different works done in the production of transportation fuels via pyrolysis. Thermal and catalytic pyrolysis has been suggested to be the possible routes for obtaining high grade aviation fuels. Catalytic pyrolysis has the advantage of reducing the activation energy for the process; it has also been reported to contribute to high selectivity of the products. The high cost of catalyst and the contamination of feed stock are challenges facing the commercialization of aviation fuels via catalytic pyrolysis. There is therefore need for more comprehensive work to be done towards developing a catalyst that is cheap possibly from renewable sources, e.g activated carbon from biomass that would not increase operational cost.

REFERENCES

Aadhik, A., Athmanathan, Hari, N. (2016) *Synthesis of Fuel from waste plastic* Report project Mechanical Engineering Anna University, p53

Aida Isma M.I, Salmiaton A, and Nur Dinie K.B (2015) *Mixed Plastic Wastes Pyrolysis in a Fluidized Bed Reactor for Potential Diesel Production* Int. J. Env. Sci. Dev. 6**,** 606-609

Almeida D. and Maria de Fatima Marques (2016) *Thermal and Catalytic Pyrolysis of Plastic Waste.* Polimeros, 26(1), 44-51

Anene Azubuike Frances, Siw Bodil Fredriksen,Kai Arne Saetre and Lars-Andre Tokheim (2018) *Experimental Study of Thermal and Catalytic Pyrolysis of Plastic Waste Compounds* Sustainability 10(11), 3979

Archana Saxena,Hitesh Sharma, and Girish Ratni (2017) *Conversion of Waste Plastics to Fuel:Pyrolysis-An Efficient Method :A Review* https:www.researchgate.net/publication/ 313349450.

Bajus, M., Hajekova (2010) *Thermal cracking of the model seven components mixed plastics into oils/waxes* Petroleum and Coal 52, 3

Butler.E, G.Devlin and K.McDonnel (2011) *Waste Polyolefins to Liquid Fuels via Pyrolysis: Review of Commercial State of the Art and Recent Laboratory Research* Waste Biomass Valor 2, 227-255.

Chen Dezhen, Lijie Yin, Huan Wang, and Pinjing He (2014) *Pyrolysis Technologies for Municipal Solid Waste: A Review* Waste Management 34, 2466-2486.

Chuck Christopher J and Donelly Joseph (2014) *The Compactibility of Potential Bioderived Fuels with Jet A-1 Aviation kerosene* Applied Energy 118(c), 83-91.

Gandidi I.M, M. D Susila and H. Rustamaji (2018), *Effect of Natural Catalyst in the Isothermal – Catalytic Cracking of Real Municipal Solid Wastes (SMSW) for Bio-oil Production*. IOP Conference Series Earth and Environ.Sci 160, 1-15.

Ghodrat Maryam, Dharmappa Hagare, Richard Yang and Bijan Samali (2019) *Economic Feasibility of Energy Recovery from Waste Plastic using Pyrolysis Technology an Australian Perspective* International Journal of Environmental Science and Technology 16, 3721.

Gutierrez, C. et al. (2012) *Recycling of extruded polystyrene wastes by dissolution and supercritical CO2 technology* Journal of Materials Cycles and Waste Management 14, 308-316

Ikebude C.F (2017*) Feasibility Study of Solid Waste Management in Port Harcourt Metropolis: Causes, Effects and Possibilities* Nigerian Journal of Technology 36(1), 276-281.

Kumar S., Prakash R., Murugan S., Singh R (2013) *Performance and emission analysis of blends of waste plastic oil obtained by catalytic pyrolysis of waste HDPE with diesel in a CI engine* Energy Convers Manag 74, 323-31.

Lpez A. de Marco I., Cabellero B., Laresgoiti M., Adrados A. (2011) *Influence of time and temperature on pyrolysis of plastic wastes in a semi-batch reactor* Chem Eng J 173, 62-71

Miandad R., Mohamed Rehan, Asad.S.Aburizaiza, Hizbullah Khan,Iqbal M.I Ismail, Jeya Dhavamani, Jabbar Gardy, Ali Hassan pour and Abdul-Satter Nizani (2019) *Catalytic Pyrolysis of Plastic Waste : Moving Towards Pyrolysis Based Refineries*. Frontiers of Energy Research 7, 1-27.

Miandad, R., Barakat, M. A., Aburiazaiza, A. S., Rehan, M., and Nizami, A. S. (2016). Catalytic pyrolysis of plastic waste: a review. Process Safety Environ. Protect. 102, 822–838.

Mohammad Chika, Jude A O and Paul T W (2015a) *Catalytic Pyrolysis of Waste Plastic from Electrical and Electronic Equipment* (Leeds, United Kingdom: Energy Research Institute, Faculty of Engineering, University of Leeds) 113,332-339.

Mohammad Chika, Jude A Onwudili and Paul T Williams (2015b) *Thermal Degradation of Real World Waste Plastics and Simulated Mixed Plastics in a Two Stage Pyrolysis-Catalysis Reactor for Fuel Production* Energy and Fuels 29 (4), 2601-2609.

Oghenefejiri B., Nwagozie Ify L, and Agunwamba J.C (2016*) Exploratory Factor Analysis and Assessment of Energy Potential of Generated Solid Waste in Nigeria* International Journal of Civil Engineering and Technology 7, 274-289.

Panda A. K, Singh R. K, Mishra D. K. (2010) *Thermolysis of waste plastics to liquid fuel A suitable method for plastic waste management and manufacture of value-added products- A world prospective* Renewable and Sustainable Energy Reviews 14,233-248

Patni N., Shah Pallav, Agarwal Shruti and Singhal Piyush (2013) *Alternative Strategies for conversion of Waste Plastics to Fuels* ISRN Renewable Energy 2013.1-7.

Sharma.K.Brajenbra,Bryan R Moses, Karl E Vermillion, Kenneth M Doll, and Nandakishore Rajago Palan (2014) *Production of Fuel Properties of Alternative Diesel Fuel from Pyrolysis of Waste Plastic Grocery Bags* Food Proceeing Technology 122,79-90.

Sogancioglu, M., Ahmetli, G., Yel., E. (2017) *A comparative Study on Waste Plastics Pyrolysis Liquid Products Quantity and Energy Recovery* Potential Energy Procedia 118, 221-226

Syamsiro Mochamad, Shuo Cheng, Zainal Alinmuddin,] and Kunio Yoshikawa (2014) *Fuel Oil Production From Municipal Plastic Wastes in Sequential Pyrolysis and Catalytic Reforming Reactors* Energy Procedia 47,180-188.

Tadda M.A., A. Ahsan, A. Shitu, M. ElSergany, T. Arunkumar, Bipin Jose, M. Abdur Razzaque, and N.N. Nik Daud (2016) *A review on activated carbon: process, application and prospects. Journal of Advanced Civil Engineering Practice and Research, 2(1):7*

Thahir Ramli, Altway Ali, Sri Rachmania Juliastuti (2019) *Production of Liquid Fuel from Plastic Waste Using Integrated Pyrolysis Method with Refinery Bubble Cap Plate Column.*Researchgates10.1016/j.egyr.2018.11.004.

Xue, Y., Kelkar, A., Bai, X. (2016) *Catalytic co-pyrolysis of biomass and polyethylene in a tandem micropyrolyzer*, Fuel 166, 227-236

Zhang Yayan, Denggle Duan, Hanwu Lei, ElmarVillota, and RogerRuan (2019) *Jet Fuel Production from Waste Plastics via Catalytic Pyrolysis with Activated Carbon* Applied Energy 251,113337

Proceedings of the 49th NSChE Annual Conference
KADA 2019: pp 346-354

P2B-02: A REVIEW THERMAL ENERGY STORAGE SYSTEMS USING PHASE CHANGE MATERIALS

[1]Muhammad Ahmad, [2]Ibrahim Shehu Diso, [3]Usman Aminu
[1,2]Department of Mechanical Engineering, Faculty of Engineering, Bayero University Kano, Nigeria.
[3]Usman Aminu, Department of Mechanical Engineering, Nuhu Bamali Polytechnic Zaria, Kaduna State, Nigeria
Corresponding Author: mailafiya09@gmail.com

ABSTRACT
Thermal energy storage being a relatively old area of research has gained special attention from researchers around the globe. The problem of global warming, ozone layer depletion, acid rain, environment pollution among other issues resulting from continuous use of conventional fossil fuel have necessitate the need for alternative energy sources which are cleaner, cheaper and more sustainable. One of the available options is to develop energy storage systems so as to aid in energy conservation by improving the efficiency and performance of energy systems. This paper looked deeply into the literature and presents a review of latent heat thermal energy storage systems with phase change materials. It is discovered from this study that Thermal energy storage system has proved its potential in addressing the mismatch between energy demand and supply in energy systems. Sustainable development requires that energy resources be used as efficiently as possible so as to maximize the benefits it derived from utilizing energy resources, while minimizing the negative impacts (such as environmental damage) associated with their use.

Key-words: thermal energy storage:-, phase change materials:-, latent heat thermal storage

1.0 INTRODUCTION
Energy storage plays important roles in conserving available energy and improving its utilization, since many energy sources are intermittent in nature. Several forms of energy are stored using different technologies such as electrical energy in batteries, mechanical energy in flywheels, chemical energy storage in form of organic molecular storage, biological storage, magnetic storage and Thermal Energy Storage (Dincer and Rosen,2011). Thermal energy storage (TES) has become extremely important in the recent years since it balances the energy demand and improves the efficiency of energy systems. Thermal energy can mainly be stored using three technologies namely; sensible heat storage, latent heat storage and thermo-chemical storage (Sharma et al, 2009). Sensible heat storage is a developed technology which can be done in different storage media such as water, rocks, concrete etc. Water as a sensible heat storage medium has an edge over other sensible storage media because of its large specific heat capacity. However, low energy storage density and dependence on temperature gradient among other problems have limited its application. Thermo-chemical energy storage has large energy storage density but its large change of volume pose containment problem (Dincer and Rosen, 2011).

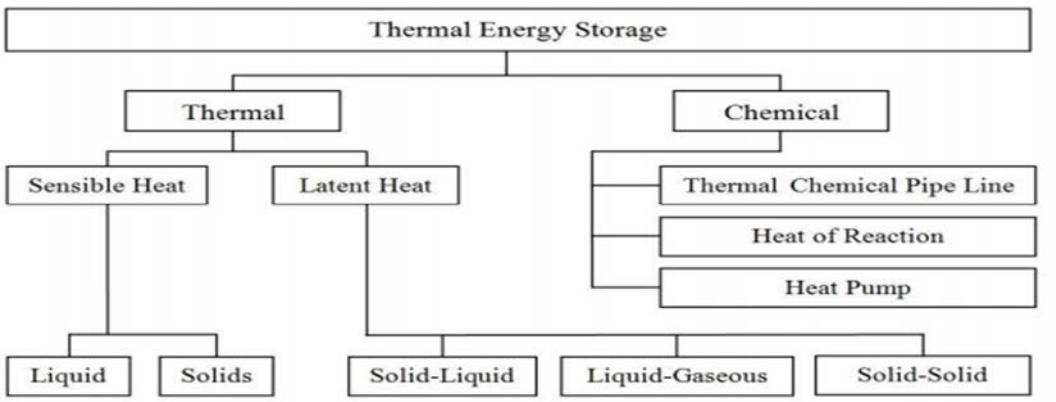

Figure 1: Methods of thermal energy storage. (Simone, 2015)

1.1 LATENT HEAT THERMAL ENERGY STORAGE

Latent heat thermal energy storage is characterized with high energy storage density and constant temperature. The main principle in latent heat thermal energy storage is that heat is absorbed by a material at its transition temperature which causes change of phase from one state to another (i.e solid- liquid, liquid-gas, solid-gas and vice versa) (Tatsidjodoung *et al,* 2013). This heat is released for use at a later time causing the material to change phase to its original state. Latent heat thermal energy storage takes advantage of constant transition temperature which corresponds to the desired operation temperature and substantial latent heat of fusion/melting of phase change materials (PCMs) (Dincer and Rosen, 2011). Usage of Phase Change Materials (PCM) for energy storage provides a great benefit but, their low thermal conductivity becomes a major drawback. This problem can be mitigated using various heat transfer improvements methods such as metallic fillers, metal matrix construction and finned tubes (Thamaraikannn et al 2017).

1.2 PHASE CHANGE MATERIALS (PCMs)

Phase change materials (PCMs) are substances that can store and release heat during the change from one phase to another at a known temperature range. Phase change can be between any of the phases solid, liquid or gas. Large amount of heat is absorbed as change in phase occurs at nearly constant temperature. So also, equal amount of energy is released when it changes back to the initial phase. Its ability to store high amount of latent heat as compared to conventional materials gives more heat storage capacity per unit volume. The classification of phase change materials is depicted in figure 2 below.

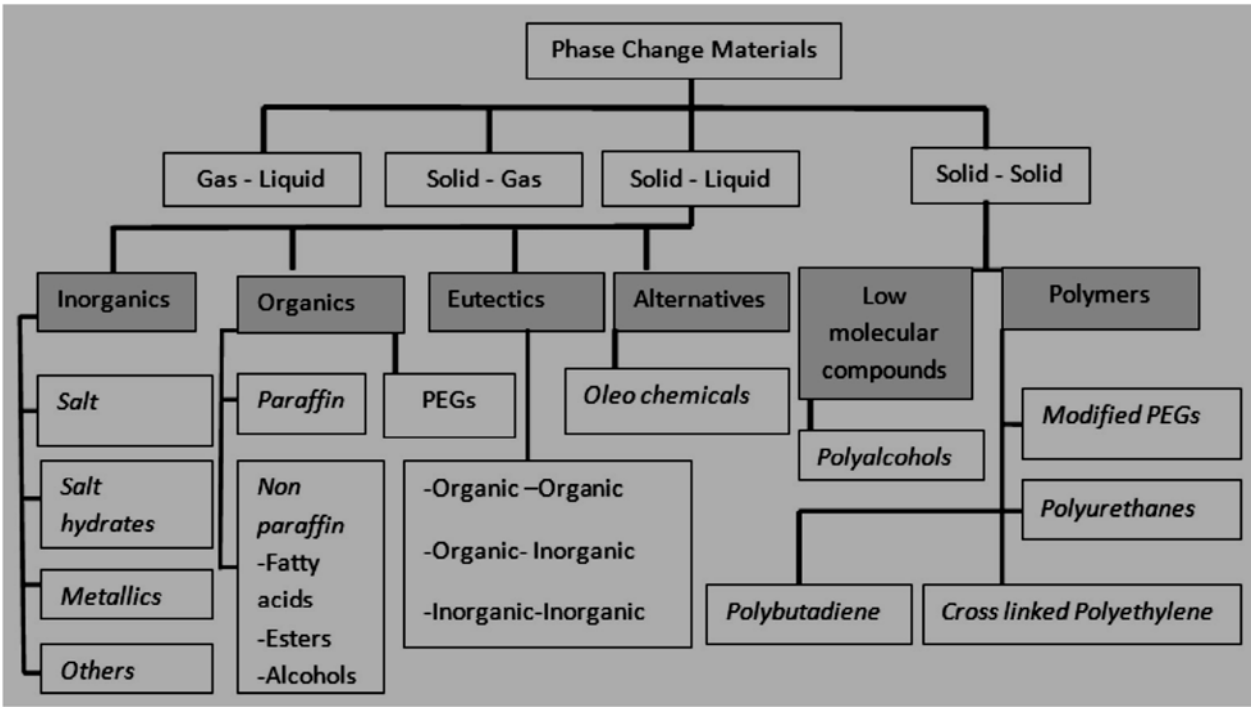

Figure 2: Classification of PCMs (Kapsalis and Karamanis, 2016).

2.0 RELATED LITERATURE ON LATENT HEAT THERMAL ENERGY STORAGE SYSTEMS

According to Sharma and Sagara (2005), Latent heat storage is a relatively old area of research and pioneered by Telkes M. in the 1940s. It did not receive much attention, however, until the energy crisis of the late 1970s and early 1980s. The first application of PCM described in the literature as asserted by Sharma and Sagara (2005) was their use for heating and cooling in buildings. Telkes et al. (1978) published the idea of using PCMs in walls, better known as Trombe walls.

Over the years, latent heat thermal energy storage systems have been developed for cooling, low temperature and high temperature applications. Areas of applications include solar water heating, waste heat recovery, power plants, cooling of electronic devices and buildings. Koca et al. (2008) developed a latent heat storage flat-plate solar collector with phase change material ($CaCl_2.6H_2O$). The designed collector combines in a single unit solar energy collection and storage. PCMs are stored in a tank, which is located under the collector. They observed that the average net energy and exergy efficiencies are of 45% and 2.2%, respectively. Eman-Bellah et al. (2006) investigated the performance of a compact solar collector with an absorber plate–container unit. Both absorbing and storing operations of solar heat in a paraffin wax were examined, experiments were conducted for conducted for different water mass flow rates in the range 8.3 – 21.7 kg/h. They observed that the heat transfer coefficients increases sharply with increasing molten layer thickness as the natural convection grows strong during the charging process while in the discharge process, the useful heat gain was found to increase as the water mass flow rate increases. Also a solar collector consisting of two adjoining sections, one filled with water and the other with paraffin wax of melting point range of about 45-50^{0}C as a PCM was developed and investigated by Kurklu et al (2002). The result of the study indicated that the water temperature exceeded 55^{0}C during a typical day of high solar radiation and was kept over 30^{0}C during the whole night. Instantaneous thermal efficiencies achieved were between 22% and 80%.

Canbazoglu et al. (2005) tested the performance of solar thermal energy storage using sodium thiosulfate pentahydrate as PCM in a solar water-heating system. They founded that the storage time of hot water, the produced hot water mass and total heat accumulated in the system were approximately 2.59–3.45 times that of solar water-heating system without PCM.

Castell et al. (2008) experimentally investigated a TES with PCM in 3 different modules, without fins, with 8 fins of length 20mm, and with 8 fins of length 40mm to determine the heat transfer coefficient through natural convection. It has been proved that bigger fins resulted in a faster heat transfer process.Ye et al. (2011) studied thermal storage and release process in an aluminium plate-fin storage unit. The results show that larger temperature differences lead to shorter melting time. Ehsan et al. (2013) designed a TES made of corrugated copper panels with increased surface to volume ratio. Six square corrugated copper panels were soldered together to the center at 60° forming six corrugated fins. The experimental results obtained with the corrugated TES were compared with a multi-tube system and was found that the corrugated TES had better results due to higher surface to volume ratio.

Nallusamy et al (2007) investigated experimentally the thermal behavior of a packed bed of combined sensible and latent heat thermal energy storage (TES) unit. A TES unit is designed, constructed and integrated with constant temperature bath/solar collector to study the performance of the storage unit. The TES unit contains paraffin as phase change material (PCM) filled in spherical capsules, which are packed in an insulated cylindrical storage tank. Charging experiments are conducted on the TES unit to study its performance by integrating it with constant temperature source/varying temperature source (solar energy). It is observed that in the case of constant inlet temperature of heat transfer fluid, mass flow rate has little effect on the charging rate and the rate of heat transfer increases in direct proportion with the increase in inlet temperature of the HTF. In the case of the storage unit integrated with solar flat plate collector, the mass flow rate has significant effect on the heat extraction rate from the collector, which in turn affects the rate of charging of the TES tank. Experiments are conducted for continuous discharging and batchwise discharging for both sensible heat storage system (SHS) system and combined storage system. It is concluded that the combined storage system gives better performance than the conventional SHS system where there is a direct mixing of the HTF with the hot water in the storage tank.

Agyenim et al. (2010) designed a horizontal shell and tube heat exchanger containing a medium temperature PCM with a melting temperature of 117.7^0C. Two experimental configurations consisting of single tube control unit and a multi tube systems were studied. Temperature gradients in the two configurations along three directions (radial, axial and angular directions) were analyzed and compared. The temperature gradients recorded for the single and multi-tube systems in the axial direction during change of phase were found to be respectively 2.5 and 3.5% that of radial direction. The results of the investigation proved that the multi-tube system performed better than the single tube system.

Hosseini et al. (2012) investigated experimentally and numerically a shell and tube heat exchanger to determine the effect of buoyancy during the melting of PCM contained within the heat exchanger. The effect of inlet temperature of heat transfer fluid on the performance of the thermal storage system was investigated. The results shows that heat transferred to PCM is largely influenced by natural convection and increase in the inlet temperature of heat transfer fluid to 80^0C reduced the melting time by 37%.

El-Kaddadi and Asbik (2017) carried out experimental study of heat transfer during latent heat storage cycle (charging/discharging) in a vertical cylindrical system. The experimental setup consists of two cylindrical tanks filled respectively with hot and cold water, a test bench, and measurement instruments. They observed that the convective heat transfer coefficient between the heat transfer fluid (HTF) and the annular space is improved by increasing of the mass flow rate of the heat transfer fluid. Furthermore, Jesumathy et al. (2014) evaluated the thermal behavior of 0.7 kg of commercial paraffin in a shell-and-tube heat exchanger, placed both horizontally and vertically, under the influence of different heat transfer fluid (HTF) (water) mass flow rates and inlet temperatures during the melting and solidification processes. Results showed no subcooling of the paraffin and demonstrated that the modification of the HTF operating conditions has a higher influence during melting than during solidification.

The energy and exergy efficiencies of a seasonal thermal energy storage using paraffin wax as a PCM with the latent heat storage technique developed to heat the greenhouse of 180 m2 floor area was experimentally evaluated by Ozturk (2005). The system consists mainly of five units: flat plate solar air collectors (as heat collection unit), latent heat storage (LHS) unit, experimental greenhouse, heat transfer unit and data acquisition unit. The LHS unit was filled with 6000 kg of paraffin, equivalent to 33.33 kg of PCM per square meter of the greenhouse ground surface area. The rate of heat transferred in the LHS unit ranged from 1.22 to 2.63 kW, whereas the rate of heat stored in the LHS unit was in the range of 0.65–2.1 kW, average net energy and exergy efficiencies were found to be 40.4% and4.2%, respectively

Gu et al. (2004) developed a heat recovery system using PCM to recover the rejected heat of air conditioning systems and produce low temperature hot water for washing and bathing. They concluded that the heat recovery system decreases not only the consumption of primary energy for heating domestic hot water but also the calefaction to the surroundings due to the rejection of heat from air conditioning systems. It was observed that the efficiency ratio of the system is improved effectively when all the rejected (sensible and latent) heat from air conditioning systems is recovered.

Buddhi (1997) designed and fabricated a shell and tube type heat exchanger for low temperature waste heat recovery using PCM. Stearic acid (59 °C, 198 kJ/kg) was used as a PCM for this study. To enhance the effective thermal conductivity of the system, the radial distance between the tubes was kept at 3 to 4 cm. The shell was filled with 50 kg commercial grade stearic acid. Hot and cold water was used as a Heat Transfer Fluid for charging / discharging of the PCM. Ambient temperature, flow rate and PCM temperatures were measured simultaneously at an interval of 15 minutes. He concluded that the experimental results show the feasibility of using PCM as storage media in heat recovery systems.

Recently, Thirugnanam and Marimuthu (2013) have investigated experimentally the feasibility of using PCM in heat recovery system, in their study, a double pipe type heat exchanger was designed and fabricated for low temperature heat recovery system using paraffin wax as PCM. Two mass flow rates of 15lph and 20lph were used in the experiment. It is observed that the heat stored in 20lph is higher than 15lph.So when flow rate is increased the heat storing as well as heat releasing capacity increased. Their result shows the feasibility of using PCM in heat recovery system.

Niu et al (2019) carried out experimental investigations on thermal storage performance of a shell and tube unit with a metal-foam composite heat exchanger (Mtube) with pure paraffin (smooth tube) as the basis of comparison. The complete heat storage time of the Mtube unit was found to be 63.6% shorter than the smooth tube unit at the same flow rates. By comparing the temperature distribution of the two heat storage units, flow rate is found to have little effect on metal-foam-tube unit and relatively strong influence on the smooth-tube unit. The result also shows that compared to the smooth tube unit, the M-tube unit due to the expanded heat transfer area have improved heat transfer coefficient and weakened natural convection hence the bottom PCM in the M-tube unit melts faster.

Bayomy et al (2019) developed a three dimensional numerical model of a water based thermal storage thank using phase change material. A computational fluid dynamics CFD numerical code was developed for a domestic hot water tank using PCM to the demand of a family of one, two, three and four. It was observed that for a given hot water supply, increasing the number of families increases the efficiency from 35% for family of one to 82% for four families. Also, increasing the hot water supply during the charging periods increased the storage efficiency from 35% to 39%. It was observed that increase in family demands improve the thermal efficiency of the storage system due to the increase in the portion of energy recovered during the night time. Cabeza et al. (2002) reported that the PCM can be used for transporting temperature sensitive medications and food because of the PCM's capability to store heat and cold in arrange of several degrees. Several companies are engaged in the research of temperature sensitive transporting PCMs for various applications. Vasiliev et al. (2000) developed the latent heat storage module for motor vehicles so the heat is stored when the engine is stopped, and can be used to preheat the engine on a new start. It is possible to reach an optimized working temperature within the engine in a much shorter time using heat storage than without heat storage. Pal and Joshi (1996; 1997) recommended the PCM to restrict the maximum temperature of electronic components. Tan et al. (2004) conducted an experimental study on the cooling of mobile electronic devices, such as personal digital assistants (PDAs) and wearable computers, using a heat storage unit (HSU) filled with the phase change material (PCM) of n-eicosane inside the device. The high latent heat of n-eicosane in the HSU absorbs the heat dissipation from the chips and can maintain the chip temperature below the allowable service temperature of 50 °C for 2 h of transient operations of the PDA.

Sun and Wang (2016) conducted a research on heat transfer performance of passive solar collected-storage wall with PCMs. The energy saving characteristics was investigated theoretically and experimentally. The experimental result shows that ordinary room temperature is lower than the indoor temperature of the passive solar phase change room (PSPCR). They concluded that indoor can be improved by using passive solar collector wall system with PCMs to promote air thermal circulation and good heat storage capacity of PSPCR improves energy-saving characteristic for occupancy. A numerical study was conducted by Zhinuo Zhou et al. (2015) to explore the effectiveness of $NH_4(SO_4)_2.12H_2O$ as a new inorganic phase change material used for solar thermal energy storage in residential building in cold climate. The heat transfer pattern was studied both experimentally and simulation. The charging heat efficiency was optimized when the heat source temperature was 26.5C higher than the phase transition temperature. This helps satisfy the storage demand and also the utilization of solar thermal energy.

3.0 DISCUSSION

This paper presents a review of various applications of latent heat thermal energy storage systems. Based on the number of literatures reviewed, latent heat thermal energy storage have proved its potential to address the intermittent nature of solar energy and suitability in different applications such as space heating and cooling, heating and cooling of greenhouses and air conditioning among others. Most of phase change materials used for thermal energy storage have low thermal conductivity which causes incomplete melting and solidification of the PCM during operation. This negatively affects the performance of thermal storage systems and cause local accumulation of heat which might distort the thermal properties of the PCM and result to system failure. Efforts should therefore be focused on developing new PCMs with high thermal conductivity and methods of improving the thermal conductivity of available PCMs at affordable cost.

It is observed from this review that majority of developed thermal storage systems are evaluated based on energy efficiency without considering exergy efficiency. Exergy being a measure of quality of energy is more significant than energy in the analysis of thermal storage system and should therefore be considered. Exergy analysis takes into account the loss of availability of heat in storage operations and hence it more correctly reflects thermodynamic and economic value of the storage system.

Thermal energy storage will go a long mile in contributing to Nigeria energy security and energy sustainability. Over the years different researchers around the globe have committed time and resources and researches in the field have advanced to a higher level. Unfortunately, researchers in Nigeria have not given the deserved attention to this area which undermines their quest towards sustainable energy.

4.0 CONCLUSION

Based on the number of literature reviewed, it can be concluded that the usage of PCM integrated energy storage applications leads to improved performance, efficiency, and as well as the energy storage capacity of the total system. But the major drawback of the PCMs is low thermal conductivity. Performance improvement can be obtained through proper consideration of the material with high thermal conductivity, design with higher heat transfer areas and several parameters such as input temperature, dimensions, and flow rate. Use of pins, fins and avoiding edges corners in TES promotes melting and solidification rate.

REFERENCES

Agyenim F., Eames P., Smyth M. "Heat transfer enhancement in medium temperature thermal energy storage system using a multitube heat transfer array," Renewable Energy. 35 (2010) 198–207.

Bayomy A., Davies S., and Saghir Z. (2019) "Domestic hot water Tank utilizing phase change materials (PCMs): Numerical Approach" Energies 12(2019) 2170.

Buddhi, D. (1997). "Thermal performance of a shell and tube pcm storage heat exchanger for industrial waste heat recovery." *Proc ISES Solar World Congress*. Taejon, Korea. August 24–29

Canbazoglu S, Sahinaslan A, Ekmekyapar A, Aksoy YG, Akarsu F. "Enhancement of solar thermal energy storage performance using sodium thiosulfate pentahydrate of a conventional solar water-heating system." Energy Build 2005; 37: 235–42.

Castell A., Sole C, Medrano M., J Roca J., Cabeza L. F, Garcia D., "Natural convection heat transfer coefficients in phase change material(PCM) modules with external vertical fins, Applied thermal engineering." 28 (2008) 1676-1686.

Dinc'er I and Rosen M. A (2011)"THERMAL ENERGY STORAGE SYSTEMS AND APPLICATIONS, SECOND EDITION" A John Wiley and Sons, Ltd., Publication (2011).

Dan Sun, Lijiu Wang; Research on heat transfer performance of passive solarcollector-storage wall system with phase change materials, 2016, Dalian, 116024, China

E.M.Languri, C.O.Aigbotsua, J. L.Alvarado, Latent thermal energy storage system using phase change material in corrugated enclosures, Applied Thermal Engineering. 50 (2013) 1008-1014.

EL-Kaddadi L., Asbik M.(2017) "Experimental study of latent thermal energy storage by using phase change materials (PCM) enclosed in a vertical cylindrical annular space"13ème Congrès de Mécanique 11 - 14 Avril 2017

Gu, Z., Liu, H., Li, Y. (2004).Thermal energy recovery heat recovery system calculation and phase change material development. *Applied Thermal Engineering* 24: 2511–2426.

Hosseini M. J, Ranjbar A. A, Sedighi K, Rahimi M., "A combined experimental and computational study on the melting behavior of a medium temperature phase change storage material inside shell and tube heat exchanger," International Communications in Heat and Mass Transfer. 39 (2012) 1416–1424.

Jesumathy, S.P.; Udayakumar, M.; Suresh, S.; Jegadheeswaran, S. "An experimental study on heat transfer characteristics of paraffin wax in horizontal double pipe heat latent heat storage unit." J. Taiwan Inst. Chem. Eng. **2014**, 45, 1298–1306.

Koca A, Oztop HF, Koyun T, Varol Y. "Energy and exergy analysis of a latent heat storage system with phase change material for a solar collector." Renew Energy2008;33:567–74

Kurklu, A., O' Zmerzi, A., Bilgin, S. (2002). "Thermal performance of a water- phase change material solar collector."*Renewable Energy* 26: 391–399.

Lane GA, Glew DN, Clark EC, Rossow HE, Quigley SW, Drake SS, et al. 'Heat of fusion system for solar energy storage subsystems for the heating and cooling of building.' Chalottesville, Virginia, USA, 1975.

Niu Z, Yu J., Cui X., Yang X., Sun Y., and Yan J. (2019) "Experimental investigation on the thermal energy storage performance of shell and tube unit with composite phase change materials" Energy Procedia 158 (2019) 4889-4896

Pal, D., Joshi, Y. (1996). Application of phase change materials for passive thermal control of plastic quad flat packages: a computational study. *Numerical Heat Transfer Part A*30: 19–34.

Pal, D., Joshi, Y. (1997). Application of phase change materials to thermal control of electronic modules: a computation study. *Trans ASME* 119: 40–50.

Sharma S.D and Sagara K. (2005) "Latent Heat Storage Materials and Systems: A Review", International Journal of Green Energy, 2:1, 1-56

Simone A. (2015)"Modeling, design and analysis of innovative thermal energy storage systems using PCM for industrial processes, heat and power generation." PhD Thesis, University of Cagliari, Italy.

Tan, F.L., Tso, C.P. (2004). Cooling of mobile electronics devices using phase change materials. *Applied Thermal Engineering* 24: 159–169.

Telkes, M. (1978). "Trombe wall with phase change storage material." *Proceedingss of the 2nd national passive solar conference.* Philadelphia, PA, USA.

Thirugnanam.C, Marimuthu.P (2013) 'Experimental Analysis of Latent Heat Thermal Energy Storage using Paraffin Wax as Phase Change Material' International Journal of Engineering and Innovative Technology (IJEIT) Volume 3, Issue 2, August 2013.

Tatsidjodoung P., Le Pierres N, Luo L. (2013) "A review of potential materials for thermal energy storage in building applications" Renewable and Sustainable Energy Reviews 18 (2013) 327–349.

Oztu¨rk H. H "Experimental evaluation of energy and exergy efficiency of a seasonal latent heat storage system for greenhouse heating" Energy Conversion and Management 46 (2005) 1523–1542

V. Kapsalis, D. Karamanis;(2016) "Solar thermal energy storage and heat pumps with phase change." Applied thermal Engineering, 99 (2016) 1212-1224.

Ye W., Zhu D., Wang N., "Numerical simulation on phase-change thermal storage/release in a plate-fin unit," Applied Thermal Engineering. 31 (2011) 3871-3884.

Zhihua Zhou, ZhimingZhang, JianZuo, KeHuang, and LiyingZhang; Phase change materials for solar thermal energy storage in residential buildings in cold climate, 2015, Adelaide 5000, Australia

Proceedings of the 49th NSChE Annual Conference
KADA 2019: pp 355-372

P2B-03: PROSPECTS OF HIGH-TEMPERATURE SOLAR THERMAL (HTST) TECHNOLOGY DEPLOYMENT IN NIGERIA

S.N. Mumah*, O. Olaniyan, H.F. Akande, M.K. Yusuf, T.M. Garba, Usman Rumah and Francis Samuel
College of Engineering, Kaduna Polytechnic, Kaduna, Nigeria
***Corresponding author:** mumahsndoyi@kadunapolytechnic.edu.ng

ABSTRACT
The major aim of this paper is to stimulate discussion into an alternative form of energy for Nigeria - high-temperature solar thermal (HTST) energy source. The power supply situation in Nigeria is precarious, and while other countries are researching in alternative forms of energy, we must not be left behind. It has been established that economic growth is directly proportional to the growth in energy use. How we harness our energy sources indicates how serious we want the economy to grow. If we don't, we will be importing the technologies in the future. The paper firstly evaluates the energy production and consumptionpatterns in Nigeria and the need to shift focus to alternative forms of energy. Secondly, it examines high-temperature solar thermal (HTST) technology, with emphasis on the four main designs being considered: parabolic trough, parabolic dish, power tower, and linear Fresnel and the drawbacks of HTST technology. Thirdly, the need to include energy storageis explored, and finally, the limitations of HTST technology are outlined, and the barriers to implementation in Nigeria are discussed.

The paper concludes that HTST has many benefits and is a potential energy source for Nigeria. However, the high installation cost, a lack of right policies at both the federal and state government levels and the required incentives needed to bolster growthare obstacles identified to the deployment of this energy source. Advocacy, anincrease of the funding regime for renewable energy sources, especially high-temperaturesolar systems and coordinated research efforts on the utilization of HTST are recommended strategies to fast-track this technology in Nigeria.

Keywords: Energy production, High-TemperatureSolar thermal (HTST) Technology, Energy Storage

Introduction
The access to energy plays a crucial role in the economic growth of communities, which can contribute to poverty alleviation, provision of basic human services, and overall human well-being. Due to the worldwide population growth and industrialization, the demand for energy has been dramatically increasing. Renewable energy, which can be obtained from natural resources such as wind, solar, biomass and geothermal, has been encouraged by many countries due to the advantages of being sustainable and not contributing to the world's CO_2 greenhouse gas emissions.

Nigeria's estimated population is 180 million (2015 figures). This population is expected to rise to 260 million by 2030 (http://edition.cnn.com/2017/06/25/africa/africa-population-growth-un/index.html). This large and rapidly growing population demands greater energy consumption each year.However, Nigeria's economic expansion is held back by the continual under-performance of the country's energy sector. According to the Oil and Gas Journal (OGJ), Nigeria

had an estimated 37 billion barrels of proved oil reserves by the end of 2015—the second-largest amount in Africa after Libya and holds the largest natural gas reserves on the continent (http://www.marcon.com/library/country_briefs/Nigeria/nigeria.pdf). Nigeria is the largest oil producer in Africa and is the world's fourth-largest exporter of liquefied natural gas (LNG) in 2015 (*2016 World JNG Report, www.igu.org/sites/default/.../IGU-World%20LNG%20Report-2015%20Edition.pdf*). Nigeria became a member of the Organization of the Petroleum Exporting Countries (OPEC) in 1971, more than a decade after oil production began in the oil-rich Bayelsa State in the 1950s. Although Nigeria is the leading oil producer in Africa, production is affected by sporadic supply disruptions, which have resulted in unplanned outages of up to 500,000 barrels per day (b/d) http://www.marcon.com/library/country_briefs/Nigeria/nigeria.pdf).

Nigeria's oil and natural gas resources are still the mainstay of the country's economy though diversification to other areas such as agriculture is now being pursued aggressively.This therefore means thatthe Nigerian economy is greatly affected by variation in crude prices.The IMF reported that Nigeria's oil and natural gas exports earned $52 billion in 2015, $35 billion less than in 2014, which is mostly attributed to the fall in oil prices (http://www.offshoreenergytoday.com/report-shell-evacuates-workers-in-nigeria-after-security-threat/). This decline in revenue has continued unabated through 2015, 2016 and presently. Figure 1 shows Nigeria Petroleum and other liquids production and consumption.

Nigeria's oil and natural gas industry is primarily located in the southern Niger Delta area, where it has been a source of conflict. Prospecting in the north-east has been hampered by Boko Haram insurgency. Furthermore, aging infrastructure and poor maintenance have also resulted in dwindling production and oil spills. Natural gas flaring has continued unabated contributing adversely to serious pollution challenges in the south-south. This has been further compounded by protests from environmental groups and locals over damages to the environment resulting from oil. This has led to pollution to water and land resulting in lack of portable drinking water, degraded land which is no more suitable for agriculture and decrease in fish stocks. The resultant effecthas been a further decrease in oil and gas revenues accruing to the nation and poverty increase.

Energy Consumption in Nigeria

For Nigeria to sustain the high growth in population, the country would require a substantial increase and improvement of its current energy situation to meet forecasted demand. Presently, Nigeria cannot meet its energy needs. This is due principally to inadequate infrastructure in the sector, lack of proper planning and poor policy implementation and very low investment in the Energy sector.

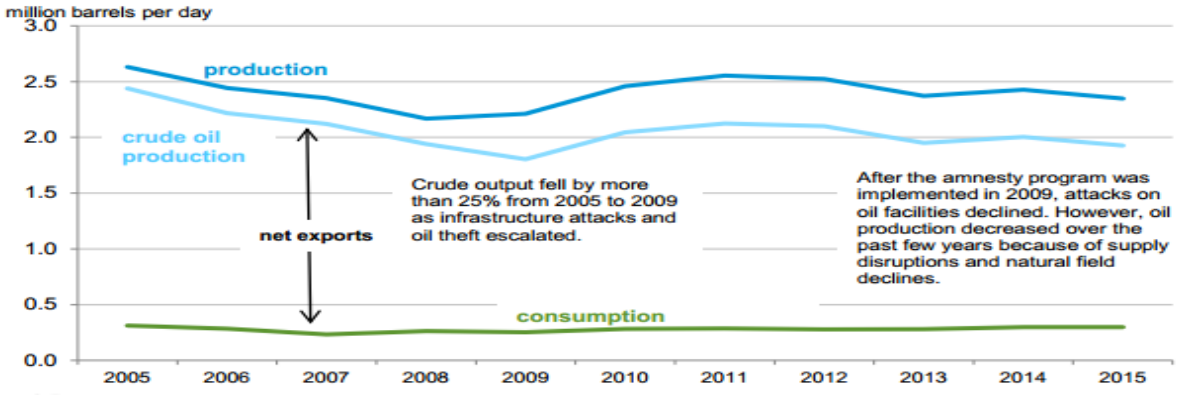

Figure 1. Petroleum and other liquids production and consumption in Nigeria
Source: U.S. Energy Information Administration

The U.S. Energy Information Administration (EIA) estimated that in 2013 total primary energy consumption in Nigeria was about 4.8 quadrillion British thermal units (Figure 2) (Country Analysis Brief: Nigeria - Marcon International, Inc.www.marcon.com/library/country_briefs/Nigeria/nigeria.pdf). Of this amount, traditional biomass and waste (typically consisting of wood, charcoal, manure, and crop residues) accounted for 74%. This high share represents the use of biomass to meet off-grid heating and cooking needs, mainly in rural areas. It's important to note that estimates of traditional biomass consumption are imprecise because biomass sources are not typically traded in easily observable commercial markets. The electrification rate in Nigeria is estimated at 45%—leaving approximately 93 million people in Nigeria without access to electricity (www.informationng.com/.../93-million-people-lack-access-to-electricity-in-nigeria.html).

The International Energy Agency estimates that 115 million people in Nigeria rely on traditional biomass and waste as their main sources of energy.Seasonal variations lead to theintermittent supply of water needed to power dams for hydroelectricity. Also, constant disruption of natural gas flow to power stations affects energy output. This has led to the rise of alternative power generation through the use of diesel and petrol generators.

Nigeria's electricity sector is relatively small. Brazil and Pakistan, two countries with similar population sizes, generate 24 times and 5 times more power than Nigeria, respectively. (https://amebosayso.wordpress.com/2013/06/12/us-energy-information-administration-nigeria-analysis-2012/). EIA estimates show that Nigeria's net generation was 18.8 billion kilowatt-hours (KWh) in 2009.9 The graph below clearly illustrates the abysmal population to power ratio in Nigeria (5GW to 170 million people) (geni.org/globalenergy/research/...nigeria/100-percent-renewable-energy-Nigeria.pdf). Even when compared with other countries in Africa, Nigeria has not fared better. Figure 3shows the country population to power generation ratio for selected African countries.

The installed power capacity has remained relatively flat over the last decade 10,396.0 MW, although net energy generation has slightly decreased from its peak of 23 billion kWh in 2004, mainly due to a decline in hydroelectric power. The majority of electricity generation in Nigeria comes from thermal power plants (79%) (Charles, 2014), with about two-thirds of thermal power being derived from natural gas and the rest from oil. Hydroelectricity (21%), the only other source

of power generation, has decreased from its peak of 8.2 billion kWh in 2009, slightly less than generation, Most of the remainder of the remainder of the hydroelectricity is being exported to Niger through an agreement under the West African Power Pool IEA data for 2009 indicates that the electrification rate for Nigeria was 50 percent for the country as a whole – leaving approximately 80 million people without access to electricity in Nigeria (Charles, 2014); geni.org/globalenergy/research/...nigeria/100-percent-renewable-energy-Nigeria.pdf). Other estimates place the countrywide electrification rate as low as 45 percent.

Nigeria has however set ambitious goals to increase generation capacity. Nigeria plans to increase generation from fossil-fuel sources to more than 20,000 MW by 2020 and to increase hydroelectricity generation capacity to 5,690 MW by 2020, almost tripling the capacity from the 2012 level. This includes upgrading current hydroelectricity plants and constructing new plants: Gurara II (360 MW), Zungeru (700 MW), and Mambilla (3,050 MW). In late 2013, the Nigerian government announced a $1.3 billion deal with China to build the 700 MW Zungeru hydropower project. The Export-Import Bank of China will finance 75% of the cost, and the Nigerian government will finance the remaining amount. The project was initially scheduled to be completed in 2017, but that date has been pushed back because legal challenges that have delayed construction work (http://www.marcon.com/library/country_briefs/Nigeria/nigeria.pdf).

In Nigeria, more than 70% of the population are rural dwellers. Since the energy production level of any community dictates her pace of development, it is possible to alleviate thepoverty of the large community of Nigerians by providing alternative renewable energy (solar) for them.

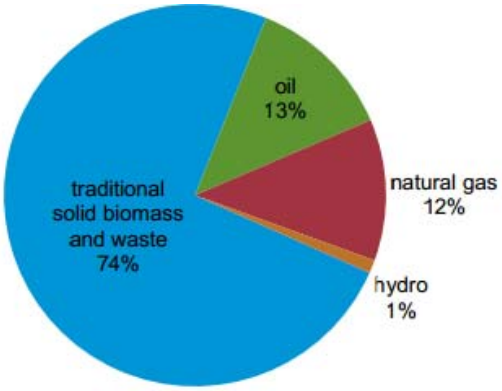

Figure 2. Nigeria's total primary energy consumption, 2013
(Source: U.S. Energy Information Administration, International Energy Agency)

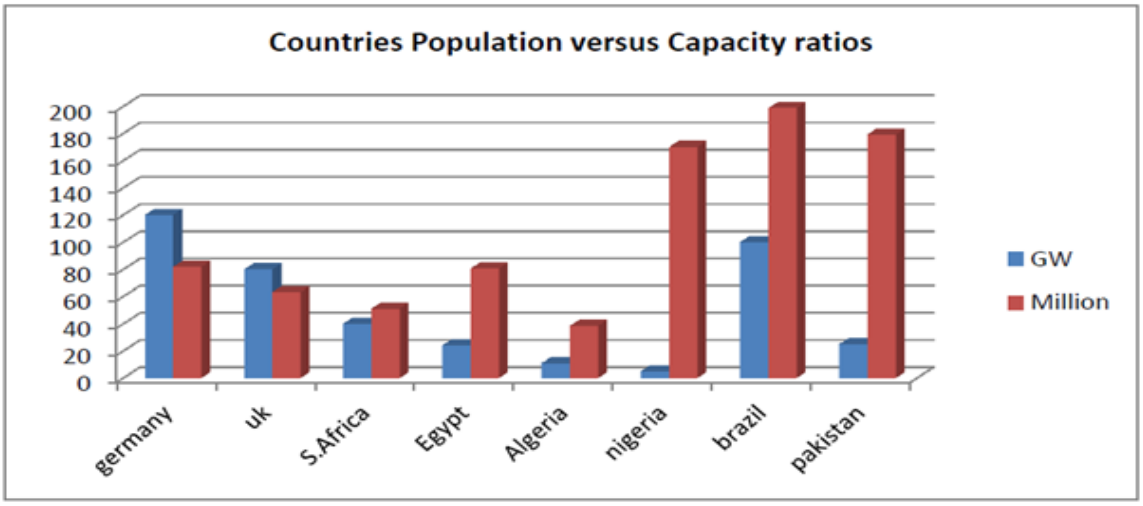

Figure 3: Countries Population to Generation Capacity Ratios (http://geni.org/globalenergy/research/renewable-energy-potential-of-nigeria/100-percent-renewable-energy-Nigeria.pdf)

Solar Energy Utilization Challenges

Nigeria is strategically located within a high sunshine belt with a fairly evenly distributed solar radiation across the country (Figures 4 and 5). The annual average of total solar radiation varies from about 12.6 MJ/m2/day (3.5 kWh/m2-day) in the coastal latitudes to about 25.2 MJ/m2-day (7.0 kWh/m2-day) in the far north. Thus, over a whole year, an average of 6,372,613 PJ/year (≈1,770 thousand TWh/year) of solar energy falls on the entire land area of Nigeria. This is about 120 thousand times the total electrical energy generated by the National Electric Power Authority for the whole country for the year 2002. This then is an estimated potential solar thermal energy resource base(Renewable Electricity Action Program (REAP), December 2006, iceednigeria.org/backup/workspace/uploads/dec.-2006-2.pdf)

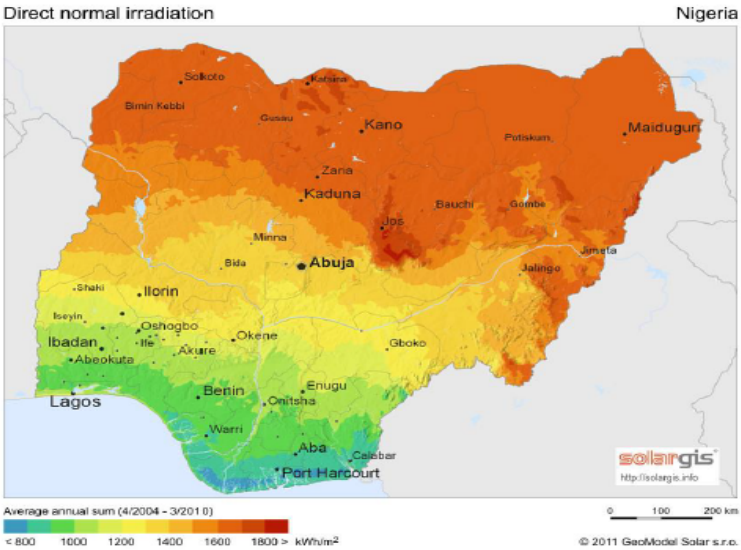

Figure 4: Nigeria's Average Solar Radiation Map (http://solargis.com/products/maps-and-gis-data/free/download/nigeria)

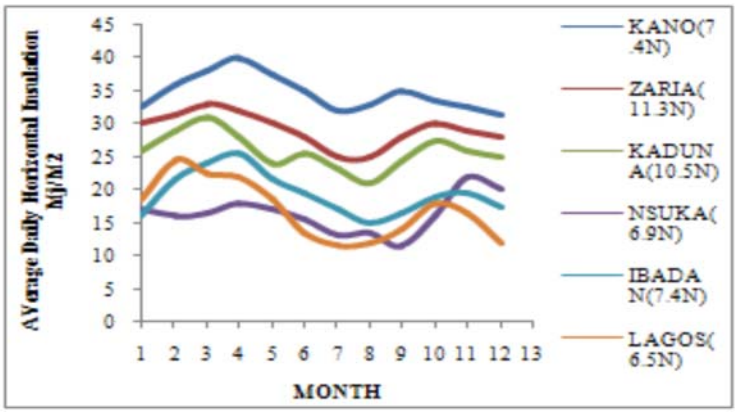

Figure 5: Average daily Horizontal Radiation
(http://geni.org/globalenergy/research/renewable-energy-potential-of-nigeria/100-percent-renewable-energy-Nigeria.pdf)

The use of solar Energy is growing fast, and despite its huge potential, many are still skeptical about its prospects as a viable energy source. The principal reasons are cost and its intermittent nature. Nigeria stands to gain tremendously if solar energy use is pursued as an alternative energy source to petroleum and gas. The reasons are obvious; Nigeria location and its large land area. Also, the use of solar energy helps to reduce the greenhouse gases that are a major cause of climate change though it is usually considered that its use does not significantly reduce greenhouse gases emission.

The sun is the most readily and widely available renewable energy source capable of meeting the energy needs of thewhole world. One of the greatest assets that Nigeria has that can facilitate solar energy generation in Nigeria is her geographical location, that is, the equatorial region which is full of alarge quantity of solar radiation. Solar radiation is fairly well distributed in Nigeria with average solar radiation of about 19.8 MJm–2 day-1 and average sunshine hours of 6 hours a day; ranging between about 3.5 hrs at the coastal areas and 9.0 hrs at the far northern boundary.(http://sweetcrudereports.com/2012/12/25/solar-energy-for-sustainable-power-supply-in-nigeria/). Nigeria lies within a high sunshine belt and thus has enormous solar energy potentials. If solar collectors or modules were used to cover 1% of Nigeria's land area, it would be possible to generate 1850 ×103 GWh of solar electricity per year; this is over one hundred times the current grid electricity consumption level in the country.35 Generally, the solar capacity for Nigeria ranges between 3.5kW/m/day – 7.0kW/m/dayand average sunshine daily of 4 – 7 hours(http://www.careerhubafrica.com/blog/solar-energy-a-substitute-for-gas-in-power-generation/)

Challenges Confronting Solar Installation in Nigeria

1. Affordability
According to a Fitch Report (https://www.ripplesnigeria.com/nigerias-poverty-level-index-hits-72-2016-fitch-reports), the level of poverty (productivity index) in Nigeria has maintained a constant rise, reaching its all-time high of 72 percent by August 2016.The report stated that the productivity scale, used in assessing the GDP and other developing indexes of countries, was said to have maintained a constant decline in the past five years in most countries under reference, with Nigeria recording its worst, jumping from 60 percent in 2015 to 72 per cent in the second

quarter of 2016. With a poverty level this high, it is quite evident why installation of solar energy devices is very low in the country.

2. Lack of Awareness

Government investment in the energy sector has concentrated on fossil fuels and hydropower. Investments in solar powered systems are still very low as policies needed to fast-track diversification into other energy sectors are either lacking or not implemented. To appreciate the capacity of solar energy to solve the energy challenges in Nigeria, there is need to expose policy makers to the full potential of this energy source. Presently in Nigeria, solar Energy has been reducing as anenergy source for street lighting and powering small homes through inverter and PV system. However, in countries that have lower solar energy penetration that Nigeria, solar energy is now used to power cities. The USA and Spain have made tremendous advances in solar energy utilization for electricity power production as is presented later. Creating awareness on the use of solar energy at high-temperature level is therefore not only essential but important to Nigeria development. The energy availability situation in Nigeria is a serious factor contributing negatively to the country very low development index. Expansion into solar energy is not only an option but a necessity. Educating both policy makers and thepopulace on the need for research, development, and utilization of solar energy systems is therefore very crucial as awareness will make the development and implementation of energy policies much easier. As state in the 2016 National Human Development Report for Nigeria,a fundamentalprecondition for sustainable development is theempowerment of people, referring to their education. By educating them, the key barrier to human development – human mind – can be surpassed.

3. Low-Performance System

The use of fossil energy sources seems seamless and without complication, while the use of solar energy seems complicated and not guaranteed. One seems to forget the amount of research that has gone into fossil fuel utilization over the last two centuries to take us this far. As with any new system being introduced, there are always challenges. We must decide to continue to research on how to solve thesechallenges, or we remain with fossil fuels which are expected to run out someday

4. Cost of generation

Couple to low efficiency is generally the cost of generation. Installing High-temperature solar systems are very costly.This isparticularlyso if many components cannot be purchased locally or off the shelf and has to be fabricated to specification when needed. Solar energy systems have alongbreak-even period. However, the lifespan is considerable longer after this couple with the low maintenance cost. For example, typical PV systems have an average fouryears period to breakeven. The main challenge, therefore, is securing the initial investment for purchasing and installing solar systems. With a high poverty index, it is not had to see why solar systems are not very popular in the country.

5. Political Will

Energy policies are generallyspelt out in plans. A review of the renewable energy policies of the countryreveals poorly draft policies on solar energy utilization. Unrealistic energy policies only mean one thing, poor or none implementation. This is compounded in Nigeria by non-continuity in policy implementation as regime changes. It is not difficult to see why despite the advantage of Nigeria's geographical position, she cannot boost of any solar plant.

6. Low Research Effort in Solar Energy development and Utilization

Many of the energy research centres in the country concentrate on low-temperature solar energy utilization. For meaningful progress to be made in this sector, there is need to upgrade our research effort to medium and high-temperature solar energy utilization. It is only at this level electric energy can be produced to meet national grid demands. Low temperature and PV solar systems are well known and can only contribute to areas like streets lighting, borehole powering and individual household electricity power provision. However serious and cutting-edge research does not come cheap, and government public sector must be ready to invest into solar energy development utilization research.

High-Temperature Solar Systems

Many people associate solar electricity generation directly with photovoltaics and not with solar thermal power. Large, commercial, concentrating solar thermal power plants have been generating electricity at reasonable costs for more than 15 years.The easy integration of thermal energy storage (TES) makes concentrating solar power (CSP) dispatchable and unique among all other renewable energy generating alternatives. CSP technologies generate electricity by concentrating the solar radiation beam onto a small area, where a heat transfer fluid(HTF) is heated up, and this energy is ultimately transferred to the steam.

Solar thermal technologies are categorized as low-temperature, medium-temperature, or high-temperature. High-temperature solar thermal (HTST), also known as concentrating solar thermal (CST), is used for electrical power generation. HTST power plants are a lot like traditional fossil fuel power plants, but the important difference is that they obtain their energy input from the sun, instead of from fossil fuels. HTST systems have two main components: the collector/concentrator, and the receiver/absorber. The collector is a mirror with the function of collecting solar energy and concentrating this energy (by reflection) toward a centralized receiver, which contains a working fluid that absorbs the concentrated solar energy.

HTST has advantages over some other renewable energy options (http://www.solarthermalworld.org/sites/gstec/files/HTSolar%20thermal%20roadmap.pdf).
These include:

a. It can integrate well with conventional thermodynamic cycles and power generation equipment as well as complementary renewable technologies such as geothermal energy.
b. It offers dispatchable power when integrated with thermal storage and/or gas co-firing, and thus good matching between solar insolation and the growth in electrical demand in many countries that is driven by air conditioning loads during summer.
c. The collector technology itself is constructed of predominantly conventional materials (glass, steel, concrete) — no scientific breakthroughs are required for the cost to continue to drop as the volume of megawatts deployed increases.

High-temperature solar thermal systemsare those collectors that work at temperatures above 500 ° C. They are used for electric power generation.
The technologies used in high-temperature solar thermal energy are:

a. Parabolic trough solar collectors
b. Central tower
c. Parabolic dishes or parabolic reflector
d. Linear Fresnel concentrators

Parabolic trough solar collectors

Parabolic trough solar collectors concentrate sunlight using parabolic mirrors in an absorber pipe which passes through the axis of the parabola. Within this absorbing pipe a fluid is heated and can reach temperatures as high as 450 º C.

Depending on the application and the temperature at which you want to achieve a type of fluid, or another is used. To a maximum temperature of 200 ° C can be used demineralized water or ethylene glycol as working fluids and for higher temperatures of up to 450 º, C synthetic oils are used.

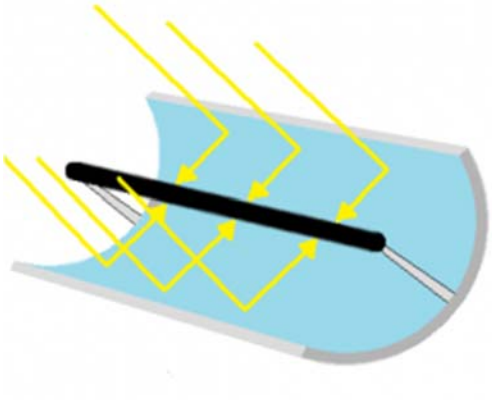

Figure 4: Parabolic trough solar collectors

This type of getter concentration should be modifying their position adapting to the sun's position by rotating around the axis parallel to its focal line to take advantage of direct sunlight position.

Solar power tower

Tower systems or central receiver tower consist of a field of heliostats (movable mirrors over two axles). The heliostats capture and concentrate the direct sunlight onto a receiver, installed on the top of a central tower. Operation of the plant is simple. The central solar receiver generates high-temperature steam. The steam generated is then used to drive a turbine that produces electricity.

Parabolic dish reflector

The parabolic dishes are systems that concentrate solar energy in a point where the solar receiver is located and a Stirling engine or a microturbine that is coupledto an alternator. The fluid located in the receiver is heated to temperatures above 750 ° C thereby obtaining heat energy. This heat energy generated is used by the Stirling engine or the microturbine to produce electricity.

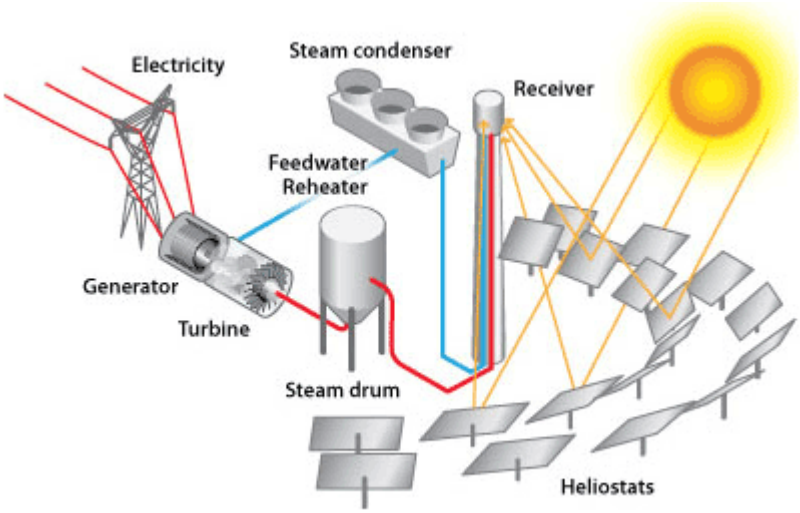

Figure 5: A power tower power plant (https://energy.gov/eere/energybasics/articles/power-tower-system-concentrating-solar-power-basics)

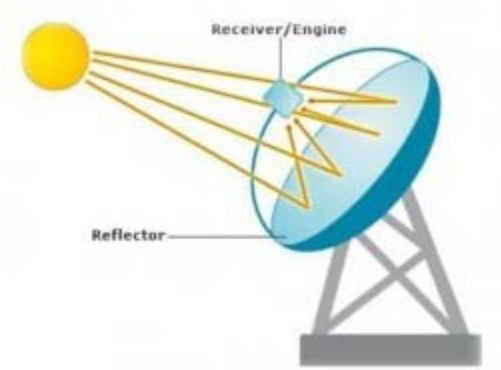

Figure6:Parabolic Dish Reflector(http://www.alternative-energy-tutorials.com / solar-hot-water/solar-dish-collector.html)

A Stirling engine is a thermal engine, which means that the energy contribution can be realized through concentrated solar energy. An alternator coupled to a Stirling engine approaches the movement generated by the engine to produce electricity. The electricity generated can be connected to the grid for sale or in most cases can be used for direct consumption.This technology is still experimental and is still less profitable than atower or parabolic mirrors.

Linear Fresnel concentrators

The reflectors lead normal flat mirrors and simulate the curvature of the parabolic mirrors (more expensive) varying the angle of each row with a single axis tracking.The main advantage of linear Fresnel concentrators system is its simple installation and low cost although the yield is less than the parabolic trough solar collectors.

Solar Energy Storage Systems

Most techniques for generating electricity from heat need high temperatures to achieve reasonable efficiencies. The output temperatures of non-concentrating solar collectors are limited to temperatures below 200°C. Therefore, concentrating systems must be used to produce higher temperatures. Due to their high costs, lenses and burning glasses are not usually used for large-scale power plants, and more cost-effective alternatives are used, including reflecting concentrators.

In contrast to photovoltaic systems, solar thermal power plants can guarantee capacity (see Figure 8). During periods of bad weather or the night, a parallel, fossil fuel burner can produce steam; this parallel burner can also be fired by climate-compatible fuels such as biomass, or hydrogen produced by renewables. With thermal storage, the solar thermal power plant can also generate electricity even if there is no solar energy available.

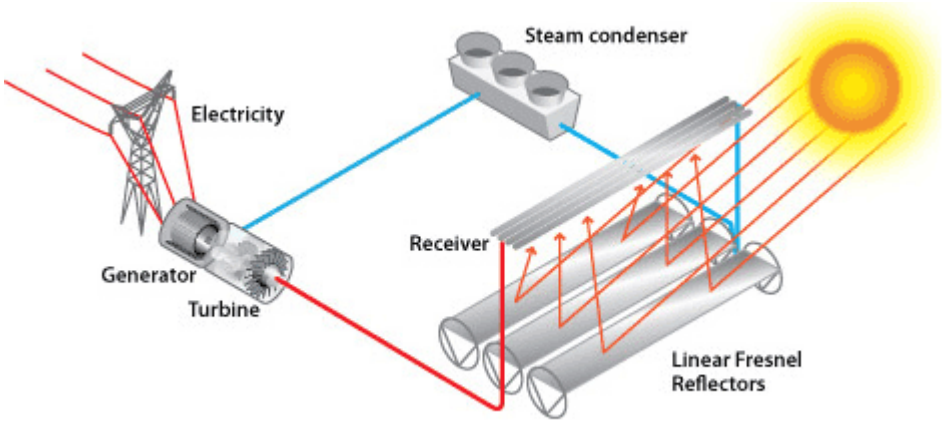

Figure 7: A linear Fresnel reflector power plant

Source:https://energy.gov/eere/energybasics/articles/linear-concentrator-system-basics-concentrating-solar-power).

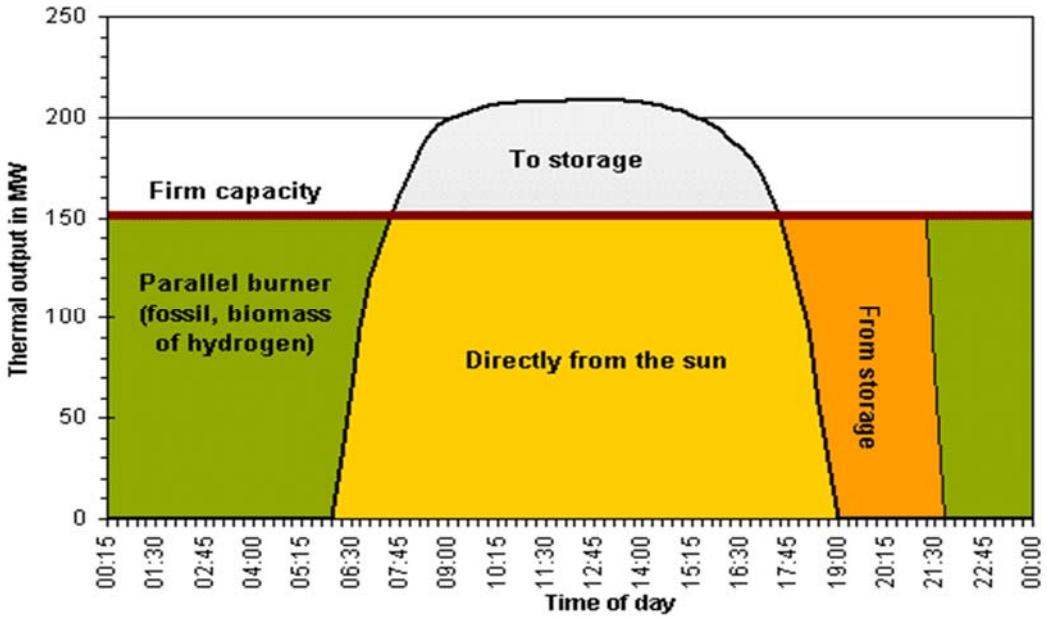

Figure8: Typical output of a solar thermal power plant with two-hour thermal storage and backup heater to guarantee capacity (https://www.volker-quaschning.de/articles/fundamentals2/index_e.php**)**

A proven form of storage system operates with two tanks. The storage medium for high-temperature heat storage is molten salt. The excess heat of the solar collector field heats up the molten salt, which is pumped from the cold to the hot tank. If the solar collector field cannot produce enough heat to drive the turbine, the molten salt is pumped back from the hot to the cold tank and heats up the heat transfer fluid. Figure 9 shows the principle of the parabolic trough power plant with thermal storage. Potential storage media for HTST are presented in Table 1.

Commercial Status of HTST

The USA and Spain are world leaders in HTST deployment. HTST faces strong competition with fossil fuel and wind power. So far, government incentives have been inadequate. If Nigeria is to take advantage of its abundant solar resources, new national and state energy policies must be introduced. Such policies would include a national target for installed HTST capacity and a feed-in tariff for HTST power.

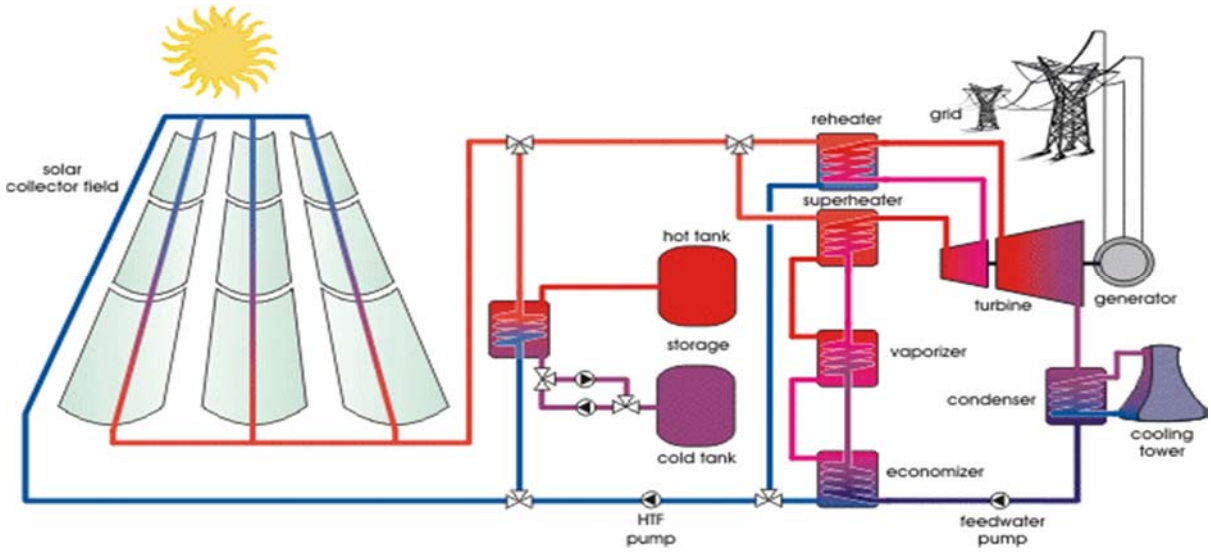

Figure 9: Schematic of a concentrated solar thermal trough power plant with thermal storage (https://www.volker-quaschning.de/articles/fundamentals2/index_e.php)

One of the main barriers to wider adoption of HTST technology is the high cost of solar-generated electricity. At its current level of development, HTST generates electricity at a higher cost than some existing renewable energy technologies. The Concentrating Solar Power generating cost is expected to reduce by 50–60% through technical improvement and scaling up and volume production (https://www.irena.org/DocumentDownloads /Publications/RE_Technologies_Cost_Analysis-CSP.pdf). For this happen considerable research effort has to be continuously funded by various countries including Nigeria to make CSP more cost-effective.Table 2 shows thecurrentlist of solar thermal power plants around the world. This list is expanding fast as another tap in into the potentials of HSTS.

Challenges in Setting up HTST Systems

HTST requires large areas of cleared flat land and can cause significant environmental damage if inappropriately sited. Best-practice would prescribe that HTST installations be located away from fragile ecosystems, and preferably on already degraded land. Water use is another issue that must be considered, particularly in desert / dry locations. The potential environmental and aesthetic impacts of HTST are generally more than offset by the benefits, which include significant reductions in greenhouse gas emissions and other air pollutants, and increased energy security. Consequently, HTST has a high level of public acceptance.

The cost of HTST is projected to decrease significantly over the next 10 to 15 years due to production volume increases, plant size scale up, and technological advance. HTST projects are labor intensive and thus could be especially beneficial during times of higher unemployment, such as now.

Table 1: Melting Point and heat capacities of Salt Mixtures for HTST Systems

S/N	System	Temperature °C		Cp, J/g.°C at 600 °C
		Cal	Experimental	
1	LiF-K_2CO_3	456	482	1.85
2	LiF-Li_2CO_3	612	608	1.88
3	NaF-Na_2CO_3	694	690	1.78
4	Li_2CO_3-K_2CO_3	503	503	2.03
5	Li_2CO_3- Na_2CO_3-K_2CO_3	397	398	1.70
6	LiF-Na_2CO_3-K_2CO_3	386	389	1.74
7	LiF-NaF- K_2CO_3	414	422	1.81
8	LiF-KF- K_2CO_3	412	438	
9	LiF-NaF-Na_2CO_3- K_2CO_3	373	423	1.85
10	LiF-NaF-Li_2CO_3-Na_2CO_3	444	444	1.88
11	NaCl-KCl-$MgCl_2$ (24-21-55)		393	1.0
12	LiF-BeF_2(66-34)		457	2.38
13	LiF-NaF-KF(46.5-11.5-42)		454	1.88
14	LiF-NaF-BeF_2(31-31-38)		326	2.20
15	NaF-$NaBF_4$(8-92**)**		384	1.506
16	KF-ZrF_4(58-42)		390	1.00
17	KCl-$MgCl_2$**(68-42)**		435	1.16
18	$NaNO_3$-KNO_3**(Solar Salt) (66-34)**		222	(1396.044+0.172T)/1000.0
	$NaNO_3$-$NaNO_2$-KNO_3(Hitec®)(7-49-44)			

Source: https://energy.gov/sites/prod/files/2014/01/f7/csp_review_meeting_042413_reddy.pdf, https://arxiv.org/pdf/1307.7343.pdf

Table 2: Current List of Solar Thermal Power Plants

S/N	Name	Design Capacity (MWe)	Country	State
1	HassiR'mel integrated solar CC Power Plant	25	Algeria	Laghouat
2	Shiraz Solar Power Plant	0.25	Islamic Republic of Iran	Fars
3	Noor OuarzazateCSP Power Station (OSPS)	160	Morocco	Meknes-Tafilalet
4	Andasol I Solar Power Plant	50	Spain	Andalusia
5	PS10 Solar Power Plant	11	Spain	Andalusia
6	PS20 CSP Power Plant	20	Spain	Andalusia
7	Andasol II Solar Power Plant	50	Spain	Andalusia
8	Andasol III Solar Power Plant	50	Spain	Andalusia
10	Solnova CSP Power Plant	150	Spain	Andalusia
11	Valle 1 and 2 CSP Power Plant	100	Spain	Andalusia
12	Gemasolar CSP Power Plant	19.9	Spain	Andalusia
13	Lebrija 1 CSP Power Plant	50	Spain	Andalusia
14	Palma del Rio CSP Power Plant	100	Spain	Andalusia
15	Helioenergy 1 and 2 CSP Power Plant	100	Spain	Andalusia
16	Solacor I and II CSP Power Plant	100	Spain	Andalusia
17	MorÃ³n CSP Power Plant	50	Spain	Andalusia
18	Soluz Guzman CSP Power Plant	50	Spain	Andalusia
19	La Africana CSP Power Plant	50	Spain	Andalusia
20	Manchasol-1 and 2 CSP Power Plant	100	Spain	Castile-La Mancha
21	Helios I and II CSP Power Plant	100	Spain	Castile-La Mancha
22	Puertollano CSP Power Plant	50	Spain	Castile-La Mancha
23	Aste 1A 1B CSP Power Plant	100	Spain	Castile-La Mancha
24	Borges Termosolar Power Plant	25	Spain	Catalonia
25	Alvarado (La Risca) CSP Power Plant	50	Spain	Extremadura
26	Extresol CSP Power Plant	150	Spain	Extremadura
27	Olivenza 1 CSP Power Plant	50	Spain	Extremadura
28	Majadas CSP Power Plant	50	Spain	Extremadura
29	Solaben CSP Power Plant	200	Spain	Extremadura
30	Orellana CSP Power Plant	50	Spain	Extremadura
31	Termosol I and II CSP Power Plant	100	Spain	Extremadura
32	La Florida (Semcasol 1) CSP Power Plant	50	Spain	Extremadura
33	La Dehesa CSP Power Plant	50	Spain	Extremadura
34	Astexol II CSP Power Plant	50	Spain	Extremadura
35	Casablanca CSP Power Plant	50	Spain	Extremadura
36	Puerto Errado 1 Thermosolar Power Plant	1.4	Spain	Murcia

37	Puerto Errado 2 Thermosolar Power Plant	30	Spain	Murcia
38	EnerstarVillena CSP Power Plant	50	Spain	Valencia
39	Shams-1 CSP Power Plant	100	UAE	Abu Dhabi
40	Solana CSP Power Plant AR	280	USA	Arizona
41	SEGS I (Daggett) Solar Power Station	13.8	USA	California
42	SEGS II (Daggett) Solar Power Station	30	USA	California
43	SEGS III (Kramer Junction) Solar PP	33	USA	California
44	SEGS IV (Kramer Junction) Solar Power Plant	33	USA	California
45	SEGS IX (Harper Lake) Solar Power Plant	80	USA	California
46	SEGS V (Kramer Junction) Solar Power Plant	33	USA	California
47	SEGS VI (Kramer Junction) Solar Power Plan	33	USA	California
48	SEGS VII (Kramer Junction) Solar Power Plant	33	USA	California
49	SEGS VIII (Harper Lake) Solar Power Plant	80	USA	California
50	Ivanpah SEGS Power Plant	392	USA	California
51	Mojave CSP power Plant CA	280	USA	California
52	Martin Next Generation Solar Energy Center	75	USA	Florida
53	Nevada Solar One Power Plant	64	USA	Nevada
54	ISCC Kuraymat (ISCC Kuraymat)	20	Egypt	Kuraymat

4.2.1 Source: https://en.wikipedia.org/wiki/List_of_solar_thermal_power_stations

4.2.2 http://thermal-powerplant.blogspot.com.ng/2010/06/list-of-solar-thermal-power-plants.html,
https://www.solarpowerauthority.com/high-temperature-solar-thermal/

Recommendations

It is estimated that a large-scale market should be available to HTST technologies by 2030 (and possibly muchearlier) provided that HTST continues to reduce its cost of generation, which is likely in a global sense given the rapid growth in announced commercial projects overseas. The best prospects forcost reductions are in thesolar field and thermal storage sub-systems, which make up a large component of capital costs. Increasing plant size may also reduce operating costs through economies of scale. It is also clear that in many market contexts,development of cost-effective thermal storage or siting HTST plants near gas pipelines to utilise gas as a co-firing fuel is crucial for the long-term prospects for this technology.

There is a range of solar concentrator (linear Fresnel reflector, parabolic trough, power tower and parabolic dish), thermal receiver/heat transfer fluid (hot oil, molten salts, direct steam), heat storage and power generation (steam turbine, Stirling engine) technologies that are Proceedings through innovation and/or commercialisation pathways. There is no clear-cut 'winner' today in HTST system configurations — and it will take many years and multiple commercial-scale projects for lowest cost configurations to be identified.

Indeed it is possible that most, if not all, HTST concentrator approaches will prove to provideeconomical solutions for zero or low emission electricity generation. It therefore is prudent, within a sensible strategic approach, for industry and governments to continue to

support promising HTST system and component technologies through their innovation and commercialisation paths and processes.

Large sums of money have been, and continue to be, invested overseas in HTST-related RDandD and again now in commercial deployment of utility-scale systems. To date,Nigeria has not invested comparably to investigate the opportunities that HTST may offer for a clean energy future. Nigeria does not have locally-developed and innovative HTST technologies or a strong RandD reputation in the field.This strongly suggests that a policy regime is required in Nigeria that will promote industry investment in local deployment of commercial HTST technologies and associated supply-chain infrastructure/capability.Large-scale demonstration of less-mature HTST technologies; and ongoing RandD of next-generation HTST technologies at the system and key sub-system/component levels to reduce cost and expand market options. Achieving this will require the development of a favourable policy framework for clean energy in Nigeria, knowledge building in consumers, utilities, financiers, industry, regulators, and governments about HTST. Also market development efforts to promote the sector and to remove barriers to deployment, development of Nigerian supply-chains for viable near-term applications and large-scale demonstration programs; and training and competence building in human resources and technology capability and capacity are other major requirements. Investing in these activities will enable Nigerian governments, industry, researchers and the broader community to position Nigerian industry and technologies in the strongly-growing, global HTST sector and to exploit HTST as a key component of Nigeria's energy future.

While acknowledging the importance of building on and extending the RandD capability and capacity in Nigeria for HTST and related areas (particularly manufacturing RandD to reduce key component production costs), stakeholders' top five priorities focused primarily on market and supply-chain development activities, as follows:

1. Large-scale demonstrations will pull and underpin: RandD; technology, industry and policy development; removal of implementation barriers; and overseas interest in Nigeria as a market.
2. Capacity and capability building, particularly in manufacturing and engineering areas relevant to HTST systems and components.
3. Establishment of an advocacy group to be a champion for HTST in Nigeria.
4. The establishment now of long-term public policy that both pulls and pushes progress in Nigeria in HTST, particularly market-support mechanisms and removal of specific or inadvertent barriers to market entry for HTST.
5. Exploit viable near-term markets, which will enable (in conjunction with large-scale demonstrations) establishment of sustainable supply chains in Nigeria for HTST system design, implementation, and operation.

Conclusion

The major aim of this paper is to stimulate discussion into an alternative form of energy for Nigeria. The power supply situation in Nigeria is precarious,and while other countries are researching on alternative forms of energy, we must not be left behind.It has been established that economic growth is directly proportional to the growth in energy use. How we harness our energy sources indicates how serious we want the economy to grow. If we do not, we will be importing the technologies in the future.

Presently, theparabolic trough has a greater market share than other high temperature solar thermal collectors. It is envisaged that parabolic dishes will dominate the high temperature solar thermal scene in the future if thecost can be drastically reduced. However, power tower and linear Fresnel systems are also finding increasing use. Despite its high efficiency, the cost of parabolic dishes has proved to be a serious drawback. The introduction of storage systems in HTST installations has greatly enhancedits acceptability as an independent power system.

The drawbacks for HTST are the large areas of cleared flat land required, the amount of water required and the impact on the environment if not properly sited. However, Nigeria has so much unused and degraded lands that are far from our fragile ecosystems and so best suited for HSTS installations. The potential environmental and aesthetic impacts of HTST are generally more than offset by the benefits, which include significant reductions in greenhouse gas emissions and other air pollutants, and increased energy security. Consequently, HTST will a high level of public acceptance, especially when compared to installation of nuclear power stations has already been mooted, and many regions in the country have kick again its construction (https://www.solarpowerauthority.com/high-temperature-solar-thermal/). The cost of HTST is projected to decrease significantly over the next 10 to 15 years due to production volume increases, plant size scale up, and technological advance. HTST projects are labor intensive and thus could be especially beneficial during times of higher unemployment, such as now.

HTST presently faces strong competition with fossil fuels, and government incentives have been lacking. If the HSTS sector is given the right incentive by thegovernment, this may become major electric power generation contributor in the very near future.Nigeria, therefore, should take advantage of its abundant solar resources by introducing new and implementable policies on energy power production by both the federal and state governments and increase investment and research in HSTS Systems.

High-temperature solar systems are the future in energy. The raw material, the sun, is very abundant in Nigeria. Nigeria is best placed to maximize its advantages due to its geographical location. It will, however, take courage from our policymakers to venture into it. Initial investments may seem huge, but the reward in the future is great. Prospecting for more crude oil zones in the country seems easy, but we must not forget the changing energy use scenario. There are advance researches to replace petrol vehicles with electric powered ones. Many countries have set targets for such replacement. Nigeria must, therefore,start investing researching into alternative forms of energy. High-temperature solar systems are expensive now, but it is the future.

Acknowledgement

The funding for writing this Research and presentation is provided by Tertiary Education Trust Tund (TETFund) under the National Research Fund (NRF) Window(TETFund NRF PCM Solar Powered Refrigeration Project).

References

Charles A. (2014); How is 100% renewable energy possible for Nigeria?, Global Energy Network Institute (http://geni.org/globalenergy/research/renewable-energy-potential-of-nigeria/100-percent-renewable-energy-Nigeria.pdf)

Douglas T. (2016) Dynamic modeling andsimulationof a solar-PVhybridbatteryand hydrogenenergystoragesystem; Journal of Energy Storage, 7. 104-114

https://en.wikipedia.org/wiki/List_of_solar_thermal_power_stations
http://thermal-powerplant.blogspot.com.ng/2010/06/list-of-solar-thermal-power-plants.html,
https://www.solarpowerauthority.com/high-temperature-solar-thermal/
https://amebosayso.wordpress.com/.../us-energy-information-administration-Nigeria-a..
http://geni.org/globalenergy/research/renewable-energy-potential-of-nigeria/100-percent renewable-energy-Nigeria.pdf
http://geni.org/globalenergy/research/...nigeria/100-percent-renewable-energy-Nigeria.pdf
Ikeagwuani I., Olusola Bamisile, Serkan Abbasoglu and Arua Julius, Performance Comparison of PV and WindFarm in Four Different Regions of Nigeria,
https://www.academia.edu/28657624/Performance_Comparison_of_PV_and_Wind_Farm_in_Four_Different_Regions_of_Nigeria
Renewable Energy Technologies: Cost Analysis Series, Volume 1: Power Sector, Issue 2/5, June 2012, Concentrating Solar Power (https://www.irena.org/DocumentDownloads/Publications/RE_Technologies_Cost_Analysis-CSP.pdf)
SOLAR ENERGY – A SUBSTITUTE FOR GAS IN POWER GENERATION, careerhubafrica July 15, 2016; http://www.careerhubafrica.com/blog/solar-energy-a-substitute-for-gas-in-power-generation

Proceedings of the 49th NSChE Annual Conference
KADA 2019: pp 373-380

P2B-04: ELECTROCHEMICAL PERFORMANCE OF MELON SEED HUSK WASTE BIOCHAR IN A DIRECT CARBON FUEL CELL

Ijagbulu O.M., *Adeniyi, O.D., Uthman H., Adeniyi, M.I., and Yakubu E.,
Chemical Engineering Department, Federal University of Technology, Minna, Nigeria
*Corresponding author: o.adeniyi@futminna.edu.ng

ABSTRACT
This paper reports the study on the use of the direct carbon fuel cell (DCFC) technology to convert the chemical energy of melon seed husk (MSH) waste to electrical energy with the aim of alleviating the problem of power instability in the country. Pyrolysis was carried out on the MSH at 500°C and a heating rate of 10°C/min to produce carbon biochar used in the DCFC to produce electricity. The pyrolysed biomass was used to determine the electrochemical performances of the DCFC using molten carbonate salts as the electrolyte and five different resistor loads. The electrochemical performances of the MSH waste were investigated at a temperature of 500°C to 800°C. The biochar from the MSH waste gave an open circuit voltage of 0.68 V, a current density of 32.65 mA/cm^2 and power density of 7.51 mW/cm^2. Scanning electron microscopy (SEM) results of the carbon fuel show the morphological structures of the biofuel used in the DCFC. The phase composition using X-ray diffraction (XRD) of the biochar show some level of amorphous structure.

Keywords: Direct Carbon Fuel Cell, Melon seed husk, biochar, pyrolysis, power density

1.0 INTRODUCTION
The requirement for electrical energy for industrial and commercial need has been on the increase and according to the World Energy Council (WEC), the global demand for energy supplies will increase by over 65% in 2050 going by the current trend (WEC, 2015). Energy production from fossil fuel is on the decline as the world reserves of crude oil is declining with increase in greenhouse gas emissions. This has led to different researches in finding alternatives for electricity generation process. One of the promising alternative available is the use of fuel cell technologies particularly the direct carbon fuel cell (DCFC). A fuel cell is an electrochemical device that can convert chemical energy to electrical energy. There are different types of fuel cells but this paper focuses on the direct carbon fuel cell (Dudek *et.al.,* 2018; Adeniyi *et.al.,* 2014; Adeniyi and Ewan, 2012; Jain *et.al.,* 2009,2007).

A direct carbon fuel cell is an electrochemical device that efficiently converts the chemical energy of a carbon rich fuel (like the one present in MSH waste) directly to electrical energy without burning the fuel. The DCFC technology offer a viable technique that can produces electricity that is safe, efficient and environmentally friendly (Kacprzak *et al.,* 2017; Munnings *et.al.,* 2014; Arenillas *et.al.,* 2013; Li *et.al.,* 2010; Cooper and Berner, 2005).

Scarcity of traditional petroleum fuels and its over-dependence by nations like Nigeria, increasing emissions of combustion generated pollutants and their increasing costs have made renewable energy sources the focal point of some researchers. The world petroleum reserves are finite in nature and reducing quickly, melon seed husk a popular waste in Nigeria is a good alternate to investigate. It is an agricultural waste which is combusted in open air or dumped in refuse dumps and landfill sites thereby worsening the prevalence of greenhouse gases and becomes an

environmental burden of pollutant emissions. There is a growing need to explore more routes for the conversion of agricultural waste such as melon seed husk for present and future clean bioenergy application (Giddey *et al.,* 2012; Jia *et.al.,* 2010; Declaux *et.al.,* 2010; Cooper and Cherepy, 2008; Cao *et al.,* 2007; Dicks, 2006; Cherepy *et al.,* 2005; Zecevic *et al.,* 2004; Larminie and Dicks, 2003; Hoogers, 2003). This paper is aimed at producing electrical energy from waste generated from MSH thereby solving the problems of environmental pollution and climate change.

2.0 METHODOLOGY

Pretreatment such as sorting, drying and size reduction were carried out for the purpose of conversion of the melon seed husk (MSH) to produce biochar from the waste using pyrolysis process. The melon seed husk waste was obtained from Kasuan Gwari, Minna, Niger State. The sample was sorted to remove impurities, dried for 48 hours, the melon seed husk was (Plates I and II) then reduced to smaller sizes of 10-15 mm. The ground samples were further sieved. The sieving process was carried out by putting the sample in the sieve with mechanical shaker to achieve uniform particle size of 8-10 mm. This process was repeated to obtain reasonable size. The ground melon seed husk was pyrolysed at 600 ^{o}C at Badeggi Research Institute, Bida, Niger State. The biochar produced after pyrolysis was ground to finer particles. Proximate analysis was carried out using an ELTRA CHS-580 Analyser (Netherlands). Samples of the biochar produced were used to determine the carbon, hydrogen, sulphur, nitrogen and oxygen contents. The proximate analyses gave the ash content, volatile matter, fixed carbon content, and moisture content using ELTRA CHS-580 Analyzer (Netherlands).

Scanning electron microscopy (SEM) (Nova NanoSEM 200 FEI, Netherlands) was used to examine the morphological structure (amorphous or crystalline structures) of the pyrolysed melon seed husk and its elemental compositions for its application as fuel in a DCFC. X-ray diffraction (Siemens D500 XRD, Netherlands) analysis was equally carried out to determine structural changes related to pyrolysed melon seed husk. XRD analysis gave the structure of the biochar produced.

The carbon biochar particles (Plate III) used for the electrochemical reaction according to procedures described in literatures (Adeniyi and Ewan, 2012; Cooper and Cherepy, 2008) was mixed with carbonate salt (15 wt.% of biomass, 46.6 wt.% of Na_2CO_3 and 53.4 wt.% of K_2CO_3. Sodium carbonate (13.98 g) and potassium carbonate (16.02 g) were mixed together and later mixed with 4.5 g of the carbon particle to form fuel for the DCFC. The electrolyte was prepared using molten carbonate of sodium and potassium based on information from literatures (Adeniyi *et al.*, 2014; Cooper and Berner, 2005). 9.5 g of Na_2CO_3 and 15.5 g of K_2CO_3 were measured and mixed together and later transferred to a stainless steel. The mixture was stirred continuously to ensured homogeneity. The molten state of the salts was observed at a temperature range of 1159^{o}C to 1310^{o}C. The 25 mm aluminum wire mesh was saturated with the molten carbonate. Upon cooling, the molten carbonate stuck to the aluminum wire mesh and it was used as the electrolyte. Plates I to III show the raw MSH waste, the ground MSH and the pyrolysed MSH to produce the biochar used in the electrochemical performance in the DCFC.

Plate I: Melon seed husk

Plate II: Ground Melon Seed Husk

Plate III: Pyrolysed Melon Seed Husk

3.0 RESULTS AND DISCUSSIONS

Table 1 shows the proximate analysis results on the pyrolysed MSH showing the chemical composition. This includes the percentage of the volatile content (VC), ash content (AC), moisture content (MC), and fixed carbon (FC). Ultimate analysis was performed to determine the elemental composition of the MSH biofuel giving the Carbon (C), Nitrogen (N_2), Hydrogen (H_2), Oxygen (O_2) and Sulphur (S). The proximate and ultimate analyses were carried out at the National Cereal Research Institute (NCRI), Badeggi, Niger State. The higher heating value (HHV) is also presented. The carbon and the higher heating values are significant for the performance of this biomass in the DCFC.

Table 1: Proximate and ultimate analyses for Melon Seed Husk (MSH) waste

MC wt.%	AC wt.%	VC wt.%	FC wt.%	HHV MJ/kg	C wt.%	H wt.%	S wt.%	N wt.%	O wt.%
2.5	5.0	66.0	26.5	18.7	41.2	3.6	39.6	1.2	0.3

Figure 1 shows the SEM micrograph for the carbon fuel particle of the biomass. The SEM results show differences in the particle sizes and porosity of the biochar. Results of the XRD from the analyses conducted on the pyrolysed MSH waste biochar are shown in Figure 2, these revealed a disordered carbon fuel structures, this is what will enhance oxidation of the carbon fuel and in turn enhance the electrochemical conversion in the DCFC. These results obtained can be used to explain variation in the size distribution and structure of the MSH biochar. Figure 2 shows the XRD of pyrolysed melon seed husks used in fuel cell. The highest peak occurred at angle of 33.1 (2θ axis) and relative intensity of 100 %. The XRD pattern reveals that the MSH biochar is amorphous in nature, which will enhance the electrochemical conversion of the fuel during fuel cell operations. There are also indications of crystalline structures in the figure suggesting the presence of impurities like silica.

Table 1 show the MSH waste proximate and ultimate values, of significant interest is the HHV and the carbon content which are important parameters for the fuel used in the DCFC. Tables 2 and 3 show the open circuit voltage (OCV) result from the electrochemical conversion of the MSH biochar in the DCFC. The OCV is the voltage of the fuel cell when current and power densities

are not taken out of the system. The OCV increases with the increase in temperature indicating that the oxidation of the MSH waste biofuel is favoured by temperature (Kacprzak *et al.,* 2017; Hackett *et al.*, 2007). Table 3 shows the results obtained from the electrochemical performance of the DCFC at different temperatures.

Table 2: Open Circuit Voltage (OCV) readings for Melon Seed Husk waste

S/No	Time (min)	Temperature (°C)	OCV (V)
1	24	100	0.02
2	48	200	0.04
3	66	300	0.05
4	96	400	0.06
5	124	500	0.18
6	132	600	0.35
7	140	700	0.38
8	144	800	0.68

The OCV increased with increase in temperature of the DCFC, this is because carbon oxidation is favoured by increase in temperature (Cao *et al.,* 2007; Zecevic *et al.,* 2004). The maximum OCV was observed at 800 °C to give 0.68 V. From Table 3, the maximum current density of 32.65 mA/cm^2 was obtained at 800 °C, the same was observed for the peak power generation and efficiency.

Table 3: DCFC Electrochemical performance at different temperature

	Temperature (°C)			
Cell parameters	**500**	**600**	**700**	**800**
OCV (V)	0.18	0.35	0.38	0.68
Peak power density (mW/cm^2)	1.71	3.82	5.33	7.51
Max. current density (mA/cm^2)	16.33	20.57	24.49	32.65
Voltage at peak power (V)	0.08	0.17	0.19	0.46
Efficiency at peak power (%)	22.0	49.0	50.0	68.0

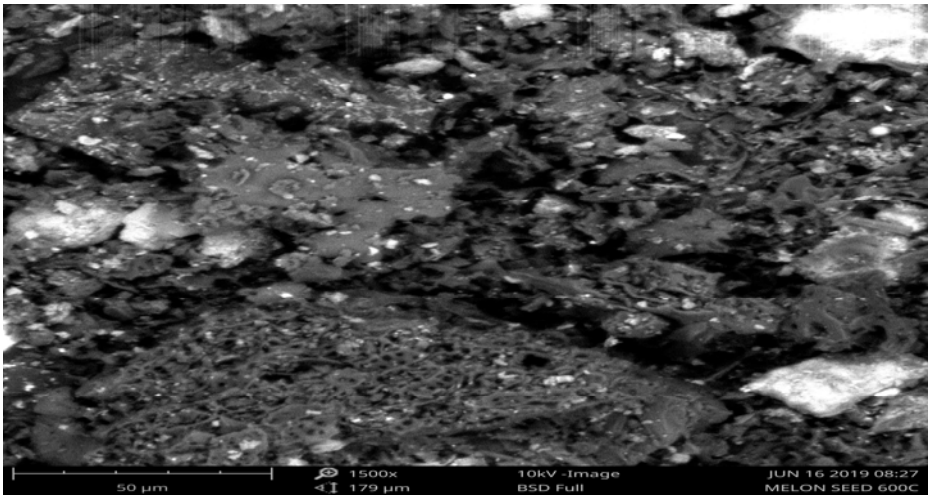

Figure 1: SEM Melon Seed Husk waste biofuel

Figure 3 shows the OCV results obtained from the experiment carried out on the DCFC at varying temperature from 100 °C to 800 °C. As the temperature increase from 100–800 °C it was observed that there was an increase in value but a reasonable increase was noticed from 400 °C to 800 °C, this was as a result of the electrons movement and conduction of electricity, leading to the biochar reaching the electrolytes assembly to take part in the electrochemical conversion. It has been reported that carbon oxidation is favoured by temperature (Dudek *et.al.,* 2018; Adeniyi *et.al.,* 2014; Jain *et.al.,* 2009, 2007).

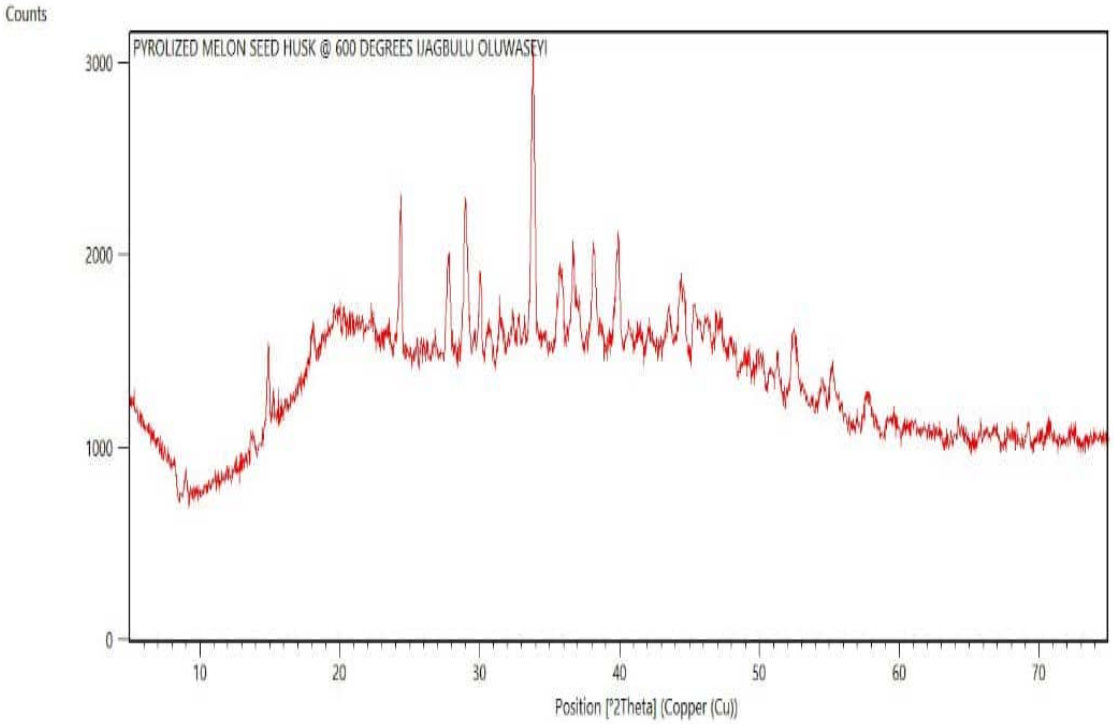

Figure 2: XRD of Melon Seed Husk waste biofuel

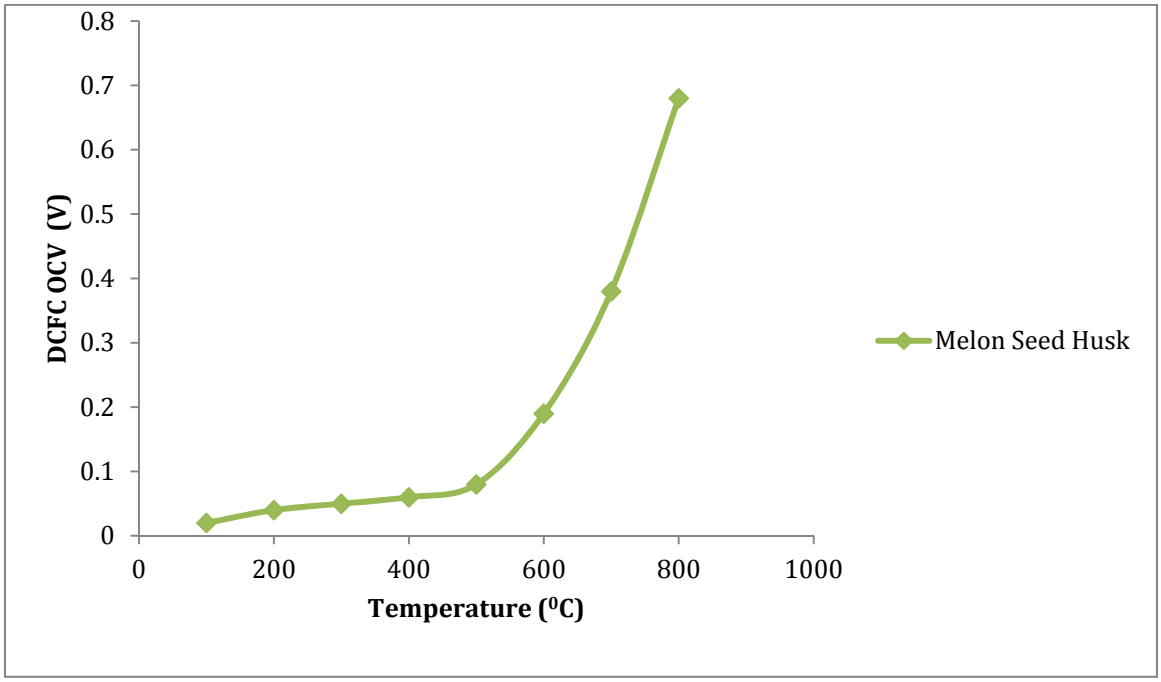

Figure 3: DCFC-OCV for the MSH waste biofuel at various temperatures.

Figure 4 presents the results obtained from the electrochemical performance of the MSH biochar in the direct carbon fuel cell. The tests were conducted at various temperatures of 500 °C, 600 °C, 700 °C and 800 °C. From Figure 4, the DCFC current density and power density increases with increase in the operating temperature. These observations were similar to those in the literature (Li *et al.*,, 2010; Hackett *et al.*, 2007). At 800 °C, the electrochemical performance was much better and improved as a result of the improvement in the conduction rate of the ions of the electrolyte and the electrochemical reactions at the two electrodes of the DCFC (Li *et al.*,, 2010; Hackett *et al.*, 2007).

Figures 3 and 4 present the electrochemical performances of the MSH waste biochar utilized in the molten carbonate direct carbon fuel cell. The open circuit voltage increased (0.18 V at 500 °C) with the increase in the temperature until it reached its maximum (0.68 V at 800 °C). At 800°C the peak values obtained for the current density and power density were 32.65 mA/cm^2 and 7.51 mW/cm^2. At 800 °C, the greater part of the carbon fuel was consumed requiring a refill for further electrochemical reactions (Munnings *et al.*, 2014; Jia *et al.*, 2010; Jain *et al.*, 2009).

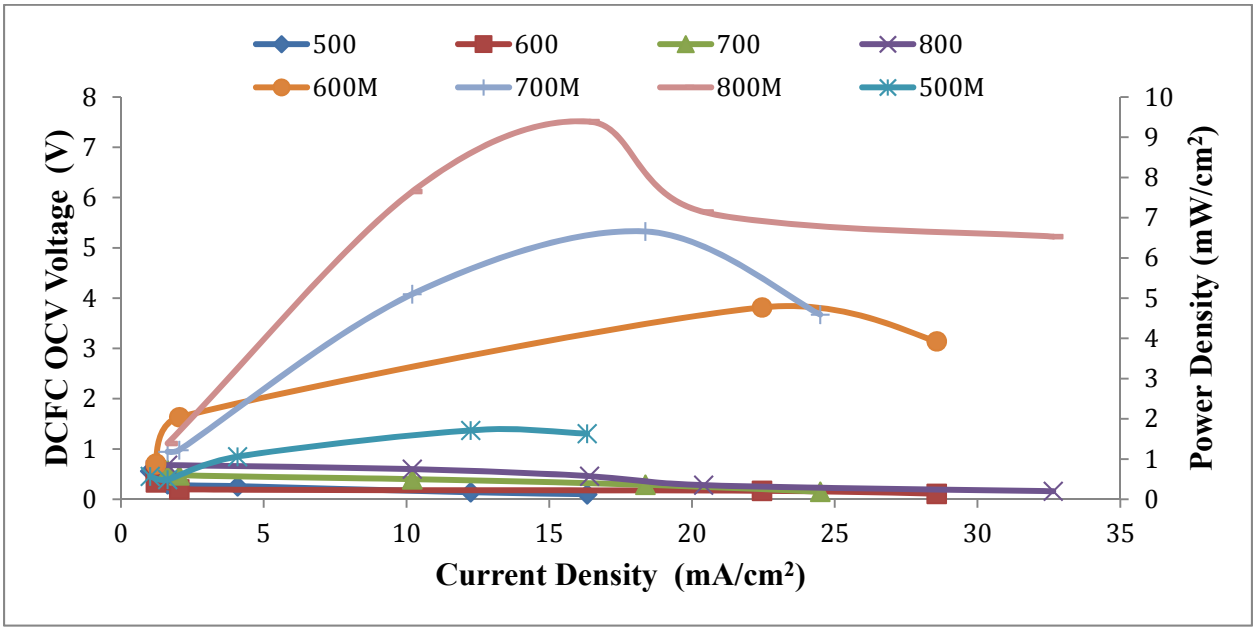

Figure 4: DCFC performances using MSH biochar at different temperatures

4.0 CONCLUSIONS

The study of the molten carbonate direct fuel cell showing the electrochemical performance of melon seed husk (MSH) waste biochar was carried out. The highest open circuit voltage of the biochar was 0.68 V showing the viability of using MSH waste biochar to power the DCFC. The optimum peak power density recorded for the biochar is 7.51 mW/cm^2, maximum current density of 32.65 mA/cm^2. An efficiency of 68 % was obtained from the MSH waste biochar which enhances the electrochemical performance in the direct carbon fuel cell operations. The scanning electron micrograph and X- ray diffraction reveals that the MSH biochar contain various sized particles with amorphous structures. It was observed that finer particle morphology led to enhanced current density and the presence of non-crystallites carbon product improved the current and power densities achievable with the direct carbon fuel cell.

REFERENCES

Adeniyi, O.D. and Ewan, B.C.R. (2012). Electrochemical conversion of switchgrass and poplar in molten carbonate direct carbon fuel cell. *International Journal of Ambient Energy*, 33:4, 204-208.

Adeniyi, O.D., Ewan, B.C.R., Adeniyi, M.I. and Abdulkadir, M. (2014). The behaviour of biomass char in two direct carbon fuel cell designs, *Journal of Energy Challenges and Mechanics,* 1(4) 6, 1-6.

Arenillas, A., Menéndez, J.A., Marnellos, G.E., Konsolakis, M., Kyriakou, V., Kammer, K., Jiang, C., Chien, A. and Irvine, J.T.S. (2013). Direct coal fuel cells (DCFC).The ultimate approach for a sustainable coal energy generation. *Bol. Grupo Español Carbón*, 29, 8-11.

Cao, D., Sun, Y., Wang, G. (2007). Direct carbon fuel cell: Fundamentals and recent developments. *Journal of Power Sources*, 167(2), 250-257.

Cherepy, N.J., Krueger, R., Fiet, K.J., Jankowski, A.F. and Cooper, J.F. (2005). Direct conversion of carbon fuels in a molten carbonate fuel cell. *Journal of the Electrochemical Society*, 152(1) A80-A87.

Cooper, J.F., and Berner, K. (2005). The carbon/air fuel cell, conversion of coal-derived carbons" in: *The Carbon fuel Cell Seminar*, Palm Spring, CA, Nov. 14th, UCRL-PRES-216953, 1-16

Cooper, J.F., and Cherepy, N. (2008). Carbon fuel particles used in direct carbon conversion fuel cells. *US Patent Publication,* No. US 2008/0274382 A1.

Desclaux, P., Nürnberger, S., and Stimming, U. (2010). Direct carbon fuel cells", in R. Steinberger-Wilckens, W. Lehnert (eds.) *Innovations in Fuel Cell Technologies*, RSC Energy and Environment Series No. 2, Royal Society of Chemistry, Cambridge, 190-210.

Dicks, A.L. (2006). The role of carbon in fuel cells. *Journal of Power Sources*, 156, 128-141.

Dudek, M., Adamczyk, B., Sitarz, M., Sliwa, M., Lach, R., Skrzykiewicz, M., Raźniak, A., Ziąbka, M., Zuwala, J. and Grzywacz (2018). The usefulness of walnut shells as waste biomass fuels in direct carbon solid oxide fuel cells, *Biomass and Bioenergy*, 119, 144–154.

Giddey, S., Badawal, S.P.S., Kulkarni, A. and Munnings, C. (2012). A Comprehensive Review of Direct Carbon Fuel Cell Technology. *Progress in Energy and Combustion Science*, 38, 360 – 399.

Hackett, G. A., J. W. Zondlo, and R. Svensson. (2007). Evaluation of Carbon Materials for use in a Direct Carbon Fuel Cell. *Journal of Power Sources*, 168: 111–8.

Hoogers, G. (2003). Fuel Cell Technology Handbook. *CRC Press LLC*, Florida.

Jain, S.L., Lakeman, J.B., Pointon, K.D. and Irvine, J.T.S. (2007). A novel direct carbon fuel cell concept. *Fuel Cell Science and Technology.* 4, 280-282.

Jain, S.L., Lakeman, J.B., Pointon, K.D., Marshall, R. and Irvine, J.T.S. (2009). Electrochemical performance of a hybrid direct carbon fuel cell powered by pyrolysed MDF. *Energy Environ. Sci.* 2,687-693.

Jia, L., Tian, Y., Liu, Q., Xia, C., Yu, J., Wang, Z., Zhao, Y., and Li, Y., (2010). A direct carbon fuel cell with (molten carbonate)/(doped ceria) composite electrolyte. *J. Power Sources*, 195:5581-5586.

Kacprzak, A., Kobyłecki, R. and Bis, Z. (2017). The effect of coal thermal pretreatment on the electrochemical performance of molten hydroxide direct carbon fuel cell. *Journal of Power Technologies* 97 (5) (2017) 382–387.

Larminie, J. and Dicks, A. (2003). Fuel cell systems explained. 2nd edition, John Wiley and Sons Ltd., England.

Li, X.,Zhu, Z.H., de Marco, R., Bradley, J. and Dicks, A. (2010). Evaluation of Raw Coals as Fuels for Direct Carbon Fuel Cells. *Journal of Power Sources*, 195 (13): 4051 – 458

WEC (2015) The World Energy Scenario: Composing Energy Future to 2015 http://www.worldenergy.org/publications/2013/world-energy-scenarios-

Munnings, C., Kulkarni, A., Giddey, S., and Badwal, S.P.S. (2014). Biomass to power conversion in a direct carbon fuel cell. *International Journal of Hydrogen Energy*, 39, 12377-12385.

Zecevic, S., Patton, E.M., and Parhami, P. (2004). Carbon-air fuel cell without a reforming process. *Carbon*, 42, 1983-1993.

Proceedings of the 49th NSChE Annual Conference
KADA 2019: pp 381-389

P2B-05: SUGARCANE BAGASSE AND GROUNDNUT SHELL DENSIFICATION FOR THERMAL ENERGY APPLICATIONS

Augustina Almai and Binta Zakari Bello[1]
Department of Chemical Engineering Ahmadu Bello University, Zaria, Nigeria

ABSTRACT
In view of the prevailing global economic crisis, utilization of readily available agricultural wastes and by-products is widely acclaimed. Consequently, the search for new and improved methods for the most efficient utilization of such materials is on the increase. Biomass densification is a way of increasing the energy density of biomass, so as to make it more effective as a fuel for thermal energy applications. In this work, briquettes were made via densification of sugarcane bagasse and groundnut shells, both of which are wastes associated with major cash crops of Nigeria. The physicochemical analysis carried out, shows the effect of the materials' properties as well as that of the binder, on the physical and thermal characteristics of the briquettes'. The analysis of physicochemical characteristics indicate that the biomass briquettes produced from groundnut shells have better qualities for thermal applications.

INTRODUCTION
Due to prevailing socio-economic and (most especially) environmental reasons, the utilization of biomass for a variety of energy applications is becoming increasingly popular. However, biomass in general has very low energy density. Hence, densification is used to significantly increase the energy density of different biomass materials, so as to make them more malleable for both domestic (like cooking and space heating) and industrial like (steam and power generation) applications.

Biomass densification is one of the processes through which biomass residues and agricultural wastes or by-products can be converted into higher energy density biomass briquettes (Olorunnisola, 2007). Biomass densification is an easy and environmentally friendly means of briquetting agricultural wastes into low-cost replacements of the fire wood, twigs and charcoal. Thus, in addition to turning the wastes into useful products, productions of the briquettes will help in avoid cutting off of trees which is a major contributor to soil erosion and desert encroachment (Olorunnisola, 2007).

Briquetting is a densification process for compacting loose residues (of a material) into a product of higher density (Wilaipon, 2007; Kaliyan and Morey, 2009). Biomass briquettes can conveniently replace fire wood, twigs and charcoal – which collectively account for about 51% of the total energy sources for domestic cooking in Nigeria (Kwadzah and Ogbeh, 2013).

Sugar cane bagasse and groundnut shells constitutes part of agricultural wastes in Nigeria. About 0.41 Million tons of bagasse and 1.81 Million tons of groundnut shells are regarded as waste residues globally (Bhattacharya *et al.*, 1993). This work is about production of briquettes from bagasse and groundnut shells obtained in northern Nigeria, using starch based organic binder.
Sugarcane, a cash crop cultivated in more than 90 countries, is the world's largest crop by production quantity. By 2018, the annual production of sugarcane in Nigeria, was estimated as 80,000 metrics tonnes. The sugarcane bagasse, is the residual, pulpy fibrous dry matter obtained as the leftover, after sugar juice is extracted from sugarcane.

As both sugarcane and groundnuts are seasonal crops, shortly after harvest, their supply normally reach their peaks, requiring strategic management and storage for use all year round. Thus, making briquetting via densification a very attractive approach for both sugarcane bagasse and groundnuts shells.

This work was carried out to investigate the effects of key parameters in the briquetting process on the quality of briquettes made from groundnut shells and sugar cane bagasse as well as a composite of the two in different ratios.. The parameters studied include variations in the moisture content, biomass to binder ratio, as well as the composting ratio on the calorific values and the potency of the briquettes for thermal energy applications.

1.1 Biomass Briquetting

The technological process of briquetting is relatively well known. However, there are few studies on briquettes developed from agricultural wastes because of the different types and quantities of agricultural wastes generated worldwide. Briquetting is essentially a mechanical process often seen as a relatively high-cost high-pressure technology. This is not always the case because it is possible to use a low-cost low-pressure technique to produce acceptable briquettes of reasonable quality that will perform the task for which it is intended (Russell, 1997).

1.2 Evaluation of a Briquette

Producing a biomass briquette is mostly for the purpose of its utilization as a fuel. Burning a substance as a fuel is a combustion process which follows a sequence of exothermic chemical reactions between the fuel and an oxidant. Materials used as fuels, exhibit different combustion behaviours depending their physio-chemical properties like bulk density, moisture content, proximate and ultimate analysis, etc (Shuaibu *et al.*, 2016). Likewise, the quantity of heat released from the exothermic reaction depends on the fuel's properties like calorific value and burning rate.

Briquettes are generally evaluated by assessing their physical characteristics like moisture content, bulk density, proximate and ultimate properties, gross calorific values, etc.

2.0 METHODOLOGY

2.1 Waste Biomass Collection and Preparation

The Groundnut shell was gathered from local farmers in Samaru and Bagasse was obtained from sugar cane juice point in Danfodio hostel, ABU Zaria. Groundnut shells and bagasse were sun-dried for 1 week to remove moisture. The bagasse was further oven-dried for 4 hours at 70^{o}C to aid size reduction. Both groundnut shells and the sugarcane bagasse were grinded and sieved to have uniform particle sizes using a 4mm sieve.

Eleven samples of briquettes were made using different combinations of the waste biomass and/or different binders as shown in Table 1

The various samples were made by weighing the required amounts of biomass and binder in accordance with the given mass ratios (Table 1). Each sample was then thoroughly mixed and poured into a mold. Then a hydraulic press was used to compress the samples by applying a pressure of 5.0 bar. The briquettes formed were then detached from the molds. The briquettes were then weighted and sun-dried for 14 days.

Table 1. Samples compositions

Sample Label	Composition	Mass Ratio
GG1	Groundnut shell with gum Arabic	3:1
GG2	Groundnut shell with gum Arabic	5:1
GS1	Groundnut with starch binder	3:1
GS2	Groundnut with starch binder	5:1
BG1	Bagasse with gum Arabic	3:1
BG2	Bagasse with gum Arabic	5:1
BS1	Bagasse with starch binder	3:1
BS2	Bagasse with starch binder	5:1
GBG1	Groundnut shell, bagasse and gum Arabic	1:2
GBG2	Groundnut shell, bagasse and gum Arabic	1:3
GBG3	Groundnut shell, bagasse and gum Arabic	1:1

2.2 EVALUATION OF BRIQUETTES

2.2.1 Percentage Volatile Matter (PVM)

3g of oven dried sample of each of the briquettes was pulverized, and heated in an oven at 500 ^{o}C for 10 mins. After cooling and weighing, the PVM was calculated using equation 4

2.2.2 Percentage Moisture Content (PMC) and Percentage Ash Content (PMC)

5g of oven dried sample of each of the briquettes were dried and then burned to ash. PMC was calculated using equation 2 while PAC was calculated using equation 5
Equation 6 was then used to determine Percent fixed carbon (PFC) for each sample

2.2.3 Calorific value and Burning Rate

3g of each sample was taken and placed inside an O-Bomb Calorimeter. Galvanometer deflections were taken for deflections without sample and with sample respectively. Calorific value of each sample was calculated using equation 7 and recorded.

For the burning rate, 10g of each sample was taken and placed on an insulated wire gauze, and then placed on a burner to burn. The sample and the insulated wire gauze were measured at 20 seconds interval. The burning rates were calculated using equation 10

3.0 RESULTS AND DISCUSIONS

3.1 Nature and Appearance of Briquettes

Plate 1 shows the briquettes produced from Groundnut shell and sugar cane bagasse with gum Arabic and Starch binders. The briquettes produced from the compaction machine were strong and well formed. The briquettes had a light brown coloration. From a physical examination of the briquettes some have a rough look due to the small amount of binder under pressure of 5 MPa while others appear smoot because of sufficient amount of binder under pressure of 5 MPa. It was observed that the briquettes compaction and strength increased with binder concentration also, the briquettes produced from bagasse have weak and lighter weight compared to groundnut shell briquettes. Finally, it was noticed that bacteria and fungi formation occurred with increase in binder concentration and it is more pronounced on the sugarcane bagasse samples.

Plate 1: Sugarcane bagasse and ground shell briquettes

Table 2: Physical observation of strength of briquettes

Samples	Strength			Degree of cracking		
	Poor	Average	Good	Severe	Average	No crack
GG1			✓			✓
GG2			✓			✓
GS1			✓			✓
GS2		✓			✓	
BG1			✓			✓
BG2	✓				✓	
BS1		✓			✓	
BS2	✓			✓		
GBG1			✓			✓
GBG2		✓				✓
GBG3	✓					✓

Effects of properties of briquette produced on the quality of briquette

The quality of briquettes is one of the most influencing factor affecting the burning of briquettes. The qualities are expressed in form of calorific values, densities and resistance to humidity. Calorific values affect the burning of briquettes greatly. The higher the calorific value, the easier and better the burning.

Briquette density influences their burning too as high density briquettes tends to have a longer burning time and releases more heat. The raw material particle size and moisture content have direct effect on the density of the briquette. Smaller particle sizes and low moisture content increases density of briquettes. From Figure 1, GG1 has the highest bulk density (1.156 g/cm^3) which is agreeable because it also shows low moisture content (23.66%). In terms of resistance to humidity, briquettes are going to get damaged when subjected to humidity because lignin and majority of binders added to briquettes are water soluble. When the briquettes absorb moisture, they crumble too quickly during combustion hence, briquettes with low moisture content are better than those with very high moisture content (Cutz *et al.,* 2016). Other factors that affect the quality of briquette are Ash content and compacting pressure and temperature. Low ash

content is desired for briquette so that low amount of waste will be produced hence reducing environmental pollution. From Figure 2, GBG 2 has the lowest ash content (0.04%).

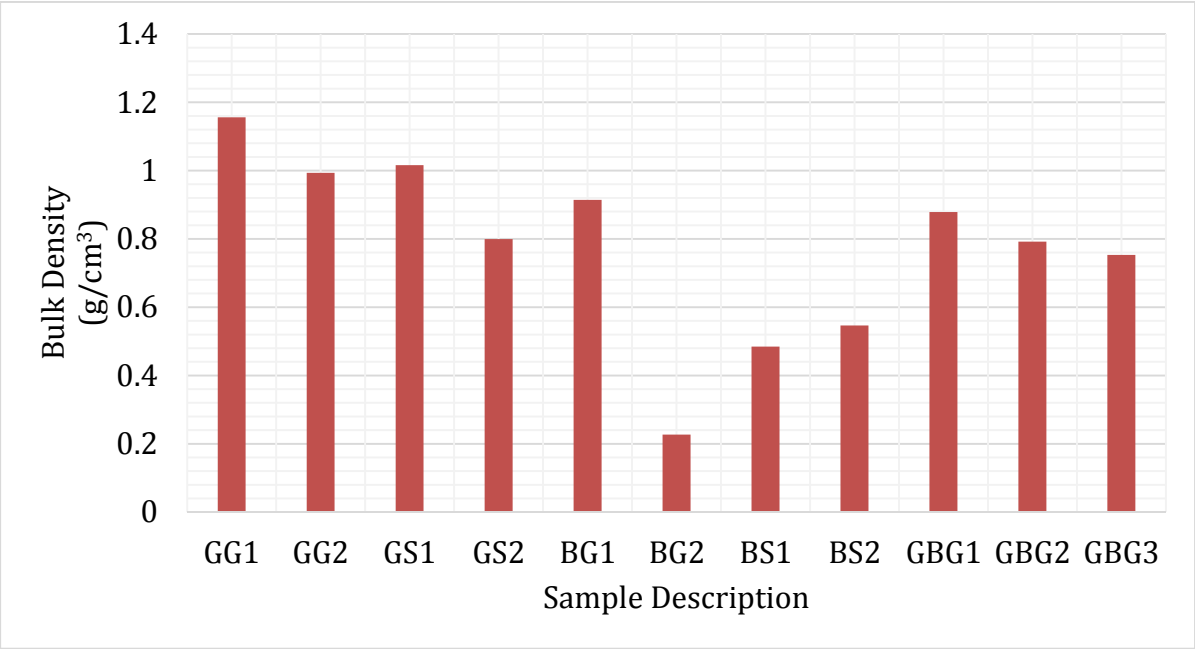

Figure 1: Graph of bulk densities of briquettes

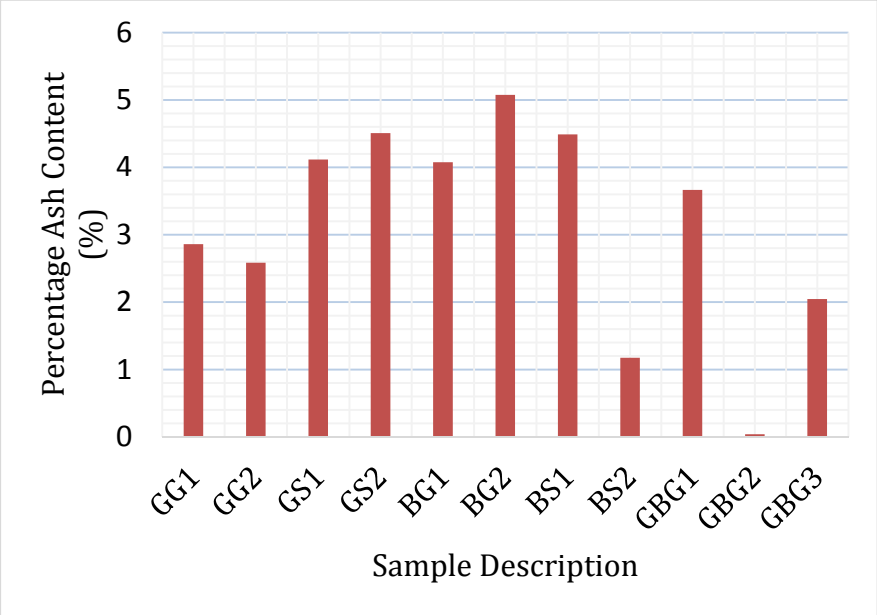

Figure 2: Graph showing Percentage Ash Content of samples

From Figure 3, sample GG1, GG2, GS1, BS1, GBG2 and GBG3 gave good results which were above 16.0 MJ/kg (Lubwama and Yiga, 2017). The briquette showing the highest calorific value was GS1 because of high concentration of binder and also starch binder has better binding properties than gum Arabic (Ismaila and Sadiq, 2013).

Effect of binder ratio and composting ratio on the performance of briquettes

From Figure 3, it can be seen that higher ratios of binder gave higher calorific values. This was consistent with the report of David and Jason (2013). In as much as suitably high amount of binder is required, it has its own side effect on the appearance of briquettes as too much binder yields fungi and bacteria on the briquettes. Figure 3 shows that GBG 2 has the highest calorific (16.382 MJ/kg) value when considering the composting ratio. This can be attributed to the suitable blending of properties of the two materials.

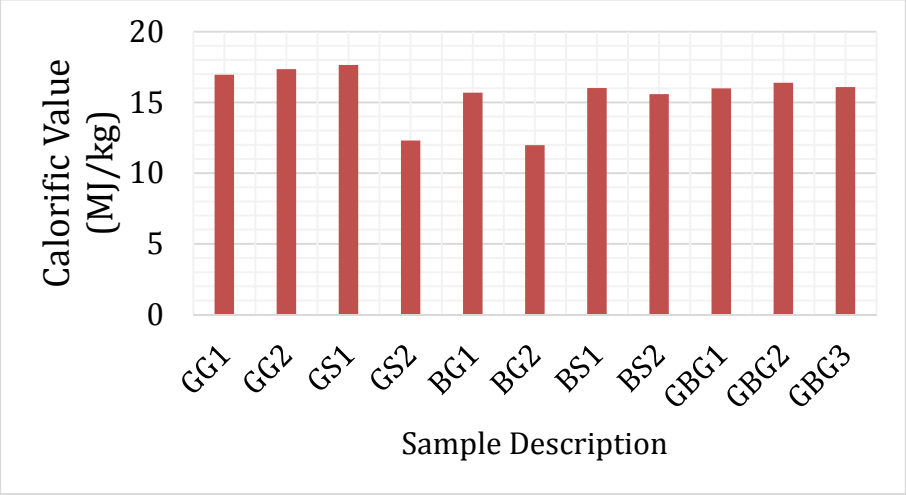

Figure 3: Plot of calorific values of briquettes

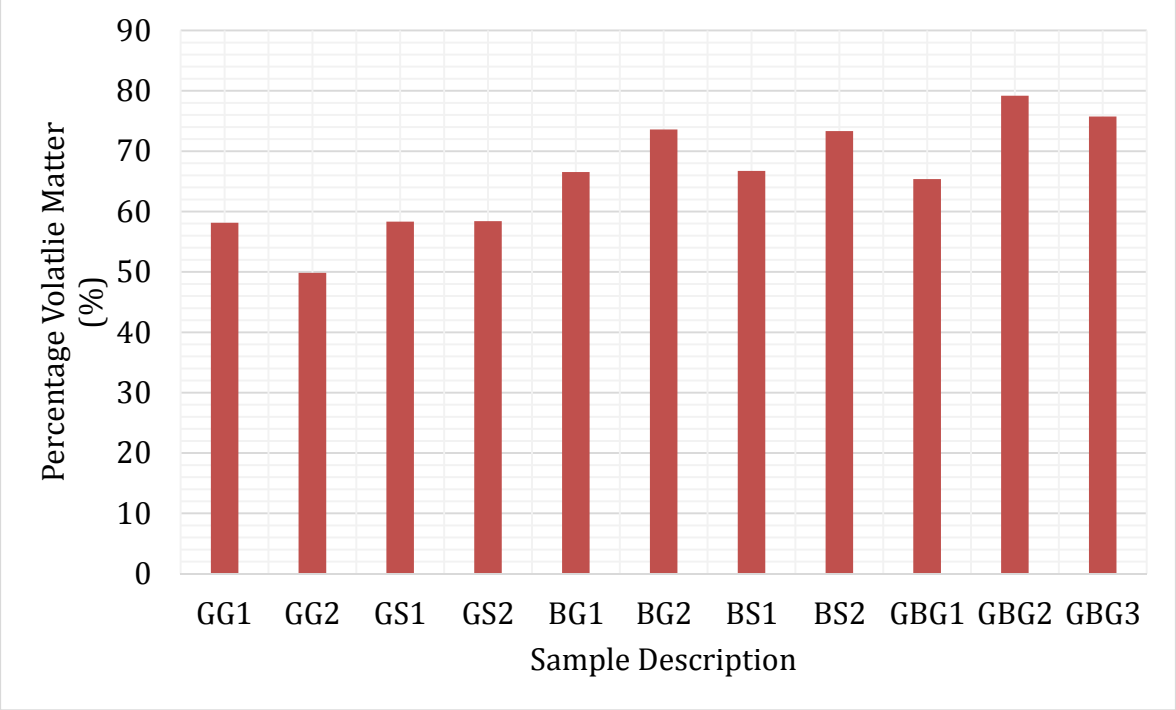

Figure 4: Graph showing percentage volatile matter of briquettes

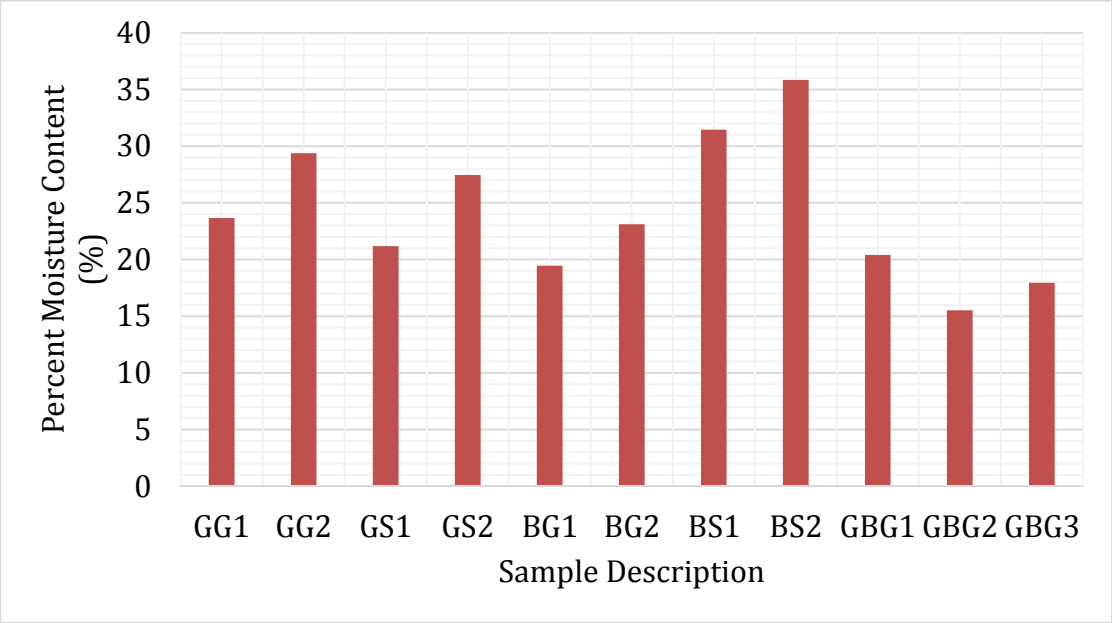

Figure 5: Graph showing percent moisture content of samples

Effect of moisture content on briquettes

Moisture content is generally affected by the kind of feed stock and its properties. The optimal moisture content is around 10-18% according to Siddiqui (2000). When the moisture content is lower than 10% or higher than 18%, the particles will not be consistent and briquette may show tendencies of falling into pieces. From Figure 5, BG 1, GBG 2 and GBG 3 fall between this optimum range with GBG 2 having the lowest moisture content (15.52 %). This may be due to mixture of properties between the two kind of material used for the briquetting.

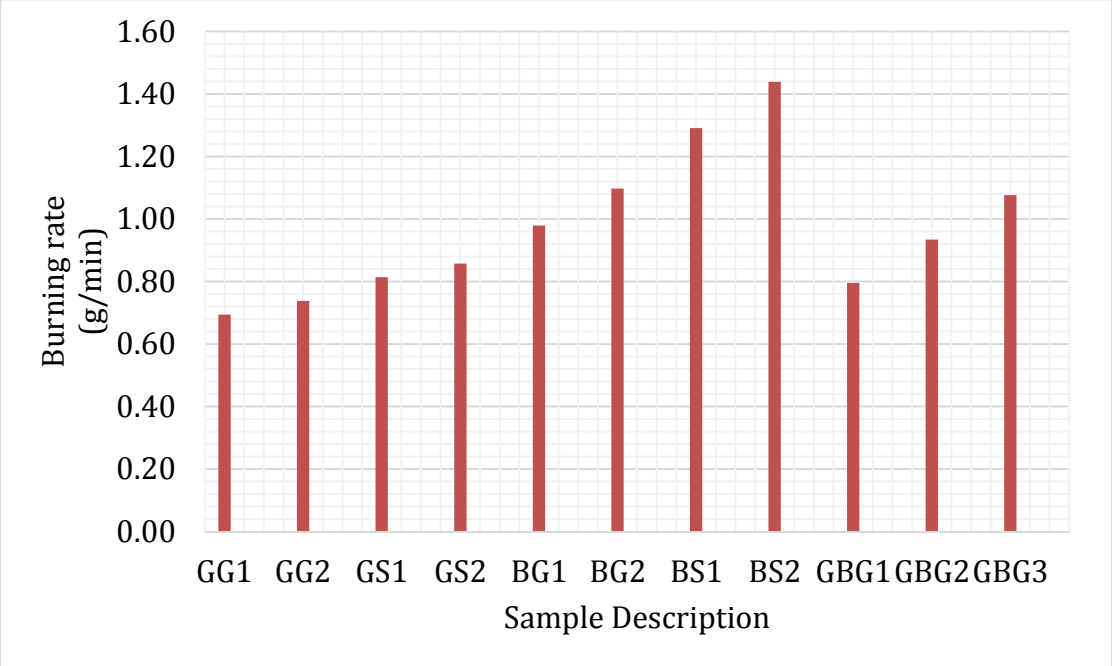

Figure 6: Graph showing burning rates of briquette samples

Evaluation of overall performance of briquette as source of thermal energy

The quality of any fuel briquette depends on its ability to provide sufficient heat at the necessary time, to ignite easily without any danger, generate less ash as this will constitute nuisance during cooking. Groundnut shells and bagasse can be a significant alternative fuels to be used most especially for domestic purposes. It can be noticed from Figure 3, the calorific energy values for most of the samples are within a reasonable range. Also, the percentage of ash removal too is suitable most especially for sample GBG 2. Despite the good qualities observed, it was also noticed that the briquettes produced smoke especially at the start of ignition. This was more pronounced with GBG 2 and it also shows from Figure 4 that it has high percent of volatile matter.

CONCLUSION

In this study, briquettes from groundnut shells and sugar cane bagasse were developed using wheat starch and gum Arabic as binders. This was accomplished by varying the amount of the binders and also varying the relative mass ratios of the two raw materials. Increasing the amount of binder increased the calorific values and volatile matter content. Sample BG 2 produced high amount of ash while GBG 2 has the lowest ash content. Sample GBG 2 showed desirable characteristics in terms of physical appearance, ash removal (0.039%), calorific value (16.382 MJ/kg), moisture content (15.52%) and a suitable value of burning rate (0.93 g/min). It also has a bulk density of 0.7918 g/cm^3. Despite its good characteristics, it also has high percentage of volatiles (79.19%) and produced smoke at ignition. The developed briquette could be used as fuel especially for domestic uses and its production could help alleviate the wastage of groundnut shells and sugar cane bagasse.

REFERENCES

Amrit, K. (2017). Benefits and amp; Uses of Biomass Briquettes. Retrieved April 30, 2019. Available at https://hitechagroenergy.wordpress.com/2017/07/16/benefits-uses-of-biomass-briquettes/

Bhattacharya S.C; Sett S, Shrestha RM. (1989). State of the art for Biomass Densification. *Energy Sources*, 5, pp. 161-182.

Chandra, K. (2014). Various Types of Briquettes. *Biomass Briquetting Plant*. Retrieved May 2, 2019. Available at https://briquettingplantsindia.wordpress.com/2014/12/20/various-types-of-briquettes/

Finelib. (2017). Sugarcane Production And The States That Grows It In Nigeria. Retrieved May 1, 2019. Available at https://www.finelib.com/about/nigeria-cash-crops/sugarcane-production-and-the-states-that-grows-it-in-nigeria/149

Jittabut, P. (2015). Physical and Thermal Properties of Briquette Fuels from Rice Straw and Sugarcane Leaves by Mixing Molasses.pdf. Thailand: Elsevier.

Kaliyan, N. and Morey, R. V. (2009) "Factors Affecting Strength and Durability of Densified Biomass Products" *Biomass and Bioenergy,* 33, pp.337-359

Kathuria, R. S. (2012). Using Agricultural Residues as a Biomass Briquetting: An Alternative Source of Energy. *IOSR Journal of Electrical and Electronics Engineering*, *1*(5), 11–15. https://doi.org/10.9790/1676-0151115

Kwadzah, T. K., and Ogbeh, G. O. (2013) "A Comparative Study of the Thermo-Physical Properties of Fuel Briquettes of Sawdust and Rice Husk" *Journal of Engineering and Applied Science*, 5, pp.147-158

Maxton. (2018). binders for briquette making, learn and choose the right one. Retrieved May 2, 2019. Available at https://briquettesolution.com/all-about-binders-make-briquette-with-proper-binder/

Mckendry P. (2002). Energy Production from biomass (part 1); overview of biomass. *Bioresource Technology*; 83(1): pp.37-46

Njenga, M., Karanja, N., Jamnadass, R., Kithinji, J., Sundberg, C., and Jirjis, R. (2013). Quality of Cooking Fuel Briquettes Produced Locally from Charcoal Dust and Sawdust in Kenya, *7*(3). https://doi.org/10.1166/jbmb.2013.1355

Olorunnishola, A. (2007). "Production of Fuel Briquettes from Waste Paper and Coconut Husk Admixtures" Agricultural Engineering International: *The CIGR E-Journal* Manuscript EE, 6, pp.123-128

Onukak, I. E., Mohammed-dabo, I. A., Ameh, A. O., Id, S. I. R. O., and Fasanya, O. O. (2017). Production and Characterization of Biomass Briquettes from Tannery Solid Waste. https://doi.org/10.3390/recycling2040017

RADHE Group. (2013). Easily Available Raw Materials for biomass Briquettes. Retrieved May 1, 2019. Available at http://www.biomassbriquetting.com/raw-materials.php

Russell, A. (1997). Using Biomass residue for Energy. Issue 39. Briquetting Agricultural Residues (knowledge Bank). Hedon Household Energy Network. http://hedon.info/BP39_UsingBiomassResiduesForEnergy

Sharma, M. K., Priyank, G., and Sharma, N. (2015). Biomass Briquette Production: A Propagation of Non-Conventional Technology and Future of Pollution Free Thermal Energy Sources. *American Journal of Engineering Research (AJER)*, 4, pp.44–50. Available at www.ajer.org

Shuaibu, N., Dandakouta, H., and Bello, A. A. (2016). Evaluating Groundnut Shell Briquettes as High Grade Fuels for Domestic Cooking ; Part 2 : Modeling the Effect of Processing Parameters on the Combustion Characteristics of the Briquettes, *2*, pp.1–7.

Wilaipon, P. (2007). Physical Characteristics of Maize Cob Briquettes under Moderate Die Pressure. *American Journal of Applied Science*, 4, pp.995-998

Zhang, G., Sun, Y., and Xu, Y. (2018). Review of briquette binders and briquetting mechanism. Renewable and Sustainable Energy Reviews, 82, pp.477–487. https://doi.org/10.1016/j.rser.2017.09.072

Zotero, Whitehead, D., Chen, L., Xing, L., Han, L., Tamilvanan, A., and Vinothkumar, M. (2016). Biomass Briquetting Process. *Renewable and Sustainable Energy Reviews*, *13*(2), pp.229. https://doi.org/10.1016/j.rser.2009.06.025

Proceedings of the 49th NSChE Annual Conference
KADA 2019: pp 390-397

P2B-06: PRODUCTION OF RENEWABLE ENERGY FUEL FROM WASTE VEGETABLE OIL USING HETEROGENEOUS CATALYST DERIVED FROM TERMITE CLAY

[1*]**Babatunde E. O., [2]Olutoye M. A., [2]Akpan U.G. and [2]M. Auta.**

[1*]Chemical Engineering Department, Faculty of Engineering and Technology, University of Ilorin, Nigeria

[2]Chemical Engineering Department, Federal University Of Technology, Minna, Nigeria

ABSTRACT

This paper reports the synthesis and characterization of heterogeneous catalyst from mixture of cow-bone and termite clay for the transesterification of waste vegetable oil (WVO) using simple 2^k factorial design method for the optimization of process parameters. Four factors Viz methanol to oil ratio, reaction temperature, catalyst loading and reaction time were investigated. It was found that the most significant factor on the biodiesel production was reaction time based on the factorial design method. The optimum FAME yield of 98.5% were achieved at methanol to oil ratio 6:1; catalyst loading of 2.0 wt%; reaction temperature of 65℃ and reaction time of 1 h. The biodiesel produced with the optimized process parameters meets the global standard for biodiesel ASTM and thus could be considered as suitable substitute for conventional diesel in unmodified diesel engine application.

1.0 Introduction

The alarming global twin problems of fossil fuel depletion and environmental pollution has called for attention of researchers to seek an alternative fuel in which biodiesel, a renewable fuel is one of the key solution. Global economy majorly depends on transportation of goods and services while transportation depends on energy from petroleum product which results in high increase in fuel consumption. Energy is an important aspect and it plays a principal and irreplaceable role in the economy of all country of the world. Majority of these energy requirements are supplied by coal, petroleum resources, natural gas and nuclear energy (Zhang, Dube, McLean, and Kates, 2003). Among all the conventional fuels, petroleum is the most important in the growth of industries, transportation and agricultural sector to satisfy all the needs of human beings (Alvarez, Lopez, Amutio, Bilbao, and Olazar, 2014).

Biodiesel which is also known as fatty acid methyl ester (FAME) serve as an alternative to petrol-diesel due to several advantages (Erum *et al.*, 2014). Crude oil or petroleum fuels that the world solely depends on are non-renewable energy source which is highly degradable and poisonous and it greatly affects both the safety of humans and the environment. This negative impact led researchers to find an alternative energy source and one of the breakthroughs achieved was the invention of biofuels. According to Olutoye and Hameed, (2016) the introduction of an eco-friendly green technology is the current focus of the human society in the production of energy. Biodiesel has become more important because of its environmental benefits such as its biodegradability and nontoxicity, thereby making it environmentally beneficial due to its low emission profiles. Also, Yusuff *et al.* (2018) reported that biodiesel being the most promising substitute fuel to the fossil fuel is as a result of aforementioned benefits and advantages.

The FAME can be synthesized through a transesterification of vegetable oil or animal fat and alcohol in the presence of a catalyst. The catalyst which may either be homogenous or heterogeneous catalyst. Homogenous catalyst are mostly used for industrial production of

biodiesel but leads to high cost of production because of waste water generation and difficulty in separation (yusuff *et al.*, 2018). The high cost of biodiesel is the major challenge in the commercialization of the process (Dhawane *et al.,* 2018) and the use of waste vegetable oil (WVO) instead of virgin oil is a way of reducing the cost, as WVO estimated to be about half the price of virgin oil (Ali et al.,2018).

In this present study, heterogeneous catalyst was prepared from mixture of cow-bone and termite clay which was used for transesterification of WVO to produce biodiesel. Reaction parameters were optimized by varying the reaction time, methanol to oil molar ratio, catalyst loading and reaction temperature.

2.0 Materials and method

Termite clay was harvested from the locality of Tanke Iledu, Ilorin, Nigeria. Cow-bone was gathered from Ipata market, Ilorin. WVO used as feedstock for the production of the FAME was obtained from item 7 restaurant Oke-odo, Ilorin, Nigeria. Ethanol, KOH, distilled water, Petroleum ether, methanol (analytical grade, 99.5%) were obtained from Central Research Laboratory B, University of Ilorin Road, Ilorin Nigeria.

2.1 Catalyst preparation

The cow bone collected were thoroughly washed and cleaned with soap and water to remove dirt, sand and any unwanted materials on it. Thereafter, the bone was boiled at a temperature of 100℃ and rinsed with distilled water to get rid of left over mucous inside the bone. Then, the washed bone was oven dried at 110℃ for 48 h to remove moisture. The bone was later crushed into powder using mechanical grinding machine. The powdered bone was sieved with the use of 75 µm mesh which was kept in a desiccator to avoid moisture. Similarly, the harvested clay was initially washed using the distilled water to remove the impurities. It was further dried at 100 ℃ for 4 h. The clean clay was further crushed using ceramic mortar and pestle. The particles were sieved using 75 µm mesh. The cow-bone and fine clay were weighed and mixed in 50-50% proportion into a beaker. Adequate amount of distilled water was added to the mixture to form suspension and stirred for 4 h on a magnetic stirrer for proper mixing. The mixture was kept for 48 h for ageing and later dried in an oven at 110℃. Thereafter, calcined in a muffle furnace at 900℃ for 4 h (Babatunde *et al.*, 2015), this synthesized catalyst is refer to as SC9 (that is silica/cowbone mixture calcined at 900 ℃) catalyst in this paper.

2.2 Characterization of Catalyst

The catalyst was analyzed to know its morphology, elemental composition and crystallinity by Scanning Electron Microscopy, Energy Dispersive X-Ray Spectroscopy and X-Ray Diffraction respectively. Elemental analysis of the catalyst surface was done and all the elements present on the surface were quantified by using X-ray energy dispersive analysis (EDAX) using OXFORD Instrument INCAX-sight.

2.3 Transesterification of Waste Vegetable Oil

The transesterification reaction was carried out in a batch reactor (250 ml round bottom flask) with magnetic stirrers inserted. 40 ml of Waste vegetable oil measured into the flask. A calculated amount of methanol was added to a known amount of catalyst (2.0 wt% - 4.0 wt%) to ease miscibility and speed up the rate of the reaction. Afterwards, the mixture (with methanol to oil ratio of 6:1- 9:1) was stirred rigorously at constant agitation speed, temperature (50℃ - 65 ℃) and reaction time (1 h - 4h), the experimental matrix used was presented in Table 4.The effects

of methanol-oil ratio, reaction time, reaction temperature and catalyst loading, were investigated for a range of values. At the end of the transesterification reaction, 30 ml of distilled water was added to the products; biodiesel and glycerol, giving rise to two distinct phases which were separated from each other using a separating funnel, catalyst was separated through a filter paper which was aimed at preventing the catalyst from being lost in the mixture. The glycerol was drained out from the bottom of the funnel and left with only the biodiesel.
The yield was obtained using Equation 1 below:

$$\text{Yield}(\%) = \frac{\text{weight of biodiesel}}{\text{weight of oil}} \times 100 \quad (1)$$

2.4 Design of experiment

The biodiesel production was optimized using simple factorial design which was used to build the experimental design of four variables Viz methanol-oil ratio, reaction temperature, catalysts loading and reaction time were considered at two levels as shown in Table 1. Hence, it is important to analyze the parametric effects on biodiesel production process and their optimization to obtain the desired waste vegetable methyl ester (WVME) yield.

Table 1: The selected process parameters and their values at two levels for factorial design

Variables	Parameters	Low	High
A	Methanol/oil ratio	6:1	9:1
B	Temperature (℃)	50	65
C	Time (h)	1	3
D	Catalyst loading (wt%)	2.0	4.0

2.5 Determination of physicochemical properties of biodiesel produced

The density, viscosity, flash point, pour points, cetane number and iodine value of the WVME produced were determined and compared by the standard method of American Standard for Testing Materials (ASTM).

3.0 RESULTS AND DISCUSSION

3.1 Characterization of Waste Vegetable Oil

The WVO used as feedstock was characterized based on its physicochemical properties and the result obtained was presented in Table 2. From acid value and free fatty acid (FFA) content, the feedstock can be used directly since the FFA was below 2%.

Table 2: Physicochemical properties of Waste Vegetable Oil

S/N	Properties	Units	Value
1	Density	g/cm^3	0.873
2	Kinematic viscosity at 40℃	mm^2/s	34.65
3	Acid Value	Mg KOH/g	3.366
4	Iodine Value	g/100 g	125.32
5	Molecular Mass	g/mol	1380.02
6	FFA	%	1.683
7	Flash Point	℃	159

3.2 Characterization of Synthesized Catalyst

The results of SEM-EDX analysis for SC9 catalyst calcined at 900 °C can be seen in Figure 1 and 2. The various elemental compositions were presented in Table 3. Fiqure 1 revealed that the catalyst are rough in surface and contains large pores which is good enough for transeterification process to occur. The result is in agreement with Yusuff *et al* (2018). Figure 2 revealed the elemental composition and the major element present in the catalyst is calcium in form of oxide which is the major element for conversion of triglycerides into FAME. Elements like magnessium, silicon, iron, carbon, phosphorus were also found. The presence of calcium and silicon as the major constituent was an indication that the mixture of cow-bone and termite clay comprised of calcium carbonate and silica and upon calcination can be completely converted to calcium oxide and silicon oxide respectively. The XRD analysis was presented in Figure 3. The result shows that the sharp peaks at 2θ =23.6° and 29.5° indicate the presence of calcium oxide and silica oxide respectively. The peaks are similar to those reported by Cheng *et al* (2016).

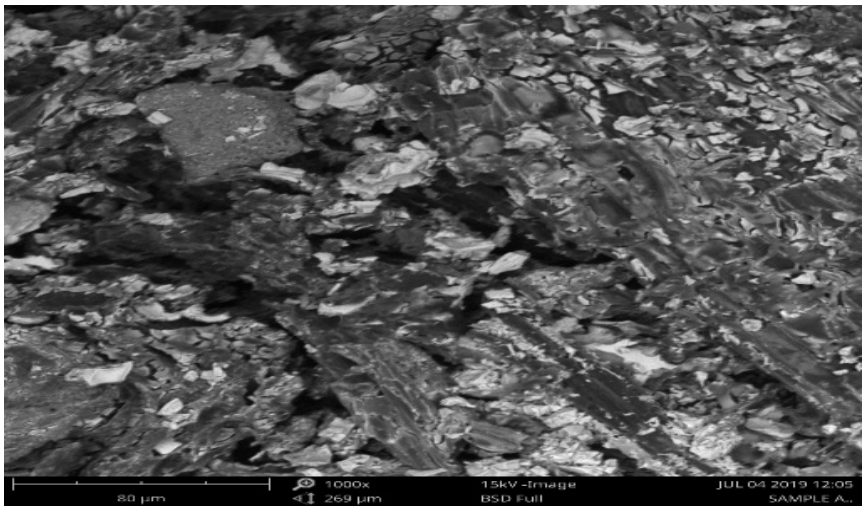

Figure1. SEM image of calcined SC9 catalyst

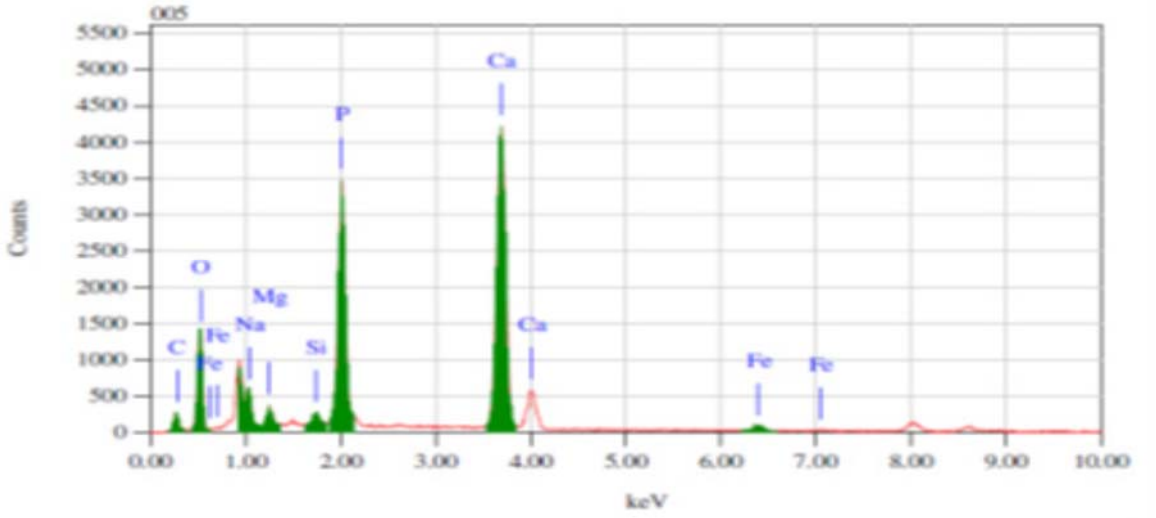

Figure2. EDX Analysis of calcined SC9 catalyst

Table 3. EDX analysis showing the elemental composition of SC9 catalyst

Element	Ca	P	Fe	S	Mg	Al	Si	O	Na	Cr	Ti	Total
Wt. %	46.06	26.83	6.80	0.03	2.07	0.85	3.61	11.59	0.29	1.17	0.69	100

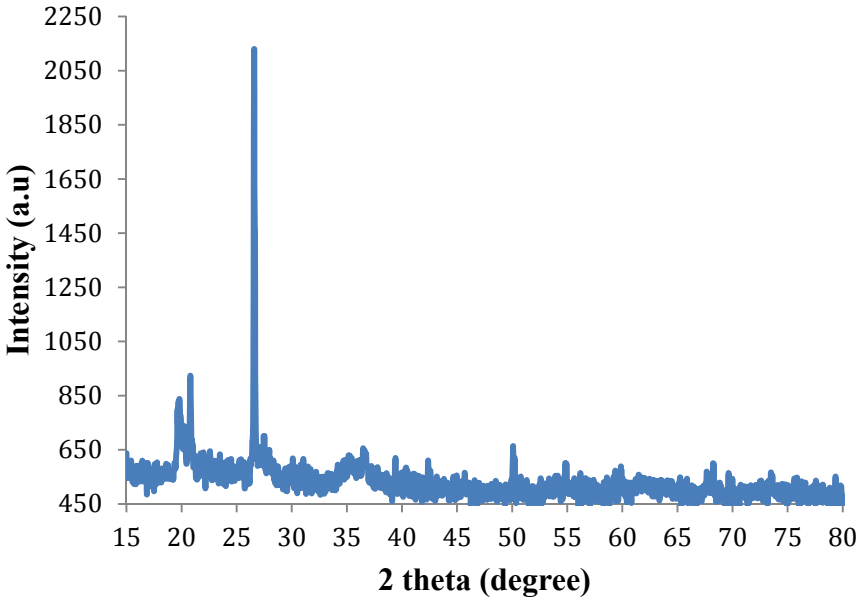

Figure 3.XRD Analysis of calcined SC9 catalyst

The result obtained on the influence of the operating parameters on the yield of biodiesel is summarized in Table 4. These effects are discussed in details below;

Table 4. Factorial design matrix for operating variables with biodiesel yield

Run	Temp (°C)	Time (h)	Catalyst (wt%)	MeOH/Oil	Biodiesel yield
1	65	1.00	2.00	12:1	96.8
2	45	1.00	2.00	6:1	85.5
3	45	1.00	4.00	6:1	84.3
4	45	3.00	2.00	12:1	84.6
5	65	1.00	4.00	6:1	94.6
6	65	1.00	4.00	12:1	95.6
7	45	1.00	2.00	12:1	87.5
8	65	1.00	2.00	6:1	98.5
9	45	3.00	2.00	12:1	83.7
10	65	1.00	4.00	12:1	97.9
11	65	1.00	2.00	6:1	94.8
12	45	3.00	4.00	6:1	82.3
13	65	3.00	4.00	6:1	97.2
14	65	1.00	2.00	6:1	98.4
15	45	3.00	4.00	12:1	88.6
16	45	1.00	4.00	12:1	85.9

3.3 Effect of Process Conditions on Biodiesel Yield

The effective production of biodiesel and energy efficient are affected by various operating parameters viz. Temperature, reaction time, catalyst loading and methanol to oil ratio.

3.3.1 Effect of methanol to oil ratio

Since the stoichiometric molar ratio of alcohol to oil for the transesterification is 3:1 and the reaction is reversible, higher molar ratios are required to increase the miscibility and to enhance contact between the alcohol molecule and the triglyceride. For this study, the molar ratio of methanol to WVO was varied from 6:1 and 12:1. Figure 4(a) shows increase in methanol to oil ratio results in slight decrease in biodiesel yield. Therefore, the yield of biodiesel increases with increase in the concentration of methanol up to certain concentration. However further increase of alcohol content (12:1) was found to result in excess unreacted methanol after separation of products which resulted into increase in the cost of methanol recovery. Ratio 6:1 relatively yields high at high temperature (run 8 and 14) and is recommended as the optimum for similar works of this kind (Taufiq-yap *et al*., 2014).

3.3.2 Effect of reaction temperature

The temperature was varied from 45^{o}C to 65^{o}C. The result from Figure 4(b) shows that there was increase in the biodiesel yield with increase in temperature. This was because higher reaction temperatures increase the rate of reaction. Considering run 8 at 65^{o}C the yield was 98.5% this is confirmed by the work of Ajala *et al* (2019). This result is expected as the rate of transesterification reaction depends on temperature (Ho, Ngo, and Guo, 2014).

3.3.3 Effect of catalyst loading

Catalyst loading is one of the most influencial parameter affecting the yield of biodiesel. This parameter was varied at two levels viz. 2 and 4 wt% ,from Figure 4(c) it was observed that catalyst loading at 2 wt% gave highest yield compared to 4 wt% .Considering run 8 and 14 where highest biodiesel yield was obtained, catalyst loading of 2 wt% was used. Futher increase in catalyst loading from 2 to 4 wt% slightly brought about decrease in the yield,which is in agreement with the work of Dhawane *et al* (2016).This decrease in yield can be attributed to leaching of the excess catalyst at higher concentration of catalyst and leading to saponification during the reaction.

3.3.4 Effect of reaction time

The dependence of the biodiesel yield on the reaction time was studied. As shown in Figure 4(d), the effect of reaction time on the yield was investigated in the range 1–3 h, the yield of biodiesel increased (98.5%) as the reaction time increased from 1 h to 3 h. This is because reaction time of 1-3 h was sufficient for completion of transesterification reaction with base catalyst (Nasim *et al*., 2014). For higher reaction time leaching of catalyst may increase and thereby lower the catalyst active sites, this was in agreement with the report of Dhawane *et al* (2017).

3.4 Properties of WVME produced

The major properties of WVME produced were estimated and presented in Table 5. The reported properties namely density, viscosity, acid value, iodine value, flash point and cetane number were compared with ASTM standard for biodiesel. The results show that all the properties of WVME were found to meet the global standard; hence WVME could be a substitute to fossil diesel.

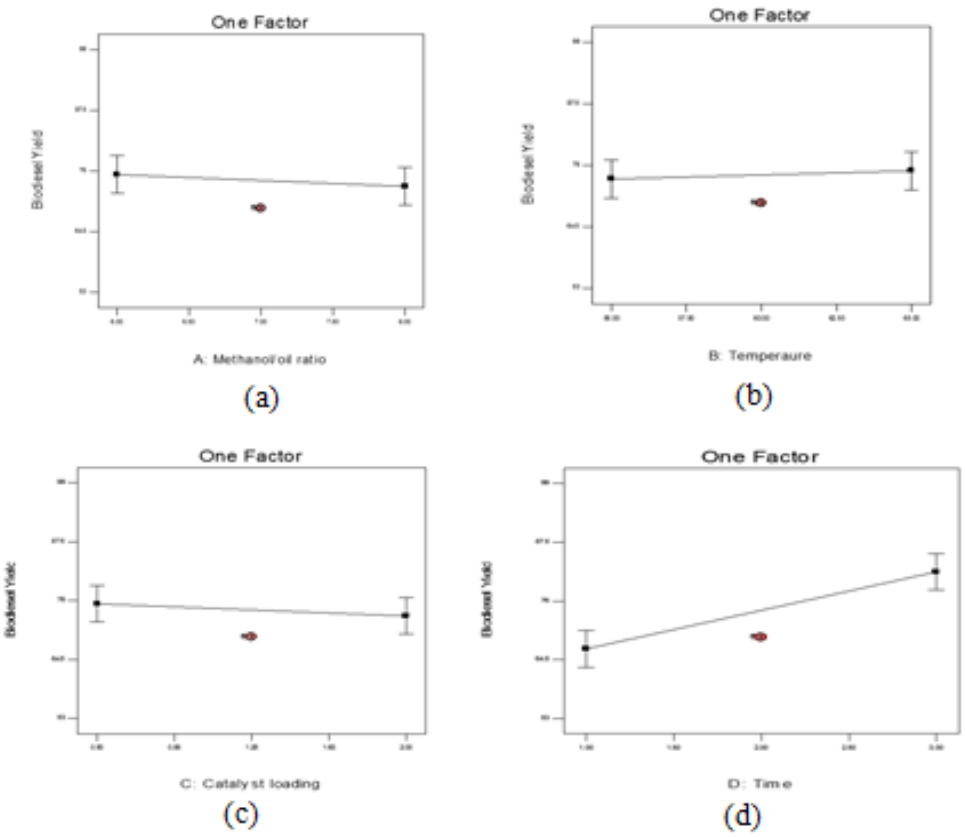

Figure 4. (a) Effect of methanol/oil ratio on WVME yield, (b) Effect of temperature on WVME yield, (c) Effect of catalyst loading on WVME yield (d) Effect of time on WVME yield

Table 5. Properties of waste vegetable methyl ester (WVME) in comparison with biodiesel standard (ASTM)

Properties	WVME	ASTM Limit	Testing procedure
Density at 15℃ (g/cm^3)	0.875	0.875-0.900	ASTM D4052
Viscosity(mm^2/s)	4.56	5-6	ASTM D445
Acid value (mg KOH/g)	0.14	0.8	ASTM D974
Flash point(℃)	165	>130	ASTM D93
Pour point (℃)	-6	-	ASTM D97
Cetane number	52	>47	ASTM D975
Iodine value (g iodine/100 g)	63.5	<120	AOAC CD1-25

4.0 Conclusion

In this present study a composite of calcined cow-bone and termite clay obtained after calcination of mixture of cow-bone and termite clay (SC9) catalyst has shown excellent activity for transesterification of WVO with FAME yield of 98.5% under optimal conditions. This study has tackled environmental and economic aspects of FAME production by using waste materials as both feedstock and catalyst. The effects of various parameters have been studied in which the most significant parameter is time and FAME produced showed conformance with the ASTM

standard. Studies on leaching of catalyst and its reuse need to be carried out, the kinetics of the process also need to be analysed as well as detailed modeling and optimization.

References

Ajala E. O., Ajala M. A., Okedere O. B., Aberuagba F. and Awoyemi V. (2019): Synthesis of solid catalyst from natural calcite for biodiesel production: Case study of palm kernel oil in an optimization study using definitive screening design, *Biofuels*, *1-12*.DOI:10.1080/17597269.2018.1532752

Alvarez, J., Lopez, G., Amutio, M., Bilbao, J., and Olazar, M. (2014). Bio-oil production from rice husk fast pyrolysis in a conical spouted bed reactor. *Fuel, 128*, 162-169. Doi: http://dx.doi.org/10.1016/j.fuel.2014.02.074

Babatnde E. O., David I., Olutoye M. A., Akpan U. G. and Eterigho E. J. (2015), Catalytic Degradation of Polyethylene to gas oil using synthesized clay based copper modified catalyst. *Nigerian Journal of Engineering and Applied Science (NJEAS*), 2(1): 19-27.

Cheng, S., Wei, L., Zhao, X., and Julson, J. (2016). Application, Deactivation, and Regeneration of Heterogeneous Catalysts in Bio-Oil Upgrading. *Catalysis A*. https://doi.org/10.3390/catal6120195

Dhawane, S. H., Bora, A. P., Kumar, T., and Halder, G. (2017). Parametric optimization of biodiesel synthesis from rubber seed oil using iron doped carbon catalyst by Taguchi approach. *Renewable Energy*, *105*, 616–624. https://doi.org/10.1016/j.renene.2016.12.096

Dhawane, S. H., Karmakar, B., Ghosh, S., and Halder, G. (2018). Parametric optimisation of biodiesel synthesis from waste cooking oil via Taguchi approach. *Journal of Environmental Chemical Engineering*, *6*(4), 3971–3980. https://doi.org/10.1016/j.jece.2018.05.053

Erum, Z., Rehana, S., Mehwish, A. H., and Anjum, Y. (2014). Study of physicochemical properties of edible oil and evaluation of frying oil quality by Fourier Transform-Infrared (FT-IR) Spectroscopy. *Arabian Journal of Chemistry*, 3870–3876. https://doi.org/10.1016/j.arabjc.2014.05.025

Gashaw, A., and Teshita, A. (2014). International Journal of Renewable and Sustainable Energy Production of biodiesel from waste cooking oil and factors affecting its formation: A review. *International Journal of Renewable and Sustainable Energy*, *3*(5), 92–98. https://doi.org/10.11648/j.ijrse.20140305.12

Ho, D. P., Ngo, H. H., and Guo, W. (2014). A mini review on renewable sources for biofuel. *Bioresource Technology, 169*, 742-749.

Nasim, M. N., Pervez, M. S., Yarasu, R., and Lotia, N. (2014). Recycling waste automotive engine oil as alternative fuel for diesel engine: A Review. *Journal of Mechechanical and Civil Engineering*, 46-50.

Olutoye, M. A., and Hameed, B. H. (2016). Kinetics and deactivation of a dual-site heterogeneous oxide catalyst during the transesterification of crude jatropha oil with methanol. *Journal of Taibah University for Science*, *10*(5), 685-699.

Yusuff, A. S., Adeniyi, O. D., Olutoye, M. A., and Akpan, U. G. (2018). Development and Characterization of a Composite Anthill chicken Eggshell Catalyst for Biodiesel Production from Waste Frying Oil. *International Journal of Technology*, 1, 1-11

Zhang, Y., Dube, M. A., McLean, D., and Kates, M. (2003). Biodiesel production from waste cooking oil: 1. Process design and technological assessment. *Bioresource Technology, 89*(1), 1-16. doi:

Proceedings of the 49th NSChE Annual Conference
KADA 2019: pp 398-405

P2B-07: DESIGN AND DEVELOPMENT OF A NEW TECHNOLOGY TO MITIGATE PREVALENCE OF FUEL ADULTERATION IN NIGERIA

***Olotu O. O[1, 2], Haruna B.[1], Isehunwa S. O[2]**
[1] Project Design and Development, Federal Institute of Industrial Research, Oshodi (FIIRO)
P.M.B 21023, Ikeja, Lagos, Nigeria.
[2] Department of Petroleum Engineering, University of Ibadan. Oyo-State
***Corresponding author**: bisi_olusanya@yahoo.com, olotu.olabisi@fiiro.gov.ng,
+234-803-567-3267

ABSTRACT
With the increase in fuel demand and consumption but decrease in supply, an increase in the level of fuel adulteration has also been observed and confirmed in Nigeria. Lower priced adulterants are commonly added to our conventional fuel which contributes towards the increase in damages mostly on cars, generators, industrial machines, Human Health and some other electrical Gadget in the society. This paper ascertains fuel adulteration and introduces a prototype design of a new technology for real time detection of fuel from any source.

A survey was conducted by administration of a questionnaire given to each Respondent to complete in the 6 geopolitical zone of Nigeria in order to ascertain prevalence of fuel adulteration: North-Central (NC), South-East (SE), North-East (NE), South-South (SS), North-West (NW) and South-West (SW) From data, it was ascertained that the most significant items were as follows. 90% major fuel consumers are between the ages of 21-60 years. 86% of the respondent have experienced fuel Adulteration at one time or the other, 32% Civil Servant, 28% Professionals, 12%Students, 12% Businessmen. 10% Artisan, 10% Trader all spread across the 6-geopolitical zone of Nigeria. In the second section, 66% of Respondent are frequent users of Petrol, 8% uses Diesel more than Fuel, and 26% uses Kerosene more often. Adulteration of fuel is obvious in the survey, 16% experienced Adulteration on a daily basis, 76% every week, 8% monthly.78% has attempted to check for adulteration, 46 % of the adulterated fuel was bought from Road Vendor, 48% from Pump Station, 6% from Pipeline Vandals. A mathematical relation was developed and validated using response surface methodology. The model was simulated into a design of a portable and simple technology. Results of the model revealed that consumers prefer a new technology effective and simple enough to detect any form of adulteration.

Keywords: Prototype design, Petroleum Products, Adulteration, Modelling, New Technology

INTRODUCTION
Fuel adulteration problems have become increasingly rampant in recent times. It is a common knowledge that purity of fuel holds crucial significance mainly for automobile, power generation and engineering industries (2). In Nigeria, adulteration during production, through transportation, right up to the point of sale has become an acute problem.

The introduction of a foreign substance into motor spirit / high speed diesel, or kerosene illegally or unauthorized with the result that the product does not conform to the requirements and specifications of the product is called adulteration (4). The foreign substances are called

adulterants which when introduced alter and degrade the quality of the base transport fuels. Specific types of adulteration may be broadly classified as follows: Small amount of distillate fuels like diesel or kerosene into Petrol. Variable amount (as much as 30%) of hydrocarbons such as industrial solvents into Petrol. Waste industrial solvent such as used lubricants, which would be costly to dispose of in an environmentally approved manner into Petrol and diesel. A blend of kerosene into diesel, often as much as 20-30 percent. The use of such adulterants is not only affecting the quality of the conventional automobile fuels but also contribute towards environmental and health hazard. (1). The work aims at investigating and generate reliable mathematical model using the Physical Parameters sensitive enough to detect and determine an adulteration in fuel from any source.

MATERIALS AND METHODS

Population and Sampling

A survey was conducted in the 6 geopolitical zone of Nigeria which are North Central(NC), South East(SE), North East(NE), South South(SS), North West(NW), South West(SW) of Nigeria. The purpose of the survey was to analyze using Statistical package for the Social Sciences (SPSS) software and study the Effect of Adulteration of Conventional Fuel on the environment.

Data Collection

The most significant items are as follows. 90% major fuel consumers are between the age of 21-60 years. 86% of the respondent have experienced fuel Adulteration at one time or the other, 32% Civil Servant, 28% Professionals, 12%Students, 12% Businessmen. 10% Artisan, 10% Trader all spread across the 6-geopolitical zone of Nigeria.

In the second section, not surprisingly, 66% of Respondent are frequent users of Petrol, 8% uses Diesel more than Fuel, and 26% uses Kerosene more often. Adulteration of fuel is obvious in the survey, 16% experienced Adulteration on a daily basis, 76% every week, 8% monthly.78% has attempted to check for adulteration, 46% of the adulterated fuel was bought from Road Vendor, 48% from Pump Station, 6% from Pipeline Vandals. 90% of the respondent use physical examination to detect Adulteration, 74% of the 90% complained that the physical examination method is not effective enough, 88% needs a more Technical approach to detect Adulteration, 72% preferably wants a new technology with cost ranging between N2000-N10,000.

Model Development

According to Isehunwa and Falade (1993), any volumetric or thermodynamic property of a fluid may be expressed as:

$$f = f(P, T, X) \quad \text{----------(1)}$$

Where,

P= Pressure
T= Temperature
X=Composition

At atmospheric conditions, equation 1 can be reduced to:

$$f = f(T, X) \quad \text{----------(2)}$$

If we treat an adulterated petroleum product as a fluid mixture, Kay's mixing rule (Kay, 1936) may be applied at any fixed temperature:

$$A = \Sigma XiAi \text{----------(3)}$$

Where, A = Any physical property of the mixture component i.

Therefore, in an adulterated fluid system, the degree of adulteration can be expressed by Xi such that:

$$Xi = f(A/Ai) \text{ ----------(4)}$$

If we select some properties of the mixture (Ai) such as Specific gravity (SG) and/or Interfacial Tension (IFT), at any temperature, we have:

$$Xi = f(S.G, IFT)\text{----------(5)}$$

Equations 4 and 5 implies that the degree of adulteration in a mixture can be related to the physical properties of the pure fluid and the mixture.

RESULT AND DISCUSSION

Frequency of Adulteration: The figure 1 below shows the problem of Adulteration has become a global problem and the detail of its frequency is analyzed below that 16% of the respondent has a daily experience of adulteration of any one of the petroleum product sample, also 76% of the respondent has her own experience of adulteration weekly likewise very few about 8% has their own experience monthly

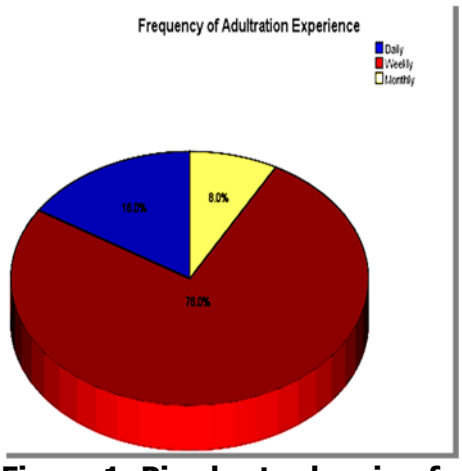

Figure 1: Pie charts showing frequency of Adulteration in the society

Desperation towards Adulteration Solution: The figure 2 shows that most of the respondent about 88% desire a quick intervention on resolving the problem of Adulteration, due

to the fact that the available methods are not readily available.

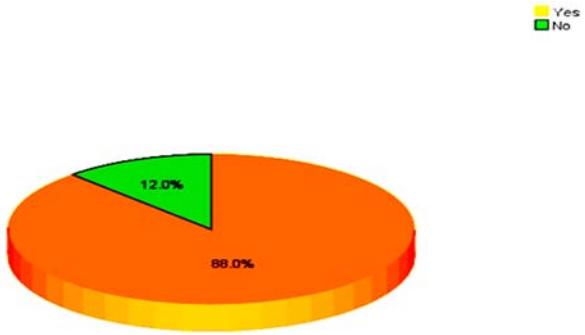

Figure 2: Pie Chart showing respondent is in need of Intervention

Type of Intervention needed: In figure 3 below it was observed that 72 % of the respondent desired a new but simple approach in form of a new technological innovation to tackle the problem of Adulteration.

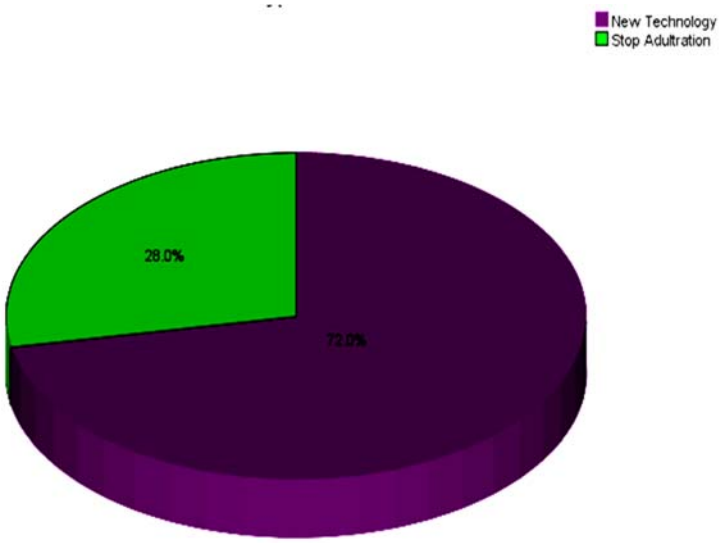

Figure 3: Pie Chart showing type of Intervention needed

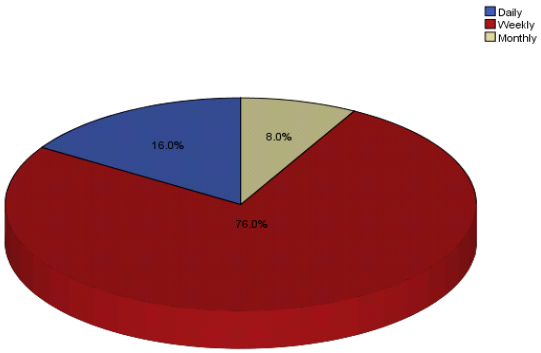

Figure 4: Pie Chart showing the frequency of how respondents have experienced Fuel Adulteration.

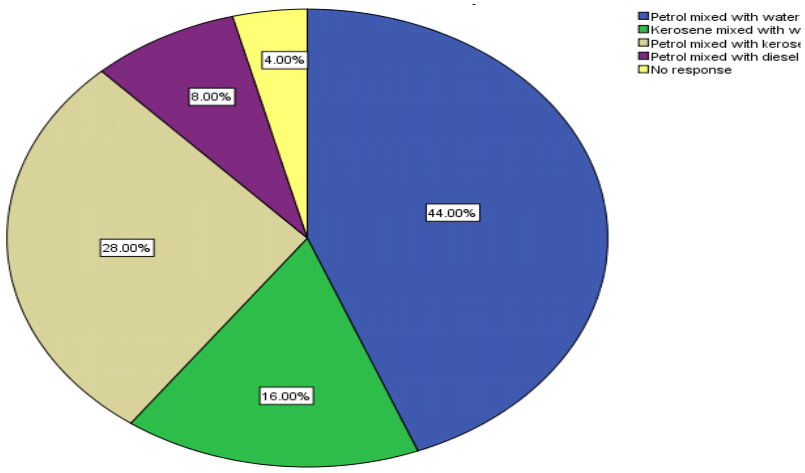

Figure 5: Shows the form of adulteration experienced by the respondent.

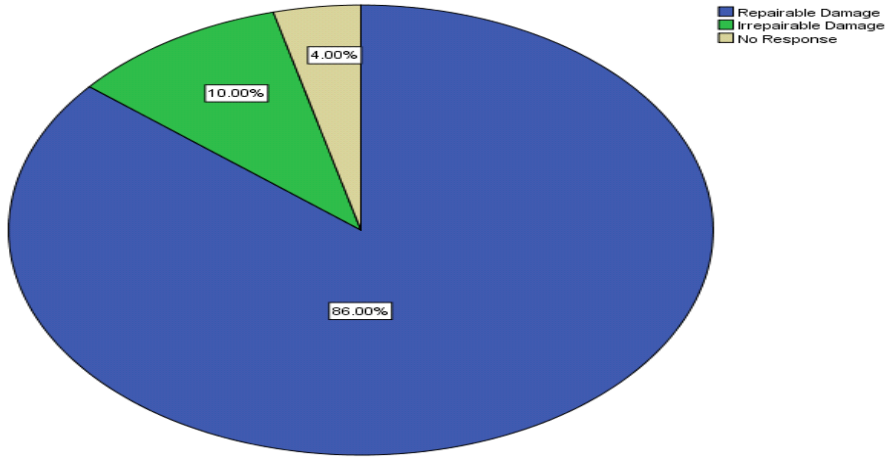

Figure 6: The pie chart showing the effect of damage resulting from fuel adulteration

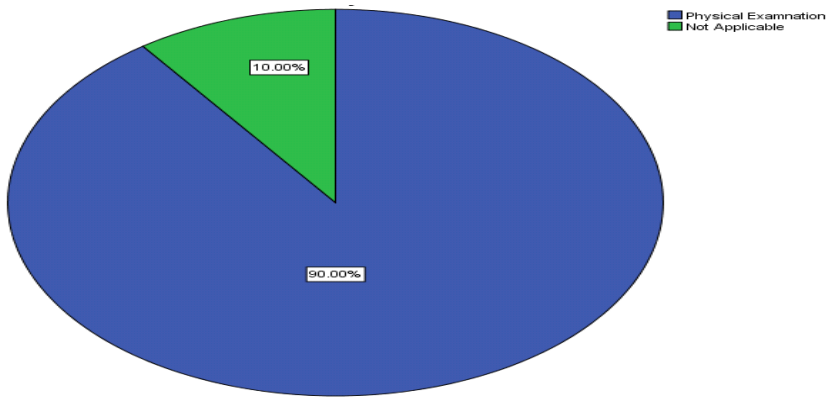

Figure 8: This Pie chart shows how respondent has been checking for Adulteration.

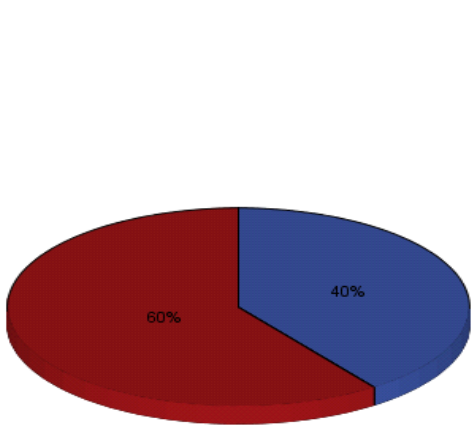

Figure 9: Pie Chart showing if respondents have been able to solve the problem of Fuel Adulteration.

Response Surface Methodology model (RSM)

The fitted second-order model for specific gravity from the experimental data using RSM can be expressed as:

$$Y(x) = b_0 + b_1X_1 + b_2\mathbf{X_2} - + b_3X_3 + b_{12}X_1X_2 + b_{13}X_1X_3 + b_{23}X_{23+} b_{123}X_{123}$$

where**:**

$Y_{RESPONSE\ (model2)} = SG_{Experiment}$

,

$X_{1=}$ Interfacial Tension,

X_2 =Temperature,

$X_{3=}$%Adulteration by Volume.

Table 1: $Y_{RESPONSE} = SG_{MODEL(A)}$ $X_{1=}$Interfacial Tension, X_2 =Temperature, $X_{3=}$%Adulteration by Volume

S/N	YRESPONSE	1	X1	X2	X3	X1X2X3	X12	X22	X32		ϵ(Truncation Error).
1	0.833	1	22.5	28	0	0	0	0	0	-	ϵ1
2	0.840	1	23.0	27	20	12420.0	529.0	729.0	400	b0	ϵ2
3	0.880	1	24.0	26	40	24960.0	576.0	676.0	1600	b1	ϵ3
4	0.903	1	24.0	25	60	36000.0	576.0	625.0	3600	b2	ϵ4
5	0.908	1	24.6	24	50	29420.0	605.16	576.0	2500	b12	ϵ5
6	1.020	1	25.5	23	80	46920.0	650.25	529.0	6400	b22	ϵ6
7	1.000	1	22.0	22	100	48400.0	484.0	484.0	10000	-	ϵ7

Table 2: Descriptive model Summary using Response Surface Methodology (RSM)

	b_0	b_1	b_2	b_3	b_{12}	b_{13}	b_{23}	b_{123}
MODEL A	1.005	1.040	1.050	1.020	1.080	-1.060	0.902	-0.001
MODEL B	1.000	-1.000	-1.050	-1.000	-1.020	1.040	-1.047	0.001
MODEL C	1.000.	-0.900	0.900	1.080	-1.070	-1.000	1.070	-0.001
MODEL D	1.050	-1.080	1.040	-1.200	-1.200	-1.020	1.080	-0.001
MODEL E	1.030	-0.990	1.050	1.050	-0.100	-1.130	1.200	-0.001
MODEL F	1.030	-1.030	1.000	-1.050	-1.050	-1.070	1.100	-0.003

CONCEPTUAL DESIGN IN TWO AND THREE DIMENSIONAL AUTOCAD DRAWINGS.

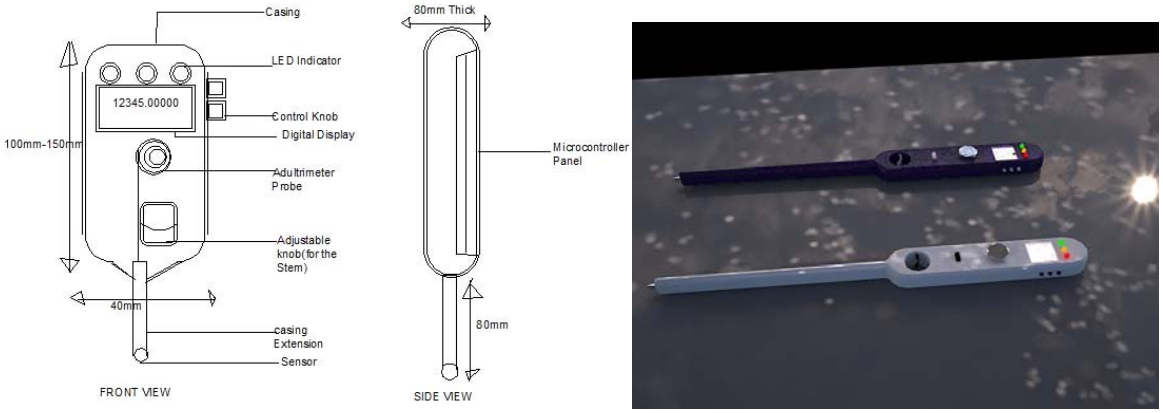

Figure 1: 2 and 3 Dimensional Design and Isometric View

CONCLUSION

The challenges posed by adulteration of fuel in Nigeria was investigated by carrying out a survey in the 6 geopolitical zones in the country. Results from the survey indicated that majority of respondents in the society prefers a new, simple and readily available technology effective enough to detect any form of adulteration. Based on the results of the survey, a mathematical model was developed, simulated into a design of a new technology. Results and analysis, showed the sensitivity of the new technology, which detected adulteration between 20 - 40% concentration by volume of contamination.

References

Cuckow, F.W. A new method of high accuracy for the calibration of reference standard hydrometers, MWG7, Workshop on Hydrometers Querétaro, (México) 2006, 68, 44–49.

Gupta, R. K.; Sharma, A new method for estimation of automobile fuel adulteration, Vanda Villainy (Ed.), Intec Publishers, 2010,40, 357-370.

Isehunwa, S. O. and Falade, G. K. (1993). A Type Curve Approach to Quantitative Description of Reservoir Fluids. Paper SPENC 9309, Proceedingss of the 17th Annual Conference of the Society of Petroleum Engineers, Warri, Nigeria. Pp 91-97.

Lorefice, S.; Heinonen, M.; Madec. Bilateral comparisons of hydrometer calibrations between the IMGC-LNE and the IMGC-MIKES. Metro logia 2000, 37, doi:10.1088/0026-1394/37/2/6.

Murty, B.S,; Rao, R.N Global optimization for prediction of blend composition of gasolines of desired octane number and properties, Fuel Processing Technology, 85, 2004, 1595-1602.

Nikkos, P. G. Vasilis, Octane number prediction for gasoline blends, Fuel Processing Technology, 87(6), 2006, 505–509.

Peña, L.M.; Pedraza, J.C.; Becerra, L.O.; Galvan, C.A. A New Image Processing System for Hydrometers Calibration Developed at CENAM. In Proceedingss of the 20th TC3, 3rd TC16 and 1st TC22 International Conference, Cultivating Metrological Knowledge (IMEKO), Mérida, Yucatan, México, 27 November 2007.

Roy. S, Fiber optic sensor for determining adulteration of petrol and diesel by kerosene, Sensors and Actuator, 55, 1999, 212–216.

Proceedings of the 49th NSChE Annual Conference
KADA 2019: pp 406-418

P2C-01: TACKLING THE UNEMPLOYMENT 'SAGA' OF THE YOUNG CHEMICAL ENGINEERS – THE ROLE OF COST ENGINEERING PROFESSIONAL CERTIFICATIONS

Johnson Awoyomi
Engineering and Technology Division, NNPC, Abuja

ABSTRACT
Unemployment of the young professionals such as chemical engineers continue to be a source of great concerns to all meaningful Nigerians – especially the parents who have sweated to train their wards in higher education. Government and private sector are also not left out in the fight against the unemployment. This paper will showcase the massive opportunities that exist in Cost Engineering Professional Certifications to our young and up-coming chemical engineers. According to the Association for the Advancement of Cost Engineering (AACE) International, Cost Engineering is the area of engineering practice where engineering judgment and experience are utilized in the application of scientific principles and techniques to problems of Cost estimating, Cost control, Profitability analysis, Project management and Planning and scheduling. Cost Engineering is the art and science of Total Cost Management. It is a very important tool for project management in the successful delivery of their capital project/programs – on schedule, within budget and at the right quality. Currently, in Nigeria and abroad, there is a great demand for certified cost professionals – certified estimating professional, certified cost engineers, planning and scheduling professional, etc. Out of the over 4,000 AACE Certified Cost Professionals in the globe, less than 40 are Nigerians. This is a clarion call to all the young chemical engineers to consider a professional certification in Cost Engineering. The benefits of earning the cost engineering professional certifications are many and include the following: is a proof you are worth more, enhances your professional image, leads to more career opportunities, demonstrates initiative and it improves your skill and knowledge.

INTRODUCTION
Unemployment of the young professionals such as chemical engineers continue to be a source of great concerns to all meaningful Nigerians – especially the parents who have sweated to train their wards in higher education. Government and private sector are also not left out in the fight against the unemployment. The benefits of earning an AACE Certifications in the following:

- Is a proof you are worth more: Individuals holding AACE certification earn on average USD 15,000 more than the non-certified individuals with the same amount of work related experience
- Enhances your professional image: Having AACE Certification helps you stand out in the crowd. It helps you showcase your expertise – that you can provide resolutions to your company and your clients and that you can successfully complete a project
- Leads to more career opportunities: being able to prove your mastery of specific skills require d to earn an AACE certification will open your professional door for a greater number of career opportunities
- Demonstrate initiative: Earning AACE certifications will show your employer and your clients that you have the leadership initiative to invest in your professional stature. If you can invest in yourself, it demonstrates you will invest your best efforts for your company and clients.

- Improves your skill and knowledge: Holding an AACE certification means you have to maintain your credentials to stay up to date with industry best practices, learn through continuing education, and adhere to the AACE Canons of Ethics throughout the recertification process

DEFINITION OF COST ENGINEERING

Another word for Cost Engineering is "Project Controls. Project Controls is that Element of a Project that keeps it on-Track, On-Time and Within Budget and can be responsible for projects, programs, or portfolios that contribute to the company's bottom-line (AACE International).
According to Bechtel Incorporation; Cost Engineering is a critical Bechtel function that provides a behind-the-scene- view of projects evolutions as well as exposure to both the technical and business aspects of engineering construction (AACE Int 2015 Annual Meeting).

KEY ELEMENTS OF COST ENGINEERING

The key elements of Cost Engineering are Cost Engineering and Cost Controls, Cost estimating and Planning and Scheduling as depicted in Figure 1.

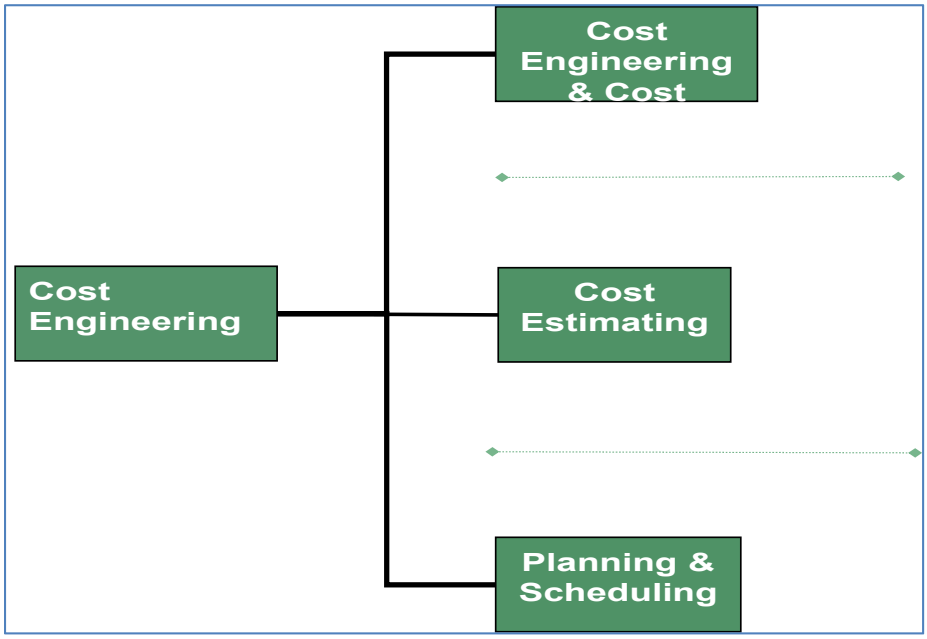

Figure 1: Key Elements of Cost Engineering

Good capital management efficiency and cost control occur when we abide by the principle of what is in the Figure 2.

The Cost Engineering and Cost Control deals with cost control side of cost engineering and is very key because no matter how reliable and competitive your estimate (cost and schedule are), without emplacing robust cost monitoring and control, you have your budget ballooned and overrun in no time and the project get bankrupt. Cost Control will minimize the impact of changes to the base scope and budget and schedule thus helping your project to e successful. The elements of cost control are as in Figure 3.

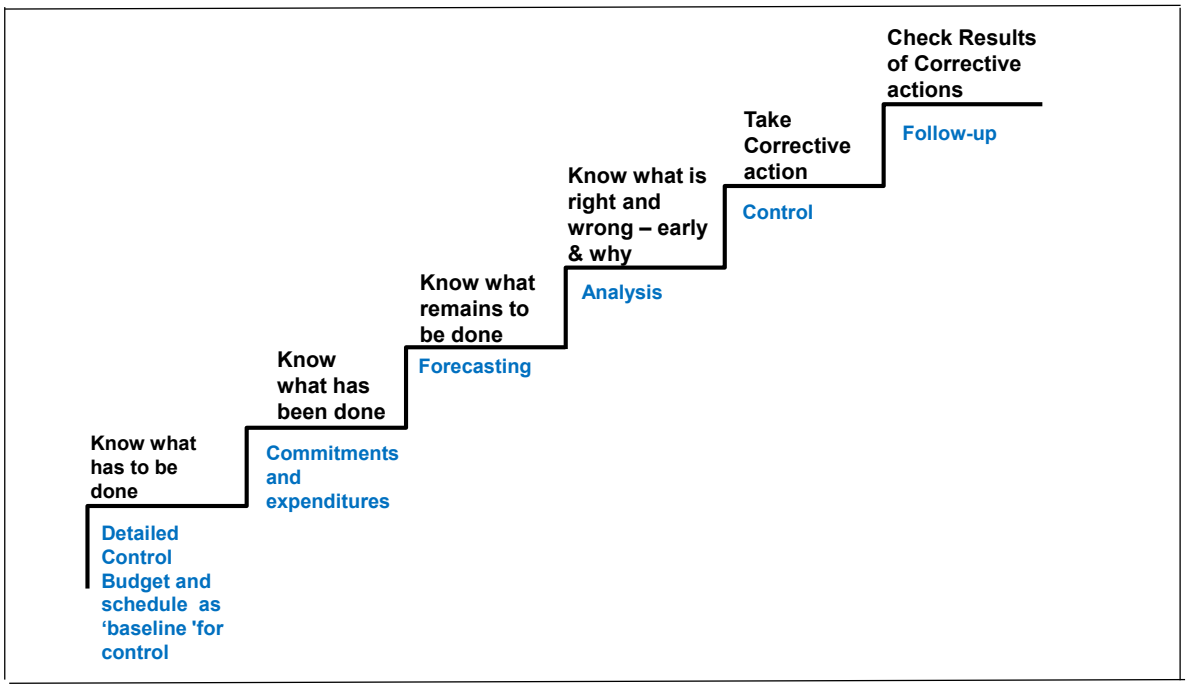

Figure 2: Elements of Good Cost Control

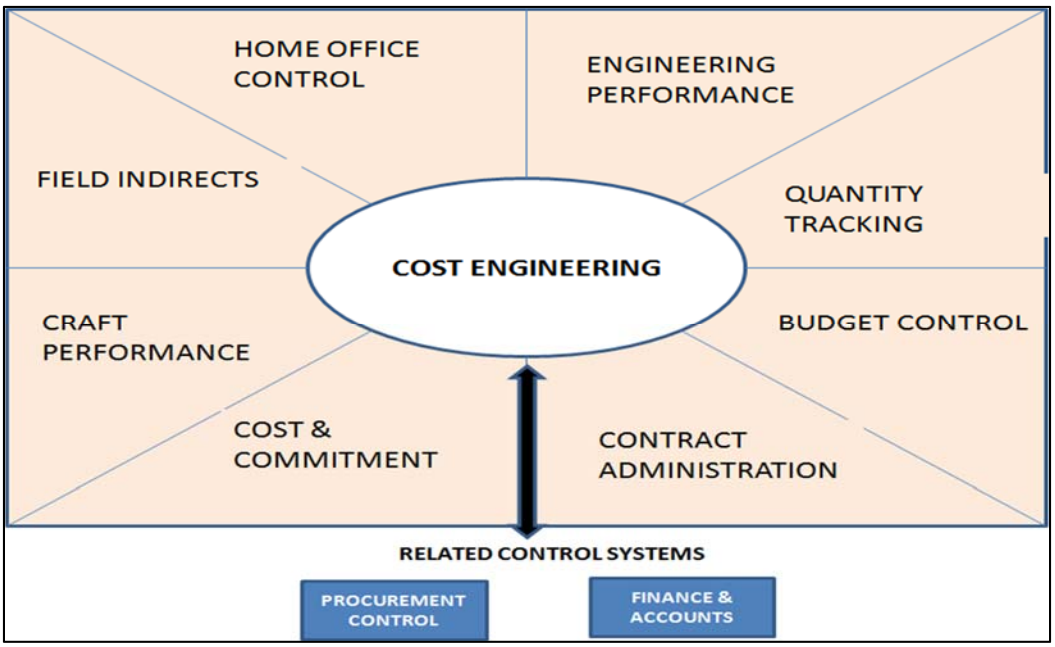

Figure 3: Cost Engineering and Cost Control Modules

There are techniques of controlling project costs (which is outside the scope of this paper). Cost control entails – what to control, methods to be deployed to control and who and how to control. In order to ensure proper control of project cost and schedule it is imperative that a cost engineering professional is assigned on to the project – both from owners' side as well as contractors' side.

From experience, a lot of resources are expended during the planning phase of the projects but alas, very little attentions are devoted to proper execution of the propjets in terms of emplacing proper project controls. One quickest gap you notice is lack of Cost Engineering Professionals on the project and thus, regular project monitoring, progress reporting and cost controls are thrown to fate and emotions. In fact most contracts' Invitation To Bid (ITB) have no detailed/ specific scope for Cost Engineering.

Therefore, it is recommended that in order to have full cost engineering requirements emplaced in the tendering documents, the inclusion Cost Engineering Requirements inside the ITB Docs should be effected in such a way that (see Figure 4):

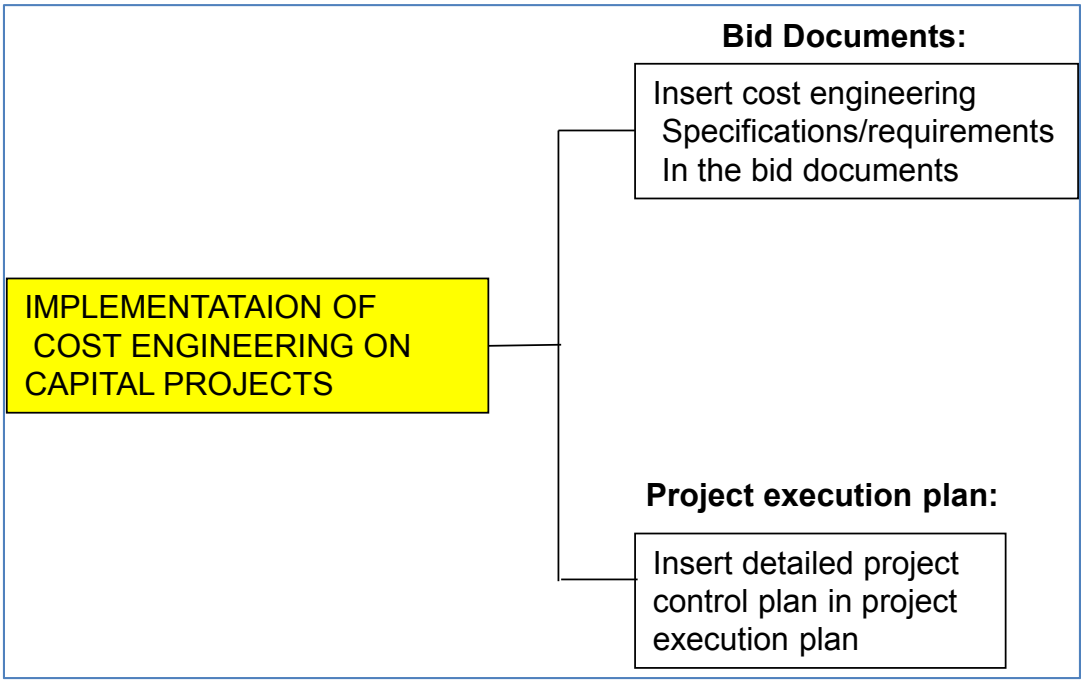

Figure 4: Inclusion Cost Requirements inside Tendering Documents

Cost Estimating.

Estimating refers to both the money required for the project execution and the length of time (days, weeks, months or years) that the project will take to finish from start. The reliability and the believability of these estimates go a long way to determine how successful the project in question will be. Sometime ago, I was directed to review a variation on a project that grew to over 400% of the awarded budget and in the course of my diagnosis/analysis, it was noted that the estimate right from the planning stage was wrong – as it was neither validated nor benchmarked. If your capital project must succeeded, you must deploy project control best practices of reviewing, validating and benchmarking your estimates (money and time) prior to sanctioning.

One thing we are all sure of is that estimate will be wrong because is an estimate and is never a figure but a range, a probability distribution with contingency. AACE International defined a cost estimate as a compilation of all the probable costs of the elements of a project or effort included *within an agreed upon scope*. The key word here is 'an agreed scope'. Without an agreed scope of work, the estimate is baseless. Cost Estimate is a prediction of quantities, cost, and/or price of

resources required by the scope of an asset investment option, activity, or project. Larry Dyssert during the 2018 AACE International Annual meeting in San Diego, USA recommended a revised definition of an estimate to include the location element – by defining a cost estimate as the prediction of the probable costs of a project, for a given and documented scope, to be completed at a *defined location and point of time in the future*.

AACE International Classification of Cost Estimate

It should be noted that as a prediction, an estimate must address risks and uncertainties. An estimate predicts what a project will cost, not what it should cost. For every project phase, there is a corresponding estimate class premised on the project definition level. By AACE International Classification standards, there are five Classes of Cost estimate as shown in Figure 5.

	Primary Characteristic	*Secondary Characteristic*				
ESTIMATE CLASS	**LEVEL OF PROJECT DEFINITION** Expressed as % of complete definition	**END USAGE** Typical purpose of estimate	**METHODOLOGY** Typical estimating method	**EXPECTED ACCURACY RANGE** Typical +/- range relative to best index of 1 [a]	**PREPARATION EFFORT** Typical degree of effort relative to least cost index of 1 [b]	
Class 5	0% to 2%	Screening or Feasibility	Stochastic or Judgment	4 to 20	1	**Owner Only**
Class 4	1% to 15%	Concept Study or Feasibility	Primarily Stochastic	3 to 12	2 to 4	**Owner Only**
Class 3	10% to 40%	Budget, Authorization, or Control	Mixed, but Primarily Stochastic	2 to 6	3 to 10	**Owner/FEED Contractor**
Class 2	30% to 70%	Control or Bid/ Tender	Primarily Deterministic	1 to 3	5 to 20	**Owner/ Contractor**
Class 1	50% to 100%	Check Estimate or Bid/Tender	Deterministic	1	10 to 100	**Contractor Only**

Figure 5: AACE Cost Estimate Classification (Source: AACE International)

a) Class 5 -screen estimate
b) Class 4 - conceptual
c) Class 3 - Budget Estimate
d) Class 2 - Control or Bid/Tender Estimate and
e) Class 1 - Check Estimate.

The primary criterion to classify a cost estimate is the level of project definition – usually given as the percentage of Engineering design completed as at the time the estimate is being prepared. Another classification of cost estimates and their uses are shown in the Figure 6

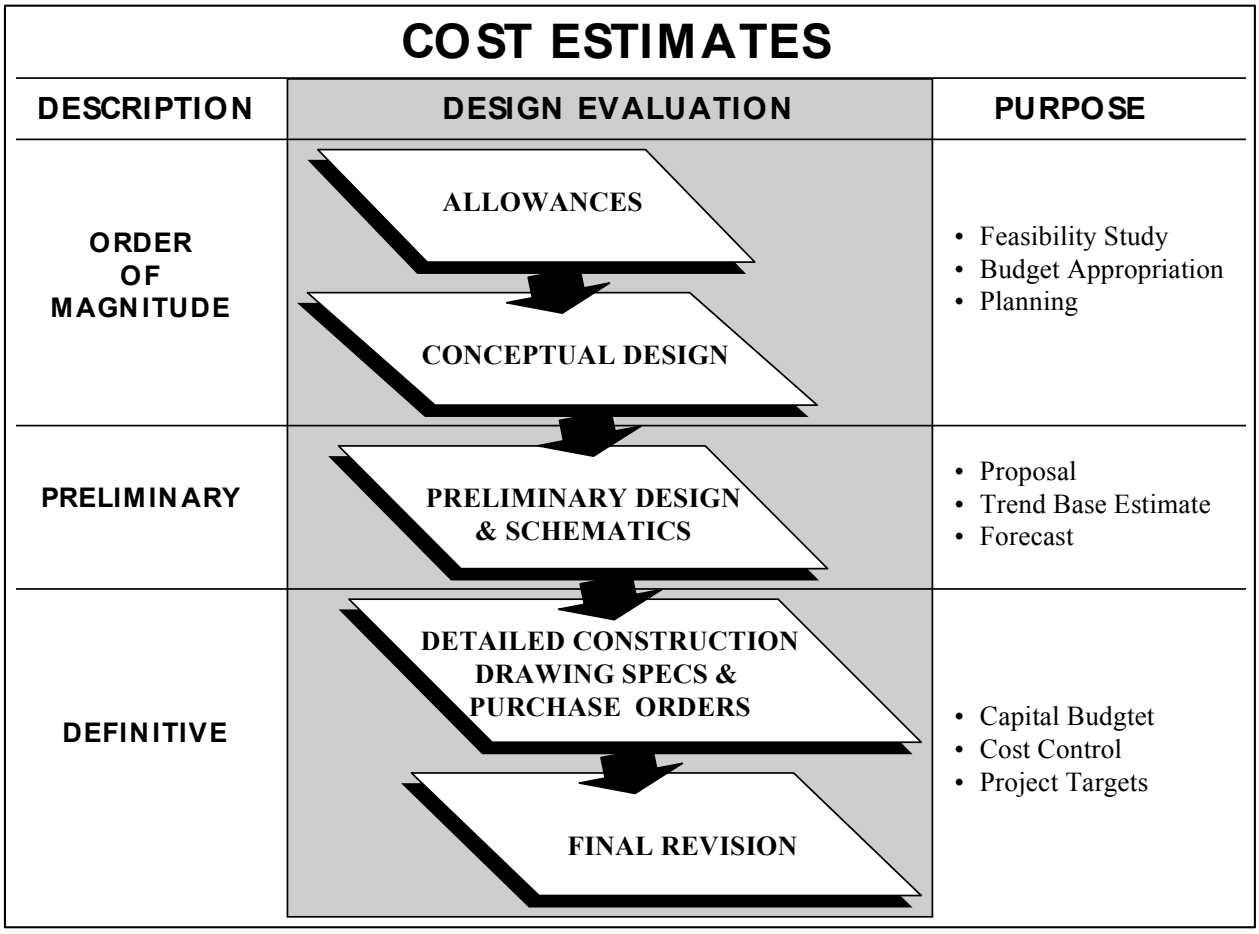

Figure 6: Type of cost Estimates

Planning and Scheduling:

Without proper planning and scheduling, no success can be achieved on any project. Planning defines all the project activities and links the activities into a network structure to show interdependencies. Scheduling takes the plan and assigns dates on which each activity will be performed. The Critical path method (CPM) technique uses a network schedule to determine the activities that combine to make a "critical path" such that if one activity on the critical path slips, the project end date will slip. A resource loaded critical path schedule should be developed prior to full funding of a project. The actual schedule during the execution phase of the project should be compared to the target schedule, and corrective actions should be taken on an ongoing basis - through regularly schedule review meeting. There are various level of schedules based on the kind of information that a stakeholders requires as shown in Figure 7

a) Level I: Milestone / Executive Master Summary schedule/ One-pager, time scaled bar chart
b) Level II: Contract Master / Detailed Integrated schedule CPM to plan, implement and control overall project.
c) Level III: Area Master / Contract schedules Subcontract / phased / element CPM schedules
d) Level IV: Control / 2-3 Week Look-Ahead schedules, Spreadsheets / Bar Chart field plans
e) Level V: Daily / Hourly Work schedules, Field supervision planning and execution listings

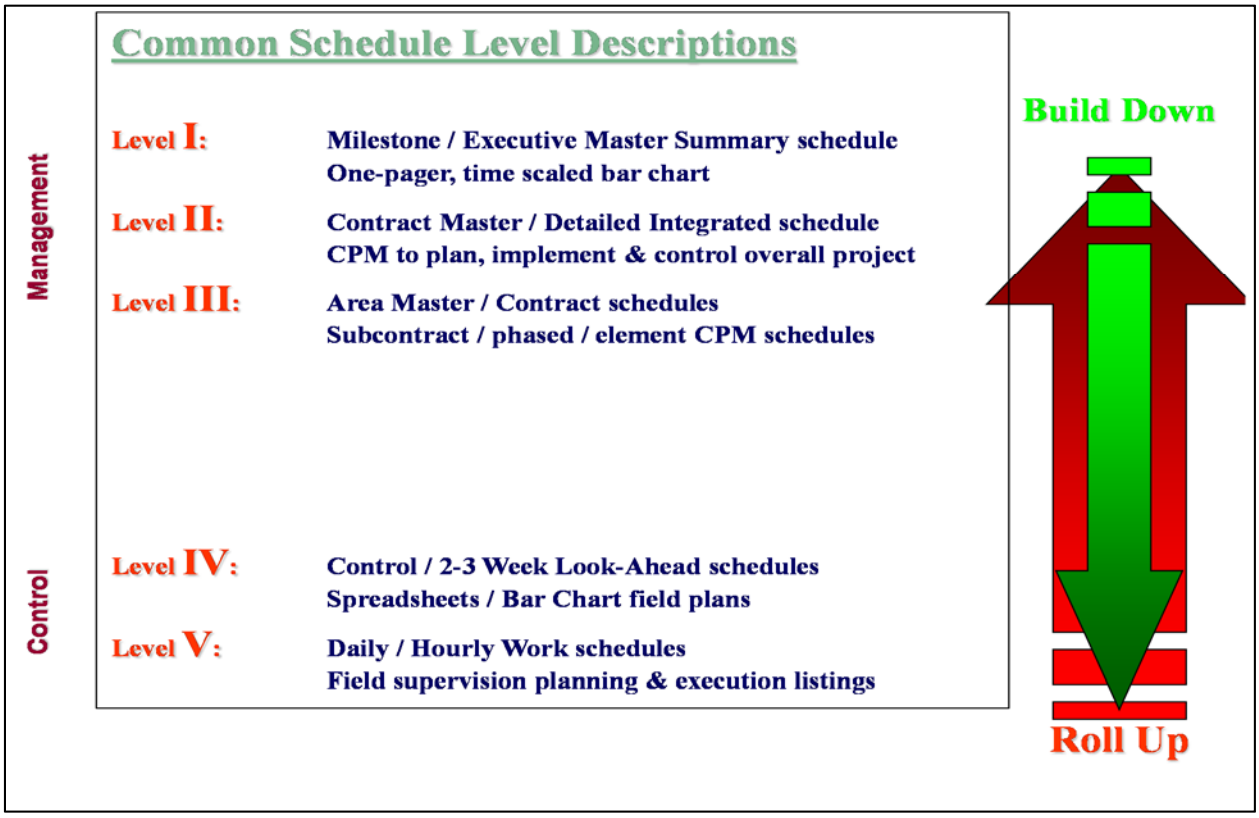

Figure 7: Level of Schedule

THE AACE'S TOTAL COST MANAGEMENT (TCM) CONCEPT

TCM is a process for applying the skills and knowledge of cost engineering [1]. It is the effective application of professional and technical expertise to plan and control resources, costs, profitability and risks. Simply stated, it is a systematic approach to managing cost throughout the life cycle of any enterprise, program, facility, project, product, or service. This is accomplished through the application of cost engineering and cost management principles, proven methodologies and the latest technology in support of the management process.

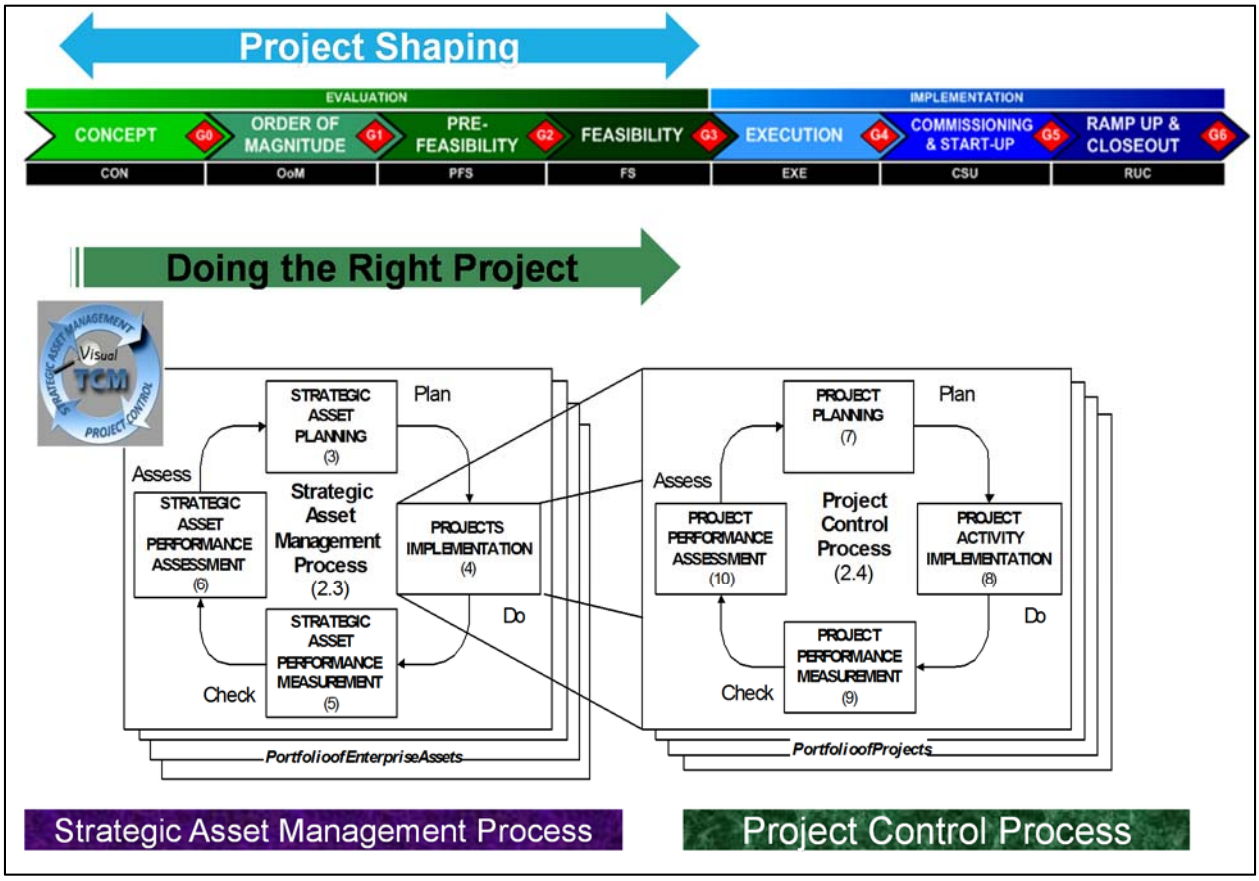

Figure 8: Total Cost Management Framework (Source: AACE International)

TCM ties all the Cost Engineering skills and knowledge areas together into a single process and it establishes Cost Engineering as a unique discipline that supports business and project management alike. For Business, TCM is an Integrated Recipe for Managing Portfolios, Programs, and Projects in Alignment with Business Strategy! TCM Combines Asset and Project Life Cycle Management and afford both the owners and contractors a good understanding on how to manage and control the costs of their projects over the entire project life cycle.

The Value of the TCM Framework for Industry

TCM provides a strategic model that can help an organization design its own processes related to cost management. For individuals, the *TCM Framework* provides a "map" to help them understand all the practice areas while also helping guide their career planning. In the academic arena, the *TCM Framework* provides a model for developing cost engineering education and training products and curricula that will serve those individuals and enterprises in need of a broader, more integrated perspective.

CAREER PATHS IN COST ENGINEERING

The list of AACE International Certifications that anyone interested in progressing his/her career are can go for are as listed in Tale 1. It is recommended that anyone interested in any of the AACE Certification should endeavor to access the AACE official website – (www.aacei.org) to confirm recent requirements and fees chargeable.

Table 1: Career Paths in Cost Engineering

S/N	AACE Certification	Status	Requirements
1	Certified Cost Technician (CCT)	Junior	First degree
2	Certified Schedule Technician (CST).	Junior	First degree
3	Certified Cost Professional (CCP)	Professional	Min of 4 Years' experience after graduation
4	Certified Estimating Professional (CEP)	Professional	Min of 4 Years' experience after graduation
5	Planning and Scheduling professional (PSP)	Professional	Min of 4 Years' experience after graduation
6	Certified Forensic Claims Consultant (CFCC),	Advanced	Min of 4 Years' experience after graduation
7	Earned Value Professional (EVP)	Professional	Min of 4 Years' experience after graduation
8	Decision Risk and Management Professional	Advanced	Min of 4 Years' experience after graduation
9	Etc.		

Nigerian AACE Certificants Versus Global Certificants

Globally today, there are so many engineers – chemical, electrical, civil, structural etc but there are very few certified cost engineers. As at the time of writing this paper by AACE standards there are just about 4,200 AACE certified cost professionals all over the globe out of which 32 are Nigerians as shown in Table 2 - Certified cost engineering professionals (www.aacei.org).

Table 2: List of current AACE Certificants globally (source: www.aacei.org)

NIGERIA AACE INT. ACTIVE CERTIFICANTS		
Description	Global	Nigeria
Certifed Cost Technicians (CCT)	201	1
Certified Schedule Technician (CST)	125	0
Certified Cost Professionals (CCP)	1,756	21
Planning and Schedulig Professional) (PSP)	1,269	3
Certifed Estimating Professional (CEP)	322	5
Earned Value Professional (EVP)	443	2
Decision and Risk Management Professional (DRMP)	22	0
Certified Forensic Claims Consultnt (CFCC)	73	0
OVERALL	4,211	32
Percentage of the Nigerian Certified Cost Professionals by AACE International is less than 1%	0.76%	
Souces: AACE Internationa website @ July 2019		

Without doing too much analysis less than 1% of the AACE Global certififcants are Nigerians. Could this explain why 'costs are really our issues and not technical'? What Table 2 is showing is that developing economy like Nigeria is full of opportunities for aspired and would-be AACE International cost professionals. The list of the opportunities are listed in the Table 3.

Table 3: List Opportunities as Certified Cost Professionals

S/N	Career Opportunity	Roles
1	Cost Engineer	Works with various disciplines and functional areas to capture and record all relevant costs Considers historical records and current trends to establish reliable cost forecasts
2	Cost Estimator	During conceptual stages, prepares initial estimates for project sanction; Works with Cost Controller to formulate a project budget Validates or produces cost estimates for changes to the project scope
3	Planner/Scheduler	Works with Project Manager and disciplines to create a work breakdown structure (WBS) Sequences project work activities and monitors critical and sub-critical activities
4	Claims analysts	Investigate facts and circumstance surrounding disputes
5	Project risk analysts	Often use detailed tools and analysis to conduct scenario analysis and probabilistic modeling of cost and schedule
6	Project Controls Manager (Supervisor)	Oversees the actions of assigned cost engineers, estimators, and planners/schedulers Anticipates changes to keep the project on schedule and within budget Serves as the project's overall commercial advisor and works hand-in-hand with the Project Manager to ensure accomplishment of cost, time, and quality considerations
7	Project Manager	Responsible for the success of the project. A good cost engineering professional will grow to become an excellent Project Manager
8	Etc	

COST ENGINEERING CERTIFICATIONS AND BENEFITS OF THE CERTIFICATION? (www.aacei.org)

The intent of the AACE International certification is to recognize specialists who meet a demanding set of criteria by a rigorous examination, experience, education and ethical qualifications. For ease of AACE Certifications entry, there are 2 levels – Junior entry levels and Professional driven by level of experience as at the time the candidate is applying for certification:

Why should you become a Certified Cost Professional (Certified Cost Engineer, Certified Estimating professional, Planning and Scheduling Professional ,Etc)?

Professional Certification is and is an investment in your career. In today's world of intense competition in the workplace, total cost management is the concern of all businesses and companies. It is therefore, essential to have employees that are proficient in the principles and practices of total cost management. Certification is a verification of that proficiency. It provides assurance that the person performing the work is qualified and up-to-date on the latest skills and techniques and has the experience and knowledge to apply them [AACE International].

Some of the benefits for people seeking to get certified include the following:

- Confirm your skills are current
- Demonstrates initiative
- Enhances your professional image
- Improves skills and knowledge
- Leads to more career opportunities
- Helps you master key industry competences
- Grants you professional credentials
- Means greater earning potentials

How to get certified?

The AACE certification program encompasses specialties in cost estimating, project controls, planning and scheduling, earned value, and other related cost management disciplines. The initial certifications, the Certified Cost Professional (CCP) cover all areas of total cost management and require 8 full years of relevant experience or 4 Years if is a degree holder. The Certified Cost Technician (CCT and CST) covers the fundamentals and basic skills and knowledge, and requires 4 full years of relevant experience or a first degree qualification. The CCT/CST provides junior-level cost engineering professionals with the opportunity to attain recognition in the industry prior to possessing the minimum 8 years of related professional experience or 4 years if having a degree required to become fully certified [www.aacei.org].

Cost Engineering and Project Management

According to the AACE International, "Engineers" are always responsible for creating functional things that is strategic assets as we call them in TCM such as designs of a refinery, bridge, high rise building, develop software, etc But beyond the physical dimension of design (e.g., the refinery, bridge structure), there are other important dimensions *of money, time and other resources that* are invested in the creation of the designed asset. This is what cost professionals get concerned about. Using the above illustration, the job of a cost professional can be illustrated better as per the Figures 2.4a, 2.4b and 2.4c.

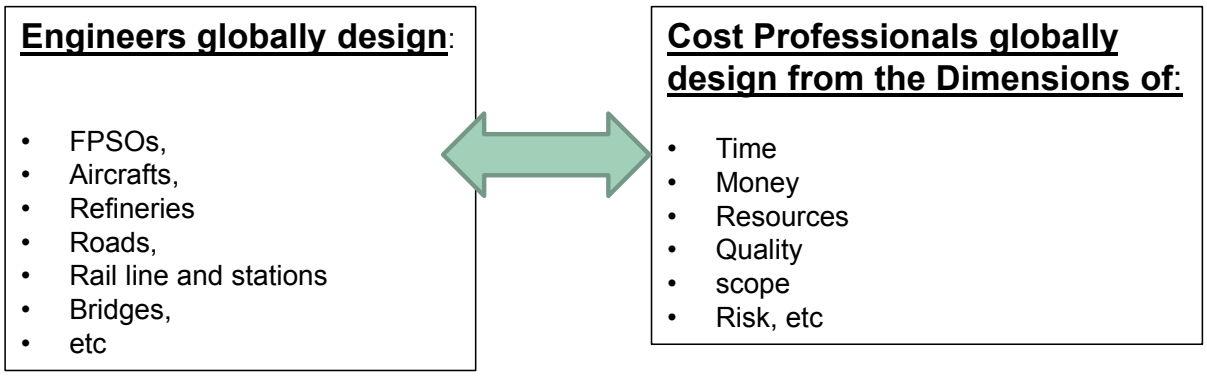

Figure 2.4a: What Does a Cost Engineer do?

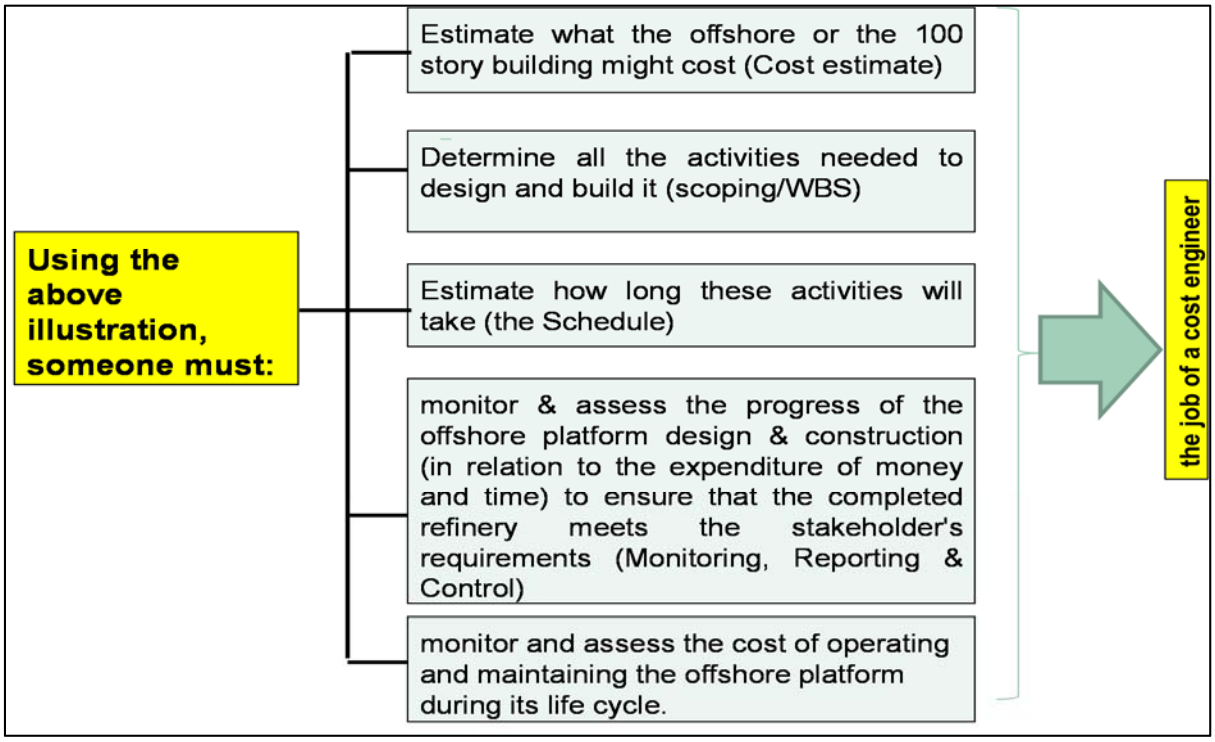

Figure 2.4b: What Does a Cost Engineer do?

Other typical roles of a cost professional include but not limited to:

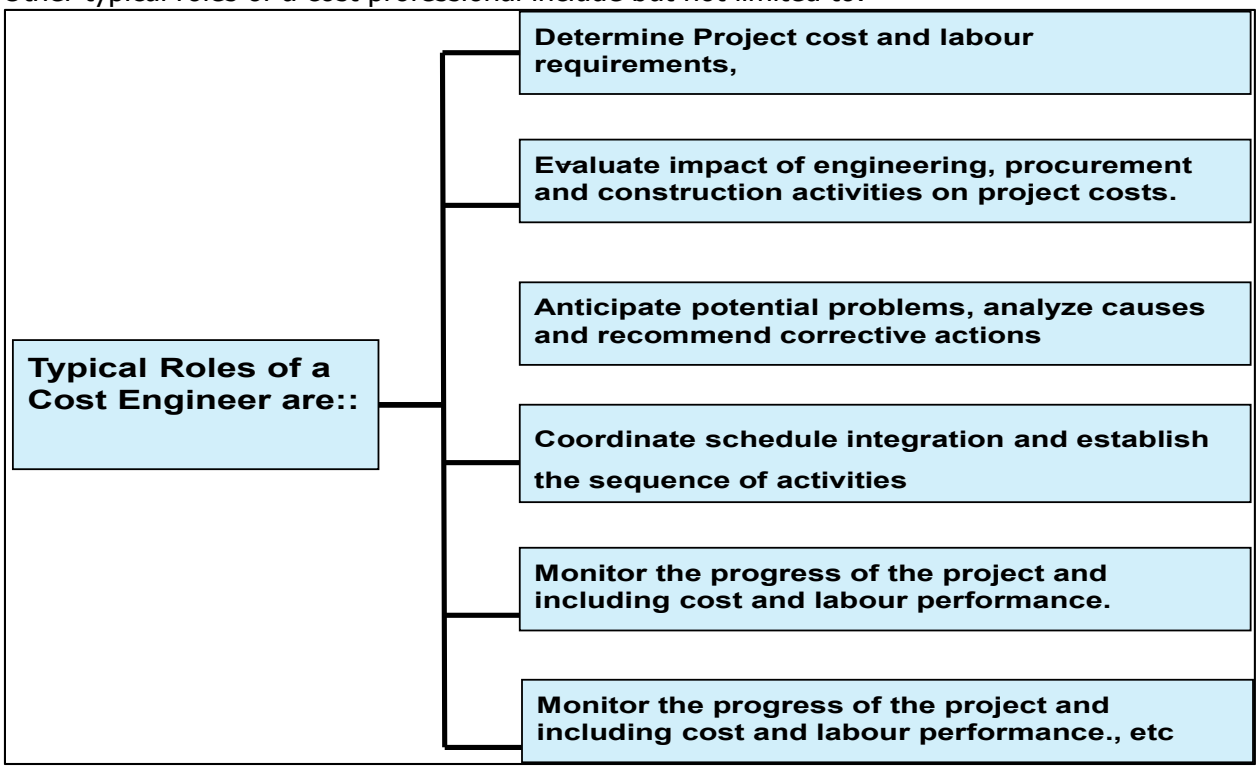

Figure 2.4c: What Does a Cost professional do?

CONCLUSION

By this paper, it is hoped that the appetites of our young chemical engineers present here today have been wetted for them to take the abundant opportunities that are lying fallow through the Cost engineering professional certifications. Better opportunities pay, exposures, etc exist both onshore and offshore for certified cost professionals. The few Nigerian certified cost professionals are on daily basis being bombarded with lots of offshore job offers. It is never too late to get certified!! One man says 'the thing' will start when you start 'the thing'.

References

Hollmann, John K. (editor), Total Cost Management Framework, AACE International, Morgantown, WV, 2006.

AACE International - The Association for the Advancement of Cost Engineering. (2012). Total Cost Management Framework (First Edition, Revised ed.). (P. C. John K. Hollmann, Ed.) Morgantown, WV: AACE® International.

U.S. GAO, United States Government Accountability Office;. (March 2009). GAO-09-3SP, Cost Estimating and Assessment Guide: Best Practices for Developing and Managing Capital Program Costs. Washington, DC: Govt. Accountability Office

AACE International - The Association for the Advancement of Cost Engineering. (2009). AACE Recommended Practice 10S-90, Cost Engineering Terminology. Morgantown, WV: AACE® International

AACE International - The Association for the Advancement of Cost Engineering. (Revised November, 2011). AACE International Recommended Practice No. 17R-97, Cost Estimate Classification System

(Revised November 29, 2011 ed.). Morgantown, WV: AACE® International.

Proceedings of the 49th NSChE Annual Conference
KADA 2019: pp 419-426

P2C-02: STUDENTS' PERFORMANCE AT FOUNDATION LEVEL AS A PREDICTOR OF ACADEMIC SUCCESS

Dabai F.N.*, Galadima M.S. and Jibril B.Y.
Chemical Engineering Department, Ahmadu Bello University, Zaria, Nigeria
***Corresponding author**: email address: fndabai@abu.edu.ng, +2348168706410

ABSTRACT
Engineering curricula designs are based on the belief of a strong relationship between the level of knowledge of foundation level courses and academic success. This study aims at substantiating such belief; using the students Cumulative Grade Point Average-CGPA at the end of 100 level (as an indicator of knowledge of foundation courses) and CGPA at the end of 500 level (as an indicator of academic success). The study used students' data from 2002 to 2018 at the Chemical Engineering Department of Ahmadu Bello University, Zaria, Nigeria. There were strong correlations (average R^2=0.7639) between CGPA at 100 level and at 500 level. This supports the supposition that indication of early abilities in mathematics and sciences may suggest high level of acquisition of the expected learning outcomes of Chemical Engineering, by the time of graduation. The initial and final CPGA(s) for students, who gained 'direct entry' at 200 level, were also investigated to have a comparative study between students who had basic knowledge of science and mathematics, and were admitted into 100 level, and those who had some extra tuition to prepare them for specific courses at 200 level. The study showed that there is no significant difference in the performance of the two different groups of students. Nevertheless, the findings suggest that engineering educators should pay more attention to the foundation levels courses as success at foundation level seems to predict final academic success.

Keywords: Academic success, Foundation level, CGPA, Chemical Engineering Education.

1.0 Introduction
Undergraduate Engineering curricula are biased to mathematics and science courses, especially at the foundation level. This is because engineering educators consider students' abilities to know, understand and apply mathematics and sciences, as strong indicators of attaining the learning outcomes. There are several studies that have attempted to substantiate the supposition of the direct relationship between students' performance at the foundation level and the final level academic successes (Murtaugh *et al.* (1999), Thomas *et al.* (2009), Tumen *et al.* (2008), Stinebrickner and Stinebrickner (2013)). There have also been studies that have attempted to relate students' final performance to other factors, such as prior knowledge, classroom attendance, success in specific foundation subjects/modules, gender, and personal factors, such as financial or accommodation issues (Lee *et al.* (2008), Kauffman *et al.* (2018), Murdoch-Eaton *et al.* (2007), Alfan and Othman (2005), Roy and Chadalawada (2014), Dewhurst *et al.* (2016)).

This study is focused on exploring the relation between the performance at the foundation level and the final performance (academic success) of students; using students of the Chemical Engineering Department of Ahmadu Bello University, Zaria, Nigeria, as the case study.

2.0 Methodology

In this study, students' data from 2002 to 2018 at the Chemical Engineering Department of Ahmadu Bello University, Nigeria, was used to investigate the existence of statistically significant relationship between the knowledge of the foundation level courses and overall (final) academic successes of the students. The data used in the study was obtained from the Examination Office of the Department of Chemical Engineering, ABU, Zaria. The names of the students were expunged from the data, and the raw data, which gives the cumulative grade point average (CGPA) of each student, was used for the analysis.

In Ahmadu Bello University (ABU), an undergraduate engineering degree, which leads to a Bachelor in Engineering (B.Eng.) award, is a five-year program. The first and second year courses tend to be science and mathematics courses taken by all Engineering students at the Faculty (Science and Engineering) levels. These are considered foundation courses; which each (Science and Engineering) degree program will build on in the subsequent years. During the first year (i.e. 100 level), Chemical Engineering students take 36 core credit hours/units, which comprises of Mathematics (12), Sciences (12), Engineering (9) and others (3). More credit units are taken during the second, third, fourth and fifth year(s). It is expected that at the end of the fifth year (500 level) each student would have taken a minimum of 173 credit units and maximum of 182 credit units. The knowledge gained is assessed and indicated by the cumulative grade point average (CGPA) at the end of each session (academic calendar, which comprises of two semesters). It may be important to note that some students gain 'direct entry' to the second (200 level) or third year (300 level) instead of the first year (100 level), and are therefore subject to different minimum and maximum credit units at the end of their degree program.

For each student that graduated at the expected time, the student's CGPA at 500 level was obtained and the corresponding 100 level CGPA was also obtained from the archives. The obtained values were then plotted against each other, for all the students in that particular graduating year, and the chart obtained was subjected to statistical analysis. Thus, the relation between the CGPA at the 100 level and the CGPA at 500 level was investigated. The initial and final CPGA(s) for students, who gained direct entry at 200 level, were also investigated for the existence of statistically significant relationship between the knowledge of the foundation level courses and overall (final) academic success; in order to have a comparative study between students who had basic science and mathematics knowledge and were admitted into 100 level, and those who had some extra tuition to prepare them for specific courses at 200 level.

3.0 Results and Discussion

Table 1 shows the yearly (2004 to 2018) distributions of the registered students at the different levels (100 to 500) at the Chemical Engineering department of ABU.

Table 1 shows that in 2004 there appeared to be a surge in the number of students admitted to 100 level. The number more than doubled that of students at any other level. On investigation, it was realized that the university (ABU) was not in session in 2003/2004 due to a strike action, thus the students that should have been admitted in 2003 where not admitted; instead in 2004, more students than usual were admitted for the 2004/2005 session. Over the next 13 years, the number of students at 100 level was maintained at an average of 148 students. Such a surge without commensurate increase in teaching resources and student supports may have dire consequences, such as bad quality teaching and learning, which may lead to increase (decrease) in students' failures (performance), and eventually 'delays' in students graduations.

Table 1 Distribution of students based on registration at different levels (2004 – 2018)

Year (Session)	Students registered at different levels				
	100	**200**	**300**	**400**	**500**
2004/2005	142	61	48	57	60
2005/2006	114	137	47	46	92
2006/2007	135	112	137	38	84
2007/2008	134	154	102	104	89
2008/2009	157	152	146	113	111
2009/2010	197	195	182	109	159
2010/2011	121	208	184	169	195
2011/2012	114	139	217	179	212
2012/2013	121	131	137	220	243
2013/2014	180	145	156	141	315
2014/2015	170	149	163	146	255
2015/2016	158	143	169	150	237
2016/2017	168	155	143	157	231
2017/2018	158	151	157	124	228

It is important to note that ABU operates a system in which students 'carry over' failed courses to another session, rather than another semester. Due to limited number of lecturers, teaching auditoriums and laboratories, each course is offered only once per year. Thus if a student fails a 100 level course, the student will take that course again when he/she is at 200 level. If the course is a pre-requisite to a 200 level course, it implies that the student will not be able to take the 200 level course and it will have to be taken at 300 level, if the student passes the prerequisite course at 200 level. If not, the student will take the 100 level course at 300 level. For example, MATH 105 (Differential and Integral Calculus), is a prerequisite for MATH 241 (Calculus I) and MATH 242 (Calculus II). Thus as long as the student fails MATH105, he/she will be unable to take MATH 241 and MATH 242, and will have to continue to take MATH 105 until he/she passes it. Unfortunately this 'carry over' course (MATH 105) may continue to feature for years. This implies that a 500 level student may still have 100, 200, 300 and/or 400 level(s) courses being taken concurrently with 500 level courses. Thus a build-up of these 'carry over' courses can lead to a student being stagnant (delayed) at 500 level for a number of years, until the 'residency permit' of the student expires, at which stage, the student is withdrawn from the university. This 'delay' is exhibited by the exponential increase in the number of student registered at 500 level. However, in 2014, the increasing trend of the number of students in 500 level was broken. On investigation, it was realized that the university carried out an 'Amnesty' program to try to clear the back-log of delayed students. The program allowed students to take a course concurrently with its pre-requisites. Thus it was possible to take, for example, MATH 105, MATH 241 and MATH 242 in the same session. This allowed some of the students to offload a number of courses at the same time, without waiting for subsequent years to take the course/graduate. This may have accounted for the drop in the number of 500 level students in the next session (2014/2015 session).

Relation between performance (CGPA results) at foundation level and at final level

Figure 1 shows a sample of the chart obtained for the variation of students CGPA at 500 level with their CGPA at 100 level. Based on the chart obtained, it is obvious that the CGPA at 500 level and CGPA at 100 level have a strong linear relationship. The chart was plotted for all the students that graduated from 2008 to 2018, and the obtained charts were analysed. The results of the analysis are shown in Table 2.

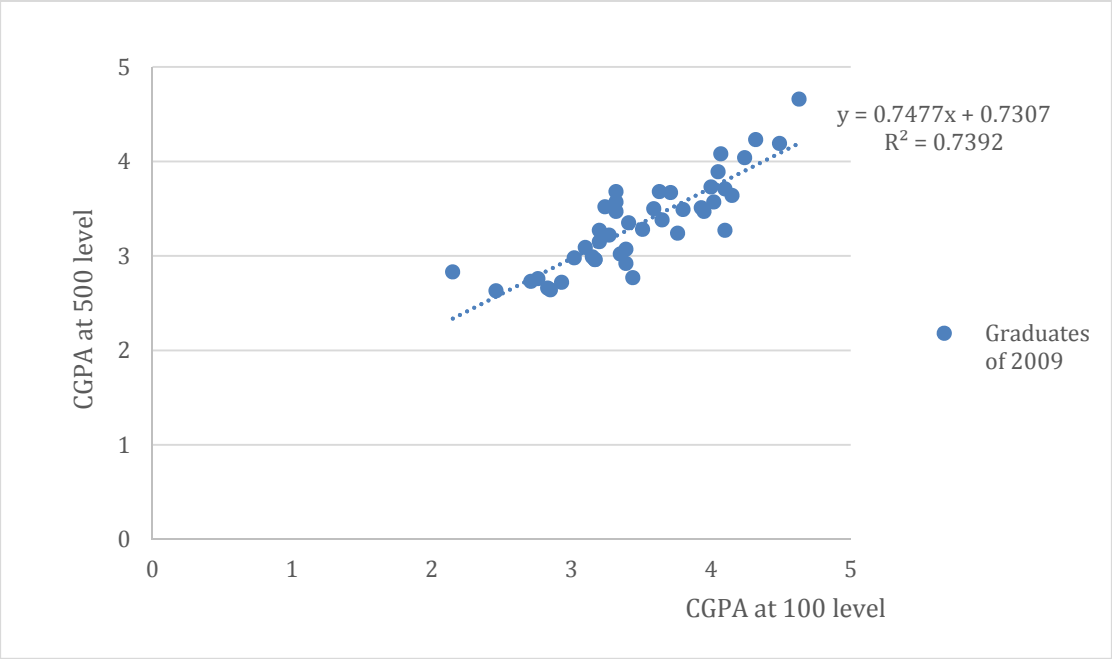

Figure 1. Variation of CGPA at 500 level with that at 100 level for 2009 graduates (i.e. students admitted in 2004/2005 session).

Table 2 summarizes the linear equation parameters obtained for students admitted from 2002 up to 2018 (i.e. students who graduated from 2008 to 2018 at the appropriate time).

Table 2. Parameters of linear relationship between CGPA-100 level and CGPA-500 level

Graduation Year	Parameters of linear equation: Y = aX + b		
	R^2	a	B
2008	0.7683	0.9138	0.0663
2009	0.7392	0.7477	0.7307
2010	0.6321	0.6591	1.1872
2011	0.8245	0.7834	0.6669
2012	0.7593	0.7076	1.1541
2013	0.7251	0.6939	1.0891
2014	0.8300	0.7785	0.9365
2015	0.8185	0.6254	1.6554
2016	0.7315	0.7175	0.9953
2017	0.7591	0.6163	1.5639
2018	0.8154	0.6707	1.3924
Average	0.7639		

The CGPA at 100 level and CGPA at 500 level, show a good relationship, as indicated by the goodness of fit parameter (R^2) in Table 2. The year with the worst R^2 value, which does not show a very good fit, is 2010. It is difficult to explain this sudden drop in R^2 value, especially considering that for the students that graduated in that year, a fewer number of students were initially admitted compared to the year before (as shown in Table 4). Nevertheless, the average R^2 value (for all the years analysed) is 0.7639, which implies a strong correlation between the CGPA at 100 level and the CGPA at 500 level.

The analysis was also carried out for students with direct entry into the 200 level. These students have undertaken a foundation (remedial) course before admission into 200 level. Generally, they are students who were unable to get entry to 100 level, possibly due to a shortfall in meeting the requirements for direct entry at 100 level or due to the limited available resources, which limits the number of students that can be admitted. The analysis also shows a good fit for the relationship between CGPA at 200 level and CGPA at 500 level, with a slightly higher average R^2 value of 0.8058, as shown in Table 3.

Table 3. Parameters of linear relationship between CGPA-200 level and CGPA-500 level for students with 'direct' entry into 200 level

Graduation Year	**Parameters of linear equation: Y = aX + b**		
	R^2	**a**	**B**
2008	N/A	N/A	N/A
2009	0.6468	0.6175	1.4725
2010	1.0000	0.8190	0.9380
2011	0.7970	0.6915	1.2099
2012	0.8305	0.9484	0.4964
2013	0.7705	1.0118	0.3410
2014	0.9680	1.0121	0.4863
2015	0.8964	0.7394	1.0541
2016	0.7244	0.5114	1.9401
2017	0.7444	0.7339	1.2262
2018	0.6799	0.8417	0.6913
Average	0.8058		

Delays in Graduation

Table 4 shows the pass rate(s) as a function of the admission/graduation year(s). Students are supposed to graduate after five years of studies. Thus students admitted in 2004, for the 2004/2005 session, are supposed to graduate in 2009. However, only 33.3% of the students admitted in 2004 graduated in 2009, the others were delayed for varying years depending on their outstanding courses. Encouragingly, after 2009, the number of students (as a percentage of the number admitted) that graduated on time, increased to slightly above 40% until 2014, when the percentage began to increase steadily. This sudden increase in 2014, may be associated with the 'Amnesty' program introduced to clear up the backlog of student as mentioned earlier. This steady increase in pass rate was noticed up to 2018, when there was a sudden drop in the rate. On investigation, it was realized that the policy changed for students admitted for the 2013/2014 session. The students were no longer permitted to graduate with a 'pass degree', as such the minimum graduation CGPA increased from 1.0 to 1.5. This may have contributed to the sudden significant drop in pass rate noticed in 2018. However, it is important to note that from 2018, the policy has been changed again, so that students admitted after 2018, i.e. students

admitted for the 2018/2019 session will have the opportunity to graduate with the lesser grade of 'pass' degree (CGPA of 1.0). In other words, there has been a reversal in the earlier policy; which can lead to inconsistencies and dissatisfaction.

Table 4. Student pass rate, as a function of year of admission and the number of students admitted

Graduation year	Admission year	No. of students admitted at 100 level	No. of students that graduated on time	% of students that graduated on time (%)
2008	2002	52	25	48.1
2009	2004	132	44	33.3
2010	2005	95	41	43.2
2011	2006	134	54	40.3
2012	2007	135	63	46.7
2013	2008	156	65	41.7
2014	2009	185	103	55.7
2015	2010	117	71	60.7
2016	2011	113	74	65.5
2017	2012	113	77	68.1
2018	2013	156	63	40.4
Average				49.4

It may be interesting to note that although in 2004, 132 students were admitted, and the pass rate (for these group of students) was only 33.3%, subsequent high number of student admission did not seem to have the same impact as the initial surge of students. For example, when the pass rates of other years are compared to that of the 52 students that were admitted in 2002, the pass rates are not much worse than theirs. Nevertheless, from 2014 there was a sudden surge in the pass rate, i.e. the students admitted from 2009, did consistently better, in terms of having a higher pass rate than subsequent years. It is possible that the 'Amnesty' program was responsible for the initial increase in the pass rate, but the subsequent increase cannot be explained easily. By 2018, the pass rate suddenly dropped, possibly as a result of the change in policy (pass mark), as already mentioned above. These findings are contrary to the expectation that large numbers of student intake/admission will automatically lead to increase in student failure.

In the course of this study, it was observed that during the period under study, there has been frequent changes in policies, which have included the number of students admitted, pass mark, sequence of taking courses, 'amnesty', school calendar, etc., which makes it very difficult to know the effect of only one variable on say pass rate. Since it would seem that at any one time, more than one variable is changing. Nevertheless, one thing that is evident in this study, is the fact that for those students that graduated at the expected time, the relationship between their foundation level CGPA and final level CGPA is very strong.

The analysis of the student pass rate was also carried out for students with direct entry into 200 level. The results are as shown in Table 5.

Table 5. Student pass rate, as a function of year of admission and the number of students admitted for 200 level direct entry students

Graduation year	Admission year	No. of students admitted at 200 level	No. of students that graduated on time	% of students that graduated on time (%)
2008	2004	16	0	0.00
2009	2005	11	4	36.4
2010	2006	9	2	22.2
2011	2007	16	9	56.3
2012	2008	16	7	43.8
2013	2009	26	12	46.2
2014	2010	18	10	55.6
2015	2011	10	5	50.0
2016	2012	12	12	100.0
2017	2013	41	34	82.9
2018	2014	21	12	57.1
Average				50.0

The analysis for the direct entry students shows that on average no much difference exists in the pass rate between students admitted at 100 level and those admitted via direct entry at 200 level. However, there are two years (2016 and 2017) that show exceptional high pass rate for 200 level direct entry students. In particular, 100% of the students admitted via direct entry in 2012 graduated on time (2016). Again, due to the inconsistencies in procedures, it is difficult to justify this result.

4.0 Conclusions

This study has shown that the performance of students in the foundation level courses can be a strong indicator of the students' later academic success. On average, the goodness of fit parameter (R^2), for the relationship between the CGPA at 100 level and CGPA at 500 level, is 0.7639, and the average R^2 value between CGPA at 200 level (for direct entry students) and CGPA at 500 level is 0.8058, which shows that both values indicate good fit(s) between foundation level CGPA and final level CGPA. Also, the study showed that there are no significant difference(s) in the performance of the two different groups of students, as the average pass rate (as a percentage of the initial number of students admitted) was about 50% for both students that were admitted at 100 level and those admitted at 200 level. Nevertheless, the findings suggest that engineering educators should pay more attention to the foundation level courses as success at foundation level seems to predict final academic success.

References

Alfan, E., and Othman, M.N. (2005). "Undergraduate students' performance: the case of University of Malaya", *Quality Assurance in Education*, 13 (4), 329-343, https://doi.org/10.1108/09684880510626593

Dewhurst, P., Rix J., and Newell, D. (2016). Influence of year-on-year performance on final degree classification in a chiropractic master's degree program, *J Chiropr Educ*, 30 (1), 14-19, DOI 10.7899/JCE-14-26

Kauffman, C.A., Derazin, M., Asmar, A., and Kibble, J.D. (2018). Relationship between classroom attendance and examination performance in a second-year medical pathophysiology class, *Adv. Physiol. Educ.*, 42: 593–598, doi:10.1152/advan.00123.2018.

Lee, S., Harrison, M.C., Pell, G. and Robinson, C.L. (2008). Predicting performance of first year engineering students and the importance of assessment tools therein, *Engineering Education*, 3 (1), 44 - 51, DOI: 10.11120/ened.2008.03010044

Murdoch-Eaton, D.G., Pel,l R.G. and Roberts, T.E. (2007). Changing approach to undergraduate studies documented during annual appraisal of medical students, Medical Teacher. *Carfax Publishing Limited*, 29 (2), 111-118.

Murtaugh, P.A., Burns, L.D., and Schuster, J. (1999). "Predicting the retention of university students", *Research in Higher Education*, 40 (3)

Roy, S.S. and Chadalawada J. (2014). Predictors of academic performance of medical undergraduate students of microbiology class in Kolkata. *International Journal of Medicine and Public Health*, 4 (4), 392-5

Stinebrickner R. and Stinebrickner, T. (2013). "Academic Performance and College Dropout: Using Longitudinal Expectations Data to Estimate a Learning Model", *The National Bureau of Economic Research NBER, Working Paper No. 18945*

Thomas, G., Henderson, A., and Goldfinch, T. (2009). "The Influence of University Entry Scores on Performance in Engineering Mechanics", 20th Australasian Association for Engineering Education Conference, Adelaide, SA, Dec 6-9, 2009

Tumen, S., Shulruf, B., and Hattie, J. (2008). "Student pathways at the university: patterns and predictors of completion", *Studies in Higher Education*, 33(3), 233-252

Proceedings of the 49th NSChE Annual Conference
KADA 2019: pp 427-435

P2C-03: CHEMICAL ENGINEERING EDUCATION AND PROBLEM LEARNING PLATFORM: FOCUS AND DEVELOPMENTS

Nnadi, C. N, Ogulu, E.O and Oduola, M.K
Centre for Oilfield Chemical Research, World Bank Africa Centre for Excellence, University of Port-Harcourt. Choba, Port-Harcourt

ABSTRACT
This study reviewed Chemical Engineering Education and Problem Base Learning that involved innovative approaches for effective and efficient result-oriented. The study reviewed the various element needed for Chemical Engineering Education learning platform that will enhance rapid knowledge acquisition. Modern techniques in Chemical Engineering education was identified that includes e-learning platform, flowsheets, process flowsheet, schematic diagram and computer software applications. The modules of these techniques and function were discussed for easy accessibility to the learners. Project organized problem base learning, problem base learning and project base learning were considered as part of the difficulties to address in Chemical Engineering Education. Historical background, previous works, best practice and focusing priorities etc were briefly explained as relate to this study. The study concluded by emphasizing on the need of making learning of Chemical Engineering effective by caring out training and retraining of staff for efficient impartation of knowledge. Learning is a search for meaning, which requires understanding of the whole framework in order to relate the parts of the context. The problem base learning in Chemical Engineering education is viewed from different point which are data collection, analysis of data and the materials for the learning process. Various units and column that are involved in conversion of raw-materials into finished products were reviewed for easy understanding. The chemical engineering discipline is still fragmented due to the fact that necessary ingredients for learning are not either under-utilized or not available for usage.

Keywords: Chemical Engineering Education, Learning and Problem-Based

INTRODUCTION
Chemical Engineering education is a process of learning that involves the conversion of raw materials into finished product by application of chemical science. Chemical Engineering nowadays needs to evolve in order to produce marketable Chemical engineering graduates. Traditional Chemical engineering instruction is deductive, beginning with theories and progressing to the applications of those theories. The traditional methods alone do not seem to be able to cultivate required skills by the industries since the demand of the industries on the graduate's skill keeps on changing from time to time. To address these challenges, industries need skilled personnel with good oral and written communication skills, tuned to modern technology and adept at teamwork. However, rising costs, reduced budgets, difficulties in retaining high quality students and lack of technical and laboratory resources are some of the challenges that beset universities. Further exigencies include time constraints and clashes within a flexible semester system offering multiple options. Therefore, innovative teaching methods such as Project organized problem-based Learning which is based on constructivist learning theory seem the best methods to resolve this issue(Duch,2001). Chemical Engineers are increasingly finding more non -traditional type employment in order to make ends meet for survival. From a student's perspective, an essential factor in student learning is motivation. Studies from Dahlgren (2003) note the limitations of traditional classroom teaching in today's changing environment. The

student's desire to learn can be enhanced by involving them in the education process and by presenting the course material in an attractive format, relevant to today's needs. The curriculum designer on the other hand needs to focus on specifying the desired graduate attributes and matching course content with those attributes to be finally imparted to the learner (Schon,1997). **Project organized problem-based Learning** is hybrid model that consists of two types of inductive(student centered) learning methods, which are project based learning and problem based learning .The terms project-based learning and problem-based learning are each used to describe a range of instructional strategies.

Problem-based learning begins when students are confronted with an open-ended, ill-structured, authentic (real-world) problem and work in teams to identify learning needs and develop a viable solution, with instructors acting as facilitators rather than primary sources of Information (Barrows,1980) while **Project-based learning** begins with an assignment to carry out one or more tasks that lead to the production of a final product—a design, a model, a device or a computer simulation. The culmination of the project is normally a written and/or oral report summarizing the procedure used to produce the product and presenting the outcome. Project-based learning is similar to problem-based learning in several respects. Both normally involve teams of students in open-ended assignments that resemble challenges the students are likely to encounter as professionals, and both call for the students to formulate solution strategies and to continually re-evaluate their approach in response to outcomes of their efforts. There are differences in the two approaches as they have traditionally been implemented, however. A project typically has a broader scope and may encompass several problems. In addition, in project-based learning the end product is the central focus of the assignment and the completion of the project requires primarily application of previously acquired knowledge, while solving a problem requires the acquisition of new knowledge and the solution may be less important than the knowledge gained in obtaining it (Woods,1994). In other words, the emphasis in project-based learning is on applying or integrating knowledge while that in problem-based learning is on acquiring it. In practice, however, the distinction between the two methods is not necessarily that clean, and programs have recently adopted approaches that include features of both of them. The main principles of project organized problem-based learning can be described as in figure 1. Problem-based learning in chemical Engineering profession can easily by handle with experimental and descriptive approach through effective and coherent reasoning. Scientifically, Chemical Engineering has to do with conversion of raw-materials into finishes products by application of physical and chemical processes.

Historical Background

In higher education concepts such as "self-directed-learning," "case-based learning," "inquiry based learning," "experiential learning," "service learning," "project-based service learning," "active learning," CDIO (Conceive, Design, Implement, and Operate), "project-based learning," and "problem-based learning" were introduced in the decades after the Second World War. All these new learning concepts come under the umbrella of learner-centered or student-centered learning models. Problem-based and project-based learning, both known as PBL, originate from the reform universities, and the new educational models, established between 1965 and 1975.

In problem-based learning, problems form the starting point for students' learning emphasizing a self-directed learning process in teams. The educational model problem-based learning was introduced at curriculum scale at the medical faculty of McMaster University, Canada, followed by Maastricht University in the Netherlands and many others. Project-based learning shares the

aspect of students working on problems in teams, but with the added component that they have to submit a project report completed collaboratively by the project team. The problem- and project-based/project organized model adopted at Aalborg University and Roskilde University, Denmark, was inspired by the critical pedagogy in Europe after the student revolts of the 1960s.

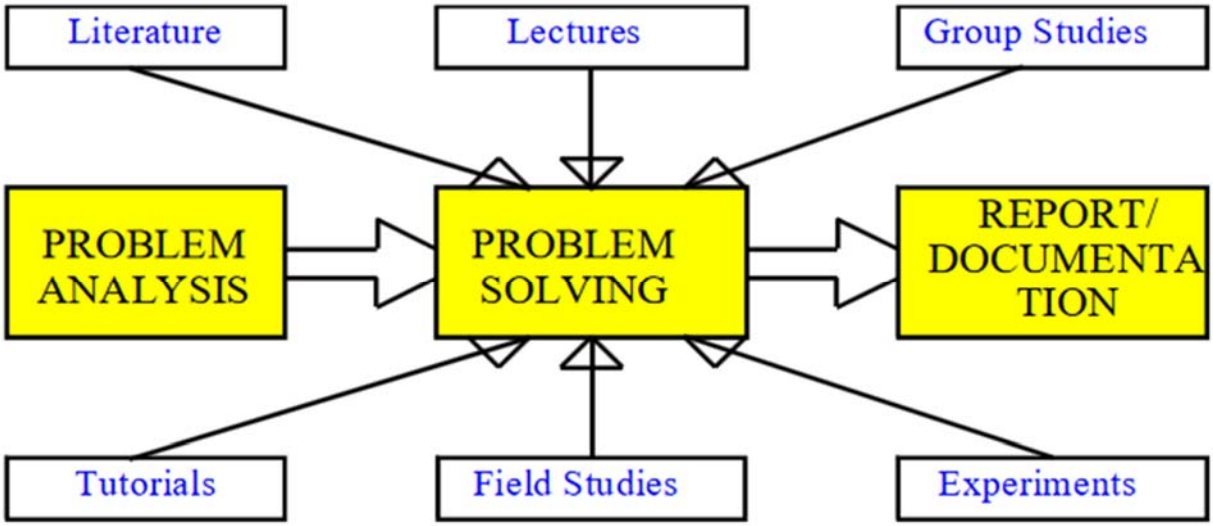

Figure 1: Principles of project-organized problem-solving (Kjærsdam and Enemark, 1994)

At Aalborg University both models of PBL were eventually combined in problem-based project organized learning, which was practiced at all faculties – the Faculty of Engineering and Science being the largest. The problem- and project-based/project organized model adopted at Aalborg University and Roskilde University, Denmark, was inspired by the critical pedagogy in Europe after the student revolts of the 1960s. At Aalborg University both models of PBL were eventually combined in problem-based project organized learning, which was practiced at all faculties – the Faculty of Engineering and Science being the largest. The problem- and project-based/project organized model adopted at Aalborg University and Roskilde University, Denmark, was inspired by the critical pedagogy in Europe after the student revolts of the 1960s. At Aalborg University both models of PBL were eventually combined in problem-based project organized learning, which was practiced at all faculties – the Faculty of Engineering and Science being the largest. The problem- and project-based/project organized model adopted at Aalborg University and Roskilde University, Denmark, was inspired by the critical pedagogy in Europe after the student revolts of the 1960s. At Aalborg University both models of PBL were eventually combined in problem-based project organized learning, which was practiced at all faculties – the Faculty of Engineering and Science being the largest. The problem- and project-based/project organized model adopted at Aalborg University and Roskilde University, Denmark, was inspired by the critical pedagogy in Europe after the student revolts of the 1960s. At Aalborg University both models of PBL were eventually combined in problem-based project organized learning, which was practiced at all faculties – the Faculty of Engineering and Science being the largest.

The problem- and project-based/project organized model adopted at Aalborg University and Roskilde University, Denmark, was inspired by the critical pedagogy in Europe after the student revolts of the 1960s. At Aalborg University both models of PBL were eventually combined in problem-based project organized learning, which was practiced at all faculties – the Faculty of

Engineering and Science being the largest. This combined approach is the central point of reference for this work.

Previous Work

Lars et al (2003) research on Project Organized problem-based learning in distance Education was an empirical work that dwelled on how Chemical Engineering degrees can be obtained using distance learning methods such as online. Another study by Fink(1999) was on Problem Organized base learning in Engineering Education, dealt on the need of advancing Engineering Education through rigorous approaches adopting a an approach that will advance the discipline of Engineering through Industry-academia related approach. Lehmann et al (2008) researched on Problem-Oriented and project-based learning (POPBL) as an innovative learning strategy for sustainable development in Engineering Education, this work was based on to advance knowledge acquisition in Chemical Engineering so as to meet global trends and development. Authors such as Kalmos et al (2004) worked on The Aalborg PBL Model: progress, diversity and challenges. This topic was able to identify various challenges that are to be encountered by student in cause of Chemical Engineering Education but the limitation to the research is the way forward that was not revealed by this publication. Mills (2003) Talked on Engineering Education: Is problem-based or learning-based the answer? Which pose as a pointer to both the teaching and leaning audience of the Engineering Profession. This question asked by the author is essential to knowledge acquisition in Engineering considering the time involved in Engineering training. Hadim et al (2002) researched on Enhancing the Engineering Curriculum through project-based learning researched on repositioning the Engineering profession through knowledge impartation in correlation with trends in society and innovative reasoning. This authors considered some important factors that are essential in enhancing Engineering knowledge but this not go into details on how this can be effectively implemented in our present day society.

Jasiek et al (2010) researched on Identifying opportunities for collaboration in International Engineering Education Research on Problem-and project-based learning, this study was anchored on the for effective collaboration on Engineering knowledge acquisition for the growth of society. This empirical review see the need for implementation of ideas in Engineering Education in general and Chemical Engineering education in particular knowledge impartation and acquisitions. This present study is intended to tackle the issue of problem-base learning platform in Chemical Engineering Education that will advance the growth of society through value-chain and effective collaboration. Chemical Engineering education essential for the advancement of the 21st century economy in areas like Agriculture ,energy, power, mines and steel etc. In advancing value chain economy Chemical Engineering education is vital to the achievement of the needed growth and priority need to be place in knowledge acquisition so as to boost manpower input and output.

Best Practice

Chemical Engineering education has evolved since its origins. One of the strongest features of engineering education, in fact, has been its resilience and flexibility, and its ability to adapt and evolve as new challenges, opportunities and new realities become apparent. Some have attempted to provide pathways to the future of engineering [5]. Despite the appearance of confusion that sometimes seems to be associated with chemical engineering education, there are discernable trends. Many of these trends are discussed here, where they are grouped into several categories: refocusing priorities, enhancing professionalism, advancing teaching and learning methods.

Refocusing Priorities

The main future trends around chemical engineering education priorities, which I anticipate may be modified or expanded, relate to creativity, innovation, design, engineering methods and fundamentals, multidisciplinary studies and independent learning in chemical engineering education, given those factors are crucial to chemical engineering design, and yield more competent and productive engineers.

Enhancing Professionalism

Several future trends around professionalism are likely in the future, the principal ones of which involve the environment, ethics, professional attributes, business, management, entrepreneurship and globalization. As environmental issues and concerns continue to grow, we anticipate that, Chemical Engineering education will place a greater emphasis on ensuring that chemical engineers have a broad awareness of the implications of their actions on the environment, and a better understanding of their role in environmental stewardship and responsible environmental behavior.

Advancing Teaching and Learning Methods

The main future trends around teaching and learning methods in chemical engineering education are likely to new teaching and learning methods, information and communications technologies and virtual and simulated laboratories. I anticipate that there will be expanded use of new methods to facilitate teaching and learning, taking advantage of the many new methods being proposed or tried to improve educational activities and student learning. For instance, active learning and reflection have been in various areas of engineering education.

MATERIALS AND METHODS

In achieving the aim and objectives of the study, we considered various learning platforms such as Schematic diagrams, Process diagram, Flowsheets, e-learning platforms and Computer Software Applications. These materials were reviewed on their various mode of application to the Chemical Engineering profession. The methods adopted in the application of this materials for effective knowledge impartation on Chemical Engineering are review on various modules of operation. Schematic diagrams are applied for illustrating the process involves in various conversion of raw-material such as distillation column for fractionation of crude and other fluids. The usage of e-learning system involves digital application either through electronic mails, projector and visual form of learning. This study considered of projector and electronic mails in teaching and getting of feedback from students in transfer of Chemical Engineering knowledge. Computer Software Applications such CHEMCAD, Auto-CAD,HYSYS, PRO11,MATLAB and Excel are constantly applied in teaching innovative knowledge in the Chemical Engineering Profession. These software are used in designs, simulation and modeling of chemical Engineering processes. Flow sheet are necessary in show different steps involved in conversion of raw-materials into finished products like production of beer.

DISCUSSION

The Flow diagram is illustrated below for production of Ethyl alcohol were 95% ethanol was recovered with molasses serving as feedstock. The flow diagram the column and units that are involved in the production.

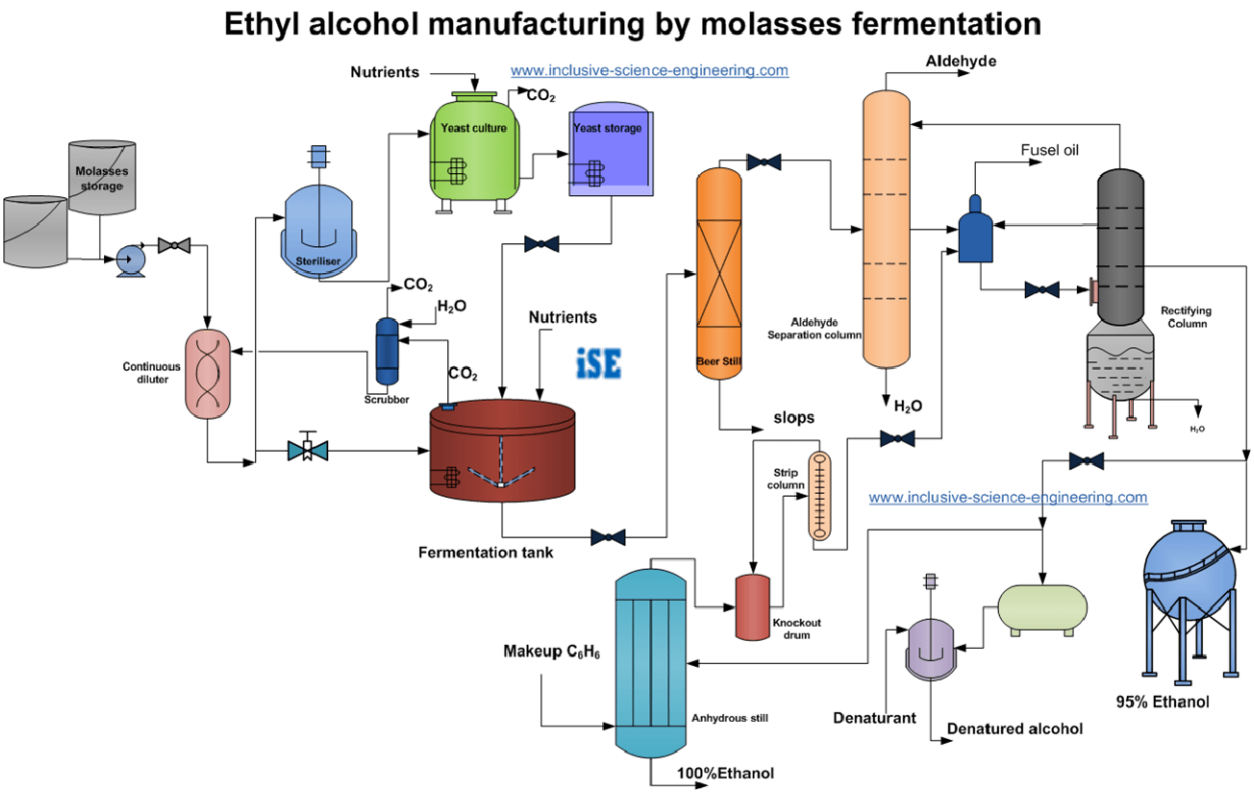

Figure1.2: Flow Diagram for Ethyl alcohol Production

The schematic diagram below shows the production process of bioethanol from grains and sugar solution. The schematic diagram is a teaching aid that gives detail information of the process of production of any products. The various units in the bioethanol production then related through the schematic diagram.

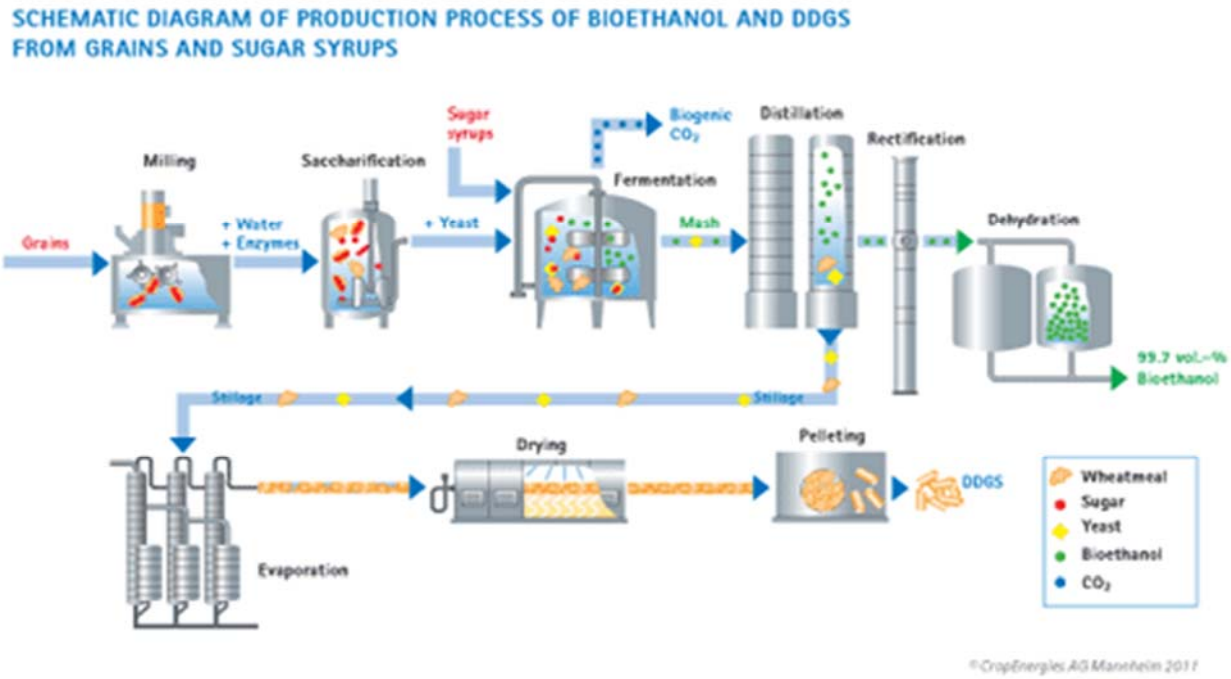

Figure1.3: Schematic Diagram for Bioethanol Production from Sugar and Grains

Process diagram is block diagram that gives information on the various stages of production of any products such as bioethanol that is illustrated below. Process diagram is an important teaching aid in Chemical Engineering and help solve the problem of understanding the steps in producing a particular products.

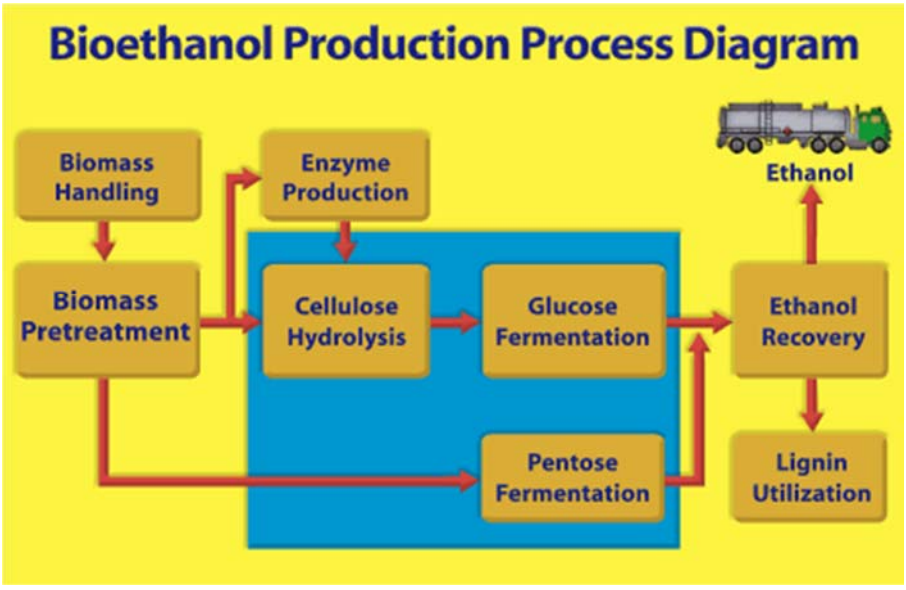

Figure1.4: Process Diagram for Bioethanol Production

This is a flow diagram for PP Powder production, with catalyst as feedstock and PP powder as end product. The flow diagram as a teaching aid is viewed on this study as an illustrative material that shows the production step of desired product.

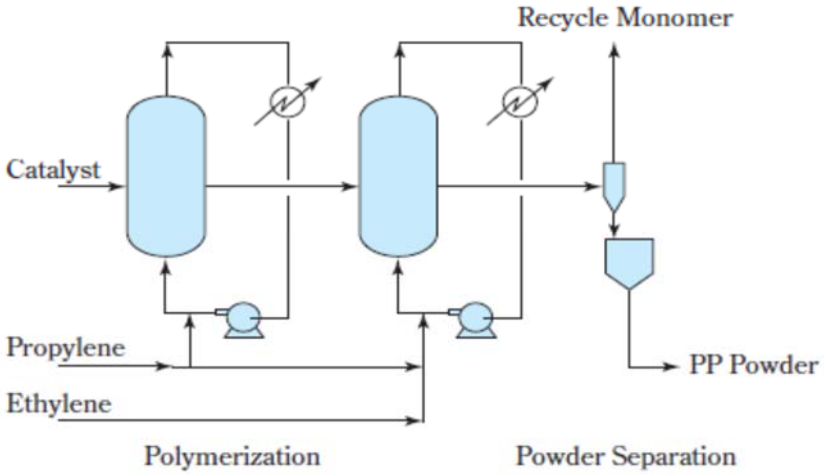

Figure 1.5: Flow Diagram for PP powder

CONCLUSION

Many challenges and opportunities faces chemical engineering education, a change to **project organized problem based learning** may be an expensive and time consuming endeavor but given visionary and supportive management and well-trained, committed and dedicated staff, the change may lead to results in terms of student competences that are worth the effort. It is a known fact that Chemical Engineering is an innovative discipline that entail modern way of knowledge acquisition. This study reviewed various Chemical Engineering Education and problem base learning which also suggest possible solution to this problems. The various modern tools that are involved in Chemical Engineering Education were related to Problem base learning and modules were also reviewed. This study concluded that Chemical Engineering Education is vital for advancement of innovative society and problem base learning are urgent in need of attention.

RECOMMENDATIONS

1. Teaching staff involved in teaching the project organized problem based learning curriculum should be provided with ample opportunities for discussions and deliberations, leading to mental comfort about the change, as well as ample training leading to cognitive skills in mastering the PBL teaching tasks, such as problem crafting and facilitation.
2. Dynamic approach should be used in teaching Chemical Engineering courses by using vigorous modern methods in their knowledge impartation on students.
3. Staff who are interested in participating in the delivery of the PBL curriculum should be involved in the first phases of the change processes so that it can lead to sustainable change.
4. Interdisciplinary collaboration among teachers should be secured in order to provide interdisciplinary real-life problems for students to work with.
5. Real-life problems should be introduced early on in the study program, when the motivational factor is the greatest.
6. Provision should made in utilization of the tools to solve the problem base learning through effective training and retraining of staff.
7. Student should be regularly expose to these modern tools so as to enable them see the problem learning as one of the challenge to overcome before becoming a Chemical Engineer.

REFERENCES

Barrows, H.S., and Tamblyn, R., Problem-Based Learning: An Approach to Medical Education, New York: Springer, 1980.

Boud, D., and Feletti, G., The Challenge of Problem-Based Learning, 2nd ed., London: Kogan Page, 1997.

Dahlgren, M.A., "PBL through the Looking-Glass: Comparing Applications in Computer Engineering, Psychology and Physiotherapy," Intl. J. Engr. Education, Vol. 19, No. 5, 2003, pp. 672–681.

Duch, B.J., Groh, S.E., and Allen, D.E., The Power of Problem-Based Learning, Sterling, VA: Stylus, 2001.

Duch, B.J., "Models for Problem-Based Instruction in Undergraduate Courses," in Duch et al. [49], Ch. 4.

Institution of Engineers, Australia Task Force , Changing the Culture: Engineering Education into the Future: Review Report, Institution of Engineers, Australia: Canberra, 1996

Norman, G.R., and Schmidt, H.G., "The Psychological Basis of Problem-Based Learning: A Review of the Evidence," Academic Medicine, Vol. 67, No. 9, 1992, pp. 557–565

Schon, D., "Educating the Reflective Practitioner: toward a new design for teaching and learning in the professions," Jossey-Bass, San Francisco, 1987

Tan, O.S., Problem-Based Learning Innovation, Singapore: Thomson, 2003

Woods, D. R., Felder, R. M., Rugarcia, A., and Stice, J. E. The Future of Engineering Education - Developing Critical Skills, Chem. Eng. Ed., 34(2), 108-117 , 2000.

Weiss, R., "Designing Problems to Promote Higher-Order Thinking," in D.S. Knowlton and D.C. Sharp, eds., Problem-Based Learning in the Information Age, New Directions for Teaching and Learning, #95, San Francisco: Jossey Bass, Fall 2003, pp. 25–30.

Woods, D.R., Problem-Based Learning: How to Gain the Most from PBL, Waterdown, ON: Donald R. Woods, 1994.

Proceedings of the 49th NSChE Annual Conference
KADA 2019: pp 436-453

P2C-04: REVIEWING THE CHEMICAL ENGINEERING CURRICULUM FOR RELEVANCE

S.N. Mumah
Department of Chemical Engineering, Kaduna Polytechnic, Kaduna, Nigeria
Correspodence: mumahsndoyi@kadunapolytechnic.edu.ng, +234 -8037619719

ABSTRACT
This paper reviews the case of the chemical engineering curriculum and proposes ways and areas that need urgent attention. It recommends the need to develop an appropriate action plan for the review, the introduction of new courses that are in consonance with new trends in the chemical industry and the need to develop instructional materials to make the implementation of the curriculum easier for both the lecturers and the students and the reintroduction of the periodic industrial attachments for lecturers to keep them abreast with the new developments in the industry. It further calls for an implementable timetable to ensure regular reviews of the curricula of the programmes of Nigerian tertiary institutions and for all institutions to strengthen their strategies and specific initiatives designed to support the development of quality teaching since pedagogy is a central enabler of the implementation of all academic curricula. The paper finally recommends that Nigerian tertiary institutions consider the hiring of adjunct lecturers from critical industries to join regular staff for a period of time as this will go a long way in inculcating the appropriate real life skills and competences in students. Such symbiotic collaboration between industry and academia are key ingredients of a successful curriculum implementation.

Key words: Curriculum Revision, Industrial Trends, Chemical Engineering

Definition of Curriculum
According to United Nations Educational, Scientific and Cultural Organization (UNESCO), Curriculum is a systematic and intended packaging of competencies (i.e. knowledge, skills and attitudes that are underpinned by values) that learners should acquire through organised learning experiences both in formal and non-formal settings. Good curriculum plays an important role in forging life-long learning competencies, as well as social attitudes and skills, such as tolerance and respect, constructive management of diversity, peaceful conflict management, promotion and respect of Human Rights, gender equality, justice and inclusiveness.

Curriculum development is defined as a planned, purposeful, progressive, and systematic process to create positive improvements in the educational system. Every time there are changes or developments happening around the world, the curricula are affected. There is a need to update them to address the society's needs. According to Bilbao et al. (2008), curriculum is considered the "heart" of any learning institution which means that the Polytechnics or Universities cannot exist without a curriculum for each of their programmes. Since there are constant changes in the society, curriculum development has become a dynamic process. The curriculum can therefore be considered the total learning experiences of individuals not only in the institutions but the society as well. The critical question we need to ask is, do we have to wait for society to change before we prepare a curriculum to match it or can we be innovative enough to keep pace?

The truth is that we have to develop the curriculum around the challenges in the Chemical Industry. Wrongly defined trends lead to wrongly defined challenges to non-relevant curriculum. What type of Curriculum are we preparing? Is it a community curriculum, regional curriculum, national curriculum or global curriculum?

Importance of Curriculum Development

Curriculum development has a broad scope because it is not only about the Institution, the learners, and the teachers; It is also about the development of society in general. In today's knowledge economy, curriculum development plays a vital role in improving the economy of a country. It also provides answers or solutions to the world's pressing conditions and problems, such as environment, politics, socio-economics, and other issues of poverty, climate change, and sustainable development. There must be a chain of developmental processes to develop a society. First, the curriculum must be developed to preserve the country's national identity and to ensure its economy's growth and stability. Thus, the president of a country must have a clear vision for his people and the country as well. For instance, in Nigeria, Mr. President in his Change Agenda may want the country to be self sufficient in food and also produce its fuel so as not to rely on importation. The curriculum should therefore be reviewed to support these initiatives by, for example, the introduction of storage and processing systems and bio-fuel studies.

There are issues of illegal processing of stolen crude oil. The mineral sector needs to be developed to enable us move from oil dependency. How will this influence the curriculum development and review? Then the curriculum must be developed along that line. Curricula programs for higher education can be crafted in such a way that graduates can fit easily in the relevant sectors to boost the food, oil industry and mineral sector. For example, different models may arise such as a curriculum that emphasizes renewable energy, bio-energy, returning to coal energy, producing fuel from methane. Questions like, will there be more emphasis on gas. Should government and industry support the building of more modular refineries? How about the introduction of mineral processing systems or emphasizing multidisciplinary approaches in the curriculum? In Singapore, for example, water is a key issue and there are more water related programmes and research. Poor curriculum means precious time is wasted by industry for on-the-job training.

If Polytechnics or Universities have curricular programmes that are innovative and in demand in the local or global markets, many students even from foreign countries will enroll. A higher number of enrollees would mean income on the part of the Institutions. As a result, if the income is big, it can be used for teachers' promotion, scholarship, and remuneration. It can also be used in funding research and development endeavors, and in putting up school facilities, libraries, and laboratories. The country's economy can improve the people's way of life through curriculum development. And to develop it, curriculum experts or specialists should work hand in hand with lawmakers such as senators, the local government officials, governors among others.

Likewise, business communities and industries, and other economically oriented players in society may be engaged in setting and implementing rules and policies for educational reforms. Hence, curriculum development matters a lot in setting the direction of change in an Institution, not only at the micro but also at macro levels. As long as the goals and objectives of curriculum development are clear in the planner's mind, cutting-edge achievements in various concerns can be realized. Why is Massachusetts Institute of Technology (MIT) or Harvard University, etc, considered a brand? This can be traced to, among others, the quality of the programmes they run, which can further be traced to the curricula they use.

Development Relevance of Curriculla

The following are key considerations when developing a curriculum:

i. What does the country/community want to achieve with regard to the personal development of learners and societal well-being and advancements? And how well does the curriculum reflects that education vision?
ii. What are the mechanisms for making the curricula to respond to national development policies and strategies? Is there evidence that the mechanisms work effectively?
iii. How well are the key/core/cross-cutting competencies identified in the curricula aligned to education policy goals?
iv. Is there evidence that such key competencies have been at the core of curriculum development?
v. How are education stakeholders (teachers, learners, private sector, and civil society) involved in developing the curriculum vision and appropriate curriculum policies?
vi. Is there evidence of their involvement having made a difference?

STAKEHOLDERS IN CURRICULUM DEVELOPMENT

As we all know, curriculum development is a complex and iterative process with a great number of activities that involve many stakeholders. This therefore means that a variety of stakeholders should be consulted in order to collect invaluable feedback regarding their needs and requirements related to education processes. Two distinct groups of stakeholders have been indentified: curriculum stakeholders and professional stakeholders. Curriculum stakeholders are key informers and drivers of the content, method of delivery, evaluation requirements and scope of curriculum that qualifies for a certain profession. Professional stakeholders have a broader interest in specific professions, professional attributes of graduates, their work capabilities and conditions, specialty career development, knowledge and competencies. Curriculum stakeholders are essential to curriculum development. Collaboration with stakeholders and an open dialogue that calls for recommendations, feedback, critique and advice that can provide a significant contribution in combining the content and method of delivery of the curriculum to meet the needs of the wider community (Matkovic *et al*., 2014).

A modified curriculum development master process based on analysis, design, development, implementation and evaluation model was proposed by Matkovic *et al*. (2014). The model recognize the importance of different stakeholders, how to identify and select key curriculum stakeholders whose contribution can be of great importance for the curriculum development process, how to collect and process their requirements, the activities of the analysis phase, and utilize their input for curriculum innovation.

In identifying the stakeholders involved in curriculum development, the following pertinent question must be answered:

a. Why do you need to develop or review the curriculum?
b. Who is developing the curriculum?
c. Who will use the curriculum?
d. Where is it to be used?
e. Who will deliver the curriculum?
f. Where will the students who use the curriculum go to when they graduate?
g. The students you enroll, where are they coming from (pre-knowledge of the field)?
h. How is the curriculum development team selected?

Curriculum development for programmes in Nigerian tertiary institutions has not been a regular exercise in many cases. Why this is so can be traced to many factors but the most important is not the funds to conduct the exercise but to the lack of the knowledge of the importance of such exercise by the institutions administrators and supervisor agencies to the institution in particular and the country in general. It is important for all tertiary institutions to assess themselves by asking the following questions:

a. Who is the primary initiator of curriculum development?
b. Is the Institution reviewing or developing a curriculum because the supervisory bodies (National Universities Commission (NUC) or National Board for Technical Education (NBTE) say so?
c. What internal quality assurances measures do Nigerian tertiary institutions have to improve the curriculum of their programmes?
d. Do Nigerian tertiary institutions have tracer programmes for graduates to see if the skills and competencies imparted are relevant to their future endeavors?
e. Are Nigerian tertiary Institutions ready to phase out programmes that the skills and competences are no longer required by industry?
f. Are tertiary Institutions innovating enough to produce graduates for the industry of the future or we only think about past and present gaps?
g. Are Nigerian tertiary Institutions' curricula producing regional, national or global graduates?

National Board for Technical Education(NBTE) Curriculum criteria: Polytechnics

Before any programme in the Polytechnic in Nigeria can be accredited, the National Board for Technical Education (NBTE) has laid down the following conditions:

a. The curriculum in use for the programme should be adequate and therefore, not inferior to the NBTE's approved minimum curriculum and course specification for the level of training.
b. It should reflect the requirements of the relevant industry and employers, and adequate in content to prepare students at the appropriate level in the particular field to acquire skills, that is, sound theoretical background and competences to fulfill the requirements for specific job objectives, in addition to social and communication skills necessary to understand the environment and to live, work and make useful contributions as a citizen.
c. There is a curriculum for the programme designed by the department/institution. Its structure includes professional and general education courses and students' industrial work experience scheme (SIWES).
d. The curriculum developed by NBTE is just a minimum requirement. Additional curriculum content must be developed by the Department to meet local/regional needs.
e. The content of each course should be adequate and similar to those contained in the NBTE curriculum.
f. The curriculum content is clear to the lecturers teaching the courses.
g. Skill and professional components are adequate for the level of programme.
h. The mode of teaching the curriculum is effective and includes lecture/recitation, practical exercises/projects and written exercise.

It is further expected that general studies courses should be included so that students may improve their communication skills, oral and written and their understanding of themselves, and their environment where they will live, work and make useful contributions as worthy citizens of the country and the world at large. General studies courses will also inform the student on how to relate his skills to the society and the economy. The general studies courses account for 10% - 15% of the contact hours allocated to the programme distributed by courses in the arts and

humanities, social and behavioral sciences, mathematics and basic sciences and physical and health education. All students in all programmes are expected to take all the modules in Use of English, Communication in English, Physical and Health Education, Contemporary Social Problems and Outline History of Nigeria (Citizenship).

Other courses are taken as elective courses depending on the professional programme and the resources available to the institution to mount them. Students' practical/project works are of good standard and quality. They reflect adequate preparation of the students for entry level employment in his chosen field.

In addition, the Board shall confirm that:

a. All laboratory/workshop/farm practical exercises listed for each course were accomplished by the end of each semester;
b. Simulated work related problems in each core modules are solved;
c. Projects undertaken by the students are related to the discipline, useful in the Nigerian environment and are of good standard;
d. All new equipment, are properly installed and commissioned;
e. All equipment in the laboratories, workshops and farm/field facilities are functioning;
f. Safety provisions are adequate and are being maintained; and;
g. Adequate volumes of books, journals, periodicals and non-book items are available in the library for the programme.

NATIONAL UNIVERSITIES COMMISSION (NUC): CURRICULUM CRITERIA: UNIVERSITIES

Before any programme in the University in Nigeria can be accredited, the National Universities Commission (NUC) has laid down the following conditions:

1. The Curriculum of the programme to be accredited should be adequate to prepare graduate at an appropriate level in the particular field;
2. It should include adequate theoretical knowledge and skills to fulfill the requirements for the specific job objectives;
3. It should be designed to equip the graduates with adequate communication skills (written and oral) and a sound knowledge of the social, political and economic environment in which the graduate shall live, work and make useful contribution as a citizen;
4. The curriculum must be in compliance with the NUC Benchmarks Minimum Academic Standards (BMAS);
5. The environment of the university must be suitable for the implementation of the curriculum;
6. The must adequate infrastructure such as lecture rooms, theatres, laboratories and workshops with the relevant equipment, etc to support the implementation of the curriculum;
7. There must be evidence of individual course content, textbooks, students' work, lecture notes and descriptive materials and annual external examiners' reports of final examinations for three years preceding the accreditation visit.

PRESENT DAY TRENDS ISSUES THAT AFFECTS CURRICULUM DEVELOPMENT

Scanning the present day industry and socio-economic landscape, the following are predominately the catch phrases or words trending:

A. Climate Change,
B. Changing Ecology,
C. Nanotechnology,

D. Increasing Population,
E. High Speed Computers,
F. Fracking,
G. Global Warming,
H. Job Loss Due To The Influence Of Technology,
I. Deforestation,
J. Desertification,
K. Multidisciplinary Approach And Team Work,
L. Sustainable Development,
M. Equity,
N. Finite Resources,
O. New Sustainable Energy Sources, Etc.

Is the current chemical engineering curriculum in use abreast with these new trends? A review shows that it is highly defici**ent.**

Scope and Emerging Career Options in Chemical Engineering

The chemical and related industries including pharmaceuticals and health, agriculture and food, phosphate and fertilizers, environment, oil and energy production, textile, iron and steel, bituminous, building materials, glass, surfactants, cosmetics and perfume, and electronics, etc; are today in a phase of rapid evolution. Engineering, Procurement and Construction (EPC) companies, which are contractors who complete projects from start to finish for their clients, routinely hire chemical engineers for design related jobs such as designing petrochemical, industrial plants, refineries etc using various software tools. Electronics companies also hire chemical engineers for jobs such as material development, production and process control equipment design. In case you are good at number crunching and analytics, you may also join banks or analytics companies and be involved in their financial modeling and quantitative research work. A glance at the Chemical Industry identifies the following fields, some emerging (*https://books.google.com.ng/books?isbn=0309165806)*:

i. Upstream Oil and Gas, Energy

Many integrated oil companies consist of an upstream organization and a downstream organization. The former focuses on exploration and production and the latter refines crude petroleum into usable products (gasoline, lubricants, etc.). Within upstream, processes and departments are often separated by subsurface work and surface facility work. Generally, most Chemical Engineers upstream are found on the facility side, managing projects related to tanks, pumps, pipelines and separators. Besides, there are options in sub stream as well. As we attempt to tackle the current national energy challenges, oil and gas will continue to be a key factor in the equation.

ii. Chemical Engineering Informatics

Chemical engineering informatics is the application of information technology to help engineers investigate new problems and organize, analyze and understand scientific data in the development of novel compounds, materials and processes. Chemical informatics is the application of information technology to chemistry and chemical engineering. Major aspects of chemical informatics are information acquisition, information management, information use, chemical computation and biopharmaceutical computation.

iii. Genetic farming and consumer goods

Chemical engineers who work in the food industry can work in agriculture or in manufacturing. Those working in agriculture may study the genetic modification of fruits and vegetables and attempt to increase yields and make them more desirable and thus more profitable. The career may also include researching methods of making agriculture more environment friendly, trying new methods of processing waste and conserving soil and water. Farmers of the future will not only raise livestock and agricultural crops, they will also grow plants that have been genetically engineered to grow therapeutic proteins, pharmaceuticals and chemicals. All consumer products involve chemicals; consumer product development depends upon research to develop and improve a product – work that would fall to a chemical engineer. Such a career may involve improving such consumer goods as hygiene products, chemical cleaning products, and electronics.

iv. *Bio-technology*

Chemical engineers working in biotechnology typically work in conjunction with researchers in molecular biology, biochemistry, genetics, embryology, and cell biology. A career in biotechnology may overlap with work in health care, crop production, agriculture, and the environment. A researcher may use chemical engineering to advance procedures in genetic testing and gene therapy. Chemical engineers in medicine may also work on engineering organisms and microorganisms to be used in applications, such as degrading wastes and converting chemicals into more useful ones.

v. *Green Processes*

The focus of all chemical engineers is to work sustainably. Corporations and consumers worldwide are increasingly embracing green technology and celebrating achievements in sustainable technology, water management and energy efficiency. Every organization would have a role of green process engineer who will develop environmentally benign chemical processes and products, select processes that minimize pollution, use less hazardous materials and develop alternative reactions. This will all need to be done while meeting emerging regulations and laws.

The Changing Work Environment:

Trends to Innovation

The emerging trend is toward open innovation: solutions to problems are externalized more, instead of having all the people inside a company available to work on every problem. There is more effort to reach out to the world to get answers. Companies are emerging around this idea, such as Nine-Sigma and Intercentive. These are places where problems can be posted for a bounty. Some 20 or 30 years ago, this might have been impossible to manage or handle. Now it is very easy. A web page can be accessible to almost everyone who might be interested in providing a solution.

Digitalization will drive a tremendous wave of innovation. Recent advancements in digital technology offer unprecedented levels of connectivity, granularity, and speed in accessing, processing, and analyzing huge amounts of data. Besides mobility, cloud and in-memory computing, the Internet of Things, machine learning and block-chain will start acting as game-changers in the chemical industry. All three trends are coming together to challenge existing

strategies and create a perfect storm for the chemical industry. In addition, computer modeling is changing how chemical engineering and experimentation are thought about. They can quickly pinpoint how something is going to react, where it is going to react, and what issues the reaction presents. It is remarkable how this is changing.

Supply centers are shifting due to the challenges in the Niger-Delta Region of Nigeria, advent of shale gas in the U.S. or coal to olefins in China. Also, demand centers are shifting thanks to a rapidly growing middle class in the emerging countries. In addition, new market entrants drive shrinking lifecycles and rapid commoditization of products. Key raw materials are getting scarce. Regulatory requirements exponentially increase as the environmental impact of emissions and waste becomes more and more evident. Chemical companies are in the driver's seat to respond to this, and some are already extending their ecosystems with the purpose to establish end-to-end concepts.

Challenges for the New Graduates

As markets change swiftly and as many other fields also move quickly, people who cannot go from one field to another become stranded in the company. They are experts, with expertise that is no longer needed. To perform well in the commercial process in a global environment, people have to understand how they fit into the whole value-creation process and how they connect to people around the world. Obviously, for top talent, international people skills and being able to lead diverse teams are going to be essential for personal growth and success. Broader language skills are also desirable but not requisite. When chemical engineers need all these high-value skills to perform well in a company, however, a lot is asked from them. Most at the top of the company now cannot provide this sort of capability, but it will be expected of the next generation. They will have to be better.

To address these challenges, institutions must be ready to answer these questions: What role can or should the polytechnics and universities play in selecting and developing students, or is it solely the role of industry to find the right people? Are engineers being prepared to use teams and external resources to supplement what they can do and what they are doing? Does the entire graduate-school process take students down a slightly different path that must be unlearned once they go into industry? Is industry making full use of the new skills and capabilities that new graduates have, and how well are chemical engineers being trained to understand how their craft will be practiced when they get into industry.

Green Process Engineering

Capentier (2016) pointed out that today's industries are confronted by 4 challenges:

a. The globalization of the markets,
b. Acceleration of partnerships and innovation,
c. Fight against environmental destruction and
d. Non-sustainable behaviour of the today world production.

Capentier (2016) proposed that the chemical and related industries militate for the evolution of chemical engineering in favour of a modern process engineering voluntarily concerned by sustainability (the green process engineering). New challenges and stakes arise because of the complex systems at the molecular scale, at the product scale and at the process scale. Therefore existing and the future processes will be progressively adapted to the principles of the " green chemistry" which involves a modern approach of chemical engineering that satisfies both the

market requirements for specific nano and microscale end-use properties of competitive targeted green (sustainable) products, and the social and environmental constraints of sustainable industrial meso and macroscale production processes at the scales of the units and sites of production.

These last constraints require an integrated system approach of complex multidisciplinary, non-linear, non-equilibrium processes and transport phenomena occurring on the different time and length scales of the chemical supply chain. This means a good understanding of how phenomena at a smaller length-scale relates to properties and behaviour at a longer length-scale, from the molecular and active aggregates-scales up to the production-scales. This modern scientific multiscale approach of chemical engineering " the green approach of process engineering" that combines both market pull and technology push is strongly oriented on process intensification and on the couple green products/green processes "to produce much more and better in using much less", and to sustainably produce molecules and products responding to environmental and economic challenges, with the help of technical innovation and sustainable technologies for efficient mass and energy utilization and for a better quality of life. This modern green approach of chemical and process engineering will concern the eco-efficient "Factory of Future".

The success of this integrated multiscale approach for process innovation is mainly due to the considerable developments in the analytical scientific techniques coupled with image processing, in the powerful computational tools and capabilities (clusters, supercomputers, cloud computers, graphic processing units, numerical codes parallelization etc.) and in the development and application of descriptive models of steady state and dynamic behaviour of the objects at the scale of interest (Capentier, 2016).

Qualities of a Good Chemical Engineer

a. What will be the qualities of the future workforce for those operating in this increasingly global environment? This has to do with know-who and know-how.
b. To be a good engineer in the future will mean competing with an extraordinary number of good engineers around the world. To be differentiated from the rest, it will be important to have expertise, of course, but it will also be necessary to have the ability to go out and find things and to connect with others.
c. Willingness to be a team player is essential. This is where communication Skills comes in. There are only a few jobs and a few opportunities for people who are lone experts. In most industrial companies, value is created by multifunctional teams. The ability to perform and provide knowledge and expertise to such teams is critical.
d. Flexibility is another important quality for success as a chemical engineer of the future. One must be able to adapt to new areas and learn to integrate knowledge from other fields. That is manifested in terms of a low-growth environment. The narrow people, however, are not as fortunate.

The Present HND Chemical Engineering Curriculum

The success of any chemical engineering curriculum will depend on the realization of the following students outcomes (*maeweb.ucsd.edu/.../AE%20STUDENT%20OUTCOMES*):

a. An ability to apply knowledge of mathematics, science, and engineering,
b. An ability to design and conduct experiments, as well as to analyze and interpret data,

c. An ability to design a system, component, or process to meet desired needs within realistic constraints such as economic, environmental, social, political, ethical, health and safety, manufacturability, and sustainability,
d. An ability to function in multidisciplinary teams,
e. An ability to identify, formulate, and solve engineering problems,
f. An understanding of professional and ethical responsibility,
g. An ability to communicate effectively,
h. The broad education necessary to understand the impact of engineering solutions in global, economic, environmental, and societal context,
i. A recognition of the need for, and an ability to engage in life-long learning,
j. A knowledge of contemporary issues,
k. An ability to use the techniques, skills, and modern engineering tools necessary for engineering practice.

The present ND and HND curricula were reviewed as far back as 2002 and there is little hope that the above listed outcomes can be achieved with the present curriculum. The curriculum for the HND Chemical Engineering is presented in Table 1. A look at the content of the curricula shows that many aspects in the emerging areas in chemical engineering were left out. This shows that the curricula are grossly deficient. Of course, this can be traced to the lack of regular review of the chemical engineering curriculum. More importantly, the ICT components are scanty and in a very dynamic area as Information technology *vis-a-vis* the rapid changes taking place in the chemical industry, a review is needed at least every two years. Table 2 presents a list of new courses that can be considered for addition to the curriculum during review. In coming up with the list, the trends in chemical industry have been considered and the peculiar need of the country.

There is therefore the need to constantly review the content of each course to keep up with new developments in the industry. To ensure this is done, an implementable plan of action for regular value-added curriculum review should be put in place and followed religiously. Since the curriculum of the NBTE is just the minimum standard, there must be a forum for institutions to share what each has added to the curriculum. This type of cross fertilization will help those institutions that are weaker in this area.

TABLE 1: THE PRESENT HND CHEMICAL ENGINEERING CURRICULUM: 2002

CODE	COURSE TITLE	CU
MTH 311	Advanced Algebra	2.0
MTH 312	Advanced Calculus	2.0
CHE 301	Engineer in Society	2.0
CHE 303	Unit Operations 111	2.0
CHE 305	Chemical Engineering Laboratory 111	3.0
CHE 307	Heat Transfer 11	2.0
CHE 309	Chemical Engineering Thermodynamics 11	2.0
CHE 311	Mass Transfer 11	2.0
MTH 313	Engineering Statistics	2.0
GNS 301	Use of English 11	2.0
		21.0
MTH 321	Advanced Numerical Methods	2.0
COM 321	Computer Programming	3.0

GLT 301	Instrumentation	2.0
CHE 302	Unit Operations IV	2.0
CHE 304	Fluid Mechanics 11	2.0
CHE 306	Chemical Reaction Engineering 11	2.0
CHE 308	Chemical Engineering Laboratory IV	3.0
CHE 310	Polymer Science and Technology	2.0
CHE 312	Strength of Materials	2.0
GNS 302	Communication in English	2.0
		22.0
CHE 401	Process Design	3.0
CHE 403	Chemical Plant Economics Unit	2.0
CHE 405	Operations V	2.0
CHE 407	Food Science and Technology Chemical	2.0
CHE 409	Engineering Laboratory V Chemical	3.0
CHE 411	Engineering Analysis Project	2.0
CHE 413	Engineering Management	2.0
CHE 415		2.0
	Elective 1	
	Pulp and Paper Technology	
CHE 417	Process Metallurgy	
CHE 419		
		22.0
CHE 402	Unit Operations VI	2.0
CHE 404	Equipment Design	2.0
CHE 406	Chemical Process Dynamics and Control	2.0
CHE 408	Health, Safety and Environment II	2.0
CHE 410	Chemical Engineering Entrepreneurship	2.0
CHE 412	Plant Services and Maintenance	2.0
CHE 414	Petroleum Refining and Petrochemical Technology	2.0
CHE 416	Project	2.0
	Elective II	
CHE 418	(i) Biochemical Engineering	
CHE 420	(ii) Gas Processing Technology	
CHE 422	(iii) Reserviour Engineering.	
		20.0

A look at the content of the curriculum shows that it is highly deficient. Key areas trending in the chemical Engineering field are not covered. A complete review of the curriculum is very necessary to correct these anomalies.

Challenges for Reviewing the Chemical Engineering Curriculum

In reviewing the chemical engineering curriculum, it is important to note the following challenges:

i. The need to keep core chemical engineering knowledge;
ii. The need to emphasize fundamentals: basis life-long learning;

iii. The need to modernize the curriculum and add flexibility by emphasizing the following;
iv. Increase exposure molecular level,
v. Increase exposure to energy (alternative/renewable) sustainability issues,
vi. Expose students to new process technology,
vii. Introduce product design as complement of process design,
viii. Emphasize process operations, enterprise planning,
ix. Increase link to other industrial sectors (e.g. pharmaceuticals and electronics).
x. The need to recognize that "bio-area" While important will not be dominant force in chemical engineering, emphasis should be on bio processing;
xi. Environmental engineering increasingly important and requires chemical engineering (water use efficiency, pollution control, etc.);
xii. Need closer interaction with industry; otherwise risk being irrelevant;
xiii. Need to provide excitement to recruit the very best young people to join chemical engineering.

Table 2: List of New courses to be considered when reviewing the Chemical Engineering Curriculum

S/No	New Courses to be introduced or modified
1	Energy Technology and Management
2	Renewable Energy Engineering
3	Energy Engineering and Technology
4	Industrial Pollution Prevention
5	Industrial Pollution Control
6	Introduction to Biochemical Principles
7	Programming Using MATLAB
8	Biology for Engineers
9	Biochemical Process Design
10	Enzyme Engineering and Technology
11	Bioreactor Analysis
12	Bioreactor Design
13	Fertilizer Technology
14	Petroleum Refining Technology
15	Polymer Technology
16	Drug and Pharmaceutical Technology
17	Pulp and Paper Technology
18	Petrochemical Technology
19	Food Technology

20	Chemical Plant Safety and Occupational Hazard
21	Electrochemical Engineering
22	Computational Fluid Dynamics
23	Introduction to Statistical Thermodynamics
24	Equilibrium Stage Operations
25	Chemical Plant Utilities
26	Chemical Process Optimization
27	Basic Mechanical Engineering
28	Basic Electrical Engineering
29	Basic Electronics Engineering
30	Value Education
31	Basic Civil Engineering
32	Classical and Instrumental Methods of Analysis Laboratory
33	Computational Methods
34	Chemical Process Equipment Design and Drawing Laboratory
35	Chemical Reaction Engineering and Process Control Laboratory
36	Chemical Process Equipment Design and Drawing Laboratory
37	Process Modeling and Simulation
38	Sustainable Refinery and Bio-Refinery.
39	Process and Product Design
40	Biological Systems Engineering
41	Food Engineering Operations
42	Food and Pharmaceutical Separations
43	Environmental Engineering
44	Mineral Processing Technology
45	Bioprocess Engineering
46	Autocad PandID
47	Computer Aided Process Dynamic and Control
48	Project and Business Management
49	Communication

CHALLENGES OF CURRICULUM DEVELOPMENT

To carry out a thorough review of the curriculum, we must strive to overcome the following challenges:

i. The infusion of the ICT gene into the workers of the future who are the present students.
ii. The lecturers cannot afford to be analogue and trying to raise digital graduates.
iii. Be innovative on how to tackle the conservatives (If it is not in Levenspiel, it is bad CRE)
iv. What to do with lecturers who do not have the knowledge to implement the revised curriculum: (*Reskilling and Upskilling?)*
v. Deciding on the best way for selecting the appropriate team for curriculum development.

Importance of Pedagogy in Curriculum Implementation

Despite the frenetic call for regular curriculum review for most programmes in Nigerian tertiary institutions, it is highly questionable to what extent classrooms have changed as little attention has been paid to teacher development. It is important that all institutions should strengthen their strategy and specific initiatives be designed to support the development of quality teaching. Therefore pedagogy can be viewed as a central enabler of the implementation of all academic curricula.

Pedagogy can be considered as the dynamic relationship between learning, teaching and culture. Teachers' actions in the classroom, in relation to learning and teaching, are underpinned by the ideas and values that they have about education. Pedagogy interacts with and draws together beliefs about learners and learning, teacher and teaching, and curriculum. It also includes consideration of the context in which learning and teaching takes place. Pedagogy is often shaped by a teacher's own experience of learning. For many this was simply knowledge being transmitted by their teacher. Their role as students was to receive this knowledge without question or other interaction (*https://www.unesco.org.uk/wp-content/uploads /2017/06/pedagogy.pdf)*.

Teachers' own beliefs about learning and teaching, teachers' experience of and expertise in alternative learning and teaching approaches and the alignment between curriculum, pedagogy and assessment expectations (leading, for example, to 'teaching to the test') are considered critical challenges in realizing education targets. In addition, learning and teaching space and resources, the quality of teacher education and ongoing support for teachers' professional learning; and teacher educators' understanding of different pedagogical approaches are also important considerations

To improve pedagogy which will ensure that the curriculum is well implemented, teachers need support in the following areas (*https://www.unesco.org.uk/wp-content /uploads /2017/06/pedagogy.pdf)*:

a) High quality pre-service and in-service teacher education. Teacher education and mentoring must be viewed as an on-going process, continuing throughout a teacher's career and helping teachers to understand and apply different pedagogical principles.
b) Alignment of curriculum, pedagogy and assessment. Examinations need to be designed to ensure a better fit of the assessment to the different types of knowledge and skills required for the 21st century globalised world.
c) Alignment of new pedagogical approaches sensitively with existing cultural practices. Educational stakeholders and community leaders should develop equal partnerships and joint visions to meet the educational targets.

Importance of Industrial Training for Lecturers in Curriculum Implementation

Teachers are seen to be vital in not only developing greater understanding about industry needs and expectations but also in the transfer of those workplace-related skills and competencies to their work with students. Concerns have been expressed about teachers' knowledge and abilities to make this link effective. This has resulted in a significant focus being placed on teacher professional development programmes that increase teachers' understanding about the world of work (Perry and Ball,1998). Whilst there has been an increasing recognition of the value of programmes that create links or partnerships between education and industry, the main emphasis of these programmes has been on provision of work placements for students. There has been less emphasis placed on school-industry link programmes that focus on teacher professional development. Those programmes that do involve linking teachers and industry more often relate to curriculum materials production and seminar or liaison group discussions with industry personnel than they do on focusing on teachers actually working in industry. It is therefore paramount that the programme of lecturers spending quality time in the industry be reintroduced and followed religiously.

The Role of Adjunct Positions in the Success of Curriculum Implementation

Industry managers think that Nigerian tertiary institutions are not properly preparing students to enter the workforce. However, it is important that industry managers appreciate the enormity of the task of inculcating skills and competencies to students. It is easy to criticize the quality of the product of tertiary institutions but it is more productive if industry managers are more involved in improving the quality of the graduates. It will do industry managers a world of good if they can spend some quality time in tertiary institution to teach students real life experiences.

Many tertiary institutions abroad hire adjunct lecturers who are currently employed in the industry they are teaching about. This allows the institution to gain the insight of the person's practical knowledge and allows the professional to share their real-world experience with students because they want to, not because they have to *(https://www.cornerstoneondemand.com/rework/adjunct-solution-using-industry-knowledge-teach-must-have-skills-workplace)*. With a strong understanding of how skills are being used in their industries on a practical level, adjunct lecturers are quickly becoming the norm in tertiary institutions abroad. The key to getting students the best education possible lies in striking the right balance between adjunct and full-time academic staff. Adjunct staff gives the student real-world examples which are critical ingredient of an industry compliant graduate.

It is therefore important that Nigerian tertiary institutions are encouraged to hire adjunct lecturers from critical industries to join regular staff for a period of time as this will go a long way in inculcating the appropriate real life skills and competences in students. Such symbiotic collaboration between industry and academia are key ingredients of a successful curriculum implementation.

Lessons from UNESCO-Nigeria TVE Revitalisation Project

During the years 1998 – 1999, NBTE, recognized that most Technical and Vocational Education (TVE) curricula have been operated for more than a decade without updating and were far out of synchrony with the world of work. Subsequently, a Project Document and Plan of Operation were signed on 15 December 2000 by UNESCO and the Federal Government of Nigeria for the "Support for Revitalisation of Technical and Vocational Education in Nigeria – Phase I". The Phase

I was instrumental to the first ever review of TVE curricula in the country, about 57No curricula were reviewed and updated to international standards, as well as integrating industry needs and current technologies. These curricula and their formats were adopted by other ECOWAS countries. In the Phase II of the Project, a total of 346 learning/training e-packages for thirteen programmes at the National Diploma level were produced in the areas where the curricula have been developed. At the same period, about 25 additional curricula were reviewed or developed in new and emerging fields, which are being adopted by West African countries through collaboration with the ECOWAS Commission. Furthermore, some 500 new Learning, Teaching and Training Materials (LTTMs) were developed for other subject areas. More importantly, the Project had a well-structured approach to curriculum review and development.

Recommendations

In order to come up with a workable and implementable chemical engineering curriculum, the following recommendations have been made:

a. Developing an action plan for the immediate review of not only the chemical engineering curriculum but the curricula of all engineering programmes in the polytechnics and universities. The last review of the chemical engineering curriculum was done in 2002.
b. Requesting Tertiary Education Trust Fund (Tetfund) and other sponsors to support the development of curricula of new programmes identified in this study and the review of the old ones. This will ensure that they support Institutions whose programmes contribute to the growth of the economy.
c. To ensure that the revised curriculum is satisfactorily deployed, Tetfund and other sponsors should support Instructional Materials development to assist the lecturers in the implementation of the new curricula. Textbook are scarce these days.
d. The lessons learnt in the curriculum development programme of the UNESCO-Nigeria Technical and Vocational Education (TVE) Project should be evaluated and those that can assist the curriculum development process implemented.
e. There is the need to identify the redundancies and gaps in the chemical engineering workplace and then deciding which new programmes to introduce and which old ones to phase out. This will require identifying knowledge gaps which need to be filled for an evidence-based policy and practice of curriculum development.
f. There is the need for a special team to identify the key areas and binding constraints to be addressed urgently to achieve major improvements in the quality of the curricula.
g. The need to develop an innovative approach to curriculum development by identifying the skills and knowledge required for the future chemical engineering industry.
h. Identifying key electives with the immediate regions in mind.
i. Ensuring that research and design activities are industry related and ICT tools are appropriately used.
j. An implementable timetable should be developed to ensure regular review of the curricula of the programmes of Nigerian tertiary institutions.
k. The need for proper funding, the provision of the required equipment and facilities to support the implementation of the curriculum and maintenance of infrastructure and policies that ensure a serene environment conducive for teaching and learning is available.
l. The upgrading of virtual library facilities to support the implementation of the curriculum.

Conclusion

This paper has analyzed the present chemical engineering curriculum used by Nigerian tertiary institutions and has found it to be deficient and therefore cannot be used to produce employable

graduates for Nigerian industries in particular and the world of work in general. This is because a critical review of the curriculum has revealed that the curriculum is out of tune with the state of the present industry. The deficiency is traced to the lack of regular review and revision of the curriculum. It was noted that regular review is important in order for the curriculum to keep pace with the developments of the industry and the lack of it has led to the production of graduates with obsolete skills and competencies which make them work-place and industry non-compliant. It is further revealed that, in many cases, industry has to spend huge resources retraining new employees before they could be useful in the industry. The paper points out that the classrooms have not changed significantly as little attention has been paid to teacher development. It therefore calls for all institutions to strengthen their strategies and specific initiatives designed to support the development of quality teaching since pedagogy is a central enabler of the implementation of all academic curricula. Major recommendations proposed include the development of a curriculum review plan with set timelines, the selection of knowledgeable curriculum review teams and updating of the curricula of not only the chemical engineering curriculum but the curricula of all engineering programmes of tertiary institutions so that new areas and trends occurring in the industry and workplace are captured.

The paper further recommends the development of an appropriate action plan for the review and introduction of new courses that are in consonance with new trends in the chemical industry and proposes the development of curriculum-linked instructional materials to make the implementation of the curriculum easier for both the lecturers and the students. Other recommendations include the development of an implementable timetable to ensure regular review of the curricula of the programmes of Nigerian tertiary institutions and the reintroduction of the periodic industrial attachments for lecturers to keep them abreast with the new developments in the industry.

The paper finally recommends that Nigerian tertiary institutions consider the hiring of adjunct lecturers from critical industries to join regular staff for a period of time as this will go a long way in inculcating the appropriate real life skills and competences in students. Such symbiotic collaboration between industry and academia are key ingredients of a successful curriculum implementation.

Acknowledgement

The Powerpoint version of this paper was presented at the Chemical Engineering Curriculum Workshop, Organised by the Nigerian Society of Chemical Engineers (NSChE), held at the University of Lagos, Akoka, Lagos, on the 21st of June, 2018

References

Charpentier, Jean-Claude (2016) What kind of Modern "green" Chemical Engineering is required for the Design of the "Factory of Future"? "SYMPHOS 2015", 3rd International Symposium on Innovation and Technology in the Phosphate Industry; Procedia Engineering 138, 445 – 458

https://simplyeducate.me/2014/12/13/the-meaning-and-importance-of-curriculum-development/

http://www.unesco.org/new/en/education/themes/strengthening-education-systems/quality-framework/core-resources/curriculum/

https://www.ncbi.nlm.nih.gov/books/NBK83654/

http://www.digitalistmag.com/digital-economy/2017/12/18/major-trends-for-chemical industry-in-2018-05652353

https://www.researchgate.net/publication/272294393_University_Stakeholders_in_the_Analysis_Phase_of_Curriculum_Development_Process_Model [accessed Jun 24 2018].

Matkovic, Predrag, Pere Tumbas, Marton Sakal, Veselin Pavlićević (2014) University Stakeholders in the Analysis Phase of Curriculum Development Process Model; 7th International Conference of Education, Research and Innovation (ICERI 2014), At Seville, Spain

Perry, Chris and Ian Ball (1998) What do teachers really know about work? Professional development through education-industry links, Teacher Development, 2:1, 73-86

Proceedings of the 49th NSChE Annual Conference
KADA 2019: pp 454-460

P2C-06: THERMAL CHARACTERIZATION OF GBETIOKUN OIL SHALE VIA ROCK-EVAL PYROLYSIS AND THERMOGRAVIMETRIC ANALYSIS

Obadiah Pagu Bitrus, A. G. Olugbenga and M. U. Garba
Petroleum and Gas Engineering Program, Chemical Engineering Department Federal University of Technology, Minna, Niger State, P. M. B. 65, Nigeria.
Corresponding author: realobd@gmail.com

ABSTRACT
The pyrolysis characteristics of Gbetiokun oil shale were investigated with rock-eval pyrolysis and thermogravimetry analysis (TGA). The Rock-Eval pyrolysis outlined the hydrocarbon potential of the oil shale sample via total organic carbon (TOC) value, hydrogen Index (HI) and production index (PI). The TGA was investigated at different heating rates of 10, 20 and 30 °C/min in the temperature range of 29-950°C (Figure 1). From the Rock-eval pyrolysis, it was deduced that the oil shale sample has a total organic carbon (TOC) value of 0.51wt% more than 0.5wt% which is the minimum standard required for the generation of hydrocarbon. The hydrogen index (HI) value of 208 mg HC/gTOC falls within the range of 150-300 mg HC/gTOC indicating that the sample is oil and gas prone. While PI value for the sample is 0.05 which is less 0.1 signifying that the organic matter is immature. The TGA shows the main stage of mass loss at temperature range of 200-620°C and higher corresponding to the release of oil and gas, further weight loss was due to decomposition of carbonate. It was also observed that increasing the heating rate shifted the weight loss to higher temperatures. It can be concluded that Gbetiokun oil shale has high potential to generate hydrogen and both Rock-Eval pyrolysis and TGA show that the sample is oil and gas prone.

Keywords: Rock-Eval pyrolysis, Thermogravimetric Analysis, Total Organic Carbon, Hydrogen Index, Production Index, Differential Thermogravimetric Analysis.

1.0 INTRODUCTION
In this time of global market uncertainty, the world needs energy and in increasing quantities, since the world population is growing rapidly, which is used to support economic and social progress and build a better quality of life especially in developing countries (Imperial Oil Limited, 2019). Energy is the key input in economic growth since it is essential in various production processes. The process of economic development requires the use of various higher levels of energy consumption. Almost everything in the world today can be traced to the use of energy in one form or another. And most of the energy is from the Sun to earth. Apart from direct solar energy, the sun's energy shown in different ways such as in wind power, water power, tidal power, fossil fuels, nuclear energy, coal, natural gas and petroleum, etc.

Petroleum is a naturally occurring liquid located beneath the Earth's surface which can be refined into fuel. Petroleum is a fossil fuel i.e. it has been created by the decomposition of organic matter over millions of years ago. Its formation is in sedimentary rocks under intense heat and pressure for so long. Petroleum may be used as fuel to power vehicles, heating units and machines of all sorts, as well as being converted into plastics and other materials (*Tissot et al., 1984)*. Exploration and production of oil and gas from various 'unconventional' sources (such as methane from coals, shale gas, underground coal gasification, and oil shale) are most likely to have significantly different land-use planning impacts to 'conventional' onshore oil and gas. The alternative sources such as oil shale are available globally which may breach the gap developing between remaining

conventional resources and demand (Crown Onshore Oil and Gas, 2011). The inland basins in Nigeria comprises of the following; Anambra Basin, the Dahomey Basin, the Lower, Middle, and Upper Benue Trough, the Chad Basin, the Bida Basin, and the Sokoto Basin (Aizebeokhai, 2012). Nigerian is blessed with an abundant resource of crude oil and its alternatives such oil shale, oil sand, tar, asphaltite, shale gas which can be transformed to increase supply of energy (Kok and Ozgur, 2016). However, petroleum potentials of Nigeria have not been fully explored, especially hydrocarbon resources in the inland basins. The underutilized basins include Anambra Basin, Benue Trough, Benin Basin, Bida Basin, Borno Basin, Niger Delta Basin and Sokoto Basin (Geologin, 2012). Therefore, there is need to utilized the use of energy sources to meet huge energy demand.

Oil shale is an organic-rich sedimentary rock that can be considered as a source of alternative energy. The organic matter enclosed in the oil shale is largely an insoluble solid matter referred to as kerogen. Thermal degradation of the kerogen at a temperature in the range of 400-600 ^{o}C will volatilize from oil, gas and a solid residue of coke (Tissot *et al.,* 1978). The yield of the oil during pyrolysis depends on the quantity or quality of the kerogen contained in the oil shale and its evolution (Tissot *et al*., 1978). Understanding the behavior of the thermal degradation of the kerogen in oil shale and its geochemical features are very vital for effective exploitation of this natural resource as alternative source of energy.

Pyrolysis is a general technique used for the decomposition of complex organic material at elevated temperatures in the absence of oxygen (or any halogens). In such a way that low energy kerogen can be transformed into high energy hydrocarbon (shale oil). Shale oil is close to oil crude when its composition is compared. It can be utilized as a fuel or feedstock for the production of derivatives of oil and chemicals. However, shale oil usually contains olefinic and polar heteroatomic compounds which makes it less attractive than the crude oil. However, further treatment to increase the content of desirable compounds in shale oil may be necessary (Akash, 2003; Bai *et al*., 2015; Lai *et al*., 2016). The characterization of organic matter for oil shale is a crucial step in the evaluation of hydrocarbon potentials of oil shale. Moving on to this ground, this study provides insight for the hydrocarbon potential Gbetiokun oil shale sample with Rock-Eval Pyrolysis and TGA.

2.0 Experimental

2.1. Sample

The oil shale used in this study was collected from Gbetiokun Delta South Local Government Delta in the southeastern part of Nigeria. The sample was treated with hydrochloric acid and rinsing with hot water to remove the potential contaminants from drilling mud and evaporative loss. The oil shale samples were grounded to particle size <100 meshes which is a standard procedure according to ASTM (ASTM D 2013-72).

2.2 Rock-Eval Pyrolysis

The Rock-Eval pyrolysis was performed on the Gbetiokun oil shale sample in Getamme Laboratories Nigerian Limited, Port Harcourt. This analysis was done in order to determine the hydrocarbon generative potential of the organic matter (TOC), to determine the maturity of the source rock (PI) and to evaluate the relative proportion of the hydrocarbon (HI) in the samples. The samples are then introduced into the combustion oven and the amount of carbon is measured

as carbon dioxide by Infra-Red Detector. The programmed temperature applied in pyrolysis mode is 300^0C (3min) and 650^0C (25min) (detected by Final Investment Decision). HI and PI can be deduced from the following expression in equation 1 and 2:

$$HI = S2 \times 100/TOC \quad 1$$

$$PI = S1/(S1 + S2) \quad 2$$

Where S1 represents the quantity of free hydrocarbon present in the source rock sample that can be volatile with kerogen decomposition while S2 represents the number of hydrocarbons obtained through thermal cracking of nonvolatile organic matter.

2.3 Thermogravimetry Analysis

The TGA is an instrument used for measuring mass a sample while heating the it. A sample is heated, it reacts and released mass inform of gas. There are two main types of TGA. The open system and closed systems. An open system is exposes the sample to a sweep substance that constantly replaces the medium around the sample and sweeps the product away while closed systems have to do with isolated sample in a reaction cell and reaction products persist around the sample. Most systems make use of a controlled atmosphere of gases but a unique form of a closed TGA makes use of water as the medium and a magnetic balance commonly mass loss measurement, is made at either isothermal condition or constant heating rate.

3.0 Results and Discussion

3.1 Rock-Eval analysis

Source rock analysis (SRA) also known as Rock-Eval analysis is a quick and conventional technique used in the field of petroleum exploration to assess different source rocks, their petroleum potential, maturity and to characterize the degree of evolution of gas/oil, type of kerogen and depositional environment. The standard parameters for generative potentials of source rocks are shown in Tables 1 and 2. The total organic carbon (TOC) serves as a measure to determine the amount of organic matter. S1 represents the quantity of free hydrocarbon present in the source rock sample that can be volatilized with kerogen decomposition (S1= 0.05). S2 represents the quantity of hydrocarbons obtained through thermal cracking of nonvolatile organic matter which is 1.04. S2, therefore, represents the existing potential of rock to generate petroleum. The Tmax is the measure of the organic matter potential and maturity. Tmax is equivalent to the temperature of the maximum production of hydrocarbon during pyrolysis (S2 peak maximum). Tmax value relies on the kerogen type. Tmax result of 414^0C signifies immature to early mature stage. Tmax further gives detail explanations of where does the maturity fall in relation to oil generation window. It can either be immature for oil generation, mature for oil generation or overmatured for oil generation.

HI: is the normalized hydrogen content. From the standard parameters for generative potentials listed in Table 2, The hydrogen index (HI) of 208 mg HC/gTOC indicates that the sample is prone to oil and gas. The analysis signifies that the source rock contains type II kerogen, since the HI fall within the range of 150 to 300 mg HC/gTOC. Production index defines the thermal maturity of the hydrocarbons. The PI value of 0.05 in this study is below 0.1 which signifies organic matter is immature.

Table 1. Standard geological parameters for generative potentials of immature source rocks (Peters and Cassa 1964)

Petroleum Potential	TOC (wt%)	S1 mg HC/g rock	S2 mg HC/g rock	Tmax
This study	0.51	0.05	1.04	414^0C
Poor	<0.5	<0.5	0-2.5	
Fair	0.5-1	0.5-1	2.5-5	
Good	1-2	1-2	5-10	
Very Good	2-4	2-4	10-20	
Excellent	>4	>4	>20	
Standard				

Table 2. Standard parameters for HI and PI (Peters and Cassa 1964)

Stage of oil maturity	Production Index	Temp
immature	<0.1	<435
Early mature	0.1-0.15	435-445
Peat mature	0.25-0.40	445-450
Late mature	>0.4	450-470
Post mature	-	>470
HI generative potential	Values (mgHC/gTOC)	
	Standard	This study
No generative potential	<50	
Gas prone	50 to 150	
Oil and gas prone	150-300	208
Oil prone	300	

3.2 Thermogravimetry Analysis

Figure 1 shows the overall profile of weight loss in oil shale. The overall profile can be divided into three stages: water removal (stage I), organic decomposition (stage II) and inorganic decomposition (stage III). Stage II can be further divided into two sub-stages I and II of weight loss. These two sub-stages occurring during pyrolysis process can be identified as bitumen and oil regimes. The first sub-stage decomposition occurs generally until 350 °C and represents organic decomposition; where degradation of kerogen produces bitumen (Al-Harahsheh *et al.*, 2011). This stage produces gas, bitumen, and carbon residue. In the second sub-stage, the produced gas, bitumen and carbon residue are de-volatilized further to produce oil, coke, and gas. This occurs between 350 and 600 °C. (Al-Harahsheh *et al.*, 2009; Fang-Fang, Ze *et al.*, 2010; Qing *et al.,* 2007).

The third stage refers to the inorganic decomposition regime and occurs generally between 600 °C and 800 °C. In this stage, mass loss is observed due to the decomposition of carbonates in the inorganic compounds of oil shale. At higher temperatures the carbon dioxide formed during carbonate decomposition reacts with residual coke and forms carbon monoxide. This process adds to the final weight loss (Qing *et al.*, 2007).

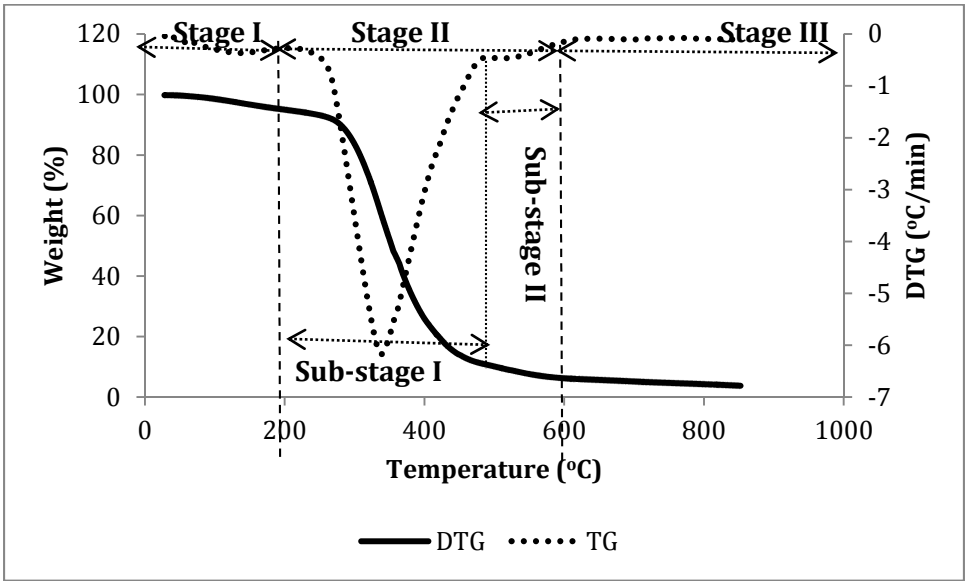

Figure 1. TG/DTG profile for the oil shale sample.

3.3 Effect of Heating Rate on Weight Loss

Figure 2 showed the oil shale thermographs of weight loss (Figure 2) and derivative weight loss (Figure 3) at corresponding different heating rates of 10, 20 and 30 °C/min (Extrapolation of Sedimentary Basin) respectively. At higher heating rate, the curves shift to highest temperatures and maximum weight loss shift to higher temperatures. The heat transfers across the oil shale particles (at a higher heating rate) is more effective but restricted by the heat transfer resistances. However, at a lower heating rate, the time was sufficient enough for heat to infuse steadily into the oil shale particles. These observations are in agreement with what was in the literature (Idris *et al.*, 2010). The corresponding peak temperatures of weight loss were 345, 401 and 430°C for 10, 20 and 30 °C/min heating rate respectively from the derivative weight loss curves in Figure 3.

Though the oil shale undergone two stages of pyrolysis, the results of the first and second stage weight loss of the oil shale pyrolysis in Table 3 are compatible as in Figure 3. The twin stages of the shale's deferential mass loss at the different temperature ranges showed the complex nature of the oil shale pyrolysis. In stage II, the broad peaks signified the high activity that rapidly pyrolyzed the shale through increased ability to overcome the resistance layer of mass transfer. The scenario can be explained by the chemical reaction that controlled the shale de-volatilization leading to the release of heat energy. Therefore, the stage wise decomposition activities of the shale particles are consistent with the literature (Wu *et al.*, 2014).

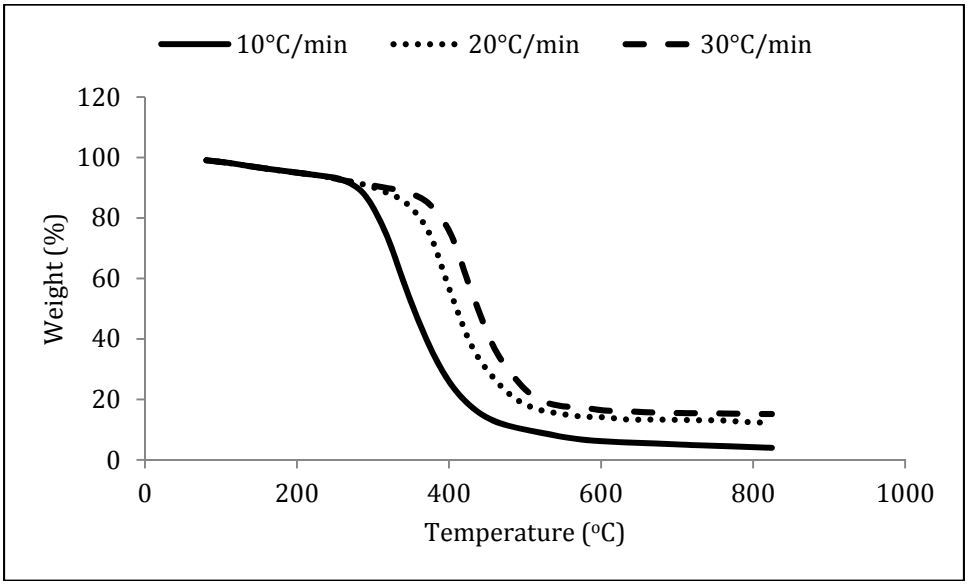

Figure 2. Weight loss profile for the oil shale sample at different heating rates.

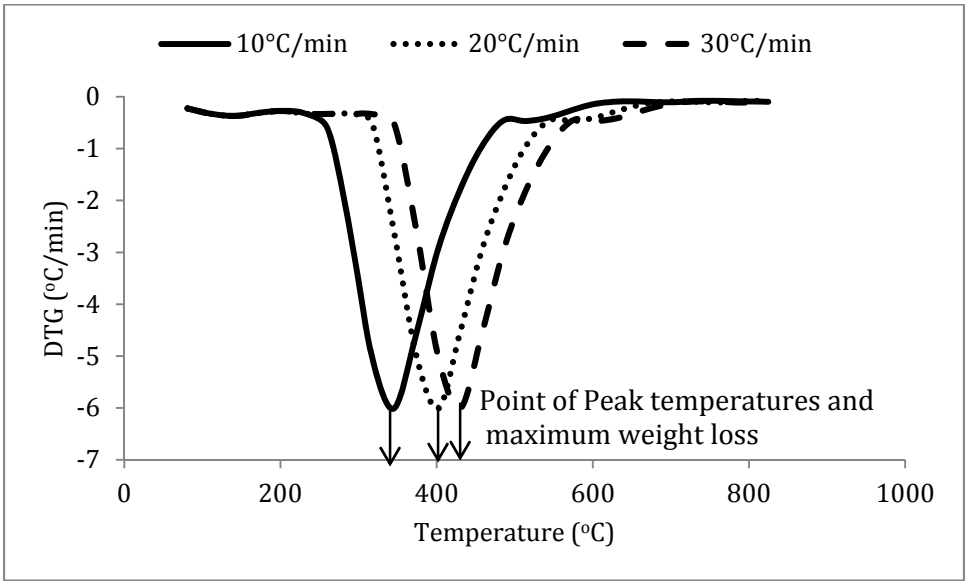

Figure 3. Derivative weight loss profile for the oil shale sample at different heating rates.

Conclusion

The pyrolysis characteristics of Gbetiokun oil shale was investigated with rock-eval pyrolysis and TGA. It deduces that the oil shale sample has total TOC value more than the minimum standard required for the generation of hydrocarbon. The HI value falls within the standard range indicating that the sample is oil and gas prone. While PI value was below the minimum standard signifying organic matter is immature. The TGA shows the main stage of mass loss corresponding to release bitumen and oil in the temperature range and at higher temperatures, further weight loss was due to decomposition of carbonate. It was also observed that increasing the heating rate shifted the weight loss to higher temperatures.

Reference

Wu, K. *et al.*, (2014). Pyrolysis characteristics and kinetics of aquatic biomass using the thermogravimetric analyzer. Bioresour. Technol. 163, 18–25.

Idris, S.S. *et al.*, (2010). Investigation on thermochemical behavior of low-rank Malaysian coal, oil palm biomass, and their blends during pyrolysis via thermogravimetric analysis (TGA). Bioresour. Technol. 101 (12), 4584–4592

Tissot BP, Welte DH (1978). Petroleum formation and occurrence. 3rd ed. Heidelberg, Berlin, New York: Springer- Verlag. P. 231.

Kok, M.V., and Ozgur .E. (2016).Combustion Performance and Kinetics of oil shales. Energy sources, part A:Recovery utilization and environmental effects 38:8,1039 1047.Doi:10.1080/15567036.2015.1098749.1039 – 1040.

B. A. Akash, Energy Source **25** (2003) 1171

F. Bai et al. (2015) Fuel **146** p. 111

D. Lai et al. (2016) Fuel **173** p. 1383,5

Thakur, D. S., and Nuttall, H. E. (1987). Kinetics of pyrolysis of Moroccan oil shale by thermogravimetry. Ind. Eng. Chem. Res., **26**(1932), 1351–1356.

Al-Harahsheh, M., Al-Ayed, O., Robinson, J., Kingman, S., Al-Harahsheh, A., Tarawneh, K.

Barranco, R. (2011). Effect of demineralization and heating rate on the pyrolysis kinetics of Jordanian oil shales. Fuel Processing Technology, **92**(9), 1805–1811. doi: 10.1016/j.fuproc. 2011.04.037

Fang-Fang, X., Ze, W., Wei-Gang, L., and Wen-Li, S. (2010). Study on Thermal Conversion of Huadian Oil Shale Under N2 and Co2 Atmospheres. Oil Shale, **27**(4), 309. doi: 10.3176/oil.2010.4.04

Qing, W., Baizhong, S., Aijuan, H., Jingru, B., and Shaohua, L. (2007). Pyrolysis characteristics of Huadian oil shales. Oil Shale, **24**(2), 147–157.

Proceedings of the 49th NSChE Annual Conference
KADA 2019: pp 461-471

P2C-07: INVESTIGATION INTO THE KINETICS OF ALKALI HYDROLYSIS OF CRYSTAL VIOLET

Nurudeen Salahudeen[1]* and Adamu A. Rasheed[1]
[1]Department of Chemical and Petroleum Engineering, Bayero University, Kano
***Corresponding author**: nusdeen@yahoo.co.uk

ABSTRACT
Kinetics of alkali hydrolysis reaction of crystal violet (CV) was studied at 21°C and varying concentrations of NaOH. Three concentrations of NaOH were used; 0.008, 0.016 and 0.024 M. The study shows that the reaction rate depends largely on the concentration of NaOH and the rate constant is stable only at certain range of NaOH concentration. The values of rate constant determined were 0.32 $\left(\frac{mol}{L}\right)^{-0.6} min^{-1}$ *and 0.41*$\left(\frac{mol}{L}\right)^{-0.9} min^{-1}$ *for NaOH concentration ranges of 0.008 – 0.016 M and 0.016 and 0.024 M respectively.*
Keywords: Kinetics; Alkali Hydrolysis Reaction; Rate Constant; Rate Order.

1.0 INTRODUCTION
Crystal violet is a cationic triphenyl methane dye chemically known as hexamethyl pararosaniline chloride. It is a highly demanded industrial raw material used in far-reaching industrial and medical applications. It is used as dye; in textile materials such as cotton and silk, in ternary materials such as leather and animal skin. It is used as an external disinfectant due to its toxic effect on cells. In medical and veterinary applications it is used as the active ingredient in Gram's Stain, employed in classifying bacterial (Ram and Bharagava, 2016; Wu *et al*., 2009).

Despite its huge economic benefits, crystal violet constitutes a major environmental threat as it is a key constituent of the waste water from the textile, ternary, and plastic industries. It has also been reported that uncontrolled exposure to crystal violet poses genotoxic and carcinogenic effects on humans and aquatic lives (Goswani *et al*., 2001; Mobacken *et al*., 1974). Hence, the need for effective treatment of CV in industrial waste water before disposal cannot be over emphasize. In waste water treatment, the removal of color from wastewaters is often more important than the removal of the soluble colorless organic substances, especially for industries using large quantities of water such as textile, leather, paint, acrylic, cosmetic, plastic and pharmaceutical industries, etc.

The alkali hydrolysis of CV can be expressed as Equation (1). Progress of the reaction can be physically monitored as the deep violet CV stock solution gradually losses its colour as the reaction progresses. At the completion of the reaction the CV solution becomes colourless.

$$C_{25}H_{30}N_3Cl(aq) + NaOH(aq) \longrightarrow C_{25}H_{31}ON_3(aq) + NaCl(aq) \quad (1)$$

The crystal violet color is due to the extensive system of alternating single and double bonds which extends over all three benzene rings and the central carbon atom. This alternation of double and single bonding is termed hydrolysis, and molecules which have extensive hydrolysis are usually highly colored. Trace the hydrolysis in the crystal violet structure and note that in the reaction product, the three rings are no longer in hydrolysis with one another, and hence, the material is colorless. The stoichiometry of the complete reaction is as shown in Figure (1).

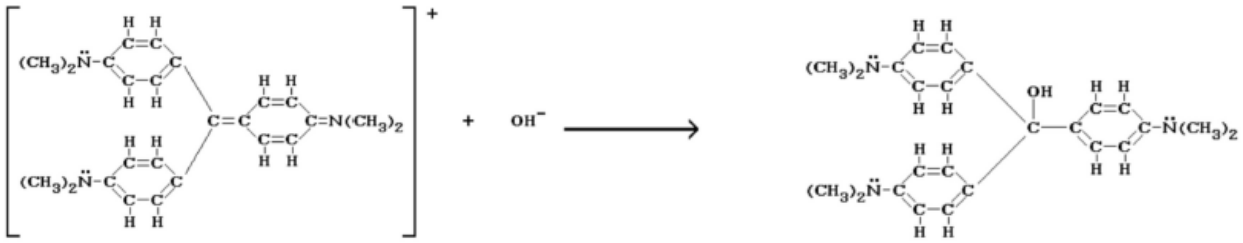

Figure 1: Stoichiometry of the Reaction between Crystal Violet and NaOH (Ram and Bharagava, 2016)

For the hydrolysis reaction in Eq. (1), it follows that;

$$\text{Rate} = k\,[CV]^x\,[OH^-]^m \quad (2)$$

$$-r_A = \frac{-dC}{dt} = k\,C_{Ao}{}^x\,[OH^-]^m \quad (3)$$

where; $-r_A$ = the rate of reaction with respect to the reactant CV

k = the rate constant of the reaction.

C = [CV], the concentration of the crystal violet.

n = the order of the reaction with respect to CV.

m = the order of the reaction with respect to OH^-

In this experiment, the initial $[OH^-]$ is made much greater than the initial [CV]. Thus, the $[OH^-]$ change, during the time that the CV is consumed, is negligible.

Therefore, since $[OH^-] >> [CV]$, Equation (3) can be written as follows

$$-r_A = \frac{-dC}{dt} = k'C^x \qquad \text{where } k' = k[OH^-]^m \quad (4)$$

The constant, k' is called a *pseudo rate constant* because it is a constant that relates the reaction rate to C^n only. Note that k' would have different values depending on the value of different $[OH^-]$. Therefore, the actual rate constant is expressed as;

$$k = \frac{k'}{[OH^-]^m} \quad (5)$$

For the two set of experiments carried out at different values of $[OH^-]$, it follows that two sets of equation hold;

$$k'_1 = k\,[OH^-]_1{}^m \quad \text{and} \quad k'_2 = k\,[OH^-]_2{}^m \quad (6)$$

$$\frac{k'_1}{k'_2} = \frac{k\,[OH^-]_1 m}{k\,[OH^-]_2 m} \quad (7)$$

$$m = \frac{log\frac{k'_1}{k'_2}}{log\frac{[OH^-]_1}{[OH^-]_2}} \quad (8)$$

Literature information on the kinetics of crystal violet are scanty, although, some researchers have reported some information about the reaction of crystal violet with sodium hydroxide (Chen *et al*., 2008; Cho *et al*., 2003; Du *et al*., 2013; Kabir and Susan, 2008; Karayil and Sreejith, 2017), the depths of most of the reports are not sufficient to give extensive information on the rate law of the reaction. This work is aimed at defining the extensive kinetic rate law of the alkali hydrolysis of crystal violet at a defined reaction conditions.

2.0 MATERIAL AND METHODS

2.1 Materials

The materials used include; analytic grade Crystal Violet (Sigma Aldrich, Darmstardt, Germany), analytic grade Sodium Hydroxide Pellets (98% Loba Chemie, Mumbai, India), distilled water was produced using water distiller water (SZ-96, Mon Scientific), stop watch and glassware.

2.2 Calibration Curve

A stock solution of crystal violet was prepared by weighting 0.1 g of the powder using weighing balance (Ohaus SP202 Scoutt Pro) and dissolved in 1000 ml of distilled water. Six (6) samples containing 0, 2, 4, 6, 8 and 10 mg/L of CV were prepared by diluting the stock solution with appropriate volumes of distilled water. The absorbance of each of the six (6) samples was measured with a Spectrophotometer (Zuzi; Model 4201/20, France) at a wavelength of 565 nm.

2.3 Kinetic Reaction

Runs of alkali hydrolysis at three different NaOH concentrations; 0.008, 0.016 and 0.024 M were carried out at 21°C in a 250 ml glass beaker used as the batch reactor. Progress of the reaction was monitored from the beginning to the end of the reaction by taking the spectrophotometer absorbance in intervals of 30 s.

Figure 2: Image of the physical view of the decolourization associated with the hydrolysis reaction of CV

3.0 RESULTS AND DISCUSSION

Figure 3 shows the calibration curve for the measurement of concentrations of the CV used in the reaction using spectrophotometer as the analytical technique.

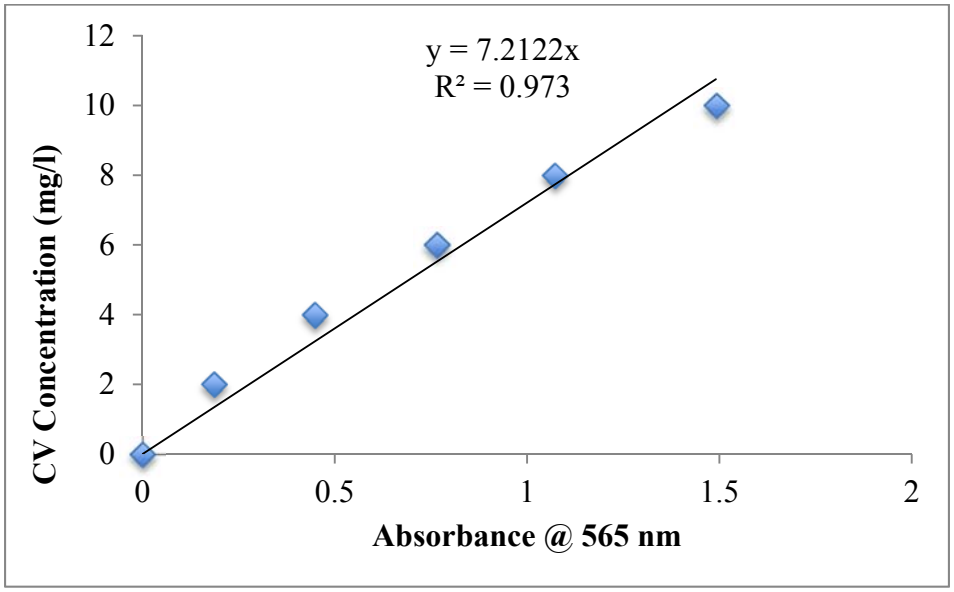

Figure 3: Calibration curve

Using the straight line graph equation of Figure 3, it was established that;

$$C = 7.212 \times \text{Absorbance} \quad (9)$$

where C = concentration of CV

Table 1 presents CV concentration variation against time for the alkali hydrolysis reaction carried out at 0.008 M NaOH and at 21°C. Figure 4 shows the concentration vs time curve for the hydrolysis reaction. Typical of concentration, time graph, it can be observed that the CV concentration depletes as the reaction time progresses, until the reaction was almost completed.

Table 1: Concentration, time data for the alkali hydrolysis reaction of CV at 0.008 M NaOH

Time (min)	C_A x 10^{-6} (mol/L)	Time (min)	C_A x 10^{-6} (mol/L)	Time (min)	C_A x 10^{-6} (mol/L)	Time (min)	C_A x 10^{-6} (mol/L)
0.00	26.35	7.00	9.36	14.00	3.58	21.00	1.56
0.50	23.30	7.50	8.70	14.50	3.35	21.50	1.49
1.00	21.53	8.00	8.13	15.00	3.15	22.00	1.42
1.50	20.34	8.50	7.55	15.50	2.94	22.50	1.36
2.00	19.05	9.00	7.03	16.00	2.78	23.00	1.29
2.50	17.72	9.50	6.56	16.50	2.64	23.50	1.24
3.00	16.50	10.00	6.13	17.00	2.45	24.00	1.19
3.50	15.42	10.50	5.71	17.50	2.30	24.50	1.13
4.00	14.30	11.00	5.35	18.00	2.16	25.00	1.10
4.50	13.33	11.50	4.98	18.50	2.06	25.50	1.03

5.00	12.49	12.00	4.66	19.00	1.95	26.00	0.97
5.50	11.62	12.50	4.34	19.50	1.84	26.50	0.92
6.00	10.83	13.00	4.08	20.00	1.74	27.00	0.90
6.50	10.05	13.50	3.83	20.50	1.65		

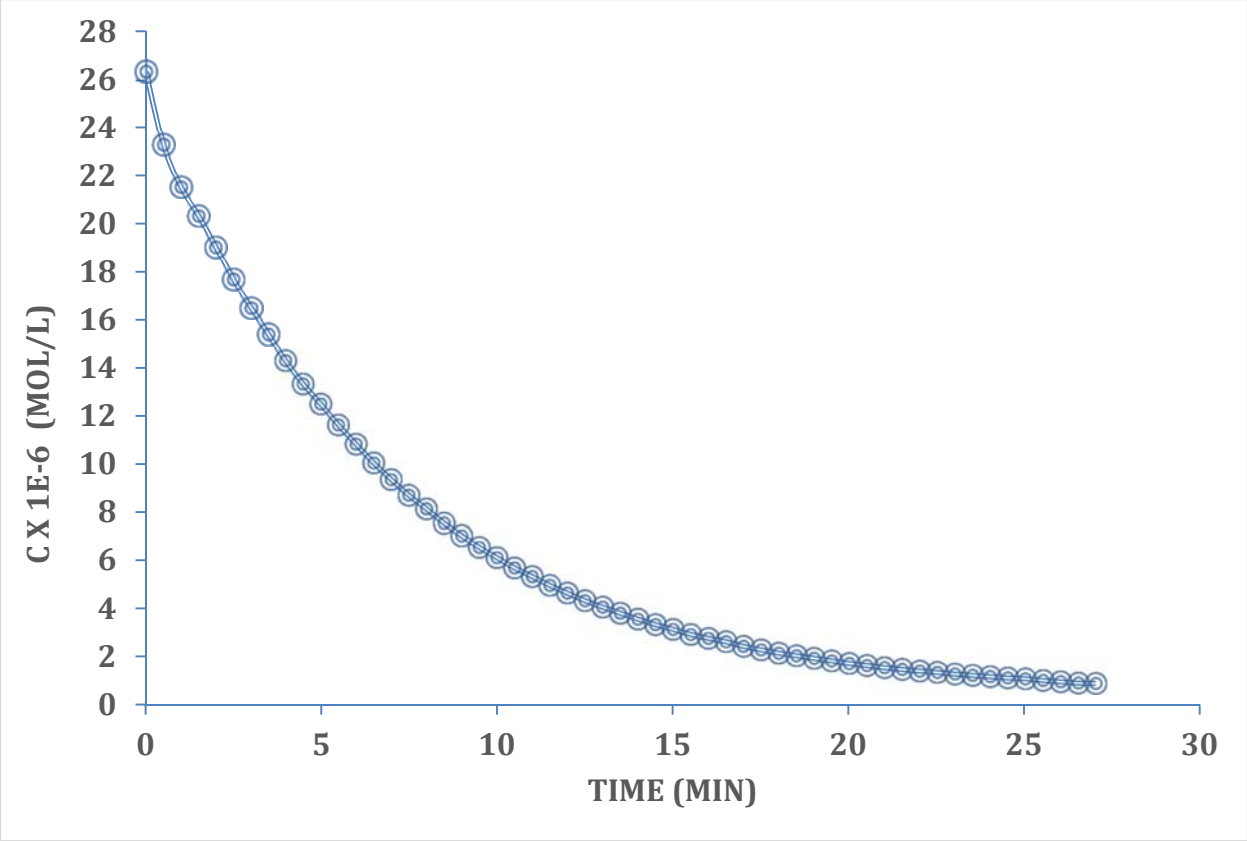

Figure 4: Concentration, time graph for the alkali hydrolysis of crystal violet 0.008 M NaOH and 21°C

The generalized kinetic formula for nth order reaction (Levenspiel, 1999) can be written as;

$$t_F = \left(\frac{F^{1-n}-1}{k\,(n-1)}\right) C_{Ao}^{1-n} \quad (10)$$

$$\log t_F = \log\left(\frac{F^{1-n}-1}{k\,(n-1)}\right) + (1-n)\log C_{Ao} \quad (11)$$

Taking the F factor as 0.5, we have;

$$\log t_{0.5} = \log\left(\frac{0.5^{1-n}-1}{k\,(n-1)}\right) + (1-n)\log C_{Ao} \quad (12)$$

Table 2 presents the variable values of C_{Ao} and their corresponding $t_{0.5}$ derived from Figure 4. Analyzing the plot of log $t_{0.5}$ against log C_{Ao} shown in Figure 5, it can be observed that the slope is zero. Therefore, from Equation (12), we can deduce that;

$$(1 - n) = \text{slope} = 0 \quad (13)$$

$$n = 1 \quad (14)$$

Hence, it is established that the reaction is 1st order reaction

Table 2: Values of C_{Ao} and $t_{0.5}$ for the hydrolysis of CV at 0.008 M NaOH

C_{Ao} x 10^{-6} (mol/L)	$t_{0.5}$ (min)	**Log C_{Ao}**	log $t_{0.5}$
26	4.8	1.41	0.68
20	4.8	1.30	0.68
16	4.8	1.20	0.68
10	4.8	1.00	0.68

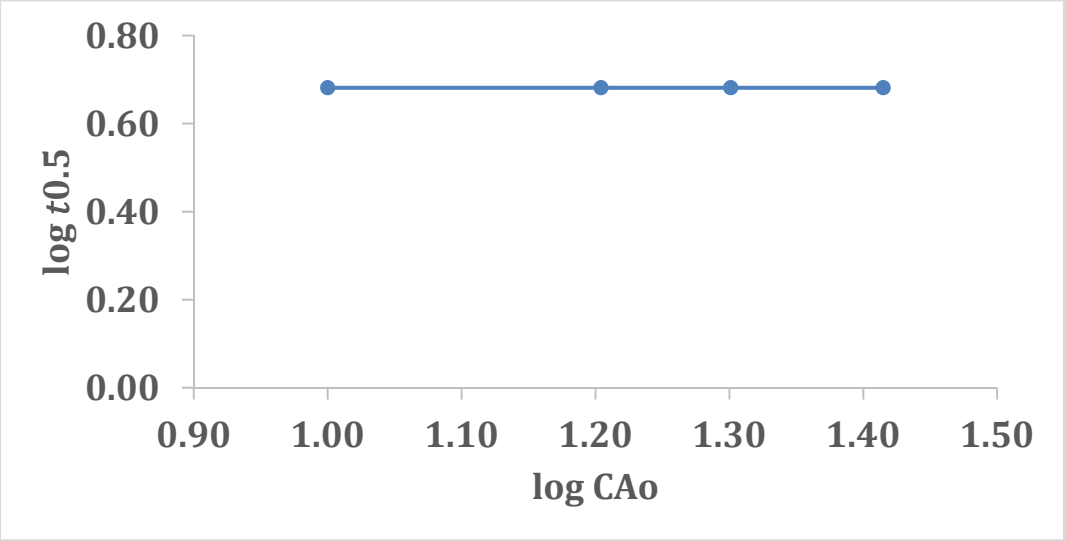

Figure 5: log $t_{0.5}$ vs log C_{Ao} graph

5 FOR 1ST ORDER REACTIONS, EQUATION (4) CAN BE SIMPLIFIED AS FOLLOWS;

$$\frac{-dC}{dt} = k'C \quad (13)$$

$$\int_{C_{Ao}}^{C_A} \frac{-dC}{C} = \int_0^t k'\mathrm{d}t \quad (14)$$

$$-\ln \frac{C_A}{C_{Ao}} = k't \quad (15)$$

Using the raw kinetic data in Table 1, values of $\ln \frac{C_A}{C_{Ao}}$ were derived at variable time as shown in Table 3. A plot of $-\ln \frac{C_A}{C_{Ao}}$ against time gave a straight line graph as shown in Figure 6. From Equation (15), the slope of the graph is equal to k', the pseudo rate constant of the alkali hydrolysis reaction. Hence, at NaOH concentration of 0.008 M and 21°C k_1' = 0.146 min^{-1}.

Table 3: Values of -ln $\frac{C_A}{C_{Ao}}$ at variable times for the alkali hydrolysis reaction at 0.008 M NaOH

Time (min)	-ln $\frac{C_A}{C_{Ao}}$	Time (min)	-ln $\frac{C_A}{C_{Ao}}$	Time (min)	-ln $\frac{C_A}{C_{Ao}}$	Time (min)	-ln $\frac{C_A}{C_{Ao}}$
0.00	0.00	7.00	1.04	14.00	2.00	21.00	2.83
0.50	0.12	7.50	1.11	14.50	2.06	21.50	2.87
1.00	0.20	8.00	1.18	15.00	2.12	22.00	2.92
1.50	0.26	8.50	1.25	15.50	2.19	22.50	2.96
2.00	0.32	9.00	1.32	16.00	2.25	23.00	3.01
2.50	0.40	9.50	1.39	16.50	2.30	23.50	3.06
3.00	0.47	10.00	1.46	17.00	2.38	24.00	3.10
3.50	0.54	10.50	1.53	17.50	2.44	24.50	3.15
4.00	0.61	11.00	1.59	18.00	2.50	25.00	3.18
4.50	0.68	11.50	1.67	18.50	2.55	25.50	3.24
5.00	0.75	12.00	1.73	19.00	2.60	26.00	3.30
5.50	0.82	12.50	1.80	19.50	2.66	26.50	3.35
6.00	0.89	13.00	1.87	20.00	2.72	27.00	3.37
6.50	0.96	13.50	1.93	20.50	2.77		

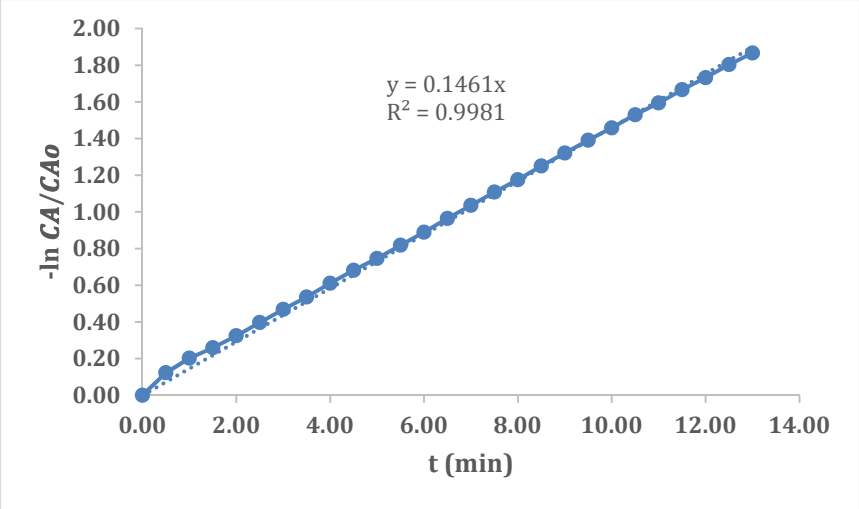

Figure 6: -ln $\frac{C_A}{C_{Ao}}$ vs time graph for CV hydrolysis reaction at 0.008 M NaOH

Table 4 presents the concentration, time data for the alkali hydrolysis reaction carried out at 0.016 M NaOH and at 21°C. Values of -ln $\frac{C_A}{C_{Ao}}$ were derived and plotted against time as shown in Figure 7. The slope of the straight line graph obtained is equal to k_2', the pseudo rate constant of the alkali hydrolysis reaction. Hence, at NaOH concentration of 0.016 M and 21°C k_2' = 0.216 min^{-1}.

Table 4: Values of -ln $\frac{C_A}{C_{Ao}}$ at variable times for the reaction at 0.016 M NaOH

Time (min)	C_A x 10^{-6} (mol/L)	-ln $\frac{C_A}{C_{Ao}}$	Time (min)	C_A x 10^{-6} (mol/L)	-ln $\frac{C_A}{C_{Ao}}$
0.00	26.35	0.00	8.50	3.51	2.02
0.50	22.19	0.17	9.00	3.19	2.11
1.00	19.74	0.29	9.50	2.89	2.21
1.50	17.51	0.41	10.00	2.60	2.31
2.00	15.59	0.52	10.50	2.37	2.41
2.50	13.82	0.65	11.00	2.18	2.49
3.00	12.30	0.76	11.50	2.00	2.58
3.50	10.92	0.88	12.00	1.86	2.65
4.00	9.66	1.00	12.50	1.74	2.72
4.50	8.58	1.12	13.00	1.63	2.78
5.00	7.65	1.24	13.50	1.54	2.84
5.50	6.79	1.36	14.00	1.47	2.89
6.00	6.08	1.47	14.50	1.40	2.94
6.50	5.40	1.58	15.00	1.33	2.99
7.00	4.84	1.70	15.50	1.29	3.01
7.50	4.31	1.81	16.00	1.28	3.03
8.00	3.88	1.92			

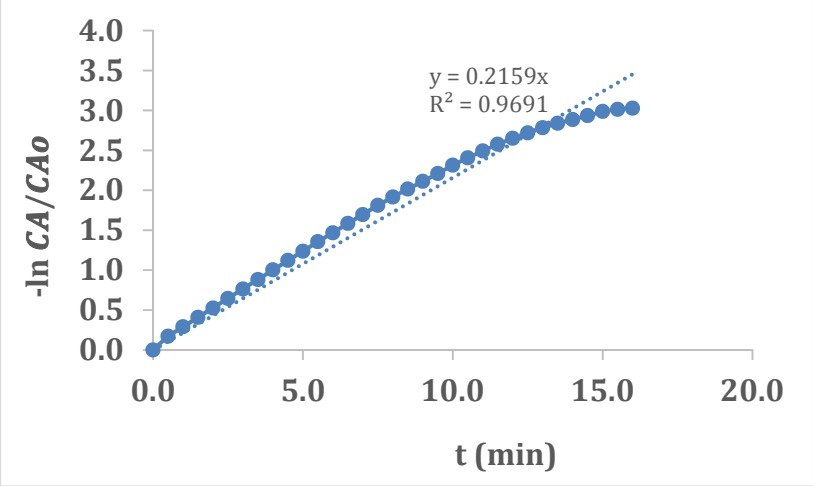

Figure 7: -ln $\frac{C_A}{C_{Ao}}$ vs time graph for CV hydrolysis reaction at 0.016 M NaOH

Table 5 presents the concentration, time data for the alkali hydrolysis reaction carried out at 0.024 M NaOH and at 21°C. Values of -ln $\frac{C_A}{C_{Ao}}$ were derived and plotted against time as shown in Figure 8. The slope of the straight line graph obtained is equal to k_3', the pseudo rate constant of the alkali hydrolysis reaction. Hence, at NaOH concentration of 0.024 M and 21°C k_3' = 0.313 min^{-1}.

Table 5: Values of -ln $\frac{C_A}{C_{Ao}}$ at variable times for the reaction at 0.024 M NaOH

Time (min)	C_A x 10^{-6} (mol/L)	-ln $\frac{C_A}{C_{Ao}}$	Time (min)	C_A x 10^{-6} (mol/L)	-ln $\frac{C_A}{C_{Ao}}$
0.00	26.35	0.00	7.00	2.37	2.41
0.50	21.62	0.20	7.50	2.04	2.56
1.00	18.29	0.37	8.00	1.75	2.71
1.50	15.42	0.54	8.50	1.54	2.84
2.00	12.99	0.71	9.00	1.36	2.96
2.50	10.37	0.93	9.50	1.24	3.06
3.00	9.14	1.06	10.00	1.10	3.18
3.50	7.67	1.23	10.50	1.01	3.26
4.00	6.43	1.41	11.00	0.92	3.35
4.50	5.40	1.58	11.50	0.85	3.43
5.00	4.55	1.76	12.00	0.80	3.50
5.50	3.85	1.92	12.50	0.76	3.54
6.00	3.28	2.08	13.00	0.73	3.59
6.50	2.75	2.26			

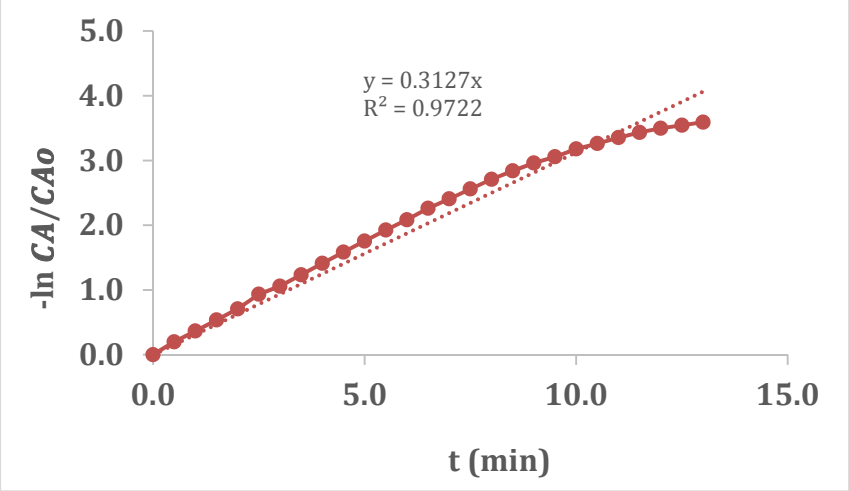

Figure 8: -ln $\frac{C_A}{C_{Ao}}$ vs time graph for CV hydrolysis reaction at 0.024 M NaOH

Table 6 presents the various values of the pseudo rate constant of the alkali hydrolysis reaction carried out at 21°C and at variable concentrations of NaOH. The values of k' increases generally with NaOH concentration. At NaOH concentration of 0.008 M k' value was 0.146 min^{-1}. The value increased by 48% when the NaOH concentration was doubled and increased by 114% when the NaOH concentration was tripled.

Table 6: Values of the pseudo rate constant at variable NaOH concentration

Reaction run	NaOH concentration ($[OH^-]$ in M)	k' (min^{-1})
1	0.008	0.146
2	0.016	0.216
3	0.024	0.313

The actual rate constant, K, of the alkali hydrolysis reaction can be obtained from Equation (5).

To determine this, the pseudo rate order with respect to [OH^-], m, is first of all determine using Equation (8). Therefore, Table 7 presents values of m and K for the alkali hydrolysis reaction at NaOH concentration range of 0.008 – 0.016 M and 0.016 – 0.024 M. It can be observed that k' has no constant value within a particular NaOH concentration range, but K value is constant within a particular NaOH concentration range. The reaction rate order of NaOH was 50% higher than that of CV at NaOH concentration of 0.008 – 0.016 M, and 800% higher at NaOH concentration of 0.016 – 0.024 M.

Table 7: Values of the actual rate constant of alkali hydrolysis reaction at various NaOH concentration range

[OH^-] range (M)	m	x	K ($\left(\frac{mol}{L}\right)^{-m} min^{-1}$)
0.008 – 0.016	0.6	0.4	0.32
0.016 – 0.024	0.9	0.1	0.41

4.0 CONCLUSION

The overall kinetic rate order of the reaction of alkali hydrolysis of crystal violet has been determined as 1st order reaction. The study shows that the reaction rate was largely dependent on the concentration of NaOH. The individual rate order with respect to the two participating reactants depend on the concentration range of NaOH. The values were 0.4 and 0.6 for CV and NaOH, respectively, at NaOH concentration of 0.008 – 0.016 M. And 0.1 and 0.9 for CV and NaOH, respectively, at NaOH concentration of 0.016 – 0.024 M. The rate laws for the reaction at the NaOH concentration range of 0.008 – 0.016 M and 0.016 – 0.024 M are as presented in Equations (16) and (17), respectively.

$$-r_A = 0.32\left(\frac{mol}{L}\right)^{-0.6} min^{-1}\ {C_{Ao}}^{0.4}\ [OH^-]^{0.6} \quad (16)$$

$$-r_A = 0.41\left(\frac{mol}{L}\right)^{-0.9} min^{-1}\ {C_{Ao}}^{0.1}\ [OH^-]^{0.9} \quad (17)$$

REFERENCES

Chen ZY, Zhao JH, He W, An XQ, Shen WG (2008) Study of association thermodynamic between crystal violet and sodium bis(2-ethylhexyl)-sulfosuccinate and kinetics of basic fading of crystal violet in microemulsions. Inter J Chem Kinet 40: 294-300.

Cho B, Yang T, Blankenship LR, Moody JD, Churchell M, et al. (2003) Synthesis and Characterization of N-dimethylated Metabolites of Malachite green and Leucomalachite green. Chem Res Toxicol 16: 285-294.

Du Z, Mao S, Chen Z, Shen W (2013) Kinetics of the reaction of crystal violet with hydroxide ion in the critical solution of 2-Butoxyethanol + water. J Phys Chem A 117: 283-290.

Goswani G, Kothari S, Benerji KK (2001) Kinetics and mechanism of the oxidation of some diols by benzyltrimethylammoniumtribromide. J Chem Sci 113: 43-54.

Kabir AR, Susan MB (2008) Kinetics of the alkaline hydrolysis of crystal violet in aqueous solution influenced by anionic surfactants. J Saud Chem Soc 12:543-554.

Karayil J, Sreejith L (2017) Catalytic action of CTAB/KBr/C9OH micellar media on the basic hydrolysis of crystal violet. J Dispersion Sci Technol 38:854-851.

Latona Dayo Felix (2018). Kinetic Study of the Discoloration of Crystal Violet Dye in Sodium Hydroxide Medium. Journal of Chemistry and Applied Chemical Engineering, 2:1; 11-4.

Mobacken H, Ahonen J, Zederfeldt B (1974) The effect of Cationic triphenylmethane Dye (Crystal violet) on rabbit granulation tissue. Oxygen Consumption and RNA and Protein Synthesis in tissue Slices. Acta Derm Venereol 54: 343-347.

Levenspiel, O. (1999). Chemical Reaction Engineering, 3rd ed. John Wiley and Sons, Inc. New York.

Ram, M. S., Bharagava, N. (2016). Exposure to Crystal Violet, Its Toxic, Genotoxic and Carcinogenic Effects on Environment and Its Degradation and Detoxification for Environmental Safety. Reviews of Environmental Contamination and Toxicology Volume 237 pp 71-104.

Wu, J., Jung, B., Kim, K., Lee, Y., Sung, N. (2009). Isolation and characterization of pseudomonas otitidis and its capacity to decolorize triphenylmethane dyes. J Environ Sci (China) 21: 960-964.

Proceedings of the 49th NSChE Annual Conference
KADA 2019: pp 472-478

P2C-08: EFFECTS OF SOIL BACTERIA ON LUFFA FIBER REINFORCED WASTE POLYSTYRENE FOAM COMPOSITE

Tajudeen Kolawole BELLO* **and Mohammed AKABE**
Department of Chemical Engineering, Ahmadu Bello University, Zaria.
***Corresponding author**: tkbello@abu.edu.ng, 09092547792*

ABSTRACT
This paper presents studies of biodegradation due to soil bacteria on polystyrene composite. The composite was formed from treating luffa cylindrical fiber with 10 wt% sodium hydroxide before using it as reinforcement in waste polystyrene foam. The loading of the luffa fiber was from 0 wt% (unreinforced polystyrene) to 50 wt%. The composites were buried for 14 weeks and effect of bacteria activity on the composites' weight loss studied. It was observed that degradation was highest (14.66%) for composite with highest luffa fiber (50 wt%). The microorganism identified in the soil was bacillus sp. which had a cell count of 4.0 × 10^7 CFU/gm. It can be concluded that reinforcing polystyrene foam with luffa, produces bio composites that are environmentally friendly.

Keywords: ***p****olystyrene, luffa fiber, composite, soil bacteria, reinforcement.*

1.0 INTRODUCTION
The use of bio-composites as a replacement to conventional synthetic composites has been gaining attention in recent years. This is because they degrade easily (compared to the synthetic ones) into the environment thereby decreasing waste management issues. Natural fillers used in bio composites are cheap, light weight, renewable and environmentally friendly (Bandyopadhyay-Ghosh and Ghosh, 2015; Pickering *et al.*, 2016; Ghori *et al.*, 2017). They however have drawbacks due to compatibility issues with the matrix they are used to reinforce. Most bio fillers are hydrophilic while synthetic matrices are hydrophobic. This makes the materials used for fabricating bio composites not only incompatible but having problems of swellings thereby leading poor mechanical properties (Ali *et al.*, 2016). These problems can be solved if the fillers morphology are treated or modified to improve the interfacial properties between the filler and matrix as well as filler dispersion in the matrix (La Mantia and Morreale, 2011). Treatments such as alkaline, maceration, benzoate, saline isocyanate, corona as well as thermal treatment have been studied and found to improve compatibility of natural fillers with synthetic matrices (; Li *et al.*, 2007; Ponnusamy *et al.*, 2019). The improved compatibility has also made them candidate materials for mechanical and structural applications as well as maintaining their low carbon footprint (Sanjay *et al.*, 2017).

Non-biodegradable plastics litter everywhere from blocking drains to suffocating aquatic lives. They have made several Environmental pressure groups to ask scientist and Engineers to help the planet from these excessive carbon footprints. The production of biodegradable composites from natural fiber and synthetic fillers will not only increase the overall biodegradability of the synthetic filler but also reduce waste plastic accumulations. The degradation of the composites by biological processes involves living organism such as bacteria, fungi and algae to breakdown the organic substances present in the composite into simpler and smaller structures such as

carbon dioxides, water, methane etc as end products (Shah *et al.*, 2008; Pelissari *et al.*, 2019). The simpler end products are easily disposed thereby reducing the menace caused by non-biodegradable plastics which litter the environment. A reduction in plastic production is directly related to low carbon dioxide emission due to production synthetic matrix from fossil fuel byproducts (Adamcova *et al.*, 2017).

This research work therefore focuses on the study of biodegradation by burial method of a bio-composite formed from Luffa fiber and waste polystyrene foam. The soil organism was identified and degradation rate due to the organism monitored and modelled.

2.0 METHODOLOGY

2.1 Materials, Chemicals and Equipment

The materials and Chemicals used in this research are polystyrene foam, luffa fiber, soil sample, methylated spirit, distilled water, nutrient agar, cotton wool, crystal violet, iodine, ethanol, safranin, paper towel, foil paper, and sodium hydroxide.
The equipment/apparatuses used are measuring cylinder, beaker, conical flask, glass rod, pipettes, glass slide, sterile bottle (test tubes), staining rack, culture plates (petri plates), sterile syringes, forceps, wire loop, digital weighting balance, electric heating mantle, Bunsen burner, incubator, autoclave, microscope, and humidity and temperature meter.

3.0 Procedure

3.2.1 Composite Preparation

Luffa fiber sourced from Ahmadu Bello University, Dam area was first cut, dried then treated with 10 wt% NaOH. It was then washed and dried in the oven at 60 ^{o}C for two hours. The fiber was then used to reinforce waste polystyrene foam in a 2 roll mill after which it was then compressed at 100 ^{o}C and 4psig. It was then cooled and removed. 0 to 40 wt% fiber loading at an interval of 10 wt% was used as reinforcement as described in Table 1. Three samples each of size 25 x 30 x 5 cm were cut from saples A to E, weighed and taken for biodegradation test using burial method.

Table 1: Description of fabricated composite samples.

Sample	Weight percent (wt%) of luffa used to reinforce polystyrene matrix
A	0; i.e 100% polystyrene
B	10
C	20
D	30
E	40
F	50

3.2.2 Biodegradation test using burial method

In this research, a land space of 2 × 1 x 0.1 m was cleared at Kaduna Polytechnic Demonstration Farm, Kaduna. A mixture of soil samples taken from the cleared ground and then taken for microbial analysis. The composite samples were then buried at a depth of 5 cm maintained at average temperature and humidity of 27 and 20% respectively by sprinkling water (Haider *et al.*, 2018). The cleared site and composite samples are shown in Plate 1. After seven days (a week),

all samples were removed, washed, cleaned and dried in the oven at 60 °C for and 4 hrs before calculating the biodegradation due to weight loss using equation 1:

$$\text{Degradation rate due to weight loss } (\%) = \frac{(\text{Mo} - \text{Ms})}{\text{Mo}} \times 100 \quad \text{.....(1)}$$

where; Mo is the initial mass, and Ms is the mass of buried composite after reference days.

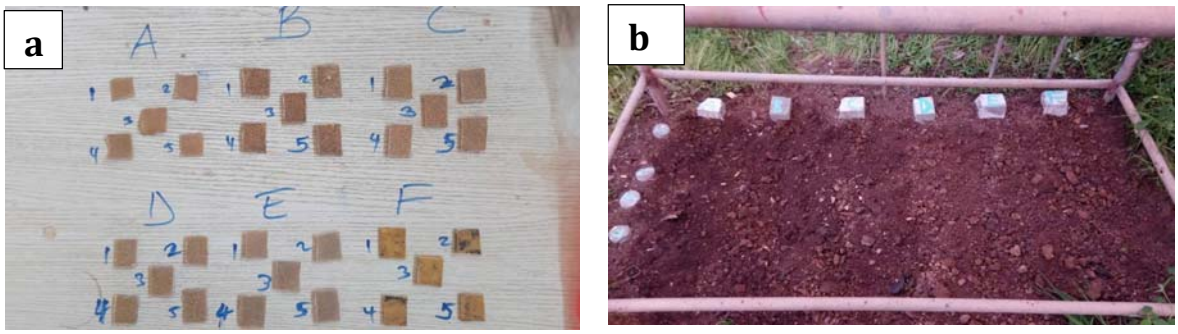

Plate 1: Image showing (a) Composite samples (b) burial site for the samples

2.2.3 Microbial analysis of soil sample

Serial dilution method was used to prepare nutrient agar and poured into the petri dish. The soil was then plated and incubated for 24 hours after which bacteria growth was counted and thereafter identified by microscopic morphology. Equation (2) was used to calculated the number of colonies unit (CFU). Coliform count between 20-200 is usually recommended and therefor was used in this study (Bio Resource, 2016).

$$\text{NCU}(\text{CFU/gm}) = \frac{\text{Number of Colonies Count (Average)} \times \text{Recip.of Dil.Factor}}{\text{ml plated}} \quad \text{.....(2)}$$

where; CFU/gm is colonies forming units per ml, and ml plated used is 0.1 ml.

A smear and gram staining process was then carried out on the coliform unit. Shape and colour were observed under the microscope to identified the species of the bacteria present. The biodegradation analysis was carried out based on ASTM D6691, 2001 (Muller, 2005).

4.0 RESULTS AND DISCUSSIONS

4.1 Biodegradation analysis of the composites.

Figure 1 shows the rate of biodegradation of the composite samples. It was observed that the un-reinforced composites which served as the control sample degraded by only 1.23% after 14 weeks. It had the lowed degradation rate among all the samples. Sample E (50/50) had the highest degradation rate (14.66%) after 14 weeks because of its high natural fiber content. It was generally observed that the degradation rate increased with increase in fiber content (Gomez and Michel, 2013; Bello *et al.*, 2019). This is expected before of the biodegradation nature of natural fibers which makes them attractive for application in production of bio degradation polymers (Lucas *et al.*, 2008).

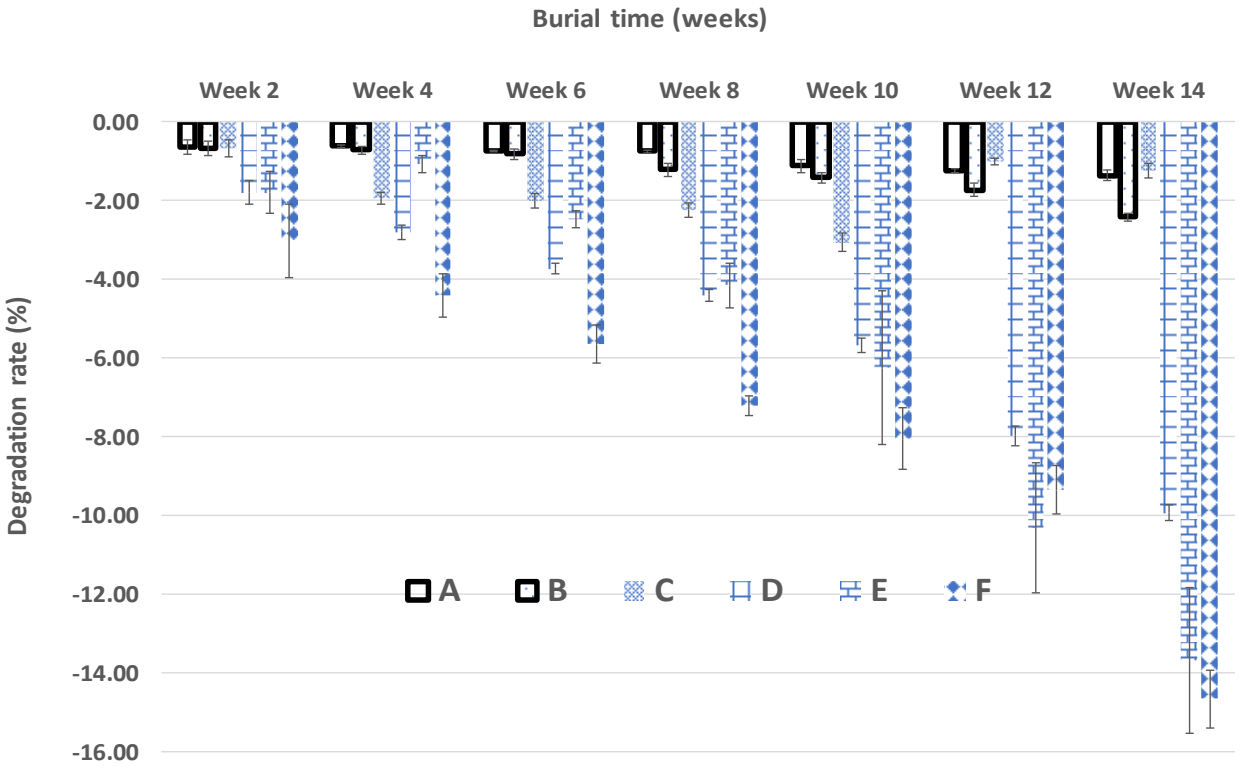

Figure 1: Degradation rate of the composites samples for 14 weeks

The sample degradation rate was further analyzed using Microsoft excel, the trendline was generated and fitted as summarized in Table 2. The samples degradation rate easily fitted into a polynomial model (with R^2 greater than 0.93) of order 2 (quadratic) except for sample C which had an order 5 polynomial. This behavior may be due to moisture diffusion in the composite leading to alternating increase and decrease in weight of the sample (Krauklis *et al.*, 2019).

Table 2: Modelling of degradation rate of composite samples buried for 14 weeks.

Samples	Equation	R^2	Model	Order
A	$R_D = -0.0165t^2 - 0.0025t - 0.5802$	0.9441	Polynomial	2
B	$R_D = -0.0463t^2 + 0.0884t - 0.7097$	0.9852	Polynomial	2
C	$R_D = -0.04t^5 + 0.7864t^4 - 5.7285t^3 + 19.148t^2 - 29.291t + 14.476$	0.9357	Polynomial	5
D	$R_D = -0.152t^2 - 0.0952t - 1.7643$	0.9922	Polynomial	2
E	$R_D = -0.4124t^2 + 1.2317t - 2.3547$	0.9949	Polynomial	2
F	$R_D = -0.2197t^2 + 0.07t - 3.3656$	0.9493	Polynomial	2

Where R_D is degradation rate and t is burial time in weeks

3.2 Microbial count in the soil

Table 1 shows the count of the coliform forming unit (CFU) observed in the plate of incubated soil sample collected from the sample burial site.

Table 1: Quantification Number of Colonies Forming Unit (CFU)

Dilution Series	Plate	Number of Colonies Count	Average of Number of Colonies Count	Colony Forming Unit (CFU/gm)
10^{-1}	1	+++		
	2	+++		
	3	+++		
10^{-2}	1	+++		
	2	+++		
	3	+++		
10^{-3}	1	+++		
	2	+++		
	3	+++		
10^{-4}	1	48		
	2	63		
	3	90		
10^{-5}	1	34		
	2	41	40	4.0×10^{7}
	3	45		
10^{-6}	1	18		
	2	25		
	3	28		

+++ too numerous to count

The counts for serial dilution for 10^{-1} to 10^{-3} was neglected because the count was uncountable. The serial dilution for 10^{-4} was also neglected because of the wide variation in counts. 10^{-5} was used for the calculations because it did not have wide variations like $10^{-}4$ or a count below 20 as the case of $10^{-}6$ (Bio Resource, 2016). The average total number of bacteria counted of the colonies forming unit was calculated to be 4.0×10^{7} CFU/gm of soil.

3.2 Identification of Microorganisms in the Soil Sample

The identification of the species of microorganisms in the soil sample was carried out under the microscopy observation. The type of microorganisms observed in the soil sample was gram positive bacteria, which showed the present of Bacillus because of its rod-like structure and purple color as shown in Plate 2.

5.0 CONCLUSIONS

The following conclusions can be drawn from this study.

1. The degradation increased with increase in fiber content with 50 wt% (Sample F) recorded the highest at 14.66 % while the lowest degradation of 1.23 % was observed for the un-reinforced composite.
2. The degradation rate followed mostly a quadratic model.
3. The microorganism responsible for the degradation behavior of the composite was the *bacillus* sp of bacteria.
4. The average coliform forming unit was 4.0×10^{7} CFU/gm of soil.

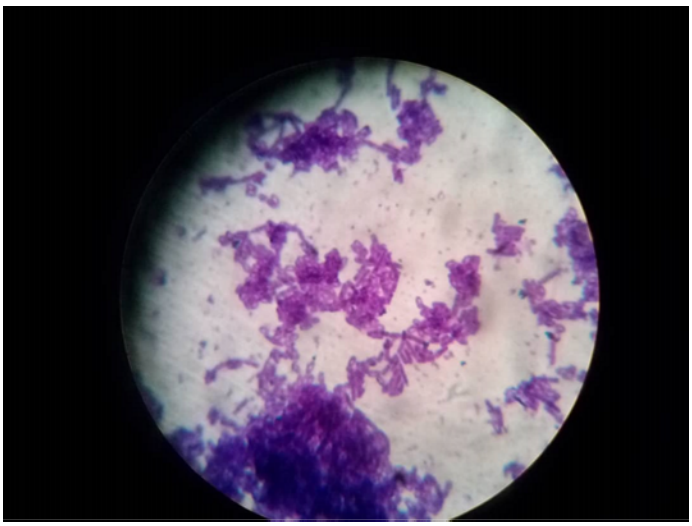

Plate 2: Rod like bacillus specie observed in the stained colonies

Acknowledgement
The research team is grateful to Kaduna State Polytechnic for granting permission to use their microbiology laboratory during the microbial analysis.

REFERENCES

Adamcova, D., Radziemska, M., Fronczyk, J., Zloch, J., and Vaverkova, M. D. (2017). Research of the Biodegradability of Degradable/Biodegradable Plastic Material in various Types of Environments. Scientific Review Engineering and Environmental Sciences. 26. 3-14. 10.22630/PNIKS.2017.26.1.01.

Ali, A., Shaker, K., Nawab, Y., Jabbar, M., 2, Hussain, T., Militky, T., and Baheti, V. (2016). Hydrophobic treatment of natural fibers and their composites—A review. Journal of Industrial Textiles. DOI: 10.1177/1528083716654468. jit.sagepub.com.

ASTM D6691 (2001). Standard Test Method for Determining Aerobic Biodegradation of Plastic Materials in the Marine Environment by a Defined Microbial Consortium.

Bandyopadhyay-Ghosh, S and S. B. Ghosh, S. B. (2015) The use of biobased nanofibres in composites. In *Biofiber Reinforcements in Composite Materials* (pp. 571-647). Woodhead Publishing.

Bello, T. K., Isa, M. T., Gideon, T. J. and Al-Bashir, U. A. (2019). Mechanical and Biodegradability studies of Toluene-2-4-Diisocynate (TDI) modified Okra fiber reinforced polyester composite. Nigerian Journal of Engineering, Vol 26 No3 pp 28-34.

Bio Resource (2016). CFU: Colony Forming Unit and Calculation http://technologyinscience.blogspot.com/2011/11/cfu-colony-forming-unit-calculation.html.

Ghori, W., Saba, N., Jawaid, M., and Asim, M. (2017). A review on date palm (phoenix dactylifera) fibers and its polymer composites presented at The Wood and Biofiber International Conference (WOBIC 2017). Published at IOP Conf. Series: Materials Science and Engineering **368** (2018) 012009.

Gomez, E. F, and Michel, F. C. (2013). Biodegradability of Conventional and Bio-based Plastics and Natural Fiber Composites during Composting, Anaerobic Digestion and long-term Soil Incubation. Polymer Degradation and Stability. Vol. 98(12): Pp. 2583–2591.

Haider, T., Völker, C., Kramm, J., Landfester, K, and Wurm, F. R. (2018). Plastics of the future? The Impact of Biodegradable Polymers on the Environment and on Society. Angewandte Chemie (International Ed. In English).

Krauklis, A. E., Gagani, A. I., and Echtermeyer, A. T. (2019). Prediction of Orthotropic Hygroscopic Swelling of Fiber-Reinforced Composites from Isotropic Swelling of Matrix Polymer. J. Compos. Sci. 2019, 3, 10; pp 1-14 doi:10.3390/jcs3010010

La Mantia, F. P and Morreale, M (2011). Green composites: A brief review. Composites: Part A 42 (2011) 579–588.

Li, X., Tabil, L. G., Panigrahi, S. (2007). Chemical Treatments of Natural Fiber for Use in Natural Fiber-Reinforced Composites: A Review. J Polym Environ 15:25–33.

Lucas, N., Bienaime C., Belloy C., Queneudec, M., Silvestre, F., and Nava-Saucedo, J. E. (2008). Polymer Biodegradation: Mechanisms and Estimation Techniques. Chemosphere. Vol. 73(4): Pp. 429–442.

Muller R. (2005). "Biodegradability of Polymers: Regulations and Methods for Testing". In Steinbüchel A (Ed.). Biopolymers. Wiley-VCH.

Pickering, K. L., Aruan Efendy, M. G., Le, T. M. (2016). A review of recent developments in natural fibre composites and their mechanical performance. Composites: Part A 83 (2016) 98–112. http://dx.doi.org/10.1016/j.compositesa.2015.08.038.

Pelissari, F. M., Ferreira, D. C., Louzada, L. B., dos Santos, F., Corrêa, A. C., Moreira, F. K. V., Mattoso, L. H. (2019). Chapter 10 - Starch-Based Edible Films and Coatings: An Eco-friendly Alternative for Food Packaging, Editor(s): Maria Teresa Pedrosa Silva Clerici, Marcio Schmiele, Starches for Food Application, Academic Press, 2019, Pages 359-420.

Ponnusamya,V. K., Nguyenc, D.B., Dharmarajad, J., Shobanae, S., Banuf, J. R., Sarataleg, R. G., Changc, S. W., Kumarh, G. (2019). A review on lignin structure, pretreatments, fermentation reactions and biorefinery potential. Bioresource Technology 271 (2019) 462–472.

Sanjay, M. R., Madhu, P., Jawaid, M., Senthamaraikannan, P., Senthil, S., Pradeep, S. (2017). Characterization and Properties of Natural Fiber Polymer Composites: A Comprehensive Review, Journal of Cleaner Production (2017), doi: 10.1016/j.jclepro.2017.10.101.

Shah, A.A.; Hasan, F.; Hameed, A.; and Ahmed, S. (2008). Biological Degradation of Plastics: A Comprehensive Review. Biotechnology Advances, Vol. 26(3), Pp. 246-265.

Proceedings of the 49th NSChE Annual Conference
KADA 2019: pp 479-488

P2C-09: SYNTHENSIS AND CHARACTERIZATION OF BIO-SYNTHESIZED NEEM-BASED ZINC OXIDE (ZnO) PHOTOCATALYST

Gana[1,2*] I. N., Ohageria[1] V.U., Akpan[1*] U.G and Ani[1] I.J.
[1]Department of Chemical Engineering, Federal University of Technology, Minna, Nigeria
[2]Headquarters Central Armament Depot, Tactical Air Command, Nigerian Air Force Base, Makurdi, Nigeria
[*]Corresponding Author: ugaekon@futminna.edu.ng; ganaisraelndamawo@gmail.com

ABSTRACT
Today, nanotechnology is gaining high recognition as a vital area of research going by its remarkable applications in the fields of photochemistry, engineering, medicine and pharmacy. This technology of nanomaterial involves the materials and their applications having one dimension in the range of 1–100 nm. On the other hand, biosynthesis of nanoparticles (NPs) is gaining much attention from researchers and has been suggested as possible replacement for chemical and physical methods because of the numerous challenges associated with known conventional methods. In this study, an active photocatalyst, dogonyaro (Azadirachta indica)-based zinc oxide (ZnO) was biosynthesized from zinc acetate dihydrate precursor using sol gel and precipitation methods. The synthesized samples were characterized using FTIR, XRD, BET, EDS and SEM characterization techniques. The SEM and XRD analysis of the green synthesized and non-green synthesized ZnO demonstrated the formation of hexagonal wurtzite crystalline structure and agglomerated morphology. EDX analysis demonstrated the existence of Zn and O as the major constituents of the as-synthesized nanoparticles with traces of carbon which could be attributed to the carbon tape of the sample holder. The BET analysis displayed that the surface area of the ZnO nanoparticles increased from 23.75cm^3/g to 97.08 cm^3/g after the green synthesis. Based on the surface area values, it can be derived that neem leaf extract enhanced the surface area of the green synthesized sample.

1.0 INTRODUCTION
Nanotechnology could be defined as the manipulation of matter through certain physical and/or chemical processes to produce materials that have specific properties which can be used in particular applications. Nanoparticles can be defined as particles that have at least one dimension less than 100 nm in size (Thakkar *et al*., 2014). On the other hand, (Ahmed *et al*., 2015) defined "Nanomaterials" as those particles whose size lies in the dimension area of 1–100 nm. Nanomaterials are found to show enhanced properties based on morphology, size and distribution.

Nanotechnology is no doubt emerging as a vital area of study with its incredible applications in the areas of science, engineering, medicine, catalysis, pharmacy, electrochemistry, sensors, biomedicines, food technology, cosmetics, textile industry, optics, electronics, space industry, mechanics, energy science, optical devices etc. Zinc oxide and silver NPs have attracted much interest in the research community among metal and metal oxide NPs, owing to their outstanding properties in terms of use in different areas such as antimicrobial, optical and catalytic properties (Espitia *et al*., 2016 and Khan *et al*., 2016). ZnO NPs have shown different physical and chemical properties depending on the morphology. ZnO NPs have been synthesized by different methods such as sol–gel method, electrophoretic deposition, laser ablation, hydrothermal methods, electrochemical depositions, co-precipitation, ultrasound, chemical vapor deposition, thermal

decomposition, and combustion method, microwave-assisted combustion method (Ahmed *et al*., 2015). These physical and chemical methods have major shortcomings such as chemical poisoning and low surface area of the synthesized material. Therefore, any method that is environmentally friendly and could result to improvement in the surface area of the synthesized ZnO nanoparticle is urgently needed. However, in recent researches, ZnO NPs have also been synthesized by biological method using biological agents as reducing agents (Madhumitha *et al*., 2016 and Ahmed *et al*., 2015). ZnO NPs are non-toxic, semi-conducting materials having good photocatalytic behavior and high transparency. In addition, ZnO NPs produced from biological method have shown remarkable photocatalytic degradation of many dye pollutants like methylene blue, reactive dyes, direct dyes, disperse dyes, methyl orange,basic dyes, azo dyes, rhodamine blue amongst others (Ghaly *et al*., 2014). Worthy of note is that ZnO NPs has gained special attention due to environmental concerns and it ability to degrade leading water pollutants particularly those in industrial effluents (Bhuyan *et al*., 2015).

Recently, (Ahmed *et al*., 2015) in a meta-analysis reported the use of plant extract in the green synthesis of photocatalysts. These extracts include those of Ziziphora tenuior (Sadeghi and Gholamhoseinpoor, 2015), Abutilon indicum (Ashokkumar *et al*., 2013), Solanum tricobatum (Logeswari et al., 2013), Erythrina indica (Sre *et al*., 2015), Ocimum tenuiflorum (Logeswari et al., 2013), Spirogyra varians (Salari *et al*., 2014), Melia dubia (Ashokkumar et al., 2013), leaf extract of Acalypha indica. with high antibacterial activities (Krishnaraj *et al*., 2010), Also, extracts of Sesuvium portulacastrum with nanoparticle size ranging from 5 to 20 nm (Nabikhan *et al*., 2010) have been identified as a source for the synthesis of nanoparticles as an alternative to the conventional methods. Azadirachta indica (Neem) leaf extract have been studied by Ahmed *et al*., (2015) and reported that the extract plays an important role in synthesis of ZnO NPs functioning as capping and stabilizing agent. They also noted that different capping agents can be used to stabilize ZnO particles imparting different properties, like size and morphology. They further reported that different surfactants have been employed in the synthesis of ZnO NPs, but the challenge with these surfactants is that they are difficult to degrade and are environmentally hazardous. Hence; the need to introduce green capping agents in the synthesis of ZnO NPs becomes imperative. Again, it's important to bear in mind that synthesis of NPs is entirely dependent on biochemicals present in the precursor materials such as alkaloids, and others. Actually, the biochemicals present in the neem leaf extract can be a viable alternative.

The 'green' environment friendly methods being talked about in chemical and chemistry technologies are becoming increasingly popular and are much needed now because of the worldwide problems associated with environmental health (Thuesombat *et al*., 2014; Ahmed *et al*., 2015). In the last ten years or more, researchers have showed interest in biological method to synthesize metal and metal oxide nanoparticles and the development of this biologically stimulated technique is growing as an important branch in the field of nanotechnology and nanoscience (Sharif *et al*., 2017). These so-called green syntheses of nanoparticles is gaining importance and has recently been suggested as potential alternative to physical and chemical methods because it is eco- friendly, non-toxic and safe reagents during the green-synthesis process while the use of dogonyaro (Neem) leaf extract offers a biological method for the controlled and precise synthesis of several metallic nanoparticles with well-defined various shapes and sizes.

The bio-reduction of zinc ions into respective nanoparticles mediated by dogonyaro leaf extract is chemically complex but environmentally benign. The role of neem leaf extract as reducing and

mediating agent in the biosynthesis of ZnO nanostructures makes it indispensable in green technology (Bhuyan *et al.,* 2015). On a general note, plant-extract-based and sodium hydroxide (NaOH)-enhanced simple precipitation processes are the most commonly used procedure in the synthesis of ZnO nanoparticles with NaOH as pH adjuster for the reaction mixture (Vishnukumar *et al.,* 2018).

The wide variability of metabolites present in the dogonyaro leaf extract have reducing properties or antioxidant that helps in the immediate reduction of the zinc ions into nanostructured ZnO photocatalyst. Flavones, ketones, organic acids, amides and aldehydes are the main phytochemicals present in the dogonyaro leaf extract which acts as bio-reductant out of which flavones, organic acids and quinones are water soluble phytochemicals that are actually responsible for the direct reduction of zinc ions into their respective nanostructures (Prathna *et al*., 2010, Bhuyan *et al*., 2015). Previous studies have further demonstrated that mild heating followed by subsequent incubation of three types of benzoquinones (namely, cyperoquinone, dietchequinone and remirin) present in neem (mesophyte) leaf extract end up in the activation of quinones which results in particle size reduction (Bhuyan *et al*., 2015). Green synthesis is employed in this research because it is cheap, eco-friendly, and highly efficient method since it does not use toxic precursor as compared with the physical and chemical synthesis approach. No doubt, the green synthesis of (ZnO) using extract solution from Azadirachta indica will help to increase the surface area. This study seeks to synthesize ZnO nanoparticles through green synthesis, characterized and compare with the non-green synthesized one.

2.0 MATERIALS AND METHODS

Chemical and reagents such as the precursor [Zinc acetate dihydrate [$Zn(CH_3COO)_2$]-$2H_2O$], and sodium hydroxide (NaOH) were of analytical grade as supplied by Panlac Chemicals Nigeria Limited and were used directly without further purification.

2.1 Dogonyaro (*Azadirachta indica*) Leaf Sample Collection

Fresh leaves of Dogonyaro (*Azadirachta indica*) were randomly collected from different locations in Gidan Kwano, Bosso Local Government Area, Minna, Niger Sate, Nigeria. The collected leaves were gently washed with tap water and subsequently with de-ionized water, cut into pieces, sundried for seven days afterward grounded using plastic mortar and pestle. The resulting powdered was stored in an air tight container for subsequent uses.

2.2 Preparation of Dogonyaro Leaves Extract

About thirty grams (30 g) of the powdered leaves were weighed into a beaker containing 300 ml of de-ionized water. The mixture was for 15 minutes at 60 °C on a heating mantle. The extract was then allowed to cool at room temperature, filtered using Whatman No.1 filter paper. The obtained extract (filtrate) was poured into a bottle and stored in a refrigerator at a temperature of 4^{o}C for further use.

2.3 Non-Green Synthesis of Zinc Oxide (ZnO) Nanoparticles

One molar (1 M) of aqueous sodium hydroxide (NaOH) was prepared by adding 40 g of the crystals in 1000 ml of de-ionized water. To synthesized the non-green ZnO nanoparticles; 20 g of the Zinc acetate [$Zn(CH_3COO)_2$]-$2H_2O$] was added to 60 ml of de-ionized water in a beaker and stirred at 50 rpm for 60 min. The mixture then was divided into three equal volumes and with controlled drops of aqueous NaOH into each beaker, pH values of 8, 10 and 12 where measured using a pH meter. 20 ml of de-ionized water was subsequently added to each of the 3 beakers,

stirred rigorously and allowed to settle for 30 min and then decanted after which the same volume of water was repeatedly added twice and decanted. The gel obtained were properly dried in electrically heated oven over the night at 150^{o}C and then calcined at 350^{o}C using muffle furnace for 2 h, cooled and stored for use.

2.4 Green Synthesis of Dogonyaro-Based Zinc Oxide (ZnO) Nanoparticles

In the green synthesis of the dogonyaro-based ZnO nanoparticles; 20 g of the Zinc acetate was added to 60 ml of de-ionized water in a beaker followed by 30 ml of the dogonyaro (*Azadirachta indica*) extract and stirred for 60 min at a rotation speed of 50 rpm. The mixture then was divided into three equal volumes and with controlled drops of aqueous NaOH into each beaker, pH values of 8, 10 and 12 where measured using a pH meter. 20 ml of de-ionized water was subsequently added to each of the 3-beakers stirred rigorously and allowed to settle for 30 min and then decanted after which the same volume of water was repeatedly added twice and decanted. The gel obtained were properly dried in electrically heated oven over the night at 150 ^{o}C and then calcined at 350^{o}C for 2 h in a muffle furnace, cooled and stored for use.

2.5 Characterization of the Green Synthesized and Non-Green Synthesized ZnO Photocatalysts

The morphology, elemental composition, crystallography, Surface area and adsorption bands of the non-green synthesized and green synthesized ZnO nanoparticles were comprehensively examined using SEM, EDS, XRD, FT-IR and BET characterization techniques.

3.0 RESULTS AND DISCUSSION

3.1 Surface Electron Microscopy (SEM) Analysis

Synthesized ZnO and (B) Non – Green Synthesized ZnO

SEM was employed to analyze the structure of nanoparticles that were synthesized. The SEM images in Figure1 (a–b) show the changes in morphology of ZnO NPs. The photocatalysts formed are fairly spherical in shape and agglomerated tiny rods. However, the agglomeration was less for the green synthesized sample as compared with the non-green synthesized photocatalyst, and the particle sizes are generally smaller for the green synthesized than the non-green synthesized photocatalyst. Similar result was also obtained by Ungula and Dejene (2016).

3.2 Energy Dispersive X-ray Spectroscopy (EDXS) Analysis

EDX analysis (Table 1, Figs. 2 and 3) was carried out to determine the elemental composition and stereochemistry of the synthesized zinc oxide nanoparticles. The EDS spectra in Figure 2 and Figure3 indicate that the synthesized samples are composed of zinc and oxygen and the route has pure ZnO phases. Theoretically, expected stoichiometric mass percent of Zn and O are 80.3% and 19.7% (Bari *et al*. 2009). The green synthesized sample showed a closer theoretical value of Zn and O as shown in Table 1. This high purity of the ZnO NPs was further confirmed by XRD spectra. However, some traces of carbon element were found in the sample, which could be attributed to the carbon tape of the sample holder. Similar result was also reported by Gnanasangeetha and Thambwani (2013).

Table 1: Elemental Composition of the modified (M-ZnO) and unmodified (U-ZnO) ZnO samples

Photocatalyst	Zn	O	Total (%)
G-ZnO	88.19	11.81	100
N-ZnO	91.57	8.43	100

G = Green synthesized, N = Non-green synthesized

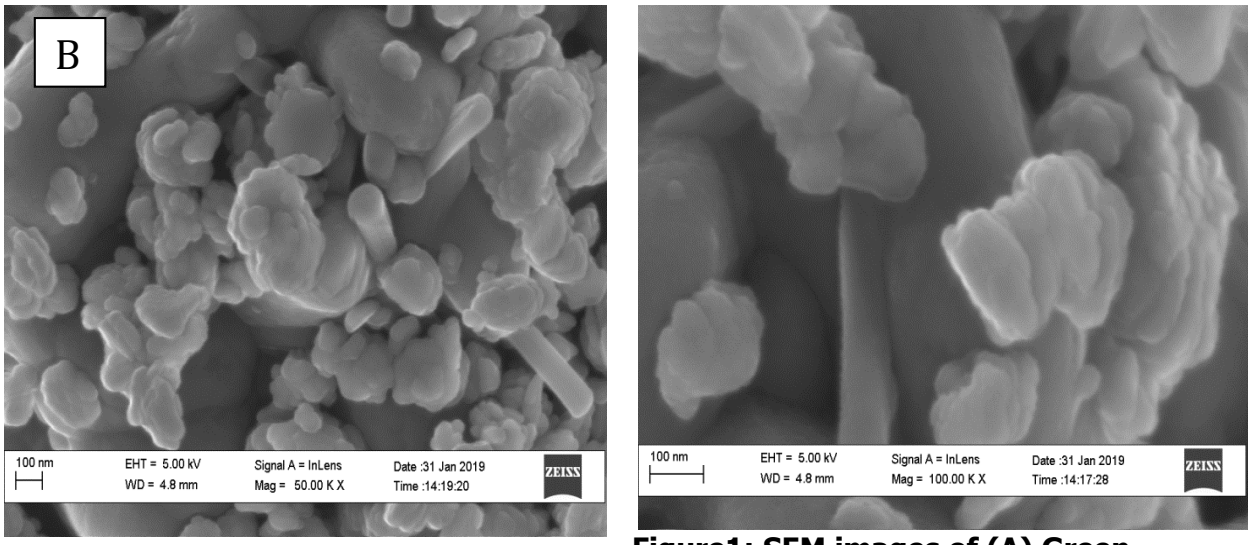

Figure1: SEM images of (A) Green

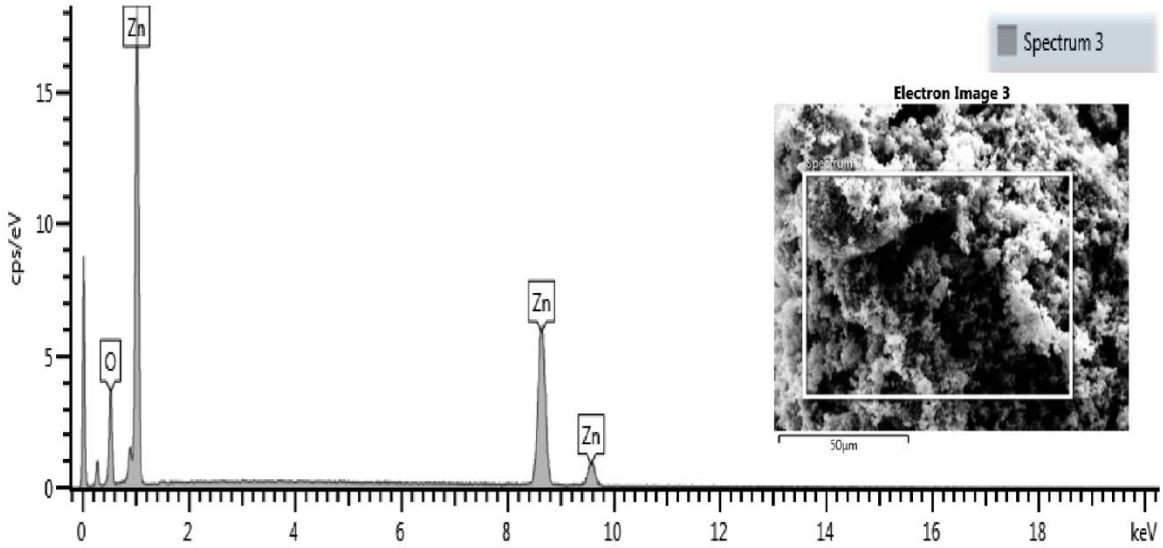

Figure 2: EDX Spectrum of Green synthesized ZnO

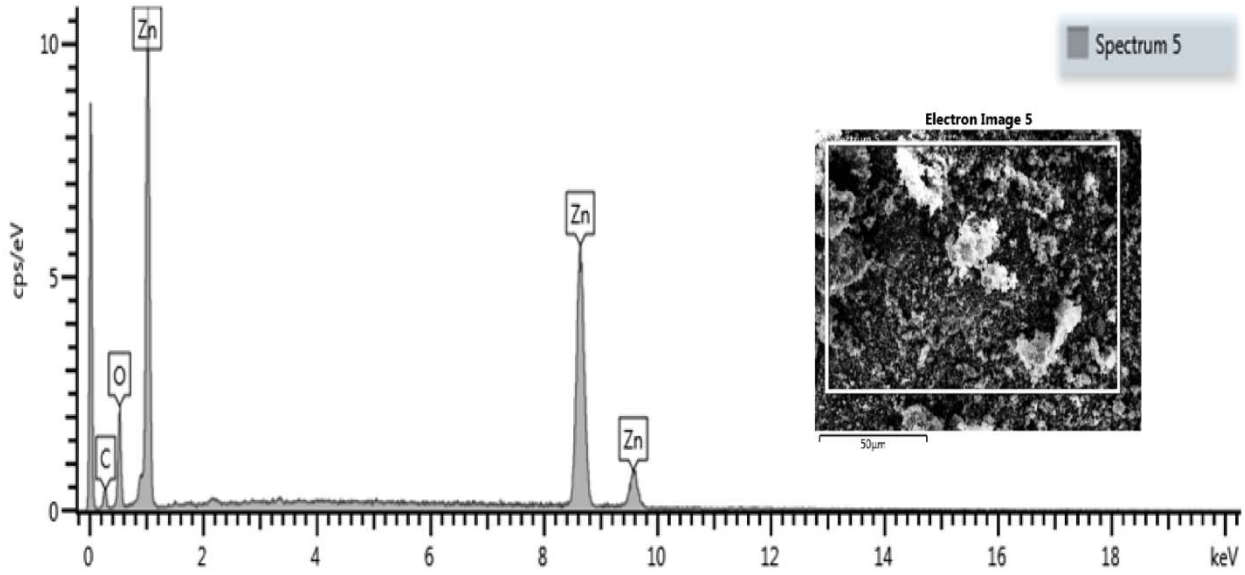

Figure 3: EDX Spectrum of the non-green synthesized ZnO

3.3 X-Ray Diffraction (XRD) Analysis

XRD analysis (Figure 4) was performed to investigate the crystal structure of the synthesized photo catalysts. The XRD patterns of the samples were recorded in the diffraction angle range 5° to 80°. Figure4 displays the XRD pattern of the synthesized ZnO samples. All of the diffraction peaks at the characteristic planes (1 0 0), (0 0 2), (1 0 1), (1 0 2), (1 1 0), (1 0 3), (1 1 2) and (2 0 1) can be directly indexed to a hexagonal wurtzite crystalline structure of ZnO (Otal *et al.*, 2011). This Wurtzite crystalline structure also matched well with the Joint Committee on Powder Diffraction Studies Standards (JCPDS standard Card No.: 01-036-1451). No other peaks are detected, indicating a high phase purity of the samples. The sharp and strong diffraction peaks in the XRD patterns of the zinc oxide nanoparticles synthesized confirm the high crystalline nature of the samples. Figure4 also shows that the peak intensity increases for the green synthesized ZnO sample, which indicates an increased crystallinity of the modified sample compared to the non-green synthesized one. Similar result was also obtained by Xing *et al*. (2017).

3.4. BET Surface Area Analysis

The BET surface area values of the synthesized ZnO nanoparticles are shown in Table 2. It can be seen that the BET surface area of 97.08 m^2/g was obtained for the green synthesized (G-ZnO) sample, an increase of four folds compared to the value of 23.75 m^2/g for the non-green synthesized (N-ZnO) sample. Based on the surface area values, it can be derived that neem leaf extract enhanced the surface area of the modified sample.

3.5 Fourier Transform Infrared (FT-IR) Analysis

To characterize stretching vibrations of the prepared samples, FT-IR spectra for the green synthesized and non-green synthesized ZnO samples were studied and the results are shown in Figure 5.

The spectrum in the 459 cm^{-1} and 400 cm^{-1} identifies the bending vibration of Zn-O in the green synthesized and non-green synthesized samples respectively. In addition, the result clearly indicates that –OH stretching around 3042 cm^{-1} and –CH stretching around 2340 cm^{-1} are responsible for strong capping on the geen synthesized ZnO nanoparticles. This result matches

with the already reported result of biosynthesis of ZnO nanoparticles using Acalypha indica leaf extract (Gnanasangeetha and Thambwani 2013).

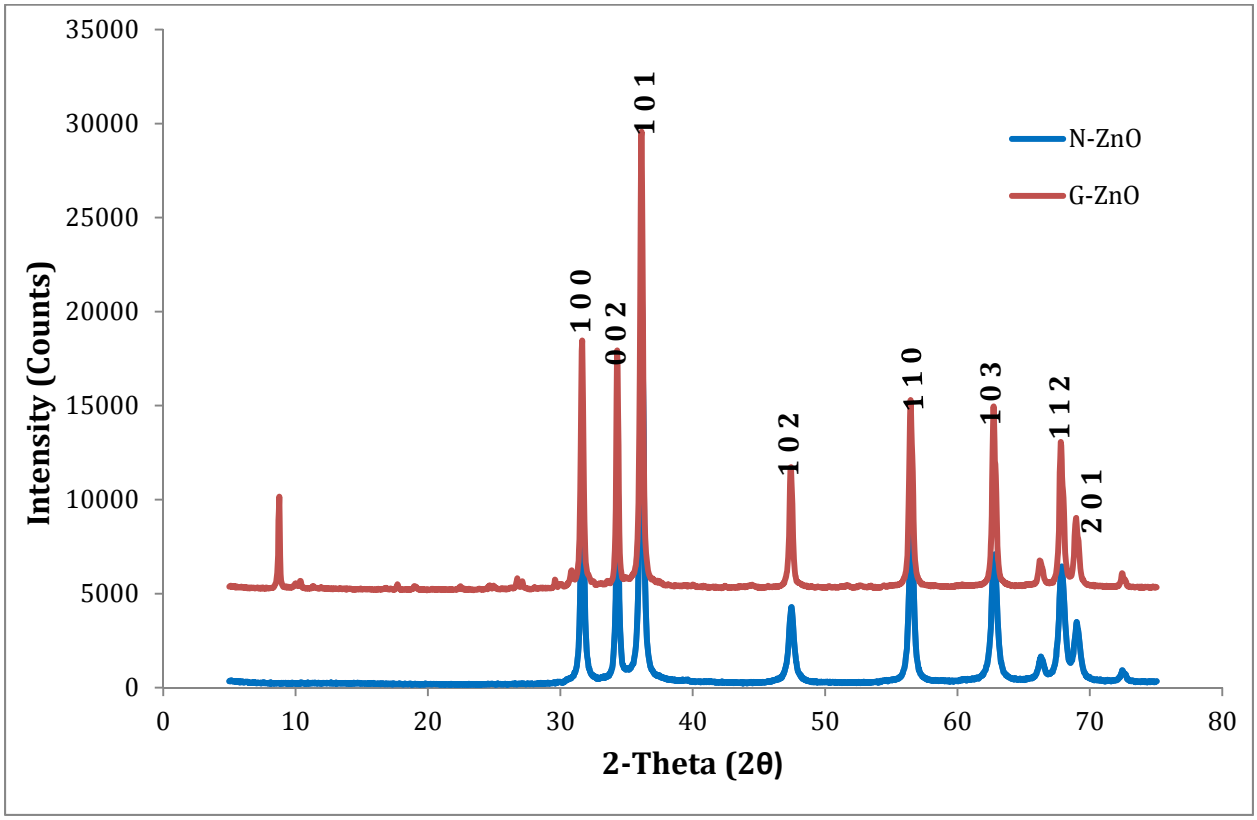

Figure 4: XRD patterns of the green synthesized (G-ZnO) and non-green synthesized (N-ZnO) ZnO samples

Table 2: The BET specific surface area, pore volume and pore size of the photocatalysts

Photocatalyst	BET Surface Area (m^2/g)	Pore Volume (cm^3/g)	Pore Size (nm)
N-ZnO	23.75	0.01431	2.138
G-ZnO	97.08	0.04949	2.105

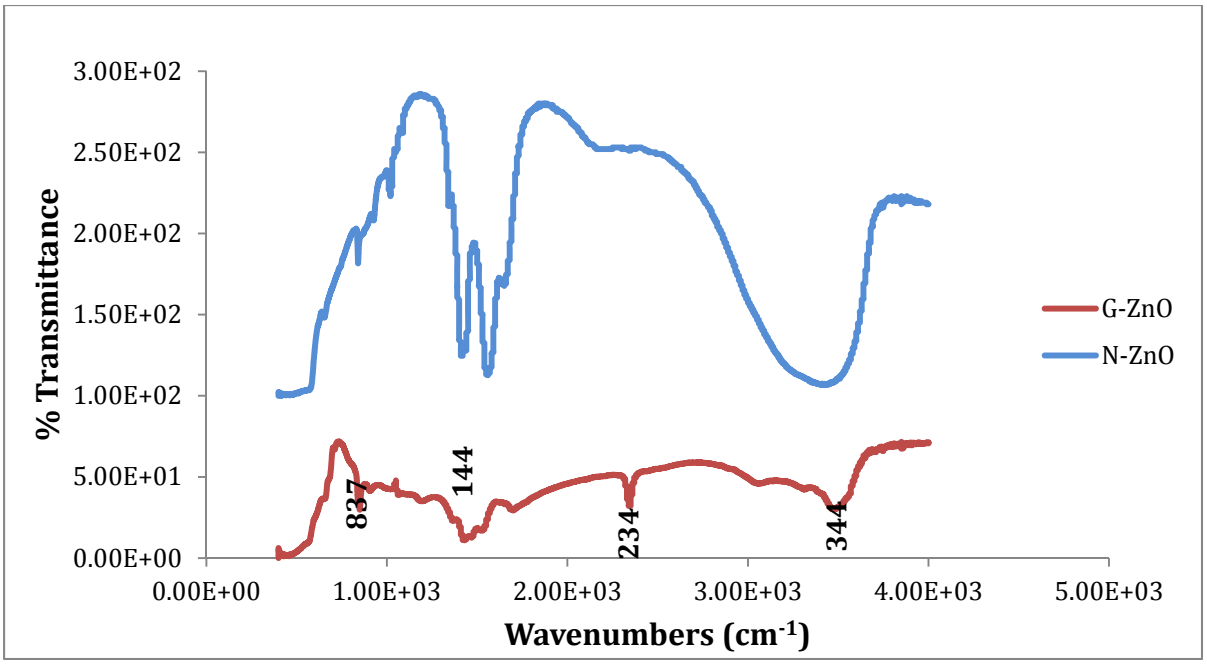

Figure 5: FT-IR spectra of the green synthesized (G-ZnO) and non-green synthesized (N-ZnO) nanoparticles

4.0 CONCLUSION

Zinc oxide nanoparticles have been successfully synthesized via green route, an eco-friendly and inexpensive method for the bio-synthesis of ZnO using aqueous leaf extracts of dogonyaro (*Azadirachta indica)*, and characterized using different techniques. The extracts act as reducing and stabilizing agents for the synthesis of shape and size controlled ZnO nanoparticles: an eco-friendly route which would invariably eliminate the cost of buying chemical reducing agents which are toxic in nature. The sharp and strong diffraction peaks in the XRD patterns of the zinc oxide nanoparticles synthesized confirm the high crystalline nature of the samples. The EDS result revealed a successful synthesis of ZnO NPs, while the FT-IR spectra indicates the presence of –OH and –CH stretching which are responsible for strong capping on the green synthesized ZnO NPs. In addition, the BET characterization shows an obtained ZnO nanoparticle with improved surface area which is 4-folds higher than the non-green synthesized one. The improved surface area of the green synthesized ZnO NPs could be attributed to the effect of the neem leaf extract which enhanced the surface area. From the results obtained, the ZnO nanoparticle is hereby proposed to be applied in the degradation of organics in wastewater especially industrial effluents. This therefore, will be gainfully employed in environmental remediation.

Acknowledgement

The authors wish to acknowledge the support of TETFund in conjunction with Federal University of Technology, Minna for providing 2017 IBRG grant No.: TETFUND/FUTMINNA/2016-20177/6THIBRP/12.

References

Ahmed, S., (2015). Green synthesis of silver nanoparticles using Azadirachta indica aqueous leaf extract, *Journal of Radiation Research and Applied Sciences*, http://dx.doi.org/10.1016/j.jrras.2015.06.006

Ashokkumar, S., Ravi, S., and Velmurugan, S. (2013). Green synthesis of silver nanoparticles from Gloriosa superba L. leaf extract and their catalytic activity. Spectrochimica Acta Part A: Molecular and Biomolecular Spectroscopy, 115, 388-392.

Bari, A. R., Shinde, M. D., Vinita, D. and Patil, L. A. (2009). Effect of Solvents on the Particle Morphology of nanostructured ZnO. *Indian Journal of Pure and Applied Physics*, 47, 24-27.

Bhuyan, T., K. Mishra, M. Khanuja, R. Prasad, A. Varma, (2015). Biosynthesis of zinc oxide nanoparticles from Azadirachta indica for antibacterial and photocatalytic applications, Mater. Sci. Semicond. Process. 32 55–61.

Espitia, P.J., C.G. Otoni, N.F.F. Soares, (2016). zinc oxide nanoparticles for food packaging applications, Antimicrob. Food Packag, pp. 425–431.

Ghaly, A.E., Ananthashankar, R., Althab, M., and Ramakrishnam, V.V. (2014). Production, characterization, and treatment of textile wastewaters: a chritical review. Journal of chemical engineering process technology, 5,182-187.

Gnanasangeetha, D., Thambwani, D.S. (2013). Biogenic production of zinc oxide nanoparticles using Acalypha indica. *Journal of Chemistry, Biology and Physical Sciences*, 1, 238–246.

Khan, S.T., J. Musarrat, A.A. Al-Khedhairy, (2016) . Countering drug resistance, infectious diseases, and sepsis using metal and metal oxides nanoparticles: current status, ColloidsSurf. B: Biointerfaces 146,70–83.

Krishnaraj, C., Jagan, E. G., Rajasekar, S., Selvakumar, P., Kalaichelvan, P. T., and Mohan, N. (2010). Synthesis of silver nanoparticles using Acalypha indica leaf extracts and its antibacterial activity against water borne pathogens. Colloids and Surfaces B: Biointerfaces, 76, 50-56.

Logeswari, P., Silambarasan, S., and Abraham, J. (2013). Ecofriendly synthesis of silver nanoparticles from commercially plant powders and their antibacterial properties, Sciencia Iranica, 20, 1049-105

Madhumitha, G., G. Elango, S.M. Roopan, (2016). Biotechnological aspects of ZnO nanoparticles: overview on synthesis and its applications, Appl. Microbiol. Biotechnol. 100, 571–581.

Otal, E.H., Yoon, S., Aguirre, M., Weidenkaff, A. (2011). Metastability of heavy lanthanides in the ZnO wurtzite structure. *Journal of Alloys and Compounds*. 509, 364-366.

Prathna, T.C., L. Mathew, N. Chandrasekaran, A.M. Raichur, A. Mukherjee, (2010). Biomimetic synthesis of nanoparticles: science, technology and applicability, Biomimetics Learning from Nature, (Chapter1).

Salari, Z., Danafar, F., Dabaghi, S., and Ataei, S. A. (2014). Sustainable synthesis of silver nanoparticles using macroalgae Spirogyra varians and analysis of their antibacterial activity. Journal of Saudi Chemical Society. http:// dx.doi.org/10.1016/j.jscs.2014.10.004.

Sharif,M.M., F.-H. Shah,M.S. Butt, H.R. Sharif, (2017). Role of nanotechnology in enhancing bioavailability and delivery of dietary factors, Nutr. Deliv, 587–618.

Sre, P. R. R., Reka, M., Poovazhagi, R., Kumar, M. A., and Murugesan, K. (2015). Antibacterial and cytotoxic effect of biologically synthesized silver nanoparticles using aqueous root extract of Erythrina indica lam. Spectrochimica Acta Part A: Molecular and Biomolecular Spectroscopy, 135, 1137-1144.

Tamanna Bhuyan, Kavita Mishra, Manika Khanuja, Ram Prasad, Ajit Varma (2015). Biosynthesis of zinc oxide nanoparticles from Azadirachta indica for antibacterial and photocatalytic applications. Materials Science in Semiconductor Processing, 32, 55–61.

Thakkar KS, Mhatre SS, Parikh RY (2014) Biological synthesis of metabolic nanoparticles. Nanomedicine 2:257–262

Thuesombat, P., Hannongbua, S., Akasit, S., and Chadchawan, S. (2014). Ecotoxicology and environmental safety effect of silver nanoparticles on rice (Oryza sativa L. cv. KDML 105) seed germination and seedling growth. Ecotoxicology and Environmental Safety, 104, 302-309.

Ungula, J. and Dejene, B.F. (2016). Effect of solvent medium on the structural, morphological and optical properties of ZnO nanoparticles synthesized by the sol–gel method. Physica B, 480, 26–30

Vishnukumar, P., S. Vivekanandhan, M. Misra, A.K. Mohanty, (2018). Recent advances andemerging opportunities in phytochemical synthesis of ZnO nanostructures. Materials Science in Semiconductor Processing 80, 143–161

Xing, Z., Chen, Y., Liu, C., Yang, J., Xu, J., Situ, Y., Huang, H. (2017). Synthesis of core-shell ZnO/oxygen doped g-C3N4 visible light driven photocatalyst via hydrothermal method. *Journal of Alloys and Compounds.* 708, 853-861.

Proceedings of the 49th NSChE Annual Conference
KADA 2019: pp 489-498

P2C-10: DEVELOPMENT AND CHARACTERIZATION OF LOW-DENSITY POLYETHYLENE REINFORCED PINEAPPLE LEAVES FIBRE COMPOSITES

A.I. Isah[1], P. E. Dim[2], I. Dahiru[3] and M.B. Umar[4]
[1,2]Department of Mechanical Engineering, Nuhu Bamalli Polytechnic, PMB 1061 Zaria
[2]Department of Chemical Engineering, Federal University of Technology, Minna, Niger State
[3]Department of Agric Education, Nuhu Bamalli Polytechnic, PMB 1061 Zaria, Kaduna State
Phone: 08104019228, email: abufaseehah@gmail.com

ABSTRACT
Pineapple leaves are agricultural wastes that are found in abundance in Nigeria but its potentials have not been fully harnessed. It is a natural fibre with high cellulose content and low lignin and hemicellulous composition which indicates its possession of high mechanical properties. This research was aimed at developing a biodegradable composite from pineapple leave fibre (PALF) by reinforcing it with low density polyethylene (LDPE) based plastic as matrix. Alkaline treatment based on NaOH was used to clean and modify the surface of fibre to promote enhanced fibre-polymer adhesion. The composite was developed using compression moulding process. Mechanical analysis of the composites was carried out to determine its range of usefulness and service life expected, and thermal analysis was also carried out to determine its response on application of heat. Finally burial test was conducted to determine the level of biodegradability at various loading. The composite formed was used to produce a poor panel that can be used as automotive parts. The maximum tensile strength reinforced composite was obtained at 30wt% of PALF loading of 14.09136 MPa while composite of ratio 50:50 of LDPE/PALF was found to have the lowest flexural strength of 4.2 MPa. Also the FTIR results after burial showed that there was the shift of band from the 1033cm^{-1} to 1021cm^{-1} and the peak changed from sharp to broad. Hence PALF is an efficient fibre for the production of biodegradable composites that can replace synthetic fibres, help to safe cost and other resources.

.

Keywords: Pineapple, Composites, Natural fibres, Polyethylene, Environment.

1.0 Introduction
Nowadays, polyethylene based plastic materials are being extensively used for commercial and household purposes. However, these polyethylene-based plastics are substantially resistant to biodegradation. Thus, their increasing accumulation in the environment is proving to be an ecological threat to the world (Liu et al., 2013). Pineapple is a fruit crop that can grow in every part of Nigeria, fibres gotten from the leaves are found to contain high cellulose content enough to be used as reinforcement for polymers. Pineapple leaves can be used for fibre production (Dey et al., 2014). The comparative value of the chemical composition of pineapple leave fibres and other major plant fibres indicates that pineapple leave fibres has about the same Pentosen contents as wood fibre. Since pineapple leave fibres has less lignin and more cellulose than wood fibre. Pineapple leave fibres have only a small quantity of both lignin and pectin. It can be said that the unique features of pineapple leave fibres are its relatively large cellulose contents and extremely low contents of lignin and pectin which is the major inter-cellular components. This low content of lignin and pectin makes it very different from other fibres. Blending PAPF with LDPE will increase the mechanical properties of the composites as they have satisfactorily high specific

strength and modulus light weight (Roshafima et al,.2017).It is therefore expected that pineapple leave fibres can be easily made into composite under mild treatment conditions giving good yield.

Table 1: **Chemical compositions of pineapple leave fibres**

Constituents	Percentage
Ash Content	4.5
Cellulose Content	66.2
Hollocellulose Content	85.7
Hemicellulose Content	19.5
Lignin Content	4.2
Moisture Content	81.6
Hot water soluble Content	32.5
1% NaOH Solubility Content	

(Faruk et al., 2012)

Low density polyethylene has been used in hybrid composite formulations because it is the least expensive polyethylene. It was also reported that low density polyethylene has the ability to photodegrade in sunlight and photo-degradation is found to be important in biodegradation (Basu and Roy, 2007). Polymer matrix composite materials are formed into shape using different processing technologies such as extrusion, compression, rotational, and injection moulding techniques. Processing of natural short fibre reinforced polymer composites is based on mixing of short natural fibres and polymer matrix followed by subsequent moulding (Kim et al., 2014). Although composites reinforced with synthetic fibres possess superior mechanical properties, they have some severe drawbacks that include high cost, poor recyclability and non-biodegradability (Mohammed et al., 2015).

Surface treatment of fibres is used to reduce their tendency for moisture absorption and thereby facilitates greater compatibility with the polymer matrix (Kabir et al., 2014). Mercerization is an economical and effective method used for improving the interfacial incompatibility between the matrix and the fibre. It has also proven to reduce water uptake of fibres. It improves the adhesive characteristics of the fibre surface by removing natural waxy materials, hemicellulose and artificial impurities, and produce good surface topography (Jacob et al., 2014). However, mercerization of natural fibres by alkali is the most popular method nowadays to improve fibre/matrix interactions by reducing the hydrophilicity of the natural fibre (AbdulMotalib et al., 2018). To minimize this threat, there is need to improve the biodegradability properties of polyethylene. This study focuses on the production of polyethylene reinforced pineapple leaves fibres composites.

2.0 Materials and Methods

2.1. Materials

Ten (10) kg of pineapple leaves fibre were collected from Station market in Barnawa area of Kaduna state, Nigeria. Low density polyethylene (LDPE) was supplied by Nigeria Institute of Leather and Science Technology (NILEST) Samaru-Zaria, Kaduna state, Nigeria. Sodium hydroxide (NaOH) pellets (98% purity, analytical grade) and distilled water (100% purity) were supplied by a vendor. All chemicals were used as received.

2.2. Method

2.2.1. Extraction and pre-treatment of pineapple leaves fibres

Ripe and mature pineapples were bought from the market and the leaves were removed mechanically using a metal cutter. The leaves were washed in a running tap water to remove sand and other impurities and then allowed to dry for 24h. Pineapple fibres were then extracted through scrapping the pineapple leaf with a sauce plate.

2.2.1. Chemical treatment (Mercerization)

The extracted pineapple leaves fibres were subjected to alkaline treatment to clean and modify the surface and to promote enhanced fibre-polymer adhesion. Five (5) wt% of NaOH solution was prepared; pineapple leave fibres were soaked in the prepared 5 wt% of NaOH solution and heated at 40 ℃ for 20mins on a regulated hot plate under a continuous stirring to ensure even modification. These concentrations were chosen to preserve the cellulose part of the fibres but dissolving the hemicellulose and the lignin portions (Elanga et al., 2013). Distilled water was used to rinse the fibres until a neutral pH was achieved, and then the treated fibre was allowed to dry.

2.2.2 Size Reduction

The dried PALF fibres were subjected to size reduction by grinding using local milling machine. The ground fibres were sieved. Fibres with sizes of 2mm-4mm were taken for this study as the size was the highest amount from sieving

2.2.3. Formulation and production of Composites

The composites were produced through mixing the treated pineapple leaves fibres and low density polyethylene according to the composition: 10 wt%, 20 wt%, 30 wt%, 40 wt% and 50 wt% of pineapple leave fibres with the corresponding 90 wt%, 80 wt%, 70 wt%, 60 wt% and 50 wt% matrices of low density polyethylene. The mixing was achieved by a way of compounding using two-roll mill. The two-roll mill machine was heated to a temperature of 120℃ for 30 minutes, which is the melting temperature of low density polyethylene. At the end of this period, 50 wt% of LDPE was poured into the preheated two-roll mill to melt the LDPE for about 5 min, followed by gradual pouring of 50 wt% PALF into the melted LDPE until a complete mixing of the fibre with the matrix was achieved. Finally, the compounded PALF/LDPE was scraped from the mill to form a sheet. A total of five samples were made. After mixing, the samples were introduced to the extruding machine, where uniformly mixed extrudates were produced. The processing parameters used were: motor current = 6.5 A, melt pressure = 0.1 MPa, screw speed = 320 rpm and feeder speed = 25 rpm.

2.2.4. Characterization of polymer composites

The composites formed were characterized in order to have a complete understanding of their behaviours. Different mechanical and thermal were carried out. This includes tensile test, water absorption measurements and FTIR respectively to know the level of strength and functional group.

2.2.4.1 Tensile Test

The tensile test was conducted according to ASTM D638 using the Instron universal testing machine. The dimensions, gauge length and cross-head speeds are chosen according to the ASTM D638 standard. The test specimens were cut into dog-bone shape of dimension 150 mm × 20

mm × 3.2 mm using a hydraulic cutter. Five specimens were tested for each composite formulation with a load cell of 5 kN and crosshead speed of 5 mm/min.

2.2.4.2 Flexural Test

Flexural strength was measured under a three-point bending approach using a universal testing machine according to ASTM D790. The dimensions and gauge length were chosen according to the ASTM D790 standard. Samples measuring 127 mm × 12.7 mm × 3.2 mm were tested at a crosshead speed of 4 mm/min, which was determined using equation 2.1 (AbdulMotalib et al., 2018).

$$R = \frac{ZL2}{6d} \qquad 2.1$$

where;
Z which is a constant, is the rate of straining of the outer fibre, while
L is the support span, and
d is the thickness of the sample.

2.2.4.3 Impact Test

The impact test was conducted according to ASTM D256 using the charpy V-notch impact testing machine. The dimensions, gauge length and V-notch were chosen according to the standard. The specimen was placed between a special holder with the notch oriented vertically and towards the origin of impact. The specimen was struck by a "tup" attached to a swinging pendulum. The specimen breaks at its notched cross-section upon impact, and the upward swing of the pendulum was used to determine the amount of energy absorbed in the process.

2.2.4.4 Hardness Test

The hardness of the polyethylene reinforced baobab fibre composites were measured with the aid of Shore Duro-meter testing machine according to ASTM. The samples were indented following the various fibre compositions in the composites. The reading on the machine was noted and recorded.

2.5 Biodegradability behaviours of composites (Burying Process)

The masses of the PALF reinforced polyethylene composite samples were weighed using digital weighing balance before burying in the soil sample collected from the dump site. 4.4g, 5.0g and 4.51g for 100:0, 80:20 and 70:30 sample ratios of LDPE to PALF respectively were weighed before burial. The mean total bacteria count (TBC) of the soil sample is 8.0 x 10^7cfu/g (colony forming unit per gram) of soil. Also, the mean total fungal count (TFC) of the soil sample is 22 x 10^5cfu/g of soil. After two weeks, the samples were removed from the soil and then cleaned. They were then dried inside the oven for good three (3) hours at 50 ℃ for the removal of moisture contents from the samples after drying the samples were weighed again and their masses recorded. The same procedure was repeated for the next two weeks, and the interval of two weeks was continued up to the end of 90 days consecutively. The soil samples were kept moist always by addition of small amount of water to it, when they tend to dry.

2.6 Water Absorption Test

The samples were weighed and submerged in a 250-ml beaker containing water for 24 h. After the samples stayed for 24 h, they were then taken out of the water, dried and weighed according to ASTM D570-98. The percentage water absorbed was calculated using the Equation (2.2)

$$\frac{Wf - Wi}{Wi} \times 100 \quad (2.2)$$

where,

W_f is the weight of the sample after immersion in water.
W_i is the weight of the sample before immersion in water.

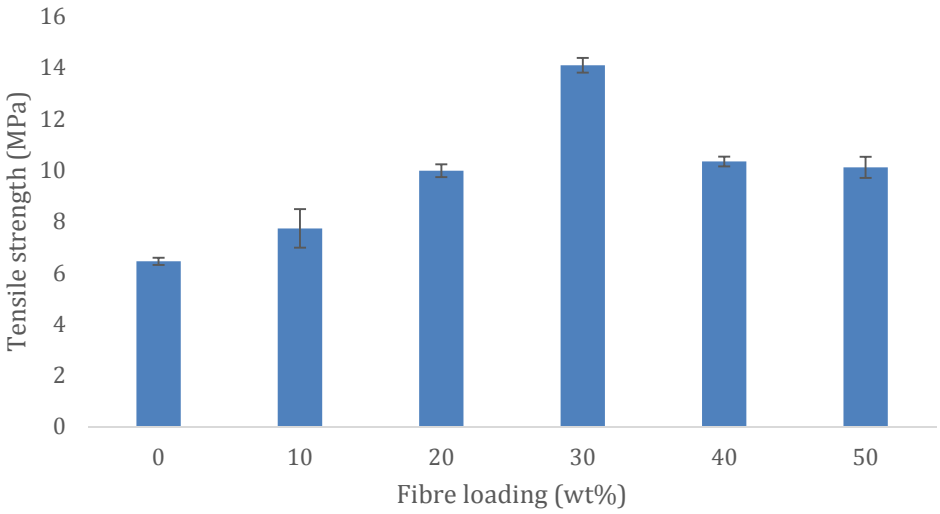

Figure 1: Tensile strength at varying fibre loading.

3.0 Results and discussion

3.1 Mechanical Properties of LDPE/PALF composite.

3.1.1 Tensile Strength

The maximum tensile strength reinforced composite was obtained at 30wt% of PALF loading as shown in Figure 1. While 10 wt% gave the lowest tensile strength of 7.73MPa on reinforcing with PALF. The tensile strength of the entire reinforced composite was higher than the un-reinforced LDPE as shown. The maximum tensile strength obtained at 30wt% might be due to proper binding between the fibre and matrix and the decrease in tensile strength as shown in Figure 3.1 after 30wt% might be due to agglomeration between the fibre and the matrix in the composite. The maximum tensile strength obtained at 30 wt% PALF loading is higher than 7.1 MPa obtained by Kuburi, (2017) for coir fibre-LDPE composite at 30 wt%.

3.1.2 Flexural Strength

The flexural strength of unreinforced LDPE composite gives the highest value of 13.69 MPa when compared to the other composites. The composite of ratio 50:50 of LDPE-PALF has the lowest flexural strength of 4.2 MPa. It was observed that on reinforcement, the flexural strength is reduced as the PALF loading was increased. The highest flexural strength of 13.69 MPa in the unreinforced LDPE is lower than 25 MPa obtained by Oluyemi et al., (2017) for unreinforced polyester. The nature of the two materials and their molecular structures may differ and this could lead to their differences in flexural strengths. The highest flexural strength of 11.84 MPa obtained

on reinforcing with 10 wt% fibre content is low when compared with 17 MPa at 10 wt% obtained by Kuburi et al., (2017) for Coir fibre-polyethylene composite.

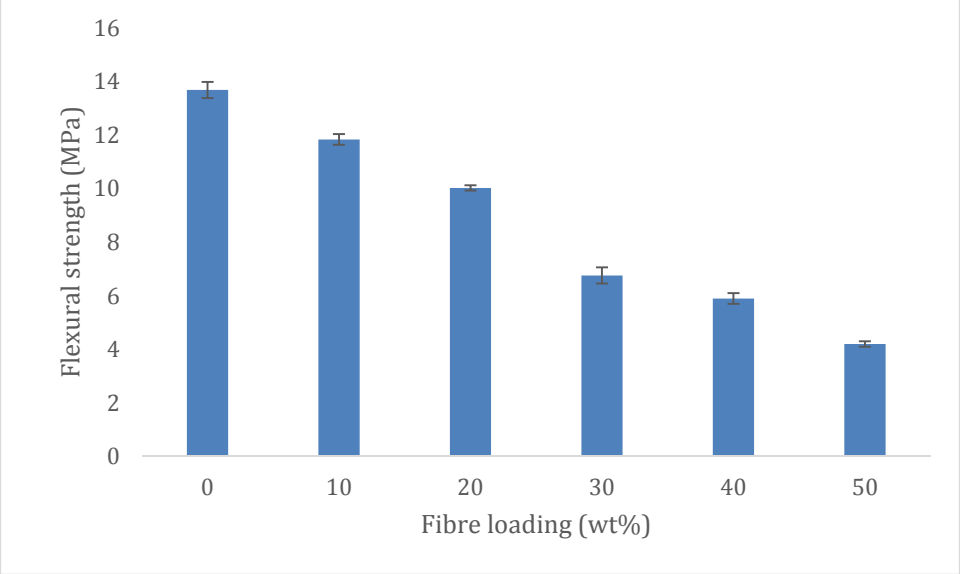

Figure 2: Flexural strength of composite at varying fibre loading

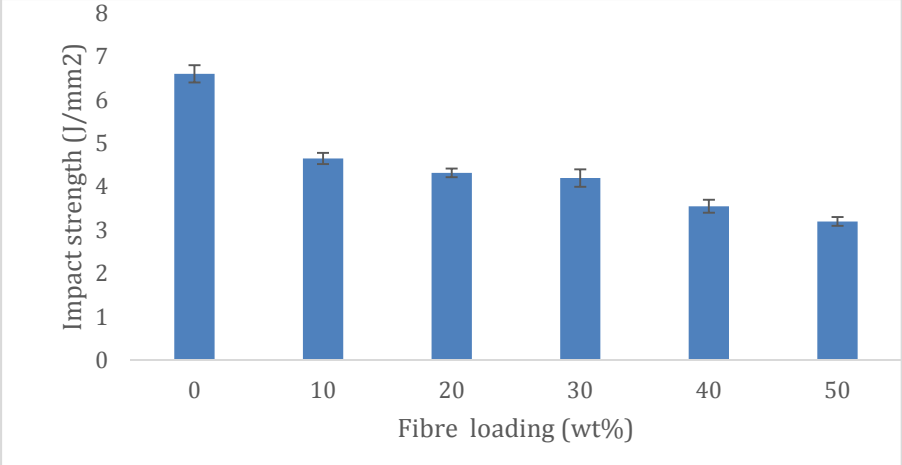

Figure 3: Impact strength of composite of varying PALF loading

3.1.3 Impact Test

The impact strength is higher on virgin LDPE than the reinforced composites. The impact strength of 4.65 J/mm^2 obtained at 10 wt% PALF loading is higher than 3.8 J/mm^{2}obtained by Shehu (2016) for untreated baobab fibre loading at 10 wt%. There is enhancement in mechanical properties of reinforced composite when the reinforcing fibre is being treated with alkali. The Figure 3 above reveals that the impact on composite decreases as the percentage of PALF increases. Impact properties decrease due to poor interfacial adhesion between the matrix and the fibre. The fibre loading increases the brittleness of the composite. The error bar overlapped between 20 wt% and 30 wt% fibre loading shows that there is no significant change in impact strength between the two composites.

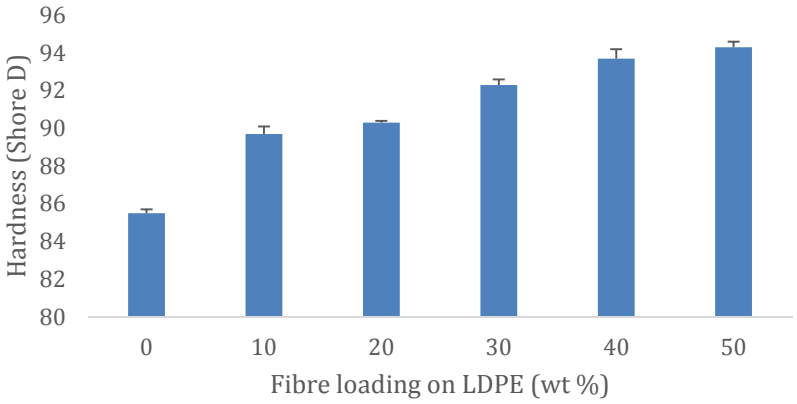

Figure 4: Hardness of composite of varying PALF loading

3.1.4 Hardness Test

Hardness is the resistance of a material to surface indentation. Figure 4 revealed the hardness of the PALF-LDPE composites. It was observed that the addition of fibre to polyethylene increases the hardness property. The lowest hardness strength of 85.5 shore D obtained at 10 wt% of PALF loading was lower than 86 shore D obtained by Kuburi et al, (2017) for Coir fibre loading-polyethylene composite. The overlapped in the error bars between 10 wt% and 20 wt% shows that there were no significant differences in the hardness strength between them and also between 40 wt% and 50 wt% baobab loading shows no significant differences in the hardness strength between the two.

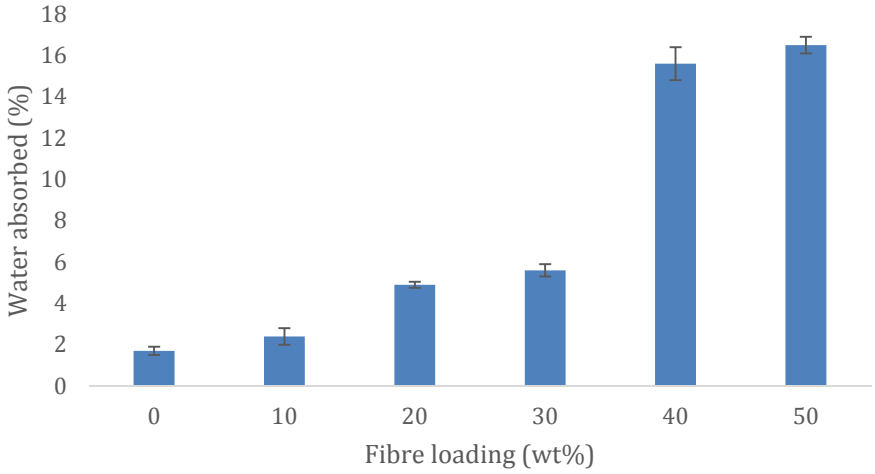

Figure 3: Water absorption on different loading for LDPE/PALF composite.

3.2 Water absorption analysis of LDPE/PALF composites.

The water absorption on virgin low density polyethylene is very low due to the hydrophobic characteristic. While on the reinforced composite of ratio 50:50 of low density polyethylene to pineapple leave fibres shows the highest water absorption than the remaining composites, this is due to the presence of higher percentage of pineapple leave fibres in the composite than the rest. This is a clear indication that water absorption increases with the increase in percentage

fibre loading in the composite, the increase is due to the hydrophilic behaviours of the pineapple leave fibres.

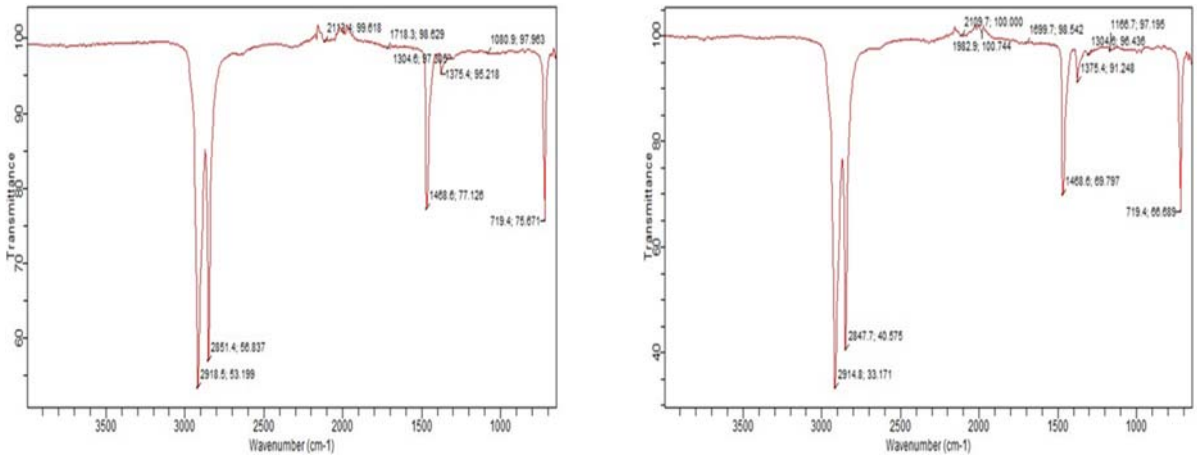

(a) (b)

Figure 4: FT-IR spectra of 100% LDPE (a) Before and (b) After burial

3.3 FT-IR Analysis for LDPE/PALF composites

It was observed from the Figure 4. which shows the FTIR spectra of 100% LDPE (a) Before burial and (b) After burial, that the peaks 1469 cm^{-1}, 1375 cm^{-1} and719 cm^{-1}, which were attributed to the stretching vibration of C=C, bending of -C-H and C-H respectively were appeared at both (a) before the burial and (b) after the burial, this shows no significant degradation has taken place throughout the period of 90 days of burial.

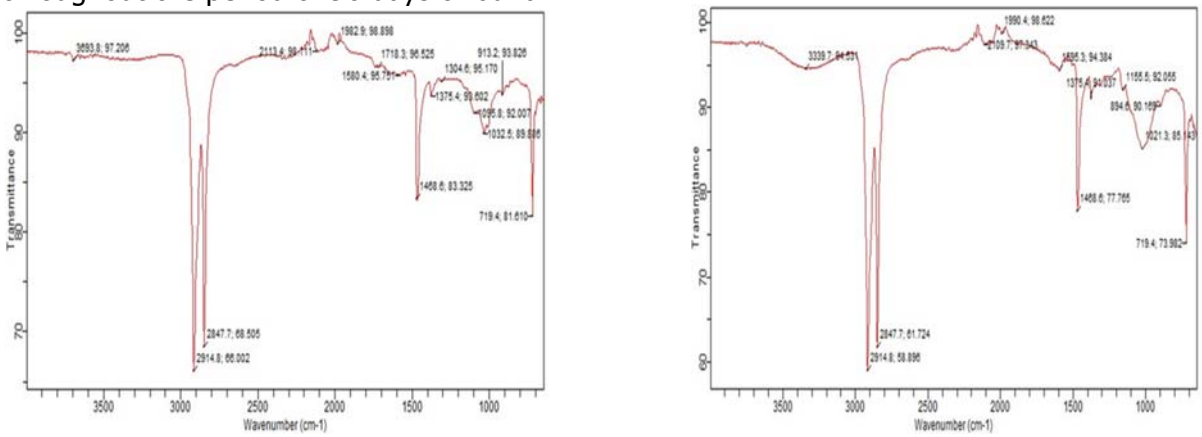

(a) (b)

Figure 5: FT-IR spectra of LDPE/PALF of ratio 70:30 (a) Before and (b) After burial

It was observed from Figure 5.which shows the FT-IR spectra of low density polyethylene to pineapple leave fibres of ratio 70:30 (a) Before burial and (b) After burial: that before burying sample 70:30 the peak at the band of 1033 $cm^{-1}$with stretching vibration of C-O was sharp. But, after burying the sample there was the shift of band from the 1033cm^{-1} to 1021$cm^{-1}$and the peak changed from sharp to broad. And the band at 1718cm^{-1} with stretching vibration of C=O in Figure 5(a) disappeared after the burial. The changes that occurred from 1033$cm^{-1}$to 1021cm^{-1} before and after the burial, and also the disappearance of the 1718cm^{-1} in 5(b) showed that degradation occurred.

4.0 Conclusion

Production of biodegradable composites from Pineapple leaves fibres was carried out using compression moulding and the following conclusions were drawn. The 30wt% and10wt% pineapple fibres loading exhibited the high tensile and low tensile strength of 14.09MPa and 7.73MPa respectively. Also, it was observed that the composite with the highest percentage of pineapple leaves fibres has the highest level of water absorption. Consequently, from the FTIR result it was concluded that significant biodegradation has occurred after burial for LDPE/PALF of ratio 70:30. Consequently, it can be concluded that pineapple leave fibre is an effective fibre that can be used as reinforcement for low density polyethylene to increase its biodegradability.

References

AbdulMotaleb K. Z. M., SharifulIslam, M. D., and Mohammad B. H. (2018). "Improvement of Physicomechanical Properties of Pineapple Leaf Fibre Reinforced Composite". Hindawi International Journal of Biomaterials, pp.2–3, doi.org/10.1155/2018/7384360

Basu G. and Roy A.N. (2007). " Blending of jute with different natural fibres". Journal of Natural Fibres, 4 (4); 13–29.

Dey. S. K. and Satapathy. K. K. (2011). "A Combined Technology Package for Extraction of Pineapple Leaf Fibre- An Agro waste, Utilization of biomass and for application in Textiles". National Institute of Research on Jute and Allied Fibre Technology Indian Council of Agricultural Research 1-9.

Elenga, R. G.; Djemia, P.; Tingaud, D.; Chauveau, T.; Maniongui, J. G.; Dirras, G.(2013) Effects of Alkali Treatment on the Microstructure, Composition, and Properties of the Raffia textilis Fiber. Bioresour. Peer-reviewed online J. 8, 2934–2949

Faruk, O., Bledzki, A. K., Fink, H. P., and Sain, M. (2012), "Bio composites reinforced with natural fibres: 2000-2010". Program Polymer Science. , 37, 1552–1596.

Jacob, M., Varughese, K. T., Thomas, S. (2005). "Water sorption studies of hybrid biofibre reinforced natural rubber biocomposites. Biomacromolecules" 6, 2969–2979.

Kaczmar, J. W.; Pietrzak, K.; Wlosinski, W. (2000). "The production and application of metal matrix composite materials". J. Mater. Process. Technol. 106, 58–67.

Kabir, M. M.; Wang, H.; Lau, K. T.; Cardona, F. (2012). "Chemical treatments on plant-based natural fibre reinforced polymer composites: An overview". Compos. Part B Eng. 43, 2883–2892.

Kim, S. W.; Lee, S. H.; Kang, J. S.; Kang, K. H. (2006). Thermal conductivity of thermoplastics reinforced with natural fibres". Int. J. Thermophys. 2006, 27, 1873–1881

Kuburi, L.S., Dauda M., Obada, D.O., Umaru S., Dodoo-Arhin, D., Iliyasu I., Balogun M.B. and Mustapha, S. (2017). "Effect of coir fibre loading on the physio-mechanical and morphological properties of coconut shell powder filled low density polyethylene composites." Science Direct. 7(2017):138-144

Liu W., Wang Y.J., Sun Z., (2003). "Effects of Polyethylene-grafted-Maleic Anhydride (PE-g-MA) on Thermal Properties, Morphology and Tensile Properties of Low Density Polyethylene (LDPE) and Corn Starch Blends". Journal of Applied Polymer Science 88, 2904-2911.

Mohammed, L. Ansari, M. N. M. Pua, G.; Jawaid, M. Islam, M. S. (2015). "A Review on Natural Fibre Reinforced Polymer Composite and Its Applications". Int. J. Polym. Sci. doi:10.1155/2015/243947

Oluyemi, O. D., Adeolu, A. A., Benjamin,O.A. and Adewole, O. (2017). "Mechanical properties and water absorption behaviour of treated pineapple leaf fibre reinforced polyester matrix composites". Leonardo Journal of Sciences 1583(0233):15-3

Roshafima R.A., Wan A., Wan A. R., Rafiziana M.K., Norazana I., Hasrinah H., Aziatul N.S., Umi A.A., Ebrahim A. (2017) "Pineapple Peel Fibre Biocomposite: Characterisation and Biodegradation Studies". Chemical engineering transactions. .doi:10,3303/set1756223

Shehu, U. and Isa, M. T. (2017). "Effects of NaOH modification on the mechanical properties of baobab pod fibre reinforced LDPE composites". Nigerian Journal of Technology (NIJOTECH), 36, 87 – 95.

Proceedings of the 49th NSChE Annual Conference
KADA 2019: pp 499-502

P3A-01: NOVEL METHOD OF PRODUCTION OF HYDROXYMETHYL FURFURAL FROM CASSIA SIEBERIANA LEAVES BY ACID HYDROLYSIS

*Haruna Ibrahim[1], Suleiman Magaji[1], Muhammad Olufade[2]
[1]Ibrahim Shehu Shema Centre for Renewable Energy Research, Umaru Musa Yar'Adua University, Katsina
[2]Department of Pure and Industrial Chemistry, Umaru Musa Yar'Adua University, Katsina
*Corresponding author: ibrahimhauna@gmail.com

ABSTRACT
The quest for alternative to petroleum products for industrial feedstocks is receiving attention in research on biomass which are biodegradable, environmental friendly, renewable and sustainable. Hydroxymethyl furfural (HMF) is a very useful organic compound for the production of the biofuel, dimethylfuran (DMF) and other important molecules such as levulinic acid, 2,5-furandicarboxylic acid (FDA), 2,5-diformylfuran (DFF), dihydroxymethyl furan and 5-hydroxy-4-keto-2-pentenoic acid. It has been known to be produced from glucose and fructose with low yield of not more than 57%. Besides, its low yield the process is expensive hence discourage the commercial production of the compound. In this study, 5-Hydrxymethyl furfural was produced from fallen dead leaves of Cassia sieberiana by hydrolysis of the pulverized leaves with 3% sulphuric acid solution. 5-Hydrxymethyl furfural constituted 82.4% among the extracts. The process is less expensive, less labour intensive yet achieved higher production from the waste product.

Keywords: dead leaves of *Cassia sieberiana*, hydrolysis, hydroxymethy furfural, sulphuric acid.

INTRODUCTION
Increasing renewable sources as chemical feedstocks has increased researches in biomass in recent years due to crises and prices rise in petroleum products (Gomes et al,. 2015). Wood comprises of cellulose, hemicellulose and lignin of which the first two components are most important were first considered for the production of bioethanol for fuel and other purposes at the beginning of 19th century (Rosatella et al., 2011). Biomass can be converted into biofuels and feedstocks chemicals that can replace fossil-based chemical (Zhao et al., 2015). Cellulose is formed by anhydro-D-glucopyranose units linked by b-1→4-glycosidic bonds while hemicellulose is a polymer formed by different sugar units such as glucose, galactose, mannose, xylose and arabinose (Rosatella et al., 2011). Both can be hydrolytic degraded into simple monomers. Hydrolysis of cellulose yields simple sugars (glucose) but that of hemicellulose which is faster yields hexoses and pentoses (galactose, mannose, xylose and arabinose) (Rosatella et al., 2011). Synthesis of 5-hydroxymethylfurfural (HMF) was based on the triple dehydration of hexoses and now include oligo- and polysaccharides as well as converted industrial wastes (Lewkowski 2001). HMF is a cyclic aldehyde produced by sugar degradation through the Maillard reaction (a nonenzymatic browning reaction) during food processing or long storage of honey (shapla et al, 2018). HMF is also prepared from the fructose portion of the sugar molecule and can also be obtained by acid-catalyzed dehydration of hexoses. It can be obtained by acid-catalyzed dehydration of different carbohydrates such as fructose, glucose, sucrose, cellulose or inulin (Gumes et al., 2015). Peng and Wu [2014], reported the production of HMF from glucose and cellulose via an arylboronic acid-catalyzed dehydration in ionic liquid (13AJOC947). de Souza *et al.,* (2012) reported that hydroxymethyl furfural can be prepared through catalyzed dehydration

of largely available carbohydrates, such as glucose and transformed into highly valuable intermediates, such as 2,5-furandicarboxylic acid (FDCA). Numerous important scientific groups are carrying out studies on the synthesis, and applications of HMF and its derivatives (Lewkowski**,** 2001).

HMF is a six-carbon heterocyclic organic compound containing both aldehyde and alcohol (hydroxymethyl) functional groups (shapla et al., 2018). HMF is one of the most interesting organic compounds from biomass. Menegazzo et al., (2018) described HMF as a multifunctional molecule for it is at the same time an aromatic aldehyde, an aromatic alcohol and a furan ring system. de Sauza (2012) reported that, among the organic compounds that can be obtained from biomass, HMF is probably one of the most important platform molecules It is an organic compound obtained from the dehydration of hexoses (glucose and fructose) (Rosatella et al., 2011), melts at 32-35^{o}C and boils at 291-292^{o}C. An organic compound known as HMF is formed from reducing sugars in honey and various processed foods in acidic environments when they are heated through the Maillard reaction (Shapla et al., 2018). It is very soluble in water and alcohol. It has aldehyde and alcohol functionalities which possibly makes it soluble in water. Freely soluble in water, methanol, ethanol, acetone, ethyl acetate, dimethylformamide; soluble in ether, benzene, chloroform; less soluble in carbon tetrachloride; sparingly soluble in petroleum ether. It has specific gravity of 1.243 at 25^{o}C, refractive index of 1.562 at 20^{o}C and flash point of 79.4^{o}C. It has a molecular weight of 126.12 and molecular formula of $C_6H_6O_3$. Figure 1 depicts the structural formula of HMF. In particular, HMF has been considered an important platform chemical in a biorefinery because it is a precursor for the production of various high-volume plastics and biofuels (Gomes, et al., 2015). HMF is very useful not only as intermediate for the production of the biofuel dimethylfuran (DMF) and other molecules, but also for important molecules such as levulinic acid, 2,5-furandicarboxylic acid (FDA), 2,5-diformylfuran (DFF), dihydroxymethylfuran and 5-hydroxy-4-keto-2-pentenoic acid [Rosatella et al].

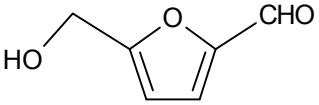

Figure 1: Structural formula of 5-hydroxylmethyl furfural.

HMF can be converted to 2, 5-Dimethylfuran (DMF), which is a liquid biofuel that in certain ways is superior to ethanol. Oxidation of HMF also gives 2,5-Furandicarboxylic acid, which can be used in place of terephthalic acid for the production of plastics. It is used in the synthesis of dialdehydes, glycols, ethers, amino alcohols and acetals. As an aqueous acid it catalyzes ring opening. It has been reported by Ibrahim et al., (2017) that the blend of HMF with fossil fuel gave smooth engine performance with significant reduction in sooth emissions from vehicles. HMF is not stable for long periods and therefore it cannot be stored for extended periods (Menegazzo et al., 2018).

In this study, HMF was produced via the acid hydrolysis of *Cassia sieberiana* fallen dead leaves. The dead leaves of cassia sieberian that fell off to the ground were collected from the premises of Umaru Musa Yar'Adua University, Katsina, Nigeria cleaned, pulverized, sieved and hydrolyzed with 3% solution of concentrated sulphuric acid at 100^{o}C for 30 minutes.

MATERIALS AND METHODS

The material used in this investigation include; pulverized dead leaves of Cassia sieberiana, ceramic mortar and pestle, sieve, measuring cylinder, distilled water ,weighing balance, 1000 ml conical flask, filter paper, Gallen kamp hot plate magnetic stirrer and thermometer. The reagents used was concentrated sulphuric acid.

The dead leaves of *Cassia sieberiana* was collected from the premises of Umaru Musa Yar'Adua University Katsina, cleaned pulverized in a ceramic mortar. It was sieved and the fine particles was parked in nylon bag and labelled. 50 g of the pulverized leaves was poured into 1000 ml conical flask containing 500 ml 3% solution of concentrated sulphuric acid. The content was heated to 100^{o}C and maintained at this temperature for 30 minutes (Ibrahim et al., 2017). The hydrolyzed product were filtered and the filtrates were analyzed with GCMS to determine the chemical components and their compositions.

RESULTS AND DISCUSSION

Table 1 presents the hydrolytic products of dead leaves of *cassia sieberiana* carried out with sulphuric acid at 100^{o}C for 30 minutes. The component with the highest composition in the product was 5-hydoxymethyl furfural which constitute 82.4%. Besides the 5-hydroxymethyl furfural, there were 11 other component compounds as presented in Table 1.

Table 1: The Acid Hydrolytic Products of Dead Leaves Cassia Sieberiana

Components	MF	% Composition
Furfural	$C_2H_4O_2$	3.6
Furanmethanol	$C_5H_6O_2$	1.5
5-Hydroxymethyl furfural	**$C_6H_6O_3$**	**82.4**
3-ethy-2-methyoxylpyrazine	$C_7H_{10}N_2O$	0.2
5-(ethoxymethylfuran)-2-carbaldehyde	$C_8H_{10}O_3$	2.4
5.(methoxymethylfuran) 2-carbaldehyde	$C_7H_8O_3$	1.3
Butric acid	$C_4H_8O_2$	0.5
2,3-dihydro-3,5-dihydroxy-6-methyl-4H-pyran-4-one	$C_6H_8O_4$	4.2
Glycolaldehyde	$C_2H_4O_2$	0.6
5-Methylfurfural	$C_6H_6O_2$	0.2
4,5-Dimethyfurfural	$C_7H_8O_2$	1.3
3-isobutyl-2-methoxypyrazine	$C_6H_{14}N_2O$	1.8
Total		**100**

Despite the versatile application profile of HMF derived intermediate chemicals, HMF is not yet produced on an industrial scale, mainly because of the high production costs (Gumes et al., 2015). Lewkowski [2001] reported that, despite numerous methods, which are being reported, no one has found an inexpensive and easy-to-use mode of the preparation of HMF. Going by this process of ours, its production cost is significantly reduced and easy to achieve. The residue from filtration constitutes sulphuric acid which can be neutralized with calcium oxide and use as fertilizer. The production of 5-HMF from glucose and fructose has been known since at end of 19th century, but not without difficulty (de Souza et al., 2012) and low yield. The highest yield of 5-HMF obtained from ionic liquid 1-H, 3-methyl imidazolin chloride and then recovered using diethyl ether was

85% after several methods attempted (de Souza et al., 2012). The production HMF from dead leaves of *Cassia sieberiana* is purely from lignocellulose material. This raw material of production does not affect the plant life as the falling dead leaves which are considered as wastes (or rather agricultural residue). It has been suggested that, for both commercial and sustainable issues efforts should focus on HMF production from lignocellulosic biomass rather than from edible products (Menegazzo et al., 2018). The highest HMF ever produced as reported by Lewkowski (2001) was that produced by Salomon and co-workers who tested catalytic properties of tributylstannoxane in the hydrolysis of HMF carried out in benzene for 8 hours at 80 °C and led to HMF in 92% yield. This method is not only expensive but harmful because it involves the use of benzene which is toxic.

CONCLUSION

5-Hydroxymethyl furfural was produced from *cassia sieberenna* leaves by hydrolysis with sulphuric acid yielded 82.4 %. The waste from this process constitutes sulphuric acid and the residue of the leaves after neutralizing the acid with calcium oxide can be used as fertilizer. The process we used is not only inexpensive and easy but also converts waste to wealth. Exploring and exploiting our forest resources would provide jobs, empower people and provide raw materials for our small, medium and even large scale industries.

REFERENCES

de Souza R. L., Yu H., Ratabou F. and Essayem N. (2012). 5-Hydroxymethylfurfural (5-HMF) Production from Hexoses: Limits of Heterogeneous Catalysis in Hydrothermal Conditions and Potential of Concentrated Aqueous Organic Acids as Reactive Solvent System. Challenges, 3, 212-232; doi: 10.3390/challe3020212 pp 212-232

Gomes F. N. D. C., Pereira L. R., Ribeiro N. F. P. and Souza M. M. V. M. (2015). Production of 5-Hydroxymethylfurfural (HMF) via Fructose Dehydration: Effect of Solvent and Salting-out. Brazilian Journal of Chemical Engineering, Vol. 32, No. 01, pp. 119 - 126,

Ibrahim H., Ayilara S., Nwanya K. O., Zanna A. S., Adegbola O. B. and Nwakuba D. C. (2017). Exploring *Gmelina arborea* leaves for Biofuels and Petrochemical and Pharmaceutical Feedstocks.

Lewkowski J. (2001). Synthesis, chemistry and applications of 5-hydroxymethylfurfural and its derivatives. General papers, ISSN 1424-6376, pp17-54

Menegazzo F., Ghedini E. and Signoretto M. (2018). 5-Hydroxymethyl Furfural production from Real Biomass, Molecule, pp1-18.

Rosatella A. A., Simeonov S. P., Frade R. F. M. and Afons C. A. M. (2011). 5-Hydroxymethylfurfural (HMF) as a building block platform: Biological properties, synthesis and synthetic applications. The Royal Society of Chemistry, Green Chem., 13, 754-793

Shapla U. M., Solayman M, Alam N, Khalil M. I.and Gan S. H. (2018). 5-Hydroxymethylfurfural (HMF) levels in honey and other food products: effects on bees and human health. *Chemistry Central Journal) 12:35* pp1-18

Zhao S., Xu G., Chang J., Chang C., Bai J., Fang S. and Liu Z. (2015). Direct Production of Ethyl Levulinate from Carbohydrates Ctatalyzed by H5-ZSM-5 Supported Phosphtungstic acid. Bioresources 10 (2) 2223-2234.

Peng X. and Wu J. (2014). Five-Membered Ring Systems, Progress in Heterocyclic Chemistry. Pp 1-12

Proceedings of the 49th NSChE Annual Conference
KADA 2019: pp 503-519

P3A-02: BATCH ADSORPTION STUDY OF PHENOL FROM AQUEOUS SOLUTION ONTO CHITOSAN FROM CRAB SHELL

[1]Idris Misau Muhammad, [1]Surajudeen Abdulsalam, [1]Usman Aliyu El-Nafaty, [2]Muhammad Abbas Ahmad Zaini, [2,3*]and Asokogene Oluwadayo Francis

[1]Department of Chemical Engineering, Abubakar Tafawa Balewa University, Bauchi, Bauchi State, Nigeria

[2]Centre of Lipid Engineering and Applied Research (CLEAR), Ibnu-Sina Institute for Scientific and Industrial Research (ISI-SIR), Universiti Teknologi Malaysia, Johor Bahru, Johor, Malaysia

[3]Department of Mineral and Petroleum Resources Engineering, Federal Polytechnic, Auchi, Edo State, Nigeria

ABSTRACT

Synthesized chitosan from crab shell was successfully used as promising adsorbent for phenol removal from water. The chitosan was screened to coarse (CC, 600 µm), medium (MC, 300 µm) and fine (FC, 150 µm) aggregates sizes. The samples were characterized for surface chemistry, surface morphology and surface texture. Primary and secondary amine/amide groups with specific surface area ranging from 191 to 226 m^2/g were displayed by chitosan characteristics. The effects of initial concentration, adsorbent dosage, contact time, temperature and solution pH were evaluated in phenol removal. The coarse chitosan (CC) displayed maximum adsorption capacity of 59.3 mg/g, in which mesopore filling and ionic interaction are the possible adsorption mechanisms. Sips model showed the best fit to the equilibrium data, suggesting the adsorption onto heterogeneous surface through adsorbate-adsorbent interactions. Kinetics data were best described by pseudo first-order model, indicating external diffusion as the significant step in phenol adsorption.

Keywords: Adsorbent, crab shell, chitosan, equilibrium, kinetics

1.0 Introduction

The increasing toxicity of phenol and phenolic compounds mostly present in wastewater of pharmaceutical, paint, leather and textile, oil refinery, disinfectant and lubricant industries (Shany and Giora, 2018; Long-Fei *et al*., 2017) and their impacts on the biosphere has become a subject of increasing concern (El-Zokm *et al*., 2015; Okbah *et al*., 2015). This could be attributed to the progressing increase in the adoption of industrial lifestyle as a result of increasing world population. The existence of phenol in water and the environment for a long period potentially affects human health (Wenjue *et al*., 2018; Mehdi *et al*., 2018). Therefore, phenolic pollutants in wastewater must be seriously treated. Treatment methods of phenolic pollutants include ion exchange, precipitation, biodegradation, ozone treatment, membrane filtration, photocatalysis, coagulation and flocculation, oxidation, and adsorption among others (Rajasulochana and Preethy, 2016). However, adsorption is considered to be inexpensive, easy to operate and effective among these treatment methods (Chang *et al*., 2018; Apurva *et al*., 2018; Lakshmi *et al*., 2016).

The quest for low cost adsorbents for effective removal of phenol at low concentrations has become a subject of burgeoning interest among adsorption scientists. A number of natural materials such as sodium zeolite (Saravanakumar and Kumar, 2013), pomegranate peels ash (Najafpoor *et al*., 2016), sewage sludge (Zhu *et al*., 2015), rice straw (Sarker and Fakhruddin, 2017), banana leaf ash (Rahdar *et al*., 2017) and activated carbon (Anisuzzaman et al., 2016)

have been evaluated for phenol adsorption because they are promising adsorbent candidates for the treatment of most wastewater contaminants (Annaduzzaman, 2015).

Chitosan is among the most abundant biopolymer in nature after cellulose. It can be produced through deacetylation of chitin extracted from the shells or scales of shrimp, prawns, crabs, insects and other crustaceans (Ramasamy and Shanmugam, 2015; Hajji *et al*., 2015). It is an effective adsorbent due to its low cost and high contents of amino and hydroxyl functional groups, endowing significant adsorption potential for the removal of various aquatic pollutants (Tondwal and Singh, 2018; Zdarta *et al*., 2015), and has been used in wastewater treatment (Pestov and Bratskaya, 2016; Wang *et al*., 2017). It is also biocompatible, biodegradable and non-toxic (Shukla *et al*., 2013; Lee, 2013). Recent studies showed that chitosan exhibit substantial removal of heavy metals, dye and phenol in batch mode. Wang *et al*. (2017) and Negm *et al*. (2015) reported removal of Cu^{2+} at 146 mg/g and 280 mg/g, respectively in batch mode. Liang *et al*. (2017) reported a 212 mg/g removal of dyes, while Nair *et al*. (2014) reported a 111 mg/g removal of remazol brilliant blue R in batch mode. Similarly, the capacities of 130 mg/g reactive red (Mahmoodi and Mokhtari-Shourijeh, 2015) and 190 mg/g for reactive black 5 (Cinar *et al*., 2016) was removed from their solution in batch mode. In a related work, about 78.4% to 90.4% of phenol solution was treated by chitosan (Moosa *et al*., 2016) in batch mode.

Therefore, to broaden the existing body of knowledge on chitosan applications in wastewater treatment, this present work is aimed at evaluating the adsorption performance of produced chitosan from Pessu river crab shell on phenol. The material was characterized and the batch adsorption was performed at different operating conditions. The adsorption data were evaluated using isotherm and kinetics models, and the possible mechanisms governing the adsorption were discussed.

2.0 Methodology

2.1 Preparation and characterization of chitosan

Fresh crab shell was collected from Pessu river in Warri, Delta State, Nigeria and washed to remove soluble organic substances, proteins and impurities. It was crushed and kept in a polyethylene bag at 25 °C for 24 h for partial autolysis. The crab shell chitosan was synthesized according to the methods described elsewhere (Moosa *et al*., 2016; Hossain and Iqbal, 2014; Toan 2009). Briefly, the shell was mixed in a 1 M NaOH solution at a ratio of 1:10 (w/v), at 25 °C for 24 h to remove proteins. The solid was washed with distilled water to remove excess NaOH, and dried in an oven at 70 °C for 2 h. The dried solid had to undergo demineralization (mainly calcium carbonate) in 0.25 M HCl solution at a ratio of 1:10 (w/v) for 15 min at 25°C. The solid (chitin) was washed to remove excess acid, and dried at 90 °C for 1 h. Chitin was converted into chitosan via deacetylation process. It was mixed in a concentrated sodium hydroxide solution at 80 °C for 1 h. The residue (chitosan) was washed and dried at 80 °C for 2 h. The crab shell chitosan was ground and sieved into 600, 300 and 150 µm aggregates designated as coarse chitosan (CC), medium chitosan (MC) and fine chitosan (FC), respectively.

A Nicolet ISI 10 FTIR spectrometer (Thermo Scientific, USA) was used to characterize the surface functional groups of crab shell chitosan at a frequency range of 4000 to 400 cm^{-1}. The elemental composition of chitosan was determined using a Brucker energy dispersive X-ray (EDAX) analyzer (Ghannam *et al.,* 2016). The surface morphology of chitosan was observed using a Karl Zeiss scanning electron microscope (SEM). A Micromeritics ASAP 2010 analyzer (Thermo Scientific, USA) was used to measure the textural properties of chitosan.

2.2 Batch adsorption studies

Working phenol concentrations of 10 to 300 mg/L solution were prepared by appropriate dilution of analytical grade phenol crystals (99%, Scharlab). A 50 mL solution of each concentration was added to 50 mg of crab shell chitosan in beatson bottle. The bottles were sealed and shaken for 72 h on SYSTEC™ homogenizer at 30 °C and a speed of 110 rpm to attain equilibrium (Hui and Zaini, 2015). The phenol concentrations of 10, 30 and 50 mg/L were evaluated for adsorption kinetics. At the pre-set time interval between 0 to 120 min, the supernatant was withdrawn from the solution for residual concentration measurement. In adsorption thermodynamics, the adsorbate-adsorbent mixture was agitated in a temperature-controlled water bath shaker at 20, 30, 40, 50, 60 and 70 °C. The residual concentrations were determined using a DU 8200 UV-Vis spectrophotometer (Shanghai Drawell Scientific Instrument) at a wavelength of 269 nm. The adsorption capacity, q_e (mg/g) was calculated from the mass balance equation as,

$$q_e = \left(\frac{C_o - C_e}{m}\right) \times V \qquad (1)$$

where, C_o and C_e (mg/L) are the initial and equilibrium concentrations, respectively, V (L) is the volume of solution and m (g) is the mass of adsorbent.

3.0 Results and Discussion

3.1 Adsorbent characteristics

Figure 1 represents the FTIR spectrum of crab shell chitosan. The peaks in the region of 3693 - 3198 cm^{-1} could be attributed to hydrogen bonded O—H and N—H stretching vibration of primary and secondary amines/amides (Kumari *et al.,* 2017). The peak at 2121 cm^{-1} is due to C≡C stretching. The peaks within the region of 1990 - 1826 cm^{-1} could be assigned to C—H bending of aromatic structures. Also, the C—C ring stretching is the characteristic of peaks at 1479 - 1401 cm^{-1}. The peaks centred in the region of 1156 - 1029 cm^{-1} and 902 - 869 cm^{-1} signify the presence of aliphatic amines group of C—N stretching and primary/secondary amine of N—H wagging. Meanwhile, the peaks at 1651 cm^{-1} and 1402 cm^{-1} could be due to the deacetylation of chitin and the formation of α-chitosan (Al Sagheer *et al.,* 2009; Younes *et al.,* 2014; Trung *et al.,* 2006).

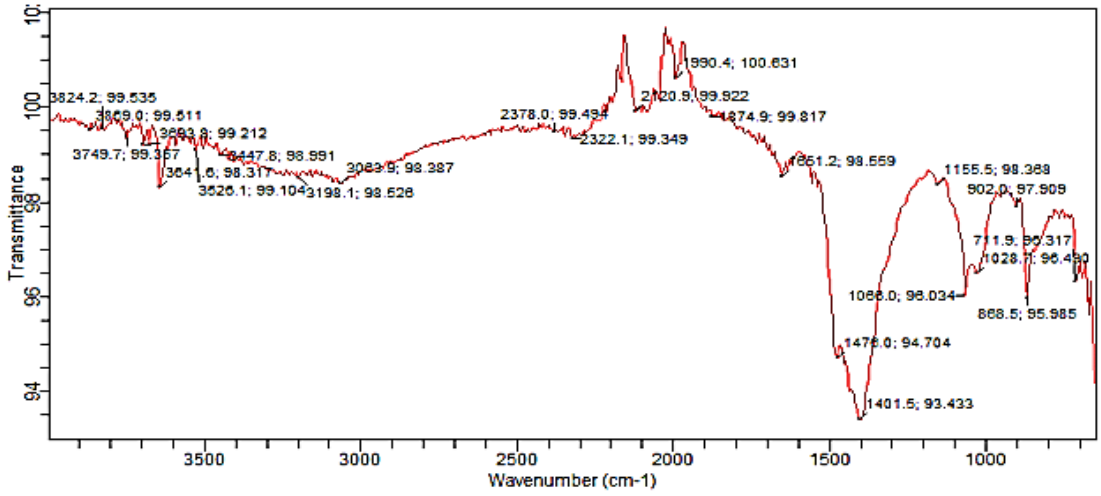

Figure 1: FTIR spectrum of crab shell chitosan

EDAX spectrum of crab shell chitosan presented in Figure 2 shows major peaks which correspond to calcium (Ca), strontium (Sr), nickel (Ni) and oxygen (O) elements. The presence of alkaline metals (Ca, Sr) and transition metals (Ag, Ni, Rh, Fe) is in agreement with the elemental composition of commercial chitosan (Shavandi *et al.*, 2015). The presence of these elements within the matrix could improve the adsorptive properties of chitosan. Rehman *et al.* (2013) reported that the transition metals within the concentration range of 0.01 - 0.31 % could enhance the adsorption of cationic dye.

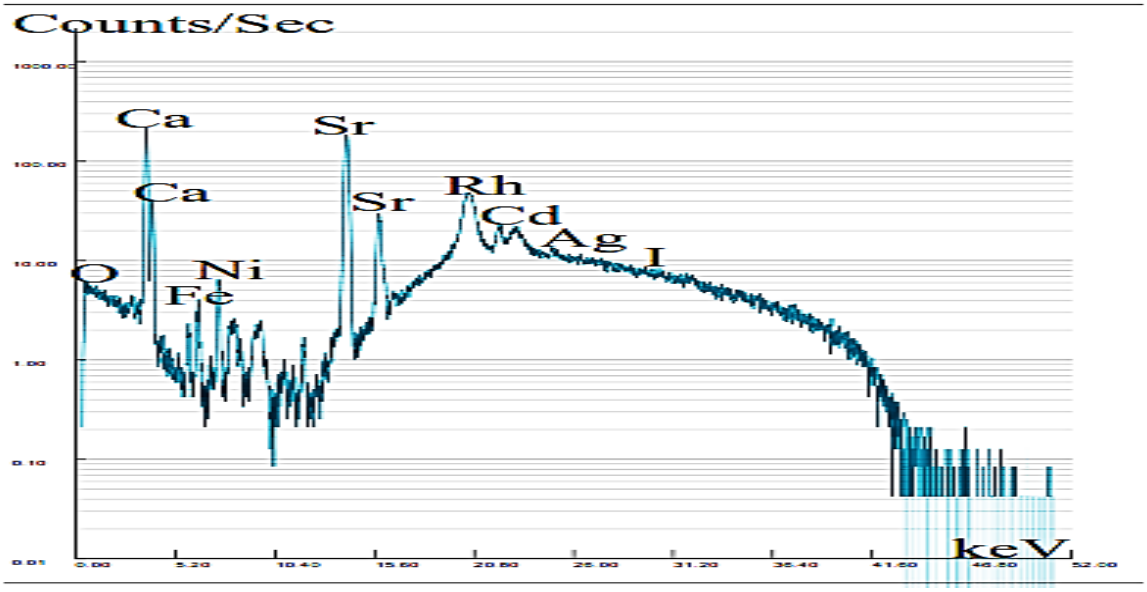

Figure 2: EDAX spectrum of crab shell chitosan

The SEM images in Figure 3 illustrate the surface morphology of crab shell chitosan. The images show rough surface with visible pores. The flaky particles with porous, fractured and fibril structures and irregularities are promising attributes of adsorbent for adsorption.

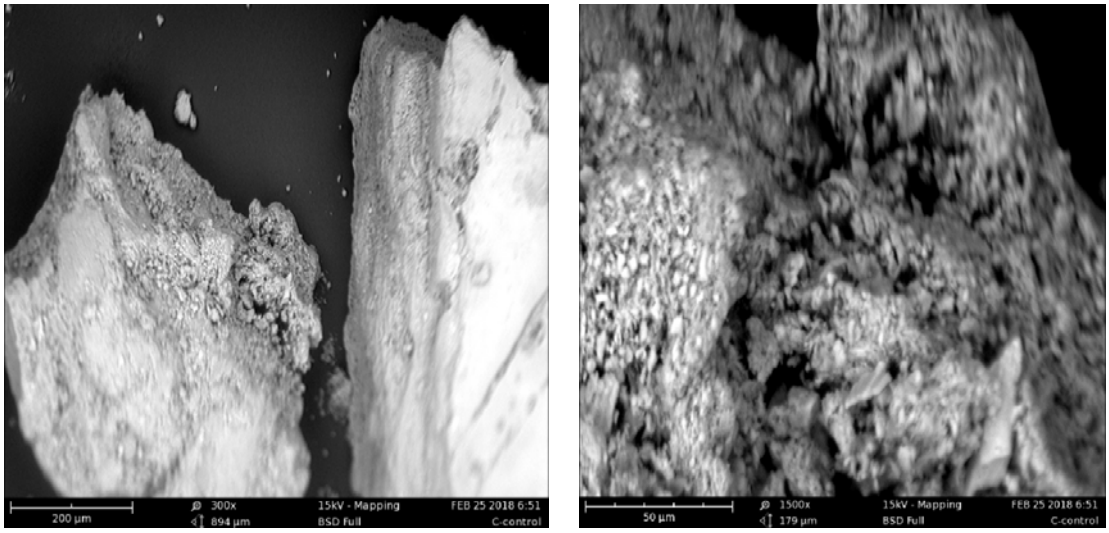

Figure 3: SEM images of crab shell chitosan

The textural properties of crab shell chitosan are summarized in Table 1. The surface area of chitosan is in the range of 191 - 226 m^2/g. Generally, there is no obvious trend of textural properties with respect to the particle sizes of chitosan. The material is highly mesoporous with pore width about 2.0 nm. The presence of mesoporous texture allows easy penetration of ions and macromolecules into the pore channels (Hu *et al.,* 2003; Budsaereechai *et. al.,* 2012). In a related work, the mesoporous biopolymer sorbent exhibits a promising removal of phenol from aqueous solution (Wan *et al.*, 2010).

Table 1: Textural properties of crab shell chitosan

Sample	BET surface area (m^2/g)	Total pore volume (cm^3/g)	Micropore volume (cm^3/g)	Average pore width (nm)	Mesoporosity (%)
CC	191	0.126	0.037	1.85	70.6
MC	226	0.125	0.036	2.12	71.3
FC	209	0.130	0.039	2.14	70.0

3.2 Batch adsorption study

Figure 4 shows the effect of initial concentration on phenol adsorption by chitosan aggregates derived from crab shell. Adsorption capacity generally increases as the initial concentration of phenol increased from 10 to 300 mg/L. This is attributed to the surface affinity of chitosan towards phenol molecules and also the mass transfer phenomenon (diffusion) due to chitosan-phenol concentration gradient. At low concentration, the active sites of chitosan are readily occupied by phenol molecules. As the phenol concentration increases, the concentration gradient offers a driving force for phenol molecules to overcome solid mass transfer resistance, resulting in a collision, thereby increasing the removal capacity (Soni *et al.*, 2017; Kumar *et al.,* 2011; Patil *et al.,* 2011). CC displays a better removal performance than MC and FC, which is pronounced at concentrations between 100 mg/L and 300 mg/L. Although it is expected that fine chitosan particles (150 µm) could endow an improved external surface for phenol contact and interaction, their dispersion and agglomeration in solution may partly complicate the attainment of equilibrium, hence decreasing the removal performance.

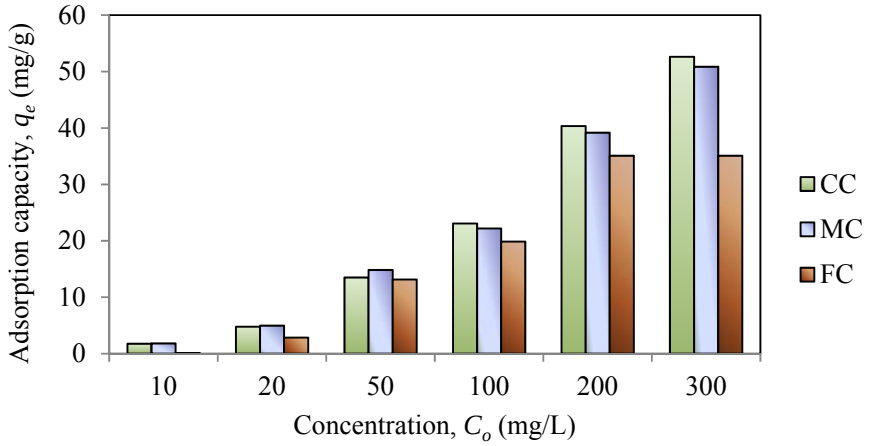

Figure 4: Effect of initial concentration on phenol adsorption by crab shell chitosan

Figure 5 presents the effect of CC dosage on phenol adsorption. Increasing CC dosage would normally increase active adsorption sites. However, there is a decrease in phenol adsorption

as dosage increased from 20 mg to 100 mg. It implies the possible overlapping, swelling and/or aggregation of the active sites which reduces the access of phenol molecules. As a result, the dosage becomes the limiting factor in adsorption. Meanwhile, at low adsorbent dosage, the adsorbate molecules can easily lodge onto the active sites, leading to a higher adsorption capacity (Agarwal *et al.,* 2013). From Figure 5, phenol adsorption capacity at a dosage of 25 mg is 17.3 mg/g.

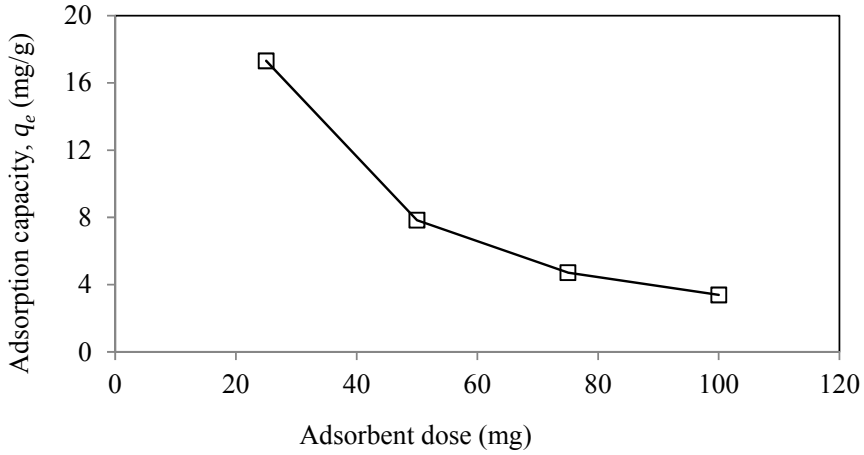

Figure 5: Effect of adsorbent dosage on phenol adsorption by CC (C_o = 30 mg/L)

The effect of contact time on phenol adsorption at a concentration of 30 mg/L is presented in Figure 6. Adsorption was found to increase with increasing contact time. Meanwhile, equilibrium was attained in about 40 min with the specified operating conditions. The adsorption capacity at equilibrium (q_e) of CC was 7.3 mg/g. A rapid adsorption was observed during the first 20 min, after which the adsorption rate (slope) decreased with increasing contact time to a point of equilibrium. The high adsorption rate could be prompted by the physicochemical properties of adsorbent and adsorbate which brought about weak Van der walls forces and interactions for phenol removal. A progression in contact time resulted in a decrease of active sites, and the formation of strong bonds between the adsorbate and adsorbent, leading to a slowdown in the process prior to equilibrium (Villarante *et al*., 2017; Poedji *et al*., 2015; Manoj and Arvind, 2012).

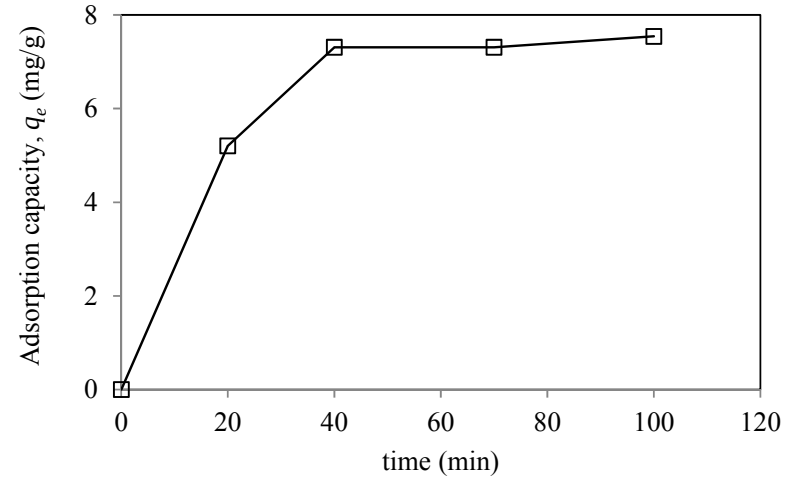

Figure 6: Effect of contact time on phenol adsorption onto CC (C_o = 10 mg/L)

The effect of pH on phenol adsorption by CC is presented in Figure 7. Adsorption of phenol is poor at a pH of 2.6 and increased as the solution pH becomes less acidic to a pH of 7.8. Further increase in solution pH has resulted in a slight decrease in adsorption capacity. This could be attributed to the solubility of chitosan in acidic media as the material tends to swell, thereby decreasing the available adsorption sites. In excessive basic environment, amine groups of chitosan form hydrogen bonds with OH^- ions, thereby increasing the ionic strength of solution and decreasing in the number and diameter of pores (Ngah *et al.*, 2011; Al-Anber *et al.*, 2011; Vucurovic *et al.*, 2012).

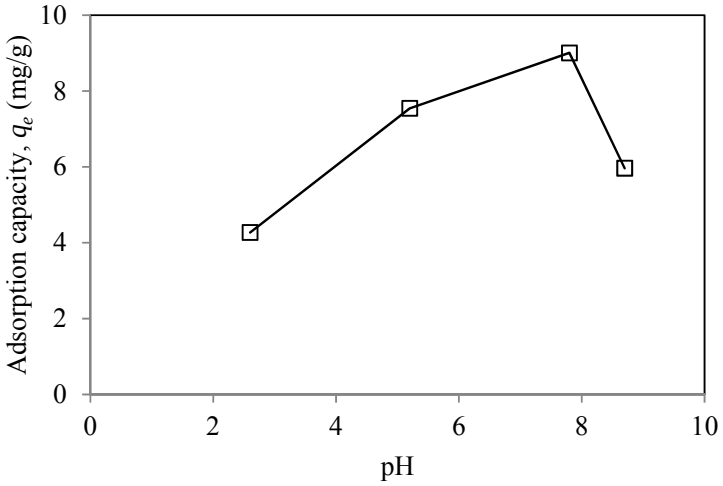

Figure 7: Effect of pH on phenol adsorption onto CC (C_o = 10 mg/L)

The removal of phenol by CC at varying solution temperatures is presented in Figure 8. The adsorption of phenol decreased with increasing temperature, although there is a small increase in adsorption from 20 ºC to 30 ºC. It implies that the adsorption is exothermic in nature. At this temperature range, the phenol molecules become mobile as a result of reduced viscosity, and interact more with the external boundary layer and internal pores, thereby increasing the adsorption capacity. Meanwhile, a further increase in the solution temperature to 70 ºC leads to the weakening of adsorptive forces between the adsorbate and adsorbent which resulted in a decreased of adsorption capacity (Aluigi *et al.*, 2014; Yagub *et al.*, 2014).

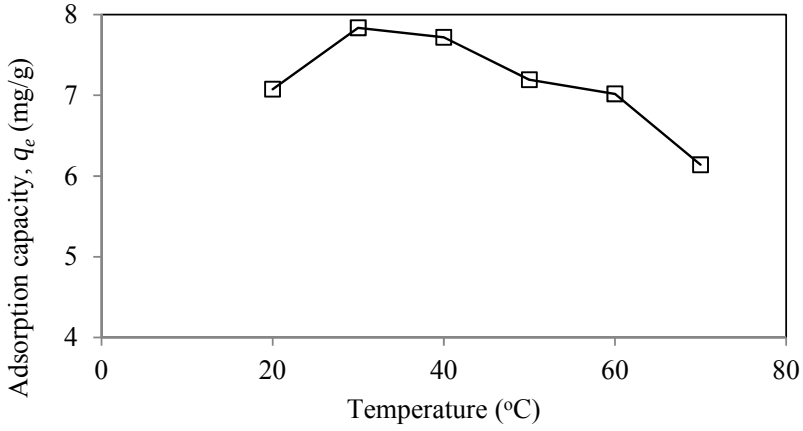

Figure 8: Effect of temperature on phenol adsorption onto CC (C_o = 10 mg/L)

3.3 Models fitting

Equilibrium adsorption was described using non-linear Langmuir, Freundlich, Temkin, Redlich Peterson and Sips isotherm models. The models were used to fit the equilibrium data. The equations for these models are given as follows,

$$q_e = \frac{Q_m K_L C_e}{1 + K_L C_e} \quad (2)$$

$$q_e = K_F C_e^{\frac{1}{n}} \quad (3)$$

$$q_e = \frac{RT}{b} \ln(aC_e) \quad (4)$$

$$q_e = \frac{Q_m (K_S C_e)^{n_S}}{1 + (K_S C_e)^{n_S}} \quad (5)$$

$$q_e = \frac{AC_e}{1 + BC_e^{\beta}} \quad (6)$$

For all isotherm models, q_e (mg/g) is the equilibrium capacity, C_e (mg/L) is the concentration of phenol in solution at equilibrium, Q_m (mg/g) and K_L (L/mg) are Langmuir isotherm constants which are the monolayer adsorption capacity and intensity, respectively. The Langmuir model is based on the assumptions that the adsorbed layer is of one molecule thickness, and the process occurs at localized sites with no lateral interaction and steric hindrance between the adsorbed molecules (Vijayaraghavan, *et al.,* 2006). The Freundlich constants, K_F (mg/g)(L/mg)$^{1/n}$ and $1/n$ are indicative of the relative adsorption capacity and intensity of surface heterogeneity, respectively. The Freundlich model is applicable to low adsorbate concentration (Fosso-Kankeu, *et al.,* 2014) and that which describes a multilayer adsorption on a heterogeneous surface (Vhahangwele and Mugera, 2015). The Temkin isotherm considers the interaction between the adsorbent and adsorbate based on uniformly distributed binding energy, where the heat of adsorption decreases linearly with increasing adsorbate coverage (Kavitha and Namasivayam, 2007; Wang and Qin, 2005). In Temkin model, T (K) is the absolute temperature, and R (= 8.314 J/mol.K) is the universal gas constant, b (J/mg) is a constant related to the heat of adsorption and a (L/mg) is the equilibrium binding constant. The Sips isotherm is a combination of Langmuir and Freundlich models that is suitable for predicting the adsorption on a heterogeneous surface. At low adsorbate concentration, the Sips model satisfies the Freundlich model, but at high adsorbate concentration, it becomes the Langmuir model (Elmorsi, 2011). In Sips model, K_S (L/mg) is the affinity constant and n_S describes the surface heterogeneity, wherein these parameters are dependent on pH, temperature and concentration (Chen, 2012). The Redlich-Peterson model is an empirical three parameters model which combines the features of the Langmuir and Freundlich models (Kolodynska *et al.,* 2009). A (L/g), B (L/mg)$^{\beta}$ and β are the Redlich-Peterson constants. The Redlich-Peterson model reduces to Freundlich model at high concentration, becomes Langmuir model at β = 1, and follows Henry model at β = 0.

Microsoft Excel *Solver* was applied to solve the model equations through non-linear regression. The fitting of isotherm models with the equilibrium data is shown in Figure 9(a) for the removal

of phenol onto CC, while Table 2 summarizes the models constants. The Sips isotherm is the best fitted model to the equilibrium data at the experimental conditions with the coefficient of determination (R^2) value of 0.988. Hence, the equilibrium data and removal behaviour of phenol onto CC could be sufficiently described by Sips model, followed by Redlich-Peterson and Langmuir models. The close agreement of Sips model with the equilibrium data is visualized in Figure 9(b). Accordingly, it suggests a heterogeneous process of phenol adsorption onto chitosan by mesopore filling and ionic interaction. Nevertheless, the adsorption intensity ($1/n$) of Freundlich model is between 0 and 1, indicating a favourable physical process. The R_L values from Langmuir isotherm are greater than 1 ($R_L > 1$), suggesting an unfavourable shape of Langmuir isotherm to describe the chemical adsorption for this process (Kumar *et al.,* 2010).

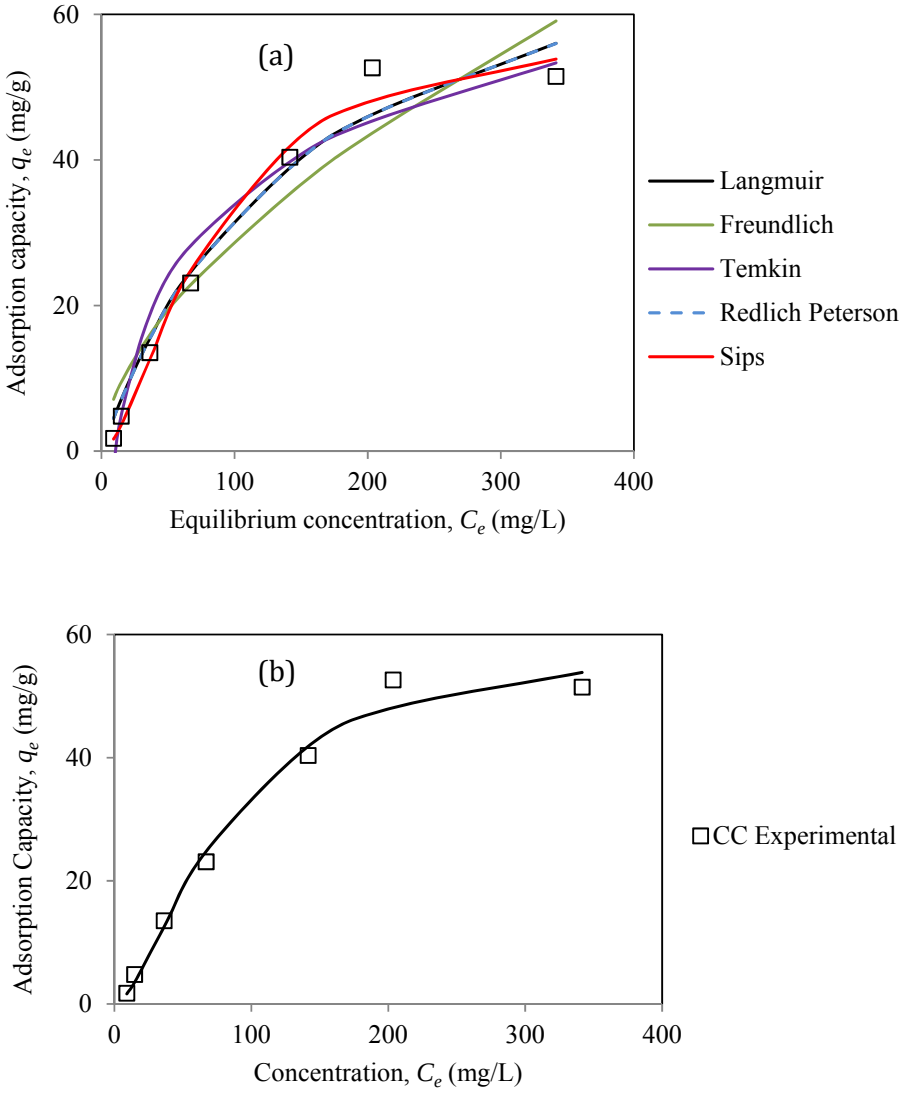

Figure 9: Equilibrium adsorption of phenol onto CC (a) isotherm models fitting and (b) Sips equilibrium isotherm

The adsorption kinetics was evaluated using non-linear pseudo-first-order, pseudo-second-order and intraparticle diffusion models. The model equations can be expressed as follows,

$$q_t = q_e\left(1 - e^{-K_f t}\right) \quad (7)$$

$$q_t = \frac{K_s q_e^2 t}{1 + K_s q_e t} \quad (8)$$

$$q_t = K_{id} t^{0.5} \quad (9)$$

For all models, q_e and q_t (mg/g) are the adsorption capacities at equilibrium and at time t (min), respectively, K_f (min^{-1}) is the rate constant of pseudo-first-order model, K_s (g/mg.min) is the rate constant of pseudo-second-order model and K_{id} ($mg/g.min^{0.5}$) is the rate constant of intraparticle diffusion model.

Table 2: Parameters of isotherm models fitting for phenol adsorption onto CC

Isotherm model	Parameters	CC
Langmuir	Q_m (mg/g)	81.4
	K_L (L/mg)	0.00647
	R^2	0.975
	R_L	1.90
Freundlich	K_F (mg/g)(L/mg)$^{1/n}$	1.97
	$1/n$	0.583
	R^2	0.927
Temkin	b (J/mg)	163
	a (L/mg)	0.0928
	R^2	0.953
Redlich Peterson	A (L/g)	0.527
	B (L/mg)$^{\beta}$	0.00647
	β	1
	R^2	0.975
Sips	Q_m (mg/g)	59.3
	K_s (L/mg)	0.0122
	n_s	1.61
	R^2	0.988

The rate of phenol adsorption by CC is shown in Figure 10 and the kinetics constants are summarized in Table 3. The results showed that the pseudo-kinetics models fitted the kinetics data well. However, the pseudo-first-order model shows better correlation with $R^2 \geq 0.978$ and good agreement between the experimental ($q_{e,exp}$) and predicted ($q_{e,cal}$) values. Furthermore, the calculated error function (SSE) is relatively lower than that of pseudo-second-order model. Therefore, it can be inferred that the external diffusion is a significant step in phenol adsorption by CC; hence, the rate of adsorption depends highly on the solution

concentration and the number of available adsorption sites. Poor regression by intraparticle diffusion model indicates that the rate limiting step is not solely controlled by intraparticle diffusion. Accordingly, it is suggested that the adsorption of phenol is governed via a weak interaction with reversible character (Gupta and Bhattacharyya, 2011; Maria *et al.,* 2009).

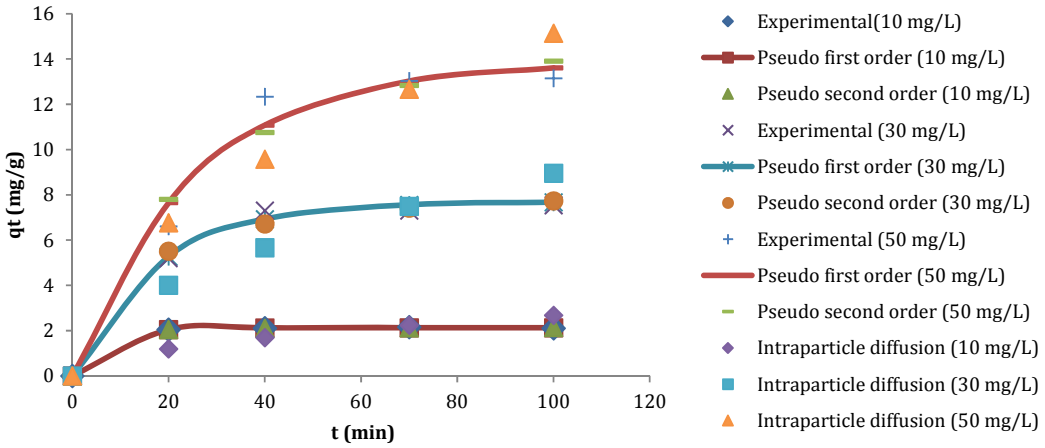

Figure 10: Adsorption kinetics of phenol onto CC, curves fitting by pseudo-first-order model

Table 3: Rate constants of pseudo-kinetics and intraparticle diffusion models for phenol adsorption

		Pseudo first order					Pseudo second order				Intraparticle diffusion		
Sorbent	C_o (mg/L)	$q_{e,exp}$ (mg/g)	$q_{e,cal}$ (mg/g)	K_f (min^{-1})	SSE	R^2	$q_{e,cal}$ (mg/g)	K_s (g/mg . min)	SSE	R^2	K_{id} (g/mg . min$^{0.5}$)	SSE	R^2
CC	10	2.20	2.13	0.16	0.002	0.999	2.16	0.436	0.002	0.999	0.27	1.22	0.735
	30	7.54	7.70	0.06	0.228	0.995	8.60	0.010	0.491	0.988	0.90	6.18	0.878
	50	13.2	13.9	0.04	2.88	0.978	17.3	0.002	4.55	0.966	1.51	11.7	0.916

3.4 Comparison with literature

Comparison of equilibrium and kinetics results of phenol adsorption using various adsorbents is shown in Tables 4 and 5, respectively. The maximum adsorption capacity of phenol onto CC at 30 ºC as predicted by Sips model is 59.3 mg/g (Table 4). Adsorbents such as crab eye activated carbon (Lallan *et al*., 2017), heat-treated activated carbon (Saenz-Alanis *et al.,* 2017), granulated activated carbon (Saenz-Alanis *et al*., 2017) and chitosan-carbon based biocomposite (Soni *et al*., 2017) exhibit greater removal performance than crab shell chitosan. This could be due to the presence of aromatic-graphitic structure of activated carbon that prompts the π-π interaction with phenol molecules. Meanwhile, crab shell chitosan (CC) exhibits a higher adsorption capacity than pyrolytic tire char, powdered coconut shell activated carbon, granulated coconut shell activated carbon, Ca-bentonite/chitosan composite, activated carbon/chitosan composite and chitin. Generally, higher surface area of adsorbent endows greater adsorbate-adsorbent interaction probabilities for adsorption. Nevertheless, the physicochemical properties of adsorbent such as pore size, functional groups and surface

charge, and that of adsorbate such as polarity, solubility and molecular dimension could in some way impede the adsorption due to pore restriction and inherent repulsion.

The rate constant reflects the speed of adsorption at any concentration. Normally, the value is higher for adsorption at lower concentration due to minimum competition to lodge onto active sites. Maria *et al*. (2009) reported that the pseudo-first-order kinetics model is the rate controlling mechanism of phenol adsorption. For comparison, the rate constant (K_f) value is 0.0075 min^{-1} for C_o = 10 mg/L that yields 0.24 mg/g of phenol removal (Maria *et al*., 2009). In this present study, the corresponding values at the same concentration are 0.16 min^{-1} and 2.20 mg/g, respectively. Meanwhile, at higher concentrations, the patterns of rate constant varied with increased adsorption capacity. Therefore, adsorption capacity is not necessarily a function of rate constant, but interplay of concentration and other physicochemical properties of the adsorbent and adsorbate.

The availability and ease of processing crab shell which is readily available and abundant with no market value renders it as promising chitosan source for wastewater treatment (Zwain *et al*., 2014). The processing of chitosan adsorbent is simple, cheap and requires less energy as compared with crab eye activated carbon, heat-treated activated carbon, granulated activated carbon and chitosan-carbon based biocomposite.

Table 4: Comparison of adsorption of phenol by various adsorbents

Adsorbent	Surface area (m^2/g)	Adsorbent dosage (mg)	C_o (mg/L)	pH	Temp. (ºC)	Q_m (mg/g)	Reference
Pyrolytic tire char	135	50	2-100	6	25	51.9	Makrigianni *et al.* (2015)
Crab eye activated carbon	265	40	50-150	8	30	169	Lallan *et al.* (2017)
Powdered coconut shell activated carbon	1344	50	35	6	30	4.31	Latinwo and Agary (2015)
Heat-treated activated carbon	619	40	10-200	7	25	197	Saenz-Alanis *et al.* (2017)
Granulated activated carbon	677	40	10-200	7	25	158	Saenz-Alanis *et al.* (2017)
Granulated coconut shell activated carbon	1076	50	35	6	30	7.58	Latinwo and Agary (2015)
Ca-bentonite/chitosan composite	-	100	50-150	7	-	12.5	Poedji *et al*. (2015)
Activated carbon/chitosan composite	-	30	20-250	Natural	30	37.2	Liu *et al.* (2014)
Chitin	-	40	10-100	2	25	16.1	Pigatto *et al*. (2013)
Chitosan-carbon based biocomposite	-	50	200-800	-	30	409	Soni *et al*. (2017)
CC	191	50	10-300	Natural	30	59.3	Present Study

4.0 Conclusion

Chitosan was produced from crab shell for phenol removal from simulated wastewater. The surface chemistry of chitosan shows the presence of N—H and hydrogen bonded O—H groups, with specific surface area of 191 m^2/g. The adsorption study in batch mode revealed that phenol adsorption increased with increasing concentration to a point of saturation, contact time to a point of equilibrium, and pH to a value of 7.8. Meanwhile, phenol adsorption

decreased with increasing adsorbent dosage and temperature. Sips model fitted well the equilibrium data with maximum value of 59.3 mg/g. Kinetics data fitted well to pseudo-first-order model, suggesting physical adsorption of phenol onto the heterogeneous surface of chitosan. Therefore, chitosan from crab shell is a promising adsorbent candidate for phenol removal from wastewater.

Table 5: Comparison of pseudo kinetics and intraparticle diffusion rate constant of phenol adsorption by various adsorbents

Adsorbent	C_o (mg/L)	pH	q_e (mg/g)	K_f (min^{-1})	K_s (g/mg.min)	K_{id} (mg/g.min)	Reference
Chitosan	10		0.24	0.0075	0.0243	0.0025	Maria *et al.* (2009)
	30		1.49	0.0033	0.0008	0.0110	
	50		2.33	0.0063	0.0005	0.0173	
Chitosan-carbon based biocomposite	100	-	33.6	3.9×10^{-2}	-	-	Soni *et al.* (2017)
Crab eye activated carbon	50	8	12.2	0.0185	0.0012	0.755	Lallan *et al.* (2017)
	100	8	28.9	0.0186	0.0005	1.30	
	150	8	33.0	0.0170	0.0008	7.33	
CC	10	Natural	2.20	0.16	0.44	0.21	Present Study
	30	Natural	7.54	0.06	0.01	0.90	
	50	Natural	13.2	0.04	0.002	1.51	

Acknowledgement

This work was supported by Tertiary Education Trust Fund (TETFund) of Nigeria through Academic Staff Training and Development (ASTandD) grant, and Ministry of Education Malaysia and Universiti Teknologi Malaysia through Fundamental Research Grant Scheme (FRGS) No. 4F995

References

Agarwal, B., Majumder, C.B. and Thakur, P.K. (2013). Simultaneous co-adsorptive removal of phenol and cyanide from binary solution using granular activated carbon. *Chemical Engineering Journal,* 228, 655-664.

Al-Anber Z.A., Al-Anber M. A., Matouq M., Al-Ayed O. and Omar N. M. (2011). Deffated Jojoba for the removal of Methylene blue from aqueous solution: thermodynamic and kinetic studies. *Desalination,* 276, 169-174.

Al Sagheer, F.A., Al Sughayer, M.A., Muslim, S. and Elsabee, M.Z. (2009). Extraction and characterization of chitin and chitosan from marine sources in Arabian Gulf. *Carbohydrate Polymer,* 77.

Aluigi, A., Rombaldoni, F., Tonetti, C. and Jannoke, L. (2014). Study of methylene blue adsorption on keratin nanofibrous membranes. *Journal of Hazardous Materials,* 156-165.

Anisuzzaman, S. M., A. Bono, D. Krishnaiah, and Y. Z. Tan, (2016). A study on dynamic simulation of phenol adsorption in activated carbon packed bed column. *Journal of King Saud University-Engineering Sciences,* 28, 47-55.

Annaduzzaman, M. (2015). Chitosan biopolymer as an adsorbent for drinking water treatment-investigation on arsenic and uranium. TRITA-LWR LIC., 2-26.

Apurva A. Narvekar, J.B. Fernandes, and S.G. Tilve, (2018). Adsorption behavior of methylene blue on glycerol based carbon materials. *Journal of Environmental Chemical Engineering,* 6(2), 1714-1725.

Budsaereechai, S., Kamwialisak, K. and Ngernyen. Y. (2012). Adsorption of lead, cadmium and copper on natural and acid activated bentonite clay. *KKU Research Journal,* 17(5), 800-810.

Chang Zhu, Jiena Yun, Qian Wang,et al. (2018). Adsorption of ion pairs onto graphene flakes and impacts of counterions during the adsorption processes. *Applied Surface Science,* 435, 329-337.

Chen C. (2012). Evaluation of equilibrium sorption isotherm equations. *Open Chemical Engineering Journal,* 7(1), 24-44.

Çinar S., Kaynar Ü. H., Aydemir T., Çam Kaynar S., and Ayvacikli M. (2016). An efficient removal of RB5 from aqueous solution by adsorption onto nano-ZnO/Chitosan composite beads. *International Journal of Biological Macromolecules,* 96, 459-465.

Elmorsi T. M. (2011). Equilibrium isotherms and kinetic studies of removal of methylene blue dye by adsorption onto miswak leaves as a natural adsorbent. *Journal of Environmental Protection,* 2(6), 817-827.

El-Zokm, G.M., Okbah, M.A. and Younis, A.M. (2015). Assessment of heavy metals pollution using AVS-SEM and fractionation techniques in Edku lagoon sediments, Mediterranean sea, Egypt. *Journal of Environmental Science and Health Part A,* 50, 1-14.

Fosso-Kankeu, E., M. Reitz, and F. Waanders. (2014). Selective adsorption of heavy and light metals by natural zeolites. 6th International Conference on Green Technology, Renewable Energy and Environmental Engineering, Cape Town (SA), 167-170.

Ghannam H.E., Talab, A.S., Dolganova, N.V., Hussein, A.M.S. and Abdelmaguid, N.M. (2016). Characterization of chitosan extracted from different crustacean shell wastes. *Journal of Applied Sciences,* 16(10), 454-461.

Gupta, S. S., Bhattacharyya, K. G. (2011). Kinetics of adsorption of metal ions on inorganic materials: A review. *Advance in Colloid and Interface Science,* 162, 39-58.

Hajji, S., Ghorbel-Bellaaj, O., Younes, I., Jellouli, K. and Nasri, M. (2015). Chitin extraction from crab shells by bacillus bacteria: Biological activities of fermented crab supernatants. *International Journal of Biological Macromelecules,* 79, 167-173.

Hossain, M.S. and Iqbal, A., (2014). Production and characterization of chitosan from shrimp waste. *Journal of Bangladesh Agricultural University,* 12(1), 153-160.

Hu, Z., Guo, H., Srinivasan, M.P. and Yaming, N.A., (2003). A simple method for developing mesoporosity in activated carbon. *Separation Purification Technology,* 31, 47-52.

Hui, T. S. and M. A. A. Zaini. 2015. Isotherm studies of methylene blue adsorption onto potassium salts-modified textile sludge. *Jurnal Teknologi (Science and Engineering),* 74(7), 57-63.

Kavitha, D. and Namasivayam, C. (2007). Experimental and kinetic studies on methylene blue adsorption by coir pith carbon. *Bioresource Technology,* 98, 14-21.

Kołodyńska, D., Skwarek, E., Hubicki, Z. and Janusz, W. (2009). Effect of adsorption of Pb (II) and Cd (II) ions in the presence of EDTA on the characteristics of electrical double layers at the ion exchanger/NaCl electrolyte solution interface. *Journal of Colloid and Interface Science,* 333(2), 448-456.

Kumar, P.S., Ramalingam, S., Senthamarai, C., Niranjanaa, M., Vijayalakshmi, P. and Sivanesan, S. (2010). Adsorption of dye from aqueous solution by cashew nut shell: studies on equilibrium isotherm, kinetics and thermodynamics of interactions. *Desalination,* 261, 52-60.

Kumar, S., Zafar, M. , Prajapati, J.K. , Kumar, S. and Kannepalli, S. (2011). Modeling studies on simultaneous adsorption of phenol and resorcinol onto granular activated carbon from simulated aqueous solution. *Journal of Hazardious Materials,* 185, 287-294.

Kumari, S., Annamareddy, S.H.K., Abanti, S. and Rath, P.K. (2017). Physicochemical properties and characterization of chitosan synthesized from fish scales, crab and shrimp shells. *International Journal of Biological Macromolecules,* 104, 697-1705.

Lakshmi, S., M. Harshitha, G. Vaishali, S. R. Keerthana, and R. Muthappa. (2016). Studies on different methods for removal of phenol in wastewater – Review. *International Journal of Science, Engineering and Technology Research,* 5(7), 2488-2496.

Lallan, S.Y., Bijay, K.M. and Arvind, K. (2017). Batch and column studies of phenol removal from aqueous solutions using laboratory prepared low-cost activated carbon as an adsorbent. *Chemical Technology Indian Journal,* 12(2), 114.

Latinwo, G.K. and Agary, S.E. (2015). Removal of phenol from paint wastewater by adsorption onto phosphoric acid activated carbon produced from coconut shell: isotherm and kinetic modeling studies. *Chemistry and Material Research Journal.* 7(5), 123-137

Lee, D.W., Lim, C. Israelachvili, J.N. and Hwang, D.S. (2013). Strong adhesion and cohesion of chitosan in aqueous solutions. *Langmuir,* 29(46), 14222-14229.

Liu, Q., Bingchao, Y., Lujie, Z. and Ruihua, H. (2014). Simultaneous adsorption of phenol and Cu^{2+} from aqueous solution by activated carbon/chitosan composite. *Korean Journal of Chemical Engineering*, 31(9), 1608-1615

Liang, X., Duan, J., Xu, Q., Wei, X., Lu, A., and Zhang, L. (2017). Ampholytic microspheres constructed from chitosan and carrageenan in alkali/urea aqueous solution for purification of various wastewater. *Chemical Engineering Journal,* 317, 766-776.

Long-Fei Ren, Rui Chen, Xiaofan Zhang, et al., (2017). Phenol biodegradation and microbial community dynamics in extractive membrane bioreactor (EMBR) for phenol-laden saline wastewater. *Bioresource Technology,* 244, 1121-1128.

Mahmoodi, N. M., and Mokhtari-Shourijeh, Z. (2015). Preparation of PVA-chitosan blend nanofiber and its dye removal ability from colored wastewater. *Fibers and Polymers,* 16, 1861-1869.

Makrigianni, V., Aris, G., Yiannis, D. and Ipannis, K. (2015). Adsorption of phenol and methylene blue from aqueous solutions by pyrolytic tire char: Equilibrium and kinetic studies. *Journal of Environmental Chemical Engineering,* 3, 574-582

Manoj, Kumar Mahapatra and Arvind, Kumar (2012). "Phenol removal from aqueous solution by adsorption using granular activated carbon" National conference on Technological advancements in chemical and environmental engineering (TACEE2012), BITS, Pilani.

Maria, Aparecida L. Milhome, Denis, de Keukeleire, Jefferson,P. Ribeiro e Ronaldo, F. Nascimento, Tecia, Vierira Carvalho and Danilo, Caldas Queiroz, (2009). Removal of phenol and conventional pollutants from aqueous effluent by chitosan and chitin. *Quim Nova,* 32(8), 2122-2127.

Mehdi Mohammadi, Mohammad Ali As'habi, Peyman Salehi,et al. (2018). Immobilization of laccase on epoxy-functionalized silica and its application in biodegradation of phenolic compounds. *International Journal of Biological Macromolecules,* 109, 443-447.

Moosa, A. A., A. M. Ridha, and N. A. Kadim, (2016). Use of biopolymer adsorbent in the removal of phenol from aqueous solution. *American Journal of Materials Science,* 6(4), 95-104.

Nair, V., Panigrahy, A., and Vinu, R. (2014). Development of novel chitosan-lignin composites for adsorption of dyes and metal ions from wastewater. *Chemical Engineering Journal,* 254, 491-502.

Najafpoor, A. A., S. Dousti, A. J. Jafari, and A. Hosseinzadeh, (2016). Efficiency in phenol removal from aqueous solutions of pomegranate peel ash as a natural adsorbent. *Environmental Health Engineering and Management,* 3(1), 41-46.

Negm, N. A., El-Sheikh, R., El-Farargy, A. F., Hefni, H. H. H., and Bekhit, M. (2015). Treatment of industrial wastewater containing copper and cobalt ions using modified chitosan. *Journal of Industrial and Engineering Chemistry,* 21, 526-534.

Ngah, Wan W.S., Teong, L.C. and Hanafiah, M.A.K.M. (2011). Adsorption of dyes and heavy metal ions by chitosan composites: A review. *Carbohydrate Polymer,* 83, 1446-1456.

Okbah, M.A., El-Zokm, G.M. and Younis, A.M. (2015). Heavy metals fractionation and acid volatile sulfide (AVS) in the Bardawil lagoon sediments, Northern Sinai, Egypt. *Developmental Analytical Chemistry Journal,* 2, 1-9.

Patil, S., Deshmukh, V., Renukdas, S. and Patel, N. (2011). Kinetics of adsorption of crystal violet from aqueous solution using different natural materials. *International Journal of Environmental Sciences,* 1, 6.

Pestov, A., and Bratskaya, S. (2016). Chitosan and its derivatives as highly efficient polymer ligands. *Molecules,* 21

Pigatto, G., Alessandra, L., Elisabetta, F. and Mauri, S.A.P. (2013). Chitin as biosobent for phenol removal from aqueous solution: Equilibrium, kinetic and thermodynamic studies. *Chemical Engineering and Processing Journal,* 70, 131-139

Poedji, Leokitowati Hariani, Fatima, Fahma Riyanti and Hesti, Ratnasani (2015). Adsorption of phenol pollutants from aqueous solution using Ca-Bentonite/chitosan composite. *Jurnal Manusia Dan Lingkungan,* 22(2), 233-239.

Rahdar, S., M. Ahamadabadi, R. Khaksefidi, M. Saeidi, M. R. Narooie, A. Salimi, H. Biglari, and M. M. Baneshi, (2017). Evaluation of phenol removal from aqueous solution by banana Leaf ash. *Journal of Global Pharma Technology,* 3(9), 20-28.

Rajasulochana P, and Preethy V. (2016). Comparison on efficiency of various techniques in treatment of waste and sewage water- A comprehensive review. *Resource Efficient Technologies,* 2, 175-184.

Ramasamy, P. and Shangmugam, A. (2015). Characterization and wound healing property of collagen-chitosan film from sepia kobiensis. *International Journal of Biological Macromolecules,* 74, 93-102.

Rehman, M. S. U., Munir, M., Ashfaq, M., Rashid, N., Nazar, M. F., Danish, M. and Han, J. I. (2013). Adsorption of brilliant green dye from aqueous solution onto red clay. *Chemical Engineering Journal,* 228, 54-62.

Saenz-Alanis, A. Carina, Refugio, B. Garcia-Reyes, Eduardo, Soto-Regalado and Alcione, Garcia-Gonzalez (2017). Phenol and methylene blue adsorption on heated-treated activated carbon: characterization, kinetics and equilibrium studies. *Adsorption Science and Technology,* 1-17.

Saravanakumar, K., and A. Kumar, (2013). Removal of phenol from aqueous solution by adsorption using zeolite. *African Journal of Agricultural Research,* 8(23), 2965-2969.

Sarker, N. and A. N. M. Fakhruddin, (2017). Removal of phenol from aqueous solution using rice straw as adsorbent. *Applied Water Science,* 7, 1459-1465.

Shany Ben Moshe, and Giora Rytwo (2018). Thiamine-based organo-clay for phenol removal from water. *Applied Clay Science,* 155, 50-56.

Shavandi, Amin, Adnan, A. Bekhit, Alaa El-Din, A. Bekhit, Zhifa, Sun and Ali, M. Azam, (2015). "Preparation and Characterisation of Irradiated Crab Chitosan and New Zealand Arrow Squid Pen Chitosan." *Materials Chemistry and Physics,* 1-8.

Shukla, S. K., Mishra, A. K., Arotiba, O. A., and Mamba, B.B. (2013). Chitosan-based nanomaterials: A state of the art review. *International Journal of Biological Macromolecules,* 59, 46-58.

Soni, Usha, Jaya, Bajpai, Sunil, Kumar Singh and A.K. Bajpai (2017). Evaluation of chitosan-carbon based biocomposite for efficient removal of phenol from aqueous solutions. *Journal of Water Process Engineering,* 16, 56-63.

Toan, N.V. (2009). Production of chitin and chitosan from partially autolyzed shrimp shell materials. *Open Biomaterials Journal,* 1, 21-24.

Tondwal, R., and Singh, M. (2018). Chitosan functionalization with a series of sulfur-containing α-amino acids for the development of drug-binding abilities. *Journal of Applied Polymer Science,* 135(12), 46.

Trung, T.S., Thein-Han, W.W., Qui, N.T., Ng, C.H. and Stevens, W.F. (2006). Functional characteristics of shrimp chitosan and its membranes as affected by the degree of deacetylation. *Bioresource Technology,* 97(4), 659-663.

Vhahangwele, M., and G. W. Mugera. (2015). The potential of ball-milled South African bentonite clay for attenuation of heavy metals from acidic wastewater: Simultaneous sorption of Co^{2+}, Cu^{2+}, Ni^{2+}, $Pb^{2+}$and Zn^{2+} ions. *Journal of Environmental Chemical Engineering,* 3(4), 2416-2425.

Vijayaraghavan, K., Padmesh, T. V. N., Palanivelu, K. and Velan, M. (2006). Biosorption of nickel (II) ions onto Sargassum wightii: application of two-parameter and three-parameter isotherm models. *Journal of Hazardous Materials,* 133(1), 304-308.

Villarante, N.R., Bautista, A.P.R. and Sumalapao, D.E.P. (2017). Batch adsorption study and kinetic profile of Cr(VI) using lumbang (Aleurites moluccana)-derived activated carbon-chitosan composite crosslinked with epichlorohydrin. *Oriental Journal of Chemistry,* 33(3), 111-1119.

Vucurovic, V. M., Razmovski R. N. and Tekic M. N. (2012). Methylene Blue (cationic dye) adsorption onto sugar beet pulp: Equilibrium isotherm and kinetic studies. *Journal of the Taiwan Institute of Chemical Engineers,* 43, 108-111.

Wan, Chi-Chu M. W. Kan, B.D. Rogel and M.L.P. Dalida, (2010). Adsorption of copper (II) and lead (II) ions from aqueous solution on chitosan-coated sand. *Carbohydrate Polymers,* 80, 891-899.

Wang, B., Zhu, Y., Bai, Z., Luque, R., and Xuan, J. (2017). Functionalized chitosan biosorbents with ultra-high performance, mechanical strength and tunable selectivity for heavy metals in wastewater treatment. *Chemical Engineering Journal,* 325, 350-359.

Wang, X.S. and Qin, Y. (2005). Equilibrium sorption isotherms for of Cu^{2+} on rice bran. *Process Biochemistry,* 40, 677-680.

Wenjue Zhong, Donghong Wang, and Zijian Wang (2018). Distribution and potential ecological risk of 50 phenolic compounds in three rivers in Tianjin, China. *Journal of Environmental Pollution,* 235, 121-128

Yagub, M., Sen, T., Afroze, S. and Ang, H. (2014). Dye and its removal from aqueous solution by adsorption: A review. *Advances in Colloid and Interface Science,* 1(13).

Younes, I., Hajji, S., Frachet, V., Rinaudo, M., Jellouli, K. and Nasri, M.. (2014). Chitin extraction from shrimp shell using enzymatic treatment. Antitumor, antioxidant and antimicrobial activities of chitosan. *International Journal of Biological Macromolecules,* 69, 489-498.

Zdarta, J., Klapiszewski, L., Wysokowski, M., Norman, M., Kolodziejczak-Radzimska, A., Moszynski, H., Ehrlich, H., Maciejewski, A., Sterling, D. and Jesionowski, T. (2015). Chitin-lignin material as a novel matrix for enzyme immobilization. *Marine Drugs,* 13(4), 2424-2446.

Zhu, W., W. Yao, Y. Zhan, and Y. Gu, (2015). Phenol removal from aqueous solution by adsorption onto solidified landfilled sewage sludge and its modified sludges. *Journal of Material Cycles and Waste Management,* 17, 798-807.

Zwain, H. M., Vakili, M. and Dahlan, I. (2014). Waste material adsorbents for zinc removal from wastewater: A comprehensive review. *International Journal of Chemical Engineering.*

Proceedings of the 49th NSChE Annual Conference
KADA 2019: pp 520-537

P3A-03: ADSORPTION OF PHENOL FROM AQUEOUS SOLUTION ONTO CHITOSAN FROM CRAB SHELL IN A FIXED BED COLUMN

[1,3]**Asokogene Oluwadayo Francis, [2]Idris Misau Muhammad, [2]Surajudeen Abdulsalam, [2]Usman Aliyu El-Nafaty and [3]Muhammad Abbas Ahmad Zaini,**
[1]Department of Mineral and Petroleum Resources Engineering Technology, Federal Polytechnic, Auchi, Edo State, Nigeria
[2]Department of Chemical Engineering, Abubakar Tafawa Balewa University, Bauchi, Bauchi State, Nigeria
[3]Centre of Lipid Engineering and Applied Research (CLEAR), Ibnu-Sina Institute for Scientific and Industrial Research (ISI-SIR), Universiti Teknologi Malaysia, Johor Bahru, Johor, Malaysia
Correspondence: asokogenedayo@yahoo.com

ABSTRACT
The characteristics of coarse chitosan (CC, 600 µm) aggregates from crab shell as prospective adsorbent for phenol removal was studied in a fixed bed column. Surface chemistry of the CC showed characteristics attributed to the primary and secondary amine/amide groups with specific surface area of 191 m^2/g. Surface morphology exhibited rough surface with visible pores, and flaky particles with porous, fractured and fibril structures. The effects of varying inlet concentrations, flow rates and bed heights were evaluated for phenol adsorption. Maximum adsorption capacity of the CC at optimum conditions was 190.21 mg/g. Thomas and Yoon-Nelson kinetics model showed good correlation with experimental data and best described the breakthrough behavior of the phenol removal. External and internal diffusion were the rate controlling mechanism as predicted by Thomas model, while the entire system kinetics as predicted by Adams-Bohart model was a simultaneous steady state process of intraparticle diffusion and chemical reaction.

Keywords: Adsorption, crab shell, chitosan, fixed bed column, diffusion, phenol

1.0 Introduction
Wastewater from pharmaceutical, paint, leather, textile, oil refinery, disinfectant and lubricant industries (Shany and Giora, 2018; Long-Fei *et al.*, 2017) mostly contain phenol and phenolic compounds as pollutants. A phenolic pollutant potentially affects human health because it is toxic, carcinogenic, teratogenic and mutagenic, and can also exist in the environment for a long time (Wenjue *et al.*, 2018; Mehdi *et al.*, 2018; Gholizadeh *et al.*, 2013). Phenolic compounds are listed among priority pollutants by many Environmental Protection Agencies (Hameed and Rahman, 2008; Jia and Lua, 2008).Therefore, wastewater containing phenol should not be disposed in open water without treatment. Consequently, several conventional methods for their removal from aqueous solution include ion exchange, precipitation, biodegradation, ozone treatment, membrane filtration, photocatalysis, coagulation, flocculation, oxidation and adsorption (Rajasulochana and Preethy, 2016, Aslam *et* al., 2017; Aysan *et* al., 2016; Luo *et* al., 2017; Wang *et* al., 2017; Ihsan, 2013). Most of these methods are expensive, lead to the formation of hazardous by-products and require high energy (Tabari *et al.*, 2012; Yazdanbakhsh *et al.*, 2011). However, adsorption method is considered to be simple, highly effective, fast, inexpensive and easy to operate among the treatment methods (Chang *et al.*, 2018; Apurva *et al.*, 2018; Lakshmi *et al.*, 2016; Aysan *et* al., 2016; Pathania *et al.*, 2017; Tahir *et* al., 2017).

The development of a low-cost adsorption method for highly effective removal of phenol is increasingly becoming attractive. Adsorption of contaminants onto different solids is essential from environmental, purification and hazardous waste product disposal point of view (Anku *et al*., 2017; Gavrilescu, 2004; Mellah *et al*., 2005; Benavente, 2008). Many researchers used a number of materials as adsorbents, such as sodium zeolite (Saravanakumar and Kumar, 2013), pomegranate peels ash (Najafpoor *et al*., 2016), solidified landfilled sewage sludge (Zhu *et al*., 2015), rice straw (Sarker and Fakhruddin, 2017), banana leaf ash (Rahdar *et al*., 2017) and activated carbon (Anisuzzaman *et al*., 2016). However, natural products are seen as alternative and novel adsorbent materials for most wastewater contaminants (Annaduzzaman, 2015). Therefore, the search for low-cost and easily available adsorbents has led many researchers to search for more economic and efficient natural and synthetic materials as adsorbents.

Chitosan has gained wide attention as an effective biosorbent due to its low-cost and high contents of amino and hydroxyl functional groups which showed significant adsorption potential for the removal of various aquatic pollutants (Arbia *et al.,* 2013; Tondwal and Singh, 2018; Zdarta *et al*., 2015). It is also biocompatible, biodegradable and nontoxic (Shukla *et al*., 2013; Lee *et al*., 2013). This biopolymer is the most abundant in nature after cellulose, produced by deacetylation of chitin extracted from the shells/scales of shrimp, prawns, crabs, insects and other crustaceans (Ramasamy and Shanmugam, 2015; Hajji *et al*., 2015) and widely used in wastewater treatment (Pestov and Bratskaya, 2016; Wang *et al*., 2017). Recent studies showed the removal of phenol using a fixed bed column by various adsorbents. Rocha *et al*. (2015) reported the adsorption capacity of phenol in a fixed bed column at bed height of 5 cm and flow rate of 18 mL/min of 86.9, 72.0, 55.8 and 46.9 mg/g at initial concentrations of 200, 300, 400 and 500 mg/L, respectively, using corn cobs treated activated carbon. Karunarathne and Amarasinghe (2013) reported the removal of phenol in a fixed bed column using sugarcane bagasse activated carbon at initial concentration of 20 mg/L and flow rate of 33.3 mL/min as 12.02 and 12.34 mg/g at bed weight of 5 and 10 g, respectively. Similarly, Muthamilselvi *et al*. (2018) also reported the adsorption of phenol onto garlic peel powder at initial concentration of 50 mg/L and bed height of 15 cm of 21.36, 17.66 and 17.29 mg/g at flow rate of 15, 20 and 25 mL/min, respectively. Meanwhile, no known study on the removal of phenol in fixed bed column using chitosan prepared from Pessu river crab shells for phenol adsorption has been carried out. The availability at little cost of Pessu river crab shell waste which is the primary raw materials for the preparation of chitosan adsorbent in this study could be good alternatives to present day adsorbents.

Therefore, to broaden the existing body of knowledge on phenol removal in fixed bed mode, chitosan synthesized from Pessu river crab shell has been applied for the removal of phenol from simulated wastewater at parametric conditions in fixed bed mode and the dynamic behaviour of fixed bed adsorption predicted and analysed using Adams-Bohart, Thomas and Yoon-Nelson models.

2.0 Methodology

2.1 Preparation and characterization of chitosan

Fresh crab shell was collected from Pessu river in Warri, Delta State, Nigeria and washed to remove soluble organic substances, proteins and impurities. It was crushed and kept in a polyethylene bag at 25 °C for 24 h for partial autolysis. The crab shell chitosan was synthesized according to the methods described elsewhere (Moosa *et al*., 2016; Hossain and Iqbal, 2014; Toan 2009). Briefly, the shell was mixed in a 1 M NaOH solution at a ratio of 1:10 (w/v), at 25 °C for 24 h to remove proteins. The solid was washed with distilled water to remove excess NaOH, and dried in an oven at 70 °C for 2 h. The dried solid had to undergo demineralization

(mainly calcium carbonate was demineralized) in 0.25 M HCl solution at a ratio of 1:10 (w/v) for 15 min at 25°C. The solid (chitin) was washed to remove excess acid, and dried at 90 °C for 1 h. Chitin was converted into chitosan via deacetylation process. It was mixed in a concentrated sodium hydroxide solution at 80 °C for 1 h. The residue (chitosan) was washed and dried at 80 °C for 2 h. The produced chitosan was ground and sieved into 600 µm aggregates and designated as coarse chitosan (CC).

A Nicolet ISI 10 FTIR spectrometer (Thermo Scientific, USA) was used to identify the surface functional groups of crab shell chitosan at a frequency range of 4000 to 400 cm^{-1}. The elemental composition of chitosan was determined using a Brucker energy dispersive X-ray (EDAX) analyzer (Ghannam *et al.,* 2016). The surface morphology of chitosan was observed using a Karl Zeiss scanning electron microscope (SEM). A Micromeritics ASAP 2010 analyzer (Thermo Scientific, USA) was used to measure the textural properties of chitosan.

2.2 The adsorption study in a fixed bed column

The adsorption study was carried out in a 0.75 cm inner diameter and height of 56.7 cm Pyrex Technico, England glass column with steel sieve supported by plastic wool inserted at the bottom of the column. Coarse chitosan (CC) was packed into the column at required bed heights of 1.75 cm (0.5 g) and 3.5 cm (1.0 g). Steel sieve supported by glass wool was also introduced at the top of the bed in the column to avoid loss of adsorbent and to allow for uniform flow of the solution. Known phenol concentrations of 100 and 200 mg/L was injected at the bottom of the vertical column at fixed and controlled discharge rates (2.17 and 2.90 mL/min) upward through the column by a peristaltic pump (supplied by Baoding longer, China). The solution was pumped upward to avoid channeling due to gravity. Treated phenol solution was collected at the column outlet at regular time intervals and their concentrations analyzed using a UV-Vis spectrophotometer (Drawell (DU 8200) Scentific, China) at 269 nm. The experiment was carried out at room temperature (30°C) and natural pH of adsorbate. Breakthrough curve which shows mass transfer zone or the interaction between adsorbate and adsorbent (Afroze *et al.*, 2016), was determined from the plot of C_t/C_o against t (min), where C_t is the effluent concentration, C_o is the influent concentration and t is the service time. Inlet concentrations and flow rates of adsorbates were varied and the amount adsorbed was determined from the area under the plot by integrating the amount of phenol adsorption expressed as C_{ads} ($C_{ads} = C_o - C_t$) for a given time t (min). The amount of phenol adsorbed in the fixed bed column [q_{total} (mg)] was evaluated using equation 1 (Yagub *et al.*, 2014).

$$q_{total} = \frac{QA}{1000} = \frac{Q}{1000}\int_{t=0}^{t=t_{total}} C_{ad}\,dt \quad (1)$$

where t_{total}, Q and A are the total flow time (min), volumetric flow rate (mL/min) and the area under the breakthrough curve, respectively. Equilibrium uptake ($q_{o,eq}$) (mg/g) is determined using equation 2.

$$q_{o,eq} = \frac{q_{total}}{m} \quad (2)$$

where m (g) is the amount of adsorbent in the fixed bed column. The amount of phenol passed into the column [M_{total} (mg)] is determined by equation 3.

$$M_{total} = \frac{C_o Q t_{total}}{1000} \quad (3)$$

Percentage of phenol removed is the quotient of the maximum capacity of the column (q_{total}) divided by the total amount of phenol sent to the column (M_{total}) expressed in equation 4.

Total removal = $\frac{q_{total}}{M_{total}} \times 100$ (4)

At equilibrium, the unadsorbed phenol concentration [C_{eq} (mg/g)] in the continuous flow system is expressed in equation 5.

C_{eq} (mg/L) = $\frac{M_{total} - q_{total}}{V_{eff}} \times 1000$ (5)

At equilibrium, effluent volume [V_{eff} (mL)] collected is expressed in equation 6.

$V_{eff} = Q \times t_{total}$ (6)

where, Q and t_{total} are volumetric flow rate (mL/min) and total flow time (min), respectively.

3.0 Results and Discussion

3.1 Adsorbent characteristics

Figure 1 represents the FTIR spectrum of the chitosan. The peaks in the region of 3693 - 3198 cm^{-1} could be attributed to hydrogen bonded O—H and N—H stretching vibration of primary and secondary amines/amides (Kumari *et al.,* 2017). The peak at 2121 cm^{-1} is due to C≡C stretching. The peaks within the region of 1990 - 1826 cm^{-1} could be assigned to C—H bending of aromatic structures. Also, the C—C ring stretching is the characteristic of peaks at 1479 - 1401 cm^{-1}. The peaks centred in the region of 1156 - 1029 cm^{-1} and 902 - 869 cm^{-1} signify the presence of aliphatic amines group of C—N stretching and primary/secondary amine of N—H wagging. Meanwhile, the peaks at 1651 cm^{-1} and 1402 cm^{-1} could be due to the deacetylation of chitin and the formation of α-chitosan (Al Sagheer *et al.,* 2009; Younes *et al.,* 2014; Trung *et al.,* 2006).

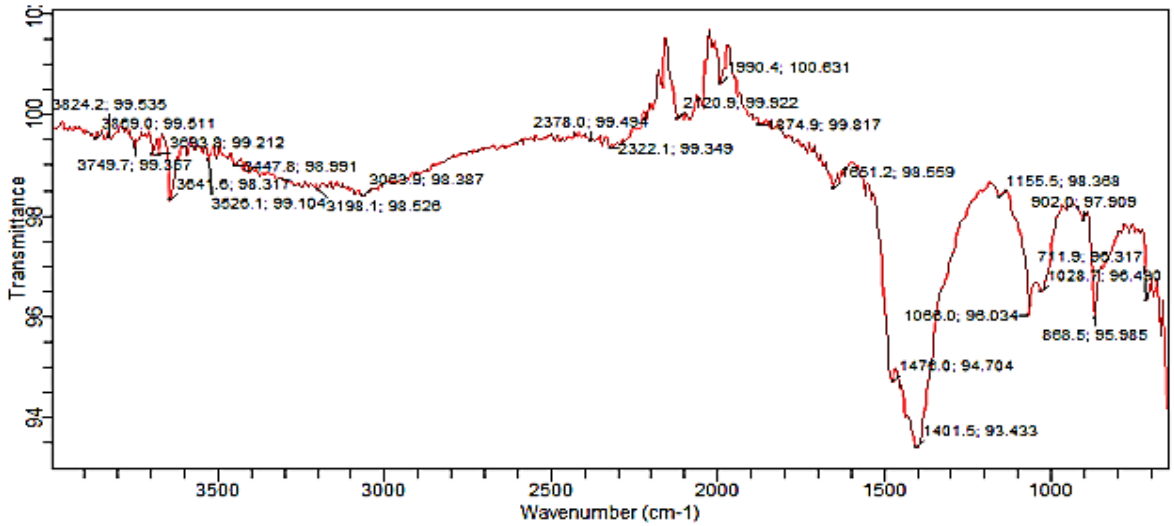

Figure 1: FTIR spectrum of the chitosan

EDAX spectrum of the chitosan presented in Figure 2 shows major peaks which correspond to calcium (Ca), strontium (Sr), nickel (Ni) and oxygen (O) elements. The presence of alkaline metals (Ca, Sr) and transition metals (Ag, Ni, Rh, Fe) is in agreement with the elemental

composition of commercial chitosan (Shavandi *et al.*, 2015). The presence of these elements within the matrix could improve the adsorptive properties of the chitosan. Rehman *et al.* (2013) reported that the transition metals within the concentration range of 0.01 - 0.31 % could enhance the adsorption of cationic dye.

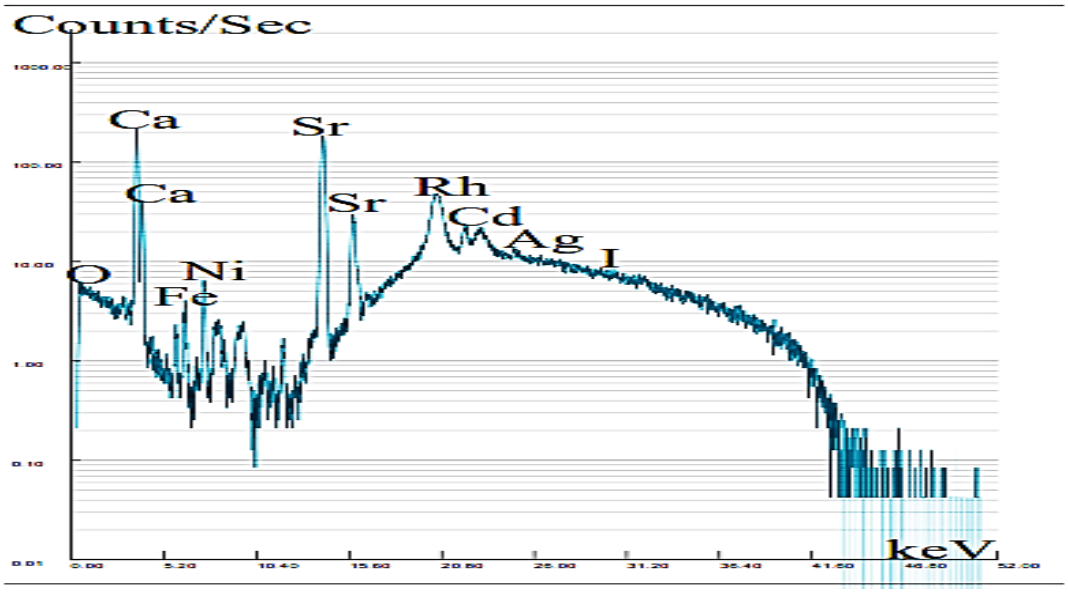

Figure 2: EDAX spectrum of the chitosan

The SEM images in Figure 3 illustrate the surface morphology of crab shell chitosan. The images show rough surface with visible pores. The flaky particles with porous, fractured and fibril structures and irregularities are promising attributes of adsorbent for adsorption.

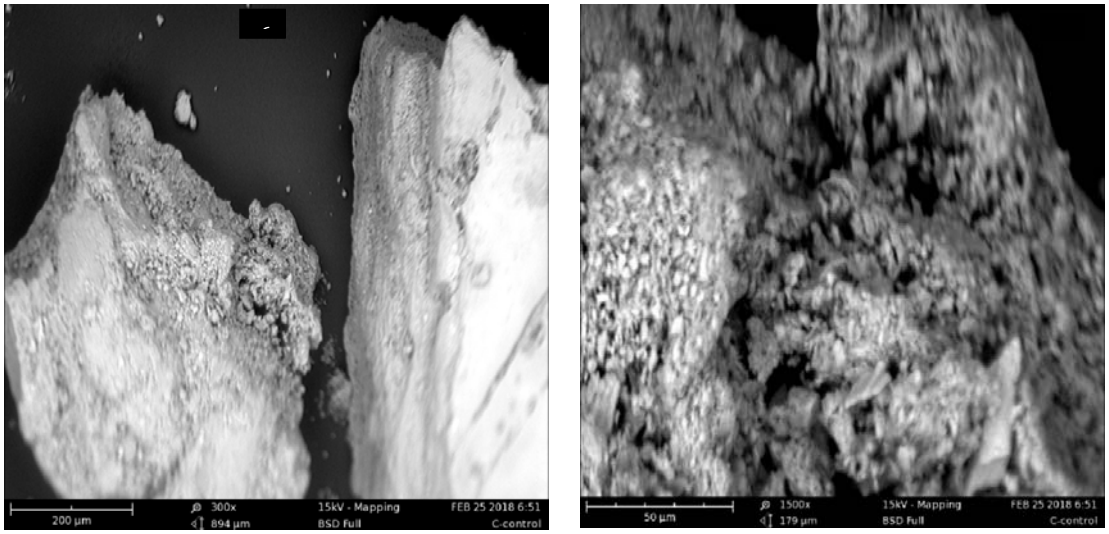

Figure 3: SEM images of the chitosan (a) 300x magnification, and (b) 1500x magnification

The textural property of CC is summarized in Table 1. The specific surface area of CC is 191 m^2/g. The material is highly mesoporous with pore width about 2.0 nm. The presence of

mesoporous texture allows easy penetration of ions and macromolecules into the pore channels (Hu *et al.,* 2003; Budsaereechai *et. al.,* 2012). In a related work, the mesoporous biopolymer sorbent exhibits a promising removal of phenol from aqueous solution (Wan *et al.*, 2010).

Table 1: Textural properties of the chitosan

Sample	BET surface area (m^2/g)	Total pore volume (cm^3/g)	Micropore volume (cm^3/g)	Average pore width (nm)	Mesoporosity (%)
CC	191	0.126	0.037	1.85	70.6

3.2 Fixed bed adsorption study

The effect of adsorbate inlet concentration at varying concentrations of 100 and 200 mg/L at constant flow rate (2.17 mL/min), temperature (30°C), pH of 6.2±0.4 and bed height (3.5 cm) is presented in sorption breakthrough curve shown in Figure 4. Phenol inlet concentration of 100 mg/L showed prolong breakthrough curve and longer breakthrough time (140 min), hence larger volume of phenol treatment (1334.55 ml); meanwhile, for phenol inlet concentration of 200 mg/L, shorter breakthrough curve and time (99 min) signifying smaller volume of phenol treatment (928.76 ml) was observed. Similar effect was observed by Nouri and Ouederni (2013). However, the values of q_{total}, M_{total}, $q_{o,eq}$, C_{eq} and percentage removal increased from 41.89 to 59.42 mg, 128.77 to 173.15 mg, 41.89 to 59.42 mg/g, 65.10 to 122.45 mg/L and 32.53 to 34.32 %, respectively, with increasing inlet concentration from 100 to 200 mg/L (Table 2).

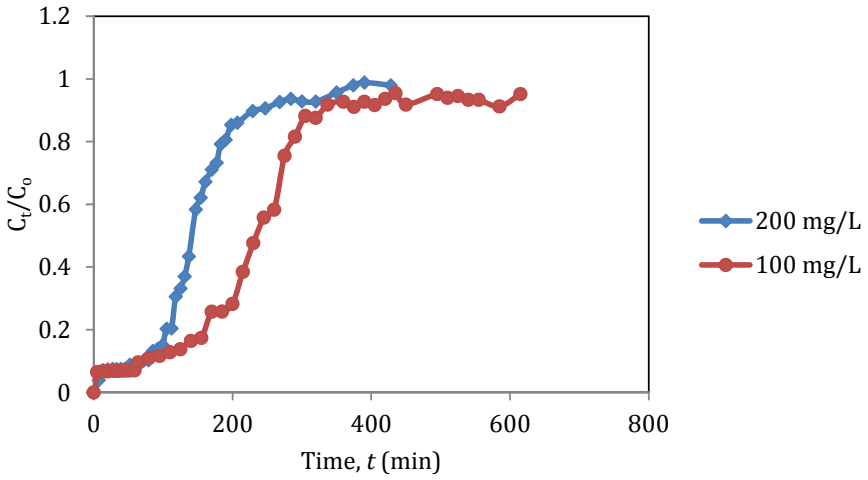

Figure 4: Experimental breakthrough curves (BTC) for adsorption of phenol onto CC at varying initial inlet concentrations

The effect of varying adsorbent bed height (1.75 cm and 3.5 cm) at constant flow rate of 2.17 mL/min, temperature of 30°C, pH of 6.2±0.4 and influent concentration of 200 mg/L is presented in sorption breakthrough curve shown in Figure 5. The results presented in Figure 5 and Table 2 suggest that there was an increase in the breakthrough time from 30 to 99 min as the bed height was increased from 1.75 to 3.5 cm. Meanwhile, the equilibrium sorption capacity ($q_{o,eq}$) decreased from 190.21 to 59.42 mg/g as the bed height increased from 1.75 to 3.50 cm. This suggests that at smaller bed height, the effluent adsorbate concentration ratio increased more rapidly and saturates in less time than at higher bed height. Similar observation was reported by Nwabanne and Igbokwe (2012).

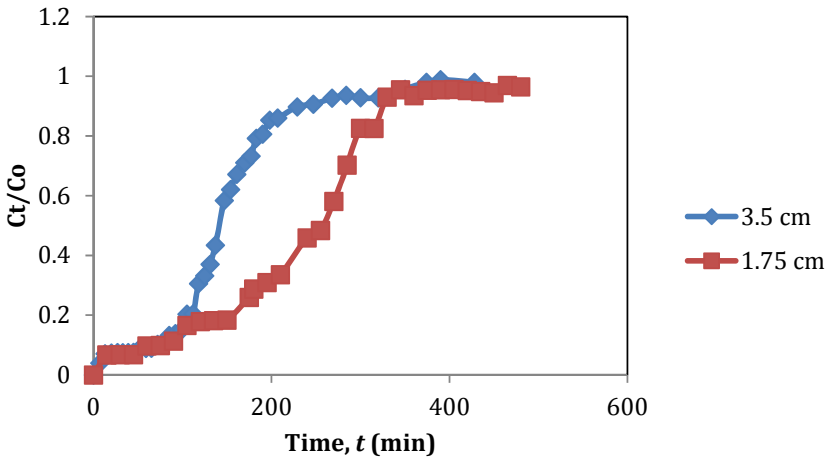

Figure 5: Experimental breakthrough curves (BTC) for adsorption of phenol onto CC at different bed height

The effect of varying adsorbate flow rate (2.17 and 2.90 mL/min) at constant bed height (3.5 cm), temperature(30°C), pH of 6.2±0.4 and influent concentration (200 mg/L) presented in sorption breakthrough curve (Figure 6) showed rapid initial adsorption for both flow rates due to possible availability of vacant active adsorption sites and ionic interactions; meanwhile, as adsorption proceeded, there was reduction in the rapidity of adsorption as a result of gradual occupancy of the vacant active sites (Afroze *et al.*, 2016). However, the best adsorption capacity of phenol onto CC of 148.85 mg/g was found at the higher flow rate of 2.90 mL/min (Table 2). This may be attributed to higher mass transfer of the adsorbate and protonation of more amine group in the adsorbent (Auta and Hameed, 2012).

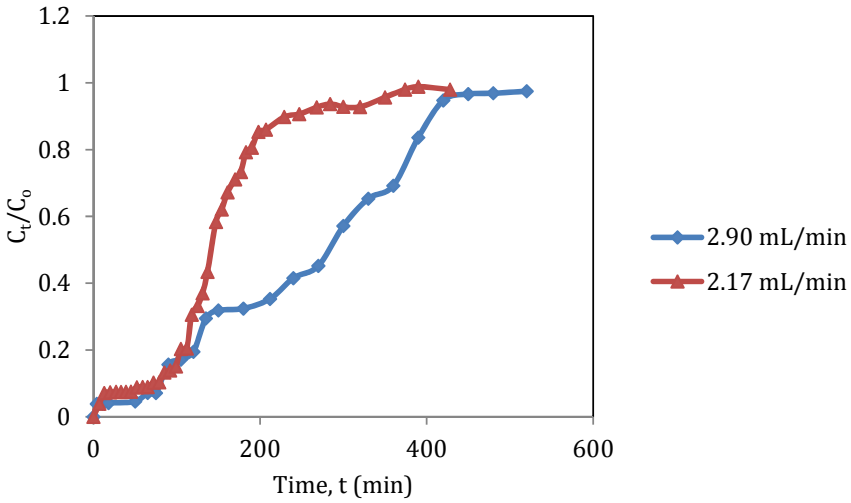

Figure 6: Experimental breakthrough curves (BTC) for adsorption of phenol onto CC at different flow rate

The mathematical description of the column adsorption parameters of phenol onto CC from the plots in Figures 4 - 6 are presented in Table 2.

Table 2: Mathematical description of column parameters for the adsorption of phenol at different operating conditions

Adsorbate	Adsorbent	Bed Height (cm)	C_o (mg/L)	Q (mL/min)	q_{total} (mg)	M_{total} (mg)	V_{eff} (ml)	Total removal (%)	$q_{o,eq}$ (mg/g)	C_{eq} (mg/L)
Phenol	CC	1.75	200	2.17	95.10	199.79	1041.60	47.60	190.21	100.51
		3.50	200	2.90	148.85	295.25	1508.00	50.42	148.85	97.08
		3.50	200	2.17	59.42	173.15	928.76	34.32	59.42	122.45
		3.50	100	2.17	41.89	128.77	1334.55	32.53	41.89	65.10

Fixed bed adsorption modeling

Thomas, Yoon-Nelson and Adams-Bohart kinerics models have described the fixed bed column behavior. These models were adopted to fit experimental data and analysed the sorption performance of phenol. The linearized form of Thomas, Yoon-Nelson and Adams-Bohart kinetics models are given in equations 7, 8 and 9, respectively (Chowdhury *et al.*, 2016).

$$\ln\left[\left(\frac{C_o}{C_t}\right) - 1\right] = \left(\frac{K_{Th}q_o m}{Q}\right) - \left(\frac{K_{Th}q_o V_{eff}}{Q}\right) \quad (7)$$

$$\ln\left[\frac{C_t}{C_o - C_t}\right] = K_{YN}t - \tau K_{YN} \quad (8)$$

$$\ln\left(\frac{C_t}{C_o}\right) = k_{AB}C_o t - k_{AB}N_o\frac{Z}{F} \quad (9)$$

where, K_{Th} is Thomas rate constant (mL/min. mg), q_o is equilibrium adsorbate (mg/g), m is the amount of adsorbent packed in the column (g), K_{YN} is Yoon-Nelson rate constant (min^{-1}), τ is the time required for 50% adsorbate breakthrough (min), k_{AB} is Adams-Bohart rate constant (L/mg.min), F is the linear velocity calculated by dividing the flow rate by the column section area (cm/min), Z is column bed depth (cm), N_o is the maximum adsorption capacity (mg/L), C_o is inlet concentration and C_t is adsorption concentration at time, t. Thomas model adsorption rate constant, K_{TH} (mL/min.mg) and maximum solid phase concentration, q_o (mg/g) were calculated from the slope and intercept of linear plot $\ln[(C_o/C_t)-1]$ against t (= V_{eff}/Q) according to equation 7 at different flow rates (2.17 and 2.90 mL/min), inlet concentrations (100 and 200 mg/L) and bed heights (1.75 and 3.5 cm). Similarly, Yoon-Nelson model adsorption rate constant, K_{YN} (min^{-1}) and time required for 50% sorbate breakthrough, τ (min) were determined from the slope and intercept of the plot of $\ln[C_t/(C_o - C_t)]$ against t according to equation 8, and Adams-Bohart model adsorption rate constant, K_{AB} (L/mg.min) and saturation concentration, N_o (mg/L) were determined from the slope and intercept of the plot of $\ln[C_t/C_o]$ against t according to equation 9.

Breakthrough curves predicted by Thomas, Yoon-Nelson and Adams-Bohart models at different experimental conditions are shown in Figures 7- 9 and their calculated parameters presented in Table 3.

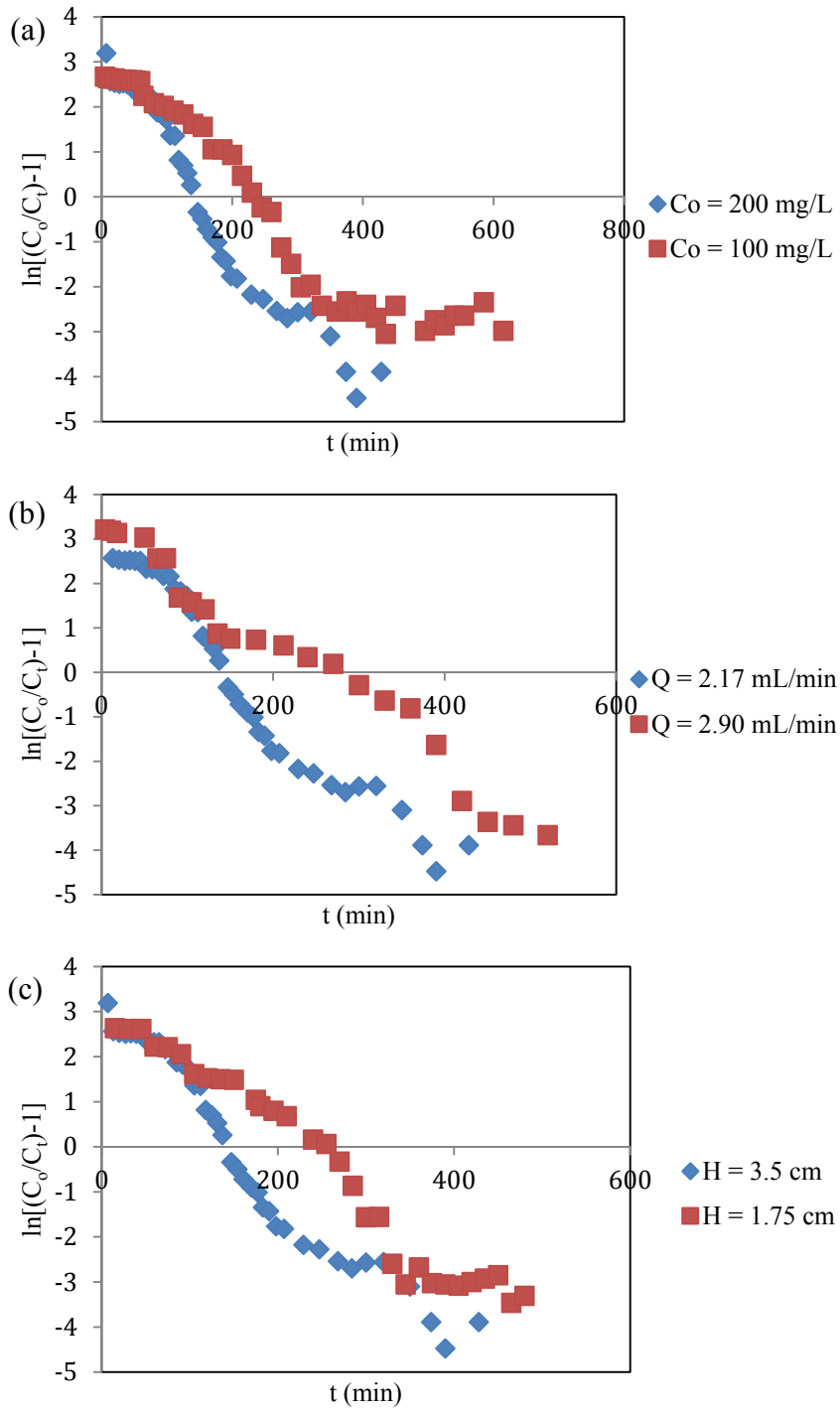

Figure 7: Thomas kinetics plots for the adsorption of phenol onto CC, (a) effect of influent concentrations (flow rate = 2.17 mL/min; bed height = 3.5 cm), (b) effect of flow rates (influent concentration = 200 mg/L; bed height = 3.5 cm) and (c) effect of bed heights (influent concentration = 200 mg/L; flow rate = 2.17 mL/min)

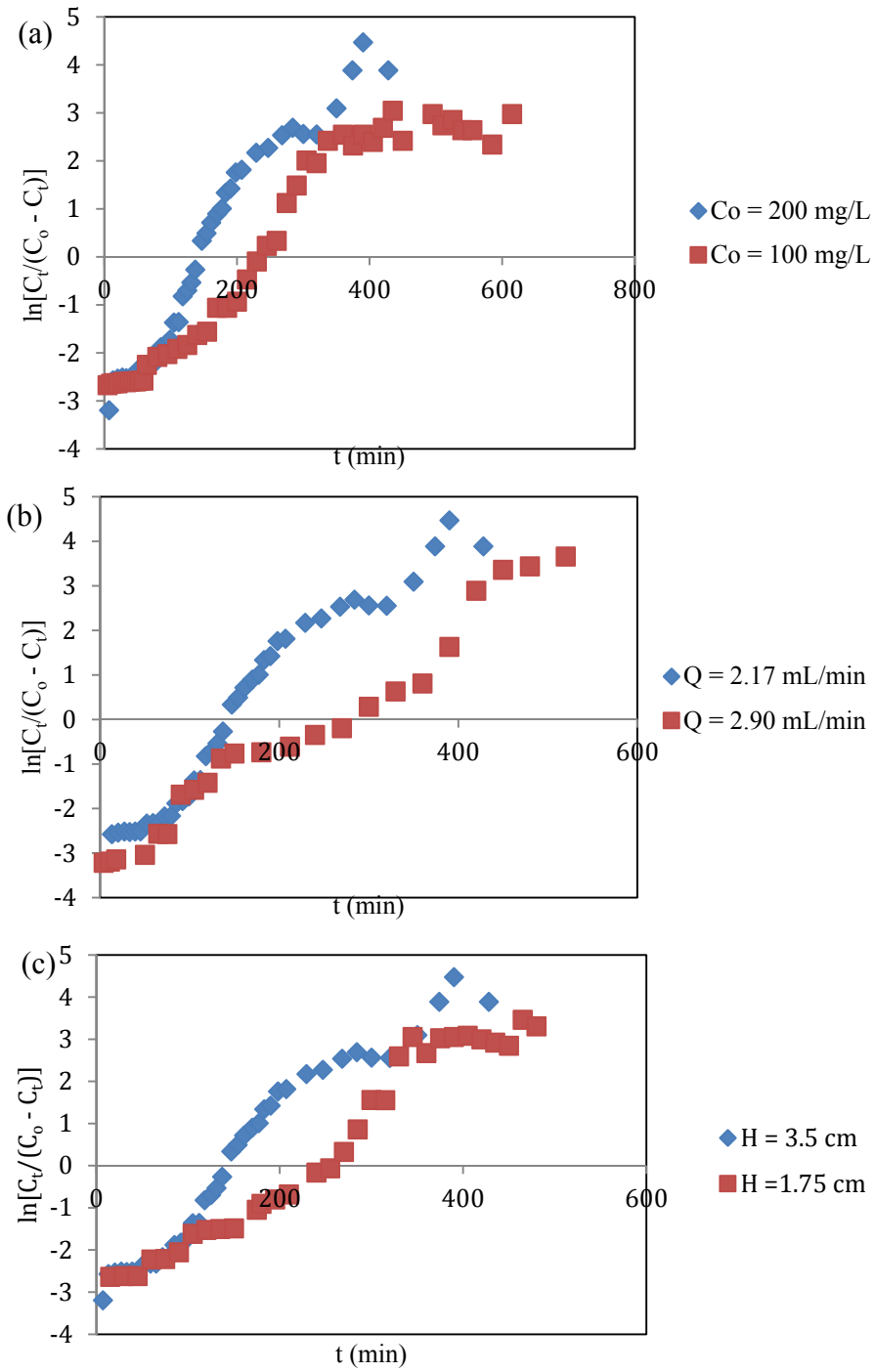

Figure 8: Yoon-Nelson kinetics plots for the adsorption of phenol onto CC, (a) effect of influent concentrations (flow rate = 2.17 mL/min; bed height = 3.5 cm), (b) effect of flow rates (influent concentration = 200 mg/L; bed height = 3.5 cm) and (c) effect of bed heights (influent concentration = 200 mg/L; flow rate = 2.17 mL/min)

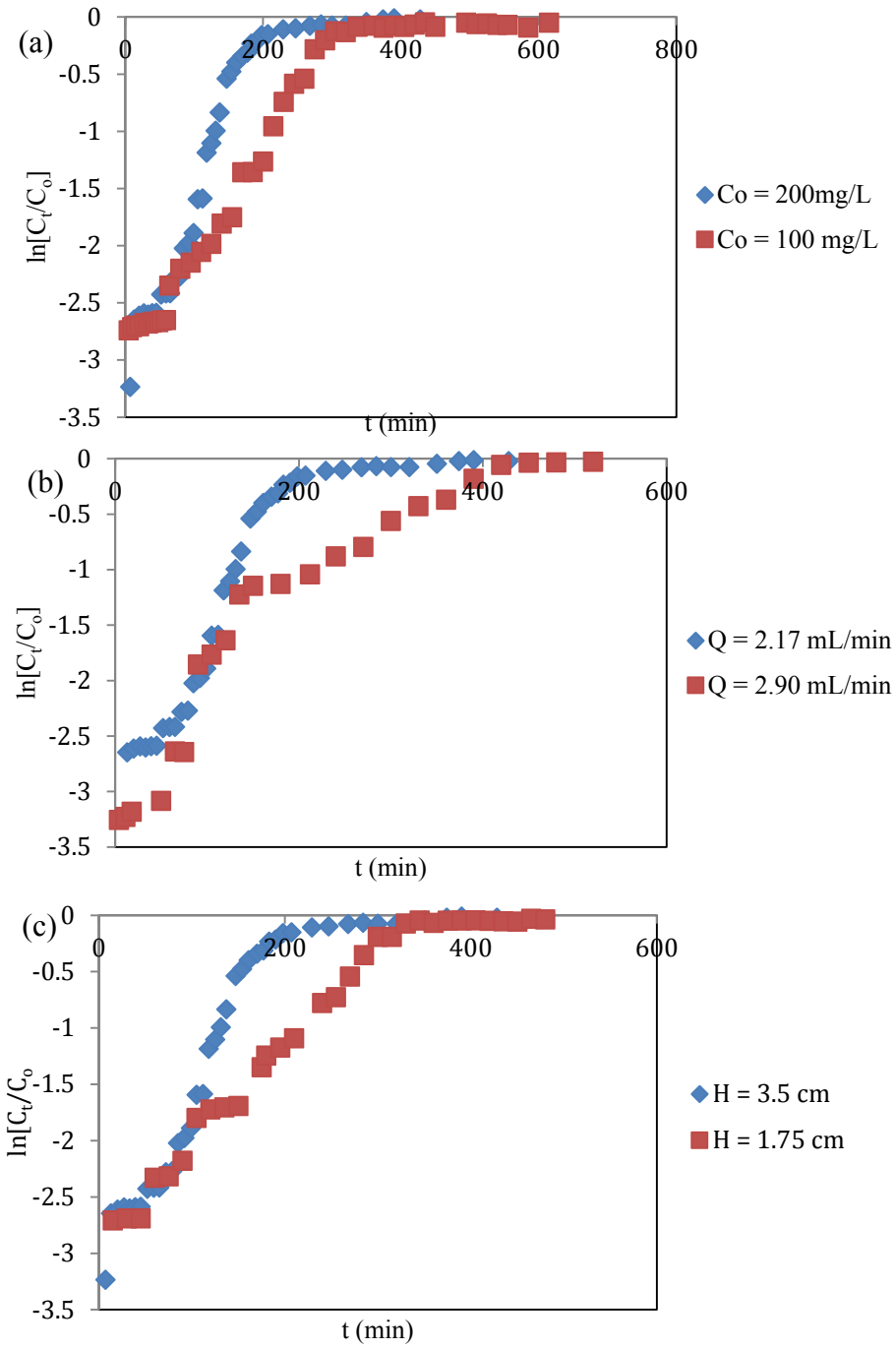

Figure 9: Adams-Bohart kinetics plots for the adsorption of phenol onto CC, (a) effect of influent concentrations (flow rate = 2.17 mL/min; bed height = 3.5 cm), (b) effect of flow rates (influent concentration = 200 mg/L; bed height = 3.5 cm) and (c) effect of bed heights (influent concentration = 200 mg/L; flow rate = 2.17 mL/min)

Table 3: Model parameters for continuous adsorption of phenol at different initial concentrations, flow rates and bed height

				Thomas model			Yoon-Nelson model			Adams-Bohart model		
Adsorbate	Initial conc. (mg/L)	Flow rate (mL/min)	Bed height (cm)	K_{TH} (mL/min.mg)	q_o (mg/g)	R^2	K_{YN} (min^{-1})	τ (min)	R^2	K_{AB} (L/mg.min)	N_o (mg/L)	R^2
Phenol	200	2.17	3.5	1.05×10^{-4}	2.94×10^{4}	0.942	0.020	158	0.942	4.51×10^{-5}	552	0.767
	200	2.90	3.5	6.84×10^{-5}	4.82×10^{4}	0.968	0.013	246	0.968	3.37×10^{-5}	1093	0.866
	200	2.17	1.75	7.92×10^{-5}	8.44×10^{4}	0.956	0.015	220	0.956	3.39×10^{-5}	1511	0.920
	100	2.17	3.5	1.2×10^{-4}	2.35×10^{4}	0.916	0.012	244	0.916	5.7×10^{-5}	445	0.855

Thomas model (Table 3) shows that for phenol adsorption breakthrough analysis, increasing flow rate from 2.17 to 2.9 mL/min at constant inlet concentration (200 mg/L) and bed height (3.5 cm), led to a decrease in K_{Th} value from 1.05×10^{-4} to 6.84×10^{-4} mL/min.mg and increased q_o value from 2.94×10^{4} to 4.82×10^{4} mg/g. Similarly, increasing inlet concentration from 100 to 200 mg/L at constant flow rate (2.17 mL/min) and bed height (3.5 cm) resulted in decreased K_{Th} value from 1.2×10^{-4} to 1.05×10^{-4} mL/min.mg and increased q_o value from 2.35×10^{4} to 2.94×10^{4} mg/g. Furthermore, increasing bed height from 1.75 to 3.5 cm at constant inlet concentration (200 mg/L) and flow rate (2.17 mL/min) resulted in increased K_{Th} value from 7.92×10^{-5} to 1.05×10^{-4} mL/min.mg and decreased q_o value from 8.44×10^{4} to 2.94×10^{4} mg/g. Meanwhile, the q_o values estimated from experimental data (Table 2) are smaller than those calculated using Thomas model (Table 3). This could be attributed to lower diffusion of solute (Chowdhury *et al.*, 2015).Similar results were reported by Biswas and Mishra (2015). The correlation coefficient (R^2) values ranges between 0.916 - 0.968. This is a good correlation of Thomas model with experimental data and shows that Thomas model best described the breakthrough behavior of phenol adsorption process in which external and internal diffusion constraints were absent (Biswas and Mishra, 2015). Yoon-Nelson model however suggested that increased inlet concentration and bed height resulted in increased K_{YN} values and decreased τ values, while increased flow rate resulted in decreased K_{YN} values and increased τ values. The correlation coefficient (R^2) values ranges between 0.916 – 0.968. This also shows good correlation of Yoon-Nelson model with experimental data and best described the breakthrough behavior of phenol. Adams-Bohart model shows that the values of K_{AB} decreased while N_o increased with increased flow rate and inlet concentration. Meanwhile, increased bed height resulted in increased K_{AB} and decreased N_o values. This shows that the entire system kinetics was a simultaneous steady state process of intraparticle diffusion and chemical reaction. Klaewkla *et al*. (2011), Biswas and Mishra (2015) and Jock *et al*. (2017) reported similar behavior. The poor R^2 values of Adams-Bohart model show its lesser suitability to describe the breakthrough data.

Table 4 shows comparison in fixed bed column adsorption of phenol onto CC to other adsorbents from selected literatures at varying inlet concentrations, flow rates and bed heights. The column capacity of CC is relatively lower than all adsorbents column from literatures. However, it possesses higher adsorption capacity at optimum conditions. Therefore, the ease and availability of raw materials for the synthesis of CC and its adsorption potential in this present study has made it promising alternative low-cost adsorbent for phenol removal from wastewater.

Table 4: Comparison in fixed bed column adsorption of phenol onto CC to other adsorbents

Adsorbent	C_o (mg/L)	Bed height (cm)	Bed weight (g)	Flow rate (mL/min)	Adsorption capacity, q_o (mg/g)	References
Corn cobs treated activated carbon	200	5	-	18	86.9	Rocha *et al*. (2015)
	300	5	-	18	72.0	
	400	5	-	18	55.8	
	500	5	-	18	46.9	
	500	5	-	18.3	104.5	
	500	5	-	25.6	54.9	
	500	5	-	33.0	57.1	
Sugarcane bagasse activated carbon	20	-	5 g	33.3	12.02	Karunarathne and Amarasinghe (2013)
	20	-	10 g	33.3	12.34	
Modified coal fly ash (MCFA)	1039.9	7.5	-	1.0	69.88	Talib *et al*. (2018)
	1039.9	13.5	-	1.0	84.64	
	1039.9	27.5	-	1.0	111.0	
	1039.9	13.5	-	0.375	39.38	
	1039.9	13.5	-	0.75	34.31	
	1039.9	13.5	-	1.0	21.84	
	70	13.5	-	1.0	6.930	
	292.7	13.5	-	1.0	26.81	
	651.2	13.5	-	1.0	58.60	
	1039.9	13.5	-	1.0	77.68	
Garlic peel powder	50	15	-	15	21.36	Muthamilselvi *et al*. (2018)
	50	15	-	20	17.66	
	50	15	-	25	17.29	
	50	15	-	15	21.35	
	100	15	-	15	31.08	
	150	15	-	15	34.69	
	50	5	-	15	17.60	
	50	10	-	15	16.40	
	50	15	-	15	21.95	
CC	200	1.75	-	2.17	190.21	Present study
	200	3.50	-	2.90	148.85	
	200	3.50	-	2.17	59.42	
	100	3.50	-	2.17	41.89	

4.0 Conclusion

Chitosan prepared from Pessu river crab shell was successfully used as potential promising alternative and environmentally friendly low-cost adsorbent for the removal of phenol in fixed bed

mode. The surface chemistry of the coarse chitosan showed the presence of N—H and hydrogen bonded O—H groups, with specific surface area of 191 m^2/g. Results revealed that adsorption capacity was considerably affected by inlet concentrations, bed heights and flow rates. Maximum adsorption capacity was 190.21 mg/g. Breakthrough behavior kinetics models revealed external and internal diffusion, and simultaneous steady state process of intraparticle diffusion and chemical reaction as the rate controlling mechanisms. The experimental data obtained in this adsorption study using a fixed bed column would be beneficial for the commercialization of the process.

Acknowledgement

This work was supported by Tertiary Education Trust Fund (TETFund) of Nigeria through Academic Staff Training and Development (ASTandD) grant, and Ministry of Education Malaysia and Universiti Teknologi Malaysia through Fundamental Research Grant Scheme (FRGS) No. 4F995

References

Afroze, S., Sen, T. K., and Ang, H. M. (2016). Adsorption performance of continuous fixed bed column for the removal of methylene blue (MB) dye using Eucalyptus sheathiana bark biomass. *Research on Chemical Intermediates*, 42(3), 2343-2364.

Al Sagheer, F.A., Al Sughayer, M.A., Muslim, S. and Elsabee, M.Z. (2009). Extraction and characterization of chitin and chitosan from marine sources in Arabian Gulf. *Journal of Carbohydrate Polymer*, 77.

Annaduzzaman, M. (2015). Chitosan biopolymer as an adsorbent for drinking water treatment-investigation on arsenic and uranium. TRITA-LWR LIC., Pp.2-26.

Anisuzzaman, S.M., Bono, A., Krishnaiah, D. and Tan, Y.Z. (2016). A study on dynamic simulation of phenol adsorption in activated carbon packed bed column. *Journal of King Saud University-Engineering Sciences,* 28, 47–55

Anku, W. W., M. A. Mamo, and P. P. Govender, (2017). Phenolic Compounds in water: Sources, reactivity, toxicity and treatment methods. *INTECH,* 17, 419-443.

Apurva A.N., Fernandes, J.B. and Tilve, S.G. (2018). Adsorption behavior of methylene blue on glycerol based carbon materials. *Journal of Environmental Chemical Engineering*, 6 (2), 1714-1725.

Arbia, W., Arbia, L., Adour, L. and Amrane, A. (2013). Chitin extraction from crustacean shells using biological methods-a review. *Food Technology and Biotechnology Journal,* 51(1), 12-25.

Aslam, S., Zeng, J., Subhan, F. *et al.* (2017). In-situ one-step synthesis of Fe_3O_4@MIL-100(Fe) core-shells for adsorption of methylene blue from water. *Journal of Colloid and Interface Science,* 505, 186–195.

Auta, M. and Hameed, B.H. (2012). Coalesced chitosan activated carbon composite for batch and fixed-bed adsorption of cationic and anionic dyes. Colloids and Surfaces B: Biointerfaces, 105, 199-206

Aysan, H., Edebali, S., Ozdemir, C., Karakaya, M. C. and Karakaya, N. (2016). Use of chabazite, a naturally abundant zeolite, for the investigation of the adsorption kinetics and mechanism of methylene blue dye. *Microporous and Mesoporous Material,* 235, 78–86

Benavente, M. (2008). Adsorption of metallic ions onto chitosan: equilibrium and kinetic studies. *TRITA Chemical Engineering Report,* 44**.**

Biswas, S. and Mishra, U. (2015). Continuous fixed-bed column study and adsorption modeling: removal of lead ion from aqueous solution by charcoal originated from chemical

carbonization of rubber wood sawdust. *Journal of Chemistry*, art. 907379, 9 pp. doi:10.1155/2015/907379.

Budsaereechai, S., Kamwialisak, K. and Ngernyen. Y. (2012). Adsorption of lead, cadmium and copper on natural and acid activated bentonite clay. *KKU Research Journal*, 17(5), 800–810.

Chang, Z., Jiena, Y., Qian, W. *et al*. (2018). Adsorption of ion pairs onto graphene flakes and impacts of counterions during the adsorption processes. *Journal of Applied Surface Science*, 435, 329-337.

Chowdhury, S., Yasin, M., Uddin, M.T. and Islam, M.A. (2016). Batch and continuous (fixed bed column) adsorption of methylene blue by rubber leaf powder. *International Journal of Integrated Sciences and Technology,* 2, 24-28.

Chowdhury, Z. Z., Hamid, S. B. and Zain, S. M. (2015). Evaluating design parameters for breakthrough curve and kinetics of fixed-bed columns for Cu(II) cations using lignocellulosic wastes. *BioResources,* 10(1), 732–749.

Gavrilescu, M. (2004). Removal of heavy metals from the environment by biosorption. *Engineering and Life Science Journal,* 4(3), 219–232.

Ghannam H.E., Talab, A.S., Dolganova, N.V., Hussein, A.M.S. and Abdelmaguid, N.M. (2016). Characterization of chitosan extracted from different crustacean shell wastes. *Journal of Applied Sciences,* 16(10), 454-461.

Gholizadeh, A., Kermani, M., Gholami, M. and Farzadkia, M. (2013). Kinetic and isotherm studies of adsorption and biosorption processes in the removal of phenolic compounds from aqueous solutions: comparative study. *Journal of Environmental Health Science Engineering,* 11, 29

Hajji, S., Ghorbel-Bellaaj, O., Younes, I., Jellouli, K. and Nasri, M. (2015). Chitin extraction from crab shells by bacillus bacteria: Biological activities of fermented crab supernatants. *International Journal of Biological Macromelecules*. 79, 167-173.

Hameed, B.H. and Rahman, A.A. (2008). Removal of phenol from aqueous solutions by adsorption onto activated carbon prepared from biomass material. *Journal of Hazardous Materials,* 160, 576–581.

Hossain, M. S. and Iqbal, A. (2014). Production and characterization of chitosan from shrimp waste. *Journal of Bangladesh Agricultural University*, 12(1), 153-160

Hu, Z., Guo, H., Srinivasan, M.P. and Yaming, N.A., (2003). A simple method for developing mesoporosity in activated carbon. *Separation Purification Technology,* 31, 47-52.

Ihsan, H.D. (2013). Removal of phenol from industrial wastewater using sawdust. *International Journal of Engineering and Science,* 3(1), 25-31

Jia, Q. and Lua, A.C. (2008). Effects of pyrolysis conditions on the physical characteristics of oil-palm-shell activated carbons used in aqueous phase phenol adsorption. *Journal of Analytical Applied Pyrolysis,* 83, 175–179.

Jock, A. A., Zaini, M. A. A., Surajudeen, A., El-Nafaty, U. A. and Aroke, U. O. (2017). Multi-metals column adsorption of lead(II), cadmium(II) and manganese(II) onto natural bentonite clay. Water Science and Technology, 76(8), 2232-2241.

Karunarathne, H. D. S. S., and Amarasinghe, B. M. W. P. K. (2013). Fixed bed adsorption column studies for the removal of aqueous phenol from activated carbon prepared from sugarcane bagasse. *Energy Procedia*, 34, 83-90.

Klaewkla, R., Arend, M. and Hoelderich, W. F. (2011). A review of mass transfer controlling the reaction rate in heterogeneous catalytic systems. In: *Mass Transfer-Advanced Aspects* (H. Nakajima, ed.). InTech Open, Shanghai, pp. 667–684.

Kumari, R., Sharma, R. K. and Singh, A. P. (2017). Cellulose based grafted biosorbents- Journey from lignocellulose biomass to toxic metal ions sorption applications - A review. *Journal of Molecular Liquids*, 232, 62-93

Lakshmi, S., Harshitha, M., Vaishali, G. Keerthana, S.R. and Muthappa, R. (2016). Studies on different methods for removal of phenol in wastewater – Review. *International Journal of Science, Engineering and Technology Research,* 5(7), 2488–2496.

Lee, D.W., Lim, C. Israelachvili, J.N. and Hwang, D.S. (2013). Strong adhesion and cohesion of chitosan in aqueous solutions. *Langmuir Journal,* 29(46), 14222-14229.

Long-Fei R., Rui, C., Xiaofan, Z. *et al*., (2017). Phenol biodegradation and microbial community dynamics in extractive membrane bioreactor (EMBR) for phenol-laden saline wastewater. *Journal of Bioresource Technology*, 244, 1121-1128

Luo, X.P., Fu, S.Y., Du, Y.M., Guo, J.Z. and Li, B. (2017). Adsorption of methylene blue and malachite green from aqueous solution by sulfonic acid group modified MIL-101. *Microporous and Mesoporous Materials*, 237, 268-274.

Mehdi, M., Mohammad, A.A., Peyman, Salehi,*et al*. (2018). Immobilization of laccase on epoxy-functionalized silica and its application in biodegradation of phenolic compounds. *International Journal of Biological Macromolecules,* 109, 443-447.

Mellah, A., Chegrouche, S. and Barka, M. (2005). The removal of uranium(VI) from aqueous solutions onto activated cabon: Kinetic and thermodynamic investigations. *Jounal of Colloid and Interface Science,* 296, 434-441.

Moosa, A.A., Ridha, A.M., and Kadim, N.A. (2016). Use of biopolymer adsorbent in the removal of phenol from aqueous solution. *American Journal of Materials Science*, 6(4), 95-104.

Muthamilselvi, P., Karthikeyan, R., Ashish, K. and Prabhakar, S. (2018). Continuous fixed bed studies for adsorptive remediation of phenol by garlic peel powder. *International Journal of Industrial Chemistry,* 9, 379-390

Najafpoor, A.A., Dousti, S., Jafari, A.J. and Hosseinzadeh, A. (2016). Efficiency in phenol removal from aqueous solutions of pomegranate peel ash as a natural adsorbent. *Environmental Health Engineering and Management,* 3(1), 41–46.

Nouri, H. and Ouederni, A. (2013). Modeling of the dynamics adsorption of phenol from an aqueous solution on activated carbon produced from olive stones", *International Journal of Chemical Engineering and Applications*, 4(4), 254-261.

Nwabanne, J.T. and Igbokwe, P.K. (2012). Adsorption performance of packed bed column for the removal of lead (II) using oil palm fibre. *International Journal of Applied Science and Technology,* 2(5), 106 -115

Pathania, D., Sharma, S. and Singh, P. (2017). Removal of methylene blue by adsorption onto activated carbon developed from Ficus carica bast. *Arabian Journal of Chemistry*, 10, 1445-1451

Pestov, A., and Bratskaya, S. (2016). Chitosan and its derivatives as highly efficient polymer ligands. *Molecules,* 21

Rahdar, S., Ahamadabadi, M., Khaksefidi, R., Saeidi, M., Narooie, M.R., Salimi, A., Biglari, H. and Baneshi, M.M. (2017). Evaluation of phenol removal from aqueous solution by banana Leaf ash. *Journal of Global Pharma Technology,* 3(9), 20-28.

Rajasulochana, P. and Preethy, V. (2016). Comparison on efficiency of various techniques in treatment of waste and sewage water- A comprehensive review. *Resource Efficient Technologies,* 2, 175-184

Ramasamy, P. and Shangmugam, A. (2015). Characterization and wound healing property of collagen-chitosan film from sepia kobiensis. *International Journal of Biological Macromolecules*, 74, 93-102.

Rehman, M. S. U., Munir, M., Ashfaq, M., Rashid, N., Nazar, M. F., Danish, M. and Han, J. I. (2013). Adsorption of brilliant green dye from aqueous solution onto red clay. *Chemical Engineering Journal*, 228, 54-62.

Rocha, P. D., Franca, A. S., and Oliveira, L. S. (2015). Batch and column studies of phenol adsorption by an activated carbon based on acid treatment of corn cobs. *International Journal of Engineering and Technology*, 7(6), 459.

Saravanakumar, K., and Kumar, A. (2013). Removal of phenol from aqueous solution by adsorption using zeolite. *African Journal of Agricultural Research,* 8(23), 2965–2969.

Sarker, N. and Fakhruddin, A.N.M. (2017). Removal of phenol from aqueous solution using rice straw as adsorbent. *Applied Water Science,* 7, 1459–1465.

Shany, B.M. and Giora, R. (2018). Thiamine-based organo-clay for phenol removal from water. *Journal of Applied Clay Science,* 155, 50-56

Shavandi, Amin, Adnan, A. Bekhit, Alaa El-Din, A. Bekhit, Zhifa, Sun and Ali, M. Azam, (2015). "Preparation and Characterisation of Irradiated Crab Chitosan and New Zealand Arrow Squid Pen Chitosan." *Materials Chemistry and Physics,* 1-8.

Shukla, S.K., Mishra, A.K., Arotiba, O.A., and Mamba, B.B. (2013). Chitosan-based nanomaterials: A state of the art review. *International Journal of Biological Macromolecules,* 59, 46-58

Tabari, T., Tavakkoli, H., Zargaran, P. and Beiknejad, D. (2012). Fabrication of Perovskite type oxide $BaPbO_3$ nanoparticles and their efficiency in photodegradation of methylene blue. *South African Journal of Chemistry,* 65, 239-244

Tahir, N., Bhatti, H. N., Iqbal, M. and Noreen, S. (2017). Biopolymers composites with peanut hull waste biomass and application for Crystal Violet adsorption. *International Journal of Biological Macromolecules*. 94, 210-220

Talib, M.I., Chauhan, Y.P. and Parate, V.R. (2018). Packed bed adsorption study on phenol removal and its modeling. Conference paper presented in January, 2018 and retrieved from *https*://www.researchgate.net/publication/322757361 on 14/07/2019

Toan, N.V. (2009). Production of Chitin and Chitosan from Partially Autolyzed Shrimp Shell Materials. *Journal of Open Biomaterials,* 1, 21-24.

Tondwal, R., and Singh, M. (2018). Chitosan functionalization with a series of sulfur-containing α-amino acids for the development of drug-binding abilities. *Journal of Applied Polymer Science*, 135(12), 46000.

Trung, T. Si., Thein-Han, W. W., Nguyen Thi Qui, Chuen-How Ng and Willem F. Stevens (2006). Functional characteristics of shrimp chitosan and its membranes as affected by the degree of deacetylation. *Journal of Bioresource Technology*, 97, 659-663.

Wan, Chi-Chu M. W.. Kan, B.D. Rogel and M.L.P. Dalida, (2010). Adsorption of copper (II) and lead (II) ions from aqueous solution on chitosan-coated sand. *Journal of Carbohydrate Polymers*, 80, 891–899

Wang, F., Zhang, L., Wang, Y., Liu, X., Rohani, S., and Lu, J. (2017). Fe_3O_4@SiO_2@CS-TETA functionalized graphene oxide for the adsorption of methylene blue (MB) and Cu(II). *Applied Surface Science*. 420, 970-981.

Wenjue, Z., Donghong, W. and Zijian, W. (2018). Distribution and potential ecological risk of 50 phenolic compounds in three rivers in Tianjin, China. *Journal of Environmental Pollution,* 235, 121-128

Yagub, M., Sen, T., Afroze, S. and Ang, H. (2014). Dye and its removal from aqueous solution by adsorption: A review. *Advances in Colloid and Interface Science Journal*, 1(13).

Yazdanbakhsh, M., Tavakkoli, H. and Hosseini, S.M. (2011). Characterization and evaluation catalytic efficiency of $La_{0.5}Ca_{0.5}NiO_3$ nanopowders in removal of reactive blue 5 from aqueous solution. *Desalination,* 281, 388-395

Younes, I., Hajji, S., Frachet, V., Rinaudo, M., Jellouli, K. and Nasri, M. (2014). Chitin extraction from shrimp shell using enzymatic treatment. Antitumor, antioxidant and antimicrobial activities of chitosan, *International Journal of Biological Macromolecles*, 69(0).

Zdarta, J., Klapiszewski, L., Wysokowski, M., Norman, M., Kolodziejczak-Radzimska, A., Moszynski, H., Ehrlich, H., Maciejewski, A., Sterling, D. and Jesionowski, T. (2015). Chitin-lignin material as a novel matrix for enzyme immobilization. *Marine Drugs*, 13(4), 2424-2446.

Zhu, W., Yao, W., Zhan, Y. and Gu, Y. (2015). Phenol removal from aqueous solution by adsorption onto solidified landfilled sewage sludge and its modified sludges. *Journal of Material Cycles and Waste Management,* 17: 798–807.

Proceedings of the 49th NSChE Annual Conference
KADA 2019: pp 538-551

P3A-04: ADSORPTION OF HEAVY METALS CONTAMINANTS IN USED LUBRICATING OIL USING PALM KERNEL AND COCONUT SHELLS ACTIVATED CARBONS.

[1,2,3]Boadu K.O[1] Joel, O.F[2], Essumang D.K[3] and Evbuomwan B.O[4]

[1] World Bank Africa Centre of Excellence, Centre for Oil Fields Chemicals, Institute of Petroleum Studies, University of Port Harcourt, Nigeria

[2]Department of Chemistry, University of Cape Coast, Cape Coast, Ghana

[3]Department of Chemical Engineering, University of Port Harcourt, Port Harcourt, Nigeria

(koboadu@ucc.edu.gh, boadu.kwasi@aceuniport.org)

ABSTRACT

This research work investigated the adsorption of some heavy metals contaminants in used lubricating oil using chemically activated carbon produced from palm kernel and coconut shells. The adsorption mechanism was able to remove heavy metals such as zinc, chromium, cadmium and magnesium contaminants from the used lubricating oil to appreciable levels. For instance, zinc from initial concentrations of 16.475±0.950 ppm before to 10.375±0.171 ppm after treatment processes for used lubricating oil sample A. Also, for coconut shell from an initial concentration of 14.575±0.272 ppm to 5.450±0.3000 ppm after treatment processes. It was found out that the coconut shell activated carbon was effective in the removal of lead metal while palm kernel cannot. However, the activated carbons produced from palm kernel and coconut shells were not able to remove both copper and iron metals. For example, after the treatment process with the palm kernel shell activated carbon, the mean concentration of copper metal increases for virgin (C) 0.001± 0.000 to 0.075±0.013 ppm and used lubricating oil samples (AandB) from 0.150±0.008 to 0.400±0.018 ppm and from0.220±0.096 to 0.230±0.008 ppm respectively. In the case of coconut shell activated carbon, the mean concentration of copper in virgin lubricating oil remains the same 0.001±0.000 whereas for used lubricating oils samples (i.e. AandB) it increases from 0.150±0.008 to 0.780±0.014 and from 0.220±0.096 to 0.790±0.026 respectively. The equilibrium adsorption data were analysed using the Langmuir isotherm model. The fit of this isotherm model to the adsorption data was determined, using the linear coefficient of correlation (R^2). The following R^2 values were obtained; Copper (0.8185), Cadmium (0.8347), Lead (0.9349), Chromium (0.9378), Iron (0.9927), Zinc (0.9953), and Magnesium (0.9997) respectively. From the results obtained and statistics point of view, it can be concluded that the Langmuir model fit well due to the high coefficient of correlation ($R^2 \approx 1$). The recovered oil could be re-used.

Keywords: *Activated Carbons, heavy metals, contaminants, used lubricating oils, adsorption, Langmuir isotherm model, Correlation co-efficient.*

Introduction

Intensive research works have proven that activated carbons are most effective, efficient, reliable and suitable adsorbents for the removal of contaminants from polluted gas, liquid streams, wastewater, dyes, used lubricating oils etc. These are made possible because of the characteristic nature of the activated carbon which have a large active surface area, high adsorption capacity, well developed porous morphology and good mechanical properties [Sumathi *et al.*, 2009 and Arami-Niya *et al.,* 2012]. Activated carbons are most extensively preferred because of its chemical (e.g. surface groups) and physical properties (e.g. surface area and pore size distribution). They are normally designed and adjusted according to their required application [Xie *et al.,* 2014]. Further, the adsorption on activated carbon appears to be most common techniques because of

its ease of operation since the adsorbents material can be made extremely efficient, stress-free to handle and in some cases they can be able to be regenerated [Viswanathan *et al.,* 2009].
The best substances used for the preparation of activated carbons are organic materials that have high carbon content. Therefore, the development of methods to recycle waste materials such as activated carbons is significantly desired and offers a promising future. Agricultural wastes, for example coconut shell and palm kernel shell can be converted into activated carbons because of their hardness, high strength and desired properties as a result of its high lignin, high carbon content and low ash content of their materials [Arami-Niya *et al.,* 2012; Lehmann and Joseph, 2009]. The most widely method used for the production of activated carbon is the carbonization of the char at high temperature in an inert atmosphere followed by the activation process. The activation process is divided into physical and chemical. Physical activation process involves treatment of char obtained from carbonization with oxidizing gases, normally steam or carbon dioxide at high temperature (400-1000^{o}C) [Matali *et al.,* 2013]. In the chemical activation process, the starting material is mixed with a chemical activation reagent and the mixture is heated in an inert atmosphere [Ioannidou and Zabanioutu, 2007; Allwar, 2012; Hidayu and Muda, 2016]. This process is usually done at lower temperature and relative time interval, producing higher surface area and better porosity compared to physical activation. The aim of this research work were to produce activated carbons from palm kernel shell and coconut shell using chemical activation from potassium carbonate (K_2CO_3) and sodium bicarbonate ($NaHCO_3$) to adsorb some heavy metals from used lubricating oil samples. The surface area of the impregnated activated carbons was analyzed using Brunauer, Emmett and Teller (BET). In other to further improve the adsorption efficiency of the activated carbons produced, the data obtained were model to suit the heavy metal parameters.

Materials and Methods

Raw material

Among the agriculture waste materials, palm kernel shell (PKS) and coconut shell (CS) were used for activated carbon preparation. PKS was obtained from a Palm oil Mill Industry that is located in Aluu, and CS was obtained from the Local Community Market in Choba, all suburbs in Port Harcourt, Rivers State, Nigeria. The materials (palm and coconut shells collected) were thoroughly cleaned with tap water, then further with distilled water several times to remove dust and all other impurities. The PKS and CS samples were later dried in the spray drying oven at 110^{o}C for 24h to remove any trace of surface moisture and were then ground to the desired size that can pass through 500 µm mesh size.

Figure 1. (a) Palm kernel shell; (b) Coconut shell

Chemical Activation and Activated carbon preparation

Activated carbons were produced from the palm kernel and coconut shells using a chemical activation method used by [Evbuomwan *et al.,* 2013 and Boadu *et al.,* 2018]. 30g of the powdered samples each (that is palm kernel and coconut shells) were impregnated with 1M solution of K_2CO_3 and $NaHCO_3$ and left in the room temperature for 3 hours. The samples were chemically activated for 40 mins at a high carbonization temperature of 800^0C using Carbolite Muffle Furnace. The activated carbons produced were treated with 0.5 M glacial acetic acid solution, then rinsed thoroughly with distilled water until the pH's were within 6-7. The samples were dried in the sun and sieved with 500 µm mesh. Portions of the activated carbons remained on the mesh were dried in the oven for 1 h, then removed and stored in air-tight containers. According to the literature, the surface area of chemical activated carbons can range from 250 to 2500 $m^2\ g^{-1}$, depending on the precursor and the type of treatment used for the production of the activated carbon. However, the most common values are around 600 to1000 $m^2\ g^{-1}$ [Cabal *et al*., 2009; Olivares-Marín *et al*., 2009 and Magriotis *et al*., 2010]

Characterization of the Activated Carbon Samples.

Surface Area Determination by Brunauer, Emmett and Teller (BET)

The specific surface area of the chemical activated carbons from the palm kernel and coconut shells were determined using the pore size distribution by means of adsorption and desorption of nitrogen at 77 K using the method of Brunauer, Emmett and Teller (BET) with a model ASAP 2020 Micromeritics Analyzer (Dublin, Ireland) [Boadu *et al.,* 2018].

Oil Samples Collection, Preparation, Digestion and Elemental Analysis

5 litres of used lubricating oil samples (Total quartz 20 W 50) that have been used for 3 and 6 months were collected from Total Service Stations at East-West road, Port Harcourt, Rivers State, Nigeria. The 3 and 6 months old used lubricating oils were labels as sample **A** and **B** respectively. Also, 5 litres of fresh sealed lubricating oil (Total quartz 20 W 50) were purchased from the same source and label as control sample **C**. Used lubricating oil samples **A** and **B** were stored for several days to allow large suspended particles and small particles to settle under gravity.

Preparation of Oil Samples

Filtration of the used lubricating oil samples **A** and **B** were carried out under gravity using Buchner funnel and filter paper to remove contaminations such as sand, metal chips, micro impurities etc. that polluted the lubricating oil. The used lubricating oils were allowed to settle for 24 hours and samples were further filtered.

Oil Samples Digestion and Elemental Analysis

According to the acid digestion method used by [McKenzie *et al*, 1981 and Boadu *et al.,* 2018], 0.5 g each of the fine oil samples were weighed into a Kdjedahl digestion flask and 5 mL concentrated H_2SO_4 was added to each of the oil samples and heated in a fume hood until the oil samples started to char. Then, 10 ml of H_2O_2 were added to the charred mixture and were heated for 5 min and the mixture turned colourless when the digestion was completed. The used and virgin lubricating oil (control) samples were digested using the same procedure**.** The digested samples were transferred into a 100 ml volumetric flask and made up to the mark**.** The samples were then transferred into a cleaned plastic container for AAS analyses. The digested samples were analysed using Perkin Elmer Atomic Absorption Spectrophotometer model number Buck

Scientific 210 at the Pollution Control and Environmental Management Limited, Port Harcourt, Nigeria.

Determination of Heavy Metals Present

Perkin Elmer Atomic Absorption Spectrophotometer model number buck Scientific 210 were used to determine the heavy metals that were present in the oil samples before and after analyses with the activated carbons.

Adsorption Isotherms

Adsorption isotherm reveals the relationship between the amount of a solute adsorbed at constant temperature and its concentration in the equilibrium solution. It provides essential physiochemical data for assessing the applicability of the adsorption process as a complete unit operation (Aydin and Baysal, 2006). Langmuir isotherm models are widely used to investigate the adsorption process (Chan *et al,* 2008). The model parameters can be construed further, providing understandings on sorption mechanism, surface properties, and an affinity of the adsorbent (Sagar Nayak and Kumar Singh, 2007). The Langmuir isotherm was develope on the assumption that the adsorption process will only take place at specific homogenous sites within the adsorbent surface with uniform distribution of energy level. Once the adsorbate is attached on the site, no further adsorption can take place at that site; which concluded that the adsorption process is monolayer in nature. The Langmuir adsorption model further based on the assumption that all the adsorption sites are energetically identical and adsorption occurs on a structurally homogeneous adsorbent. The linearized form of the Langmuir equation based on those assumptions is given as (Langmuir, I., 1918 and Xunjun Chen, 2015).

$$\frac{\mathbf{1}}{\boldsymbol{q_e}} = \frac{\mathbf{1}}{\boldsymbol{Q^o}} + \frac{\mathbf{1}}{\boldsymbol{bQ^oC_e}}$$

Where $\boldsymbol{q_e}$ is the amount of solute adsorbed on the surface of the adsorbent (mmol g^{-1}), $\boldsymbol{C_e}$ is the equilibrium ion concentration in the solution ($mmol^{-1}$), $\boldsymbol{Q^o}$ is the maximum surface density at monolayer coverage and b is the Langmuir adsorption constant (L $mmol^{-1}$). The plots of $1/\boldsymbol{q_e}$ versus $1/\boldsymbol{C_e}$ give a straight line and the values of $\boldsymbol{Q^o}$ and $\boldsymbol{b}$ can be calculated from the intercept and slope of the plots, respectively. In general, the coefficient of correlation (R^2) is between 0.0 and 1.0, and the quality of fitting increases with the nearness of R^2 to 1.0. From the statistics point of view, it can be concluded that the Langmuir model shows a better fit due to the high coefficient of correlation ($R^2 \approx 1$). Durbin-Watson Test (D. W. T.) is another parameter considering the difference between the real and model amount in every point knowing as residual. This parameter determines the relation adsorption on both sizes of activated carbon.

Methods for Data Analysis and Presentation

IBM SPSS version 23 statistical analysis software's was used to analyse the data generated in the experiments. The results obtained were recorded in the tables below. Also, the constants of all models were obtained by an ordinary correlation coefficient of the parameter (least square method) using the Quantitative Micro Software LLC., Eviews 4 User's Guide, 2002 and Jan 15(2018), XLSTAT version.1. In both Eviews software" version 3.1 and XLSTAT version 2018.1 software, several examinations were performed for analysing and fitting of data. The models are developed based on the statistical function such as coefficient of correlation (least square) parameter (R^2) and Durbin-Watson Test (D. W. T.).

Results and Discussion

Table 1: Mean, ±SD, of virgin and used lubricating oil samples before treatment with palm and coconut shells activated carbons.

Samples/Parameters	Control	Sample A	Sample B
Cu (ppm)	0.001±0.000	0.150 ±0.008	0.220±0.096
Fe (ppm)	1.502±0.092	4.650±0.159	3.350±0.289
Zn (ppm)	2.833±0.034	16.475±0.950	14.575±0.272
Cd (ppm)	0.020±0.008	0.020±0.008	0.030±0.008
Pb (ppm)	1.000±0.093	1.045±0.478	1.525±0.222
Cr (ppm)	0.410±0.051	0.400±0.065	0.445±0.039
Mg (ppm)	41.900±0.258	5.450±0.265	21.475±0.650

Table 2: Mean, ±SD of virgin and used lubricating oil samples after treatment with Palm Kernel Shell Sample

Samples/Parameters	Control	Sample A	Sample B
Cu (ppm)	0.075±0.013	0.400±0.018	0.230±0.008
Fe (ppm)	1.150±0.129	8.500±0.258	3.400±0.183
Zn (ppm)	8.325±0.275	10.375±0.171	5.450±0.300
Cd (ppm)	0.000±0.000	0.018±0.009	0.000±0.000
Pb (ppm)	1.650±0.039	1.648±0.097	2.388±0.070
Cr (ppm)	0.065±0.013	0.210±0.026	0.135±0.013
Mg (ppm)	0.350±0.026	0.900±0.025	0.505±0.013

Table 3: Mean, ±SD of virgin and used lubricating oil samples after treatment with Coconut Shell Sample

Samples/Parameters	Control	Sample A	Sample B
Cu (ppm)	0.001±0.000	0.780±0.014	0.790±0.026
Fe (ppm)	3.650±0.625	13.500±0.942	14.125±0.618
Zn (ppm)	0.6700±0.071	5.838±0.344	5.400±0.280
Cd (ppm)	0.001±0.000	0.001±0.000	0.001±0.000
Pb (ppm)	0.563±0.172	0.410±0.037	0.438±0.222
Cr (ppm)	0.348±0.049	0.388±0.046	0.528±0.055
Mg (ppm)	1.475±0.171	3.625±0.222	0.645±0.037

Table 4: Analysis of Variance of Variables and Summary for all Y's for the various Heavy Metals (Langmuir Model Parameter Results)

S/N	(Cu)	(Fe)	(Zn)	(Cd)	(Pb)	(Cr)	(Mg)
R^2	0.8185	0.9927	0.9953	0.8347	0.9349	0.9378	0.9997
F	15.2181	459.5948	715.9685	17.0436	48.4738	50.8595	11356.9041
Pr > F	< 0.0001	< 0.0001	< 0.0001	< 0.0001	< 0.0001	< 0.0001	< 0.0001
Filtration process	20.9543	864.8179	1058.5040	51.4600	164.4045	171.7839	26526.6506
	< 0.0001	< 0.0001	< 0.0001	< 0.0001	< 0.0001	< 0.0001	< 0.0001
Samples	13.1799	696.8264	978.8792	3.1714	17.1650	14.7779	5447.8007
	0.0001	< 0.0001	< 0.0001	0.0579	< 0.0001	< 0.0001	< 0.0001
Filtration process* Samples	13.3691	138.3674	413.2453	6.7714	6.1629	8.4382	6726.5826
	< 0.0001	< 0.0001	< 0.0001	0.0007	0.0012	0.0001	< 0.0001

Table 5: Brunauer, Emmett and Teller (BET) Summary

Parameters	Palm Kernel shell	Coconut shells
Surface area (m^2/g)	717.142	1177.524
Correlation coefficient (r)	0.9994	0.9963
Slope	3.063	2.121
Intercept	1.793e+00	8.361e-01
Constant	2.706	3.537

Discussions

Adsorption of Heavy Metals in Used Lubricating Oil using Palm Kernel and Coconut Shells as Adsorbents.

From the results obtained, it can be seen that both the palm kernel and coconut shells were not suitable for the removal of copper metal in the fresh and used lubricating oil samples. Because, the initial mean concentrations of copper in virgin (C) and used lubricating oil samples (i.e. A andB) were 0.001±0.000 ppm, 0.1500±0.008 ppm and 0.220±0.096 ppm respectively before treatment processes. But after the treatment process with the palm kernel shell activated carbon, the mean concentration of copper metal increases for virgin (C) to 0.075±0.013 ppm and used lubricating oil samples (AandB) are 0.400±0.018 ppm and 0.230±0.008 ppm respectively. In the case of the coconut shell activated carbon, the mean concentration of copper also in virgin lubricating oil remains the same 0.001±0.000 whereas for used lubricating oils samples (i.e. AandB) it increases to 0.780±0.014 and 0.790±0.026 respectively. The increase in mean concentrations after the treatment processes with both the palm kernel and coconut shells activated carbons can be attributed to leaching of copper ions already present in the bed of the adsorbents as ascertain in the physio-chemical characterization analysis of the adsorbent beds by [boadu *et al.,* 2018 and Odisu *et al.,* 2019]. Though, the percentage leached in palm kernel was small compared to that of coconut shells. Hence, there is the need to further search for better and potential raw materials for the production of activated carbons that can meet industrial needs of removal of copper metals in both fresh and used lubricating oil samples. However, Nabil, *et al.,* 2010 reported that date palm kernel can slightly reduce copper metals in used lubricating oils from 7mg/kg to 6mg/kg. But several works of literature have shown that chemical activated carbons from palm kernel and coconut shells are effective in the removal of pollutants in muddy water and colour from wastewater [Inegbenebor, *et al.,* 2012 and Akpen *et al.,* 2017]. Also, Kwakye-Awuah *et al.,* 2018 reported that laboratory-synthesized zeolite types LTA and LSX successfully removed heavy metals, particularly lead, copper and iron that was in the spent oil.

Also, it can be observed from the results obtained that the concentrations of iron metal increases after treatment processes with both the chemically activated carbons produced from coconut and palm kernel shells. The concentrations of iron metal before the treatment processes were 1.502±0.092 ppm for virgin and 4.650±0.159 ppm and 3.350±0.289 ppm for both used oil samples AandB. However, after treatment processes with chemically activated carbons produced from palm kernel and coconut shells, the concentrations of the iron metal increases. For the palm kernel activated carbon, the values obtained are 1.150±0.129 ppm for virgin, 8.500±0.258 ppm

for sample A and 3.400±0.183 ppm for sample B respectively. In the case of the coconut activated carbons, the observed values are 3.650±0.625 ppm for virgin, 13.500±0.942 ppm for sample A and 14.125±0.618 for sample B respectively. The level of increase was not much in palm kernel as compared to coconut shells. The concentration increase in iron metal after the treatment process with both the coconut and palm kernel shells might be due to leaching of the iron metal concentration already present in the adsorbent beds by [Boadu *et al.,* 2018 and Odisu *et al.,* 2019]. According to their research works reported, chemically activated carbons produced from coconut and palm kernels contain a high amount of iron metal concentration. Though, the analyses of iron revealed that palm kernel shell activated carbon performed better followed by coconut shell activated carbon respectively. Because of this reason, activated carbons produced from palm kernel and coconut shells as adsorbents are not recommended for the removal of iron metals present in used lubricating oil samples.

In general, zinc is added to fresh lubricating oil as zinc diethyl dithiophosphate (ZDDP), zinc dithiophosphates, and zinc dialkyl dithiocarbamates. This was added to the base oil as part of multi-functional additives for improving oil's performance [Kwakye-Awuah *et al.,* 2018]. From all the tests conducted on the zinc before treatment with activated carbons produced from coconut and palm kernel shells the results were for virgin was 2.833±0.275 ppm and used lubricating oil samples AandB are 16.475±0.950 ppm and 14.57±0.272 ppm respectively. But after the treatment process with palm kernel shell activated carbon the values recorded were for virgin was 8.325±0.275 ppm and used lubricating oil samples AandB are 10.375±0.171 ppm and 5.450±0.300 ppm. For coconut shell activated carbon, the results obtained were for virgin was 0.670±0.071 ppm and used lubricating oil samples AandB are 5.838±0.344 ppm and 5.400±0.280 ppm respectively. Comparing the various results obtained, it proved that coconut shell activated carbon has a better adsorption capacity than palm kernel shell activated carbon. lnegbenebor *et al.* 2012, conducted similar research using activated carbons from palm kernel and coconut shells for purification of polluted water for drinking but reported that palm kernel was rather effective than coconut shells. The disparity might due to the used lubricating oils sample instead of the polluted water for drinking. Kwakye-Awuah *et al.,* 2018 reported that the recycling of the used oil was possible with metakaolin and the zeolites. Their results led to a reduction in zinc content by 94.96 %, 96.76 % for zeolite LTA and 93.88 % for zeolite LSX. This shows that coconut shell activated carbon produced can be used effectively and efficiently as an alternative to those prepared by other researchers.

Analysis of the heavy metal such as cadmium from Tables 1, 2 and 3 revealed that both coconut and palm kernel shells activated carbons are very efficient and effective in the adsorption processes (i.e. almost 100%). Because the concentrations of cadmium metal before the treatment process with palm kernel and coconut shells activated carbons were for virgin 0.020±0.008 ppm and used samples AandB lubricating oils are 0.0200±0.008 ppm and 0.030±0.008 ppm respectively. But after the treatment with palm kernel shell activated carbon the concentrations of cadmium metal reduces, for lubricating oils; virgin 0.000±0.000 ppm and used samples AandB to 0.018±0.009 ppm and 0.000±0.000 ppm lubricating oils respectively. Also, with the coconut shells activated carbon after the treatment processes, they all drop in the concentrations of the cadmium metals, with lubricating oils; virgin 0.001±0.000 ppm and used samples are AandB the recorded values are 0.001±0.000 and 0.001±0.000 respectively. This affirmed what Nabil, *et al.,* 2010 had reported earlier that, date palm kernel powder was a good adsorbent for removal of cadmium metal in used lubricating oils.

However, Okafor *et al.,* 2012 reported that coconut shell adsorbed Pb^{2+}, Cu^{2+} Cd^{2+} and As^{3+} ions from aqueous solutions and the concentration of the metal ions adsorbed increased with increase in concentrations, increase in contact time, increase in temperature and increases in pH for each metal. He concludes that coconut shell could serve as a cheap, readily available effective adsorbent for the removal of $Pb,^{2+}$ $Cu,^{2+}$ $Cd,^{2+}$ and As^{3+} from wastewater as a way of treatment before discharge into the environment. From the literature findings reported earlier, it can be concluded that chemically activated carbons produced from both coconut and palm kernel shells are good adsorbents for removal of heavy metal such as cadmium from used lubricating oils.
From the analysis of chromium metal in Tables 1;2 and 3, it was observed that concentrations of chromium metal before the treatment processes with both palm kernel and coconut shells activated carbons were, for lubricating oils; virgin 0.410±0.051 ppm, used samples AandB are 0.400±0.065 ppm and 0.445±0.039 ppm respectively. But after treatment with palm kernel shells activated carbon, the values obtained were 0.065±0.013 ppm for virgin, 0.210±0.026 ppm for used sample A and 0.135±0.013 ppm for used sample B lubricating oils respectively. In the case of after treatment with coconut shell activated carbons, the values recorded are 0.348±0.049 ppm for virgin, 0.388±0.046 ppm for used sample A and 0.528±0.055 ppm for used sample B. From all the results obtained, it revealed that palm kernel shell activated carbon was a good adsorbent compared to coconut shell activated carbon because the palm kernel shell reduces the concentrations of chromium metal compared to coconut shell activated carbons. Babayemi, 2017 revealed that palm kernel shell being an agricultural waste could be converted to useful and efficient adsorbent through the use of activating chemicals, particularly H_2SO_4. Also, Nabil, et al., 2010 reported a similar phenomenon with chromium metal.

However, Hidayu and Muda, (2016) reported that palm kernel and coconut shells can be used as the perfect raw material to prepare activated carbon with the high surface area for CO_2 adsorption rate. Also, Mehr *et al.,* 2019 found out that palm kernel shell, an inexpensive and easily available material, was very effective to remove Cr (VI) from aqueous solutions. He reported that the tested activated carbon produced from palm kernel shells showed higher adsorption capacities compared to those of some coconut shell and other activated carbons found in the works of literature. Odisu *et al.,* 2019 reported that palm kernel husks, coconut and groundnut shells could be used as an alternative to available commercial adsorbents for cement wastewater treatment. They also affirmed that the combination of physical and chemical treatment of these adsorbents could enhance their adsorption capabilities due to their resultant high surface area and increased depth of pore spaces.

From the Tables 1,2 and 3, the analysis of heavy metal such as lead (Pb) concentrations before treatment processes with both chemically activated carbons produced from palm kernel and coconut shells gave the following results for the lubricating oil samples; for virgin 1.000±0.093 ppm, used sample **A** 1.045±0.478 ppm and used sample **B** 1.525±0.222 ppm respectively. But after the treatment process with the chemically activated carbon prepared from palm kernel shells, the values recorded were as follows, for virgin 1.650±0.039 ppm, used sample **A** 1.648±0.099 ppm and used sample **B** 2.388±0.070 ppm lubricating oils in that order. However, with the chemically activated carbon produced from coconut shells, the results obtained after the filtration process were as follows, for virgin 0.563±0.172 ppm, used sample **A** 0.410±0.037 ppm and used sample **B** 0.438±0.220 ppm lubricating oils respectively. From all the test results recorded, it shows that coconut shell activated carbon as have a better adsorption capacity for lead metals after the treatment processes with various types of lubricating oil samples compared to palm kernel shells activated carbons. This proved that coconut shell activated carbon was

effective and efficient adsorbent. Therefore, it can be used as a suitable adsorbent for the removal of lead metal concentration in used lubricating oils. Hence, coconut shell is preferred to palm kernel shell activated carbons because of its large surface area as shown in Table 5.
In the case of palm kernel shell activated carbon, the concentration of lead metals increases. Nabil *et al.,* 2010, also reported an increase in lead metal concentration with activated carbon prepared from date palm kernel. Jodeh *et al.,* 2015, found out that concentration of heavy metal lead in used lubricating oil is higher than the concentration of other metals and adsorption of lead increases with increase adsorbent dosage, temperature and time of contact.

Finally, the adsorption results obtained for magnesium heavy metal analysed indicated that activated carbons produced from the coconut and the palm kernel shells can be used as a high-performance adsorbent with higher adsorption capacity. It was worthy of note that from all the analysis performed, the magnesium metal contents of the used lubricating oil samples were generally far below the general range reported in the literature with both palm kernel and coconut shells activated carbons. From Tables 1, 2 and 3, the results obtained for the analysis of magnesium concentrations before the treatment process was as follows for the various lubricating oils, for virgin was 41.900±0.258 ppm, used sample A was 5.450±0.265 ppm and used sample B was 21.475±0.650 ppm respectively. But after the treatment process with activated carbon produced from palm kernel shells, the values obtained for the respective lubricating oils were, virgin 0.350±0.026 ppm and used samples AandB are 0.900±0.025 ppm and 0.505±0.013 ppm in that order. In the case of the coconut shell activated carbon, the results recorded for the various types of lubricating oils are as follows, virgin 1.475 ±0.171 ppm, used sample A 3.625±0.222 ppm and used sample B 0.645±0.645 ppm respectively. Nabil *et al.,* 2010 reported a similar trend of decrease in magnesium metal concentration from fresh to used lubricating oil samples with activated carbons prepared from date palm kernel powder. Also, Siti *et al.,* 2015, found that the increase of chitosan dosage from 0.5 to 1.0 g decrease the metals such as sodium, magnesium, calcium and zinc removal percentage in used lubricating oils. Furthermore, they observed that the increase of temperature from 30 to 70°C and the increase of contact time from 2 to 10 min resulted in a decrease of metals removal from used lubricating oils.

Adsorption Model

Table 4, shows that copper have the R^2 (0.8185), DW (1.4546) and Pr > F (< 0.0001). In this model, the amounts of R^2 are close to 1 for the adsorbate and D. W. T. is more than 1 for the solute which confirms the definition of modelling basis. Also, in the ANOVA, the lesser the Pr > F value, the more significant the results. The adsorption data obtained after the analysis fitted well to the Langmuir model and adsorptive surface area of 717.120 m^2/g for palm kernel and 1177.524 m^2/g for coconut shells as shown in Table 5.

From the results in Table 4, iron metal have R^2 (0.9927), DW (2.6443) and Pr > F (< 0.0001) respectively. In this model, the amounts of R^2 are close to 1 for the adsorbate and D. W. T. is more than 1 for the solute which confirms the definition of modelling basis. Also, in the ANOVA, the lesser the Pr > F value, the more significant the results. The iron metal revealed that it conforms to a straight line Langmuir adsorption isotherm [Kamal *et al.,* 2014].

The values recorded in Table 4, zinc have R^2 (0.9953), DW (2.2315) and Pr > F (< 0.0001) respectively. In this model, the amounts of R^2 (0.9953) are close to 1 for the adsorbate and D. W. T. (2.2315) was more than 1 for the solute which confirms the definition of modelling basis.

Also, in the ANOVA, the lesser the Pr > F value, the more significant the results. Hence, the zinc metal was found to conform to a straight line Langmuir adsorption isotherm [Kamal *et al.,* 2014]. Also from the results obtained in Table 4, cadmium has R^2 (0.8347), DW (2.7000) and Pr > F (0.0001). From the statistic point of view, R^2 is the most important parameter to obtain the model ability in the fitting of various conditions provided based on experimental data. Therefore, these results showed that cadmium metal conforms to a straight line Langmuir adsorption isotherm [Kamal *et al.,* 2014].

In Table 4, lead recorded values of R^2 (0.9349), DW (2.3732) and Pr > F (< 0.0001) respectively. It can be seen from the results obtained in the tables that, the Langmuir isotherm best fitted to the experimental data. This data has revealed that activated carbons produced from palm kernel and coconut which are agricultural waste, can be used as an adsorbent for lead metal [A.E. Ofomaja, 2010].

From the results obtained in Table 4, chromium has R^2 (0.9378), DW (2.1824) and Pr > F (< 0.0001). The results recorded showed that chromium metal conforms to a straight line Langmuir adsorption isotherm (Kamal *et al.,* 2014) and it proved that activated carbons produced from the coconut and the palm kernel shells can be used as a high-performance adsorbent with higher adsorption capacity [A.E. Ofomaja, 2010].

Finally, from Table 4, magnesium recorded the following results R^2 (0.9997), DW (2.4396) and Pr > F (< 0.0001). R^2 is the most important parameter to ascertain the model ability in the fitting of various situations provided based on experimental data. In this model, the amounts of R^2 (0.9997) are close to 1 for the adsorbate and D. W. T. (2.4396) was more than 1 for the solute which confirms the definition of modelling basis. Also, in the ANOVA, the lesser the Pr > F value, the more significant the results. This revealed that magnesium metal conforms to a straight line Langmuir adsorption isotherm [Kamal *et al.,* 2014]. This result obtained for magnesium proved that activated carbons produced from the coconut and the palm kernel shells can be used as a high-performance adsorbent with higher adsorption capacity [Ghorbanian *et al.,* 2016].

Conclusions

The adsorption results obtained for some of the heavy metals analysed indicated that activated carbons produced from the coconut and the palm kernel shells can be used as a high-performance adsorbent with higher adsorption capacity. This research work further ascertained that the some of the heavy metal contents in the used lubricating oil samples were reduced considerably to appreciable concentrations through re-refining with the chemically activated carbons produced from both palm kernel and coconut shells. Particularly, magnesium, cadmium and chromium contents in the used lubricating oil samples respectively. However, the activated carbons produced from palm kernel and coconut shells were not suitable for the removal of both copper and iron metals. From the R^2 values obtained and statistics point of view, it can be concluded that the Langmuir model shows a better fit due to the high coefficient of correlation ($R^2 \approx 1$). Also, the recovered oil could be re-used. Finally, agriculture waste such as palm kernel and coconut shells can be converted to a high-performance adsorbent.

Acknowledgements

Authors acknowledge the research grant provided by the University of Cape Coast, Cape Coast, Ghana and World Bank Africa Centre of Excellence, Centre for Oilfield Chemicals Research, Institute of Petroleum Studies, University of Port Harcourt, Nigeria under the PhD. research grant.

References

Akpen, G.D. Okparaku, L.A. and Odoh, F.O (2017). Removal Of Colour From Wastewater By Raffia Palm Seed Activated Carbon, *Journal of Emerging Trends in Engineering and Applied Sciences (JETEAS),* Vol. 8(1), pp. 25-29

Allwar, (2012)."Characteristics of micro- and mesoporous structure and surface chemistry of activated carbons produced by oil palm shell," presented at the International Conference on Chemical, Ecology and Environmental Science (ICEES'2012), Bangkok.

Aydin, H. and Baysal, G. (2006). Adsorption of acid dyes in aqueous solutions by shells of bittim (pistacia khinjuk stocks), *Desalination,* Vol.196, pp.248–259

Arami-Niya, A., Wan, W. M. A, Daud, F. S., Mjalli, F. Abnisa, and Shafeeyan, M. S. (2012). Production of microporous palm shell-based activated carbon for methane adsorption: Modeling and optimization using response surface methodology, *Chemical Engineering Research and Design*, Vol.90, pp.776-784.

Babayemi, A.K. (2017) Performance Evaluation of Palm Kernel Shell Adsorbents for the Removal of Phosphorus from Wastewater. *Advances in Chemical Engineering and Science*, Vol.7, pp.215- 227.

Bentum, JK; Anang, MA; Boadu, KO; Koranteng-Addo, EJ; (2011). Assessment of heavy metals pollution of sediments from Fosu lagoon in Ghana, *Bulletin of the Chemical Society of Ethiopia*, Vol.25 (2), pp.191-196.

Boadu, K.O; Joel, O.F; Essumang, D.K; Evbuomwan, B.O, (2018); Comparative Studies of the Physicochemical Properties and Heavy Metals Adsorption Capacity of Chemical Activated Carbon from Palm Kernel, Coconut and Groundnut Shells*, J. Appl. Sci. Environ.Manage.*Vol.22 (11) pp.1833–1839.

Cabal, B., Budinova, T., Ania, O. C., Tsyntsarski, B., Parra, B. J., and Petrova, B. (2009). Adsorption of naphthalene from aqueous solution on activated charcoals obtained from bean pods. *Journal of Hazardous Materials*, Vol.34, pp. 1150-1156

Chan, L.S., Cheung, W.H., McKay, G. (2008). Adsorption of acid dyes by bamboo-derived activated carbon, *Desalination*, Vol. 218, pp. 304–312

Evbuomwan, B.O; Agbede, A.M; Atuka, M.M (2013); A Comparative Study of the Physico-Chemical Properties of Activated Carbon from Oil Palm Waste (Kernel and Fibre). *Inter. J. Sci. Engineer. Investigate*, 2(19),pp.75-79

Ghorbanian, Sohrab A; Bagheri, Nafiseh; Khakpay, Amir (2016). Investigation of Adsorption Isotherms of Aniline on Activated Carbon Investigation of Adsorption Isotherms of Aniline on Activated Carbon, 1st National Conference on Industrial Water and Wastewater Treatment. Tehran, Iran

Hidayu, A.R and Muda, N. (2016). Preparation and characterization of impregnated activated carbon from palm kernel shell and coconut shell for CO_2 capture, *Procedia Engineering*, Vol.148, pp. 106 – 113

IBM SPSS version 24 (May 22, 2016) Statistical Software

Ioannidou, O. and Zabaniotou, A. (2007).Agricultural residues as precursors for activated carbon production—A review, *Renewable and Sustainable Energy Reviews*. Vol.11, pp.1966-2005.

lnegbenebor Adedayo I, Inegbenebor Anthony 0, Boyo Henry. I (2012). Comparison of the Adsorptive Capacity of Raw Materials in Making Activated Carbon Filter for Purification of Polluted Water for Drinking; *ARPN Journal of Science and Technology*, Vol 2, (9), pp. 754-760

Jodeh, S., Odeh, R., Sawalha, M., Abu Obeid, A., Salghi, R., Hammouti, B., Radi, S., Warad, I. (2015). Adsorption of lead and zinc from used lubricant oil using agricultural soil: equilibrium, kinetic and thermodynamic studies, *J. Mater. Environ. Sci.* Vol. 6 (2), pp. 580-591

Kamal, Muhammad Ashraf, Syed Mumtaz Danish Naqvi, and Fasihullah Khan (2014). Optimized liquid-liquid extractive re-refining of spent lubricants, *Scientific World Journal*, Volume2014, Article ID 458789, pp. 1-10

Kwakye-Awuah, B., Kwakye, R., Sefa-Ntiri, B., Nkrumah, I., Von-Kiti, E., and Williams, C., (2018). Comparison of the Recycling Efficiency of Metakaolin and Laboratory-Synthesized Zeolite Types LTA and LSX on Used Lubricant Engine Oil, *Applied Physics Research*; Vol. 10, Vol. 4; pp. 1916-9639.

Langmuir, I. (1918). J. Am. Chem. Soc. 40 (9) pp. 1361

Lehmann, J. and Joseph, S (2009). Biochar for environmental management: *Earthsca*

Magriotis, Z. M., Leal, P. V. B., Sales, P. F., Papini, R. M., and Viana, P. R. M. (2010). Adsorption of ether amine on kaolinite: a cheap alternative for the treatment of mining effluents. *Journal of Hazardous Materials*, Vol. 184, pp. 465-47

Maryam Razavi Mehr, Mohammad Hossein Fekri, Faezeh Omidali, Noushin Eftekhari, Behrouz Akbari-adergani, (2019). Removal of Chromium (VI) from Wastewater *by* Palm Kernel Shell-based on a Green Method*, Journal of Chemical Health Risks*, Vol.9(1), pp. 75-86

Matali, S., Khairuddin, S. A., Sharifah, A. S. A. K and Hidayu, A. R (2013)."Removal of selected gaseous effluent using activated carbon derived from oil palm waste: An Overview," in 2013 IEEE Symposium on Business, Engineering and Industrial Applications, Kuching, Sarawak

McKenzie, T., (1981, Atomic absorption spectrophotometry for the analysis of wear metals in oil samples, Varian Instruments at Work, Varian atomic Absorption AA-10, *Techtron Pty*., Ltd., Australia, pp: 1-9

Nabil M. Abdel-Jabbar, Essam A.H. Al Zubaidy, and Mehrab Mehrvar (2010). Waste Lubricating Oil Treatment by Adsorption Process Using Different Adsorbents; *International Journal of Chemical and Biological Engineering*; 3(2), pp. 70-73

Odisu, T; Edomwonyi-Otu, L.C; Anih, E.C (2019). Comparative Studies of Adsorption of Heavy Metals from Cement Waste Water Using Activated Carbon from Palm Kernel Husk, Coconut and Groundnut Shells, *J. Appl. Sci. Environ. Manage*. Vol. 23 (5) pp.967-975

Ofomaja, A.E. (2010). Equilibrium studies of copper ion adsorption onto palm kernel fibre, *Journal of Environmental Management*, Vol. 91, pp.1491-1499

Olivares-Marín, M., Del-Prete, V., Garcia-Moruno, E., Fernandez-Gonz?ales, C., Macías-García, A., and Gomez-Serrano, V. (2009). The development of activated charcoal from cherry stones and it uses in the removal of ochratoxin a from red wine. *Food Control*, Vol. 20, 298-303

Okafor, P.C; Okon, P.U; Daniel, E.F; Ebenso, E.E (2012). Adsorption Capacity of Coconut (Cocos nucifera L.) Shell for Lead, Copper, Cadmium and Arsenic from Aqueous Solutions, *Int. J. Electrochem. Sci.*, 7, pp. 12354 – 12369

Sagar Nayak, P. and Kumar Singh, B. (2007). Removal of phenol from aqueous solutions by sorption on low-cost clay, *Desalination*, Vol. 207, pp. 71–79.

Siti Munira Jamil, Mohamad Wijayanuddin Ali, Adnan Ripin and Arshad Ahmad, (2015). Adsorption of Sodium, Magnesium, Calcium and Zinc from Recovered Base Oil of Used Lubricants Using Chitosan. *Journal of Applied Sciences,* Vol.15, pp.516-523.

Sumathi, S., Bhatia, S., Lee, K. T. and Mohamed, A. R (2009). Optimization of microporous palm shell activated carbon production for flue gas desulphurization: Experimental and statistical studies, *Bioresource Technology*, Vol. 100, pp.1614-1621.

Viswanathan, B., Neel, P. I. and Varadarajan, T. K (2009). "Methods of activation and specific applications of carbon materials," National Centre for Catalysis Research Department of Chemistry, Indian Institute of Technology Madras, Chennai.

Xie, J., Yan, N., Liu, F., Qu, Z., Yang, S., and Liu, P. (2014). CO2 adsorption performance of ZIF-7 and its endurance in flue gas components, *Frontiers of Environmental Science and Engineering,* Vol.8, pp.162-168.

XLSTAT version .1, (2018), Microsoft Excel, Copyright Addinsoft 1995-2018

Xunjun Chen,(2015), "Modeling of Experimental Adsorption Isotherm Data", *Information*, 6, pp.14-22; DOI:10.3390/info6010014.

Proceedings of the 49th NSChE Annual Conference
KADA 2019: pp 552-561

3A-05: PRODUCTION AND CHARACTERIZATION OF LIGNIN PEROXIDASE ENZYME AS A GREEN AND SUSTAINABLE AGROCHEMICAL FOR ENHANCED BIOETHANOL PRODUCTION FROM AGRO-WASTES

Justice Obinna Osuoha*[a], Bene Willie Abbey[b], Evans Chidi Egwim[c] and Eucharia Oluchi Nwaichi[b]

[a] World bank Africa Centre of Excellence in Oilfield Chemical Research, University of Port Harcourt Choba, Rivers State, Nigeria
[b] Department of Biochemistry, University of Port Harcourt Choba, Rivers State, Nigeria
[c] Department of Biochemistry, Federal University of Technology, Minna, Niger State Nigeria
*Corresponding author: osuoha.justice@aceuniport.org; justice_osuoha@uniport.edu.ng

ABSTRACT

Agro-wastes are the most auspicious feedstock for the production of renewable products like bioethanol. The enzymatic hydrolysis of these substrates is sacrosanct. In this study, lignin peroxidase production from microorganisms and their capacity to hydrolyze lignocellulose biomass was evaluated. Isolation and screening for lignin peroxidase activity from the microbial strains were done using standard techniques. The enzyme was produced in broth medium and purified using standard methods. The purified enzyme was immobilized in sodium alginate and was used for degradation of lignocellulose materials. Twelve microbial strains were isolated from oil contaminated soils. Among 12 isolates, Yeast, Trichorderma sp. and Micrococcus were selected for enzyme production and characterization. Results revealed that the immobilized enzyme significantly hydrolyzed lignocellulosic biomass and showed high affinity for other biomass constituents. The findings highlight the capacity of local enzyme production in Nigeria and promote a cost effective means of obtaining useful products from locally available agro-wastes.

1.0 Introduction

Agro-wastes abundant in lignocellulose biomass are the most promising feedstock for the generation of renewable, carbon neutral substitutes for synthetic materials (e.g. bioethanol, biofuel, building materials etc.). One of the biggest renewable reservoir of potentially fermentable carbohydrates in the world is lignocellulose biomass, and its exploitation for bioethanol production lingers to be a topic of global interest (Ahmadi *et al.*, 2010; Mtui and Nakamura, 2005). These lignocellulose biomasses are made up of hemicelluloses and cellulose that are very hard to convert to simple sugars because of their recalcitrant nature. Due to food shortages and incessant depletion of oil reserves, bioethanol production from cellulosic biomass still provokes a global interest. This has invariably made the exploitation of agro-wastes for the production of sugars by enzymatic hydrolysis an attractive venture. Hydrolysis of this biomass to fermentable sugars makes them attractive and useful as a feedstock for production of single cell protein, alcoholic fermentation and numerous industrial activities (Louime and Uckelmann, 2008).

In bioethanol production from agro-wastes, the conversion of lignocellulose biomass to bioethanol involves four distinct stages: pretreatment, enzymatic degradation, fermentation and lastly the isolation of the produced ethanol (Amadi *et al.*, 2017). The removal of hemicelluloses, deconstruction of lignin barriers and decrement of crystallinity is achieved in the pretreatment stage (Balat, 2011). After the pretreatment stage, the next stage which involves enzymatic hydrolysis of the substrate is the most significant stage because if the polysaccharides are not broken down to simple sugars, there would be no fermentation. When this happens, the overall aim of the process is defeated, relying on indigenous enzymes to hydrolyze the pretreated

biomass is the initial strategy used and it made the production of ethanol from agro-waste unattractive as a result of low yield, however, this drawback was surmounted through introduction of exogenous enzymes.

Peroxidase enzymes expressed by microorganisms are required for the hydrolysis of lignin into simple sugars which can be fermented (Egwim *et al*., 2015). The first lignolytic enzyme to be discovered in the world is lignin peroxidase (Tien and Kirk, 1983). Lignin peroxidase are glycosylated enzymes containing two calcium ions, a single heme with a molecular weight ranging from 27 to 50 kDa (Egwim *et al*., 2015; Hammel and Cullen, 2008). They breakdown lignin with the help of hydrogen peroxidase with a catalytic cycle common to all peroxidase enzymes (Wong, 2009; Hammel and Cullen, 2008). This enzyme is treasured in the industry because it has numerous applications.

Presently, industrial enzymes are not produced in Nigeria commercially. Consequently, lots of diverse enzymes are imported yearly to satisfy the demand of indigenous industries. The indigenous industrial sectors in Nigeria had increased enormously in the last decade, thus, it is a demand of time to locally produce industrial enzymes to cut down expenses on importation and at the same time boost export earnings. In this study, we isolated and produced lignin peroxidase locally and evaluated the applicability of the enzyme in the degradation of cellulosic biomass.

2.0 Methodology

Sample collection

Oil contaminated soil samples were collected from Tai Local Government Area in Ogoni, River State Nigeria using an Auger as described by Osuoha *et al*. (2018).

Isolation and Identification of Lignolytic Microorganisms from Oil Contaminated Soil

A tenfold serial dilution of the soil sample was done till a 10^3 dilutions was obtained according to the technique previously illustrated by Agu (2017). The method reported by Osuoha *et al*. (2019) was used to isolate the microorganisms under aseptic conditions after serial dilution. In brief, 1 mL from serially diluted 10^3 test tube was inoculated into a molten Saubourand dextrose agar petri dish. The plates were allowed to solidify after mixing on the bench before incubation. Afterwards, the petri dishes were incubated for three days at a temperature of 25 ºC to 28 ºC. The petri dishes were monitored for production of colonies and they produced colonies were distinguished based on their appearance, elevation, opacity, size, color, and shape. In other to obtain pure cultures, the separated colonies were sub-cultured into different Saubourand dextrose agar. The petri dishes were incubated as described earlier after sub-culturing until the isolates became pure. The obtained pure cultures were reserved in bijou bottles after due identification via the macroscopic and morphological characteristics.

Screening for Lignin Peroxidase Producing Microorganisms

Preliminary screening for lignin peroxidase production of all microbial isolates was done based on the zones of clearance produced by the organisms on the solid media (Osuoha *et al*., 2019). All the isolated and identified organisms were cultured on petri dishes containing Saubourand dextrose agar media supplemented with 1 v/v of olive oil as substrate for lipase. The petri dishes were incubated for 72 h as described earlier and then screened for the formation of zones of clearance around the colonies. Organisms that showed zones of 5 mm and above were selected and used for further studies (Osuoha *et al*., 2019).

Enzyme Production from Selected Strains

Microbial isolates for lipase production were selected based on the magnitude of zones of clearance formed around the colonies. Standard inoculums of the identified microbial isolates were aseptically inoculated into 500 mL conical flasks containing 500 mL of broth productive medium which contain the following: peptone 5 g, yeast extract 5 g, glucose 10 g, $MgSO_4.7H_2O$ (0.6g), $FeSO_4.7H_2O$ (0.4g), $CuSO_4.5H_2O$ (0.4g), glycine (0.4g), $NH_4.SO_4$ (0.6g) and progallol (1 g) for lignin peroxidase production. They were incubated at 25 ºC to 28 ºC on a rotary shaker (150 rpm) for 4 days. The broth was centrifuged to remove viable cells at 3000 rpm for 10 min before used for analysis and purification.

Lignin peroxidase activity

Lignin peroxidase activity was determined by measuring the rate of H_2O_2-dependent oxidation of the substrate pyrogallol to purpurogallin (Egwim *et al*., 2015). The reaction mixture contained 2 mL of Sodium acetate buffer (10 mM) pH 5.0, 0.8 mL of pyrogallol (2 mM) and 0.1 mL of enzyme source. The reaction was initiated through the addition of 0.1 mL of H_2O_2 (0.15 M). The initial absorbance was recorded at 450 nm using a spectrophotometer and the reaction mixture was incubated at 30 ºC for 30 min, after which the final absorbance was recorded at 450 nm (Jhadav *et al*., 2009). Distilled water was used instead of the enzyme source in the blank.

$$\text{Enzyme activity in U/secs} = \frac{\text{Final Absorbance of sample} - \text{Initial Absorbance of sample}}{\text{Time (secs)}}$$

The amount of enzyme needed to oxidize 1 µmol of pyrogallol is defined as one unit of lignin peroxidase. Lignin peroxidase activity in U/mL was extrapolated using the molar coefficient of pyrogallol (2470 $M^{-1}cm^{-1}$).

Purification of Lignin peroxidase enzyme

The crude lignin peroxidase enzyme was purified through ammonium sulfate precipitation, dialysis and Sephadex G-75 column chromatography as described by Osuoha *et al* (2019). During all stages of enzyme purification, enzyme activity and total protein concentration were assayed periodically. Twenty fractions were obtained during the chromatographic separation, and the fractions that had low protein concentration and high enzyme activity were pooled together and used for subsequent experiments (Osuoha *et al*., 2019).

Stabilization studies

The optimum pH for lignin peroxidase activity was established by varying the pH of buffer (3, 3.5, 4, 4.5, 5, 5.5, 6, 6.5, 7) while the influence of temperature on the activity of lignin peroxidase was established by incubating the reaction medium comprising of 2 mL of Sodium acetate buffer (10 mM) pH 5.0, 0.8 mL of pyrogallol (2 mM) and 0.1 mL of enzyme at diverse temperature ranges (20, 25, 30, 35, 40, 45, 50), for 30 min. Other reaction conditions were kept constant and the lignin peroxidase activity was determined as described earlier.

Immobilization of lignin peroxidase on sodium alginate using entrapment technique

The produced purified lignin peroxidase enzyme was immobilized following the protocol reported by Osuoha *et al*. (2019). In brief, sodium alginate (0.1g) was dissolved in 10 mL of distilled water with continuous stirring to obtain sodium-alginate solution. Then exactly 10 mL

of the purified lignin peroxidase enzyme was mixed with the prepared solution for 20 min in a ratio of 1:1. Afterwards, the resultant solution was gradually introduced drop-wise into 50 mL of calcium chloride (100 mM) resulting to the formation of calcium alginate beads. The beads were allowed to harden, and was subsequently rinsed with phosphate buffer and distilled water (Osuoha *et al*., 2019).

Hydrolysis of lignocellulosic biomass using the immobilized lignin peroxidase

Different agro- wastes of lignocellulose origin (plantain pseudo stem waste, pumpkin pod) were used as substrate for lignin peroxidase activity. Other reaction conditions were kept constant as described earlier.

3.0 Results and Discussion

Microorganisms can easily thrive in oil contaminated environments and utilize the hydrocarbon present in the medium as a source of carbon for growth and development because of their chemotactic capacity (Osuoha *et al*., 2019). Oil contaminated environments could harbor some beneficial microorganisms that can be utilized for the production of novel secondary metabolites, hence the proponent for the exploration of this biodiversity in this study. In this study, we isolated and identified ten different microorganisms based on their morphological and macroscopic characteristics. The identified isolates were primarily screened for possible lignin peroxidase production based on the magnitude of the zones the expressed. Three isolates: *Yeast, Trichorderma* sp. and *Micrococcus* were selected among the twelve isolates as demonstrated in (Table 1).

Table 1 Zone of clearance produced around microbial colonies for lignin peroxidase production

S/N	Name of organism	Zone of clearance (mm)
1	*Aspergillus flavus*	3.8
2	Yeast*	11.3
3	*Aspergillus niger*	3.4
4	*Micrococcus lutes**	8.7
5	*Staphylococcus aureus*	3.7
6	*Penicillum* sp.	4.3
7	*Trichorderma* sp*	9.4
8	*Lactobacillus* sp.	2.1
9	*Verticillium* sp.	4.5
10	*Bacilus subtilis*	2.6

**selected for enzyme production*

The expression of zones of clearance around the colonies of microorganism was used by previous authors (Dajanta *et al*., 2009; Roy *et al*., 2014; Osuoha *et al*., 2019) as the initial screening for microbial enzyme production because it has been established to have a direct relationship with enzyme production by the microorganism (Roy *et al*., 2014). The lignin peroxidase enzyme was produced in broth and lignin peroxidase activity was evaluated to corroborate the presence of lignin peroxidase enzyme using pyrogallol as the substrate. After examination of lignin peroxidase activity, the isolate *Yeast, Trichorderma* sp. and *Micrococcus lutes* that revealed the highest lignin peroxidase expression was selected for enzyme production and characterization.

The final screening of the identified isolates was achieved based on the magnitude of the lignin peroxidase activity. Pyrogallol is the prevalent substrate utilized for the evaluation of *in vitro* lignin peroxidase activity (Egwim *et al.*, 2015). In the lignin peroxidase determination assay, lignin peroxidase expressed by *Yeast* demonstrated the highest enzyme activity (Table 2) in comparison to the other organisms. Based on that, it was selected for enzyme purification and further characterization.

Table 2 Final screening for lignin peroxidase production from identified isolates

S/N	Name of organism	Lignin peroxidase activity (U/sec)
1	*Trichorderma* sp.	5.6
2	*Yeast**	8.5
3	*Micrococcus lutes*	4.9

**selected for purification and further characterization*

On the basis of the results obtained during the final screening of lignin peroxidase activity, the lignin peroxidase enzyme expressed by *Yeast* was selected for further characterization. The crude lignin peroxidase enzyme was partially purified using ammonium sulfate precipitation and sephadex G-75. The data recorded during the purification steps are presented in Table 3. The specific activity of lignin peroxidase was initially 1.59 but was observed to improve to significantly 9.83 after purification as demonstrated in Table 3.

From the results in Table 3, the lignin peroxidase enzyme was purified to obtain a purification fold of 2.27 and a total yield of 52.29 %. Furthermore, twenty fractions were obtained during the column chromatographic separation, and the fractions 3, 6, and 16 (Figure 1) which were observed to have low total protein concentration with high lignin peroxidase activity were joined together and used for further characterization (Osuoha *et al.*, 2019).

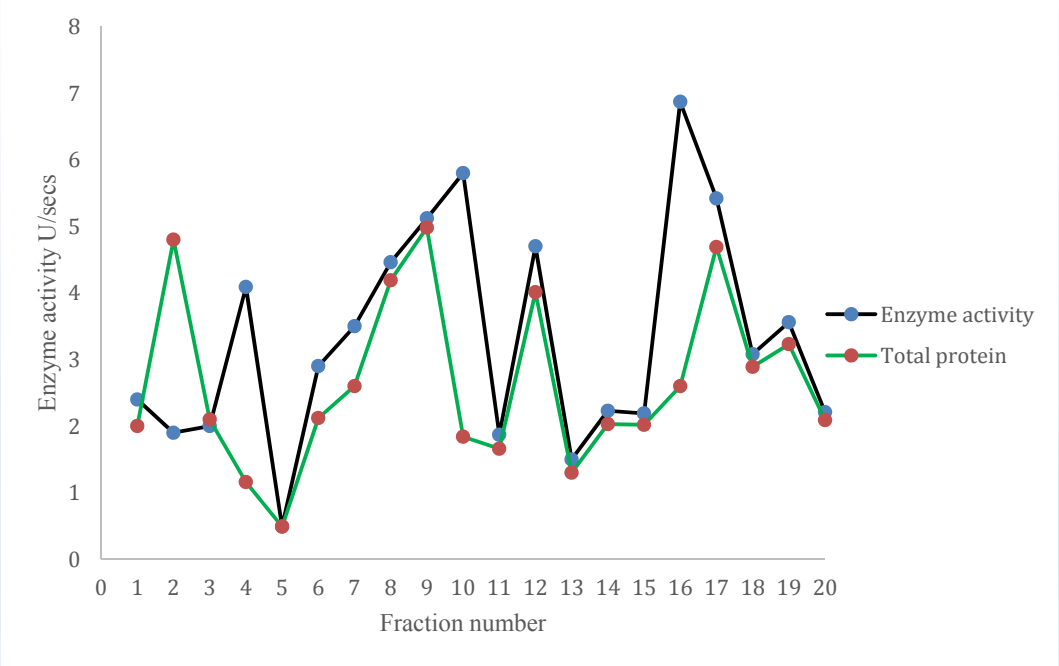

Figure 1: Elution profile of fractions collected during chromatographic separation

When the fractions that were joined together were characterized, we observed that the lignin peroxidase enzyme further purified to get a specific activity of 9.81 with a yield of 33.61 % and purification fold of 6.18.

More so, the expression of enzymes by microorganism has been reported by Osuoha *et al*. (2019) to be regulated by temperature, pH and the availability of enzyme inducers. One of the unique properties for fascinating industrial biotechnological utilization of microbial enzymes is their capacity to retain activity at different environmental conditions. Hence, the optimum conditions for lignin peroxidase activity were optimized. The optimum pH recorded for liginin peroxidase expressed by *Yeast* is 5 (figure 2). The optimum pH of 5 recorded in this work is in consonance with the work of Egwim *et al*. (2015), who also recorded optimum pH of 5 for lignin peroxidase expressed by *Bacillus subtilis*. However, it was vaguely lower than those established by Bibi and Bhatti (2012) who reported the optimum pH of 6.8 for partially purified lignin peroxidase. Microbial enzymes that can resist extreme pH are valuable in several industries (Singhal *et al*., 2012).

Table 3 Purification steps of lignin peroxidase enzyme expressed by *Yeast*

Stages	Volume (mL)	Tyrosinase activity (U/sec)	Protein concentration (mg/mL)	Total enzyme activity	Total Protein Concentration	Specific activity (U/mg)	Purification fold	Yield (%)
Crude enzyme	200	9.4	5.89	1880	1178	1.59	1	100
Ammonium sulphate precipitation	12	11.18	3.08	134.15	36.96	3.62	2.27	52.29
Sephadex G-75 column chromatography	10	19.47	1.98	194.7	19.8	9.83	6.18	33.61

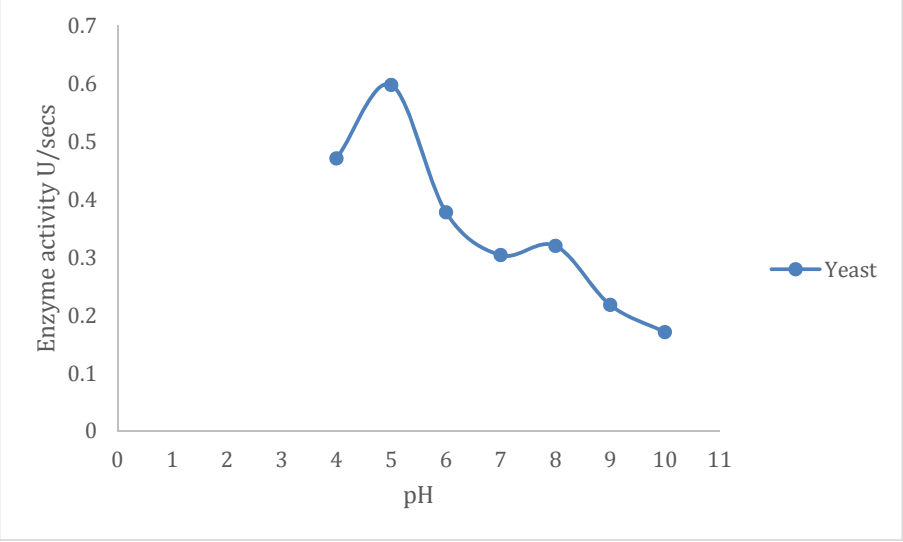

Figure 2 Optimum pH for lignin peroxidase activity

The optimum temperature recorded for lignin peroxidase in this study is in contrast with the report of Ekrem *et al*. (2008) and was slightly lower than those 40 °C and 45 °C reported by Asgher *et al*. (2007) and Bibi and Bhatti (2012) respectively for lignin peroxidase. However, the optimal temperature of 35 °C (figure 3) established in this study is in agreement with those reported by Egwim *et al*. (2015) who reported an optimum temperature of 35 °C for lignin peroxidase.

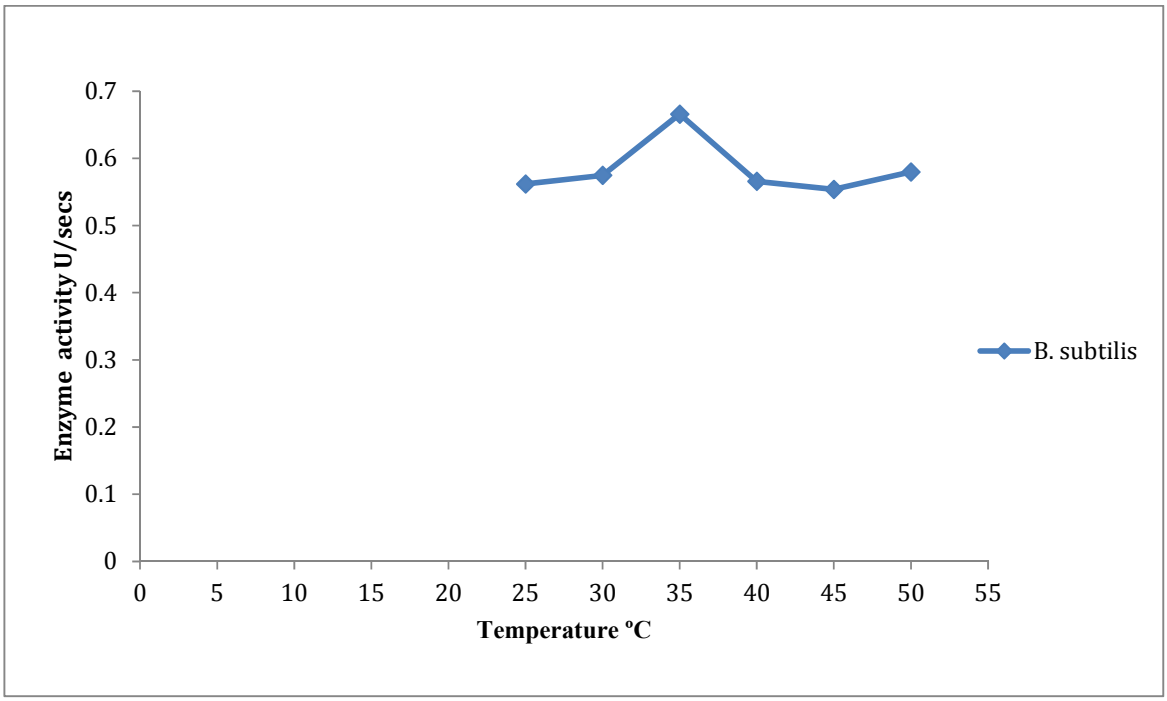

Figure 3 Optimum temperature for lignin peroxidase activity

The immobilization of enzymes provides the enzyme with diverse advantages for its application for different industrial purposes because the stability and catalytic rate of the enzyme is usually improved. Furthermore, the immobilized enzyme can be reused and this alone gives the enzyme a wide advantage when compared to free enzymes. Numerous protocols have been used for lignin peroxidase immobilization viz a viz. adsorption, covalent binding, encapsulation and entrapment. In this study, the produced lignin peroxidase was immobilized via entrapment technique using sodium alginate. The immobilized lignin peroxidase enzyme was characterized and used for the hydrolysis of lignocellulose biomass for enhanced bioethanol production. Immobilized enzymes show improved efficacy regarding the issue of reusability, stability and viability (Bevilaqua *et al*., 2002; Molina *et al*., 2003; Kameda *et al*., 2006). The utilization of available and cost effective support for immobilization is economical and essential for industries (Osuoha *et al*., 2019). For this reason, sodium alginate was used to immobilize the produced lignin peroxidase enzyme in order to improve the efficacy of the enzyme for the hydrolysis of lignocellulosic biomass. In this study, the breakdown of the polysaccharides present in the agro-waste was monitored within 4 h. the agro-wastes utilized for the enzymatic hydrolysis were plantain pseudo stem (PSM) and pumpkin pod (PP). Due to the heterogenous nature of the compounds in the agro-wastes, the had very low reducing sugar content after pretreatment. The pretreatment must have induced the presence of indigenous enzymes that was able to release the sugars in low concentration.

After the introduction of the immobilized lignin peroxidase, the concentration of the reducing sugars increased drastically and was highest after four hours as demonstrated in (Figure 4).

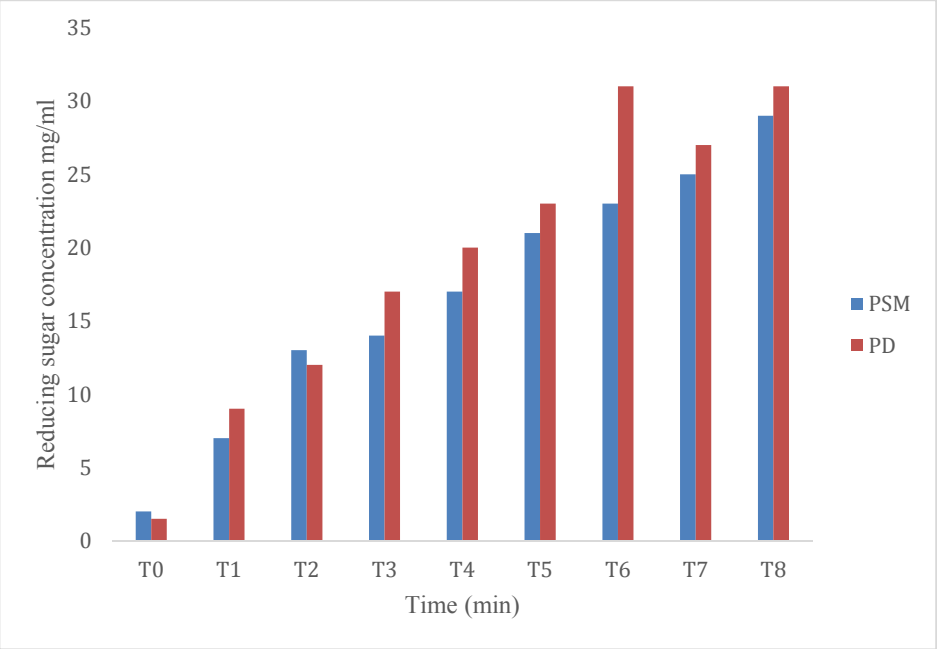

Figure 4: Total reducing sugar content of plantain pseudo-stem waste (PSM) and pumpkin pod waste (PD) before and after addition of immobilized lignin peroxidase, at different time intervals

The high presence of reducing sugars in the agro wastes as a result of the immobilized enzyme highlights the suitability of the enzyme for bioethanol production because the presence of reducing sugars at high concentration will improve the ethanol yield when *Yeast* is introduced into the medium for fermentation. The activity of yeast completes the biochemical process of bioethanol production. Interestingly, after the enzymatic hydrolysis, the immobilized lignin peroxidase still retained activity, which shows that the enzyme can be reused for further hydrolysis of other biomass.

4.0 Conclusion

In conclusion, the microorganism *Yeast* isolated from oil contaminated soil were established to be potent lignin peroxidase enzyme producers. The produced lignin peroxidase demonstrated high catalytic activity and was very stable at diverse temperature and pH. Immobilization of lignin peroxidase in sodium alginate improved the catalytic rate, reusability and stability of the enzyme. The immobilized lignin peroxidase was successful in the hydrolysis of lignocellulose biomass to simple sugars. These findings promote the utilization of indigenous microorganism for local enzyme production and advocate for a cost effective means of local bioethanol production from agro-wastes.

REFERENCES

Agu, I. V. (2017). Monitoring and optimization of biodegradation of organic pollutants in refinery biodisks. A Thesis Submitted to the Department of Microbiology, Faculty of Science, School of Graduate Studies, University of Port Harcourt, Nigeria

Ahmadi AR, Ghoorchian H, Hajihosaini, R. (2010). Determination of the amount of protein and amino acids extracted from the microbial protein (SCP) of lignocellulosic wastes. Pakistan J Biol Sci. 13(8):355–361.

Amadi, P. U., Ifeanacho, M. O. and Agomuo, E. N. (2017). The effects of different heating periods and exclusion of some fermentation conditions on bioethanol production from plantain pseudo-stem waste using the digestive juice of Archachatina marginata, garlic and Saccharomyces cerevisiae. Biofuels, DOI: 10.1080/17597269.2017.1292018

Asgher, M., Asad, M. J. and Bhatti, H. N. (2007). Hyperactivation and thermostabilization of Phanerochaete chrysosporium lignin peroxidase by immobilization in xerogels. *World Journal of Microbiology and Biotechnology*, 23, 525-531.

Balat M. (2011). Production of bioethanol from lignocellulosic materials via the biochemical pathway: A review. Energ Convers Manage, 52:858–875

Bevilaqua, J. V., Freire, M. C, Anna, S. (2002). Phenol removal through combined biological and enzymatic treatments. Braz J Chem Eng, 19 (2): 151–158

Bibi, I. and Bhatti, H. N. (2012). Enhanced biodecolorization of reactive dyes by basidiomycetes under static conditions. *Applied Biochemistry and Biotechnology*, 166 (8), 2078–2090.

Dajanta, K., Wongkham, S., Thirach, P., Baophoeng, P., Apichartsrangkoon, A., Santithum, P., Chukeatirote, E. (2009). Comparative study of proteolyticactivityofprotease-producingbacteriaisolatedfromThua nao. Maejo Int J Sci Technol, 3: 269–276

Egwim, E. C., Kabiru, A. Y. and Tola, A. J. (2015). Partial characterization of lignin peroxidase expressed by bacterial and fungal isolates from termite gut. *Biokemistri*, 27 (1), 33–38

Ekrem, K and Ilhami, G. (2008). Purification and characterization of Peroxidase from cauliflower (Brasica oleracea.L.var.botrytics) buds. *Protein and Peptide Letters*, 15,300-320.

Hammel, K.E. and Cullen, D. (2008). Role of fungal peroxidases in biological ligninolysis. Current Opinion in Plant Biology. Vol. 11, No. 3, (June 2008), pp. 349-55, ISSN 1369-5266.

Kameda, E., Langone, M. A. and Coelho, M. A. (2006). Tyrosinase extract from Agaricus bisporus mushroom and its in natura tissue for specific phenol removal. Environ Technol, 27(11): 1209–1215

Louime C, Uckelmann H. Cellulosic ethanol: securing the planet future energy needs. Int J Mole Sci. 2008;9 (5):838–841.

Molina, L. P., Hiner, A. N. P., Tudela, J., Garcı'a-Ca'novas, F., Rodrı'guezLo'pez, J. N. (2003). Enzymatic removal of phenolsfrom aqueous solution by artichoke (Cynara scolymus L.) extracts. Enzyme Microb Technol, 33(5): 738–742

Mtui G, Nakamura Y. Bioconversion of lignocellulosic waste from selected dumping sites in Dar es Salaam, Tanzania. Biodegradation. 2005;16(6):493–499.

Osuoha, J. O., Abbey, B. W., Egwim, E. C., and Nwaichi, E. O. 2019. Production and Characterization of Tyrosinase Enzyme for Enhanced Treatment of Organic Pollutants in Petroleum Refinery Effluent. Society of Petroleum Engineers. doi:10.2118/198791-MS

Osuoha, J., Iheka, C., Amadi, P., Archibong, I., Adeoti, O. 2018. Distribution and Toxicological Risk Evaluation of Pb, Cd, As and Zn from Surface Soils of Selected Marts in Port Harcourt, Rivers State, Nigeria. *Journal of Chemical Health Risks*, JCHR, 8(4), 255-264

Roy, S., Das I., Munjal, M., Karthik, L., Kumar, G., Kumar, S., Rao, K.V.B. 2014. Isolation and characterization of tyrosinase produced by marine actinobacteria and its application in the removal of phenol from aqueous environment. Front. Biol. 9(4): 306–316

Roy, S., Das I., Munjal, M., Karthik, L., Kumar, G., Kumar, S., Rao, K.V.B. (2014). Isolation and characterization of tyrosinase produced by marine actinobacteria and its application in the removal of phenol from aqueous environment. Front. Biol. 9(4): 306–316.

Singhal, P., Nigam, P. and Vidyarthi, A.S. (2012). Studies on production, characterization and application of microbial alkaline protease. *International Journal of Advanced Biotechnology and Research*, 3, 23-29.

Tien M and Kirk T (1983). Lignin-degrading enzyme from the hymenomycetes Phanerochaete chrysosporium. Science, 22: 661–63.

Wang, W. and Wen, X. (2009). Expression of lignin peroxidase H2 from Phanerochaete chrysosporium by multi-copy recombinant Pichia strain. Journal of Environmental Sciences.21: 218-22

Proceedings of the 49th NSChE Annual Conference
KADA 2019: pp 562-571

P3A-06: POTENTIAL APPLICATION OF AGRO-WASTE (TERMINALIA MANTALY GUM) AS VISCOSIFIER FOR DRILLING MUD FORMULATION

Inemugha O., [a]* Chukwuma F., [a] Uyigue L., [a] Akaranta, O., [b] Ajienka J A.[c]
[a]Department of Chemical Engineering, World Bank Africa Center of Excellence, Center for Oilfield Chemicals Research, University of Port Harcourt, Nigeria.
[b]Department of Industrial Chemistry, World Bank Africa Center of Excellence, Center for Oilfield Chemicals Research, University of Port Harcourt, Nigeria
[c]Department of Petroleum and Gas Engineering, World Bank Africa Center of Excellence, Center for Oilfield Chemicals Research, University of Port Harcourt, Nigeria.
*Email of the Corresponding author: oinemugha@yahoo.com

ABSTRACT
Eco-friendly polymers are used as viscosifier or fluid loss control agent in drilling mud due to positive impact in the environment but have limitations in modifying viscosity in thermal environment. This study reports the potential of using Terminalia mantaly (TM gum) biopolymer as a viscosifier in water based drilling mud. The rheological properties of water-based drilling mud modified with the biopolymer were studied. The effect of concentration and temperature on the rheological properties of mud formulation with this biopolymer was reported. The mud was compared with conventional polymers. Result obtained show that as polymer concentration increased from 0.5v/w to 2v/w, the drilling mud rheological properties; apparent viscosity increased by 23.1%, plastic viscosity increased by 25% and yield point increased by 25.6%. Also, an increase in temperature (299.82 K – 333.15 K) slightly decreased the rheological properties of the mud. The mud was found to obey Hershel Bulkley model. The polymer in the mud had comparable rheological properties with conventional polymers and proved to be a good viscosifier in a water-based mud.

Keywords: max. Rheological properties; Agro Waste; Drilling Mud; Viscosifier

1. INTRODUCTION
Water based drilling mud are still preferred more that than the oil-based mud because of the negative impact of oil based mud on the environment. In recent years, some reports have been conducted on the effective use of water-based mud in drilling fluid (Abduo et al, 2016; Udoh and Okon, 2012; Behnamanhar et al, 2014). A good number of these reports have revealed the uses of polymers in water-based mud to improve viscosity and control fluid loss (Akeem et al., 2018). Experimental examination at several API standards, temperature and pressure are used to explain the practical behaviour of polymers in the mud.

The composition of water based drilling mud contains a base fluid, suspended solid particles and chemicals. The suspended solid particles react chemically with the base fluid to control the properties of the mud (Annis and Smith, 1996). Some of the major additives like polymers are used in water-based mud to improve the rheological properties (apparent viscosity, plastic viscosity, yields point) or control the loss of fluid in the mud. These rheological properties are used to define the flow behaviour of the mud.

The molecular size and shape of polymers are responsible for their ability to absorb water and turn viscous. (Nwosu & Ewulonu, 2014). The viscosity in a solution is influenced by polymer chain entanglement and polymer solvent interaction which can be described by hydrodynamic volume (HDV). HDV of a polymer is determined by the polymer structural parameters such as chain toughness, chain length and polymer-solvent interactions and polymer associations or

repulsions which depend on the concentration, temperature, molecular weight and deformation rate of the polymer (Kong and Ziegler, 2014).

Terminalia mantaly gum is a non-food agricultural waste gotten from the incised of the bark of the tree. It is seen as an agricultural waste because its economic values are less than processing it for human benefit. The aim of this work is to study the effect of the concentration and temperature on the rheological properties of drilling mud formulation with terminalia mantaly gum and compare with mud formulation with conventional polymers such as Xanthan gum and Polyanionic cellulose.

The uses of terminalia mantaly gum in pharmaceutical industries as binding agent in tablet have been studied. Studies have shown that the molecular structure of this water soluble gum contain highly branched polysaccharides consisting of galacturonic, glucuronic and 4-O-methylglucuronic acids, as well as galactose, arabinose, rhamnose, mannose and xylose but neutral sugars and total uronic acid content may vary with different type of Terminalia gum (Oluyemisi et al., 2012; Michael et al., 2017). The physicochemical properties is presented in Table 1.

Table 1. Physicochemical properties of Terminalia mantaly exudate (Michael, Babatunde, and Oluyemisi, 2017).

Parameters	Terminalia mantaly exudates
Particle diameter (μm)	263.10
Angle of repose (°)	57.80
Particle density	1.32
Bulk density (g/cm^3)	0.090
Tapped density (g/cm^3)	0.139
Hausner's ratio	1.54
Carr's index	35
Swelling index	8.4
Water absorption capacity	10.71

2. MATERIALS AND METHODS

2.1 Purification of Terminalia Mantaly Gum

The purification of TM exudates was first reported by (Michael et al., 2017). TM gum was collected from the incised of the tree and allowed to dry for five days. 100.0g of dried gum was washed with deionized water to remove the initial foreign bodies from its body surface. The washed gum was kept in a hot air oven at a temperature of 50^{O}C for 50 hours. The gum was hydrated in a double strength chloroform and water mixture in the ratio of 0.5%:95.5% for 5 days to soften and extract the mucilage. A straining exercise was carried out with use of a white muslin cloth to further remove the remaining viscous mucilage from the gum. Precipitation of the gum was conducted with use of an absolute ethanol for extra purification process. 100ml of Dimethyl ether was used to wash the precipitated gum after that the gum was kept at a temperature of 50^{O}C in a hot air oven for 10 hours. The precipitated gum was pulverized with the use of blender into powdery form. 50.0g of the powdery TM gum was stored in an air tight container.

2.2 Drilling mud formulation

Formulations of water-based mud with few additives were performed in this section. The following additives were used for the water-based drilling mud formulation: Pre-hydrated bentonite, soda Ash, caustic soda, terminalia mantaly gum, xanthan gum, potassium chloride, low viscosity poly anionic cellulose and barite. Table 2 presents drilling mud formulation components and their functions. Water-based mud were formulated according to API American Petroleum Institute) standard.

Table 2 Component of drilling mud formulation

Component	Functions
Deionized water	Base fluid
Pre-hydrated Bentonite	Viscosifier, Filtration Control
Soda Ash	Treat contamination
Caustic Soda	Alkalinity control
Xanthan gum	Viscosifier
Terminalia mantaly gum	-
Potassium chloride	Inhibition Source of K+ion
PAC L	Filtration control
Barite	Weighing material

2.3 Rheological measurement

Rheological properties were performed to describe the flow behavior of the mud at different concentrations and temperature. 22.5 g of bentonite was put in a weighing plate and weighed with electronic balance. The weighed material was added to a 350 ml of deionized water in a mud cup and Hamilton beach mixer was used to stir the suspension for 20 minute in which a spatula was used to scrap the mud on the walls of the cup making sure that proper mixing is carried out. The same procedure was used to prepare four other pre-hydrated muds. Pre-hydrated mud functions better in the presence of salt (Annis and Smith, 1996). Water-based drilling mud formulation was carried by first adding 155.6 ml of pre-hydrated bentonite (PHB) in a mud cup containing 194.4 ml of deionized water and stirred for five minutes using Hamilton beach mixer. Soda Ash and caustic soda of 0.1g each were added to the mixture every five minutes. Xanthan gum, PAC L and TM gum of 1.7g were added in the order presented in Table 3 together with 10.5g of potassium chloride, and 19g of Barite.

Table 3 Different drilling mud formulation

Mud A	Mud B	Mud C
Deionized water	Deionized water	Deionized water
Pre-hydrated Bentonite	Pre-hydrated Bentonite	**Pre-hydrated Bentonite**
Soda Ash	Soda Ash	Soda Ash
Caustic Soda	Caustic Soda	Caustic Soda
Xanthan gum	-	-
-	**Terminalia mantaly gum**	-
Potassium chloride	Potassium chloride	Potassium chloride
PAC L	-	-
Barite	Barite	Barite

Rheological properties were calculated from 600 and 300 rpm readings using the following equations 1, 2 and 3 from API Specification for drilling fluid material.

Apparent Viscosity (*AP*) = ½ θ600 (1)

Plastic Viscosity (*PV*) = θ600 – θ300 (2)
Yield point (YP) = θ300 – PV (3)

where,
Apparent Viscosity in equation (1) is measured in centipoise (cp)
Plastic Viscosity in equation (2) is measured in centipoise (cp)
Yield Point or *Yield Stress* in equation (3) is measured in lb/100ft^2
θ600 is the dial reading at 600 rpm and θ300 is the dial reading at 300 rpm

2.4 Shear stress and shear rate

Shear stress and shear rate relationship data obtained were described using Bingham plastic model and power law model and Herschel Bulkley mode;l

Bingham plastic model
The Bingham model is a two parameter model used to describe flow characteristics in many types of muds. This model can be expressed mathematically as;

$$\tau = \tau_o + \mu_p \gamma \quad (4)$$

where, τ is the shear stress in lb/100ft^2, τ_o is the yield point with the unit lb/100ft^2, μ_p is the plastic viscosity in (centipoise (cp)) and the γ is the shear rate in sec^{-1} (Per second).
Power law model

The Power law model or Ostwald-De-Weale model is another two parameter model that are used to describe fluids with pseudo-plastic behavior in which the relationship between the shear stress and shear rate of a fluid is easily presented;

$$\tau = K\gamma^n \quad (5)$$

where, K and n are consistency index and flow indices respectively, τ is the shear stress and γ is the shear rate in sec^{-1}. The logarithm of the equation is obtained by the following;

$$\log \tau = \log K + n \log \gamma \quad (6)$$

From the equation, n = slope and K = intercept

Herschel-Bulkley Model
The Herschel-Bulkley describes the behaviour of pseudo-plastic fluids using three parameter model

$$\tau = \tau_o + K\gamma^n \quad (7)$$

where, τ is the shear stress, τ_o is the yield stress, K is the consistency index, γ is the shear rate, n and is the flow index.

2.5 Rheology Test on Temperature

Mud formulation with TM gum was subjected to rheology test for different concentration (0.5g, 1g, 1.5g, 2g) in the mud. The mud sample of each concentration was poured into the

viscometer cup to the mark inscribed inside the cup. The viscometer cup was kept inside a thermocouple and placed on the viscometer stand and lifted to immerse the rotating sleeve. The thermometer was inserted into the viscometer cup allowed to heat up to the specified temperature. Thereafter, the respective dial reading for each temperature was recorded. At every concentration, rheology test was conducted for different temperatures (299.82 K – 333.15 K)

3 RESULTS AND DISCUSSION

3.1 Rheological Characterization

The shear stress and shear rate plot is presented in Figure 1. From the figure, there was an initial high stress which later reduced as the shear increased. This type of behavior indicates a pseudo-plastic fluid behavior described by the Herschel Bulkley model. Fluids that allow initial stress to kick-start the flow but less shear as it increases are described by Herschel-Bulkley (Nwosu and Ewulonu, 2014). Equation 7 was used to fit in the experimental data. The result achieved from Figure1 is in agreement with Khalil and Jan, 2012. As TM gum increased, the yield stress of the drilling mud also increased with an increase in the resistance to flow. An increase in shear stress increased the yield stress with concentration which resulted in breaking the gel structure of the mud before flow started.

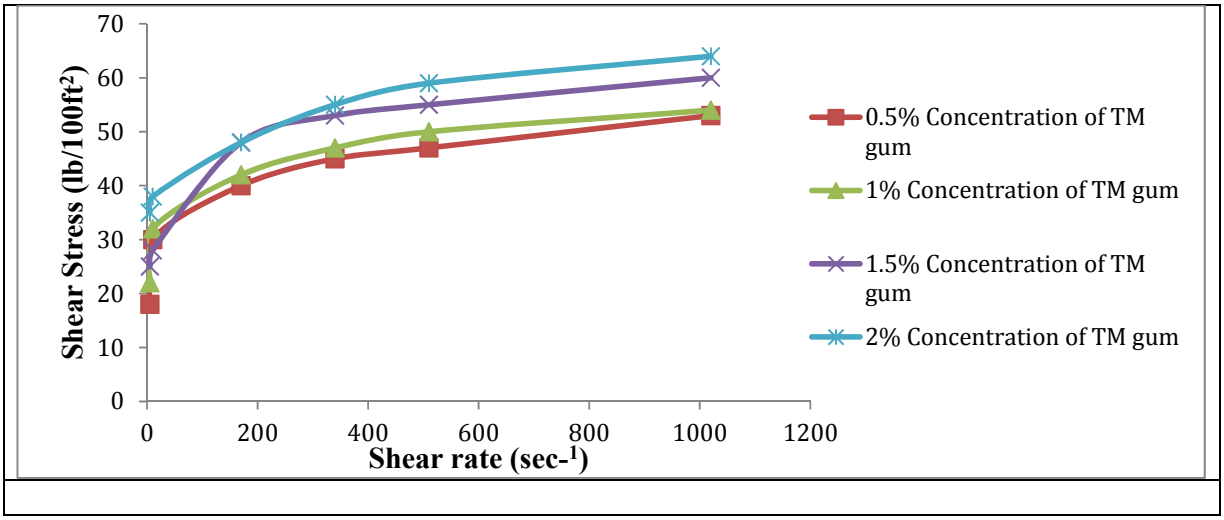

Figure1 Shear stress flow behavior for concentration of TM gum in Drilling mud

Table 3 Rheological Properties of Water Based Drilling fluid with TM gum

Concentrations of TM gum	**0.5 g**	**1 g**	**1.5 g**	**2 g**
Apparent Viscosity (cp)	26	27	30	32
Plastic Viscosity (cp)	4	4	5	5
Yield Point (lb/100ft^2)	43	46	50	54
Flow index, n	0.19	0.14	0.10	0.24
Consistency index, k	12.53	20.37	17.69	6.75

3.2 Effect of Concentration of TM gum

Drilling mud rheological properties were studied on drilling mud as a function concentration of the TM gum. TM gum was the additive used to improve the properties of the mud. From the result shown in Figure2, it can be seen that the apparent viscosity, plastic viscosity, and the yield point of the drilling mud gradually increased by 23.1%, 25%, and 25.6% respectively with increase in concentration of the TM gum in the mud. As the concentration of the mud increased, the rheological properties of the drilling mud increased slowly showing concentration-dependence behavior which is mostly attributed to the chain entanglement density and gel formation as polymer network is formed in the drilling mud.

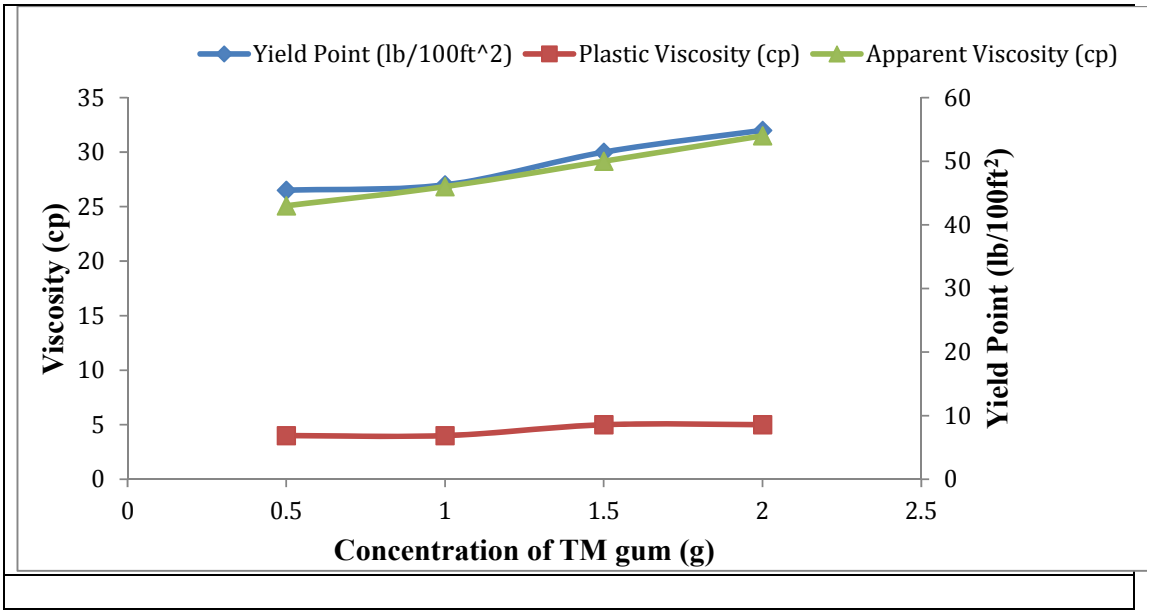

Figure 2 Rheological Properties as function TM Concentration of Drilling Mud

3.3 Effect of Temperature on the Rheological properties of TM gum

The studies of the effect of temperature on the rheological properties of TM gum in the drilling mud were presented in Figure3 to 5. The rheological properties slowly decreased as temperature increased. This could be attributed to the degradation of the polymer in the mud as heat is applied. The degradation of the polymer caused the clay platelets to dehydrate and link each other so closely thereby making the attractive forces dominate resulting in a state of dispersion with edge to face contacts of the platelets (Makinde et al., 2010). Therefore, an increase in temperature increased the intermolecular distanced of the molecules of the polymers in the mud which lead to a state of degradation and flocculation of clay platelets resulting to decreased flow properties. In Figure 3, the apparent viscosity of higher polymer concentration decreased slowly with increase in temperature showing favorable thermal stability. In Figure 4, Sharp decrease in the plastic viscosity was observed with different concentration as temperature increased while in Figure 5, a slow decrease in yield was observed as temperature increased also showing encouraging resistance in thermal environment.

.

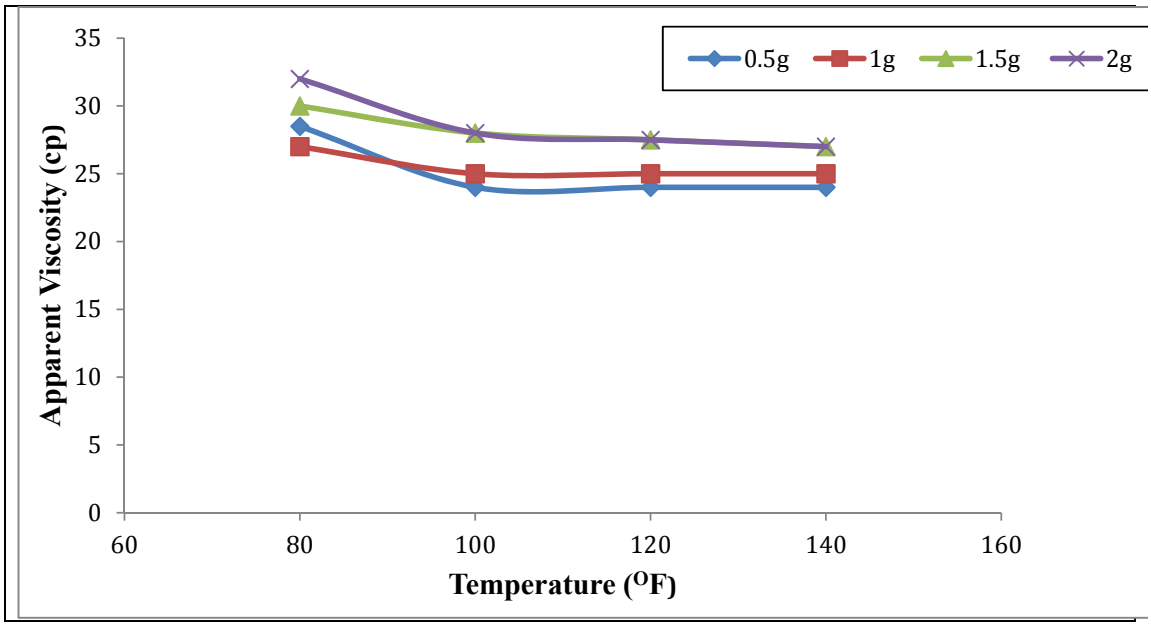

Figure 3 Effect of Temperature on the Apparent Viscosity of TM gum Drilling Mud

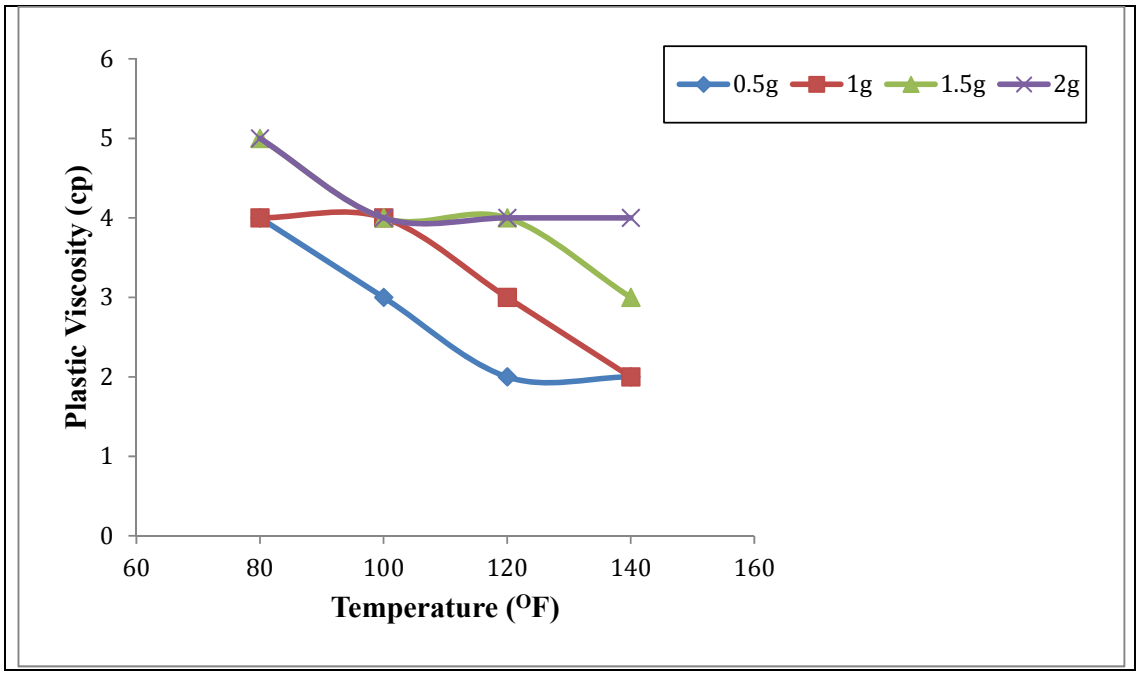

Figure 4 Effect of Temperature on the Plastic viscosity of TM gum Drilling Mud

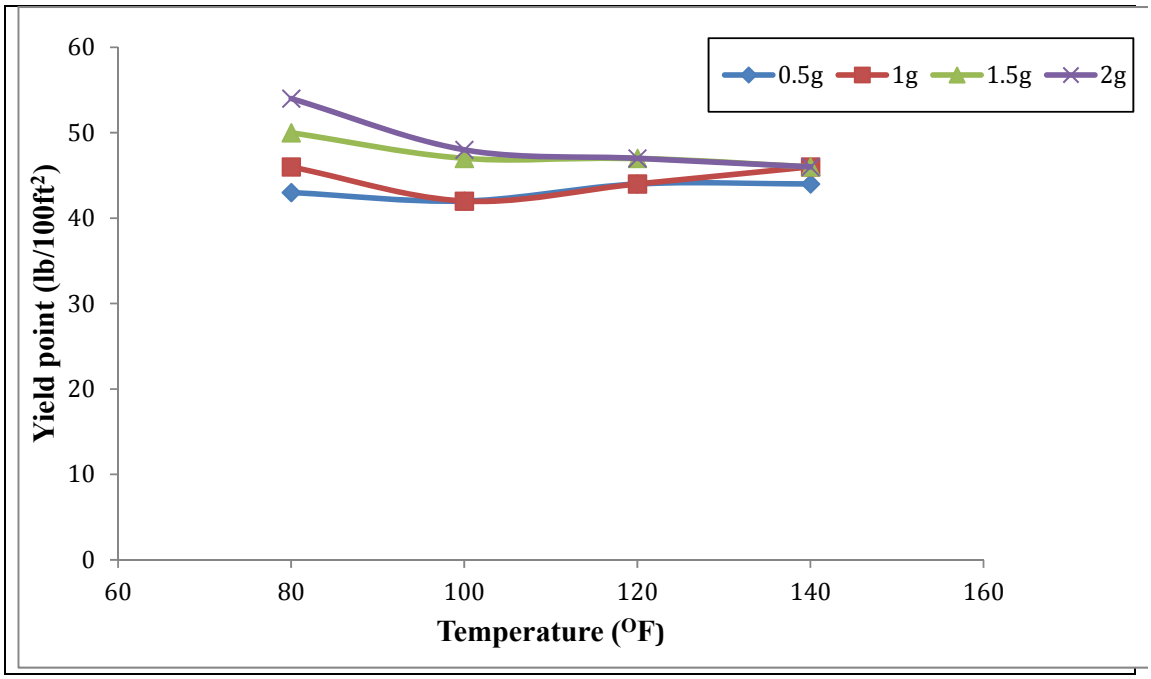

Figure 5 Effect of Temperature on the Yield point of TM Drilling Mud

3.4 Effect of TM gum on the Rheological Properties of the Mud

In this section, the rheological properties of three different muds were studied. Mud A, Mud B and Mud C. Mud A was prepared with Xanthan gum as the viscosifier and PAC L as the fluid control agent. Mud B was prepared with only Terminalia mantaly gum. This agricultural waste was used as a viscosifier and fluid loss control agent while Mud C was prepared with only pre-hydrated bentonite. From Figure 6, Mud B had better rheological properties than Mud A and Mud C. Terminalia mantaly gum used for the formulation of Mud B acted as a good viscosifier and fluid control agent. It was observed that Mud B had a lower plastic viscosity and a higher yield point. In drilling, the plastic viscosity is a vital function of the viscosity of the liquid and volume of solids found in the mud. It tells how the mud behaves around the bit. Higher plastic viscosity is never desirable because an increase in plastic viscosity can increase pressure drop down the drill string which can hinder the rate of flow and offset any increase in lifting ability. Higher yield point favors good hole cleaning and pressure control capability especially during the initial stages of drilling operation.

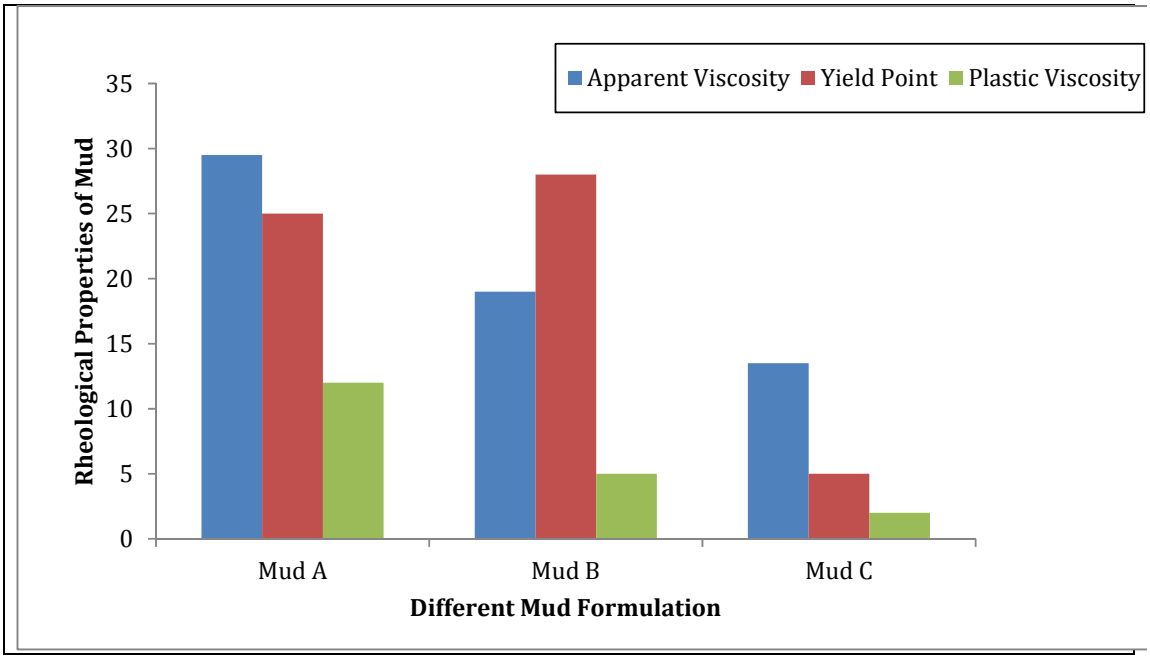

Figure 6: Rheological Properties of Three (Mud A, Mud B and Mud C) Different Drilling Mud

4.0 CONCLUSIONS

This work has demonstrated the potential use of terminalia mantaly biopolymer in the formulation of water based drilling mud. Drilling mud formulation with Terminalia mantaly gum exhibited shear thinning behavior and obeyed the Herschel Bulkley model. The rheological properties increased with increase in polymer concentration in the mud. The effect of temperature on the apparent viscosity and yield point of the mud initially decreased sharply and gained slight thermal stability as temperature increased. The new Terminalia mantaly gum drilling mud acted as a better viscosifier owing to the negative charges it possesses with good rheological properties. Comparing drilling mud with terminalia mantaly gum with conventional polymers confirms the potential use of Terminalia mantaly gum as a good viscosifier in water-based drilling mud.

REFERENCES

Abduoa, M. I., Dahab, A. S., Abuseda, H., Abdulaziz, A. M., and Elhossieny, M. S. (2016). Comparative study of using water-based mud containing multiwall carbon nanotubes versus oil-based mud in HPHT fields. *Egyptian Journal of Petroleum*, 25(4), 459-464.

Akeem, O. A., Olalekan, S. T., Salam, K. K., Omoloa, J. M., and Gafar, A. O. (2018). Potential evaluation and optimization of natural biopolymers in water-based drilling mud. *Journal of Chemical and Petroleum Engineering*, 52(1), 1-12.

Alsabagh, A. M., Abduoa, M. I., Khalil, A. A., Hamed, H. E., and Aboulrous, A. A. (2014). Investigation of some locally water-soluble natural polymers as circulation loss control agents during oil fields drilling. *Egyptian Journal of Petroleum*, 23(1), 27-34.

Annis, M. R., and Smith, M.V. (1996). Drilling Fluid Technology. *Revised edition, USA: EXXON COMPANY*.

Behnamanhar, H., Noorbakhsh, S. S., and Maghsoudloojafari, H. (2014). Environmentally friendly water-based drilling fluid for drilling of water-sensitive formations. *Journal of Petroleum and Gas Exploration Research*, 4(4), 60-71.

Collins, N., Kharitonov, A., Harliburton, C. T., Mitchell, R., Ahmadishin, F., and Tatneft, I. G. (2011). First application of new polymer viscosifier with a non-damaging drill-in fluid. *American Association of Drilling Engineers*, *National Technical Conference and Exhibition*, *Houston, Texas*, 1-8

Khalil, M., and Jan B. M. (2012). Herschel-Bulkley rheological parameters of a novel environmentally friendly lightweight biopolymer drilling fluid from xanthan gum and starch. *Journal of Applied Polymer Science*, 124, (1), 595-606.

Kong, L., and Ziegler, G. R. (2014). Molecular Entanglement and Electrospinnability of Biopolymers*. Journal of Visual Experiment*, (91), 1-7.

Makinde, F. A., Adejumo, A. D., Ako, C. T., and Efeovbokhan, V. E. (2011). Modeling the effects of temperature and aging time on the rheological properties of drilling fluids. *Journal of Petroleum and Coal,* 53(3), 167-182.

Michael, A. O., Babatunde, M. O., and Oluyemisi, A. B. (2017). Native and microwave-modified Terminalia mantaly gums as sustained-release and bioadhesive excipients in naproxen matrix tablet formulations. *Polymers in Medicine*, 47(1), 35-42.

Nwosu, U. O., and Ewulonu, C. M. (2014). Rheological Behavior of Eco-friendly Drilling Fluids from Biopolymers. *Journal of Polymer and Biopolymer Physics Chemistry*, 2(3), 50-54.

Oluyemisi, B. A., Oluwatoyin, O. A., Vivek, S. R., and Ruchita, K. (2012). Terminalia Gum as a Directly Compressible Excipient for Controlled Drug. *AAPS Pharmaceutical Science Technology*, 13(1), 16-23.

Udoh, F. D., Okon, A. N. (2012). Formulation of Water-based Drilling Fluid Using Local Materials. *Asian Journal for Microbial Biotech Environmental Science*, 14(2), 167-174.

Proceedings of the 49th NSChE Annual Conference
KADA 2019: pp 572-578

P3B-01: STUDY ON THE EFFECT OF PARTICLE SIZE AND CONTACT TIME ON EXTRACTION OF OLEORESIN FROM GINGER

Shehu U. H.*, Ameh A.O. and Olakunle M.S.
*Chemical Engineering Department, Kaduna Polytechnic, Kaduna
Chemical engineering Department, Ahmadu Bello University, Zaria
*Corresponding author: habibashehu016@gmail.com /08028619921

ABSTRACT
The effect of particle size and extraction time on the solvent extraction of ginger oleoresin was investigated to obtain data for process control and optimization. The extraction was carried out using ethanol as solvent at a constant temperature of 40°C and solid-liquid ratio of 10g/100ml and various extraction times of 10, 20, 30, 40, 50, 60, and 70 minutes. Ginger particle sizes of 1200, 850, 600, 425 and 250 microns were considered. Experimental data generated were fitted into Patricelli's model equation to determine the kinetics parameters. It was found out that, for each particle size the yield of oleoresin increases with increasing extraction time up to 70mins after which the yield remained constant. Also, the maximum oleoresin yield was found to be dependent on the particle size; smaller particle size range of 250 microns favored greater yield (10.4% at 70min). These results were reflected in the constants of the Patricelli equation (K and τ). The optimum k and τ values were 10.29 and 6.315 respectively. Fitting the data to the Patricelli's model indicated a goodfit of the model as represented by the R^2 value of 0.9622.

Keywords: Extraction, Ginger, Particle size, Oleoresin, Modeling.

INTRODUCTION
Zingiber officinale Roscoe, commonly known as ginger, is a member of *Zingeberaceae* family. Ginger is the underground rhizome of the ginger plant with a firm, striated texture. Most *Zingiberaceae* family spices are fibrous rooted perennial herb which is widely cultivated in some tropical regions such as India, China, Nigeria, Australia and Jamaica (Bartley and Jacobs, 2000).

Ginger species possesses aromatic properties. There are two extracts of ginger, essential oil which varies as 0.8–4.2% and oleoresin in the range of about 5-8% depending on its origin habitat and agronomic treatment of culture (Azian *et al.,* 2001). The pungent taste of ginger rhizome is due to its oleoresin content, which is an oily viscous liquid containing oxymethyl phenol like shagoal, zingerone and gingerol that are probably responsible for its antioxidant property (Mbaeyi-Nwaoha *et al.,* 2013).

Oleoresin compounds, such as *6-gingerol* and its derivatives obtained from the root of ginger possess high antioxidant activity (Stoilova *et al.,* 2007). The antioxidants are micronutrients that have gained interest in recent years due to their ability to neutralize the actions of free radicals (Carenas and Packer, 1996). Mbaeyi-Nwaoha *et al.,* (2013) states that free radicals are potentially harmful products generated during a number of natural processes in the body, and are associated with the ageing of cells and tissues. Ginger oleoresin has widely reproduced the character of the ginger and ginger oil fully. It contains the volatile and the non-volatile constituents of the ginger. It can replace whole ground ginger without impairing any flavor and aroma characteristics. Ginger oleoresin has widespread uses as a flavoring agent in foods, beverages, and medicines. The increased prominence of oleoresins over natural spices is due to increased economy in use, more uniform flavor and concentration, and lack of microbial contamination.

Solvent extraction is a widely employed technique designed to separate soluble polyphenols from plant tissue using a solvent. Commonly used solvents for extraction of oleoresin from plant tissue are water, ethanol, methanol; acetone etc. (Jakopic *et al.,* 2009). Research has shown that there is a scientific curiosity and certain popularity with regard to screening essential oils and extracts from plants to detect natural compounds characteristics and antioxidant activity as well as antimicrobial activity, used medicinally all over the world (Hassan *et al.*, 2012).

Although many studies have been carried-out on the determination of the active compounds of ginger and on the development and implementation of the different operating conditions for ginger oleoresin recovery, little attention seems to have been given to the optimization of the various extraction variables. This gives the motivation for the present study; to focus on ginger which is abundant in Nigeria and also considering its benefits to the pharmaceutical and food industry. Hence, the aim of this research is to determine the effect of particle size and extraction time on the extraction yield of oleoresin from ginger rhizome and also modelling of prediction equation for the process using principle of curve fitting with the aid Matlab software.

METHODOLOGY

The ginger rhizomes used for the extraction of oleoresin was sourced from Kachia local government in southern part of Kaduna state, Nigeria. The samples were identified at Biological Science Department of Ahmadu Bello University (ABU) Zaria. Proximate analysis was carried out on the ginger rhizome at Agronomy Department ABU Zaria. Other materials used such as distilled water, ethanol, and ethyl acetate were sourced from Chemical Engineering Department of ABU Zaria, Nigeria.

Ginger Pre-treatment

Ginger rhizomes were washed thoroughly with tap water to remove sand and dirt. The ginger was cut into tiny pieces using a knife. All samples so prepared were then dried in an air-circulating oven at a temperature of 40 ^{0}C in the laboratory and grinded manually into power, using a grinder and screened into different particle size ranges using a set of sieves (1200, 850, 650, 425 and 250µm). The grinded samples were stored in an air-tight polythene bag as stock sample in a cool dry place until required for extraction.

Extraction of Ginger Oleoresin

Ten grams (10g) of 1200µm powdered ginger was placed directly into a round bottom flask containing 100ml of the solvent (95% ethanol); the round bottom flask was placed in a hot water bath which sat on a combined hot plate and stirrer. The solvent and ginger was stirred throughout the extraction time of 10min. The temperature was kept constant at 40±2^{o}C and the system was operated at atmospheric pressure. After the extraction, the solvent was recovered by distillation method using a soxhlet extractor to obtain a solvent free oleoresin. The recovered oleoresin was then cooled and weighed. The same procedure was repeated using various time of 20, 30, 40, 50, 60 and 70 minutes. The extraction was carried out for other particle size ranges 850, 600, 425 and 250µm of the ginger powder using the same conditions and procedure to study the effect of particle size.

Kinetic Studies

The mass transfer of oleoresin during solvent extraction can be described by a first order model (Ozkal *et al.,* 2005). The kinetics model equation is:

$$\tau \frac{dY}{dt} = (K - Y) \qquad \text{(i)}$$

Where;
Y = g of oleoresin extracted per 100 g dry ginger (initially at time, t= 0, Y = 0)
K = the maximum g of oleoresin which can be extracted in the process per 100 g dry ginger
t = the extraction time (min), and τ is the time constant for the process (min).
This model is a lumped form of Fick's Law of Diffusion (Halim *et al.,* 2012). Solving the differential equation gives:

$$Y(t) = K[1 - e^{-\frac{t}{\tau}}] \qquad \text{(ii)}$$

The maximum yield (K) and time constant (τ) depend on the solvent used and the ratio (R, amount of solvent used per g dry ginger used). This equation matches Patricelli *et al.* (1979) model without a washing stage.

An algorithm in Matlab software was used to write an algorithm to curve fit the experimental data collected into the theoretical models stated in Equation ii. From which the curve fitted was then subjected to statistical analysis, the validity and accuracy of the model developed were examined using R-squared and Adjusted R-squared value. This was done for different sets of experimental data collected for the different particles sizes.

The oleoresin extracted was then characterized using FTIR (ABB3000) at the Center for Mineral Research and Development, Kaduna Polytechnic, Kaduna, Nigeria.

RESULTS AND DISCUSSIONS

The ginger was identified as *zingeber officinale* (card number: 2261). Proximate analysis of the ginger rhizome is as shown in Table 1.

Table 1: Proximate Analysis of Dry Ginger Rhizome

Nutrients	Composition (%)
Moisture content	6.41
Crude Carbohydrate	59.76
Dietary fiber	9.74
Crude Protein	9.82
Crude Fat	8.81
Ash	5.46

Values are average of three replications.

The proximate composition of the dry ginger rhizome (Table 1) compares favourably with those in literature, with a slight variation. These variations could actually be attributed to the species of the ginger, season, climate and storage condition. The dry ginger sample has a high total carbohydrates content of 59.76% and crude fiber content of 9.74%. It showed a moisture content of 6.41% which is lower compared to that obtained by El-Ghorab *et.al.* (2010), but closely similar to that obtained by Otunola *et al.* (2010). It has a protein content of 9.82%, the protein content is very important from the nutritional point of view. The works of Mbaeyi-Nwaoha *et al*. (2013) and Otunola *et al.* (2010) showed a relatively low protein content compared to this value, while some others Latona *et al* (2012) showed higher value. It should be noted that the low moisture content of the ginger samples significantly raises the other constituents. The crude fat content of the dry ginger sample was 8.81%, whereas the

ash content is 5.46%, which is comparable to values obtained in literature 6.1% (El-Ghorab *et al*. 2010).

Effects of Extraction Time and Particle Size on Oleoresin Extraction from Ginger

The effect of particle size (Y) and extraction time (x) were evaluated with the aid of the statistical plot represented on Figure 1 which shows the relationship between various variables.

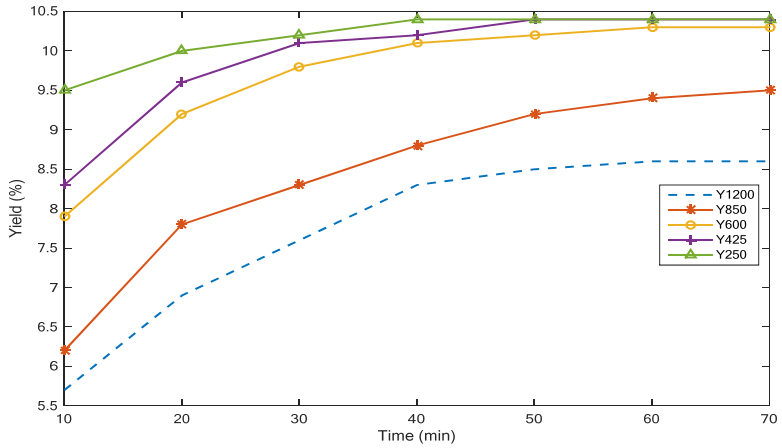

Figure 1: Plot of Yield against Time

The extraction curves in Figure 1 indicated the exponential increase of extraction rate for all the examined particle classes (range 250 to 1200 microns). The highest yield of extracted oleoresin was obtained during extraction from the smallest particle class (250 microns) in the amount of 10.4% at 70mins; this could be attributed due to the large surface area possessed by the smaller particle size. The lowest yield of 8.6% was obtained in the case of the biggest particle size class (1200-850 microns) at 70mins. It was observed that the yield of 5.7, 6.2, 7.9, 8.3 and 9.5% were obtained for 1200, 850, 600, 425 and 250 microns respectively after 10 minutes of extraction which confirms that the lower particle size class of 250 microns gave a highest yield.

In addition to that, high initial rate of oleoresin extraction (first 10 min) can be seen from extraction curves, followed by slower extraction rate, and asymptotically approaching the equilibrium concentration. This could be due to the concentration gradient of solute and the viscosity of the solvent.

The results of the coefficients of the model developed, R-squared value and Adjusted R-squared value from the model validation analysis carried-out in Matlab are presented on Table 2.

Table 2: Model Parameters for Different Particle Size of Ginger using Ethanol as solvent

Particle size (microns)	K	τ	R-Square	Adj. R-Square
1200	8.457	10.22	0.9259	0.9111
850	9.192	9.851	0.9309	0.9171
600	9.686	7.03	0.9437	0.9324
425	10.29	6.315	0.9622	0.9546
250	10.32	4.031	0.8519	0.8223

From the results presented in Table 2, it can be deduced that the K (the maximum g of oleoresin which can be extracted in the process per 100 g dry ginger) decreases as the particle sizes of the ginger increase which agrees with curve presented on Figure 2 (showing the effect of particle size on yield). It was found that 250 micron recorded the highest maximum extractable oleoresin from a 100 g of dry ginger as 10.32 while 1200 micron recorded the least as 8.457 oleoresin per 100 g of dry ginger.

Also, it was deduced from Table 2 that the higher the particle size of the ginger, the larger the time constant (τ) becomes. That is, as the particle size rises from 250, 425, 600, 850 to 1200 microns, their time constant values increases from 4.032, 6.315, 7.030, 9.851, to 10.22 minutes respectively. From which it was concluded that 1200 microns recorded the highest time constant while 250 microns recorded the least time constant.
Moreover, Table 2 shows that the extraction yield model for 1200, 850, 600, 425 and 250 microns shows R-squared values of 92.6, 93.1, 94.4, 96.2 and 85.2% while the adjusted R-squared values were 91.1, 91.7, 93.2, 95.5 and 82.23% respectively.

Based on the R-squared and adjusted R-squared values in Table 2, it can be concluded that model for the extraction of oleoresin from 425 microns ginger will give a best prediction and its output will be reliable due to its high R-squared and adjust R-squared value recorded as 96.2 and 95.5 % respectively. Although, other models for 1200, 850 and 600 microns will also give good predictions but it cannot be compared to that of 425 microns.

FTIR Analysis
The characteristic absorption bands in the infrared absorption spectrum of gingerol is shown in Figure 2 and a summary of the description of the characteristic IR bands for gingerol are described in Table 3. Similar results were reported by Purnomo *et al*. (2010) and Jayanudin and Rochmadi (2017) on FTIR analysis of ginger extract.

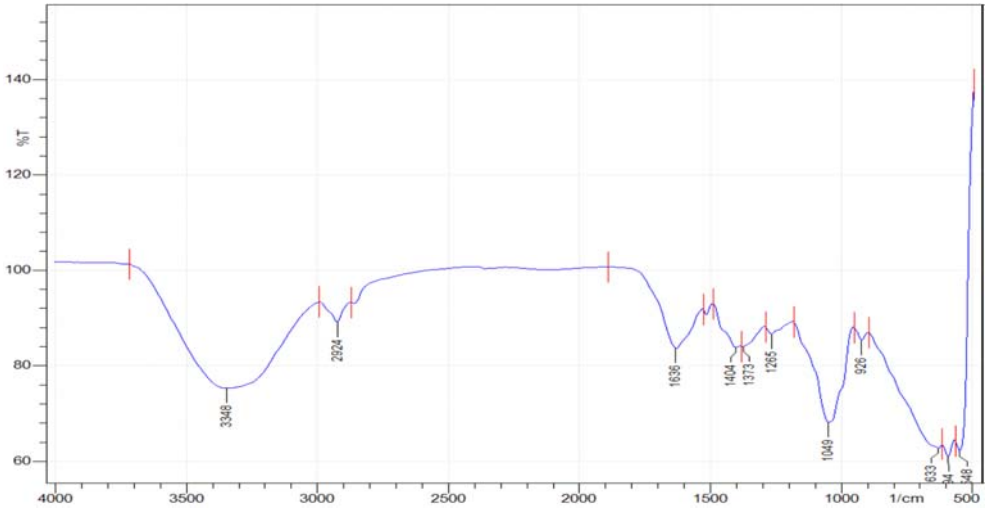

Figure 2: FTIR spectra of the ginger oleoresin.

CONCLUSION
This work showed that for each particle size, yield of oleoresin increases with increasing extraction time up to an optimum time after which the yield remained constant. Also, the

optimum extraction was found to increase with decreasing particle size: thus, the Patricelli's parameter K was found to be particle size dependent, i.e. smaller particle size range (< 250 microns) favored greater yield with K-value of 10.32 and a lower **τ** value of 4.031, the kinetics of extraction showed a good fit of the model used with an R^2 value of 0.9622. The kinetics of the extraction showed a good fit to the Patricelli equation.

Table 3: Functional groups of ginger oleoresin analyzed using FTIR

No.	Wavelength (cm^{-1})	Vibration type	Functional groups
1	633	O-H bend	Phenol
2	926	=C-H bend	Alkene
3	1265, 1049	C-O stretch	Ether (R-O-R)
5	1373	C-O bend	Alkanes
6	1404	CH stretch	C=C aromatic
7	1636	C=O Stretch	Ketones
8	2924	OH stretch; H-bonded	Carboxylic acid (RCOOH)
9	3348	OH stretch; H-bonded	OH

REFERENCES

Azian N.M., Sazalina M. S. and Rizan H. M. R.(2001). Essential Oil and Active Ingredients Extraction from Ginger Plants*. Annual Progress Report Centre of Lipids Engineering and Applied Research.* Kuala Lumpur, Malaysia.

Bartley J.P. and Jacobs A.L.(2000). Effects of drying on flavor compounds in Australian- grown ginger (Zingiber officinale). *J. Sci. Food Agric. (80)*: 209–215.

Carenas E, Packer L (1996). *Hand Book of Antioxidants.* Plenum, New York. 127-131.

El-Ghorab, A.H., Nauman, M., Anjum, F.M., Hussain, S. and Nadeem, M. (2010). A Comparative Study on Chemical Composition and Antioxidant Activity of Ginger (*Zingiber officinale*) and Cumin (*Cuminum cyminum*). *J. Agric. Food Chem. 2010, (58)*: 8231–8237 8231, DOI:10.1021/jf101202x

Hasan H.A., Rasheed R AM, Abd Razik B.M, Rasool Hassan B.A (2012). Chemical Composition and Antimicrobial Activity of the Crude Extracts Isolated from Zingiber Officinale by Different Solvents. *Pharmaceut Anal Acta. (3)*: 184.

Jakopič, J., Veberič, R., Štampar, F. (2009): Extraction of phenolic compounds from green walnut fruits in different solvents. *Acta Agriculturae Slovenica. 93 (1)*:11 – 15.

Jayanudin J. and Rochmadi R. (2017) Encapsulation of red ginger oleoresin (*Zingiber Officinale Var Rubrum*) with chitosan as wall material, *International Journal of Pharmacy and Pharmaceutical Sciences. 9(8)*: 29 – 34.

Latona, D.F., Oyeleke, G.O. and Olayiwola, O.A. (2012). Chemical Analysis of Ginger Root. *IOSR Journal of Applied Chemistry*. *1(1)*: 47-49.

Mbaeyi-Nwaoha, I.E., Okafor, G.I. and Apochi, O.V., (2013). Production of oleoresin from ginger (*Zingiber officinale*) peels and evaluation of its antimicrobial and antioxidative properties, *African Journal of Microbiology Research*, *7(42):* 4981-4989, DOI: 10.5897/AJMR2013.6125

Otunola, G.A., Oloyede, O.B., Oladiji, A.T. and Afolayan, A.J. (2010). Comparative analysis of the chemical composition of three spices – Allium sativum L., Zingiber officinale Rosc. And Capsicum frutescens L. commonly consumed in Nigeria. *African Journal of Biotechnology, 9(41)*: 6927-6931. DOI: 10.5897/AJB10.183.

Ozkal S.G., Yener M.E., Bayindirli L. (2005). Mass Transfer Modeling of Apricot Kernel Oil Extraction. *LWT-Food Sci. Technol, (38)*: 611.

Patricelli A., Assogna A., Casalaina A., Emmi E., Sodini G. (1979), "Fattori che influenzano l'estrazoine dei lipidi da semi decorticate di girasole", *La Rivista Italiana Delle Sostanze Grasse, (56)*: 136-142.

Purnomo, H., Jaya, F. and Widjanarko, S. B. (2010) The effects of type and time of thermal processing on ginger (*Zingiber officinale* Roscoe) rhizome antioxidant compounds and its quality, *International Food Research Journal, (17)*: 335-347.

Stoilova I., Krastanov A., Stoyanova A., Denev P. and Gargova S., (2007). Antioxidant Activity of a Ginger Extract *(Zingeber Officinale). Food Chem, (102)*: 764—770.

Proceedings of the 49th NSChE Annual Conference
KADA 2019: pp 579-586

P3B-02: OPTIMIZATION OF GINGER OLEORESIN YIELD USING BOX-BEHNKEN DESIGN OF EXPERIMENT

Shehu U. H.*, Ameh A.O. and Olakunle M.S.
*Chemical engineering Department, Kaduna Polytechnic, Kaduna
Chemical engineering Department, Ahmadu Bello University, Zaria
*Corresponding authors Email/GSM: habibashehu016@gmail.com /08028619921

ABSTRACT
The study aim to maximize the extraction of oleoresin from ginger (Zingiber officinale) through the statistical optimization of three influential process parameters temperature (°C), extraction time (min) and solid-liquid ratio (g/100ml using ethanol as solvent. Response Surface Methodology (RSM) was employed to design experiments and study the interaction effects of these parameters on the extraction process. Analysis of Variance (ANOVA) was used for the analysis of regression coefficient, prediction of equation and case statistics. The optimum conditions for the maximum yield of oleoresin from each gram of ginger were found to be 43.25 °C, 42.1 minutes and 11.30g/100ml respectively. The order of relative importance of these three parameters was: solid-liquid ratio > temperature > time. Total phenolic content of the extracted oleoresin using optimized parameters was 126mg/l determined using Folin-Ciocalteau colorimetric method.

Keywords: Extraction, Ginger, Optimization, RSM, Oleoresin, Yield, Phenolic.

Introduction
Ginger is well known spice for its medicinal properties and health benefits through ages in almost all system of medicines against many diseases and infections. Ginger is the underground rhizome of the ginger plant with a firm, striated texture. Most *Zingiberaceae* family spices are fibrous rooted perennial herb which is widely cultivated in some tropical regions such as India, China, Nigeria, Australia and Jamaica (Bartley and Jacobs, 2000).

Ginger species possesses aromatic properties and has a commercial importance. There are two extracts of ginger, essential oil which varies from 0.8–4.2% and oleoresin in the range of about 5-8% depending on its origin habitat and agronomic treatment of culture (Azian *et al.,* 2001). The pungent taste of ginger rhizome is due to its oleoresin content, which is an oily viscous liquid containing oxymethyl phenol like shagoal, zingerone and gingerol that are probably responsible for its antioxidant property (Mbaeyi-Nwaoha *et al.,* 2013). Oleoresin compounds, such as *6-gingerol* and its derivatives obtained from the root of ginger possess high antioxidant activity (Stoilova *et al.,*2007).

The antioxidants are micronutrients that have gained interest in recent years due to their ability to neutralize the actions of free radicals (Carenas and Packer, 1996). Mbaeyi-Nwaoha *et al., (*2013) states that free radicals are potentially harmful products generated during a number of natural processes in the body, and are associated with the ageing of cells and tissues. Ginger oleoresin reproduced the character of the respective ginger and ginger oil fully. It contains the volatile and the non-volatile constituents of the spices. It can replace whole ground ginger without impairing any flavor and aroma characteristics. Ginger oleoresin has widespread uses as a flavoring agent in foods, beverages, and medicines. The increased prominence of oleoresins over natural spices is due to increased economy in use, more uniform flavor and concentration, and lack of microbial contamination.

Research has shown that there is a scientific curiosity and certain popularity with regard to screening essential oils and extracts from plants to detect natural compounds characteristics and antioxidant activity as well as antimicrobial activity, used medicinally all over the world (Hassan *et al.*, 2012).

Solvent extraction is a widely employed technique designed to separate soluble polyphenols from plant tissue using a solvent. Commonly used solvents for extraction of oleoresin from plant tissue are water, ethanol, methanol; acetone etc. (Jakopic *et al.,* 2009). The poly-phenolic components in ginger are proven beneficial in treating health problems. But recovery of the poly-phenolic components at the same time has not been possible by conventional separation processes, because of longer contact time of extraction and thermal degradation of the active components.

Response surface methodology (RSM) is a statistical technique used to determine the optimum values of the independent variables to achieve the maximum response, and enables the user to investigate the interaction of the individual variables, which is considered more efficient than the traditional single parameter optimization because of the saving in time, space, and raw materials. Jung-Hoon *et al.,*(2014). For these reasons, RSM has been employed in the extraction of chemical compounds from herbal medicines (Hossain *et al.,* 2011).

In this research, Solvent extraction was adopted for extraction of oleoresin from ginger rhizome. The effect of temperature, time, and solid-liquid ratio was investigated using ethanol as solvent. The extraction process was optimized in terms of oleoresin yield using statistical analysis. Implementation of optimized process parameter will lead to effective extraction process.

Design of Experiments for Extraction

The experimental design was chosen to study the optimization of three selected parameters: temperature, time and solid/liquid ratio. Yield optimization was carried out based on the experimental matrix defined using Box-Behnken Design approach (BBD). The experimental design was developed using STATISTICA 7 software. The design has 3 factors, 1 block and 15 runs. The coded and uncoded levels of the independent variables were shown in Table 1.

Table 1: Box-Behnken Design Variables for Ginger Oleoresin Extraction.

Independent variables	Symbol		Coded levels		
	Coded	Uncoded	-1	0	1
Temperature, ^oC	X_1	Z_1	30	40	50
Time, min.	X_2	Z_2	20	40	60
Solid-Liquid ratio, g/100ml	X_3	Z_3	10	20	30

The relationship between the output response and the input process variables (temperature, time and solid/liquid ratio) are defined using RSM modeling approach.

Materials and Methods

The ginger rhizomes used for the extraction of oleoresin was sourced from Kachia local government area in southern part of Kaduna state, South-Central region of Nigeria. The ginger sample was identified at Biological Science Department of Ahmadu Bello University (ABU) Zaria. Other materials used were distilled water, ethanol, and were sourced from Chemical Engineering Department of ABU Zaria Nigeria.

Ginger pre-treatment

Ginger rhizomes were washed thoroughly with tap water to remove sand and dirt. The ginger rhizome was cut into tiny pieces using a knife. The sample so prepared was then dried in an air-circulating oven at a temperature of $40^{O}C$ in the laboratory and ground manually into power, using a mortar and pestle. The powdered ginger was sieved using a set of sieves to obtained different particle size range. A particle sized range of 425- 250µm was used. The sample was stored in an air-tight polythene bag as stock sample in a cool dry place until required for extraction.

Extraction of Oleoresin

The dry ginger powder was put directly into the solvent (95% ethanol) and heated under reflux inside a round bottom flask. The round bottom flask was placed in a hot water bath which sat on a combined hot plate and stirrer. A water bath makes temperature control easy and it ensured uniform heating. The solvent and the ginger mixture were stirred throughout the extraction. The round bottom flask had three ports. The water cooled condenser was connected directly to the round bottom flask using one of the ports. The other ports were used to insert/remove a thermometer for checking the temperature. The system was operated at atmospheric pressure. The operating conditions for the extraction are done according to the design of experiment shown in Table 1. After extraction, the round bottom flask was allowed to cool down, the ginger oleoresin were then separated using filtration. Whatman number 1 filter paper was used for the filtrations. After filtering, the oleoresin and solvent were recovered using a soxhlet extractor. The mass of oleoresin recovered were determined and used to calculate the extraction yield.

Determination of Total Phenolic Contents

The total phenolic content of oleoresin was determined using Folin-Ciocalteu reagent as described by Singlaton and Rossi (1965). Sample was inserted into a test tube and mixed thoroughly with 5ml Folin-Ciocalteu reagent (pre-diluted 10 times with distilled water). After 5 min, 4 ml of 7.5% sodium carbonate (Na_2CO_3) was added and allowed to react for 2hrs at room temperature. The absorbance was measure at 765 nm using spectrophotometer (6061 Jenway, England). Determination of total phenolic compounds was carried out in a duplicate and calculated from the calibration curve obtained with gallic acid, which was used as a standard and results were expressed as mg GAE/l.

RESULTS AND DISCUSSION

The ginger sample was identified as *zingeber officinale* (card number: 2261).

Response Surface Methodology Modeling of Ginger Oleoresin Production

The result of optimization of yield of oleoresin produced for each experimental run of the input parameters (temperature, time and solid/liquid ratio) using ethanol as a solvent are shown in Table 2. The experimental and predicted values for the response parameter (yield) at the design points and all the three variables in coded form are shown.

Table 2: Input Parameter for Oleoresin Extraction at Various Runs and Yield

Run	Temperature(° C)	Time (min)	Solid/liquid ratio (g/100ml)	Experimental yield	Predicted yield
1	30	20	20	7.10	7.16367
2	50	20	20	7.95	8.88617
3	30	60	20	7.00	7.71117
4	50	60	20	9.57	9.43367
5	30	40	10	9.00	9.74492
6	50	40	10	12.20	11.46742
7	30	40	30	5.60	5.12992
8	50	40	30	5.870	6.85242
9	40	20	10	10.00	10.33242
10	40	60	10	10.50	10.87992
11	40	20	30	5.80	5.71742
12	40	60	30	5.97	6.26492
13	40	40	20	9.30	8.29867
14	40	40	20	9.32	8.29867
15	40	40	20	9.30	8.29867

The predicted values obtained from the model fitting technique were seen to be sufficiently correlated to the observed values.

Figure 2 Presents the plot of observed verses predicted values of the model.

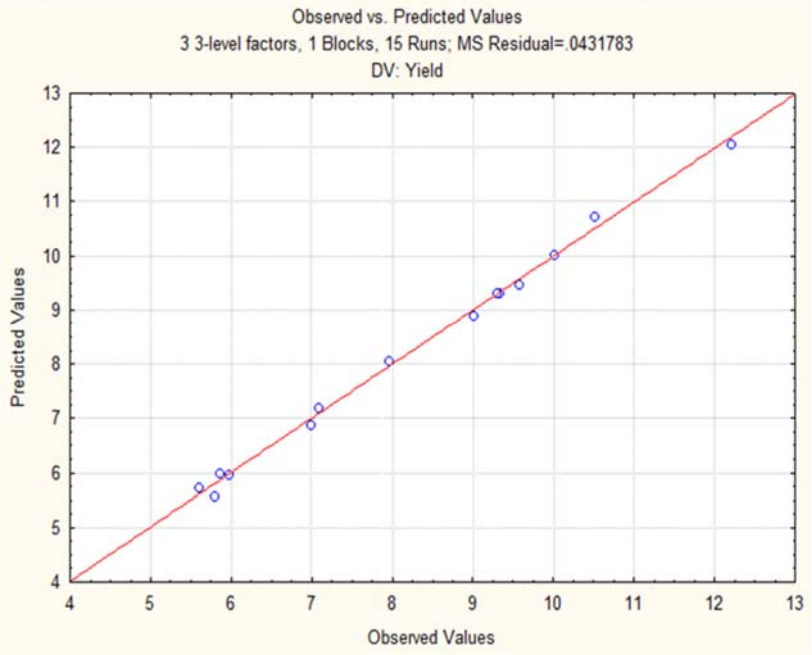

Figure 2: Plot of predicted values versus actual (observed) values of oleoresin yield

Multiple Regression Summary of Optimum input Parameter for Ethanol Extract
The input values of temperature (A), time (B) and solid-liquid ratio (C) in coded and uncoded term are presented in Table 3.

Table 3: Multiple Regression Summary of Optimum input Parameter for Ethanol Extract

Factor	Coded optimum parameter(X)	Uncoded optimum parameter(Z)
Temperature	0.324914	43.2491
Time	0.103275	42.0655
Solid/ Liquid Ratio	-0.870526	11.2947

The general model equation in term of the actual (uncoded) factor is shown in Equation (1)

$$Yield = -8.19083 + 0.6672Z_1 + 0.08610Z_2 + 00.27408Z_1 + 0.00215Z_1Z_2 - 0.00733Z_1Z_3 - 0.00041Z_2Z_3 - 0.00651{Z_1}^2 - 0.00188{Z_2}^2 - 0.00488{Z_3}^2 \quad \text{(i)}$$

Analysis Of Variance for Ethanol Extract

Statistical analysis of the model was performed. ANOVA is used to check the adequacy of the empirical model. The results of ANOVA for fitting the quadratic response surface model by a mean square method are summarized in Table 4.

Table 4: ANOVA for Response Surface quadratic Model

Factor	SS	DF	Mean Square	F-value	P-value
A-Temp	5.93401	1	5.93401	137.4303	0.000079
A^2	1.56400	1	1.56400	36.2219	0.001821
B-Time	0.59951	1	0.59951	13.8846	0.013624
B^2	2.08154	1	2.08154	48.2080	0.000952
C- S/L Ratio	42.59645	1	42.59645	986.5237	0.000001
C^2	0.88050	1	0.88050	20.3922	0.006307
AB	0.73960	1	0.73960	17.1290	0.009008
AC	2.14622	1	2.14622	49.7061	0.000887
BC	0.02723	1	0.02723	0.6305	0.463166
Lack of Fit	0.21563	2	0.07188	59.1	0.42600
Pure Error	0.00027	3	0.00013		
Total SS	56.20957	14			
R^2= 0.99616	R^2_{adj} =0.99925				

The significance of each of the coefficients are checked from p-values (probability of error value), which also indicates the interaction strength of each parameter. According to Table 4 the p-value of the model is <0.05, demonstrating high significance in predicting the response values and the suitability of the model. The high F-value with very low p-value indicated the high significance of the fitted model. The value of regression coefficient R^2 for the model was 0.99616 and adjusted R^2 is 0.99925 both indicating good fit of the model with an insignificant lack of fit.

Figure 3 presents the Pareto chart of the standardized effect for oleoresin yield response.

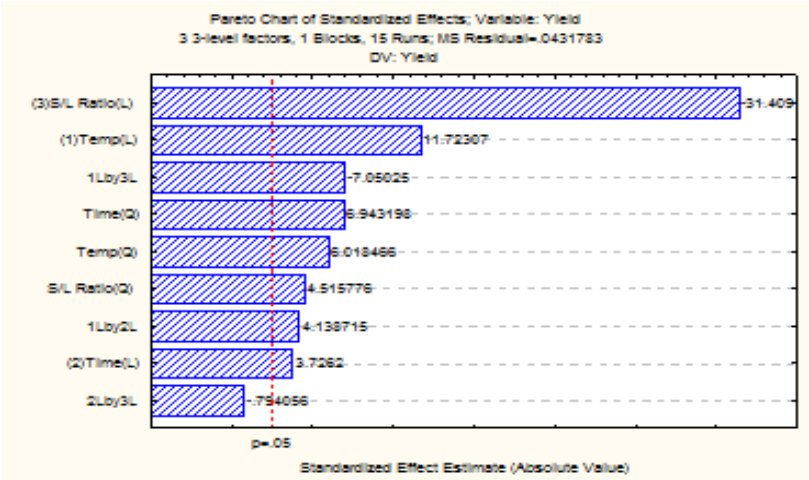

Figure 3: Pareto Chart of Standard Effects.

From Figure 3 it can be observed that all the linear effect, all the quadratic effect and all the interactive effect are significant because the p-values are less than 0.05. The largest effects are linear terms of solid-liquid ratio and temperature because they extend the farthest. The quadratic effects of solid-liquid ratio, temperature and time are less significant.
The Response surface plots in Figure 4, 5 and 6 Show the variation of the percentage oleoresin yield with respect to the variables for extraction using ethanol.

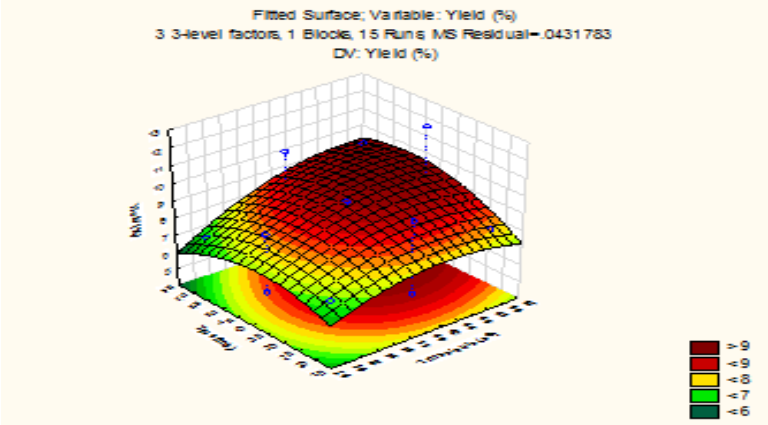

Figure 4: Effect of temperature and time on oleoresin Yield

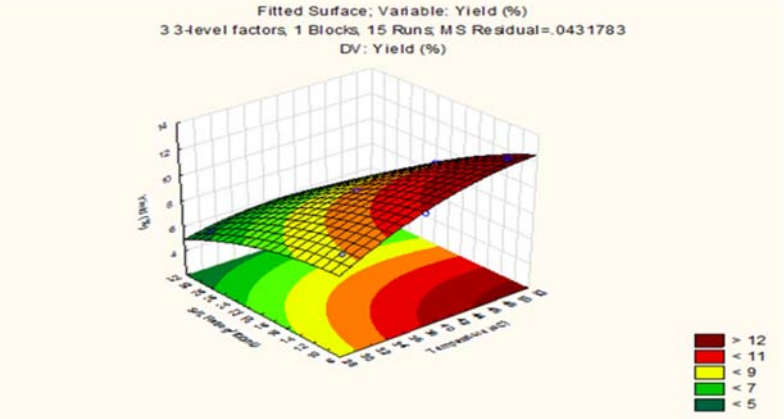

Figure 5: Effect of S/L ratio and temperature on oleoresin Yield

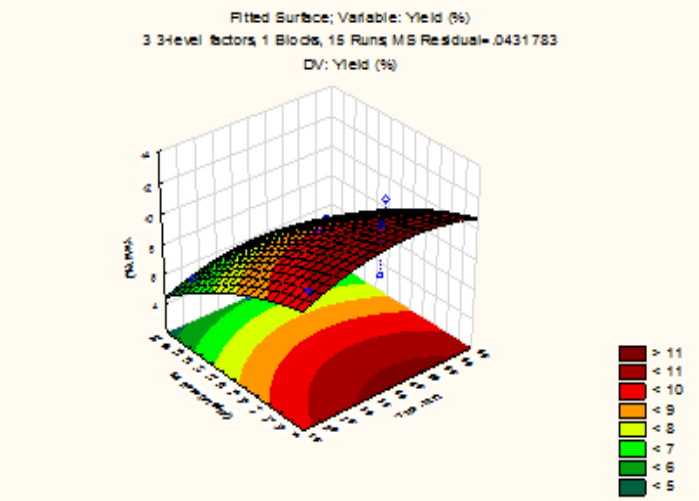

Figure 6: Effect of Solid/Liquid ratio and Time on oleoresin Yield

The response surface plots shown in Figure 4-6 show the optimal condition between independent variables in different fixed parameters. The 3D plots shows the effect of interaction among the variables, extraction time and temperature, solid-liquid ratio and temperature and solid-liquid ratio and extraction time on yield of oleoresin respectively. From the Figures, it can be seen that the oleoresin yield increases with decrease in solid-liquid ratio and increases with increase in temperature and extraction time.

Table 5: Physical Properties of Oleoresin

Properties	Oleoresin Extracted	Oleoresin Requirement (BIS)
Odour	Spicy and aromatic	Spicy, sweet and aromatic
Colour	Dark brown	Dark brown or reddish brown
Appearance	Viscous liquid	Viscous liquid
Density	0.8579	-
Specific Gravity at 30°C	0.8604	0.8640 – 0.8758
Refractive Index at 27°C	1.4879	1.4880 – 1.4970
Phenolic Content (mg/l)	126	-

From Table 5 all the values of the physical properties fall within the requirements for ginger oleoresin reported by the Bureau for Indian standard (1996). The ginger oleoresin has a total phenolic content of 126mg/l compared to 136 mg/l reported by (Ercan *et al.,* 2016). This study showed that the ginger oleoresin demonstrated effective antioxidant properties and its consumption may reduce or delay the progression of diseases that oxidate stress to take place due to lack of antioxidant supplement.

CONCLUSIONS

The optimal values of the parameters that maximizes the oleoresin yield are; temperature, extraction time and solid-liquid ratio; 43.25°C, 42.1min and 11.30g/100ml using ethanol solvent with an optimum yield of 11.4110% respectively. The most significant effect is the

linear effect. The quadratic effect and the interactive effects of all the parameters are less significant. The order of relative importance of these parameters are Solid-Liquid Ratio > Temperature > Time.

REFERENCES

Azian N.M., Sazalina M. S. and Rizan H. M. R.(2001). Essential Oil and Active Ingredients Extraction from Ginger Plants*. Annual Progress Report Centre of Lipids Engineering and Applied Research.* Kuala Lumpur, Malaysia

Bartley J.P. and Jacobs A.L.(2000). Effects of drying on flavor compounds in Australian- grown ginger (Zingiber officinale). *J. Sci. Food Agric. (80)*: 209–215

Bureau of Indian standards (1996). *Indian standard specification for ginger oleoresin,* Zafar Marg, New Delhi, India

Carenas E. and Packer L. (1996). *Hand Book of Antioxidants*. Plenum, New York. 127-131

Ercan B., Ekram K. and Ilhami G. (2016). Antioxidant activity and phenolic compounds of ginger (*Zingiber Officinale rosc.*) root determined by holc and ms/ms. *Journal of food measurement and characterization.* Doi: 10.1007/s11694-016-9423-

Hasan H.A., Rasheed R AM, Abd Razik B.M, Rasool Hassan B.A (2012). Chemical Composition and Antimicrobial Activity of the Crude Extracts Isolated from Zingiber Officinale by Different Solvents. *Pharmaceut Anal Acta (3)*: 184

Hossain M.B., Barry-Ryan C., Martin-Diana A.B., Brunton N.P.(2011). Optimization of Accelerated Solvent Extraction of Antioxidant Compounds, From Rosemary *(Rosmarinus officinalis L.),* Marjoram *(Origanum majorana L.) and* Oregano *(Origanum vulgare L.)* using Response Surface Methodology. *Food Chem, (126)*: 339–346.

Jakopič, J., Veberič, R., Štampar, F. (2009): Extraction of phenolic compounds from green walnut fruits in different solvents. *Acta Agriculturae Slovenica*, *93 (1)*:11 – 15.

Jung-Hoon K., Hyeun-Kyoo S., and Chang-Seob S., (2014). Optimization of the Extraction Process for the Seven Bioactive Compounds in Yukmijihwang-Tang, An Herbal Formula, using Response Surface Methodology*, Pharmacogn Magazine. 10(3)*: S606–S613. doi: 10.4103/0973-1296.13979

Mbaeyi-Nwaoha, I.E., Okafor, G.I. and Apochi, O.V., (2013). Production of oleoresin from ginger (*Zingiber officinale*) peels and evaluation of its antimicrobial and antioxidative properties, *African Journal of Microbiology Research*, *7(42)*: 4981-4989, DOI: 10.5897/AJMR2013.6125

Mukherjee S., Mandal N., Dey A., and Mondal B. (2014). An approach towards optimization of the extraction of polyphenolic antioxidants from ginger (Zingiber officinale), *J Food Sci Technol. 51(11)*: 3301–3308.

Singlaton V. and Rossi J. (1965). Colorimetry of Total Phenolic Compounds with Phosphomolybdic-Phosphotungstic Acid Reagents. *American Journal of Enology and Viticulture. (16)*: 144-158

Stoilova I., Krastanov A., Stoyanova A., Denev P. and Gargova S., (2007). Antioxidant Activity of a Ginger Extract *(Zingeber Officinale). Food Chem, (102)*: 764—770.

Proceedings of the 49th NSChE Annual Conference
KADA 2019: pp 587-593

P3B-03: STUDY ON THE EFFECTS OF PARTICLE SIZE ON THE YIELD OF ESSENTIAL OIL EXTRACTED FROM EUCALYPTUS (*CITRIODORA*) USING PILOT PLANT STEAM DISTILLATION TECHNIQUE

***[1]Akuso, S. A., [1]Kabiru M., [1]Victor O., [1]Abubakar, G., [1]Nwobi, B. E., [2]Apugo-Nwosu, T. U., and [1]Batari, M. L.**

[1]National Research Institute for Chemical Technology (NARICT), Zaria, Kaduna State
[2]Department of Chemical Engineering, Michael Okpara University of Agriculture, Umudike, Abia State
***Corresponding author**: alkaliakuso@gmail.com or alkalisamuel1962@yahoo.com

ABSTRACT

The effect of particle size on volume and yield of oil extracted from eucalyptus leaves (citriodora) with time was studied using steam distillation technique via a pilot plant. The effect of particle sizes of 10, 20, 30, 40 and 50 cm of the eucalyptus leaves were used to find the best particle size that could achieve maximum oil yield. The results showed that particle size of 10 cm for 60 minutes extraction gave the highest percentage yield of oil (0.6177 wt %) compared to particle size of 50 cm with percentage yield of oil (0.3291 wt %) for the same extraction time of 60 minutes. The results showed that, increasing extraction time beyond sixty minutes had no effect on the amount and yield of the oil as long the capacity of the tank remains constant. Physicochemical properties of the extracted oil revealed that; refractive index at 25°C was 1.4425, specific gravity at 25°C was 0.9015 and acid value was 19.465 ml/gram.

Keywords: Essential Oil, Eucalyptus (*citriodora*) leaves, Extraction, Oil yield, Particle size, Steam Distillation Technique,

INTRODUCTION

Essential oils are volatile, natural base products, which are found in spices, aromatic and medicinal plants. The extraction of essential oils is well known from ages when pure essential oil and crude extract of essential oil bearing plants, herbs and grasses were in use for various medicinal and fragrances, flavors, preservatives and insect repellants purposes [1-2], flavoring chemicals, aromatic in pharmaceutical products, food, perfume and industrial [3]. Eucalyptus plant is commonly grown in tropical and sub-tropical regions because of its resistance to many pest and adaptability to various climatic conditions. These include South Africa, China, Congo Republic, Angola, India and West Africa. The plant has up to 700 species and can grow as high as 40 m tall in an altitude of 600 m. The principal component of the essential oil extracted from eucalyptus *citriodora* leaf is cineola which is up to 70 - 80%. The oil is mainly used in medicinal, industrial and perfumery applications. The yield of essential oil is naturally constrained (usually less than 2 %) but with high market value [4]. Eucalyptus oil has many biological effects such as, antiviral, antifungal and antibacterial components and also uses against the effect of influenza, cold, arthritis and other respiratory infection, rhinitis and sinusitis [3, 5].

Inspite of the abundant deposit of untapped raw materials for the production of essential oils, Nigeria is still importing essential oils to meet the demand of the end users of the product. This study aimed at investigating the effect of particle size on the yield of essential oil from plant material eucalyptus (*citriodora*) leaves by steam distillation using pilot plant.

MATERIALS AND METHODS

Material Sourcing and Preparation

Fresh eucalyptus *citriodora* leaves were obtained from National Research Institute for Chemical Technology (NARICT) plantation in Zaria, Kaduna State, Nigeria. The leaves were pretreated and freed from foreign (dirt) materials. 15 kg each of the eucalyptus leaves of particle sizes of 10, 20, 30, 40 and 50 cm were weighed for five batch operations. Figure 1 shows picture of eucalyptus *citriodora* leaves plant.

Figure 1: Eucalyptus *citriodora* leaves

Extraction of Essential Oil

The experimental pilot plant set-up for steam distillation extraction as shown in Figure 2 is situated at National Research Institute for Chemical Technology (NARICT), Zaria-Kaduna State, Nigeria. The plant consists of cylindrical tank still, condenser, steam generation and cooling water units. 25 litres of water was charged into the steam generation unit of the tank still which is situated directly at the bottom of the tank still. The oil extraction chamber is separated from the boiler section by a stainless steel weir mesh. 15 kg of the leaves was then charged into the tank still from the top and the lid was properly tight to avoid steam-oil leakage. The fuel used is fire wood as source of energy to generate the steam used in the extraction. The extraction time of the process was sixty minutes per batch operation.

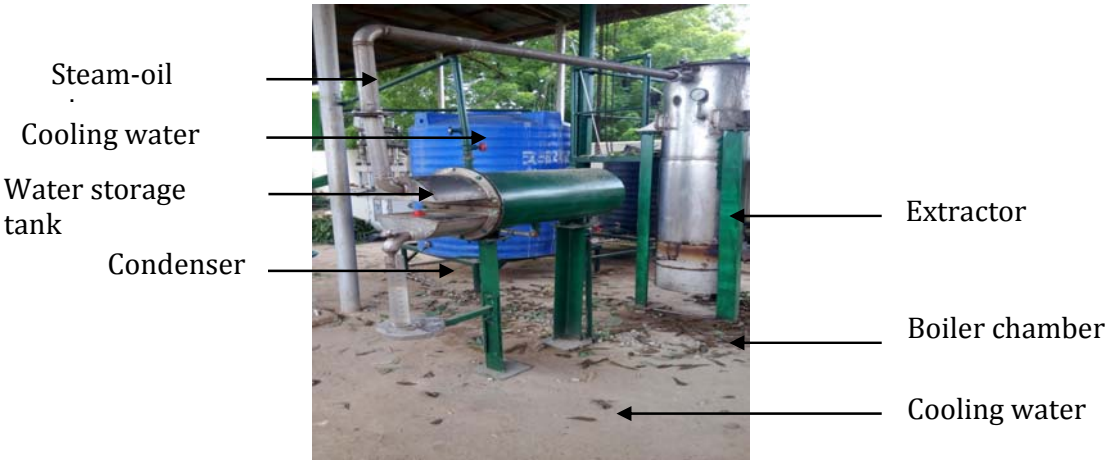

Figure 2: Essential oil extraction pilot plant set-up

The steam generated from the boiler section travelled across the packed bed of leaves and ruptured the plant cell and extracted the oil which was carried away by the stream of steam to the condenser. The flow of steam-oil mixture in the condenser and cooling water was counter current for effective condensation. The condensate (oil-steam water mixture) was collected in a separating flask at various time intervals and separated through decantation process as shown in Figure 3. The volume of oil collected were determined every sixty minutes and recorded.

Figure 3: Separating process of essential oil and water

The block diagram for the extraction of essential oil using steam distillation pilot plant is as shown in Figure 4 below.

Determination of Physicochemical Properties of the Extracted Oil

Physicochemical properties of the extracted essential oil from eucalyptus leafy plant such as refractive index, specific gravity, solubility in ethanol and acid value were determined according to the methods described by [3, 6].

RESULTS AND DISCUSSION

Effect of Particle Size on Oil Volume

The effect of particle size was studied for five different samples of 10, 20, 30, 40 and 50 cm per batch of production cycle of sixty minutes until equilibrium was reached. As seen from Table 1 below that the amount of essential oil extracted was higher for particle size of 10 cm when compared to the largest particle size of 50 cm. This shows that particle size has a

significant effect on the amount of oil extracted as long the capacity of the tank still remains constant. The higher the particle size the more the packing density of the plant material in the tank still which results in resistance to flow of steam and oil across the packed bed. In each extraction circle, the oil collected, extraction time, weight and yield of oil were all recorded as shown in Table 2 below. The same procedure was repeated for 20, 30, 40, and 50 cm of particle sizes of leaves. The weight (wt) and percentage yield (%) of the extracted oil was calculated using Equations (1) and (2) below.

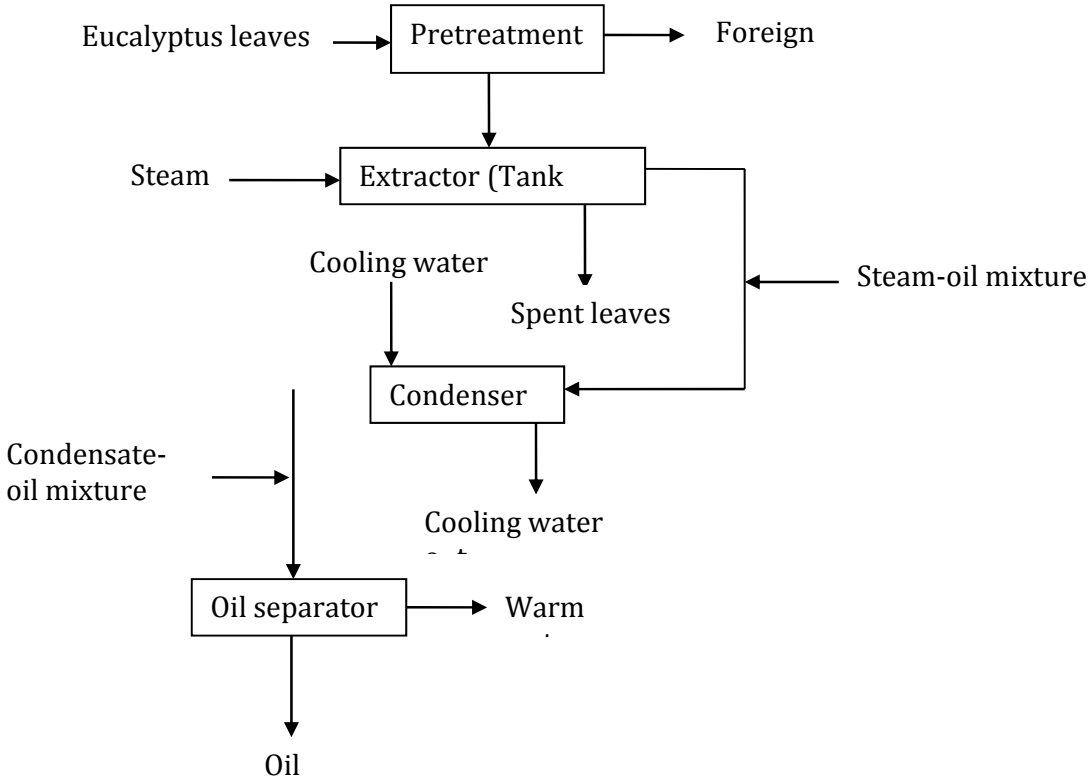

Figure 4: Block diagram of essential oil extraction

Table 1: Oil volume (ml) extracted at various particle sizes

S/N	Time (minute)	Oil volume (ml) at various particle sizes of leave				
		10 cm	20 cm	30 cm	40 cm	50 cm
1	10	21	17	13	11	9
2	20	55	48	31	27	21
3	30	78	67	44	40	37
4	40	95	84	56	52	48
5	50	105	91	66	61	56
6	60	107	93	67	62	57

$$\text{Weight of oil} = \text{density of oil} \times \text{volume of oil} \quad (1)$$

$$\text{Oil Yield } (\%) = \frac{\text{Weight of oil}}{\text{Weight of leaves}} \text{ x } 100 \quad (2)$$

Table 2: Oil yield (%) extracted at various particle sizes

S/N	Time (min)	Weight and oil yield at various particle sizes of leave (%)									
		10 cm		20 cm		30 cm		40 cm		50 cm	
		Wt	Yield	Wt	Yield	Wt	Yield	Wt	Yield	Wt	Yield
1	10	18.18	0.1212	14.72	0.0981	11.26	0.0751	9.53	0.0635	7.79	0.0520
2	20	47.63	0.3175	41.57	0.2771	26.85	0.1790	23.38	0.1559	18.19	0.1212
3	30	67.55	0.4503	58.02	0.3868	38.10	0.2540	34.64	0.2309	32.04	0.2136
4	40	82.27	0.5485	72.74	0.4850	48.50	0.3233	45.03	0.3002	41.57	0.2771
5	50	90.93	0.6062	78.81	0.5254	49.50	0.3810	52.83	0.3522	48.50	0.3233
6	60	92.66	0.6177	80.54	0.5369	58.02	0.3868	53.69	0.3579	49.36	0.3291

Effect of Particle Size on Oil Yield

The results presented in Figure 5 shows that the yield of the oil extracted decreases with increase in particle size. There was an increase in the oil yield to a maximum value of 0.6177 wt % due to reduction in particle size. Further increase in the particle size resulted in a decrease in the oil yield. It was also observed from Figure 5 below that the minimum particle size of 10 cm has maximum oil yield whereas the larger particle size of 50 cm has minimum oil yield of 0.3291 wt %. This could be attributed to the fact that the smaller particle size has greater interfacial surface area between the leaves and surrounding space within the tank still and therefore the rate of diffusion of the oil-steam mixture was higher as compared with larger particle size that are high in packing density which resulted to less amount of oil being transferred from inside the larger particle to the surrounding tank still. The results were in agreement with the report obtained by [5-6].

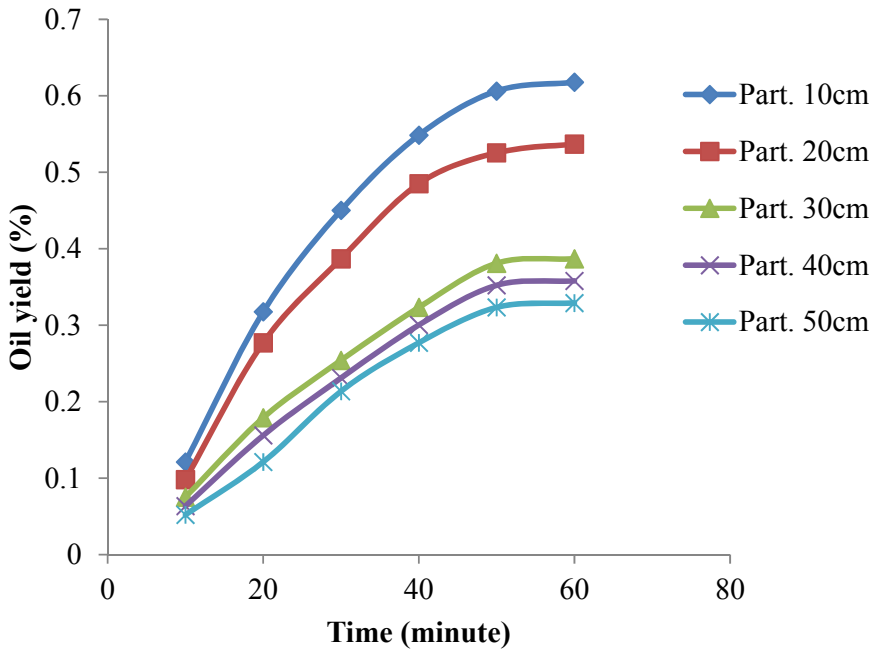

Figure 5: Effect of particle size on oil yield as a function of time.

Physicochemical Properties of Eucalyptus Oil Extracted

The physicochemical properties of eucalyptus oil extracted using steam distillation pilot plant were as shown in Table 3 below as determined according to the methods described by [3-4].

The results from this study indicated that refractive index was 1.4425, specific gravity was 0.9015 and acid value was 19.465 ml/g which are in agreement with the results obtained by [6-7].

Table 3: Physicochemical properties of eucalyptus oil extracted values and unit

Physical properties	Results	Unit	Standard values
Colour	Pale yellow	-	Pale yellow
Odour	Aromatic	-	Aromatic and camphoraceous
Taste	Spicy	-	Spicy
Solubility in alcohol	Soluble	-	Soluble in alcohol
Molecular formula	$C_{10}H_{18}O$	-	$C_{10}H_{18}O$
Refractive index at 25^{o}C	1.4425	-	1.4550 – 1.4670
Specific gravity at 25^{o}C	0.9015	-	0.9060 – 0.0.9250
Acid value	19.465	ml/gram	19.635

CONCLUSIONS

The results showed that the yield of oil was more with smaller particle sizes of eucalyptus leaves and vice versa. Particle size of 10 cm gave oil yield of 0.6177 wt %, while particle size of 50 cm gave less oil yield of 0.3291 wt % all within the same amount of time sixty minutes. Smaller particle sizes has high diffusion rate of the oil from inside the packed bed of materials compared with the larger particle sizes which resulted in low oil yield. From Figure 5, we can see that increasing time of extraction beyond sixty minutes has little or no effect on the amount and yield of the oil extracted. Physicochemical properties of the extracted oil were determined among other parameters has refractive index at 25 ^{o}C was 1.4425, specific gravity at 25 ^{o}C was 0.9015 and acid value was 19.465 ml/gram, these are in agreement with literature values obtained by [6-7].

ACKNOWLEDGEMENTS

The authors would like to express their deepest gratitude to the Director-General/CEO of National Research Institute for Chemical Technology (NARICT), Zaria for his moral and financial supports towards this project. The corporation and support by members of staff of Pilot Plants and Fabrication Technology Department, NARICT, Zaria are also highly appreciated.

RECOMMENDATION

A further study on the quality of extracted essential oil from the eucalyptus using GC-MS and HPLC should be investigated.

REFERENCES

Weiss, E. A. (1997). Essential Oil Crops, *CAB International, USA*

Panda, H. (2011). Essential Oils Handbook, *National Institute of Industrial Research, Delhi*.

Khalid M. A. and Tariq M. N. (2018). Extraction of Essential Oil from Iraqi Eucalyptus Camadulensis Leaves by Water Distillation Methods. *International Conference on Materials Engineering and Science*, 454, 0121613

UNIDO, (1983). Practical Manual on Essential Oils Industry (UNIDO, *Vienna, Austria)*, 3-5.

Basma A. A-M, Asrar A. H. and Badoor M. K. (2013). Extraction of Oil from Eucalyptus Camadulensis Using Water Distillation Method. *Iraqi Journal of Chemical and Petroleum Engineering*, 14(2), 7-12.

Galadima, M.S. (2004). Design and fabrication of a pilot plant for steam distillation of essential oil, *M.Sc. thesis, Department of Chemical Engineering, Ahmadu Bello University, Zaria, Nigeria*, 4-6

Meaza K. (2016). Extraction and Characterization of Essential Oil from Eucalyptus Leaves Using Steam Distillation, *M.Sc Thesis. Addis Ababa University, Addis Ababa Institute of Technology, Department of Chemical Engineering, Ethopia.*

Proceedings of the 49th NSChE Annual Conference
KADA 2019: pp 594-609

P3B-04: TECHNO-ECONOMIC ANALYSIS OF AN INTEGRATED LOW TEMPERATURE BIOGAS UPGRADING AND POWER GENERATION PLANT

A. O. Olanrewaju[1] and S. M. Waziri[2,*]
[1]OAO Technologies, Kaduna, Nigeria: oaotechnologies2016@gmail.com
[2]Chemical Engineering Department, Ahmadu Bello University, Zaria – Kaduna, Nigeria
[*]Corresponding author: smwaziri@abu.edu.ng

ABSTRACT
The primary objective of the study was to simulate and analyse low-temperature CO_2 removal process with an integrated gas power plant using Aspen HYSYS. The energy efficiency of the process as well as sensitivity analysis of the operating conditions and economics of the process were also examined. The simulation result indicated that concentration of CH_4 increases from 60.233to95.848 mol. % with a recorded 0.0062% CH_4 loss, while CO_2 increases from 37.467 to99.815 mol.% in the liquid CO_2 stream. Also, the net power generation of the process is 23035.97kW with a thermal efficiency of 47.387%. The sensitivity analysis of the operating conditions showed that fuel pressure, temperature and compressor exit pressure affect quantity of power generated.Furthermore, the specific investment cost of the combined low temperature biogas upgrading technique and the integrated power plant is US$ 1,661,705.53/MW of power generated, which showed that biogas utilization for power generation is a viable option to mitigate power challenges in Nigeria.

1.0 INTRODUCTION
Globally, energy is recognized to be an indispensable part of any developed economy. It has been a fundamental factor in the poverty alleviation effort of any society (Aderemi *et al.*, 2009). The availability and access to energy are ingredients of national development and improvement in the standard of living of any nation. However, global energy demand has continued to rise due to economic and population expansion, while availability and access to energy are dwindling. The present energy system is greatly dependent on fossil fuels such as coal, oil and gas. The dependence on fossil fuels and derivatives as the main source of energy has led to global warming and its attendant adverse climatic changes which have led to ice melting and sea level rise, environmental degradation and pollution with its adverse effects on public health (Eze and Agbo, 2010). These challenges have led to global efforts on sustainable, "green" energy.

In the global push for sustainable energy alternatives, Africa cannot be left behind due to the energy challenges to its socio economic development. It is indeed unfortunate that less than 43% of the total population of 21 sub-Saharan African countries have access to electricity (Moussa and Malcolm, 2019). Thus, the need for sustainable energy generation from renewable local resources cannot be over emphasized. In addition to its considerable deposits of fossil fuels, the continent's floral diversity and abundance, sunshine and winds give it potential for the production of sustainable energy. Nigeria, the most populous country on the African continent remains stunted economically due to inadequate and epileptic electrical energy supply.

Nigeria recorded 6803 MW generating capability in 2017 and a wheeling capacity of 6700 MW by the Transmission Company of Nigeria (TCN) while less than 4,000 MW of the over 6803 MW generated in 2017 get in to Nigerians (Olawoyin, 2017). However, as at 2016, the estimated energy demand of the country is put at over 98,000 MW while supply is about 6% of estimated demand (Wijeratne and Omontuemhen, 2016). This shows that the demand is far greater than the supply which is gotten from fossil fuels and hydro power. This resulted in the need to seek alternative sources of power by turning towards sustainable and renewable

sources. One key and possible alternative source of power generation is the use of biogas resources. However, biogas utilization in Nigeria is on the low side despite huge reserves of biogas feedstock from agricultural and animal waste with biogas potential of 25.53 billion m^3 biogas and potential to produce 169541.66 MWh and 88.19 million tons of bio fertilizer per year (Ngumah *et al.*, 2013). This implies that a large proportion of Nigeria's power requirement can be sourced from biogas.

Biogas, a renewable and sustainable source of energy can be produced from several readily available waste materials such as sewage sludge and agricultural waste by anaerobic degradation. Biogas comprises mainly of methane (45 – 75% vol.), carbon dioxide (25 – 55% vol.) and traces of other compounds including hydrogen sulfide, water, nitrogen, carbon monoxide as well as volatile organic gases (Zhao *et al.*, 2010). Carbon dioxide and carbon monoxide generated from biogas are a potent greenhouse gas (GHGs) if emitted into the atmosphere. Therefore, in order to upgrade raw biogas to a higher purity of methane to ensure environmentally friendly and energy efficient power generation, the more potent GHG and lower heating value gas, CO_2 needs to be removed.

The main biogas upgrading techniques which are Pressure Swing Adsorption (PSA), absorption with water (water scrubbing), Amine based absorption, membrane separation and cryogenic separation have been reported by several authors (Rochelle, 2009; Cheng-Hsiu*et al.*, 2012; Bauer *et al.*, 2013; Alhassan*et al.*, 2017; Sutanto *et al.*, 2017). Amine based absorption is the most applicable technique for CO_2 removal. However, studies have shown that amine-based absorption of CO_2 are associated with several drawbacks which include high regeneration energy requirement, high equipment corrosion, degradation of amines and large absorber volume requirement (Rochelle, 2009; Murshid *et al.*, 2011; Cheng-Hsiu*et al.*, 2012). In addition, although, membranes separation technique has a low thermal energy usage, it requires power for compression of feed and/or permeate gas. Furthermore, limited selectivity of membranes towards CO_2 leads to methane being emitted along with the CO_2. This issue can largely be overcome by the use of a line-up with two or more stages, but comes with additional costs for permeate recompression (Sutanto *et al.*, 2017).

The upgrading of biogas by a low temperature CO_2 removal processes have been reported by Berstad *et al.* (2011), Mori and Forsyth (2013), Sipöcza *et al.* (2013) and Yousef *et al.* (2016), as an interesting energy-efficient, high capacity alternative to conventional upgrading technologies. However, no studies have been in relevant current extant literature on the techno-economic analysis of an integrated low temperature CO_2 removal biogas upgrading and power generation plant. Therefore, this study aims to fill this gap.The objectives of the study are simulation of a low-temperature CO_2 removal process with an integrated biogas power plant, analysis of CO_2removal and upgraded biogas, evaluation of the energy efficiency of CO_2 removal and power generation of the integrated power plant, sensitivity analysis of the operating conditions and economic analysis of the integrated process.

1. METHODOLOGY

Aspen HYSYS 8.8 and Microsoft Excel 2013 software packages were used in the course of this study for the simulation and analysis of the biogas upgrading technique and the power plant. The feed composition used in this study was adopted from Rakican (2007) and Abdulsalam (2018) as presented in Table 1 for the raw biogas composition used for the low temperature biogas upgrading process.

Table 1: Compositions of raw biogas produced.

Component	Value
Methane (CH_4), mol. %	55.68
Carbon (IV) Oxide (CO_2), mol. %	34.62
Carbon monoxide (CO), mol. %	1.26
Oxygen (O_2), mol. %	8.39
Hydrogen Sulphide (H_2S), mol. %	0.05
Flowrate, kmol/hr	1000
Temperature, ^oC	30
Pressure, kPa	220

2.2 Process Simulation of Low Temperature CO_2 Removal Process and Integrated Power Plant

Aspen HYSYS Process Simulator was used for the process simulation of the low-temperature CO_2 removal integrated with a power plant. To assess the technical and economic feasibility of the proposed low temperature CO_2 removal process, a complete modeling and simulation of the process was carried. The process simulation software package used is Aspen HYSYS V9.0. This is because Aspen HYSYS provides reliable and comprehensive thermodynamic packages, vast component library and advanced calculation techniques. The procedure for the simulation mainly involves component and thermodynamic model selection, and design basis as well as the temperature, pressure and mass flow rates of the input streams. Figure 1 present the simulated model of the low temperature biogas upgrading technique. The upgraded biogas from the low-temperature $CO_2$was fed into an integrated combine cycle power plant for power generation. The power plant was simulated using data presented in Table 2.

Table 2: Power plant Process for Power Plant

Parameter	Value
Air Compressor Exit Pressure, bar	15 – 23
Fuel Concentration (% CH_4)	92 – 100
Fuel Temperature, ^oC	20 - 30
Fuel Pressure, bar	20 – 30
Combustion Temperature, ^oC	≤ 1500
Steam Pressure Cycle, bar	≤ 150
Gas Turbine Exit Temperature, ^oC	600 – 800
Gas Turbine Exit Pressure,atm	1
Steam Turbine Exit Pressure, bar	1

The CO_2 removal plant model was simulated in Aspen HYSYS and consists of 2compressors with inter-stage cooler that receives raw biogas at 30 ^oC and 220 kPa to deliver an exit pressure of 4900 kPa and temperature of 108^oC. The resulting compressed was cooled by exchanging heat with the upgraded biogas from the distillation column. The compressed raw biogas was further cooled by exchanging heat in a chiller to – 50 ^oC before entering the distillation column. The cooled and compressed raw biogas was then upgraded to 95.848% $CH_4$and the higher purity liquid CO_2 stream (99.815%) from the bottom of the distillation column. Figure 1 shows the simulated CO_2 removal plant.

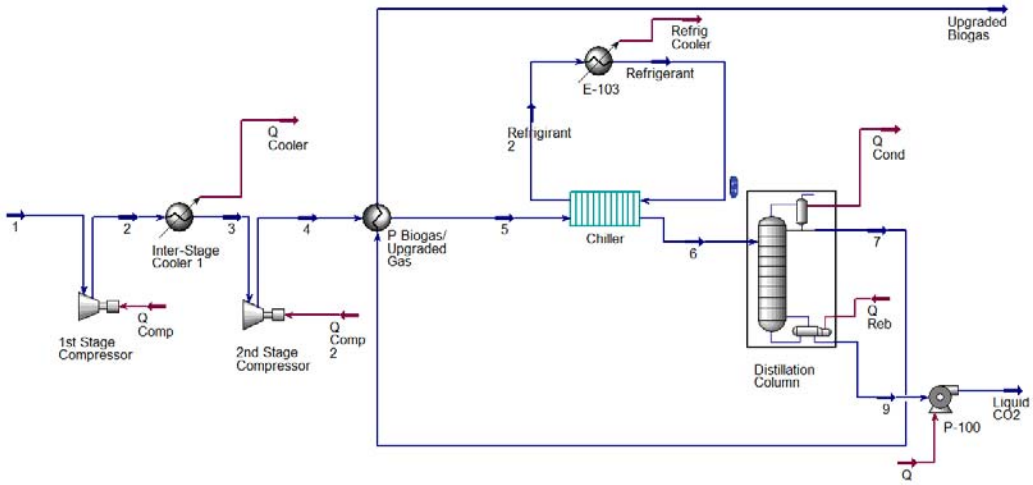

Figure 1: Model and Simulation of Low Temperature Biogas Upgrading

The power plant model was simulated in Aspen HYSYS and consists of a compressor that receives air at ambient conditions to deliver an exit pressure of 18 bar. The resulting compressed air is introduced together with pressurized fuel at 25 bar (upgraded biogas) into a Gibbs reactor that simulates the combustion chamber of the gas turbine. The gases leaving the combustion chamber are introduced into the gas turbine where they are expanded to atmospheric pressure. The work generated by the gas turbine is used to move the compressor and to generate electricity which is simulated by an energy balance. The exhaust gases are sent to a Heat Recovery Steam Generator (HRSG) that is used to generate more steam, and simulated as a regular heat exchanger. The steam generated at 125 bar is introduced into the steam turbine where they are expanded to a pressure of 1 bar. Figure 2 shows the simulated combine cycle power plant.

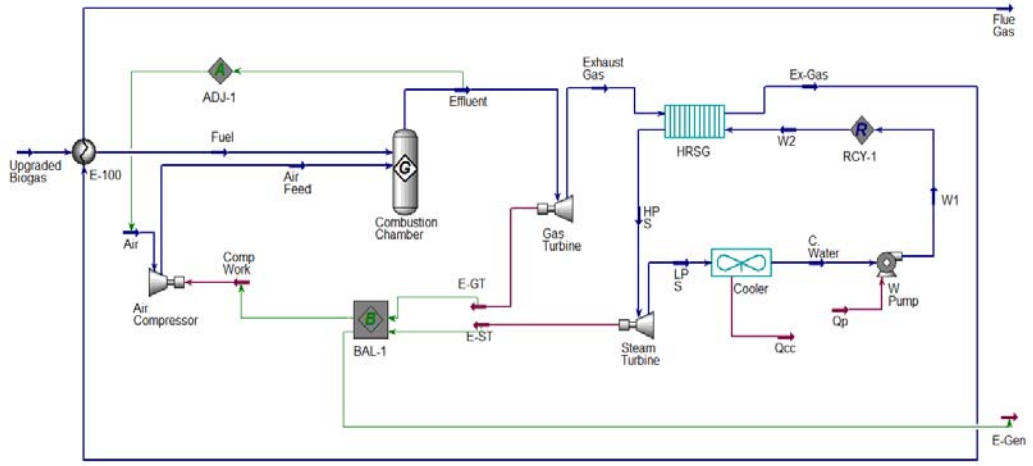

Figure 3: Simulated Combine Cycle Upgraded Biogas Power Plant

3.0 RESULTS AND DISCUSSION

3.1 Analysis of CO_2 Removal and Upgraded Biogas

The low temperature CO_2 removal technique and the integrated power plant simulated are shown in Figures1and 2. Data used for the simulation are presented in Tables1 and 2. The feed pressure and temperature to the distillation column are established as 4800kPa and–50^oC, respectively, to avoid freeze-out of CO_2 which is often a challenge encountered with low

temperature CO_2 removal. From the CO_2 freeze-out analysis carried out, it was established that at a pressure of 4800kPa, CO_2 will freeze-out to solid at-63.9962^oC, thus at 4800kPa, a significant decrease in the feed temperature beyond 223 K (-50^oC) will increase the risk of CO_2 freeze-out(Berstad *et al.,* 2013; De-Guido *et al.*, 2014; Babar *et al.*, 2018). However, for this study, the low temperature process is designed to operate at a temperature that does not poses any risk of CO_2 freeze-out, as there is a wide margin between the operating temperature and the freeze-out temperature. Table 3 presents the distillation column results.

Table 3: Distillation Column Result

Parameters	Value
CO_2 Removal Efficiency, %	99.002
Liquid CO_2 (mol. %)	99.815
Methane Loss, %	0.0062
Upgraded Biogas (mol. %)	95.848
Number of Stages	9
Feed Stage	5
Feed Pressure (kPa)	4800
Feed Temperature (K)	213
Condenser Pressure, kPa	2950
Reboiler Pressure, kPa	2970

From Table 3, it can be seen that the concentration of CH_4 increases from 60.233 to 95.848 mol% for the upgraded biogas. The purity of 95.848 mol% upgraded biogas obtained is higher than 94.5 mol% CH_4 reported by Yousef *et al.* (2016) for similar a low temperature CO_2removal. However, the value obtained in this study is slightly lower than 98 mol% CH_4 purity of upgraded biogas reported by Bauer *et al.* (2013) for a four column Pressure swing adsorption (PSA) unit, 97 mol% CH_4reported by Ryckebosch *et al.* (2011) for pressurised water absorption and 97 mol% upgraded CH_4 from Cryogenics process (Warren, 2012), while high CH_4 purity of almost 100 mol% has been reported for chemical absorption processes (Warren, 2012). Although, the most common technologies are PSA, pressurized water absorption and chemical absorption due to their higher product purity, the 95.848 mol.% CH_4 purity obtained in this study qualifies it for use as natural gas fuel in gas-fueled plant or gas fueled power plant as well as injecting to the national gas grid. The process at the established condition recorded 0.0062% CH_4loss (Table 3), which is low when compared to 0.3% CH_4 loss reported by Yousef *et al.*(2016) and 0.8% for a three stage membrane-based biogas upgrading plants in Austria (Miltner *et al.*, 2016). The concentration of CO_2 increases from 37.467 mol% in raw biogas to 99.815mol% in the liquid CO_2 stream at the simulated column condition. The high purity of 99.815mol% liquid CO_2 obtained in this study is slightly higher than 99.7 mol% liquid CO_2 reported by Yousef *et al.* (2016). The high purity liquid CO_2 obtained in this process is the primary advantage of the process compared to other conventional technologies, since high purity liquid CO_2 is a valuable by-product. The simulated low temperature biogas upgrading process was able to remove 99.002% of the CO_2 from the raw biogas feed stream (Table 3), with the column designed to operate at acceptable column internal hydraulic condition.

Unlike other conventional upgrading technologies where CO_2 are recovered in gaseous form and requires intensive energy to regenerate and transport the CO_2 gas by compression, the low temperature processes recovers liquid CO_2which can be pressurized and transported by pumping at substantially lower energy cost. Furthermore, removal and recovery of CO_2 in

liquid form as a by-product rather than releasing same to the atmosphere as in the case of some conventional technologies make the low temperature upgrading process more environmentally friendly. The recovery of high purity liquid CO_2 (Table 3) is highly economical as it found a lot of usage, such as a sterilant with several potential benefits in sterilization of implants to prevents infections (Zhang *et al.*, 2006). Liquid CO_2found wide usage in the food industry for freezing meats, poultry, vegetables, and fruits, as well as to increase recovery from oil and gas wells (Air Products and Chemicals, 2014). The produced liquid CO_2, can be used for algae production for renewable and high valued fuels, chemical and fertilizers, as well as fire extinguisher because it is heavier than air and extremely stable. Liquid CO_2, also offers the ease of transportation to locations of its utilization which is a crucial advantage of the low temperature CO_2 removal technology.

3.2 Energy Analysis and Efficiency

Table 4 presents the energy requirement of the low temperature biogas CO_2 removal process. From the table it can be observed that the LHV and HHV rises from 20.5983MJ/m^3 to32.7178 MJ/m^3 and 22.8702MJ/m^3 to 36.3268 MJ/m^3, respectively, which is slightly lower than 21.5 MJ/m^3LHV and 23.5 MJ/m^3 LHV for raw biogas reported by Ilaboya *et al.* (2010) and Burkard (2009), respectively. Similarly, the HHV of the upgraded biogas which increased to 36.3268 MJ/m^3after treatment compared closely with 40 MJ/m^3reported by Burkard (2009) and Ilaboya *et al.* (2010).

Table 4: Energy Requirement of the low temperature CO_2 removal process

Parameters	Value
Power Consumed in terms of Raw Biogas (kW.hr/m^3)	0.1861
Power Consumed in terms of Upgraded Biogas(kW.hr/m^3)	0.2962
Power Consumed in terms of CO_2 Captured(kW.hr/m^3)	0.5009
LHV of Raw Biogas (MJ/m^3)	20.5983
HHV of Raw Biogas (MJ/m^3)	22.8702
LHV of Upgraded Biogas (MJ/m^3)	32.7178
HHV of Upgraded Biogas (MJ/m^3)	36.3268

The power and energy requirement of the low temperature CO_2 removal and biogas upgrading technique is depicted in Figure 4. From the figure, it can be seen that the total utilities energy requirement of the 1000 kmol/hr biogas plant is 6680.89 kW, with cooling utilities accounting for 5059.22 kW (75.74% of total utilities). This is because the process is a low temperature technology which requires more cooling to lower the operating temperatures at adjourning plant units. The established total utilities energy requirement of 6680.89 kW, is comparable to 5000 kW – 8000 kW reported by Beil *et al.*(2013) for chemical absorption technologies with organic solvents.

The power requirement of the established low temperature CO_2 removal process requires a total power consumption of 4401.05 kW (Figure 4), with the raw biogas compression accounting for 67.78% (2983.05 kW) of the total power required for the operation. This value is lower than the total power consumption of 6148 kW and biogas compression power consumption of 3598kW reported by Yousef *et al.*(2016) for same low temperature CO_2 removal technology. The operating conditions established in this work reduces the total power consumed by 28.41% when compared to that reported by Yousef *et al.*(2016). Also, from Figure 4, it was observed that the power requirement for the refrigeration cycle in this study is 1368 kW. This gives 45.50% reduction when compared to 2510 kW for the same

refrigeration cycle (Yousef *et al.*, 2016). However, the power consumption for liquid CO_2 pumping to 110 bar, which is the targeted export pressure for transport, is 50 kW for this study. This is higher compared to 40 kW reported by Yousef *et al.*(2016) to accomplish the same purposes. The power consumed by the liquid CO_2 account for 1.14% of the total power consumed by this low temperature technique.

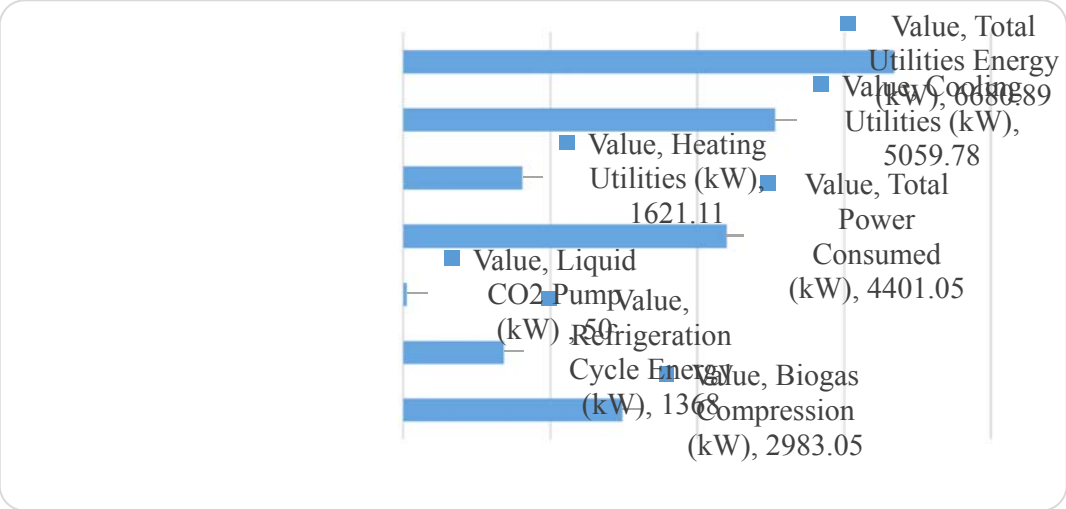

Figure 4: Energy Requirement for 1000 kmol/hr Low Temperature CO_2 Removal and Biogas Upgrading.

The specific power consumption by the process for both raw biogas and upgraded biogas are also presented in Table 4. This study shows that the specific power requirement for low temperature CO_2 removal and biogas upgrading technique is 0.1861 kW.hr/m^3 of raw biogas (Table 4). Yousef *et al.*(2016) reported the specific power consumed by the same process as 0.26 kW.hr/m^3 of raw biogas. The specific power consumption of 0.1861 kW.hr/m^3 of raw by the low temperature CO_2 removal and biogas upgrading technique compared favourably with 0.15 – 0.3 kW.hr/m^3 of raw biogas for PSA, 0.20 – 0.30 kW.hr/m^3 of raw biogas for membrane separation and 0.18 – 0.2.8kW.hr/m^3 of raw biogas for physical absorption processes by the manufacturers (Bauer *et al.*, 2013; Miltner *et al.*, 2016). However, 0.1861kW.hr/m^3 of raw biogas established for the low temperature biogas upgrading technique is higher than 0.12 – 0.14 kW.hr/m^3 of raw biogas for amines based absorption processes and 0.05 – 0.10 kW.hr/m^3 of raw biogas for water scrubing processess, but lower than 0.76 kW.hr/m^3 of raw biogasfor cryogenic separation (Bauer *et al.*, 2013), this shows that the low temperature upgrading technique compared favourably with existing processes. The variation in these processes are due to operation at lower and high plant capacity.

From Table 4, it can be seen that the power consumed by the low temperature biogas upgrading technique in terms of the upgraded biogas is 0.3228 kW.hr/m^3 of upgraded biogas. The power consumption of 0.3228 kW.hr/m^3 of upgraded biogas established in this study is lower compared to 0.41kW.hr/m^3 of upgraded biogas reported by Yousef *et al.*(2016). The 0.2962kW.hr/m^3 upgraded biogaspower consumption compared favorably with 0.2 – 0.46 kW.hr/m^3 upgraded biogas for water scrubbing, 0.13 – 0.56kW.hr/m^3 upgraded biogas for chemical absorption process, 0.32 – 0.67kW.hr/m^3 upgraded biogasfor physical absorption process, 0.21 – 0.46 kW.hr/m^3 upgraded biogas forPSA process and 0.19 – 0.43 kW.hr/m^3 upgraded biogas formembrane separation (Niesner *et al.*, 2013). Similarly, the power consumed in terms of the reported CO_2 captured or removed by the low temperature biogas upgrading technique in this study is 0.5009 kW.hr/m^3 CO_2 captured, which is lower compared

to 0.6590 kW.hr/m^3 CO_2 captured (Yousef *et al.*, 2016). From the energy analysis carried out in this study, it can be established that low temperature biogas upgrading technique is feasible and compared favorably with other available technologies in terms of energy and power requirement and consumption of the process.

A comparison of energy requirement of existing biogas upgrading technologies with the low teperature CO_2 removal technology considered in this study was carried to examine the technicalities of its operation in comparison to existing technologies. From Table 5, it can be seen that the Low Temperature CO_2 Removal (LTCR) technology compete favorably with other existing technology with the lowest CH_4 loss and heat requirement. However, the LTCR technology requires high pressure operation which is due to the raw biogas compression to liquid. Despite the high pressure operation, power requirement and heating requirement is one of the lowest, which make the LTCR technology technically viable and energy efficient. Table 5 futher shows that biogas upgrading using chemical absorption requires less power but has a high heat demand (particularly, with amine scrubber) which none of the other technologies have.

Table 5: Comparison of energy requiremet of biogas upgrading technologies

Parameters	LTCR	PSA	PWS	PA	CA	MS	CS
Power Requirement (kW.hr/m^3 BG)	0.1861	0.2 – 0.25	0.2 – 0.3	0.23 – 0.33	0.06 – 0.15	0.18 – 0.25	0.18 – 0.33
Heating Requirement (kW.hr/m^3 BG)	0.07	NA	NA	0.3	0.5 – 0.8	0	0
Process Pressure (bar)	1 – 49	4 – 7	5 – 10	4 – 7	0.1 – 4	4 – 10.	8 – 80
CH_4 Loss (%)	0.0062	1 – 5	0.5 – 2	1 – 4	0.1	2 – 8	NA
Chemical Requirement	No	No	No	Yes	Yes	No	No

LTCR= Low Temperature CO_2 Removal, PSA= Pressure Swing Adsorption, PWS= Pressurized Water Scrubing, PA = Physical Absorption with organic solvent, CA = Chemical Absorption with organic solvent, MS= Membrane Separations, CS= Cryogenic Separation, NA= Not Available

The energy consumption and power generated from the integrated power plant are presented in Table 6. The energy requirement of the compressor and the net power generated from the integrated power plant are 8985.67kW and 23035.97 kW (23.036 MW), respectively. Furthermore, the total utilities requirement of the power plant is 9216.08 kW (9.216 MW). Conversely, the thermal efficiency of the power plant is 47.387%, which is higher than 39.02 – 41.08% reported by Paoli (2008) and 40 – 45% for Olorunsogo Thermal Power Plant in Nigeria reported by Okoye *et al.* (2017) for similar combine cycle gas power plant. Similarly, the efficiency of the modeled power plant is comparable to 36.78 – 56.49% for GateCycle combined cyclegas power plant (CCGT) in Singapore (Liu and Karimi, 2018). However, the slightly low efficiency of the power plant (47.387%) compared to acceptable standard of 35 – 50 for thermal power plant could be attributed to the presence of 4.15 per cent of other non combustible gases in the the upgraded biogas. Therefore, the thermal efficiency of the modeled power plant is comparable to that of existing combine cycle power plant.

3.3 Sensitivity Analysis

Sensitivity analysis was carried out using the case study tool in Aspen HYSYS software package. The effect of fuel (Upgraded Biogas) temperature and pressure on power generated by the gas turbine were investigated. The temperature effect was examined between 20 – 120^oC and pressure in the range of 1000 – 4000 kPa. Figure 5(a) depict the effect of fuel (biogas) preesure on gas turbine power generated. It can be seen from Figure 5(a) that the power generated increases rapidly as pressure increases from 1000 – 2000 kPa maximum. However, from 2000 – 4000 kPa, there was no any change or effect on the power

generated.Figure 5(b) depict the effect of fuel (biogas) temprature on gas turbine power generated. It can be seen from Figure 5(b) that the power generated decreases rapidly and linearly as temperature increases from 20 – 120°C. This implies that increase in fuel (biogas) temperature have negative implication on the power generated by the gas turbine.

Table 6: Energy Utilized and Generated from The Power Plant

Parameters	kW	MW
Compressor Work	8985.67	8.986
Gas Turbine Power Generated	28993.12	28.993
Steam Turbine Power Generated	3028.52	3.029
Net Power Generated	23035.97	23.036
Pump Power	73.37	0.073
Total Utilities	9216.08	9.216
Overall Efficiency of Power Plant, %	47.387	47.387

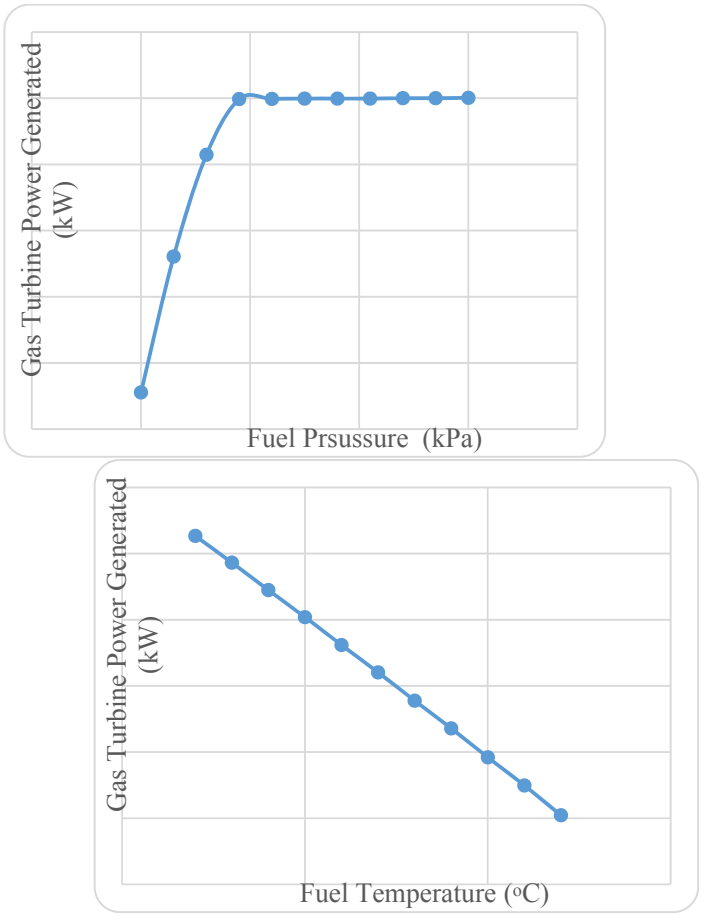

Figure 5: Effect of Fuel (Biogas) Preesure (a) and Temperature(b) on Gas Turbine Power Generated.

Also, the effect of air compressor exit pressure on gas turbine power generated was investigated in this study. From Figure 6(a), it was observed that as the air compressor exit pressure increases from 1000 – 1800 kPa, the power generated increases to a maximum and remain almost constant till 2400 kPa. Howeevr, as the pressure increases beyond 2400 kPa, the power generated reduces rapidly and linearly, this can be attributed to the fact that increase in pressure above 2400 kPa, rises the pressure ratio which inturn lower the efficiency of the gas turbine.This signifies that the best exit pressure for the air compressor is 1800 kPa, as presure below or above reduces the power genearated by the gas turbine (Figure 6b). Figure 6(b) depicted the effect of cycle water pressure on steam turbine power generation. From Figure 6(b), it can be seen that the power generated remain almost constant as the water pressure increases from 8000 – 13000 kPa and then decreases rapidly from 3017.108 – 1376.670kW as the water pressure increases from 13000 – 15000 kPa. However, the power generated remain constant as the water pressure increases to 17000 kPa. This signifies that the best cycle water pressure for maximum power output is in the range of 10000 – 12000 kPa, as presure above reduces the power genearated by the gas turbine.

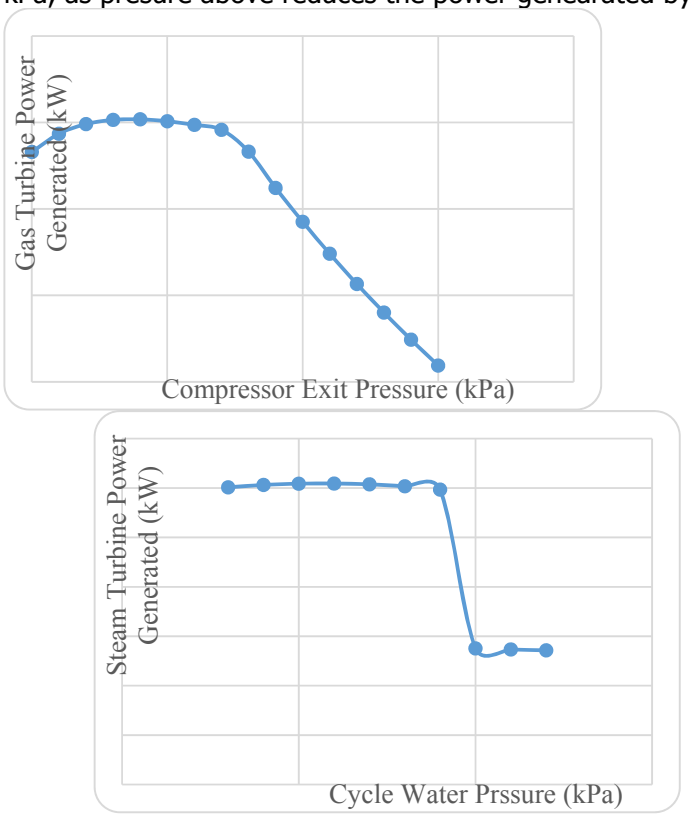

Figure 6: Effect of Compressor Exit Pressure (a)and Cycle Water Pressure(b) on Gas Turbine Power Generated

3.4 Economic Analysis

The economic evaluation of low temperature CO_2 removal and biogas upgrading technology was carried out to analyse the investment and economic fesibility of the process. The economic evaluation was carried by comparing the captial cost estimate (CAPEX) and Operating cost estimate (OPEX) with those of other available technologies. Table 7 present the economic evaluation of the low temperature CO_2removal and biogas upgrading technology. It can be seen that the total capital investment cost (CAPEX) needed for the project is estimated asUS$12,352,000, while the total operating cost (OPEX) is US$4,234,590

per year. The Operating cost makes up the cost of the total of raw material, utility, operating labor, maintenance, operating charges, plant overhead and the general and administrative costs associated with engineering, materials, and construction work.

Table 7: Parameters for Economic Evaluation of Low Temperature CO_2 Removal

Parameter	Cost (US$)	Cost (₦)
Total Project Capital Cost	12,352,000	3,952,640,000
Total Operating Cost(USD/Year)	4,234,590	1,355,068,800
Total Utilities Cost(USD/Year)	2,421,420	774,854,400
Desired Rate of Return (%)	20	20
Economic life	20 yrs.	20 yrs.
Total Cost of Project (CAPEX + OPEX)	16,586,590	5,307,708,800

The viability of the economics of the low temperature biogas upgrading technology was also carried and compared to other available technologies in terms of the the specific investment cost (comprises of total project capital cost and total operating cost). Figure 7 present a comparative analysis of the of low temperature biogas upgrading with other available technologies. From the figure, it was observed that water scrubbing technology has the lowest specific investment cost, followed by the low temperature biogas upgradingtechnology. However, amine based absorption has the highest specific investment cost, followed by physical absorption, membrane separation and PSA technology.Bauer*et al*. (2013), also reported that, amine based absorption is higher in specific investment cost in the lower to mid capacity, and the membrane technology is slightly lower in specific investment cost in the lower to mid-scale range capacity, however, at higher throughputs the investment costs tends to slightly reduce. It can also be seen from the figure that there is little difference from an investment point of view between the PSA, membrane separation and the physical absorption technologies. Therefore, it can be concluded that the low temperature biogas upgrading technology is compared favourably with other available technologies and can be said to be economically competative and feasible.

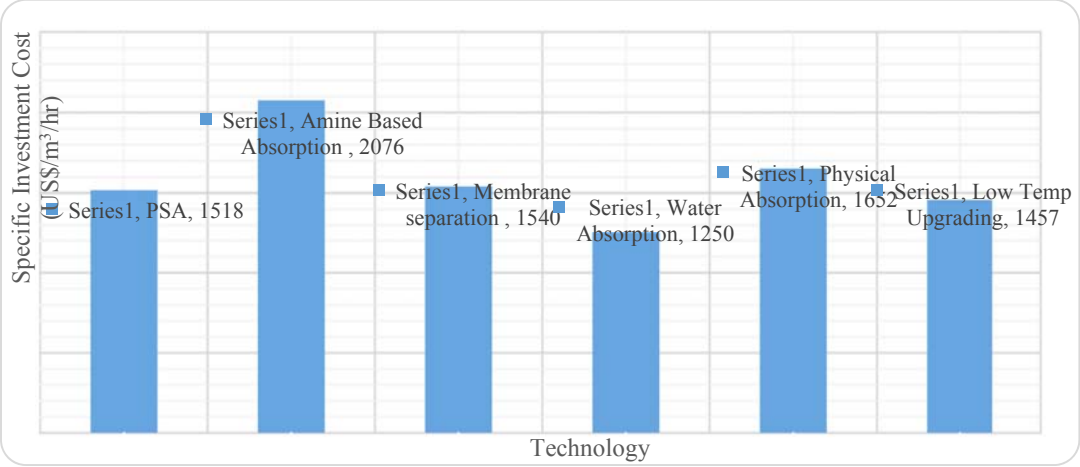

Figure 7: Comparative Analysis of the Economy of Low Temperature Biogas Upgrading and Other Available Technology

Table 8 presents the investment analysis of the integrated power plant. It can be seen from the table that the investment cost for the generation of 23035.97 kW (23.036 MW) is US$ 25,927,000.00 (₦8,296,640,000.00). This gives a specific investment cost of US$ 1,125,500.65/MW (₦ 360,160,206.62/MW). The specific investment of the modelled

integrated and upgraded biogas combined cycle power plant of US$ 1,125,500.65/MW is slightly higher than US$ 1,000,000.00 US$ 1,094,000.00/MW and slightly lower than US$ 1,150,000.00/MW recommended by National Electricity Regulatory Commission, International Energy Agency (IEA) and American Energy Organization (AEO) respectively in 2017 for combined cycle gas turbine power plant (Roche *et al.*, 2017). Thus, the obtained investment cost in this study compared favorably with internationally recommended cost per megawatt of combined cycle power plant.

Table 8:Economic Evaluation of the Integrated Power Plant

Parameter	Cost ($)	Cost (₦)
Exchange Rate	1	320
Total Capital Cost	25,927,000.00	8,296,640,000.00
Total Operating Cost/Year	8,861,900.00	2,835,808,000.00
Total Utilities Cost/Year	6,455,000.00	2,065,600,000.00
Desired Rate of Return /Year	20.00	20.00
Equipment Cost	15,814,300.00	5,060,576,000.00
Total Installed Cost	18,556,200.00	5,937,984,000.00
Specific Investment Cost/MW	1,125,500.65	360,160,206.62

A comparative study of the investment cost of the modelled power plant with other existing technologies was carried out. Figure 8 presents the result of the comparative analysis of the various sources of power generation. It can be seen from the figure that the combined cycle gas power plant (CCPP) has the lowest investment cost (CAPEX) of US$ 1,063,000.00/MW and could range from 0.76 – 1.51 million US$/MW. This shows that combined-cycle gas power plants are much cheaper and easier to build than coal and nuclear plants and are therefore more acceptable to local populations and if the economics are right, much more investable (WEC and BNEF, 2013; Roche *et al.*, 2017). The modelled power plant in this study is a CCPP, with a US$ 1,125,500.65/MW, which compared favorably with the CAPEX cost for the CCPP.

Figure 8: Comparative Analysis of Specific Investment Cost of The Modelled Power Plant With Other Power Generation Sources

FC=Fuel Cells, **GPP** =Geothermal Power Plant, **OnWPP**= Onshore Wind Power Plant, ***OfWPP***=*Offshore Wind Power Plant,* ***HPP***=*Hydropower Plant,* ***RPP***= *Renewable/ Biomass Power Plant,* ***STP***=*Solar Thermal Plant,* ***SPP***=*Solar Photovoltaic Plant,* ***SPCP***= *Standard Pulverized Coal Plant,* ***CCPP***=*Combined Cycle Power Plant,* ***NNPP***=*New Nuclear Power Plant,* ***MPP***=*Modelled Power Plant.*

The capital cost of a power generating plant can vary widely depending upon the technology.Of the established and conventional technologies presented in Figure 8, including nuclear, fossil fuel and hydropower-based generating plants the cheapest by a wide margin is the CCPP. On the higher side of the CAPEX, a modern nuclear plant is likely to cost over US$ 6,350,000 – US$ 8,375,000/MW and US$7,350,000.00/MW on average. Of all the advanced and renewable/biomass technologies, geothermal power plant stands to be the cheapest at US$1,666,000.00 on average, with wind power plant close behind(WEC and BNEF, 2013; IEA and NEA, 2015; Roche *et al.*, 2017). Therefore the integrated biogas power plant is economically feasible and compared favourably with the developed process.

Table 9 present the economic analysis of the low temperature biogas upgrading and an integrated power plant. From the table, it can be seen that the combined CAPEX of the low temperature CO_2 removal and the integrated power plant is US$ 1,661,705.53/MW which is comparable with the cost of other power generation technologies presented in Figure 8. Therefore, biogas generation for power generation in Nigeria is a viable option to meet the power availability challenges in Nigeria especially with the high biodegradable waste generated across cities and communities in Nigeria.

Table 9: Economic Analysis of the Low Temperature CO_2 removal with the Integrated CCPP

Parameter	CO_2 Removal	Power Plant	CO_2 Removal and Power Plant
Total Capital Cost [US$]	12,352,000	25,927,000.00	38,279,000.00
Total Operating Cost [US$/Year]	4,234,590	8,861,900.00	13,096,490.00
Total Utilities Cost [US$/Year]	2,421,420	6,455,000.00	8,876,420.00
Equipment Cost [US$]	3,565,100	15,814,300.00	19,379,400.00
Total Installed Cost [US$]	5.957,100	18,556,200.00	24,513,300.00
Specific Investment Cost, $/MW		1,125,500.65	1,661,705.53

4.0 CONCLUSION

Low temperature CO_2 removal technique was successfully simulated and the feed pressure and temperature to the distillation were established as 4800 kPa and 223 K (–50°C) respectively to avoid freeze-out of CO_2 which is often a challenge encountered with low temperature CO_2removal.The concentration of CH_4 increases from 60.233 mol.% in raw biogas to 95.848 mol.% in upgraded biogas at the simulated column condition with a recorded 0.0062% CH_4 loss, while the concentration of CO_2 increases from 37.467 mol.% in raw biogas to 99.815 mol.% in the liquid CO_2 stream. The high purity liquid CO_2 obtained in this process is the primary advantage of the process compared to other conventional technologies, since high purity liquid CO_2 is a valuable by-product used as sterilant, freezing meats, vegetables and fruits, algae production for renewable and high valued fuels, chemical and fertilizers as well as to increase recovery from oil and gas wells, which makes the process more environmentally friendly.

The low temperature CO_2 removal technique rises the LHV and HHV from 20.5983 MJ/m^3 to 32.7178 MJ/m^3 and 22.8702 MJ/m^3 to 36.3268 MJ/m^3, respectively with a specific power requirement of 0.1861 kW.hr/m^3 of raw biogas and 0.3228 kW.hr/m^3 of upgraded biogas, which compared favorably with the other available biogas upgrading technologies in terms of power requirement and consumption of the process. Similarly, the net power generated from the integrated power plant is 23035.97 kW (23.036 MW) with a thermal efficiency of 47.387%

that comparedcompetatively with existing combine cycle power plants.The sensitivity analysis of the operating conditions showed that power generated is maximum at 2000 kPa fuel (Biogas) pressure, decreases rapidly from 20 – 120^{o}C fuel temperature, maximum at 1800 kPa air compressor exit pressure and maximum between 12000 – 13000 kPa.

The economic evaluation of low temperature CO_2 removal technology showed that the specific investment cost (comprises of total project capital cost and total operating cost) is US$ 1457/m^3/hr and compared favourably with other available technologies for CO_2 upgrading, while the specific investment cost for the integrated power plant is US$1,125,500.65/MW of power generated which also compete favorably with internationally recommended cost per megawatt of combined cycle power plants. Conversely, the specific cost of the combined low temperature biogas upgrading technique and the integrated power plant is US$ 1,661,705.53/MW of power generated, which showed that biogas utilization for power generation in Nigeria is a viable option to meet the power availability challenges in Nigeria especially with the high biodegradable waste generated across cities and communities in Nigeria.

ACKNOWLEDGEMENT

The researchers wish to acknowledge the management of Egbin power plant, Lagos for granting usthe opportunity to use their plant data for our research.

REFERENCES

Abdulsalam A., Mohammed, A., Abubakar, G. I., Kovo, A. S. and Olanrewaju, A. O. (2018). Comparative Studies on the Kinetics of Biogas Purification Using Activated Carbon and Zeolite, *2nd International Conference on Science and Sustainable Development*, IOP Conference Series: Earth and Environmental Science: 1 – 15.

Aderemi, A. O., IIori, M. O., Aderemi, H. O. and Akinbami, J. F. K. (2009). Assessment off Electrical Energy use Efficiency in Nigeria food Industry. *African Journal of food Science*. Vol. 3(8): 206-216.Air Products and Chemicals, 2014

Alhassan, M., Andrew, I., Auta, M., Umaru, M., Garba, U. G., Isah, A. G. and Alhassan, B. (2017). Comparative studies of CO_2 capture using acid and base modified activated carbon from sugarcane bagasse, *Biofuels*, DOI:10.1080/17597269.2017.1306680.

Babar, M., Bustam, M. A., Ali, A. and Maulud, A. S. (2018). Identification and Quantification of CO2 Solidification in Cryogenic CO_2 Capture from Natural Gas, *International Journal of Automotive and Mechanical Engineering*, Vol. 15, Issue 2: 5367 – 5376.

Bauer, F., Hulteberg, C., Persson, T. and Tamm, D. (2013). Biogas Upgrading – Review of Commercial Technologies, *Swedish Gas Technology Centre (SGTC)*, Malmo, Sweden.

Beil, M., Beyrich, W., Holzhammer, U. and Krause, T. (2013). Biomethane, Federal Ministry of Food, Agriculture and Consumer Protection, FachagenturNachwachsendeRohstoffee. V. (FNR): Germany: 15 – 30. Available from www.druckerei-weidner.de, accessed: 21/11/2018Berstad *et al.* (2011),

Berstad, D., Anantharaman, R. and Nekså, P. (2013). Integrated Low-Temperature CO2 Capture from IGCC Power Plant by Partial Condensation and Separation of Syngas, *Chemical Engineering Transactions*, Vol. 35, p. 355 – 60.

Burkard, Thilo (2009): Project cases of Biogas-plants in Kenya. Presentation for Biogas Delegation Trip, Agritechnica 2009. Clearly presented detailed analysis of the technical and economic aspects of 5 biogas power plants in Kenya.

Cheng-Hsiu, Y., Chih-Hung, H. and Chung-Sung, T. (2012). A Review of CO_2 Capture by Absorption and Adsorption, *Aerosol and Air Quality Research*, Taiwan 12: 745–769. doi: 10.4209/aaqr.2012.05.0132.

De-Guido, G., Langè, S., Moioli, S. and Pellegrini, L. A. (2014). Calculation of CO_2 freezing points in mixtures using SRK and PR EOSs, *Journal of Energy Challenges and Mechanics*, Vol. 1, Issue 4, Article 3: 185 – 191.

Eze, J. I. and Agbo, K. E. (2010). Maximizing the potentials of biogas through upgrading, *American Journal of Scientific and Industrial Research*. 1(3): 604-609. (Mshandete and Parawira, 2009)

Ilaboya, I. R., Asekhame, F. F., Ezugwu, M. O., Erameh, A. A. and Omofuma, F. E. (2010). Studies on Biogas Generation from Agricultural Waste; Analysis of the Effects of Alkaline on Gas Generation, *World Applied Sciences Journal*, 9 (5): 537-545, 2010

International Energy Agency (IEA) and Nuclear Energy Agency (NEA) (2015). Projected Costs of Generating Electricity 2015 Edition, *Organisation For Economic Co-Operation And Development*, France: 111 – 113.

Liu, Z. and Karimi, I. A. (2018). Simulating combined cycle gas turbine power plants in Aspen HYSYS, *Energy Conversion and Management*, 171: 1213–1225.

Miltner, M., Makaruk, A. and Harasek, M. (2016). Selected Methods of Advanced Biogas Upgrading, *Chemical Engineering Transactions*, Vol. 52: 463 – 468. Available from www.aidic.it/cet.

Mori, Y. and Forsyth, J. (2013), High Performance CO_2 Capture by Autothermal AGR, Energy Procedia, Proc. 11th International Conference on Greenhouse Gas Control Technologies (GHGT-11), Kyoto, Japan, p. 9.

Moussa, P. B. and Malcolm, C. D. (2019). Electricity Access in Sub-Saharan Africa: Uptake, Reliability and Complementary Factors for Economic Impact. Africa Development Forum of World Bank Group.

Murshid, G., Shariff. A. M. and Keong, L. K. (2011). Thermo physical analysis of 2-amino-2-methyl-1-propanol solvent for carbon dioxide removal. ChemEngTrans.;25:45–50. DOI:10.3303/CET1125008.

Ngumah, C. C., Ogbulie, J. N., Orji, J. C. and Amadi, E. S. (2013). Biogas potential of Organic Waste in Nigeria. *Journal of Urban and Environmental Engineering*, Vol. 7, No. 1, p. 110 – 116.

Niesner, J., Jecha, D. and Stehlík, P. (2013). Biogas Upgrading Technologies: State of Art Review in European Region, *Chemical Engineering Transactions*, Italy, Vol. 35: 517 – 522.

Okoye, C. U., Adeniji, O. A. and Sunmonu, A. O. (2017). A Study and Performance Evaluation of Olorunsogo Thermal Power Plant in Nigeria, *International Journal of Engineering Sciences and Research Technology (IJESRT)*, 6(12), December: 151 – 158.

Olawoyin, O. (2017). Nigeria's current electricity generating capacity is 6,803 MW, Premium Times: August 15. Available at https://www.premiumtimesng.com/news/more-news/240258-nigerias-current-electricity-generating-capacity-6803-mw-fashola.html, Accessed: 15/04/2018

Paoli, N. (2008). *Simulation Models for Analysis and Optimization of Gas Turbine Cycles*, MSc. Thesis in Chemical Engineering, Università di Pisa: 68 – 88.

Roche, M. Y., Ude, N. and Ofoegbu, I. D. (2017). Comparison of Costs of Electricity Generation in Nigeria, Report of Nigerian Economic Summit Group and Heinrich BöllStiftung Nigeria, Abuja, June: 20 – 34.

Rochelle, G. T. (2009). Amine Scrubbing for CO_2 Capture. *Science*, 325: 1652–1654.

Ryckebosch, E. Drouillon, M., Vervaeren, H. (2011). Techniques for Transformation of Biogas to Biomethane. Journal of Biomass and Bioenergy 35, 1633-1645.

Sipöcza, N., Hernandez-Nogales, A., Gonzalez-Salazar, M. A., Shisler, R. and Lissianski, V. (2013). Low Temperature CO_2 Capture for Near-Term Applications, *Energy Procedia*, 37: 1228 – 1238.

Sutanto, S., Dijkstra, J. W., Pieterse, J. A. Z., Boon, J., Hauwert, P. and Brilman, D. W. F. (2017). CO_2 Removal from Biogas with Supported Amine Sorbents: First Technical Evaluation Based on Experimental Data, *Separation and Purification Technology*, 184: 12–25

Warren, K. E. H. (2012). A techno-economic comparison of biogas upgrading technologies in Europe, M.Sc. Thesis in Biological and Environmental Science, University of Jyväskylä, p. 9 – 13.

Wijeratne, D. and Omontuemhen, P. (2016). Powering Nigeria for the Future: The power Sector in Nigeria July 2016, *pwc*. Available from, www.pwc.com/gmc, accessed: 27/08/2019.

World Energy Council (WEC) and Bloomberg New Energy Finance (BNEF) (2013). World Energy Perspective: Cost of Energy Technologies: 1 – 44.

Yousef, A. M. I., Eldrainy, Y. A., El-Maghlany, W. M. and Attia, A. (2016). Upgrading Biogas by a Low-Temperature CO_2 removal Technique, Alexandria Engineering Journal, 55(2): 1143–1150. http://dx.doi.org/10.1016/j.aej.2016.03.026

Zhang, J., Davis, T. A., Mattews, M. A. Drews, M. J., Laberge, M. and An, Y. H. (2006). Sterilization Using High-Pressure Carbon Dioxide, *Journal of Supercritical Fluids*, Science Direct, 38: 354 – 372.

Zhao, Q., Leonhardt, E., MacConnell, C., Frear, C. and Chen, S. (2010). *Purification Technologies for Biogas Generated by Anaerobic Digestion*, Climate Friendly Farming, CSANR Research Report, 001: 1 – 20.

Proceedings of the 49th NSChE Annual Conference
KADA 2019: pp 610-617

P3B-05: EFFECT OF FERRIC SULPHATE:CAO/Al_2O_3 RATIO ON CONVERSION OF JATROPHA CURCAS OIL TO BIODIESEL

Nelson Jack Evangnum [1], Suleiman Yunusa[1]*, Abdulkareem Abubakar [1] and Haruna Ibrahim[2]
[1]**Dep**artment of Chemical Engineering, Ahmadu Bello University, Zaria, Nigeria
[2]Langtang Outstation, National Research Institute foe Chemical Technology, Langtang-Nigeria
*Email: slmnyunus@gmail.com, +2348038951472

ABSTRACT
Mixture of Ferric sulphate and Calcium oxide supported with alumina were employed as catalysts in this study. Calcium Oxide was synthesised from cow bone and supported with alumina for single step simultaneous esterification and transesterication of jatropha curcas oil and the result was compared with commercial Calcium oxide (CaO). Effect of $Fe_2(SO_4)_3$: CaO/Al_2O_3 was studied using 1:1, 2:1, 3:1 and 4:1 at 5 weight % catalyst loading, 15:1 methanol to oil mole ratio, 60 °C reaction temperature and 2 hour reaction time. Ratio of 4:1 $Fe_2(SO_4)_3$: CaO/Al_2O_3 gave optimum conversion as indicated by gas chromatography and mass spectrometry (GCMS) analysis. The catalyst was analysed using BET machine while produced biodiesel were analysed using FTIR and GCMS machine respectively. The GCMS gave a fatty acid methyl ester (FAME) conversion of 96.72% for biodiesel from CaO derived from cattle bone and 97.01% for commercial CaO at optimum condition. Mixture of $Fe_2(SO_4)_3$ and CaO/Al_2O_3 was found to produce high biodiesel yield in a one-step esterification and transesterification process.
Keywords: Biodiesel; *Jatropha curcas*; Calcium Oxide; Aluminium Oxide; Transesterification

1.0 INTRODUCTION
Fossil fuel has played a very vital role as energy in our day to day activities. Due to the depletion of fossil fuel reserve and the adverse effect of fossil fuel in the environment, there is need for a renewable source with no negative effect to the environment. Biodiesel is a renewable fuel which serves same purpose as conventional diesel fuel. Biodiesel is environmental friendly because it has low carbon dioxide emission, biodegradable fuel, high cetane number and combustion efficiency, lower aromatic and sulphur content unlike petroleum diesel (Gemma *et al*., 2004). Addition of Alumina support is to affect its surface area and increase the basic sites. Biodiesel is usually produced through esterification and transesterification reactions of vegetable oils and/or animal fats with an alcohol. Methanol or ethanol is usually the alcohol for biodiesel preparation in the presence of either homogeneous or heterogeneous catalyst. The use of CaO for transesterification of oil with high FFA (above 1%) is difficult. The amount of free fatty acid (FFA) is important in order to select the appropriate catalyst (Fangrui *et al*., 1999).

One step simultaneous esterification and transesterification is a method of producing biodiesel in just a single reaction. The conventional method of biodiesel production requires a first step reduction of high FFA content of oils by acid-catalysed esterification followed by an alkali-catalysed transesterification which is the second step(Zhang *et al*., 2003). Homogeneous catalysts are difficult to recover, hence increasing the cost of biodiesel production (Endalew *et al*., 2011). Heterogeneous acid catalysts are an alternative to avoid the alkaline pathway for producing alkyl esters from oils with a high content of free fatty acids (Policano *et al*., 2016). In the conventional two steps, Sulphuric acid which is a homogeneous catalyst and not easily recoverable is often used in the first step because of its high conversion and low cost

(Zhang *et al*., 2003). These disadvantages and high cost of metal oxides have caused research for different sources of heterogeneous catalysts (Sabat *et al*., 2017). Bones among other raw materials are several sources of calcium such as eggshells and mollusks. Bone consists of organic and inorganic materials (Sabat *et al*., 2017). Bones consists of inorganic materials such as calcium phosphate (65-70%), protein and collagen matrix (30-35%). Inorganic materials of natural sources contain the main components of calcium phosphate and calcium carbonate, with little magnesium, fluoride, and sodium, phosphorus, manganese, tin and copper (Prasuna *et.al*, 2004).

Ferric sulphate is a substitute for sulphuric acid for the esterification of FFA since it is heterogeneous hence, easy to recover (Wang *et al*., 2006). It is environmental friendly and easy to separate. Ferric sulphate has much higher catalytic activity compared to sulphuric acid (Wang *et al*., 2006). *Jatropha Curcas* is an oil bearing plant that has high oil yield compared to other non-edible plants and it is drought resistant (Achten *et al*., 2007 and Becker *et al*., 2008). *Jatropha Curcas* is non-edible and can grow in non-arable land without causing food crisis since its non-edible (Ibrahim *et al.,* 2014). In this study, one step esterification and transesterification of *Jatropha curcas* oil and methanol was carried out using ferric sulphate and cow bone ash as source of CaO. Result was compared with commercial calcium oxide bought from Cardinal scientific supplier Zaria. The products obtained were analyzed with GC-MS and FTIR for esters yield and viscometer for viscosity. Also the acid value, iodine value, saponification value, cloud point, pour point and density were analyzed.

2.0 METHODOLOGY

2.1 Materials/ Equipment

The *Jatropha Curcas* oil (JCO) used for this research were supplied by National Research Institute for Chemical Technology (NARICT). Cow bones were sourced from Abattoir, Zango, Zaria, Kaduna State. Methanol, Calcium Oxide and Ferric Sulphate were obtained from Cardinal Chemicals, Zaria. Alumina was collected from the Chemical Engineering Departmental store. Equipment used are gallenkamp hot plate magnetic stirrer, 500 ml one neck flat bottom flask, funnel, filter paper and thermometer.

2.1 Preparation of Cow Bone Ash (CBA)

Calcium Oxide was prepared from cow bone collected from Abattoir, Zango, Zaria, Kaduna State. The Cow bones were first washed with water to remove dirt from the bones. The bones were boiled with water for 1 hour at 120 ^oC to aid the removal of oil, fats, tissues and flesh from the bones. The cow bones were oven dried at 105 ^oC for 24 hour, crushed using an electric crushing machine and further ball milled and sieved with 125 µm. The sieved cow bone was calcined at 900 ^oC for 2 hour.

2.2 Preparation of CBA/Al_2O_3 Catalyst

The wet impregnation method was employed for the preparation of CBA/Al_2O_3 catalyst. Alumina was used as support on the prepared catalyst because of its high surface area and high thermal stability. 80 % Alumina was mixed with 20 % CaO in 40ml distilled water. The solution was first evaporated at 70 ^0C for 60 min on a water bath and oven dried at 120 ^0C for 90 minutes and calcined at 700 ^oC for 90 minutes

2.3 Determination of FFA

1.0 g of *Jatropha Curcas* oil sample was dissolved in 25 ml of propan-2-ol with addition of two drops of phenolphthalein to the solution. The solution was titrated against 0.1M potassium hydroxide till pink colour is seen. A separate titration (blank) was performed by titrating 25

ml of propan-2-ol against 0.1M potassium hydroxide. The difference of the two titre values (V) was used to determine the FFA of the oil.

$$\text{FFA} = \frac{0.1M \; x \; V \; x \; 56.1 \; g/mol}{1.0 \; g} \quad \text{..... (1)}$$

$$\%\text{FFA} = \frac{FFA}{2} \quad \text{..... (2)}$$

2.4 One Step Esterification and Transesterification

One step esterification and transesterification was carried out for methyl ester production from *Jatropha Curcas* oil. The use of one step as against the conventional two step is to reduce the overall time of reaction, reduce cost of materials and energy consumption. In this work, reaction temperature of 60 ^oC, 120 minutes reaction time, 15:1 methanol to oil ratio (mole ratio) and agitation rate of 400 rpm were kept constant while Ferric Sulphate: CaO/Al_2O_3 ratio were varied. 50 g of oil was weighed and placed in a 500 ml flat bottom flask and was heated using a gallenkamp hot plate magnetic stirrer at 60 ^oC for 60min. Mixture of $Fe_2(SO_4)_3$ and CaO/Al_2O_3 with methanol was added to the oil, magnetic stirrer was dropped into the reactor and the reaction mixture was allowed to react for 120 minutes. After the end of each reaction time, the catalyst was filtered off and the filtrate was transferred into a separating funnel and allowed to separate overnight. The glycerol which is denser than the biodiesel was collected at the bottom while the biodiesel was washed with hot water to remove impurities after which it was taken for FTIR and GCMS analysis.

2.5 Catalyst characterization and biodiesel analysis

The catalyst CaO/Al_2O_3 was characterised for BET surface area, pore size and pore volume using a NOVA 4200e BET machine. FTIR and GCMS were used for analysis of the biodiesel produced.

3.0 RESULTS AND DISCUSSIONS

3.1. BET Surface Area of Calcined Cow Bone Supported with Alumina

The catalyst surface area was analysed using NOVA 4200e BET machine. The multipoint BET surface area of the supported cow bone with alumina was found to be 533.9 m^2/g with pore volume of 0.2722 cc/g and width of 2.647nm. The high surface area of the supported catalyst was due to high ratio (80% alumina) of alumina on the precursor catalyst. Kouzu *et al*, (2009) and Zabeti *et al,* (2010) reported that high surface area reduces leaching of precursor to medium and produced a high fatty acid methyl ester conversion. The high fatty acid methyl ester conversion is due to alumina's large specific area which enhances high dispersion of active sites (Theodoro *et al*., 2017). Xie *et al* (2006) reported that alumina-supported potassium iodide gave the highest catalytic activity and highest conversion compared to non-supported catalyst. Zabeti *et al,* (2010) used an alumina support on heterogeneous catalyst and confirmed the supported catalyst has the highest conversion. High surface area, large pore volume and smaller pore sizes allow triglycerides of different sizes to enter the pores of the catalyst, which gives a large surface for proper transesterification (Sulaiman N.B, 2017).

3.2. Transesterification

The FFA of the raw *Jatropha curcas* oil was calculated to be 6.3 using equation 1 above hence %FFA is 3.15. FTIR and GCMS were used to analyse the biodiesel produced for conversion obtained. GCMS analysis gave FAME conversion of 96.72% for CaO from cattle bone ash and 97.01% for commercial CaO at 2 hour reaction time, 15:1 methanol to oil ratio, temperature of 60^oC and 5wt% catalyst at 4:1 Ferric sulphate: CaO/Al_2O_3 ratio.

One step transesterification of JCO using CaO/Al_2O_3 and ferric sulphate as catalyst was done using CaO sourced from cow bone ash and commercially sourced CaO. The FTIR peaks of JCO at 1744.4 confirm the presence of Fatty acid methyl ester. These methyl esters were also confirmed in a GCMS analysis where all the esters and the masses of the esters present were listed as shown in table 2. The biodiesel samples had specific gravity of 0.89 and 0.88 which are within range of 0.86-0.9 EN standard (Barabás and Todoruţ, 2011). Their viscosity was 4.78 also fall within the range 3.5 -5.0 EN standard and 1.6-6.0 ASTM standard (Barabás and Todoruţ, 2011).

Table 1. Physical Properties of *Jatropha Curcas* oil Biodiesel

Property	JCO	Biodiesel from CBA	Commercial CaO	ASTM D6751 -02 STANDARD/ EN 14214
Ester content		96..72 %	97.01 %	96.5 %
Density at 40^0C (g/cm^3)	0.92	0.89	0.88	0.875-.900
Viscosity at 40^0C (mm^2/s)	32.50	4.78	4.78	1.9 – 6.0
Acid value (mg KOH/g)	12.6	0.264	0.12	0-0.5
Pour point ^{0}C	-	4	3	−15 to 16
Cloud point ^{0}C	-	13	10	−3.0 to 12
Iodine value (mg I/100g oil)	102	104	105	120

Their acid values are lower than the minimum standard for both EN and ASTM 0.5 mg KOH/g (Ibrahim et al, 2018); hence they are suitable for use in any diesel engine. The physicochemical properties are shown in Table 1. The GCMS analysis gave a FAME conversion of 97.01% for biodiesel using commercial CaO and 96.72% biodiesel using cow bone ash supported on alumina. The biodiesel produced from synthesized cow bone and commercial CaO meets minimum ASTM standard of 96.5 % for conversion.

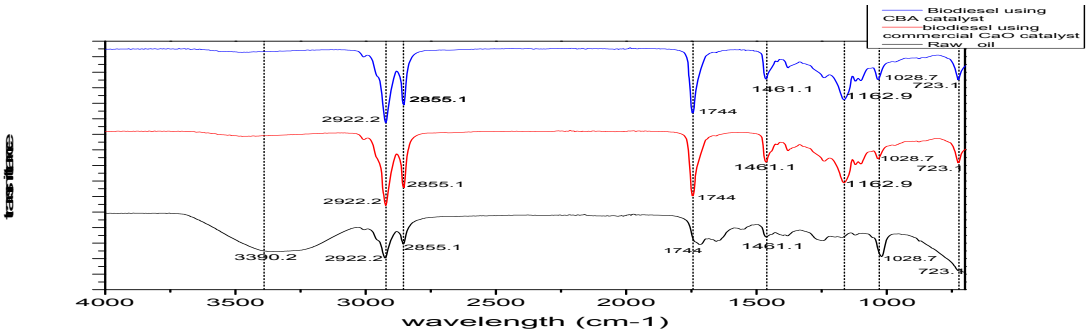

Figure 1: FTIR analysis of JCO at optimum

3.3. FTIR analysis

The presence of fatty acid methyl esters can be detected by the FTIR analysis. The spectra of raw oil and biodiesel produced using CaO/Al_2O_3 and CBA/Al_2O_3 is shown in Figure 1. The most intense and broad peaks occur at 2922 cm^{-1}, 2855 $cm^{-1,}$ 1744 $cm^{-1,}$ 1461 $cm^{-1,}$ 1162 cm^{-1} and 723 cm^{-1}. From the plot, the peaks corresponding to presence of metal carboxylates were absent as depicted by a flat profile within the expected range of 1580 – 1541$cm^{-1.}$ Tanwar *et al.,* (2013) independently reported that peaks corresponding to 1750 – 1730cm^{-1} represent the presence of fatty acid methyl esters which are essentially biodiesel. Peaks at 1744 cm^{-1} is the case of produced biodiesel which has low peak for the raw oil. The differences observed between the spectra of raw oil and biodiesel is small since the product of the transesterification process (FAME) is chemically similar to its precursor (*Jatropha curcas oil*). The peaks at 1461 cm^{-1} corresponds to the asymmetric stretching of -CH3 present in the biodiesel spectrum and absent in the raw oil spectrum (Soares *et al.*, 2008). The stretching of O-CH3, represented by the absorbance at 1162 cm^{-1}, is typical of biodiesel. Region between 1075–1100 cm^{-1} is present only in the raw oil spectrum and absent in biodiesel. This findings are similar to previous ones for products of biodiesel.

3.4. Effect of ferric sulphate:CaO/Al_2O_3 ratio on conversion

The effect of ratio of ferric sulphate to supported calcium oxide was studied on conversion of biodiesel at reaction condition of 60 ^{0}C reaction temperature, 120 min reaction time and 15:1 methanol to oil ratio. At 5 wt % catalyst loading, ratio of ferric sulphate to CaO/Al_2O_3 at 1:1 gave a conversion of 89.72% for biodiesel using commercial CaO and 88.23% using CaO synthesized from cow bone. Ratio of ferric sulphate to CaO/Al_2O_3 was adjusted to 2:1 and a noticeable increase in yield of biodiesel was confirmed and soap formation was reduced from product formed. The optimum conversion was at 4:1 ferric sulphate to CaO/Al_2O_3 ratio as shown in figure 3. Alumina supported CaO with ferric sulphate enhanced high fatty acid methyl ester conversion for single step transesterification. These findings concurs with Theodoro *et al.*, (2017) who reported that alumina has very large specific area which enhances high dispersion of active sites.

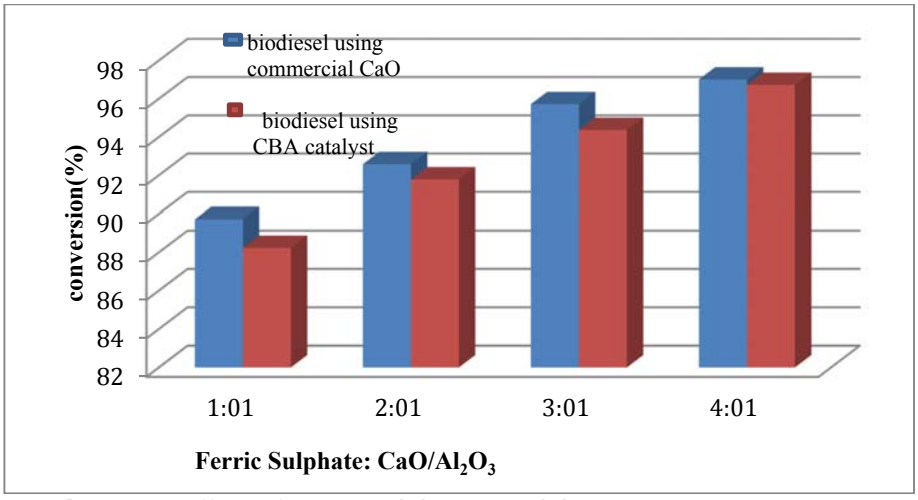

Figure 3: Effect of Ferric Sulphate:CaO/Al_2O_3 Ratio on Conversion

Table 2: GCMS Analysis for Produced Biodiesel

CMS result for biodiesel using cow bone derived CaO catalyst on alumina support as catalyst				**GCMS result for biodiesel using commercial CaO catalyst on alumina support as catalyst**			
S/N	**Compound**	**Molecular Formula**	**Conversion %**	**S/N**	**Compound**	**Molecular Formula**	**Conversion %**
1	*Methyl hexadecanoate	$C_{17}H_{34}O_2$	5.47	1	*Methyl heptadecanoate	$C_8H_{10}O_3$	5.46
2	2-Methyl-Z,Z-3,13-octadecadienol NE	$C_{19}H_{36}O$	0.63	2	* Methyl Linoleate	$C_{19}H_{34}O_2$	4.75
3	* Methyl Palmitate	$C_{17}H_{34}O_2$	21.69	3	Ethylene glycol monooleate NE	$C_{20}H_{38}O_3$	0.78
4	*Methyl Margarate	$C_{18}H_{36}O_2$	2.17	4	*Methyl pentadecanoate	$C_{21}H_{42}O_2$	4.06
5	*Methyl Tridecanoate	$C_{14}H_{28}O_2$	0.78	5	* Methyl Oleate	$C_{19}H_{36}O_2$	12.09
6	*Methyl Behanate	$C_{23}H_{46}O_2$	1.65	6	*Methyl Myristate	$C_{15}H_{30}O_2$	5.90
7	*Methyl Arachidate	$C_{21}H_{42}O_2$	0.12	7	* Methyl Palmitate	$C_{17}H_{34}O_2$	10.56
8	* Methyl Oleate	$C_{19}H_{36}O_2$	17.06	8	* Methyl Stearate	$C_{19}H_{38}O_2$	11.19
9	*Methyl Myristate	$C_{15}H_{30}O_2$	0.21	9	* Methyl hexadecanoate	$C_{24}H_{48}0_2$	6.36
10	n-Octacosane NE	$C_{28}H_{58}$	0.76	10	*Methyl Heneicosanoate	$C_{22}H_{44}O_2$	3.27
11	* Methyl Stearate	$C_{19}H_{38}O_2$	17.22	11	*Methyl trans-9-octadecanoate	$C_{25}H_{48}O_2$	21.05
12	* Methyl Tetracosanoate	$C_{24}H_{48}0_2$	2.23	12	*Methyl 9-octadecenoate	$C_{18}H_{36}O_2$	12.32
13	*Methyl Heneicosanoate	$C_{22}H_{44}O_2$	5.31	13	Hexadecanenitrile NE	$C_{16}H_{31}N$	1.04
14	*Methyl Eicosadienoate	$C_{21}H_{38}O_2$	4.34	14	2,6-Dimethoxyphenol NE	$C_8H_{10}O_3$	1.17
15	*Methyl trans-9-octadecanoate	$C_{25}H_{48}O_2$	15.12	-	-	-	-
16	*Methyl Margarate	$C_{18}H_{36}O_2$	2.56	-	-	-	-
17	*Methyl Melissate	$C_{31}H_{62}O_2$	0.79	-	-	-	-
18	Tetracosane NE	$C_{24}H_{50}$	1.17	-	-	-	-
19	Z-8-Methyl-9-tetradecenoic acid NE	$C_{15}H_{28}O_2$	0.72	-	-	-	-

4.0 CONCLUSIONS

One step simultaneous esterification and transesterification method using heterogeneous catalysts (ferric sulphate, commercial calcium oxide and synthesized calcium oxide from cow bone) both anchored on alumina was carried out on *Jatropha curcas* oil. High biodiesel quality of 97.01 and 96.72 % methyl esters yields were obtained from that catalysed by commercial and synthesized calcium oxide catalysts respectively. These were achieved at 2 hours with mole ratio of 15:1 methanol to oil at 60°C. This method reduces cost and time as the catalysts used are recoverable by simple filtration. Biodiesel of high ester yield was successfully

produced using One step simultaneous esterification and transesterification with ferric sulphate:CaO/Al_2O_3 at 4:1.

4. REFERENCES

Achten W.M.J, Mathijs E, Verchot L, Singh VP, Aerts R, Muys B (2007). Jatropha biodiesel fueling sustainability: A perspective. Biofuels Bioprod Biorefin.1, 283-291.

Barabás I. and Todoruţ I. (2011). Biodiesel Quality, Standards and Properties, Biodiesel-Quality, Emissions and By-Products, Dr. Gisela Montero (Ed.), ISBN: 978-953-307-784-0, InTech, Available from: http://www.intechopen.com/books/biodiesel-quality-emissions-and-by-products/biodiesel-qualitystandards-and-properties

Fangrui M, Milford A, H. (1999). Biodiesel production: A review. Bio resources Technology., 70: 1-15.

Gemma V., Martınez M, Jose A. (2004). Integrated biodiesel production: a comparison of different homogeneous catalysts systems. Bioresource Technology 92, 297–305

Ibrahim H., Chika E, Aminu H, Deborah C.U.N, Olabode O, Amina A, Amina M.I (2014) : Comparison of palm oil and *Jatropha curcas* oil for biodiesel production in Nigeria using bulk CaO catalyst. International Journal of emerging technologies and engineering 1, 28-32.

Ibrahim H., Ahmed A. S., Bugaje I. M. and Mohammed-Dabo I. A. (2018). Product Qualities of Biodiesel Produced from a Process Intensify Pilot Plant. *Chemical Science International Journal 22(2): 1-13, 2018; Article no.CSIJ.40501 ISSN: 2456-706X*

Policano M. D., Rivaldi J. D., de Castro H. F., Carneiro L. M (2016). Simultaneous esterification and transesterification of andiroba oil using niobium oxide-sulfate as catalyst. International Journal of Engineering Research and Science 2, 2395-6992.

Prasuna. C.P.L., Narasimhulu. K.V., Gopal. N.O., Rao. J.L., Rao. T.V.R.K. (2004). The Microstructures of Biomineralized Surfaces: a Spectroscopic Study on the Exoskeletons of Fresh Water (Apple) Snail, Pila Globosa. Spectrochimica Acta Part A, 60, 2305-2314.

Sabat O.C.S, Risfidian M (2017): Preparation of calcium oxide from cattle bones as catalyst for conversion of waste cooking oil to biodiesel. Science and Technology Indonesia, 2, 77-79.

Soares I. P., Rezende T. F., Silva R. C., Castro E. V. R., and Forte I. C. P. (2008). Multivariate calibration by variable selection for blends of raw soybean oil/biodiesel from different sources using Fourier Transform Infrared spectroscopy (FTIR) spectra data, *Energy Fuels* (22), 2079-2083.

Sulaiman, N. B. (2017). Response surface methodology for the optimum production of biodiesel over Cr/Ca/r-Al2O3 catalyst: catalytic performance and physicochemical studies. *Renewable energy, 113*, 697-705.

Tanwar, D., Ajayta, D., Mathur, Y., and Sharma, D. (2013). Production and Characterization of Neem Oil Methyl Ester. *International Journal of Engineering Research and Technology. 2*(5), 1896 -1902.

Theodoro, P., Pedro, A., and Silva, E. A. (2017). Synthesis of bifunctional calcium oxide supported on gamma alumina for biofuel production from the transesterification of crambe oil . *Acid base catalysis*, 7-10.

Wang, Y., Ou, S., Liu, P., and Zhang, Z. (2006): Preparation of biodiesel from waste cooking oil via two-step catalyzed process. Energy Conversion and Management.

Xie, W. and Li, H. (2006). Alumina-supported potassium iodide as a heterogeneous catalyst for biodiesel production from soybean oil. *Journal of Molecular Catalysis A: Chemical*, 255: 1-9.

Zhang Y, Wong, W.T, Yung K.F, (2013). One-step production of biodiesel from rice bran oil catalysed by chlorosulfonic acid modified zirconia via simultaneous esterification and transesterification. Bioresource Technology 147, 59-64.

Zabeti, M., Daud, W. M. A. W. and Aroua, M. K. (2010). Biodiesel production using alumina-supported calcium oxide: An optimization study. *Fuel Processing Technology*, 91: 243–248.

Proceedings of the 49th NSChE Annual Conference
KADA 2019: pp 618-627

P3B-06: UTILISATION OF RESPONSE SURFACE METHODOLOGY FOR THE OPTIMIZATION OF OIL EXTRACTION FROM *ALBIZIA LEBBECK* SEEDS

Sani Inuwa Lamido, Ibrahim Muazu , Hawawu Salami and Murtala Mohammed
Department of Chemical Engineering, Kaduna Polytechnic, Kaduna, Nigeria
e-mail:i.lamido@kadunapolytechnic.edu.ng, Phone no.: +2348030632639

ABSTRACT
Oil from Albizia lebbeck was successfully extracted considering three factors (particle size, solvent volume and time of the extraction) at three levels. Response Surface Methodology (RSM) with Box-Behnken Design (BBD) was performed using STATISTICA v10 software to determine the optimum operating conditions for the oil extraction process using oil yield as the response. The maximum predicted percentage yield was 26.86% at particle size of 0.17 mm, solvent volume of 262 ml and 4.8 hrs extraction time. Analysis of variance (ANOVA) indicates that the model was significant as evidenced from R^2 of 0.99998. Hence the model can be used for prediction of Albizia lebbeck seed oil yield in essential oil extraction. Analysis on physicochemical properties of the oil showed that the oil has a pH, refractive index, acid value, iodine value and saponification value of 7.28, 1.474, 13.46mgKOH/g, 65.7g/100g, and 223mgKOH/g respectively The results of GCMS analysis of the extracted Albizia lebbeck seed oil shows that the oil majorly contain linoleic acid (41.9%).
Key words: *Albizia lebbeck, Essential Oil, Response Surface Methodology (RSM), Box-Behnken Design (BBD).*

1. INTRODUCTION

The extraction of essential oil for consumption and medicinal use in Nigeria is still inadequate in view of a huge gap between demand and supply of such oil. Trading Economics (2019), reported that Nigeria's import of essential oils, perfumes, cosmetics was at $327.2 million in 2018 according to the United Nations COMTRADE data base on international trade.
Oil from plants source especially their seed have recently gained prominence and attention because of their wide range of applications. In addition to them being the major source of essential oils, they are also good source of raw materials for industries for the production of lubricants, fuels for paraffin lamps, additives for paint formation and soap production (Attenberger *et al*., 2005, Rozzi *et. al.,* 2002 and Fadel *et. al.,* 1999).

Albizia lebbeck (L.) Benth. (Mimosaceae) is a medium- sized deciduous tree native to India (Tripathi et al., 1979; Lowry et al., 1998). The trees have compound leaves, flat oblong fruits, round cream colored seeds (Ghani, 2003). It can grow five meters (5m) in one year and produce 100-120 kg edible dry matter per year (Lowry et al.,1998). *A. lebbeck* is a fodder tree for semi-arid regions in the tropics and subtropics (Orwa et al., 2009). The seedlings develope to a long stout taproot at an early age and are drought-tolerant. *A. lebbeck* has many common names such as Lebbeck, Karana, Walnutt; Siris tree, Kokko, fry wood, woman's tongue and Rattle tree. It is commonly known in Nigeria as "*eshegeshege*" in Bini and "*igbagbo*" in Yoruba dialects. The bark is used for tanning fishing nets, treating boils, as a soap, anthelmintic, anti-inflammatory and in treatment of bronchitis, toothache and leprosy (Rashid et. al., 2003; Kirtikar and Basu, 1980); leaves and seeds were used for eye problems (Orwa et. al., 2009).

In Nigeria, *A. lebbeck* is planted on road sides as shade trees, in village as forests for fuel wood production and in front of schools or college premises as ornamental tree. (Lawan *et. al.,* 2017 and Mohammed *et. al*., 2007).

Design of experiment (DOE) is a systematic method to determine the relationship between factors affecting a process and the output of the process. This information is needed to manage process input in order to optimize the output (response) (Rahman *et. al.,* 2007, Box *et. al.,* 1978 and Dong *et. al.,* 2009).

Current literature markedly lacked enough data and information about the oil content and composition of *Albizia lebbeck* widely grown in Nigeria; this study aimed to identify the physicochemical properties of oil extract from the seed of *A. lebback* through statistical optimization of the extraction process.

2.0 METHODOLOGY

Seed Pre-treatment

Albizia lebbeck seed was obtained from the trees in Kaduna polytechnic main campus, Kaduna state, Nigeria. The pod was broken to obtain the seeds that were washed thoroughly to remove dirt and impurities. These seeds were decorticated by winnowing to remove the hull from the seeds. The weight of the seeds (W1) was measured and then placed in an oven at 50 ^{o}C for drying until constant weight (W2) was obtained. The dried seeds were grounded and the sample was expressed on a standard sieve screen of 0.154 mm, 0.30 mm and 0.45mm to obtain the different particle sizes.

Experimental Procedure

Oil extraction was performed using soxhlet apparatus and was performed at least twice to minimize error, with ethanol as solvent. Fifty gram of dried *Albizia* seed sample (0.154 mm) was measured and placed in a filter paper. The prepared sample was inserted into the thimble and placed in the inner tube of the soxhlet apparatus. The apparatus was fitted with a 250 ml round bottom flask containing 150 ml of the solvent. The setup was then placed on a heating mantle and then boiled for 4 hrs at 80^{o}C and then the flux was trapped in the condenser. The oils were obtained after refluxing at 80^{o}C so as to remove any excess solvent used for the oil extraction. The extracted Albizia lebbeck oil was isolated from the solvent (Ethanol) using the same soxhlet extractor but with the leachate removed. The same procedure was repeated for other runs from the design of experiment presented in Table 1.

The amount of solvent recovered was measured using a measuring cylinder as well as the mass of the oil was also measured. The percentage of oil yield was calculated and tabulated for each round.

Design of Experiment

Box-Behnken Design (BBD), with three factors (Particle size, Solvent volume, and Time) and percentage oil yield as response, was chosen for the experimental design. The coded and un-coded levels of the independent variables were shown in Table 2. For statistical analysis, the relationship between the coded and actual (un-coded) variables can be represented by Equation (1).

$$X_{\mathrm{i}} = \frac{Z_{\mathrm{i}} - Z*}{\Delta Z} \qquad (1)$$

Where X_i = the coded i^{th} variable, Z_i = the actual i^{th} variable, ΔZ = step change of Z variable, $Z*$ = center point values for the i^{th} variable, Number of variable, i= 1 – 3

The design of the experiment based on Box-Benkhen Design having 3 factors and 15 runs is shown in Table 1 using STATISTICA Version 10.0 Software package for implementing RSM methodology. The percentage oil yield for each experimental run of the input parameters (i.e., particle size, time and solvent volume) are also shown in the same table.

Table 1: Box-Behnken Design for the Extraction of *Albizia lebbeck* Seed Oil

	1 Particle Size (mm)	2 Solvent Volume (ml)	3 Time (hr)	4 Yield (%)	5 Var5
1	0.154000	150.0000	4.000000	22.28	
2	0.450000	150.0000	4.000000	13.24	
3	0.154000	350.0000	4.000000	26.86	
4	0.450000	350.0000	4.000000	13.92	
5	0.154000	250.0000	2.000000	21.24	
6	0.450000	250.0000	2.000000	12.24	
7	0.154000	250.0000	6.000000	28.02	
8	0.450000	250.0000	6.000000	15.91	
9	0.300000	150.0000	2.000000	14.1	
10	0.300000	350.0000	2.000000	14.83	
11	0.300000	150.0000	6.000000	18.95	
12	0.300000	350.0000	6.000000	19.28	
13	0.300000	250.0000	4.000000	16.14	
14	0.300000	250.0000	4.000000	16.1	
15	0.300000	250.0000	4.000000	16.12	

Table 2.1: Coded and Un-coded Level of the Independent Variables

Factors	**Low (-1)**	**Centre (0)**	**High (1)**
Particle size (mm)	0.154	0.30	0.45
Solvent Volume (ml)	150	250	300
Reaction Time(hr)	2	4	6

Polynomial Modeling of oil extraction from Albizia lebbeck seed

The 15 designed experimental runs were conducted and the results (response) was analysed with ***STATISTICA V10***. The following quadratic model equations (Equation 2 and Equation

3), in uncoded terms, are the equations that correlates the oil yield to various process parameters. The intercept and coefficient of the linear effects, quadratic effects and interaction effects are presented in Table 3.

Table 3: Regression Coefficient of Predicted Quadratic Polynomial Model for Oil Yield

Regr. Coefficients; Var.:Yield (%); R-sqr=.99215; Adj:.97803 (Albezia 3 3-level factors, 1 Blocks, 15 Runs; MS Residual=.5066982
DV: Yield (%)

Factor	Regressn Coeff.	Std.Err.	t(5)	p	-95.% Cnf.Limt	+95.% Cnf.Limt
Mean/Interc.	26.4636	4.30819	6.14262	0.001661	15.389	37.5381
(1)Particle Size (mm)(L)	-87.6593	12.91806	-6.78580	0.001057	-120.866	-54.4524
Particle Size (mm)(Q)	129.2939	16.91609	7.64325	0.000610	85.810	172.7781
(2)Solvent Volume (ml)(L)	0.0198	0.02127	0.92946	0.395313	-0.035	0.0745
Solvent Volume (ml)(Q)	0.0000	0.00004	0.52977	0.618945	-0.000	0.0001
(3)Time (hr)(L)	1.2005	0.94534	1.26987	0.260018	-1.230	3.6305
Time (hr)(Q)	0.1184	0.09261	1.27886	0.257084	-0.120	0.3565
1L by 2L	-0.0654	0.02405	-2.71937	0.041806	-0.127	-0.0036
1L by 3L	-2.6199	1.20236	-2.17896	0.081219	-5.711	0.4709
2L by 3L	-0.0005	0.00178	-0.28097	0.789991	-0.005	0.0041

The oil yield (OY) equation in terms of significant parameters for the un-coded factors is given in Equation 2 as:

$$OY = 26.4636 - 87.6593*A + 0.0198*B + 1.2005*C + 129.2939*A^2 + 0.1184*C^2 - 0.0654*A*B - 2.6199*A*C - 0.0005*B*C \quad (2)$$

Where A = Particle size, B= Solvent volume, and C=Time

Both the quadratic and linear terms of the Particle size have significant effect on the response parameter with p-value < 0.05 so as the interactive effect between the linear terms of particle size and solvent volume. The linear and quadratic effect of both solvent volume ant time of extraction appears to have no significant effect on the response with p-values > 0.05. Also, the interactions between the linear terms of particle size and solvent volume, and that of solvent volume with time are also non-significant on the yield of oil. This can further be visualized in Figure 1 Pareto chart where the linear effect of particle size is the most significant. This is followed by the linear effect of time. Other significant terms in hierarchy of being more significant are quadratic effect of particle size, linear effect of solvent volume, then the interactive effects of the particle size and solvent volume.

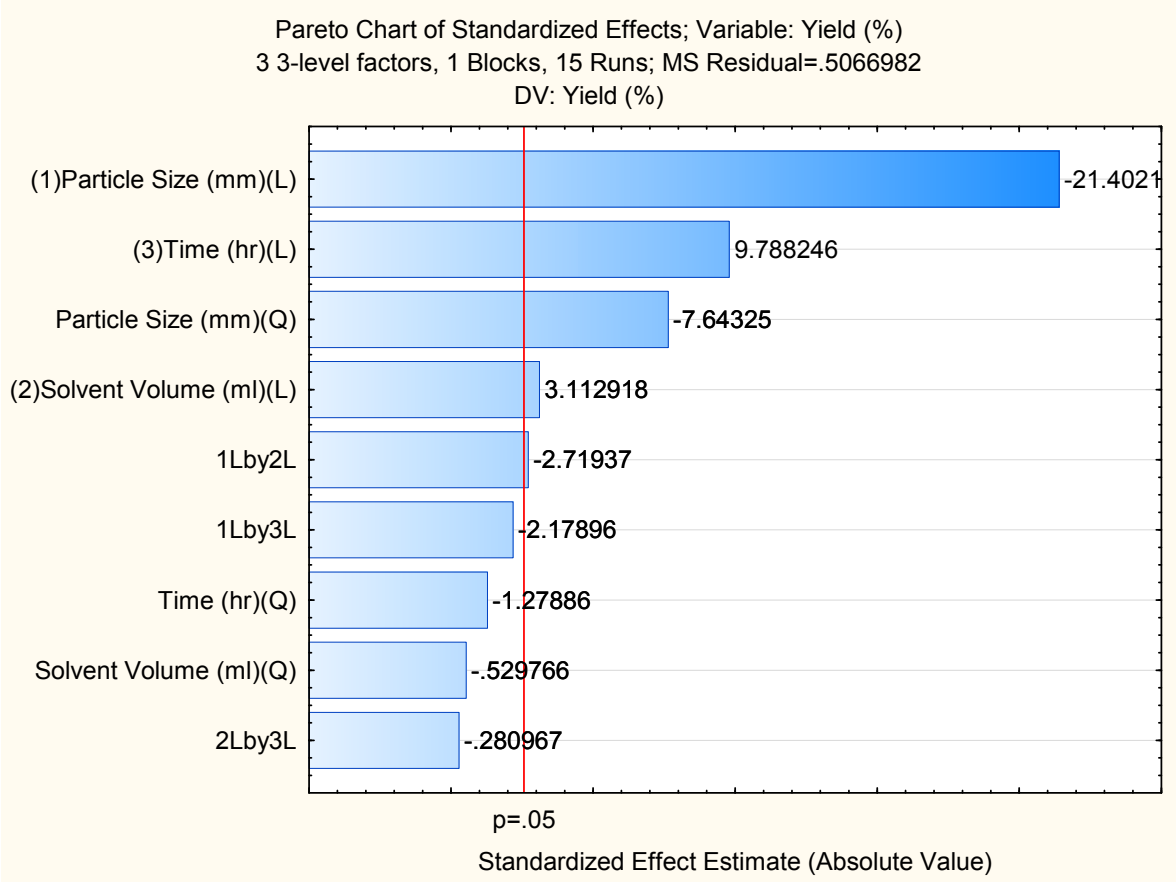

Figure 1: Pareto Chart of the Standardized Effects of variables on Oil yield.

To further confirm the validity of the model, residual analysis and normal probability plot was done. Figure 2 shows the plot of predicted values against observed values. This shows how closed the assumed model is to the predicted values as all observed values are fitted. This is also the reason behind the high R^2 value observed.

Analysis of Variance (ANOVA)

Statistical analysis of the model was performed to evaluate the ANOVA and check the adequacy of the empirical model. The result of ANOVA for fitting the quadratic response surface model by a mean square method are summarized in Table 4. The coefficient of the response surface model as provided by Equation 2 in the un-coded factor were also evaluated. The significance of each of the coefficient are checked from P-value (probability of error value) which also indicate the interaction strength of each parameter. According to Table 4, the p-values of the investigated parameters are all less than 0.05, demonstrating high significance in predicting the response values and the suitability of the model. The high F-values with corresponding very low probability value indicate the high significance of the fitted model. Table 4 presents the significance of all coefficient established by p-values.The value of the R^2 was 0.99215 and adjusted R^2 was 0.97803 which shows model significance.

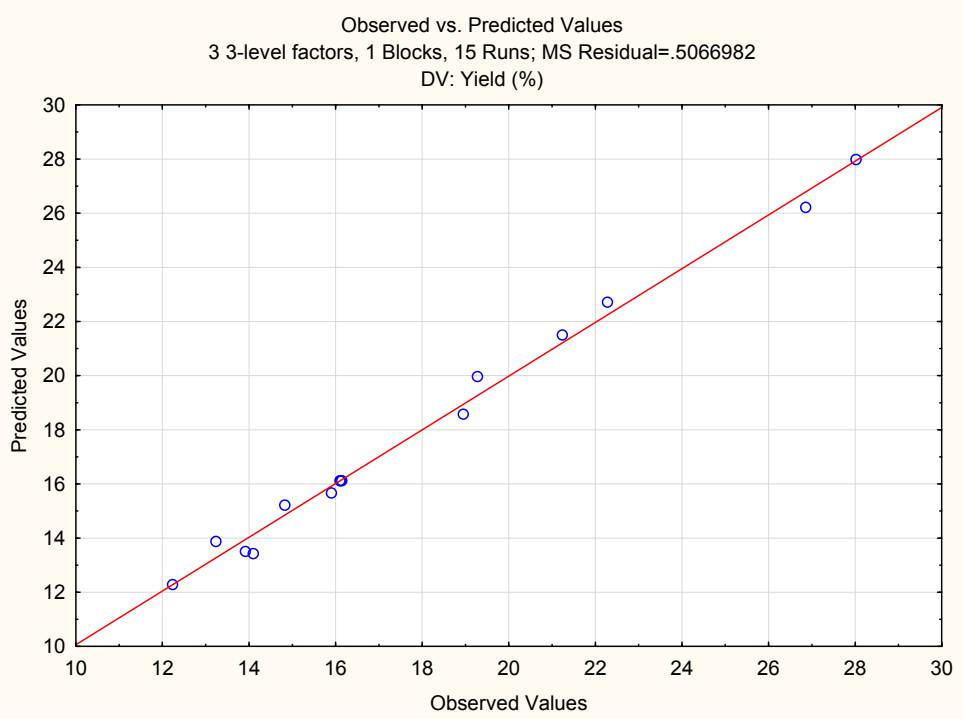

Figure 2: Predicted Values Vs Observed Values

Analysis of Variance (ANOVA)

Statistical analysis of the model was performed to evaluate the ANOVA and check the adequacy of the empirical model. The result of ANOVA for fitting the quadratic response surface model by a mean square method are summarized in Table 4. The coefficient of the response surface model as provided by Equation 2 in the un-coded factor were also evaluated. The significance of each of the coefficient are checked from P-value (probability of error value) which also indicate the interaction strength of each parameter. According to Table 4, the p-values of the investigated parameters are all less than 0.05, demonstrating high significance in predicting the response values and the suitability of the model. The high F-values with corresponding very low probability value indicate the high significance of the fitted model. Table 4 presents the significance of all coefficient established by p-values.The value of the R^2 was 0.99215 and adjusted R^2 was 0.97803 which shows model significance.

Response Surface Analysis

The effects of process variables on the response variable can be further elaborated by visualization using response surface plots. Figure 3a shows the effect of particle size and solvent volume on oil yield, as the particle size decreases with increasing volume of solvent as oil yield increases. Thus, the curve nature of the graph indicates the significance of the quadratic terms. In Figure 3b a similar trend was observed for the effects of particle size and the time of extraction. Oil yield increases with a decreasing particle size as the time of extraction increases.

Whereas Figure 3c, the effect of the quadratic terms on oil yield is of less significance as compared to Figure 3a and 3b. As time increases, oil yield increase but a little change was noticed for an increase in solvent volume oil yield. Thus, the interactive effect of time and solvent volume is more dominant by the linear terms.

Table 4: ANOVA for response surface quadratic model

Factor	ANOVA; Var.:Yield (%); R-sqr=.99215; Adj:.97803 (Albezia Oil New) 3 3-level factors, 1 Blocks, 15 Runs; MS Residual=.5066982 DV: Yield (%)				
	SS	df	MS	F	p
(1)Particle Size (mm) L+Q	260.1946	2	130.0973	256.7550	0.000009
(2)Solvent Volume (ml) L+Q	5.0522	2	2.5261	4.9855	0.064462
(3)Time (hr) L+Q	49.3753	2	24.6877	48.7226	0.000526
1*2	3.7470	1	3.7470	7.3950	0.041806
1*3	2.4057	1	2.4057	4.7479	0.081219
2*3	0.0400	1	0.0400	0.0789	0.789991
Error	2.5335	5	0.5067		
Total SS	322.9300	14			

.

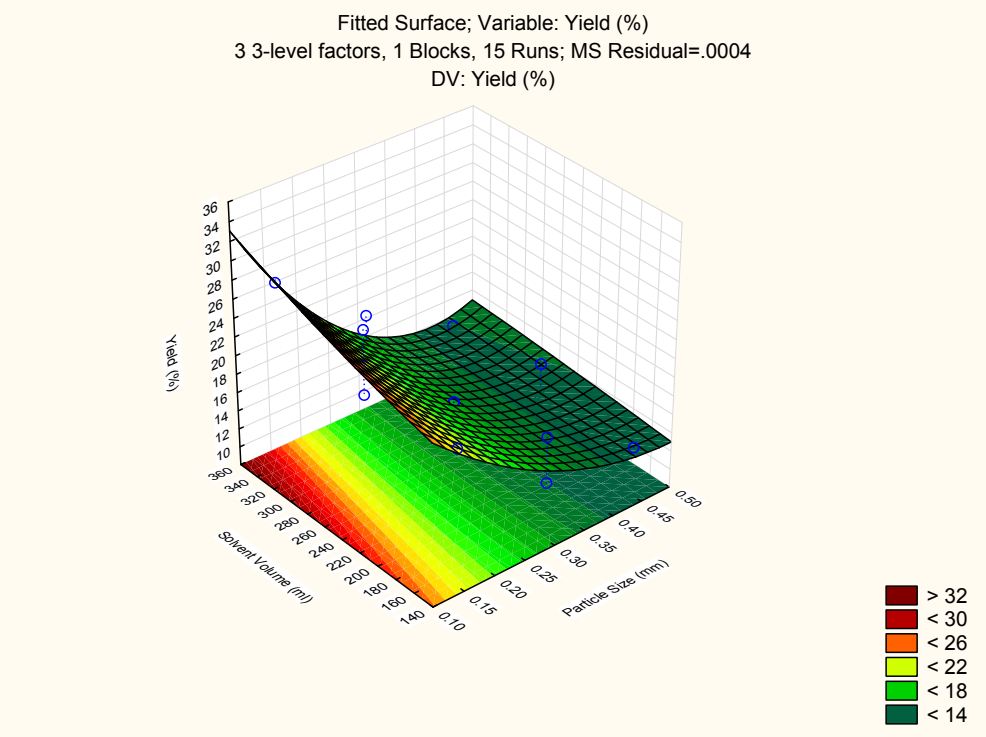

Figure 3(a): Effect of Particle Size (mm) and Solvent Volume (ml) on Oil Yield

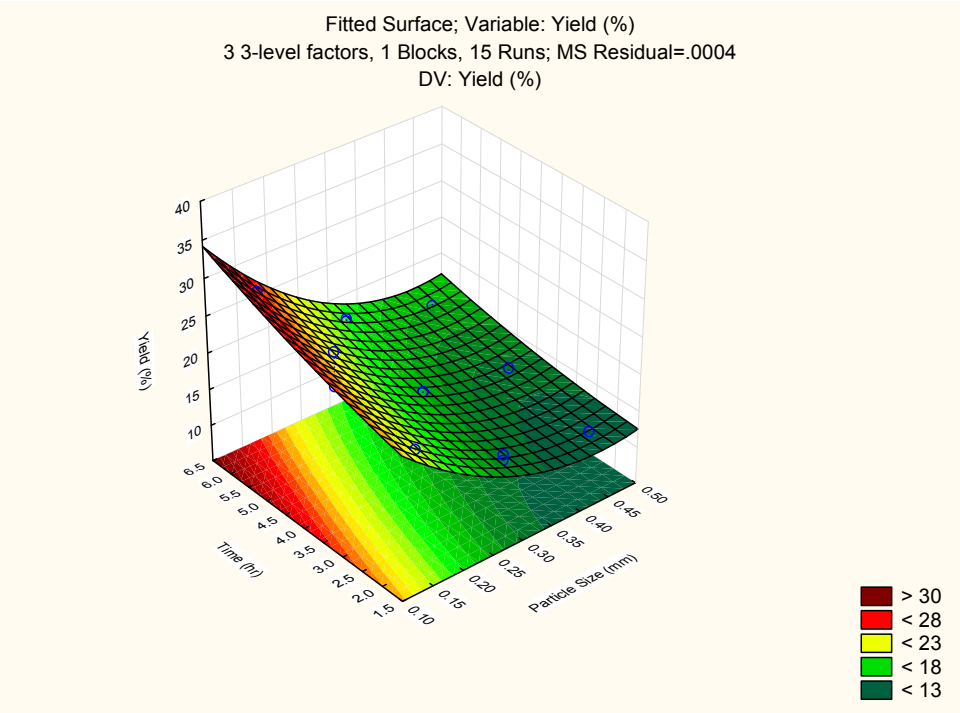

Figure 3(b): Effect of Time (hr) and Particle Size (mm) on Oil yield

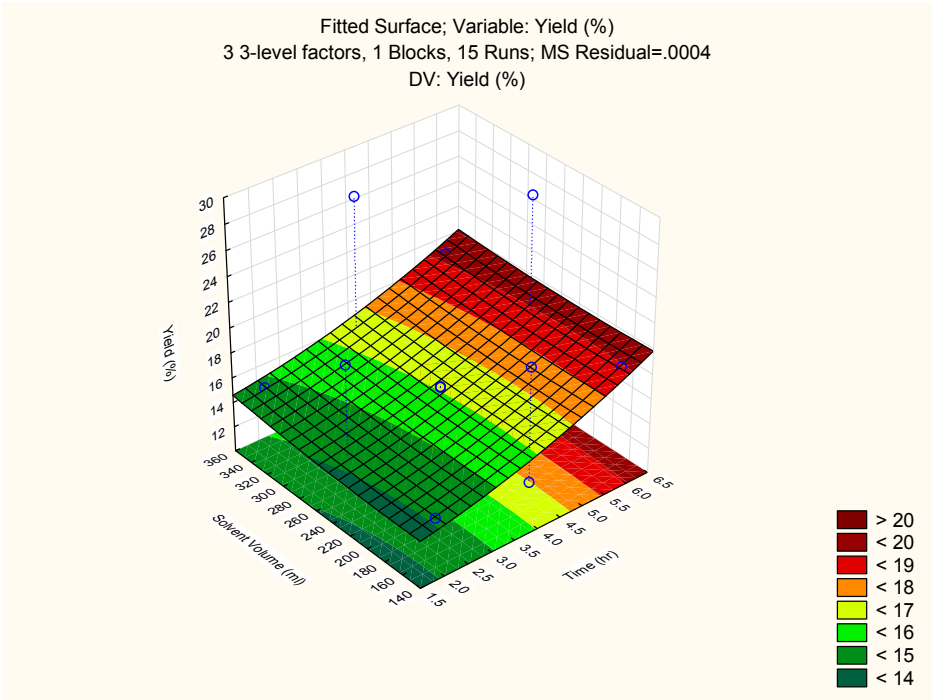

Figure 3(c): Effect of Solvent Volume (ml) and Time (hr) on Oil Yield

Optimization and Validation of the Model

Multiple regression analysis was employed for the prediction of the optimum parameters from the experimental result. From the regression analysis result generated by STATISTICA V10 software, the optimum input values of particle size (A), solvent volume (B) and time (C) are given in coded and uncoded terms as presented in Table 5. The uncoded variables were evaluated using Equation. (1).

Table 5: Coded and Uncoded values for the three Optimum Variable Factors.

Factors	Coding	Xi	Z*	ΔZ	Zi	
Particle Size (mm)	A	-0.8450	0.3	0.15	0.1733	
Solvent Volume (ml)	B	0.1243	250	100	262.43	
Time (hr)	C	0.3886	4	2	4.78	

The optimum parameters of 0.1733, 262.43 and 4.78 are substituted into Equation 2 to obtain the optimum values of the response (Oil Yield) as 15.35%. Confirmatory experiments were conducted in triplicate using the optimum values, to confirm the validity of the model, and the average OY from the confirmatory test was calculated to be 15.02%.

Physicochemical Properties of extracted oil

The oil extracted was analysed so as to characterize it. The physicochemical properties of the oil are given in Table 6.

Table 6: Physiochemical properties of the extracted *Albizia lebbeck* seed oil

Properties	**Extracted Oil**	**Literature Values** (Ajay, 2014 and Maryam et. al., 2009)
Acid Value, mgKOH/g	13.46	12 – 15
Free Fatty Acid (FFA), %	6.73	< 7.0
Saponification value, mgKOH/g	223	201 – 235
Peroxide Value, mg/100g	57.3	30– 70
Iodine value, g/100g	65.7	57 – 113
Specific gravity, 28°C	0.964	0.850 – 0.969
Density, mg/ml	0.903	0.890
Refractive Index, 28 °C	1.474	1.3 – 1.67
Viscosity, cp	4.800	4.600 – 4.900
pH	7.28	7.0 – 8.0

CONCLUSION

The optimization of oil extraction through the application of response surface methodology from locally grown *Albezia lebbeck* seeds was successfully carried out. A quadratic model was developed and the effect of parameter interactions was also examined. Optimum model parameters such as particle size of 0.1733 mm, solvent volume of 262.43 ml and time of 4.78 h were established for the extraction of oil from seeds of *Albizia lebbeck* within the experimental limits. The oil extracted at optimum conditions shows characteristics and properties such as acid value of 13.46 mgKOH/g, FFA of 6.73%, saponification value of 223 mgKOH/g and iodine value of 65.7 g/100g similar to that essential oils.

REFERENCES

Ajay, K. (2014). Physico-chemical and natural products investigations of essential oil from the rhizomes of Kaempferia galangal, Pelagia Research Library, Der Chemica Sinica, 5(2):91-94.

Attenberger A., Matthäus B., Brühl L., Remmele, E. (2005). Research into the influencing factors on the quality of cold pressed rapeseed oil used as edible oil and determination of a quality standard. Eigenverlag, Technologie-und Förderzentrum, pp 84–91

Box, G. E. P., Hunter, W. G. and Hunter, J. S. (1978). Statistic for Experimenters, John Wiley and Sons, New Yo rk, NY, USA.

Dong, C. H., Xie, X. Q., Wang, X. L., Zhan, Y. and Yao, Y. J. (2009). Application of Box-Behnken design in optimisation for polysaccharides extraction from cultured mycelium of Cordyceps sinensis,"Food and Bioproducts Processing, vol.87, no.2, pp.139–144.

Fadel, H., Marx, F., El-Sawy, A. and El-Gorab, A. (1999). Effect of extraction techniques on the chemical composition and antioxidant activity of Eucalyptus camaldulensis var. brevirostris leaf oils, 208: 212-216.

Ghani, A., (2003). Medicinal Plants of Bangladesh with Chemical Constituents and Uses. 2nd Ed., Asiatic Society of Bangladesh, Dhaka, Bangladesh, pp: 603.

Kirtikar, K.R. and Basu, B.D. (1980). Indian Medicinal Plants. 2nd Ed., MP Singh and BP Singh, UK.

Lawan, S. A., Saleh, A., Sani, B. G., Fa'iza, A. M. and Sadiya, A. Z.(2017). Preliminary Phytochemical Constituents and Phytotoxic Effect of *Albizia Lebbeck* (L.) Benth on Sorghum bicolor, Bayero Journal of Pure and Applied Sciences, 10(1): 405 - 408 ISSN 2006 – 6996, http://dx.doi.org/10.4314/bajopas.v10i1.79S

Lowry, J. B., Prinsten, J.H. and Burrows, D.M. (1998). *Albizia Lebbeck*-A Promising Forage Tree for Semiarid Regions. In: Forage Tree Legume in Tropical Agriculture, Gutteridge,and Shelton (Eds.). CAB International, Wallingford, UK., pp: 7-14.

Maryam, J., Mahdi, K., Javad, K. (2009). Detection of Adulteration in Iranian Olive Oils Using Instrumental (GC, NMR, DSC) Methods, J Am Oil Chem Soc (2009) 86:103–110, DOI 10.1007/s11746-008-1333-8.

Mohammad, B. U., Romel, A., Sharif, A. M. and Mohammad, K. H. (2007): Inhibitory effects of *Albizia lebbeck* (L.) Benth. Leaf extracts on germination and growth behavior of some popular agricultural crops. Journal of Forestry Research, 18(2): 128-137.

Orwa, C., Mutua, A., Kindt, R., Jamnadass R. and Anthony, S. (2009). Agroforestry Database: A Tree Reference and Selection Guide. Version 4.0, World Agroforestry Centre, Nairobi, Kenya, pp 6.

Rahman, S. A., Choudhury, J. P., Ahmad, A. L., and Kamaruddin, A. H. (2007). Optimizati on studies on acid hydrolysis of oil palm empty fruit bunch fiber for production of xylose,"Bioresource Technology, vol. 98, no. 3, pp. 554 –559.

Rashid, R.B., Chowdhury, R., Hasan, C. M. and Rashid, M. A.(2003). Constituents of A*lbizzia lebbek* and antibacterial activity of an isolated flavone derivative. Saudi Pharm. J., 11: 52-56.

Rozzi, N. L., Phippen, W., Simon, J. and Singh, R. (2002). Supercritical fluid extraction of essential oil components from lemon-scented botanicals. Lebensm.- Wiss. U. Technol., 35: 319-324

Trading Economics (2019). Nigerian imports of essential oils, perfumes, cosmetics, toiletries, Retrieved from: http://tradingeconomics.com/nigerian/imports/essential-oils-perfumes-cosmetics-toiletries, on 20th August, 2019.

Tripathi, R.M., Sen, P.C. and Das, P.K. (1979). Studies on the mechanism of action of *Albizia lebbeck* L. an Indian indigenous drug used in the treatment of atopic allergy. J. Ethnopharmacol., 1: 385-396.

Proceedings of the 49th NSChE Annual Conference
KADA 2019: pp 628-638

P3B-07: OPTIMIZATION OF EPOXIDIZED COTTON SEED OIL VIA TAGUCHI DESIGN OF EXPERIMENT FOR INDUSTRIAL QUENCHING

R.M. Dodo*, T. Ause, E. T. Dauda, U. Shehu, K. A. Bello and Z. Musa
Department of Metallurgical and Materials Engineering, Ahmadu Bello University, Zaria, Nigeria
*Correspondence: rdmamuda@abu.edu.ng, ray.dodo@yahoo.com

ABSTRACT
The present study focused on optimizing process parameters for cotton seed oil (CSO) epoxidation via Taguchi approach. The epoxidation process was carried out with peroxy acid generated in situ by using hydrogen peroxide and acetic acid. The epoxidation process was conducted by varying the input variables which include temperature, mole ratios of hydrogen peroxide to double bond concentration (DBC), acetic acid to DBC and amount of catalyst. The optimum parameters' setting obtained was 50°C temperature, mole ratio of hydrogen peroxide to DBC of 1.5:1, mole ratio of acetic acid to DBC of 0.75:1 and 3 wt% of catalyst. The maximum relative per cent conversion to oxirane (RPCO) achieved was 72.20 %. This agreed closely with the predicted value identified (68.173 %). The epoxidized cotton seed oil (ECSO) was characterized by Fourier transforms infrared (FTIR) and ^{1}H NMR spectra. Similarly TGA/DTA and cooling curve analyses on ECSO was carried out to ensure the attainment of improved oxidative stability and cooling characteristics respectively. The result of FTIR and ^{1}H NMR analyses confirmed the formation of oxirane in the ECSO. Furthermore, the ECSO produced was found to have superior heat transfer rate compared to raw cotton seed oil (RCSO).
Keywords: Epoxides, heat transfer coefficient, optimization, Taguchi, acetic acid, hydrogen peroxide, temperature, cotton seed oil

1.0 Introduction
Bioquenchants (vegetable oils and animal fats) have been in use for many centuries ago as quenchants for hardening steels. However, when mineral oils were discovered in the late 1800s, the use of these liquids as quenchants rapidly decreased. This was mainly due to, but not exclusively, their usually high thermal-oxidative instability and the difficulty in formulating them with differing consistent quenching performance (Otero *et al.,* 2014). Nonetheless, in the recent years, vegetable oils have started regaining its lost position in the industry due to its environmental friendliness (biodegradable and non-toxic nature); but then their high thermal oxidative instability which lead to low heat transfer ability still remain a major challenge in their usage in heat treatment industries. In addition, by modifying the molecular structure of the oils through chemical means, in which the unsaturated fraction of the fatty acids molecules is epoxidized; a quenchant with high resistance to oxidation and thermally stable is anticipated to be developed capable of extracting heat from the hot component at high rate, and at the same time satisfies nearly all the desired requirement of a quenchant. Epoxidation is one of the effective chemical modification processes used by many researchers in improving oxidative stability of vegetable oils (Darfizzi and Jumat, 2014; Liew *et al.,* 2015). Efforts have been made to improve the low oxidative stability of the soybean oil for quenching application by epoxidation process (Otero *et al.,* 2014). Additionally, many attempts have been made to improve the oxidative stability and high temperature performance of cottonseed and rapeseed oils by the same process (Dinda et al., 2008; Milchert and Smagowicz, 2009).

In the synthesis of bio-based quenchant, the double bonds in the vegetable oils, after epoxidation, are converted to epoxy group which eventually raises the oxidative stability of the oils. However, in the epoxidation process, the peroxy acid generated *in situ* spontaneously

reacts with the oil's double bonds, forming an epoxy group and releasing carboxylic acid. Besides the main reactions of peroxidation and epoxidation, the acid catalysed side reactions of the epoxy group opening with nucleophilic agents also occur during the process (Arumugam *et al.,* 2014; Goud *et al.,* 2011). The conversion of double bonds to epoxides and selectivity of the process are strongly influenced by the process parameters, therefore, their optimization is needful regardless of which carboxylic acid or catalyst is used in the process. Hence, the optimal operating condition in the epoxidation process must be clearly defined to achieve high content of epoxy groups. Consequently, in the present study, optimization of epoxidation process parameters for cotton seed oil (CSO) based on Taguchi method is reported.

2.0 Materials and Methods

2.1 Epoxidation Process

In the present investigation, epoxidation reaction was used to convert the unsaturated fractions of fatty acids in CSO into oxirane rings (epoxide). The degree of conversion of double bonds to oxirane rings is determined by per cent of oxirane oxygen content (OOC). From the oxirane oxygen content, the per cent relative conversion to oxirane (RPCO) was determined using Equation (1):

$$RPCO = \frac{OO_{ex}}{OO_{th}} x\ 100 \quad (1)$$

Where: OO_{ex} is the experimentally determined per cent content of oxirane oxygen
OO_{th} is the theoretical maximum per cent content of oxirane oxygen in 100 g of oil, which was calculated using Equation (2)

$$OO_{th} = \left\{\frac{{}^{IV_o}/_{2A_i}}{100+({}^{IV_o}/_{2A_i})A_o}\right\} 100A_o \quad (2)$$

Where: IV_o = Initial iodine value of the oil
A_i = Atomic weight of iodine = 126.9 g/mol
A_o = Atomic weight of oxygen = 16.0 g/mol

The experimental design for the epoxidation process parameters using the L9 orthogonal array and RPCO results are illustrated in Table 1. Subsequently, Taguchi method was used to find the mean S/N ratio response for each process parameter at each level. The RPCO results were converted into S/N ratio using MINITAB 16 software based on the larger-the-better characteristics.

Table 1: DOE Results for Epoxidation process of CSO

Expt. No.	Factors				Response
	Temperature (°C)	H_2O_2 (ratio)	Acetic Acid (ratio)	Catalyst (wt %)	RPCO (%)
1	50	1.5	0.50	2	63.11
2	50	3.0	0.75	3	64.23
3	50	4.5	1.00	4	59.00
4	60	1.5	0.75	4	60.09
5	60	3.0	1.00	2	52.33
6	60	4.5	0.50	3	62.51
7	70	1.5	1.00	3	63.11
8	70	3.0	0.50	4	57.92
9	70	4.5	0.75	2	59.53

The amounts of each level for all the epoxidation input variables were calculated based on the double bond concentration of the CSO. The calculated amount is depicted in Table 2.

Table 2: Calculated Amount of Parameters for CSO

Amount (g)	**DBC (mole)	Hydrogen peroxide			Acetic acid		Catalyst (H_2SO_4) (%)
		Ratio	Amount (g)	AI30S (g)	Ratio	Amount (g)	
40	0.103152	1.5	5.2608	17.536	0.50	3.095	2*
		3.0	10.5215	35.072	0.75	4.642	3*
		4.5	15.782	52.607	1.00	6.189	4

Where: DBC is acronym for double bond concentration
AI30S is acronym for amount in 30% solution

Note: * is the total mass of hydrogen peroxide and acetic acid. For example, raw 1 and 2 will have 2% catalyst (2% of [5.2608+3.095]) and 3% catalyst (3% of [10.5215+4.642]) respectively.

** the Gas-liquid chromatographic analysis done revealed that the oil contains 59.1 and 13.2 % linoleic and oleic acids respectively. Therefore, the DBC was determined as follows:

DBC = total number of moles of double bond = $\eta = \eta_{linoleic} + \eta_{oleic}$

For 40 g of oil,

$$\eta_{linoleic} = \frac{\frac{59.1}{100} \times 40}{280} = 0.0844286\ mol$$

$$\eta_{oleic} = \frac{\frac{13.2}{100} \times 40}{282} = 0.0187234\ mol$$

$$\therefore \eta = 0.103152\ mol$$

280 and 282 are the respective molar mass (in g/mol) of linoleic and oleic acids.

In the optimization event, the epoxidation process was carried out as follows:
The epoxidation reaction was performed in a 2000 ml glass beaker on a heated magnetic stirrer using peroxy acetic acid produced *in situ*. In the epoxidation process, the experimental factors shown in Table 1 were used. The calculated catalyst mass (H_2SO_4) was slowly added to the measured acetic acid drop wise and then the mixture was poured into the oil sample. At a steady speed of 450 rpm, the mixture was stirred continually; the required quantity of hydrogen peroxide was added slowly. The mixture was heated to the desired temperature gradually. Mixing acetic acid with hydrogen peroxide simultaneously generated peroxide acid *in situ*. The mixture was poured into a separate funnel after 2.5 hours and the aqueous layer was immediately drained. With 15 per cent NaOH solution, the product was neutralized, washed carefully with hot water and lastly dried by evaporation.

2.2 Characterization Techniques

The spectra of the FTIR were obtained using the technique outlined by Dodo *et al.,* (2019a). Likewise, the cooling curves and the corresponding coefficient of heat transfer (HTC) for the oil were obtained according to the method adopted by Dodo *et al.* (2019a). On the other hand, ^{1}H NMR spectrum was generated at 125.77 MHz in CDCl3 solvent using an Ascend NMR spectrometer (model 500) with a 5 mm broad band inverse probe head fitted with protected z-gradient accessories.

The oxidative stability of ECSO and RCSO was investigated in the ambient to 600^{o}C temperature. In the TA instruments Q500 TGA model, the non-isothermal thermogravimetric analysis was performed. Oxygen atmosphere at a flow rate of 100 ml / min was used as a reactive gas together with nitrogen as a purging gas. Different amounts of samples (in mg) were used in the analysis, but in an open silica crucible (less than 10 mg), TG curves and derivatives curves were used for identifying the oxidation start temperatures.

3.0 Results and discussion

3.1 Effect of reaction conditions on the epoxidation

Table 3: S/N ratios response Table for RPCO of CSO

Level	Temperature	H_2O_2	Acetic Acid	Catalyst
1	35.86	35.86	35.73	35.29
2	35.29	35.26	35.74	36.03
3	35.58	35.61	35.26	35.42
Delta	0.57	0.60	0.48	0.73
Rank	3	2	4	1

Table 3 demonstrates the mean S/N ratio response for RPCO on epoxidation of CSO. The Table presents the ranking which shows that conversion to oxirane is influenced by catalyst, hydrogen peroxide, temperature and acetic acid in decreasing order of significance of the process parameters. Rank 1 indicates that catalyst substantially affected the conversion to oxirane followed by rank 2 which means that hydrogen peroxide also has a considerable effect on the process. Rank 3 and 4 in the same table indicate that temperature and acetic acid had less effect on the process. On that account, the most influencing epoxidation parameter is the catalyst and least is the acetic acid. The catalyst increases the rate of epoxidation reaction rapidly because of the active moieties (H^+) present in it. The result supports the finding of Dinda *et al.,* (2008) who reported that sulfuric acid do have a great influence on the epoxidation process and boost the formation of the oxirane. The result further reveals that conversion to oxirane oxygen is almost independent of acetic acid concentration. This is similar to the result of investigation done by Ferra *et al.,* (2012).

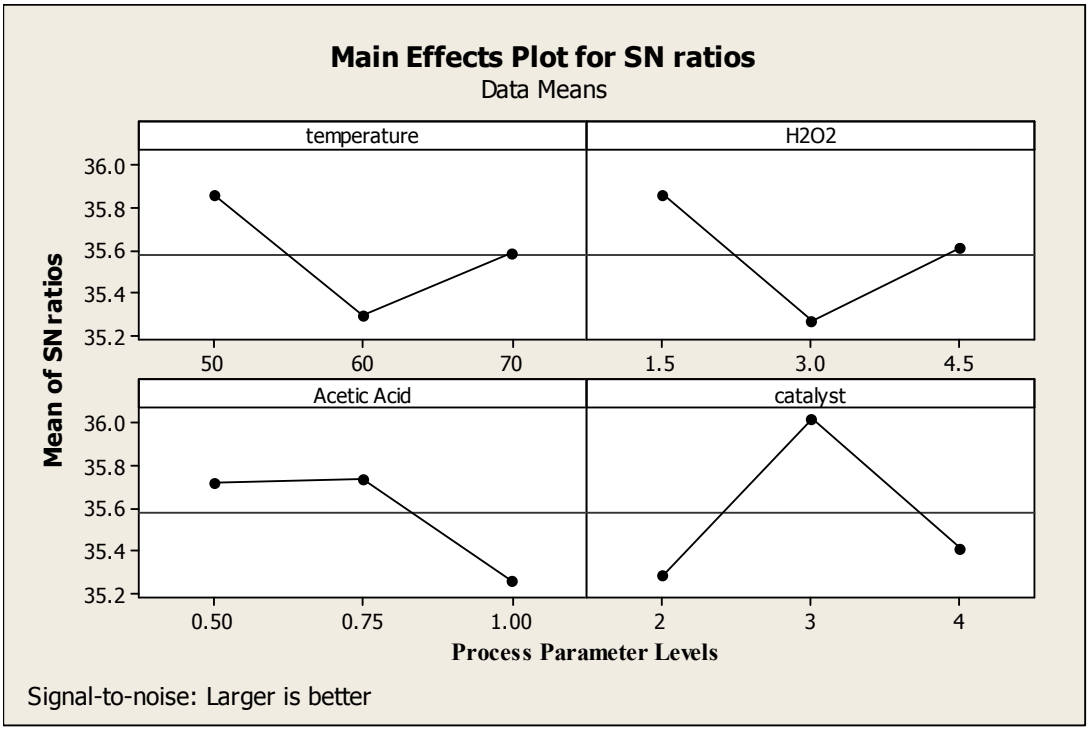

Figure 1: Influence of epoxidation process parameters on RPCO for CSO

The main effects plot of S/N ratio for RPCO of CSO is shown in Figure 1. The graph infers that mean conversion to oxirane oxygen was found to decrease dramatically before a gradual rise with the increase in reaction temperature and hydrogen peroxide. Nevertheless, a gentle increase and then a considerable decline were observed in the conversion with acetic acid concentration whereas more catalyst addition led to marked increment and decrement in the conversion. From main effects plot, it is clearly evident that the reaction temperature (50 ^{o}C), H_2O_2 to DB (double bond) molar ratio (1.5:1), acetic acid to DB molar ratio (0.75:1) and catalyst concentration of 3 wt% are the promising conditions to maximize RPCO for CSO. This is close to the observation of Dinda *et al.,* (2008) who concluded that reaction conditions favourable for epoxidation of cottonseed oil catalysed by inorganic acids are temperature (50 to 60 ^{o}C), molar ratio between peroxide to unsaturation in the oil (1.5 to 2.0) and about 2% of catalyst loading.

3.2 Confirmation of Experimental Results

Confirmation experiment was carried out in this study to validate the experimental results obtained during the optimization analysis and at the same time to verify the Taguchi models' prediction. The confirmation experiment was conducted by running a new experiment using the best experimental conditions obtained for optimum RPCO. The optimal parameter combinations were used to predict S/N ratios and mean values of RPCO through the following prediction model equations (3-4):

$$\bar{Y}_{cO} = Y_{cO} + (\overline{T_1} - Y_{cO}) + (\overline{H_1} - Y_{cO}) + (\overline{A_2} - Y_{cO}) + (\overline{C_2} - Y_{cO}) \quad (3)$$

$$\bar{y}_{cO} = y_{cO} + (\overline{t_1} - y_{cO}) + (\overline{h_1} - y_{cO}) + (\overline{a_2} - y_{cO}) + (\overline{c_2} - y_{cO}) \quad (4)$$

Where: $\bar{Y}_{cO}$ and $\bar{y}_{cO}$ represent the predicted RPCO S/N ratio and mean value at optimum conditions.

$\overline{T_1}$ $\overline{H_1}$, $\overline{A_2}$, $\overline{C_2}$, and $\overline{t_1}$, $\overline{h_1}$, $\overline{a_2}$, $\overline{c_2}$ are the mean responses of S/N ratio and mean values for factors at designated optimum levels respectively.
Y_{cO} and y_{cO} demonstrate the average of the S/N ratios and mean values.

The predicted epoxide conversions as per the obtained model are shown in Table 4. In order to make comparison between the predicted values and the experimental results, the Table illustrated the two values. Additionally, the per cent errors of the Taguchi-predicted results with respect to the experimental values as reference are also presented in the Table.

Table 4 Analysis of confirmation Experiment for DB conversion to oxirane

Best parameter combination	Prediction		Experimental		Prediction Error (%)		Improvement	
	Mean value (%)	S/N ratio (dB)	Mean value (%)	S/N ratio (dB)	Mean value error	S/N ratio error	Value	(%)
$T_1H_1A_2C_2$	68.173	36.753	72.200	37.171	5.578	1.125	7.970	13.238

Where TiHiAiCi represent the respective amount (degree) of temperature, hydrogen peroxide, acetic acid and catalyst at level i.

The calculated predicted conversion at the optimum conditions based on the model was found to be 68.173% and the experimental observations were 72.200% conversions. Also, from Table 4, the average deviation between experimental and predicted epoxide conversion values were found to be less than 10%. For this reason, the proposed models are validated and confirmed. Furthermore, a substantial improvement in the conversion to oxirane was observed from the confirmation experiments.

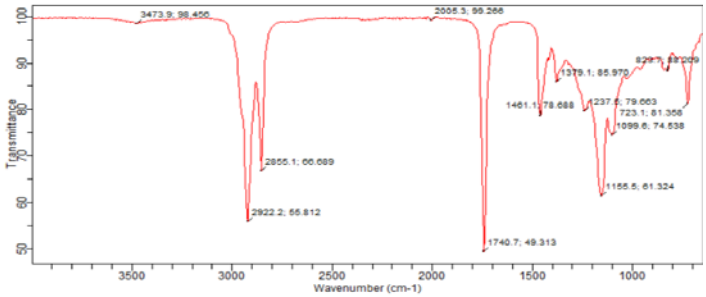

Figure 2: FT-IR spectrum of ECSO

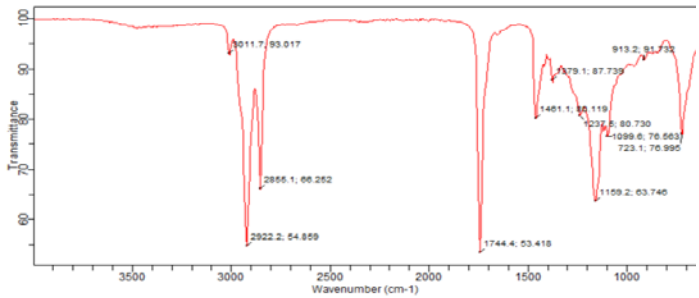

Figure 3: FT-IR spectrum of RCSO
(Source: Dodo *et al.,* 2019b)

3.3 characterizations Result

In Figures 2-3, the spectra of ECSO and RCSO showed an overtone stretching vibration peak of C=O for ester at wavenumber 3473.9 cm^{-1}. Based on the comparison between ECSO and RCSO FTIR, there is stretching vibration peak of C–H bond attached to unsaturation bond (3011.7 cm^{-1}) and unsaturation peak of HC=CH at wavenumber 1650 cm^{-1} in Figure 3. However, the characteristic peaks (Figure 2) that indicate the presence of epoxide groups in the ECSO can be observed at 823 cm^{-1} (Venu and Vaibhav, 2014). Furthermore, the unsaturation and stretching vibration peaks of =CH are completely absent in Figure 2. This confirmed a near complete conversion of unsaturation in RCSO to epoxides.

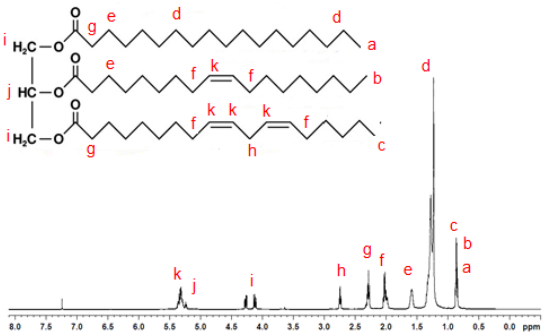

Figure 4: ^{1}H-NR spectrum of RCSO

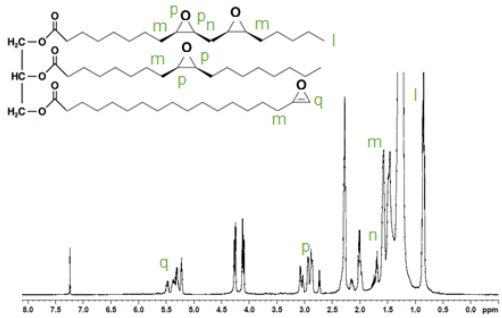

Figure 5: ^{1}H-NMR spectrum of ECSO

The peak assignments of the proton NMR spectra of the RCSO and ECSO are shown in Figures 4-5. Two sets of peaks from 4.10-4.28 ppm were generated as a result of the glycerol four methylene protons while the glycerol β-methine proton gave rise to peaks at 5.21-5.25 ppm. Due to the protons on the double bonds, peaks at 5.30-5.38 ppm were produced. The 2.2-2.3 ppm peaks show the existence of methylene groups next to carboxyl group. Peaks in the 2.7-2.8 ppm region belong to groups of methylene surrounded by double bonded atoms of carbon. Furthermore, the peaks at 1.97-2.04 show the presence of methylene groups next to double bonded carbon atoms. The ^{1}H NMR spectrum of the ECSO shows that there is no double allylic proton of $=CCH_2C=$ (2.7-2.8 ppm), however, a new band of around 1.7 ppm is produced which is attributable to epoxy -CH_2 -epoxy in the ECSO (Figure 5). In the same manner, the peak at 0.97 ppm indicating the presence of linolenic acid (attributable to terminal methyl homoallylic in linolenate glyceride) present in the RCSO is absent in the ECSO while a new peak occurs at 0.98-1.0 due to terminal methyl of a diepoxystearate (Figure 5). The epoxidized oil has no olefinic proton signals in the region 5.2-5.3 ppm, but shows the epoxy protons in 2.8-3.2 ppm region. Epoxide with single unsaturation (epoxy-octadecenoic) as remnant of double bond generated a peak at 5.4 ppm. The solvent used (chloroform) is shown

by a chemical shift peak of about 7.26 ppm in Figures 4 - 5. The ^{1}H NMR spectra observed are close to the report of Akintayo (2007).

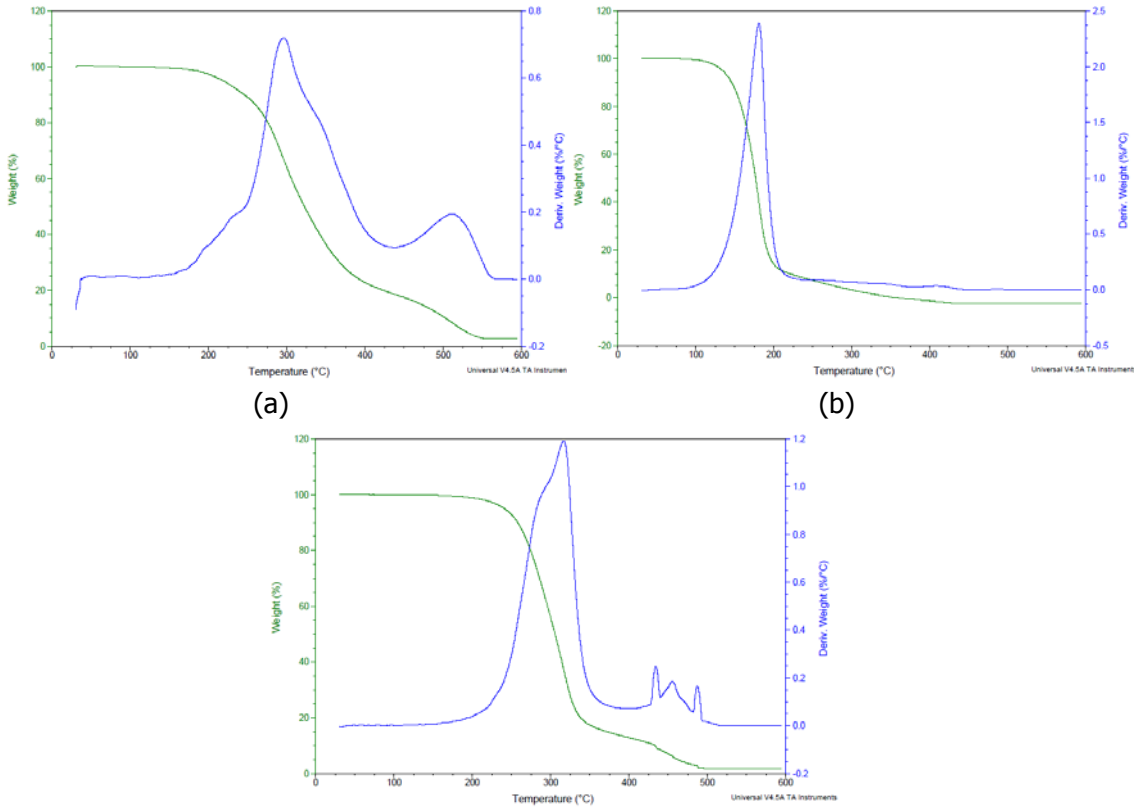

Figure 6: TGA-DTA thermogram of a) ECSO, b) RCSO, c) *SAE40 in O_2 atmosphere (*Source: Dodo *et al.*, 2019b)

Table 5: Oxidative stabilities (onset temperatures) of the oils

Bioquenchants	Oxidative stability (Under O_2)	
	T_{onset} (°C)	T_o (°C)
ECSO	240[a]	300[a]
RCSO	155	180
*SAE40	255	320

[a] *There is second thermal event with 460 and 510 °C for T_{onset} and T_o respectively.*
*(*Source: Dodo et al., 2019c)*

The oxidative stability of the oils was analyzed by extrapolated onset Temperatures for the initiation of the oxidative events according to ASTM E2550 – 17 standards. The oxidative stability was identified from the oxidative onset temperatures under oxygen atmosphere (reactive atmosphere). TGA and DTA curves of the oils are illustrated in Figure 6. During the analysis, large degradation was observed for all the samples. Oxidation onset temperatures (T_{onset}) were inferred from the corresponding TGA/DTA curves (Figure 6) and shown in Table 6. It can be noted that ECSO resist oxidative deterioration up to 240 °C. Nevertheless, RCSO and SAE40 were stable up to 155 and 255°C respectively. After the onset temperature with gradual increase in temperature, temperature at which maximum mass loss rate (T_o) occurred

was observed. From the TGA curves, it was observed that process of oxidative deterioration of ECSO started and ended within a temperature range close to that of SAE40. The improved oxidative stability could be linked to the removal of unsaturation in the fatty acid composition of ECSO. Alike observations were reported by Venu and Vaibhav (2014).

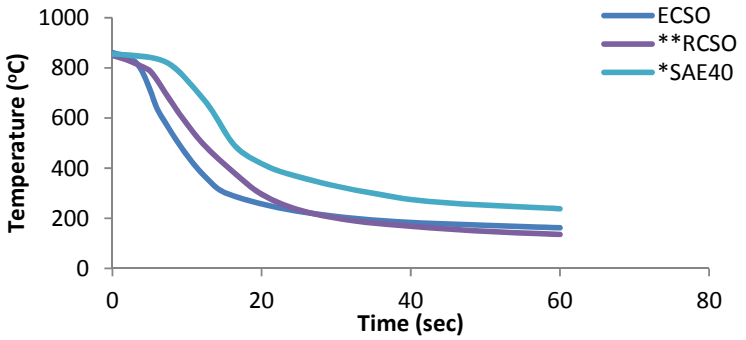

Figure 7: Cooling curves of the oils using INCONEL 600 probe
(Source: *Dodo *et al.,* 2019a, **Dodo *et al.,* 2019b)

In Figure 7, it is evident that ECSO have the shortest stage I (vapour blanket stage); which was estimated to last for three seconds, whereas stage II was observed to complete at 13 seconds. Notwithstanding, vapour blanket ruptured at longer time in RCSO. Accordingly, the data suggests that epoxidation of the RCSO significantly speed up vapour blanket collapse. In a similar occurrence, Simêncio, *et al.,* (2016) recorded shorter vapour blanket in palm oil due to improved thermal-oxidative stability as a consequence of antioxidant addition. SAE40 mineral oil presented a longer vapour blanket and boiling stage enabling it to have slower cooling than ECSO and RCSO. This is in line with what was established by Komatsu *et al.* (2009).

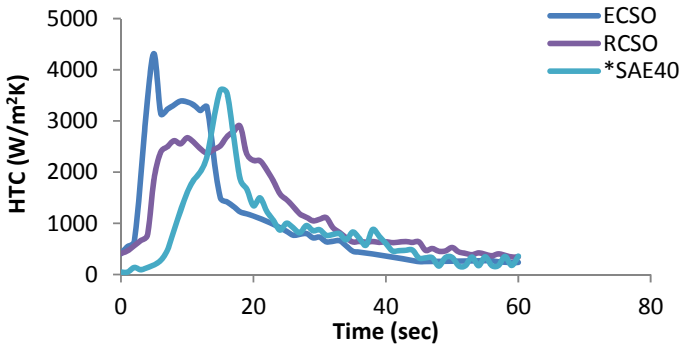

Figure 8: HTC as a function of time for the oils*(*Source*: Dodo *et al.,* 2019c)

In contrast to RCSO and SAE40 (Figure 8), it is evident that ECSO has outstanding heat transfer ability. HTC of the ECSO rise rapidly. However, after reaching peak value at 5 seconds of immersion, HTC decreases considerably. Similarly, Figure 8 revealed that RCSO offered maximum HTC at around 18 seconds which is lower compared to that exhibited by ECSO. Additionally, SAE40 exhibited maximum peak HTC at about 15 seconds. The superior heat transfer ability displayed by ECSO is attributable to the improved oxidative stability because product of oil oxidation which results to sludge has poor HTC (MacKenzie, 2013).

4.0 Conclusions

Synthesis of epoxidized cotton seed oil via Taguchi approach has been carried out successfully. The promising experimental conditions for optimum conversion of unsaturation to oxirane was found to be at temperature of 50 ^{o}C, 1.5:1 molar ratio of hydrogen peroxide to DBC, 0.75:1 molar ratio of acetic acid to DBC and 3 wt% catalyst. Among the process parameters tested, amount of catalyst has largest influence. Second in significance is amount of hydrogen peroxide. Confirmation experiment gave 72.2 % conversions. However, the error recorded with reference to the predicted conversion value was 5.578 %. Therefore, the model equation developed for predicting optimum RPCO is reliable. FT-IR and ^{1}H NMR analyses confirmed the formation of epoxides in the ECSO produced using the best combination of experimental parameters. TGA-DTA thermograms indicated the improved oxidative stability achieved in ECSO. Furthermore, from the cooling curves and HTC graphs; ECSO exhibits superior heat transfer ability compared to RCSO and SAE40. Thus, ECSO is recommended to be used as fast quenching oil, since it shows splendid heat extraction ability.

Acknowledgments

The authors express their deep and sincere gratitude to the Management of Ahmadu Bello University, Zaria, Nigeria for the financial support given through Tertiary Education Trust Fund (TETFund) throughout the research work.

References

Akintayo, E.T. (2007). Ethylmethyldioxirane Epoxidation of Plukenetia Cononophora Oil, *Bulletin of Chemical Society of Ethiopia,* 21(1), 95-102.Dinda S., Patwardhan, A.V., Goud, V.V. and Pradhan, N.C. (2008). Epoxidation of cottonseed oil by aqueous hydrogen peroxide catalysed by liquid inorganic acids. *Bioresource Technology* 99(9): 3737-3744.

Arumugam S. Sriram G., Rajmohan T., Multi-Response Optimization of Epoxidation Process Parameters of Rapeseed Oil Using Response Surface Methodology (RSM)-Based Desirability Analysis, Arab J. Sci Eng (2014) 39:2277–2287, DOI 10.1007/s13369-013-0789-5.

Darfizzi D., Jumat S., Waled A. A. (2014). Preparation of Epoxidized Palm Olein as Renewable Material by using Peroxy Acids, *The Malaysian Journal of Analytical Sciences,* 18 (3): 584 – 591.

Dinda, S., Patwardhan, A.V., Goud, V.V. and Pradhan, N.C. (2008). Epoxidation of cottonseed oil by aqueous hydrogen peroxide catalyzed by liquid inorganic acids. *Bioresource Technology,* 99: 3737-3744.

Dodo R.M., Ause T., Dauda E. T., Shehu U. and Popoola A. P. I., (2019a). Multi-response optimization of transesterification parameters of mahogany seed oil using grey relational analysis in Taguchi method for quenching application, 5 (8), August 2019a, e02167, https://doi.org/10.1016/j.heliyon.2019.e02167

Dodo R.M., Ause T., Dauda E. T., Shehu U. and Popoola A. P. I., (2019b). Multi-response Optimization of Transesterification Parameters of Cotton seed oil using Grey Relational Analysis in Taguchi Method for Quenching Application, under review in FUDMA Journal of Sciences (FJS), Federal University Dutsin-Ma, Katsina State.

Dodo R.M., Ause T., Dauda E. T., Shehu U. and Kasim A. (2019c). Optimization of epoxidized mahogany seed oil using the taguchi Approach for quenching applications, under review for Nigerian Metallurgical Society (NMS) 35th Annual Conference.

Ferra N., Robiah Y., Tinia Idaty M. G. and Irmawati R. (2012). Synthesis of Epoxidized Palm Oil-Based Trimethylolpropane Ester by *In Situ* Epoxidation Method, Pertanika Journal of Science and Technology 20 (2): 331 - 337.

Goud,V.V.; Mungroo, R.; Pradhan, N.C.; Dalai, A.K.: Modification of epoxidized canola oil. Asia-Pacific J. Chem. Eng. **6**, 4–22 (2011)

Komatsu, D., Elki C.S., Lauralice F.C.C., and Geoge, E.T. (2009). "Effect of Corrosion Inhibitors on Cooling Curve Behavior of Soybean Oil-Based Quenchants", *Conf. Proceed. New Challenges in Heat Treating and Surface Engineering – Conference in Honor of Božidar Ličić, June 9-12, 2009*, Cavtat Croatia, Publ. by Croatian Society for Heat Treatment and Surface Engineering, Zagreb, Croatia, 37-44.

Liew K. H., Rahimi M. Y., Nadia S. and Jumat S. (2015). Optimization of the in situ epoxidation of linoleic acid of jatropha curcas oil with performic acid, The Malaysian Journal of Analytical Sciences, 19 (1) (2015): 144 – 154.

MacKenzie, S. (2013). The Mechanism of Quench Oil Oxidation, Houghton International, Inc. Valley Forge, PA, USA 19482.

Milchert, E. and Smagowicz, A. (2009). The influence of parameter on the epoxidation of rapeseed oil with peracetic acid. *Journal of the American Oil Chemists' Society*, 86:1227-1233.

Otero, R. L. S., Canale L. C.F. and Totten G. E. (2014). Bioquenchants Formulated from Epoxidized Soybean Oil: Evaluation of Metal Quenching and Heat Transfer Performance *International Journal of Mechanical Engineering Autom.* 1(2): 101-110.

Simêncio, E., Otero, R. Canale, L. and Totten, G. (2016). Stabilization of vegetable oil-based quenchants to thermal-oxidative degradation: experimental strategy and effect of oxidation on quenching performance. *La Metallurgia Italiana,* 3.

Venu B. B. and Vaibhav V. G. (2014). Epoxidation of castor oil fatty acid methyl esters (COFAME) as a lubricant base stock using heterogeneous ion-exchange resin (IR-120) as a catalyst, *Energy Procedia,* 54, 75 – 84.

Proceedings of the 49th NSChE Annual Conference
KADA 2019: pp 639-642

P3B-08: EFFECT OF TEMPERATURE AND TIME ON THE OIL YIELD OF ALMOND SEED

Ojiagho R, Ebhodaghe S.O, Akhihiero E.T, Ogbeide S.E.
Department of Chemical Engineering, University of Benin.
Presenting author:samuel.ebhodaghe@eng.uniben.edu, 08051662808.

ABSTRACT
There is need for deeper understanding of the variables with significance affects oil yield from food crops such as almond seeds. This study seeks to examine the effects of temperature and time on oil yield from almond seeds. Using hexane, the solvent method of extraction was used to separate the oil from seeds. At constant temperature and time of 40 ^{0}C and 40 minutes, the highest yield of oil extracted were 61.46 % (43.02 g) and 68.64 % (48.05 g) respectively. Therefore, this result reveals that oil yield increases with temperature and time. This implies that oil yield can be maximized at higher process conditions of temperature and time.
Keywords: Hexane, almond seed, temperature, time.

Introduction
Almond (Prunus dulcis, family: Rosaceae) is a common tree nut and oil source which is characterized by large seed size and high oil content. It has several applications such as in cosmetics, as food source, medication and health promoting properties because of its bioactive compounds (Fernandes *et al*., 2017; Rabadan et al 2018). Almond seeds are commonly found in the Middle East countries such as Iraq and Iran, Spain, North America, Mediterranean countries, California, Northwest Mexico, Australia (FAO 2015; Fernandes *et al*., 2017). Almond seeds are made up of several components such as fibre, soluble sugars, phytochemicals and mineral fraction (Roncero et al 2016). Commercial production process of almond seed oil has been in the USA (62 %), Spain and Australia (5 %) (Fernandes *et al*., 2017). The oil obtained from these countries generally differs due to several factors including conditions of processing. Samples of almond seeds and its' fruits are shown in Plates 1 and 2.

Research has shown that factors such as temperature, time duration on fatty acid and phenolic compositions, antioxidants, time of harvest significantly affects the oil yield and quality of almond seeds (Kazantzis et al 2003; Piscopo et al 2010; Rabadan *et al*., 2018). Also, the effects of storage conditions and atmosphere have been investigated (Raisi et al 2015; Lin et al 2016). Therefore, it is evident that the effects of process variables have attracted significant research attention. While more recent studies have explored the production processes of biodiesel production from almond seeds as well as determination of physico-chemical properties (Fadhil and Mohammed 2018; Esonye *et al*., 2019a; Esonye *et al* 2019b), attention has also being given to the different methods of extraction (Roncero *et al*, 2016; Fernandes et al, 2017; Ojolo *et al*, 2018).

Studies have shown that differences in methods of oil extraction significantly affect the oil yield of such plants (Gomez *et al*, 1996). More research is needed to examine this idea since previous research has only highlighted the use of extraction methods in oil production. To this end, this study will examine the influence of hexane solvent extraction method while determining the effect of time and temperature variables on the oil yield from almond seeds.

Plate 1: Almond fruit

Plate 2: Almond seeds

2.0 Methodology

2.1 Pre-Treatment of Samples.

The almond seed was sun dried for three days to remove moisture from it and thereafter was oven dried at 100°C for an hour. Moisture removal is significant because it determines the time that will be required for drying, and this consequently affects oil yield as investigated in this study. Because of the need to determine effect of temperature variation, this study applied sun-drying and oven to examine the effect on oil yield since they provide different temperature conditions. The almond seeds were grinded into fine particles.

2.2 Extraction of Almond seed oil.

Solvent extraction method was used to extract oil from Almond seed, using hexane as the extracting solvent and Soxhlet extractor as the extracting medium. This method has previously been illustrated by Roncero et al, 2016.

2.3 Characterization of Almond Oil

The following properties were characterized for in the almond oil: density, specific gravity, viscosity, acid value, saponification value, peroxide value and iodine value. These methods of characterization are detailed in literature (Esonye et al, 2019).

3.0 Results and Discussion

3.1 Extraction of Almond Seed Oil at Varying Temperature

Table 1 Effect of temperature on oil yield at 40 minutes

Temperature (°C)	Yield (g)	Yield (%)
30	0.00	0
40	43.02	61.46
50	38.94	55.63
60	36.69	52.41
70	34.77	49.67
80	32.08	45.83
90	30.96	44.23

Heating temperature has a significant effect on oil yield. From the effect of extraction temperature on the yield of oil from almond seed at a constant time of 40^{0}C shown in Table 1, the highest yield of oil extracted was at 40°C was 61.46 % (43.02g). It is observed that as temperature increased, the oil yield was found to reduce. The findings of Gomez et al (1996) corroborate this result. Though previous studies have shown that oil yield from almond seeds depends on the extent of moisture content in the seeds (Ajibola et al 1993; Olajide et al 2014)

and on the heating time duration (Adeeko and Ajibola 1990), the results from this present study indicate that the method of oil extraction may also have contributed to the increase in yield at a low temperature value of 40^0C. This view is supported by Aremu et al (2016). From their experiments, they discovered that the oil content of African oil bean seeds was 86.8% using a soxhlet extractor. Similarly, Sodiq (2012) reported a 60.6% oil yield using solvent extraction. In their experiment, Gomez et al (1996) revealed that differences in methods of oil extraction have a significant effect on oil extraction yields. They also found that the use of hexane solvent in conventional extraction guarantees maximum extraction efficiency. At 30°C no extraction occurred, this could be because there is insufficient heat for the extraction to occur.

3.2 Extraction of Almond Seed Oil at Varying Time

Table 2: Effect of time on Oil Yield at 40°C

Time (minutes)	Yield (g)	Percentage yield
30	36.67	52.39
35	40.72	58.17
40	43.23	61.76
45	45.95	65.64
50	46.72	66.74
55	47.32	67.60
60	48.05	68.64

The effect of extraction time on the yield of oil from almond seed at constant temperature of 40°C is shown in Table 2. Within the time range examined in this study, the highest oil yield is found to be 68.64% (48.05g) at 60^0C. It is evident from these results that the time of extraction increases with the oil yield. Ajibola et al (1993) and Adeeko and Ajibola (1990) also showed from their research that increase in time brings about a corresponding increase in oil yield. Heating time duration is a factor that has been shown to have a directly affect oil yields irrespective of the type of extractor utilized (Adeeko and Ajibola 1990).

4.0 Conclusion

The effect of temperature and time has been reported in this study. Though different feedstock has previously been investigated, this study has examined the effect of common process variables – temperature and time on the oil yield of almond seed. It is evident from these results that the temperature and time of extraction increases with oil yield. Besides, the results confirms that the extent of oil yield is determined by corresponding process conditions of temperature and time. Future studies can explore the effect of other process variables on oil yields of non-edible plants to examine their potential for biodiesel production.

References

1. Adeeko K.A, Ajibola O.O. (1990) Processing factors affecting yield and quality of mechanically expressed groundnut oil. Journal of Agricultural Engineering Res. 45; 31-43
2. Ajibola O.O, Owolarafe O.K, Fasina O.O, Adeeko K.A. (1993). Expression of oil from sesame seeds. Canadian Agricultural Engineering. 35 (1).Kazantzis I, Nanos G.D, Stavroulakis G.G. (2003). Effect of harvest time and storage conditions on almond kernel oil and sugar composition. Journal of the Science of Food and Agriculture. 83: 354-9. DOI: 10.1002/jsfa.1312

3. Akubude V.C, Maduako J.N, Egwuonwu C.C, Olaniyan A.M, Ozumba I.C, Nwosu C, Ajala O.E. (2017). Effect of process parameters on oil yield mechanically expressed from almond seed (Using Response Surface Methodology). American Journal of Food Science and Nutrition Research. 4(1): 1-8.
4. Aremu, Ademola K, Ogunlade C.A. (2016). Effect of operating parameters on mechanical oil expression from African oil bean seed. Global Journal of Science Frontier Research. 16 (1).
5. Esonye C, Onukwuli O.D, Ofoefule A.U. (2019). Optimization of methyl ester production from Prunus Amygdalus seed oil using response surface methodology and Artificial Neural Networks. Renewable Energy. 130: 61-72. DOI: 10.1016/j.renene.2018.06.036
6. Esonye C, Onukwuli O.D, Ofoefule A.U. (2019). Characterization and oxidation modeling of oils from *Prunus amygdalus, Dyacrodes eduliss* and *Chrysophyllum albidium.* Industrial Crops and Products. 128:298-307.
7. Fadhil A.B, Mohammed H.M. (2018). Co-solvent transesterification of bitter almond oil into biodiesel: optimization of variables and characterization of biodiesel. Transport. 33(3); 686-98. DOI: 10.3846/16484142.2018.1457568Lin J-T, Liu S-C, Hu C-C, Shyu Y-S, Hsu C-Y, Yang D-J. (2016). Effects of roasting temperature and duration on fatty acid composition, phenolic composition, Maillard reaction degrees and antioxidant attribute of almond (Prunus dulcis) kernel. Food Chemistry. 190: 520-8. DOI: 10.1016/j.foodchem.2015.06.004
8. Fernandes G.D, Gomez-Coca R.B, Perez-Camino M.C, Moreda W, Barrera-Arellano D. (2017). Chemical characterization of major and minor compounds of nuts oils: Almonds Hazelnut and Pecan Nut. Journal of Chemistry. DOI: 10.1155/2017/2609549Raisi M, Ghorbani M, Mahoonak A.S, Kashaninejad M. (2015). Effect of storage atmosphere and temperature on the oxidative stability of almond kernels during long term storage. Journal of Stored Products Research. 62: 16-21. DOI: 10.1016/j.jspr.2015.03.004
9. Gomez A.M, Lopez C.P, de la Ossa E.M/ (1996). Recovery of grape seed oil by liquid and supercritical carbon dioxide extraction: a comparison with conventional solvent extraction. The Chemical Engineering Journal. 61; 227-31
10. Olajide J.O, Afolabi T.J, Adeniran J.A. (2014). Optimization of oil yield from groundnut kernel (Arachis hypogeae) in an hydraulic press using response surface methodology. Journal of Scientific Research and Reports. 3(14); 1916-26
11. Ojolo S, Ogundare A, Adesina A, Ibhadode O. (2018). Development of almond seed extractor for whole kernel recovery. Agricultural Engineering International. 20 (4); 195-201
12. Piscopo A, Romeo B, Poiana M. (2010). Effect of the harvest time on kernel quality of several almond varieties (Prunus dulcis (Mill.) D.A. Webb). Scientia Horticulturae. 125: 41-6. DOI: 10.1016/j.scienta.2010.02.015.
13. Roncero J.M, Alvarez-Orti M, Pardo-Gimenez A, Gomez R, Rabadan A, Pardo J.E. (2016). Virgin almond oil: Extraction methods and composition. Grasasy Aceites. 67 (3). DOI: 10.3989/gya.0993152
14. Rabadan A, Pardo J.E, Gomez R, Alvarez-Orti M. (2018). Effect of almond roasting, light exposure and addition of different garlic cultivars on almond oil stability. European Food Resources Technology 244:219-24. DOI: 10.1007/s00217-017-2947-6
15. Sodiq O.M. (2012). Effect of microwave heating as a pretreatment on quality and quantity of African oil bean seed. Unpublished MSc Project, Department of Food Technology, University of Ibadan.

Proceedings of the 49th NSChE Annual Conference
KADA 2019: pp 643-655

P3B-09: OPTIMIZATION OF PROCESS PARAMETERS FOR THE ALKALI TREATMENT OF ALPHA CELLULOSE FROM GROUNDNUT HUSK (ARACHIS HYPOGAEA)

Hassana. A. G, Ameh .O. A and Mohammed T. I
Department of Chemical Engineering, Ahmadu Bello University, Zaria.
Auduhassana27@yahoo.com **+2348034530264**

ABSTRACT
Microcrystalline cellulose (MCC) is described as purified, partially depolymerised cellulose prepared by treating α-cellulose, obtained as a pulp from fibrous plant with mineral acids. Groundnut husk of 1.00mm particle size was selected for the alkali treatment using sodium hydroxide. Response Surface Methodology (RSM) was used to optimize the extraction of alpha cellulose from groundnut husk known as Arachis hypogaea. Sodium Hydroxide was for this extraction. The independent variables time, concentration and temperature were optimized using central composite design (CCD). Analysis of variance (ANOVA) showed that temperature was the most influential factor for hydrolyzing the amorphous sections of cellulose. Under optimal conditions, the percentage yield and percentage purity of the alpha cellulose obtained were 76.44 % and 40.89 % respectively. The theoretical values for the percentage yield of the extracted alpha cellulose were close to the experimental one, resulting in small error percentages of 2.73 % and 0.18 %, respectively. Thus, it can be concluded that the RSM technique based on CCD design is suitable for optimizing the variables influencing the hydrolyzing and extraction of alpha cellulose.

Key words: Groundnut husk (GH), microcrystalline cellulose (MCC), groundnut husk (Arachis hypogaea)

1.0 INTRODUCTION
Microcrystalline cellulose is a purified, partially depolymerised non-fibrous form of cellulose. It is widely use in cosmetic, pharmaceutical and food industry as fat substitute, stabiliser, thickener, filler-binder, anticaking agent and adsorbent (*Matrosovich et al*, 2006) are used for counting viruses, as an alternative to carboxymethyl cellulose (Hindi, 2016). Microcrystalline cellulose are obtained from both softwood and hardwood which has different chemical composition (cellulose, hemicelluloses, and lignin) and structure. Sources of cellulose and its derivatives obtained from Agricultural waste are: cotton linters, orange peel, rice husk, corn cob, groundnut husk, sugar cane bagasse, calabash, bark of palm nut trees (Chukwuemeka, 2012).

The chemical composition of groundnut husk is 14.7- 18.7% of hemicellulose, 37.5 - 40.5% cellulose, 26.4 - 30.2% lignin and 0.4 – 5.9% of ash contents. The process of extraction of microcrystalline cellulose utilizes the removal of hemicellulose and lignin which constitutes the matrix for cellulose micro fibrils. The isolation and characterization of microcrystalline cellulose from different sources like corn stalk (Reddy et al. 2005), rice husk (Reddy and Yang, 2005), wood (Orts, 2005), sugar cane bagasse (Sun, 2005), coconut husk (Rosa, 2010), etc. have been previously reported. However, the optimization of alpha cellulose from groundnut husk has not been reported.

This work aim to study the effect of process variables for the extraction of alpha cellulose from groundnut husk. Response surface methodology (RSM) base on the central design composite will be used to optimise the process variables. Statistical significance of the experimental observations shall be investigated in terms of Analysis of Variance (ANOVA).

2.0 METHODOLOGY

2.1 Materials: Groundnut husk was obtained from Institute of Agricultural Research A.B.U Zaria, Nigeria and then identified in Biological Sciences Department and Biochemical Laboratory as the raw material. The chemicals used was NaOH.

2.2 Proximate Analysis:

1 g of the treated groundnut husk was used to examine the percentages of Acid Detergent Fiber (ADF) and Neutral Detergent Fiber (NDF) to calculate percentages of cellulose, hemicellulose, lignin and ash content as shown in Table 1.

2.3 Production of Alpha Cellulose

Groundnut husk was washed with distilled water and dried for three days at room temperature. The dried groundnut husk was ball milled and sieved to obtain 1.00 mm particle size. The groundnut husk were measured for 25 g and treated with Sodium Hydroxide (500 ml distilled H_2O, 0.5 M of NaOH) for twenty runs. The factors obtained from the Central Composite Design (CCD) as presented in Table 2 were the temperature, time and concentration that were used to optimize the process. The dark slurry obtained was then filtered and washed several times with distilled water until pH 7 was recorded and then oven dried at 70^0 C for 2 hrs. Finally, the dried alpha cellulose was stored in plastic containers. The responses of the percentage yield of the extracted alpha cellulose and the percentage purity were recorded as shown in Table 2.

Table 1: Coded Values for the Central Composite Design

Coded Symbols	Variables	Levels			
		Low	High	-Alpha	+Alpha
		-1	1	-α	+ α
X_1	Time (hr)	1	2	0.659104	2.3409
X_2	Temperature (^{0}C)	80	98	73.8639	104.136
X_3	Concentration (g/ml)	0.25	0.9	0.0284173	1.12158

2.3 Percentage Yield

Percentage yield was calculated using the following equation:

Percent yield (%) = X 100 …… Equation (1)

Where:
W3 is the weight of oven dried treated sample (alpha cellulose).
W1 is the weight of oven dried untreated sample.

2.4 Central Composite Design

Research Surface Methodology was employed to maximize the production of alpha cellulose from groundnut husk by optimization of operational factors. The interaction among process variables was determined by statistical techniques. Central composite design was employed to investigate the effect of critical parameters; temperature, time, and concentration of the process. The yield and purity percentages of the alpha cellulose were selected as the response variables as shown in Table 1

The three variables and their value range were selected based on preliminary studied. Three dimensional surface were applied to investigate and validate the influence on process variables

on the treatment of alpha cellulose. The reaction time (1 to 2 hours), temperature (80 to 98^0C) and sodium hydroxide concentration (0.25 to 0.90 g/ml) were the input variables. The percentage alpha cellulose and percentage purity of the alpha cellulose were coded Y_1 and Y_2 in the statistical analysis as the response values. The factors were coded in values (-1 and 1).

2.5 Statistical Analysis

The data were analyzed using Design Expert Software version 10.0.7.0(Stat- Ease Minneapolis, MN, USA). The mathematical relationship between the response of these variables and the independent variables can be expressed as the second order polynomial equation (Li *et al, 2*014):

$$y = b_0 + (b_1x_1 + b_2x_2) + b_3x_3 + b_4x_4 + b_{11}x_1^2 + b_{22}x_2^2 + b_{33}x_{33}^2 + b_{44}x_{44}^2 + b_{12}x_1x_2 + b_{13}x_1x_3 + b_{14}x_1x_4 + b_{23}x_2x_3 + b_{24}x_2x_4 + b_{34}x_3x_4 \quad \textbf{..... (2)}$$

Where Y is the predicted value, b is the constant, χ1 is the time, χ2 is the temperature and χ3 is the concentration

3.0 RESULTS AND DISCUSSION

3.1 Proximate Analysis

The Chemical composition of the untreated groundnut husk was investigated using a gravimetric method to determine the proximate properties. Table 2.0 presents the results obtained.

Table 2: Proximate Properties of Untreated Groundnut Husk

S/No.	Parameter	Value (%)
1	Ash	6.1
2	Hemicellulose	9.48
3	Lignin	35.78
4	Alpha Cellulose	44.16
5	Moisture Content	2.3

3.2 Actual Design of the Experiment

The Central Composite Design (CCD) is based on factorial design (time, temperature and concentration) which was used to investigate the responses of percentage yield and purity of the alpha cellulose as shown in Table 3.

3.3 Percentage Yield of Alpha Cellulose

Table 3 shows the statistical analysis of the response of the percentage yield of alpha cellulose after alkaline treatment. The results indicated an extensive extraction of alpha cellulose using equation 1 and the response recorded as presented in Table 3. These values were feed into the design of experiment (DOE) using central composite design (CCD) to compute for the results and the model equation of the ANOVA shows that the model is significant having the probability value of 0.0027 which is less than 0.0500. The lower the p- value the higher the significant of the corresponding p-value coefficient. The coefficient of variation (CV) indicated the degree of precision with which the treatment was compared. A relatively low value of CV

(1.98 %) indicate a better precision and the reliability of the experiment (Hon *et al.*, 2018). The time represented by (A), temperature (B) and concentration (C) are the factors of interest for the model equation. However in this case, the time (A), time and temperature (AB), doubled temperature (B^2) and doubled concentration (C^2) are significant model terms AS SHOWN IN Table 4. The statistical analysis indicates that the model is adequate, possessing no significant lack of fit and with a satisfactory value for the R-Squared (0.8631) indicating that a statistical model can explain 86.31 % of the variability of the response. Normally a regression model with an R-Square higher than 0.90 (90 %) is considered to have a higher correlation (Jinbao *et al*,. 2014). The closer the value to unity, the better the empirical model fits the actual data (Sathavornvichit, 2006). Therefore, the proposed model fit the experimental data and the independent variables or parameters has considerable effects on the response.

Table 3: The Actual Design of the Experiment and Response of Percentage Yield and Percentage Purity of the Alpha Cellulose

ACTUAL DESIGN						
Std	Run	Factor 1 A:Time (hr)	Factor 2 B:Temperature (0C)	Factor 3 C: Concentration (g/750ml)	Response 1 Percentage Yield of Alpha Cellulose (%)	Response 2 Percentage Purity of Alpha Cellulose (%)
9	1	0.66	89.00	0.57	73.00	45.45
16	2	1.50	89.00	0.57	70.00	45.66
18	3	1.50	89.00	0.57	72.19	37.65
19	4	1.50	89.00	0.57	74.00	50.93
3	5	1.00	98.00	0.25	73.00	47.80
10	6	2.34	89.00	0.57	68.00	47.86
17	7	1.50	89.00	0.57	72.00	46.60
7	8	1.00	98.00	0.90	70.00	35.85
6	9	2.00	80.00	0.90	75.00	44.98
2	10	2.00	80.00	0.25	70.00	43.57
8	11	2.00	98.00	0.90	75.00	53.20
4	12	2.00	98.00	0.25	74.00	44.65
5	13	1.00	80.00	0.90	80.00	43.30
12	14	1.50	104.00	0.57	76.00	38.08
13	15	1.50	89.00	0.28	74.00	49.32
14	16	1.50	89.00	1.12	76.00	43.35
1	17	1.00	80.00	0.25	78.00	45.68
11	18	1.50	73.86	0.57	75.00	39.30
15	19	1.50	89.00	0.57	73.00	43.03
20	20	1.50	89.00	0.57	73.00	41.07

Table 4: Statistical ANOVA Analysis of Response for the Percentage Yield of Alpha Cellulose

ANOVA for Response Surface Quadratic model						
Analysis of variance table [Partial sum of squares - Type III]						
Source	**Sum of Squares**	**df**	**Mean Square**	**F Value**	**p-value Prob > F**	
Model	133.26	9	14.81	7.01	0.0027	Significant
A-Time	17.39	1	17.39	8.23	0.0167	
B-Tempt	6.36	1	6.36	3.01	0.1135	
C-Conc	5.12	1	5.12	2.42	0.1506	
AB	45.13	1	45.13	21.35	0.0009	
AC	6.13	1	6.13	2.90	0.1195	
BC	10.12	1	10.12	4.79	0.0535	
A^2	4.00	1	4.00	1.89	0.1992	
B^2	22.20	1	22.20	10.50	0.0089	
C^2	16.33	1	16.33	7.73	0.0195	
Residual	21.14	10	2.11			
Lack of Fit	11.90	5	2.38	1.29	0.3939	not significant
Pure Error	9.24	5	1.85			
Cor Total	154.40	19				

Std.Dev--------- 1.45 R-Square ---------- 0.8631
Mean --------- 73.56 Adj-Square ---------- 0.7399
C.V. % --------- 1.98 Pred R-Square --------- 0.3276
PRESS --------- 103.82 Adeq Precision -------- 10.196

The Model Equation

The mathematical relationship of the second order polynomial equation in terms of coded factors were used to make predictions about the response for given levels of each factor. By default, the high levels of the factors are coded as +1 and the low levels of the factors are coded as -1. The coded equation is useful for identifying the relative impact of the factors by comparing the factor coefficients. Equation 3 presents the predicted response (72.34 %) which is the percentage yield of the alpha cellulose.

Percentage Yield = 72.34

$-1.13A - 0.68B + 0.61C + 2.38AB + 0.88AC - 1.12BC - 0.53A^2 + 1.24B^2 + 1.06C^2$..... (3)

3.4 Percentage Purity of Alpha Cellulose

Proximate Analysis method was used to obtain the response for the percentage purity of alpha cellulose as tabulated in Table 2. The response was computed using ANOVA and presented in Table 5. The p-value is 0.2433 which is greater than 0.050 indicating a non-significant model. This means that the independent variables time, concentration and temperature has no considerable effect on the response in the term of purity. The R- square is 0.5869 also indicating that a statistical model can explain 58.69 % of the variability of the response. While the coefficient of variation (CV) 8.91 shows a fair precision and reliability of the experiment.

Table 5: Statistical ANOVA Analysis of Response for the Percentage Purity of Alpha Cellulose

ANOVA for Response Surface Quadratic model						
Analysis of variance table [Partial sum of squares - Type III]						
	Sum of		**Mean**	**F**	**p-value**	
Source	**Squares**	**df**	**Square**	**Value**	**Prob > F**	
Model	221.81	9	24.65	1.58	0.2433	not significant
A-Time	23.26	1	23.26	1.49	0.2503	
B-Tempt	0.27	1	0.27	0.017	0.8981	
C-Conc	15.21	1	15.21	0.97	0.3470	
AB	26.75	1	26.75	1.71	0.2198	
AC	73.75	1	73.75	4.72	0.0549	
BC	0.74	1	0.74	0.047	0.8323	
A^2	17.27	1	17.27	1.11	0.3177	
B^2	42.71	1	42.71	2.74	0.1292	
C^2	13.88	1	13.88	0.89	0.3679	
Residual	156.14	10	15.61			
Lack of Fit	48.90	5	9.78	0.46	0.7955	not significant
Pure Error	107.24	5	21.45			
Cor Total	377.95	19				

Std.Dev--------- 3.95 R-Square ---------- 0.5869
Mean --------- 44.37 Adj-Square ---------- 0.2151
C.V. % --------- 8.91 Pred R-Square --------- -0.5360
PRESS --------- 580.52 Adeq Precision -------- 4.417

The Model Equation

The second order polynomial equation (eq. 2) is used to express the predicted percentage purity of the alpha cellulose. Equation 4 presents the predicted response of the percentage purity of the alpha cellulose given as 44.12 %. Which compares favourable with the experimented value.

Percentage Purity = 44.12
$1.13A + 0.14B - 1.06C + 1.83AB + 3.04AC - 0.30BC + 1.09A^2 - 1.72B^2 + 0.98C^2$..... (4)

3.5 Plots on Percentage Yield and Percentage Purity of the Alpha Cellulose

The plots presents the interaction between the process parameters; Time, Temperature and Concentration on the percentage yield and percentage purity of the alpha cellulose.

The Perturbation plot in Figure 1 shows that at Point A (time) decreases while points B (temperature) and C (concentration) increases. However, at deviation from reference point 0.00 (coded units) both Point A, B and C coincided to give optimal percentage yield of 72.6% of alpha cellulose which is slightly above the predicted response (72.34 %). The different between the experimented and predicted response is 0.26 %. Similarly, the optimal percentage purity of the alpha cellulose is 44% as shown in Figure 2. However the predicted response from equation (4) was 44.12 % having the different between the experimented and predicted response as 0.12 %.

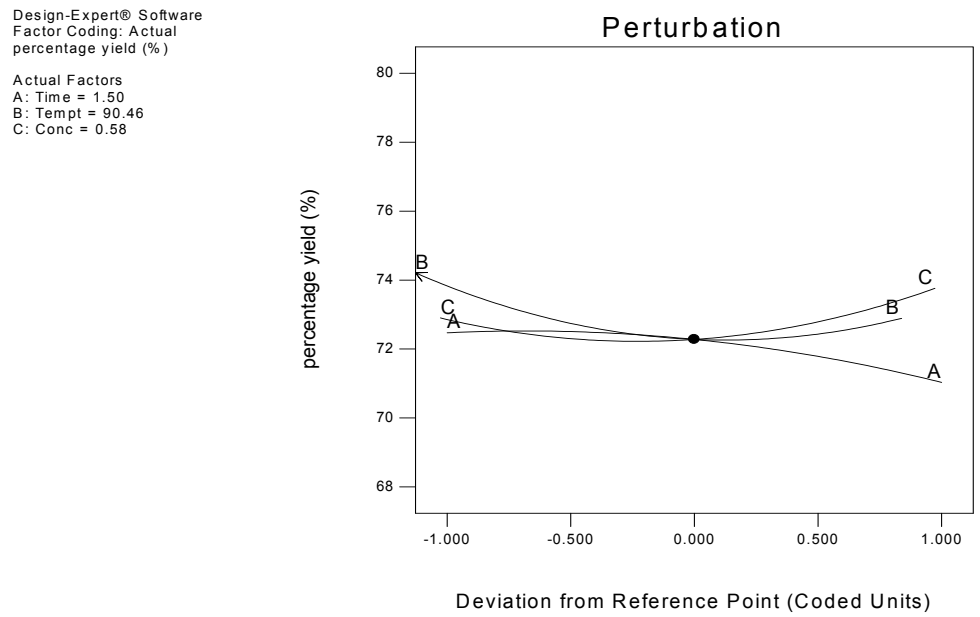

Figure 1: Perturbation Plot showing the effect of time, temperature and concentration on the percentage yield of alpha cellulose

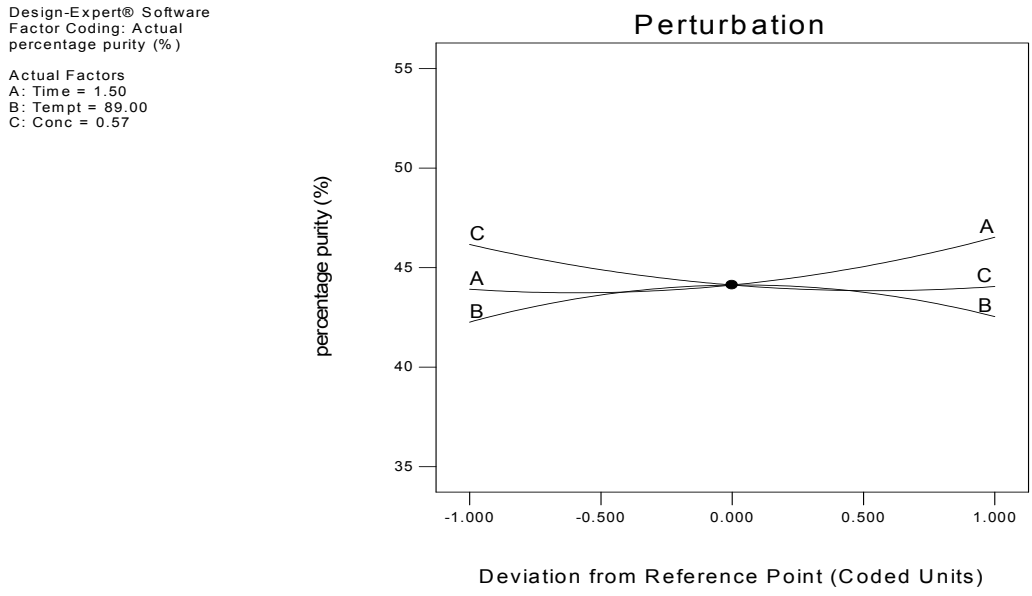

Figure 2: Perturbation Plot showing the effect of time, temperature and concentration on the percentage purity of alpha cellulose

The Predicted versus Actual Plot

The predicted against actual plot shows the effect of the model and compares against the null model. For a good fit the points should be close to the fitted line, with narrow confidence bands. The experimented percentage yield 72.6% and the predicted 72.34 % of alpha cellulose are very close. This is clearly seen from the plots on Figure 3 that the points on the left and right are close to the regression line. The R- Square value of 0.8631 (86.31%) and 73.99% adjusted R- Square value are also close. The outliers points affect the fit (*Garvasio et al.* 2008).

However, in Figure 4 the R- Square value for the percentage purity is 0.5869 (58.69%) and a low adjusted R- Square value of 21.51%. However, some of the points are a bit far from the line of regression. Also, the variables have no significant effect to the response.

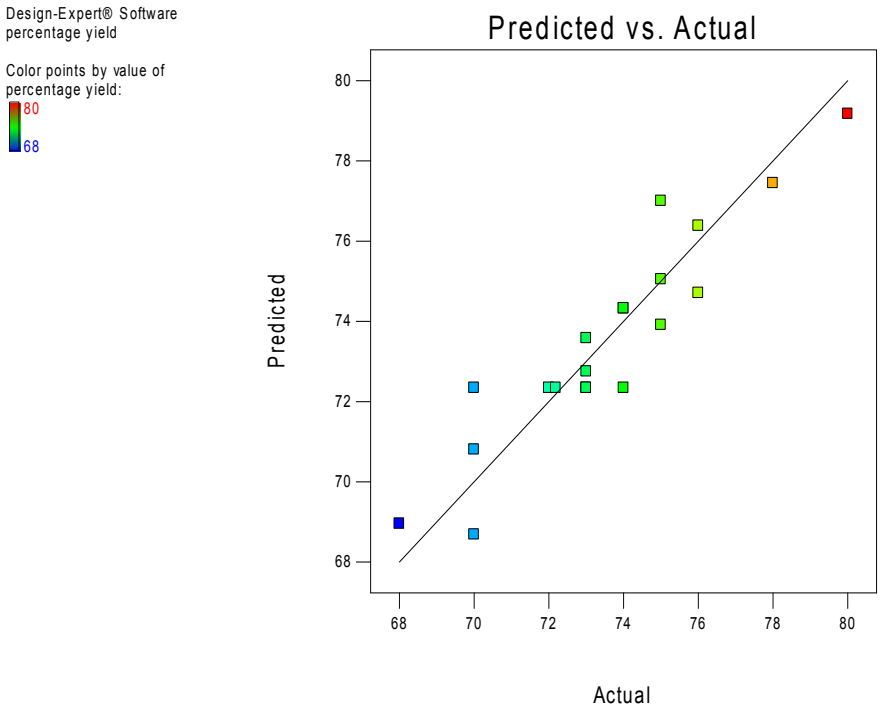

Figure 3: Plot of Predicted verses Actual on the percentage yield of the alpha cellulose

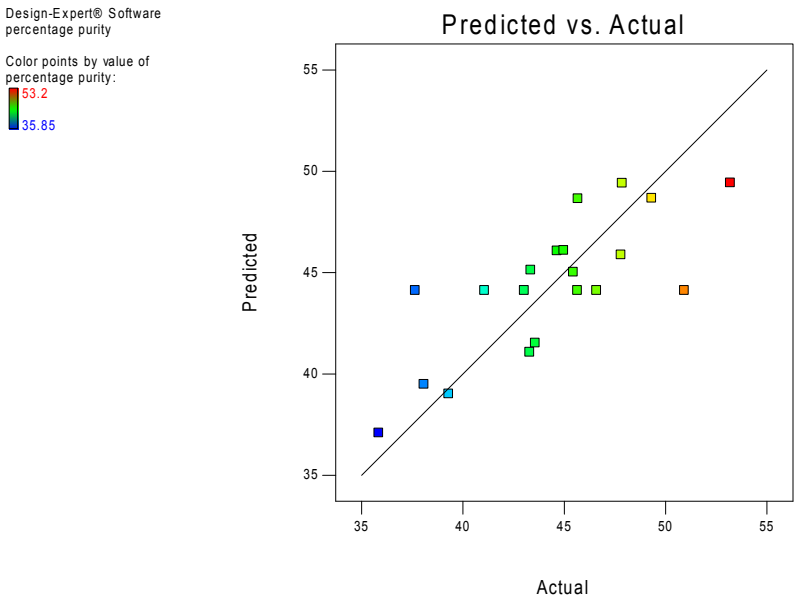

Figure 4: Plot of Predicted verses Actual on the percentage purity of the alpha cellulose

The 3-Dimensional Design

In Figure 5, the 3-Dimensional plot shows the response surface of percentage yield of alpha cellulose. The percentage of alpha cellulose is the function of temperature and time. The optimal percentage yield of alpha cellulose is greatly influenced by temperature. Therefore, increase in temperature greatly increase the percentage yield of the alpha cellulose at a lower time. However, in Figure 6, the percentage purity of alpha cellulose is not affected by the independent variables.

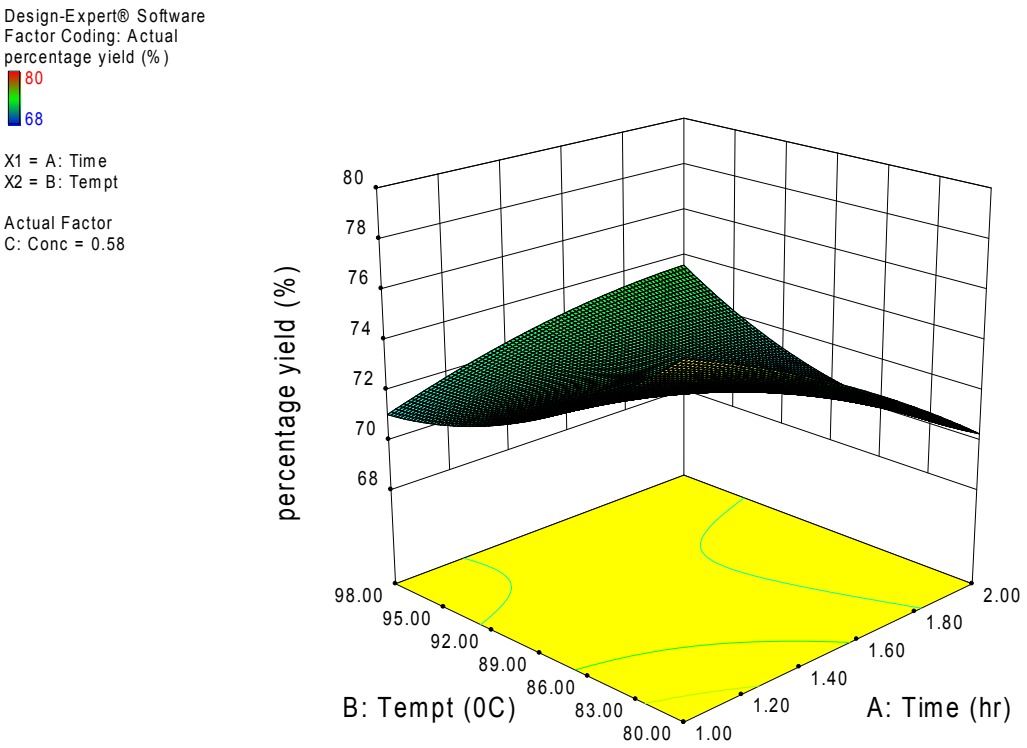

Figure 4: 3D plot of percentage yield and percentage purity of alpha cellulose

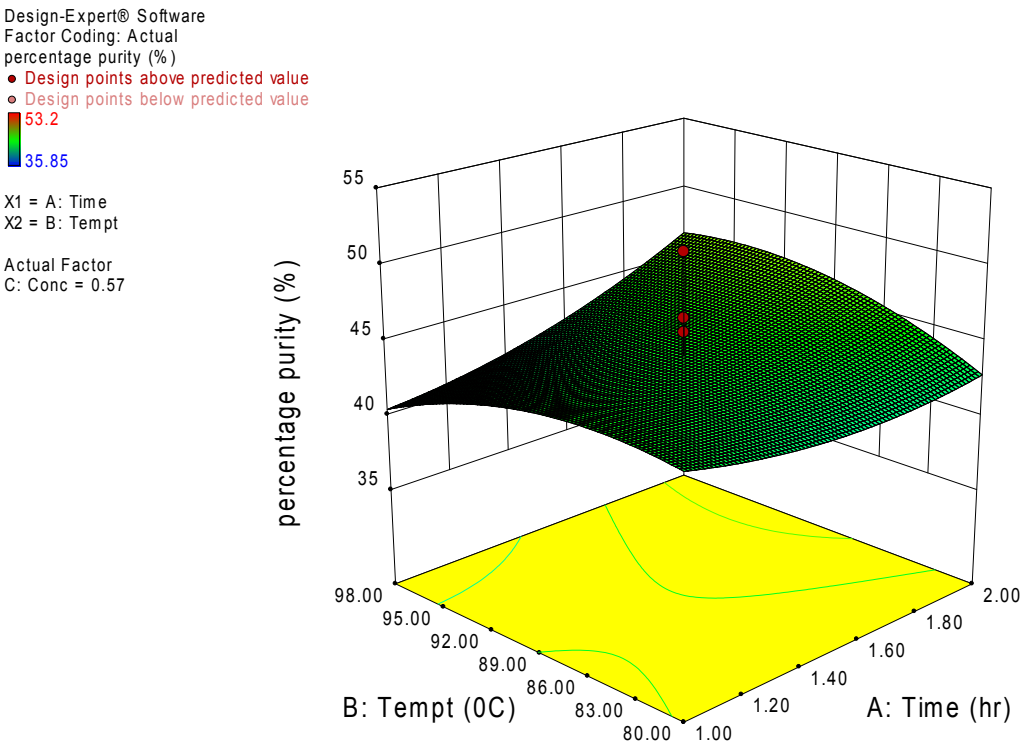

Figure 5: 3D plot of percentage purity and percentage purity of alpha cellulose

In Table 6, the responses were computed and analyzed which present the optimized solutions. However, these conditions were used to validate the optimized data and recorded in Table 7. Therefore, under optimal conditions, the percentage yield and percentage purity of the alpha cellulose obtained were 76.44 % and 40.89 % as seen in Table 7 of number 1. This optimal value as seen present the most favourable result.

Table 6: Solutions of the optimization of the extraction of Alpha Cellulose

OPTIMIZE SOLUTION OF ALPHA CELLULOSE							
Number	**Time (hr)**	**Tempt (⁰C)**	**Conc (g/ml)**	**Percentage yield (%)**	**Percentage purity (%)**	**Desirability**	
1	1.00	80.00	0.90	79.17	41.07	0.93	Selected
2	1.01	80.00	0.90	79.15	41.07	0.92	
3	1.00	80.00	0.89	79.13	41.09	0.92	
4	1.02	80.00	0.90	79.11	41.08	0.92	
5	1.00	80.08	0.90	79.10	41.08	0.92	

Table 7: The validated Solutions of the optimized of Alpha Cellulose

OPTIMIZE SOLUTION OF ALPHA CELLULOSE							
Number	**Time (hr)**	**Tempt (⁰C)**	**Conc (g/ml)**	**Percentage yield (%)**	**Percentage purity (%)**	**Desirability**	
1	1.00	80.00	0.90	76.44	40.89	0.93	Selected
2	1.01	80.00	0.90	76.40	39.75	0.92	
3	1.00	80.00	0.89	77.16	38.28	0.92	
4	1.02	80.00	0.90	78.60	36.56	0.92	
5	1.00	80.08	0.90	76.16	39.13	0.92	

4.0 CONCLUSION

The Analysis of variance (ANOVA) showed that temperature is the most influential factor for alkali treatment and extraction of alpha cellulose. Under optimal conditions, the percentage yield and percentage purity of the alpha cellulose obtained were 76.44 % and 40.89 % respectively. The theoretical values for the percentage yield of the extracted alpha cellulose were close to the experimental results having an error difference of 2.73 % percentage yield and 0.18 % percentage purity respectively. Therefore, RSM technique based on CCD design is suitable for optimizing the variables influencing the extraction of alpha cellulose.

REFERENCES

Achor M, Oyeniyi YJ and Yahaya A., Extraction and characterization of microcrystalline cellulose obtained from the back of the fruit of *Lageriana siceraria* (water gourd), Journal of Applied Pharmaceutical Science Vol. 4 (01), pp. 057-060, January, 2014 DOI 10.7324/JAPS.2014.40109 ,ISSN 2231-3354

Alidadi Shamsabadi, T. Behzad, R. Bagheri.,Optimization of acid hydrolysis conditions to improve cellulose nanofibers extraction from wheat straw, Fibers and Polymers.March 2015, Volume 16, Issue 3, pp 579–584

Ansel CH, Popovich GN. *Ansel's Pharmaceutical Dosage Forms and Drug Delivery Systems.* New York: Lippincott Williams and Wilkins; 2005. p. 189.

Audu-Peter JD, Ojile JE, Bhatia PG. Physicochemical and Powder Properties of Alpha- and Microcrystalline cellulose derived from Maize Cobs. J Pharm Biores 2004; 1:41-5.

Chukwuemeka P. A, Odulaja, J.O. and Okhamafe A.O, Physicotechnical, spectroscopic and thermogravimetric properties of powdered cellulose and microcrystalline cellulose derived from groundnut shells Journal of Excipients and Food Chemicals. 2012; 3(3): 106-115

Chukwuemeka P. A, Okhamafe A.O, Physicochemical, spectroscopic and thermal properties of microcrystalline cellulose derived from corn cobs. International Journal of Recycling of Organic Waste in Agriculture. 2012; 1(1): 9

Chukwuemeka P. A, Silva B.O. and Okhamafe A.O. Pharmacopoeial and physicochemical properties of cellulose and microcrystalline cellulose powders derived from cornstalks. International Journal of Green Pharmacy. 2012; 6(3): 193-198

Duret X, Fredon E, Masson E, Deshamus L, and Gerardin P, Optimization of acid pretreatment in order to increase the phenolic content of picea abies by surface research methodology, Bioresources 2013, 8 (1), 1258-1273.

Gervasio David Feria, Jean-Roch Mouret, Nathalie Gorret, Gérard Goma, Stéphane E. Guillouet, Oleic acid delays and modulates the transition from respiratory to fermentative metabolism in *Saccharomyces cerevisiae* after exposure to glucose excess, Applied Microbiology and Biotechnology, February 2008, Volume 78, Issue 2, pp 377–377.

Gregory Thoorens, Microcrystalline cellulose, a direct compression binder in a quality by design environment—A review. International journal of pharmaceutics, volume 474, issue 1-2, October 2014, page 64-72

Hindi, S.S.Z. Microcrystalline Cellulose: Its specifications and pharmaceutical processing Biocrystals Journal.1 March 2016, (1): 26-38 improvement of drug photostability in solid dosage forms. Expert Opinion on Drug Delivery. 2013; 10(10): 133

Hou X.J and Chen W., Optimization of extraction process of crude polysaccharides from wild edible Bachus mushroom by research surface methodology, carbohydrates polymers, 2008, 72 (1), 67-74.

Javad Shokri and Khosro Adibkia, Application of Cellulose and Cellulose Derivatives in Pharmaceutical Industries, 29 August 2013, DOI: 10.5772/55178

Jinbao Li, Xiangrongrong Zhang, Meiyun Zhang, Huijuan Xin, and Hany He, Optimization of selective acid hydrolysis of cellulose for microcrystalline cellulose using $FeCL_3$, Bioresources

, 2014, 9 (1), 1334-1345Matrosovich M, Matrosovich T, Garten W, Klenk HD., New low-viscosity overlay medium for viral plaque assays. *Virol J.* Aug 31; 3:63. (2006).

Ohwoavworhua FO, Kunle O.O, Extraction and characterization of microcrystalline cellulose derived from Luffa cylindrica plant. African J Pharm Res December 2004; 1:1-6.

Ohwoavworhua, F.O. and Adelakun, T.A, Some Physical Characteristics of Microcrystalline Cellulose Obtained from Raw Cotton of Cochlospermum planchonii, Tropical Journal of Pharmaceutical Research, Vol. 4, No. 2, December 2005, pp. 501-507

Orts W.J, Shey J, Imam S.H, Glenn G.M, Guttman M.E, Application of Cellulose Microfibrils in Polymer Nano composites, Revol. J. Polymer. Enviroment., 13,2005, 301-306

Qi B.K., Chen X.R., Shen F., Su Y., and Wan Y. H., Optimization of enzymic hydrolysis of wheat straw pretreated by alkaline peroxide using research surface methodology, industrial and engineering chemistry research, 2000, 48 (15), 7346-7353.

Rani K. P, Sreejith M. P and E. Purushothaman., Isolation of microcrystalline and nano cellulose from peanut shells, Journal of Chemical and Pharmaceutical Sciences ISSN: 0974-2115 JCHPS Special Issue 1: January 2016

Reddy N, Yang Y, Properties and potential applications of natural cellulose fibers from cornhusks, Green Chem.,7, 2005, 190-195.

Reddy N, Yang Y, Structure and properties of high quality natural cellulose fibers from cornstalks, Polymer, 46, 2005, 5494-5500.

Rojas .J, Ospina L., Fonseca S., International Journal of Pharmaceutical Sciences Review and Research. 2012; 13(1): 1-8

Rosa M.F, Medeiros E.S, Malmonge J.A, Gregorski K.S, Wood D.F, Mattoso L.H.C, Glenn G, Orts W.J, Imam S.H, Cellulose nano whiskers from coconut husk fibers: Effect of preparation conditions on their thermal and morphological behavior, Carbohydrate. Polymer, 81, 2010, 83-92.

Sathavornvichit, N., Bookkamana, P., and Plubin, B. "Central Composite Design in Optimization of the Factors of Automatic Flux Cored Arc Welding for Steel ST37" in *Proceedingss IMT-GT Regional Conference on Mathematics, Statistics and Applications*, Penang, Malaysia 2006.

Sun J.X, Mao F.C, Sun X.F and Sun R.C., Comparative study of hemicelluloses isolated with alkaline peroxide from lignocellulosic materials. J. Wood Chem. Technol, 2004, 24, 239-262.

Proceedings of the 49th NSChE Annual Conference
KADA 2019: pp 656-672

P3B-10: DETERMINATION OF OPTIMAL MASS SEPARATING AGENT FOR THE REMOVAL OF POLLUTANT FROM INDUSTRIAL WASTES USING MASS EXCHANGER NETWORKS SYNTHESIS

G.B. Adebayo O. S., Azeez[1]* and A.S. Abdulkareem[2]*

Department of Chemical Engineering, School of Infrastructure,Process Engineering and Technology, Federal Universityof Technology, P.M.B 65, Main Campus, Gidan-Kwano Minna, Niger State, Nigeria

Corrresponding author: agracebosede@yahoo.com

ABSTRACT

Wastes and Emissions from chemical plants have over the years contributed to the environmental pollutions. End-of-pipe treatments alonecannot effectively mitigatethe effects of chemical processing facilities because of their complexity, it is important for pollution prevention to be considered from the beginning of chemical process synthesis steps. Therefore, this study focuses on the determination of optimal mass separating agent(MSA) for the removal of a pollutant from industrial wastes using mass exchanger networks synthesis(MENS). Pinch y-y tool was used to determine the most suitable external MSA for MENS problem with multiple MSAs (S_3, S_4, S_5 and S_6) and to target for capital cost and total annual cost (TAC) for the network before actual design. From the result of the designs, MSA (S_3) shows to be the most suitable and economical, followed by S_6, S_4 and S_5 respectively. It can be inferred from the results that these methods can be used to screen and select MENS problems with multiple MSAs options quickly and effectively. This also reduces the design cost as well as minimising the emission of pollutants into the environment.*

Keywords- Capital cost targets; Mass exchanger networks; Mass separating agent; Pinch technology, Pollution

1.0 INTRODUCTION

Research in process synthesis over the years has been driven by the desire to enhance process performance and profitability while reducing the environmental impact. The effort to improve yield and profitability will have to be simultaneously achieved along with reductions in energy consumption, impressive process flexibility, process and environmental safety, product quality enhancement,waste recycling and reuse and pollution prevention (Keller and Bryan, 2000).Industrial wastewater can be used for irrigation to increases agricultural production, thus contributing to food safety. The nutrients that arepossibly contained in wastewatercan thus allow for savings on purchase of fertiliser. Nevertheless, the risks of industrialwaste water re use in agriculture and other activities can be extensive in terms of public health problem if necessary steps are not taken before and after re use. The prevention of pollution can therefore, be a greatbenefit associated with industrial waste reuse but necessary steps will have to be taken to ensure safety of public health.

Chemical processing facilities vary from simple connections of units to complex networks of units of equipments and streams.The environmental issues emanating from such complex system cannot be effectively mitigated by just end-of-pipe treatments.Pollution prevention through system integrationshould be taken into account from the beginning of process synthesis steps. The environmental performance and cost effectiveness of a process will depend on the performance of the various unit operations and process integration. Achieving global insights into the nature of heat and mass flow of processing facilities enable pollution reduction at the source as well as cost effectiveness of the process(Linnhoff and Ahmad, 1989; Agrawal and Sikdar, 2012; Azeez, 2011).

Chemical process synthesis involves the systematic development of process flow sheets that can effectively transform available raw materials into desired products that will meet specified performance criteria of minimum cost of productions, energy efficiency, maximum raw material recovery, minimum waste production and excellent operability (Smith, 2016). It answers the question of which unit operation should be used and the way it should be approached in order to provide the best possible solution to a synthesis problem. One of the design approaches that have been adopted in recent times is the integration of the systems that make up the processes. Process integration is a tool that have been used to accomplish some of the goals in process optimization. Some of the task that have been accomplish using the process integration include improved sustainability by reducing the process waste discharge, effective use of raw materials,reduction in the purchase of external energy utilities and mass separating agents and minimising the generation of emissions and wastes (Kaggerud et al, 2006). It is a system-oriented, thermodynamics-based, integrated approach to the analysis, synthesis and retrofit of process plants. (El-Halwagi, 1997; Linnhoff et al., 1982; Linnhoff and Ahmad, 1989).

There are two main approaches to process integration; the pinch technology approachandthe mathematical optimization approach. In pinch technology, the designer uses physical and thermodynamic concepts to set up and optimise the task to be synthesised (Linnhoff and Vredeveld, 1984).Mathematical programming approach involves setting up a mathematical framework which is supposed to embed all possible alternative structures using different types of mathematical constraints. The framework is subsequently optimised subject to the constraints in order to obtain the optimum structure (Azeez, 2011; Isafiade, 2008).

In theapplication of process integration, several optimisation techniques have been developed in order to reduce the usage of material and energy resources as well as discharge of wastes (Wang and Smith, 1994; Hallale and Fraser, 2000aandb; Tjan et al., 2010; Ponce-Ortega et al., 2010;Papalexandri et al.,1994; Azeez, 2011 ; Foo et al., 2005).

Heat Exchanger Network Synthesis (HENS) had been given more attention over MENS;this was due to the rising cost of energy in the seventies (Gundersen andNaess, 1988; Linnhoffand Ahmad, 1989; Yee and Grossmann., 1990). Also, concern has been raised by various regulatory bodies on the effect of process industries emissions into the environment.This has necessitated the development of integration methods for mass exchange network synthesis (El-Halwagi, 1997; Hallale and Fraser, 2000aandb).Mass exchanger networks has now become parts of the separation networks of the chemical plants, MENS seeks to clean the emanating process streams before they are released to the environment. MENS reduces the amount of external MSAs required for cleaning and the cost of the end-of-pipe waste treatments. It serves as a direct pollution prevention goalsuch as removal of phenol and many other harmful wastes that may be present in streams coming out of industrial processes.

Mass-exchange operation is common in industrial processes, a mass exchanger is any direct-contact mass-transfer unit that employs a mass-separating agent (MSA) or a lean phase (such as solvent, adsorbent, stripping agent, ion exchange resin) to selectively remove specific components (pollutants, products, byproducts) from a rich phase (a waste or a product) (Isadfiade, 2008; Hallale, 1998; El-Halwagi, 1997). Mass-exchange operations include absorption, adsorption, stripping, solvent extraction, leaching, and ion exchange. Multiple mass exchange operations can be involved in many industrial situations, and several candidate MSAs may have to be considered especially where there are several rich streams from which mass has to be transferred through the employment of MSAs for the removal of the targeted

species. Therefore, applying the mass exchanger networks synthesis approach can provide both technical and economic benefits. In this research, approach of Hallale (1998) and those of Hallale and Fraser (2000a and b) are investigated in the screening and optimising the use of external mass separating agents in the removal of phenol from waste streams.

The MENS problem statement can be stated as follows (El-Halwagi, 1997; Isafiade, 2008; Hallale, 1998):
Available are a number of rich streams and a number of lean streams, otherwise known as the mass separating agents, the requirements is to synthesise a cost-effective network of mass exchangers thatcan transfer certain materials from the rich streams to the lean streams. Available also are the flow rate of each rich stream as well asthe supply and target composition.Also, the supply and target compositions are given for each MSA. The mass transfer equilibrium relations are also made available for each MSA. The flow rate of each lean stream is not given and will have to be calculated

The process MSA is already available on the plant and can be used for the removal of certain materials at a low or no cost (often free).The flow rate of each process MSA available for mass exchange is bounded by the availability in the plant. On the other hand, the external lean stream can be purchased from the market and their flow rates are subject to economic considerations.

The design questions to be addressed in the research includethe following; MSAs to be selected, the optimal flow of such MSAs, stream pairings to be selected and the optimal system configuration?

BACKGROUND

The mass exchanger networks analogue of the pinch synthesis method for heat exchanger networks was developed in El-Halwagi and Manousiouthakis (1989) and extended to El-Halwagi (1997). The authors targeted for the minimum MSA required to accomplish a separation task and also presented design methods needed to meet these targets. Hallale (1998) and Hallale and Fraser (2000a and b) developed the $y - y^*$ tools for targeting the mass exchange area and capital cost for both stage-wise and continuous contact columns that were not available in the studies of El-Halwagi and co-worker. One of the important areas of MENS problems which have not been given much attention is the optimal selection of MSAs in MENS when there are multiple MSAs.This constitutes the purpose of this studythrough the use of the tools developed by the aforementioned researchers in this background.

2.0 METHODOLOTY

Pinch analysis as applied to MENS, involves targeting before actual design which include; minimum mass separating agent (MSA) targeting, the minimum number of units targeting (El-Halwagi, 1997), capital and total cost targeting (Hallale and Fraser, 2000a and b), then network designs.Hallale, (1998)'s y-y* tool will be employed in solving a problem with multiple external MSAs. The following factors will be used to determine the most suitable MSA to be used; the lowest overall cost of removing mass load of the contaminant, the minimum flow rate required for the selected MSAs, operating cost of the MSAs, capital and total cost targets and also the capital and total costs of the design network will be accounted for to enable proper selection between the multiple external MSAs.

2.1 Mass Separating Agent Targets

Pinch technology strives to optimize the use of the process MSAs to recover mass from the process before employing the external MSAs. If the mass removed with process MSAs is maximized, lesser external MSAs will be required. The pinch diagram approach for targeting the minimum external MSA requirement is an analogy to that of the pinch in HENS.A composite of all the rich streams is obtained by plotting each rich streamcontaining the mass to be removed against its supply and target compositions on a single graph (Isafiade, 2008). Addition of the mass loads of the rich process streams in the synthesis task in each concentration intervalis accomplished and a new line drawn across the interval equivalent to the sum of the mass load (El-Halwagi and Manousiouthakis, 1989). Lean streamswere treated the same wayusing the same steps. Both composite curves were drawn on the same axes as presented by El-Halwagi and Manousiouthakis, and it is shown in Figure 1.

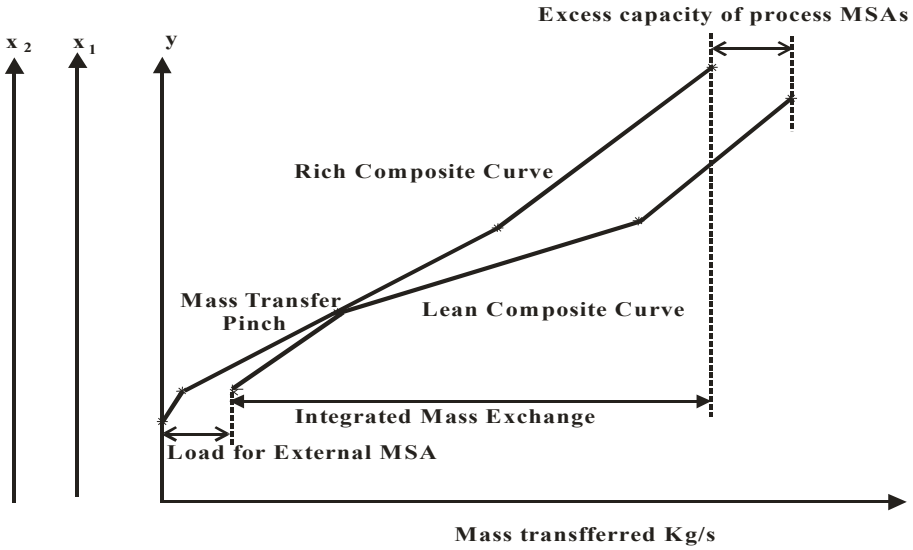

Figure 1: Mass exchange composite curves(El-Halwagi and Manousiouthakis, 1989).

The point at which the rich and lean composite curves have contact is known as the *mass transfer pinch.* The two curves touch each other not because there is zero or no driving force but the ε valueis built into the lean stream compositions using the equilibrium relation shown in Equation (1) (Hallale and Fraser, 1998).

$$y = m_j(x_j + \varepsilon_j) + b_j \quad (1)$$

where y and x are the rich and lean stream compositions, m_j is the mass transfer equilibrium relation for MSAs, ε_j is minimum allowable composition difference, which is also the driving force and bj is the equilibrium constant.

According to Hallale and Fraser (2000a), for a MENS problem where each lean stream has separate composition scales, it is important to point out that they are not equivalent because of the different equilibrium relations.For all MSA compositions to have a common basis therefore, an MSA composition, x_j, will have to be expressed as the rich stream composition

with which it would be in equilibrium, y*. The equilibrium relations transformation is as follows;

$$y^* = m_j x_j + b_j (2)$$

The driving forces for exchanger sizing is expressed in terms of y and y* values. The minimum composition difference between y and y* is represented as Δy_{min} and is related to the composition difference in the MSA, Δx, through the equilibrium constant.The authors then constructed the lean composite curve in terms of y* values correspond to the x^s and x^t values for the MSAs.Both the rich and lean streams composite curves were then presented on the same axes against mass transfer load and shifted together until a pinch was noted (Figure 2). Plotting lean streams in term of y* values prevented thecomposite curvesfromtouching at the pinch but now separated by a composition difference of Δy_{min} (Hallale and Fraser, 2000a).

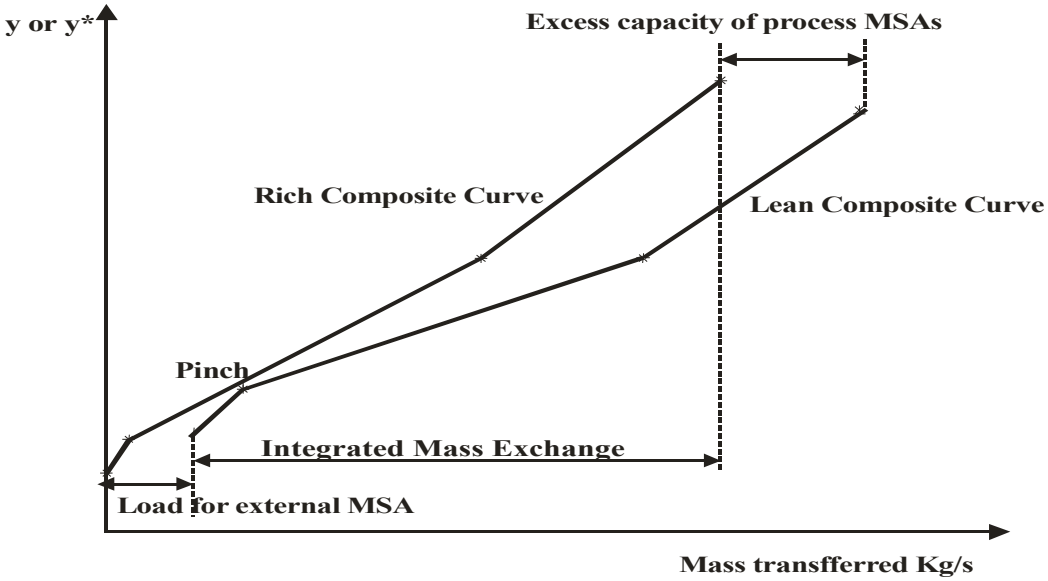

Figure 2: Mass transfer composite curves with lean stream compositions y* (Hallalae and Fraser, 2000a)

The region ofcomplete vertical overlap of the rich composite curve over the lean composite curve in Figure 2 shows the optimum amount of species that can be removed by the process MSAs. The overshoot of the lean composite curve over the rich composite curve indicates the excess capacity of the process MSAs that can remove load available. Details of the process is contained in Hallale (1998). The external MSAs flow rate targets is established by drawing y-y* composite curves for these MSAs.

2.2 Capital Costs Targets

To determine the capital cost of a mass exchanger network, factors like the number of mass exchangers, the size, number of transferunit or number of stages of the exchangers, and the material of construction have to be accounted for as these contribute to the capital cost of a mass exchange network (Hallale, 1998).

2.3 Number of Transfer unit Targets

Targeting for the capital cost of mass exchange networks include factors such as: the target for the number of equilibrium stages in the network, total number of transfer unit, exchanger diameters, transfer height, inactive heights, distribution of units between streams and other relevant information regarding number of staged are contained in Hallale, (1998). The mass transfer composite curves which represent the entire network do not show the composition differences that can be used for the number of transfer unit targetingand to predict equipment sizes. A new plot, y-y* composite curve developed by Hallale (1998) and used in Hallale and Fraser (2000a) which shows the composition differences and still representing the entire network was seen to be useful and will be used in this work. The tool as developed in Hallale (1998) is shown in Figure (3).

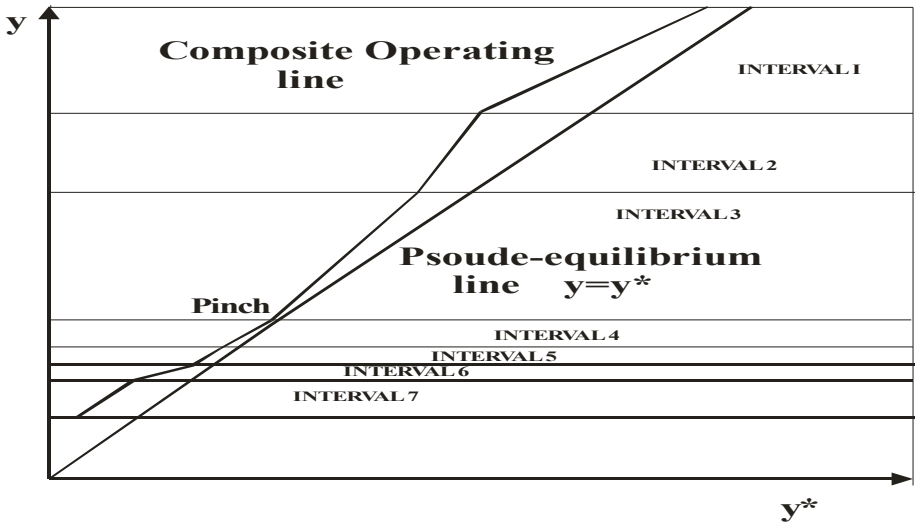

Figure 3: The *y-y composite curve of Hallale, (1998).**

The y-y* composite curve plot developed by Hallale (1998)shows the profile for vertical mass transfer andmanyothermaterialsneededfor mass exchanger sizing. The plot presents the analogy between HENS and MENS using pinch technology. The ratio of the composite operating line slope to the equilibrium line slope is the removal factors A, and the differences between the operating line and the pseudo- equilibrium line is Δy values (driven force). The detail of the tool is contained in Hallale (1998).The number of stages can be determined for each composition interval using graphical approach or Kremser equation for stage wise exchanger while for continuous contact columns transfer unit approach used for the height targeting. In this study, the continuous contact exchanger is used and the minimum network height, *Hmin*, was determined for each interval as follows (Hallale and Fraser 2000b):

$$H_{min} = \sum_{i}^{\text{Rich streams}} HTU_i + \sum_{k \propto i} NTU_i = \sum_{i} H_i \quad (3)$$

where NTU and HTU are number and height of theoretical units respectively. NTU is a function of Δy_{min} is given as:

$$NUT = \frac{y^{in} - y^{out}}{\left(y_i - y_j^*\right)_{logmean}} (4)$$

Δy_{lm} is the log means rich-phase composition differences, given by:

$$\left(y_i - y_j^*\right)_{logmean} = \frac{\left(y^{in} - y^{*out}\right) - \left(y^{out} - y^{*in}\right)}{\log\left[\frac{\left(y^{in} - y^{*out}\right)}{y^{out} - y^{*in}}\right]} (5)$$

Δy^{in} and Δy^{out} are driving forces, the differences between the operating line and equilibrium line.

2.4 Capital Cost and Total Annual Cost Estimation

Hallale (1998) targeted for total number of exchangerheight by summing up the contributions from each rich stream using a method similar to that of shell targeting in HENS (Ahmad and Smith, 1989). Because of the pinch division, the author subdivided the rich stream contributions in to contributions above and below the pinch. The total target as presented by Hallale,(1998) is thus:

$$H_{min} = \sum_{i}^{Rich} H_{i,above\ pinch} + H_{i,below\ pinch} (6)$$

2.5 Minimum Number of UnitTargets

The minimum number of units is also required for capital cost targeting for the purpose of practicality and operability. Minimum number of stages is assumed to be achievable in the minimum number of units. The minimum number of mass exchanger N_{unit} is simply one less than the total number of streams in the network as presented by Hallale (1998). For network where there is pinch division, this should be applied to each side of the pinch separately as done by Hallale (1998):

$$N_{units} = (N_R + N_S - 1)_{\text{Above pinch}} + (N_R + N_S - 1)_{\text{Below pinch}} \quad (7)$$

where N_R and N_S are the number of rich process streams and MSAs, respectively.

Capital and total annual cost target are estimated as follows;

$$Capital\ cost\ target\ (cost)_{capital} = \sum_i \sum_j C_{ij} H_{ij} \quad (8)$$

Where $C_{ij,}$ is the annual cost of each column plate and its value depends on the mass exchanger's type and size. N_{ij} is the number of transfer height.

$$Total\ annual\ (cost)_{total} = capital\ cost + operating\ cost \quad (9)$$

2.6 Network Design

In order to meet the MSA cost targets in design, stream matching should start at the pinch since this is the most constrained part of the network (El-Halwagi and Manousiouthakis, 1989). For capital cost targets, Hallale, (1998) recommends that a low number of units should be used to approach as closely as possible the ideal profile. The feasibility criteria applicable to pinch matches presented by El-Halwagi and Manousiouthakis, (1989) and Hallale, (1998):

2.7 Stream Population: This recommendation of Hallale (1998) was observed in the stream population technique.

2.7 .1 Operating line versus equilibrium line: This was also observed as recommended by Hallale (1998)

2.7 .2 The Driving Force (y-y*) Plot

The driving force plot is constructed from the *y-y** composite curve plot as done for MENS in Hallale (1998), the selected matches between rich and line stream is evaluated on the *y-y** composite curve by comparing the operating line of each potential match with the composite operating line.

2.7 .3 Remaining Problem Analysis

A selected match is evaluated based on the penalty incurred when the remaining problem is analysed. Penalty means the use of more stages above the target in design, and it is expressed in terms of efficiency, α_{match}.

The methodology outlined above is applied to an industrial problem for the purpose of pollution prevention, removal of pollutant from wastes generation by the plant to a satisfactory level in the most economical way and selection of most suitable external MSA for the removal of the pollutant.

2.0 Problem Specification

This problem specified here involves the removal of phenol from two aqueous streams, R_1 and R_2 by solvent extraction. Removal of phenol from the waste streams is necessary because of its harmful effects when released into nearby streams or rivers. Two process MSA_S gas oil (S_1) and lube oil S_2 are available. It is specified in the problem that the entire gas oil stream should be used. Four external MSAs (S_3, S_4, S_5 and S_6) which are activated carbon, ion exchange resin, air and light oil respectively are available also available for phenol removal.

Stream and cost data for the problem are given in Tables 1 and 2, with all compositions in mass fractions. S_1 and S_2 are available free and the cost of the external MSAs are given in Table 2. The annual operating time for the plantwas assumed to be 8600h. The capital cost of mass exchangers for a continuous contact mass exchanger is assumed to be $4245 per year per height (Papalexandri and Pistikopoulos, 1994). The minimum composition difference, Δy_{min} is specified to be 0.001.

Table 1: Rich Streams Data (Isafiade, 2008)

Stream	G (kg/s)	y^s	y^t
R_1	2	0.05	0.01
R_2	1	0.03	0.006

$G_i$in Table 1 is the flow rate of process stream i, y^s_i and y^t_i are the supply and target concentrations (mass fractions) of the pollutants respectively. L^c is the upper bound on the flow rate of process MSA j, x^s_j and x^t_j are the supply and target concentrations of the MSAs, respectively. m_j is the mass transfer equilibrium relation for MSAs while ε_j is minimum allowable composition difference as earlier mention in this paper.

Table 2: Lean Streams Data (Isafiade, 2008)

Stream	L^c(kg/s)	x^s_j	x^t_j	m_j	b_j	Cost($/kg)
S_1	5	0.005	0.015	2	0	0
S_2	3	0.01	0.03	1.53	0	0
S_3	∞	0	0.11	0.02	0	0.081
S_4	∞	0	0.50	0.09	0	2.55
S_5	∞	0	0.029	0.04	0	0.06
S_6	∞	0.0013	0.015	0.71	0.71	0.01

3.0 RESULTS AND DISCUSSION

3.1 Determination of the Minimum Mass Separating Agent

Hallale (1998) analysed this problem for S_6 scenario using the stagewise column but the problem will now be analysed for all the external MSAs in this paper. In the problem specifications above each lean MSA has its individual composition scales as mentioned in the introduction and are not equivalent due to different equilibrium relations. Then the MSA composition x_i is stated as rich stream equilibrium composition, y*, as expressedin equation (2), this allows all the MSAs composition to be transformed to a general basis as shown in table (3) corresponding scale for y* (Hallale and Fraser. 2000a).

Table 3: Rich Streams Data shown (Δm_i)capacity flow rate

Stream	G (kg/s)	y^s	y^t	Δm_i(kg/s)
R_1	2	0.05	0.01	0.08
R_2	1	0.03	0.006	0.024

Corresponding Scale for y* and process MSAs capacity flowrate

Stream	(L^c_j/m_j)(kg/s)	y^{*s}	y^{*t}	Δm_j(kg/s)
S_1	2.5	0.01	0.03	0.05
S_2	1.961	0.0153	0.0459	0.06
S_3	∞	0	0.0022	-
S_4	∞	0	0.0459	-
S_5	∞	0	0.00116	-
S_6	∞	0.00192	0.01165	-

Following the steps in Figure (2), Mass transfer pinch point wasseen to be at y and y* values of 0.0163 and 0.0153 respectively which were the values obtained in the work of Hallale (1998). The minimum external MSA duty is 0.00964kg/s and the excess capacity flow rate of S_2 is 0.0156kg/s. Excess capacity flow rate can be eliminated by lowering the flow rate or the outlet compositions of process MSA. In this case, only the capacity flow rate of the process MSA S_2 was reduced from 1.961 to 1.451kg/s.The target capacity flow rate (L_j/m_j) for external MSAs were determined to be 4.382kg/s for S_3, 0.630kg/s for S_4, 8.31kg/s for S_5 and 0.992kg/s for S_6. The MSAs actual flow rate (L_j) targets are: S_1, 5kg/s, S_2, 2.22kg/s, S_3, 0.0876kg/s, S_4, 0.0567kg/s and S6, 0.704 kg/s.

The first criterion to be considered in screening, of MSAs is their allowable concentration range, both the supply and the target composition. Pinch rule implies that no external MSA should be used above the pinch; that means y^{*pinch} 0.0153 is the target composition for all the MSAs. MSA with target composition below this is thermodynamically feasible; MSA with supply composition below pinch but target composition above can be reduced to pinch composition.

While MSA with supply composition above pinch, composition is thermodynamically and economically inferior. In this problem S_3, S_5 and S_6 have target composition below pinch 0.0022, 0.00116 and 0.1165 respectively, while S_4 with 0.0459 target composition was reduced to y^{*pinch} 0.0153, which is corresponding to 0.17 x_4 values.

The second criterion for selecting MSA is based on the cost of removing 1kg of mass load of phenol, which depends on both the cost of the MSA and its allowable concentration range as follows (Fraser et al. 2005).

$$\text{Cost of removing mass load } \left(C_j^r\right) = \frac{\text{Cost of the MSA } \left(C_j\right)}{\left(y_j^{*\text{target}} + y_j^{*\text{supply}}\right)}$$

The removal cost of the MSAs S_3, S_4, S_5, and S_6were calculated to be: \$0.730kg, \$0.736kg, \$1.5kg and \$2.069kg respectively.

Also, operating cost is another criterion for screening external MSAs, the flow rate of MSAs can be used to determine their minimum operating cost (MOC) as follows:

$$\text{Operating cost, [cost]}_{\text{operating}} = \text{cost of MSA} \times \text{flow rate} \times \text{operaring hours}$$

For 8600 operating hours per year, S_3MOC was determined to be \$219,680yr, \$447,635yr for S_4, 617,466for S_5, and \$217,958yr for S_6.

4.0 Capital and Total Cost Targets

Capital cost targetswere estimated for all the MSAs using the target for the number of transfer unit (NTU)in the network (Equations 4 and 5).In this problem specification, the cost of the exchanger had been given, thus, there is no need for targeting for the height of theoretical units (HTU).The number of transfer unitfor each MSA is represented on a grid diagram in Figure (4). Notice that Figure 4d was similarly obtained in Hallale (1998) which implies that the method is correctly applied in this study. The intervals are represented as the vertical line with pinch marked with a dotted line. The rich streams are shown running from right to left on the diagram, while the lean streams run from left to right with their corresponding compositionsas shown in the figures below.

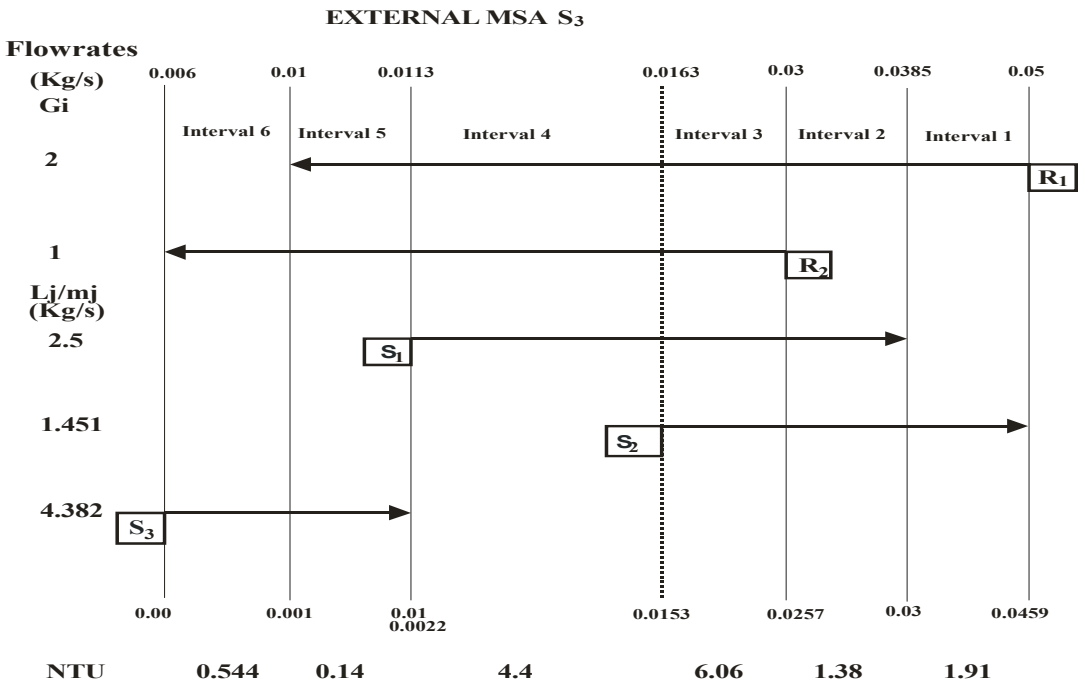

Figure 4a: Grid diagram showing external MSA S_3

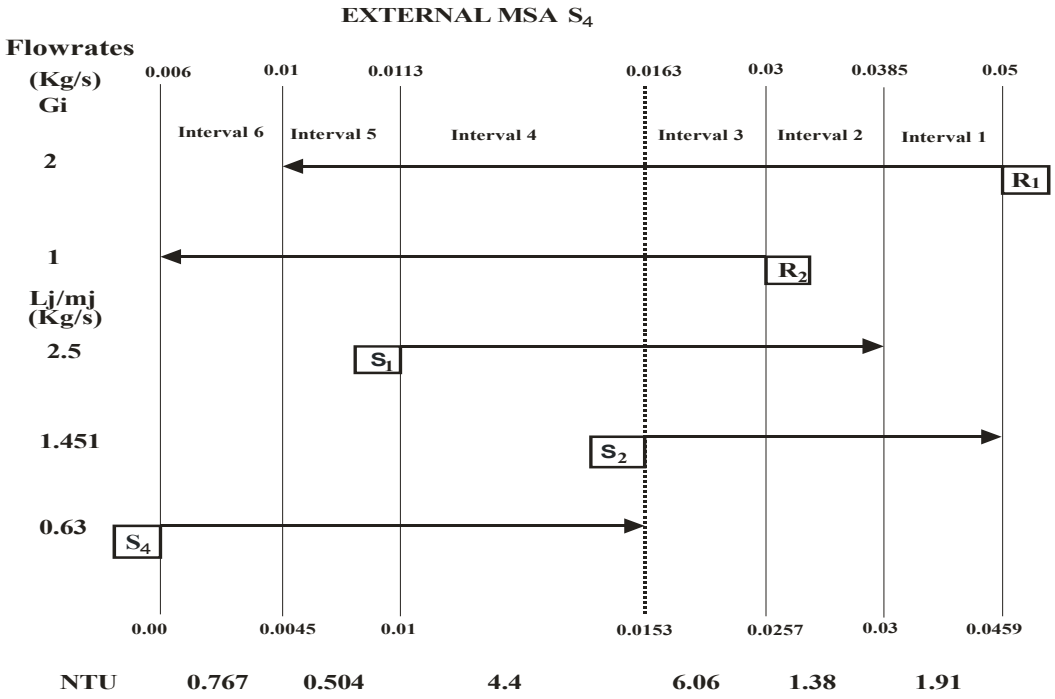

Figure 4b: Grid diagram showing external MSA S_4

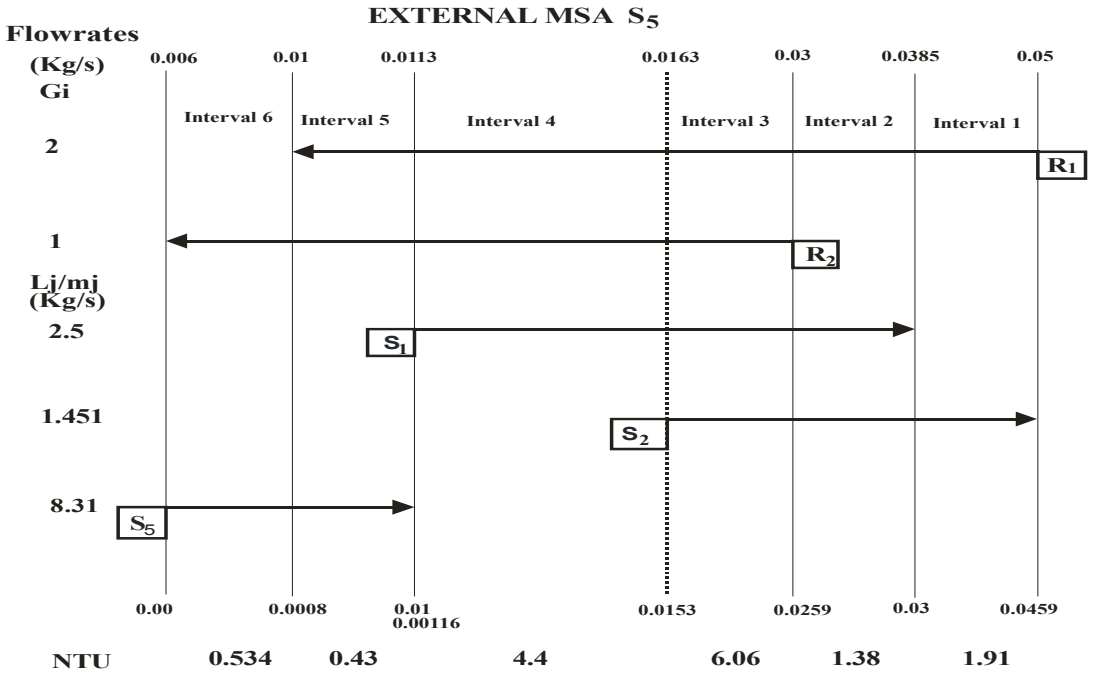

Figure 4c: Grid diagram showing external MSA S_5

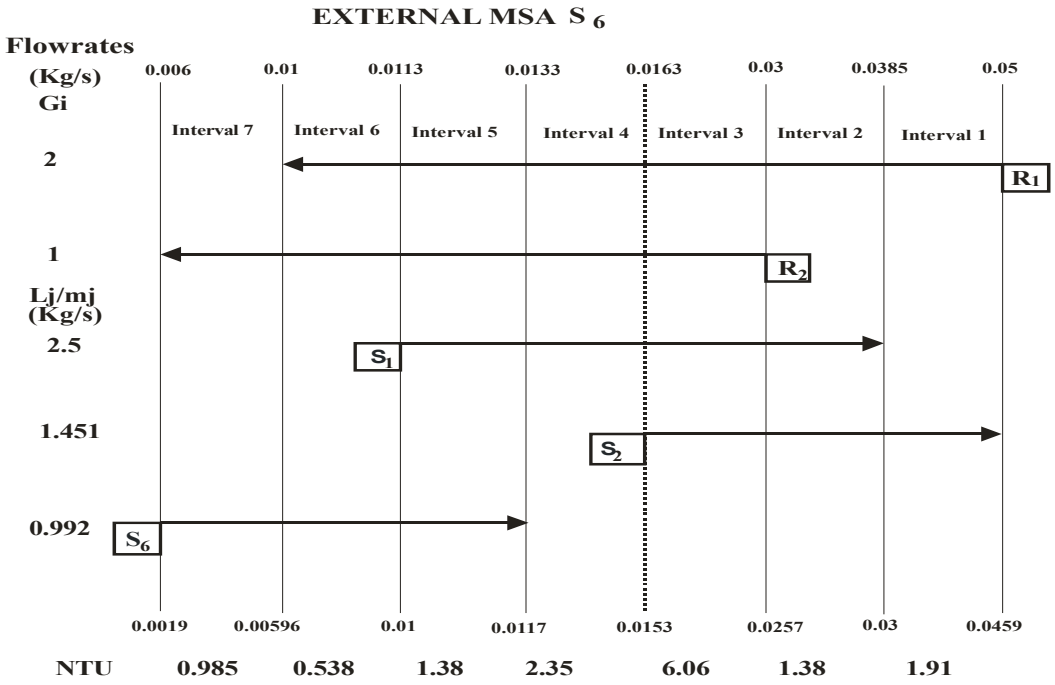

Figure 4d: Grid diagram showing external MSA S_6.

The targets for the total number of units for all MSAs were obtained by summing up the contributions from each rich stream using Equation (6).The total number of units targeting for the MSAs are: for S_3, 27, S_4, 26, S_5, 27 and S_6, 26.

4.1 Targeting for Minimum Number of Mass Exchanger Units(N_{unit})

Targeting for minimum number of mass exchanger unit, capital and total annual cost target are estimated using Equations (7) (8) and (9), respectively in manners similar to that of Hallale (1998). The results are shown in Table (4) as follows:

Table 4: Capital and Total Cost Targets

MSA	Capital cost ($/yr)	Total cost ($/yr)
S_3	110,370	330,050
S_4	114,615	562,250
S_5	110,370	727,836
S_6	114,615	332,525

4.2 Network Design

The whole network design is obtained by combining the designs in the two regions using the feasible criteria and the techniques of Hallale (1998), these were used to obtain the minimum MSA target, the number of unitsand the corresponding capital costs of the networks. The network designs are presented in Figures 6a to d, matches between streams connected by vertical lines represent the exchangers.Figure 6d was similarly obtained where Hallale (1998) applied the tool to S_6. The number of units for each match was calculated using Equation (4 and 5) and the total number of units for each design is the sum of the number of units for each match as shown in Table (5).

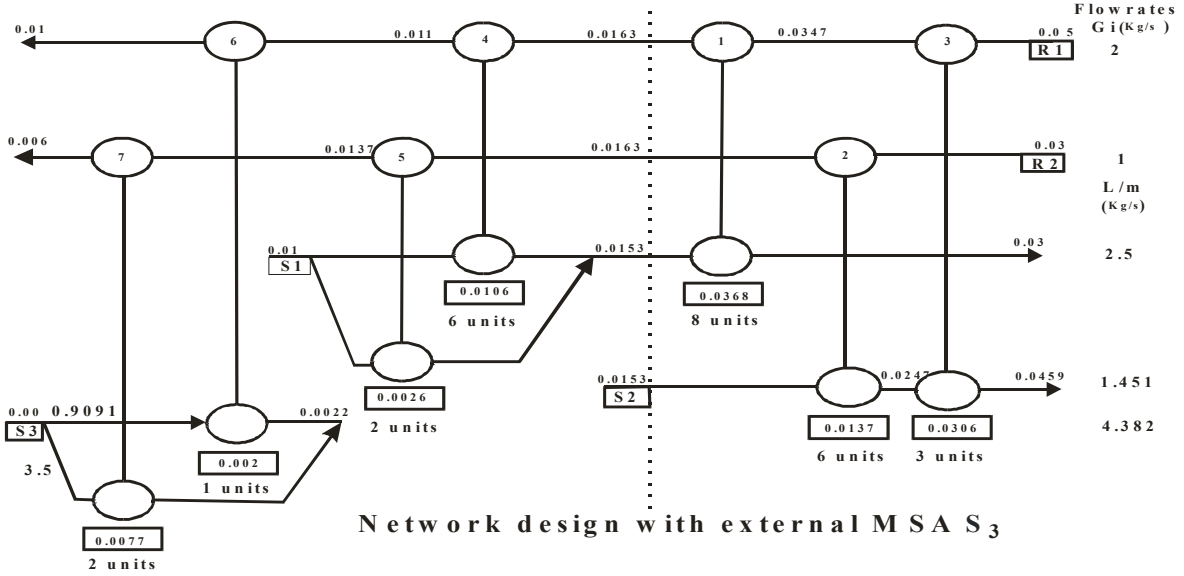

Figure 5a: Network design featuring external MSA S_3

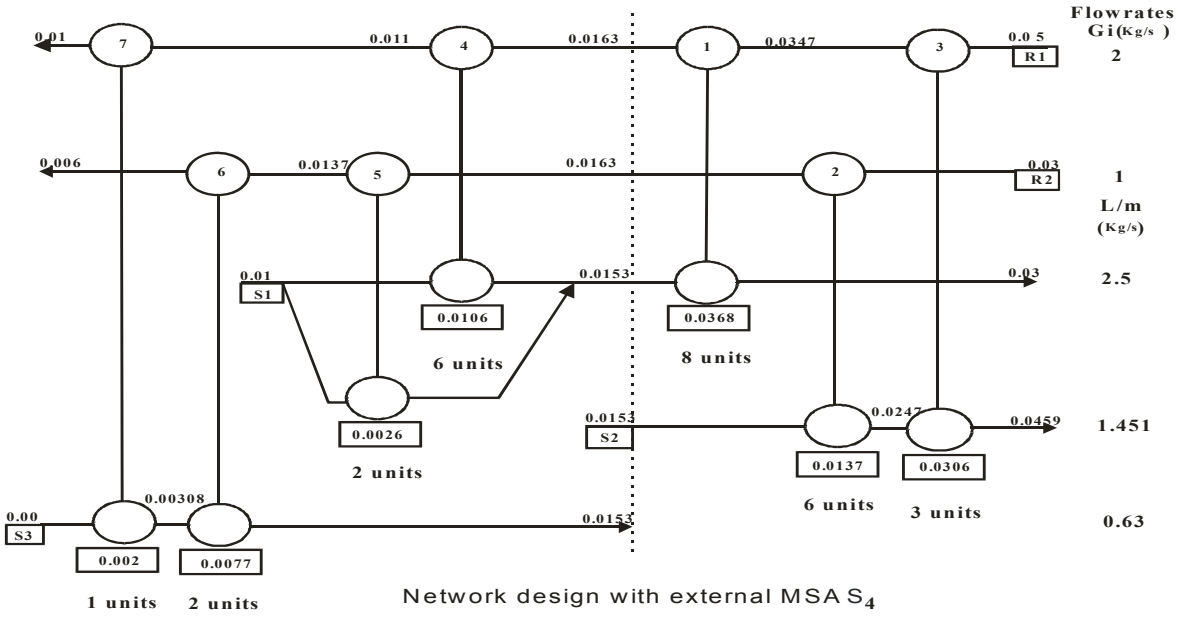

Figure 5b: Network design featuring external MSA S_4

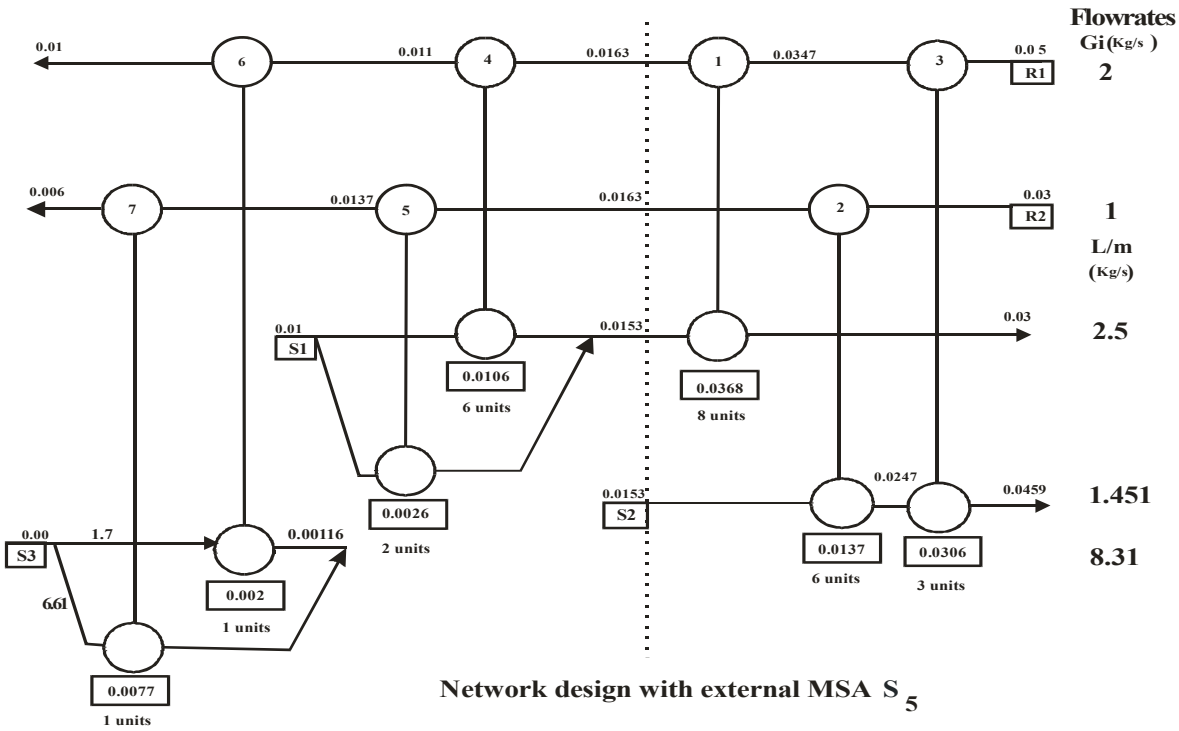

Figure 5c: Network design featuring external MSA S_5

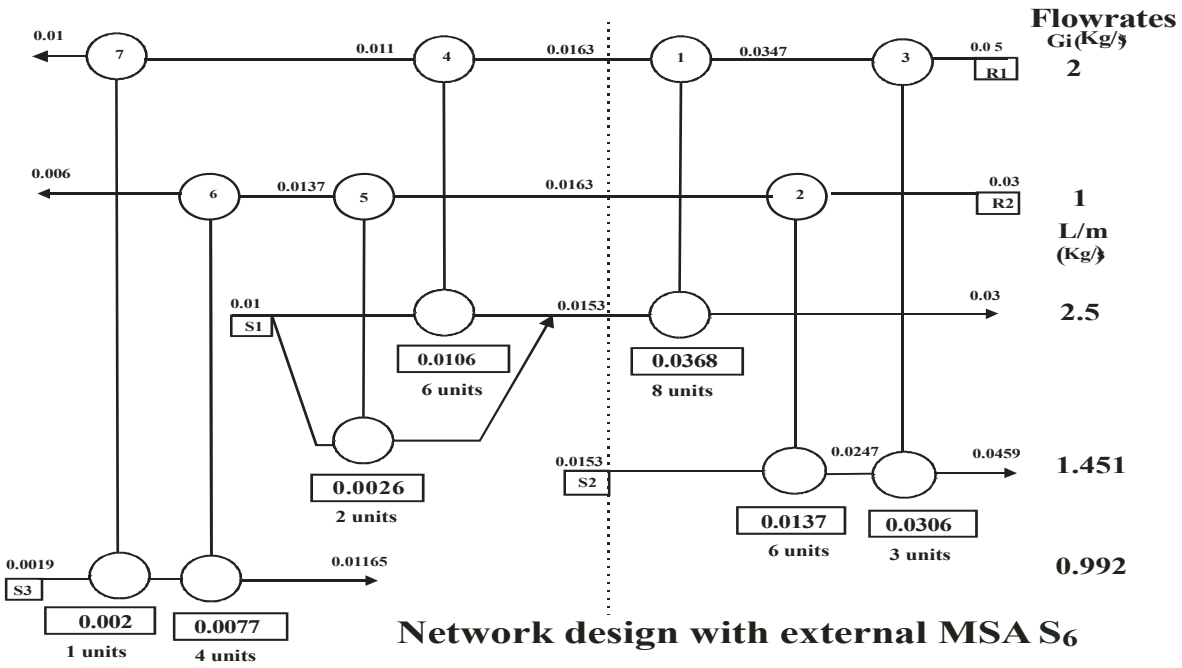

Figure 5d: Network design featuring external MSA S_6

The total number of units used in the actual design are; 30, 28,28 and 27units for S_3, S_4, S_5 and S_6 respectively.Capital cost and total annual cost for the networks design, were estimated using the same approaches for targeting (Table 5);

Table 5: Capital and Total Cost of Networks Design

MSA	Capital cost ($/yr)	Total cost ($/yr)
S_3	118,860	338,540
S_4	118,860	566,495
S_5	114,615	732,081
S_6	127,350	345,310

The table (6) below gives the summary of the MSAs; the cost of each MSAs, removal cost of 1kg of phenol, the flow rates, capital cost and total annual cost targeting and networks design and their discrepancies.

Table 6: Summary of the MSAs details

MSA	MSA Cos ($/kg MSA)	Removal Cost ($/kg phenol)	Flow Rat (kg/s)	Operating Coast ($/yr	Target TAC	Actual TAC	Discrepancy Target/Actual	Discrepancy MSAs
S_3	0.081	0.736	0.0876	219,680	330,525	338,540	+2.6%	0.00%
S_4	0.255	1.5	0.0567	447,635	562,250	566,495	+0.76%	67.3%
S_5	0.06	2.069	0.3324	617,466	727,836	732,081	+6%	116.2%
S_6	0.01	0.730	0.704	217,960	332,525	345,310	+3.8%	2.0%

From the detailsanalysesin the table (6) above, for the cost of each MSA that can remove 1kg of phenol and their minimal operating cost MOC, S_6 with the smallest MSA cost of $0.01kg has the lowest removal cost and MOC of $0.730kg and $217,960yr respectively. Followed by S_3 with MSA cost of $0.081 has $0.736kg and $219,680yr. S_4 with MSA cost of $0.255kg has $1.5kg and $447,635yr, while S_5 with $0.06kg has $2.069kg and 617,466yr, respectively. These results show S_6 with the cheapest cost of MSA to have the lowest removal cost and MOC. S_5 the second cheaper MSA has the highest removal cost and the MOC of about 183.4% and 183.3% respectively while S_4 with the highest cost of MSA has 105.5% and 105.4% of removal cost and MOC respectively, was discovered to be better and preferable to S_5. The Screening and selection of suitable external MSA for this particular problem based on the removal cost and MOC of the MSAs as analysed above, S_6 is preferable followed by S_3 with removal cost and MOC of 0.6% and 0.8% respectively above S_6.

Total annual cost (TAC) was another criterion used for ranking external MSAs which is a function of the operating cost and the capital cost of the mass exchangers used in the design. For this problem specification, TAC of the MSAs S_3, S_4, S_5 and S_6, were calculated to be 338,540, 566,495, 732,081, and 345,310($/yr) respectively. From these results, S_3 has the lowest TAC, followed by S_6 with 2.0%, S_4 with 67.3% and S_5 with 116.2% respectively above S_3.

5.0 CONCLUSION

In this study, pinch technology using the graphical approached together with y-y* tool had been employed in solving MENS problem with multiple external MSAs in order to determine the most suitable and economical external MSA for the removal of phenol from the rich streams below the pinch point. From the results of this study, it can be concluded that selection of external MSA to be used for MENS problem with multiple MSAs should not be based on the MSA with lowest cost. Although S_6 with the lowest cost of MSA was found to be the cheapest based on the removal cost and the minimum operating cost of the MSA while S_5 with lower cost was discovered to be the most expensive among all the external MSA. It can also be inferred from the analysis of the results that the selection of MSA should be better based on the TAC of the network design as capital cost of the network also contribute significantly to the TAC. This can be deduced from the TAC of S_3 which was more expensive among the MSAs but was discovered to be thelower TAC at the end of the network design.

REFERENCES

Ahmad, S. and Smith, R. (1989). Targets and design for minimum number of shells in heat exchanger networks, *Tran IChemE,* **67**, 481-494.

Agrawal, R., andSikdar, S. K. (2012). Energy, environment and sustainability challenges and opportunities for chemical engineers. *Current Opinion in Chemical Engineering,* 1, 201-203.

Azeez, O.S. (2011). Supply and target based superstructure synthesis of heat and mass exchange networks. Ph.D. Thesis, ChemicalEngineering Department, University of Cape Town, South Africa.

El-Halwagi, M. M. (1997). Pollution Prevention through Process Integration: Systematic Design Tools. San Diego CA, Academic Press.

El-Halwagi, M. M. andManousiouthakis, V. (1989). Synthesis of mass exchange Networks. *AICHE Journal* **35**(8): 1233-1244.

Foo, D. C. Y., Manan, Z. A., and Tan, Y. L. (2005). Synthesis of maximum water recovery network for batch process systems. *Journal of Cleaner Production,* 13, 1381-1394.

Fraser, D. M., Howe, M., Hugo, A. and Shenoy, U.V. (2005). Determination of mass separating agents flows using the mass exchange grand composite curve. *Chem. Eng. Res. Des.* **83**(A12): 1381-1390.

Gundersen, T andNaess, L. (1988). The synthesis of cost optimal heat exchanger networks: an industrial review of the state of the art, *Comp. Chem. Eng.*, **12**(6), 503-530.

Hallale, N. (1998), Capital cost targets for the optimum synthesis of mass exchange networks. Ph.D. thesis. Department of Chemical Engineering, University of Cape Town.

Hallale, N. and Fraser, D. M. (2000a). Capital and total cost targets for mass exchange networks, Part 1: Simple capital cost models. *Comp. and Chem. Eng.* **23**:1661-1679.

Hallale, N. and Fraser, D. M. (2000b). Capital and total cost targets for mass exchange networks, Part 2: Detailed capital cost models." *Comp. and Chem. Eng.* **23**:1681-1699.

Hallale, N. and Fraser, D. M. (1998). Capital cost targets for mass exchange networks, a special case: Water minimization, *Chem. Eng. Sci*. **53**(2) 293-313.

Isafiade, A. J. (2008). Interval based MINLP superstructure synthesis of heat and mass exchange networks, Ph.D Thesis, Chemical Engineering Department, and University of Cape Town, South Africa.

Kaggerud, K. H.; Bolland, O. and Gundersen, T. (2006). "Chemical and process integration: Synergies in co-production of power and chemicals from natural gas with CO2 capture", *Applied Thermal Engineering*, 26, 1345–1352.

Keller, G. E. and Bryan, P. F. (2000). Moving in new directions. *Chemical Engineering Progress.* 96,41-50.

Linnhoff, B. and Ahmad, S. (1989). Supertargeting: Optimum synthesis of energy management systems, *ASME J. Energy Resources Tech.*, **111**(3) 121-1130.

Linnhoff, B. andVredeveld, D.R. (1984). Pinch Technology has come of age, *Chem. Eng. Prog.*, **80**(7): 33-40.

Linnhoff, B., Townsend, D.W., Boland, D., Hewitt, G.F., and Thomas, B.E.A., Guy, A.R. and Marshland, R.H.(1982), *User Guide on Process Integration for the Efficient use of Energy*. IChemE, Rugby, U.K.

Papalexandri, K.P. andPistikopoulos, E.N. (1994). A multiperiod MINLP for the synthesis of flexible heat and mass exchange networks, *Comp. Chem. Eng.,* **18**(11/12), 1125-1139.

Ponce-Ortega, J. M., Hortua, A. C., El-Halwagi, M., andJimenez-Gutierrez, A. (2009). A Property-Based Optimization of Direct Recycle Networks and Wastewater Treatment Processes. *AIChE Journal,* 55, 2329-2344.

Smith, R. (2016). Chemical process design and integration. Chichester, West Sussex, United Kingdom: John Wiley and Sons, Inc.

Tjan, W., Tan, R. R., and Foo, D. C. Y. (2010). A graphical representation of carbon footprint reduction for chemical processes. *Journal of Cleaner Production.* 18, 848-856.

Wang, Y. P. and Smith, R. (1994). Wastewater Minimization, *Chem. Eng. Sci.,* 49,981-1006

Yee, T.F. and Grossmann, I.E. (1990). Simultaneous optimization models for heat integration-II. Heat exchanger network synthesis, *Comp. and Chem. Eng.*, **14**(10): 1165 - 1184.

Proceedings of the 49th NSChE Annual Conference
KADA 2019: pp 673-676

P3C-01: EFFECT OF SODA ASH PRE-TREATMENT ON RHEOLOGICAL AND THIXOTROPIC PROPERTIES OF DRILLING MUD FORMULATED FROM ORGANOPHYLLIC CLAY DEVELOPED FROM LOCAL NIGERIAN BENTONITIC CLAY

Bala Usman[1], Suleiman Muhammad Shuwa[1] Sabiu Bilal[1]
[1] Department of Chemical Engineering, Ahmadu Bello University, Zaria-Nigeria
*Email: balausman87@gmail.com

ABSTRACT
Nigerian bentonitic clays are lower grade due to high calcium oxide. However, rheological properties would be improved when activated with soda ash. In this work, organophillic clay was developed from locally sourced Nigerian bentonitic clay sourced from Sabon Garin Ngalda and an API grade Wyoming bentonite. An emulsion based drilling mud was formulated using the three clay samples with oil to water ratio of 90:10 and drilling mud formulated from organophillic clay developed from API grade Wyoming bentonite was used as standard for comparison. The drilling mud developed from organophillic clay developed from locally sourced bentonitic clay has shown poor rheological and thixotropic properties but was seen to improve after soda ash pre-treatment. The developed drilling mud using the raw local organophyllic clay has shown plastic viscosity (PV) and apparent viscosity (AV) of 11 cP and 11 cP respectively but was seen to improve to 17 and 18 cP respectively after soda ash pre-treatment and viscosifier treatment. The 10 s and 10 min gel strength for the raw local organophillic formulation was 1 lbf/100 ft2 but improved to 5 lbf/100 ft2 after soda ash pre-treatment and viscosifier treatment these properties compare very well with API grade organophillic clay formulation.

Key Words: rheological, thixotropic, API, organophillic clay and emulsion

1.0 Introduction

Drilling mud is fluid used in drilling operation in which the mud is circulated from the surface, down the drill string, through the bit and back to the surface via the annulus with objective removal of cuttings, cooling and lubricating drill bit, supporting some portion of the drill bit and controlling corrosion. Drilling mud is divided generally into three that is, water- based mud where water is the continuous phase, oil-based mud where oil is the continuous phase and emulsion-based mud where oil and water are mixed to form a single phase in the presence of an emulsifier (Bourgouyne *et al.,* 1991).

Drilling muds in use are made up of fluid components such as water, oil, chemical additives like viscosifiers and fluid loss control additives such as clay, dispersants and weighting agents such as barite. Sodium-based bentonitic clays have shown better viscosity control and fluid loss with good cutting carrying capacity or gel strength. The calcium-based type has shown low swelling capacity and consequently poor rheological and thixotropic properties

North eastern Nigeria is blessed with more than 700 million metric tonnes with the average consumption of 100 000 tones drilling fluid development alone (RMRDC, 2010). Organophillic clay is a material formed from treatment of the bentonic clay with the cationic surfactant. Organophillic clay is characterised by good swelling capacity when mixed with oil or emulsion. It has the advantage of being oil-wet, low fluid loss and lower vulnerability to structural collapse when used as drilling mud constituent.

In this study, organophyllic clay was developed by introduction of quaternary ammonium surfactant to a pre-treated soda ash calcium based-bentonite. The effect was investigated by

formulating an emulsion-based mud, testing the resultant mud and comparing its properties with properties of mud formulated from organophyllic API grade Wyoming bentonite.

2. Materials Equipment and Methods

2.1 Materials Equipment

The materials used are bentonitic clay sourced from Sabon Garin Ngalda in Fika formation, API grade Wyoming bentonite, Hexadecyltrimethyl ammonium bromide (CTAB), Sorbitan mono Oleate, water, diesel, 200 mesh size sieves and homogeniser, FANN35SA viscometer and thermometer.

The modified clay sample was developed by adding an equivalent weight of the cationic surfactant (CTAB) based on Cation Exchange Capacity (CEC) of the clay, and the resultant clay was sun-dried, ground to required particle size, and characterised.

The clay sample was then beneficiated by adding 12 wt% soda ash (Bilal, 2015) and allowed to stand for 24 hours (Ibrahim, 2016)

The CEC of the clay samples was determined using the ammonium acetate saturation method

The mud was formulated by adding the 1 wt% of oil as viscosifier to 90 %vol followed by adding 7 wt% of the total fluid phase as modified clay to the oil followed 10 %vol of water (Schmidt *et al* 1987). The volume of oil and water was taken to be 350 ml.

3.0 Result and Discussion

3.1 Result

Variation of dial readings with dial speed for 90:10 formulations is shown in Figure 1

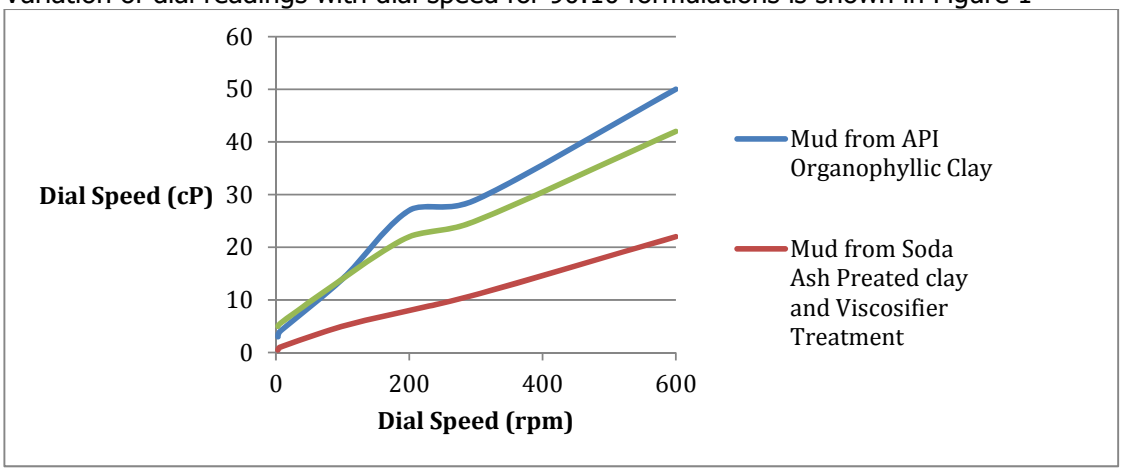

Figure 1: Variation of dial readings with dial speed for 90:10 formulations

Comparison of rheological and thixotropic properties for 90:10 formulations is shown in Figure 2.

3.2 Discussion

Figure 1 shows the variation of dial reading with dial speed for drilling mud formulated from raw local organophyllic clay without prior treatment with soda ash or viscosifier, modified API grade Wyoming bentonite and that with soda ash activated sample. The 12 wt% soda ash activated sample treated with 1 wt% viscosifier was seen to compare very well with the modified API grade Wyoming bentonite as shown by the light green line in Figure 1

In all the formulations it was observed that the dial readings increased with increase in dial speed. This implies that at higher dial readings there would be higher shear stress with a corresponding increase in shear rate, this property characterises shear thinning drilling mud which is an an important property for drilling mud. This increase in dial reading with dial speed agrees with the findings of Bilal (2015) and Ibrahim (2016)

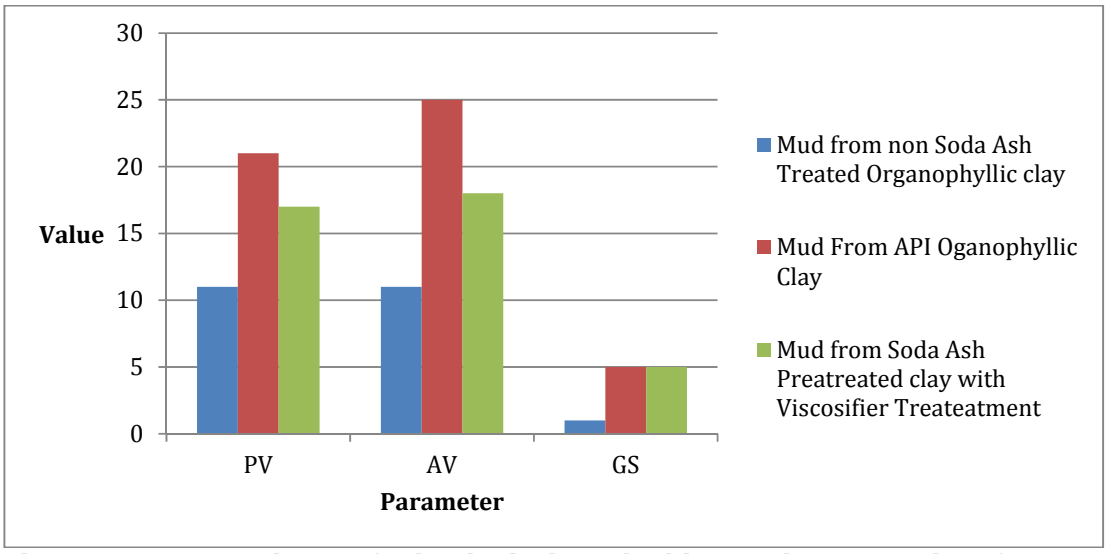

Figure 2: Comparison of rheological and thixotropic properties for 90:10 formulations

Comparison of properties of modified API grade, raw local organophyllic clay and soda ash pre-treated sample formulation is shown in Figure 2. It can be seen that the soda ash pre-treated sample compares very well with the organophillic API grade in terms plastic viscosity. This agrees with the findings of Shuwa (2010) that soda ash activation of calcium based bentonite improves its rheological properties. There was also an increase in AV of the raw organophyllic clay from 11cP to about 18 cP attributed to increase in dial readings at 600 rpm. Both the soda ash pre treated and the API grade organophyllic clay formulations have shown almost equal gel strength of 5 $lb_f/100\ ft^2$ hence, the cutting suspension potential for the two formulations is the same

4.0 Conclusions

From the research carried out, it can be concluded that soda ash pre-treatment of raw local sample before conversion to organophyllic clay improve the rheology and thixotropic properties of the formulated mud making it compare well with organophillic (modified) API grade Wyoming bentonite.

Reference

1. Bilal, S., (2015): Investigation and Enhancement of Quality Of Nigerian Bentonitic Clay Samples for Oil and Gas Drilling Operation. Unpublished PhD Thesis, Department of Chemical Engineering Ahmadu Bello University, Zaria, Nigeria.
2. Bourgouyne, A. T., Millhiem, K.K., Chenevert, M.E., Young, F.S. (1991). Applied Drilling Engineering, 2nd edition, Society of Petroleum Engineers, Richardson, Texas
3. Ibrahim, A.O., (2016): Enhancement of Gambe Bentonic Clay using Fermentable and Unfermentable Polymers for Drilling Fluid Application Unpublished MSc Thesis, Department of Chemical Engineering Ahmadu Bello University, Zaria, Nigeria

4. Shuwa (2010): Beneficiation and Evaluation of the Potentials of Dikwa Bentonitic Clays for Oil Well Drilling Fluids Formulation. Unpublished M.Sc. Project, Department of Chemical Engineering Ahmadu Bello University, Zaria, Nigeria
5. RMRDC. (2010). *Non-Metallic Mineral Endowments in Nigeria: Bentonite.* Abuja: Raw Materials Research and Development Council
6. Schmidt D. O.,Roos A.F and Cline J.T, (1987) Interaction of Water With Organophilic Clay in Base Oils to Build Viscosity. A conference paper presented at the 62nd Annual Technical Conference and Exhibition of the Society of Petroleum Engineers held in Dallas, TX September 27-30. 1987.

Proceedings of the 49th NSChE Annual Conference
KADA 2019: pp 677-687

P3C-02: MODELING AND SIMULATING THE CONSEQUENCES DUE TO LIQUEFIED PETROLEUM GAS LEAKAGE FROM FUEL PIPE SUPPLYING A FIRED HEATER

H., Jamilu[1], U. Abubakar Zaria[1,*], and S. M. Shuwa[1]
[1]Department of Chemical Engineering, Ahmadu Bello University, Zaria
*E-mail: uabubakar@abu.edu.ng/augayya@yahoo.com; Tel.: +2348033690787

ABSTRACT
Crude oil fired heaters are associated with considerable fire and explosion hazards. The heaters present higher risks at later operational life due to ageing, wear and obsolescence. It is therefore important to re-evaluate such heaters to determine the adequacy or otherwise of the existing safeguards. This paper presents results of studies on hazard levels in aged fired heaters through quantitative consequence modeling method. A number of credible failure scenarios were considered. In particular, characteristics of potential jet fires due to Liquefied Petroleum Gas (LPG) leaks from hole sizes: 15, 30, 50 and 100 mm were investigated. For the 100 mm hole size, it was found that thermal radiation level of up to 37.5 KW/m^2 could be experienced within 25 m radius of the heater, which is enough to affect nearby operators severely and could also adversely affect critical pieces of equipment around. Fireball potential with peak thermal density of about 12.5 KW/m^2 was also observed within 2 m radius. For the 100 mm hole size, lower flammability limit of the fuel could be attained within 16 m downwind which poses flash fire risks. Overpressures of 1.02, 1.14 and 1.21 bar could be experienced at 30, 6 and 4 m respectively away from the fired heater which could result in partial demolition of structures that are within the radius. Overall, the results indicate that the risk profile is very sensitive to leak sizes, operating and atmospheric conditions as well as the fuel quantity being held, among others. For the chosen case study, higher integrity protection layers, in form of safety instrumented systems, relief, blow down and alarm systems, are recommended.

Keywords: *Downwind distance; Consequence modeling; Radiation intensity; Flame length; Overpressure; Liquefied Petroleum Gas*.

INTRODUCTION
Fire is the most frequently reported process-related incident in Nigerian petroleum industry (DPR annual report, 2017). Fire may result in no damage/loss, medium to catastrophic damage/loss, depending upon the fire characteristics (type of fire, mode of occurrence and potential of escalation). Leakage or spillage of flammable material can lead to a fire that is triggered by any number of potential ignition sources (sparks, open flames, etc.). Depending upon the types of leakage scenarios, fires are mainly categorized into four types, jet fire, pool fires, flash fires and fire balls, therefore there is need to study the risk associated with fire (Usama *et al*. 2016). Figure 1 is a schematic flowchart showing a typical risk assessment process.

Consequence analysis predicts magnitude, direction vulnerability zones of negative effects of incidents. Once these zones are identified, the risk analysis suggests measures of mitigation or prevention that can be proposed to eliminate damage to plant and potential injury to personnel. Estimation of vulnerability zone of such an incident plays an important role in preparing a realistic emergency plan (Ravichandran *et al*., 2010). Table 1 gives the effect of various radiation intensities. Consequence modelling refers to the calculation or estimation of numerical values (or graphical representations of these) that describe the credible physical

outcomes of loss of containment scenarios involving flammable, explosive and toxic materials with respect to their potential impact on people, assets, or safety functions (Risk Assessment Data Directory 2010).

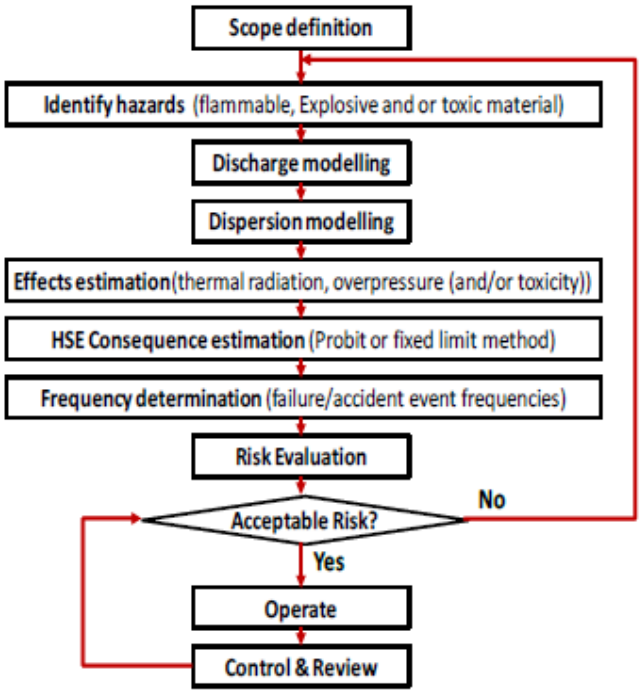

Figure 1. Typical risk assessment procedure (Abubakar *et al.,* 2017)

Estimation of vulnerability zone due to credible scenarios via consequence analysis would play important role in preparing realistic preventive and mitigative measures- including emergency response and evacuation plan. Physical models can be used to estimate hazards zones in case of accidents (Osman *et al.*, 2015). For these reasons, it is important to determine consequences due to accidental leak or rupture of a component at various locations around the heater. The following section highlights the methodology involved in this study.

Case Study of Kaduna Refinery

The most Hazardous unit of the crude distillation column (CDU1) is the crude heating section (Fired Heater 10H01) where the crude is heated to distillation temperature before it is finally sent to fractionator. This is because the fired heater contains a naked flame and handles crude in the pipe which is highly flammable. In this work our emphasis will be on hazard resulting from fire that is associated with crude discharge fired heater (10H01) of Kaduna Refining and Petrochemicals Company (KRPC) Crude distillation unit (CDU).

The fired heater is an exchanger that transfers heat from the combustion of fuel to fluids contained in tubular coils within an internally insulated enclosure. The fired heaters are an essential component of CDU (I), KRPC. The functions served by fired heaters in chemical plants are many ranging from simple heating or providing sensible heat and raising the temperature of the charge to heating and partial evaporation of the charge, where equilibrium is established between the unvapourised liquid and the vapour. The charge leaves the furnace in the form of a partially evaporated liquid in equilibrium. Fired heaters may also be used to provide the heat required for cracking or reforming reactions. Fired heaters process fluids flowing inside tubes mounted inside the furnace, the fluid is heated by gases produced by the combustion of a liquid or gaseous fuel. The major advantage of fired heaters is the achievement of continuous operation (Garg, 1997). These heaters are widely used for heating purposes in petroleum refining, petrochemical plants and other chemical process industries.
Fired heaters present high safety risks as the process streams contain highly flammable hydrocarbons with potential catastrophic fire incidents. Due to ageing (over 30 years after commissioning of the refinery), wear and obsolescence, the fire risk profile of the crude charge fired heater (10H01) of KRPC CDU needs to be reevaluated. For instance, in the year 2017 there was explosion at fired heater 12H01 of CRU KRPC due to tube rupture which led to the breakdown of the unit for about two years. Therefore, it is important to determine the vulnerability zone of other heaters in the company.

METHODOLOGY

The calculation of risk is dependent on the Probability of failure (P_f) combined with the expected Consequence $E(C)$ of failure and can be estimated from:

$$\boldsymbol{R = P_f \times E(C)} \qquad \text{Eqn. 1}$$

The overall risk may be fully quantitative (reported as number), qualitative (e.g. graded as low, medium or high) or semi quantitative (e.g.in form of a risk matrix). The risk is usually in terms of health and safety, environment and/or assets. Determination of the parameters such as flame dimensions, release rates, heat flux and distances to radiation levels is an important aspect of the risk assessment process (Abubakar *et al.,* 2017).

PHAST (Process Hazard Analysis Software Tool) is a quantitative risk assessment tool that is widely used in the chemical process industry and has shown good agreement with experimental results in validation exercises (Spouge and Pitblado, 1998). The tool is able to simulate various release scenarios such as leaks, line rupture, long pipeline releases and tank roof collapse in pressurized and unpressurised vessels or pipes (Nishant *et al.*, 2014). This software is used to account for a range of practical factors such as pipeline location, geographical coordinates, prevailing atmospheric conditions and leak source characteristics. Key data used for the study are:

Table 1 gives the effect of various radiation intensities:

Table 1. Effect of Various Radiation Intensities

Intensity of heat radiation kw/m^2	Various effect
1.6	Insufficient to cause discomfort for long exposure
2.2	Threshold pain. No reddening or blister
4.2	First degree burn
8.3	Second degree burn
10.8	Third degree burn
15.0	Piloted ignition of wood
25.0	Spontaneous ignition of wood
4.0	Glass crack
12.0	Plastic melt
19.0	Cable insulation degrade
37.5	Damage to process equipment
100.0	Steel structure fail

Source: (Alche/CCPS, 2000)

Table 2 gives various overpressure effects of explosion

Table 2: Overpressure Effects of Explosion

Pressure (psig)	Damage
0.02	Annoying noise (137 dB if of low frequency 10-15 Hz).
0.03	Occasional breaking of large glass windows already under strain.
0.04	Loud noise (143 dB), sonic boom glass failure.
0.1	Breakage of small windows under strain.
0.15	Typical pressure for glass breakage.
0.3	"Safe distance" (probability 0.95 no serious damage beyond this value).
0.4	Limited minor structural damage.
0.5-1.0	Large and small windows usually shattered; occasional damage to window.
0.7	Minor damage to house structures.
1.0	Partial demolition of houses, made uninhabitable.
1-2	Corrugated asbestos shattered; corrugated steel or aluminium panels, fastenings.
1.3	Steel frame of clad building slightly distorted.
2	Partial collapse of walls and roofs of houses.
2-3	Concrete walls, not reinforced, shattered.
2.3	Lower limit of serious structural damage.
2.5	50% destruction of brickwork of houses.
3	Heavy machines in industrial building suffered little damage; steel frame.
3-4	Frameless, self –framing steel panel building demolished; rupture of oil storage.
4	Cladding of light industrial buildings ruptured.
5	Wooden utility poles snapped; tall hydraulic press in building slightly damaged.
5-7	Nearly complete destruction of houses.
7	Loaded train wagons overturned.

7-8	Brick panels, 8-12 in. thick, not reinforced, fail by shearing or flexure.
10	Probable total destruction of buildings, heavy machines tools moved and badly damaged, very heavy machine tools (12,000lb) survived

(Source: M/s. SV Enviro labs and consultants)

Table 3: Required input parameters and specification

Parameter	Specification
Location under consideration:	KRPC
Location coordinate:	10.41159N,7.49065E
Time:	10:44 am
Material:	LPG
Wind speed:	5 m/s maximum
Wind direction:	SSW/208.150 upper angular limit
Solar radiation flux:	1 KW/m^2
Ambient temperature:	28 ^{0}C maximum
Pasqual stability:	Assumed to be neutral/D
Humidity:	78 %
Cloud cover:	67 % cloud level
Terrain/Ground roughness:	Assumed 30 mm-open flat terrain, grasses, few isolated objects
Pipe diameter:	0.16 m
Height/elevation:	2.65 m
Temperature at burner:	45 ^{0}C
Pressure at burner:	1.5 bar
Phase/state of release:	Vapor
Inventory/consumption rate:	0.35 kg steam/kg oil
LPG Composition:	85 % Butane, 15 % Propane
Radius of interest:	200 m
Outdoor release direction:	Assumed to be horizontal
Leak sizes identified (from field data):	15 mm, 30 mm, 50 mm, and 100 mm
Scenario:	Pipe leak
Intensity levels:	4, 12.5 and 37.5 KW/m^2
Lethality levels:	0.01, 0.1 and 0.99 fractions

These input data were used in the identified scenario i.e. LPG leak as shown in Figure 2 and was simulated. After the simulation, the result of the different fire models was selected and analyzed considering wind speed and atmospheric stability.

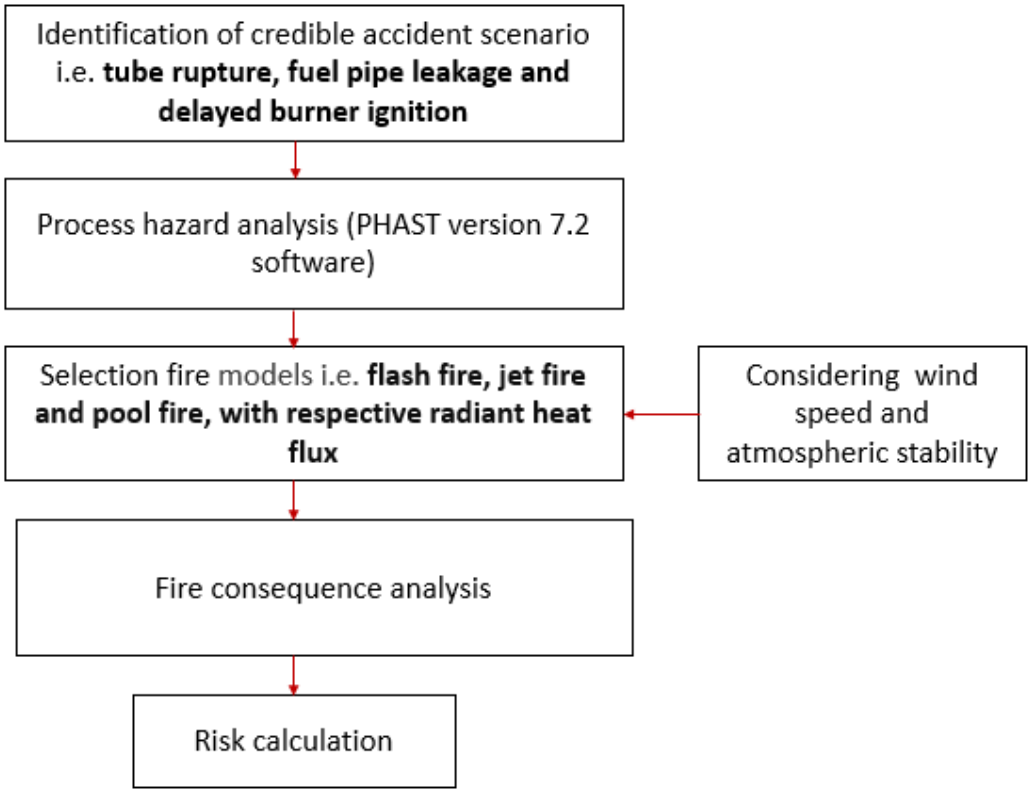

Figure 2. Research Methodology (adopted from Usama *et al.*, 2016)

RESULTS AND DISCUSSIONS

Table 4 gives the jet fire downwind distance to experience 4, 12.5 and 37.5 KW/m^2 radiation intensities and scenarios flame length.

Table 4: Jet fire downwind distance to experience defined radiation levels, for Weather

	Category 5/D			
Scenario	Down Distance [m]to Radiation Levels and Flame Length			
	Flame length	4 KW/m^2	12.5kw/m^2	37.5 KW/m^2
15mm Leak	5.219	n/a	n/a	n/a
30mm Leak	9.956	10.95	n/a	n/a
50mm Leak	15.7	20.65	15.53	n/a
100mm leak	27.26	40.77	32.55	25.41

Figure 4 gives the radiation levels and respective downwind distance for jet fire.

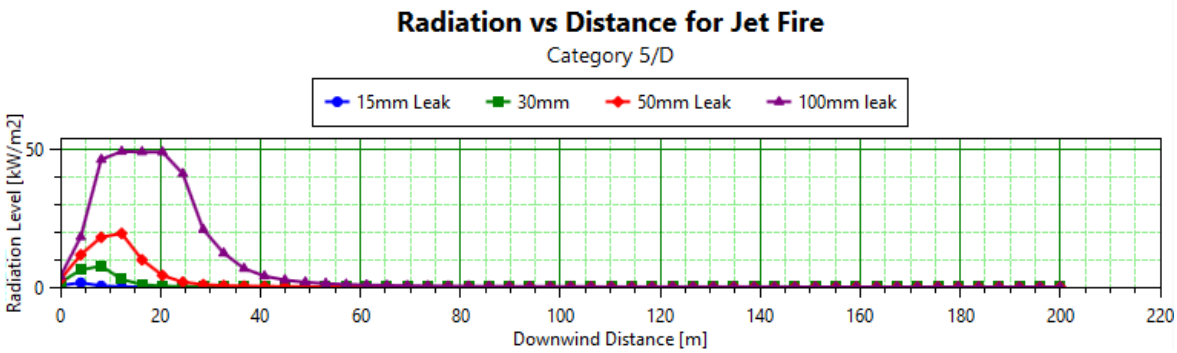

Figure 3: Radiation vs Distance for Jet fire

For Jet Fire, using PHAST the radiation level was plotted for the leakage sizes of 15, 30, 50, and 100 mm in 5/D climate weather as shown in Figure 3, the result of the flame length, radiation levels and calculated distance in downwind direction are presented in Table 4. As depicted in Table 4, the 100 mm leak size has the highest flame length followed by 50 mm, 30 mm and least 15 mm leak size. 4, 12.5 and 37.5 KW/m^2 intensity could not be experienced at 15 mm leak size, 12.5 and 37.5 KW/m^2 intensity could not be experienced at 30mm leak size, 37.5 KW/m^2 could not be experienced at 30 mm leak size and all the defined radiation levels could be experience at 100 mm leak size.

The following equipment; tank, LAB flare knockout drum, VDU heater, NHU heater, CRU heater, column, column, desalter, and heat exchangers were identified to be surrounding the heater at approximate and respective distances of 80, 55, 30, 150, 181, 16, 43, 92, 166 and 200 m away from the heater (10H01) as shown in Plate 3. These fall within the defined distance (200 m) of interest. Hence 10C01 fractionator that is in the wind direction could experience 37.5 KW/m^2 radiation at 100 mm leak size which could result in catastrophic damage of the column while 10C07 may experience 4 KW/m^2 radiation intensity which could result in first degree burn on the personnel around as highlighted in Table 1. It can be observed that radiation consequences are concentrated more toward the downwind direction due to flame tilt caused by the wind as equally reported by (Ravichandran *et al.*, 2010). Table 5 gives the fireball downwind distance to experience 4, 12.5 and 37.5 kw/m^2 radiation intensities and fireball diameter.

Table 5: Fireball downwind distance to experience defined radiation levels, for Weather

	Category 5/D			
Scenario	**Down Distance [m]to Radiation Levels and Fireball Diameter**			
	4 kw/m^2	**12.5 kw/m^2**	**37.5kw/m^2**	**Fireball Diameter**
15mm Leak	7.128	1.756	n/a	4.607
30mm Leak	7.128	1.756	n/a	4.607
50mm Leak	7.128	1.756	n/a	4.607
100mm leak	7.128	1.756	n/a	4.607

Figure 4 gives radiation levels and respective downwind distance for fireball

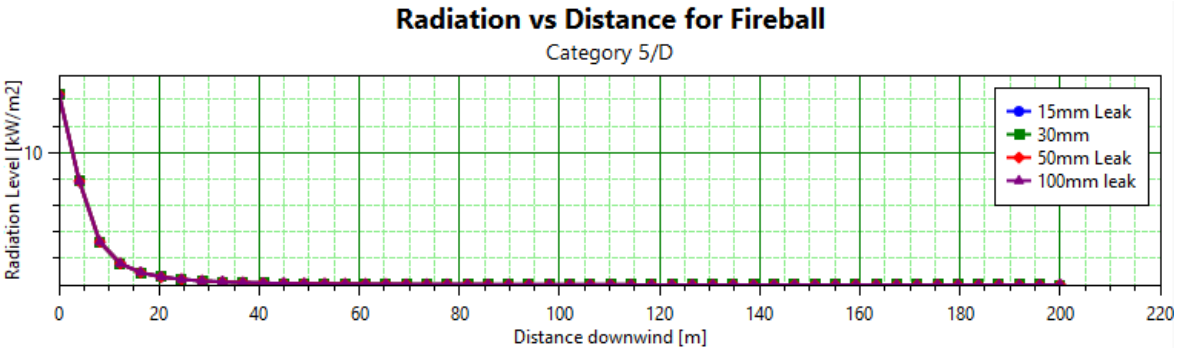

Figure 4. Radiation vs Distance for Fireball

For the fireball, 15, 30, 50 and 100 mm leak size show the same fire ball diameter of 4.607 m also the same downwind distance of 7.128 m to 4kw/m^2 intensity level, and 1.756 m to 12.5 kw/m^2 intensity. 37.5 kw/m^2 intensity could not be experienced for the different leak sizes as shown in Figure 4 and Table 5. The 12 KW/m^2 radiation intensity which could be experienced up to a distance of 1.756m from the epicenter may result in damaging of plastic materials and second degree burn to operators that are within the radius.
Table 6 gives scenarios downwind distance to lower and upper flammability limit of flash fire

Table 6: Flash fire downwind distance to defined concentrations, for Weather Category 5/D

Scenario	Down Distance [m]to LFL, LFL Fraction and UFL		
	LFL[m]	**LFL[Fractions]**	**UFL**
15mm Leak	3.211	5.644	0.6181
30mm Leak	5.17	10.45	1.224
50mm Leak	9.92	16.15	2.026
100mm leak	16.25	22.46	4.01

Figure 5 shows the flash fire envelope downwind distance for different scenarios at concentration of 8000 ppm

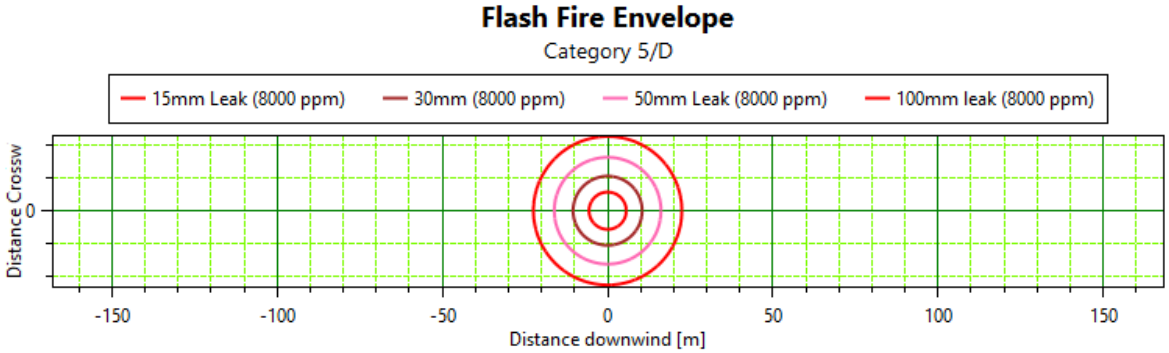

Figure 5. Flash Fire Envelope

Table 6 and Figure 5 shows that 15, 30, 50 and 100 mm leak sizes have the maximum downwind distance to lower flammability limit (LFL) of 5. 644, 10.45, 16.15 and 22.46 m

respectively with 100 mm leak scenario having the highest distance, the increase of LFL is due to increase in leak size. The LFL gives the idea of where the ignition will started

Plate I gives the flash fire envelope at concentration of 8000 and 16000 ppm for different scenarios

Plate I. 10H01 LPG Fuel Pipe Flash Fire Envelope

Plate I show that 15, 30, 50 and 100 mm leak sizes have the maximum downwind distance to lower flammability limit (LFL) of 5. 644, 10.45, 16.15 and 22.46 m respectively at 8000 ppm concentration with 100 mm leak scenario (contour) having the highest distance and been clearly captured in table 6 and figure 5.

Table 7 gives downwind distance to defined explosion overpressure for the different scenarios

Table 7: Late explosion overpressure downwind distance to experience defined overpressures, for Weather Category 5/D

Scenario	Max. Distance [m]to Overpressure		
	1.02068 bar	**1.1379 bar**	**1.2068 bar**
15mm Leak	0	0	0
30mm Leak	25.15	12.94	12.21
50mm Leak	29.01	13.7	12.77
100mm leak	0.0	0.0	0.0

Figure 6 gives downwind distance to defined explosion overpressure

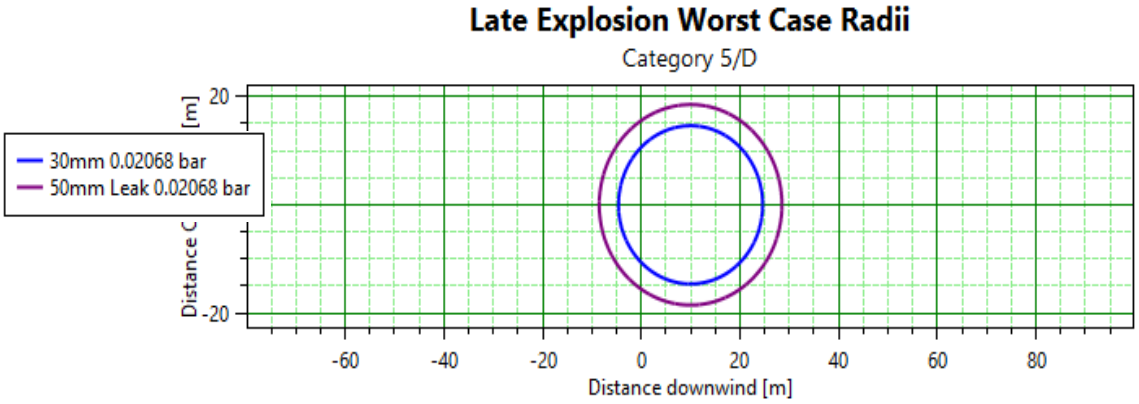

Figure 6. Late Explosion Worst Case Radii

Table 7 and Figure 6 shows that at overpressure of 1.2068 bar 30, and 50 mm leak sizes scenarios has the overpressure downwind distance of 12.21 and 12.77 m respectively with 15 and 100 mm leak size scenario having no overpressure hazard at this pressure. For the 15 and 100 mm leak size, all the overpressure scenarios ((1.02068-1.2068 bars)) may be experienced right at the epicenter. The 1.2068 bar overpressure could result in minor damage to structures, partial demolition of houses and shattering of corrugated asbestos as highlighted in Table 2.

Table 8 gives downwind distance to defined explosion overpressure for the different scenarios

Table 8: Maximum overpressure distance to experience defined overpressures, for Weather Category 5/D

Scenario	Max. Distance [m]to Overpressure		
	1.02068 bar	**1.1379 bar**	**1.2068 bar**
15mm Leak	0	0	0
30mm Leak	30.3	5.9	4.4
50mm Leak	38.0	7.4	5.5
100mm leak	0.0	0.0	0.0

For leak size 30 mm, overpressures of 1.02, 1.14 and 1.21 bar could be experienced at about 30, 6 and 4 m respectively away from the fired heater which could result in partial demolition of structures that are within the radius as highlighted in Table 2. For the15 and 100mm leak size, all the overpressure scenarios (1.02 - 1.21 bars) may be experienced right at the epicenter. It can be concluded that, physical models can be used to estimate hazards zones in case of accidents as equally reported by (Osman *et al.*, 2015).

CONCLUSION

After analysis of the result it was observed that the flame length and downwind distance to radiation intensity of a jet fire increase with increase in leak size and for 100 mm leak size, any equipment or personnel that is within the downwind distance of 25 m could experience a catastrophic damaged. For fire ball, the leak size does not affect the fire ball diameter and downwind distance to radiation intensity, and any personnel or plastic material within a

downwind distance of about 2 m could be damaged. Radiation consequences are concentrated more toward the downwind direction due to flame tilt caused by the wind. Overpressures of 1.02, 1.14 and 1.21 bar could be experienced at 30, 6 and 4 m respectively away from the fired heater which could result in partial demolition of structures that are within the radius. Leak size plays a significant role in fire accident. Therefore, leak should be prevented by minimizing number of joints, elbows, bend, using corrosion resistant pipe and proper maintenance practice. Ignition sources, such as like sparks, heat surfaces and open flames should be eliminated. Mitigative measures such as bund/dike and emergency response arrangement such as fire fighters, high integrality protection layers, such as safety instrumented systems, relief, blow down and alarm systems, should be put in place to reduce the negative outcome in case the accident happened.

REFERRENCES

1. Abubakar, U. Hamisu A. A., S. Bilal S and B. Dan-asabe (2017). Effects of Operating Conditions on Gas Release Thermal Consequences: a case study of the Trans-Saharan Gas Pipeline. NJTR 12(2): 27-33.
2. AIChE/CCPS, Guideline for chemical process quantitative risk analysis, second edition, New York, 2000.
3. Aushtosh Garg (1997). Optimize Fired Heater Operations to Save Money Furnace Improvements, Sugar Land, Texas
4. Assessment, R., and Directory, D. (2010). Flickr Architecture | High Scalability, (434). Retrieved from http://highscalability.com/flickr-architecture
5. DPR, (2017). Oil and Gas Annual report
6. M/s. SV Enviro labs and consultants 'Quantitative Risk Analysis' SY. no: 274P, 275P, 236/2CP, 239/2P and 249/2P Vakalapudi (v), Kakinada, east Godavari district, Andhra Pradesh
7. Nishant Pandya, Eric Marsdena, Pascal Floquet and Nadine Gabas (2014), Toxic Release Dispersion Modelling with PHAST: Parametric Sensitivity Analysis
8. Osman, K., Geniaut, B., Herchin, N., and Blanchetiere, V. (2015). A review of damages observed after catastrophic events experienced in the mid-stream gas industry compared to consequences modelling tools, (160), 1–12.
9. Pula, Ravichandra, Faisal I. Khan, Brian Veitch, and Paul R. Amyotte. "Revised fire consequence models for offshore quantitative risk assessment." Journal of loss prevention in the process industries 18.4-6 (2005): 443-454
10. Spouge, J. R., and Pitblado, R. M. (1998). 'Consequence modelling of the hydrocarbon fire' (147), 1–15.
11. Usama Muhammad Niazi, Mohammad Shakir Nasif, Masdi bin Muhammad and Muhammad Imran (20016). Modelling of pool fire and injury prediction considering different wind speeds and directions in offshore platform, ARPN Journal of Engineering and Applied Sciences, vol. 11, no. 22, ISSN 1819-6608

Proceedings of the 49th NSChE Annual Conference
KADA 2019: pp 688-704

P3C-03: THERMODYNAMIC ANALYSIS OF PRODUCTS DISTRIBUTION FOR PROPANE AROMATIZATION PROCESS

E.E. Peter, A.Y. Atta, B.Mukhtar, B.O. Aderemi, B.J. El-Yakub
Department of Chemical Engineering, Ahmadu Bello University, Zaria, Nigeria
e-mail: emapeteum@gmail.com

ABSTRACT
The aromatization process of light alkanes is one of the major ways of adding value to the lower saturated hydrocarbons obtained from the refining process and Liquid Petroleum Gas, LPG. The thermodynamic analysis based on Gibbs free energy minimization subject to certain constraints was used to reduce the number of proposed species from thirty-six to thirteen at reaction conditions of 550 °C and 1 bar. The process of minimizing the Gibbs free energy equation was done using Aspen Plus software in a carbon-free atmosphere. Influence of temperature, pressure and flow rate was studied on product distribution in the form of selectivity, yield and conversion of propane. It was observed that the formation of aromatics was least favoured as seen from the yield at various temperature. The hydrocarbon selectivity and yield were reported on a carbon basis. It was discovered that methane formation was most favoured. Yield and selectivity of aromatics were found to be independent of pressure at 1 to 10 bar, and m-xylene was found to be the most favoured of the isomers of xylene. This work also presented the computational justification for assuming that isomers of products obtained from propane aromatization are in quasi-equilibrium. The temperature which determines the maximum yield of the desired product was determined.

Keywords: Aromatization, Chemical-thermodynamics, Aspen Plus, Carbon-free, Selectivity, Conversion

INTRODUCTION
The aromatization process has been studied both industrially and academically with the aim of transforming abundant and relatively low-cost LPG to more valuable products in the form of benzene, toluene and xylene (BTX) (Lmutairi, 2013).

$$C_3H_8 \leftrightarrow C_6H_6, C_{10}H_8, \ldots + H_2 \quad (1)$$

Industrially, Cyclar process developed by Universal Oil Petroleum (UOP) together with the British Petroleum (BP), the M2-forming process by Mobil, the Alpha process developed by a Japanese company, Sanyo and Asahi, and Aroforming process by IFP Salutec have been used successfully for commercial transformation of light alkanes using a modified Zeolite into aromatics (Baradaran *et al.*, 2015). The mentioned processes use modified ZSM-5 with metals such as Gallium, Zinc and Platinum. It was reported that a modified ZSM-5 increased selectivity towards the formation of aromatics, which are used as either feedstock in the chemical and petrochemical industries or as finished products (Muteib, 2013). The aromatization of light alkanes being a complex reaction, the nature of the metals used for modifying ZSM-5 has been the subject of intense research during the last three decades (Nguyen *et al.*, 2006). To reduce the complexity of the light alkanes aromatization reaction, many authors have broken it down into several key steps. Nguyen et al.,(2006) divided into different steps: dehydrogenation, cracking, oligomerization, cyclization and aromatization. The products from the reaction may be produced from more than one process of the reaction (*Lukyanov et al., 1994*).The author reported forty-two components from the kinetic model for ethene and propene aromatization over HZSM-5 and Ga-ZSM-5. Another author reported thirteen

components from kinetic studies of propane and n-butane aromatization over H-ZSM5 at 500 ^{o}C (Nguyen *et al.*, 2006). The number of species may be reduced by considering product distribution at equilibrium. Some of the species may be constrained by thermodynamics to eliminate reactions that occur in a trace amount. The investigation of chemical distribution has been studied for many types of reactions, e.g. simultaneous partial oxidation and steam reforming of natural gas (Chan, 2000; Zhu, Zhang and King, 2001; Aishah, Amin and Peng, 2009; Ávila-Neto *et al.*, 2009). For Fischer-Tropsch synthesis, the thermodynamic molecular weight distribution was observed to correlate well with experimentally determined product distribution (Stenger and Askonas, 1986). Though most chemical reactions are often carried out far from equilibrium, which is an interesting area of research to find impacts of thermodynamics on the kinetics of chemical reactions. Chemical reactions in non-equilibrium thermodynamics bring thermodynamics and kinetics into a common point (Walz and Caplan, 1995; Rao and Esposito, 2016).

However, the thermodynamic equilibrium calculation of chemical reaction helps in investigating the maximum possible conversion of reactant, selectivity and yield that can be attained at specified external variables of temperature and pressure (Mazzotti, 2015; Soto *et al.*, 2016). Though for practical purpose, the reaction pathway can be altered for selectivity and yield of desired products using a catalyst. Equilibrium constant estimation has been the traditional approach for simple problems. For a complex reaction which occurs simultaneously, a more sophisticated calculation is required. These complex reaction requires energy minimization of the Gibbs function subject to constraint by incorporating Lagrange multiplier (Ebel *et al.*, 2000; Lwin, 2000; Silva and Heck, 2008; Koukkari, 2014). Few studies had been reported on the thermodynamic analysis of light alkanes aromatization which may show the equilibrium conversion and product distribution and the possible maximum yield of desired products at pre-determine temperature. (Moghimpour;Sohrabi ;Sahebdelfar, 2014) studied the effect of water, carbon-monoxide and carbon-dioxide on product selectivity from propane aromatization. His work was limited to studies of both saturated hydrocarbon and olefins. This study focuses on energy maximization to investigate products distribution subject to the prevailing external conditions such as temperature and pressure. In this study, an emphasis was placed on benzene, toluene and isomers of xylene distribution and the temperature to obtain the maximum quantity of the said products. Also,computational investigation of the assumptions made by several researchers on the quasi- equilibrium of isomers was studied.

METHODOLOGY

The first step was to propose several chemical species obtained from the aromatization of light alkanes (Lukyanov *et al.*,1994; Bhan and Delgass, 2008). In this work, about thirty-five chemical species were proposed, and the reaction was carried-out under carbon-free atmosphere which is a realistic condition for propane aromatization. The proposed chemical species and their molecular formula is presented in the appendix:

Thirty-five products suspected to be obtained from aromatization of propane were investigated to determine the equilibrium contribution, which was used as a parameter for its reduction to about thirteen components. The process was achieved based on energy minimization of Gibbs free energy at constant temperature and pressure, subject to a constraint of elemental balance

$$nG = \sum_{i=1}^{N} n_i \bar{G}_i = \sum n_i \bar{\mu}_i \qquad (2)$$

The chemical thermodynamics may be written as a function of composition, temperature and pressure

$$\bar{\mu}_i = G_i^0 + RT \ln \frac{\hat{f}_i}{f_i^0} \tag{3}$$

$$nG = \sum n_i G_i^0 + RT \sum n_i \ln \frac{\hat{f}_i}{f_i^0} \tag{4}$$

The assumption of a single-phase was made. This was justified by the fact that the overall aromatization of light alkanes is an endothermic reaction and requires a temperature of about 500 °C for the formation of aromatics (Hassanusi, 2013).
For a single-phase, the total Gibbs free energy is:

$$\left(G^t\right)_{T,P} = g\left(n_1, n_2, n_3, \ldots, n_N\right) \tag{5}$$

For a gas phase reaction:

$$\hat{f}_i = \hat{\phi}_i \, y_i P \tag{6}$$

For a standard state of pure gas at 1 bar, the fugacity of pure component equals the pressure. The standard Gibbs free energy, G_i^0 for each element, equals zero. Then for a compound, $G_i^0 = \Delta G_i^0$

The general expression of $nG\left(n_{is}, T, P\right)$ as a function of temperature, pressure and composition becomes:

$$nG\left(n_{is}, T, P\right) = \sum n_i \Delta G_{f_i}^0 + \sum n_i RT \ln P + \sum n_i RT \ln y_i + \sum n_i RT \ln \hat{\phi}_i \tag{7}$$

The main objective here is to find the n_{is} which minimizes the objective function at constant temperature and pressure subject to a constraint of elemental balances:

$$\sum n_i a_{ik} = A_k \qquad \text{(k=1,2, 3, …, z)} \tag{8}$$

Where subscript k stands for an identity of the atom, a_{ik} is the number of atoms of the kth element present in each molecule of chemical species i.
The next step was to introduce Lagrange multipliers λ_k implemented by multiplying each element by λ_k :

$$\lambda_k \left(\sum n_i a_{ik} - A_k\right) = 0 \tag{9}$$

A combination of equations 5 and 9 resulted in a new formation which changes with the number of moles. The resulting equation was minimized to obtain

$$\Delta G_{f_i}^0 + RT \ln\left(y_i \hat{\phi}_i \frac{P}{P^0}\right) + \sum_k \lambda_k a_{ik} = 0 \tag{10}$$

P^0 is usually 1bar, though the operating reaction condition was at high temperature and low pressure of 1bar, Peng-Robinson thermodynamic package was used to calculate the compressibility factor so that fugacity coefficient can be found for determination of the molar flowrates of the proposed compounds.

These procedures were implemented using an R- Gibbs reactor from the Aspen Plus

The Aspen Plus simulation was initially carried out at the reacting temperature of 550 °C and pressure of 1 bar. The basis for the calculation was 1 molar flow rate of the reactant, propane. The equilibrium molar flowrate calculated was used to reduce the number of species to about thirteen. The Selectivity and yield were calculated based on carbon balance,

$$S_i = \frac{x_i C_{x_i} H_{y_i}}{3C_3H_8} \quad (11)$$

$$Y_i = \frac{x_i C_{x_i} H_{y_i}}{\sum x_i C_{x_i} H_{y_i}} \quad (12)$$

and sensitivity analysis were carried out to see the effect of varying temperature, pressure and flow rate was investigated.

RESULTS AND DISCUSSION

The reduction of the components from thirty-five to thirteen at a temperature of 550 °C and a pressure of 1bar was based on the reported output from AspenPlus. The molar flowrate of less than 1.0 $x10^{-7}$ was reported as a trace. The conversion was almost 100% at this temperature. This is the constraint by thermodynamics which means that higher molecular weight of straight-chain hydrocarbon obtained from propane as a reactant seems to be insignificant. The higher olefins which were formed by oligomerisation occur in traced quantity. The higher olefins which are secondary products are highly reactive and react to form cyclo compounds which undergo hydride transfer to form the aromatics. Several investigators had always assumed that isomers are at equilibrium, justifying the reason for ignoring the isomers *(Lukyanov et al., 1994*). However, no known work had presented quantitative data to justify the claimed. In this work, the mole fraction of n-butane and i-butane is of magnitude 10E-9. The same trend can also be seen from the isomer of 2,4 and 2,5 dimethyl-2,4-hexadiene. The formation of methane is most favoured thermodynamically because the Gibbs free energy of methane is -50,460J /mol K at 298. 15K (Liu *et al.*, 2004). Methane is formed from different reaction steps, mainly cracking of propane and higher olefins, and dealkylation of toluene and xylene.

The selected components were investigated to see the effect of temperature on its molar flowrate as shown in Figure 1

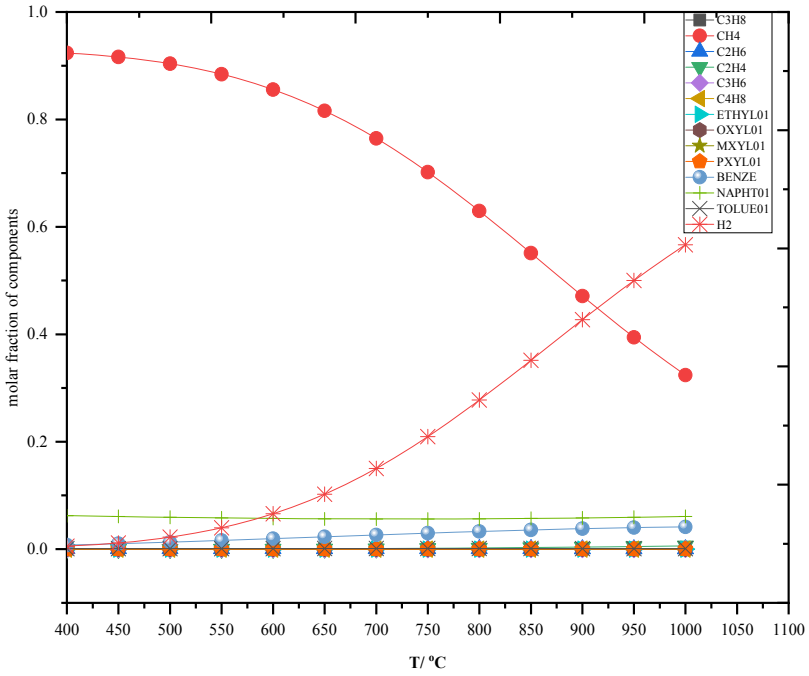

Figure 1: Effect of temperature on molar fraction of components at 1 bar

The molar fraction of methane is seen to decrease as temperature increases. This may be attributed to the decomposition of methane to form several radicals as the temperature increases to form other products. This assumption is justified by the fact that the molar fraction of hydrogen is seen to increase with the increase in temperature to about 920 °C, where methane and hydrogen molar fraction is at equilibrium. Beyond this temperature, hydrogen is seen to grow exponentially with temperature. Hassanusi (2013) reported similar findings of hydrogen production varying with operating temperature. This result established that propane decomposed to its elemental components at 920 ^{0}C. The relationship for other components which may not be clearly interpreted from Figure 1 can be observed clearly by expanding the cluster region as seen in Figure 2.

Benzene and naphthalene are observed to be the dominant components of propane aromatization (Figure 2). The molar fraction of naphthalene, which is seen to be almost independent of higher temperature indicates the beginning of the formation of carbon soot, which, in this case, is in a gaseous phase. Benzene is seen to increase with temperature as higher oligomers that are formed react readily to form the simplest aromatic (benzene). This information is important, if the objective of the researcher is to produce more benzene which is thermodynamically favoured among the BTX. Catalyst, such as a modified ZSM-5 may be used to change the reaction pathway, if toluene, xylene and ethylbenzene are to be produced in significant quantity. The molar fraction of other aromatics with temperature which is not clearly illustrated in Figure 2 due to its low molar fraction is illustrated in Figure 3.

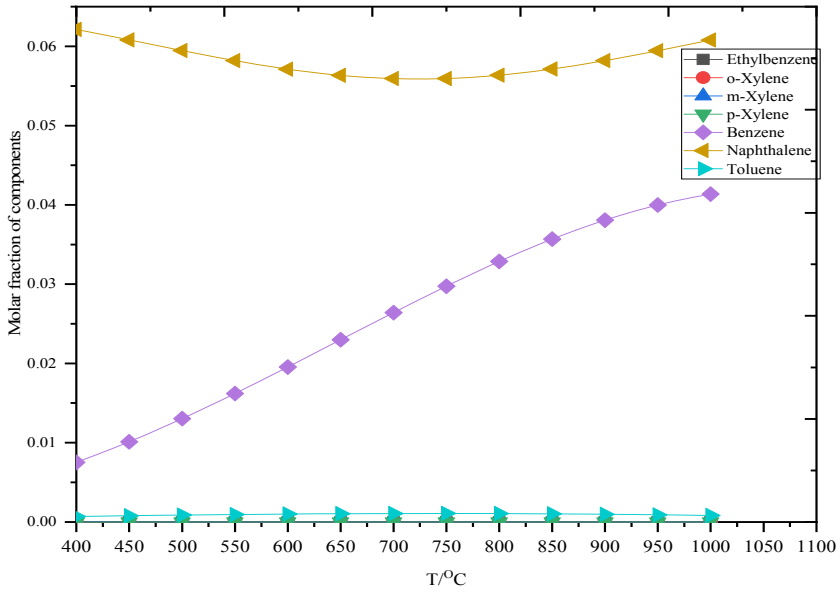

Figure 2: Equilibrium distribution of Aromatics at the various temperature at 1 bar

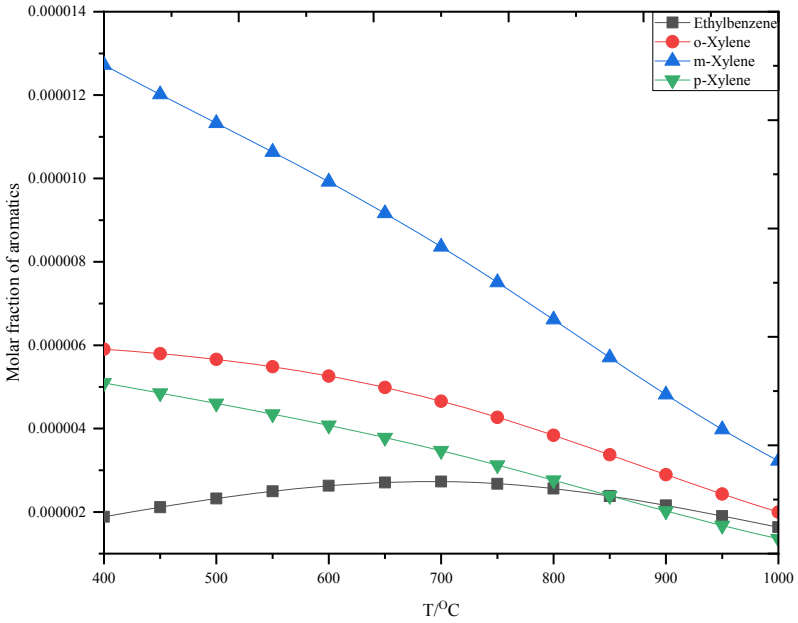

Figure 3: Equilibrium distribution of aromatics (excluding benzene) at various temperatures at 1 bar.

The molar fraction of m-xylene is most affected by temperature as the curve slides downward as the temperature increases. Other components such as ethylbenzene, ortho and para-xylene are less affected by temperature. The molar fraction of ethylbenzene is seen to be almost independent of temperature. This pattern may be attributed to the stability of the intermediates. The decrease in molar fractions of the aromatics (Figure 3) may be due to dealkylation which may be justified by an increase in the molar fraction of benzene (Figure 2).

The effect of temperature and pressure on the yield of aromatics was also studied as illustrated in Figure 4

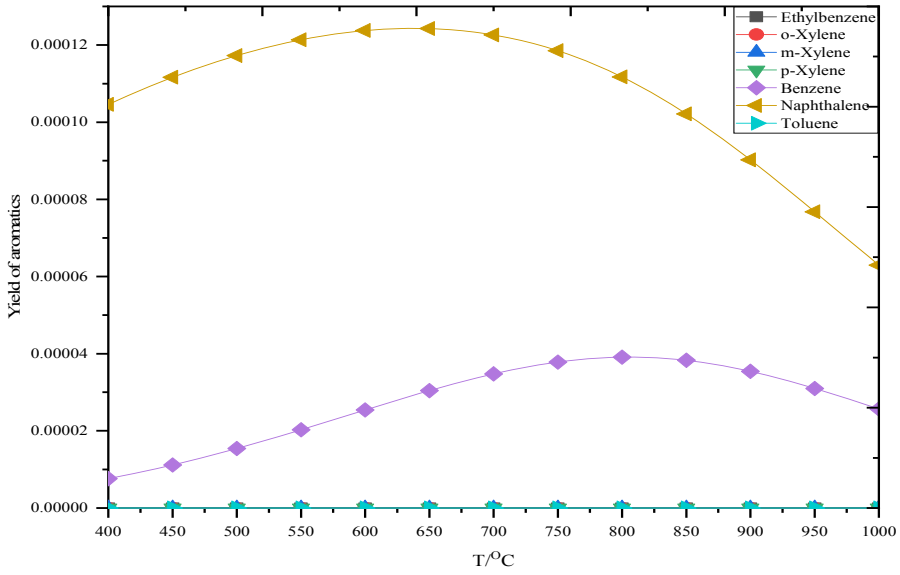

Figure 4: Effect of temperature on aromatics distribution at 1bar

Benzene and naphthalene are observed to be the dominant components. The yield of naphthalene was noticed to increase slightly and later dropped linearly as the temperature increased. Benzene yield is seen to increase to some extent with temperature, with its maximum yield at 800 ^{0}C. Beyond this temperature, the yield is seen to decrease as the temperature increases. The yield of other components which are not so significant may be observed by expanding the scale of the lower portion of Figure 4.

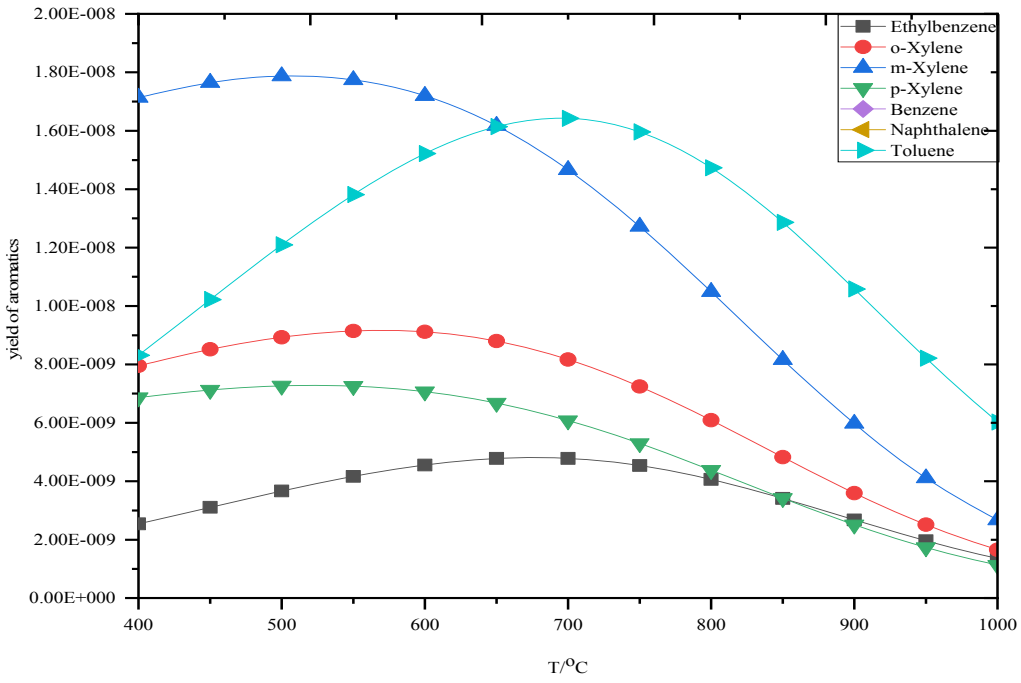

Figure 5: Effect of temperature on the yield of selected aromatics

The yield for m-xylene was observed to drop significantly as the temperature increased. At higher temperature (> 900 °C), the yield of m-xylene, O-xylene, p-xylene and ethylbenzene is similar. The yield for toluene increased gradually until it exceeded that of m-xylene, the maximum yield occurred at 700 °C. At much higher temperature, the yield starts to slide downward. The sudden decrease in the formation of m-xylene may be due to dealkylation leading to the increase in the yield of toluene and benzene (Figure 5).The Effects of temperature on the selectivity of the aromatics were also studied (Figure 6)

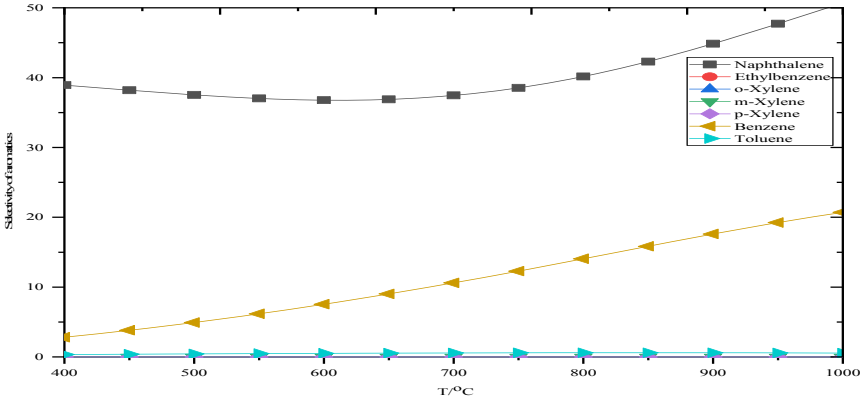

Figure 6: Effect of temperature on the selectivity of aromatics.

The selectivity for naphthalene is the most favoured thermodynamically, though it seems to be independent of temperature up until 600 °C. Beyond 600 °C, the selectivity increases exponentially. The selectivity for benzene increases linearly with temperature. From this observation, it is clear that there is a correlation between yield and selectivity. For o-xylene m-xylene, p-xylenes, toluene and ethylbenzene, the relationship is shown in Figure 7

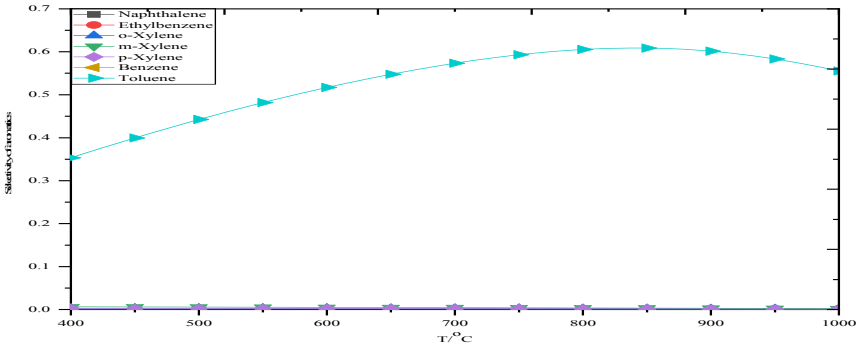

Figure 7: Effect of temperature on the selectivity of some aromatics

The selectivity for toluene is seen to be thermodynamically favoured. The maximum selectivity was obtained at 800 ^{0}C. The lower portion (Figure 7) is expanded (Figure 8).

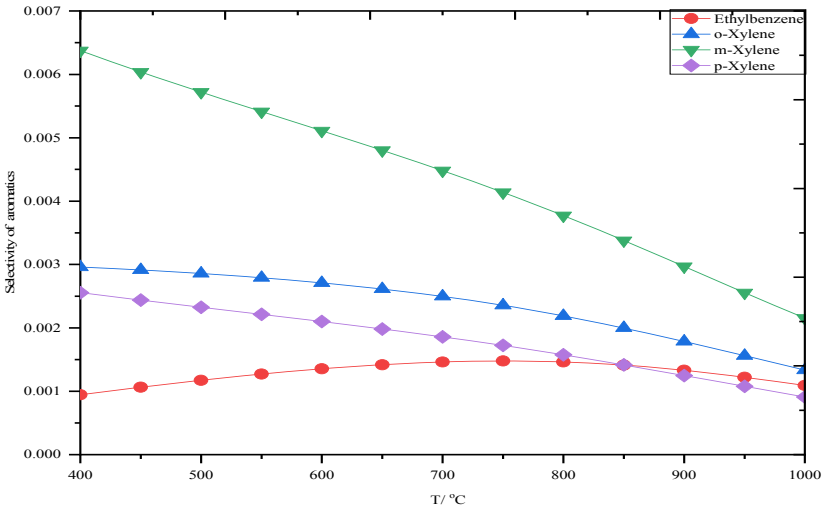

Figure 8: The selectivity of selected aromatics component with temperature

The selectivity of isomers of xylene and ethylbenzene shows that m-xylene is strongly affected by temperature. The selectivity of ethylbenzene is almost similar to that of p-xylene at 900 °C The effect of changing the flow rate of propane on product distribution at 550 °C was also studied thermodynamically as shown in Figure 9.

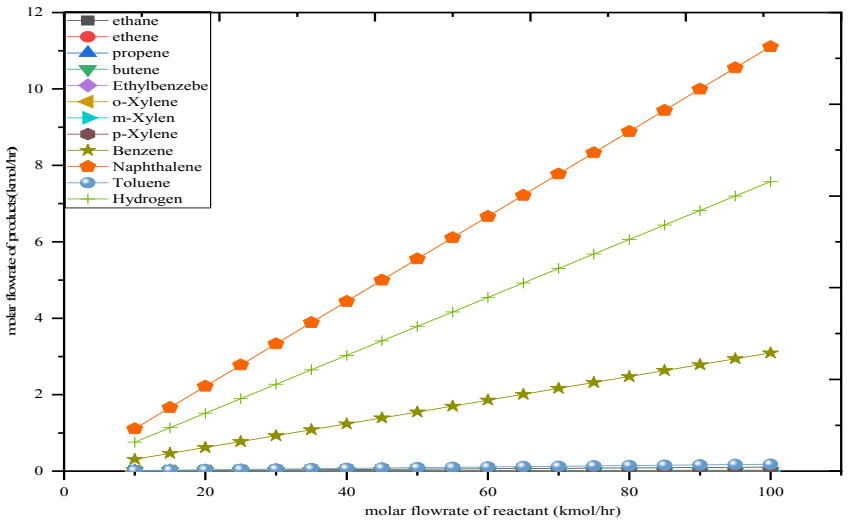

Figure 9: Product distribution due to changes in the molar flowrate of propane at 550 ºC

The product distribution shows linear relationship at a temperature of 550 ºC and a pressure of 1 bar with Naphthalene having the highest molar flowrate. The formation of naphthalene may indicate the formation of soot which may have to be taken into consideration during catalyst formulation. This assumption may be deduced from the formation of hydrogen which designates that cracking of propane to form various radicals is the dominant reaction

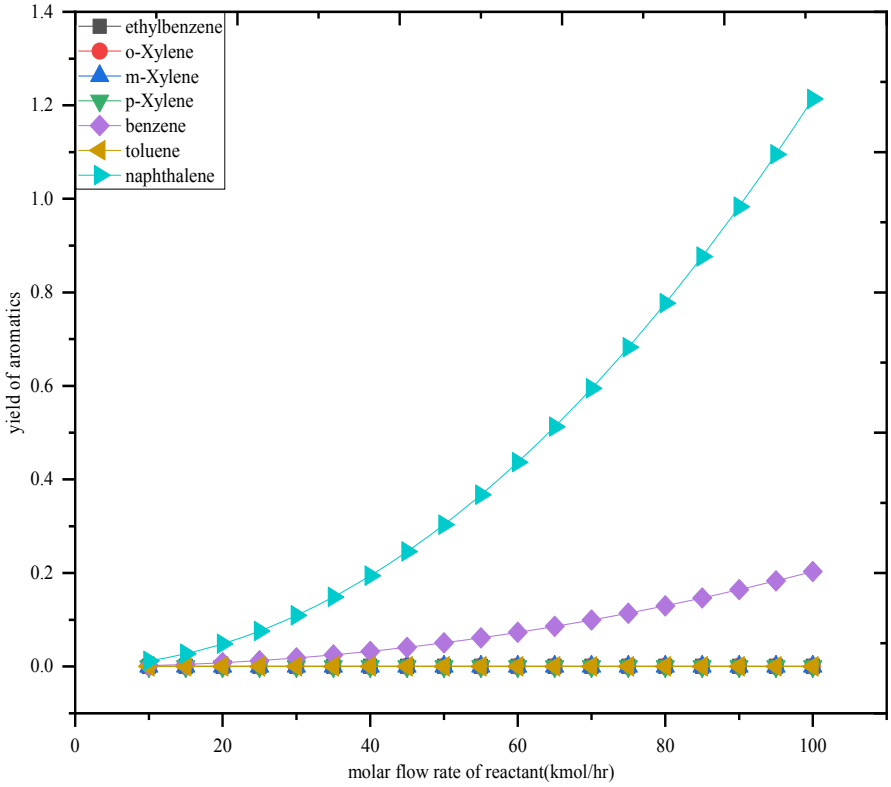

Figure 10: Yield of aromatics in response to changes in propane flowrate at 550 °C and 1bar.

It was observed that the yield of Naphthalene increased exponentially with the reactant flowrate at 550 °C. The yield of benzene shows little response in a linear pattern with propane flow rate. Other aromatics show almost zero yield but the lower portion can be expanded to study the relationship as shown in Figure 11.

With the exception of ethylbenzene, the aromatic yield shows an exponential relationship as the molar flowrate of the propane increases. The yield of toluene is lower than m-xylene with increase in propane flowrate. The reverse is the case when temperature was used as parameter to study products distribution (Figure 2).

The distribution of benzene as the flowrate of the reactant changes at various temperatures was also studied (Figure.12).

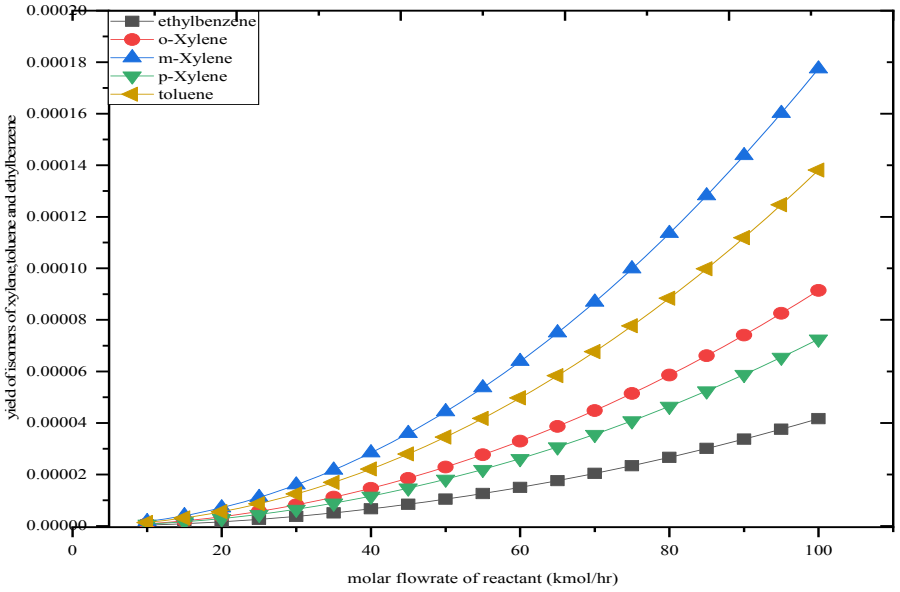

Figure 11: Yield of aromatics in response to changes in propane flowrate at 500 °C and at 1bar.

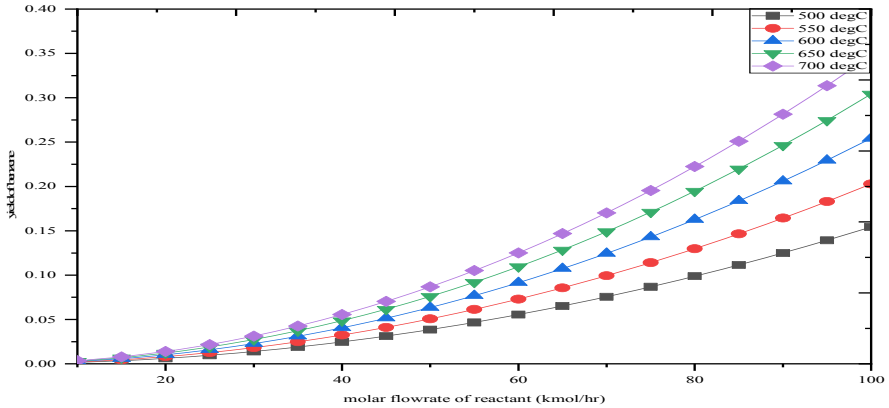

Figure 12: Yield of benzene with changes in molar flowrate of reactant(propane) at several temperature and 1bar

The formation of benzene is seen to be significant at a higher temperature as the flowrate of propane increases. Electrons are highly delocalised at higher temperature and this account for the stability of benzene. At lower flowrate, the yield of benzene is insignificant and independent of temperature. At lower flowrate, there may be lower formation of cyclic compounds which undergo protonation and dehydrogenation to form benzene.

The yield of toluene with an increase in propane flow rate at various temperature was also studied (Figure 13)

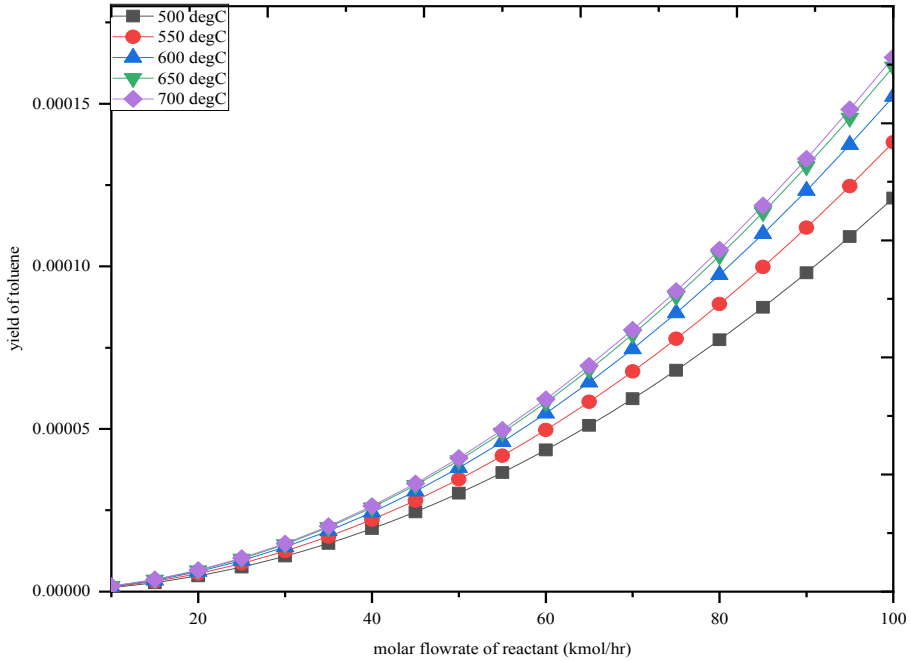

Figure 13: Toluene yield with changes in propane molar flowrate at various temperature and 1bar.

Changes in temperature have little effect on the yield of toluene as the molar flowrate of the reactant increases. Due to the stability of benzene at high temperature as explained previously (Figure 12), temperature may play little effects on the yield of toluene.

The effect of varying pressure on the yield of selected aromatics at 550 °C was also studied. This justified the reason why Pen-Robinson thermodynamic package was used.

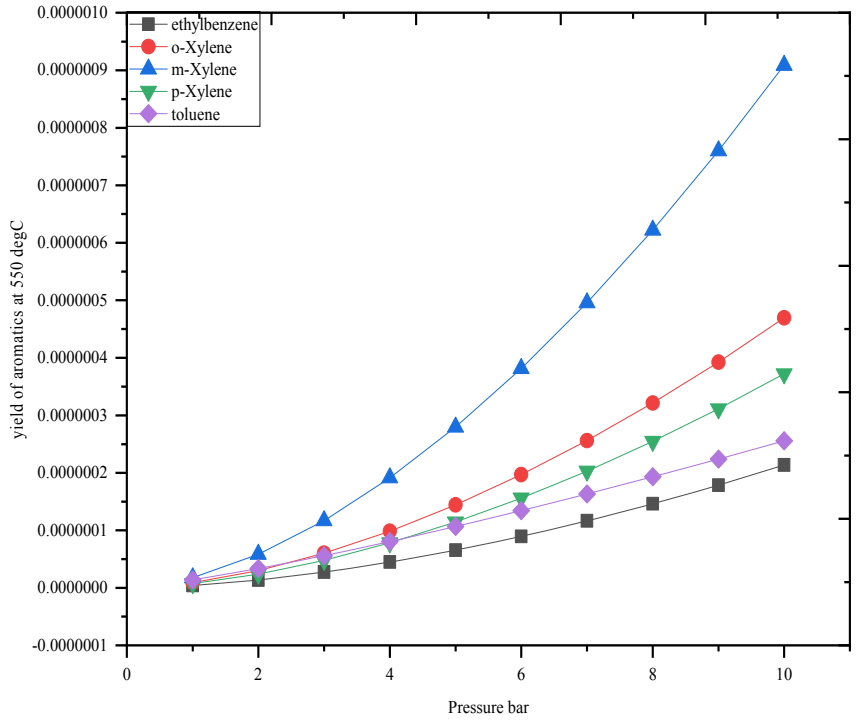

Figure 14: Effect of pressure on the yield of selected aromatics at 550 °C

The yield of m-xylene was observed to increase almost linearly with pressure. For instance, at a pressure of 10 bar, the yield of m-xylene to o-xylem is 2 to 1. The ratio was observed to even-out at a pressure of 1-bar. The formation of toluene is strongly affected by pressure as its yield to m-xylene is seen to be in the ratio of 1 to 4 at a pressure of 10 bar. It may be assumed that the formation of the carbocation is favourable at the meta position of toluene which abstract the reactive methyl group from the gaseous phase to form m-xylene. This claimed may be seen from Figure 14 which clearly shows low yield of toluene with pressure. The lower yield of ethylbenzene may be due to low concentration of ethylene.

Benzene was chosen as a representative of the aromatics to see the effect of pressure change of reactant on its molar flowrate at various temperature (Figure15).

Though the flowrate of benzene is seen to increase with increased in temperature, it was observed that changes of reactant pressure at various temperature has little or no effect on the molar flowrate of benzene. The fugacity of benzene within the specified pressure interval may be insignificant from the ideal pressure which reduces the fugacity coefficient to one. This may be the reason why aromatics formation is favourable at a lower pressure and a higher temperature.

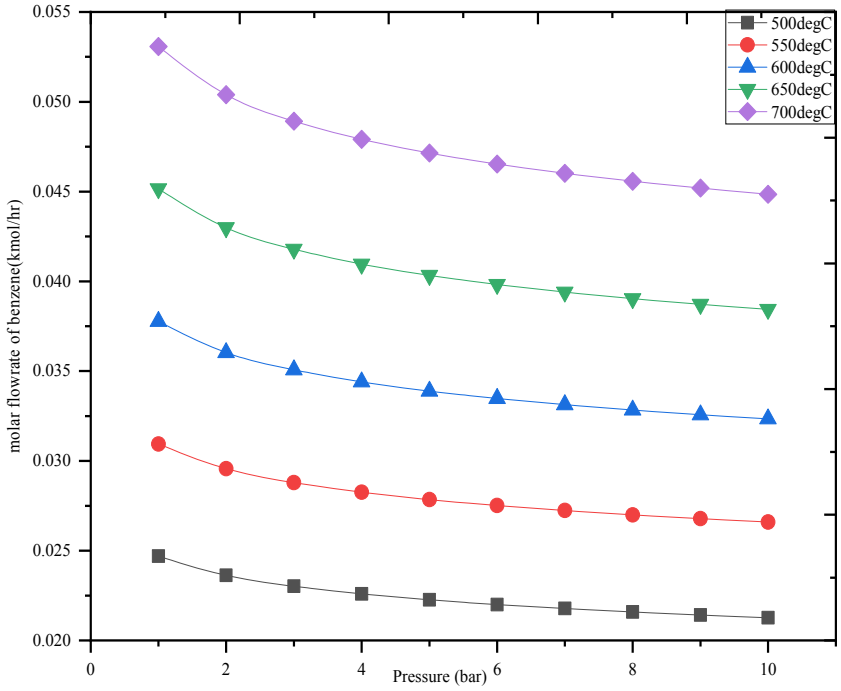

Figure 15: Effect of pressure changes of reactant on benzene flowrate at different temperature.

CONCLUSION

The study of light alkanes aromatization by energy minimization has helped to reduce the number of proposed products from thirty-five to thirteen. Though Nguyen et al (2006) had reported thirteen components from propane and n-butane aromatization from kinetic studies, this research investigated thirteen components from propane aromatization after using thermodynamic analysis at equilibrium. The effect of temperature on product distribution at equilibrium was found to have effect on the formation of methane and hydrogen. Though aromatization of light alkanes involves several reaction processes, it was observed that the cracking process was the domineering reaction process. The effect of pressure at various temperature on the molar flow rate of benzene was studied. It was found that pressure had little or no influence on aromatic distribution. The assumption of the isomers of certain product being in quasi-equilibrium was quantified computationally. To alter the reaction pathway towards the formation of desired products, for instance, to produce more of p-xylene, which is in high demand, a search for the right metal for the modification of the ZSM-5 must be intensified which would alter the reaction pathway.

ACKNOWLEDGEMENT

The Researchers wish to acknowledge the support of the Petroleum Technology Development Fund PTDF for funding the research from the annual oil and gas research grant and the Chemical engineering Department, Ahmadu Bello University, Nigeria for the provision of materials for the successful completion of the research work.

REFERENCES

Aishah, N., Amin, S. and Peng, S. E. (2009) '*A Thermodynamic Equilibrium Analysis on Oxidation of Methane to Higher Hydrocarbons*', *Pertanika J. Sci. and Technol.*, pp. 363–370.

Ávila-Neto, C. N. *et al.* (2009) *'Hydrogen production from methane reforming: Thermodynamic assessment and autothermal reactor design*', *Journal of Natural Gas Science and Engineering*, 1(6), pp. 205–215. doi: 10.1016/j.jngse.2009.12.003.

Baradaran, S. *et al.* (2015) '*Experimental and modelling study of propane aromatization over H-ZSM-5 catalysts prepared by different silica sources*', *Canadian Journal of Chemical Engineering*. doi: 10.1002/cjce.22160.

Bhan, A. and Delgass, W. N. (2008) *'Propane aromatization over HZSM-5 and Ga/HZSM-5 catalysts', Catalysis Reviews - Science and Engineering*. doi: 10.1080/01614940701804745.

Bijani, P. Moghimpour;Sohrabi, M; Sahebdelfar, S. (2014) *'Petroleum Science and Technology Thermodynamic Analysis of Propane Aromatization'*, (April 2015), pp. 37–41. doi: 10.1080/10916466.2012.678539.

Chan, S. (2000) *'Thermodynamic analysis of natural-gas fuel processing for fuel cell applications', International Journal of Hydrogen Energy*, 25(5), pp. 441–449. doi: 10.1016/S0360-3199(99)00063-4.

Dmitri B. Lukyanov, t N. Suor Gnep, and M. R. G. (1994) *'Kinetic Modeling of Ethene and Propene Aromatization over HZSM-5 and GaHZSM-5', Industrial and Engineering Chemistry Research*, 33, pp. 223–234.

Ebel, D. S. *et al.* (2000) *'Gibbs Energy Minimization in Gas + Liquid + Solid Systems', Journal of Computational Chemistry*, 21(4), pp. 247–256. doi: 10.1002/(SICI)1096-987X(200003)21:4<247::AID-JCC1>3.0.CO;2-J.

Guisnet, M. *et al.* (1992) *'Conversion of light alkanes into aromatic hydrocarbons VI . Aromatization of C and C , alkanes on H-ZSM-5 - Reaction mechanisms', Applied Catalysis A,* 87, pp. 255–270.

Hassanusi, Q. B. (2013) *Thermodynamic Study of Propane Dehydrogenation into propylene*. Universiti Malaysia Pahang.

Koukkari, P. (2014) *Introduction to constrained Gibbs energy methods in process and materials*. Edited by V. Technology. JULKAISIJA – UTGIVARE.

Liu, M. *et al.* (2004) '*Theoretical Study on Thermodynamic Properties of C 1 - C 16 Alkanes : A 3-Parameter Least-Squared Calibration*', *J. Phys. Chem. A*, 108(eq 4), pp. 6784–6787.

Lmutairi, S. ami m uteib a (2013) .*The role of Lewis and Brønsted acidity for alkane activation over zeolites*. Eindhoven Univerdity of Technology.

Lukyanov, D. B., Gnep, N. S. and Guisnet, M. R. (1994) '*Kinetic modeling of ethene and propene aromatization over HZSM-5 and GaHZSM-5*', *Industrial and Engineering Chemistry Research*, 33(2), pp. 223–234. doi: 10.1021/ie00026a008.

Lwin, Y. (2000) *'Chemical Equilibrium by Gibbs Energy Minimization on Spreadsheets'*, *International Journal of Engineering Education*, 16(4), pp. 335–339. Available at: https://www.ijee.ie/articles/Vol16-4/Ijee1157.pdf.

Mazzotti, M. (2015) *Introduction to Chemical Engineering: Chemical Reaction Engineering*, *ETH Swiss federal institute of technology Zurich separation processes laboratory*. Zurich. doi: 10.1246/nikkashi1898.64.10_1693.

Nguyen, L. H. *et al.* (2006) *'Combined experimental and kinetic modelling studies of the pathways of propane and n -butane aromatization over H-ZSM-5 catalyst'*, *Chemical Engineering Science*, 61, pp. 5881–5894. doi: 10.1016/j.ces.2006.05.017.

Paula Yurkanis, B. (2003) *An Introduction to the Study of Organic Chemistry.*

Rao, R. and Esposito, M. (2016) *'Nonequilibrium thermodynamics of chemical reaction networks: Wisdom from stochastic thermodynamics'*, *Physical Review X*, 6(4). doi: 10.1103/PhysRevX.6.041064.

Silva, A. da and Heck, N. (2008) *`To Compute Equilibrium Concentrations in Multicomponent Systems By Gibbs Energy Minimization on Spreadsheets', Materiales-Sam.Org.Ar*. Available at: http://www.materiales-sam.org.ar/sitio/biblioteca/CONAMET-SAM2008/pdfs/f15.pdf.

Soto, R. *et al.* (2016) *'Equilibrium conversion, selectivity and yield optimization of the simultaneous liquid-phase etherification of isobutene and isoamylenes with ethanol over Amberlyst™ 35'*, *Fuel Processing Technology*, 142, pp. 201–211. doi: 10.1016/j.fuproc.2015.09.032.

Stenger, H. G. and Askonas, C. F. (1986) *'Thermodynamic Product Distributions for the Fischer-Tropsch Synthesis'*, *Industrial and Engineering Chemistry Fundamentals*, 25(3), pp. 410–413. doi: 10.1021/i100023a018.

Walz, D. and Caplan, S. R. (1995) *'Nonequilibrium thermodynamics and kinetics', in Bioelectrochemistry: General Introduction*. Basel: Birkhäuser Basel, pp. 1–48. doi: 10.1007/978-3-0348-7318-5_1.

Zhu, J., Zhang, D. and King, K. D. (2001) *`Reforming of CH4 by partial oxidation: Thermodynamic and kinetic analyses'*, *Fuel*, 80(7), pp. 899–905. doi: 10.1016/S0016-2361(00)00165-4.

Proceedings of the 49th NSChE Annual Conference
KADA 2019: pp 705-713

P3C-04: PARTICLE SIZE DISTRIBUTION AND EFFECT OF ATTRITION ON A COMMERCIAL GRADE CATALYST USED FOR INDUSTRIAL FCC OPERATION

Okwonna, Obumneme O.[1*], Otaraku, Ipeghan J.[2], Oduola, Koyejo M.[2] and Okeke, Eric O.[3]

[1]Africa Centre of Excellence for Oilfield Chemicals Research (ACE-CEFOR), University of Port Harcourt, Choba, Nigeria
[2] Department of Chemical Engineering, University of Port Harcourt, Choba, Nigeria
[3]Mercogas Group, Port Harcourt, Nigeria
*Email of the Corresponding author: obumneme_okwonna@uniport.edu.ng

ABSTRACT

In this work, an investigation has been made on the effect of attrition on the particle size distribution of a commercial-grade catalyst used forindustrial Fluid Catalytic Cracking (FCC) operation. It considers the technical evaluation of a commercial FCC unit in Nigeria using both design and production data drawn from 5 continuous run operations from where the catalyst loss due to attrition was evaluated. Furthermore, physicochemical property test of the catalyst was used to analyse the effect of attrition on them. The attrition rate of the catalyst was modelled with an empirical model, whereas, the specific attrition rate has been modelled with an exponential decay model. Analysis of the particle size distribution, total surface area (118 m^2/g) and apparent particle size (75 µm) all indicate the effect of attrition on the catalyst. The least sized particles were most attrited. The attrition indices for the fresh and spent catalyst were found to be 58.9 and -2.50 respectively. The specific attrition rate had R^2 value of 0.999, Standard Error of 0.000908 and RSS value of $1.403 * 10^{-5}$*. These results show that the exponential decay model presents a suitable description of attrition of this catalyst and that catalyst attrition is dependent on particle size.*

Keywords: Fluid Catalytic Cracking, Catalyst Attrition, Particle Size Distribution, Mathematical Modelling

1.0 INTRODUCTION

Attrition is a significant source of catalyst deactivation in the fluid catalytic cracking (FCC) process. It occurs due to particle motion and inter-particle collision resulting from gas flows and the bed-to-wall impact on the process. Although these collisions are required for the efficient performance and operation of fluidised-bed reactors, the resulting attrition is a major drawback in the operation of these units. The main consequence of catalyst attrition is the generation of fines which eventually pass as dust leading to the loss of valuable catalytic materials (Wu *et al*., 2015, Wei *et al*., 1977). This loss has both operational and economic implications on the running of the FCC units. Loss of catalyst particle fines increases the coarseness of the bed particle size distribution hence the need for addition of makeup catalyst in order to keep the system at a required level of fines (Kramp *et al*., 2011; Wether and Hartge, 2003). While an increased coarseness is undesirable, having large amount of particle fines within the system could give rise to a fluidised-bed whose particle size distribution may be too fine to achieve the desired result.

Various models have been used to describe attrition in the FCC unit. Wei *et al.,* (1997), Wether and Hartge (2003), Puttmann *et al*., (2006), Hartge *et al.,* (2010), Kramp *et al.,* (2011), Thon *et al.,* (2013), Wu *et al.,* (2016) among others have all made various predictions on the effect of particle size distribution on the attrition process based on different lab-scale investigations. Because particle size is of significant consideration in the attrition process, it is necessary to investigate the extent to which attrition could affect the size distribution of catalyst particles,

especially, in an industrial scale FCC operation. This investigation will give a proper guide on the material strength and their ability to withstand attrition. It will also be of great significance to predict the rate of attrition of these catalysts using some available models so at understand the relationship between the particle size distribution and the attrition process. The aim of this work is therefore, to evaluate the effect of attrition on the particle size distribution of a commercial-grade catalyst for an industrial process and condition.

2.0 METHOD

The methods used in this work include: technical evaluation, catalyst characterisation, data analysis and mathematical modelling.

2.1 Technical evaluation

Technical evaluation of the design and operation of a selected FCC unit in Nigeria was done. Data from 5 continuous run operations were used to study the effect of attrition on the commercial-grade catalyst under consideration. The catalyst level inside the regenerator during the operation was evaluated from the pressure exerted by the catalyst at each point in time and recorded on a 6 hr interval while the amount of the makeup catalyst was deducted to evaluate the catalyst loss in the process.

2.2 Catalyst Characterization

The commercial-grade catalyst used in this work consists mainly of Y-zeolite with an Alumina base built on Nickel support. Its length and bulk density were 3 – 6mm and 0.8g/cm^{3}respectively. Particle size and total surface area analyses were used to characterise the fresh and spent catalysts. These analyses were done using mechanical sieves and BET water adsorption method respectively.

2.3 Attrition measurement

Using the data obtained from the technical evaluation of this FCC process as reported in the work of Okwonna *et al.,* (2019), the rate of catalyst attrition was predicted using the model presented by Wu *et al.,* (2015) while parameter estimation was done using Data Fit version (9.0). Rate of attrition on the unit was assessed from the change in mass of the catalyst bed within the regenerator where attrition was assumed to be solely responsible for the catalyst loss within the unit. The catalyst which comprises of various particle size distributions (as shown in Table 2) was considered with the assumption that there was no form of interaction among these particles. Hence, predicting the mass of the full-sized sample implied a linear combination of these fractions with the correlation of Equation 1.

$$M = \sum_{i=1}^{n} x_i * m_i \quad (1)$$

Where:
M = Mass of catalyst; x_i = mass fraction of various particle sizes;m_i = average mass of the particle at time t; n = particle class size
Therefore, the attrition rate is given by Equation 2:

$$R = \frac{dM}{dt} = \sum_{i=1}^{n} x_i * \frac{dMi}{dt} = \sum_{i=1}^{n} x_i * R_i \quad (2)$$

The specific attrition rate of the catalyst particles which is a ratio of attrition rate to the change in mass of the catalyst bed as shown in Equation 3.

$$R_b = \frac{R}{M_0 - M} = \frac{\sum_{i=1}^{n} x_i * R_i}{M_0 - \sum_{i=1}^{n} x_i * m_i} \quad (3)$$

Where:
R= Attrition rate; R_b = specific attrition rate; R_i = attrition rate for particle i
Note: x_i was obtained from particle size analysis (Table 2), whereas m was determined during the operation (see Section 2.1).

Furthermore, the specific attrition rate was modelled with the exponential decay model of Equation 4 as presented by Wu *et al.,* (2016)

$$R_b = R_c + De^{-\frac{1}{\tau}} \quad (4)$$

Where: R_c = steady-state specific attrition rate; D = total decay value of the specific attrition rate; τ = decay time parameter

Where D and τ were obtained from a least-square nonlinear fit of the technical data.
The initial specific attrition rate (at time τ = 0) is given by Equation 5

$$R_0 = R_c + D \quad (5)$$

Also, the percentage error values between the observed and predicted values for the specific attrition rate would be obtained using Equation 6.

$$AbsoluteRelativeError(\%) = \frac{\sum y_{predicted} - \sum y_{observed}}{\sum y_{observed}} * 100 \quad (6)$$

3.0 RESULTS AND DISCUSSION

The results obtained from the technical evaluation, catalyst mass loss, catalyst characterisation and attrition study have been presented and discussed as follows:

3.1 Catalyst loss on the system

The mass of catalyst within fluid bed was evaluated from the pressure exerted by the catalyst inside the regenerator and monitored from the control unit. The catalyst loss for the runs1 and 4 are shown in Figure 1, whereas plots for run 2, 3 and 5 are shown in Figure 2.

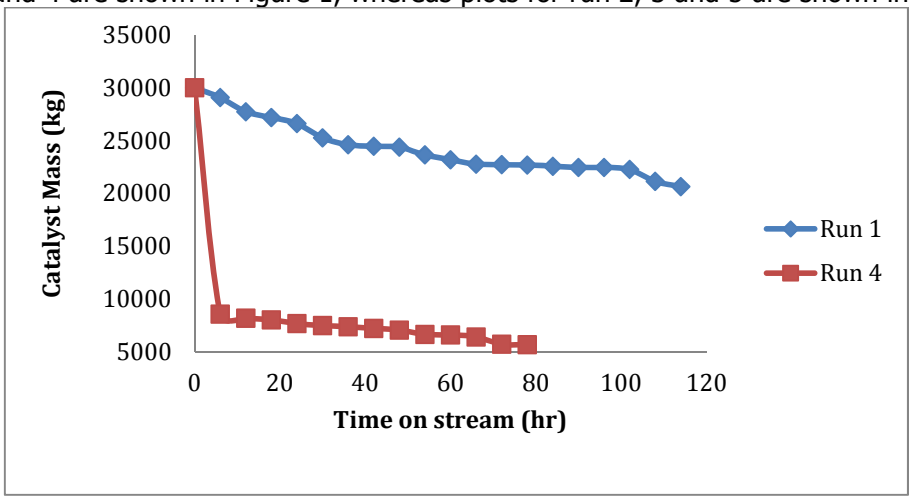

Figure 1: Catalyst Mass Vs Time for Run 1 and 4

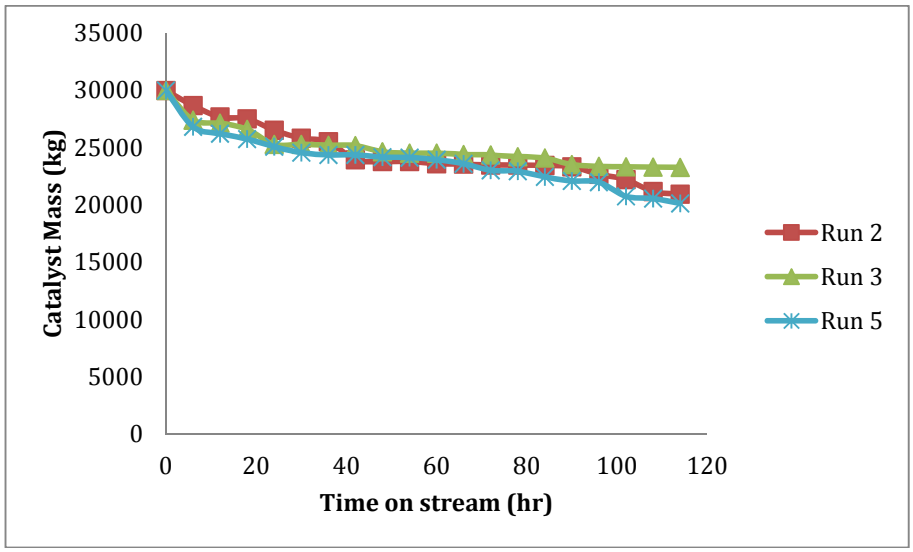

Figure 2: Catalyst Mass Vs Time for Run 2, 3 and 5

Figures 1 and 2 show a general decline in the mass of the catalyst bed inside the regenerator for all the cases considered. In this study, the amount of makeup catalyst 3000kg/day (3tons/day) was first deducted. The sharp decline observed in the 4th run could be due to the high pressure of the operation which might have had some consequence on the catalyst loss and attrition process. This decline could also be indicative a technical fault in the unit; although a gradual decline in mass was observed in the 1st, 2nd, 3rd and 5th run operations. The gradual decline in the mass of the catalyst implies a steady loss of elutriated fines within this unit which Wu *et al.,* (2016) had ascribed to characteristic loss of smaller fines in the catalyst bed and according to Kramp *et al.*, (2011) also leads to increased coarseness of the fluid-bed. With continuous removal of the surface layer from the parent material, these coarse particles could undergo further attrition over time (Chiranjeevi *et al.*, 2014). The initial sharp decline could infer the unsteady state process described by Wu *et al.,* (2010). Moreover, whereas increased pressure within the regenerator could have a significant impact on the catalyst loss and attrition process, the same cannot be said of temperature. In other words, mechanical stress rather than thermal stress could be responsible for attrition in this unit; although there is need for further research in this area. Also, considering the performance of this unit in terms of catalyst loss, data from the first run operation have been used to model the attrition rate of the catalyst.

3.2` Catalyst Characterization

Particle size and surface area analyses were used to characterise the fresh and spent catalyst samples. As stated earlier, analyses on the particle size and total surface area of the catalyst were done using mechanical sieves and BET water adsorption methods respectively and the results presented in Table 1 as shown.

Table 1: Catalyst particle analysis

Property	Fresh Catalyst	Spent Catalyst
Apparent Particle Size (μm)	71	75
Total Surface Area (m^2/g)	251	118
Attrition Index	58.9	-2.5

***Note**: values for the spent catalyst were the average from 5 run operations*

Table 1 shows that there were variations in the properties of the fresh and spent catalysts. Increase in the apparent particle size of the catalyst from 71 µm for the fresh catalyst to 75 µm for the spent catalyst is an evidence of the attrition of the smaller sized particles thereby leading to an increment in the coarseness of the catalyst bed and hence corroborates the work of Kramp *et al.,* (2011). An increase in apparent particle size gave rise to a corresponding decrease in the reaction surface area from 251 to 118 m^2/g, and this could affect the product yield as suggested by Meyer *et al.,*(2018) and Fiske (2013).

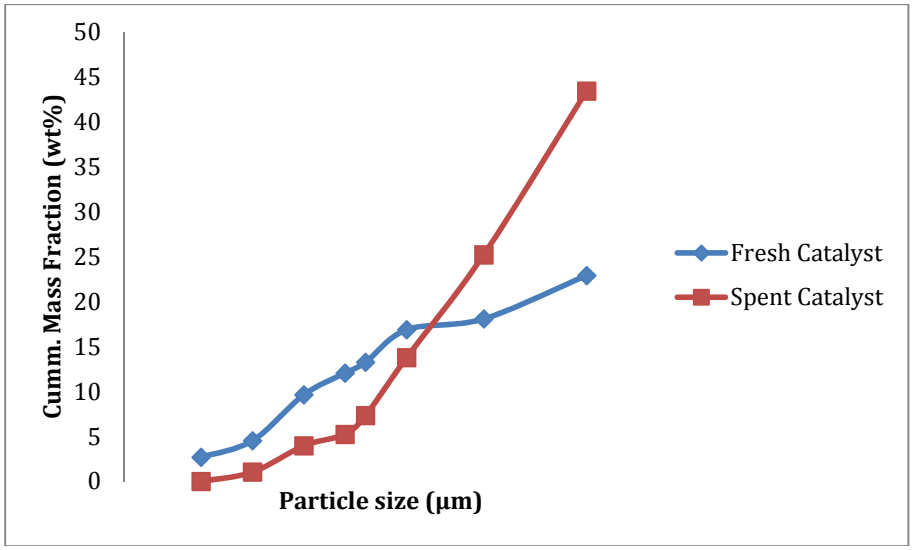

Figure 3: Effect of catalyst attrition on the Particle size distribution

The particle size distribution of the catalyst before and after the FCC operation is shown in Figure 3. This figure shows a reduction in the mass fraction of the 0 - 60 µm sized particles of the spent catalyst as compared to the fresh catalyst. These results, therefore, show that the least sized particles were more attrited than the larger sized particles in line with the work of Thon *et al.,* (2013) and therefore a further proof to the increased coarseness of the catalyst bed due to attrition. According to Coco *et al.,* (2010), the resistance of this catalyst to attrition can be predicted by the ratio of the attrition indices (AI). AI (20) and AI (44) corresponding to the weight of particles generated by attrition below 20µm and 44µm. Therefore, the attrition indices for the fresh and spent catalyst from Figure 6 were found to be 58.9 and -2.50 respectively.

The mass fraction of the particle size fractions retained on each sieve was obtained and presented in Table 2.

Table 2: Particle size analysis for fresh catalyst and spent catalyst

Particle	Diameter (µm)	Nominal Average Diameter (µm)	Mass fraction (x)	
			Fresh (wt%)	Spent (wt%)
1	0 – 20	-	2.69	0
2	0 – 30	25	4.54	1.052
3	0 – 40	35	9.644	3.97
4	0 – 45	43	12.05	5.2449
5	0 – 50	47	13.25	7.34
6	0 – 60	55	16.87	13.78
7	0 – 80	70	18.079	25.21
8	0-100	90	22.89	43.41

***Note**: values for the spent catalyst were the average from 5 run operations*

Between the fresh and spent catalysts, a reduction in the mass fraction of Class 1 - 6 (0 - 60µm) particles and an increase in that of Class 7 - 8 (81 - 100µm) particles were observed from the particle size distribution shown in Table 2. These results show that the least sized particles were more attrited than the larger sized particles. This attrition pattern provides further proof on the increment in the coarseness of the catalyst bed due to attrition in line with the work of Wei *et al.,* (1977). Sadeghbeigi (2000) further corroborated this view and also reported an adverse effect of increased coarseness of the fluid-bed on the fluidization process.

3.3 Rate of attrition

The rate of the attrition of the catalyst particle has been evaluated by employing Equation 2, and the resultant time dependence of this rate is presented in Figure 4.

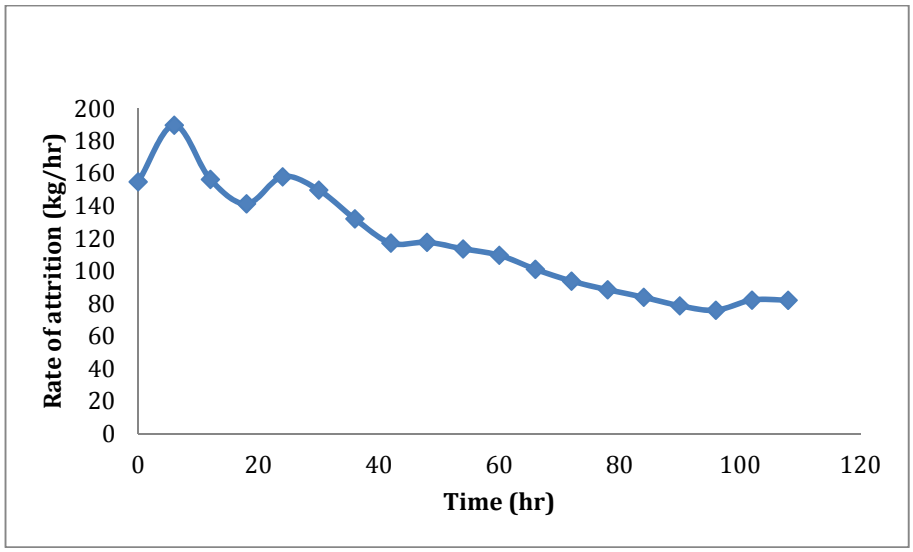

Figure 4: Time dependence of the catalyst attrition rate.

From Figure 4 it can be seen that the rate of attrition of the catalyst increased within the first 6 hours after which a decline was observed. The initial increase could be attributed to early non-steady state stage of attrition as well as the amount of small-sized particles contained in the catalyst composition which are easily lost as microfine due to attrition. According to Sadeghbeigi (2000), catalyst particles of 0 - 40µm size distribution are easily lost at this stage and in addition to the inherent properties of the catalyst; this loss could also be a function of the cyclone efficiency. An unstable process was observed within the first 30hrs of operation after which a steady-state process emerged.

A plot of the specific attrition rate obtained from Equation 3 is shown in Figure 5.

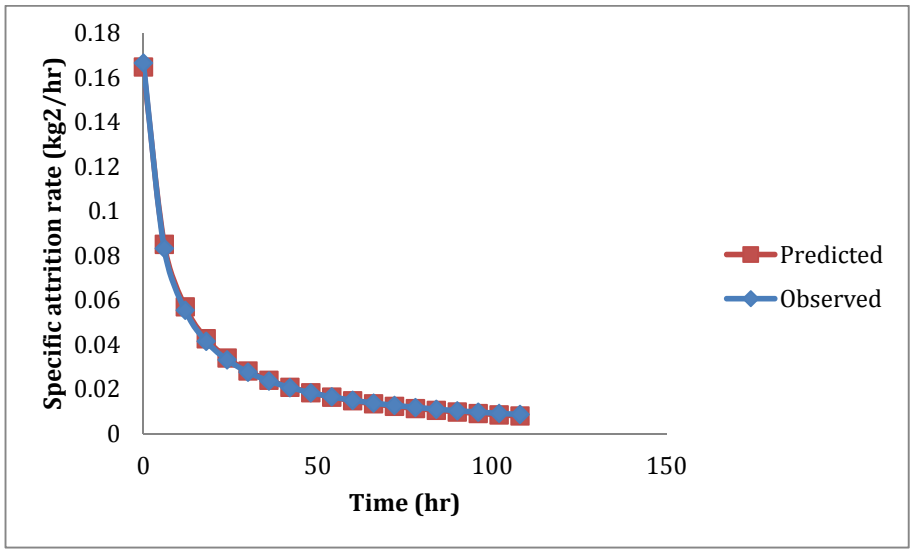

Figure 5: Specific attrition rate vs Time

The specific attrition rate as proposed by Wu *et al.,* (2015) is a property used to study attrition behaviour of catalysts which describes how the attrition rate changes with continuous change in the mass of the catalyst bed. Figure 5 shows that there was also a sharp decline in this property during the early turbulent-phase of this process, after which the decline became gradual and almost constant in the steady-state stage of attrition. The non-linear fitting of the technical data to Equation 4 was used to model the specific attrition rate. The estimated statistical parameters of the regression coefficient, standard errors, T-ratio, residual sum, and residual average were also determined.

Table 3: Parameter estimates for the prediction of specific attrition rate of FCC catalyst

R_c(kg²/hr)	D	R_0 (kg²/hr)	R^2	Standard Error	Residual Sum	Residual Average	RSS
1.08115	-1.08251	-0.00136	0.9994	0.000908	-1.77983E-15	-9.36751E-17	1.40304E-05
(0.0059)	(0.0061)						
182.1219#	-176.9888#						

Hence for the attrition time considered, the modelled equation predicting the specific attrition rate on this unit is as shown in Equation 7:

$$R_b = 1.08115 - 1.08251e^{-\frac{1}{t}} \quad (7)$$

Where: t is the attrition time (h).

Table 3 presents the results of parameter estimates of model fittings for the specific attrition rate. The fittings gave high correlation coefficient of determination, R^2, of 0.999 whereas low values of the standard errors across the parameters implies that the exponential decay model adequately describes the specific attrition rate of the catalyst. The R^2 value from this work was higher than 0.989 reported in the work of Wu *et al.,* (2016). From the model fitting, the attrition rate on this unit at steady state was found to be 1.08115 kg²/hr; this could be

attributed to the loss due to activities at the bubble phase, particle motion, inter-particle collision and gas flows necessary to keep the bed fluidized in accordance with the works of Thon *et al.,* (2013) and Werther and Reppenhagen (1999). The initial specific attrition rate was -0.00136kg^2/hr, whereas a total decay of 1.08251kg^2/hr was recorded for this unit over this operation. Standard Errors of 0.0059 and 0.0061 were obtained for the parameters R_c and D respectively. T-values 182.1219 and -176.9888 respectively give the ratio of the sample regression coefficient to the standard erroracross these parameters. Also, the Standard Error of 0.000908 over the unit indicates the statistical accuracy of the model prediction. RSS value of $1.403 * 10^{-5}$ shows very low discrepancy between the data and the estimation model hence a proof of the extent of its accuracy. Moreover, the percentage error of $7.90 * 10^{-3}$shows the closeness of the observed and predicted specific attrition values and therefore provides further confirmation of the precision and accuracy of these modelled parameters.

4.0 Conclusion

FCC unit operation results in catalyst attrition and this work have successfully evaluated the effect of attrition on the particle size distribution of a commercial-grade catalyst in an industrial operation. The changes observed in the particle size distribution and surface area of the catalyst both indicate the effect of attrition on the catalyst particle by this process. Attrition indices of 58.9 and -2.50 for the fresh and spent catalysts respectively are indicative of the material strength of these catalyst samples. Modelling of the specific attrition rate using the exponential decay model gave R^2 value of 0.999, SE 0.000908 and RSS value of $1.403 * 10^{-5}$. The percentage error between observed and predicted models of the specific attrition rates was 7.90 * 10^{-3}. These results show that the exponential model adequately predicted the rate of attrition of this catalyst grade. This study also shows that the least-sized particles were more attrited than the larger sized particles and hence a proof that catalyst attrition leads to an increased coarseness of the catalyst bed inside the regenerator.

Acknowledgement

The authors acknowledge the World Bank Africa Centre of Excellence for Oilfield Chemicals Research (ACE-CEFOR), University of Port Harcourt, Nigeria, for their support in carrying out this research.

References

Chiranjeevi, T., Ravichander, N., Gokak, D.T., Ravikumar, V., Choudary, N.V. (2014). The Selection of Fluid Catalytic Cracking Catalysts and Additives: The Significance of Attrition Studies, *J.Petroleum Science and Technology*, 32:470–478.

Coco, R., Arrington, Y., Hays, R., Findlay, J., Karri, S. (2010). Jet Cup Attrition Testing, *J. Powder Technology*, 200: 224-233.

Fiske, T.H. (2013). Correlation of Catalyst Morphology with Attrition Resistance and Catalytic Activity of Fischer Tropsch Catalysts, Thesis submitted to the Department of Chemical Engineering, Norwegian University of Science and Technology (unpublished).

Hartge, E.U., Heinrich, S., Werther, J., Puttmann, A., Thon, A., Patience, G., Bockrath, R. (2010). Prediction of catalyst attrition in an industrial Fluidized bed plant based on lab-scale attrition tests, refereed Proceedingss the 13th International Conference on Fluidization - New Paradigm in Fluidization Engineering, 1-8.

Kramp, M., Thon, A., Hartge, E.-U., Heinrich, S., Werther, J. (2011). The Role of Attrition and Solids Recovery in a Chemical Looping Combustion Process, *Oil and Gas Science and Technology – Rev. IFP Energies nouvelles,*66 (2): 277-290.

Meyer, A.J., Angwafor, J., Prytz, A.K., Tveten, E., Dyrøy, A. (2018).The Effect of Alumina Attrition Index on Breakage in Transport and Handling,Travaux 47, Proceedingss of the 36th International ICSOBA Conference, Belem, Brazil, 29 October - 1 November 2018**.**

Okwonna, O. O., Otaraku, I.J., Oduola, M.K., Okeke, E.O. (2019). Study of the Effect of Attrition on the Properties of Catalyst Used for Industrial FCC Operation, *International Journal of Engineering Science Invention (IJESI)*, 8(7): 53-66.

Püttmann, A., Hartge, Werther, J. (2006). E. U., simulation of the selective oxidation of n-butane to maleicanhydride in a riser/regenerator system, www.researchgate.net/publication/268287351.

Sadeghbeigi, R. (2000). Fluid Catalytic Cracking Handbook Design, Operation and Troubleshooting of FCC facilities. *Gulf Professional Publishing, Houston*, *2*, 234-275.

Tamjid, S., Hashemabadi, S.H., Shirvani, M. (2010). Fluid catalytic cracking: Prediction of catalyst attrition in a regeneration cyclone, Filtration+Separation September/October 2010, pg 29 – 33.

Thon, A., Kramp, M., Hartge, E., Heinrich, S., Werther (2013). Catalyst attrition in the CFB riser**,** 10th International Conference on Circulating Fluidized Beds and Fluidization Technology - CFB-10", T. Knowlton, PSRI Eds, ECI Symposium Series, (2013). http://dc.engconfintl.org/cfb10/78.

Vogt, E. T. C., Weckhuysen, B. M. (2015). Fluid catalytic cracking: recent developments on the grand old lady of zeolite catalysis, *J.Chem. Soc. Rev*, 44: 7342—7370.

Wei, J., Lee, W., Krambeck, F.J. (1977). Catalyst Attrition and deactivation in Fluid Catalytic Cracking system, *J. Chemical Engineering Science*, 32: 1211 – 1218.

Werther, J., Hartge, E. U. (2003). Modelling of Fluidized Bed Reactors, International Journal of Chemical Reactor Engineering, 9: 1-47.

Werther, J. and Reppenhagen, J. (1999). Catalyst Attrition in Fluidized-Bed Systems, AIChE J., 45(9): 2001- 2010.

Wu, D. F., Gu, Z. D., Li, Y. D. (2015). Attrition of catalyst particles in a laboratory-scale fluidised bed reactor. Chem Eng Sci. 2015: 135: 431–440.

Wu, D., Wu, F., Li, Y. (2016). Particle Size Effect on the Catalyst Attrition in a Lab-Scale Fluidized Bed, *AIChE Journal*, DOI 10.1002/aic.15458.

Wu, J. S., Li, X. G., Gong, M. Y., Zhang, Z. H., Guo, J. T. (2010). Kinetics and mechanism of several FCC catalysts. *J Chinese Soc Corros Protect*, 30(2):135–140.

Proceedings of the 49th NSChE Annual Conference
KADA 2019: pp 714-719

P3C-05: INVESTIGATING THE QUALITY PARAMETERS IN THE PRODUCTION OF EMULSION PAINT

H., Jamilu[1, *] and B. Mukhtar[1]
[1]Department of Chemical Engineering, Ahmadu Bello University, Zaria
E-mail: jharuna@abu.edu.ng/jamiluharuna220@yahoo.com; Tel.: +2349027346561

ABSTRACT
A critical issue faced by today's paint formulators is the rising cost and stringent quality standards. This has generated renewed interest in improving quality of the paint at an affordable cost. Thus, the need to study the parameters that affect the quality of paint for better formulation. In this paper, parameters that affect quality of paint in the production of emulsion paint were investigated. Six paint samples were produced based on difference in quantity of titanium dioxide, polyvinyl acrylic and sequence of mixing. The pH, drying time, viscosity and opacity of the samples as quality control parameters were analyzed and compared with the standard given by the Nigerian Industrial Standard (NIS). The main difference in the mixing sequence was indicated in the methodology. Results revealed that samples A to F had range of values for pH (9.5 – 10), drying time (45 – 50 min), viscosity (24 – 25 cP) and opacity (5.1 – 7.01 m^2/L), which were all within the (NIS 278) limit. However, sample F had the highest coverage area due to unique sequence of mixing.

Keywords: Opacity; viscosity; drying time; pH; sequence of mixing; binding power

1.0 INTRODUCTION
Paint is any liquefiable or mastic composition that, after application to a substrate in a layer, converts to a solid film. It is commonly used to protect, colour or provide texture to objects. Paint can be made or purchased in many colours and in many different types, and it is typically stored, and applied as a liquid, but dries into a solid (Benedson, 1989).

Paint was first used as a protective coating by the Egyptians who applied pitches and balsams to exposed wood of their ships. During the middle ages, some inland wood also received protective coatings of paint, but due to the scarcity of paint, this practice was generally limited to store front and signs. Around the same time, artist began to boil resin with oil to obtain highly miscible (mixable) paint and artist of the fifteenth century were first to add drying oils to paint, thereby hastening evaporation. They also adopted a new solvent, linseed oil, which remained the most commonly used solvent until synthetics replaced it during the twentieth century (Benedson, 1989).

Paint generally exist in two forms; water-based paint and solvent-based or oil-based paint. A water-based paint is a type of paint in which the solvent is mainly water, it is classified into an emulsion paint (smooth paint) and a texture/texcoat paint. While oil-based paint is a form of paint in which the solvent is kerosene related, example of this paint is gloss finish paint and matt finished paint.

Emulsion paint is a water-based paint principally used for internal and external surface coatings, mostly in buildings for appearance and protection. The processes involved in paint production, and quality of emulsion paint depend largely on the properties of its constituents and the ratios of these constitutions. The constituents generally used for the production of emulsion house paints include; prime pigments, solvents, extenders pigments, binders and additives (Surajudeen and Yahaya 2010). Solvent is used to mix the other components and

blend it together in order to have a uniform solution while extender is used for improvement of adhesion, ease of sanding and film strength, example is calcium carbonate. Binder is used to hold the pigment particles together and help them to adhere to the surface, it is also largely responsible for the protective qualities and durability of the paint (Douglas, 1989). Pigments give colour and opacity to paints. Amongst the organic pigments, particularly important are anthraquinone derivatives while the most inorganic pigment is Titanium dioxide. Additives are used to modify the properties of the paint, depending on the type of paint and intended use. Additive may include, ammonia, kalgon, formaline and genepurl.

Abdullah (1997) reported that titanium dioxide which is a major ingredient in paint manufacturing is imported. Nigeria only provides 25% of the paint industry Kaolin and lime stone (calcium carbonate). Most of the chemicals needed for paint production in Nigeria are imported with the fright rates and import duties, increasing the prices of paint raw materials. Abdullah (1997) noted that Nigeria paint manufacturing has been highly dependent on foreign equipment, machinery and raw material partly sue to technological backwardness and the industrialization policies particularly import substitution, of the raw materials. In recent times, with the fluctuating economy people now appear to patronize locally made products, including paints produced with a high percentage of local raw materials (Opara, 2014). Therefore, it is important to investigate the quality parameters of emulsion paint

The quality of an emulsion paint depends solely on the quality of ingredients, composition of the formulation and sequence of mixing. All ingredients used in the production of emulsion paint play a vital role in ensuring the quality of the paint. In this paper, the most important ingredients which include, titanium dioxide, polyvinyl acrylic and calcium carbonate were considered. In the constituents for production of emulsion house paints, binder (PVA) usually takes between 17 to 33% total cost of production depending on the paint type and this raw material is not available locally, therefore imported. Hence the high cost of this raw material (PVA – binder) leads to high cost of paint production (Surajudeen and Maiwada 2015). This has generated renewed interest in improving quality of the paint at an affordable cost. Thus, the need to study the parameters that affect the quality of a paint for better formulation.

2.0 MATERIALS AND METHOD

2.1 Material: The raw materials were obtained from EMMYBIZ chemicals, Sabon Gari, Zaria.

Table 1. Materials and their brand name

Material	**Brand**
Calcium Carbonate	Calco, freedom groups
Titanium dioxide	Du Poun Ti Pure
Polyvinyl Acetate (PVA)	Pexi Chem Private Lmtd. New Delhi
Natrosol (thickner)	Natrosol performax™ Ashland
Defoamer	SAF 130
Ammonia (28%)	Bird brand Ammonia
Water	Laboratory tap water
Kalgon	Kalgon

Equipment: Some of the equipment used are; Digital weighing balance HZ-2003, AI521 PH800 Laboratory Benchtop pH Meter, Rotary Viscometer Viscosity Tester (NDJ-1), Beakers, measuring cylinders, Plastic containers, Brush, stop watch, Wall and Ceiling board.

The quality control parameters were pH, drying time, viscosity and opacity.

2.2 Procedure for the Production of the Emulsion Paint Samples

For sample A, B, C, D and E, required amount of water was initially measured and put into a mixer with a mechanical stirrer, measured amount of Calgon was dispersed into the mixer and the stirrer was switched on. Required quantity of calcium carbonate was gradually added into the mixer and stirring was continued at 420 rev/min. Then measured quantity of Titanium dioxide was gradually added into the mixer and allowed to grind, measured quantity of Natrosol was gradually added and the resultant mixture was stirred continuously for about 20 min (Opara, 2014) to be well mix after which PVA and other ingredients were then added orderly as itemized in Table 2 in their measured quantity and the mixture was allowed to mix properly before packaging. For sample F, the sequence of addition of ingredient was as itemized in Table 3 and the same procedure was applied as in Sample A. Different colours were however formed by different choices of colour paste.

Table 2: Materials (in order) used in Production of 0.5 L Sample A paint

S/N	Material	Quantity
1	Water	0.27 L
2	Calgon	0.0027 kg
3	Calcium carbonate	0.34 kg
4	Titanium dioxide	0.0125 kg
5	Natrosol	0.0025 kg
6	PVA	0.025 L
7	Genepur	0.0005 L
8	Ammonia	0.001 L
9	Yellow Iron Oxide	0.004 kg
10	Deformer	0.00042 L

2.2.1 Production of 0.5 L of Sample A

Applying the same procedure as in Sample A paint, Samples B and C were produced with the same quantity of materials as itemized in Table 2 except that the quantity of titanium dioxide was replaced with 0.0120 kg, 0.0130 kg respectively, sample C and D were also produced with the same quantity of materials as itemized in Table 2 except that the quantity of PVA was replaced with 0.020 L and 0.030 L respectively. Different sequence of mixing was used in the production of sample F as it is orderly itemized in Table 3 but the same formulation as in Sample A in Table 2.

Table 3. Materials (in order) used in production of 0.5 L Sample F paint

S/N	Material	Quantity
1	Water	0.27 L
2	Ammonia	0.001 L
3	Genepur	0.0005 L
4	Calgon	0.0027 kg
5	Titanium dioxide	0.0125 kg
6	Calcium carbonate	0.34 kg
7	PVA	0.025 L
8	Deformer	0.00042 L
9	Yellow Iron Oxide	0.004 kg
10	Natrosol	0.0025 kg

.

2.3 Analysis of Paint Properties

2.3.1 pH Test
Fifty (50) ml of the paint produced was poured into a beaker and the pH was determined using a pH meter. The same procedure was also used to determine the pH of the other samples, the measurement were taken six times.

2.3.2 Drying Time
One hundred (100) ml of the paint produced was painted on a wall and allowed to dry at room temperature recoding the time it took for the paint sample to dry. The same procedure was also used to determine the drying time of the other samples.

2.3.3 Viscosity Test
Fifty (50) ml of the paint produced was poured into a beaker and the viscosity was determined using viscometer. The same procedure was also used to determine the viscosity of the other samples.

2.3.4 Opacity Test
One hundred (100) ml of paint was poured on to a beaker. It was used to paint the wall and the area of the painted surface was measured to find the opacity of the paint.

Opacity (m^2/L) = area of painted surface/volume of paint used 1 (Flick, 1989)

3.0 RESULTS

3.1 Measured Parameters
Table 4 gives the values for the measured quality parameters.

Table 4. pH, drying time, viscosity and opacity of different samples

S/N	Sample	pH	Drying time (min)	Viscosity (cP)	Opacity (m^2/L)
1	NIS	8-10	30-50	15-25	5-8
2	Sample A	9.5	45	24.5	5.2
3	Sample B	9.8	46	24	5.1
4	Sample C	9.9	49	25	5.6
5	Sample D	10	48	24.5	5.2
6	Sample E	9.5	49	24.5	5.2
7	Sample F	10	50	24	7.0

From Table 4, the six different samples of paint produced had pH values within the range approved by the Nigerian Industrial Standard as in SON (2005). Even though all the pH values are within the NIS range, there was a slight variation in the pH values among the paint samples produced which was due to difference in formulation.

The paint is usually basic because most of the materials used in the formulation are basic in nature and should by any means the paint happens to be acidic it will not stay properly on the surface on which it is applied because it will affect the binding ability of the binder (Talbert, 2008).

The drying time from Table 4 shows that the paint produced with sequence of ingredient addition indicated in Table 3, sample F, took longer time to dry than the paint produced with sequence of ingredient addition indicated in Table 2, sample A, even though all the values were within the NIS range. Low drying time is preferred because, should it fail to dry fast there is tendency that dust, insect, and possibly rain (when used outside) may affect the appearance of the paint (Bently, 1990).

Sample A has viscosity of 24.5 cP while sample B and C had viscosity of 24 and 25 cP respectively, which was due to increase and decrease in quantity of titanium dioxide used. Sample F had viscosity of 24 cP, this was due to difference in the sequence of mixing used. In satin emulsion paint the higher the quantity of titanium dioxide used the higher the viscosity of the paint and the higher the coverage. In this research work, the calcium carbonate content was kept constant, therefore the higher the viscosity the better the paint. Water can be used to reduce the viscosity during application, but it is applied only to high quality paint.

Opacity refers to the ability of a coat of paint, when applied at a given thickness, to hide the substrate. From Table 4 it can be seen that the paint produced with higher quantity of titanium dioxide as in sample C had lager coverage than the samples with low quantity titanium dioxide as in sample A and B. However, sample F had the highest coverage even though small quantity of titanium dioxide was used most probably due to the difference in its formulation sequence. The opacity was measured without any application of water to the paint. However, it can be increased by addition of water to the paint. All the parameters measured are in conformity with that of NIS

3.0 CONCLUSION

From the findings of this study on the production of different samples of emulsion paint it was noted that, sample F had the highest coverage area followed by sample C, sample E, sample A, sample D and then sample B with the following opacity values 7.01, 5.6, 5.23, 5.2, 5.2, and 5.1 m^2/L respectively. The variation in the quantity of titanium dioxide used resulted in the change in opacity and viscosity of the paint and led to sample C to have higher opacity and viscosity than sample A, B, C, D and E. Even though sample F had less quantity of titanium dioxide than sample C and less volume of PVA than sample E, due to difference in the sequence of mixing it produced paint with higher coverage/opacity and higher binding power. Though the binding power was not experimentally measured but it was assessed by the use of hand on the applied paint. Conclusively, it is more qualitative and cheaper to produce emulsion paint using the formulation and sequence of mixing applied to sample F as it required less PVA and titanium dioxide which are expensive to yield a desired product. Finally, sequence of mixing/addition of raw materials play a significant role in the production of emulsion paint.

REFERENCES

1. Douglas J.M. (1998) Conceptual design of chemistry process, McGraw Hill, New York
2. Flick, E.W., (1989) Handbook of paint raw materials, 2nd ed. Noyes Data corp.
3. Grant, E.L., (2000) Statistical quality control McGraw Hill, New York
4. Rushton J.H, Costich E.W and Everett H.J. (1950) Emulsion and water-soluble paint *Chemical Engineering Progress* volume 46, No. 9, September.
5. S. Abdulsalam, Zebulu D. M., (2015) "Production of Emulsion House Paint Using Polyvinyl Acetate and Gum Arabic as Binder" *International Journal of Materials Science and Applications*. Vol. 4, No. 5, 2015, pp. 350-353. doi: 10.11648/j.ijmsa
6. Standard Oganization of Nigeria (SON) 2005

7. S. Abdulsalam, and Yahaya, Y. U. (2010), "Effectiveness of Gum Arabic as a Binder in Emulsion House Paint", *Global Journal of Engineering Research*, 10 (1 and 2): pp. 83-89, 2010.
8. Talbert, R., (2008). ''Paint technology handbook" volume 1, CRC press New York.
9. Nigerian Industrial Standards, NIS, (1990) Test Methods for Paints and Varieties, NIS 278
10. Opara Patrick N 'Production of Textcoat and Emulsion Paints Stainless for Youth Skill and Entrepreneurship Empowerment Program' Journal of Educational Policy and Entrepreneurial Research (JEPER) www.iiste.org Vol.1, N0.1, September 2014. Pp 96-102
11. Benedson A.M., (1989). Marine painting manual, London
12. Bentley J. and turner, G.P.A. (1990). Introduction to paint chemistry and principle of paint

Proceedings of the 49th NSChE Annual Conference
KADA 2019: pp 720-726

P3C-06: COMPARING THE PERFORMANCES OF NATURAL AND SYNTHETIC DRAG-REDUCTING POLYMERS IN HORIZONTAL PRODUCED WATER FLOWS

A. Ahmed[1], A. Abubakar[1*], L. C. Edomwonyi-Otu[1,2], N. Yusuf[3]
[1]Department of Chemical Engineering, Ahmadu Bello University, Zaria, Nigeria
[2]Department of Chemical and Petroleum Engineering, Delta State University, Abraka, Nigeria
[3]Department of Chemical and Petroleum Engineering, Bayero University, Kano, Nigeria
*Corresponding Author, Email: abubakara@abu.edu.ng, +2348036951137

ABSTRACT
Enormous amount of energy is dissipated in pumping oil-water emulsion along pipelines over a long distance especially in petrochemical industries. Energy loss in form of pressure loss occurs due to skin friction and turbulence in the flow. The use of drag reducing polymers (DRPs) in transporting fluids is known to offer large economic advantage in maintenance and transportation cost. This research focused on comparing the performances of synthetic (polyethylene oxide (PEO), MW = 8 x 10^6) and natural (okra mucilage with MW = 1.76 x 10^6) drag-reducing polymers in horizontal produced water (a depleted dispersed oil-water mixtures) flows in 12- and 20-mm ID horizontal pipes. The dispersed oil-water flows here refer to tap water mixed with Bonny Light crude oil of fractions α = 0, 0.005, 0.01 and 0.02, respectively. The piping network for the experimental flow rig was made of unplasticized polyvinyl chloride (uPVC). Master solutions of the polymers in water were prepared with the following compositions: 1000 ppm of PEO and 2000 ppm of okra mucilage. More dilute solutions were subsequently achieved when these master solutions were injected at controlled flow rates during the flow experiments. Drag reductions (DRs) were measured at different oil-water emulsion flowrates in the range 10 – 40 liters/min. The results showed maximum DRs of 75.23 % with 30 ppm of PEO and 66.44 % with 400 ppm of okra mucilage for undiluted tap water (α = 0). Furthermore, analyses of the results for depleted oil-water emulsions (α = 0.005, 0.01 and 0.02) showed that drag reduction with the synthetic PEO was about 10- 15.2% higher than that for the natural okra mucilage.

Keywords: Oil-water emulsion, drag reduction, PEO, okra mucilage

1.0 INTRODUCTION
Transporting oil-water emulsions in pipelines is ubiquitous in chemical and petroleum industry operations. These include long distance fluid transport, petroleum products loading and offloading in refineries, and fire-fighting. All these have associated energy losses. Drag reducing agents reduce these losses consequently increasing pipeline capacity and power savings.

Even though the concentrations of the oil- water emulsion affect the pumping energy loss because higher concentrations have higher viscosities and thus higher viscous losses when transported through pipelines, more of the pumping power is dissipated in overcoming and suppressing the turbulence structures in the flow. Therefore, oil viscosity, concentrations and droplets size in pipes are essential in understanding any drag reduction investigation in oil-water or water-oil emulsion. Extensive investigations have been reported mostly on 10 – 98% water-oil/oil-water emulsions (Angeli and Hewitt, 1998; Lum *et al.*, 2004; Al-Yaari *et al.*, 2009; Al-Sarkhi, 2010; Al-Wahaibi, 2012; Al-Wahaibi *et al.*, 2013; Al-Yaari *et al.*, 2013; Al-Wahaibi *et al.*, 2014). The need to further study the produced water emulsion in the drag reduction phenomena is of great importance. The work, which is still ongoing, seeks to compare the drag reduction of two types of polymers in depleted or dilute oil-water emulsions (0 – 2 %), investigate the mechanism(s) involved and consequently suggest possible applications of drag

reducing agent (DRA) in produced water (a depleted oil-water emulsion) flows. Also, factors affecting DRA in turbulent flow and types of drag reducing agents will be discussed. Most importantly, the effect of PEO and okra mucilage polymer in produced water (water separated from the oil during oil exploration) in horizontal pipe will be investigated. However, this paper only compares the performances of two polymers (PEO and okra mucilage) in reducing pressure drops in the depleted oil-water emulsions.

Drag-reducing agents are polymeric chemicals which when added in minute quantity drastically reduces turbulent mode of transporting fluids. The different categories of these agents are surfactants, polymers and fibers (Edomwonyi-Out, 2014). There are different theories that described their mechanisms of action. Lumley (1969), postulated that the increased extensional viscosity due to the stretching of randomly coiled polymers to give rise to the drag reduction. De Gennes (1990) argued that the elastic energy stored in the macromolecules causes drag-reduction.

The effectiveness of a DRA can be quantified by Equation 1 below

$$\%DR = \frac{\Delta P_{without\ DRA} - \Delta P_{with\ DRA}}{\Delta P_{without\ DRA}} - - - - - - 1$$

where $\Delta P_{without\ DRA}$ = Pressure drop without DRA, $\Delta P_{with\ DRA}$ = pressure drop with DRA

The pipe flow Reynolds number whose magnitude indicates whether the flow in the pipe is laminar or turbulent is given by Equation 2:

$$Re = \frac{\rho v d}{\mu} - - - - - 2$$

where Re = Reynold number, ρ = fluid density, v = average flow velocity, d = pipe diameter and μ = fluid viscosity.

2.0 MATERIAL AND METHODS

2.1 Materials

The experimental flow facility consists of three sections (Figure 1). The storage section consists of 250-liter capacity of separation tank and 200-liter capacity each of water and oil tanks. The drag reducing polymers used were synthetic polyethylene oxide (PEO) and natural Okra mucilage and the testing fluids were tap water and Bonny light crude oil. A centrifugal pump (model Jet102M/N.31227) was used for the circulation of the oil-water emulsion throughout the loop facilities. A 1-m long acrylic pipe with two pressure ports of 0.5 m apart was inserted along the PVC pipe for taking the pressure drop using u-tube manometer. A port just before the Y-junction was used for polymer injection.

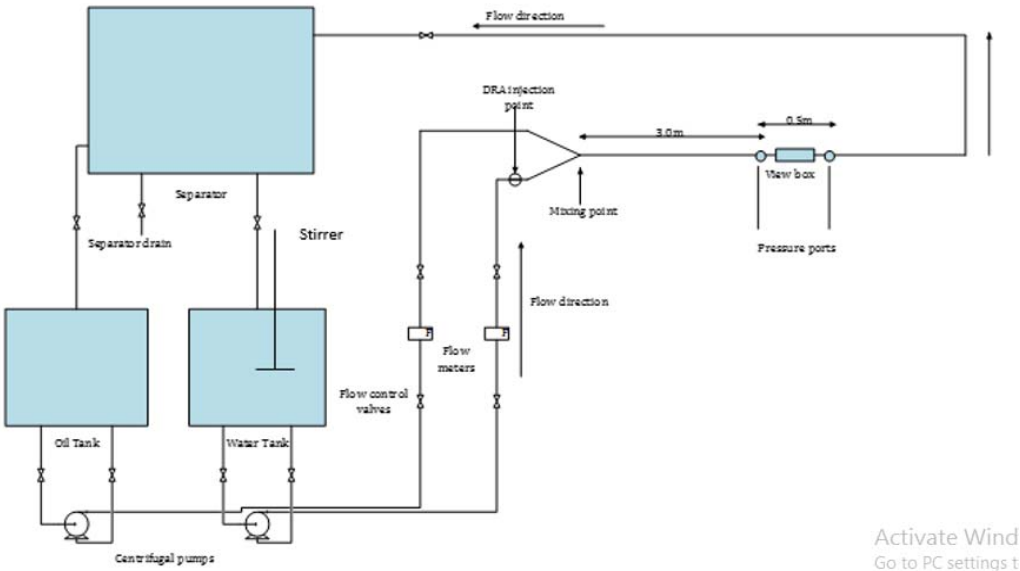

Figure 1: Schematic diagram of experimental flow loop facility

2.2 Methods

The produced water of oil fractions 0, 0.005, 0.01 and 0.02 were prepared in the water tank, and circulated through the flow system via the testing section, where pressure drop measurement was taken. To achieve stable oil-water emulsion, a mixer (HM-20) of 12400/rpm was used to agitate the mixture for 30-40 minutes in order to ensure dispersion of oil evenly into the water. A master solution of 1000 ppm PEO were prepared where 5g of polymer were sprinkle in 5 litres of distilled water and stirred until completely form a clear viscous solution. Similarly, a master of 2000 ppm of okra mucilage were prepared by soaking 10 gram of chopped okra in 5 litres of distilled water, warmed and allowed to stay overnight. The extract from the okra were sieved and a clear thick viscous colour called mucilage were produced. Calibration of flow meter (LZM-20J) and polymer injection pump (Ne-9000) were conducted to ensure accurate delivery of the require amounts of testing fluid and polymer solutions along the flow system. The experiment was initially run at 0 oil fraction (i.e. water only) at 10-50 ppm concentrations of PEO between and 30 ppm recorded the maximum DR and at 100-500 ppm concentrations of okra mucilage and 400 ppm gave a maximum DR. Each pressure drop was taken before and after polymer addition at a corresponding flowrate. The DR was calculated using Equation (1). Then the same procedure was repeated on the produced water of oil fractions of 0.005, 0.01 and 0.02 from which the effectiveness of natural and synthetic polymers on drag reduction were noted and compared.

3.0 RESULTS AND DISCUSSION

The effects of synthetic (PEO) and natural (okra mucilage) drag-reducing polymers in simulated produced water in horizontal pipe flows with different oil fractions in the range 0 to 2%, and pipe IDs of 12 and 20 mm are presented in Figures 2 – 5.

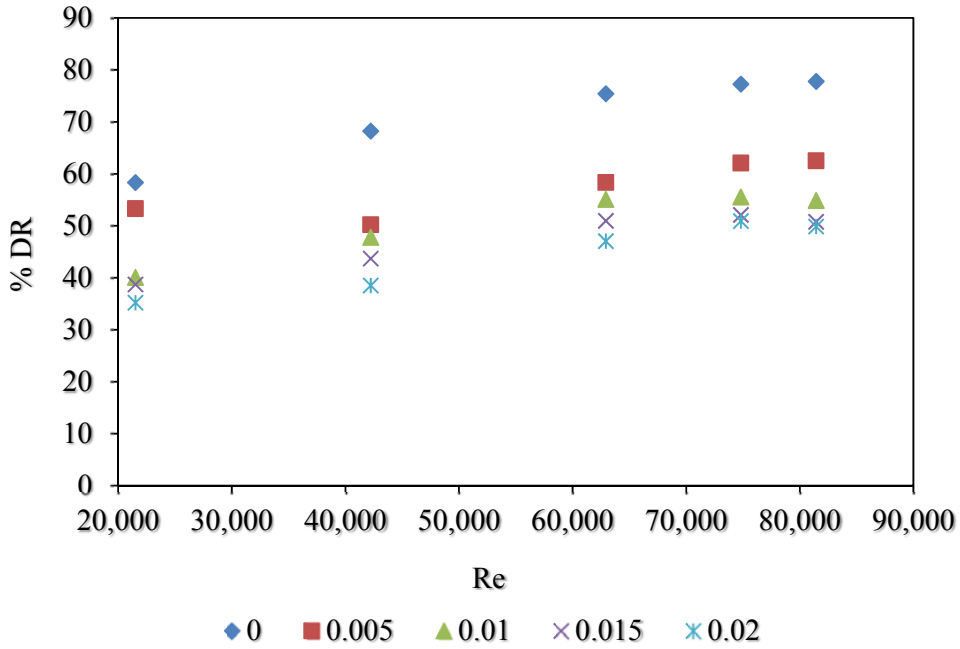

FIGURE 2: DRAG REDUCTION IN PRODUCED WATER AGAINST REYNOLDS NUMBER AS A FUNCTION OF OIL FRACTION FOR 12-MM ID PIPE USING PEO

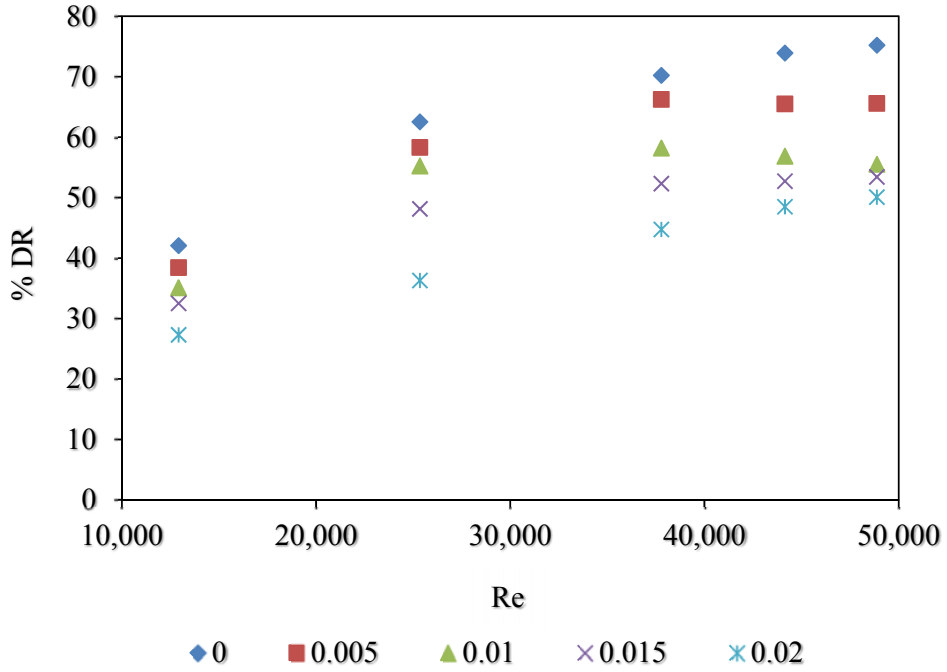

FIGURE 3: DRAG REDUCTION IN PRODUCED WATER AGAINST REYNOLDS NUMBER AS A FUNCTION OF OIL FRACTION FOR 20-MM ID PIPE USING PEO

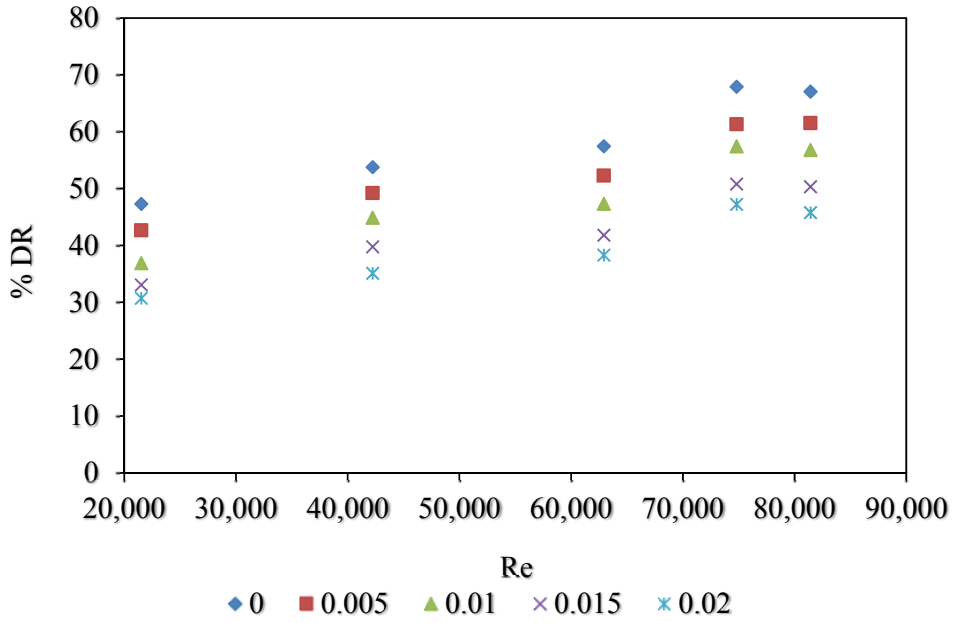

FIGURE 4: DRAG REDUCTION IN PRODUCED WATER AGAINST REYNOLDS NUMBER AS A FUNCTION OF OIL FRACTION FOR 12-MM ID PIPE USING OKRA MUCILAGE

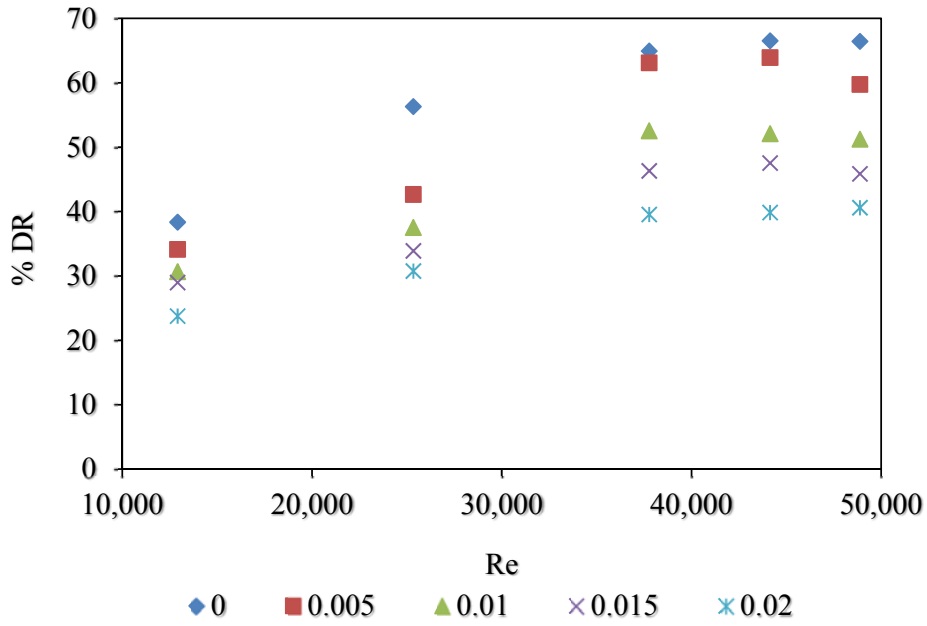

FIGURE 5: DRAG REDUCTION IN PRODUCED WATER AGAINST REYNOLDS NUMBER AS A FUNCTION OF OIL FRACTION FOR 20-MM ID PIPE USING OKRA MUCILAGE

In Figures 2 and 3, increase in DR with PEO concentration was observed until maximum drag reductions were achieved. In Figure 3 in particular, further addition of additives does not have

any significant effect on the drag reduction because the produced water had become saturated with respect to the polymer at that point (Lumley, 1969). With produced water emulsion of oil fraction 0.005 – 0.02, drag reduction decreased at same Reynold number and 30 ppm polymer concentration. This is because the concentration of the emulsions is increased with oil droplets and thus increased the pressure drop.

In Figures 4 and 5, the addition of natural polymer (okra mucilage) exhibit slightly lower drag reduction compared with that of the PEO in produced water emulsion. For instance, in Figures 3 and 5, about 66.44% maximum drag reduction was produced by okra mucilage as compared to the 75.23% produced by PEO at the same 20-mm ID pipe diameter and 0 oil fraction. The lower effectiveness of okra is due to its lower molecular weight and probably its degradability as reported by Al-Wahaibi *et al.* (2014).

4.0 CONCLUSION

The drag reduction by the two polymers studied on produced water pipe flows was pronounced in the polymer concentration range studied in this work. However, measures show a 10 – 15 % DR advantage of PEO over okra mucilage. This is attributable to possible degradation of okra mucilage and its lower molecular weight compared to PEO.

REFERENCES

Al-Sarkhi, A. (2010). Drag reduction with polymers in gas-liquid/liquid-liquid flows in pipes; A literature review. *Journal of Natural Gas Science and Engineering* 2. pp 41-48.

Al-Wahaibi, T. (2012). Pressure gradient correlation for oil-water separated flow in horizontal pipes. Experimental Thermal and Fluid Science 42: 196-203.

Al-Wahaibi, T., Al-Wahaibi, Y., Al-Ajmi, A., Yusuf, N., Al-Hashmi, A. R., Olawale, A. S. and Mohammed, I. A. (2013). Experimental investigation on the performance of drag reducing polymers through two pipe diameters in horizontal oil-water flows. Experimental Thermal and Fluid Science 50(0): 139-146.

Al-Wahaibi, Y.M., Abubakar, A., Al-Hashim A.R., Al-Ajmi A. (2014). Influence of Drag-reducing Polymer on Flow Patterns, Drag Reduction and Slip Velocity Ratio of Oil-Water Flow in Horizontal Pipe. *International Journal of Multiphase Flow, pp. 2–5.*

Al-Yaari, M., Al-Sarkhi, A., Hussein, I. A. and Abu Sharkh, B. (2013). Effect of drag reducing polymers on surfactant-stabilized water-oil emulsions flow. Experimental Thermal and Fluid Science 51(0): 319-331.

Al-Yaari, M., Soleimani, A., Abu-Sharkh, B., Al-Mubaiyedh, U. and Al-Sarkhi, A. (2009). Effect of drag reducing polymers on oil–water flow in a horizontal pipe. International Journal of Multiphase Flow 35: 516-524.

Angeli, P. and Hewitt, G. F. (1998). Pressure gradient in horizontal liquid–liquid flows. International Journal of Multiphase Flow 24(7): 1183-1203.

de Gennes, P. G. (1990). Introduction to Polymer Dynamics. Cambridge, University Press, 56.
Edomwonyi-Otu, L. C., Chinaud, M. and Angeli, P. (2014). Drag reduction in stratified oil-water flows. BHR Group - 9th North American Conference on Multiphase Technology. Canada, OnePetro: 165-173.

Lum, J. Y., Lovick, J. and Angeli, P. (2004). Low Inclination Oil-water Flows. The Canadian Journal of Chemical Engineering 82: 303-315.

Lumley, J. L. (1969). Drag reduction by additives. Annual Review of Fluid Mechanics 1: 367-384.

Proceedings of the 49th NSChE Annual Conference
KADA 2019: pp 727-738

P3C-07: HIGH TEMPERATURE NAPHTHENIC ACIDS OXIDATION OF STEELS IN CRUDE OIL REFINIING

***Cybala, A. V, Okonkwo P. C., and El-Yakubu B.J.**
Department of Chemical Engineering, Ahmadu Bello University Zaria, Nigeria.
Key words: Corrosion, Naphthenic acids, mineral oil (Paraffin oil), Benzoic acid, Steel coupons.
*Corresponding author Email: cybala_vincent@yahoo.com Phone: +2347036014812

ABSTRACT
A study was carried out on the naphthenic acid oxidation of steels in crude oil refining units. Weight loss techniques was used to examine the kinetics of corrosion of steel coupon (Cs and type 305 (Cr18)) in an aromatic naphthenic acid of benzoic acid. The finding indicates type305 (Cr18) steels are suitable for crude distillation units (CDU) and vacuum distillation units (VDU) at high concentration and temperature of naphthenic acids. The corrosion rate on the steel samples shows that the mechanism obeys the Arrhenius type equation, with temperature exhibiting a higher impact on the corrosion rate than concentration. Austenitic stainless steel of type305 (Cr18) is observed to be resistant to naphthenic acid corrosion due to the presence of high chromium (17.6 weight percent) and molybdenum (0.319 weight percent) compare to carbon steel. The SEM analysis identified forms of corrosion, which includes general corrosion, hydrogen blistering corrosion, erosive corrosion and pitting form of corrosion on the steels surfaces.

1.0 Introduction

1.1 Background of the Study

Corrosion is the deterioration of metal as a result of its interaction with the environment. Deterioration of the metal is caused by chemical or electro chemical reaction with the environment, whereas, destruction is mainly caused by mechanical wear or abrasion (Fontana, 1910). Fundamentally all crude oils consist of sulfur compounds, inorganic salts, water, organic acids and oxygen that initiate corrosion (Jayaraman *et al.,* 1993). Among these impurities, carboxylic acids, commonly known as naphthenic acids create corrosion problems during high temperature operations in petroleum refinery. Blount suggested that crude oils contained three distinct sources of corrosion in distilling equipment: Naphthenic acids, Sulfur and Magnesium Chloride (Derungs, 1956). Naphthenic acids are present in many crude oils in varying amounts and provide a class of corrosion such as pitting. With naphthenic acid constituting 50 weight percent of the total acid in crude oil (Sami, 2001). Naphthenic acids are saturates, mono-aromatics and di-aromatics (Derungs, 1956). 70% of naphthenic acid are composed of saturated ring compounds (Sarkar, 2009). The term "Naphthenic acids", as used in the petroleum industry, refers collectively to all of the carboxylic acids present in crude oil (The American Petroleum Institute Petroleum HPV Testing Group, 2012). Naphthenic acids describe a collection of organic acids containing at least one carboxylic group (COOH) (Jauseau and Nesic, 2016).

Figure 1 shows examples of different naphthenic acid compounds of ring families (Z), alkyl (R) and Carbonyl (m) side chains.

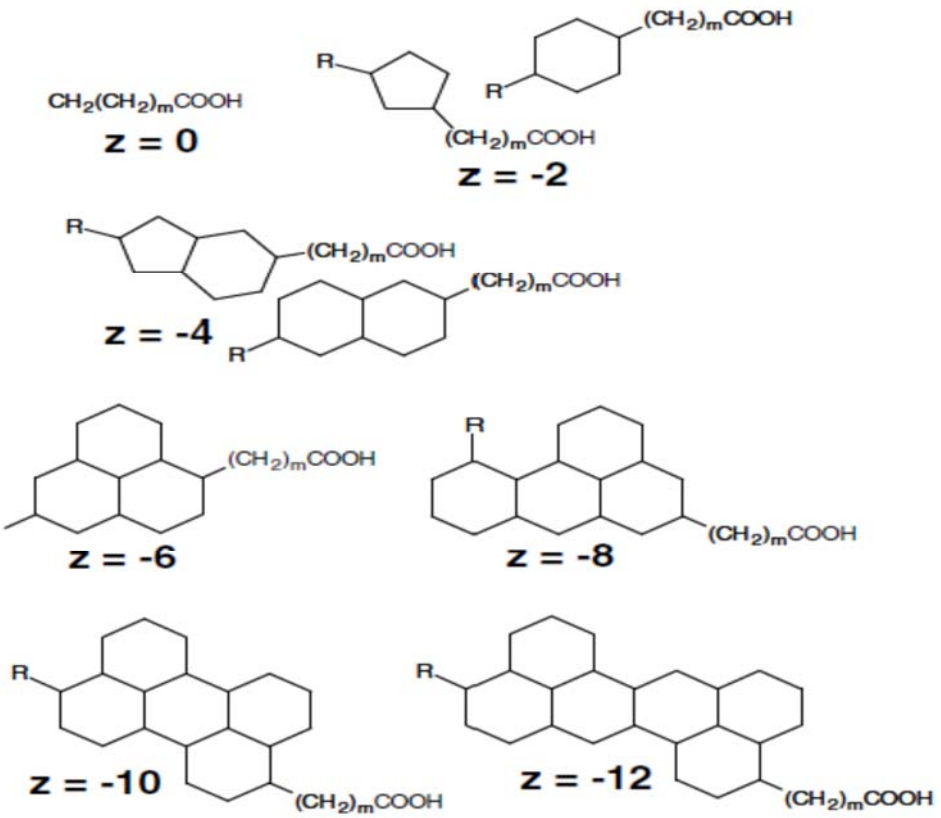

Figure 1: Example of different naphthenic acid compounds (source: Frank *et al.,* 2008).

The general mechanism accepted by the corrosion community can be expressed by the following reaction:

$Fe\ (s) + 2RCOOH\ (oil) \rightleftarrows Fe(RCOO)_2\ (oil) + H_2\ (g)$ ..... (1)

The Naphthenic Acid (NA) corrosion mechanism in reaction (1) describes the attack of naphthenic acids (RCOOH) on the iron metal (Fe) producing iron naphthenates ($Fe(RCOO)_2$), which are soluble in oil (Jauseau and Nesic, 2016).

1.1.1 Factors Affecting Naphthenic Acid Corrosion.

Naphthenic acid corrosion intensity is defined by the following factors: kind of acids or types of naphthenic acids, Total Acid Number (TAN) or concentration (in some cases), temperature, flow velocity, type of alloy and its surface condition (presence of passive layers), and duration (Groysman *et al.,* 2017).

Concentration of Naphthenic Acid.

The naphthenic acid content is commonly determined by titration with potassium hydroxide (KOH). The value obtained is referred to as neutralization number or Total Acid Number (TAN), expressed in milligrams of KOH required to neutralize the acid constituents present in 1g of sample. Crude with TAN higher than 0.5 are considered as potentially corrosive (Speight, 2014a). Values of TAN in the range of 0.1 to 3.5 mg/KOH are common but findings have shown TAN values in excess of 10 mg/KOH (Kane and Cayard, 2002). As the distributions of

naphthenic acids within crude blends varies widely, and the corrosivity of individual acids vary, primarily, with the molecular weight (Slavcheva, *et al.,* 1998). TAN measures not only the organic acids but also the acidity generated by other compounds contained in the oil such as; H_2S, CO_2, $MgCl_2$, and $CaCl_2$ (Turnbull *et al.,* 1999). Thus, prediction of crude corrosivity based on TAN could be misleading in assessment of plant corrosion effects, the naphthenic acid content needs to be determined in order to predict exact corrosion rate (Shalaby *et al.,* 1996).

Temperature of the Refining Crude.

Naphthenic acids are corrosive within the temperature range of 220-400 °C (Jauseau and Nesic, 2016). Resulting to corrosion at process temperatures (248.8ºC-398ºC) within distillation columns (Speight, 2014a). However, above 400ºC no naphthenic corrosion is found due to decomposing or coking (Derungs, 1956).

Flow Rate

The effect of fluid flow has been emphasized as an important controlling factor of naphthenic acid corrosion in transfer lines of oil refineries. At high-velocity fluid flow areas, severe acid corrosion occurs within the crude distillation units at temperature ranges of 220ºC to 400ºC (Speight, 2014b). Often very severe corrosion is found in areas with high turbulent streams, whereas at neighboring places free from extensive turbulence only little corrosion occurs. This fact is most clearly demonstrated in return bends and tube inlets of furnaces (Derungs, 1956). Figure 2 shows the process flow diagram of the laboratory corrosion monitoring rig.

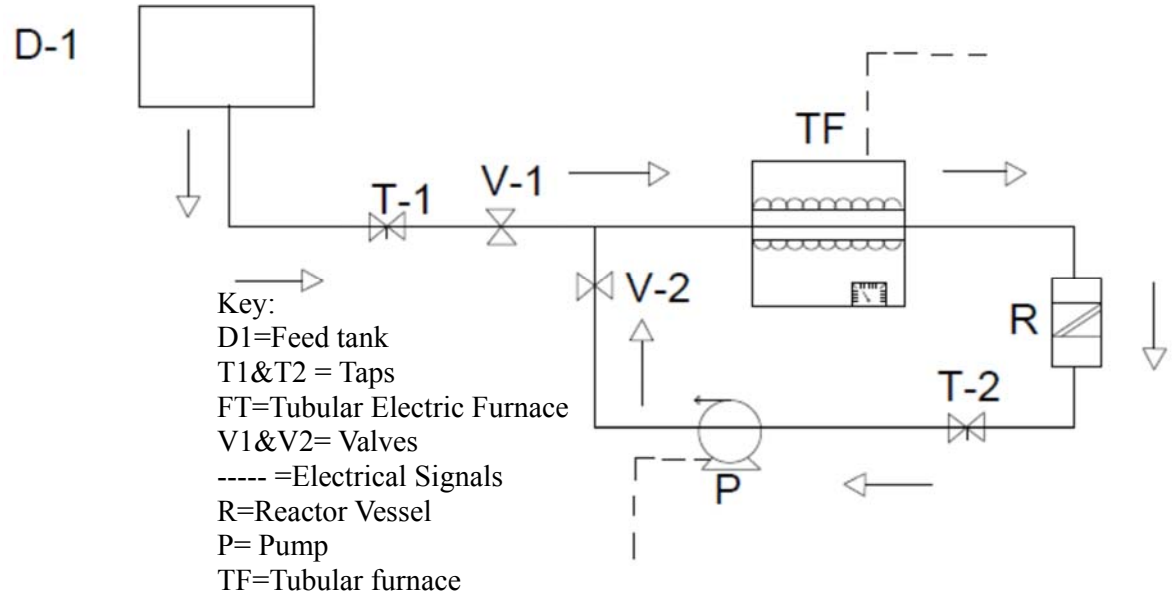

Figure 2: Process Flow Diagram (PFD).

The feed is charged from the feed tank D-1 and the quantity charged is controlled by the valve V1 as the feed passes through the Tubular electric furnace TF, which raises the feed temperature from room temperature to above 200ºC. The feed flows through the reaction chamber R where metal steel coupons are hung within the reaction chamber and are in contact with the feed passing through at varying flow rate via a pump P. T-2 is a tap used to collect samples of mock crude within the loop to confirm temperature and analytically confirm the flow within the loop. In addition to the schematic representation of laboratory corrosion monitoring rig in Figure 2. The orthographic view of the setup of the system is photographed in Plate I showing the fabricated mini laboratory corrosion monitoring rig of borosilicate glass

material piping (other than metal piping to avoid contamination/interference with the results of the metal steel coupons). That was built and connected to a pump equipped with a flow regulator to vary flowrate around the loop. The process pipe was then channeled through an Electric tube furnace, which generates the thermal heat that raises the temperature of the fluid (naphthenic acids) within the corrosion monitoring rig to the experimental process temperatures. Since in the refining industries, the influence of factors (such as temperature, TAN, fluid velocity, and material) tend to work simultaneously and cumulatively (Speight, 2014b).

Plate I: Orthographic view of corrosion monitoring rig set-up.

2.0 Materials and Method

The test fluid of naphthenic acid (Benzoic acid) was prepared in concentrations of 0.05 Mol/dm ^{3}, 0.15 Mol/dm^3, 3.5 Mo/dm^3, 4.5 Mol/dm^3, at a varying temperature of 220ºC, 280ºC, 320ºC and 360ºC . Since naphthenic acids are particularly reactive between 220ºC and 400 °C (Turnbull *et al.,* 1999). Noting that above 400°C naphthenic acids undergoes thermal decompositio. Mineral oil/white oil (paraffin) is used as a major solvent to simulate a hydrocarbon solution that can persist at liquid state at temperatures higher than 370ºC in this research. Two different experimental metal steel coupons were used, cut into dimensions of 1.5×1.5 by 0.2 inch, a Carbon steel (denoted as Cs) and type305 austenitic stainless steel denoted as (Cr18) sourced from Kaduna local metal scrap market also known as Pantaker were used to evaluate corrosion rate. All metal steel coupons surfaces were grounded using sand paper/emery paper, cleaned and degreased in ethanol and acetone then air dried and weighed immediately before corrosion tests. The original metal steel coupon weights were recorded as (Wo). Four coupons made from carbon steel (Cs) and four coupons made from type 305(Cr18) steel. Three coupons from each steel were used to measure weight change that is to determine the corrosion rate, while the fourth metal steel coupon was used as control for surface and cross-sectional analysis. After each test the coupons were removed and mechanically scrubbed with a stiff plastic brush, cleaned with ethanol and rinsed with acetone to remove lose scales (Naphthanates), the metal steel coupons were allowed to dry at atmospheric conditions and weighed again, this weight (W_f) was recorded as an average of at most three coupons with electronic weighing balance of 0.0000g. This last step of weighing was repeated if needed a few minutes until no change in the weight was recorded. The coupons re-immerse in a fresh solution, this procedure was done for a period of 7days (168hrs) on each metal steel coupons (at varying temperature, concentration) for a total of 672 hours (4weeks) to observe the corrosion rate at both short and long term exposure periods on experimental coupons. The observations were recorded, photographed and

Scanning Electron Microscopy (SEM) were done on each of the test metal steel coupons. Corrosion rates were calculated based on ASTM Standard G31-72.

The rate of corrosion is calculated as;

$$CR = \frac{Wo-Wf}{A \times t \times \rho steel} \times 24 \times 365 \qquad \ldots\ldots\ldots (2)$$

Where: CR= Rate of Corrosion in mm/yr, Wo**=** Original Coupon, Weight in g Wf**=** Final coupon weight in g ***A*** **=** Area in mm^2 , **t =** test duration in hours, ρ**Steel =** Steel density in $g/mm.^3$

3.0 Results and Discussion

XRF analysis was done prior to the exposure of the experimental metal steel coupons in order to identify the types of steels to be used on this research. This is to confirm that the steel coupons are the conventional steels applied in design and fabrication of crude distillation units, bubble caps, sieve caps, transfer lines, and pumps. Figure 3 is a carbon steel (Cs) XRF. From the chart it reveals a balanced spike of iron (fe^+) content from 0.00count/sec – 603.00count/sec at 5.10Kev- 5.13Kev, with infinitesimal/little presence of molybdenum from 0.00count/sec-0.01count/sec and 15.30Kev-15.05Kev, with no trace of chromium and nickel, which are good corrosion resistant element in refinery metal steels.

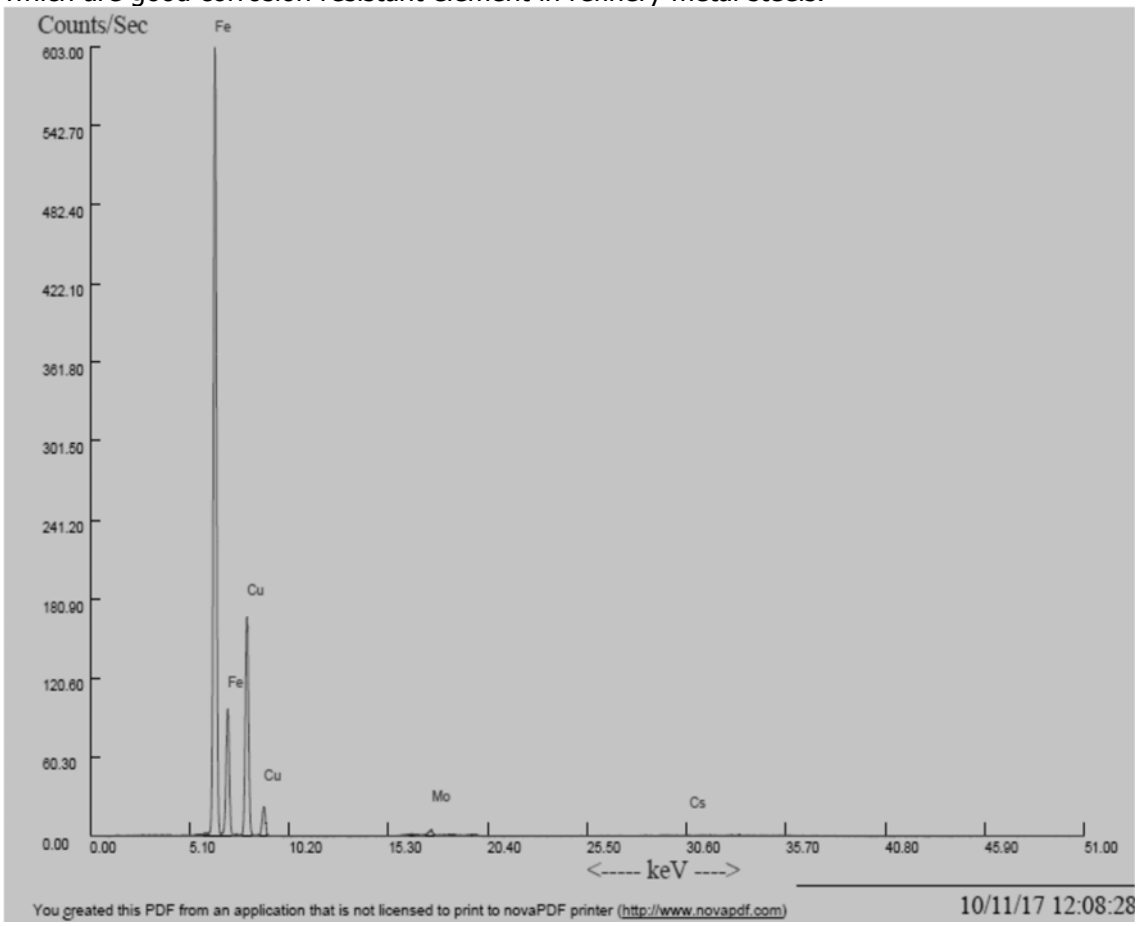

Figure 0: XRF chart of Carbon steel (Cs).

Figure 4 a type305 (Cr18) austenitic stainless steel XRF. From the chart it shows a balanced spike of iron (fe^{+}) from 0.00 count/sec.–301.00count/sec. at 5.10 keV -5.15 keV. Significant Chromium (Cr) content from 0.00 count/sec. -140.30 count/sec. at around 5.10 keV -5.12 keV with a good presence of Molybdenum (Mo) from 0.00 cont/sec. – 0.40 count/sec. at 15.10 keV -20.40 keV and significant amount of Nickel from 0.00count/sec-30.10count/sec at 5.15Kev-5.18Kev.

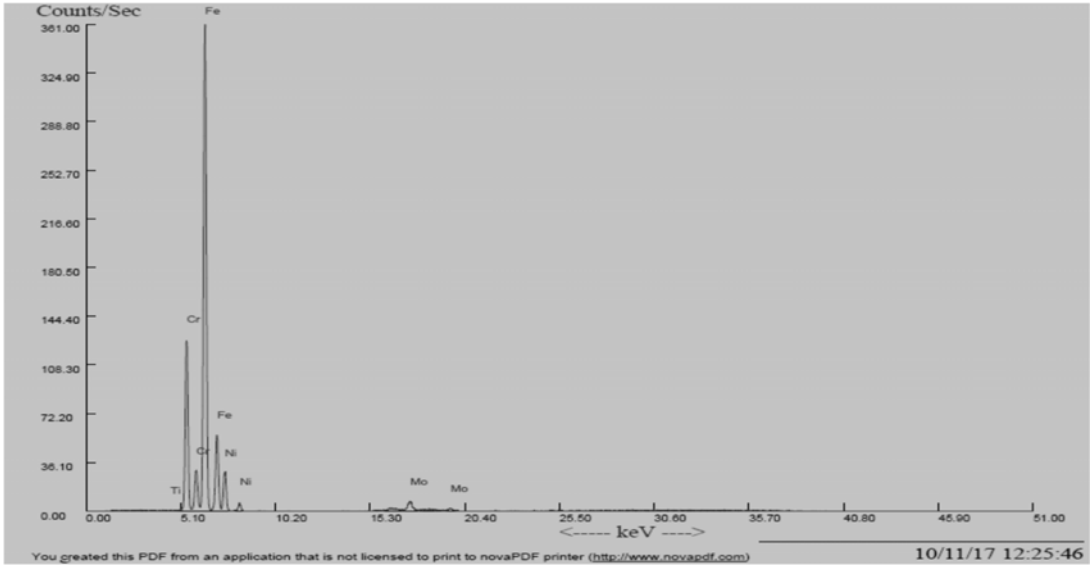

Figure 4: XRF of Type 305 (Cr18) Austenitic Stainless steel.

Molybdenum in the stainless steels limits the Fe-rich active spots and decreases the possibilityof Fe or Fe^{2+} bound with the $RCOO^{-}$ to form stable complexes (Wu et al., 2004).

Table 1: XRF weight percentage of elemental composition of metal steel coupons.

Components (W%)	Mn	Cr	Ni	Fe	Mo
Carbon steel(Cs)	0.485	-	-	65.144	0.021
Type 305(Cr18)	1.339	17.951	8.858	72.921	0.319

Chromium is a reactive element, its alloys passivate and exhibit excellent resistance to many environments. molybdenum has good corrosion resistance and is used for high temperature applications hence a good additive to stainless steels (Roberge, 2000). Plate II and III reveals the experimental steels before and after exposure to corrosive media.

Pl

Plate II and Plate III: Steel coupons before and after corrosion experiments.

3.1 Effect of Temperature:

The Table 2 shows increase in corrosion rate among steel coupons in naphthenic acids (Benzoic acid) at constant flow rate of 3.37 m^3/s and concentration of 0.15 Mol/dm^3 the *corrosion rate increased from 2.9226 mm/yr to 18.6472 mm/yr on carbon steel (Cs), from 0.04988 mm/yr to 7.3824 mm/yr on type305(Cr18) respectively. Revealing type 305 (Cr18) is the most resistant steel between the experimental steels in this present research.*

Table 2: Effect of temperature on corrosion rate of steels in naphthenic benzoic acid.

S/No	T Temp °C	corrosion rate r (mm/year)	
		Cr 18	Cs
1	220	0.04988	2.9226
2	280	1.7628	4.8597
3	320	2.7196	12.9941
4	360	7.3824	18.6472

Corrosion of most steels approximately triples with each 55ºC increase in temperature according to a field report by Gutzeit (Slavcheva *et al.,* 1998). The corrosion rate on steel coupons in Table 2 did not completely tripled but, agrees with Gutzeit. Figure 5 Shows linear increase in corrosion rate of steel coupons with increase in absolute temperature.

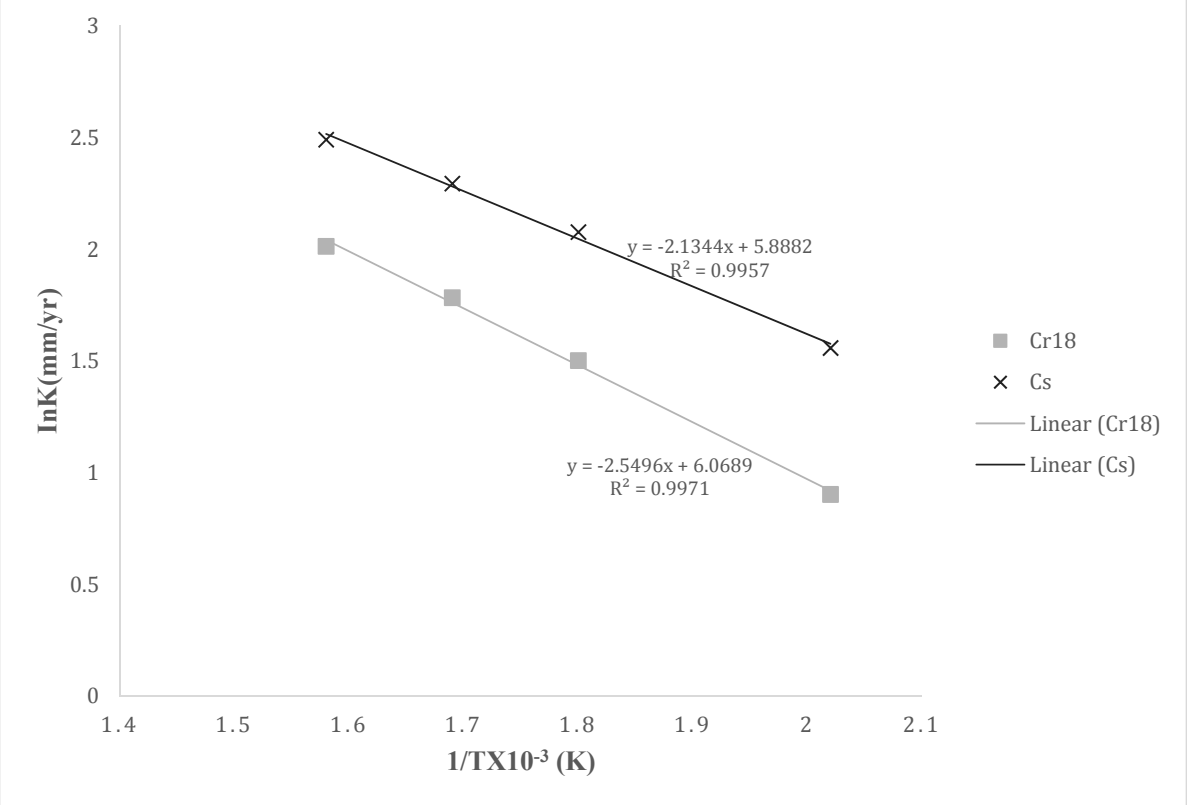

Figure 5: Variation of In K against 1/T x10^{-3}

A general correlation of the trend of the graph with other works done by researchers such as Yu et al., 2008 on carbon steels and austenitic stainless steels of type 304 and type 316 shows agreeable similarity, supporting the field studies by Gutzeit as the corrosion kinetics obeyed the Arrhenius equation.

3.2 Evaluated kinetic parameters

Using the Arrhenius equation

$$k = Ae^{-\frac{E_a}{RT}} \quad \text{.....(3)}$$

or

$$\ln k = -\frac{E_a}{RT} + \ln A \quad \text{.....(4)}$$

Gutzeit suggested that the corrosion kinetics can be represented by an Arrhenius equation, with an activation energy of 68.5kJ/mol for carbon steel and proposed that the process is controlled by chemisorption likewise Turnbull *et al.,* 1999 reported the corrosion kinetics could be represented by an Arrhenius-type equation and with an activation energy of 31.8 kJ/mol for carbon steel. However, the activation energy in this present research is 9.6 kJ/mol for carbon steel (in benzoic acid), which indicating a higher corrosion rate.

Table 3: Correlations of the Ea and R^2 in this present research with literature reviewed

steels	Models	R^2	R^2 Yu et al	Ea(kJ/ml	Yu et. al Ea(kJ/ml)	Gutzeit Ea(kJ/ml)	Turnbull Ea(kJ/ml)
Cs	Ink = -2.1344×1/T + 5.8882	0.9957	0.9798	9.6	33.8	68.5	31.8
Cr18	Ink = -2.5496×1/T+ 6.0689	0.9971		70.6	22.98		

The R^2 values agree with the result of Yu *et al.,* 2008 as it ranges within ninety percent for both carbon steel and austenitic stainless steel. The Ea of 70.6 kJ/mol and R^2 a value of 0.9971 for type305 compared to Yu *et al.,* 2008 on type 316 recorded activation energy of 22.98 kJ/mol and R^2 0.9714. Despite the difference in acid type there is a good level of similarities. Note: the lower activation energy for carbon steel, compared to the austenitic stainless steels, indicated that increased temperature accelerated the corrosion rates of carbon steel to a greater extent than the case for the stainless steels.

3.3 Effect of Concentration:

Table 4 Shows effect of varying concentration on corrosion rate of metal steel coupons in naphthenic acids of Benzoic acid at constant flow rate of 3.37 m^3/s and temperature of 320ºC.

Table 4: Effect of varying concentration of benzoic acid on corrosion rate of metal steels in.

S/No	Conc. C Mol/dm^3	corrosion rate r(mm /year)	
		Cr18	Cs
1	0.05	0.0264	2.2851
2	0.15	2.9147	5.3572
3	3.5	4.4650	8.7195
4	4.5	5.5184	13.5397

Varying concentrations of aromatic naphthenic acid of benzoic acid, the corrosion rate increased from 2.2851 mm/yr. to 13.5397 mm/yr. for carbon steel (Cs), from 0.0264 mm/yr. to 5.5184 mm/yr. on type305 (Cr18). Showing high corrosion resistance in type305 (Cr18) compare to the carbon steel in this present research. Figure 6 plot of corrosion rate against concentration, where the values of n and k can be obtained from the slopes and intercepts of these lines. The plot showing the linear dependence of corrosion rate on metal steels coupons to acid concentration.

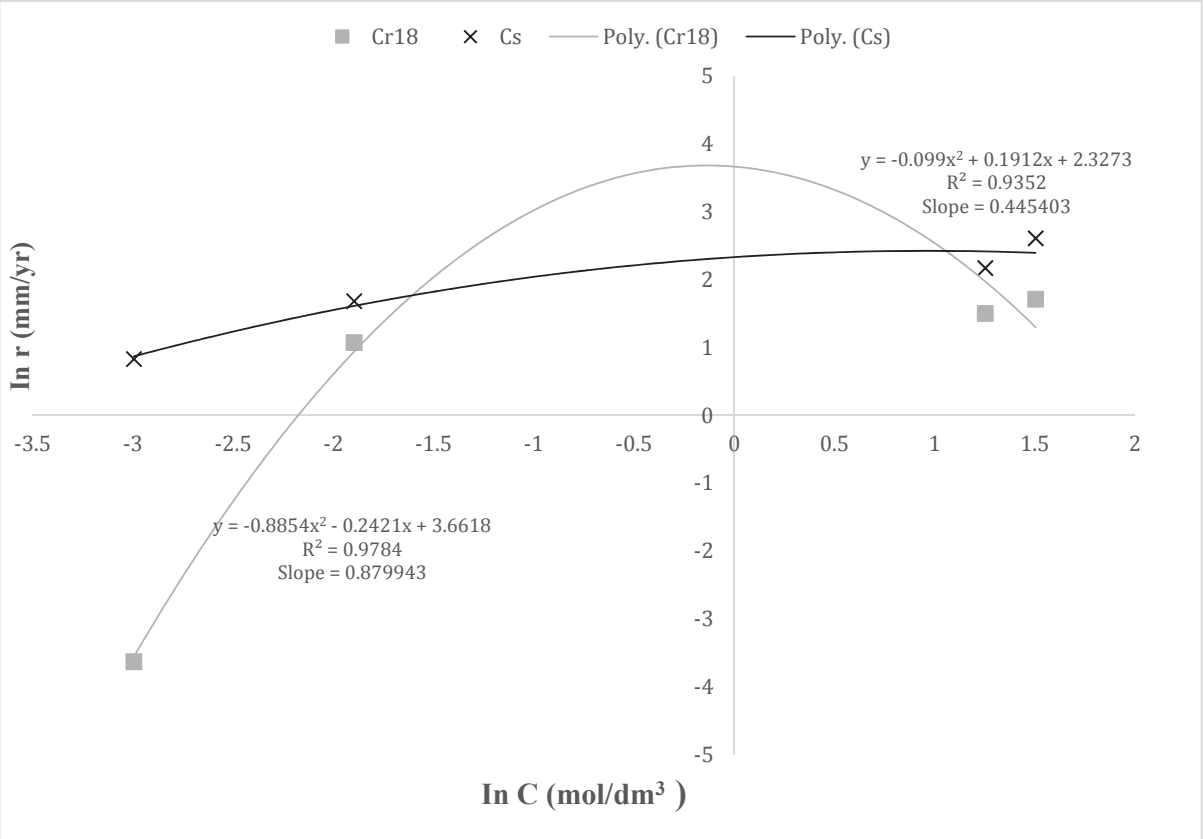

Figure 6: Variation of In r against In C.

3.7 Evaluated Kinetic Parameters:

The general order rate equation was used to evaluate the kinetics of the corrosion among the steels with regard to changes in the concentrations.

$$r = k C^{n} \quad \text{..... (5)}$$

$$\rightarrow \ln r = \ln k + n \ln c \text{ .... (6)}$$

where, n is the slope of reaction k is the reaction constant C is the concentration of the acids and r is the rate of the reaction.

Table 5 displays models, n, and R^2 values derived from the corrosion rate data applying conventional rate order equation of reaction.

Table 5: Evaluated kinetic parameter

Steel	Models	R^2	n	K
Cs	Inr = 0.099 InC^2 + 0.1912 InC + 2.3273	0.9352	0.445403	2.3273
Cr18	Inr = 0.8854 InC^2 - 0.2421 InC + 3.6618	0.9784	0.879943	3.6618

The Kinetics of corrosion rate in aromatic naphthenic acid of benzoic acid showed second order on both carbon steel (Cs) and type305 (Cr18) with an $\mathbf{R^2}$ value of 0.9352 for carbon steel and 0.9784 for type305(Cr18) stainless steel respectively indicating it fits the model. The scanning electron microscopy (SEM) were done on carbon steel (Cs) and austenitic stainless steel type305 (Cr18), which reveals in details the morphology of the nature of the type of naphthenic acid corrosion on the metal steel coupons of carbon steel and austenitic stainless steel used in this research. See Figure 7.

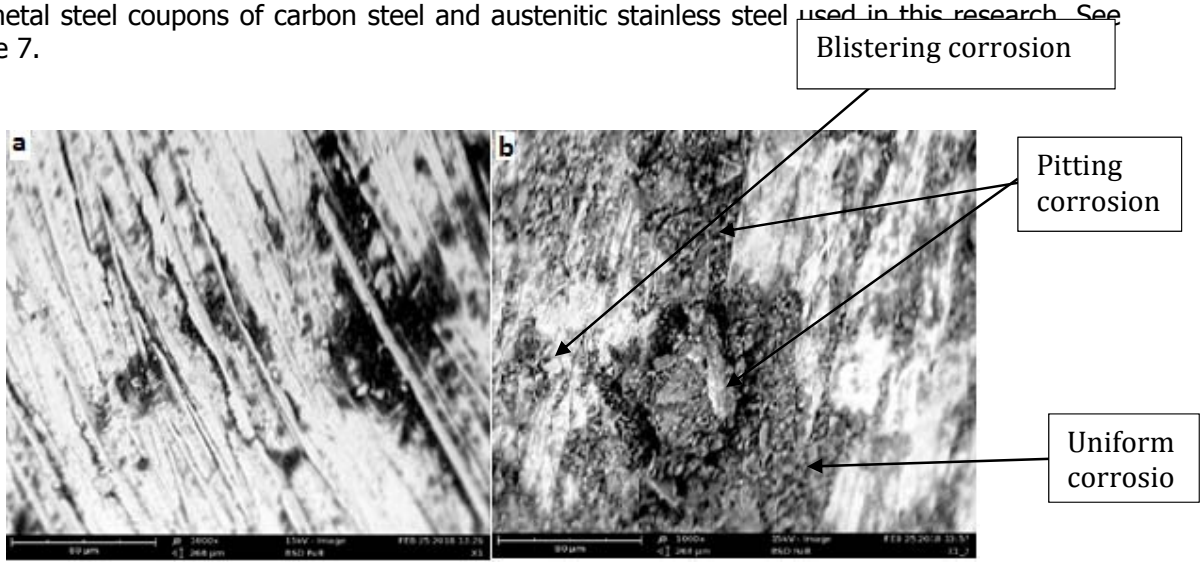

Figure 7: SEM morphology of carbon steel (a) before and (b) After

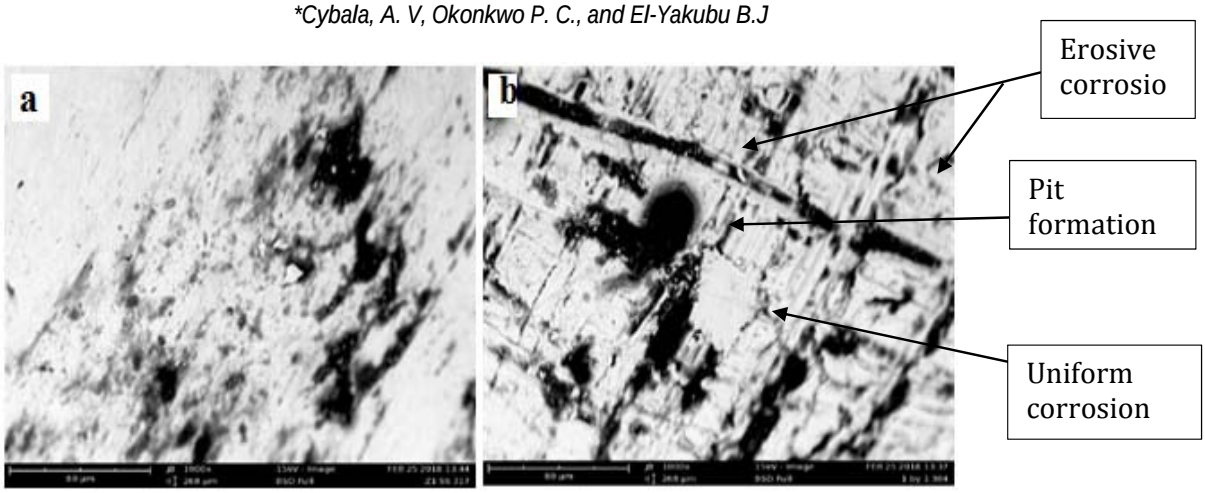

Figure 8: SEM morphology of type 305 (a) before and (b) after.

4.0 Conclusion

Using weight loss methodology and characterization of the experimental steel coupons by XRF analysis and examining the surface morphology of these steels by SEM analysis, the following conclusions were drawn:

1. At increasing temperature and concentration and flow rate, naphthenic acid corrosion increases among the carbon steel (Cs) and type305 (Cr18) stainless steels with carbon steel as the most susceptible to corrosion. The corrosion kinetics observed obeys the Arrhenius equation.
2. Models were generated to predict the corrosion rate at every varying parameter/conditions on each metal steel based upon the naphthenic acids (Benzoic acid).
3. The type305 (Cr18) stainless steel exhibit better resistance due to a high percentage of molybdenum of 0.319 w%, which form a protective passive film containing MoO_4^{2-} ions, in synergy with hydrated Cr oxyhyroxide that acts as an inhibitor thus improved the naphthenic acids corrosion resistance of the type305 (Cr18) stainless steel.
4. General forms of corrosion was observed on all the metals but the most obvious forms of corrosion are: pitting corrosion, erosive form of corrosion, and uniform type of corrosion on all the experimental metal steel coupons as revealed by the scanning electron microscopy (SEM) analysis.

REFERENCES

A. Jayaraman, K.D. Neemla, R.C. Saxena, (1993). *Inter. conference on Energy, Environment and Electrochemistry,* pp. 13-17 CECRI, Karaikudi, India.

Alec, Groysman, (2017). *Corrosion problems and solutions in oil refining and petrochemical industry*. (A. V. Gheorghe, Ed.). Nortfolk, VA USA. Springer international Publishing Switzerland. PP.1-274. doi:10.1007/978-3-319-45256-2

Derungs, W. A. (1956). Naphthenic Acid Corrosion-An Old Enemy of the Petroleum Industry. *NACE International,* 15835 Park Ten Place, Houston, TX 77084. doi:10.5006/0010-9312-12.12.41

Frank, R.A., R. Kavanagh, B.K. Burnison, G. Arsenault, J.V. Headley, K.M. Peru, G. Van Der Kraak, and K.R. Solomon. (2008). *Toxicity assessment of collected fractions from an extracted naphthenic acid mixture*. Chemosphere 72:1309-1314.

Fontana, M. G. (1987). Sanjeev R., Michael B. Beva, M. E. Shank, Charles A. West, Galth S. Welks, (Ed.). *Corrosion Engineering* (3rd Ed.) New York City McGraw Hill Book Company.

PP15-243.

Gutzeit, J. (1977). Naphthenic Acid Corrosion in Oil Refineries. Mater. Perform.pp. 24-35

Jianfei Yu Li Jiang Fuxing Gang, (2008), High temperature Naphthenic Acid Corrosion of Steel in High TAN Refining Media, *Anti-Corrosion Methods and Materials,* Vol. 55 Iss 5 pp. 257 – 263. doi:10.1108/00035590810903845

Jauseau, N., and Nesic, S. (2016). *Study of the Flow Effect on Naphthenic Acid Corrosion of Mild Steel*. Westheimer Rd. Suite 1200 Houston, TX 77042 USA, pp. 1–15.

Kane, R. D., and Cayard, M. S. (2002). Comprehensive Study On Naphthenic Acid Corrosion. *InterCorr International*, (pp. 1–16). Inc. Huston TX. Corrosion Paper No. 02555.

Roberge, P. R. (2000). *Handbook of Corrosion Engineering*. (R. Esposito and D. E. Fogarty, Eds.). New York: The McGraw-Hill Companies, Inc.

Sami Matar Lewis F. (2001). *Chemistry of Petrochemical Processes* Hatch (2nd Ed.). *Elsevier Inc.* Gulf Professional Publishing; 2 ed. Pp. 93-81. doi: 10.1016/B978-0-88415-315-3.X5000-7

Shalaby, H. M., Lowther, M., Al-Hashem, M., and Al-BesharahBy, J. (1996). Industrial Corrosion and Corrosion Control Technology. In H. M. Shalaby, A. Al-Hashem, M. Lowther, and J. Al-Besharah (Eds.), *Proceedingss of the 2nd Arabian Corrosion Conference Kuwait, Ocober 12-15, 1996* (pp. 1–684). Kuwait: Kuwait institute for Scientific Research P.O. Box 24885, 13109 Safat, Kuwait Publication Number:KISR 4890.

Slavcheva, E., Shone, B., and Turnbull, A. (1998). Factors Contolling Naphthenic Acid Corrosion. *Corrosion-NACE*, (579), 1--19. doi:10.5006/1.3284811

Speight, J. G. (2014a). Chapter 1. *Naphthenic Acids in Petroleum High acid crudes* (pp. 1–29). doi:10.1016/B978-0-12-800630-6.00001-0

Sarkar, G.N., (2009). *Advance Petroleum Refining.* Indian Oil Corporation Limited Gujarat Refinery Po: Jawahar Nagar, Baroda. KHANNA Publishers 2. B, Nath Market, Nai Sarak Delhi 11006 Fax: 3980311.

The American Petroleum Institute Petroleum HPV Testing Group. (2012). *Naphthenic Acids Category Analysis And Hazard Characterization*.

Turnbull, A., Shone, E., and Slavcheva, E. (1999). Review of Naphthenic Acid Corrosion in oil Refining. *British Corrosion Journal 1999*, *34*(2), 125–131.

Wu, X. Q., Jing, H. M., Zheng, Y. G., Yao, Z. M., and Ke, W. (2004). Resistance of Mo-bearing Stainless Steels and Mo-bearing Stainless-steel Coating to Naphthenic Acid Corrosion and Erosion – corrosion. *Elsevier*, *46*, 1013–1032. doi:10.1016/S0010-938X(03)00192-6

Proceedings of the 49th NSChE Annual Conference
KADA 2019: pp 739-743

P3C-08: STUDYING THE RHEOLOGICAL PROPERTIES OF WATER BASED DRILLING FLUID FORMULATED FROM BLENDED LOCALLY SOURCED SABON GARIN NGALDA BENTONITE AND CONVENTIONAL BENTONITE

***Sabiu Bilal[1], M.S. Adamu[1], Mustapha S. Ingawa and Bala Usman[1]**
[1] Department of Chemical Engineering, Ahmadu Bello University, Zaria-Nigeria.
*Corresponding Author Email: bilalsabiu@gmail.com

ABSTRACT
This research focused on studying the rheological properties of water-based drilling fluid formulated from blended locally sourced Sabon Garin Ngalda bentonite (SGN) and conventional bentonite (American Petroleum Institute (API) standard). Five different formulations were considered by blending SGN and conventional bentonite with ratios of A (60:40), B (65:35), C (70:30), D (75:25) and E (80:20) mixed each one with 350 mL of water and 1.5g of poly anionic cellulose. The rheological properties (apparent viscosity, plastic viscosity and yield points) as well as the mud weight of the formulated drilling fluids were determined. The results revealed that the best formulation is formulation "A" having mud weight of 8.167 lb/gal and apparent viscosity, plastic viscosity and yield point of 20 cP, 13 cP and 14 lb/100ft^2 respectively. The results are relatively close to API standard formulation. Therefore, it can be concluded that the formulated drilling fluid has a very good capacity for drilling application but still requires enhancement.

Key words: Rheological Properties, Bentonite, plastic viscosity, yield point

INTRODUCTION
Nigeria has the second largest oil reserves in Africa after Libya and is the continent's primary oil producer. Nigeria's 37.2 billion barrels of oil reserves also places it among the top 10 countries in terms of reserves on a global basis (KPMG, 2013). Drilling techniques are required to access oil and gas reserves at the extremities of existing production zones (Doug and Daryl, 2007). There was no single oil well drilled without using drilling fluid having Bentonite as a major constituent (Arabi *et al.*, 2011).

Drilling is the process of creating a passage for the discovered hydrocarbon to be produced at the surface. It involves the penetration of the earth's crust to several thousand feet where the hydrocarbons are accumulated in the reservoir using rotary drilling process. So far, from the era of cable tool rig to the use of rotary drilling rigs, a lot of technological advancements have been put forth on how best drilling operations can be carried out in the best economic and environmental possible way (Francis and Anietie, 2012).

Drilling fluids are heterogeneous mixture of chemical, water or oil and clay materials that aid drilling operations. They are vital in successful well drilling as they have common properties that facilitate safe and satisfactory completion of the well such as bottom hole cleaning, controlling high pressure zones and removal of cuttings to the surface. The importance of drilling fluid, otherwise known as 'drilling mud' cannot be over emphasized as the knowledge of drilling fluid is a requisite in the rotary drilling operation in the petroleum industry (Francis and Anietie, 2012). The drilling companies operating on the shores of the Niger Delta import bulk drilling fluid materials to carry out their respective operations. This has been a great burden and major concern to the industry since some of these drilling fluid materials cannot be recycled. Secondly, the foreign exchange involved and the high cost of drilling fluid materials also constitute a problem for the petroleum industry (Odumugbo (2005); Francis and Anietie, 2012).

The effectiveness of the drilling fluid to perform its primary functions is based on its properties, which are formulated continuously to meet the formation conditions encountered during drilling operations. Failure of the drilling fluid to meet its designed function can prove extremely costly in terms of materials and time, may jeopardize the successful completion of the well and even result in major problems such as stuck pipe, kicks or blowouts (Rabia, 2000).

The establishment of Nigerian Local Content Initiative in the Oil and Gas Sector by the Federal Government of Nigeria has necessitated the need for local substitutes to foreign drilling fluid materials. Thus, it is imperative to source for locally available drilling fluid materials and evaluate their various characteristics, then formulate fluids that can be used in drilling process (Francis and Anietie, 2012).

The search for better products for well bore drilling that will achieve a good level of performance particularly with local materials is being intensified. Although, substantial strides have been made in the development of environmentally friendly, sound performance chemistry for corrosion inhibition, etc, much has not been done in the development of such mud systems with local materials. Drilling operations rely heavily on the use of water based drilling muds. These are mixtures of solids, liquids and chemicals. Water is the continuous phase. Active solids like bentonite are added to the water (Ekeigwe *et. al.,* 2013).

Bentonite is the commercial name of a whole range of natural clays with a high water absorption capacity causing it to expand and swell. Bentonite predominantly consists of montmorillonite: a clay mineral belonging to a class of phyllosilicates called smectites. Bentonites may contain a variety of accessory minerals in addition to montmorillonite. These may include lesser amounts of other clay minerals such as kaolin, mica, illite, as well as non-clay minerals like quartz, feldspar, calcite, and gypsum. Bentonite quality, and, consequently, its applications, depend on whether it contains any of these other minerals. (Mike and Kelvin, 1998).

Bentonite acts mainly as the dispersed phase providing the main gel structure. Chemical additives are added in various proportions to control the fluid properties. The chemical additives are commonly used for the control of pH, viscosity, weight, fluid loss. The major success of every drilling operation depends solely on the performance of its drilling fluids (Ekeigwe *et. al.,* 2013).

This research work is aimed at studying the rheological properties of water-based drilling fluid formulated from a blend of locally sourced Sabon Garin Ngalda bentonite and conventional bentonite for oil and gas drilling application.

MATERIALS AND METHODS

The materials used for the research are Sabon garin Ngalda (SGN) bentonite, conventional/standard bentonite, viscosifier (poly anionic cellulose) and distilled water. The local bentonite obtained from Sabon Garin Ngalda of Yobe State and the conventional/standard bentonite obtained from Centre for Energy and Training (CERT), were blended together into five different formulations as A, B, C, C, D and E with each formulation containing 24.5 g of bentonite in the ratio of A (60:40), B (65:35), C (70:30), D (75:25) and E (80:20) for SGN and conventional/standard bentonite respectively. Table 1 depicts the blending ratio in grams and the total amount of the bentonite clays used for the research.

Table 1 The blending ratio SGN and Conventional Bentonite in grams

Sample Type	A (g)	B (g)	C (g)	D (g)	E (g)	Total Quantity of Used Bentonite (g)
SGN bentonite	14.800	16.075	17.350	18.625	19.900	86.750
Standard bentonite	9.700	8.425	7.150	5.875	4.600	35.750
Total	24.500	24.500	24.500	24.500	24.500	122.500

Each blended sample was mixed with 1.5g of poly anionic cellulose and 350ml of distilled water in a plastic container continuously stirred with an electric agitator for 30 minutes to have a homogenous mixture. After achieving homogeneity, the samples were allowed to age for 24 hours before taking the rheological properties as well as the respective mud densities of the formulated drilling fluid. The viscosity readings were recorded at 40^{o}C using Fann viscometer 35S at 3, 6, 100, 200, 300 and 600 revolutions per minutes (rpm).

RESULTS AND DISCUSSION

The viscosity consistency curves the various formulations are shown in Figure 1. The result indicates that formulation A was relatively close to the API standard, then followed by formulation B, D, E and then C, in that order.

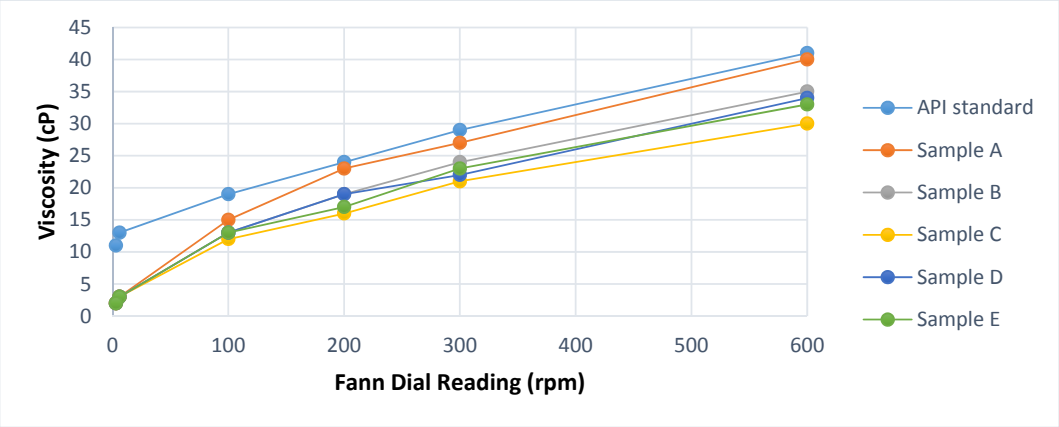

Figure 1: Viscosity consistency curve of formulated drilling fluids.

Formulation A seems to be the best with blending ratio of 60:40 which is 15.30g and 10.20g of Sabon Garin Ngalda bentonite and conventional bentonite respectively.

The mud densities of the formulated drilling fluids for the formulations A, B, C, D, E and conventional bentonite were 8.167 lb/gal, 8.58 lb/gal, 8.51 lb/gal, 8.42 lb/gal, 8.42 lb/gal and 8.60 lb/gal respectively as depicted in Figure 2. The mud density in g/cm^3 shown in the figure can be converted to mud weight in lb/gallon as API standard unit. The conversion factor is multiplication by 8.33 as explained by Bilal (2016).

The results indicate that the mud densities of the various formulations are slightly lower than API specifications (8.60 lb/gal), hence there is need to add weighing agent such as barite to enhance the density of the fluid.

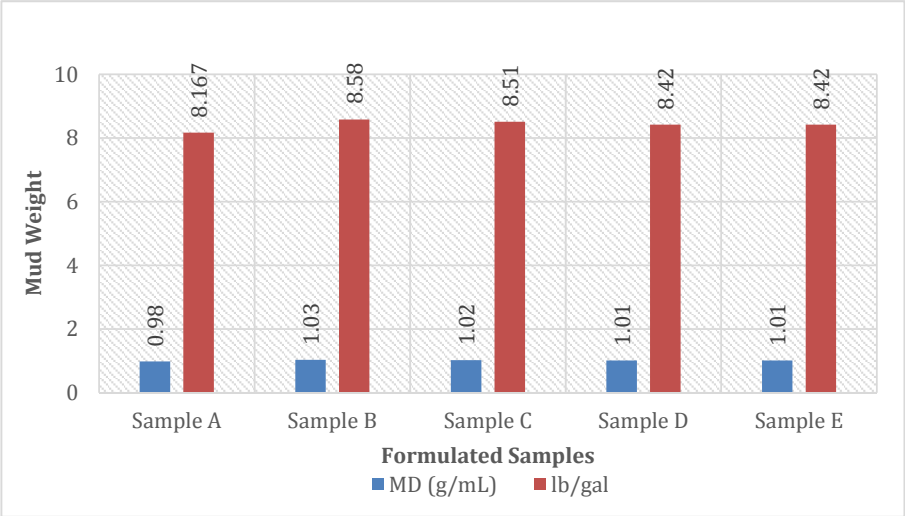

Figure 2: The mud weight/density of formulated drilling fluids

Table 1: Table showing the rheological properties of the formulated drilling fluid

Rheological Properties	Sample A	Sample B	Sample C	Sample D	Sample E	Raw SNG Bentonite	Conventional/ Standard Bentonite
Apparent viscosity (cP)	20.0	17.5	15.0	17.0	16.5	1.6	17.0
Plastic viscosity (cP)	13.0	11.0	9.0	12.0	10.0	0.9	9.0
Yield point ($lb/100ft^2$)	14.0	13.0	12.0	10.0	13.0	1.3	22.0

Rheological properties of the formulated fluid

Table 2 shows rheological properties of the formulated drilling fluids; apparent viscosity (20 cP, 17.5 cP, 15 cP, 17 cP, 16.5 cP, 1.6 cP and 17.0 cP), and plastic viscosity (13 cP, 11 cP, 9 cP, 12 cP, 10 cP, 0.9 cP and 9.0 cP), yield point (14 $lb/100ft^2$, 13 $lb/100ft^2$, 12 $lb/100ft^2$, 10 $lb/100ft^2$, 13 $lb/100ft^2$, 1.3 $lb/100ft^2$ and 22 $lb/100ft^2$) for sample A, B, C, D, E, raw SNG bentonite and standard/conventional bentonite respectively. Initially, the raw SNG bentonite has low rheological properties compared to the conventional/API standard. After blending the raw sample with the conventional bentonite there was significant increase in the rheological properties. The plastic viscosities of all the formulated samples revealed that the values obtained are higher than the value for the standard bentonite with the exception of sample C, which has similar value to standard as 9cP. This means that samples A, B, D and E have better plastic viscosity than the standard/conventional bentonite. For the yield point it was observed that the standard/conventional bentonite has higher yield point compared to all the formulations. This means in practical terms, an increasing yield point means a good and stable mud which helps in removing cuttings from the hole, while a reducing yield point means a bad and unstable mud (Adeleye *et al.,* 2012).

CONCLUSION

In conclusion, the generated results ranging from the rheological properties (apparent viscosity, plastic viscosity, yield point) and mud weight of the formulated water-based drilling fluid from blended Sabon Garin Ngalda (SGN) bentonite and conventional bentonite samples revealed that the blended samples have almost similar properties compared to the standard conventional bentonite. The best formulation is Formulation "A" having mud weight of 8.167 lb/gal and apparent viscosity, plastic viscosity and yield point of 20 cP, 13 cP and 14 lb/100ft^2 respectively. The blending ratio of "A" is 60:40 which is 15.30g and 10.20g of Sabon Garin Ngalda bentonite and conventional bentonite respectively, 1.5g of PAC and 350 mL of clean water. The information revealed that the local SGN bentonite still requires more modification for it to meet all the API specification.

REFERENCES

Adeleye, Sanmi Apaleke, Abdulaziz Al-Majed and M. Enamul Hossain (2012). State of the Art and Future Trend of Drilling Fluid: An Experimental Study. This paper was prepared for presentation at the Latin America and Caribbean Petroleum Engineering Conference16-18 April, 2012 Mexico City, Mexico. SPE -153676.

Arabi Suleiman, Abdullahi, A. A., Ibrahim, M. A., Muhammad, M. Y. Kwaya and S. Mustapha (2011). Comparative Evaluation of Rheological Properties of Standard Commercial Bentonite and a Locally Beneficiated Bentonitic Clay from a Marine Deposit in Upper Benue Basin, Nigeria*. British Journal of Applied Science and Technology* 1(4): 211-221.

Bilal Sabiu (2016). Investigation and Enhancement of the Quality of Nigerian Bentonitic Clay Samples for Oil and Gas Drilling Operation. *A P.hD., Thesis* submitted to the Department of Chemical Engineering, Ahmadu Bello University, Zaria.

Doug, Oakley, Daryl, Cullum, (2007). Down hole Fluids, Drilling Contractor. *M-I SWACO* pp 96.

Ekeigwe, O.N, Anyiam C. K., Ayo M. D. and Ekebafe L.O. (2013). the formulation of Water-Based drilling fluid from Local Materials. *Capsian Journal of Applied Sciences Research*, 2(1):18- 22.

Francis D. Udoh and Anietie N. Okon (2012). Formulation of Water-Based Drilling Fluid Using Local Materials. *Asian Jr. of Microbiol. Biotech. Env. Sc.* 14 (2): 167-174.

Mike J., Kelvin S. (1998). Origin of Bentonite. *Clay Menerology*, (2):10–21.

KPMG, (2013). Oil and Gas in Africa: Africa's Reserves, Potential and Prospects, a Cayman Islands company Limited. pp 9 available at kpmgafrica.com accessed on 12th/07/2019.

Odumugbo, C.A. (2005). Evaluation of local Bentonitic clay as oil drilling fluids in Nigeria. SPE Technical Paper, SPE 85304.

Rabia, H. (2000). Well Engineering and Constructions, Entrac Consulting, London. Graham and Trotman Ltd. 265p.

Proceedings of the 49th NSChE Annual Conference
KADA 2019: pp 744-755

P01: EVALUATION OF NATURAL GAS TRANSPORTATION APPROACHES TO MEET THE END USE DEMAND IN NIGERIA

Ogulu, E.O, Oji, A and Nwosi, H.A
World Bank Africa Centre for Excellence, Centre for Oilfield Chemical Research,
University of Port-Harcourt
Choba, Port-Harcpourt, P.M.B 2, UniPort, Rivers State. Nigeria

ABSTRACT
This study is on the various approaches by which natural gas can be transported from the point of production to the destination for end usage. With the recent revelation by Nigeria Liquefied Natural Gas (NLNG) company, on decrease in profit of about 13 % which was as a result of large offshore discovery in East Africa and shale gas emergence in United State. This paper surmises that NLNG company should diversify into Compress Natural Gas (CNG) i.e., gas at high pressure (typically 1800 psig for a rich gas to approximately 3600 Psig for a lean gas mainly methane) for the transportation sector and Liquefied Petroleum Gas (LPG) which is liquid form of natural gas that is being used in homes and offices as source of energy for cooking and other domestic activities. In achieving the essences of this paper, several computer software applications such as Aspen Hysys version 7.1 that was used in ascertaining the gas diversification capacity, Finite Element Analysis (FEA) was applied in determining the pressure distribution of the pipeline through Computational Fluid Dynamic (CFD). Carbon steel pipe of 24" was designed with the aid of Auto-CAD Software application due to its accessibilities, cost and coating options. Simulation and Process separation of heavy hydrocarbon present in the natural gas stream like C_3 and C_4 was achieved through HYSYS separation process and PandID Column. From this paper, it can be seen that 30 % local utilization either industrially or for domestically will enhance the growth of Nigeria GDP.

Keyword: Hysys, FEA, GDP, LPG, CNG, CFD, NLNG Company and Auto-CAD

1.0 Introduction/Background of the study

The natural gas business internationally has experience a robust response over years and Nigeria as a country have received her own share in the business transaction. Nigeria ranks as the largest holder of natural gas proven reserves in Africa and ninth largest holder in the globe (NNPC, 2011). The nation produced 1.2 trillion cubic feet (Tcf) of dry natural gas in 2012 and a reserve of an estimated 187 trillion cubic feet (Tcf) as of June, 2013, the production rate is increasing on daily basis making it world's 25th largest natural gas producer. The production of natural gas is restricted by lack of framework to monetize natural gas that is currently being flared. (United State, Energy Information Administration, 2017). Nigeria as a country exports to mainly Asia, Europe and America of which is being threatened Due to rising shale gas production, it is forecasted that the United State America, will be a major exporter of natural gas by the year 2020 and beyond. This may lead to LNG supplying surplus in the market and likely reduction in LNG delivery price to Asia and Europe, Nigeria's main destinations of LNG export. (Whither Nigeria's global LNG market share Business Day, 2015).Apart from the threat from the United State and Singapore, experts believe that East Africa's closeness to Asia may likely be easy access in good destination for LNG exports. The futures of Tanzania and Mozambique becoming LNG exporting nations are expected to present an alternative for Asian buyers because of the proximity compared to Nigeria. East Africa, in particular Mozambique, could be a new trending LNG exports due to its current large offshore discoveries, according to British maritime classification society, Lloyd's Register, in its 'Global Marine Trends 2030' report. This will eventually lead to decline in income generated by the LNG business in long-run and therefore leaving the company with limited

options such as prolonging the contract of long term duration to many years of LNG supply on demanding nations and developing a model for local usage of natural gas.

The first and second options are advisable for the NLNG, as the Asia nations are already complaining about the high price they are subjected to pay and would see shale gas and other eastern African's gas as a real alternative. Crashing down the exporting gas would not be a remedy either. With approximately 170 million citizens, Nigeria is the most populous country in Africa and eight most populous in the world, (Uzoh, 2011), her needs for energy is increasing and so would be preferable for natural gas to be used locally as a better option. Natural gas has great importance for transportation, industrial, commercial and cooking. To achieve this, new programs have to be develop, a good pipeline network and storage facilities have to be installed and diversification of natural gas has to be implemented as these are some of the objectives of the PIB bill.

Chronological Realization of Transporting Natural Gas

The storage of has been of numerous difficulties and so need to me move instantaneously,so as to reach its destination after being produced from a reservoir(Cranmore and Stanton,2000). Different approaches exist for transporting natural gas from oil and gas field or facilities to market(Catania,2004).These approaches includes pipelines, liquefied natural gas(LNG) and compressed natural gas(CNG).

Pipelines

Research has shown that pipelines are very suitable approach of transporting natural gas but is not flexible as the gas may leave the source of transportation and arrive at its destination. If political and economic stability can be guaranteed by the government, pipeline can become very effective and efficient in transporting natural gas.

Liquefied Natural Gas

This technology has been proved to be successful since the late 20th century. LNG is the gas that is liquid in nature and be transported in liquid form from the point of production to process plants. However, technology for liquefied natural gas need multifaceted state of the art equipment with locomotive parts and special refrigerated ship fitted for transporting the LNG to market

Compressed Natural Gas

Natural gas can be moved in containers constructed with high pressure. Scientifically 1800 psig for a rich gas to approximately 3600psig for a lean gas (mainly methane). A special dedicated transport ship transporting vast diameter in a non-conductor in a non-conductor refrigerated storage cargo package. The natural gas will be cooled, dried and compressed for storage on board.

Utilization of Natural Gas

Natural gas in Nigeria is widely used in varieties of ways such as powering of electricity, cooking at home like LPG, for preservation of food through refrigeration, cooling of homes and stadium in form of air-conditions and retrofitting of cars. It can also be used industrially in welding etc.

2.0 Materials and Method

Materials used for this dissertation are gas samples obtained from an associated well in Soku field, of which can be described as wet gas due to the presence of condensable gases contained in the natural Gas stream. The gas compositions were obtained through the application of gas chromatography technology at the Petroleum Testing Laboratory in Department of Petroleum

Engineering, Rivers State University, Port-Harcourt. The mole fraction of the different natural gas composition constituents were then recorded below in Table 3.1.

Table 3.1- Natural Gas Composition Constituents form an Associated well

COMPONENTS	MOLE FRACTION
Methane	0.8339
Ethane	0.0706
Propane	0.0395
i-Butane	0.0078
n-Butane	0.0115
i-Pentane	0.0038
n-Pentane	0.0031
n-Hexane	0.0031
n-Heptane	0.0023
n-Octane	0.0008
n-Nonane	0.0001
n-Decane	0.0001
CO2	0.0143
Nitrogen	0.0091
Total	**1.0000**

2.1.1 Pipeline Parameters and Pressure drop Models.

The transmission of fluids through pipelines requires many considerations in terms of material usage, process variables (which explicitly define the operating conditions of the fluid), the design and the topographical setting of the route.

The pipeline material used for this research, (through the various Computer software applications) is carbon steel due to its accessibility, cost, and coating options. For a 24inch pipeline, the outside diameter is 610mm, having a thickness of 6.35mm according to the ASME B36.10M19M-2004 Specification. Below is a table of different pipe size.

Table 2.1.1- Schedule of Different Pipe Sizes (ASME B36.10M19M-2004)

S/N	Sizes(Inches)	24"	28"	36"	48"
1	Outside Diameter (millimetre (OD)	610	711	914	1219.2
2	Inside Diameter (millimetre (ID) ~~	597.30	695.16	898.14	1199.10
3	Thickness (millimetres)	6.35	7.92	7.92	10.05

The relationships used in the design of the pipeline are as follows:

$$A = \frac{\pi(D_I)^2}{4} \qquad 2.1$$

Where A =Cross section of the pipeline

D_i= Inside Diameter of the pipeline

The gas is expected to have a certain flow rate which is most times based on the supply of gas (scf) per day. The relationship between the flow rate and the cross section of the pipe helps in determining the velocity of the gas stream.

$$Q = Av \qquad 2.2$$

Substituting gas supplies to NLNG from the NNPC (APPENDIX 2), if **20-50%** of the gas supplies is diverted for domestic use and taking the highest observation then it means that we can decide that the gas flow rate to be transported will be **200m³/s** maximum and 30 **m³/s** as minimum, neglecting year 2010, if that is to be considered.
equation 3.1 into 3.2 gives

$$Q = \frac{\pi (D_I)^2}{4} v \qquad 2.3$$

As the gas flows inside the pipeline, it experiences a decrease in pressure owing to the rough surface of the pipeline. The pan Handel A, pan Handle B and the Weymouth equation helps in describing this effect. This depends strictly on the material of construction as the roughness factor varies with material types of the inner wall of the pipe, the diameter of the pipe, the length of pipe, compressibility factor, pressure and temperature of the fluid. But before this can be established the Reynolds's No, the friction factor and the relative roughness must be determined.

Reynolds No, $$\mathrm{Re} = \frac{Du\rho}{\mu} \qquad 2.4$$

D: pipe ID (inside diameter), ft
u: fluid velocity, ft/sec
ρ: Fluid density, lb_m/ft^3
μ: Fluid viscosity, $lb_m/ft.sec$

Friction factor, (f): $$\frac{1}{\sqrt{f}} = 1.14 - 2\log\left(e_D + \frac{21.25}{\mathrm{Re}^{0.9}}\right) \qquad 2.5$$

Where relative roughness: $e_D = \frac{\varepsilon}{D}$ 2.6

ε = Roughness of the internal wall section, carbon steel (0.0046)

The pan Handel B equation is stated as thus:

$$\left(\frac{1}{f}\right)^{0.5} = 16.7 \times \left(\frac{\gamma_g \times Q}{D}\right)^{0.01961} \qquad 2.7$$

$$Q = 435.87 \times \left(\frac{T_b}{p_b}\right)^{1.07881} \times \left[\frac{p_1^2 - p_2^2}{\overline{Z} \times T \times L}\right]^{0.5394} \times \left(\frac{1}{\gamma_g}\right)^{0.4604} \times D^{2.6182} \qquad 2.8$$

The pan Handel A Equation..... 2.9

$$\frac{1}{f} = 52 \times \left(\frac{\gamma_g \times Q}{D}\right)^{0.1461} \qquad 2.10$$

The Weymouth Equation.....

$$f = \frac{0.00235}{d^{0.33}} \qquad 2.11$$

K= 1.162 x 10^7 2.12

2.13

$$Q_h = 3.23 \times \frac{T_b}{p_b} \times \left[\frac{\left(p_1^2 - p_2^2\right) \times D^5}{\gamma_g \times \overline{Z} \times T \times f \times L} \right]^{0.5}$$

$$Q = 435.87 \times \left(\frac{T_b}{p_b} \right)^{1.07881} \times \left[\frac{p_1^2 - p_2^2}{\overline{Z} \times T \times L} \right]^{0.5394} \times \left(\frac{1}{\gamma_g} \right)^{0.4604} \times D^{2.6182}$$

Where: Q_{SC}= flow rate,

T_{SC}= Temp standard condition

P_{SC} = Pressure standard condition

K = Sand grain- roughness

D= diameter of the pipe

γ = specific gravity of the gas

f = moody friction factor.

P_1 = Pressure in

P_2 = Pressure out

L = length of pipe

T_m = mean temperature of the gas

Z_m = Mean compressibility factor

Using the pan Handel's A, B or Weymouth's equation, we can predict the operating inlet pressure that will be required having known the critical pressure and temperature of the stream and other parameters that determine whether or not how many compressor stations will be needed for the whole process. Various results will be gotten also as the diameter of the pipe changes.

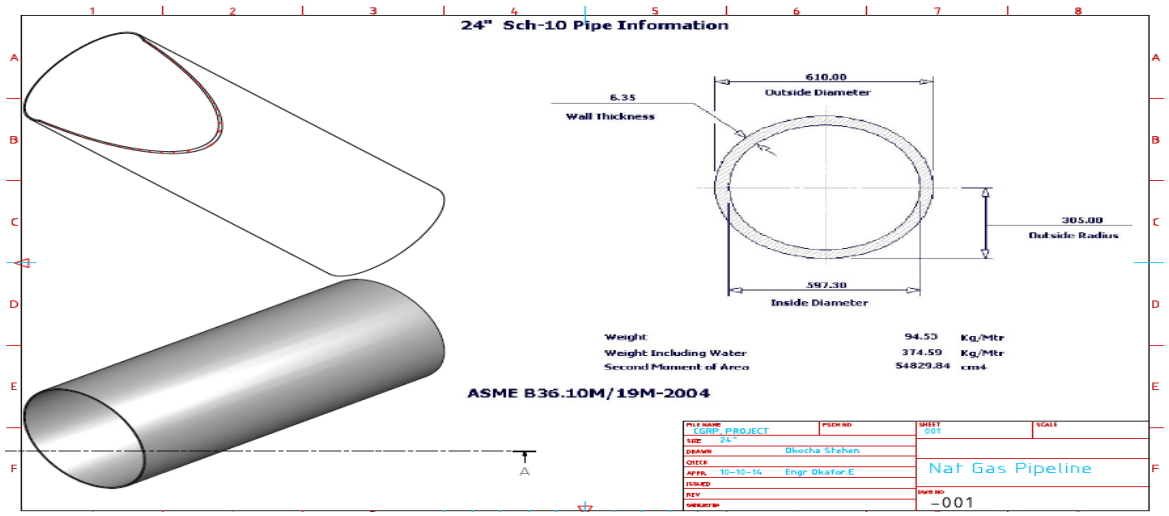

Figure2.1- Pipeline Design with ASME B36.10M Specification

As the pressure changes, the compressibility factor will also decrease, hence the natural gas stream is keeping other variables constant. The pressure and compression in connection with the specific gravity is given in table below. This was achieved with the setting of the temperature at 45^{o}C and flow rate of 200m3/s using the Peng-Robinson's fluid package in Hysys. Following this approach, the natural gas properties (both physical and chemical) changes instantly as the pressure differs. This design of the pipe was actualize with the application of Automated Computer Aided Design (Auto-CAD) 3-D, i e 3-Dimension.

Table 2.1.3- Relationship between pressure, Compressibility and Specific Gravity

(P) (Kpa)	Compressibility(Z)	specific gravity (y)
7000	0.3363	0.674
6000	0.2888	0.672
5000	0.2411	0.6715
4000	0.1932	0.6702
3000	0.1452	0.6689
2000	0.097	0.6676
1000	0.0486	0.6663
500	0	0.6631
50	0	0.00541
10	0.9952	0.0003253
5	0.9976	0.0001623

2.1.2 De-Propanizer and De-Butanizer Models

Before the natural gas is compressed and transported for domestic utilization, it must be separated of its heavier hydrocarbon components and impurities removed. This will help in reducing the possibility of hydrate (water) formation in the pipeline (Ikoku,1988). This can be achieved by de-butanizing (removing C_4) and de-propanizing (removing c_3) from the natural gas stream with the aid of PandID Column as shown in figure below(Figure3.1.2) or a heat exchanger, as such will decrease the critical temperature and pressure between liquid and vapour phase of the natural gas. The Propane liquefies at -42.1° C while butane liquefies at -0.5° C

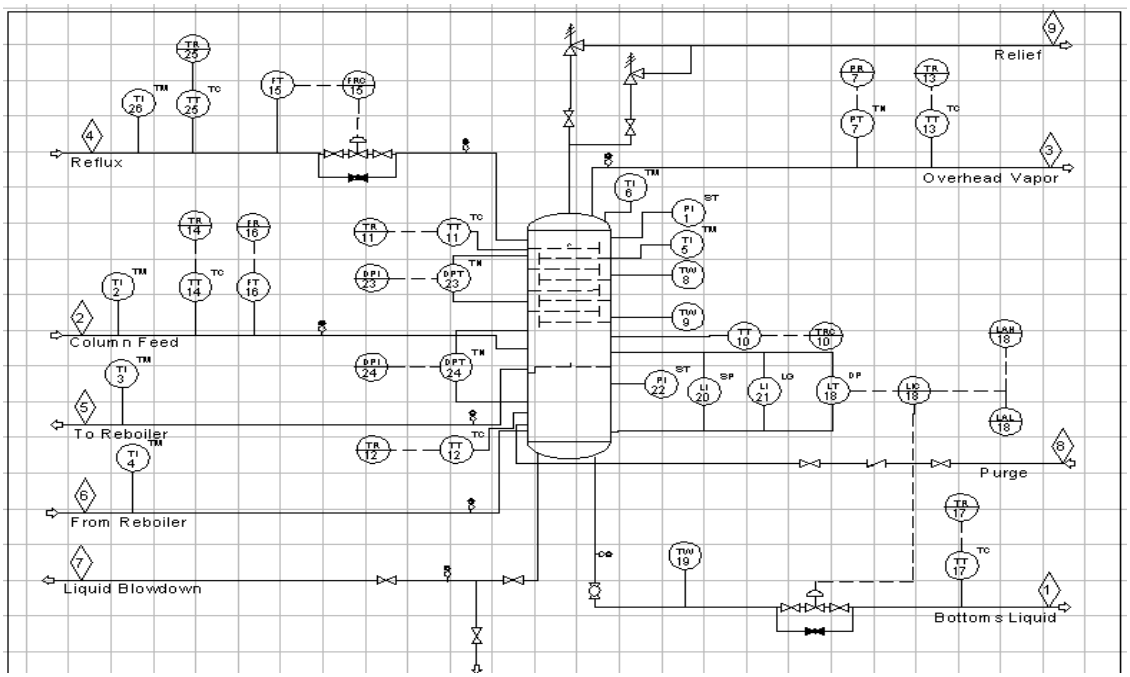

Figure2.2- Column PandID for de-Propanizer and de-Butanizer

Methods

The approaches (methods) applied in achieving the aim and objectives of this research followed series of Computer Software applications, such as Finite Element Analysis that was used in ascertaining the pressure distribution of the pipeline, through Computational Fluid Dynamics, which regulate the pressure of the fluid flowing in the pipe.

In ascertaining the composition of the natural gas constituents with their mole fractions, Liquid Gas Chromotography at the Petroleum Testing Laboratory (of Rivers State University, Portharcourt) was applied to ensure accuracy and precision of results. That is, different mole fractions of the natural gas composition constituents were obtained and recorded as in table 3.1. The diversification capacity of the natural gas was determined through hysys version 7.1, Computer Software Application, that also separate impurities present in natural gas stream, to avoid hydrate formation in the pipeline before transporting it to its market destination for utilization or consumption. Automated Computer Aided Design (Auto-CAD) 3-D, was applied to design the 24inch pipe with ASME. B36. 10M-2004, specification, with all information fully stated in the figure (Figure 2.1) above.

3.0 RESULTS AND DISCUSSION

Gas Descriptions

Natural Gas Quality and Measure

The gas characterization was achieved through the use of HYSYS (7.1) package. The components were defined as thus in table 3.1 and the fluid package used was the Peng-Robison of Equation of state. In the oil manager and environment tab, the assay data type was chromatography. The software now simulate and calculates the stream after all the components have been inputted based on molecular weights. The blend cuts the stream into hypo-components. This gives the critical pressure and temperature at which the fluid requires to function.

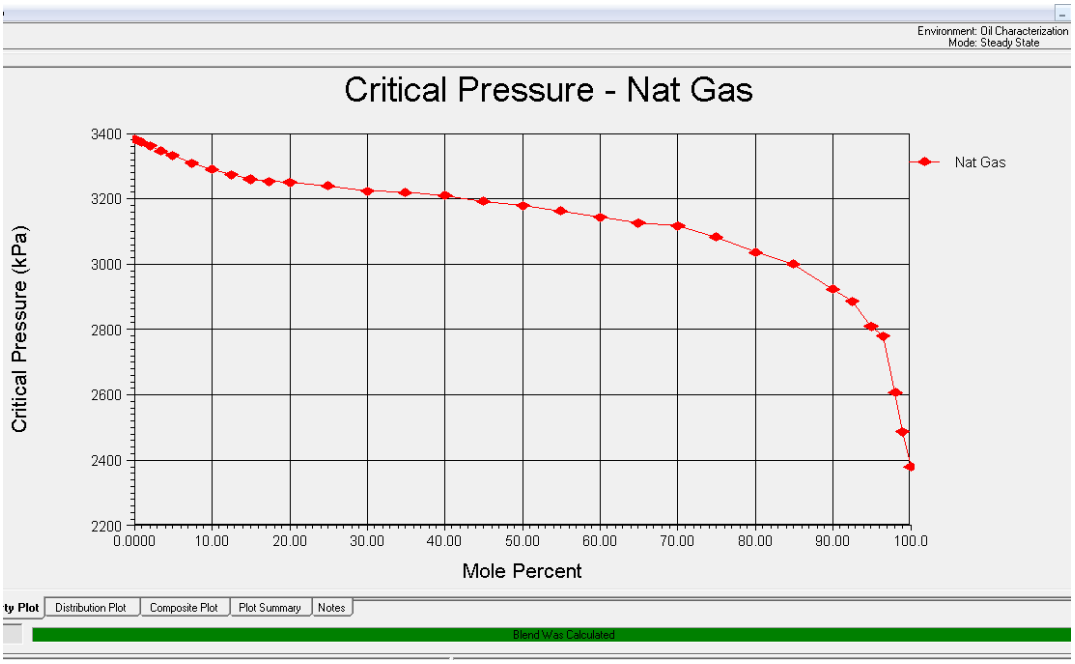

Fig3.1- Boiling point of the natural gas fractions with respect the mole %

From the diagram it shows that the highest critical pressure is 3400kpa, will bring the formation of hydrates in the pipeline, the compressor needed should compensate for the pressure. The second figure depicts the maximum temperature required of gas in the pipeline which is about 175^{o}c, this temperature is relatively high and so needs some separation to avoid hydrate formation during transportation and utilization.

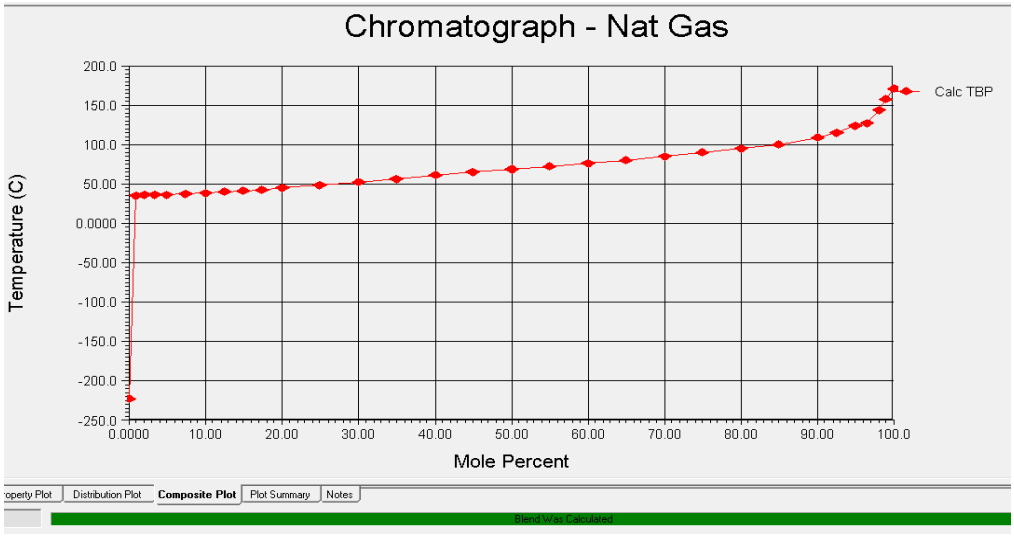

Figure3.2- Boiling point of the natural gas fractions with respect the mole %

Table 3.1- The properties of the Natural Gas Stream

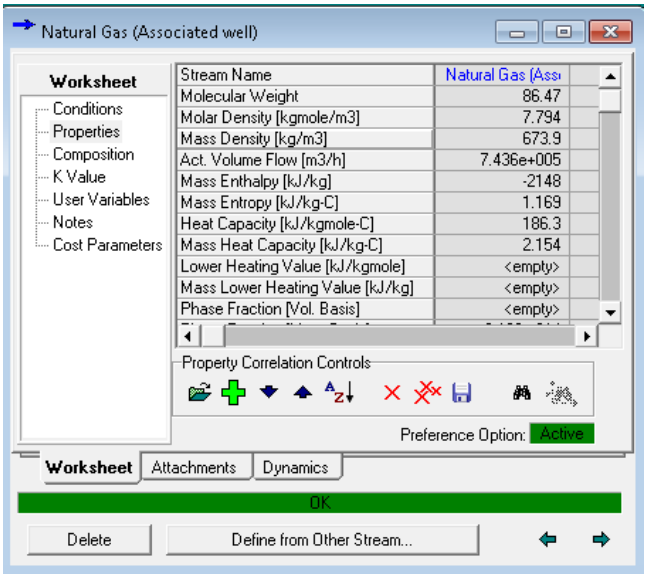

3.1.2- Potential Natural Gas separation (de-Propanizer and de-Butanizer)

Since NLNG operates in liquefying natural gas form, at a low temperature, Liquefied Petroleum Gas(LPG) can be obtained through simple separations in columns, of which are set at the boiling points of butane and propane through addition of heat energy. Using the Hysys software package, after cooling the temperature of the Natural Gas stream, such configuration can be set to separate the heavier components of the natural gas stream. Aiming the separations to take place at Propane liquefying at -42.1° C and butane liquefying at -0.5° C, the whole process flow diagram can be designed as follows:

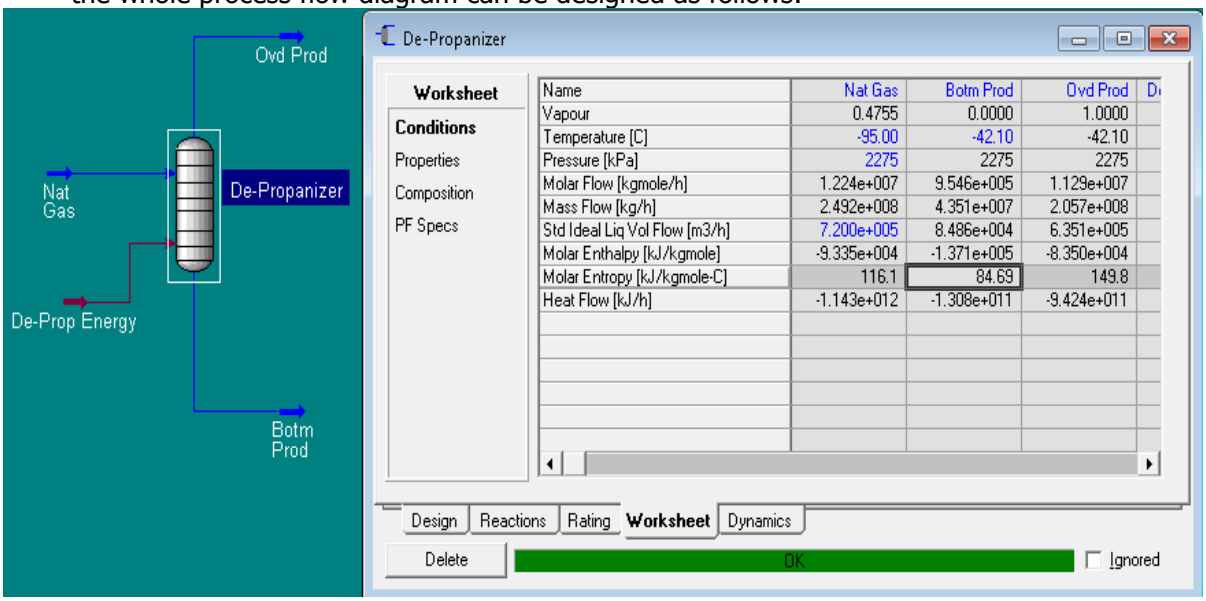

Figure3.3- A figure of the De-Propanizer and the conditions for separation

To increase the temperature to that of the boiling point of propane, a duty of about *6.9360 x 10^{10}KJ/h* of energy will be applied to accomplish it.

The over head product being rich of methane and the bottom product more of the condensate. The mole fractions between these streams as well as the properties are also shown below:

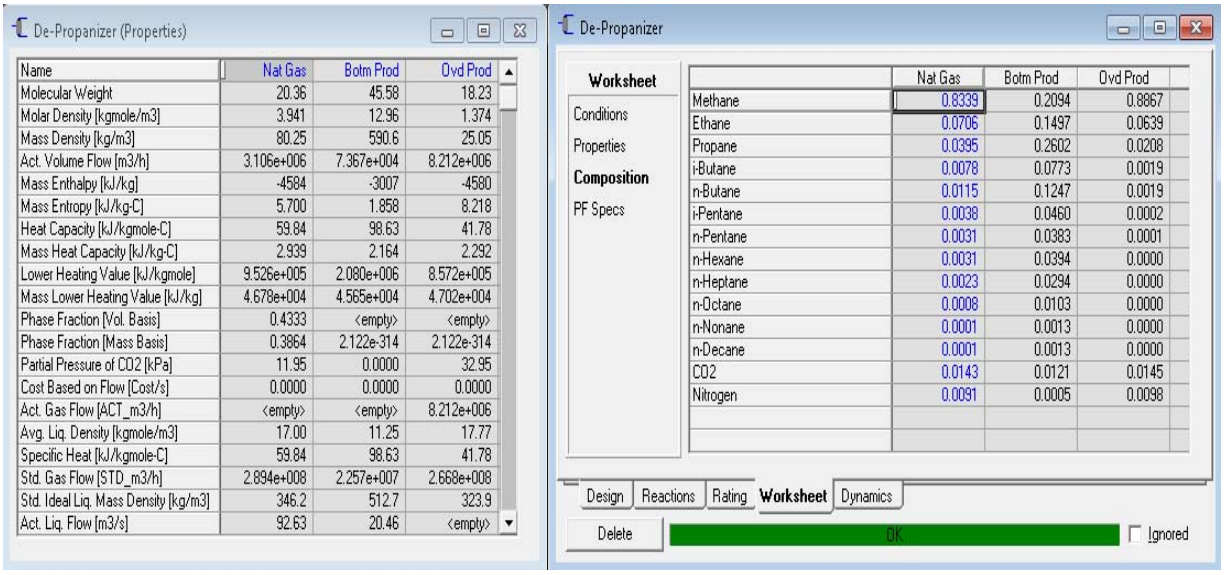

Figure3.4-properties and mole fraction of the overhead and bottom products

The result of the simulation is displayed on the excel spread sheet, presenting it in tabular form give clarity to the result achieved and for effective analysis. Separation of heavier components was done by the use of the De-butanizer simulation process of which is thus tabulated as it is on the excel spread sheet. Due to the flow rates of the two streams having the overhead stream very close to the feed, the overhead product will hence be further separated of its heavier component through the use of a De-Butanizer, this will be achieved through the same column separator as before but the set temperature will be at -0.5^{o}C. Non-return valves will be installed along the streams to prevent any form of back flow into the initial column. Also expanders were installed to help reduce pressure as well as the temperature to enable even further separation of the stream.

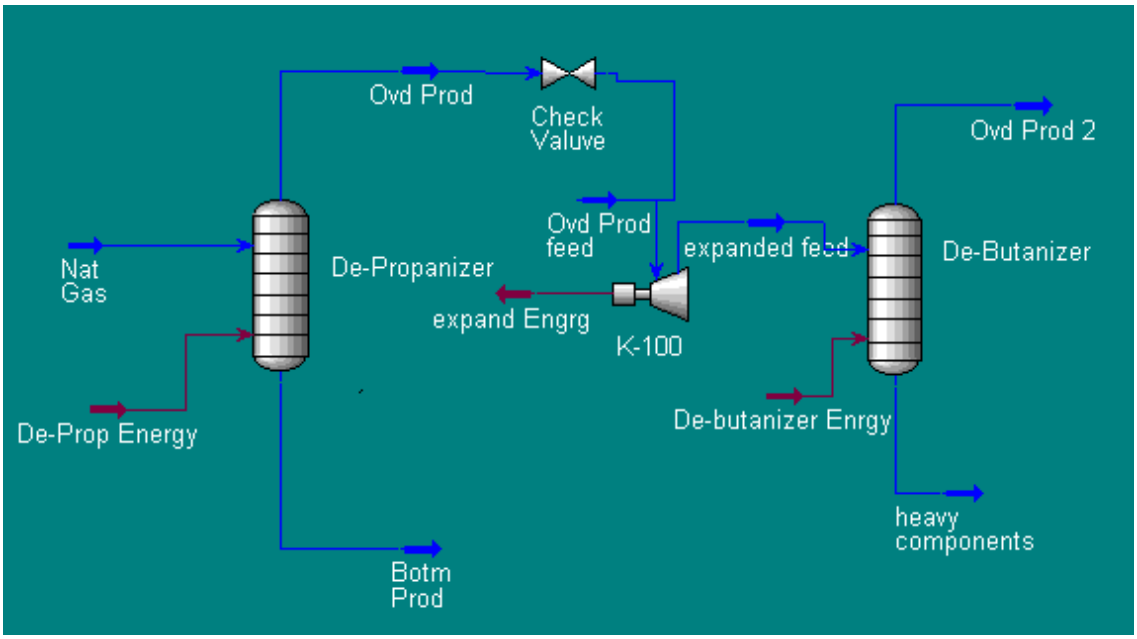

Figure3.4- Flow Diagram of De-Propanizer and De-Butanizer Configuration Separation Method

After the simulation with the use of hysys, the bottom and overhead products were determine which can be seen in the figure below, showing the De-Butanizer column is mostly contained with methane gas and its composition with a flowrate of 9.630x107 kg/hr (3.12x105m3/hr)
Presenting the mole fraction in a tabular form after the simulation details has been given below thus gives.

4.0 CONCLUSION

The domestic transportation project via pipelines and other parameters (approaches) such as LNG, and CNG can be seen as a viable solution to the many challenges faced by the NLNG in transporting natural gas. It would be of great benefit to Nigeria economy if NLNG company can invest in domestic transportation and utilization of natural gas. Domestic utilization and transportation of natural gas will promote employment to the teaming unemployed youths. It is now known that transporting natural gas from the point of production to market involved various approaches as discussed above so as to meet the aspiration of the populace. Natural gas usage cut across varieties of ways that can help boost the economy of the nation, thereby increasing the GDP. Agricultural production and other traditional occupation can be enhance through natural gas transportation for local utilization.

REFERENCES

Adesuyi, O.A., Njoku, M.O and Kolade, O.O (2015). Introduction to Oil and Gas Industry in Nigeria. *Journal of Geosciences and environmental protection*, 31,11-19, Vol 12.

ASME B36 Specification

Catania, Z.A (2004). Gas and Petroleum Application. 3rd Edition, Exnox Publishing Limited, Port Harcourt. Nigeria.

Chi,U.I (1988).Natural Gas Engineering, Penwall Publishing Company. New York, USA

Department of Petroleum Resources (2017) Annual Report. Available at http://departmentofpetroleumresources.gov.ng

Folga, S.M. (2007). Natural Gas Pipeline technology overview. United State Energy Department, Foreland. United State of America.

Idris, M.N. (2004). Review of Nigeria Oil and Gas Industry with Retrospect. 2nd Edition, Heimin Publishing company, Lagos Nigeria.

Iyagba, E. (2014). K,Natural Gas Characterization, 3rd Edition, University of Port Harcourt Press. Port Harcourt. Nigeria

Library of congress, (2011). Available at http://librarycongress.con (Retrieval, 21 June, 2017 Nigeria Extractive Industry Transparency Initiative (NEITI) Report on Gas Usage available at http:www.neti.gov.ng/gasreport (Reviewed, 28 September,2017).

NNPC Annual Report on Gas Utilization in Nigeria, 2017 Quarterly Bulletin Published by Research and Development (RandD) unit, NNPC Tower, Abuja, Nigeria. Vol. 8, 381-398.

Tunde, A.J (2003). Gas Industry in Nigeria, Retrospect and Realization. *International Journal of Applied science and Engineering.* 6 (3), 3811-3921, Vol 3.

Ubom, R.T. (2000). Energy Obligation in Nigeria, University of Benin Press, Benin City.

Uzoh, B.A (2014).Population Economics, 2nd Edition, Chibest Publishing Company, Owerri, Nigeria

Nigeria United Nation sustainable Development Goal on Energy consumption. Retrieval from http://www.uno.org/sustainabledevelopmentgoal (Viewed October 5, 2017).

Whither Nigeria Global Line Market Share, Business Day, 2017. Availableathttp://business daynewpaper.ng/gastransportationandobligation.

Proceedings of the 49th NSChE Annual Conference
KADA 2019: pp 756-766

P02: PRODUCTION OF BIOETHANOL FROM VARIOUS ARICULTURAL BIOMASS: Trends and Developments

Ogulu, E.O,[a] Oji, A[a] and Nwosi, H.A[a]
[a] World Bank Africa Centre for Excellence, Centre for Oilfield Chemical Research, University of Port-Harcourt, Port-Harcourt. Rivers State. Nigeria

ABSTRACT
Globally, investigation on bioethanol production has grown rapidly due to high energy demand and has steadily become research area of interest to government, academia and private sectors. Ethanol at the present is the most common renewable energy and it can be produced from many sources. With the availability of agricultural resources, bioethanol can be produce less expensively from agricultural base biomass. Raw materials used in the production such as sucrose base, starchy base and perennial grasses were reviewed. This paper surmises various processes at which this renewable source of energy can be produced from agricultural base biomass which includes pretreatment(physical and chemical), hydrolysis, direct fermentation and saccharification. Theses constitute the key steps in bioethanol production from agricultural base biomass which were considered. The paper also reviewed various generations of bioethanol with their component which also explained composition of some agricultural and forest residues. The agricultural sector rely on energy for effective and efficient output production that is a major component of the Nigerian economy of which bioethanol will boost the sector through energy utilization.

Keywords: Production, Bioethanol and Agricultural Biomass

INTRODUCTION
Bioethanol and biodiesel are the two main form of biofuels. Among those bioethanol produced by conversion of lignocellulosic biomass is being seen by analyst as the most promising alternative biofuel to replace fossil fuel (Ahmady*et al,* 2014). Biomass are biological materials obtained from living organisms (Ikenyiri and Oghu, 2016). It is most times refer to as plant-based materials. Biomass can be converted to other useful form of energy such as bioethanol, biogas, biodiesel and other chemicals combining both biological and chemical principles which are scientific(Ahmady *et al,*2014). The need for renewable, sustainable, cost effective and environmental friendliness is at highest rate, Shan andRahan (2014).The use of trees, crops, agricultural and forestry waste to make fuels, chemicals and generate electricity is already at advance stages in most developing and developed nations. Energy production will not only add to overcome global energy crises and environmental challenges but will also result in creating market opportunities for economic viabilities (ChumandOverand, 2001).The agricultural crops that have these biomass characteristics are sugar-based substances like sugar cane juice, sweet beets, sweet sorghum and molasses as well as starch-based materials like wheat, corn, cassava and potatoes, which are classified under first generation bioethanol materials, while second generation bioethanol materials are produced from sustainable feedstock that cannot be used directly for production. These materials are perennial grasses, agricultural waste and forest residue. The third generation bioethanol materials are direct cellulose fermentation (cellulose production, substrates hydrolysis and fermentation are accomplished in a single process steps y cellulolytic microorganism). These three generation of bioethanol materials will be extensively discuss in the literature review of this thesis. The development of alternative to fossil fuels and energy sources, has thus become a global research priority in recent time. The production of fossil fuel is capital intensive, due to high cost of refinery operating equipment (Adesuyi, 2015).The economic viability/accessibility of

these raw-materials for bioethanol production also gives high premium value to the energy sources. Bioethanol are transportation fuels that are produced from rotten garbage, agricultural and human waste which releases methane(CH_4) gases that adsorb moisture (Ogoni, 2006). Scientifically, these raw materials have high yield and selectivity in producing bioethanol due to their high moisture contents.

As it is well known, one major challenge facing the world is energy; it has being deliberated in different conferences, symposium and forums. The energy crises has affected the globe with varieties of imparts that has to do with human daily activities. This piece of crude oil dramatically has increase and decrease at some point , Energy consumption has also increase with rapid increase in human population, Due to the fact that petroleum is non-renewable resources , there is an urgent need to seek alternative energy source that are inexhaustible. With the international awareness on increasing Co2 concentration in the atmosphere and concern for global worming that is causing climate charge, the development of alternative fuel to fossil has become imperative (El-Nagger, 2014**) ,** This fuel is biofuel which are produced from biomass. Biomass are biological materials obtained from living organisms, In some cases, They are agricultural materials that are either cultivated by human or existing natural forms. Bioethanol that are produced from biomass is one of the most promising biofuel to replace fossil fuel like gasoline for future transportation vehicle**, (**El-Nagger, 2014**).** These biomasses are essential raw materials for bioethanol production. Agricultural activities involves cultivation, planting, harvesting of which biomass is part of their process. In Nigeria, the agricultural sector has suffered neglect as a result of underutilization of its potentials and bye products that serves as raw materials for the production of major products like bioethanol. The quest for renewable, sustainable, cost effective and environmental friendly source of energy for human consumption is on the increase. The source of energy independence requires strict measures for making and using such renewable source to prevent the environment. Use of trees, crops and agricultural / forestry wastes to produce fuels, chemicals and electricity is at advance stage in developed and some developing countries like Nigeria. The energy production from this source will not only help in overcoming the energy crises, but also bring in emerging market opportunities for investors, lowering environmental impacts, increasing energy security and diversity, reduce Co_2 emission (ChamsandOverend,2001).Formulation of policy for production of renewable energy sources can greatly help in overcoming environmental / energy crises facing today's society. Various renewable fuels are produced from agricultural

Sources such as; sugar base, starchy base and lignocellulose wood straw and grasses. The aim of this research is to review bioethanol production from various biomasses of agricultural products that will help solve the world energy crises. Several renewable fuels are produced from waste of different agricultural sources such as; cassava, sugarcane, and wood straws. Bioethanol is one most renewable energy source whose prospect is promising for green energy revolution. It is often used as blender with gasoline to reduce emission of Co_2, Nox and hydrocarbon after combustion. (Balan et al., 2013; Chandol et al; 2017**)**. Developmental stride in agriculture can be attributed mostly to energy availability in either making food for green plants in form of photosynthesis (thermal energy), storage of harvested products or production of other syntheses such as fertilizer etc of which makes bioethanol an important ingredient in 21st century advancement. The researchers identified the linkage between agriculture and bioethanol as simple as interaction between same species. In Nigeria, were occupation of the populace is centered around agriculture, there is need to vigorously formulate an energy-agro policy for the growth of the economy.

Generation of Bioethanol Materials

First Generation or Conventional Bioethanol

These are generation of bioethanol produced from sugar-base substances such as sugar cane juice, sugar beets and molasses as same as starch base biomass materials like corn, potatoes and cassava. Though the production of ethanol from starch biomass materials represent the most convenient and technically advance alternatives for bioenergy, which will result in competitiveness between energy and food supply. The raw-materials account for 40-70% of total ethanol production cost is based on current sugar or starch containing feedstock. Reduction on the production cost will make biofuel (bioethanol), compete with fossil fuels.

Second Generation Bioethanol

These are generation of bioethanol produced from sustainable feedstock, that can be applied directly for food production. Example are waste that can be potentially converted into bioethanol are perennial grasses, agricultural waste and forest residues. The conversion of these potential sources of feedstock for bioethanol offer several benefits of global waste reduction and development of valuable transportation fuels.

Third Generation Bioethanol

The third generation bioethanol is produced via direct cellulose fermentation (cellulose production, substrate hydrolysis and fermentation) are accomplished by a single process step by cellulolytic microorganism.

2.3 Lignocelluloses

By-products from the cultivation of corn (corn stover),wheat(wheat straw),rice straw, sorghum(sorghum stalk),barley (barley straw) and sugar cane juice(sugar bagasse) are major sources of agro-based lignocellulosic, which contains high content of cellulose and hemicellulose as described in table below(1.0). It is significant issue to dealwith agricultural waste both for comprehensive of lignocellulosic resources and for prevention of environmental pollution. One technique to overcome these challenges is the biological and chemical conversion of agricultural waste to biofuels. Production of bioethanol from renewable lignocellulosic resources (biomass) is a promising means to reduce the accumulation of green-house gases and alleviate pressure on fossil shortage(Gale and Zacchi, 2002). The main constituents of lignocellulosic nbiomass are hemicellulosic, cellulose and lignin(Kumar et al.,2009).Minor components includes ash and extractives such as waxes. On a dry weight basis, lignocelluloses contain 40-50% cellulose, 20-35%hemicellulose and 15-20% lignin. These components represent approximately 90% of dry weight of most plant materials (Brown, 2003).The cellulose chain is a linear, unbranched polymer of glucose monomers linked by β-1, 4-glucose bonds.

Table 1.0: Composition of some common and Forestry Residue

Source	Cellulose(%)	Hemicellulose(%)	Lignin(%)
Hardwood	40-55	24-40	18-25
Softwood	45-50	25-35	25-35
Corn Stover	38-40	28	7-21
Corn cob	45	35	15
Bagasse	32-48	19-24	23-32
Wheat straw	33-38	26-32	17-19
Rice Straw	28-36	23-28	12-14
Sorghum stalk	27	25	11
Barley straw	31-35	27-38	14-19

Leaves	15-20	80-85	0

Sources: Kumar *et al* (2009)

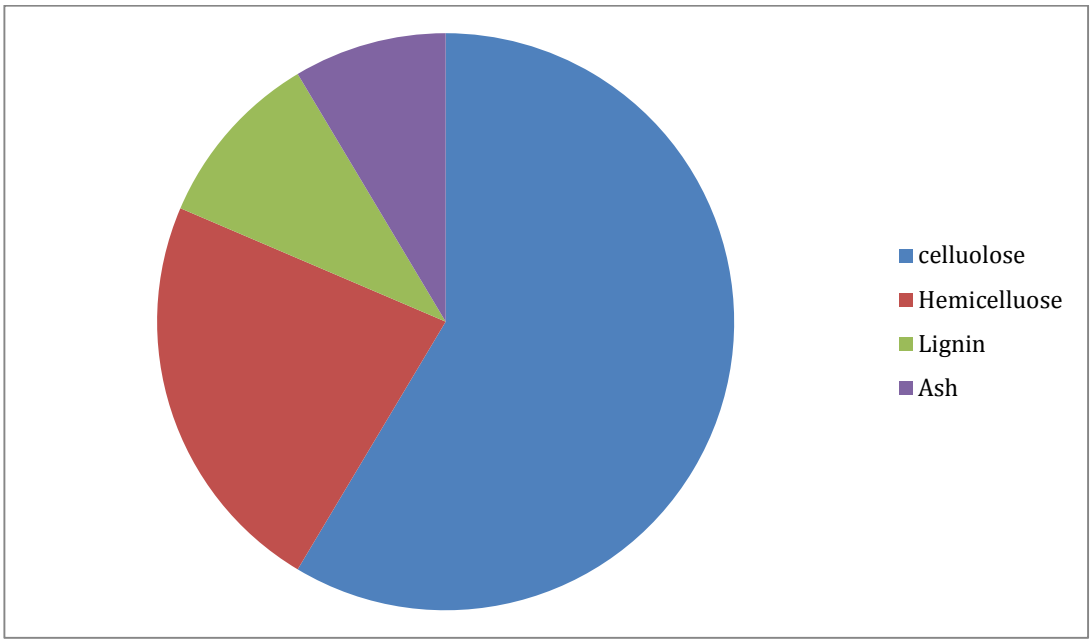

Figure 2.2: Constituents of Lignocellulose biomass

1. **Materials and Methods:**

Bioethanol is produced from several cheap materials which are mostly agricultural base raw material such as Starchy, sucrose and lignocellulose. These materials are wheat, corn cassava, sugar beet, sweat sorghum, sugar cane, wood straw and grasses**. (**Balat and Balat 2009). These materials are classified according to generation which are first, second and third generations respectively. In the production of ethanol several methods are involved such as direct fermentation, hydrolysis and simultaneous and saccharification and fermentation (SSF). The production of bioethanol using modern technological techniques is steadily undergoing innovation on daily bases due to high efficiency on thermodynamic equipment. The various materials considered in this paper essential for bioethanol production from biomass that involves some applications. These constitute majorly of agricultural characteristics and properties making suitable for this purpose. The raw-materials are Starchy-base substances such as wheat, corn, potatoes and cassava. Sucrose-base substances like sugar cane juice, sweet sorghum and molasses. Lignocellulose biomass such as wood straw and grasses.

Methods

The methods involved in the production of bioethanol from various agricultural biomass are thus described below.

Direct Fermentation;

This is usually carried out for starch base biomass because; it must be first hydrolysis to glucose before being fermented by yeast through the application of saccharomyces cerevisea. Hydrolysis process;Though acid hydrolysis of cellulose biomass is an ancient practice of converting biomass into sugar like glucose and then ethanol. This is always achieved by simple fermentation process. The flow chart for hydrolysis is given below

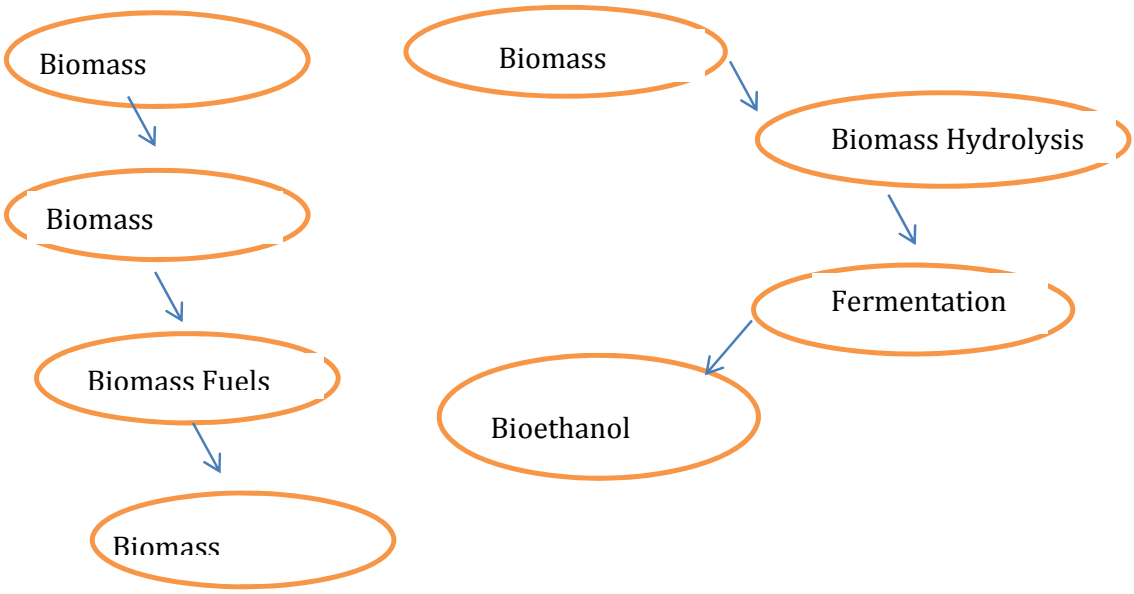

Simultaneous, Saccharification and Fermentation;

Bioethanol Production from several biomass sources (mostly agricultural) always requires pretreatment and saccharification which is mostly converted to bioethanol by simultaneous fermentation and saccharification process. It is always biological in nature because it is done by strains of yeast and bacteria's (Cao et al; 2014, Cheng et al; 2017). The selection this strains for production of bioethanol, is mostly achieve by considering their productivity, tolerance to ethanol, fermentation inhibitors and severe PH including temperature condition (Cao et al; 2014). S. ceravisiae is normally in the fermentation process. Direct cellulose fermentation is also used in a single process step by cellulolytic micro-organism. It involves cellulose production, substrate hydrolysis and fermentation in SSF which is achieve in one step.

Pretreatment Phase Involved in the Production of Bioethanol

The pretreatmentphase involved in the production of bioethanol are

Physical Pretreatment

This process increase the accessibility of the surface and size of the pore decrease the crystallinity and degree of polymerization of the cellulose. Different type of physical processes such as milling and irradiation will be applied to improve the enzymatic hydrolysis of lignocellulose waste materials.

a) Milling(cutting the lignocellulose biomass into smaller sizes) will be adopted to alter the inherent structure of lignocelluloses and degree of crystallinity and consequently make it more amenable to cellulose. Milling can improve enzymatic degradation of lignocellulose materials toward ethanol by reducing the size of the materials (Cheng and Holtzapple, 2000.,Zeng*et al.,*2007). The reduction in particle size lead to increase of specific surface and in degree of polymerization(Palmowski and Muller,1996).
b) Irradiation by example gamma rays and microwaves can can improve enzymatic hydrolysis of lignocelluloses.The combination of irradiation and other approaches such as acid hydrolysis(Mamar and Hajadj, 2000). Irradiation will enhance enzymatic degradation of cellulose into glucose. Kamara and Kaetsu(1998) research the effect of irradiation for pretreatment bagasse prior to its enzymatic hydrolysis.

Chemical Pretreatment

This treatment involves the following:

a) Dilute Acid Treatment

Treatment of lignocellulose materials with acid at high temperature can effectively and efficiently improve the enzymatic hydrolysis. Sulphuric acid (So_2) is the most acid to be use while acids such as hydrochloric (HCl), nitric etc have also reported (Taherzadeh and Karimi,2007). The acid pretreatment can operate under either high temperature, for example 180^0C for low concentration temperature(120^0C for 30-90 minutes) with high acid concentration(concentration acid pre-treatment). This is the most common approach among the chemical pre-treatment methods. It should be noticed that chemical pre-treatment have dual effect on biomass crystallinity. These effect includes

1) They remove amorphous lignin and hemicellulose components to increase to increase biomass crystallinity
2) They loosen the high packed crystalline structure through swelling to decrease crystallinity (Gharpuray*et al.,*1993).

The main benefit of dilute-acid pretreatment is the possibility to recover high portion(e.g 90%) of hemicellulose sugar. However, the main disadvantage of this pretreatment approach

(technique) is the necessity of neutrality of pH for downstream enzymatic hydrolysis (Charpuray*et al.,*2002).

b) Alkaline Pretreatment

Alkaline pretreatment refer to the usage of alkaline solution such as NAOH, $Ca(OH)_2$(lime) and NH_3 to remove lihgnin and part of hemicellulose and efficiently increase the accessibility of enzyme to the cellulose. This pretreatment can be performed at low temperature with relative long time and high concentration of the biomass.

Ozonolysis Pretreatment

Pretreatment of lignocellulosic materials can be performed with ozones, popularly ozonolysis pretreatment. This approach can effectively degrade lignin and part of hemicellulose. This pretreatment is usually performed at room temperature and does not lead to inhibitory compound(Sun and Cheng, 2002). The main parameter in ozonised pretreatment are moisture content of the sample, particle size and ozone concentration in the gas flow.

Physio-Chemical Pretreatment

This is the pretreatment approach that combine both physical and chemical process which result in electrochemical process (Chandra *et al.,* 2007).

Ammonia Fibre Explosion(AFEX)

This is an alkaline physio-chemical treatment process. The biomass will be liquid ammonia at relative high temperature(90-100^{0}C), for a period of 30 minutes, for example, followed by immediate reduction on pressure. The effective parameters in AFEX process are NH_3, loading, temperature, water loading blow down the pressure and time (Holtzapple*et al.,* 2000).

Discussion

The various steps involved in bioethanol production can be evaluated using chemical reactions to show the mechanism with a specific weight of cellulose and sugar including carondioxides. It was shown that intracellular hydrolysis minimized glucose repression of xylose fermentation allowing co-consumption of cellubiosse and xylose that improve ethanol yields. The reaction at the theoretical maximum yield is 0.51 and 0.49kg of ethanol kg -1 of C_6 or C5 sugar (Qui, 2010)

$C_6H_{12}O_6$ —Cerevisae→ $2C_2H_5OH+2Co_2$

Glucose 1kg Ethanol

Carbondioxide,

0.5kg 0.49kg

$3C_5H_{1O}O5$ —Pentose fermenting micro-→ $5C_2H_5OH + 5CO_2$

Pentose Ethanol

carbondioxide

0.49 O0.49kg 0.5kg

It is of note many processes are involved in the production method at bioethanol, which is:

-Physical pretreatment; this can increase the accessible surface and size of pore and increase the crystallining and degree of polymerization of the fermented biomass (cellulose). This is achieve through direct applications.

-Chemical Pretreatment: This is achieved by dilute acid treatment, alkaline treatment and ozonolysis.

This processes that are involved in production of bioethanol from biomass are achieved through biological and chemical principles. The Ammonia Fibre Explosion(AFEX) involves liquid ammonia in the process, but the process is not common due to the capital intensive nature of its operation.

Conclusion

With the increasing demand for renewable energy resources, bioethanol is considered as one of the most suitable and economic fuel for the future. The environmental hazard caused by the biomass can be decreased by utilizing them into useful product and generate wealth for economic empowerment. Various pretreatment processes yeast and strains of bacterial are used to convert biomass into bioethanol. In renewable processing of biomass or direct biomass production, the cost effective technologies requires further research, development and diffusion of Commercialized new technologies. The conversion of biomass into bioethanol not only can accomplish the demand for energy resources but also have positive effect on the environmental and socio economic position of Nigeria as a country. Further research and technologies development are required in the discipline of bioethanol production from biomass, so as to replace and ride the society of fossil fuel that is causing environmental and economic burden to the Nigerian society. This study will bring to the fore-burner crucial needs of seeking alternative fuel and energy sources other than fossil fuel that is a major pollution agent to the atmosphere, which threaten human existence. Furthermore the study will advance the quest for competitive energy market. The conversion of biomass to bioethanol will diversify the over dependence on crude oil that has resulted in several negative impact in society such as insecurity, laziness and neglect of other sector of the economy. Pollution which is a major threat to human health will be curtailed with the conversion of biomass to bioethanol, due to its carbon neutrality. This study will also help in encouraging Foreign Direct Investment (FDI) that will promote employment and economic growth with increase in the nation's GDP.

References

Adesuyi, A .O. (2013). Economic Impact of Biofuel in contemporary world: Important and concept. Heimann Publishing, Ibadan. Nigeria

Amin, S (2009). Review on Biofuel oil and gas production from microalgae. *Energy Conversion and Management, 50(7), 1834-1840*

Ahmady, N., Sahar, K and Ashraf, K (2014). Bioethanol production from lignocellulosic feedstock based on Enzymatic Hydrolysis: Current Status and Recent Developments*. Journal for Asian Network for Scientific Information. 13(1):1-12*

Balan, N., Chairamonti, D and Kumar, S (2013). Review of United State and European Initiatives toward development, demonstration and commercialization of lignocellulosic biofuels, bioproducts and biorefining, 7(6), 732-759

Balat, M andBalat, H (2009).Recent trend in global production and utilization of biofuel.*Applied Energy, 8(3),654-660*

Brown, A.O.(2008). Biomass potentials in 21st Century: Issues and Concepts. *Journal of Applied Energy , 86(11), 2273-2282*

Cao, L., Tang, X., Chan, E.,Tian,X.,Wang, J and Xiao, W(2014).Two stages transcription programming in sacharomycecerevisae for optimizing ethanol production form xylose. *Metabolic Engineering Journal, 24, 150-159*.

Chandel, A.K., Chana, E., Rudravaram, R., Nasau, M.L., Rao, L.V andRavindra,P(2007). Economics and Environmental Impact of Bioethanol production Technology*: An Appraisal Biotechnology and Molecular Biology Review, 2(1), 14-32*

Cheng, K.K.,G,J.R., Zhang. J.A., Ling.,H.Z., Zhou, Y.J., Yang, J.M (2007). Fermentation of pretreated sugar cane bagasse hemicellulose hydrolase to ethanol by pachysolentannophilus. *Biotechnology Journal, 29(7), 1051-1055*

Cheng, V.S andHoltzapple, A (2000). Fundamental factors affecting biomass activities.*Applied Biotechnological Journal, 84-86; 5-7*

Choi, G.W., Moon, S.K.,Kang, H.W., Min, Jand Chung, B.W(2009).Simultaneous saccharification and fermentation of sludge containing cassava for batch and repeated batch production of bioethanol by saccharomyces cerevisiae. CHF Y0321*. Journal ofChemical Technology and Biotechnology, 84(4), 547-553*

Chum, H .JandOverand, R.P (2001). Biomass and Renewable fuels.*Fuel processing technology, 71(1), 187-195*

Colins (2003). The coming oil crises: Multi Science Publishing Company, New York, United State.

Colins (2009).Economic Advantage of Biomass. Multi Publishing Company, New York. United State.

Conde-Mejia, C., Jimenez-Gutierrez, A.and El-Halwagi, M (2012). A comparison of pretreatment methods for bioethanol production from lignocellulosic materials*. Process safety and Environmental Protection, 90(30), 189 -209*

Cuzens, J.C and Miller, J.R(1997). Acid hydrolysis of bagasse for ethanol production. *Renewable Energy Journal, 10(2), 285-290*

Dagnino, E., Chamorro, E.,Romano, S.,Felissi, FandArea, M(2013). Optimization of acid pretreatment of rice hulls toobtain fermentable sugar for bioethanol production. *Industrial Crops and product Journal, 42, 363- 368.*

Dalla-Marta, A., Mancini, M., Orlando, F., Natali, Capecchi, LandF Orlandini, F(2014). Sweet sorghum for bioethanol production: Crops response for different water stress level*. Biomass and Bioenergy Journal, 64, 211-219*

Demirbas, A.(2009). Biofuel securing the planet's future energy needs*. Energy conversion and management, 50(9), 2239-2249*

Doberman,A and Fairhust, H.J(2002). Combustion of Biomass and its effects.*African Journa of Biotechnology Research, 7(13), 38010-4101.*

Di-Nasso, A., Ronucci, N., Triana, C.,Tozzini, AandBonari, E (2011). Seasonal nutrients dynamics and biomass quality of giant reed and miscanthus as energy crops. 6, 152-158

Ewanick,.S..M., Bura, R and Saddler J.N(2007).Acid catalysed steam pretreatment of lodgpole pine and subsequent enzymatic hydrolysis and fermentation to ethanol. *Biotechnology and Bioengineering Journal, 98(4), 737-747*

Galbe, H andZacchi, J(2002). A review for the production of ethanol from softwood.*Applied Biotechnology Journal,59: 618-628*

Gasper, M., Kalman, K and Reczey(2007). Corn fibre as raw material for hemicellulose and ethanol production process. *Biochem., 42:1135-1139*

Gharpuray, M., Lee, YandFan,T(1993). Structural modification of lignocellulosic by treatment to enhance enzymatic hydrolysis. *Bioengineering Journal, 25, 88-89*

Gong, C.S., Chen, L.F., Flickinger, M.C.,Chiang, L.C andTsao, G.T(2006). Production of ethanol from D-xylose by using D-xylose isomerase and yeast*. Applied Environmental Microbiology Journal, 41(2), 430-436*

Galbe, H andZacchi, J(2002). A review for the production of ethanol from softwood.*Applied Biotechnology Journal,59: 618-628*

Haghighi-Mood, S., Hossien, G.A., Tabatabaei, M., Saleh, J.G.,Najafi, G.H., Gholami, MandArdjmand, M (2013). Lignocellulose biomass to bioethanol, a comprehensive review with focus on pretreatment.*Renewable and Sustainable energy review, 27, 77-93*

Hamer, G (2003). Solid waste treatment and disposal: Effect on Public health and environmental safety. *Biotechnology Advance Journal, 22(1), 71-79*

Hammond, J.B., Egg, R., Diggings, D and Coble, C.C (1996).Alcohol from Biomass.*Bioresources Technology Journal, 51(1), 124-130*

Han, M., Kang, K. E., Kim, Y., and Choi, G.-W. (2013). High efficiency bioethanol production from barley straw using a continuous pretreatment reactor. *Process Biochemistry,(48), 488-49533*

Hari Krishna, S., Prasanthi, K., Chowdary, G., andAyyanna, C. (1998). Simultaneous saccharification and fermentation of pretreated sugar cane leaves to ethanol*. Process Biochemistry, 33(8), 825-830.*

Horn, S., Aasen, I., andØstgaard, K. (2000). Ethanol production from seaweed extract.*Journalof Industrial Microbiology and Biotechnology, 25(5), 249-254.*

Hu, G., Heitmann, J. A., and Rojas, O. J. (2008). Feedstock pretreatment strategies for producing ethanol from wood, bark, and forest residues. *BioResources Journal.* 3(1),347-268

Ikenyiri, P.NandOghu, C,Y(2016). Comparative study on the Behaviour of Biomass adsorbent used in Environmental applications: Oil and Gas industrial effluent*. Nigeria Journal of Oil and Gas Technology*

Kayler, M., Van-Dyne, Yand Blasé, A(2000). Economic feasibility of producing ethanol from lignocellulose feedstock. *Bioresources Technology,. 72,19-32*

Kheshgi,H.S., Prince, RandMarland, G(2000). The potential of biomass fuel in the context of global climate change: Focus on transportation fuel. *Energy Environ., 25,19-32*

Kumakura, M andKaetSu, I(2007). Effect of radiation pretreatment of bagasse on enzymatic and acidic hydrolysis. 3: 199-208

Levin, O.P(1996). Carbondioxide emission: effect and solutions*. Journal of Biotechnology Research, 73(5), 3801-3815*

Malherbe, LandCloete, M(2003). Lignocellulose biodegradation: Fundamental and Application. *Environmental Journal of Bioresources. 98: 815-832*

Maise, O., Eighlalian, A.,Saddler,J andMansfield, S(2002). Enhancing enzymatic hydrolysis of cellulose materials using simultaneous ball milling. 98, 815-832

Palmowski and Muller(1999).Influence of size reduction of organic waste on their anaerobic digestion*. Proceedings of the 2nd International symposium on anaerobic digestion of solid waste. June 15-17,1999, Barcelona, Spain.pp 137-144*

Sameera, V., Sameera, CandRaviteja, Y(2011). Current strategies involved in biofuel production from plant and algae. Longman Publishing, Nairobi, Kenya.

Shan and Rehan(2013). Approaches in treatment of lignocellulose materials to bioethanol.*Indian Journal Advance Scientific Research, 14, 371-378*

Sun and Cheng(2002). Hydrolysis of lignocellulose materials for ethanol production: *A BioresourcesTechnoogy, 83, 1-11*

Taherzada, MandKarimik (2007). Acid base hydrolysis process for ethanol from lignocellulose materials.*Bioresources, 2, 472-499*

Tran, A.V and Chambers, R.P(1986). Ethanol fermentation of red oak acid prehydrolysed by the yeast enzyme microbial technology. 8, 439-444

Vidal, P andMolinier, J(1998). Ozonolysis of lignin improvement of vito- digestibility of poplar saw dust*. Biomass. 16, 1-17*

Walfridsson, M., Bao, X., Anderlund, M., Lilius, G., Bülow, L., and Hahn-Hägerdal, B. (1996). Ethanolic fermentation of xylose with Saccharomyces cerevisiae harboring the Thermusthermophilusxyl A gene, which expresses an active xylose (glucose) isomerase. A*pplied and environmental microbiology*, 62(12), 4648-4651.

Wyman, C.E (2001). Handbook on bioethanol production and utilization. Taylor and Francis Press Washington D.C

Yang, B andWyman(2004). Effect of xylan and lignin removal by batch and flow through pretreatment on the enzymatic digestibility of corn stover cellulose.*Journal of Bioenginering, 86, 88-89*

Zang, M.; Mosier, N.; Haug,C.; Sherman, OandLadish, M(2007). Microscopic examination in plant cell structure in corn stove, due to hot water pretreatment and enzymatic hydrolysis. *Bioengineering Journal, 97:265-278*

Zhu, J., Pan, X., Wang, G andGleissier, L(2009). Sulfite pretreatment for robust enzymatic saccharification of sprue and red pine.*Bioresources Technology, 100, 2411-2418*

Proceedings of the 49th NSChE Annual Conference
KADA 2019: pp 767-784

P04: PHASE CHANGE MATERIAL AS ENERGY AUGMENTATION SOURCE FOR SOLAR POWERED AMMONIA-WATER ABSORPTION REFRIGERATION SYSTEM FOR AGRICULTURAL PRODUCE Storage

S.N. Mumah, O. Olaniyan, H.F. Akande, K.Y. Mudi, T.M. Garba, Usman Rumah and Francis Samuel
College of Engineering, Kaduna Polytechnic, Kaduna, Nigeria
Contact: +234-8037619719, mumahsndoyi@kadunapolytechnic.edu.ng

ABSTRACT
This paper provides an overview of the ongoing TETFUND National Research Fund project " Phase Change Material as Energy Augmentation Source for Solar Powered Ammonia-Water Absorption Refrigeration System for Agricultural Produce Storage" The goal of this project is to prove the feasibility of augmenting the power source of a solar powered ammonia-water refrigerating system by incorporating a phase change material energy storage process. This project intends to develop a holistic approach for the experimental and numerical evaluation of the thermal behavior of new thermal energy storage (TES) materials suitable for Ammonia water solar powered refrigeration system. The project also intends to construct a prototype which will be numerically and experimentally optimized. The specific research goals are to, to evaluate the usage of phase change materials as additional energy source for solar powered ammonia water absorption refrigerating system; demonstrate that phase change material energy storage system is capable of heating the working fluid (ammonia-water) up to an operating temperature of 110°C; design, fabricate and test a solar powered Ammonia-water absorption refrigerating system with a phase change material energy storage process incorporated; demonstrate that the prototype, when fully coupled, is capable of producing cooling at 5°C and below, and generate data that can be used to produce commercial solar powered ammonia water cooling systems with energy source augmented by phase change materials.

The TETFUND National Research (NRF) Project "PCM Solar Powered Refrigeration Project" is a challenging project involving researchers from different scientific backgrounds, namely Chemical, civil, and mechanical Engineering.

Keywords: Phase Change Material, Solar Powered, Ammonia-Water Absorption, Energy Storage, Thermodynamic analysis, modeling, Design and Fabrication

Introduction
The recent revelation that the country imports over 70 metric tons of tomatoes at an estimated cost of N11 billion annually while tomatoes go to waste in rural areas is not acceptable for the Nigerian economy *(http://agronigeria.com.ng/unnecessary-waste-of-agricultural-produce/)*. In Nigeria, a considerable amount of produce is wasted because of poor transportation systems and poor marketing procedures. Much produce is spoiled because it is stored beyond its inherent shelf life before marketing is completed. The challenge of feeding Nigeria's ever growing population is not really about agriculture and food production but getting the food to the people. The biggest contributors to waste are the lack of refrigerated transport and adequate high quality cold storage facilities for farmers, food manufacturers and food sellers (retailers).

Agricultural products cannot be stored indefinitely. The maximum storage duration (the shelf life) of agricultural products varies and can be only a few days for some fruits and vegetables,

a couple of months for most tubers and bulbs, and over a year for dried food grains or other seeds. The shelf life of agricultural products depends, first of all, on the product itself. Generally, fruits and vegetables perish faster than tubers and bulbs while grains and seeds last longer.

Controlling the levels of waste is beyond the capability of individual farmers or consumers. The problem is wider and involves market schemes, availability of power supply, quality of roads and focused government intervention as well as a need for a more pronounced investment in the sector. What Nigeria lacks and needs is a well-developed cold chain infrastructure. Without it, Nigeria's problems are vast and likely to grow. As an example, waste is responsible for 50 per cent of the current cost of vegetables and fruits in Nigeria *(http://agronigeria.com.ng/unnecessary-waste-of-agricultural-produce/).*While the cold storage may be the solution, the infrastructure in Nigeria is not adequate to support it. Lack of electricity in the rural areas means cold storage must be achieved by other means.

Solar powered systems have found increasing use in urban areas in Nigeria but its application to cold storage has been limited. The reasons for this are not farfetched. Solar power is intermittent and to use it efficiently, solar power storage systems must be incorporated so that the system can operate 24 hours. There is the additional challenge of low solar intensity at some periods of the year which must be solved. Furthermore, the rural electrification situation in the country is very pathetic. With the never ending threat of increase of the cost of electricity from electric power distribution companies, very few farmers can afford to pay for cold storage facilities for their produce.

The use of solar energy as alternative energy source to power refrigerating systems is well documented (Mumah, 1994; Ioan and Sebarchievici, 2015; Siddiqui and Saad, 2015). The limitation is obvious, operating alone, they can only provide cooling during periods of peak sunshine. To ensure that such systems have all day use, augmentation systems must be incorporated.

Two types of absorption refrigerating systems are commonly used, the Ammonia-Water (NH_2/H_2O) and the Lithium Bromide-Water ($LiBr_2.H_2O$) absorption systems (Mumah, 1991; Mumah, 2008; Chung *et al.*, 2014). Since the storage of most agricultural produce can be achieved at 5^oC or less, ammonia-water absorption water system will be the system best suited for this purpose.

The main trust of this work is to investigate the feasibility of incorporating phase change materials as energy storage media into a solar powered ammonia-water absorption refrigerating system. The phase change material circuit is to provide additional heat energy to the refrigerating circuit during the night and other periods when the solar intensity is low, after storing heat energy during periods of high solar radiation. This will enable the refrigerating system to operate day and night. Phase Change Materials (PCM) are substances that absorb and release thermal energy during the process of melting and freezing. When a PCM freezes, it releases a large amount of energy in the form of latent heat at a relatively constant temperature (TingXian *et al.*, 2014).

The specific objectives of the project are to;

a. carry out detailed studies to determine the appropriate phase change material to incorporate into a solar powered ammonia water absorption refrigerating system to ensure continuous performance;

b. perform analysis on absorption refrigeration system using ammonia and Water as refrigerant and to find out the influence of operating temperatures on the thermal loads of components and their coefficient of performance;
c. come up with the operating conditions where it can run by effectively utilizing both solar energy and phase change material storage systems;
d. design and fabricate a prototype to investigate the outcome of the theoretical studies;
e. evaluate and optimize the system for maximum performance;
f. generate relevant data required for the full commercialization of the project.

Conceptual framework of the Study

In solving the agricultural produce wastage problem in the country, various methods can be applied such as developing better roads infrastructure, acceleration of rural electrification or developing storage facilities that can operate efficiently in rural areas. Providing wide roads infrastructure and providing electricity to all homes in the rural areas are presently not achievable because of the huge funds required and the country lean financial resources.

The basic assumption underlying this research is that proving solar powered refrigeration can be the solution to this problem and that the ammonia-water absorption system is the system of choice based on past studies (Mumah, 1991, Mumah *et al*., 1994, Mumah, 2008, Ioan and Sebarchievici, 2015). Many cooling systems have been designed and fabricated that operate on solar energy. The major challenge with all of these systems is their intermittent nature – they can only operate during sunlight hours. Such systems must be turned off in the night.

This proposal is an attempt to solve the intermittent challenge affecting solely solar powered systems with the aim of preserving agricultural produce in rural areas where electricity power access is a challenge. We intend to solve this problem by researching on the use of phase change material as energy storage bank for ammonia-water refrigerating system.

After a critical evaluation of phase change materials as energy storage bank, there will be the need to test the outcome of our theoretical analysis. This will be achieved by designing and fabricating a prototype of a solar powered ammonia-water absorption system with a phase change material storage component incorporated. To effectively design, fabricate and evaluate such a system, there is the need to carry out extensive thermodynamic modeling and analysis of the various phase change materials that exist to determine the best one to use. After such determination, proper design, fabrication of individual components of the prototype will be done and then coupled. There is the need to incorporate various instruments like pressure gauges, temperature measuring devices, flow meters, etc, to aid in the analysis of the system.

The trust of this work is that we will be contributing to solving the food security challenge of the nation by developing a product that runs day and night without the use of electric power. Another thrust of this work is that incorporating phase change materials as heat source for solar powered ammonia-water refrigerating system has not been carried out before and in performing this study, we will be contributing something new to knowledge. The knowledge gained from this research can be translated to developing solar powered phase change material cooling devices for vaccines storage in the rural areas which is also a serious challenge in the country.

Literature Review

Reducing Nigeria's fuel dependency and environmental impact requires the development of renewable energies such as wind, hydropower biomass or solar. Thermal solar power plants represent a huge opportunity in areas where solar irradiation is of at least 2,000 kWh/m^2/year (Cavallaro, 2010). This is so in Nigeria. However, this technology has a critical limitation which is its intermittence. This inhibits the regular cooling and therefore decreases equipment performance. For this reason, it is essential that economical and effective energy storage systems are developed to augment the system.

In solar thermal generation, thermal storage is the suitable storage mode. There are three methods to storage thermal energy: sensible, latent and chemical heat. Latent heat storage systems have the potential of storing a large amount of energy per unit mass. Moreover, latent heat storage could store fusion heat at a constant temperature which is the phase transition temperature of the phase change materials (PCMs).

Unfortunately, most of the PCMs possess a low thermal conductivity (around1W/mK) which limits their deployment in large scale applications like thermal solar power plants (Pincemina *et al.*, 2008). This is the reason that has enhanced the development of different solutions whose target is improving the heat transfer from PCMs.

In sensible heat storage, the temperature of the storage material varies with the amount of energy stored. The amount of thermal energy that is stored depends on its specific heat and on the temperature variation. It has been implemented in thermal solar power plants through thermocline or two tanks systems using molten salt as storage medium (Pincemina *et al.*, 2008). Latent heat thermal energy storage is attractive due to its high energy storage density. When compared to conventional sensible heat energy storage systems, latent heat energy storage system requires a smaller weight and volume of material for a given amount of energy (Agyenim *et al.,* 2010).

Furthermore, latent heat storage stores fusion heat at a constant or near constant temperature which correspond to the phase transition temperature of the PCMs. In practice, solid-liquid phase change is preferred because of simultaneous slight volume variation and high enthalpy variation (Mumah, 2008).

Latent heat storage through PCMs has the advantage of compactness because the fusion heat of PCMs is quite larger than their specific heats. The PCMs could be classified into two groups: organic and inorganic compounds. Inorganic compounds show a volumetric latent thermal energy storage capacity thrice that of organic compounds. Nevertheless, organic substances present advantages such as their ability to melt congruently, their self-nucleation and their non-corrosive behaviour (Pya *et al.*, 2001).

An analysis of heat transfer problems in the phase change processes is complex as the solid-liquid boundary moves depending on the speed at which the latent heat is absorbed or lost at the boundary. The position of the boundary is unknown and forms part of the solution (Kurklu *et al.*,1995; Agyenim *et al.*, 2010). These types of problems are referred to as a moving boundary problems or Stefan's Problem.

Solutions to phase change problems include analytical, experimental and numerical methods using one-dimensional, two-dimensional or three-dimensional models to solve energy

formulated equation (Agyenim *et al.*,2010). A theoretical model of a shell-and-tube PCM storage unit was reported by Ismail and Alves (1986). An energy equation for the PCM was written in terms of the enthalpy. The numerical results showed the effects of the Biot number, the relative diameters of the tubes and the inlet fluid temperature on the thermal performance of the unit.

Yimmer*et al.* (1989) developed a numerical model for optimising a basic one-dimensional, shell-and-tube TES system. Lacroix (1993) developed a theoretical model to predict the transient behaviour of a shell-and-tube storage unit with the PCM on the shell side and the Heat Transfer Fluid (HTF) circulating inside the tubes. Parametric studies were performed to assess the effects of various thermal and geometric parameters on the heat transfer process and on the behavior of the system.

Many modelling publications on the problem of phase change of a PCM remain complex and require much calculation (Jian-You, 2008). Kang *et al.* (1999) used a simple analytical model to solve a heat transfer problem of conduction of a PCM in the shell, conjugated with the convection of Heat Transfer Fluid flowing in the tube. The conservation of energy method is developed for an analysis of PCM solidification and melting processes. The outlet temperature of HTF from the heat exchanger is evaluated over different periods and the solidification front of the PCM in the shell determined at different positions along the tube. This analytical method was applied and tested by Jian-You (2008). The thermal energy storage unit involved a triplex concentric tube with PCM filling in the middle channel, with a hot HTF flowing through the outer channel during the charging process and a cold HTF flowing through the inner channel during the discharging process. To test the validity of the numerical results, an experimental apparatus was designed and built by which the effect of the inlet temperature and the flow rate of a HTF on the TES were studied. Comparison between the numerical predictions and the experimental data showed good agreement.

Dincer and Rosen (2002) dealt with the problems of heat transfer with PCM in simple and complex geometries and around isothermal finned cylinders. The results were presented and validated with actual existing data. He and Zhang (2001) numerically solved a mathematical model describing the unsteady freezing problem coupled with forced convection. The method of finite difference was used to solve the equations. In their results they noted the importance of PCM thickness.

Michels and Pitz-Paal (2007) presented a numerical model to simulate different cascaded Latent Heat Storage configurations. "Dynmola/Modelica" was used to conduct the simulation using the standard library Tech-thermo. They used assumptions to simplify the heat transfer problem; the PCM was considered as a lumped mass with a uniform temperature throughout. In this work, natural convection was also considered as a type of flow regime. With their simulated results they presented experimental data to validate the model. Experimental results compared well with simulated results.

Yuksel *et al.* (2006) proposed a theoretical approach predict time and temperature during heat charge and discharge processes in the LHS, by using the average value of the mean specific heat capacities for the PCM. Analytical solutions were obtained. It was shown that the decrease of the entry temperature of the working fluid had a dominant and effect on PCM solidification time.

A PCM needs to have a set of characteristics to be selected as storage medium (Agyenim *et al.*, 2010):

a. Melting point in the desired operating temperature range.
b. High fusion latent heat per unit mass.
c. High specific heat.
d. High thermal conductivity.
e. Small volume changes during phase transition.
f. Little or no sub-cooling during freezing.
g. Chemical stability.
h. Contain non-poisonous, non-flammable and non-explosive elements/compounds.
i. Available in large quantities at low cost.

Although latent heat thermal energy storage offers a huge opportunity due to its heat storage density and there are a huge variety of PCMs whose melting point is suitable for large scale solar thermal electricity plants (Hoshi *et al*, 2005), the PCMs has not been up to the expected level and the large-scale utilization in latent heat thermal storage (LHTS) (Jegadheeswaran and Pohekar, 2010). This is because most of PCMs have a low thermal conductivity (around 1W/mK), which prolong the charging and discharging period.

Refrigerating system can be broken down into three basic stages: evaporation, absorption, and regeneration. The main components of an absorption cooling system are the absorber, pump, expansion valve, regenerator, and generator. Systems can be made more efficient by adding a stage to increase heat transfer efficiency; known as double-effect. The common refrigerant –absorbent used are ammonia/water and LiBr/water.

A single-effect refrigerating has a Coefficient of Performance (COP) of 0.6for NH_3/H2O and 0.7 for LiBr/H_2O while a double-effect chiller can have COP's ranging from 0.8 to 1.2 (Mumah,1991, Mumah *et al.*, 1994). Absorption Cooling has the advantages of a relatively high COP for solar thermal applications, as well as mature technology with several commercially available products. A disadvantage of these systems is that they are complicated, with moving parts. The process requires several different working fluids, including a cooling tower to dissipate heat.

Research Methodology

Why Absorption Refrigeration System?

Absorption refrigeration systems can be powered by solar energy. There are however obvious limitations. There are challenges during the night or period of low solar radiation. To resolve this challenge, PCM Energy Storage system can be incorporated into absorption Refrigeration Systems to provide the energy during off periods.

There is no need for electric energy from the national grid in this design. The only moving parts are three 0.5 kW pumps, two for the Refrigerating system and the System and the other for the PCM energy storage system. This will be also be powered by Solar Photovoltaic System

Why Ammonia Water System?

Today, Ammonia remains the refrigerant of choice for large industrial applications. In today's large refrigeration systems ammonia has many advantages. Ammonia(R-717) costs less. Not only is ammonia significantly cheaper than the least expensive halocarbons fluorocarbons, but because the density of ammonia is half of all halocarbons, only half as much material is

required in the system. Ammonia is more efficient since the mass flow rate of a given capacity is one-seventh that of HCFC-22(http://www.haphillips.com/ammonia.html; Ammonia Hazards; Gaps Guidelines Gap.7.2.1.2, A Publication of Global Asset Protection Services LLC, https://axaxl.com › media › gaps). This means that only one-seventh of the liquid needs to be pumped for a given refrigeration capacity. The heat transfer and thermodynamic properties are highly advantageous and provide cost savings. Ammonia requires smaller vapor line pipe sizes for large systems spread over a large area due to less drop in saturation temperatures compared to Freon Ammonia Hazards; Gaps Guidelines Gap.7.2.1.2, A Publication of Global Asset Protection Services LLC, https://axaxl.com › media › gaps). Ammonia systems are more tolerant of water contamination than Freon systems. Water concentrations of less than 100 ppm cause no adverse effects to ammonia system operation.

Ammonia /Water Absorption Refrigerating System

Details on the Ammonia-water refrigerating system are well documented (Mumah, 1991, 1994). Figure 1 shows the schematic block diagram of a simple absorption refrigeration system. It consist of an absorber, a pump, a generator and a pressure reducing valve to replace the compressor in vapour compression refrigeration system. The other components of the system are the same (condenser, evaporator and expansion valve). In this system the $NH_3$is used as a refrigerant and the water is used as an absorbent. In this system the low pressure ammonia vapour refrigerant leaving the evaporator enters the absorber, where it is absorbed by the cold water in the absorber. The water has the ability to absorb a very large quantity of ammonia vapour, and the solution thus formed is known as aqua ammonia solution. The absorption of ammonia vapour in water lowers the pressure in the absorber which turn draw the more ammonia vapour from the evaporator and thus raised the temperature of the solution. Some form of cooling arrangement (usually water cooling) is employed in the absorber to remove the heat of solution evolved here, this is necessary in order to increase the absorption capacity of water, because of higher temperature water absorb less ammonia vapour, the strong solution thus formed in absorber is pumped to the generator by the liquid pump. The pump increases the pressure of solution up to the 10 bar. The strong solution of ammonia in the generator is heated by some external source such as gas, steam, solar energy. During the heating process ammonia vapour is driven off from the solution at higher pressure and leaving behind the hot weak solution in the generator. The weak ammonia solution flows back to the absorber at low pressure after passing through the pressure reducing valve. The high pressure ammonia vapour from the generator is condensed in the condenser to high pressure liquid ammonia thus liquid ammonia is passed to the expansion valve through the receiver and then to the evaporator. This is the complete working of simple vapour absorption refrigeration cycle. The heat source for the generator Q_g will be generated from solar energy (parabolic solar collector) and phase change material energy storage system.

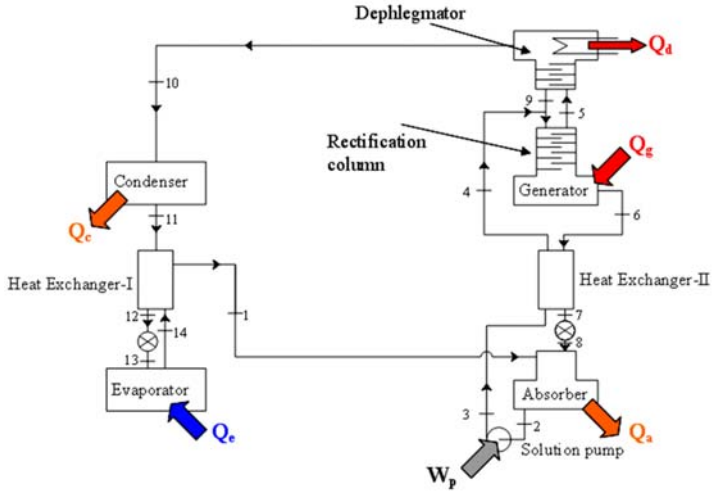

Figure 1: Schematic Diagram of Simple Vapour Absorption Refrigeration System

The process that will be executed in this project is divided in six main sections. First, establishment of the thermodynamic theories necessary for proper formulations and modeling, plus bibliographic search. Second, investigate which phase change material is appropriate for the ammonia-water absorption system. Third, gather relevant details necessary for a proper design of the various components shown in Figure 1and then perform a computer simulation of the best design of the various components. Fourth, design of the various components of the prototype. Fifth, construction and experimental modelling, with all possible scenarios taken into consideration. Sixth, test-run and gather relevant data that will assist in the fabrication of a commercial version. Typical conditions for NH_3/H_2O Absorption Refrigeration System are shown in Table 1.

Table 1: Typical Conditions for an NH_3/H_2O Absorption Refrigeration System

Capacity of system	**3.0kW**
Concentration of NH3 in refrigerant	Xr= 0.98
Concentration of NH3 in Solution	Xs = 0.42
Concentration of NH3 in absorbent	Xw= 0.38
Temperature of the evaporator	TE =2ºC
Generator or condenser pressure	PH = 10.7 bar
Evaporator pressure	PL = 4.7 bar
Temperature of the Condenser	TC=54ºC
Temperature of the Absorber	TA=52ºC
Temperature of the Generator	TG=120ºC

PCM Selection

The selection of an appropriate PCM requires the PCM to have a melting temperature within the practical range of application; so the selection was dictated by the temperature required for efficient operation of the hot side of the absorption air conditioning system.

Selection Criteria for Phase Change materials (PCMs)

The following criteria are important when selecting PCMs (Sharma et al., 2009; Agyenim*et al.*, 2010):

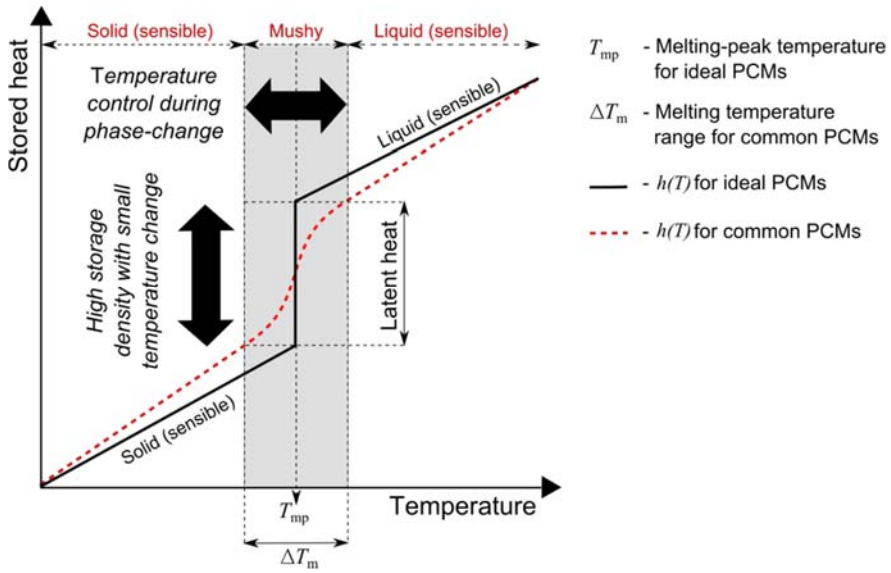

Figure 1. Potential fields of application of PCMs: (*i*) temperature control and (*ii*) storage and supply of heat with high storage density in a small quantity of material (Soares *et al.*, 2018).

Thermodynamic properties:

a. Large enthalpy of transition with respect to the volume of the storage unit;
b. High change of enthalpy near temperature of use;
c. Phase change temperature fitted to application;
d. The latent heat should be as high as possible to minimize the physical size of the heat storage;
e. High latent heat of fusion per unit mass so that a lesser amount of material stores a given amount of energy;
f. A melting point in the desired operating temperature range;
g. Fixed and clearly determined phase change temperature (freeze/melt point);
h. Congruent melting point to avoid segregation;
i. Lower change of volume during phase change;
j. High density, so that a smaller container volume holds the material
k. High thermal conductivity (both liquid and solid phases) would assist the charging and
l. High thermal con the freezing process;
m. Sufficient crystallization rates.
n. conductivity (both liquid and solid phases) would assist the charging and discharging of the energy storage high specific heat that provides additional sensible TES effect and also avoid sub-cooling.

Kinetic properties:

a. Little or no under cooling during phase change

Chemical properties:

a. No chemical decomposition, so that the latent TES system life is assured;
b. Non-corrosiveness to construction material;
c. Long term chemical stability;
d. Non-poisonous; Non-toxic;
e. Non-explosive, non-dangerous;
f Non-flammable.

Physical properties:

a. Limited changes in density to avoid problems with the storage tank;
b. High density with low density variation;
c. Small units size;
d. Low vapour pressure,
e. Favourable phase equilibrium.
f. Economic properties:
g. Available in large quantities;
h. Cheap in order to make the system economically feasible

Since Ammonia/water absorption systems operate with generator temperatures in the range of 80 to 130°C, the PCM melting temperature should be higher than the inlet generator temperature. Among the different PCMs which were summarized by Mumah(2008), Mumah *et al* (1994) and. Sharma *et al*.(2009), some PCMs are selected for investigation in this project. Those selected are listed in Table 2.

Table 2: Selected PCMs for application in solar NH_3/ water absorption systems with melting temperature in range of 80 - 150 °C

Heat storage material	Type	Melting point (°C)	Heat of Fusion(kJ/kg)	Density (g/cm^3)
Methyl fumarate	Organic(Fatty acid)	102	242	
$MgCl_2.6H_2O$	Inorganic	115	165	
Erythritol	Organic	118	339.8	
HDEP	Organic	100-150	200	
RT110	Organic (Paraffin)	112	213	
Acetanilide	Organic (non-Paraffin)	118.9	222	
Succinic anhydride	Organic (non Paraffin)	119	204	
α-Naphthol (99%) Sigma-Aldrich®	Organics	96	163	N.A.
Xylitol (99%) Sigma-Aldrich®	Organics	94	263.3	N.A.
D – Sorbitol (98%) Sigma-Aldrich®	Organics	97	185	N.A.
Acetamide(99%) Sigma-Aldrich®	Organics	81	241	1.159
$KAl(SO_4)_2{\cdot}12H_2O$	Inorganics			

(98%)Sigma-Aldrich® (CODE: APSD)	/ Hydrated Salts	91	184	N.A.
$(NH_4)Al(SO_4)_2 \cdot 12H_2O$ (99%)Sigma-Aldrich® (CODE:AASD)	Inorganics / Hydrated Salts	95	269	1.640
Plus-ICE S83 PCMprodcucts®	Inorganics / Hydrated Salts (Commercial)	83	141	1.600
Plus-ICE S89 PCMprodcucts®	Inorganics / Hydrated Salts (Commercial)	89	151	1.550
Plus-ICE A82 PCMprodcucts®	Organic (Commercial)	82	155	0.850

The selected phase change materials obtained from Table 2 will be investigated to determine their appropriateness.

Design, Fabrication and Evaluation

When the appropriate phase change material has been selected, all the components of the system will be designed and fabricated. Specifically, the components to be designed to achieve 3kW of cooling are the evaporator, condenser generator, absorber, phase change material exchanger, flat plat collector dephlegmator, and the parabolic solar collector. Schematics of the various components of system obtained from preliminary design are shown in Figures 2 to 10.

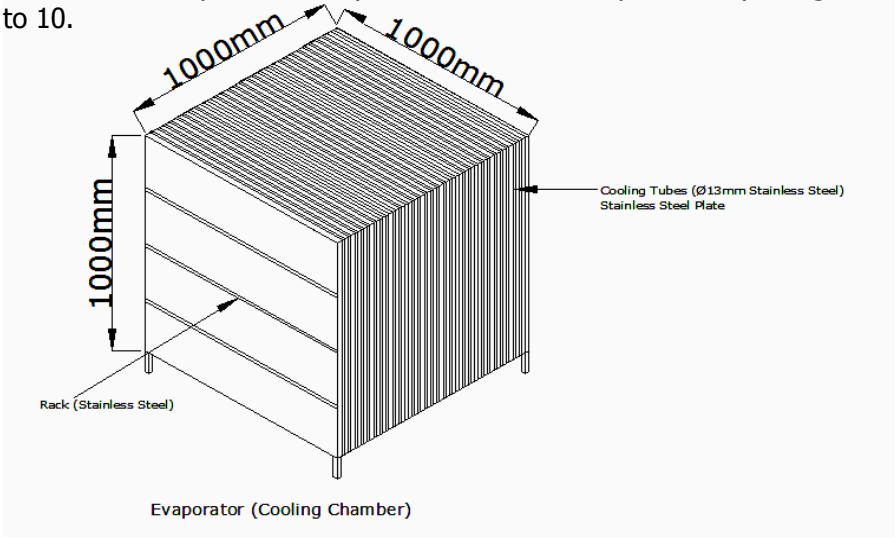

Figure 2: Evaporator

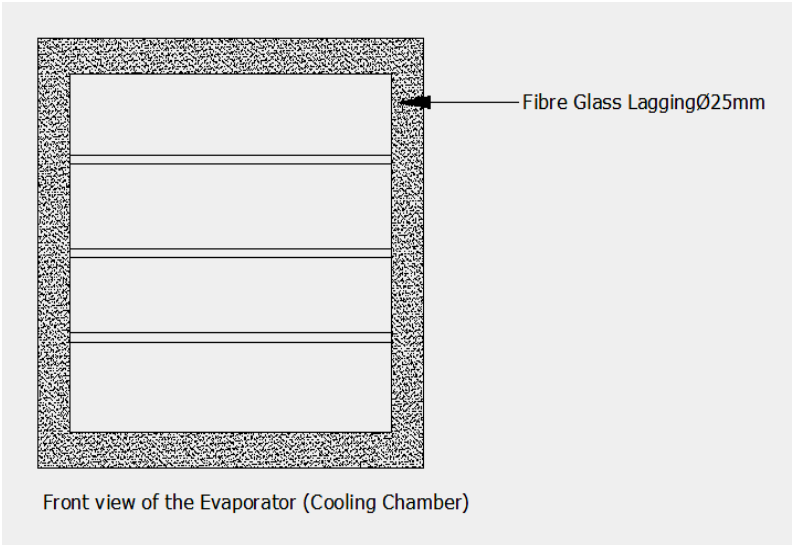

Figure 3: Front View of Evaporatpor (cooing Chamber)

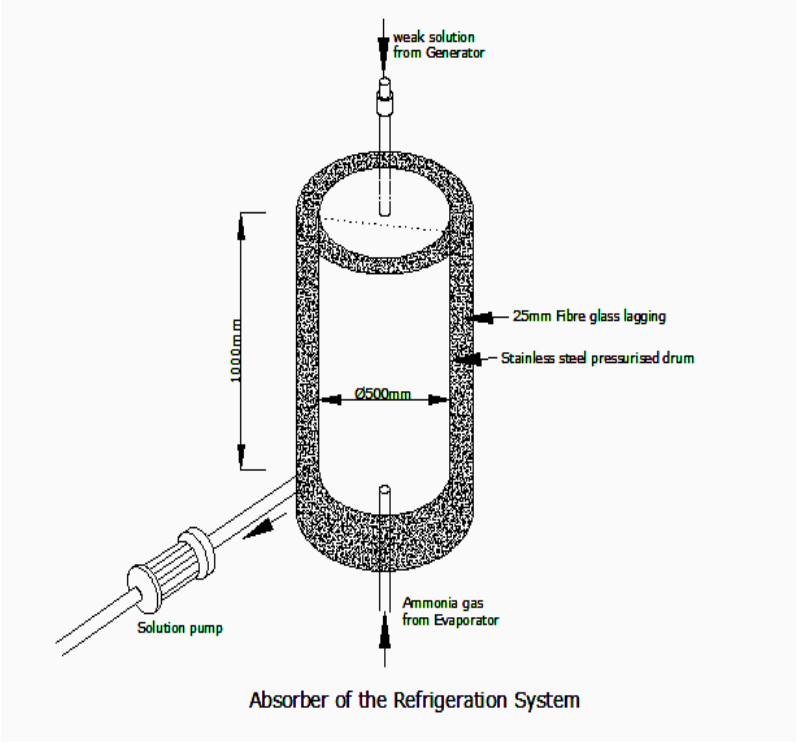

Figure 4: The Absorber

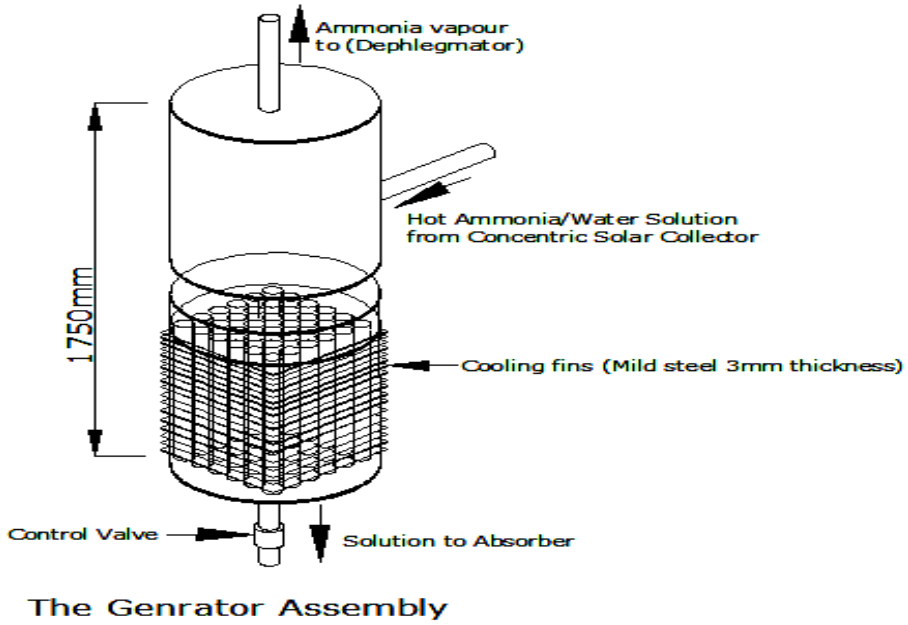

Figure 5: Generator Assembly

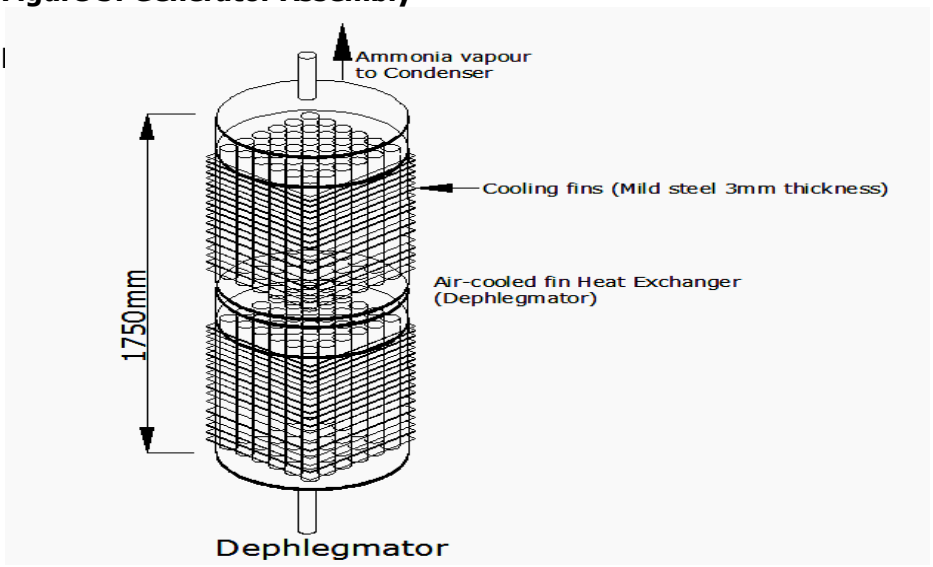

Figure 6: Dephlegmator Assembly

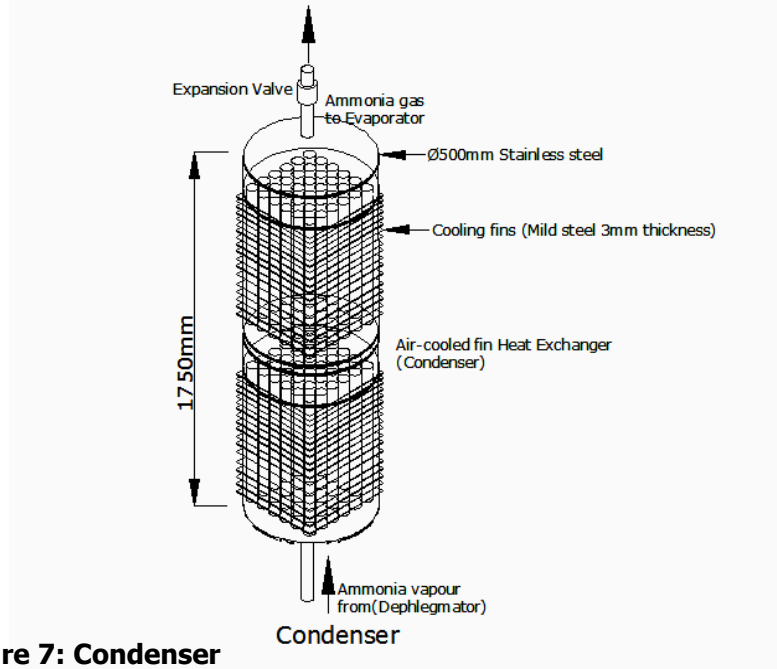

Figure 7: Condenser

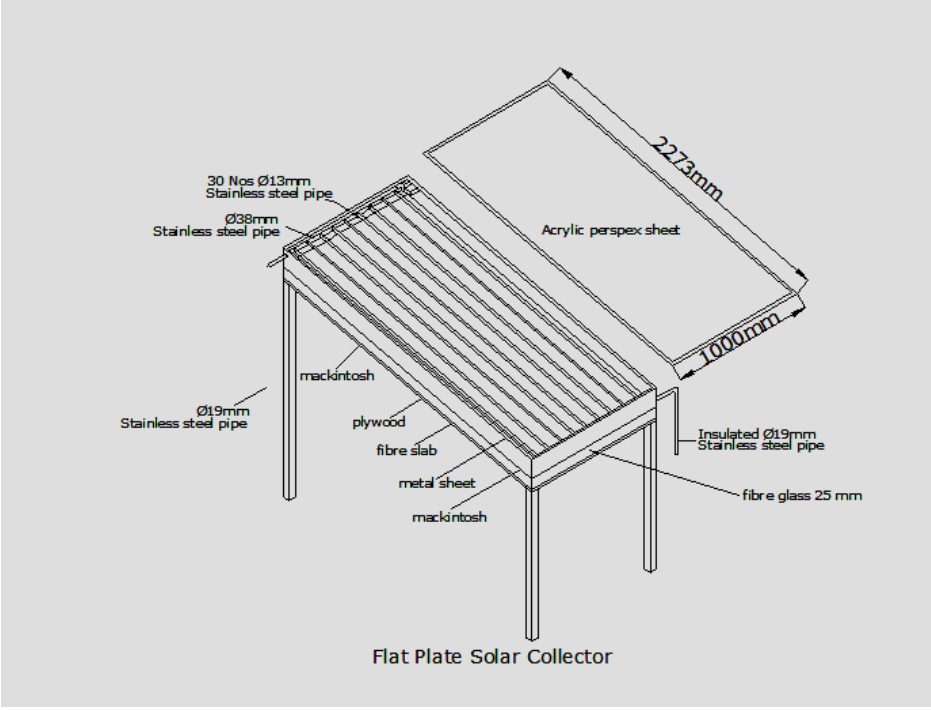

Figure 8: Flat Plate Solar Collector

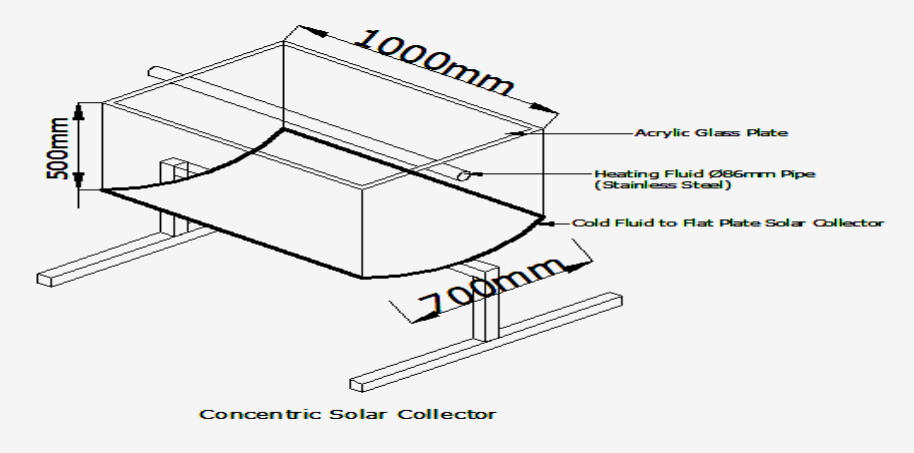

Figure 9: Concentric Solar Collector

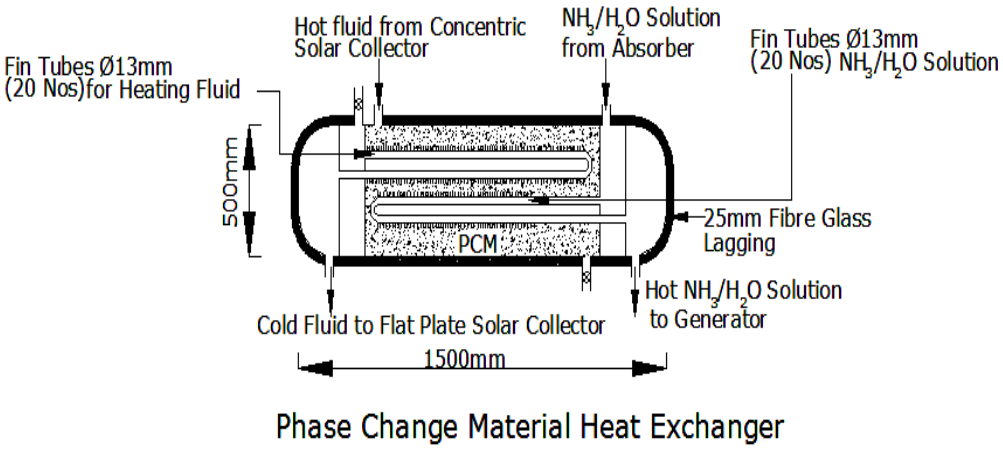

Figure 10: Phase Change Material Heat Exchanger

INSTRUMENTATION

Key issues to be considered under instrumentation include;

1. Temperature, pressure and flow rate are the main parameters measured during experimentation
2. Chromel-alumel thermocouples (K-type) will be connected to a data acquisition system and used to record temperatures.
3. Pressure transducers will be used to record pressure data directly through the data acquisition system.
4. Pressures Gauges will be are used in place of transducers while they were being repaired or for double checking.
5. Flow meters shall be installed to measure the flow rates of the interested positions.
6. Liquid level gauges shall be installed in major system components.

7. A flow indicator connects the storage tank with the system in order to monitor
8. whether liquid or vapor is flowing.
9. The solar radiation on the collector surface will be measured by a ±5% W/m^2 accuracy pyranometer and pyrheliometer.
10. Personal computer will be used as a data logger.
11. Measurement devices will be connected to a data acquisition board to obtain simultaneous readings.
12. All readings will be recorded automatically and monitored by the computer.
13. All instruments and devices used for data acquisition shall be calibrated.
14. Thermocouples shall be calibrated within ±0.5 ^oC using constant temperature bath.
15. Pressure gages shall be calibrated within ± 0.3bar using dead weight pressure tester.
16. The flow rates of the interested positions shall be measured with an accuracy of ±3% and liquid level gauges shall be calibrated within ±2%accuracy.

Project Impact

The long term Impact of the projects can be considered in the following areas:

Quality of life: By developing solely solar energy powered alternatives for cooling for rural areas, the Project will be contributing to the **improvement of quality of life** in the rural areas. First, solar energy cooling equipment or storage facilities will be directly linked to the development of rural communities and the country as a whole. It is also important to emphasize that solar energy cooling systems can be used in other areas like vaccine storage which is crucial in upgrading health facilities in rural communities. This will not only help create a greater sense of cohesion amongst communities but it will most importantly **provide hope, a sense of progress and an interest in consolidating peace and accomplishments** to those communities.

Energy security: Dependence on imported fossil fuels despite being a top producer of the crude oil leaves Nigeria vulnerable to disruption in supply and the accompanying economic and development impact. Increased use of efficient and renewables systems such as solar energy improves energy security, by boosting resource productivity, avoiding excessive dependence on imported fuels, developing local sources and diversifying energy portfolios and suppliers.

Economic development: Lack of access to sustainable energy constrains opportunities for economic development and improved living conditions. Renewables and energy efficiency systems support a sustained GDP growth by improving economic and environmental performance, enhancing technological innovation and creating new commercial opportunities.

Social equity: Access to and use of energy is marked by an uneven distribution in Nigeria, and between the rich and poor within them. Developing distributed energy generation and sustainable renewable systems can enable more equitable access to energy services and create new job opportunities, especially in rural areas.

Environmental protection: Most current energy generation and use results in serious health and environmental impacts at local and national levels – including climate change – which threatens human well-being and ecosystems. Accelerating energy efficiency improvements and deployment of sustainable renewable energy results in significantly lower environmental pollution.

CONCLUSION

Thermal energy storage is imperative to make solar energy more reliable and competitive. Further research in phase changing material can improve the efficiency of energy storage especially in Refrigeration System. Proper Design, simulation and evaluation of the system is also important in optimizing energy storage. The prospect of this project to contribute to the Nigerian Economy is great. The project is out to bring solution to a national challenge. - Agricultural produce spoilage. The project outcomes can also be applied to health care such as the storage of medicines and vaccines where constant electricity supply is a challenge.

ACKNOWLEDGEMENT

THE FUNDING FOR WRITING THIS PAPER AND PRESENTATION IS PROVIDED BY TERTIARY EDUCATION TRUST FUND (TETFUND) UNDER THE NATIONAL RESEARCH FUND(NRF) WINDOW(TETFUND NRF PCM SOLAR POWERED REFRIGERATION PROJECT).

References

Agyenim, F., N. Hewitt, P. Eames, M. Smyth,(2010).A review of materials, heat transfer and phase change problem formulation for latent heat thermal energy storage systems (LHTESS)", Renewable and Sustainable Energy Reviews, Vol. 14, pp.615-628.

Cavallaro, F.(2010).Fuzzy TOPSIS approach for assessing thermal-energy storage in concentrated solar power(CSP) systems", Applied Energy,Vol.87,pp.496-503

Chung, W. J., Seung Sun An, Yong Tae Kang. (2014) Thermal performance estimation of ammonia-water plate bubble absorbers for compression/absorption hybrid heat pump application. Energy. Online publication date: 1-Aug-2014.

Dincer, I., and Rosen, M. A. (2002).Thermal energy systems and applications. New York: Willey

He,Q. and Zhang, W. N. (2001). A study on Latent Heat Storage exchangers with the high temperature Phase Change Materials, Int.J.EnergyRes.,25:331-341.

Hoshi,A., D. R. Mills, A. Bittar, T. S. Saitoh (2005). Screening of high melting point phase change materials (PCM) in solar thermal concentrating technology based on CLFR", Solar Energy, Vol. 79, pp. 332-339.

Ioan, S., Calin Sebarchievici. (2015) General review of solar-powered closed sorption refrigeration systems. Energy Conversion and Management**105**, 403-422. Online publication date: 1-Nov-2015.

Ismail, K. A. R., Alves, C. L. F. (1986). Analysis of the shell-and-tube PCM storagesystem.Proceedingssofthe8thInternationalHeatTransferConference,1781–1786.

Jegadheeswaran, S., S. D. Pohekar, (2010). Performance enhancement in latent heat thermal storage system: A review", Renewable and Sustainable Energy Reviews, Vol. 13, pp.2225-2244.

Kang, Y.B., Zhang, Y.P., Zhu, Y.Q. (1999). A simple model for heat transfer analysis of tube and shell with Phase Change Material and its performance simulation. International Journal of Heat Mass Transfer, 45:230-236

Lacroix, M. (1993). Study of the heat transfer behavior of a latent heat thermal energy storage unit with a finned tube, International Journal of Heat and Mass Transfer, 36: 2083-2092.

Michels, H. and Pitz-Paal, R. (2007) Cascaded Latent Heat Storage for parabolic Trough Solar Power Plants. Solar energy, 81(6): 829-837.

Mumah, S.N.(1991).Simulation and Optimization of Solar-powered and Hybrid Heat Pump System for cooling. (for PhD Degree, Jan.1991)

Mumah, S.N., Adefila S.S. and Arinze E.A.; 1994, First law thermodynamic evaluation and simulation of ammonia-water absorption heat pump system; Journal of Energy Conversion and Management, Vol. 35, No.8, pp 737-750,published by Pergamon Press Exeter, England

Mumah, S. N., Adefila S. S. and Arinze E.A.(1994) Properties generation procedures for First and Second law analyses of Ammonia-water heat pump system; Journal of Energy Conversion and Management, Vol. 35, No. 8, pp 727-736; published by Pergamon Press Exeter, England.

Mumah, S. N. (2008) 'Selection of heat storage materials for ammonia-water and lithium bromide solar-powered absorption heat pump systems', International Journal of Sustainable Energy, 27:2, 81 — 93(http://www.informaworld.com/smpp/title~db=all~content=g795162769~tab=toc)

Pincemina, S., R. Olivesa, X. Pya, M. Christ, (2008). Highly conductive composites made of phase change materials and graphite for thermal storage", Solar Energy Materials and Solar Cells, Vol. 92, pp.603-613.

Pya, X., R.Olives, S. Mauran, (2001).Paraffin/ porous graphite-matrix composite as a high and constant power thermal storage material", International Journal of Heat and Mass Transfer,Vol.44,pp.2727-2737.

Kurklu, A., Wheldon, Hadley, P. (1996). Mathematical modeling of the thermal performance of a Phase Change Material (PCM) store cooling cycle. Applied Thermal Engineering, 16(7): 613-62

Sharma, A., Tyagi, V., Chen, C.,Buddhi, D.(2009).Review on thermal energy storage with phase change material sand applications. Renewable and Sustainable Energy Reviews 13, 318-345.

Siddiqui, M. U., S.A.M. Said. (2015) A review of solar powered absorption systems. Renewable and Sustainable Energy Reviews**42**, 93-115. Online publication date: 1-Feb-2015.

Soares Et Al. (2018) Systems with PCM-Filled Rectangular Cavities for the Storage of Solar Thermal Energy for Buildings: The Case of The Pcms4buildings Project, PCMs: Thermophysical Characterization and Buildings' Applications; Seminar Pcms4buildings Coimbra, 14-15 June, 2018

TingXian L., Ju-Hyuk Lee, Ru Zhu Wang, Yong Tae Kang. (2014) Heat transfer characteristics of phase change nano-composite materials for thermal energy storage application. International Journal of Heat and Mass Transfer**75**, 1-11. Online publication date: 1-Aug-2014.

Yian–You, L. (2008). Numerical and experimental investigation for heat transfer in triplex concentric tube with Phase Change Material for thermal energy storage. Solar Energy, 82(11): 977-985

Yimmer, B. and Adami, M. (1989). Parametric Study and Optimization of Phase Change Thermal Energy Storage System. National Heat Transfer Conference, HTD, Multiphase Flow, Heat and Mass Transfer, 109: 1-89.

Yuksel,N.,AvciA.,KilicM.(2006).AmodelforlatentheatenergystoragesystemsInternationalJournalofEnergyResearch, 30(14):1146–1157

Proceedings of the 49th NSChE Annual Conference
KADA 2019: pp 785-794

P05: DEVELOPMENT OF CARBON NANOTUBE ADSORBENTS FOR INDUSTRIAL WASTEWATER TREATMENT

Aliyu U, Mohammed[a,b], A. S. Abdulkareem [a,b], A.W. Hamzat[a,b]O.S. Adetayo[a,b], M.T. Bankole[a.c] and J.O. Tijani [a,c]

[a]Nanotechnology Research Group, Centre for Genetic Engineering and Biotechnology (CGEB), Federal University of Technology, P.M.B 65, Bosso, Minna, Niger State, Nigeria
[b] Department of Chemical Engineering, Federal University of Technology, P.M.B 65, Gidan Kwano, Minna, Niger State, Nigeria
[c] Department of Chemistry, Federal University of Technology, P.M.B 65, Bosso, Minna, Niger State, Nigeria
Corresponding author: sadaatualiyu238@gmail.com

ABSTRACT

Carbon nanotubes (CNTs) was produced by catalytic vapour deposition (CVD) technique The synthesized CNTs was then purified by acid treatment and modified by polyethylene glycol (PEG) to give CNTs/PEG composite. The developed composite was characterized by High Resolution Transmission Electron Microscope (HRSEM), Brunnaer Emmett Teller (BET) and Fourier Transform Infrared (FTIR) respectively. The developed CNTs/PEG was used as an adsorbent to remove iron, nickel and cadmium from battery wastewater via batch adsorption process. .Results of analysis shown that the CNTs/PEG composite produced is highly crystalline with specific surface area of 970.81 m^2/g. The batch adsorption studies revealed that the optimum conditions to achieve 93.79 % were contact time of 60 minutes, adsorbent dosage of 0.3 mg and temperature of 50°C. Freundlich model and the pseudo-second order model best described the adsorption isotherm and adsorption kinetics. The thermodynamic study preformed shows that the adsorption process was endothermic and spontaneous.

Keywords: Carbon nanotubes, Polyethylene glycol, Functionalized carbon nanotubes, Adsorption.

1.0 Introduction

Wastewater for the most part contains numerous poisonous and toxic substances, for example, heavy metals and organic contaminants. They are emitted from different industrial activities, drinking water containing these substances causes many chronic or acute diseases; therefore, these harmful substances should not be allowed in wastewater and therefore must be treated prior to discharging. The known existing strategies for water treatment incorporate coagulation, flocculation, chlorination, sedimentation, filtration, reverse osmosis and distillation just as adsorption utilizing adsorbents, for example, fly debris, silica gel, zeolite, lignin, and seaweed.

These techniques requires high energy and enormous area of land, they are likewise less viable as none of these techniques have effectively evacuate substantial metals and improve the physiochemical properties of water at the same time (Turkar *et al.,* 2011). Nanoparticles have numerous potential applications in water treatment (Aliyu et al, 2016), hydrogen storage(Yoshinori and Xinluo, 2006), drug release, medicine (Tasis et al, 2006), optics and electronics (Sharma et al, 2015), so much that the U.S National Nanotechnology activity offers government financing concentrated on nano particle research, particularly carbon nanotubes (CNTs) which has gotten impressive consideration among researchers and explored because of its distinct tubular nanostructure (Tasis et al, 2016). Nanoparticles have electrical and thermal properties, just as mechanical strength in the field of material science. Among

nanoparticles carbon nanotubes (CNTs) is of great interest, because of its astounding mechanical and electronic properties, yet in addition have well-characterized hollow interiors and biocompatibility with living systems.

CNTs is viewed as excellent candidates for some potential applications, including yet not constrained to: catalyst and catalyst supports (coville, 2011), composite materials, sensors and actuators (Balasubramanian and Burghard, 2005), field producers, tips for scanning probe microscopy, conductive films, bio-nanomaterials, energy storage mediaand nanoelectronic devices. (Physicsworld.com, 2009)

Carbon nanotubes incorporate single walled CNTs (SWCNTs), and multi walled CNTs (MWCNTs), recognized by their number of layers. Fundamentally, their large specific surface area , hollow and layered structure makes them a perfect adsorption material (Aliyu et al, 2016). The surface structure of CNTs can be improved by functionalization. This should be possible by oxidation treatment or surfactant treatment, the close tip can be opened, and their surfaces can be attached by metals, metal oxides and natural ligands, which substantially increase the dispersability and reactivity of the CNTs for application in environmental protections (Coville, 2011).Therefore, CNTs adsorbent is a promising adsorbent; because of it tubular structure which is a perfect trap for heavy metal and simultaneously improve the physiochemical properties of the water with less area of land requirements (Coville, 2011).

In this experiment, bimetallic Fe/Ni catalyst supported on kaolin was synthesized through wet impregnation method; this catalyst was used in the production of carbon nanotubes via catalytic vapor deposition (CCVD). The structure of the MWCNTs produced was modified by acid treatment and functionalized through polyethylene glycol (PEG) and Dimethyl formamide..Purified and functionalized CNTs were used for the removal of Iron (Fe), Nickel (Ni), and Cadmium (Cd) from battery industry wastewater. It also covers the investigation of effect of equilibrium contact time, adsorbent dosage, and temperature. The study also covers adsorption isotherm, kinetic and thermodynamic study, which describe the adsorption mechanism of MWCNTs.

2.0 EXPERIMENTAL METHODOLOGY

2.1. Materials

The Kaolin used in this method was sourced from Lagos state, Nigeria and without any treatment or modification.All the chemical and gases used in this study are of analytical grade with percentage purity in the range of 98 – 99.99 % . These chemical includes: Nickel nitrate hexahydrate ($Ni(NO_3)_2.6H2O$), Kaolin, Iron nitrate nonahydrate ($Fe(NO_3)_3.9H_2O$),Tetraoxosulphate (vi) acid (H_2SO_4), Trioxonitrate (v) acid (HNO_3), Dimethyl formamide(DMF) were supplied by Sigma Aldrich. Acetylene and argon gases were supplied by BOC Nigeria. The wastewater was analysedusing Atomic Absorption Spectroscopy (Perkin Elmer Analyst 700-AAS}for the iron and magnesium determination. Various CNTs were all characterized by BET method (Nova 4200), HRSEM (Tecnai G2 F20-Twin), and Fourier Transform Infra-Red (Frontier FTIR model).

2.2 Synthesis of Bimetallic Fe-Ni/Kaolin Catalyst

The Fe-Ni bimetallic catalysts supported on kaolin was prepared using a wetChemical impregnation methods described as follow: 5.05 g of Fe $(NO_3)_3.9H_2O$ and 3.64 g Ni $(NO_3)_2.6H_2O$ were weighed and mixed in a beaker. Thereafter, the weighed was grinded to fine powder and later dissolved in 50ml distilled water to make a 0.25M Fe-Ni (50:50w/w) solution. The 50ml solution was added to separately weighed 8g kaolin. The mixture was

allowed to age for 30minutes on a magnetic stirrer at a speed of 300rpm. The resulting slurry was partially dried at room temperature and later oven dried at a temperature of 140 degree Celsius for 10 hours. The mixture were later cooled to room temperature, ground and finally sieved with a 150-micrometer sieve. The catalyst powders were then calcined at 600 ^{o}C for 14 hours in a furnace to decompose the nitrates.
The yield of the catalyst was determined using the relation

$$catalystyieldbeforecalcination = \frac{weightbeforeovendrying - weightafterovendrying}{weightbeforeovendrying} x100\% \quad (1)$$

$$catalystyield\ after\ calcined = \frac{weightbeforecalcination - weightaftercalcination}{weightbeforecalcination} x\ 100\% \quad (2)$$

(Aliyu et al. 2016)

2.3 Synthesis of CNTs

The synthesis of the multiwall CNTs was carried out by the decomposition of acetylene (carbon source) on the Fe-Ni bimetallic catalyst, with kaolin as support through the CCVD (catalytic chemical vapor deposition) method. The catalyst placed in a tubular quartz tube was placed horizontally in the furnace, with the temperature maintained at 750 degree Celsius, and acetylene flow rate of 200ml per minute in the presence of Argon as the carrier gas flowing at 100ml per minute.This process continued until the reaction time of 45 min was attained .The acetylene gas (C_2H_2) flow was then stopped and the argon flow was adjusted back to 20 mL/min. The CVD machine was allowed to cool and the CNTs removed from the reactor was weighed to know the deposited synthesized CNTs.

2.3.1 Purification of CNTs

The purification of the as-synthesized CNTs were performed using the liquid phase chemical oxidation by treating the as-synthesized CNTs with H_2SO_4 and HNO_3 acid with volume ratio 1:3.. The CNTs was dissolved into 100ml of distilled water and sonicate for 90minutes at 40 ^{o}C. Suction filtration using a suitable filter was then carried out to obtained wet cake CNTs containing trace of acids. The CNTs ware then washed with deionized water. The washing continued until pH of 7 was attained.

2.3.2 Functionalization of CNTs

The dried purified CNTs was functionalized with Polyethylene Glycol (PEG) and Dimethyl formamide (DMF).5g of oxidized CNTs was mixed with 20 % PEG solution and 100ml of 10 % DMF. The solvent mixture was stirred for 8 hours at 30 ^{o}C and then centrifuged at 2000 rpm for 5 minutes.After centrifugation; the black solid obtained was washed with distilled water until the wash water was clear. The remaining black solid was retained after oven dried at 120^{o}C for 12 hours.

2.4 Batch adsorption

The wastewater sample gotten from Fogo battery manufacturing company in Ilorin, Kwara State was stored in an amber bottle and corked. The batch adsorption of manganese and iron , which incorporates: effect of contact time, adsorbent dosage and temperature on battery wastewater were performed in this study. To carryout the effect of contact time, 0.1 g of nano-adsorbent were dissoved into 100 ml glass stoppered conical flask on a rotatory shaker at 125 rpm containing 50 mL of the battery wastewater under room temperature and at pH of 1.2 The contact time was carried out at 10, 20, 30, 50 .60, 90 and 120 min respectively. The effect of dosage was performed by adding varying amount of nano adsorbents: 0.1, 0.2, 0.3, 0.4 and 0.5 g to 50 mL of battery wastewater at equilibrium time (90 min) under room temperature at 125 rpm. The effect of temperature on iron and manganese were carried out

by adding 0.1 g of nanoadsorbents in 50 mL of battery wastewater. The temperature effect was performed from 303 to 343 °K at a pH of 6 for 90 min. Each of this effect was performed in duplicate and the mean values are recorded.

3.0 Results and discussion

3.1 Characterization of Carbon nanotubes (CNTs)

The infrared spectra of the as-synthesized, purified and functionalized CNTs are shown in Figure 1. The FT-IR is used to identify the existence or absence of functional groups on the surface of the CNTs

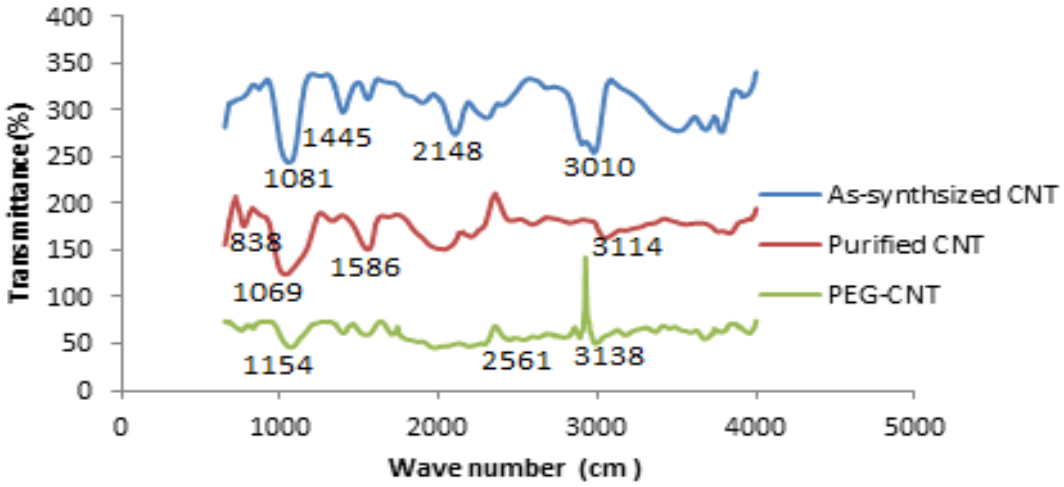

Figure 1: FTIR spectra of (i) As-synthesized CNT (ii) Purified C(iii) PEG functionalized CNT

As presented in Figure 2, an absorption band at 1081 cm^{-1}observed for the as-synthesized CNTs correspond to –OH (hydroxyl group). The band at 1445$cm^{-1}$for as-synthesizd CNTs show the presence of C-C stretching. The peak at 2148 cm^{-1} of as-synthesized-CNTs is assigned C=C bond.While the band at 3010 cm^{-1} shows the presence of –OH.After purification with acid, the band observed at 1586 cm^{-1} and 3114 cm^{-1} correspond to carboxylic functional group (-COOH) and hydroxyl group (-OH) on the surface of purified CNTs. Thefrequency band around 838 and 1069cm^{-1}represents out of plane deformation vibrations of the alkyl group and hydroxyl group attached on purified CNTssurface. After grafting PEG on CNTs surface, a new absorption bands – C= O of ester group was noticed at 1154 cm^{-1}, and also a peak at 2561 cm^{-1} which corresponds to the C-H stretching vibrations of the alkyl group of PEG . Also, an increase in the intensity of hydroxyl group on the surface of PEG-CNTs was noticed after chemical treatment, this peak was observed at 3135 cm^{-1}.

3.2 Scanning Electron Microscopy (SEM) analysis of CNTs

The surface morphology and the elemental composition of the CNTs sample were analysed using High Resolution Scanning Electron Microscopy couple with Energy dispersive spectroscopy (EDS). Figure 2 show the HRSEM images of P-CNTs and PEG –CNTs.

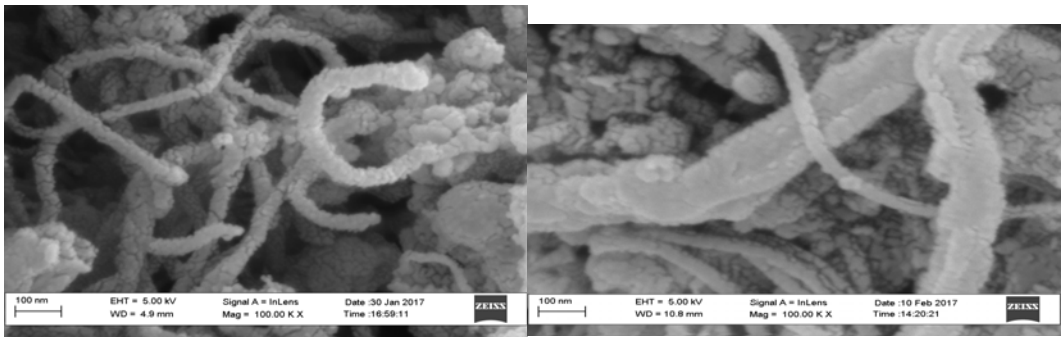

(a) (b)

Figure (2): Scanning Electron Microscopy (SEM) for (a) Purified CNTs and (b) Functionalized CNTs

As shown in Figure2 (a), the CNTs array were erect and long to form a uniform diameter tube which can be attributed to reduction of catalytic particles and amorphous carbon deposition that hinders catalyst deactivation. Similarly, the micrograph of PEG-CNTs shown in Figure 2 (b) exhibit excellent purified nanotubes by the polymer matrix after functionalization indicating dispersion of PEG on the CNTs.The diameter of the CNTs obtained slightly increased after functionalization with PEG.

3.3 Brunauer Emmett Teller (BET) surface area analysis of CNTs

The specific surface area of as-synthesized-CNTs, purified- CNT and PEG-CNTs was analyzed by BET method and is presented in Table 1

Table 1: BET surface area of as-synthesized, purified CNTs and PEG-CNTs

	As-synthesized CNTs	Purified CNTs	PEG-CNTs
BET surface area (m^2/g)	583.31	781.88	970.81
Pore volume (cm^3/g)	0.2963	0.325	0.346
Pore size (nm)	2.983	3.098	3.251

It was observed from the Table 1 that acid treatment lead to an increase in specific surface area,pore volume and pore size for purified CNTs. This is because the acid treatment process opens the end-caps and sidewall of CNTs, thereby enhancing the surface area.It can be observed that incorporation of PEG onto lattice structure of CNTs has improved surface area, pore volume and pore size as compared to as-synthesized and purified CNTs.

3.4 Adsorption Parameter

3.4.1 Effects of contact time

Figure 3 illustrates the effect of contact time on metal ions adsorption on the two adsorbents. The nanoadsorbents exhibited similar adsorption patterns, perhaps, the rate of adsorption differs. The adsorption process was first rapid for the three metals until equilibrium time of 90 minutes for purified CNTs and 60 minutes for PEG functionalized CNTs due to availability of active sites on CNTs surface. In other words, fast initial adsorption rate may be due to the higher driving force ,thus leading to fast transfer mechanism between the adsorbed metals and the active sites of the adsorbents. The functionalized CNTs shows high adsorption capacity

of 93.79%, 83.09% and 94.93% removal for Ni, Cd and Fe than P-CNTs which has removal efficiency of 92.79%, 77.7% and 78.62% for Fe, Cd and Ni respectively. This shows that PEG -CNTs successfully removed more of iron compared with other metals suggesting greater interaction between the adsorbent than the later.

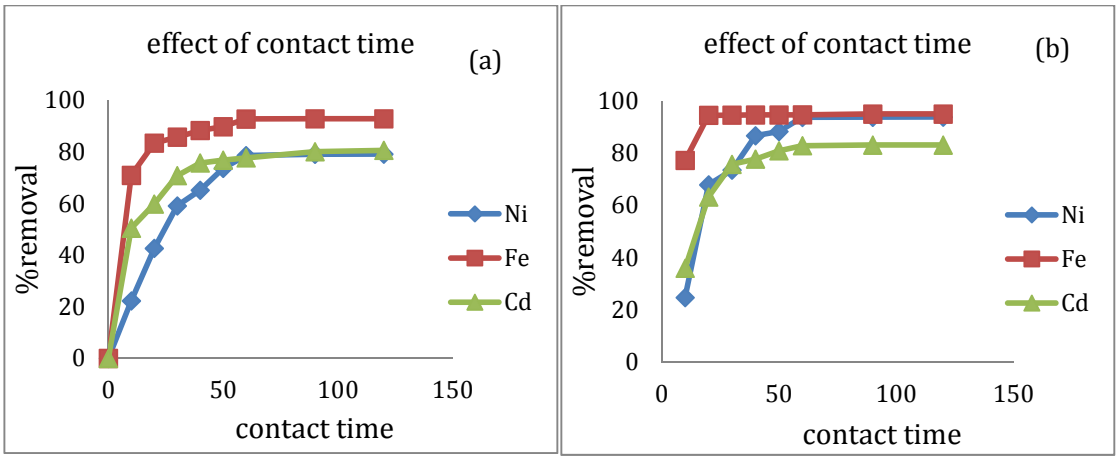

Figure 3: Effect of contact time on metals ion adsorption on (a) purified CNTs (b) PEG functionalized CNTs

3.4.2 Effect of adsorbent dosage

The effect of adsorbent dosage on the adsorption rate ofboth purified and functionalized CNTs showed similarity. As illustrated in Figure 4.3., when the mass of adsorbent was increased to 0.3grams, there was removal of 95.47, 66.67 and 95.36 % of Ni, Cd and Fe respectively. An increase in adsorbent dosage beyond 0.3grams showed slight increase in the %removal when 0.5grams of purified CNTs adsorbent was used to remove 96.918, 89.22 and 95.371 % of Ni, Cd and Fe respectively. Increase in adsorbent dosage shows a corresponding increase in adsorption rate. This is as a result of increase in adsorption capacity of the adsorbents, as more adsorbent provides wider surface area of active sites for adsorption to take place. The cessation in the percentage removal of metals beyond equilibrium isassociated with the overlapping of sorption sites due to excess of adsorbent particles (Jethave*et al,* 2017). It implies that till a certain range of initial metal concentrations, the metalremoval is associated with the soil sorption capacity. This is in correlation with the report of (Chungsying *et al*, 2004).

Similarly, for functionalized CNTs, 96.26, 92.89 and 95.07 %removal was recorded when 0.3grams of adsorbent was used for Ni, Cd and Fe respectively. Further increase in the dose of adsorbent showed an increased removal of up to 94.3627 and 98.70% removal of Cd and Ni at an adsorbent dose of 0.5grams of CNTs. However there was no significant effect of increase in dosage beyond 0.3grams for Fe uptake.

3.4.3 Effect of temperature

The effect of temperature on metal removal efficiency of iron and manganese from pharmaceutical wastewater was carryout and the result is shown in Figure 5.It was observed that the rate of iron, nickel and cadmium removal for the nanoadsorbents increases with increasing temperatures, indicating the endothermic nature of adsorption process.. Moreover, an increase in temperature resulted in a swelling effect within the internal and external structure of the adsorbent, which invariably increased the rate of penetration of the active sites on the adsorbent by the metals. The more effective uptake of metals experienced using

the functionalized CNTs can be attributed to the solubility nature of the adsorbent, and relatively larger pore space for the adsorbent to capture the metals when compared to the purified CNTs.

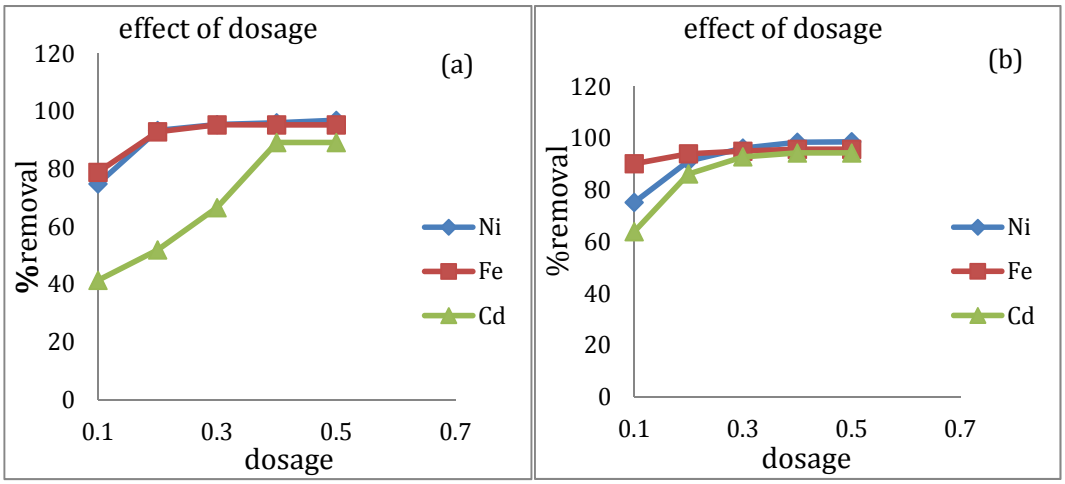

Figure 4: Effect of adsorbent dosage on metals ion adsorption on (a) purified CNTs (b) PEG functionalized CNTs

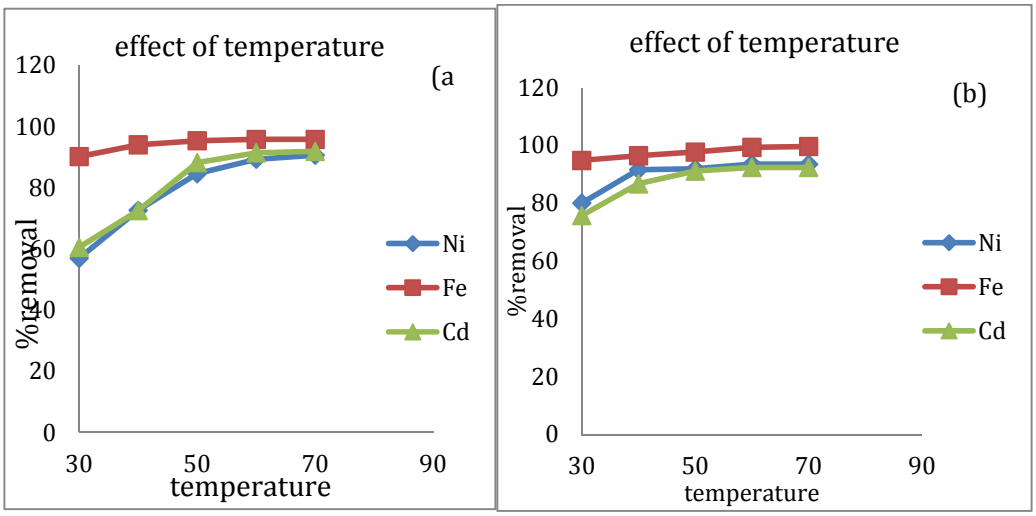

Figure4.2:(a) graph of %removal against temperature for purified CNTs. (b) Graph of %removal against temperature for functionalized CNTs.

3.5 Adsorption isotherm

The isotherm of both Lagmuir and Freundlich for the nano adsorbent are shown in Table2 and Table 3 respectively.

Table 2 :Langmuir Adsorption isotherm parameters

	Purified CNTs			functionalized CNTs		
Metals	**Q_m**	**K_l**	**R^2**	**Qm**	**K_l**	**R^2**
Ni	0.760	4.787	0.898	0.228	51.04	0.935
Fe	66.67	670.0	0.730	5.058	0.370	0.897
Cd	0.007	281.3	0.747	0.025	95.28	0.839

Table 3: Freudlich Adsorption isotherm parameters

	Purified CNTs			functionalized CNTs		
Metals	**n**	**K_f**	**R^2**	**n**	**K_f**	**R^2**
Ni	1.626	0.843	0.946	2.371	0.537	0.984
Fe	1.275	2.725	0.830	1.592	3.133	0.964
Cd	3.303	0.020	0.611	2.501	0.052	0.864

Comparing Langmuir (Table 3) and Freudlich (Table 4) adsorption isotherms parameters, it was observed that the value of R^2 for Freudlich isotherm model is higher than that of Langmuir for the adsorption of Ni on purified CNTs. hence, a value of 0.8480 and 0.9489 for Langmuir and Freudlich isotherm were accomplished respectively. Additionally, the take-up of Fe and Cd likewise takes action accordingly, with R^2 values of 0.73 and 0.747 for Langmuir, likewise 0.830 and 0.611 for Freudlich isotherm respectively. Another significant parameter to consider before concluding if the Freudlich isotherm fits the adsorption system better is the value of n. adsorption is considered as favourable when the value of Freudlich constant n falls within the scopes of 1 to 10. On the off chance that n rises to 1, this implies the adsorption process is straight; n more than 1 shows adsorption to be chemical process and n less than 0 demonstrates that the adsorption process is a physical process (Desta, 2013).

Freudlich constant "n"values of 1.626, 3.303 and 1.275 gotten for Ni, Cd and Fe show that the Freudlich model is acceptable. Also, it portrays the adsorption process better. Functionalized CNTs adsorbent likewise fits more with the Freudlich isotherm model than the Langmuir isotherm, as the value of n for Ni, Cd and Fe are 2.371, 2.501 and 1.592 respectively, which falls within the scope of 1 to 10, demonstrating that the model is acceptable. R^2 values for Freudlich isotherm are 0.984, 0.864 and 0.964 for Ni, Cd and Fe respectively, which is higher than 0.935, 0.839 and 0.899 for Ni, Cd and Fe respectively, when the Langmuir model was utilized. Chungsyinget al, (2004) revealed that Freudlich model accept that multilayer adsorption happens. This recommends why the Freudlich isotherm fits the adsorption process on the multiwall CNTs walls which has numerous layers for adsorption.

Table 4:Pseudo first order parameters.

	Purified CNTs			functionalized CNTs		
Metals	R^2	K_1	Qe	R^2	K_1	Qe
Ni	0.005	0.001	0.845	0.1	0	0.740
Fe	0.788	0.028	14.58	0.12	0.420	0.011
Cd	0.179	0.040	0.016	0.403	0.039	0.0109

Table 5 Pseudo second order parameters.

	Purified CNTs			functionalized CNTs		
Metals	R^2	K_2	Qe	R^2	K_2	Qe
Ni	0.969	0.012	3.509	0.953	0.013	3.984
Fe	0.999	0.003	100	0.999	0.01	100
Cd	0.954	0.089	0.310	0.954	0.090	0.310

3.6 Adsorption kinetics

The different adsorption isotherm parameters were determined from the plots of the kinetic model equation and outlined with correlation coefficients (R^2) in Table 4 and 5.The moderately higher value is the more relevant model to the kinetic of heavy metals adsorption onto adsorbent. For looking at the adsorption kinetic, the pseudo first order and pseudo second kinetic models were utilized. As outlined in Table 4, utilizing the purified CNTs adsorbent, the first order model have a correlation coefficients (R^2) of 0.005, 0.788 and 0.179 for Ni, Fe and

Cd respectively, which shows that the first order model is not appropriate for fitting the adsorption process, as the values are not near 1. So also, utilizing the functionalized CNTs adsorbent, the values of R^2 are 0.1, 0.12 and 0.403 for Ni, Fe and Cd, this demonstrates the second order model does not fit the adsorption kinetic process for both the purified and functionalized CNTs adsorbents.

In Table 5, the second order parameters gotten when the second order kinetic model was utilized shows great correlations . 0.969, 0.999 and 0.954 were gotten as the R^2 value for Ni, Fe and Cd respectively when the purified CNTs adsorbent was utilized. In like manner for the functionalized CNTs adsorbent, R^2 value of 0.953, 0.999 and 0.954 were gotten for Ni, Fe and Cd separately. This shows great relationship as the values are near 1. The values of Qe likewise show great correlation with the empirical values of Qe which demonstrates that the pseudo second order kinetic model fits the adsorption kinetic more than the pseudo first order kinetic model.

3.7Adsorption thermodynamics

TABLE 6: Thermodynamics parameters of heavy metals adsorption on Purified CNTs

Metals	ΔG (J/mol)					ΔH(J/mol)	ΔS (J/mol K)
	Temperature (K)						
	303	313	323	333	343		
Ni	-2254.5	-3475.6	-4696.8	-5917.9	-7139.1	34747	-122.12
Fe	-6258.0	-7064.0	-7870.0	-8676.0	-9481.9	18164	-80.599
Cd	-2438.2	-3731.4	-5024.7	-6317.9	-7611.2	36747	-129.32

TABLE 9 Thermodynamics parameters of heavy metals adsorption on functionalized CNTs

Metals	DG (J/mol)					DH (J/mol)	DS (J/mol K)
	Temperature (K)						
	303	313	323	333	343		
Ni	-48941	-49827.2	-50713.4	- 51599.6	-52485.8	22089.5`	-88.619
Fe	-130395	-132659	-134923	-137187	-139451	61796.3	-226.4
Cd	-54507.9	-55474	-56440.1	-57406.2	-58372.3	25235.5	-96.609

According to Table 6 and Table 7 shows that the values of Gibbs free energy (DG)) were both negative. The negative values of (ΔG) show that the adsorptions of Ni, Fe and Cd on the nanoadsorbents are spontaneous. This implies that the process will proceed at this temperature range. As can be seen in Table 6and Table 7 that the negative values of (ΔG)increases with increase in temperature and therefore favours the adsorption process. Also, the positive values of ΔH observed on the nanoadsorbents for the adsorption of Ni, Fe and Cd indicates the endothermic nature of the adsorption In addition, the negative values of ΔS for the adsorption of heavy metals on both purified and functionalized CNTs shows that there wasdecreasing irregular randomness as the adsorption process proceeds.

4.0 Conclusions

The present study confirmed that P-CNTs and PEG-CNTs are effective adsorbents for the removal of iron and manganese from pharmaceutical wastewater. As a function of contact time, nano-adsorbents dosage and temperature; the removal efficiency of iron, nickel and cadmium was in order of PEG-CNTs > P-CNTs and the performance of the adsorbent is surface area specific. In addition, the adsorption equilibrium data followed Freudlich model. The kinetic study revealed that pseudo second order model is fit for describing the experimental data. The thermodynamics indicated that the adsorption of the iron and manganese from battery wastewater was feasible, endothermic and spontaneous process in nature and is more favorable with increasing temperatures.

Acknowlegement

This wok was supported Tertiary Education Tax fund Nigeria (TETFUND/FUTMINNA/NRF/2014(01 and Centre of genetic Engineering and

References

Aliyu, A., Abdulkareem, A. S., Kovo, A. S., Abubakre, O. K., Tijani, J. O., andKariim, I. (2016): synthesize multiwalled carbon nanotubes via catalytic vapor deposition method on Fe-Ni bimettalic catalyst supported on kaolin. pp25.

Burghard, M. and Balasubramanian, K., (2005): Chemically Functionalized Carbon Nanotubes, (1) 2, 180 –192. www.small-journal.com

Chungsying, Lu., Yao-Lei, C., Kuan-Foo, C. (2004): Adsorption of trihalomethanes from water with carbon nanotubes. Journal *of Water Research* 39 (2005) ,1183–1189

Coville, N. J., Mhlanga, S., D., Nxumalo, E., N,,Shaikjee A. A.(2011): Review of Shaped Carbon nanomaterials. South African Journal of Sei;107(3/4), Art.418. DOI: 10.4102/sajs.vlO7i3/4.418

Carbon nanotubes. "PhysicsWorld.com. 01 January 1998. IOP publisher.31 Mar 2009.Retrieved fromhttp://physicsworld.com/cws/article/print/1761.

Jethave, G., Fegade, U., Attarde, S., Ingle, S.(2017): Facile synthesis of Lead Doped Zinc-Aluminum Oxide Nanoparticles 2 (LD-ZAO-NPs) for efficient adsorption of anionic dye: Kinetic, isotherm 3 and thermodynamic behaviors. *Journal of Industrial and Engineering Chemistry*.(3410) 1–13.

Sharma, M., Hazra, S., Basu, S.(2017): Kinetic and Isotherm Studies on Adsorption of Toxic Pollutants Using Porous ZnO@SiO2 Monolith. *Journal of Colloid and Interface Science,* doi: http://dx.doi.org/10.1016/j.jcis.2017.06.020

Sharma, R., Kumar A. and Sharma, V. (2015):Synthesis of Carbon Nanotubes by Arc-Discharge and Chemical Vapor Deposition Method with analysis of its Morphology, Dispersion and Functionalization Characteristics.Journal of *Cogent Engineering:* DOI: http://dx.doi.org/10.1080/23311916.2015.1094017

Tasis, D., Nikos T., Alberto, B., and Maurizio, P. (2005): Chemistry of Carbon Nanotubes. Chem. Rev. 2006, 106, 1105‧1136

Turkar, S., Bharti, D. B., Gaikwad, G. S., (2011): Various methods involved in waste water treatment to control water pollution. Department of Chemistry, J. L. Charturvedi College of Engineering, Nagpur, India

Yoshinori, A. and Xinluo, Z., (2006): Synthesis of Carbon Nanotube by Arc-Discharge method. New diamond and frontier carbon Technology. Vol.16,(3).

Proceedings of the 49th NSChE Annual Conference
KADA 2019: pp 795-806

P06: PINCH ANALYSIS OF HEAT EXCHANGER NETWORKS OF AN INDUSTRIAL AMMONIA PLANT FOR FERTILIZER PRODUCTION

***Dagde, Kenneth K., Iregbu, Precious O. and Tijani, Olamilekan E.**
Department of Chemical/Petrochemical Engineering
Rivers State University, Nkpolu Oroworukwo, Port Harcourt, Nigeria
**Corresponding Author Email: Dagde.Kenneth@ust.edu.ng.*

ABSTRACT
The pinch analysis of the heat exchanger networks in an Industrial Ammonia plant for the production of urea fertilizer was carried out in this work using Aspen Energy Analyzer. Process data of the heat exchanger networks (HENs) were obtained from the plant and used to formulate a thermal table after the data were entered into the software for pinch analysis of the networks. The analysis is aimed at ascertaining the energy efficiency and of the heat exchangers used in the ammonia plant. The software produced the composite, balanced, grand composite curves, the grid representation and target reports. From the results of the analysis, the following were obtained: minimum heating and cooling requirements of the entire network, the process streams not properly matched and the heat exchangers not properly placed. The analysis indicated that a total of 3.281×10^{11} *kJ/hr cold utility and* 3.217×10^{12} *kJ/hr hot utility were not utilized within the network which is as a result of poor process stream matching and wrong arrangement of the heat exchangers. Hence, the heat exchangers in the Industrial ammonia plant need to be retrofitted to ensure adequate heat recovery, process to process integration and efficient energy utilization within the heat exchanger network.*

Key words: Heat Exchanger Networks, Pinch Technology, Aspen Energy Analyzer and Ammonia Plant.

1.0 INTRODUCTION
The cost of produced products largely depends on the amount of energy consumed in the plant during production of the products. The more the amount of energy consumed in a process plant, the higher the cost of products produced from the plant and vice versa. So, energy consumption is an important factor to be considered in any process plant to reduce the cost of products for consumers' sake and to gain more profit for the company. Therefore, minimization of energy is highly important in any process plant. In the reality, it is difficult to determine the minimum amount of energy required by a process plant by using the traditional chemical engineering design (mass and energy balance, rules of thumb, good engineering judgment and creative ability of designing) without including Pinch Technology. Pinch Technology was discovered in the late 1970s and was used industrially in 1980, so it is obvious that process plants before 1980 was built and designed without performing pinch analysis on them. Therefore, the amount of energy consumed in these plants will probably be higher than required, which will lead to wastage. Pinch technology is a complete methodology based on thermodynamic principles that can be used to design new plants with reduced energy and capital costs and for existing processes; to ascertain efficiency and provide potential design modifications to improve performance. A fundamental strength of pinch analysis is that it determines the most appropriate set of heat exchange stream matches. In doing so, it minimizes energy loss, reduces the cost of hot and cold utilities and can be used to determine the minimum requirement for both hot and cold utilities in a process and thus, enhance process integration (Anozie and Odejobi, 2007). Pinch Technology can also be considered in the design of a new process plant to determine the process conditions of the core equipment of a process plant in which energy can be minimized. Heat exchanger network (HEN) is a

system of several heat exchangers connected together. It enables several process streams to exchange sufficient amount of thermal energy so they can attain their respective desired set temperature values (target), (Akpa and Okoroma, 2012). The production of Urea fertilizer requires reaction between ammonia (NH_3) and carbon dioxide (CO_2), therefore a urea fertilizer cannot be produced without an ammonia plant. The industrial ammonia plant has a production capacity of 2300 tons per day of ammonia from natural gas. The plant involves production of ammonia by first passing natural gas through the desulphurizing unit to reduce the sulphur content to below 280μg/m^3 to prevent poisoning the nickel catalyst used in the primary reformer using activated carbon or zinc oxide. The activated carbon could be regenerated by passing super-heated steam through the bed of carbon. The desulphurized natural gas is then fed into the reformer with simultaneous inflow of steam to produce carbon monoxide (CO) and hydrogen (H_2), CO is mixed with more steam to produce CO_2 and more hydrogen, the produced hydrogen from the primary reformer is then mixed with N_2 (air) to produce ammonia. Some works have been done on different sections of various plants; Akpa and Okoroma, (2012) performed pinch analysis on the heat exchanger networks of the crude distillation unit of Port Harcourt refinery and discovered pinch penalty of about 98916.1 kW hot utility and 8298.7 kW cold utility. Lukman, *et al.,* (2018), performed evaluation of Naphtha Hydro treating Unit (NHU) of Kaduna refinery using pinch technology in identification of areas requiring improvement in the heat exchanger networks of the NHU with the aim of minimizing total cost and they discovered the optimal total cost to be $263.115 from the initial target cost of $298.815 and also observed the target heating and cooling to be $1.395x10^7$kcal/h and $1.440x10^7$kcal/h respectively while the design heating and cooling are $1.228x10^7$ kcal/h and $1.273x10^7$ kcal/h. In this work, Pinch Technology was used to evaluate the heat exchanger network in Industrial Ammonia plant. The analysis will ascertain design efficiency of the existing heat exchangers network; determine appropriate number of heat exchangers and identify improper stream matching within the selected network.

2.0 MATERIALS AND METHODS

2.1 Materials

The materials used include: Aspen Energy Analyzer version 8.6 (used to produce the composite curve, balanced composite curve, grand composite curve and grid representation of the heat exchanger networks), Industrial fertilizer plant process data and process flow diagram showing the inlet and outlet temperatures, mass flow rates, specific heat capacities, enthalpy per unit temperature and enthalpy of each process streams and utilities.

2.2 Methods

The Aspen Energy Analyzer version 8.6 process tool was employed to perform a detailed and accurate pinch analysis of the heat exchanger networks in Industrial Ammonia plant. To do this, the thermal data obtained by data extraction were fed as input to the software to construct the composite curve, balanced composite curve, grand composite curve and grid representation of all networks. The following pinch rules were employed in order to achieve the minimum energy targets for the crude preheating process:

i. Heat must not be transferred across the pinch
ii. There must be no external cooling above the pinch and no external heating below the pinch (heaters must be placed above and coolers below the pinch).

Violating any of these rules will lead to cross-pinch heat transfer resulting in an increase in the energy requirement beyond the target. Any heat transfer across the pinch is excess heat which is wasted, and expressed as a pinch penalty.

2.2.1 Steps in Pinch Analysis

The pinch analysis of the industrial ammonia plant was achieved through the following steps:

a) Data Extraction

This involves extraction of the data from the process flow diagram to form thermal problem table. The data to be extracted is stated in the materials required for the work.

b) Formation of Thermal Data Table

The data table was formed from the extracted data by Aspen energy analyzer.

c) The use of Aspen Energy Analyzer Software Version 8.6

The extracted data were fed as input into Aspen energy analyzer software to complete the thermal data table.

d) Analysis of the Composite Curves and Grid Diagrams to meet the Objective of the Work

To formulate and complete the thermal data table, equation (1) was used:

$$\mathrm{Q} = \mathrm{MCp}\Delta T \quad (1)$$

where: M is the mass flow rate of the stream (kg/hr).

Cp is the specific heat capacity of the process streams $(kJ/kg°\mathrm{C})$.

ΔT is the temperature difference between inlet (supply) temperatures and the target (outlet) temperature of each stream (°C)

$$C_P = M * c_p \quad (2)$$

Cp is the heat capacity flow rate $(kJ/kg°\mathrm{C})$ and measured as enthalpy change per unit temperature difference (kJ/C-h).

2.2.2 Configurations of the Heat Exchangers and Streams

The preheating of the natural gas used for the reaction that leads to the production of ammonia was accomplished via thirteen (13) heat exchangers using hot streams from other units within the plant. For the purpose of this evaluation the thirteen heat exchangers were sectioned into two Heat Exchanger Networks (HENs), HEN-1 and HEN-2. The configurations of the two networks obtained from the Process Flow Diagram (PFD) are represented in Figures 1 and 2.

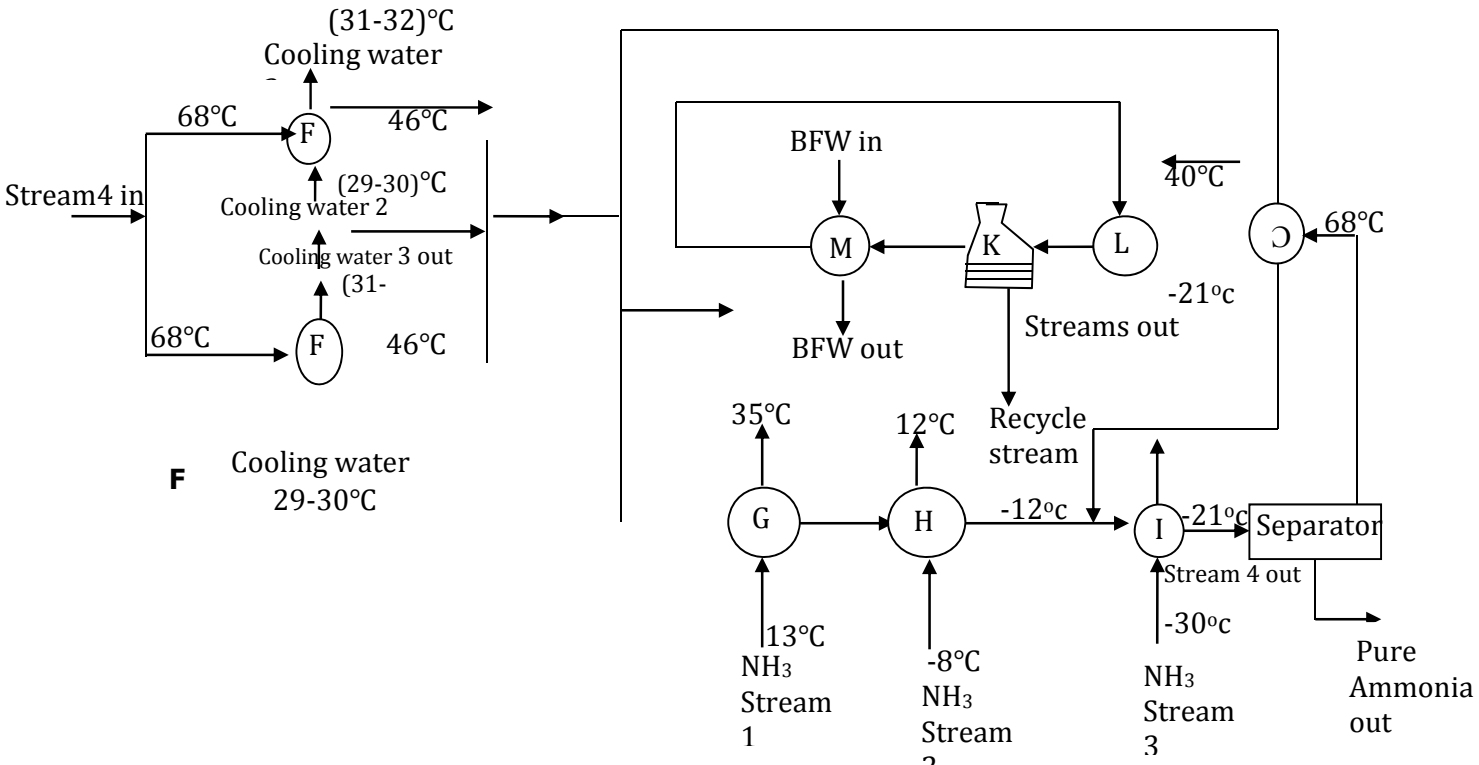

Figure 1: Flow Chart for Heat Exchanger Network 1 (HEN-1)

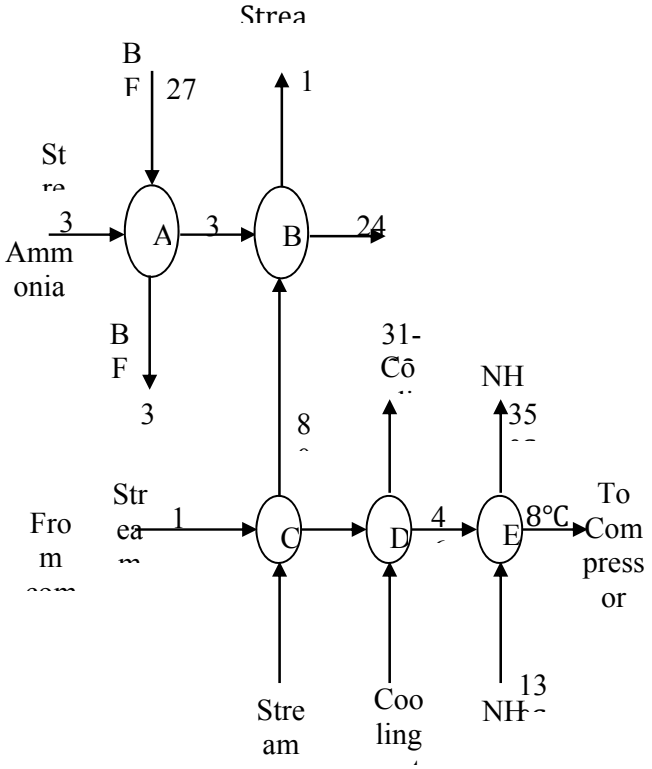

Figure 2: Flow Chart for Heat Exchanger Network 2 (HEN-2)

Table 1: Thermal Data Table for Heat Exchanger Network 1 (HEN-1)

Name	Inlet Temperature ℃	Outlet Temperature ℃	MCp $\frac{kJ}{h℃}$	Flowrate $\frac{kg}{h}$
Stream 1	375.0	242.0	2.467*10^9	1.479*10^9
Stream 2	105.0	8.0	3.125*10^9	1.479*10^9
Stream 3	70.0	116.0	7.133*10^9	1.479*10^9
NH_3	13.0	35.0	5.681*10^7	2.594*10^7
Stream 4	68.0	-21.0	1.808*10^10	-
Stream 5	68.0	40.0	5.74*10^10	-
NH_3 1	68.0	35.0	5.185*10^10	-
NH_3 2	13	12.0	5.681*10^7	2.594*10^7
NH_3 3	-8	-12.0	5.450*10^7	2.433*10^7

2.2.3 Construction of Composite Curves

A composite curve of a Heat exchanger network is a plot of enthalpy of cold streams and enthalpy of hot streams against temperature on the same graph sheet. The plot is obtained by addition of the enthalpies of the streams with respect to temperature change for both hot and cold composite curves. The composite curves determine if hot or cold utilities or both are required, and the minimum energy requirement (from the areas covered by the cold and hot composite curves) in the grand composite curves.

2.2.4 Construction of Grid Diagram

This involves the representation of heat exchanger network of a given process on a grid. The grid diagram shows all the streams on the heat exchanger network with the hot streams above the cold streams. It indicates hot streams with red color having direction from right to left and with their supply and target temperatures specified. In the grid representation the user merge two streams together with the aid of heat exchanger. Two streams are merged together based on two conditions above the pinch ($C_c \geq C_h$) and below the pinch ($C_h \geq C_c$). After the merging, the temperatures required by the software for the grid representation are put in by the user. Also, in the grid representation you can also check if hot utility or cold utility is the required target menu and HP/LP is commonly added for hot utility while cooling water is added as best cooling utility. This diagram serves as the proper measure for connecting process streams of heat exchanger network of process plant. Also, while connecting heat exchangers of a network on grid diagram, the three rules of pinch are applied which include; there must be no external heating below pinch (right hand side of the grid diagram) because it serves as heat source, no external cooling above pinch because it serves as heat sink and heat must not be transferred across pinch. If any of these rules is violated, there will be cross pinch heat transfer which will increase the minimum energy required beyond target.

3.0 RESULTS AND DISCUSSION

The results of the heat exchanger networks 1 and 2 are presented in this section. The results are shown in the composite, balance and grand composite curves for the HENs. The plots show the variation of the of enthalpy at varying temperature. The red line represents the hot stream while the blue line represents the cold stream.

3.1 Analysis of Heat Exchanger Network-1 (HEN-1)

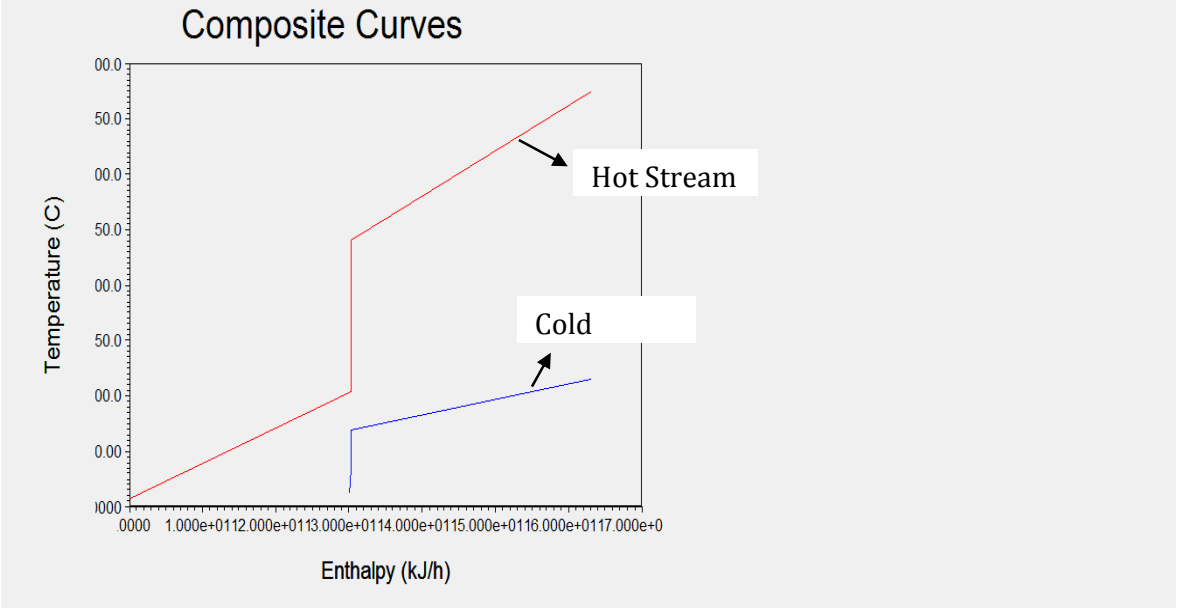

Figure 3: Composite Curve for HEN-1

From Figure 3, the left end of the cold composite and hot composite curve matches at the same enthalpy values showing that no heating utility is needed and right end of the composite curves (cold and hot) does not match at the same enthalpy value showing that cooling utility is required. The difference between the right end enthalpy value of both the hot and cold composite curves gives the minimum amount of heating utility $Q_{H,min}$ required and the difference between the left end enthalpy value of both hot and cold composite curve gives the minimum amount of cooling utility $Q_{C,min}$. From the curve, it could be seen that excess of 3.019×10^{11} KJ/hr hot duty were not utilized and all the cold duty were fully utilized in the HEN-1, these values could also be seen in the utility targets of the software where the cooling utility was the hot duty not utilized and the required heating utility was the cold duty not utilized. The minimum allowable temperature difference is found to be 10°C.

Figure 4 shows the balanced composite curve of the heat exchanger network when both hot and cold utilities have been added. The both ends of the cold and hot composite curves have the same enthalpy value in the curve meaning the cold utility required in the composite curve have been accounted for.

Figure 5 shows the amount of energy that is efficiently utilized. When a straight line is drawn from the upper end of the curve downward, the area to the right of this curve shows the amount of heat energy that was efficiently utilized while the area to the left of this curve shows the total amount of heat energy that was not utilized in the heat exchanger network.

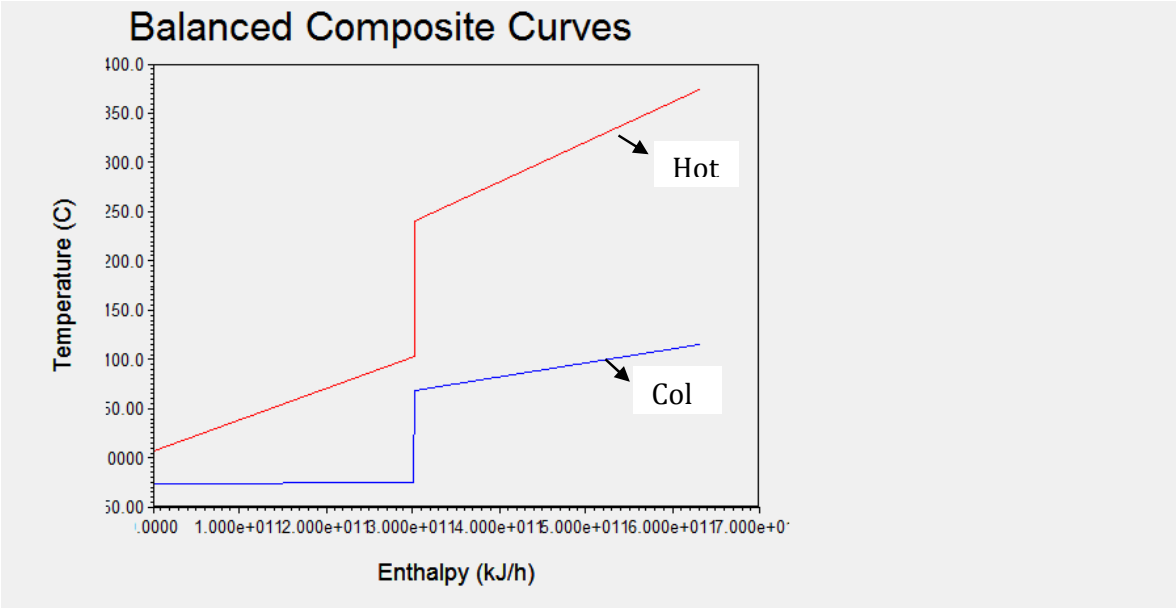

Figure 4: Balanced Composite Curve for HEN-1

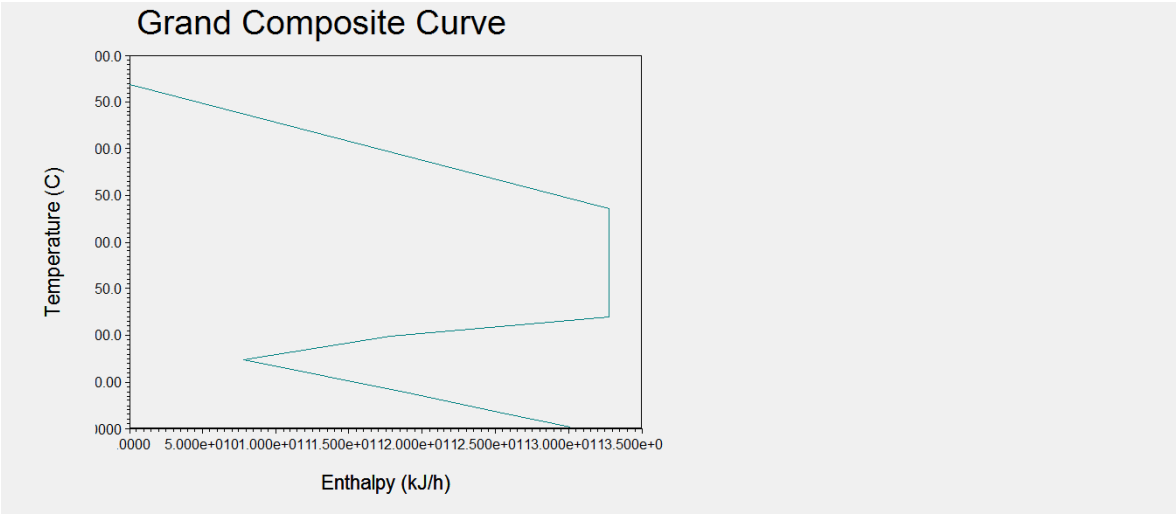

Figure 5: Grand Composite Curve for HEN-1

Table 3: Utilities used for Analysis

Name	Inlet Temperature	Outlet Temperature	Cost index	HTC	Target load
Refrigerant 1	-25	-24.0	2.739*10^6	4680	3.019*10^11

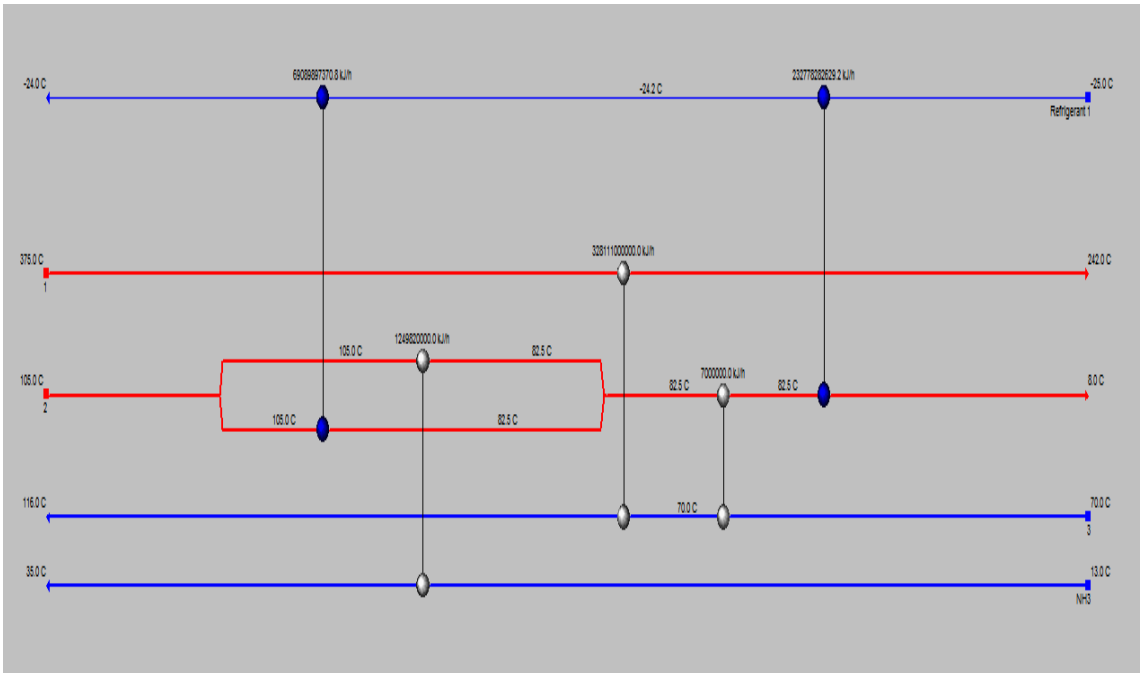

Figure 6: Grid Representation of HEN-1

From Figure 6, Heat Integration (HI) Project is used to design the grid diagram because it was discovered that there were no cold and hot pinch temperatures, so it will be so hard to design it manually or without using HI project. Since pinch temperatures were not found it shows that the streams in the network cannot be matched. HI project provides more designs near optimum design but the design that gives the lowest cost and lowest heat exchanger area is the best grid representation.

3.2 Analysis of Heat Exchanger Network-2

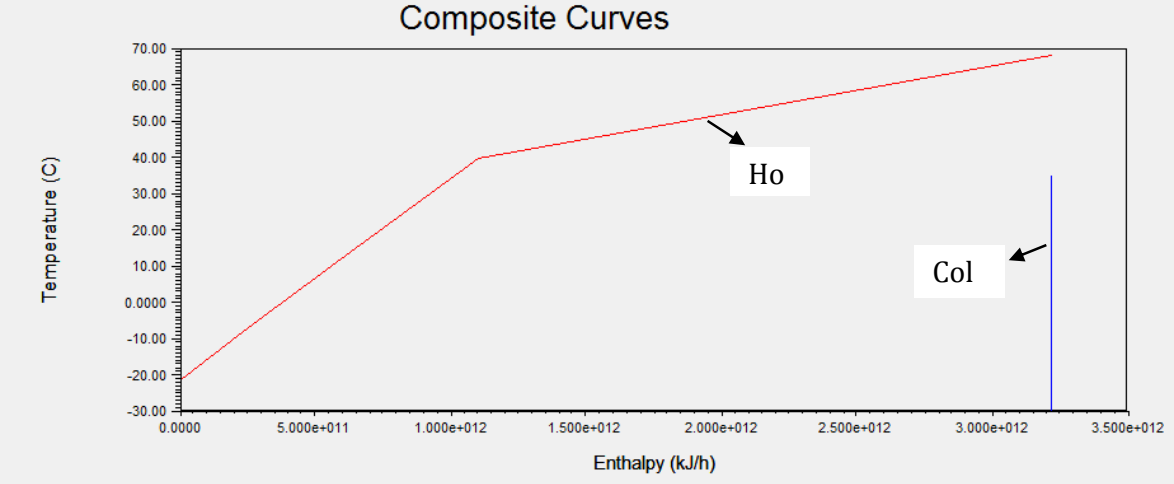

Figure 7: Composite Curve for HEN-2

From Figure 7, the curve shows that no heating utility was required since the right end of both hot and cold composite curves have the same enthalpy value and also that large amount of cooling utilities was required since the left end of the hot composite curve was far from the cold composite curve while enthalpy difference between the left ends gave the minimum amount of cooling duty required in the heat exchanger network. Also, from the composite curve, it could be seen that all the cold duty was fully used up in the network and excess of 3.215×10^{12} KJ/hr hot duty was not utilized. The minimum allowable temperature difference is found to be 10°C.

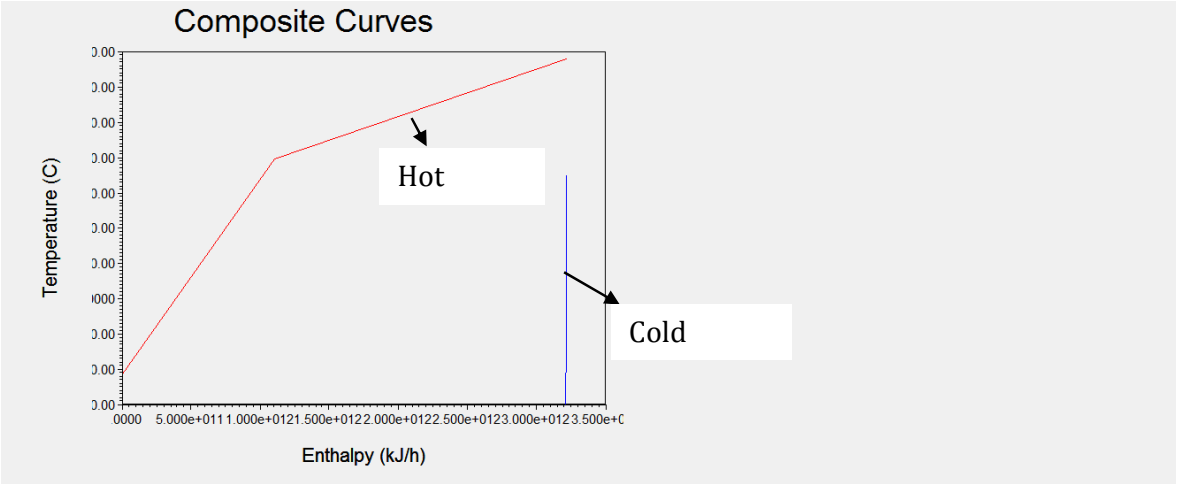

Figure 8: Balanced Composite Curve for HEN-2

Figure 8 shows the balanced composite curve of the heat exchanger network 2 when both hot and cold utilities have been added. The both ends of the cold and hot composite curves have the same enthalpy value in the curve meaning no utility requirements.

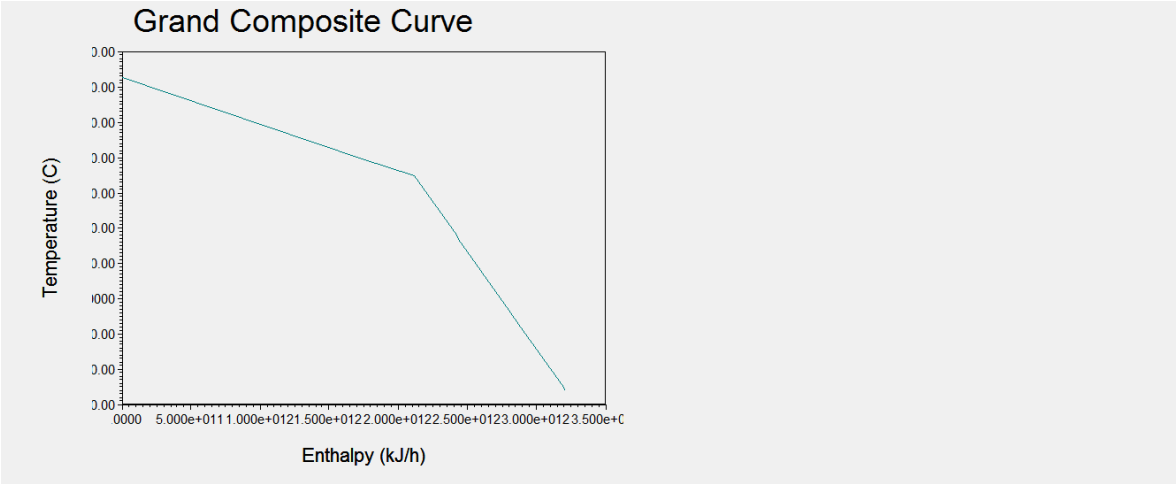

Figure 9: Grand Composite Curve for HEN-2

Figure 9 is a plot of the grand composite curve and depicts that little amount of heat energy was efficiently utilized in the heat exchanger network.

Table 4: Utility used for the Analysis

Name	Inlet Temperature	Outlet Temperature	Cost index	HTC	Target load
Refrigerant 1	-40	-39.0	3.739*10^6	4680	3.019*10^11

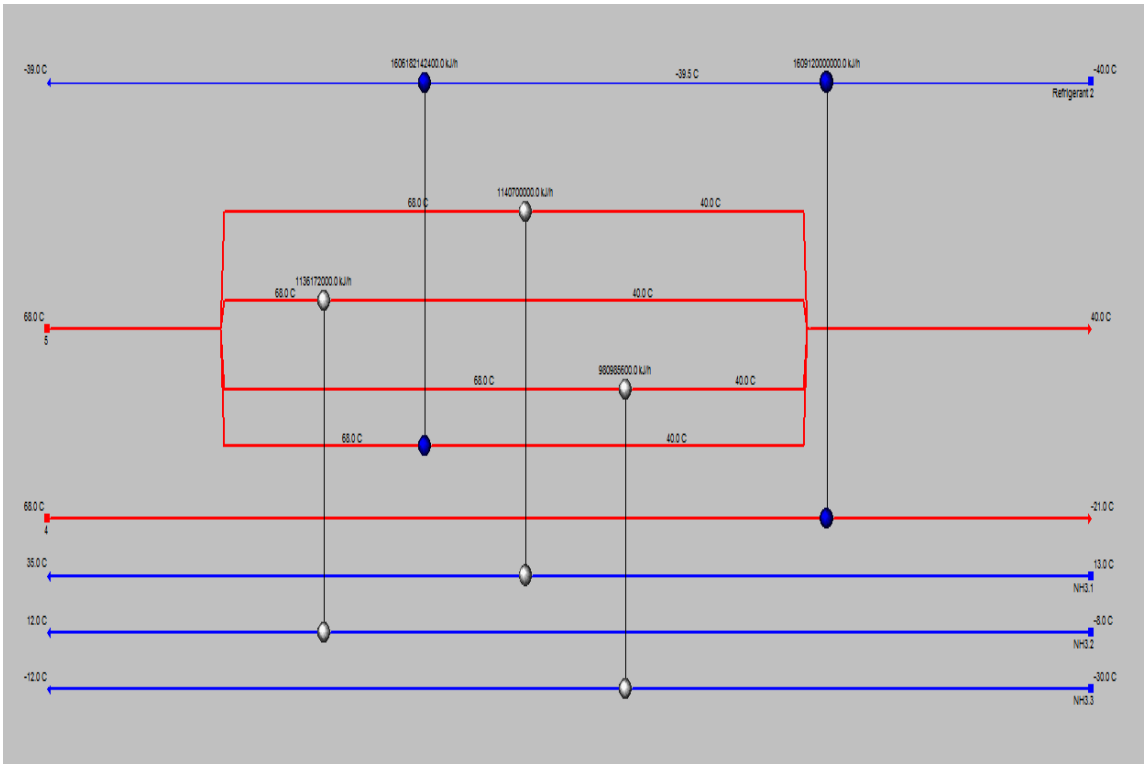

Figure 10: Grid Representation HEN-2

In designing the heat exchanger network 2, Heat Integration (HI) project was used and it gave different scenarios close to optimum design. Showing the pinch lines for all the scenarios, the stated rules of pinch principles was violated which would increase the energy requirement beyond target for the network. The grid diagram shown in Figure 10 shows the scenarios that minimally violate the rules of pinch principle and with optimal cost. Therefore, it can be concluded that the streams in heat exchanger network 2 cannot also be matched.

4.0 CONCLUSION

Pinch analysis using Aspen Energy Analyzer has been carried out on Industrial Ammonia Plant to ascertain the efficient energy utilization and process-process heat integration. The heat exchangers in the ammonia plant was divided into two heat exchanger networks (HEN-1 and HEN-2) to ascertain efficiency of heat exchanger arrangement and effective process to process heat integration and energy utilization in the networks. It was discovered that the process streams in the heat exchanger networks could not be matched because their matching violated the rules of pinch principles. The results from the analysis showed that an excess of 3.019×10^{11} KJ/hr hot duty was not utilized and all cold duty was utilized in the HEN-1 and excess of 3.215×10^{12} KJ/hr hot duty was not utilized in the HEN-2. Proper design of the heat exchanger network can ensure efficient utilization of energy in the plant. This as shown in this work can be achieved using the grid representation techniques which can give the best arrangement of heat exchangers in any process plant. Retrofit should be carried out for both heat exchanger network 1 and heat exchanger network 2 to properly match process streams so as to reduce the minimum energy requirement which would thereby reduce cost of production of products.

REFERENCES

Akpa, J.G. and Okoroma, J.U. (2012). Pinch Analysis of Heat Exchanger Networks in the Crude Distillation Unit of Port-Harcourt Refinery, *Journal of Engineering Trends in Engineering and Applied Sciences*,3(3), 475-483.

Anozie, A. N. and Odejobi O. J. (2007). "Evaluation of Heat Exchanger Network Design and Energy Efficiency in the Crude Distillation Units of Nigerian Oil Refineries", Presented at the 37th Annual Conference of the Nigerian Society of Chemical Engineers, pp 1-10.

Furman, K. C. and Sahinidis, N. V. (2002), A Critical Review and Annotated Bibliography for Heat Exchanger Network Synthesis in the 20th Century. *Industrial and Engineering Chemistry Research,* 41, 2335–2370.

Gundersen, T. and Naess, L. (1998), The Synthesis of Cost Optimal Heat Exchanger Networks—An Industrial Review of the State of the Art. *Computes Chemical Engineering*, 126, 503–530.

Lukman, Y., Yesufu, I. S. and Otoikhian, S. K. (2018). Evaluation of Naphtha Hydrotreating Unit (NHU) of Kaduna Refinery Using Pinch Technology. *Journal of Chemical Engineering and Process Technology*, 3(1), 492 – 498.

Linnhoff, B. and Flower, J. (1978), Synthesis of Heat Exchanger Networks. I. Systematic Generation of Energy Optimal Networks. *American Institute of Chemical Engineering Journal,* 244, 633– 642.

Linnhoff, B., Mason, D. R., and Wardle, I. (1979), Understanding Heat Exchanger Networks. *Computes Chemical Engineering*, 3, 295–302

Linnhoff, B., Towsend, D.W., Boland, D., Hewitt, G. F., Thomas, B. E. A., Guy, A. R., and Marsland, R. H. (1982) A User Guide on Process Integration for the Efficient use of Energy. UK: The Institute of Chemical Engineers.

Linnhoff, B., and Hindmarsh, E. (1983) The Pinch Design Method for Heat Exchanger Networks. *Chemical Engineering Science,* 38, 745–763.

Linnhoff, B. (1994), Use Pinch Analysis to Knock Down Capital Costs and Emissions. *Chemical Engineering Progress*, 32–57. 1994.

Proceedings of the 49th NSChE Annual Conference
KADA 2019: pp 807-813

P1C-05: IMPROVED SELECTIVITY EFFECT OF COBALT AND NICKEL SECOND METALCO-IMPREGNATION WITH ZINC ON ZSM-5 FOR AROMATIZATION OF PROPANE

G.G. Oseke[1,*], A. Y. Atta[1*], B. Mukhtar[1], B. J. El-Yakubu[1] and B. O. Aderemi[1]
[1]Chemical Engineering Department, Ahmadu Bello University, Zaria.
*Corresponding author email:osechemtechy@gmail.com

ABSTRACT
Conversion of light alkanes catalytically to aromatic compounds is an important research area of interest. This is because aromatic compound are the major feedstocks for petrochemical industries. Zn/ZSM-5 has been found to improve aromatic selectivity of HZSM-5 but unstable. Hence the need for stabilizing Zn with another metal. The interaction of Zn with Co and Ni on ZSM-5 shows a higher selectivity towards aromatics over 85%. This improved Zinc stability on ZSM-5 as compared to only Zinc with dwindling selectivity to 50% and HZSM-5 of 10% at TOS of ten hours. Catalyst physicochemical properties were analysed with XRD, BET, N_2-adsorption, FTIR, FTIR-Pyridine, SEM, and TEM. The XRD and FTIR characterization showed that the modified catalysts were still crystalline after metal impregnation. The products distribution also showed reduced light gases formation and formation of more aromatics. The synergistic interaction between Ni and Co with Zn metal improved the catalytic performance of Zn-Co/ZSM-5 and Zn-Ni/ZSM-5 catalysts by promoting and sustaining the dehydrogenation step and suppressing protolytic cracking step in the reaction series resulting in the recorded significant improvement in aromatic yield over the monometallic Zn/ZSM-5 catalyst.

1.0 INTRODUCTION

The conversion of propane to aromatics has been a subject of interest to industrialists and academia within the last two decades. This is not unconnected with the rising cost of naphtha, while many nations in the world like Nigeria are being declared to be more of gas rich nation. It is becoming more important and imperative to start considering ways to transform these abundant gas resources (light alkanes such as propane) to aromatic compound which are building block and feedstock to petrochemical and chemical process industries. Propane exists in large deposits in natural gas reservoirs, gas condensate, and refinery gases (Derouane *et al.,* 2006: Asaftei *et al.,* 2009).

Lots of researches have been conducted over time to understudy the kinetics and mechanism of propane transformation to aromatics (Fechete *et al.*, 2012: Armor, 2011). It was found that the reaction steps majorly includes: Protolysis, hydride transfer, beta-scission, alkylation-dealkylation, dehydrogenation, oligomerization, olefin adsorption and desorption, alkanes adsorption and desorptions, cyclization and aromatization. Most related researches from kinetic and thermodynamic views have revealed that propane protolytic cracking step is the rate limiting step and the hydride transfer which is recombination of the abstracted hydrogen with the radical intermediates further limits the progression of the reaction to form aromatics (Lindström and Lars, 2003: Bhattacharya and Sivasanker, 1996: Rane *et al.,* 2006: Xu *et al.,* 2013)

Modification of catalyst by metal anchoring on ZSM-5 catalyst had made up part of the efforts applied to solve this challenge. These include developments of monometallic zeolitic catalysts i.e. Pt/ZSM-5, Ga/ZSM-5, Zn-ZSM-5, Mo/ZSM-5 aimed at promoting protolytic scission over

C=C cracking and improve cyclization to aromatization (Bhan and Nicholas, 2008: Choudhary *et al*., 1996: Choudhary *et al*., 2006: Guisnet *et al.,* 1992: He, 2015) Zn/ZSM-5 emerged as the most promising catalyst considering cost effectiveness, selectivity toward aromatics, minimization of light gases production and environmental friendliness when compared to Ga or Pt based ZSM-5. However, it is unstable at aromatization process operating temperature and its loss is irreversible (Jiang *et al*., 1988). Also, all attempts to correct this ZSM-5 Zn-based catalyst modification can only help to enhance aromatic selectivity, but cannot inhibit severe coke formation on the catalyst which is another challenge that can be generated rather than improving the whole reaction process. These put limit to industrial application and commercialization of the process.

The need to enhance Zn/ZSM-5 catalyst stability and activity at reaction operating condition thus call for the introduction of the second metal to make bimetallic stable and active catalysts. Other approaches to mitigate this challenge include incorporating the Zn into the zeolite intra-framework or create hierarchical structure in the zeolite (Ogunronbi *et al*., 2015).

Therefore, this work studied the effect of the addition of cobalt and Nickel as a second metal due to their atomic size similarity, same oxidation states and closer electronegativity on zinc activity, aromatic selectivity and catalyst lifespan on stream on bimetallic catalyst for propane aromatization.

2. METHODOLOGY

2.1. Catalyst Preparation

NH_4-ZSM5 (Si/Al=50) was sourced commercially from Sigma Aldrich and calcined to HZSM-5 at 550^oC for five hours. Aqueous solutions containing 2 wt. % of ZnO from $Zn(NO_3)_2$ as precursor 2 wt. % of Co_3O_4 from ($Co_3(NO_3)_2$ as precursor and 2 wt. % of NiO from $Ni(NO_3)_2$ as precursor were co-impregnated by introducing them at the same time dropwise on solution of H-ZSM5 catalysts while stirring for effective mixing, and dried at 70 ^oC. The samples were further dried at 80 ^oC for 16 hours and then calcined by temperature programmed furnace at 550 ^oC (4 ^oC per minute ramping) for five hours.

2.2 Catalyst Characterization

The metallic content in the catalyst were determined by a handheld XRF machine, Thermofisher Scientific NITON XL3t Waltham, Massachusetts USA. FTIR spectra measurements were performed using Shimadzu FTIR-8400s Spectrophotometer instrument with a MCT detector (64 scans, 4cm^{-1}) at National Research Institute of Chemical Technology, Zaria. Pyridine-adsorbed Fourier Transform Infrared Spectroscopy (Py-FTIR) was used to determine the amount of Brønsted and Lewis acid sites using Shimadzu FTIR-8400s Spectrophotometer equipment. 20 mg of each catalyst was degased at 200^oC in an oven and then put in a desiccator for pyridine adsorption at atmospheric temperature. The suction was allowed for about thirty minutes after which the catalyst were re-weighed to measure the increment in mass due to pyridine adsorption and then pressed into a regular wafer and put in an infrared cell, and this spectrum was used as background for the 95 adsorbed pyridine experiments. Pyridine was then adsorbed to a 5.0×10-2 Pa equilibrium pressure at 30 °C. FTIR spectra were recorded.

The powder X-ray diffraction (XRD) patterns were obtained on a Siemens D500 X-ray Powder Diffraction (XRD) using Cu Kα. The anode was operated at 40 kV and 40 mA. X-Ray. The

catalysts were scanned in continuous mode at wavelength K_{alpha1}= 1.540598, K_{alpha2}= 1.544426 and K_{beta}=1.392218 $2\theta=10^{o}$-80^{o} at scanning speed of 12°/min°.

Nitrogen adsorption and BET analyses were performed at 77 K using Micromeritics ASAP-2020 unit at Jubilee Campus University of Nottingham, UK. Catalyst samples were vacuum-degassed at 300^{0}C for 10 hours to remove surface humidity and pre-adsorbed gases before exposure to adsorption gas. The specific surface areas of the catalyst samples were calculated from the Nitrogen isotherm data using the Brunauer–Emmett–Teller (BET) model. The micropore volumes and micropore areas were measured using t-plot analysis Brunauer, *et al.*, 1938: Lippens *et al.,* 1964: Ahmad *et al.,* 2016)

Morphology of the catalyst samples surface were obtained using Scanning Electron Morphology Machine HITACHI S4800. Resolution : 1.0 nm (15KV) Tanning Electron Morphology TEM images of the catalyst samples were obtained on a FEI Tecnai G2 Spirit STEM.

2.3 Performance Test

Performance tests of the prepared catalysts were carried out in a stainless-steel fixed bed continuous flow reactor with internal diameter of 9 mm. 0.5 g of the catalyst samples was mixed with 0.5g of silica glass beads. The catalysts were degassed under inert nitrogen flow environment as the temperature rose through the reactor to 540°C for two hours before the flowing in propane into the reactor. Propane was introduced to flow through the reactor. Aromatization reaction was carried out at 540°C and Gas Hourly Space Velocity (GHSV) of 1200 mL/g-h, pure propane and nitrogen of ratio 1:2 under atmospheric pressure. The gaseous products were analysed in-situ by an online Buck Scientific GC 910 gas chromatograph equipped with a Thermal Conductivity Detector TCD having a Molsieve 13X packed column for hydrogen, nitrogen and hydrogen detection and a flame ionization detector (FID) connected to Restek MTX1 and HAYESEP D oven packed column for hydrocarbon and aromatics detection analysis. Aromatic and other hydrocarbon selectivities were calculated based on the total carbon moles with a unit of Carbon-mole, that is ratio of each product with respect to the total moles of Carbon-containing products and carbon balance.

3.0 RESULTS AND DISCUSSIONS

3.1 Characterizations

Figure 1 shows the FTIR spectra of the catalyst sample. Peak intensities at 450 and 550 cm-1 show pentasil ring of ZSM-5 while 1100 and 1225 cm-1 correspond to bridged silanol Brönsted acid sites (Si-OH-AL) and Lewis acid sites (AL-OH) respectively. The bands at 3400 and 1700 cm-1 = stretching and bending vibration of hydroxyl (OH^{-}) group of physically absorbed water on the surface of HZSM-5 zeolite. The FT-IR spectra in the OH stretching region suggested that HZSM-5 contained Brönsted acid groups also on 3610 cm–1 associated with the framework aluminium [Si(OH)Al], isolated external silanol groups (3740 cm–1), free internal silanol groups (3730 cm–1), and delocalized hydrogen-bonded groups (3500 cm–1) of lattice defects. For Zn/HZSM-5, the introduction of Zn species has little effect on the OH groups associated with 3500 and 3740 cm–1. The silanol groups characterized by 3730 cm–1 decreased slightly, which was attributed to the interaction between the internal silanol groups and Zn (OH)+ and other loaded metal cations located in cationic positions of the zeolites. The Brönsted acid peak (3610 cm–1) decreased obviously, suggesting the replacement of the zeolite protons by the impregnated Zn and other metals (Ni and Co).

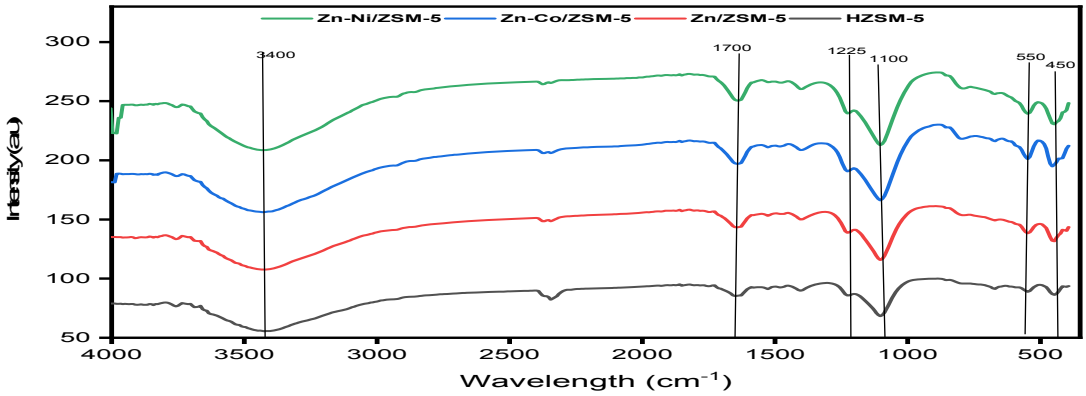

Figure 1: FTIR spectra of the catalyst samples.

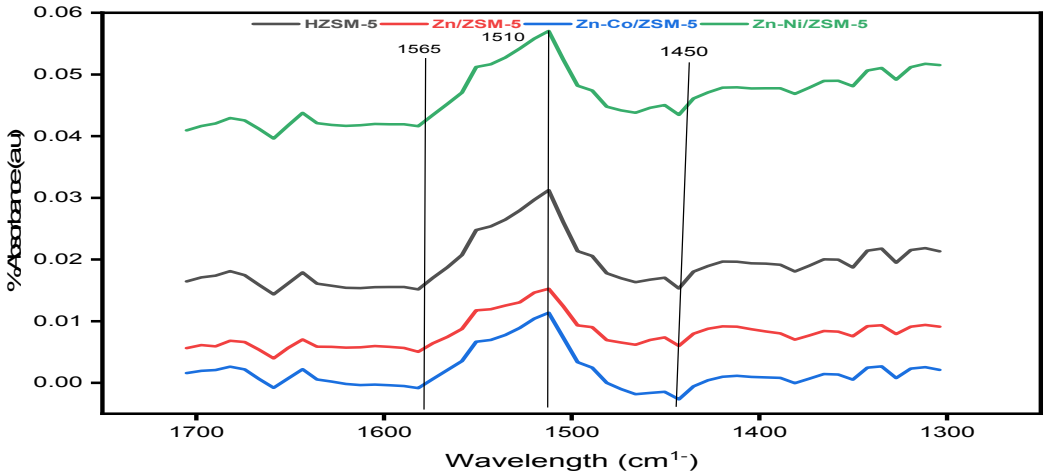

Figure 2: Pyridine-IR spectra of catalyst sample.

Figure 2 shows the Pyridine-FTIR spectra of zeolitic catalysts. Three characteristic peaks around 1450,1540 and 1490cm^{-1} are observed in all of the catalyst though there were little shifts, they represent the amount of Lewis acid sites, Bronsted acid sites and both Bronsted and Lewis acid sites respectively (He *et al.*, 2015). Lewis acid sites enhance the process of dehydrogenation and aromatization (Ni *et al.,* 2014: Cihanoglu *et al.*, 2015).

Figure 3 shows the XRD patterns of the synthesized catalysts together with ZSM-5 as control catalyst. This analysis revealed that the loading of Zn, Ni and Co oxides in accessible positions inside the zeolite matrix had no influence on its crystallinity. However, intensities of characteristic peaks were changed due to filling of metallic oxides into the zeolite matrix of ZSM-5. The characteristic peak intensities were suppressed as the X-ray absorption was fevered by the presence of Zn Co and Ni oxide particles (Wu *et al.*, 2009: Li *et al.,* 2009: El-Shall *et al.*, 2009: Yanming *et al.*, 2016).

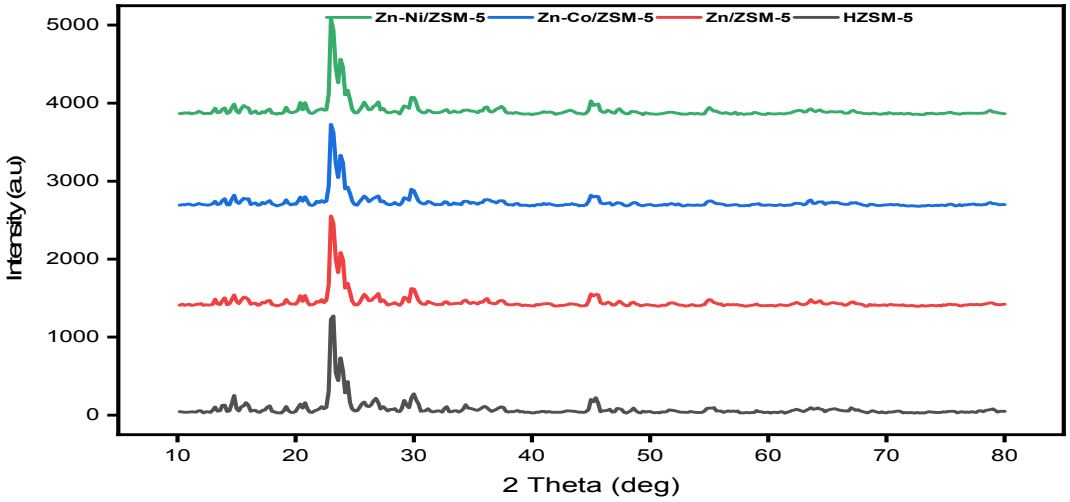

Figure 3: XRD analysis of parent and metal cation-loaded ZSM-5 zeolites

The Textural physical properties of the catalyst samples are provided in Table 1. Addition of metal oxides via co-impregnation of their precursor and their thermal decomposition during calcination had a little effect of specific surface area reduction. This decrease is attributed to the filling of the metallic oxides inside the pores and also on the surface of the matrix and decreased the pore volume, and specific area in turn. Metal co-impregnation on ZSM-5 did not affect the micro porosity of the zeolite structure (Wu et al., 2005). Thus, from the XRD and BET results of the metal incorporated catalysts compared to the parent HZSM-5, it follows that the oxides of Zn, Co and Ni might have been deposited on the outer surface of the zeolite.

Nitrogen adsorption and desorption isotherm plots are shown in Figure 4 for all the prepared catalysts. All the plots for the catalysts represent a Type I isother with high level microporosity as revealed in the BET surface area. The summary of the surface area and micropore analysis is shown in Table 1. Addition of Zn to the parent HZSM-5 decreased the total surface area, including the micropore area and the external (mesopore) surface area of the catalyst. As Co was added to Zn/ZSM-5 further decrease in the external surface area resulted.

However, their micropore area did change slightly compared to Zn/ZSM-5, suggesting that the Co metal particles did not diffuse much into the micropore structure of the zeolite. The addition of Ni to the Zn/ZSM-5 catalyst showed increased surface area. This may suggest that some Ni particles occupies sideway attachment to the external acid sites on the ZSM-5 structure while some on the surface.

The SEM and TEM study of synthesized catalyst are presented in Figure 5. The morphology of the parent ZSM-5 Figure 5 a and b was significantly changed after the addition of metallic oxides and as the loading increased as seen in a, b, c and d. The evenness of metallic oxide dispersion could be observed clearly in images in Figure 5 a-h

This also has been explained that large amount of Zn-Lewis acid sites ($ZnOH^+$ species) for dehydrogenation and aromatization, are produced more than ZnO with the introduction of Ni and Co species. This enhanced effective dispersion of the active $ZnOH^+$ as shown by TEM and SEM images thereby bringing it to tighter interaction of $ZnOH^+$ with the zeolite framework making it difficult to drain it out from the surface of zeolite as compared to ZnO. This made

more sites available for dehydrogenation and aromatization thus improving the catalysts' selectivity towards aromatics and stability.

Zn-Ni/ZSM-5 has greater stable and sustain selectivity towards aromatics because of its unique properties of same oxidation state similar atomic size and electronegativity with Zinc. Zn-Co/ZSM-5 has improved selectivity toward toluene among other aromatics in the product distribution. This is attributed to more alkylation of toluene from methane dehydrogenation. Figures 8, 9 and 10 show the effect of Ni and Co on product distribution.

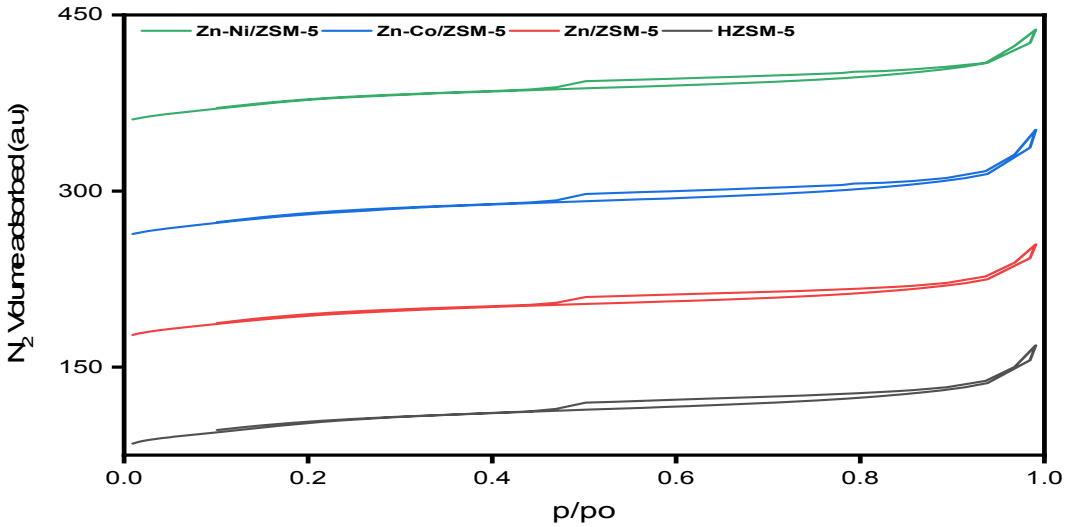

Figure 4: N2-adsorption of parent and metal cation-loaded ZSM-5 zeolites

The remarkable increase and sustained selectivity towards aromatics as seen in Figure 9 and 10 are as a result of enhanced primary aromatization through dehydroaromatization as well as suppressed cracking and subsequent H-transfer reaction.

4.0 CONCLUSION

In summary, Zinc based bimetallic catalyst containing Cobalt and Nickel were prepared and tested for propane aromatization. All physicochemical properties in characterizations revealed that the crystallinity and structure of the zeolite were preserved. The modified catalysts had strong influence on activity, aromatic selectivity and product distribution with minimized undesired products when compared to already existing catalyst. The promotional and stabilizing effect of Cobalt and Nickel on Zinc instability were observed with sustained improved and sustained selectivity towards aromatics. The introduction of these metals help to disperse zinc making more sites available for dehydrogenation reaction step and as a result improving aromatic selectivity and minimize catalyst deactivation. The developed bimetallic catalyst will contribute to the development industrial catalysts with high activity and superior stability for desired aromatic production for petrochemical and chemical process industries.

REFERENCES

Abdelsayed, V., Shekhawat, D., Poston Jr, J. A., & Spivey, J. J. (2013). Synthesis, characterization, and catalytic activity of Rh-based lanthanum zirconate pyrochlores for higher alcohol synthesis. Catalysis today, 207, 65-73.

Ahmad, M., Farhana, R., Raman, A. A. A., & Bhargava, S. K. (2016). Synthesis and activity evaluation of heterometallic nano oxides integrated ZSM-5 catalysts for palm oil cracking to produce biogasoline. Energy conversion and management, 119, 352-360.

Armor, John N. "A history of industrial catalysis." Catalysis Today 163.1 (2011): 3-9.

Asaftei, I. V., Bilba, N., Birsa, L. M., & Iofceab, G. (2009). Aromatization of industrial feedstock mainly with butanes and butenes over HZSM-5 and Zn/HZSM-5 catalysts. Acta Chennica Lasi, 17, 5-34.

Bhattacharya, D., and S. Sivasanker. "Aromatization of n-hexane over H-ZSM-5: Influence of promoters and added gases." Applied Catalysis A: General 141.1-2 (1996): 105-115.

Brunauer, S., Emmett, P. H., & Teller, E. (1938). Adsorption of gases in multimolecular layers. Journal of the American chemical society, 60(2), 309-319.

Derouane, E. G., Parmon, V., Lemos, F., & Ribeiro, F. R. (Eds.). (2006). Sustainable Strategies for the Upgrading of Natural Gas: Fundamentals, Challenges, and Opportunities: Proceedings of the NATO Advanced Study Institute, held in Vilamoura, Portugal, July 6-18, 2003 (Vol. 191). Springer Science & Business Media.

Fechete, I, Ye W, and Jacques C. V. (2012) "The past, present and future of heterogeneous catalysis." Catalysis Today 189.1: 2-27.

Lindström, Bård, and Lars J. Pettersson. "A brief history of catalysis." Cattech 7.4 (2003): 130-138.

Lippens, B. C., Linsen, B. G., & De Boer, J. H. (1964). Studies on pore systems in catalysts I. The adsorption of nitrogen; apparatus and calculation. Journal of Catalysis, 3(1), 32-37.

Ogunronbi, K. E., Al-Yassir, N., & Al-Khattaf, S. (2015). New insights into hierarchical metal-containing zeolites; synthesis and kinetic modelling of mesoporous gallium-containing ZSM-5 for propane aromatization. Journal of Molecular Catalysis A: Chemical, 406, 1-18.
Rane, N., Overweg, A. R., Kazansky, V. B., Van Santen, R. A., and Hensen, E. J. M. (2006). Characterization and reactivity of Ga+ and GaO+ cations in zeolite ZSM-5. Journal of Catalysis, 239(2), 478-485.

Wu, X. N., Zhao, H. T., Li, J., Schlangen, M., & Schwarz, H. (2014). Highly regioselective hydride transfer, oxidative dehydrogenation, and hydrogen-atom abstraction in the thermal gas-phase chemistry of [Zn (OH)]+/C 3 H 8. Physical Chemistry Chemical Physics, 16(48), 26617-26623.

Xu, Yuebing, Yoshizo Suzuki, and Zhan-Guo Zhang. "Comparison of the activity stabilities of nanosized and microsized zeolites based Fe–Mo/HZSM-5 catalysts in the non-oxidative CH4 dehydroaromatization under periodic CH4–H2 switching operation at 1073 K." Applied Catalysis A: General 452 (2013): 105-116

Zhao, Y., Liu, X., & Han, Y. (2015). Microporous carbonaceous adsorbents for CO 2 separation via selective adsorption. RSC Advances, 5(38), 30310-30330.

Proceedings of the 49th NSChE Annual Conference
KADA 2019: pp 814-822

P2C-05: PREDICTION OF FILM FRACTION IN AN ANNULAR GAS-LIQUID FLOW ACROSS A VERTICAL LARGE DIAMETER PIPE

A. M. Badeko[1,*], A. Mohammed[1], A. Mukhtar[1], J. N. Samson[2]
[1]Chemical Engineering Department Federal University of Technology, Minna, Niger State, P. M. B. 65, Nigeria.
[2]Chemical Engineering Department University of Abuja, Nigeria
Corresponding author: Email: mabadeko@gmail.com, Tel: +2348036528250

Abstract
Several research efforts were made in the past to study annular flow for both vertical and horizontal pipes, but the attention was mainly on small diameter pipes (diameter less than 100mm) with little or no emphasis laid on large diameter pipes. However, in this research work an attempt is made to develop an empirical model that can predict liquid film fraction across a vertical large diameter pipe (D = 127mm). The empirical model was based on some dimensionless numbers such as liquid and gas Renolds number and also liquid and gas Weber Number. The empirical model developed in this work for the prediction of liquid film fraction is $\varepsilon = 1.9x10^{7} Re_G^{-1.4688} Re_L^{0.0701} We_G^{-0.2276} We_L^{-0.0099}$*. There was good agreement between the predicted liquid film fraction and the experimental values when measured at different vertical positions across the vertical riser (i.e. 8.1m, 8.3m, 8.4m and 8.5m). Using the Pearson product moment correlation coefficient, the predictions were 90.6%, 84.7%, 81.1% and 98.3% respectively.*

Keywords: Dimensionless number; Empirical model; Liquid film fraction; Superficial velocity.

1.0 INTRODUCTION

Annular gas-liquid two phase flow is a very important flow configuration that occurs in many relevant applications such as in nuclear reactors, power plants, petroleum and process industries. It is a flow regime that is characterized by a high velocity gas flowing within the core of the pipe carrying some entrained liquid droplets and a thin liquid layer stationary positioned and/or moving along the internal wall of the pipe (Kaji and Azzopadi, 2010). Typically, annular gas-liquid flow are usually encountered in heat exchangers, deepwater risers in hydrocarbon production, gas condensates transport pipes, air conditioners and steam boilers used in nuclear and thermal power plants. Accurate prediction of the flow behaviour such as film fraction is very important for the safe and efficient design of heat transfer equipment, oil and gas pipelines and other process transport equipment.

Several research works have been done in the past decades on upward and downward two-phase air-water annular flow using smaller diameter pipes (i.e diameter less than 100mm) and a lot of mechanistic and empirical models have been developed to characterize the flow behaviour, however for large diameter pipes (i.e diameter greater than 100mm) not much research effort have been made as compared to the former leading to dearth of information in the literature for large diameter pipes. Consequently, data and models for small diameter pipes have been extrapolated for use in the design and operation involving large diameter pipes (Abdulkadir et al., 2019) which in most cases do not yield accurate results. However, it has been observed by other researchers such as Omebere-Iyari (2006), Kaji and Azzopadi (2010), Aliyu (2015), Lao et al. (2012) among others that the flow structures in large diameter pipes are different when compared to the small diameter pipes for instance the conventional slug flow characterised by bullet shaped Taylor bubbles does not manifest in large diameter pipes instead, there is a gradual transition from bubbly to churn flow (Aliyu, 2015).

Meanwhile, an attempt is made in this research work to develop an empirical model to predict film fraction in an annular air-water flow across a vertical large diameter pipe. The film fraction is a very important hydrodynamic parameter and is useful in determining the pressure drop and in the design of separation equipment in the petroleum industry (Ternyik et al, 1995).The models and empirical correlations that currently exist in open literature used in predicting film fraction were developed using data from small diameter pipes and cannot be applied correctly in the design of systems involving large diameter pipes such as risers used in petroleum production. There is therefore the need to develop a new film fraction correlation based on data from large daimeter pipes and this forms the gap that this research effort tries to address.

2.0 METHODOLOGY

In this research, a systematic procedure for developing an empirical dynamic model as proposed by Ljung, (1999) was used. The procedure consists of the following steps:

2.1 Formulation of model objectives

The primary objective of the empirical model to be developed is for the model to be able to predict liquid film fraction in an annular flow across a vertical large diameter pipe (127mm) using the superficial velocity, density, viscosity and surface tension of both the air and water as the input parameters. However, these input parameters were used to determine the Weber number and the Reynolds number for both phases and these dimensionless numbers were used in the model formulation.

2.2 Selection of the input and output variables for the model

The experimental data used in this research work were obtained from the work performed by Abdulkadir, (2011) at the L3 Laboratories of the Department of Chemical and Environmental Engineering at the University of Nottingham. The experiments were performed using the 127mm diameter riser where the film fraction measurements were carried out at positions 8.1m, 8.3m and 8.4m respectively along the vertical direction. Abdulkadir,(2011) reported in his work that the temperature of the air and the mains tap water were all maintained at 25^{o}C.

2.3 Evaluation of available data

The experimental data obtained from the work of Abdulkadir (2011) where measurements of film fraction were done at different combination of gas and liquid superficial velocities was analysed using the Microsoft excel. In the analysis, the Weber Number and the Reynolds Number for both the liquid phase (water) and the gas phase (air) were computed. The physical properties of the phases were obtained at the experimental conditions of 25^{o}C temperature and pressure of 2.0 bar. The density of air and that of water are 3.53kg/m^3 and 986kg/m^3 respectively. The surface tension was also obtained as 0.07199 N/m and the viscosity of air at 25^{o}C is 8.90 x 10^{-4} Pa.s

The gas Weber number was computed using equation (1) as stated below:

$$We_g = \frac{\rho_g u_{gD}^2}{\sigma}\left(\frac{\Delta\rho}{\rho_g}\right)^{\frac{1}{4}} \qquad (1)$$

But the liquid Weber Number was computed using the equation below:

$$We_L = \frac{\rho_l u_{lD}^2}{\sigma} \qquad (2)$$

The liquid and gas Reynolds Number will be computed using the equation below:

$$Re = \frac{\rho u D}{\mu} \qquad (3)$$

Where ρ = Density, kg / m^3 (subscript 'g' and 'l' for both gas and liquid respectively)
U = superficial velocity, m/s (subscript 'g' and 'l' for both gas and liquid respectively)
D = Pipe diameter, m
σ = Surface tension, N/m
μ = Viscosity, Ns/m^2

The plot of the film fraction with each of these dimensionless numbers will be made using the power law to determine the functional relationship between them.

$$\varepsilon = (We_g)^a \quad (4)$$

$$\varepsilon = (We_l)^b \quad (5)$$

$$\varepsilon = (Re_g)^c \quad (6)$$

$$\varepsilon = (Re_l)^d \quad (7)$$

where ε is the film fraction, We_g, We_l, Re_g and Re_l are the Weber Number and the Reynolds Number for both the gas and liquid phase. The exponents a, b, c, and d are determined graphically when the plot of these dimensionless numbers are made with the film fraction. The exponents from the equations were entered into a Microsoft Excel program called SOLVER as the initial values for iteration. The SOLVER is a Microsoft Excel add-in program used for 'what if' analysis. It is used to find an optimal (maximum or minimum) value for a formula in one cell called the objective cell subject to constraints or limits, on the values of other formula cells on a worksheet. SOLVER works with a group of cells, called decision variables or simply variable cells that are used in computing the formulas in the objective and constraint cells. SOLVER adjusts the values in the decision variable cells to satisfy the limits on constraint cells and produce the result you want for the objective cell. In this work, the exponents on each of the dimensionless numbers are the decision variables, the formula is the empirical model consisting of the gas and liquid Weber number and the gas and liquid Reynolds number to predict film fraction while the constraint cell is the sum of the squares of the difference between the experimental and predicted film fraction. The goal is to minimise the constraint cell as much as possible in order to improve the predictive ability of the empirical correlation.

2.4 Selection of the model structure and level of model complexity

Based on the description of the physics of the system adequately represented by the Weber Number and the Reynolds Number for the gas and liquid phases, the functional form of the empirical model to predict film fraction across a vertical pipe in an annular flow can be obtained as:

$$\varepsilon = (We_g)^a (We_l)^b (Re_g)^c (Re_l)^d \quad (8)$$

The proposed empirical model is a simple model to use because the input parameters (the superficial velocities for both the gas and liquid phase and their physical properties) can easily be obtained from laboratory measurements.

3. RESULTS AND DISCUSSION

3.1 Dependence of liquid film fraction on the gas superficial velocity at constant liquid superficial velocity

From the Figure 1, it can be observed that as the superficial velocity of the gas increases from 950m/s to 1,500m/s while keeping the superficial velocity of the liquid constant (40m/s), the

liquid film fraction which is essentially the fraction of the liquid in the riser existing as a thin film layer along the internal wall of the riser decreases from 0.06857 to 0.03382 along the 8.1m measuring position in the vertical riser and the same applies to other measuring locations in the riser. The reduction of the film fraction at constant superficial liquid velocity and increasing gas velocity is as a result of the increasing inertia force created as a result of increasing superficial velocity which potentially peels off a portion of the liquid film along the interface between the film layer and the gas core thereby increasing the amount the liquid entrained in the gas core while reducing the liquid film fraction as alluded to by other researchers such as Thome and Cioncolini (2009).

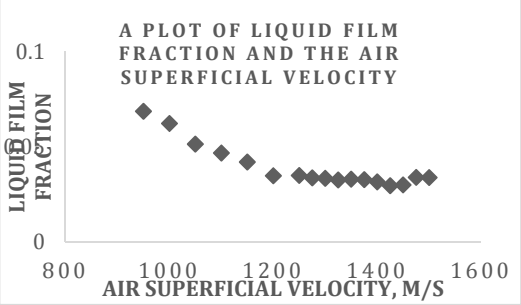

Figure 1: Gas superficial velocity versus liquid film fraction at constant superficial liquid velocity.

3.2 Dependence of the liquid film fraction on the liquid superficial velocity.

From Figure 2, it can be observed that as the superficial liquid velocity increases from 40m/s to 150m/s and at constant superficial gas velocity, the liquid film fraction increases from 0.039103 to 0.060516 though the film fraction remained almost constant between 60m/s and 150m/s superficial liquid velocity. The increase in the liquid film fraction as the superficial liquid velocity increases is as a result of the increased amount of liquid available within the measuring location which essentially increases as the superficial liquid velocity increases.

3.3 Dependence of the liquid film fraction on the gas Reynolds number (Re_G)

Figure 3 shows the plot of the liquid film fraction and the gas Reynolds Number. In order to understand the variation of the liquid film fraction as the fluid velocity increases, there is a need to understand the nature of forces at play in forming the liquid film thickness and entrained droplets within the gas core. Some of the forces include the inertia force and the viscous force. The competition between these forces determines the amount of liquid that will form the thin liquid film and equally the liquid that will be entrained into the gas core. The dimensionless number that captures the interplay between these forces is the Reynolds Number. In the Figure 4.3 above, it can be observed that as the gas Reynolds Number increases from 478,533 to 755,578 which implies a highly turbulent flow regime, the liquid film fraction decreases from 0.068568 to 0.03382. The decrease in the liquid film fraction as gas Reynold number increases is a result of the increase in the inertia force which tend to convert some layer of the liquid film into droplets in the gas core, thereby reducing its thickness and invariable the overall liquid film fraction (Berna et al, 2014).

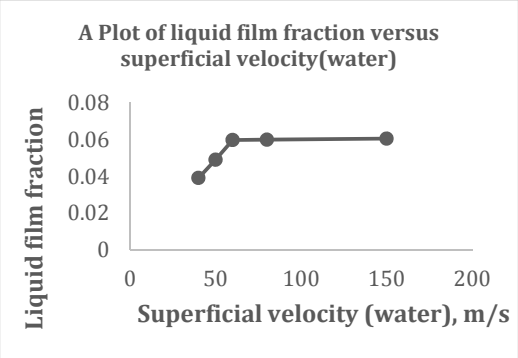

Figure 2: Liquid superficial velocity versus liquid film fraction at constant superficial gas velocity.

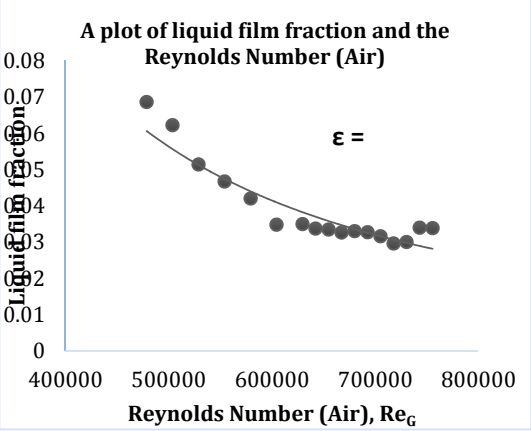

Figure 3: Liquid film fraction versus the Gas Reynolds Number.

2.4 Dependence of the liquid film fraction on the liquid Reynolds Number (Re_L)

Figure 4 shows the relationship between the liquid film fraction and the liquid Renolds Number. From the chart, it can be observed that the liquid film fraction increases from 0.039103 to 0.060516 as the liquid Reynolds Number increases from 5,627,955 to 21,104,831. The increase in the liquid film fraction as the liquid Reynolds Number increases is as a result of the increase in the superficial velocity of the liquid which tends to increase the quantity of the liquid moving into the measuring location thereby increasing the thickness of the liquid film around the internal wall of the riser and inadvertently increasing the liquid film fraction.

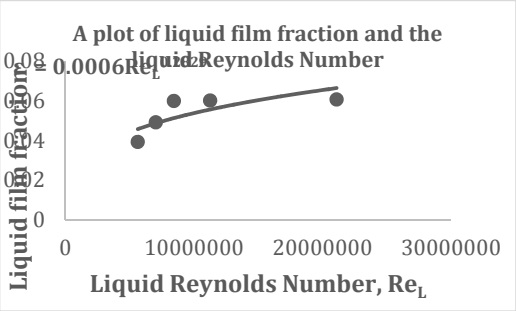

Figure 4: Liquid film fraction versus the Liquid Reynolds Number.

3.5 Dependence of the liquid film fraction on the gas weber number (We_G)

Figure 5 shows the relationship between the liquid film fraction and the gas Weber Number. The Weber Number is the dimension number that captures the interplay of inertia force and surface tension force which according to Ju (2015) governs the formation of the liquid film thickness. In fact, according to Ju (2015), the inertia force tends to break the liquid at the interface (i.e. to form droplets) while the surface tension force tends to keep the liquid at the interface (i.e. thin liquid film thickness). From Figure 5, it can be observed that as the gas Weber Number increases from 5,600,101 to 13,961,470, the liquid film fraction decreases from 0.068568 to 0.03382. The decrease in the liquid film fraction as the gas Weber Number increases is as a result of the increase in the inertia force which tends to break the thin liquid layer into tiny droplets thereby reducing the thickness of the thin liquid film and the overall reduction of the liquid film fraction.

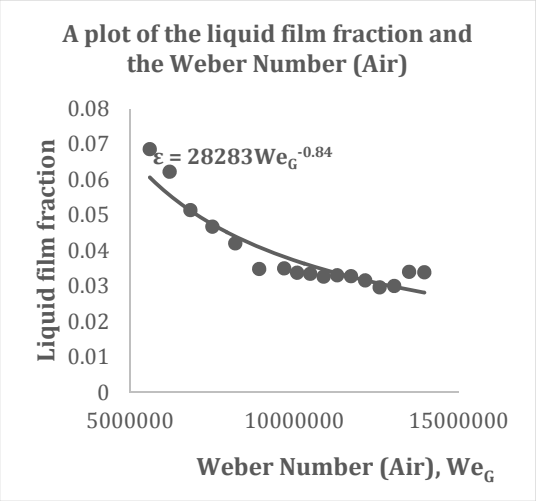

Figure 5: Liquid film fraction versus the Gas Weber Number

3.5 Dependence of the liquid film fraction on the liquid weber number (We_L)

Figure 6 shows the relationship between the liquid film fraction and the Liquid Weber Number. From the chart, it can be observed that as the liquid Weber Number increases from 2783098 to 39137311, the liquid film fraction equally increases from 0.039103 to 0.060516. The increase in the liquid film fraction as the liquid Weber Number increases is as a result of the increase in the superficial velocity of the liquid which tends to move a large quantity of the liquid and at constant gas superficial velocity, increases the thickness of the liquid film along the internal wall of the riser thereby increasing the film fraction.

The overall relationship between the liquid film fraction and the various dimensionless numbers can be summarized below:
For the gas Renolds Number:

$$\varepsilon = 2x10^{8}Re_G^{-1.68} \quad (1)$$

For the liquid Reynolds Number:

$$\varepsilon = 0.0006Re_L^{0.2829} \quad (2)$$

For the gas Weber Number:

$$\varepsilon = 28283We_G^{-0.84} \quad (3)$$

For the liquid Weber Number:

$$\varepsilon = 0.0056We_L^{0.1414} \quad (4)$$

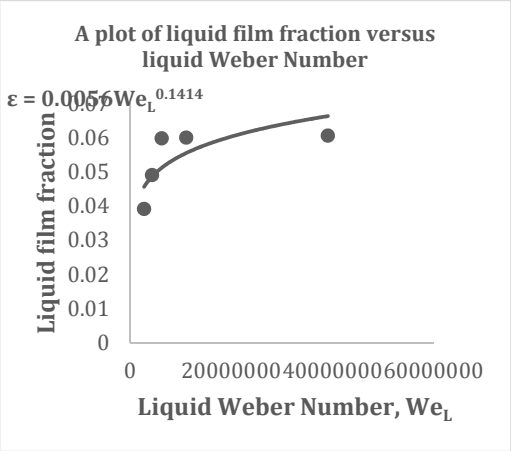

Figure 4.6: Liquid film fraction versus the Liquid Weber Number.

On combining all the dimensionless numbers to determine the overall relationship between them and the liquid film fraction, we have:

$$\varepsilon = 1.9x10^7 Re_G^{-1.68}\ Re_L^{0.2829}\ We_G^{-0.84}\ We_L^{0.1414} \quad (5)$$

The final correlation for the liquid film model can be represented as:

$$\varepsilon = 1.9x10^7 Re_G^{-1.4688}\ Re_L^{0.0701}\ We_G^{-0.2276}\ We_L^{-0.0099}$$

4.0 CONCLUSION

In this research work, the relationship between the liquid film fraction and the superficial gas and liquid velocities was investigated. It was observed that the liquid film fraction decreases as gas superficial velocity increases while it increases as the liquid superficial velocity increases. Similarly, the relationship between the liquid film fraction and the various dimensionless numbers that adequately describe the physics of the system were investigated. The dimensionless numbers include the gas and liquid Reynolds Number and gas and liquid Weber Number. It was observed that as the gas Reynolds Number and gas Weber Number increases, the liquid film fraction decreases and the reverse occur when the liquid Reynolds and Weber Numbers increases. Based on the relationships between these dimensionless numbers and the liquid film fraction, a new correlation that can predict liquid film fraction was developed, i.e. $\varepsilon = 1.9x10^7 Re_G^{-1.4688}\ Re_L^{0.0701}\ We_G^{-0.2276}\ We_L^{-0.0099}$.

REFERENCES

Aliyu, A.M., (2015). Vertical Annular Gas–Liquid Two-phase Flow in Large diameter Pipes. A PhD dissertation. Cranfield University, United Kingdom.

Aziz, K., Govier, G.W. & Forgasi, M., 1972. Pressure Drop In Wells Producing Oil And Gas. *Journal of Canadian Petroleum Technology*, 11(03).

Abdulkadir, M. (2011). Experimental and computational fluid dynamics (CFD) of gas–liquid flow in bends. PhD thesis, University of Nottingham, United Kingdom.

Abdulkadir M.,U.P. Mbalisigwe A. D. Zhao b , V. Hernandez-Perez c , B.J. Azzopardi d , S. Tahir e Characteristics of churn and annular flows in a large diameter vertical riser International Journal

Bhagwat, S.M., Mollamahmutoglu, M. & Ghajar, A.J., (2012). Experimental investigation and performance evaluation of isothermal frictional two phase pressure drop correlations in vertical downward gas-liquid two phase flow. *In Proceedings of the ASME 2012 Summer Heat Transfer Conference.* Rio Grande, Puerto Rico: ASME, 1–12.

Bhagwat, S.M., Mollamahmutoglu, M. & Ghajar, A.J., 2012. Experimental investigation and empirical analysis of non-boiling gas-liquid two-phase heat transfer in vertical downward pipe orientation. In Rio Grande, Puerto Rico: *ASME*, 1–11.

Bhagwat, S.M. & Ghajar, A.J., 2012. Similarities and differences in the flow patterns and void fraction in vertical upward and downward two phase flow. *Experimental Thermal and Fluid Science*, 39, 213–227.

Chen, L., (2006). Flow patterns in upward two-phase flow in small diameter tubes. PhD thesis, Brunel University UK.

Dalkilic, A. S., Laohalertdecha, S. & Wongwises, S., 2008. Two-phase friction factor in vertical downward flow in high mass flux region of refrigerant HFC-134a during condensation. *International Communications in Heat and Mass Transfer*, 35(9), 1147–1152.

Duns, H. & Ros, N.C.J., 1963. Vertical flow of gas and liquid mixtures in wells. *In World Petroleum Congress.* Frankfurt, Germany: World Petroleum Congress.

Hagedorn, A. & Brown, K.E., 1965. Experimental Study of Pressure Gradients Occurring During Continuous Two-Phase Flow in Small-Diameter Vertical Conduits. *Journal of Petroleum Technology*, 17(4),475 – 484.

Kaji, R. & Azzopardi, B.J., (2010). The effect of pipe diameter on the structure of gas/liquid flow in vertical pipes. *International Journal of Multiphase Flow*, 36(4), 303–313.

Lao, L., Xing, L. & Yeung, H., (2012). Behaviours of elongated bubbles in a large diameter riser. *In Multiphase 8*. Banff, Canada: BHR Group, 381–392.

Oddie, G., Shi, H., Durlofsky, L.J., Aziz, K.,Pfeffer, B., & Holmes, J.A., (2003). Experimental study of two and three phase flows in large diameter inclined pipes. *International Journal of Multiphase flow,* 29, 527 – 588.

Oliemans, R.V.A., Pots, B.F.M. & Trompe, N., 1986. Modelling of annular dispersed two-phase flow in vertical pipes. *International Journal of Multiphase Flow*, 12(5), 711–732.

Omebere-Iyari, N.K., (2006). The effect of pipe diameter and pressure in vertical two-phase flow. University of Nottingham.

Skopich, A. et al., 2015. Pipe-diameter effect on liquid loading in vertical gas wells. *SPE Production and Operations*, 30(2),164–176.

Tsoukalas, L.H., Ishii, M. & Mi, Y., 1997. A neurofuzzy methodology for impedance-based multiphase flow identification. *Engineering Applications of Artificial Intelligence*, 10(6),545–555.

Tambouratzis, T. & Pàzsit, I., 2010. A general regression artificial neural network for two-phase flow regime identification. *Annals of Nuclear Energy*, 37(5), 672–680.

Liu, Y. & Zhang, S., 2010. Local flow regime identification for boiling two- phase flow by BP neural networks approach. In *Sixth International Conference on Natural Computation*.362–366.

Zhao, X., 2005. *Mechanistic based models for slug flow in vertical pipes*. Texas Tech University.